

**ELECTROMAGNETICS,
MICROWAVE CIRCUIT AND
ANTENNA DESIGN
FOR COMMUNICATIONS
ENGINEERING**

SECOND EDITION

Peter Russer

**Electromagnetics, Microwave Circuit
and Antenna Design
for Communications Engineering**

Second Edition

For a complete listing of the *Artech House Antenna Library*,
turn to the back of this book.

Electromagnetics, Microwave Circuit and Antenna Design for Communications Engineering

Second Edition

Peter Russer



**ARTECH
HOUSE**

BOSTON | LONDON
artechhouse.com

Library of Congress Cataloging-in-Publication Data

A catalog record of this book is available from the Library of Congress.

British Library Cataloguing in Publication Data

A catalogue record of this book is available from the British Library.

ISBN 1-58053-907-6

Cover design by Igor Valdman

© 2006 ARTECH HOUSE, INC.

685 Canton Street

Norwood, MA 02062

All rights reserved. Printed and bound in the United States of America. No part of this book may be reproduced or utilized in any form or by any means, electronic or mechanical, including photocopying, recording, or by any information storage and retrieval system, without permission in writing from the publisher.

All terms mentioned in this book that are known to be trademarks or service marks have been appropriately capitalized. Artech House cannot attest to the accuracy of this information. Use of a term in this book should not be regarded as affecting the validity of any trademark or service mark.

International Standard Book Number: 1-58053-907-6

10 9 8 7 6 5 4 3 2 1

*Whatever is born,
animate or inanimate,
know them to be born
from the union of the field
and the field knower.*

Bhagadvadgita 13.26

Contents

Preface		xvii
Chapter 1	Introduction	1
	References	6
Chapter 2	Basic Electromagnetics	9
	2.1 The Electromagnetic Field Concept	9
	2.2 Field Intensities	12
	2.3 Current and Flux Densities	16
	2.4 Constitutive Relations	18
	2.5 The Charge Density	23
	2.6 The Maxwell Puzzle	24
	2.7 The Integral Form of Maxwell's Equations	26
	2.8 The Electromagnetic Wave	29
	2.8.1 The Wave Equation	35
	2.8.2 The Polarization of Electromagnetic Waves	36
	2.9 Kirchhoff's Laws	38
	2.10 Maxwell's Equations in Local Form	41
	2.11 Time-Harmonic Electromagnetic Fields	43
	2.12 Maxwell's Equations in the Frequency Domain	44
	2.13 Curvilinear Coordinates	46
	2.14 Boundary Conditions	47
	2.15 Problems	56
	References	59

Chapter 3	Potentials and Waves	61
3.1	The Electromagnetic Potentials	61
3.2	The Helmholtz Equation	65
3.3	Time-Harmonic Plane Waves	67
3.3.1	Time-Harmonic Plane Waves in Lossless Medium	69
3.3.2	Complex Waves	72
3.4	TM and TE Fields and Waves	74
3.5	Reflection and Transmission of Plane Waves	77
3.5.1	Reflection and Diffraction of a TE Wave at a Plane Boundary	80
3.5.2	Reflection and Diffraction of a TM Wave at a Plane Boundary	83
3.5.3	Total Reflection	86
3.6	Waves in Planar Layered Media	89
3.7	Thin Conducting Sheets	93
3.8	The Vector Wave Equation	94
3.9	Circular Cylindrical Waves	98
3.9.1	Excitation of a Cylindric Wave by a Uniform Current Filament	101
3.10	Spherical Waves	102
3.11	Problems	106
	References	107
Chapter 4	Concepts, Methods, and Theorems	109
4.1	Energy and Power	109
4.2	Field Theoretic Formulation of Tellegen's Theorem	116
4.3	Sources of the Electromagnetic Field	118
4.4	The Uniqueness Theorem	120
4.5	The Equivalence Principle	121
4.6	Babinet's Principle	123
4.7	Reciprocity	125
4.7.1	The Lorentz Reciprocity Theorem	125
4.7.2	The Reciprocity Theorem for Impressed Sources	126
4.8	Green's Function	128
4.9	The Integral Equation Method	133
4.10	The Free-Space Green's Dyadic Form	136
4.11	Green's Theorems	136
4.11.1	The Scalar Green's Theorems	136
4.11.2	Green's Theorems in Two Dimensions	138
4.11.3	The Vector Green's Theorems	140
4.12	Integral Formulation of the Equivalence Principle	141

4.13	The Sturm-Liouville Equation	143
4.14	Spectral Representation of Green's Functions	146
4.15	Problems	148
	References	148
Chapter 5	Static and Quasistatic Fields	151
5.1	Conditions for Static and Quasistatic Fields	151
5.2	Static and Quasistatic Electric Fields	153
5.2.1	Green's Function for the Static Electric Field	153
5.2.2	Capacitance	155
5.3	Static and Quasistatic Magnetic Fields	161
5.3.1	Green's Function for the Static Magnetic Field	161
5.3.2	Inductance	163
5.4	The Laplace Equation	169
5.4.1	Potential Separation Planes	170
5.4.2	Three-Dimensional Laplace Equation in Cartesian Coordinates	171
5.5	Conformal Mapping	174
5.5.1	Field of an Elliptic Cylindric Line	181
5.5.2	Field of a Coaxial Line	183
5.5.3	Parallel Wire Line	186
5.6	The Schwarz-Christoffel Transformation	191
5.6.1	The Coplanar Line	193
5.6.2	The Coplanar Stripline	196
5.6.3	The Stripline	197
5.7	Problems	201
	References	204
Chapter 6	Waves at the Surface of Conducting Media	207
6.1	Transverse Magnetic Surface Waves	208
6.2	Surface Currents	216
6.3	Surface Current Losses	221
6.4	Induced Surface Currents	224
6.5	Problems	227
	References	228
Chapter 7	Transmission-Lines and Waveguides	229
7.1	Introduction	229
7.2	Phase and Group Velocity	232
7.3	The Field Components	233
7.4	Waveguides for Transverse Electromagnetic Waves	235

7.5	Multiconductor Transmission-Lines	249
7.6	Quasi-TEM Modes of Transmission-Lines	254
7.6.1	Quasi-TEM Modes of Two-Conductor Transmission-Lines	254
7.6.2	Quasi-TEM Modes of Multiconductor Transmission-Lines	259
7.7	Planar Transmission-Lines	260
7.7.1	The Microstrip Line	260
7.7.2	Quasistatic Approximation for the Microstrip Line	262
7.7.3	Coplanar Waveguide and Coplanar Stripline	265
7.8	Hollow Waveguides	266
7.8.1	TE Modes	266
7.8.2	TM Modes	270
7.8.3	Modal Expansions in Waveguides	272
7.9	Rectangular Waveguides	276
7.9.1	Transverse Electric Modes	276
7.9.2	Transverse Magnetic Modes	282
7.9.3	Power Flow in the Waveguide	284
7.9.4	Orthogonality of the Waveguide Modes	285
7.9.5	Generalized Currents and Voltages in Waveguides	286
7.9.6	Attenuation Due to Conductor Losses	289
7.9.7	Attenuation Due to Dielectric Losses	291
7.10	Circular Cylindric Waveguides	292
7.10.1	The Circular Waveguide Modes	292
7.10.2	Power Flow and Attenuation in the TE_{01} Mode	298
7.11	Radial Waveguides	300
7.11.1	Radial Parallel Plate Waveguide	300
7.11.2	Wedged Radial Parallel Plate Waveguide	307
7.12	Spherical Waveguides	309
7.12.1	Conical Waveguide	311
7.12.2	Biconical Waveguide	313
7.13	Dielectric Waveguides and Optical Fibers	316
7.13.1	Homogeneous Planar Dielectric Waveguides	316
7.13.2	Dielectric Slab with Single-Sided Metallization	320
7.13.3	Circular Dielectric Waveguides with Step Index Profile	322
7.14	Problems	329
	References	333

Chapter 8	The Transmission-Line Equations	335
8.1	The Transmission-Line Concept	335
8.2	Generalized Voltages and Currents	337
8.3	Solution of the Transmission-Line Equations	341
8.4	Wave Amplitudes	344
8.5	Reflection Coefficient and Smith Chart	346
8.5.1	Impedance Matching with Lumped Elements	353
8.5.2	Impedance Matching with Stubs	355
8.6	Solution of the Multiconductor Transmission-Line Equations	356
8.7	Multimode Excitation of Uniform Hollow Waveguides	363
8.7.1	The Transverse Field Equations	363
8.7.2	Modal Field Representation	366
8.7.3	Multimode Transmission-Line Equations for Hollow Waveguides	368
8.7.4	Multimode Transmission-Line Equations of Lossless Waveguides without Internal Sources	374
8.8	Green's Functions for Transmission-Lines	375
8.8.1	Green's Function for the Transmission-Line with Matched Terminations	378
8.8.2	Green's Function for the Transmission-Line with Arbitrary Linear Passive Terminations	379
8.9	Problems	381
	References	384
Chapter 9	Resonant Circuits and Resonators	385
9.1	The Linear Passive One-Port	385
9.2	The Reactance Theorem	387
9.3	Resonant Circuits	389
9.4	The Transmission-Line Resonator	392
9.5	Cavity Resonators	395
9.5.1	The Rectangular Cavity Resonator	395
9.5.2	The Circular Cylindric Cavity Resonator	399
9.6	Coupling of Resonant Circuits and Resonators	402
9.6.1	The Loaded Quality Factor	402
9.6.2	Termination of a Transmission-Line with a Resonant Circuit	403
9.6.3	Inductive Coupling of Cavity Resonators	405
9.7	Orthogonality of the Resonator Modes	407
9.8	Excitation of Resonators by Internal Sources	409
9.9	Problems	411

References	412
Chapter 10	Passive Microwave Circuits
10.1	Linear Multiports
10.2	Source-Free Linear Multiports
10.2.1	Impedance and Admittance Representations
10.2.2	The Chain Matrix
10.2.3	The Scattering Matrix
10.2.4	The Transmission Matrix
10.3	Tellegen's Theorem
10.3.1	Connection Networks
10.3.2	Tellegen's Theorem for Discretized Fields
10.4	The Power Properties
10.5	Reciprocal Multiports
10.6	Elementary Two-Ports
10.7	Signal Flow Graphs
10.8	Lumped Element Equivalent Circuits
10.8.1	Foster Representation of Reactance Multiports
10.8.2	Cauer Representation of Radiating Structures
10.9	Obstacles in Waveguides
10.10	The Symmetry Properties of Waveguide Junctions
10.10.1	Symmetric Three-Port Waveguide Junctions
10.10.2	Symmetric Four-Port Waveguide Junctions
10.11	Problems
References	466
Chapter 11	Periodic Structures and Filters
11.1	Periodic Electromagnetic Structures
11.1.1	TE Modes in Rectangular Periodic Waveguides
11.1.2	Sinusoidal Variation of the Permittivity
11.2	Wave Parameter Theory of Two-Ports
11.3	Lumped Low-Pass Filter Prototypes
11.3.1	The Butterworth Prototype
11.3.2	The Chebyshev Prototype
11.4	Ladder Filter Networks
11.4.1	Butterworth Ladder Networks
11.4.2	Chebyshev Ladder Networks
11.5	Frequency Transformation
11.5.1	Low-Pass to High-Pass Transformation
11.5.2	Low-Pass to Band-Pass Transformation
11.5.3	Low-Pass to Band-Stop Transformation

11.6	Transmission-Line with Periodic Load	497
11.7	Plane Wave Scattering by Periodic Structures	501
11.7.1	Scattering of TE Waves by Periodic Structures	501
11.7.2	Scattering of TM Waves by Periodic Structures	505
11.8	Metamaterials	507
11.9	Problems	515
	References	517
Chapter 12	Radiation from Dipoles	519
12.1	The Hertzian Dipole	519
12.2	Aperiodic Spherical Waves	524
12.3	Vertically Oriented Electric Dipole over Lossy Half-Space	528
12.3.1	The Far-Field of the Vertical Dipole over Ground	538
12.3.2	The Surface Wave	539
12.4	Horizontally Oriented Electric Dipole over Lossy Half-Space	540
12.5	Problems	544
	References	545
Chapter 13	Antennas	547
13.1	Introduction	547
13.2	Linear Antennas	549
13.3	The Integral Equation for the Linear Antenna	555
13.4	The Impedance of the Linear Antenna	558
13.5	The Loop Antenna	560
13.6	Receiving Antennas	563
13.6.1	The Hertzian Dipole as Receiving Antenna	563
13.6.2	The Loop Antenna as Receiving Antenna	564
13.6.3	The Linear Dipole Antenna as Receiving Antenna	565
13.7	Gain and Effective Antenna Aperture	569
13.8	Antenna Arrays	575
13.8.1	Linear Antenna Arrays	575
13.8.2	Circular Antenna Arrays	577
13.9	Aperture Antennas	578
13.9.1	Radiating Apertures	578
13.9.2	Horn Antennas	582
13.9.3	Gain and Effective Area of Aperture Antennas	585
13.9.4	Mirror and Lens Antennas	587
13.9.5	Slot Antennas	589
13.10	Microstrip Antennas	591
13.10.1	Planar Rectangular Patch Antenna	593

13.11	Broadband Antennas	595
13.12	Problems	597
	References	601
Chapter 14	Numerical Electromagnetics	603
14.1	Introduction	603
14.2	The Method of Moments	605
14.3	The Transmission-Line Matrix Method	611
14.4	The Mode Matching Method	617
	References	623
Appendix A	Vectors and Differential Forms	627
A.1	Vectors	627
A.2	Differential Forms	631
A.2.1	Products of Exterior Differential Forms	632
A.2.2	The Contraction	633
A.2.3	The Exterior Derivative	634
A.2.4	The Laplace Operator	635
A.3	Stokes' Theorem	636
A.4	Curvilinear Coordinates	640
A.4.1	General Cylindrical Coordinates	646
A.4.2	Circular Cylindric Coordinates	647
A.4.3	Spherical Coordinates	650
A.4.4	Twisted Forms	653
A.4.5	Integration of Differential Forms by Pullback	653
A.5	Double Differential Forms	654
A.6	Relations between Exterior Calculus and Conventional Vector Notation	656
A.6.1	Differential Operators	656
A.6.2	Maxwell's Equations	656
	References	657
Appendix B	Special Functions	659
B.1	Ordinary Bessel Functions	659
B.2	Modified Bessel Functions	662
B.3	Spherical Bessel Functions	665
B.4	Legendre Polynomials	667
B.5	Spherical Harmonics	670
	References	672

Appendix C Linear Algebra	673
C.1 Unitary Vector Space	673
C.2 Diagonalization of a Matrix	679
C.3 Matrix Functions	681
C.4 The Hilbert Space	683
C.4.1 Linear Operators in Hilbert Space	686
C.4.2 Function Spaces	691
C.4.3 Function Spaces with Biorthogonal Basis	693
References	696
Appendix D Fourier Series and Fourier Transform	697
D.1 The Fourier Series	697
D.2 The Fourier Integral	699
D.3 The Delta Distribution	701
References	704
Appendix E Complex Integration	705
E.1 Analytic Functions	705
E.2 The Residue Theorem	707
E.3 The Saddle-Point Method	708
References	710
List of Symbols	711
About the Author	717
Index	719

Preface

The aim of this book is to deliver a comprehensive and concise introduction to the principles and basic theoretic concepts of electromagnetics. The selection of topics refers to the applications in microwave circuit and antenna design and communications engineering. It is intended as a resource for understanding electromagnetics required in current, emerging, and future broadband communications systems and high-speed analog and digital electronic circuits and systems. This second edition is enlarged by more than 300 pages. Some of the added material is of advanced character and the reader or the lecturer using the book may decide where to go into depth.

The reader is expected to attain an understanding of the principles and skills in electromagnetics that will enable him or her to apply modern electromagnetic design tools. The book attempts to provide the background for the understanding of electromagnetic wave propagation, electromagnetic interference, radio-frequency, microwave and optical circuits and systems, antennas, and high-speed digital circuits. The required mathematical framework is introduced making use of geometric concepts in the presentation of electromagnetic theory. The visual element is crucial to the method of presentation.

The book is intended to provide the framework for engineers and students to attain the necessary background in electromagnetics for solving design problems in microwave circuits and antennas. In particular, if electromagnetic CAD tools are used, the engineer needs a solid grounding in electromagnetics in order to apply the tools in a proper and efficient way. The book addresses students and engineers in communications engineering who want to acquire a working knowledge in electromagnetics for designing microwave circuits, antennas, and systems. The field of microwave engineering now is rapidly shifting toward commercial and consumer applications. Electromagnetic wave phenomena that in the past were in the domain of the microwave engineer are now becoming a limiting factor in digital circuit operation. As wireless communications is penetrating into the millimeter-wave frequencies, communications engineers need an improved background in microwaves. The study of electromagnetics is fundamental to the advancement of communications engineering and information technology to push the frontiers of the ultrafast, high bandwidth regime.

The book develops all the required concepts of electrodynamics, starting from elementary phenomena. Throughout the book, exterior differential forms are used to

describe fields. Differential forms are an extension of the vector concept. Today in the mathematics community the exterior differential calculus of Hermann Grassmann and Élie Cartan is considered to be the most suitable framework for geometrical analysis and field theory. Exterior differential calculus has simple and concise rules for computation. Furthermore, the objects of differential calculus have a clear geometrical significance and the geometrical laws of electromagnetics assume a simple and elegant form. The use of differential forms does not mean giving up the vector concept and its physical interpretations. On the contrary, the differential form representation supplies additional physical insight in addition to the conventional vector picture. Moving between the representations of exterior differential calculus and conventional vector analysis is straightforward.

Chapter 1 defines the topic of the book and comments on the rationale and method of the book.

Chapter 2 introduces the basic electromagnetic theory using exterior differential forms. For the representation of the field quantities, differential forms of order zero to three are used. The geometrical pictures of potential surfaces representing electric and magnetic field intensities and tubes representing electric and magnetic flux are introduced. The exterior derivative operator replacing gradient, curl, and divergence lends itself to geometrical interpretation and provides an easy way for a physical understanding of electromagnetics. Exterior calculus allows the introduction of orthogonal curvilinear coordinates in a most natural way. The discussion of Kirchhoff's laws establishes the link between field theory and network theory. A unified representation of normal and tangential boundary conditions is given.

In Chapter 3, scalar and vector potentials as a powerful tool to solve Maxwell's equations are introduced. The vector potentials are represented by first-order differential forms. Electromagnetic plane waves and their reflection and diffraction at plane surfaces are treated. The formulae for cylindrical and spherical waves are derived.

In Chapter 4, fundamental concepts, methods, and theorems are introduced. Poynting's theorem and stored energy and power flow in the electromagnetic field are discussed. Tellegen's theorem is the basis for the segmentation and network representation of electromagnetic structures. Equivalent field sources consisting of impressed electric and magnetic polarizations are introduced on the basis of the equivalence principle and the uniqueness theorem. The field formulations of the reciprocity theorem and the reaction concept are treated. Green's function as a fundamental tool to compute solutions of Maxwell's equations by superposition of the field contributions of point-like sources is introduced. The integral equation method allows the computation of the source distribution from the boundary conditions the excited field has to fulfill and is the basis of advanced numerical methods for electromagnetic field computations. Green's theorems are powerful tools to develop methods for the analytic solutions of Maxwell's equations. The Sturm-Liouville equation provides the fundamental for the expansion of solutions of Maxwell's equations into series of orthogonal basis functions.

In Chapter 5, static and quasistatic fields are treated. The capacitance and inductance of simple structures are computed. Solutions of the Laplace equation for static field problems are given. The conformal mapping method for the static electric and magnetic field computation of two-dimensional structures is treated. The Schwarz-Christoffel method allows field computation of polygonal structures and is applied to investigate some important planar structures.

In Chapter 6, the surface wave propagating along a plane surface of finite conductivity is treated. Based on the exact solution of this problem, surface impedance models are introduced. Skin effect, power loss due to the surface resistance, induced surface currents, and image currents are discussed.

In Chapter 7 the general principles of transmission-lines and waveguides are discussed. A general treatment of the transverse electromagnetic (TEM) waveguide modes is given. Multiconductor transmission-lines that play an important role in high speed data cables and microwave integrated circuits and planar transmission-lines are also included. The quasi-TEM waves in transversally inhomogeneous transmission-lines and planar transmission-lines are discussed. A general treatment of hollow waveguides, their field types, and the orthogonality of the modes is presented. Hollow waveguides with rectangular and circular cross-section and dielectric waveguides are discussed.

In Chapter 8, a unified presentation of transmission-line theory for TEM transmission-line modes and hollow waveguide modes is given. Generalized voltage and currents and wave amplitudes are introduced to apply the transmission-line concept to hollow waveguides as well. The Smith chart is introduced and its application to the design of impedance matching circuits is treated. Multimode transmission-line equations and methods for their solutions are discussed with respect to multiconductor transmission-lines and multimode excitation of hollow waveguides.

In Chapter 9, resonant circuits and resonators are treated. The reactance theorem characterizing lossless resonant circuits and resonators is treated from a field theoretic point of view. The orthogonality of the modes of lossless resonators and the suitability of the modal functions of the resonator as basis functions for the expansion of arbitrary field distributions inside resonators are demonstrated. The coupling of resonators to external circuits and the excitation of resonators by internal sources are discussed.

In Chapter 10, passive microwave circuits their multiport representations and their analysis by signal flow graphs are treated. The network representation of microwave circuits is discussed in detail by introducing the Foster and Cauer representations of lumped element equivalent circuits. The connection circuit is discussed on the basis of the Tellegen's theorem. Furthermore, obstacles and posts in waveguides and symmetry properties of microwave circuits are treated.

Chapter 11 on filters and periodic structures, far from giving a comprehensive treatment, is intended to introduce the fundamental concepts of this topic. Periodic structures are treated using field and network methods. The wave parameter theory of two-ports as a basis of filter theory is treated. Filter design on the basis of the insertion

loss method is presented and applied to Butterworth and Chebychev filter design. Plane wave scattering by periodic structures is treated. Metamaterials which are of growing interest for a multitude of applications are discussed on the basis of simple models.

In Chapter 12, the radiation of the Hertzian dipole is treated in frequency and time domain. The time domain treatment is crucial for the physical understanding of the process of electromagnetic radiation. Sommerfeld's theory of the electric dipole over lossy half-space is presented. The vertically and horizontally oriented electric dipoles over ground are treated. The space wave and the Zenneck surface wave are discussed.

In Chapter 13, antennas at first linear antennas are treated. The application of the integral equation method to the linear antenna for accurate computation of the antenna current distribution is demonstrated. The properties of the antenna as a receiving antenna are related to the properties of the transmitting antenna using the principle of reciprocity. Further parts of this chapter deal with antenna arrays, aperture antennas, microstrip antennas, and broadband antennas.

Chapter 14 gives an overview over numerical methods for electromagnetic field computation. The method of moments is introduced as a general method for transforming an analytic concept of solving a field problem into an associated algebraic one by expanding the field functions into a complete set of basis functions. The algebraic treatment of the field problems is based on a potentially infinite-dimensional complex linear vector space (i.e., the Hilbert space). Using Hilbert space methods to convert analytic problems into algebraic problems and solving these numerically is a powerful methodology for computational electromagnetics. The transmission-line matrix (TLM) method and the mode-matching method for numerical field computation are introduced.

I am pleased to acknowledge the assistance of many individuals in my work on this book. I thank Mahmoud Al-Ahmad, Bruno Biscontini, Klaus Fichtner, Yury Kuznetsov, Yu Lin, Petr Lorenz, Dzianis Lukashevich, Marco Ottobretti, Uwe Siart, Christoph Ullrich, José Vagner Vital, Sidina Wane, Karl Warnick, and Michael Zedler for a careful proofreading of the manuscript and checking of the formulae. I am also indebted to Leopold Felsen, Karl Warnick and Ke Wu for many helpful comments. I thank Andreas Cangellaris for the permission to use some of his material in Section 11.7. Also, for the second edition of this book the reviewer at Artech House has been of great assistance. Of course none of the above individuals is responsible for whatever inaccuracies remain. I would like to thank Michael Zedler for advice and assistance in solving \LaTeX typesetting problems and in formatting the text and Uwe Siart for making the Smith chart drawings and Dzianis Lukashevich for drawing the waveguide field visualizations. I thank Julie Lancashire, Katherine Nolan, and Tiina Ruonamaa of Artech House for their work in planning and production.

Peter Russer

Chapter 1

Introduction

A compact definition of radio-frequency engineering states that this discipline deals with methods and techniques for the generation, processing, transmission, and technical applications of electromagnetic waves. Some decades ago, radio-frequency engineering covered all aspects of circuits and systems for wireless communications and other radio frequency applications. Today, methods of radio-frequency engineering are necessary in a wide area of electrical and electronic engineering. Radio-frequency engineering has developed from a product-oriented discipline towards a method-oriented field, providing the fundamentals for dealing with high frequencies in all branches of electrical and electronic engineering.

Radio-frequency engineering is the discipline dealing with the technical applications of electromagnetic fields. It is based on Maxwell's theory of electromagnetic fields. Table 1.1 illustrates the history of the field theory from Huygens to Maxwell. In 1690, Christian Huygens published his *Traité de la Lumière* and presented there basic concepts of a wave theory of light [1]. Huygens formulated the principle that each point of an intermediate plane inserted in a propagating wave may be considered as the origin of a spherical wave. The secondary waves are determined by the envelopes of all these spherical waves.

At the end of this development, James C. Maxwell compiled all knowledge on electric and magnetic phenomena available at his time [2, 3]. Introducing the electric displacement current, he went beyond the physical experience. Maxwell's theory yielded predictions on new phenomena that could be verified in the following years and decades. In 1865 Maxwell concluded that electromagnetic waves propagating in free-space must be possible. The experimental verification of this prediction was given by Heinrich Hertz in 1888 [4]. An excellent historical survey over the development of the electromagnetic theory is presented in [5]. A *frequency band* is a continuous range of frequencies extending between two limiting frequencies. The band designations as decided upon by the Atlantic City Radio Convention of 1947 and later modified by the Comité Consultatif International des Radiocommunications (CCIR) Recommendation No. 142 in 1953 are

Table 1.1: The Development of the Field Concept

<i>Scientist</i>	<i>Invention</i>
Christian Huygens (1629–1695)	Wave theory of light Huygens' principle
Isaac Newton (1643–1727)	Law of gravitation Action over distance
Daniel Bernoulli (1700–1727)	Hydrodynamics
Leonhard Euler (1707–1783)	Flowing liquids are described by fields of velocity and acceleration
Charles Coulomb (1736–1806)	Electrostatics and magnetostatics
André Ampère (1775–1836)	Force between conductors under current
Siméon Poisson (1781–1840)	Potential theory Electrostatics and magnetostatics
Hans Ch. Oerstedt (1777–1851)	Magnetic field induced by moving electric charge
Michael Faraday (1791–1879)	Electromagnetic induction
James C. Maxwell (1831–1879)	Theory of the electromagnetic field

listed in Table 1.2. The frequency range N extends from $0.3 \cdot 10^N$ Hz to $3 \cdot 10^N$ Hz. Today the Telecommunication Standardization Sector (ITU-T) of the International Telecommunication Union (ITU) combines the standards-setting activities of the predecessor organization CCIR.

Below the 1 mm wavelength we have the submillimeter waves, succeeded by the far-infrared band, the infrared band, and the visible optical region. Due to the development of semiconductor lasers and optical fibers the infrared region has gained importance for communications and sensor applications.

There are also other frequency band designations used as well although not standardized. In the microwave and millimeter wave region a classification of frequency bands summarized in Table 1.3 is in use [6, 7].

In this book we deal with methods based on the electromagnetic theory for the modeling of microwave circuits and antennas. The necessity to use field theoretic methods for circuit modeling depends on the frequency as well as on the size of the considered structures. The modeling of antennas and wave propagation requires field-theoretic methods at low as well as high frequencies.

- At low frequencies, circuits may be described on the basis of currents and voltages. The properties of a circuit only depend on its topological structure. The theoretical framework for describing circuits at low frequencies is established by the *network concept*. The network concept is based on Kirchhoff's laws.

Table 1.2: Frequency Bands as Defined by CCIR

Region No.	Frequency	Wavelength	Name	
4	3 ... 30 kHz	100 ... 10 km	Very low frequencies	VLF
5	30 ... 300 kHz	10 ... 1 km	Low frequencies	LF
6	300 ... 3000 kHz	1000 ... 100 m	Medium frequencies	MF
7	3 ... 30 MHz	100 ... 10 m	High frequencies	HF
8	30 ... 300 MHz	10 ... 1 m	Very high frequencies	VHF
9	300 ... 3000 MHz	100 ... 10 cm	Ultra high frequencies	UHF
10	3 ... 30 GHz	10 ... 1 cm	Super high frequencies	SHF
11	30 ... 300 GHz	10 ... 1 mm	Extremely high frequencies	EHF

Table 1.3: Microwave Frequency Band Designation

Band	L	S	C	X	Ku	K	Ka	V	W
f/GHz	1–2	2–4	4–8	8–12.4	12.4–18	20–26.5	26–40	50–75	80–110

- At high frequencies, the geometric structure of the circuits plays an important role. An understanding of the circuit operation requires knowledge of the interaction of electric and magnetic fields in the circuit. The theoretical framework for describing circuits at high frequencies is established by the *field concept*. The field concept is based on Maxwell's theory.

The electromagnetic field is determined by the geometric and material properties of a structure as well as by external sources and boundary conditions. In many cases, sources exist in a given structure, and only the amplitude of the source is subject to variation. In this case we obtain an infinite number of partial solutions for the electromagnetic field. The amplitudes of these partial solutions are integral field quantities and may be considered as generalized voltages and currents.

The relation between the field concept and network concept may be illustrated by Figure 1.1. Let us first consider the resonant circuit in Figure 1.1(a). The resonant circuit is formed by an inductor and a capacitor that store magnetic energy and electric energy. The magnetic energy is concentrated within the inductor, whereas the electric energy is concentrated within the capacitor. Within the network concept the capacitor and inductor are connected via two network nodes. The circuit may be described in terms of node voltages and node currents. A field interaction between the circuit elements is not considered within the network concept. If the inductor has an inductance L and the capacitor exhibits a capacitance C , the resonant frequency f and the corresponding

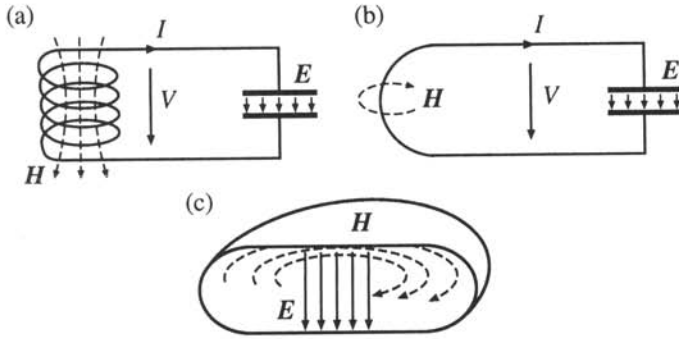


Figure 1.1: From the lumped circuit to the distributed circuit.

angular frequency ω are given by

$$\omega = 2\pi f = \frac{1}{\sqrt{LC}}. \quad (1.1)$$

Increasing the resonant frequency can be done by reducing the inductance L or the capacitance C . Reducing the inductance may be done by reducing the number of coils of the spiral inductor. In Figure 1.1(b) the inductor has been reduced to one coil. A further reduction of the inductance may be achieved by circuiting inductors in parallel. Proceeding in that way we can circularly surround the capacitor with inductor coils. Connecting all these coils will create a closed conducting surface surrounding the capacitor. Now we also reduce the capacitance by increasing the distance between the plates of the capacitor. At the end of this morphing process we obtain the pillbox-shaped resonator shown in Figure 1.1(c). Electric and magnetic fields are interacting inside the resonator. We cannot easily describe this resonator in terms of voltages and currents. Defining, for example, an electric voltage via the path integral over the electric field from the bottom to the top of the resonator, this voltage will exhibit a maximum in the center of the resonator and decrease with the radial distance from the center. The current flowing on the top and bottom surfaces of the resonator in the radial direction increases with the radial distance from the center and vanishes at the center. The electric field is generated by the surrounding alternating magnetic field due to Faraday's law. The magnetic field is generated by the vertically flowing displacement current formed by the alternating electric field. A vertical line in the center of the cavity is surrounded by maximum magnetic flux, and therefore the electric field exhibits a maximum value in the center of the cavity. The magnetic field lines of a higher radius enclose a larger displacement current, and therefore the magnetic field increases with radius.

We can distinguish between the *low-frequency* case where electric and magnetic fields may be considered to be spatially separated and stored in *capacitors* and *inductors*

respectively and the *high-frequency* case where the direct interaction of electric and magnetic fields has to be considered. Figure 1.1(a) illustrates the low-frequency case whereas Figure 1.1(c) is an example of the high-frequency case.

From this simple example we see that our conventional network concept is not applicable to describe the resonator. Circuits that are based on the direct interaction of electric and magnetic fields are called *distributed circuits*. The treatment of distributed circuits requires electromagnetic field modeling. We will, however, see later that it is possible to introduce *integral field quantities* also in the case of distributed circuits. These integral field quantities will be *generalized voltages* and *generalized currents*. Based on these generalized voltages and currents a network description is also possible for distributed circuits. Excellent textbooks on electromagnetics include Stratton [8], Schelkunoff [9], Ramo, Whinnery and Van Duzer [10], Harrington [11], Collin [7, 12, 13], Kong [14], Balanis [15], Pozar [16] and Ishimaru [17].

Adding yet another book on electromagnetics to the existing literature should not be done without good reasons. The development of communications engineering in the past decade involved a tremendous increase in the body of knowledge to be acquired by communications engineers. Over decades electromagnetics occupied a large part of the education of electrical and electronic engineers. Today for electromagnetics, less space can be allocated in electrical and electronics engineering curricula. However, the engineer developing circuits and systems for wireless communications needs a basic knowledge of electromagnetics. The goal in engineering education must be the accumulation of understanding, the stimulation of creativity and the promotion of the ability to solve problems. To solve problems in a systematic and efficient way the engineer must study the required theoretical framework. The engineer also needs intuition and creativity. These elements are strongly supported by imagery thinking [18].

The representation of electromagnetic theory can be simplified and the clarity can be improved by using geometrical methods. In 1844 Hermann Günter Grassmann published his book *Die lineale Ausdehnungslehre, ein neuer Zweig der Mathematik* [19], in which he developed the idea of an algebra in where the symbols representing geometric entities such as points, lines, and planes are manipulated using certain rules. Grassmann introduced what is now called exterior algebra, based upon the *exterior product*

$$a \wedge b = -b \wedge a. \quad (1.2)$$

The work of Grassmann already contains most of the algebraic structures of modern exterior calculus. Élie Cartan applied Grassmann algebra to the theory of exterior differential forms in his book *Leçons sur les Invariants Intégraux* [20]. Exterior calculus allows for the solution of field theoretical problems easily and directly. Furthermore it establishes a direct connection to geometrical images and supplies additional physical insight. Let us demonstrate this for the example of the electric field. The usual physical interpretation of the electric field is the force applied to a small test charge. This leads in a natural way to the vector representation of the electric field and to a picture we

may call the *force picture*. Considering the change of energy a test charge experiences as it is moved through the field yields a picture we may call the *energy picture*. The field lines in the force picture give the graphic representation of the field, and it is given by equipotential surfaces in the energy picture. The force picture is related to the vector representation whereas the energy picture is related to the differential form representation. In the differential form representation, however, the vector representation is also visible. Therefore the differential form representation provides additional physical insight.

We can represent one-forms graphically as surfaces in space. For electrostatic fields these surfaces are equipotential surfaces. Looking at the electric and magnetic flux densities and the electric current density, the differential form representation clearly points to the physical difference between field intensities and flux densities since flux densities are represented by two-forms. The graphical representation of a two-form is a bundle of tubes guiding the flux. This yields a much clearer physical interpretation than conventional vector notation. Finally, volume densities such as the charge density and the energy densities are represented by three-forms. Volume cells with cell size inversely proportional to the charge density give the geometric representation of a three-form form.

The exterior differential form calculus and its application to field theory is treated in a number of textbooks [21–30]. Textbooks on electromagnetics based on exterior calculus include [31] and [32]. Hehl and Obukhov have published an introduction to classical electrodynamics based on exterior calculus [33], and Lindell has published a comprehensive treatment of differential forms in electromagnetics [34]. An excellent approach for the use of differential forms as a tool for teaching electromagnetics has been given in [35].

In applying exterior calculus to an introductory level textbook, our goal is to develop a working knowledge of the subject with as much of a theoretical framework as necessary and as much clarity as possible.

REFERENCES

- [1] C. Huygens, *Traité de la Lumière*. Leyden, 1690.
- [2] J. C. Maxwell, *A Treatise on Electricity and Magnetism*, vol. 1. New York: Oxford University Press, 1998.
- [3] J. C. Maxwell, *A Treatise on Electricity and Magnetism*, vol. 2. New York: Oxford University Press, 1998.
- [4] H. Hertz, *Gesammelte Werke, Untersuchungen über die Ausbreitung der elektrischen Kraft*, vol. 2. Leipzig: Johann Ambrosius Barth, 1894.
- [5] R. S. Elliott, *Electromagnetics – History, Theory, and Applications*. New York: IEEE Press, 1991.
- [6] K. Lange and K. Löcherer, *Meinke Gundlach Taschenbuch der Hochfrequenztechnik*. Berlin Heidelberg New York: Springer, 1986.
- [7] R. E. Collin, *Foundations of Microwave Engineering*. New York: McGraw-Hill, 1992.

- [8] J. A. Stratton, *Electromagnetic Theory*. New York: McGraw-Hill, 1941.
- [9] S. A. Schelkunoff, *Electromagnetic Waves*. Princeton: Van Nostrand, 1943.
- [10] S. Ramo, J. R. Whinnery, and T. van Duzer, *Fields and Waves in Communication Electronics*. New York: John Wiley & Sons, 1965.
- [11] R. F. Harrington, *Time Harmonic Electromagnetic Fields*. New York: McGraw-Hill, 1961.
- [12] R. E. Collin, *Field Theory of Guided Waves*. New York: McGraw-Hill, 1960.
- [13] R. E. Collin, *Field Theory of Guided Waves*. New York: IEEE Press, 1991.
- [14] J. A. Kong, *Electromagnetic Wave Theory*. New York: John Wiley & Sons, 1986.
- [15] C. A. Balanis, *Advanced Engineering Electromagnetics*. New York: John Wiley & Sons, 1989.
- [16] D. M. Pozar, *Microwave Engineering*. Reading: Addison-Wesley, 1990.
- [17] A. Ishimaru, *Electromagnetic Wave Propagation, Radiation, and Scattering*. Englewood Cliffs, NJ: Prentice Hall, 1991.
- [18] A. I. Miller, *Imagery in Scientific Thought*. Boston: Birkhäuser, 1984.
- [19] H. Grassmann and L. C. Kannenberg, *A New Branch of Mathematics: The "Ausdehnungslehre" of 1844 and Other Works*. Chicago: Open Court Publishing, 1995.
- [20] . Cartan, *Les Systèmes Différentiels Extérieurs*. Paris: Hermann, 1945.
- [21] H. Flanders, *Differential Forms*. New York: Academic Press, 1963.
- [22] H. Cartan, *Formes Différentielles*. Paris: Hermann, 1967.
- [23] E. Heil, *Differentialformen*. Mannheim: Bibliographisches Institut, 1970.
- [24] Y. Choquet-Bruhat, C. de Witt-Morette, and M. Dillard-Bleek, *Analysis, Manifolds and Physics*. Amsterdam: North-Holland, 1977.
- [25] B. F. Schutz, *Geometrical Methods of Mathematical Physics*. Cambridge: Cambridge University Press, 1980.
- [26] R. Abraham, J. E. Marsden, and T. Ratiu, *Manifolds, Tensor Analysis and Applications*. London: Addison-Wesley, 1983.
- [27] W. L. Burke, *Applied Differential Geometry*. Cambridge: Cambridge University Press, 1985.
- [28] P. Bamberg and S. Sternberg, *A Course in Mathematics for Students in Physics 2*. Cambridge: Cambridge University Press, 1990.
- [29] T. Frankel, *The Geometry of Physics*. Cambridge: Cambridge University Press, 1997.
- [30] S. H. Weintraub, *Differential Forms – A Complement to Vector Calculus*. New York: Academic Press, 1997.
- [31] K. Meetz and W. Engl, *Elektromagnetische Felder*. Berlin: Springer, 1979.
- [32] W. Thirring, *Lehrbuch der Mathematischen Physik*, vol. 2. Wien: Springer, 1978.
- [33] F. W. Hehl and Y. N. Obukov, *Foundations of Classical Electrodynamics*. Boston Basel Berlin: Birkhäuser, 2003.
- [34] I. V. Lindell, *Differential Forms in Electromagnetics*. New York: IEEE Press, 2004.
- [35] K. F. Warnick, R. H. Selfridge, and D. V. Arnold, "Teaching electromagnetic field theory using differential forms," *IEEE Trans. Education*, vol. 40, pp. 53–68, Feb. 1997.

Chapter 2

Basic Electromagnetics

2.1 THE ELECTROMAGNETIC FIELD CONCEPT

In this chapter the framework of Maxwell's theory in differential form representation is introduced. The field quantities are discussed from a phenomenological point of view and related to the corresponding network quantities. Prior knowledge in field theory is not required but may be helpful [1–5]. The transfer of action between electrically charged matter via the *electromagnetic field* can be used to transfer energy as well as information. Electrically charged particles in rest interact via the *Coulomb force*. In the case of moving charged particles magnetic interaction also occurs. Electric and magnetic action propagates with a finite velocity, the speed of light, which is $2.998 \cdot 10^8 \text{ ms}^{-1} \cong 3 \cdot 10^8 \text{ ms}^{-1}$. To account for the finite velocity of the propagation of action the concept of the *field* has proven to be very powerful. The *field concept* means the assignment of physical quantities to the continuous space. A dynamic field is time-variable. The electromagnetic field can propagate in free-space as well as in media.

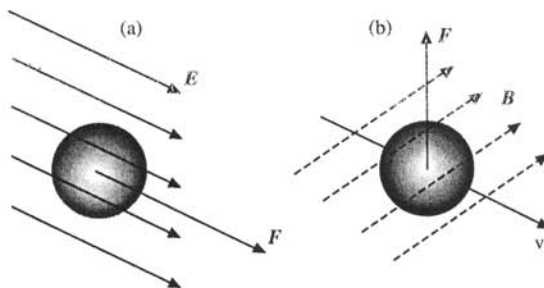


Figure 2.1: Electric and magnetic force on a charged particle.

It does not require a medium of transmission. Electrodynamics is concerned with interrelated electric and magnetic fields. This interrelation always occurs if the fields are time-varying. The electromagnetic field is generated by moving charged matter, and it acts on charged matter. Maxwell's theory summarizes the laws describing the electromagnetic field.

The complete description of the electromagnetic field is specified by two vector fields (i.e., directed fields). These fields are the electric field and the magnetic field. The electric field specifies the force on a point-like charged particle. Let us consider a particle with charge q at a point with the coordinates x , y , and z at time t . If the electric field intensity exhibits in the x -, y -, and z -direction at the point x , y , and z at time t the components $E_x(x, y, z, t)$, $E_y(x, y, z, t)$, and $E_z(x, y, z, t)$, the three Coulomb force components $F_x^{\text{el}}(x, y, z, t)$, $F_y^{\text{el}}(x, y, z, t)$, and $F_z^{\text{el}}(x, y, z, t)$ are given by

$$\begin{aligned} F_x^{\text{el}}(x, y, z, t) &= q E_x(x, y, z, t), \\ F_y^{\text{el}}(x, y, z, t) &= q E_y(x, y, z, t), \\ F_z^{\text{el}}(x, y, z, t) &= q E_z(x, y, z, t). \end{aligned} \quad (2.1)$$

The *electric field intensity* E has the unit Vm^{-1} . The action of the electric field on the charged particle is illustrated in Figure 2.1(a). We summarize the components in vectors using the notation $\mathbf{x} = [x, y, z]^T$ where the superscript T denotes the transpose (i.e., the column vector corresponding to the written line vector)

$$\mathbf{E}(\mathbf{x}, t) = [E_x(x, y, z, t), E_y(x, y, z, t), E_z(x, y, z, t)]^T. \quad (2.2)$$

This yields the more compact vector notation for (2.1):

$$\mathbf{F}^{\text{el}}(\mathbf{x}, t) = q \mathbf{E}(\mathbf{x}, t). \quad (2.3)$$

In the case of a moving charge the magnetic field also causes a force. This *Lorentz force* is proportional to the charge as well as to the velocity of the particle and has a direction orthogonal to the velocity vector as well as to the direction of the magnetic field. The action of the magnetic field on the moving charged particle is illustrated in Figure 2.1(b). Let us consider the right-handed Cartesian coordinate system with coordinates x , y , and z . If a particle with charge q is moving in the x -direction with velocity v_x and the magnetic field only exhibits a y -component B_y , the resulting Lorentz force will act in the z -direction and will be given by $F_z^{\text{mag}} = q v_x B_y$. Assuming invariance of the laws of physics under rotation in space yields a Lorentz force in the negative z -direction if the particle velocity has a y -direction and the magnetic field has an x -direction. In this case we obtain $F_z^{\text{mag}} = -q v_y B_x$. By superimposing all possible velocity components

and magnetic field components, we obtain

$$\begin{aligned} F_x^{\text{mag}} &= qv_y B_z - qv_z B_y, \\ F_y^{\text{mag}} &= qv_z B_x - qv_x B_z, \\ F_z^{\text{mag}} &= qv_x B_y - qv_y B_x. \end{aligned} \quad (2.4)$$

We can again summarize these three equations in vector notation by

$$\mathbf{F}^{\text{mag}}(\mathbf{x}, t) = q\mathbf{v} \times \mathbf{B}(\mathbf{x}, t), \quad (2.5)$$

where the symbol \times denotes the vector product

$$\begin{bmatrix} U_x \\ U_y \\ U_z \end{bmatrix} \times \begin{bmatrix} V_x \\ V_y \\ V_z \end{bmatrix} = \begin{bmatrix} U_y V_z - U_z V_y \\ U_z V_x - U_x V_z \\ U_x V_y - U_y V_x \end{bmatrix}. \quad (2.6)$$

The magnetic flux density \mathbf{B} has the unit Vs m^{-2} . It has to be pointed out that the fields \mathbf{E} and \mathbf{B} are of a different nature. \mathbf{E} is a field intensity, whereas \mathbf{B} is a flux density. The difference between these types of fields will be discussed later.

Let us now put together the electric force \mathbf{F}^{el} and the magnetic force \mathbf{F}^{mag} . In this case a test particle with charge q and velocity \mathbf{v} at point \mathbf{x} and time t is influenced by the force

$$\mathbf{F}(\mathbf{x}, t) = q(\mathbf{E}(\mathbf{x}, t) + \mathbf{v} \times \mathbf{B}(\mathbf{x}, t)). \quad (2.7)$$

For low frequencies the state of an electric circuit can be described by the currents flowing through the conductors and the voltages between the conductors. The *network concept* follows this description of circuits by voltages and currents. The properties of a circuit are only dependent on its topological structure (i.e., the connection structure of the network). The geometric arrangement of the network elements and the interconnections plays no role in a network. In the case of high frequencies, however, we make the observation that the geometric structure of the circuit may have a strong influence on the properties of a circuit or may even constitute its properties. The reason is that the abstract network describing the electrical properties of the circuit does not necessarily give a one-to-one mapping of the topology of a physical high-frequency circuit. A one-to-one correspondence between the physical network and the abstract network only will hold if all circuit elements may be described by their relations between port currents and their port voltages and these current voltage relations provide a complete description of the circuit elements.

Network theory is based on *Kirchhoff's current law* and *Kirchhoff's voltage law*. Kirchhoff's laws allow an axiomatic foundation for the network theory. However, Kirchhoff's laws are not first principles, but may be derived from Maxwell's equations. For physical

networks Kirchhoff's current law only is valid if the time derivative of the electric flux between the nodes can be neglected and if the time derivative of the magnetic flux through network loops can be neglected. The abstract network theory considers these conditions to be fulfilled exactly and takes Kirchhoff's laws as the fundamentals of the network theory.

Voltages applied to electric conductors cause an electric field between the conductors. The electric currents flowing through the conductors cause a magnetic field. At higher frequencies it is necessary also to take into consideration the electric flux between physical nodes and the magnetic flux through network loops. If frequencies are very high, it will also be necessary to take into consideration the direct interaction of electric and magnetic fields. It is possible to describe the state of a circuit by specifying the electric and magnetic fields instead of voltages and currents. The field description is more general than the description by voltages and currents. The field description is more complicated, however, since the electromagnetic field is a three-dimensional continuous quantity, and for the complete description of the electromagnetic field state it is necessary to specify the three electric field components and three magnetic field components throughout the three-dimensional continuum. Therefore, wherever electromagnetic effects may be described using the network concept, this description is much easier than a description based on the field concept.

2.2 FIELD INTENSITIES

The *electric field intensity* has the unit Vm^{-1} and is described by a vector $E(\mathbf{x}, t) = [E_x(\mathbf{x}, t), E_y(\mathbf{x}, t), E_z(\mathbf{x}, t)]^T$. As we have seen the meaning of the electric vector field is to assign some property to the space, namely to apply a force on charged matter. Let us consider in the following an electric field slowly varying with time. Moving a charged particle in the direction opposite of the direction of the field means that we have to supply *energy* equally to the product of force and distance of movement. If, for example, the electric field has an x -component E_x , the movement of a particle with charge q from position \mathbf{x} to $\mathbf{x} + \Delta\mathbf{x}$ requires an energy $\Delta W = -qE_x\Delta x$. Moving the particle in three-dimensional space along any curve from point $\mathbf{x}_1 = (x_1, y_1, z_1)$ to $\mathbf{x}_2 = (x_2, y_2, z_2)$ means that we have to sum up the infinitesimal contributions $-qE_x\Delta x$, $-qE_y\Delta y$, and $-qE_z\Delta z$. This is illustrated in Figure 2.2. The path C is approximated by infinitesimal line elements in the x -, y -, and z -direction. We are summing all contributions in the x -, y -, and z -direction and with $\Delta x, \Delta y, \Delta z \rightarrow 0$ we obtain the energy W_{21} required for moving the charge from \mathbf{x}_1 to \mathbf{x}_2 :

$$W_{21}(t) = -q \int_{\mathbf{x}_1}^{\mathbf{x}_2} E_x(x, y, z, t) dx + E_y(x, y, z, t) dy + E_z(x, y, z, t) dz. \quad (2.8)$$

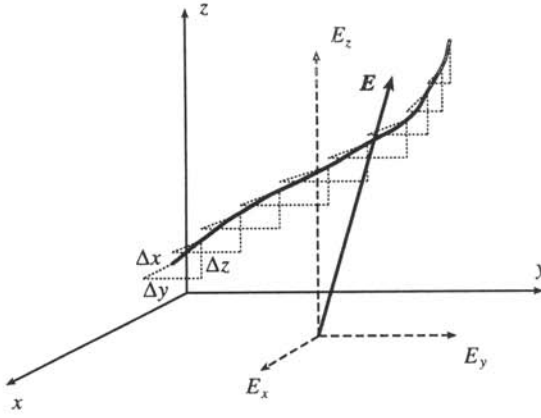


Figure 2.2: Line integral of the electric field over a curve C.

The *electric potential difference* or *voltage* v_{21} between \mathbf{x}_2 and \mathbf{x}_1 is given by

$$v_{21}(t) = - \int_{\mathbf{x}_1}^{\mathbf{x}_2} E_x(x, y, z, t) dx + E_y(x, y, z, t) dy + E_z(x, y, z, t) dz. \quad (2.9)$$

For moving a charge q from \mathbf{x}_1 to \mathbf{x}_2 the energy $W_{21}(t)$ is related to the potential difference $v_{21}(t)$ via

$$W_{21}(t) = q v_{21}(t). \quad (2.10)$$

Introducing the so-called *electric field differential form*

$$\mathcal{E} = E_x(x, y, z, t) dx + E_y(x, y, z, t) dy + E_z(x, y, z, t) dz \quad (2.11)$$

we also may write

$$v_{21}(t) = - \int_{\mathbf{x}_1}^{\mathbf{x}_2} \mathcal{E}. \quad (2.12)$$

With a differential form we mean the complete expression under an integral sign, including also the differentials (e.g., dx , dy , and dz , respectively) [6–9]. In order to distinguish the differential form (2.11) from others to be introduced later, we call this differential form a *one-form*.

Figure 2.3(a) shows the path of integration for the definition of the voltage v_{21} from node 2 to node 1. The line integral sums up the projection of the field vector on the vectorial path element. The contribution of the integrand is proportional to the product of the magnitudes of the field vector with the infinitesimal path element and the cosine of the angle enclosed between them.

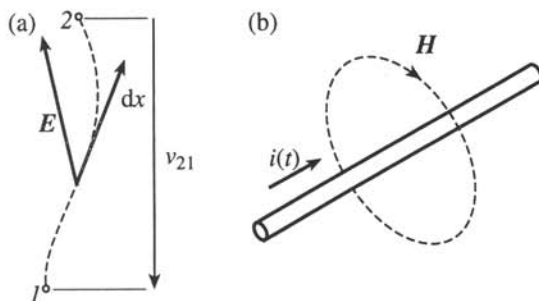


Figure 2.3: Path of integration (a) for the definition of the voltage, and (b) for the definition of the current.

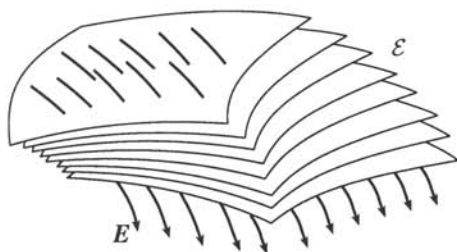


Figure 2.4: Field line and surface representations of a one-form.

The common physical interpretation of the electric field is related to the force on a point-like unit charge. This *force picture* yields in a natural way to the vector representation and to the visualization of the electric field via *field lines*. The field lines are curves having the property that the field vector is tangential at all points of the curve. Another viewpoint is to consider the energy of a charge moved through the field. We can visualize the field via the change of the energy of a test charge moved through the field. Figure 2.4 shows the representation of the field via field lines and via the surfaces of constant test charge energy or constant electric potential, respectively. The *energy picture* is more related to differential forms. For an electrostatic field the surfaces associated with the one-form \mathcal{E} are equipotentials. Since the dimension of the differential form \mathcal{E} is V the differential form \mathcal{E} expresses the change of electric potential over an infinitesimal path element. The field lines are orthogonal to the potential surfaces. Depending on the properties of the field the potential surfaces also may end or join. Figure 2.5 shows the surface representation of the three *fundamental one-forms* dx , dy , and dz . Figure 2.6 shows a situation we will encounter in time-variable fields. In the center of the structure the field intensity is higher than at its edges. In this case the integral (2.12) will depend on the path from x_1 to x_2 and we cannot assign a scalar

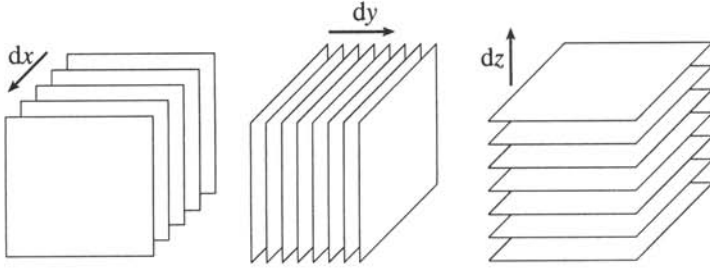


Figure 2.5: The fundamental one-forms in Cartesian coordinates.

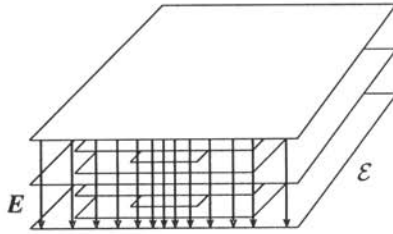


Figure 2.6: One-form with ending surfaces.

potential to the field.

The vector $\mathbf{H}(\mathbf{x}, t) = [H_x(\mathbf{x}, t), H_y(\mathbf{x}, t), H_z(\mathbf{x}, t)]^T$ describes the *magnetic field intensity* and has the unit Am^{-1} . An *electric current* i , which is slowly varying with time, and the magnetic field generated by this current are related via

$$i(t) = \oint_{\partial A} \mathcal{H} \quad (2.13)$$

with the *magnetic field differential form*

$$\mathcal{H} = H_x(x, y, z, t) dx + H_y(x, y, z, t) dy + H_z(x, y, z, t) dz. \quad (2.14)$$

The circle on the integral symbol denotes the integration over a closed boundary. Figure 2.3(b) shows the path of integration for the definition of the current i . With ∂A we denote the boundary of the surface A . The relation between the direction of reference for the current and the orientation of the path of integration is shown in Figure 2.3(b). The current is counted positive if its direction coincides with the direction of reference.

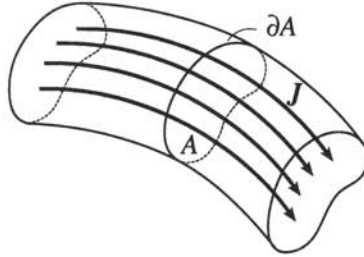


Figure 2.7: Current flow.

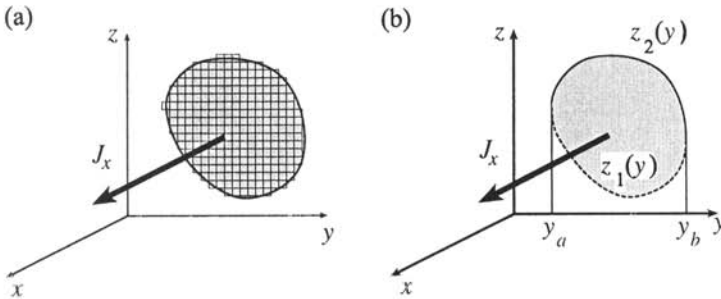


Figure 2.8: The integration over an area.

2.3 CURRENT AND FLUX DENSITIES

The current flowing through a conductor usually does not exhibit a uniform distribution over the conductor cross-section. We describe the flow of the current by a *current density* vector field $\mathbf{J}(\mathbf{x}) = [J_x(\mathbf{x}), J_y(\mathbf{x}), J_z(\mathbf{x})]^T$. Consider a current i flowing through a tube formed by the current density field lines going through the boundary ∂A of the area A as shown in Figure 2.7. Let us at first assume a current flowing in the x -direction only as shown in Figure 2.8(a). In this case, to compute the total current we have to integrate over the surface A in the yz -plane. The integration may be performed by subdividing the area A in small elements as depicted in Figure 2.8(a), multiplying the current density with the area of the area elements and summing all these contributions, so that

$$i = \int_A J_x \, dy \, dz. \quad (2.15)$$

If, for example, the boundary ∂A can be represented by two functions $z_1(y)$ and $z_2(y)$,

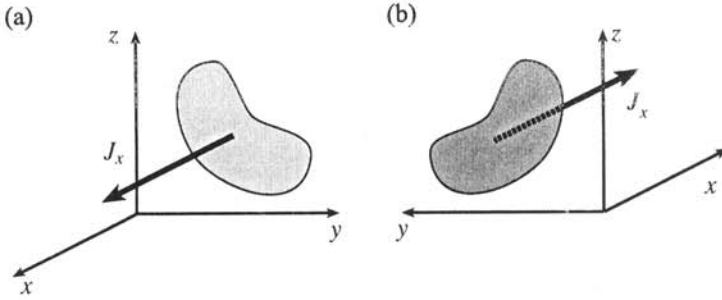


Figure 2.9: The orientation of an area.

as shown in Figure 2.8(b), we can bring the integral (2.15) into the form

$$i = \int_{y_a}^{y_b} \left[\int_{z_1(y)}^{z_2(y)} J_x dz \right] dy. \quad (2.16)$$

If we integrate a current density over an area not perpendicular to a coordinate axis we have to consider the orientation of the area. If in Figure 2.8(a) the current density J_x is positive, the current i also will be positive. Inverting the direction of J_x will yield a negative current. This inversion may be performed by mirroring the coordinates with respect to the yz -plane. How do we know whether a *surface integral* is positive or negative? The answer is: We have to define a positive orientation. A positive-oriented or right-handed Cartesian coordinate system is specified as follows: If we are looking in the z -direction on the xy -plane the x -axis may be rotated clockwise by 90° into the y -axis. In Figure 2.9 the vector component J_x is pointing in a positive orientation. On the right side of Figure 2.9 the coordinate system as well as the vector field were rotated by 180° around the z -axis. Physically nothing has changed. In the left figure, however, the vector pointing towards the observer is positive, whereas in the right figure the vector pointing away from the observer is positive.

We now introduce a notation that takes into account the orientation of a coordinate system. The so-called *exterior differential form* $dy \wedge dz$ has the property

$$dy \wedge dz = -dz \wedge dy. \quad (2.17)$$

The product denoted by the symbol \wedge is called the *exterior product* or *wedge product*. Exterior differential forms consisting of wedge products of two differentials or sums of such products are called *two-forms*. We may decide either $dy \wedge dz = dy dz$ or $dy \wedge dz = -dy dz$. Deciding

$$dy \wedge dz = dy dz \quad (2.18)$$

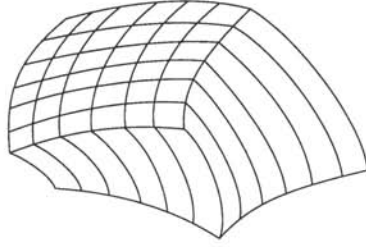


Figure 2.10: Tube representation of a two-form.

assigns to $dy \wedge dz$ the positive orientation and to $dz \wedge dy$ the negative orientation. The integral (2.15) can now be written in the orientation-independent form

$$i = \int_A J_x dy \wedge dz. \quad (2.19)$$

Figure 2.10 shows the *tube representation* of a two-form. The two-form is visualized by a bundle of tubes carrying the current. The current density is inversely proportional to the cross-sectional area of the tubes. Figure 2.11 shows the tube representations of the *fundamental two-forms* $dy \wedge dz$, $dz \wedge dx$, $dx \wedge dy$.

If the surface A is an arbitrarily oriented curved surface in three-dimensional space and the current density vector has the x -, y -, and z -components J_x , J_y , and J_z , we have to perform the integration over

$$i = \int_A J_x dy \wedge dz + J_y dz \wedge dx + J_z dx \wedge dy. \quad (2.20)$$

The first term of the integrand concerns the integration of the x -component of the current density over the projection of the surface A on the yz -plane and so forth.

Let us introduce the *current density form* \mathcal{J} by the exterior differential form

$$\mathcal{J} = J_x dy \wedge dz + J_y dz \wedge dx + J_z dx \wedge dy. \quad (2.21)$$

The current i may be expressed in a compact notation as the integral of the differential form \mathcal{J} :

$$i = \int_A \mathcal{J}. \quad (2.22)$$

2.4 CONSTITUTIVE RELATIONS

In the case of electric and magnetic field quantities we distinguish between *field intensities* and *flux densities*. A field intensity usually occurs in a path integral whereas a flux

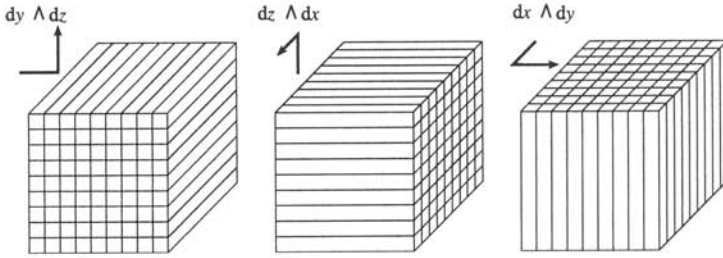


Figure 2.11: The fundamental two-forms in Cartesian coordinates.

density occurs in surface integrals. Field intensities are related to the flux densities via the *constitutive relations*. The constitutive equations depend on the metric properties of the space or the chosen coordinate system and on the *macroscopic material parameters*.

On the microscopic scale of atomic distances the electric and magnetic fields exhibit strong spatial variations. However, the knowledge of these variations is not relevant. We are dealing with the averages of fields and sources over volumes large compared with the volume occupied by a single atom. Such averaged quantities are called *macroscopic fields* [1, 2]. In a dielectric material by an applied primary electric field the negative electronic charge is shifted spatially relative to the positive background charge. This yields an *electric polarization* of the medium contributing to the *electric flux density*. In the magnetic field the *magnetic polarization* determines the relation between magnetic field intensity and magnetic flux density.

The *electric flux density* in the literature usually is called *electric displacement*, and the magnetic flux density $\mathbf{B}(\mathbf{x}) = [B_x(\mathbf{x}), B_y(\mathbf{x}), B_z(\mathbf{x})]^T$ usually is called *magnetic induction*. The denomination “flux density” stresses the geometric properties of these quantities and therefore is preferred in the following. The electric flux density $\mathbf{D}(\mathbf{x}) = [D_x(\mathbf{x}), D_y(\mathbf{x}), D_z(\mathbf{x})]^T$ and the magnetic flux density $\mathbf{B}(\mathbf{x})$ are related to the field intensities \mathbf{E} and \mathbf{H} via the *material equations* or *constitutive equations*. The electric flux density \mathbf{D} has the unit Asm^{-2} , and the magnetic flux density \mathbf{B} has the unit Vs m^{-2} . For homogeneous and isotropic media the constitutive equations are given by

$$\mathbf{D} = \epsilon \mathbf{E} , \quad (2.23a)$$

$$\mathbf{B} = \mu \mathbf{H} , \quad (2.23b)$$

where ϵ is the *permittivity* and μ is the *permeability*.

ϵ	Permittivity	$\text{AsV}^{-1}\text{m}^{-1}, \text{Fm}^{-1}$
μ	Permeability	$\text{VsA}^{-1}\text{m}^{-1}, \text{Hm}^{-1}$

In the free-space ϵ and μ assume the following values:

$$\epsilon_0 = 8.854 \cdot 10^{-12} \text{ Fm}^{-1} \cong \frac{1}{36\pi} 10^{-9} \text{ Fm}^{-1}, \quad (2.24a)$$

$$\mu_0 = 4\pi \cdot 10^{-7} \text{ Hm}^{-1}. \quad (2.24b)$$

The *relative permittivity* ϵ_r and the *relative permeability* μ_r are related to the permittivity and permeability of free-space via

$$\epsilon_r = \frac{\epsilon}{\epsilon_0}, \quad (2.25a) \quad \mu_r = \frac{\mu}{\mu_0}. \quad (2.25b)$$

The surface integral of the electric flux density \mathbf{D} over an area A yields the *electric flux* Ψ . Introducing the *electric flux form* or *electric displacement form*

$$\mathcal{D} = D_x dy \wedge dz + D_y dz \wedge dx + D_z dx \wedge dy \quad (2.26)$$

we can write

$$\Psi = \int_A \mathcal{D}. \quad (2.27)$$

The surface integral of the magnetic flux density \mathbf{B} over an area A yields the *magnetic flux* Φ . Introducing the *magnetic flux form* or *magnetic induction form*

$$\mathcal{B} = B_x dy \wedge dz + B_y dz \wedge dx + B_z dx \wedge dy \quad (2.28)$$

we can write

$$\Phi = \int_A \mathcal{B}. \quad (2.29)$$

We have seen that field intensities are described by one-forms whereas current densities and flux densities are described by two-forms. The field intensities \mathbf{E} and \mathbf{H} are related to the flux densities \mathbf{D} and \mathbf{B} via the material equations (2.23a) and (2.23b). We introduce the *star operator* \star or *Hodge operator*, defined by

$$\begin{aligned} \star f &= f dx \wedge dy \wedge dz, \\ f &= \star (f dx \wedge dy \wedge dz), \\ \star (A_x dx + A_y dy + A_z dz) &= A_x dy \wedge dz + A_y dz \wedge dx + A_z dx \wedge dy, \\ A_x dx + A_y dy + A_z dz &= \star (A_x dy \wedge dz + A_y dz \wedge dx + A_z dx \wedge dy). \end{aligned} \quad (2.30)$$

The star operator has the property

$$\star \star = 1. \quad (2.31)$$

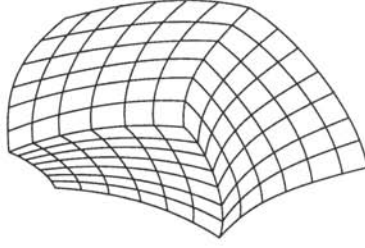


Figure 2.12: Volume element representation of a three-form.

The star operator allows to bring the material equations (2.23a) and (2.23b) into the form

$$\mathcal{D} = \epsilon \star \mathcal{E} , \quad (2.32a)$$

$$\mathcal{B} = \mu \star \mathcal{H} . \quad (2.32b)$$

In curvilinear coordinate systems the Hodge operator has a more complex form as discussed in Sections 2.13 and A.4. The Hodge operator reflects the metric properties of the space and the coordinate system. Together with ϵ_0 and μ_0 the Hodge operator expresses the metric properties of free-space.

In an *anisotropic medium* the relationships between \mathcal{D} and \mathcal{E} or \mathcal{B} and \mathcal{H} depend on the direction of \mathcal{E} or \mathcal{H} , respectively. The constitutive relationship can be expressed by a *permittivity tensor* ϵ or a *permeability tensor* μ . We obtain

$$\mathcal{D} = \epsilon \mathcal{E} , \quad (2.33a)$$

$$\mathcal{B} = \mu \mathcal{H} , \quad (2.33b)$$

with the permittivity and permeability tensors given by

$$\epsilon = \begin{bmatrix} \epsilon_{xx} & \epsilon_{xy} & \epsilon_{xz} \\ \epsilon_{yx} & \epsilon_{yy} & \epsilon_{yz} \\ \epsilon_{zx} & \epsilon_{zy} & \epsilon_{zz} \end{bmatrix} , \quad \mu = \begin{bmatrix} \mu_{xx} & \mu_{xy} & \mu_{xz} \\ \mu_{yx} & \mu_{yy} & \mu_{yz} \\ \mu_{zx} & \mu_{zy} & \mu_{zz} \end{bmatrix} . \quad (2.34)$$

To analyze anisotropic media with exterior differential forms Karl Warnick [10] has introduced the *permittivity star operator* \star_ϵ and the *permeability star operator* \star_μ . For materials described in Cartesian coordinates by symmetric permittivity and permeability tensors the permittivity star operator is defined as

$$\begin{aligned} \star_\epsilon (E_x dx + E_y dy + E_z dz) &= (\epsilon_{xx} E_x + \epsilon_{xy} E_y + \epsilon_{xz} E_z) dy \wedge dz \\ &\quad + (\epsilon_{yx} E_x + \epsilon_{yy} E_y + \epsilon_{yz} E_z) dz \wedge dx \\ &\quad + (\epsilon_{zx} E_x + \epsilon_{zy} E_y + \epsilon_{zz} E_z) dx \wedge dy , \end{aligned} \quad (2.35a)$$

$$\begin{aligned}
\star_\epsilon(D_x dy \wedge dz + D_y dz \wedge dx + D_z dx \wedge dy) &= (g_{xx}^\epsilon D_x + g_{xy}^\epsilon D_y + g_{xz}^\epsilon D_z) dx \\
&+ (g_{yx}^\epsilon D_x + g_{yy}^\epsilon D_y + g_{yz}^\epsilon D_z) dy \\
&+ (g_{zx}^\epsilon D_x + g_{zy}^\epsilon D_y + g_{zz}^\epsilon D_z) dz.
\end{aligned} \tag{2.35b}$$

The matrix elements g_{ij}^ϵ are the elements of the inverse permittivity tensor

$$\mathbf{g}^\epsilon = \boldsymbol{\epsilon}^{-1}. \tag{2.36}$$

The application of \star_ϵ to a zero-form and a three-form respectively yields

$$\star_\epsilon f = \det[\boldsymbol{\epsilon}] f dx \wedge dy \wedge dz, \tag{2.37a}$$

$$\star_\epsilon f dx \wedge dy \wedge dz = (\det[\boldsymbol{\epsilon}])^{-1} f. \tag{2.37b}$$

In the same way the permeability star operator is defined by

$$\begin{aligned}
\star_\mu(H_x dx + H_y dy + H_z dz) &= (\mu_{xx} H_x + \mu_{xy} H_y + \mu_{xz} H_z) dy \wedge dz \\
&+ (\mu_{yx} H_x + \mu_{yy} H_y + \mu_{yz} H_z) dz \wedge dx \\
&+ (\mu_{zx} H_x + \mu_{zy} H_y + \mu_{zz} H_z) dx \wedge dy,
\end{aligned} \tag{2.38a}$$

$$\begin{aligned}
\star_\mu(B_x dy \wedge dz + B_y dz \wedge dx + B_z dx \wedge dy) &= (g_{xx}^\mu B_x + g_{xy}^\mu B_y + g_{xz}^\mu B_z) dx \\
&+ (g_{yx}^\mu B_x + g_{yy}^\mu B_y + g_{yz}^\mu B_z) dy \\
&+ (g_{zx}^\mu B_x + g_{zy}^\mu B_y + g_{zz}^\mu B_z) dz.
\end{aligned} \tag{2.38b}$$

The matrix elements g_{ij}^μ are the elements of the inverse permeability tensor

$$\mathbf{g}^\mu = \boldsymbol{\mu}^{-1}. \tag{2.39}$$

The application of \star_μ to a zero-form and a three-form respectively yields

$$\star_\mu f = \det[\boldsymbol{\mu}] f dx \wedge dy \wedge dz, \tag{2.40a}$$

$$\star_\mu f dx \wedge dy \wedge dz = (\det[\boldsymbol{\mu}])^{-1} f dx dy dz. \tag{2.40b}$$

For symmetric material tensors the permittivity and permeability star operators are identical with their inverse operators,

$$\star_\epsilon \star_\epsilon = 1 \qquad \star_\mu \star_\mu = 1. \tag{2.41}$$

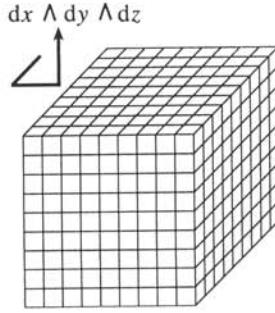


Figure 2.13: The fundamental three-form in Cartesian coordinates.

With these operators we can write the constitutive relationships for homogeneous anisotropic materials as

$$\mathcal{D} = \star_{\epsilon} \mathcal{E}, \quad \mathcal{B} = \star_{\mu} \mathcal{H}. \quad (2.42)$$

These equations are valid for symmetric as well as for unsymmetric anisotropic materials.

2.5 THE CHARGE DENSITY

The *electric charge* q is given by the volume integral over the *electric charge density* ρ . For the electric charge density we may introduce a *three-form*, the so-called *charge density form*

$$\mathcal{Q} = \rho \, dx \wedge dy \wedge dz. \quad (2.43)$$

We obtain the charge q by performing the volume integral over the three-form \mathcal{Q} ,

$$q = \int_V \mathcal{Q}. \quad (2.44)$$

We note that the exterior product $dx \wedge dy \wedge dz$ changes its sign if two factors are interchanged. Figure 2.12 shows the graphic visualization of a three-form by subdividing the volume into cells. The cell volume is inversely proportional to the charge density. Figure 2.13 shows the *fundamental three-form* $dx \wedge dy \wedge dz$.

The star operator applied to a three-form yields a *zero-form* and vice versa. A zero-form is a *true scalar* as, for example, the scalar potential. A true scalar is invariant under coordinate transformations, whereas a three-form may depend on the coordinate system.

The electric flux \mathcal{D} flowing through the boundary ∂V of a volume V is related to the charge \mathcal{Q} stored in the volume V via

$$\oint_{\partial V} \mathcal{D} = \int_V \mathcal{Q}. \quad (2.45)$$

To calculate the electric field of a point charge q we consider the point charge to be in the center of a sphere with radius r . In this way we can utilize the spherical symmetry of the problem. For symmetry reasons the flux density is homogeneous over the sphere and is directed radially. Therefore

$$\oint_{\partial V} \mathcal{D} = 4\pi r^2 D_r = q. \quad (2.46)$$

From this we obtain

$$E_r = \frac{q}{4\pi\epsilon r^2}. \quad (2.47)$$

The electric field vector is given by

$$\mathbf{E} = \frac{q\mathbf{r}}{4\pi\epsilon r^3}. \quad (2.48)$$

There exists no magnetic charge. Therefore over any closed boundary ∂V of a volume V , we obtain

$$\oint_{\partial V} \mathcal{B} = 0. \quad (2.49)$$

2.6 THE MAXWELL PUZZLE

Let us assume the electromagnetic field to be slowly varying. In this case we can consider the electric and magnetic fields to be independent from each other. In lumped element circuits we know elementary circuit elements, which are based either on electric field concentration or magnetic field concentration. Capacitors store electric field energy and inductors store magnetic field energy. Capacitors as well as inductors may be considered as lumped circuit elements within the network concept.

Ampère's law relates the current flowing through a surface A to the magnetic field tangential to the boundary ∂A of the surface A ,

$$\oint_{\partial A} \mathcal{H} = \int_A \mathcal{J}. \quad (2.50)$$

In the case of rapidly varying electromagnetic fields, however, we have to consider the direct mutual influence of electric and magnetic fields. To demonstrate this we consider the plate capacitor depicted in Figure 2.14. This capacitor is permeable for alternating

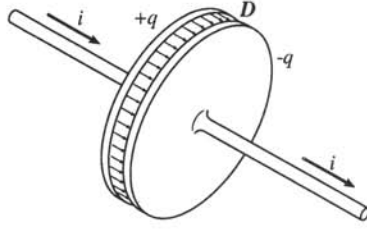


Figure 2.14: Plate capacitor.

current. The current flowing within a positive half-wave into the left capacitor plate builds up a positive charge. This positive charge influences a negative charge of equal magnitude in the right capacitor plate. The current flowing on the left side into the capacitor is equal to the current flowing out from the right side of the capacitor. With the electric field E between the capacitor plates there is a related electric flux density D given by (2.23a) and (2.32a), respectively. We assume the diameter of the plate capacitor to be large compared with the plate distance b . In this case the electric field is essentially concentrated between the capacitor plates and is homogeneous within this region. The electric flux Ψ is the product of the magnitude of electric flux density D and the capacitor area A :

$$|\Psi| = \int_A \mathcal{D} = A |D|. \quad (2.51)$$

The total electric flux Ψ is equal to the electric charge q stored in the capacitor,

$$\Psi = \int_V \mathcal{Q} = q. \quad (2.52)$$

The rate of change of the electric charge q is equal to the current,

$$i = \frac{dq}{dt}. \quad (2.53)$$

With (2.22) and (2.45) we obtain

$$\int_A \mathcal{J} = \frac{d}{dt} \int_A \mathcal{D}. \quad (2.54)$$

The time derivative of the electric flux $d\Psi/dt$ is interpreted as the *displacement current*. The displacement current was introduced by Maxwell, who considered for the first time the concept that variations in the position of bound charge were equivalent in their effect to a conduction current [1, 11]. The *conduction current* (i.e., the current carried by moving charges and flowing through the conductor) is continued by the

displacement current between the capacitor plates. Since the displacement current is equal to the rate of change of the electric flux, the displacement current is proportional to the frequency. It was the achievement of James Clerk Maxwell to recognize that the displacement current can give rise to a magnetic field in the same way as the conduction current. Therefore he added in Ampère's law (2.50) the displacement current term to the conduction current term and obtained

$$\oint_{\partial A} \mathcal{H} = \frac{d}{dt} \int_A \mathcal{D} + \int_A \mathcal{J}. \quad (2.55)$$

The displacement current can give a considerable contribution to the generation of the magnetic field, especially in the case of high frequencies.

Michael Faraday discovered that a time-varying magnetic field generates an electric field. This law is called *Faraday's law* or *law of induction*,

$$\oint_{\partial A} \mathcal{E} = -\frac{d}{dt} \int_A \mathcal{B}. \quad (2.56)$$

As a consequence, in a rapidly varying electromagnetic field the electric and magnetic fields are directly interacting in space.

2.7 THE INTEGRAL FORM OF MAXWELL'S EQUATIONS

Let us now summarize Maxwell's equations. The integral form of Maxwell's equations is given by

$$\oint_{\partial A} \mathcal{H} = \frac{d}{dt} \int_A \mathcal{D} + \int_A \mathcal{J}, \quad \text{Ampère's law} \quad (2.57a)$$

$$\oint_{\partial A} \mathcal{E} = -\frac{d}{dt} \int_A \mathcal{B}, \quad \text{Faraday's law} \quad (2.57b)$$

$$\oint_{\partial V} \mathcal{B} = 0, \quad \text{Magnetic flux continuity} \quad (2.57c)$$

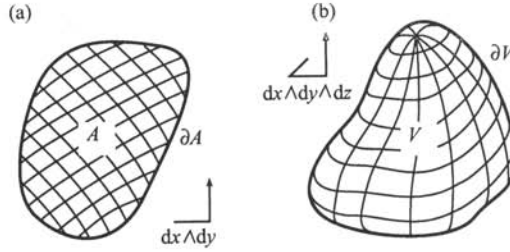
$$\oint_{\partial V} \mathcal{D} = \int_V \mathcal{Q}. \quad \text{Gauss' law} \quad (2.57d)$$

Equations (2.57a) and (2.57b) are named as Ampère's law and Faraday's law; (2.57c) describes the flux continuity and (2.57d) is named Gauss' law. The field quantities and the corresponding differential forms occurring in these equations are summarized in Table 2.1.

In (2.57a) and (2.57b) line integrals over the boundary of the surface A are related to surface integrals over the area A . Figure 2.15(a) shows the relation between the

Table 2.1: The Field Quantities

Name	Field Quantity	Dimension	Differential Form	Dimension
Electric field intensity	\mathbf{E}	Vm^{-1}	\mathcal{E}	V
Magnetic field intensity	\mathbf{H}	Am^{-1}	\mathcal{H}	A
Electric flux density	\mathbf{D}	As m^{-2}	\mathcal{D}	As
Magnetic flux density	\mathbf{B}	Vs m^{-2}	\mathcal{B}	Vs
Current density	\mathbf{J}	Am^{-2}	\mathcal{J}	A
Charge density	ρ	As m^{-3}	\mathcal{Q}	As

Figure 2.15: (a) Area A with boundary ∂A , and (b) volume V with boundary ∂V .

orientation of the area A and the contour ∂A . The line integral over the closed contour ∂A is called *circulation*. In (2.57c) and (2.57d) the surface integrals are performed over the boundary ∂V of the volume V . Figure 2.15(b) shows the orientation of the boundary surface ∂V .

The conservation of charge is embodied in the *continuity equation* following directly from Maxwell's equations. Let us apply Ampère's law (2.57a) on a surface A , which is the boundary of a volume V (i.e., $A = \partial V$). Since a boundary has no boundary it follows $\partial A = \partial(\partial V) = 0$ and therefore we obtain from (2.57a)

$$\frac{d}{dt} \oint_{\partial V} \mathcal{D} + \oint_{\partial V} \mathcal{J} = 0. \quad (2.58)$$

Inserting Gauss' law (2.57d) yields the *integral form of the continuity equation*

$$\frac{d}{dt} \int_V \mathcal{Q} + \oint_{\partial V} \mathcal{J} = 0. \quad (2.59)$$

From this it follows that any current flow through the boundary ∂V of a volume V must be accompanied by an appropriate change of the charge in V . The total charge is conserved.

Table 2.2: Field Quantities and Network Quantities

Field Quantity	Network Quantity	Name	Dimension
E	v	Electric voltage	V
H	v_m	Magnetic voltage	A
D	Ψ	Electric flux	As
B	Φ	Magnetic flux	Vs
J	i	Electric current	A
ρ	q	Electric charge	As

We shall demonstrate below that Maxwell's equations exhibit *plane wave* solutions with a free-space propagation velocity (i.e., the *speed of light* c_0), given by

$$c_0 = \frac{1}{\sqrt{\epsilon_0 \mu_0}} = 2.998 \cdot 10^8 \text{ ms}^{-1} \cong 3 \cdot 10^8 \text{ ms}^{-1}. \quad (2.60)$$

In electric conductive media the current density form \mathcal{J} is related to the electric field form \mathcal{E} via *Ohm's law*

$$\mathcal{J} = \sigma \star \mathcal{E}, \quad (2.61)$$

where σ is the *conductivity* with dimension $\text{AV}^{-1}\text{m}^{-1}$. If there also exists an *impressed current density* with the current density differential form \mathcal{J}_0 , the total current density is given by

$$\mathcal{J} = \mathcal{J}_0 + \sigma \star \mathcal{E}. \quad (2.62)$$

To every field quantity there exists a corresponding integral field quantity. The integral field quantities are obtained from the corresponding differential field quantities by integration over a one-dimensional or a multidimensional spatial domain. Integral field quantities may be interpreted as network quantities. Table 2.2 summarizes the differential field quantities and the corresponding integral field quantities or network quantities, respectively. The *voltage* v is defined by

$$v_{21} = - \int_1^2 \mathcal{E} \quad (2.63)$$

as the negative line integral over the electric field intensity. Figure 2.3(a) shows the orientation of the voltage v_{21} and the path of integration. In the same way we may define a *magnetic voltage*

$$v_{m21} = - \int_1^2 \mathcal{H}. \quad (2.64)$$

The electric flux Ψ , the magnetic flux Φ , and the current i are given by

$$\Psi = \int_A \mathcal{D}, \quad (2.65a)$$

$$\Phi = \int_A \mathcal{B}, \quad (2.65b)$$

$$i = \int_A \mathcal{J}. \quad (2.65c)$$

The electric charge q is given by

$$q = \int_V \mathcal{Q}. \quad (2.65d)$$

2.8 THE ELECTROMAGNETIC WAVE

James C. Maxwell was the first to predict the existence of *electromagnetic waves*. In 1864 he proposed that light is an electromagnetic disturbance in the form of waves [11]. In an electromagnetic wave the magnetic field is built up by the displacement current due to the time-varying electric field and, vice versa, the electric field is built up by the time-varying magnetic flux. In 1887 Heinrich Hertz provided experimental verification of electromagnetic waves [12].

Following [13], we demonstrate how a propagating *electromagnetic wave* develops by the mutual influence of electric and magnetic fields. A *uniform plane wave* is a wave that depends only on time and one space direction (i.e., the direction of propagation), and is uniform in all directions transverse to this direction of propagation. Apart from the electrostatic and magnetostatic fields, plane waves represent the simplest solutions of Maxwell's equations. For simplicity we consider the case of an electromagnetic plane wave, where the electric and magnetic field components are uniform in planes transverse to the direction of propagation. If we choose in a Cartesian coordinate system the z -direction as the direction of propagation, all field components will depend only on the coordinate z and time t . Within some finite cross-section an electromagnetic wave emitted from a far-distant source can be approximated by a plane wave.

The following considerations are not a derivation of an electromagnetic wave, since we are already making very detailed pre-assumptions. However, we want to visualize how the physical phenomena interact in order to establish wave propagation. First we assume that in a far-distant transverse plane located in the negative z -direction, at a certain moment a magnetic field \mathbf{H} is suddenly turned on. We assume that this magnetic field is directed in the y -direction and is homogeneous throughout the whole transverse plane. This may be realized when in a large conducting plane a homogeneous surface current directed in the negative x -direction is turned on instantaneously. Now let us assume that a physical action can propagate with a maximum velocity, which we

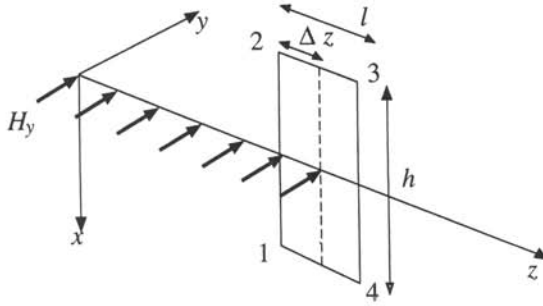


Figure 2.16: Generation of the electric field by the magnetic field.

will name c . Let us assume that a plane wave front is propagating now in the positive z -direction and that the space in front of the wave front is free of field. The space behind the wave front is filled by a homogeneous magnetic field H_y in the y -direction.

We now, in a first step, are going to show that this propagating magnetic field due to Faraday's law will induce an electric field. Let us consider an area element of height h and length l corresponding to Figure 2.16. During the time of propagation of the wave front through this area element, the magnetic flux Φ flowing through the area element is increasing linearly with time. We obtain from (2.65b)

$$\Phi = \mu h \Delta z H_y. \quad (2.66)$$

For Δz increasing with time the velocity c of the wave front is given by

$$c = \frac{d\Delta z}{dt}. \quad (2.67)$$

Therewith we obtain from (2.66) for the time interval in which the wave front is marching through the area element,

$$\frac{d\Phi}{dt} = \mu h c H_y. \quad (2.68)$$

Due to Faraday's law (2.57b) this change of the magnetic flux with time has to be related with the circulation integral of the induced electrical field E . Now we may assume that the induced electric field has no component in the z -direction, since such a field should have the same direction throughout the complete transverse plane for symmetry reasons. Such a longitudinal electromagnetic field would not be divergence-free. Therefore a component E_z cannot occur, since we did not assume any electric charge in front of the wave front. We also may assume that there is no electric field in

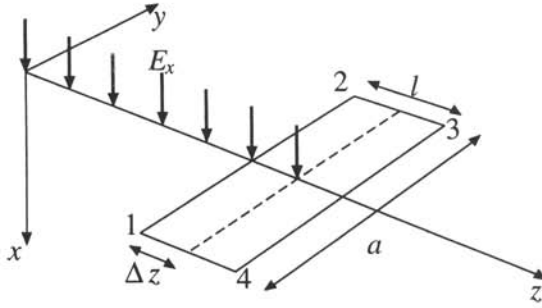


Figure 2.17: Generation of the magnetic field by the electric field.

front of the wave front. Therefore only a homogeneous electric field E_x between point 1 and point 2 of the path of integration gives a contribution to the integral, hence

$$\oint_{\partial A} \mathcal{E} = -h E_x. \quad (2.69)$$

With (2.57b) and (2.68) we obtain

$$E_x = \mu c H_y. \quad (2.70)$$

We assumed that the magnetic field propagates in the positive z -direction without discussing the rules governing this propagation. We now want to show that the propagating electric field gives rise to a magnetic field. For this purpose we consider a horizontal area element of length l and width a according to Figure 2.17. In the spatial region inside the wave front exists a homogeneous electric field E_x . In the time interval in which the wave front propagates through the area element the electric flux through this area element is given by

$$\Psi = \epsilon a \Delta z E_x. \quad (2.71)$$

With (2.67) we obtain

$$\frac{d\Psi}{dt} = \epsilon a c E_x. \quad (2.72)$$

The displacement current $d\Psi/dt$ generates a magnetic field. The circulation integral of the magnetic field over the boundary of the area element is related to the displacement current $d\Psi/dt$ according to (2.57a). Only the homogeneous magnetic field H_y between points 1 and 2 in Figure 2.17 gives a contribution to the integral, hence

$$\oint_{\partial A} \mathcal{H} = a H_y. \quad (2.73)$$

With (2.57a) and (2.72) we obtain

$$H_y = \epsilon c E_x. \quad (2.74)$$

From (2.70) and (2.74) we obtain the propagation velocity c of the plane electromagnetic wave

$$c = \frac{1}{\sqrt{\epsilon\mu}}. \quad (2.75)$$

This is the speed of light in the medium with permittivity ϵ and permeability μ . A dielectric material with $\epsilon \neq \epsilon_0$ and $\mu = \mu_0$ may be characterized by the *refractive index*

$$n = \sqrt{\epsilon_r}. \quad (2.76)$$

The refractive index gives the ratio of the free-space velocity c_0 of the transverse electromagnetic wave to its velocity c in the medium:

$$n = \frac{c_0}{c}. \quad (2.77)$$

For free-space the propagation velocity is the speed of light c_0 given in (2.60). Furthermore, from (2.74) and (2.75) we obtain the ratio of electric and magnetic field intensities, given by

$$\frac{E_x}{H_y} = \sqrt{\frac{\mu}{\epsilon}}. \quad (2.78)$$

The ratio E_x/H_y has the unit VA^{-1} . We define the *wave impedance* Z_F by

$$Z_F = \sqrt{\frac{\mu}{\epsilon}}. \quad (2.79)$$

The *free-space wave impedance* is given by

$$Z_{F0} = \sqrt{\frac{\mu_0}{\epsilon_0}} = 377 \, \Omega \cong 120\pi \, \Omega. \quad (2.80)$$

The considerations we have presented here naturally are independent from the choice of the coordinates. Therefore we may assume in general that in the case of the *plane electromagnetic wave* the direction of the electric field, the direction of the magnetic field, and the direction of propagation form an orthogonal trihedron. Up to now we only have considered a *step wave* defined by

$$E_x(z, t) = Z_{F0} H_y(z, t) \begin{cases} 0 & \text{for } ct - z < 0 \\ E_0 & \text{for } ct - z \geq 0 \end{cases}. \quad (2.81)$$

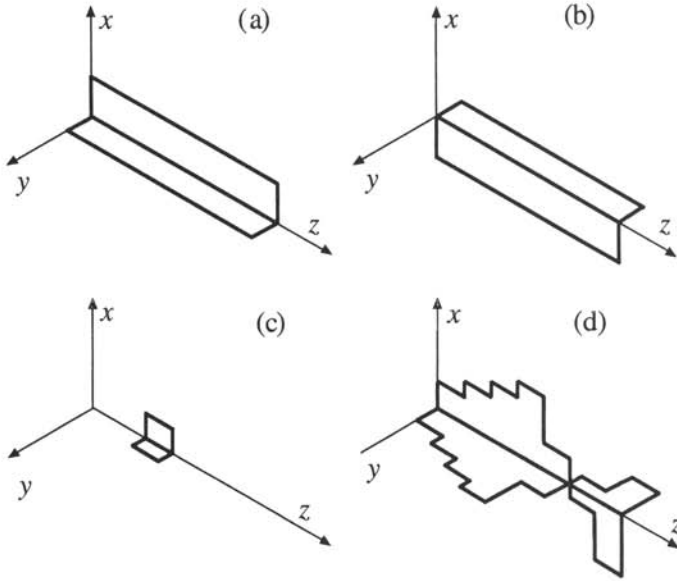


Figure 2.18: Superposition of step waves: (a) positive step wave, (b) negative step wave, (c) rectangular pulse wave, and (d) step wave train.

Due to the linearity of Ampère's and Faraday's laws, however, we can use the principle of superposition and thereby construct plane waves of arbitrary shape.

By superposition of a step wave, Figure 2.18(a), and a time-delayed step wave with opposite amplitude, Figure 2.18(b), we obtain a rectangular wave as shown in Figure 2.18(c). Putting together such rectangular waves, we can construct wave forms as depicted in Figure 2.18(d). If we reduce the width of the rectangular segments to zero, we may construct continuous waves of arbitrary shape.

We therefore may assume waves of arbitrary shape propagating at a velocity c with a stable waveform. The spatial dependence and the time dependence of a plane electromagnetic wave propagating in the positive z -direction with the electric field directed in the x -direction is given by

$$E_x(z, t) = E_x(z - ct), \quad (2.82a)$$

$$H_y(z, t) = Z_F^{-1} E_x(z - ct). \quad (2.82b)$$

If the wave is propagating in the negative z -direction, we obtain

$$E_x(z, t) = E_x(z + ct), \quad (2.83a)$$

$$H_y(z, t) = -Z_F^{-1} E_x(z + ct). \quad (2.83b)$$

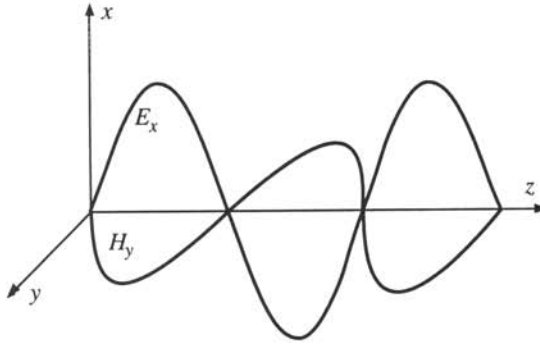


Figure 2.19: Linearly polarized time-harmonic electromagnetic wave.

Assuming a sinusoidal time dependence of the electromagnetic field, we obtain the *time-harmonic electromagnetic wave*. With frequency f , angular frequency ω , wavelength λ , and wave number k , given by

$$\omega = 2\pi f, \quad (2.84)$$

$$k = \frac{\omega}{c} = 2\pi/\lambda \quad (2.85)$$

we obtain the field components

$$E_x(z, t) = E_{0x}^+ \cos(\omega t - kz + \phi_0), \quad (2.86a)$$

$$H_y(z, t) = H_{0y}^+ \cos(\omega t - kz + \phi_0). \quad (2.86b)$$

E_{0x}^+ and H_{0y}^+ are the amplitudes of the time-harmonic electromagnetic wave propagating in the positive z -direction. The electric and magnetic field amplitudes are related via

$$E_{0x}^+ = Z_F H_{0y}^+. \quad (2.87)$$

Figure 2.19 shows the field components E_{0x}^+ and H_{0y}^+ of the time-harmonic electromagnetic wave. If the electrical field is directed in one direction only, the wave exhibits *linear polarization*. The direction of the electric field vector is always called the direction of polarization. In free-space the speed of light c_0 , the wave number k_0 , and the wavelength λ_0 are related by

$$k_0 = \frac{\omega}{c_0} = 2\pi/\lambda_0. \quad (2.88)$$

The superposition of an electromagnetic wave propagating in the positive z -direction with an electromagnetic wave propagating at the same frequency in the negative z -

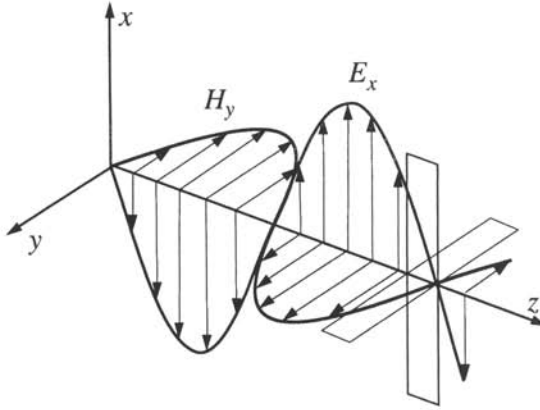


Figure 2.20: Linearly polarized time-harmonic electromagnetic wave.

direction is given by

$$E_x(z, t) = E_{0x}^+ \cos(\omega t - kz + \phi_0^+) + E_{0x}^- \cos(\omega t + kz + \phi_0^-), \quad (2.89a)$$

$$H_y(z, t) = H_{0y}^+ \cos(\omega t - kz + \phi_0^+) + H_{0y}^- \cos(\omega t + kz + \phi_0^-). \quad (2.89b)$$

The field amplitudes E_{0x}^- and H_{0y}^- of the wave propagating in the negative z -direction are related by

$$E_{0x}^- = -Z_F H_{0y}^-. \quad (2.90)$$

The negative sign in (2.90) is due to the circumstance that for the wave propagating in the negative z -direction, the directions of \mathbf{E} , \mathbf{H} , and the direction of propagation also form a right-handed orthogonal trihedron.

2.8.1 The Wave Equation

To derive a wave equation for the plane electromagnetic wave we consider the continuous plane wave according to Figure 2.20. We assume that the area elements considered in Figures 2.16 and 2.17 exhibit an infinitesimal length Δz . The magnetic flux varies continuously, and we obtain from (2.66)

$$\frac{d\Phi}{dt} = \mu h \Delta z \frac{dH_y}{dt}. \quad (2.91)$$

The circulation integral of the electric field over the contour of the vertical area element is given by

$$\oint_{\partial A} \mathcal{E} = -h (E_x(z) - E_x(z + \Delta z)). \quad (2.92)$$

From (2.57b), (2.91), and (2.92) we obtain for $\Delta z \rightarrow 0$ the differential equation

$$\frac{\partial E_x}{\partial z} = -\mu \frac{\partial H_y}{\partial t}. \quad (2.93)$$

The operator ∂ denotes the *partial derivation*. The partial derivative $\partial E_x / \partial z$ is formed as if E_x is only dependent on z . For the change of the electric flux with time we obtain

$$\frac{d\Psi}{dt} = \epsilon a \Delta z \frac{dE_x}{dt}. \quad (2.94)$$

The circulation integral of the magnetic field around the area element is given by

$$\oint_{\partial A} \mathcal{H} = a (H_y(z) - H_y(z + \Delta z)). \quad (2.95)$$

For $\Delta z \rightarrow 0$, we obtain

$$\frac{\partial H_y}{\partial z} = -\epsilon \frac{\partial E_x}{\partial t}. \quad (2.96)$$

From (2.93) and (2.96), we obtain under consideration of (2.75) the wave equation

$$\frac{\partial^2}{\partial z^2} \begin{Bmatrix} E_x \\ H_y \end{Bmatrix} - \frac{1}{c^2} \frac{\partial^2}{\partial t^2} \begin{Bmatrix} E_x \\ H_y \end{Bmatrix} = 0. \quad (2.97)$$

This wave equation is valid for E_x and H_y as well. It is easy to verify that all the above-presented solutions fulfill this equation.

2.8.2 The Polarization of Electromagnetic Waves

Let us again consider a plane electromagnetic wave propagating in the positive z -direction. We now assume that the electric field exhibits an x -component as well as a y -component given by

$$E_x^{(+)} \left(t - \frac{z}{c} \right) = E_{x0}^{(+)} \cos(\omega t - \beta z + \psi_x), \quad (2.98)$$

$$E_y^{(+)} \left(t - \frac{z}{c} \right) = E_{y0}^{(+)} \cos(\omega t - \beta z + \psi_y). \quad (2.99)$$

We allow different amplitudes $E_{x0}^{(+)}$ and $E_{y0}^{(+)}$ and different phases ψ_x and ψ_y for both electric field components. Since $E_x^{(+)}$ and $E_y^{(+)}$ may be chosen independently, every superposition of (2.98) and (2.99) is a solution of Maxwell's equations.

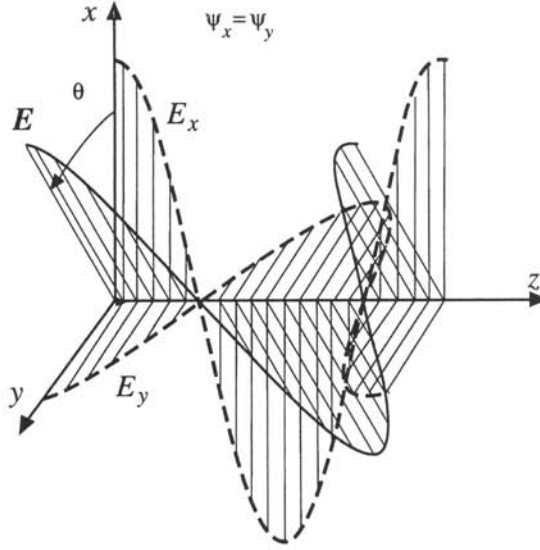


Figure 2.21: Linearly polarized plane electromagnetic wave.

Let us consider the superposition of these two waves. We first consider the case where ψ_x is equal to ψ_y (i.e., both components $E_x^{(+)}$ and $E_y^{(+)}$ have the same phase). In this case

$$\frac{E_x^{(+)} \left(t - \frac{z}{c} \right)}{E_y^{(+)} \left(t - \frac{z}{c} \right)} = \frac{E_{x0}^{(+)}}{E_{y0}^{(+)}} \quad \text{for } \psi_x = \psi_y \quad (2.100)$$

is valid. The ratio between the x -component and the y -component of the electric field is independent from space and time. Such a uniform plane wave is called *linearly polarized*. The angle

$$\theta = \arctan \frac{E_y^{(+)} \left(t - \frac{z}{c} \right)}{E_x^{(+)} \left(t - \frac{z}{c} \right)} \quad (2.101)$$

is constant. Figure 2.21 shows the direction of the field vector E and its x - and y -components E_x and E_y . In general the condition for linear polarization is given by $\psi_y = \psi_x + m\pi$ where m is an integer.

We consider the special case given by $\psi_y = \psi_x \pm \frac{1}{2}\pi$ and $E_{y0}^{(+)} = E_{x0}^{(+)} = E_0^{(+)}$. From (2.98), (2.99), and (2.100) we obtain

$$\left. \begin{aligned} |E^{(+)} \left(t - \frac{z}{c} \right)| &= |E_0^{(+)}| = \text{const.} \\ \theta &= \pm(\omega t - \beta z + \psi_x) \end{aligned} \right\} \quad \begin{aligned} &\text{for } \psi_y = \psi_x \pm \frac{1}{2}\pi \\ &\text{and } E_0^{(+)} = E_{y0}^{(+)} = E_{x0}^{(+)} \end{aligned} \quad (2.102)$$

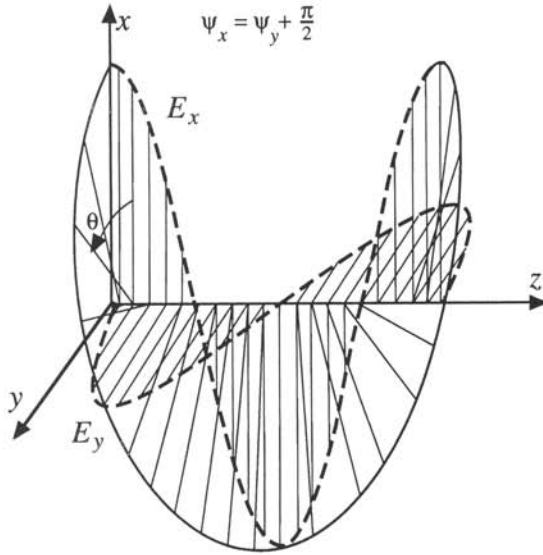


Figure 2.22: Left-hand circularly polarized plane electromagnetic wave.

The magnitude $|E^{(+)}|$ of the electrical field intensity is constant, whereas the direction of the electric field rotates around the z -axis. The rotation occurs with the angular frequency ω . The rotation in space has a period given by the wave number β . This wave exhibits *circular polarization*. Figure 2.22 illustrates this case. If we are looking into the direction of propagation of this wave, the electric field vector is rotating counter-clockwise. The wave is left-handed circularly polarized. We have to consider that the sense of rotation for constant space is opposite to the sense of rotation for constant time. For $\psi_y = \psi_x - \frac{1}{2}\pi$ the electric field vector E is rotating clockwise if we are looking in the direction of propagation. If the rotation of a circularly polarized wave with respect to time and the direction of propagation corresponds to a right-handed system, the wave is called right-handed circularly polarized. In the most general case, if $\psi_x, \psi_y, E_{x0}^{(+)}$ and $E_{y0}^{(+)}$ are arbitrary, the electric field vector performs an elliptic motion. In this case the polarization is called elliptic.

2.9 KIRCHHOFF'S LAWS

The fundamental equations of network theory may be derived from Maxwell's equations. Figure 2.23 shows a network node with n conductors. We enclose the network node in

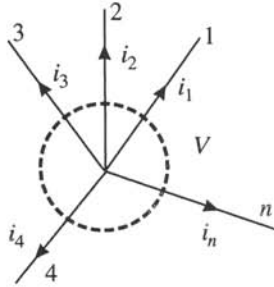


Figure 2.23: Network node.

a volume V and apply the integral form (2.59) of the equation of continuity

$$\oint_{\partial V} \mathcal{J} = -\frac{d}{dt} \int_V \mathcal{Q}. \quad (2.103)$$

On the left side of (2.103) only the integration over the surface areas of the n conductors gives a contribution. The surface integral over ∂V may be subdivided into n integrals over the cross-section areas A_k of the conductors. Each of these integrals corresponds to a current i_k flowing from the node.

$$\oint_{\partial V} \mathcal{J} = \sum_{k=1}^n \int_{A_k} \mathcal{J} = \sum_{k=1}^n i_k. \quad (2.104)$$

From (2.65d), (2.103), and (2.104) we obtain

$$\sum_{k=1}^n i_k = -\frac{dq}{dt}. \quad (2.105)$$

If the time variation of the charge on the conductors inside the volume V can be neglected, the right side of (2.105) disappears. In this case we obtain

$$\sum_{k=1}^n i_k = 0 \quad \text{for} \quad \frac{dq}{dt} = 0. \quad (2.106)$$

The sum of the node currents vanishes. This is *Kirchhoff's current law*. Since for a given charge q the magnitude of dq/dt increases in proportion to the frequency, at higher frequencies the term dq/dt may not be neglected any more. The displacement current flowing in a real network from the node may be considered by insertion of one or several capacitors in an *equivalent circuit*. Via these capacitors the displacement current

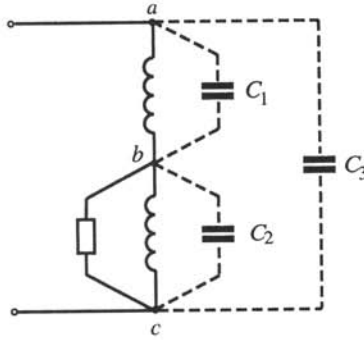


Figure 2.24: Equivalent circuit with parasitic capacitors.

flowing between the conductors of the real network are modeled. Figure 2.24 shows a network consisting of two inductors and one resistor. Three capacitors are inserted in order to consider the displacement current flowing between nodes a , b and c . The equivalent circuit contains additional circuit elements modeling the field between the physical circuit elements.

To derive Kirchhoff's voltage law we apply the integral form of Faraday's law (2.57b) to the loop depicted in Figure 2.25. The area or virtual surface bounded by this loop is A . The line integral of the electrical field intensity E over the boundary ∂A of the loop area A is equal to the negative sum of the branch voltages:

$$\oint_{\partial A} \mathcal{E} = -v_{21} - v_{32} - v_{43} - v_{54} - v_{15}. \quad (2.107)$$

From (2.57b), (2.65b), and (2.107) we obtain

$$v_{21} + v_{32} + v_{43} + v_{54} + v_{15} = \frac{d\Phi}{dt}. \quad (2.108)$$

If the time variation of the magnetic flux through the loop can be neglected, the sum of the loop voltages disappears:

$$\sum_{\text{loop}} v_{kl} = 0 \quad \text{for} \quad \frac{d\Phi}{dt} = 0. \quad (2.109)$$

This is *Kirchhoff's voltage law*. Since the quantity $d\Phi/dt$ also increases with frequency, at higher frequencies we can no longer neglect the magnetic flux through the loop. This magnetic flux may be considered by insertion of inductors into the loop branches.

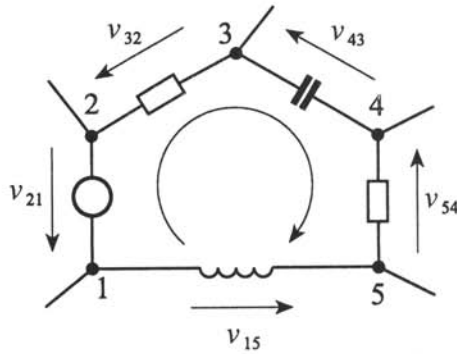


Figure 2.25: Network loop.

The voltage induced from one branch into another is thereby considered via a mutual inductance.

Inductors and capacitors, which do not correspond to real circuit elements, but are introduced via the geometry of the conductors, are called *parasitic capacitors* and *parasitic inductors*. At higher frequencies, these *parasitic network elements* cannot be neglected anymore. Usually such parasitic elements are unwanted. By careful geometric design of the circuit and the paths of the lines, such elements can be kept under control. As long as only parasitic capacitors and parasitic inductors occur, these network elements may be considered within the framework of the network concept. The situation becomes more complicated as soon as the dimensions of the circuits reach the order of magnitude of the wavelength. In this case electric and magnetic fields may be directly linked with each other. In this case it is not possible to describe the influence of electric and magnetic fields independently via equivalent capacitors and inductors. However, in these cases an equivalent circuit may also be established after solving the electromagnetic field problem.

2.10 MAXWELL'S EQUATIONS IN LOCAL FORM

Any measurement of electromagnetic field quantities is related to an integration or averaging over a finite spatial domain. However, the field concept is essentially a local concept, which means that in using the field concept we consider the local relations between field quantities within an infinitesimally small neighborhood. We will bring Maxwell's equations into their local form.

We introduce the *exterior derivative* $d\mathcal{U}$ of an exterior differential form \mathcal{U} by

$$d\mathcal{U} = \sum_i dx_i \wedge \frac{\partial \mathcal{U}}{\partial x_i} \quad \text{with } dx_i = dx, dy, dz. \quad (2.110)$$

For the exterior derivative we have the following rules:

$$d(\mathcal{U} + \mathcal{V}) = d\mathcal{U} + d\mathcal{V}, \quad (2.111a)$$

$$d(\mathcal{U} \wedge \mathcal{V}) = d\mathcal{U} \wedge \mathcal{V} + (-1)^{(\deg \mathcal{U})} \mathcal{U} \wedge d\mathcal{V}, \quad (2.111b)$$

where the *degree* of the differential form \mathcal{U} is $\deg \mathcal{U} = p$ if \mathcal{U} is a p -form.

Stokes' theorem relates the integration of a p -form \mathcal{U} over the closed p -dimensional boundary ∂V of a $p + 1$ -dimensional volume V to the volume integral of \mathcal{U} over V via

$$\oint_{\partial V} \mathcal{U} = \int_V d\mathcal{U}. \quad (2.112)$$

Applying Stokes' theorem to the integral form of Maxwell's equations (2.57a) to (2.57d), we obtain

$$\int_A d\mathcal{H} = \frac{d}{dt} \int_A \mathcal{D} + \int_A \mathcal{J}, \quad (2.113a)$$

$$\int_A d\mathcal{E} = -\frac{d}{dt} \int_A \mathcal{B}, \quad (2.113b)$$

$$\int_V d\mathcal{B} = 0, \quad (2.113c)$$

$$\int_V d\mathcal{D} = \int_V \mathcal{Q} \quad (2.113d)$$

and from this the differential representation of Maxwell's equations:

$$d\mathcal{H} = \frac{\partial}{\partial t} \mathcal{D} + \mathcal{J}, \quad \text{Ampère's law} \quad (2.114a)$$

$$d\mathcal{E} = -\frac{\partial}{\partial t} \mathcal{B}, \quad \text{Faraday's law} \quad (2.114b)$$

$$d\mathcal{B} = 0, \quad \text{Magnetic flux continuity} \quad (2.114c)$$

$$d\mathcal{D} = \mathcal{Q}. \quad \text{Gauss' law} \quad (2.114d)$$

Applying the Stokes' theorem (2.112) to the integral form of the continuity equation (2.59) yields the *local form* of the *continuity equation*

$$\frac{\partial}{\partial t} \mathcal{Q} + d\mathcal{J} = 0. \quad (2.115)$$

2.11 TIME-HARMONIC ELECTROMAGNETIC FIELDS

A *time-harmonic* electromagnetic field is an electromagnetic field with sinusoidal time dependence. As far as physical quantities are time-harmonic, a representation of these quantities by complex *phasors* can simplify the analysis [14]. The time-harmonic electric field

$$\mathbf{E}(\mathbf{x}, t) = \begin{bmatrix} E_{0x}(\mathbf{x}) \cos(\omega t + \phi_x(\mathbf{x})) \\ E_{0y}(\mathbf{x}) \cos(\omega t + \phi_y(\mathbf{x})) \\ E_{0z}(\mathbf{x}) \cos(\omega t + \phi_z(\mathbf{x})) \end{bmatrix} \quad (2.116)$$

can be represented as

$$\mathbf{E}(\mathbf{x}, t) = \Re \{ \underline{\mathbf{E}}(\mathbf{x}) e^{j\omega t} \} \quad (2.117)$$

using the *vector phasor*

$$\underline{\mathbf{E}}(\mathbf{x}) = \begin{bmatrix} E_{0x}(\mathbf{x}) e^{j\phi_x(\mathbf{x})} \\ E_{0y}(\mathbf{x}) e^{j\phi_y(\mathbf{x})} \\ E_{0z}(\mathbf{x}) e^{j\phi_z(\mathbf{x})} \end{bmatrix}. \quad (2.118)$$

We mark phasors by underlining. Due to

$$\frac{\partial}{\partial t} \mathbf{E}(\mathbf{x}, t) = \Re \{ j\omega \underline{\mathbf{E}}(\mathbf{x}) e^{j\omega t} \} \quad (2.119)$$

the partial derivation with respect to time may be replaced by a multiplication with the factor $j\omega$. We introduce the complex *differential form phasor* $\underline{\mathcal{E}}$ related to the differential form \mathcal{E} . For a time-harmonic field described by a differential form

$$\begin{aligned} \mathcal{E}(\mathbf{x}, t) = & E_{0x}(\mathbf{x}) \cos(\omega t + \phi_x(\mathbf{x})) dx + E_{0y}(\mathbf{x}) \cos(\omega t + \phi_y(\mathbf{x})) dy \\ & + E_{0z}(\mathbf{x}) \cos(\omega t + \phi_z(\mathbf{x})) dz \end{aligned} \quad (2.120)$$

we introduce

$$\underline{\mathcal{E}}(\mathbf{x}, t) = \underline{E}_{0x}(\mathbf{x}) e^{j\phi_x(\mathbf{x})} dx + \underline{E}_{0y}(\mathbf{x}) e^{j\phi_y(\mathbf{x})} dy + \underline{E}_{0z}(\mathbf{x}) e^{j\phi_z(\mathbf{x})} dz \quad (2.121)$$

and obtain

$$\mathcal{E}(\mathbf{x}, t) = \Re \{ \underline{\mathcal{E}}(\mathbf{x}) e^{j\omega t} \}, \quad (2.122a)$$

$$\frac{\partial}{\partial t} \mathcal{E}(\mathbf{x}, t) = \Re \{ j\omega \underline{\mathcal{E}}(\mathbf{x}) e^{j\omega t} \}. \quad (2.122b)$$

Table 2.3: Electric Material Properties

Material	σ/Sm^{-1}	ϵ'_r	f_c/Hz
Copper	$5.8 \cdot 10^7$	1	–
Germanium (pure)	2.2	16	$2.5 \cdot 10^9$
Sea water	4	81	$8.9 \cdot 10^8$
Water	10^{-3}	81	$2.2 \cdot 10^5$
Wet earth	10^{-3}	10	$1.8 \cdot 10^6$
Dry earth	10^{-5}	5	$3.6 \cdot 10^4$

2.12 MAXWELL'S EQUATIONS IN THE FREQUENCY DOMAIN

Replacing in (2.114a)–(2.114d) the time derivative by multiplication with $j\omega$ we obtain the complex *phasor representation* of Maxwell's equations [15]

$$d\mathcal{H} = j\omega\mathcal{D} + \mathcal{J}, \quad \text{Ampère's law} \quad (2.123a)$$

$$d\mathcal{E} = -j\omega\mathcal{B}, \quad \text{Faraday's law} \quad (2.123b)$$

$$d\mathcal{B} = 0, \quad \text{Magnetic flux continuity} \quad (2.123c)$$

$$d\mathcal{D} = \mathcal{Q}. \quad \text{Gauss' law} \quad (2.123d)$$

In a homogeneous isotropic medium with permittivity ϵ , permeability μ , and conductivity σ , we obtain with (2.32a), (2.32b), and (2.62)

$$d\mathcal{H} = (j\omega\epsilon + \sigma) * \mathcal{E} + \mathcal{J}_0, \quad (2.124a)$$

$$d\mathcal{E} = -j\omega\mu * \mathcal{H}. \quad (2.124b)$$

For insulating materials usually $\omega\epsilon \gg \sigma$ is valid. We may consider the losses in an insulator via complex permittivity $\underline{\epsilon}$.

$$\underline{\epsilon} = \epsilon' + \frac{\sigma}{j\omega} = \epsilon' - j\epsilon''. \quad (2.125)$$

If the losses in a dielectric material are due to ohmic conduction, σ will be independent from ω , and ϵ'' will be proportional to $1/\omega$. If the losses have other origins (e.g., polarization losses in a dielectric material), ϵ'' is not proportional to $1/\omega$. Sometimes the magnitude $|\underline{\epsilon}|$ and phase δ_ϵ of the complex permittivity are also specified:

$$\underline{\epsilon} = |\underline{\epsilon}| e^{-j\delta_\epsilon} = \epsilon' (1 - j \tan \delta_\epsilon). \quad (2.126)$$

Table 2.4: Complex Permittivity of Some Materials at 25°C

Material		Frequency				
		10 ²	10 ⁴	10 ⁶	10 ⁸	10 ¹⁰
Teflon	ϵ'_r	2.1	2.1	2.1	2.1	2.0
	ϵ''_r	$1.1 \cdot 10^{-3}$	$7 \cdot 10^{-4}$	$4 \cdot 10^{-4}$	$3 \cdot 10^{-4}$	$8 \cdot 10^{-4}$
Polysterine	ϵ'_r	2.56	2.56	2.56	2.56	2.54
	ϵ''_r	$1.3 \cdot 10^{-4}$	$1.3 \cdot 10^{-4}$	$1.8 \cdot 10^{-4}$	$3 \cdot 10^{-4}$	$1.1 \cdot 10^{-3}$
Quartz	ϵ'_r	3.78	3.78	3.78	3.78	3.78
	ϵ''_r	$3.2 \cdot 10^{-3}$	$2.3 \cdot 10^{-3}$	$7.5 \cdot 10^{-4}$	$4 \cdot 10^{-4}$	$4 \cdot 10^{-4}$

The phase δ_e is called the *dielectric loss angle*, and $\tan \delta_e$ is the *dielectric loss factor*: For small losses we obtain $|\underline{\epsilon}| \cong \epsilon'$ and $\tan \delta_e \cong \epsilon''/\epsilon'$. Magnetic losses may be described by a *complex permeability* $\underline{\mu}$,

$$\underline{\mu} = \mu' - j\mu'' = |\underline{\mu}| e^{-j\delta_m} = \mu'(1 - j \tan \delta_m). \quad (2.127)$$

The phase δ_m is the *magnetic loss angle*, and $\tan \delta_m$ the *magnetic loss factor*.

The *relative permittivity* is the ratio of the permittivity to the free-space dielectric constant

$$\underline{\epsilon}_r = \epsilon'_r - j\epsilon''_r = \frac{\underline{\epsilon}}{\epsilon_0}. \quad (2.128)$$

In the same way, the *relative permeability* $\underline{\mu}_r$ is given by

$$\underline{\mu}_r = \mu'_r - j\mu''_r = \frac{\underline{\mu}}{\mu_0}. \quad (2.129)$$

With the complex permittivity $\underline{\epsilon}$ and the complex permeability $\underline{\mu}$, we obtain from (2.124a) and (2.124b)

$$d\underline{\mathcal{H}} = j\omega \underline{\epsilon} \star \underline{\mathcal{E}} + \underline{\mathcal{J}}_0, \quad (2.130a)$$

$$d\underline{\mathcal{E}} = -j\omega \underline{\mu} \star \underline{\mathcal{H}}. \quad (2.130b)$$

For nonmagnetic materials $\underline{\mu} = \mu_0$ is valid. A material for which, in the considered frequency regime, $\epsilon' \gg \epsilon''$ is valid is called *quasi-dielectric*, for $\epsilon' \ll \epsilon''$ the material is called a *quasi-conductor*. The same material may be a quasi-conductor at low frequencies and a quasi-dielectric at higher frequencies. The *material cutoff frequency* f_c between these regions is given by

$$f_c = \frac{\sigma}{2\pi\epsilon'}. \quad (2.131)$$

In Table 2.3, ϵ'_r , σ and f_c are given for some materials. For metals, f_c is far beyond the optical frequency region. Table 2.4 specifies ϵ'_r and ϵ''_r for some important dielectric materials in dependence from the frequency.

2.13 CURVILINEAR COORDINATES

It is one principal advantage of vector calculus and exterior calculus that the equations defining and describing the properties may be formulated without reference to a specific coordinate system. Depending on the problem, the choice of a specific coordinate system may simplify the solution to the problem considerably. A detailed treatment of curvilinear coordinates is given in Appendix A.4.

We introduce an *orthogonal curvilinear coordinate system*

$$u = u(x, y, z), \quad v = v(x, y, z), \quad w = w(x, y, z). \quad (2.132)$$

The *coordinate curves* are obtained by setting two of the three coordinates u , v and w constant. *Coordinate surfaces* are defined by setting one of the three coordinates constant. In an orthogonal coordinate system at any point (except singular points) of the space, the three coordinate curves are orthogonal. The same holds for the three coordinate surfaces going through any point. The differentials dx , dy , dz and the differentials du , dv , dw are related by

$$dx = \frac{\partial x}{\partial u} du + \frac{\partial x}{\partial v} dv + \frac{\partial x}{\partial w} dw, \quad (2.133a)$$

$$dy = \frac{\partial y}{\partial u} du + \frac{\partial y}{\partial v} dv + \frac{\partial y}{\partial w} dw, \quad (2.133b)$$

$$dz = \frac{\partial z}{\partial u} du + \frac{\partial z}{\partial v} dv + \frac{\partial z}{\partial w} dw. \quad (2.133c)$$

The rules for transformation of the Cartesian *basis two-forms* $dx \wedge dy$, $dy \wedge dz$, $dz \wedge dx$ and the Cartesian *basis three-form* $dx \wedge dy \wedge dz$ follow directly from the above equations by applying the rules of the exterior product and are given explicitly in (A.97) and (A.98). Using the *metric coefficients* g_1^2 , g_2^2 , and g_3^2 defined in (A.104), *unit one-forms* (A.109)

$$s_1 = g_1 du, \quad s_2 = g_2 dv, \quad s_3 = g_3 dw \quad (2.134)$$

are introduced. The integral of $s_1 = g_1 du$ along any path with v and w constant yields the length of the path.

In a *circular cylindric coordinate system* defined by (A.143), the unit differential forms (A.146) are

$$s_1 = dr, \quad s_2 = r d\phi, \quad s_3 = dz. \quad (2.135)$$

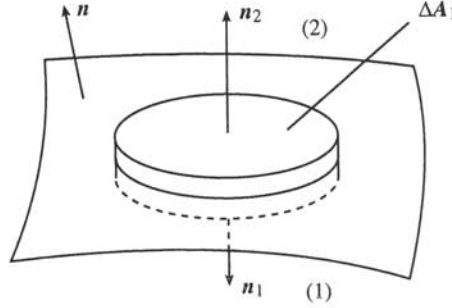


Figure 2.26: The normal boundary conditions.

In a *spherical coordinate system* defined by (A.160), the unit differential forms (A.163) are

$$s_1 = dr, \quad s_2 = r d\theta, \quad s_3 = r \sin \theta d\phi. \quad (2.136)$$

For the curvilinear unit differential forms the *Hodge operator* as defined in (2.30) is

$$\begin{aligned} *f &= f s_1 \wedge s_2 \wedge s_3, \\ *(A_u s_1 + A_v s_2 + A_w s_3) &= A_u s_2 \wedge s_3 + A_v s_3 \wedge s_1 + A_w s_1 \wedge s_2, \\ *(A_u s_2 \wedge s_3 + A_v s_3 \wedge s_1 + A_w s_1 \wedge s_2) &= A_u s_1 + A_v s_2 + A_w s_3, \\ *(f s_1 \wedge s_2 \wedge s_3) &= f. \end{aligned} \quad (2.137)$$

2.14 BOUNDARY CONDITIONS

Usually we consider electromagnetic structures assembled from various materials with different material properties. At a boundary surface between two materials the material parameters undergo a discontinuous change. At the boundary surfaces the field quantities have to fulfill *boundary conditions*. If the materials are homogeneous, we can try to find solutions of Maxwell's equations in the following way: We seek the solutions in each subdomain and fit these solutions along the boundaries. In the following we show that at boundary surfaces the tangential components of the field intensities and the normal components of the flux densities and the current density fulfill boundary conditions. Figure 2.26 shows a section of the boundary surface between spatial regions 1 and 2. We now consider an area element ΔA_1 of this boundary surface. We introduce a local orthonormal right-handed curvilinear coordinate system u, v, n with the coordinates u and v tangential to the boundary surface and the coordinate n normal to the boundary surface. In this coordinate system the magnetic flux density differential form is given by

$$\mathcal{B} = B_u s_2 \wedge n + B_v n \wedge s_1 + B_n s_1 \wedge s_2. \quad (2.138)$$

We construct a small volume ΔV that is formed as a small circular cylinder like a pillbox. The bottom surface of the cylinder is located in region 1, whereas the top surface of the cylinder is located in region 2. The pillbox encloses a volume ΔV . We now apply the magnetic flux continuity law (2.57c) to the cylinder volume ΔV . In the limit process $\Delta V \rightarrow 0$, the side surface of the pillbox will go to zero by a higher order than the bottom and top surface and may be neglected. We therefore obtain

$$\oint_{\partial(\Delta V)} \mathcal{B} = \int_{\Delta A_1} (\mathcal{B}^{(2)} - \mathcal{B}^{(1)}) = \int_{\Delta A_1} (B_n^{(2)} - B_n^{(1)}) s_1 \wedge s_2 = 0. \quad (2.139)$$

$\mathcal{B}^{(1)}$ and $\mathcal{B}^{(2)}$ are the magnetic flux density differential forms in region 1 and region 2, respectively. The above condition is fulfilled if and only if

$$n \wedge (\mathcal{B}^{(2)} - \mathcal{B}^{(1)}) = 0. \quad (2.140)$$

This is the boundary condition for the magnetic flux density.

Let us now compute the surface integral of the electric flux density over the boundary of the pillbox. Performing the same limiting process as above, we obtain

$$\oint_{\partial(\Delta V)} \mathcal{D} = \int_{\Delta A_1} (\mathcal{D}^{(2)} - \mathcal{D}^{(1)}) = \int_{\Delta A_1} (D_n^{(2)} - D_n^{(1)}) s_1 \wedge s_2. \quad (2.141)$$

We introduce a *surface charge density* ρ_A (dimension As/m^2). This means that the infinitely thin boundary surface contains a finite charge. We can describe the surface charge density by the *surface charge differential form*

$$\mathcal{Q}_A = \rho_A s_1 \wedge s_2. \quad (2.142)$$

The surface charge density is related to the volume charge density via

$$\mathcal{Q} = \delta(n) n \wedge \mathcal{Q}_A, \quad (2.143)$$

where n is the coordinate normal to the area and $\delta(n)$ is the *Dirac delta distribution* defined by

$$\int_{x_1}^{x_2} \delta(x) dx = \begin{cases} 1 & \text{for } x \in [x_1, x_2] \\ 0 & \text{for } x \notin [x_1, x_2] \end{cases}. \quad (2.144)$$

Let A be an area on the boundary surface and V be a volume supported by A and exhibiting an extension normal to the surface from $n = -\frac{1}{2}\Delta n$ to $n = +\frac{1}{2}\Delta n$. In this case

$$\int_V \mathcal{Q} = \int_A \mathcal{Q}_A \quad (2.145)$$

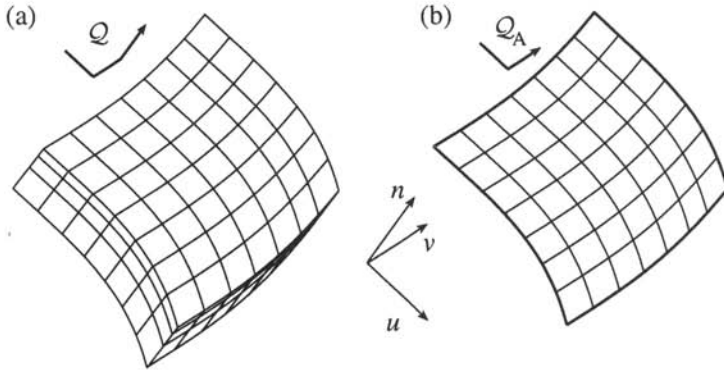


Figure 2.27: (a) Charge form \mathcal{Q} , and (b) surface charge form \mathcal{Q}_A .

is valid. Figure 2.27(a) shows the geometric picture of a charge form \mathcal{Q} and Figure 2.27(b) depicts the corresponding surface charge form \mathcal{Q}_A . Inserting this in Gauss' law (2.57d) yields

$$\oint_{\partial V} \mathcal{D} = \int_A \mathcal{Q}_A, \quad (2.146)$$

and

$$\int_{\Delta A_1} (D_n^{(2)} - D_n^{(1)}) s_1 \wedge s_2 = \int_{\Delta A_1} \rho_A s_1 \wedge s_2. \quad (2.147)$$

This yields the boundary condition for the electric flux density,

$$n \wedge (\mathcal{D}^{(2)} - \mathcal{D}^{(1)}) = n \wedge \mathcal{Q}_A. \quad (2.148)$$

Equations (2.140) and (2.148) are called the *normal boundary conditions*, since they give information about the normal components of the flux densities \mathbf{B} and \mathbf{D} .

Figure 2.28(a) shows the electric flux through the boundary for a homogeneous electric field normal to the boundaries and no surface charge in the boundary. The permittivity ϵ_2 in region 2 is assumed to be twice the permittivity ϵ_1 of region 1. The cross-section of the flux tubes remains unchanged when the flux tubes are crossing the boundary surface. For the same flux densities in both regions we obtain in region 1 twice the electric field intensity as in region 2. Therefore the potential planes in region 1 have twice the density as in region 2, see Figure 2.28(b).

We now investigate the *tangential boundary conditions*. Figure 2.29 shows a normal cut through the boundary surface. In our local coordinate system the magnetic field differential form \mathcal{H} is given by

$$\mathcal{H} = H_u s_1 + H_v s_2 + H_n n. \quad (2.149)$$

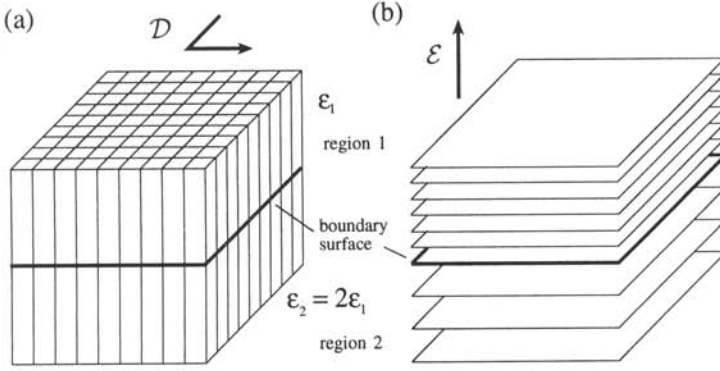


Figure 2.28: The normal boundary conditions: (a) electric flux density, and (b) electric field.

The rectangular area element ΔA_2 has the side lengths d and l , where the longer side l is parallel to u . One of these longer sides is totally embedded in region 1, and the other one in region 2. Computing the circulation integral of the magnetic field intensity over the contour ΔA_2 , we obtain for $d \rightarrow 0$

$$\oint_{\partial(\Delta A_2)} \mathcal{H} = \int_{\Delta l} (\mathcal{H}^{(2)} - \mathcal{H}^{(1)}) . \quad (2.150)$$

$\mathcal{H}^{(1)}$ and $\mathcal{H}^{(2)}$ are the magnetic field intensities in regions 1 and 2 respectively. Let us also assume a current flowing on the infinitely thin boundary layer. The current density exhibits only components tangential to the boundary layer. The current density differential form \mathcal{J} therefore is given by

$$\mathcal{J} = J_u s_2 \wedge n + J_v n \wedge s_1 . \quad (2.151)$$

If the current is concentrated in the boundary layer the dependence in the normal direction n is given by the delta distribution $\delta(n)$ and we obtain

$$\mathcal{J} = -J_{Au}(u, v) \delta(n) n \wedge s_2 + J_{Av}(u, v) \delta(n) n \wedge s_1 . \quad (2.152)$$

We introduce the *surface current density*

$$\mathcal{J}_A(u, v) = J_{Av}(u, v) s_1 - J_{Au}(u, v) s_2 . \quad (2.153)$$

The surface current density form \mathcal{J}_A and the current density form \mathcal{J} are related via

$$\mathcal{J}(u, v, n) = \delta(n) n \wedge \mathcal{J}_A(u, v) . \quad (2.154)$$

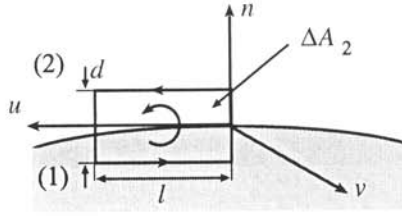


Figure 2.29: The tangential boundary conditions.

The surface current density form \mathcal{J}_A describes a finite current flowing in an infinitely thin surface. Figure 2.30 shows the geometric representation of the current density and the surface current density. The surface current density form \mathcal{J}_A is a one-form. However, unlike one-forms discussed up to now, the direction of integration is not the same as the direction of the field but is orthogonal to the corresponding field direction. We call such a one-form a *twisted one-form*. As a symbol for a twisted form we introduce a line with an arrow indicating the direction of integration with thin lines to the side of the arrow indicating the direction of the surface flux flow, as depicted in Figure 2.30(b).

To transform an ordinary one-form into a twisted one-form and vice versa, we introduce the *twist operator* by

$$\perp_n \mathcal{U} = * (n \wedge \mathcal{U}) . \quad (2.155)$$

The index n of the twist operator \perp_n denotes the axis of rotation. If u, v are the coordinates tangential to the surface and n is the coordinate normal to the surface, the application of the twist operator \perp_n to a one-form tangential to the surface rotates the one-form around n by 90° in the positive direction,

$$\perp_n (U_u s_1 + U_v s_2) = -U_v s_1 + U_u s_2 , \quad (2.156a)$$

$$\perp_n (U_v s_1 - U_u s_2) = U_u s_1 + U_v s_2 . \quad (2.156b)$$

If a current is flowing tangential to a surface, given by $n = \text{const.}$, and if the current is flowing within a small interval (n_1, n_2) , as depicted in Figure 2.30(a), we can approximate the current distribution by a surface current distribution shown in Figure 2.30(b). The surface current twisted one-form \mathcal{J}_A is obtained by integrating the current density two-form over the normal coordinate n from n_1 to n_2 . To integrate a differential form over a single coordinate we first bring the corresponding coordinate differential to the left. This follows from the circumstance that the integration is the inverse operation to the exterior derivative, and the exterior derivation attaches a coordinate differential to

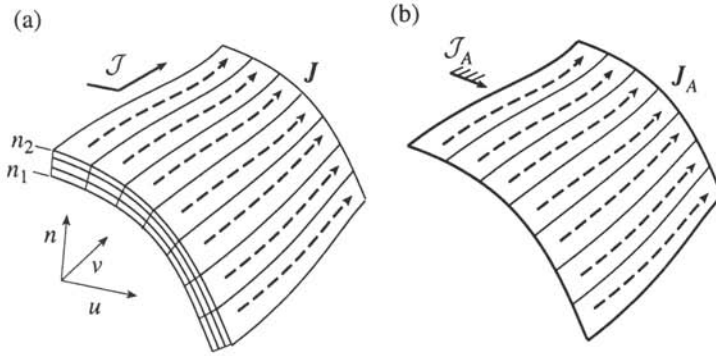


Figure 2.30: (a) Current form \mathcal{J} , and (b) surface current form \mathcal{J}_A .

the left of a differential form,

$$\mathcal{J}_A(u, v) = \int_{n_1}^{n_2} \mathcal{J}(u, v, n). \quad (2.157)$$

Inserting (2.150) and (2.154) in Ampère's law (2.57a) gives

$$\oint_{\partial A_2} \mathcal{H} = \int_{\Delta I} (\mathcal{H}^{(2)} - \mathcal{H}^{(1)}) = \int_{\Delta I} \mathcal{J}_A. \quad (2.158)$$

This yields the boundary condition for the magnetic field,

$$n \wedge (\mathcal{H}^{(2)} - \mathcal{H}^{(1)}) = n \wedge \mathcal{J}_A. \quad (2.159)$$

\mathcal{J}_A is the sum of the impressed surface current density and the surface current density induced by the field. A field-induced surface current density only may occur if we assume infinite conductivity of the medium or a finite surface impedance of the boundary surface. In case the media in both subspaces exhibit finite conductivity and if no surface current density is impressed, we obtain

$$n \wedge (\mathcal{H}^{(2)} - \mathcal{H}^{(1)}) = 0 \quad \text{for} \quad \mathcal{J}_A = 0. \quad (2.160)$$

For an *electric surface polarization* \mathcal{M}_{eA} in the boundary surface related to \mathcal{J}_A via

$$\mathcal{J}_A = \frac{\partial}{\partial t} \mathcal{M}_{eA} \quad (2.161)$$

we obtain from (2.159) the *tangential boundary condition for the magnetic field intensity*

$$n \wedge (\mathcal{H}^{(2)} - \mathcal{H}^{(1)}) = n \wedge \frac{\partial}{\partial t} \mathcal{M}_{eA}. \quad (2.162)$$

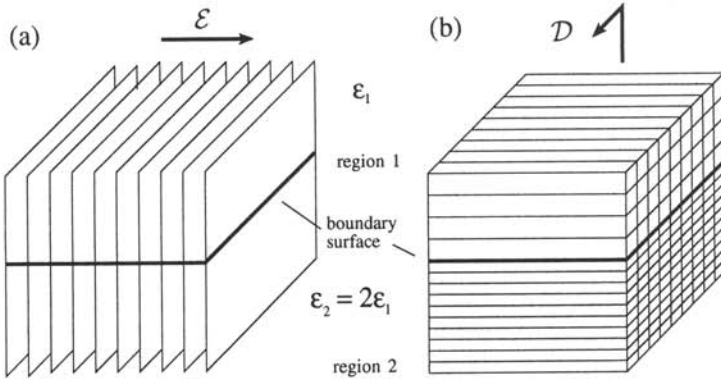


Figure 2.31: The tangential boundary conditions: (a) electric field, and (b) electric flux density.

In the same way we obtain the *tangential boundary condition for the electric field intensity*:

$$n \wedge (\mathcal{E}^{(2)} - \mathcal{E}^{(1)}) = -n \wedge \frac{\partial}{\partial t} \mathcal{M}_{mA}. \quad (2.163)$$

In this equation \mathcal{M}_{mA} is the *magnetic surface polarization* in the boundary surface. If there is no magnetic surface polarization in the boundary surface, we obtain

$$n \wedge (\mathcal{E}^{(2)} - \mathcal{E}^{(1)}) = 0. \quad (2.164)$$

In Figure 2.31 we consider an electric field parallel to the boundary for no magnetic surface polarization in the boundary. The electric potential surfaces are normal to the boundary plane and do not change their spacing when crossing the boundary. Assuming $\epsilon_2 = 2\epsilon_1$ yields twice the density of flux tubes in region 2 as in region 1.

For a field in an arbitrary direction with respect to the boundary, the spacing of the potential planes remains unchanged in directions parallel to the boundary surface whereas the spacing normal to the boundary surface becomes smaller in the region with the lower permittivity (see Figure 2.32(a)), indicating that the tangential component of the electric field remains unchanged, whereas the normal component of the electric field intensity is larger in the region with the lower permittivity. Figure 2.32(b) shows the change in tilt of the flux tubes when crossing the boundary surface. The area of the cuts of the flux tubes with surfaces parallel to the boundary remains unchanged. This indicates that the flux component normal to the boundary is maintained. The area of the cuts of the flux tubes with planes normal to the boundary surface is proportional to the permittivity.

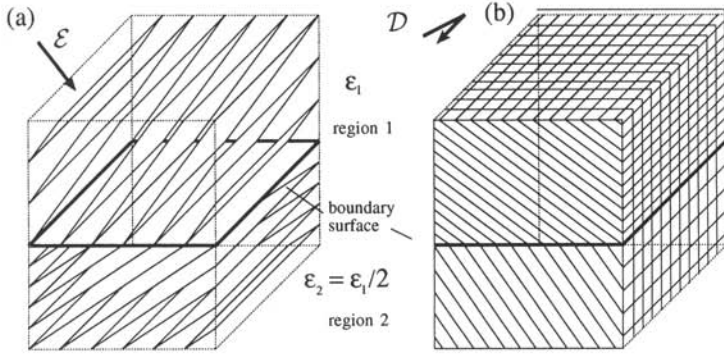


Figure 2.32: Boundary conditions for field in arbitrary direction: (a) electric field , and (b) electric flux density.

Introducing the *contraction* $\mathcal{A} \lrcorner \mathcal{B}$ of two differential forms \mathcal{A} and \mathcal{B} defined by

$$s_i \lrcorner s_j = \delta_{ij}, \quad (2.165a)$$

$$\mathcal{A} \lrcorner (\mathcal{B} \wedge \mathcal{C}) = (\mathcal{A} \lrcorner \mathcal{B}) \wedge \mathcal{C} + (-1)^{\deg(\mathcal{A})} \mathcal{B} \wedge (\mathcal{A} \lrcorner \mathcal{C}) \quad (2.165b)$$

we can bring the boundary conditions in an explicit form with respect to the sources impressed in the boundaries. The symbol \lrcorner is named “angle” and the contraction is also called the *angle product*. The angle product was introduced by Burke [7]. We use the modified form given by Warnick [16]. It may be shown easily that the following relations hold

$$\mathcal{Q}_A = n \lrcorner (n \wedge \mathcal{Q}_A), \quad (2.166a)$$

$$\mathcal{J}_A = n \lrcorner (n \wedge \mathcal{J}_A), \quad (2.166b)$$

$$\mathcal{M}_{eA} = n \lrcorner (n \wedge \mathcal{M}_{eA}), \quad (2.166c)$$

$$\mathcal{M}_{mA} = n \lrcorner (n \wedge \mathcal{M}_{mA}). \quad (2.166d)$$

The normal boundary conditions (2.140) and (2.148) now can be written as

$$n \lrcorner [n \wedge (\mathcal{B}^{(2)} - \mathcal{B}^{(1)})] = 0, \quad (2.167a)$$

$$n \lrcorner [n \wedge (\mathcal{D}^{(2)} - \mathcal{D}^{(1)})] = \mathcal{Q}_A, \quad (2.167b)$$

and the tangential boundary conditions (2.159), (2.162), and (2.163) are

$$n \lrcorner [n \wedge (\mathcal{H}^{(2)} - \mathcal{H}^{(1)})] = \mathcal{J}_A, \quad (2.168a)$$

$$n \lrcorner [n \wedge (\mathcal{H}^{(2)} - \mathcal{H}^{(1)})] = \frac{\partial}{\partial t} \mathcal{M}_{eA}, \quad (2.168b)$$

$$n \lrcorner [n \wedge (\mathcal{E}^{(2)} - \mathcal{E}^{(1)})] = -\frac{\partial}{\partial t} \mathcal{M}_{mA}. \quad (2.168c)$$

In the above notation we have brought tangential and normal boundary conditions to a unified form. We note that the expression $n \lrcorner (n \wedge \mathcal{U})$ filters the tangential component of \mathcal{U} if \mathcal{U} is a one-form, and same operation filters the normal component of \mathcal{U} if \mathcal{U} is a two-form. We obtain the tangential component \mathcal{E}_t of the one-form \mathcal{E} and the normal component \mathcal{D}_n of the two-form \mathcal{D} by

$$\mathcal{E}_t = n \lrcorner (n \wedge \mathcal{E}) = n \lrcorner [n \wedge (E_u s_1 + E_v s_2 + E_n n)] = E_u s_1 + E_v s_2, \quad (2.169a)$$

$$\begin{aligned} \mathcal{D}_n &= n \lrcorner (n \wedge \mathcal{D}) = n \lrcorner [n \wedge (D_u s_2 \wedge n + D_v n \wedge s_1 + D_n s_1 \wedge s_2)] \\ &= D_n s_1 \wedge s_2. \end{aligned} \quad (2.169b)$$

With (2.169b) the normal boundary conditions (2.167a) and (2.167b) are

$$\mathcal{B}_n^{(2)} - \mathcal{B}_n^{(1)} = 0, \quad (2.170a)$$

$$\mathcal{D}_n^{(2)} - \mathcal{D}_n^{(1)} = \mathcal{Q}_A, \quad (2.170b)$$

and with (2.169a) the tangential boundary conditions (2.159), (2.162), and (2.163) are

$$\mathcal{H}_t^{(2)} - \mathcal{H}_t^{(1)} = \mathcal{J}_A, \quad (2.171a)$$

$$\mathcal{H}_t^{(2)} - \mathcal{H}_t^{(1)} = \frac{\partial}{\partial t} \mathcal{M}_{eA}, \quad (2.171b)$$

$$\mathcal{E}_t^{(2)} - \mathcal{E}_t^{(1)} = -\frac{\partial}{\partial t} \mathcal{M}_{mA}. \quad (2.171c)$$

For complex phasors the normal boundary conditions corresponding to (2.167a) and (2.167b) are

$$n \lrcorner [n \wedge (\underline{\mathcal{B}}^{(2)} - \underline{\mathcal{B}}^{(1)})] = 0, \quad (2.172a)$$

$$n \lrcorner [n \wedge (\underline{\mathcal{D}}^{(2)} - \underline{\mathcal{D}}^{(1)})] = \underline{\mathcal{Q}}_A. \quad (2.172b)$$

The tangential boundary conditions corresponding to (2.168a), (2.168b), and (2.168c)

are

$$n \lrcorner \left[n \wedge \left(\underline{\mathcal{H}}^{(2)} - \underline{\mathcal{H}}^{(1)} \right) \right] = \underline{\mathcal{J}}_A, \quad (2.173a)$$

$$n \lrcorner \left[n \wedge \left(\underline{\mathcal{H}}^{(2)} - \underline{\mathcal{H}}^{(1)} \right) \right] = j \omega \underline{\mathcal{M}}_{eA}, \quad (2.173b)$$

$$n \lrcorner \left[n \wedge \left(\underline{\mathcal{E}}^{(2)} - \underline{\mathcal{E}}^{(1)} \right) \right] = -j \omega \underline{\mathcal{M}}_{mA}. \quad (2.173c)$$

Introducing the normal components $\underline{\mathcal{B}}_n$ and $\underline{\mathcal{D}}_n$ of the flux densities via (2.169b) and the tangential components $\underline{\mathcal{H}}_t$ and $\underline{\mathcal{E}}_t$ of the field intensities via (2.169a) yields for the normal boundary conditions

$$\underline{\mathcal{B}}_n^{(2)} - \underline{\mathcal{B}}_n^{(1)} = 0, \quad (2.174a)$$

$$\underline{\mathcal{D}}_n^{(2)} - \underline{\mathcal{D}}_n^{(1)} = \underline{\mathcal{Q}}_A \quad (2.174b)$$

and for the tangential boundary conditions

$$\underline{\mathcal{H}}_t^{(2)} - \underline{\mathcal{H}}_t^{(1)} = \underline{\mathcal{J}}_A, \quad (2.175a)$$

$$\underline{\mathcal{H}}_t^{(2)} - \underline{\mathcal{H}}_t^{(1)} = j \omega \underline{\mathcal{M}}_{eA}, \quad (2.175b)$$

$$\underline{\mathcal{E}}_t^{(2)} - \underline{\mathcal{E}}_t^{(1)} = -j \omega \underline{\mathcal{M}}_{mA}. \quad (2.175c)$$

2.15 PROBLEMS

1. Let $f(x) = x^n$ and $\mathcal{U} = df$. Compute the integral $\int_V \mathcal{U} \wedge \star \mathcal{U}$. The region of integration V is specified by the cube $x, y, z \in (0, 1)$.
2. Consider the integral $\oint_C \mathcal{U}$, where the path of integration C is a circle in the plane $z = 0$ with radius R .
 - a) Sketch the equipotential planes of \mathcal{U} and compute the integral for $\mathcal{U} = \frac{1}{\sqrt{x^2+y^2}}(y dx - x dy)$.
 - b) Sketch the equipotential planes of \mathcal{U} and compute the integral for $\mathcal{U} = \frac{1}{\sqrt{x^2+y^2}}(x dx + y dy)$.
3. Compute the integral

$$\int_C \frac{1}{\sqrt{x^2+y^2}}(ay dx - bx dy + cz dz).$$

where a and b are constant parameters. The path of integration C is a helix of radius ρ_0 and pitch h_0 with the parametric representation given by

$$x = r_0 \cos 2\pi u \quad y = r_0 \sin 2\pi u \quad z = h_0.$$

Perform the integration over the interval $u \in [0, 10]$. Hint: Apply the method of pullback discussed in Section A.4.5.

4. Let $f(x, y, z) = (x^2 + y^2 + z^2)^{-N/2}$. Compute df and $\star df$. Integrate $\star df$ over the surface of a sphere with center in the coordinate origin and radius R . Hint: Use spherical coordinates.
5. Two one-forms \mathcal{U} and \mathcal{V} are given by

$$\mathcal{U} = U_x(y) dx + U_y(x) dy, \quad \mathcal{V} = V_z(x) dz + V_x(z) dx.$$

Compute $d(\mathcal{U} \wedge \mathcal{V})$, $d(\mathcal{U} \wedge (\star \mathcal{V}))$, and $d((\star \mathcal{U}) \wedge \mathcal{V})$.

6. A plane triangular surface is defined by $x + y + z = 1$ m, $x, y, z \geq 0$. Compute the total current flowing through this surface for the current density with the components $J_x = J_y = J_z = 1 \text{ Am}^{-2}$.
7. A semi-sphere is defined by $x^2 + y^2 + z^2 = 1 \text{ m}^2$, $z \geq 0$. Sketch the current flux tubes and compute the total current flowing through this surface
 - a) for the current density given by $\mathcal{J} = 1 \text{ Am}^{-2} dx \wedge dy$,
 - b) for the current density given by $\mathcal{J} = 1 \text{ Am}^{-2} \sin \theta d\theta \wedge d\phi$.
 Give the components of the current density vector in both cases.
8. In conventional vector notation Maxwell's equations in integral form (2.57a) to (2.57d) are written as

$$\begin{aligned} \oint_{\partial A} \mathbf{H} \cdot d\mathbf{s} &= \frac{d}{dt} \int_A \mathbf{D} \cdot d\mathbf{A} + \int_A \mathbf{J} \cdot d\mathbf{A}, \\ \oint_{\partial A} \mathbf{E} \cdot d\mathbf{s} &= -\frac{d}{dt} \int_A \mathbf{B} \cdot d\mathbf{A}, \\ \oint_{\partial V} \mathbf{B} \cdot d\mathbf{A} &= 0, \\ \oint_{\partial V} \mathbf{D} \cdot d\mathbf{A} &= \int_V \rho dV. \end{aligned}$$

Use the relations (A.31) to (A.34) to show the equivalence of these notations.

9. In conventional vector notation Maxwell's equations in local form (2.114a) to (2.114d) are written as

$$\begin{aligned} \text{rot} \mathbf{H} &= \frac{\partial \mathbf{D}}{\partial t} + \mathbf{J}, & \text{rot} \mathbf{E} &= -\frac{\partial \mathbf{B}}{\partial t}, \\ \text{div} \mathbf{B} &= 0, & \text{div} \mathbf{D} &= \rho. \end{aligned}$$

Use the relations (A.31) to (A.34) and Table A.1 to show the equivalence of these notations.

10. In conventional vector notation the normal boundary conditions for the electric displacement are given by $(\mathbf{D}_2 - \mathbf{D}_1) \cdot \mathbf{n} = \rho_A$, where \mathbf{n} is a unit vector normal to the boundary surface. Derive these equations from (2.148).

11. In conventional vector notation the tangential boundary conditions for the magnetic field are $(\underline{H}_2 - \underline{H}_1) \cdot \underline{\tau}_1 = J_A \cdot \underline{\tau}_2$, where $\underline{\tau}$ is any unit vector tangential to the boundary surface. Derive these equations from (2.159).
12. Consider the following electric fields in free-space for $k = \omega\sqrt{\epsilon_0\mu_0}$:

$$\mathcal{E}(\underline{x}, t) = E_0 \cos(\omega t - kz) \, dx,$$

$$\mathcal{E}(\underline{x}, t) = \frac{1}{\sqrt{2}} E_0 \cos(\omega t - kz) (dx + dy),$$

$$\mathcal{E}(\underline{x}, t) = E_0 \cos(\omega t - kz) \, dz,$$

$$\mathcal{E}(\underline{x}, t) = E_0 \cos\left(\omega t - \frac{k}{\sqrt{2}}(z - y)\right) \, dx,$$

$$\mathcal{E}(\underline{x}, t) = \frac{1}{\sqrt{2}} E_0 \cos\left(\omega t - \frac{k}{\sqrt{2}}(z - y)\right) (dy + dz),$$

$$\mathcal{E}(\underline{x}, t) = \frac{1}{\sqrt{2}} E_0 \cos\left(\omega t - \frac{k}{\sqrt{2}}(z - y)\right) (dy - dz),$$

$$\mathcal{E}(\underline{x}, t) = \frac{1}{\sqrt{3}} E_0 \cos\left(\omega t - \frac{k}{\sqrt{2}}(z - y)\right) (dx + dy + dz).$$

Do these fields satisfy Maxwell's equations? If this is the case, compute the differential forms of the corresponding magnetic fields.

13. Consider a large plane surface, defined by $z = 0$. If we consider the close neighborhood of this plane we can assume in the following infinite extension in x - and y -directions.
- Assume an impressed uniform time-varying electric surface polarization $\mathcal{M}_{eA}(t) = M_{eAx}(t) \, dy$.
 - Compute the magnetic field on both sides of the surface. (Consider the symmetry of the problem.)
 - Compute the electromagnetic field excited by the electric surface polarization on both sides of the surface.
 - Assume an impressed uniform time-varying magnetic surface polarization $\mathcal{M}_{mA}(t) = -M_{mAy}(t) \, dx$.
 - Compute the electric field excited by the electric surface polarization on both sides of the surface.
 - Compute the electromagnetic field excited by the electric surface polarization on both sides of the surface.
 - Consider the superposition of impressed uniform time-varying crossed electric and magnetic surface polarizations $\mathcal{M}_{eA}(t) = M_{eAx}(t) \, dy$ and $\mathcal{M}_{mA}(t) = -M_{mAy}(t) \, dx$.
 - Compute the electromagnetic field excited by the crossed electric and

magnetic surface polarizations.

- ii. How must the electric and magnetic surface polarizations be chosen to excite an electromagnetic wave only in positive or only in negative z -direction?
14. Consider a transverse electromagnetic plane wave propagating in the z -direction. The electric field is given by

$$\mathcal{E}(z, t) = E_x \cos(\omega t - \beta z + \phi_x) \mathbf{d}x + E_y \cos(\omega t - \beta z + \phi_y) \mathbf{d}y.$$

- a) Give the expression for the trajectory of the electric vector in the xy -plane at $z = 0$.
- b) Determine the polarization for $E_x = E_y$ and $\phi_x = \phi_y$ and give the expression for the trajectory of the electric vector in the xy -plane at $z = 0$.
- c) Determine the polarization for $E_x = E_y$ and both cases $\phi_x = \phi_y \pm \frac{1}{2}\pi$ and give the expression for the trajectory of the electric vector in the xy -plane at $z = 0$.

REFERENCES

- [1] R. S. Elliott, *Electromagnetics – History, Theory, and Applications*. New York: IEEE Press, 1991.
- [2] J. D. Jackson, *Classical Electrodynamics*. New York: John Wiley & Sons, 1975.
- [3] H. A. Haus and J. R. Melcher, *Electromagnetic Fields and Energy*. Englewood Cliffs, NJ: Prentice Hall, 1989.
- [4] M. N. O. Sadiku, *Elements of Electromagnetics*. Orlando: Saunders, 1989.
- [5] Z. Popović and B. D. Popović, *Introductory Electromagnetics*. Englewood Cliffs, NJ: Prentice Hall, 2000.
- [6] H. Flanders, *Differential Forms*. New York: Academic Press, 1963.
- [7] W. L. Burke, *Applied Differential Geometry*. Cambridge: Cambridge University Press, 1985.
- [8] P. Bamberg and S. Sternberg, *A Course in Mathematics for Students in Physics 2*. Cambridge: Cambridge University Press, 1990.
- [9] S. H. Weintraub, *Differential Forms – A Complement to Vector Calculus*. New York: Academic Press, 1997.
- [10] K. F. Warnick, *A Differential Forms Approach to Electromagnetics in Anisotropic Media*. PhD thesis, Department of Electrical and Computer Engineering, Brigham Young University, 1997.
- [11] J. C. Maxwell, *A Treatise on Electricity and Magnetism*, vol. 2. New York: Oxford University Press, 1998.
- [12] H. Hertz, *Gesammelte Werke, Untersuchungen über die Ausbreitung der elektrischen Kraft*, vol. 2. Leipzig: Johann Ambrosius Barth, 1894.
- [13] R. P. Feynman, *Lectures on Physics 2, Electromagnetics and Matter*. London: Addison-Wesley, 1977.
- [14] L. O. Chua, C. A. Desoer, and E. S. Kuh, *Linear and Nonlinear Circuits*. New York: Mc Graw Hill, 1987.
- [15] R. F. Harrington, *Time Harmonic Electromagnetic Fields*. New York: McGraw-Hill, 1961.
- [16] K. F. Warnick, R. H. Selfridge, and D. V. Arnold, "Electromagnetic boundary conditions and differential forms," *IEE Proc., Microw. Antennas Propag.*, vol. 142, pp. 326–332, Aug. 1995.

Chapter 3

Potentials and Waves

3.1 THE ELECTROMAGNETIC POTENTIALS

Maxwell's equations (2.114a)–(2.114d) are a system of 12 coupled scalar partial differential equations. The introduction of *electromagnetic potentials* allows a systematic solution of the Maxwell's equations [1–4]. We are distinguishing between *scalar potentials* and *vector potentials*. After solution of the wave equation for a potential, all field quantities may be derived from this potential.

According to (2.114c), the magnetic flux density is free of divergence. Therefore, due to *Poincaré's lemma* (A.61), \mathcal{B} may be represented as the exterior derivative of a one-form \mathcal{A} ,

$$\mathcal{B} = d\mathcal{A}. \quad (3.1)$$

The corresponding vector field \mathbf{A} is called the *magnetic vector potential* and \mathcal{A} is called the *magnetic vector potential form*. Any two-form \mathcal{B} with a vanishing exterior derivative can be expressed as the exterior derivative of a one-form. Such a two-form describes a so-called *solenoidal field*. Such a field has neither source nor sink of flux. The flux tubes of a solenoidal field are continuous, neither originating nor ending anywhere. The flux tubes of \mathcal{B} entering any closed surface must also leave it. Inserting (3.1) into the second Maxwell's equation (2.114b) yields

$$d\left(\mathcal{E} + \frac{\partial}{\partial t}\mathcal{A}\right) = 0. \quad (3.2)$$

Since the exterior derivative of the one-form inside the brackets vanishes, we may express this one-form due to Poincaré's lemma (A.61) as the exterior derivative of the *scalar potential* Φ and obtain

$$\mathcal{E} = -d\Phi - \frac{\partial}{\partial t}\mathcal{A}. \quad (3.3)$$

The negative sign of Φ has been chosen due to the physical convention in definition of potentials. Whereas in electrostatics the electric field may be computed from a scalar potential Φ in the case of rapidly varying electromagnetic fields, we also need the vector potential \mathcal{A} .

A field that may be expressed as the exterior derivative of a scalar potential only, for example,

$$\mathcal{E} = -d\Phi \quad (3.4)$$

is called an *irrotational field*. From Poincaré's lemma (A.61) and Stokes' theorem (A.90) we obtain

$$\oint_{\partial A} \mathcal{E} = - \int_A d d\Phi = 0. \quad (3.5)$$

The circulation of an irrotational field \mathcal{E} around any closed path ∂A is identically zero. This implies that the line integral of an irrotational field \mathcal{E} is independent from the chosen path. Therefore an irrotational field is also called a *conservative field*. A vector field may be either irrotational or solenoidal or neither irrotational nor solenoidal.

The two potentials \mathcal{A} and Φ are not defined in an unambiguous way. Due to Poincaré's lemma, adding the exterior derivative of a zero-form Ψ to the vector potential \mathcal{A} does not influence the magnetic induction \mathcal{B} . The electric field \mathcal{E} also remains unchanged, if \mathcal{A} and Φ together are transformed in the following way:

$$\mathcal{A}_1 = \mathcal{A} + d\Psi, \quad (3.6a)$$

$$\Phi_1 = \Phi - \frac{\partial \Psi}{\partial t}. \quad (3.6b)$$

This transformation is called a *gauge transformation*. The one-form \mathcal{A} may be defined in an unambiguous way, if we are prescribing its exterior derivative.

Inserting (3.1) and (3.3) in consideration of (2.32a), (2.32b), and (2.62) into the first Maxwell's equation (2.114a), we obtain

$$\star d \star d\mathcal{A} + \mu \epsilon \frac{\partial^2}{\partial t^2} \mathcal{A} + \mu \sigma \frac{\partial}{\partial t} \mathcal{A} + \mu d \left(\epsilon \frac{\partial \Phi}{\partial t} + \sigma \Phi \right) = \star \mu \mathcal{J}_0. \quad (3.7)$$

Inserting (3.3) and (2.32a) into (2.114d) yields

$$\star d \star d\Phi + \star d \star \frac{\partial}{\partial t} \mathcal{A} = -\frac{1}{\epsilon} \star \mathcal{Q}. \quad (3.8)$$

Since we may choose the exterior derivative of $\star \mathcal{A}$ arbitrarily, we can make use of this option in order to decouple the differential equations for \mathcal{A} and Φ . We impose the so-called *Lorenz condition* first formulated by L. Lorenz [5, 6],

$$\star d \star \mathcal{A} + \mu \left(\epsilon \frac{\partial}{\partial t} \Phi + \sigma \Phi \right) = 0. \quad (3.9)$$

All potentials satisfying the Lorenz condition are said to be in the *Lorenz gauge*. In this way, we obtain from (3.7) and (3.8) the equations

$$(\mathbf{d} \star \mathbf{d} \star - \star \mathbf{d} \star \mathbf{d})\mathcal{A} - \mu\epsilon \frac{\partial^2}{\partial t^2} \mathcal{A} - \mu\sigma \frac{\partial}{\partial t} \mathcal{A} = - \star \mu \mathcal{J}_0, \quad (3.10a)$$

$$\star \mathbf{d} \star \mathbf{d}\Phi - \mu\epsilon \frac{\partial^2}{\partial t^2} \Phi - \mu\sigma \frac{\partial}{\partial t} \Phi = -\frac{1}{\epsilon} \star \mathcal{Q}. \quad (3.10b)$$

We define the *covariant derivative*, expressed by the operator $\tilde{\mathbf{d}}$, via

$$\tilde{\mathbf{d}}\mathcal{U} = (-1)^{\deg \mathcal{U}+1} \star \mathbf{d} \star \mathcal{U}. \quad (3.11)$$

Using the covariant derivative we introduce the *Laplace operator* Δ defined by

$$\Delta = \tilde{\mathbf{d}}\mathbf{d} + \mathbf{d}\tilde{\mathbf{d}}. \quad (3.12)$$

Applying the Laplace operator to a zero-form Φ and a one-form \mathcal{A} , respectively, yields

$$\Delta \Phi = \star \mathbf{d} \star \mathbf{d}\Phi, \quad (3.13)$$

$$\Delta \mathcal{A} = (\mathbf{d} \star \mathbf{d} \star - \star \mathbf{d} \star \mathbf{d}) \mathcal{A}. \quad (3.14)$$

With the Laplace operator Δ we can write (3.10a) and (3.10b) in the form

$$\Delta \mathcal{A} - \mu\epsilon \frac{\partial^2}{\partial t^2} \mathcal{A} - \mu\sigma \frac{\partial}{\partial t} \mathcal{A} = - \star \mu \mathcal{J}_0, \quad (3.15a)$$

$$\Delta \Phi - \mu\epsilon \frac{\partial^2}{\partial t^2} \Phi - \mu\sigma \frac{\partial}{\partial t} \Phi = -\frac{1}{\epsilon} \star \mathcal{Q}. \quad (3.15b)$$

The field intensities \mathbf{E} and \mathbf{H} derived from \mathcal{A} and Φ satisfy the four Maxwell's equations (2.114a)–(2.114d). Equations (3.15a) and (3.15b) are called *wave equations*, since their solutions describe propagating waves. Equation (3.15a) is a *one-form wave equation* or *vector wave equation*, whereas (3.15b) is a *scalar wave equation*.

Hertz has shown that it is possible to derive both potentials $\mathcal{A}(\mathbf{x}, t)$ and $\Phi(\mathbf{x}, t)$ from one vector, the so-called *electric Hertz vector* $\Pi_e(\mathbf{x}, t)$ [7, 8]. We introduce the *electric Hertz differential form*

$$\Pi_e = \Pi_{ex} dx + \Pi_{ey} dy + \Pi_{ez} dz. \quad (3.16)$$

The Lorenz condition (3.9) is fulfilled, if \mathcal{A} and Φ are derived from the electric Hertz differential form Π_e via

$$\mathcal{A} = \mu\epsilon \frac{\partial}{\partial t} \Pi_e + \mu\sigma \Pi_e, \quad (3.17a)$$

$$\Phi = -\tilde{\mathbf{d}} \Pi_e. \quad (3.17b)$$

Inserting (3.17a) into (3.15a), we obtain

$$\mu \left(\epsilon \frac{\partial}{\partial t} + \sigma \right) \left(\Delta \Pi_e - \mu \epsilon \frac{\partial^2}{\partial t^2} \Pi_e - \mu \sigma \frac{\partial}{\partial t} \Pi_e \right) = -\mu * \mathcal{J}_0. \quad (3.18)$$

For $\mathcal{J}_0 = 0$ (i.e., without impressed current sources) we obtain the *homogeneous wave equation*

$$\Delta \Pi_e - \mu \epsilon \frac{\partial^2}{\partial t^2} \Pi_e - \mu \sigma \frac{\partial}{\partial t} \Pi_e = 0. \quad (3.19)$$

The field intensity differential forms \mathcal{E} and \mathcal{H} follow from (2.32b), (3.1), (3.3), (3.17a), and (3.17b),

$$\mathcal{E} = d\tilde{d}\Pi_e - \mu \epsilon \frac{\partial^2}{\partial t^2} \Pi_e - \mu \sigma \frac{\partial}{\partial t} \Pi_e, \quad (3.20a)$$

$$\mathcal{H} = * d \left(\epsilon \frac{\partial}{\partial t} \Pi_e + \sigma \Pi_e \right). \quad (3.20b)$$

Subtracting from (3.20a) the wave equation (3.19), we obtain

$$\mathcal{E} = -\tilde{d}d\Pi_e \quad \text{for } \mathcal{J}_0 = 0. \quad (3.21)$$

Let us now consider the lossless case with impressed current sources. In this case it is advantageous to use the *impressed electric polarization* $\mathcal{M}_{e0}(\mathbf{x}, t)$ instead of the impressed current density $\mathcal{J}_0(\mathbf{x}, t)$. The corresponding differential form is

$$\mathcal{M}_{e0} = M_{ex} dy \wedge dz + M_{ey} dz \wedge dx + M_{ez} dx \wedge dy. \quad (3.22)$$

The *impressed electric polarization form* \mathcal{M}_{e0} is related to an impressed electric current \mathcal{J}_0 via

$$\frac{\partial}{\partial t} \mathcal{M}_{e0} = \mathcal{J}_0. \quad (3.23)$$

In this way it follows from (3.18)

$$\frac{\partial}{\partial t} \left(\Delta \Pi_e - \mu \epsilon \frac{\partial^2}{\partial t^2} \Pi_e \right) = -\frac{1}{\epsilon} * \frac{\partial}{\partial t} \mathcal{M}_{e0} \quad \text{for } \sigma = 0. \quad (3.24)$$

By integration over t we obtain

$$\Delta \Pi_e - \mu \epsilon \frac{\partial^2}{\partial t^2} \Pi_e = -\frac{1}{\epsilon} * \mathcal{M}_{e0} \quad \text{for } \sigma = 0. \quad (3.25)$$

Since the source of the Hertz vector field is an impressed electric polarization, the Hertz vector also is called the *electric polarization potential*. From the solution of (3.25) we obtain \mathcal{E} and \mathcal{H} via (3.20a) and (3.20b). From (3.20a) and (3.25) we obtain

$$\mathcal{E} = -\tilde{\mathbf{d}} \mathbf{d} \Pi_e - \frac{1}{\epsilon} \star \mathcal{M}_{e0}. \quad (3.26)$$

In the general case $\mathcal{J}_0 \neq 0$ and $\sigma \neq 0$, we will obtain an equation containing time derivatives up to third order. This difficulty can be avoided by using the frequency domain representation treated in the next section.

3.2 THE HELMHOLTZ EQUATION

For time-harmonic fields we can replace the operator $\partial/\partial t$ by multiplication with the factor $j\omega$. This transforms the wave equation into the *Helmholtz equation*. Using Maxwell's equations in phasor representation as introduced in Section 2.12 allows us to consider complex frequency-dependent permittivity and permeability. From (2.130a) and (2.130b) we obtain

$$\mathbf{d} \underline{\mathcal{H}} = j\omega (\underline{\epsilon} \star \underline{\mathcal{E}} + \underline{\mathcal{M}}_{e0}), \quad (3.27a)$$

$$\mathbf{d} \underline{\mathcal{E}} = -j\omega \underline{\mu} \star \underline{\mathcal{H}}, \quad (3.27b)$$

where $\underline{\mathcal{M}}_{e0}$ is the *impressed electric polarization phasor*. Also assuming a complex permeability in order to consider the magnetic losses according to (3.18) and (3.23) after transforming into the frequency domain and using (2.128) and generalizing for complex permittivity, we obtain

$$\Delta \underline{\Pi}_e + \omega^2 \underline{\mu} \underline{\epsilon} \underline{\Pi}_e = -\frac{1}{\underline{\epsilon}} \star \underline{\mathcal{M}}_{e0}, \quad (3.28)$$

where $\underline{\Pi}_e$ is the *electric Hertz differential form phasor*. This type of equation that we have obtained from the wave equation via $\partial/\partial t \rightarrow j\omega$ is called *Helmholtz equation*. In a similar way to (3.20a), (3.20b), and (3.26), we obtain the complex electric and magnetic field forms $\underline{\mathcal{E}}$ and $\underline{\mathcal{H}}$

$$\underline{\mathcal{E}} = \mathbf{d} \tilde{\mathbf{d}} \underline{\Pi}_e + \omega^2 \underline{\mu} \underline{\epsilon} \underline{\Pi}_e = -\tilde{\mathbf{d}} \mathbf{d} \underline{\Pi}_e - \frac{1}{\underline{\epsilon}} \star \underline{\mathcal{M}}_{e0}, \quad (3.29a)$$

$$\underline{\mathcal{H}} = j\omega \underline{\epsilon} \star \mathbf{d} \underline{\Pi}_e. \quad (3.29b)$$

If the electromagnetic field is generated by an impressed magnetic polarization $\underline{\mathcal{M}}_{m0}$, we obtain – instead of (3.27a), (3.27b) – the equations

$$d\underline{\mathcal{H}} = j\omega \underline{\epsilon} \star \underline{\mathcal{E}}, \quad (3.30a)$$

$$d\underline{\mathcal{E}} = -j\omega \left(\underline{\mu} \star \underline{\mathcal{H}} + \underline{\mathcal{M}}_{m0} \right). \quad (3.30b)$$

There exists a *duality* relationship [9, 10] between (3.27a) and (3.27b) on one hand, and (3.30a) and (3.30b) on the other hand. We may transform one pair of equations into a dual one by performing the substitution

$$\underline{\mathcal{E}}_2 = -Z_F \underline{\mathcal{H}}_1, \quad (3.31a)$$

$$\underline{\mathcal{H}}_2 = \frac{1}{Z_F} \underline{\mathcal{E}}_1, \quad (3.31b)$$

$$\underline{\mathcal{M}}_{m02} = Z_F \underline{\mathcal{M}}_{e01}. \quad (3.31c)$$

The field quantities of the pair of (3.27a), (3.28) are marked by the index 1, whereas the index 2 is assigned to field quantities of the pair of (3.30a), (3.30b). The *wave impedance* Z_F is given by

$$Z_F = \sqrt{\frac{\underline{\mu}}{\underline{\epsilon}}}. \quad (3.32)$$

We can make use of the duality principle to derive from one set of field solutions a dual set of field solutions with interchanged \underline{E} and \underline{H} . We also may introduce a vector potential dual to the Hertz vector. This vector potential is generated by an impressed magnetic polarization. We call this vector potential the *magnetic Hertz vector* or magnetic polarization potential. This dual magnetic Hertz vector $\underline{\Pi}_m$ is related to the electric Hertz vector $\underline{\Pi}_e$ by

$$\underline{\Pi}_m = \frac{1}{Z_F} \underline{\Pi}_e. \quad (3.33)$$

The corresponding differential forms are related via

$$\underline{\Pi}_m = \frac{1}{Z_F} \underline{\Pi}_e. \quad (3.34)$$

From (3.28) and (3.31a) - (3.31c), we obtain the inhomogeneous Helmholtz equation for the *magnetic Hertz form* $\underline{\Pi}_m$:

$$\Delta \underline{\Pi}_m + \omega^2 \underline{\mu} \underline{\Pi}_m = -\frac{1}{\underline{\mu}} \star \underline{\mathcal{M}}_{m0}. \quad (3.35)$$

After inserting (3.31a)–(3.32) and (3.34) into (3.29a) and (3.29b), we obtain

$$\underline{\mathcal{E}} = -j\omega\mu \star d\underline{\Pi}_m, \quad (3.36a)$$

$$\underline{\mathcal{H}} = d\tilde{d}\underline{\Pi}_m + \omega^2\mu\epsilon\underline{\Pi}_m = -\tilde{d}d\underline{\Pi}_m - \frac{1}{\mu} \star \underline{\mathcal{M}}_{m0}. \quad (3.36b)$$

For the source-free region with $\underline{\mathcal{M}}_{e0} = 0$ and $\underline{\mathcal{M}}_{m0} = 0$ the *homogeneous Helmholtz equation* (3.28) for the Hertz form $\underline{\Pi} = \underline{\Pi}_e, \underline{\Pi}_m$ is given by

$$\Delta\underline{\Pi} + \omega^2\mu\epsilon\underline{\Pi} = 0. \quad (3.37)$$

Using (3.12) and (3.14) yields

$$(d\tilde{d} + \tilde{d}d)\underline{\Pi} + \omega^2\mu\epsilon\underline{\Pi} = (d\star d\star - \star d\star d)\underline{\Pi} + \omega^2\mu\epsilon\underline{\Pi} = 0. \quad (3.38)$$

3.3 TIME-HARMONIC PLANE WAVES

Plane waves are the simplest wave solutions of Maxwell's equations. However their properties are significant for understanding even complex wave phenomena since electromagnetic waves of general structure may be constructed by superposition of plane waves. Consider a time-harmonic plane wave in a source-free unbounded homogeneous isotropic medium.

In Cartesian coordinates the Laplace operator for one-forms is given by

$$\Delta\underline{\Pi} = \frac{\partial^2\underline{\Pi}}{\partial x^2} + \frac{\partial^2\underline{\Pi}}{\partial y^2} + \frac{\partial^2\underline{\Pi}}{\partial z^2}, \quad (3.39)$$

where $\underline{\Pi}$ stands for $\underline{\Pi}_e$ or $\underline{\Pi}_m$. The Helmholtz equation can be put into the form

$$\frac{\partial^2\underline{\Pi}}{\partial x^2} + \frac{\partial^2\underline{\Pi}}{\partial y^2} + \frac{\partial^2\underline{\Pi}}{\partial z^2} + \omega^2\mu\epsilon\underline{\Pi} = 0. \quad (3.40)$$

The complete solution of this equation is given by

$$\underline{\Pi}(\mathbf{x}) = (\underline{\Pi}_{0x} dx + \underline{\Pi}_{0y} dy + \underline{\Pi}_{0z} dz) e^{\pm j\mathbf{k} \cdot \mathbf{x}} \quad (3.41)$$

with

$$\mathbf{k} \cdot \mathbf{k} = k^2 = k_x^2 + k_y^2 + k_z^2 = \omega^2\mu\epsilon. \quad (3.42)$$

The complete solution (3.41) of the Helmholtz equation is represented by plane waves. The wave vector $\mathbf{k} = [k_x, k_y, k_z]^T$ with dimension m^{-1} is complex for complex ϵ and

complex μ . In a lossy medium a complex wave vector \mathbf{k} describes an attenuated plane wave. The real time-dependent Hertz form is given by

$$\Pi(\mathbf{x}, t) = \Re \left\{ \underline{\Pi}(\mathbf{x}) e^{j\omega t} \right\}. \quad (3.43)$$

The quantity

$$k = \sqrt{k_x^2 + k_y^2 + k_z^2} \quad (3.44)$$

is called the *wave number*. The wave vector \mathbf{k} is the product of the wave number and the unit vector in direction of propagation. Let us now consider a plane wave propagating in the z -direction.

$$\mathbf{k} = k \mathbf{e}_z. \quad (3.45)$$

Due to (3.44), the sign of k is not determined. Since, due to (3.41), to each sign of k a corresponding solution of the wave equation exists, we may specify

$$\Re\{k\} > 0 \quad (3.46)$$

without a loss of generality. According to (3.43) and (3.45) the Hertz form

$$\Pi^{(+)}(z, t) = \Re \left\{ \underline{\Pi}_0^{(+)} e^{j(\omega t - kz)} \right\} \quad (3.47)$$

describes a *uniform plane wave* propagating in the positive z -direction. A uniform plane wave is a plane wave that is uniform transverse to the direction of propagation. The Hertz form

$$\Pi^{(-)}(z, t) = \Re \left\{ \underline{\Pi}_0^{(-)} e^{j(\omega t + kz)} \right\} \quad (3.48)$$

describes a uniform plane wave propagating in the negative z -direction. The imaginary parts of $\underline{\epsilon}$ and $\underline{\mu}$ are negative for passive media, $\epsilon'' \geq 0$ and $\mu'' \geq 0$. Hence, for a uniform plane wave under the condition given by (3.46) it follows that $\Im\{k\} \leq 0$. This means that the Hertz vector and therefore also the field quantities are decaying exponentially in the direction of propagation. Figure 3.1(a) shows the amplitude of the Hertz vector of an attenuated wave propagating in positive z -direction, and Figure 3.1(b) shows the wave amplitude of the wave propagating in negative z -direction. Instead of the *wave number* k the complex *propagation coefficient* γ is also used. The propagation coefficient γ is defined by

$$\gamma = j k. \quad (3.49)$$

The convention

$$\Im\{\gamma\} > 0 \quad (3.50)$$

corresponds to the convention specified in (3.46). The real part α and the imaginary part β of the propagation coefficient γ are given by

$$\gamma = \alpha + j\beta. \quad (3.51)$$

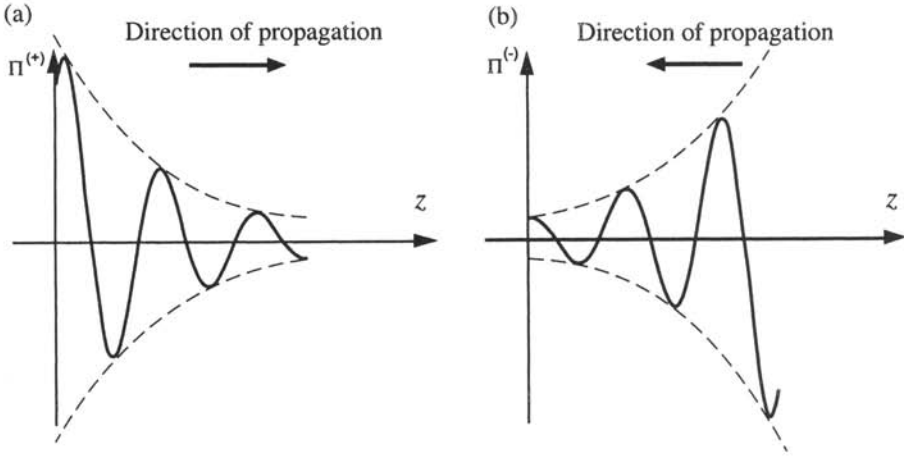


Figure 3.1: Magnitude of the Hertz vector for an attenuated uniform plane wave in (a) positive, and (b) negative z -direction.

The real part α is called the *attenuation coefficient*, and the imaginary part β is called the *phase coefficient*. The dimension of γ is m^{-1} . The attenuation coefficient α can also be specified in decibels (dB) or Nepers. For a wave propagating over a length l we obtain

$$\text{Attenuation in Nepers:} \quad \alpha l, \quad (3.52)$$

$$\text{Attenuation in decibels:} \quad 20 \log e^{\alpha l} \cong 8.69 \alpha l. \quad (3.53)$$

3.3.1 Time-Harmonic Plane Waves in Lossless Medium

Consider a time-harmonic uniform plane wave in a source-free lossless homogeneous isotropic medium. The wave number k is real in this case. We seek plane wave solutions with the wave vector $\mathbf{k} = [k_x, k_y, k_z]^T$ where the components k_x , k_y , and k_z are assumed as real. The Helmholtz equation (3.40) becomes

$$\frac{\partial^2 \underline{\Pi}}{\partial x^2} + \frac{\partial^2 \underline{\Pi}}{\partial y^2} + \frac{\partial^2 \underline{\Pi}}{\partial z^2} + k^2 \underline{\Pi} = 0, \quad (3.54)$$

where k , defined in (3.42)

$$\mathbf{k} \cdot \mathbf{k} = k^2 = k_x^2 + k_y^2 + k_z^2 = \omega^2 \mu \epsilon \quad (3.55)$$

is real and positive. The electric Hertz form corresponding to (3.41) is

$$\underline{\Pi}_e(\mathbf{x}) = \underline{\Pi}_{e0} e^{-j \mathbf{k} \cdot \mathbf{x}} \quad (3.56)$$

with the constant one-form

$$\underline{\Pi}_{e0} = \underline{\Pi}_{e0x} dx + \underline{\Pi}_{e0y} dy + \underline{\Pi}_{e0z} dz. \quad (3.57)$$

The exterior derivative of the uniform plane wave Hertz form (3.56) is

$$d\underline{\Pi}_e(\mathbf{x}) = -jk s_k \wedge \underline{\Pi}_{e0} e^{-j\mathbf{k} \cdot \mathbf{x}}, \quad (3.58)$$

where the magnitude k of wave vector \mathbf{k} is given by (3.44) and s_k is the unit one-form in the direction of propagation. With the twist operator introduced in (2.155) we obtain

$$\star d\underline{\Pi}_e(\mathbf{x}) = -jk \star s_k \wedge \underline{\Pi}_{e0} e^{-j\mathbf{k} \cdot \mathbf{x}} = -jk \perp_k \underline{\Pi}_{e0} e^{-j\mathbf{k} \cdot \mathbf{x}}. \quad (3.59)$$

This represents the projection of the Hertz form $\underline{\Pi}_e(\mathbf{x})$ on a plane orthogonal to the wave vector \mathbf{k} and subsequent rotation around \mathbf{k} by 90° in positive direction. From (3.29a) and (3.29b) we obtain for source-free medium

$$\underline{\mathcal{H}} = j\omega\epsilon \star d\underline{\Pi}_e = \omega k \epsilon \star s_k \wedge \underline{\Pi}_{e0} e^{-j\mathbf{k} \cdot \mathbf{x}} = \omega k \epsilon \perp_k \underline{\Pi}_{e0} e^{-j\mathbf{k} \cdot \mathbf{x}}, \quad (3.60a)$$

$$\underline{\mathcal{E}} = \star d \star d\underline{\Pi}_e = -k^2 \star s_k \wedge (\star s_k \wedge \underline{\Pi}_{e0}) e^{-j\mathbf{k} \cdot \mathbf{x}} = -k^2 \perp_k (\perp_k \underline{\Pi}_{e0}) e^{-j\mathbf{k} \cdot \mathbf{x}}. \quad (3.60b)$$

The magnetic field is normal to the direction of propagation and also normal to the direction of the electric Hertz vector. The electric field is normal to the direction of propagation as well as to the direction of the magnetic field. Figure 3.2 shows the wave vector \mathbf{k} and the *phase plane* that is normal to the wave vector. The electric and magnetic field vectors are parallel to the phase plane.

In explicit notation of the field components the uniform plane wave field is given by

$$\begin{aligned} \underline{\mathcal{E}} = & [(k_y^2 + k_z^2)\underline{\Pi}_{e0x} - k_x k_y \underline{\Pi}_{e0y} - k_x k_z \underline{\Pi}_{e0z}] e^{-j\mathbf{k} \cdot \mathbf{x}} dx \\ & + [(k_z^2 + k_x^2)\underline{\Pi}_{e0y} - k_y k_z \underline{\Pi}_{e0z} - k_y k_x \underline{\Pi}_{e0x}] e^{-j\mathbf{k} \cdot \mathbf{x}} dy \\ & + [(k_x^2 + k_y^2)\underline{\Pi}_{e0z} - k_z k_x \underline{\Pi}_{e0x} - k_z k_y \underline{\Pi}_{e0y}] e^{-j\mathbf{k} \cdot \mathbf{x}} dz, \end{aligned} \quad (3.61a)$$

$$\begin{aligned} \underline{\mathcal{H}} = & \omega\epsilon (k_y \underline{\Pi}_{e0z} - k_z \underline{\Pi}_{e0y}) e^{-j\mathbf{k} \cdot \mathbf{x}} dx \\ & + \omega\epsilon (k_z \underline{\Pi}_{e0x} - k_x \underline{\Pi}_{e0z}) e^{-j\mathbf{k} \cdot \mathbf{x}} dy \\ & + \omega\epsilon (k_x \underline{\Pi}_{e0y} - k_y \underline{\Pi}_{e0x}) e^{-j\mathbf{k} \cdot \mathbf{x}} dz. \end{aligned} \quad (3.61b)$$

For a magnetic Hertz form corresponding to (3.41),

$$\underline{\Pi}_m(\mathbf{x}) = \underline{\Pi}_{m0} e^{-j\mathbf{k} \cdot \mathbf{x}} \quad (3.62)$$

with

$$\underline{\Pi}_{m0} = \underline{\Pi}_{m0x} dx + \underline{\Pi}_{m0y} dy + \underline{\Pi}_{m0z} dz, \quad (3.63)$$

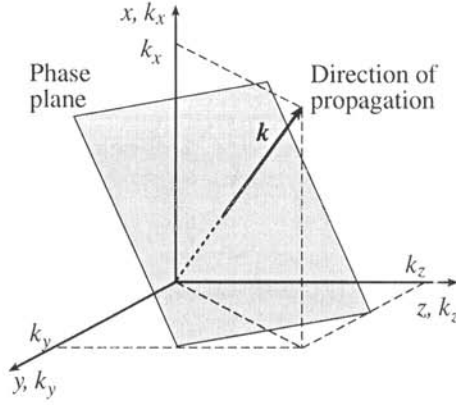


Figure 3.2: Time-harmonic uniform plane wave.

we obtain from (3.36a) and (3.36b) for source-free medium

$$\underline{\mathcal{E}} = -j\omega\mu \star d\underline{\Pi}_m = -\omega k\mu \star s_k \wedge \underline{\Pi}_{m0} e^{-j\mathbf{k} \cdot \mathbf{x}} = -\omega k\mu \perp_k \underline{\Pi}_{m0} e^{-j\mathbf{k} \cdot \mathbf{x}}, \quad (3.64a)$$

$$\underline{\mathcal{H}} = \star d \star d\underline{\Pi}_m = -k^2 \star s_k \wedge (\star s_k \wedge \underline{\Pi}_{m0}) e^{-j\mathbf{k} \cdot \mathbf{x}} = -k^2 \perp_k (\perp_k \underline{\Pi}_{m0}) e^{-j\mathbf{k} \cdot \mathbf{x}} \quad (3.64b)$$

which yields the electromagnetic field

$$\begin{aligned} \underline{\mathcal{E}} = & -\omega\mu (k_y \underline{\Pi}_{m0z} - k_z \underline{\Pi}_{m0y}) e^{-j\mathbf{k} \cdot \mathbf{x}} dx \\ & -\omega\mu (k_z \underline{\Pi}_{m0x} - k_x \underline{\Pi}_{m0z}) e^{-j\mathbf{k} \cdot \mathbf{x}} dy \\ & -\omega\mu (k_x \underline{\Pi}_{m0y} - k_y \underline{\Pi}_{m0x}) e^{-j\mathbf{k} \cdot \mathbf{x}} dz, \end{aligned} \quad (3.65a)$$

$$\begin{aligned} \underline{\mathcal{H}} = & [(k_y^2 + k_z^2) \underline{\Pi}_{m0x} - k_x k_y \underline{\Pi}_{m0y} - k_x k_z \underline{\Pi}_{m0z}] e^{-j\mathbf{k} \cdot \mathbf{x}} dx \\ & + [(k_z^2 + k_x^2) \underline{\Pi}_{m0y} - k_y k_z \underline{\Pi}_{m0z} - k_y k_x \underline{\Pi}_{m0x}] e^{-j\mathbf{k} \cdot \mathbf{x}} dy \\ & + [(k_x^2 + k_y^2) \underline{\Pi}_{m0z} - k_z k_x \underline{\Pi}_{m0x} - k_z k_y \underline{\Pi}_{m0y}] e^{-j\mathbf{k} \cdot \mathbf{x}} dz. \end{aligned} \quad (3.65b)$$

From (3.60a) and (3.60b) as well as from (3.64a) and (3.64b) together with (A.177) and (A.178) we obtain

$$\underline{\mathcal{E}} = -Z_F \star s_k \wedge \underline{\mathcal{H}} = -Z_F \perp_k \underline{\mathcal{H}}, \quad (3.66a)$$

$$\underline{\mathcal{H}} = Z_F^{-1} \star s_k \wedge \underline{\mathcal{E}} = Z_F^{-1} \perp_k \underline{\mathcal{E}} \quad (3.66b)$$

with the *wave impedance* Z_F given by

$$Z_F = \sqrt{\frac{\mu}{\epsilon}}. \quad (3.67)$$

The electric field vector, the magnetic field vector and the wave vector form a positive oriented orthogonal trihedron. Electric and magnetic fields of the uniform plane wave are transverse to the direction of propagation. Such a wave is called a *transverse electromagnetic wave* or TEM wave.

Consider a TEM wave with \mathbf{k} -vector in the xz -plane given by $\mathbf{k} = [k_x, 0, k_z]^T$. Computing this field from the electric Hertz form we obtain from (3.61a) and (3.61b)

$$\begin{aligned}\underline{\mathcal{E}} &= (k_z^2 \underline{\Pi}_{e0x} - k_x k_z \underline{\Pi}_{e0z}) e^{-j\mathbf{k}\cdot\mathbf{x}} dx \\ &\quad + k^2 \underline{\Pi}_{e0y} e^{-j\mathbf{k}\cdot\mathbf{x}} dy \\ &\quad + (k_x^2 \underline{\Pi}_{e0z} - k_z k_x \underline{\Pi}_{e0x}) e^{-j\mathbf{k}\cdot\mathbf{x}} dz, \end{aligned} \quad (3.68a)$$

$$\begin{aligned}\underline{\mathcal{H}} &= -k_z \omega \epsilon \underline{\Pi}_{e0y} e^{-j\mathbf{k}\cdot\mathbf{x}} dx \\ &\quad + \omega \epsilon (k_z \underline{\Pi}_{e0x} - k_x \underline{\Pi}_{e0z}) e^{-j\mathbf{k}\cdot\mathbf{x}} dy \\ &\quad + \omega \epsilon k_x \underline{\Pi}_{e0y} e^{-j\mathbf{k}\cdot\mathbf{x}} dz. \end{aligned} \quad (3.68b)$$

We can decompose this field into two uncoupled waves, one linearly polarized normal to the xz -plane, represented by

$$\underline{\mathcal{E}}_{\perp} = k^2 \underline{\Pi}_{e0y} e^{-j\mathbf{k}\cdot\mathbf{x}} dy, \quad (3.69a)$$

$$\underline{\mathcal{H}}_{\perp} = \omega \epsilon k_x \underline{\Pi}_{e0y} e^{-j\mathbf{k}\cdot\mathbf{x}} dz - \omega \epsilon k_z \underline{\Pi}_{e0y} e^{-j\mathbf{k}\cdot\mathbf{x}} dx \quad (3.69b)$$

and the other polarized parallel to the xz -plane:

$$\begin{aligned}\underline{\mathcal{E}}_{\parallel} &= (k_x^2 \underline{\Pi}_{e0z} - k_z k_x \underline{\Pi}_{e0x}) e^{-j\mathbf{k}\cdot\mathbf{x}} dz \\ &\quad + (k_z^2 \underline{\Pi}_{e0x} - k_z k_x \underline{\Pi}_{e0z}) e^{-j\mathbf{k}\cdot\mathbf{x}} dx, \end{aligned} \quad (3.70a)$$

$$\underline{\mathcal{H}}_{\parallel} = \omega \epsilon (k_z \underline{\Pi}_{e0x} - k_x \underline{\Pi}_{e0z}) e^{-j\mathbf{k}\cdot\mathbf{x}} dy. \quad (3.70b)$$

3.3.2 Complex Waves

Even for lossless media or free-space plane wave solutions of the Helmholtz equation with complex propagation vector exist. A wave with a complex propagation vector is called a *complex wave* [11,12]. Let the electric Hertz form of a complex plane wave be given by

$$\underline{\Pi}_e(\mathbf{x}) = \underline{\Pi}_{e0} e^{-(\alpha + j\beta)\cdot\mathbf{x}}. \quad (3.71)$$

This Hertz form satisfies the homogeneous Helmholtz equation (3.54) for

$$(\alpha + j\beta) \cdot (\alpha + j\beta) = -k^2 = -\omega^2 \mu \epsilon. \quad (3.72)$$

From this we obtain directly

$$\beta \cdot \beta - \alpha \cdot \alpha = k^2, \quad (3.73a)$$

$$\beta \cdot \alpha = 0. \quad (3.73b)$$

Without loss of generality we can assume propagation of the wave in z -direction and exponential decay of the wave in positive x -direction. This yields $\alpha = (\alpha, 0, 0)^T$ and $\beta = (0, 0, \beta)^T$, hence

$$\beta^2 - \alpha^2 = k^2. \quad (3.74)$$

We obtain the solution for this case from (3.68a) and (3.68b) by substituting β for k_z and $-j\alpha$ for k_x

$$\begin{aligned} \underline{\mathcal{E}} = & j\beta (\alpha \underline{\Pi}_{e0z} - j\beta \underline{\Pi}_{e0x}) e^{-(\alpha x + j\beta z)} dx \\ & + k^2 \underline{\Pi}_{e0y} e^{-(\alpha x + j\beta z)} dy \\ & - \alpha (\alpha \underline{\Pi}_{e0z} - j\beta \underline{\Pi}_{e0x}) e^{-(\alpha x + j\beta z)} dz, \end{aligned} \quad (3.75a)$$

$$\begin{aligned} \underline{\mathcal{H}} = & -\beta \omega \epsilon \underline{\Pi}_{e0y} e^{-(\alpha x + j\beta z)} dx \\ & + \omega \epsilon j (\alpha \underline{\Pi}_{e0z} - j\beta \underline{\Pi}_{e0x}) e^{-(\alpha x + j\beta z)} dy \\ & - j \omega \epsilon \alpha \underline{\Pi}_{e0y} e^{-(\alpha x + j\beta z)} dz. \end{aligned} \quad (3.75b)$$

The wave propagates in z -direction and exhibits longitudinal electric and magnetic field components in the direction of propagation. This solution can be decomposed in two independent parts. The first partial solution, given by

$$\underline{\mathcal{E}}_{TE} = k^2 \underline{\Pi}_{e0y} e^{-(\alpha x + j\beta z)} dy, \quad (3.76a)$$

$$\underline{\mathcal{H}}_{TE} = -\beta \omega \epsilon \underline{\Pi}_{e0y} e^{-(\alpha x + j\beta z)} dx - j \omega \epsilon \alpha \underline{\Pi}_{e0y} e^{-(\alpha x + j\beta z)} dz, \quad (3.76b)$$

is polarized normal to the zx -plane, and exhibits no longitudinal electric field components in direction of propagation. This wave therefore is called a *transverse electric wave* or TE wave. The second partial wave is polarized parallel to the zx -plane:

$$\begin{aligned} \underline{\mathcal{E}}_{TM} = & j\beta (\alpha \underline{\Pi}_{e0z} - j\beta \underline{\Pi}_{e0x}) e^{-(\alpha x + j\beta z)} dx \\ & - \alpha (\alpha \underline{\Pi}_{e0z} - j\beta \underline{\Pi}_{e0x}) e^{-(\alpha x + j\beta z)} dz, \end{aligned} \quad (3.77a)$$

$$\underline{\mathcal{H}}_{TM} = j \omega \epsilon (\alpha \underline{\Pi}_{e0z} - j\beta \underline{\Pi}_{e0x}) e^{-(\alpha x + j\beta z)} dy. \quad (3.77b)$$

This wave has no longitudinal magnetic field component and therefore is called a *transverse magnetic wave* or TM wave.

The transverse electric and magnetic field components of the TE and TM waves are related by

$$Z_{TE} = \frac{\omega\mu}{\beta} = Z_F \frac{k}{\beta} < Z_F, \quad (3.78a)$$

$$Z_{TM} = \frac{\beta}{\omega\epsilon} = Z_F \frac{\beta}{k} > Z_F. \quad (3.78b)$$

3.4 TM AND TE FIELDS AND WAVES

Consider an electromagnetic field for which the z -component of the magnetic field vanishes (i.e., $H_z = 0$). Such a field is called a *transverse magnetic* or TM field with respect to the z -axis. From (2.123c) it follows

$$\underline{d}\underline{B} = \underline{\mu} \, \underline{d} \star \underline{H} = 0. \quad (3.79)$$

From this we obtain

$$\frac{\partial \underline{H}_x}{\partial x} + \frac{\partial \underline{H}_y}{\partial y} + \frac{\partial \underline{H}_z}{\partial z} = 0 \quad (3.80)$$

and

$$\frac{\partial \underline{H}_x}{\partial x} = -\frac{\partial \underline{H}_y}{\partial y} \quad \text{for} \quad \underline{H}_z = 0. \quad (3.81)$$

This is the condition that the system of differential equations

$$\begin{aligned} \frac{\partial f}{\partial y} &= \underline{H}_x, \\ \frac{\partial f}{\partial x} &= -\underline{H}_y \end{aligned} \quad (3.82)$$

can be integrated. Due to (3.81) a function $f(\mathbf{x})$ must exist, from which \underline{H}_x and \underline{H}_y can be derived using (3.82). Making the ansatz

$$\underline{\Pi}_e(\mathbf{x}) = \frac{f(\mathbf{x})}{j\omega\epsilon} \, dz \quad (3.83)$$

for the Hertz form due to (3.29b) the condition (3.81) is fulfilled. In general in the source-free region an electromagnetic field with $H_z = 0$ can be described by a Hertz vector containing only a z -component $\underline{\Pi}_{ez}$ as

$$\underline{\Pi}_e(\mathbf{x}) = \underline{\Pi}_{ez}(\mathbf{x}) \, dz. \quad (3.84)$$

The electric and magnetic fields are computed using (3.29a) and (3.29b). For source-free regions with $\underline{\mathcal{M}}_{e0} = 0$ we obtain

$$\underline{\mathcal{H}} = j\omega\underline{\epsilon} \star d\underline{\Pi}_e, \quad (3.85)$$

$$\underline{\mathcal{E}} = -\tilde{d} d\underline{\Pi}_e = \star d \star d\underline{\Pi}_e. \quad (3.86)$$

Decomposing the electric field $\underline{\mathcal{E}}$ into a transverse part $\underline{\mathcal{E}}_t$ and a longitudinal part $\underline{\mathcal{E}}_l$,

$$\underline{\mathcal{E}} = \underline{\mathcal{E}}_t + \underline{\mathcal{E}}_l \quad (3.87)$$

we obtain

$$\underline{\mathcal{H}} = j\omega\underline{\epsilon} \left(\frac{\partial \underline{\Pi}_{ez}}{\partial y} dx - \frac{\partial \underline{\Pi}_{ez}}{\partial x} dy \right), \quad (3.88a)$$

$$\underline{\mathcal{E}}_t = \frac{\partial^2 \underline{\Pi}_{ez}}{\partial x \partial z} dx + \frac{\partial^2 \underline{\Pi}_{ez}}{\partial y \partial z} dy, \quad (3.88b)$$

$$\underline{\mathcal{E}}_l = - \left(\frac{\partial^2 \underline{\Pi}_{ez}}{\partial x^2} + \frac{\partial^2 \underline{\Pi}_{ez}}{\partial y^2} \right) dz. \quad (3.88c)$$

A wave for which the magnetic field in direction of propagation vanishes is called a *transverse magnetic wave* or TM wave. Using (3.84) we can derive a TM wave propagating in z -direction from

$$\underline{\Pi}_e(\mathbf{x}) = \underline{\Pi}_{e0z}(x, y)e^{-\gamma z} dz \quad (3.89)$$

with the complex propagation coefficient $\gamma = \alpha + j\beta$. Inserting this into the Helmholtz equation (3.37) and using (3.39) yields

$$\frac{\partial^2 \underline{\Pi}_{e0z}}{\partial x^2} + \frac{\partial^2 \underline{\Pi}_{e0z}}{\partial y^2} - (\gamma_{M0}^2 - \gamma^2) \underline{\Pi}_{e0z} = 0, \quad (3.90)$$

where γ_{M0} , the propagation coefficient of the TEM wave in the homogeneous isotropic medium with material parameters $\underline{\epsilon}, \underline{\mu}$, is defined via

$$\gamma_{M0}^2 = -\omega^2 \underline{\mu} \underline{\epsilon}. \quad (3.91)$$

Inserting (3.89) into (3.88a) to (3.88c) yields the field of the TM wave

$$\underline{\mathcal{H}} = j\omega\underline{\epsilon} \left(\frac{\partial \underline{\Pi}_{e0z}}{\partial y} dx - \frac{\partial \underline{\Pi}_{e0z}}{\partial x} dy \right) e^{-\gamma z}, \quad (3.92a)$$

$$\underline{\mathcal{E}}_t = -j\omega\underline{\epsilon} Z_{TM} \left(\frac{\partial \underline{\Pi}_{e0z}}{\partial x} dx + \frac{\partial \underline{\Pi}_{e0z}}{\partial y} dy \right) e^{-\gamma z}, \quad (3.92b)$$

$$\underline{\mathcal{E}}_l = - \left(\frac{\partial^2 \underline{\Pi}_{e0z}}{\partial x^2} + \frac{\partial^2 \underline{\Pi}_{e0z}}{\partial y^2} \right) e^{-\gamma z} dz. \quad (3.92c)$$

with the wave impedance Z_{TE} of the TM wave, given by

$$Z_{TM} = \frac{\gamma}{j\omega\epsilon} = \frac{\gamma_{M0}}{\gamma} Z_F \quad (3.93)$$

where Z_F is the wave impedance of the TEM wave in the homogeneous isotropic medium with material parameters ϵ, μ . The wave impedance of the TM wave relates the transverse electric and magnetic fields. From (3.92a) to (3.92b), (A.177), and (A.178) we obtain

$$\underline{\mathcal{E}}_t = -Z_{TM} \star dz \wedge \underline{\mathcal{H}} = -Z_{TM} \perp_z \underline{\mathcal{H}}, \quad (3.94a)$$

$$\underline{\mathcal{H}} = Z_{TM}^{-1} \star dz \wedge \underline{\mathcal{E}}_t = Z_{TM}^{-1} \perp_z \underline{\mathcal{E}}_t. \quad (3.94b)$$

An electromagnetic field for which $E_z = 0$ is valid is called a *transverse electric* or TE field with respect to z -direction. The electromagnetic field in a source-free region, fulfilling the condition $E_z = 0$, may be derived from a magnetic Hertz vector that exhibits only a z -component Π_{mz} ,

$$\underline{\Pi}_m(\mathbf{x}) = \underline{\Pi}_{mz}(\mathbf{x}) dz. \quad (3.95)$$

The electric and magnetic fields are computed using (3.36a) and (3.36b). In source-free regions with $\underline{\mathcal{M}}_{m0} = 0$ this yields

$$\underline{\mathcal{E}} = -j\omega\mu \star d\underline{\Pi}_m, \quad (3.96a)$$

$$\underline{\mathcal{H}} = -\tilde{d} d\underline{\Pi}_m. \quad (3.96b)$$

We separate the magnetic field $\underline{\mathcal{H}}$ into a transverse part $\underline{\mathcal{H}}_t$ and a longitudinal part $\underline{\mathcal{H}}_l$,

$$\underline{\mathcal{H}} = \underline{\mathcal{H}}_t + \underline{\mathcal{H}}_l \quad (3.97)$$

and obtain

$$\underline{\mathcal{E}} = -j\omega\mu \left(\frac{\partial \underline{\Pi}_{mz}(\mathbf{x})}{\partial y} dx - \frac{\partial \underline{\Pi}_{mz}(\mathbf{x})}{\partial x} dy \right), \quad (3.98a)$$

$$\underline{\mathcal{H}}_t = \frac{\partial^2 \underline{\Pi}_{mz}}{\partial x \partial z} dx + \frac{\partial^2 \underline{\Pi}_{mz}}{\partial y \partial z} dy, \quad (3.98b)$$

$$\underline{\mathcal{H}}_l = - \left(\frac{\partial^2 \underline{\Pi}_{mz}}{\partial x^2} + \frac{\partial^2 \underline{\Pi}_{mz}}{\partial y^2} \right) dz. \quad (3.98c)$$

A wave for which the electric field in direction of propagation vanishes is called a *transverse electric wave* or TE wave. As in (3.89) we assume for a TE wave propagating in z -direction

$$\underline{\Pi}_m(\mathbf{x}) = \underline{\Pi}_{m0z}(x, y) e^{-\gamma z} dz. \quad (3.99)$$

From the Helmholtz equation (3.37) and (3.39) we obtain

$$\frac{\partial^2 \underline{\Pi}_{e0z}}{\partial x^2} + \frac{\partial^2 \underline{\Pi}_{e0z}}{\partial y^2} - (\gamma_{M0}^2 - \gamma^2) \underline{\Pi}_{e0z} = 0, \quad (3.100)$$

where γ_{M0} again is given by (3.91). From (3.98a) to (3.98c) and (3.99) we obtain the field of the TM wave

$$\underline{\mathcal{E}} = -j\omega\mu \left(\frac{\partial \underline{\Pi}_{m0z}}{\partial y} dx - \frac{\partial \underline{\Pi}_{m0z}}{\partial x} dy \right) e^{-\gamma z}, \quad (3.101a)$$

$$\underline{\mathcal{H}}_t = -j\omega\mu Z_{TE}^{-1} \left(\frac{\partial \underline{\Pi}_{m0z}}{\partial x} dx + \frac{\partial \underline{\Pi}_{m0z}}{\partial y} dy \right) e^{-\gamma z}, \quad (3.101b)$$

$$\underline{\mathcal{H}}_l = - \left(\frac{\partial^2 \underline{\Pi}_{m0z}}{\partial x^2} + \frac{\partial^2 \underline{\Pi}_{m0z}}{\partial y^2} \right) e^{-\gamma z} dz \quad (3.101c)$$

with the wave impedance Z_{TE} of the TE wave, given by

$$Z_{TE} = \frac{j\omega\mu}{\gamma} = \frac{\gamma}{\gamma_{M0}} Z_F. \quad (3.102)$$

The wave impedance Z_{TE} relates the transverse electric and magnetic fields of the TE wave. From (3.101a) to (3.101c), (A.177), and (A.178) we obtain

$$\underline{\mathcal{E}} = -Z_{TE} \star dz \wedge \underline{\mathcal{H}}_t = -Z_{TE} \perp_z \underline{\mathcal{H}}_t, \quad (3.103a)$$

$$\underline{\mathcal{H}}_t = Z_{TE}^{-1} \star dz \wedge \underline{\mathcal{E}} = Z_{TE}^{-1} \perp_z \underline{\mathcal{E}}. \quad (3.103b)$$

3.5 REFLECTION AND TRANSMISSION OF PLANE WAVES

Consider a time-harmonic TEM wave incident on a plane boundary surface as depicted in Figure 3.3. The boundary surface is defined by $z = 0$. Region 1 above the boundary surface is filled with medium 1 and region 2, below the boundary surface, is filled with medium 2. Both media are assumed to be lossless, homogeneous, and isotropic and characterized by the real material parameters ϵ_1, μ_1 and ϵ_2, μ_2 . The direction of the incident wave is given by the wave vector k_i . The angle of incidence is θ_i , this is the angle enclosed by the direction of incidence and the normal to the boundary plane. The *plane of incidence* is defined by the direction of incidence and the normal to the boundary plane. The incident wave causes a reflected wave in region 1 and a transmitted wave in region 2. Electric and magnetic fields of incident, reflected, and transmitted

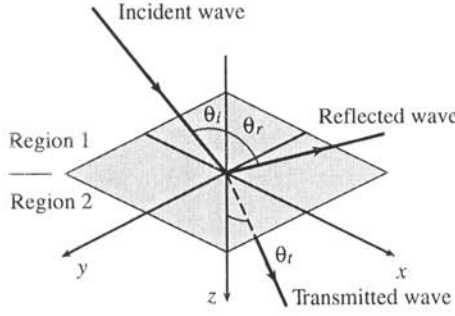


Figure 3.3: TEM wave incident on a plane surface.

waves are represented by the differential forms \mathcal{E}_i , \mathcal{H}_i , \mathcal{E}_r , \mathcal{H}_r , \mathcal{E}_t , and \mathcal{H}_t . The field in region 1 is a superposition of incident and reflected waves.

From (2.173a) and (2.173c) we obtain the transverse boundary conditions for the electric and magnetic fields:

$$n \wedge \left(\underline{\mathcal{E}}^{(i)}(x, y, 0) + \underline{\mathcal{E}}^{(r)}(x, y, 0) - \underline{\mathcal{E}}^{(t)}(x, y, 0) \right) = 0, \quad (3.104a)$$

$$n \wedge \left(\underline{\mathcal{H}}^{(i)}(x, y, 0) + \underline{\mathcal{H}}^{(r)}(x, y, 0) - \underline{\mathcal{H}}^{(t)}(x, y, 0) \right) = 0. \quad (3.104b)$$

The incident, reflected, and transmitted plane waves are described by

$$\underline{\mathcal{E}}^{(i)} = \underline{E}_x^{(i)} e^{-j(k_{ix}x + k_{iz}z)} dx + \underline{E}_y^{(i)} e^{-j(k_{ix}x + k_{iz}z)} dy + \underline{E}_z^{(i)} e^{-j(k_{ix}x + k_{iz}z)} dz, \quad (3.105a)$$

$$\underline{\mathcal{E}}^{(r)} = \underline{E}_x^{(r)} e^{-j(k_{rx}x - k_{rz}z)} dx + \underline{E}_y^{(r)} e^{-j(k_{rx}x - k_{rz}z)} dy + \underline{E}_z^{(r)} e^{-j(k_{rx}x - k_{rz}z)} dz, \quad (3.105b)$$

$$\underline{\mathcal{E}}^{(t)} = \underline{E}_x^{(t)} e^{-j(k_{tx}x + k_{tz}z)} dx + \underline{E}_y^{(t)} e^{-j(k_{tx}x + k_{tz}z)} dy + \underline{E}_z^{(t)} e^{-j(k_{tx}x + k_{tz}z)} dz \quad (3.105c)$$

and

$$\underline{\mathcal{H}}^{(i)} = \underline{H}_{0x}^{(i)} e^{-j(k_{ix}x + k_{iz}z)} dx + \underline{H}_{0y}^{(i)} e^{-j(k_{ix}x + k_{iz}z)} dy + \underline{H}_{0z}^{(i)} e^{-j(k_{ix}x + k_{iz}z)} dz, \quad (3.106a)$$

$$\underline{\mathcal{H}}^{(r)} = \underline{H}_{0x}^{(r)} e^{-j(k_{rx}x - k_{rz}z)} dx + \underline{H}_{0y}^{(r)} e^{-j(k_{rx}x - k_{rz}z)} dy + \underline{H}_{0z}^{(r)} e^{-j(k_{rx}x - k_{rz}z)} dz, \quad (3.106b)$$

$$\underline{\mathcal{H}}^{(t)} = \underline{H}_{0x}^{(t)} e^{-j(k_{tx}x + k_{tz}z)} dx + \underline{H}_{0y}^{(t)} e^{-j(k_{tx}x + k_{tz}z)} dy + \underline{H}_{0z}^{(t)} e^{-j(k_{tx}x + k_{tz}z)} dz. \quad (3.106c)$$

In region 1 the total field $\underline{\mathcal{E}}^{(1)}$, $\underline{\mathcal{H}}^{(1)}$ is given by

$$\underline{\mathcal{E}}^{(1)} = \underline{\mathcal{E}}^{(i)} + \underline{\mathcal{E}}^{(r)}, \quad (3.107a)$$

$$\underline{\mathcal{H}}^{(1)} = \underline{\mathcal{H}}^{(i)} + \underline{\mathcal{H}}^{(r)} \quad (3.107b)$$

and the field in region 2 is the transmitted field,

$$\underline{\mathcal{E}}^{(2)} = \underline{\mathcal{E}}^{(t)}, \quad \underline{\mathcal{H}}^{(2)} = \underline{\mathcal{H}}^{(t)}. \quad (3.108)$$

The wave numbers k_i and k_r in region 1 and the wave number k_t in region 2 are

$$k_i = k_r = \omega \sqrt{\mu_1 \epsilon_1} = \frac{n_1 \omega}{c_0}, \quad (3.109a)$$

$$k_t = \omega \sqrt{\mu_2 \epsilon_2} = \frac{n_2 \omega}{c_0}, \quad (3.109b)$$

where the refractive index n_i and is given by

$$n_i = \sqrt{\frac{\epsilon_i \mu_i}{\epsilon_0 \mu_0}} = \sqrt{\epsilon_{ri} \mu_{ri}}. \quad (3.110)$$

Figure 3.4 shows the wave vectors of incident, reflected, and transmitted waves and the geometrical relationship between the angle of incidence θ_i , the angle of reflection θ_r and the angle of transmission θ_t . Drawing in both region 1 the semicircle with radius $|k_1| = |k_i| = |k_r|$ and in region 2 the semicircle with radius $|k_2| = |k_t|$ we can construct the direction of the reflected and transmitted waves by considering that the x -components of the wave vectors of incident, reflected, and transmitted waves are the same:

$$k_{ix} = k_{rx} = k_{tx} = k_x \quad (3.111)$$

The x -components of the wave vectors of incident, reflected, and transmitted waves are given by

$$k_{ix} = k_i \sin \theta_i \quad k_{rx} = k_r \sin \theta_r \quad k_{tx} = k_t \sin \theta_t \quad (3.112)$$

and the z -components of these wave vectors are

$$k_{iz} = k_i \cos \theta_i \quad k_{rz} = -k_r \cos \theta_r \quad k_{tz} = k_t \cos \theta_t. \quad (3.113)$$

From (3.109a), (3.109b), (3.110), (3.111), and (3.112) we obtain $\theta_r = \theta_i$ and *Snell's law*

$$\frac{\sin \theta_i}{\sin \theta_t} = \frac{n_2}{n_1}. \quad (3.114)$$

In the following we write

$$\theta_r = \theta_i = \theta_1, \quad \theta_t = \theta_2. \quad (3.115)$$

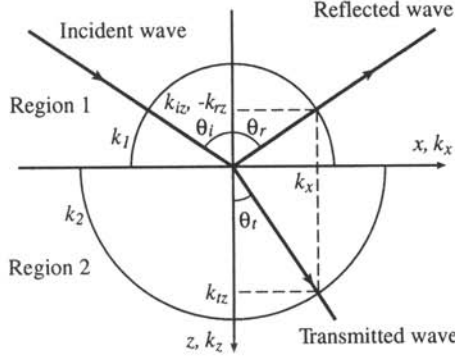


Figure 3.4: Reflected and transmitted waves.

The TEM wave impedances for media 1 and 2 Z_{F1} and Z_{F2} are given by

$$Z_{F1} = \sqrt{\frac{\mu_1}{\epsilon_1}}, \quad Z_{F2} = \sqrt{\frac{\mu_2}{\epsilon_2}}. \quad (3.116)$$

3.5.1 Reflection and Diffraction of a TE Wave at a Plane Boundary

We consider a TE plane wave incident on the boundary (i.e., a wave polarized normally to the plane of incidence). We assume the xz -plane as the plane of incidence. Incident, reflected, and transmitted waves are uniform in y -direction. That means $\partial/\partial y = 0$ holds for all field components. The resulting TE wave exhibits an electric field component in y -direction and magnetic field components in x - and z -directions. In region 1 the field of the incident wave can be derived from the magnetic Hertz form

$$\underline{\Pi}_m^{(i)} = \underline{A}^{(1)} e^{-j(k_x x + k_{iz} z)} dz. \quad (3.117)$$

With (3.36a) and (3.36b) we obtain

$$\underline{\mathcal{E}}^{(i)} = -j\omega\mu_1 \star d \underline{\Pi}_m = \omega\mu_1 k_x \underline{A}^{(1)} e^{-j(k_x x + k_{iz} z)} dy, \quad (3.118a)$$

$$\underline{\mathcal{H}}^{(i)} = -\tilde{d} d \underline{\Pi}_m = k_x k_{iz} \underline{A}^{(1)} e^{-j(k_x x + k_{iz} z)} dx + k_x^2 \underline{A}^{(1)} e^{-j(k_x x + k_{iz} z)} dz. \quad (3.118b)$$

For the reflected wave in region 1 we make the ansatz

$$\underline{\Pi}_m^{(r)} = \underline{B}^{(1)} e^{-j(k_x x - k_{iz} z)} dz. \quad (3.119)$$

This yields

$$\underline{\mathcal{E}}^{(r)} = \omega\mu_1 k_x \underline{B}^{(1)} e^{-j(k_x x - k_{iz} z)} dy, \quad (3.120a)$$

$$\underline{\mathcal{H}}^{(r)} = -k_x k_{iz} \underline{B}^{(1)} e^{-j(k_x x - k_{iz} z)} dx + k_x^2 \underline{B}^{(1)} e^{-j(k_x x - k_{iz} z)} dz. \quad (3.120b)$$

With (3.107a) and (3.107b) we obtain the total field in region 1

$$\underline{\mathcal{E}}^{(1)} = \omega\mu_1 k_x e^{-j k_x x} (\underline{A}^{(1)} e^{-j k_{iz} z} + \underline{B}^{(1)} e^{j k_{iz} z}) dy, \quad (3.121a)$$

$$\begin{aligned} \underline{\mathcal{H}}^{(1)} = & k_x k_{iz} e^{-j k_x x} (\underline{A}^{(1)} e^{-j k_{iz} z} - \underline{B}^{(1)} e^{j k_{iz} z}) dx \\ & + k_x^2 e^{-j k_x x} (\underline{A}^{(1)} e^{-j k_{iz} z} + \underline{B}^{(1)} e^{j k_{iz} z}) dz. \end{aligned} \quad (3.121b)$$

The transmitted wave we obtain from

$$\underline{\Pi}_m^{(t)} = \underline{A}^{(2)} e^{-j(k_x x + k_{iz} z)} dz. \quad (3.122)$$

With (3.36a) and (3.36b) we obtain

$$\underline{\mathcal{E}}^{(t)} = \omega\mu_2 k_x \underline{A}^{(2)} e^{-j(k_x x + k_{iz} z)} dy, \quad (3.123a)$$

$$\underline{\mathcal{H}}^{(t)} = k_x k_{tz} \underline{A}^{(2)} e^{-j(k_x x + k_{tz} z)} dx + k_x^2 \underline{A}^{(2)} e^{-j(k_x x + k_{tz} z)} dz. \quad (3.123b)$$

We express all field quantities by the electric field amplitude \underline{E}_{y0} of the incident wave. The electric field amplitudes of the transmitted and reflected waves are related to the electric field amplitude of the incident wave via the *reflection coefficient* R^\perp and the *transmission coefficient* T^\perp introduced via

$$\underline{E}_{y0} = \omega\mu_1 k_x \underline{A}^{(1)}, \quad (3.124a)$$

$$R^\perp \underline{A}^{(1)} = \underline{B}^{(1)}, \quad (3.124b)$$

$$T^\perp \underline{E}_{y0} = \omega\mu_2 k_x \underline{A}^{(2)}. \quad (3.124c)$$

We define the *wave impedances* Z_1^\perp and Z_2^\perp of the TE waves in region 1 and 2 by

$$Z_1^\perp = \frac{\omega\mu_1}{k_{iz}}, \quad Z_2^\perp = \frac{\omega\mu_2}{k_{tz}}. \quad (3.125)$$

The wave impedances Z_1^\perp and Z_2^\perp relate the electric and magnetic field components parallel to the boundary layer to the incident, reflected, and transmitted waves. Inserting (3.109a), (3.109b), and (3.113) into (3.125) yields

$$Z_1^\perp = \frac{Z_{F1}}{\cos \theta_1} \quad Z_2^\perp = \frac{Z_{F2}}{\cos \theta_2} \quad (3.126)$$

with the TEM wave impedances for media 1 and 2, Z_{F1} and Z_{F2} , given by (3.116). Inserting (3.124a) and (3.125) into (3.121a) and (3.121b) and considering (3.112) and (3.113) yields for region 1

$$\underline{\mathcal{E}}^{(1)} = \underline{E}_{y0} e^{-j k_x x} (e^{-j k_{iz} z} + R^\perp e^{j k_{iz} z}) dy, \quad (3.127a)$$

$$\begin{aligned} \underline{\mathcal{H}}^{(1)} = & \frac{1}{Z_1^\perp} \underline{E}_{y0} e^{-j k_x x} (e^{-j k_{iz} z} - R^\perp e^{j k_{iz} z}) dx \\ & + \frac{\tan \theta_1}{Z_1^\perp} \underline{E}_{y0} e^{-j k_x x} (e^{-j k_{iz} z} + R^\perp e^{j k_{iz} z}) dz. \end{aligned} \quad (3.127b)$$

For the transmitted wave in region 2 from (3.123a), (3.123b), (3.124c), and (3.125) and considering (3.112) and (3.113) we obtain

$$\underline{\mathcal{E}}^{(t)} = T^\perp \underline{E}_{y0} e^{-j(k_x x + k_{tz} z)} dy, \quad (3.128a)$$

$$\underline{\mathcal{H}}^{(t)} = \frac{1}{Z_2^\perp} T^\perp \underline{E}_{y0} e^{-j(k_x x + k_{tz} z)} dx + \frac{\tan \theta_2}{Z_2^\perp} T^\perp \underline{E}_{y0} e^{-j(k_x x + k_{tz} z)} dz. \quad (3.128b)$$

Applying the boundary conditions (3.104a) and (3.104b) to the fields (3.127a) to (3.128b) and considering (3.107a) and (3.107b) yields the *Fresnel formula*

$$R^\perp = \frac{Z_2^\perp - Z_1^\perp}{Z_2^\perp + Z_1^\perp}, \quad (3.129a)$$

$$T^\perp = \frac{2Z_2^\perp}{Z_2^\perp + Z_1^\perp}. \quad (3.129b)$$

With (3.126) we can bring these equations in the form

$$R^\perp = \frac{Z_{F2} \cos \theta_1 - Z_{F1} \cos \theta_2}{Z_{F2} \cos \theta_1 + Z_{F1} \cos \theta_2}, \quad (3.130a)$$

$$T^\perp = \frac{2Z_{F2} \cos \theta_1}{Z_{F2} \cos \theta_1 + Z_{F1} \cos \theta_2}. \quad (3.130b)$$

For the special case $\mu_1 = \mu_2$ we obtain with (3.110)

$$R^\perp = \frac{n_1 \cos \theta_1 - n_2 \cos \theta_2}{n_1 \cos \theta_1 + n_2 \cos \theta_2}, \quad (3.131a)$$

$$T^\perp = \frac{2n_1 \cos \theta_1}{n_1 \cos \theta_1 + n_2 \cos \theta_2}. \quad (3.131b)$$

The dependence of R^\perp and T^\perp on the angle of incidence θ_1 is shown in Figure 3.5. Using

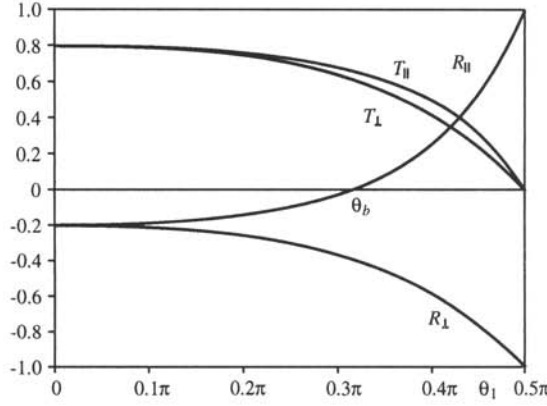


Figure 3.5: Reflection and transmission coefficient dependence on angle of incidence for $n_2 = 1.5n_1$.

Snell's law (3.114) to express θ_2 by θ_1 we obtain

$$R^\perp = \frac{n_1 \cos \theta_1 - \sqrt{n_2^2 - n_1^2 \sin^2 \theta_1}}{n_1 \cos \theta_1 + \sqrt{n_2^2 - n_1^2 \sin^2 \theta_1}}, \quad (3.132a)$$

$$T^\perp = \frac{2n_1 \cos \theta_1}{n_1 \cos \theta_1 + \sqrt{n_2^2 - n_1^2 \sin^2 \theta_1}}. \quad (3.132b)$$

The dependence of R^\perp and T^\perp on the angle of incidence θ_1 is shown in Figure 3.5.

3.5.2 Reflection and Diffraction of a TM Wave at a Plane Boundary

An incident plane wave polarized parallel to the plane of incidence yields, together with the reflected wave, a TM wave. We again assume the xz -plane as the plane of incidence. Incident, reflected, and transmitted waves are uniform in y -direction and $\partial/\partial y = 0$ holds for all field components. The resulting TM wave exhibits electric field components in x - and z -directions and a magnetic field component in y -direction. In region 1 the field of the incident wave can be derived from the electric Hertz form

$$\underline{\Pi}_e^{(i)} = \underline{C}^{(1)} e^{-j(k_x x + k_{iz} z)} dz. \quad (3.133)$$

With (3.29a) and (3.29b) we obtain

$$\underline{\mathcal{H}}^{(i)} = j\omega\epsilon_1 \star d\underline{\Pi}_e = -\omega\epsilon_1 k_x \underline{C}^{(1)} e^{-j(k_x x + k_{iz} z)} dy, \quad (3.134a)$$

$$\underline{\mathcal{E}}^{(i)} = -\tilde{d} d\underline{\Pi}_e = k_x k_{iz} \underline{C}^{(1)} e^{-j(k_x x + k_{iz} z)} dx + k_x^2 \underline{C}^{(1)} e^{-j(k_x x + k_{iz} z)} dz. \quad (3.134b)$$

The reflected wave in region 1 is obtained from the electric Hertz form

$$\underline{\Pi}_e^{(r)} = \underline{D}^{(1)} e^{-j(k_x x - k_{iz} z)} dz. \quad (3.135)$$

From this we obtain

$$\underline{\mathcal{H}}^{(r)} = -\omega \epsilon_1 k_x \underline{D}^{(1)} e^{-j(k_x x - k_{iz} z)} dy, \quad (3.136a)$$

$$\underline{\mathcal{E}}^{(r)} = -k_x k_{iz} \underline{D}^{(1)} e^{-j(k_x x - k_{iz} z)} dx + k_x^2 \underline{D}^{(1)} e^{-j(k_x x - k_{iz} z)} dz. \quad (3.136b)$$

In region 1 the total field $\underline{\mathcal{H}}^{(1)}, \underline{\mathcal{E}}^{(1)}$ is given by (3.107a) and (3.107b). This yields

$$\underline{\mathcal{H}}^{(1)} = -\omega \epsilon_1 k_x e^{-j k_x x} (\underline{C}^{(1)} e^{-j k_{iz} z} + \underline{D}^{(1)} e^{j k_{iz} z}) dy, \quad (3.137a)$$

$$\begin{aligned} \underline{\mathcal{E}}^{(1)} = k_x k_{iz} e^{-j k_x x} (\underline{C}^{(1)} e^{-j k_{iz} z} - \underline{D}^{(1)} e^{j k_{iz} z}) dx \\ + k_x^2 e^{-j k_x x} (\underline{C}^{(1)} e^{-j k_{iz} z} + \underline{D}^{(1)} e^{j k_{iz} z}) dz. \end{aligned} \quad (3.137b)$$

The transmitted wave in region 2 we obtain from

$$\underline{\Pi}_e^{(t)} = \underline{C}^{(2)} e^{-j(k_x x + k_{iz} z)} dz. \quad (3.138)$$

With (3.29a) and (3.29b) we obtain

$$\underline{\mathcal{H}}^{(t)} = -\omega \epsilon_2 k_x \underline{C}^{(2)} e^{-j(k_x x + k_{iz} z)} dy, \quad (3.139a)$$

$$\underline{\mathcal{E}}^{(t)} = k_x k_{tz} \underline{C}^{(2)} e^{-j(k_x x + k_{iz} z)} dx + k_x^2 \underline{C}^{(2)} e^{-j(k_x x + k_{iz} z)} dz. \quad (3.139b)$$

We express all field quantities by the x -component of the electric field \underline{E}_{x0} of the incident wave. The electric field amplitudes of the reflected and transmitted waves are related to the electric field amplitude of the incident wave via the reflection coefficient R^\parallel transmission coefficient T^\parallel . This yields

$$\underline{E}_{x0} = k_x k_{iz} \underline{C}^{(1)}, \quad (3.140a)$$

$$R^\parallel \underline{C}^{(1)} = \underline{D}^{(1)}, \quad (3.140b)$$

$$T^\parallel \underline{E}_{x0} = k_x k_{tz} \underline{C}^{(2)}. \quad (3.140c)$$

We define the wave impedances Z_1^\parallel and Z_2^\parallel of the TM waves in region 1 and 2, respectively, by

$$Z_1^\parallel = \frac{k_{iz}}{\omega \epsilon_1}, \quad (3.141a)$$

$$Z_2^\parallel = \frac{k_{tz}}{\omega \epsilon_2}. \quad (3.141b)$$

The wave impedances Z_1^{\parallel} and Z_2^{\parallel} relate the electric and magnetic field components parallel to the boundary layer of the incident, reflected, and transmitted waves. Inserting (3.109a) and (3.113) into (3.141a) and (3.109b) and (3.113) into (3.141b) yields

$$Z_1^{\parallel} = Z_{F1} \cos \theta_1, \quad (3.142a)$$

$$Z_2^{\parallel} = Z_{F2} \cos \theta_2 \quad (3.142b)$$

with the TEM wave impedances for media 1 and 2 Z_{F1} and Z_{F2} given by (3.116). Inserting (3.140a) and (3.141a) into (3.137a) and (3.137b) and considering (3.112) and (3.113) yields for region 1

$$\underline{\mathcal{H}}^{(1)} = -\frac{1}{Z_1^{\parallel}} \underline{E}_{x0} e^{-j k_x x} (e^{-j k_{iz} z} + R^{\parallel} e^{j k_{iz} z}) dy, \quad (3.143a)$$

$$\begin{aligned} \underline{\mathcal{E}}^{(1)} = & \underline{E}_{x0} e^{-j k_x x} (e^{-j k_{iz} z} - R^{\parallel} e^{j k_{iz} z}) dx \\ & + \tan \theta_1 \underline{E}_{x0} e^{-j k_x x} (e^{-j k_{iz} z} + R^{\parallel} e^{j k_{iz} z}) dz. \end{aligned} \quad (3.143b)$$

For the transmitted wave in region 2 from (3.139a), (3.139b), (3.140c), and (3.141b) and considering (3.112) and (3.113) we obtain

$$\underline{\mathcal{H}}^{(t)} = -\frac{1}{Z_2^{\parallel}} T^{\parallel} \underline{E}_{x0} e^{-j(k_x x + k_{iz} z)} dy, \quad (3.144a)$$

$$\underline{\mathcal{E}}^{(t)} = T^{\parallel} \underline{E}_{x0} e^{-j(k_x x + k_{iz} z)} dx + \tan \theta_2 T^{\parallel} \underline{E}_{x0} e^{-j(k_x x + k_{iz} z)} dz. \quad (3.144b)$$

Applying the boundary conditions (3.104a) and (3.104a) to (3.143a), (3.144b) and considering (3.107a) and (3.107b), we obtain the *Fresnel formula*

$$R^{\parallel} = \frac{Z_2^{\parallel} - Z_1^{\parallel}}{Z_2^{\parallel} + Z_1^{\parallel}}, \quad (3.145a)$$

$$T^{\parallel} = \frac{2Z_2^{\parallel}}{Z_2^{\parallel} + Z_1^{\parallel}}. \quad (3.145b)$$

With (3.142a) and (3.142b) we can bring these equations in the form

$$R^{\parallel} = \frac{Z_{F2} \cos \theta_2 - Z_{F1} \cos \theta_1}{Z_{F2} \cos \theta_2 + Z_{F1} \cos \theta_1}, \quad (3.146a)$$

$$T^{\parallel} = \frac{2Z_{F2} \cos \theta_2}{Z_{F2} \cos \theta_2 + Z_{F1} \cos \theta_1}. \quad (3.146b)$$

For the special case $\mu_1 = \mu_2$ we obtain with (3.110)

$$R^{\parallel} = \frac{n_1 \cos \theta_2 - n_2 \cos \theta_1}{n_2 \cos \theta_1 + n_1 \cos \theta_2}, \quad (3.147a)$$

$$T^{\parallel} = \frac{2n_1 \cos \theta_2}{n_2 \cos \theta_1 + n_1 \cos \theta_2}. \quad (3.147b)$$

Expressing θ_2 by θ_1 by Snell's law (3.114), we obtain

$$R^{\parallel} = -\frac{n_2^2 \cos \theta_1 - n_1 \sqrt{n_2^2 - n_1^2 \sin^2 \theta_1}}{n_2^2 \cos \theta_1 + n_1 \sqrt{n_2^2 - n_1^2 \sin^2 \theta_1}}, \quad (3.148a)$$

$$T^{\parallel} = \frac{2n_1 n_2 \cos \theta_2}{n_2^2 \cos \theta_1 + n_1 \sqrt{n_2^2 - n_1^2 \sin^2 \theta_1}}. \quad (3.148b)$$

Figure 3.5 shows the dependence of R^{\parallel} and T^{\parallel} on the angle of incidence θ_1 . For the TM wave the reflection coefficient R^{\parallel} becomes zero if the angle of incidence θ_1 becomes the *Brewster angle* θ_b . From (3.114) and (3.147a) we obtain

$$\theta_1 = \tan^{-1} \frac{n_2}{n_1}. \quad (3.149)$$

A TM wave incident under the Brewster angle is completely transmitted into medium 2. We obtain

$$\theta_1 + \theta_2 = \frac{1}{2}\pi \quad \text{for} \quad \theta_1 = \theta_b. \quad (3.150)$$

This means that due to the incident wave the dielectric medium 2 is polarized in the direction of the reflected wave. Since no radiation occurs in the direction of polarization, no wave is reflected.

3.5.3 Total Reflection

Let medium 1 have a higher optical density than medium 2, $n_1 > n_2$. In this case from Snell's law (3.114) follows for a wave incident under the *critical angle* θ_c given by

$$\theta_c = \sin^{-1} \frac{n_2}{n_1}, \quad (3.151)$$

that the transmitted wave propagates parallel to the boundary plane. This case is illustrated in Figure 3.6. For $\theta_1 > \theta_c$ the transmitted wave propagates parallel to the boundary plane and decays exponentially normal to the boundary plane.

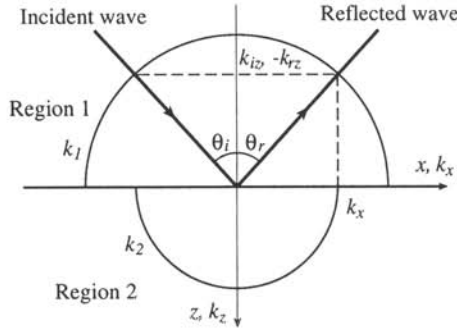


Figure 3.6: Total reflection.

In this case the incident and reflected electric and magnetic fields are still expressed by (3.105a), (3.105b), (3.106a) and (3.106b) whereas for the transmitted field (3.105c) and (3.106c) are replaced by

$$\underline{\mathcal{E}}^{(t)} = \underline{E}_x^{(t)} e^{-(j k_x x + \alpha_{tz} z)} dx + \underline{E}_y^{(t)} e^{-(j k_x x + \alpha_{tz} z)} dy + \underline{E}_z^{(t)} e^{-(j k_x x + \alpha_{tz} z)} dz, \quad (3.152a)$$

$$\underline{\mathcal{H}}^{(t)} = \underline{H}_{0x}^{(t)} e^{-(j k_x x + \alpha_{tz} z)} dx + \underline{H}_{0y}^{(t)} e^{-(j k_x x + \alpha_{tz} z)} dy + \underline{H}_{0z}^{(t)} e^{-(j k_x x + \alpha_{tz} z)} dz, \quad (3.152b)$$

where α_{tz} is the attenuation coefficient in z -direction in medium 2. Considering (3.110) the homogeneous Helmholtz equation (3.37) is fulfilled for

$$k_x^2 + k_{iz}^2 = n_1^2 k_0^2, \quad (3.153a)$$

$$k_x^2 - \alpha_{tz}^2 = n_2^2 k_0^2 \quad (3.153b)$$

with

$$k_0^2 = \omega^2 \mu_0 \epsilon_0. \quad (3.154)$$

From this we obtain for $\theta_1 > \theta_c$ the dependence of the attenuation coefficient α_{tz} from the angle of incidence

$$\alpha_{tz} = k_0 \sqrt{n_1^2 \sin^2 \theta_1 - n_2^2}. \quad (3.155)$$

Even in the case of total reflection the field penetrates exponentially decaying with a penetration depth α_{tz}^{-1} into the totally reflecting medium. The attenuation coefficient increases with increasing angle of incidence θ_1 .

For a TE wave the field in region 1 also is represented by (3.121a) and (3.121b). For the field in region 2 we obtain by substituting $\alpha_{tz} = j k_{tz}$ in (3.123a) and (3.123b)

$$\underline{\mathcal{E}}^{(t)} = \omega \mu_2 k_x \underline{A}^{(2)} e^{-(j k_x x + \alpha_{tz} z)} dy, \quad (3.156a)$$

$$\underline{\mathcal{H}}^{(t)} = -j k_x \alpha_{tz} \underline{A}^{(2)} e^{-(j k_x x + \alpha_{tz} z)} dx + k_x^2 \underline{A}^{(2)} e^{-(j k_x x + \alpha_{tz} z)} dz. \quad (3.156b)$$

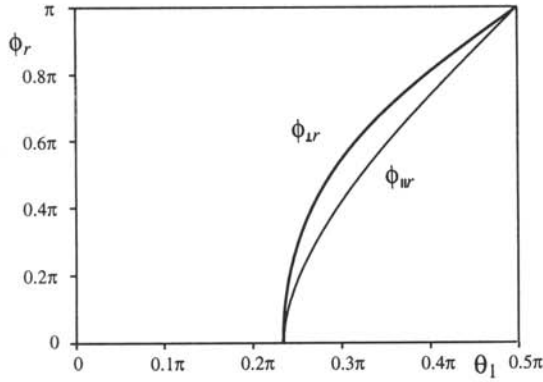


Figure 3.7: Dependence of the Goos-Hänchen shift $\phi_{\perp r}$ and $\phi_{||r}$ on angle of incidence θ_1 for $n_1 = 1.5n_2$.

Expressing all field components by the electric field amplitude E_{y0} of the incident wave we obtain again (3.124a) and (3.124c), where the wave impedance in region 1, Z_1^\perp , is given by (3.113) and (3.125) whereas the wave impedance of the *evanescent field* in region 2, Z_2^\perp , is purely imaginary. The wave impedances are given by

$$Z_1^\perp = \frac{\omega\mu_1}{k_{iz}} = \frac{\omega\mu_1}{k_0 \cos \theta_1}, \quad (3.157a)$$

$$Z_2^\perp = j \frac{\omega\mu_2}{\alpha_{tz}} = \frac{j\omega\mu_2}{k_0 \sqrt{n_1^2 \sin^2 \theta_1 - n_2^2}}. \quad (3.157b)$$

For $\mu_1 = \mu_2$ the Fresnel formula (3.129a) and (3.129b) are

$$R^\perp = \frac{n_1 \cos \theta_1 + j \sqrt{n_1^2 \sin^2 \theta_1 - n_2^2}}{n_1 \cos \theta_1 - j \sqrt{n_1^2 \sin^2 \theta_1 - n_2^2}}, \quad (3.158a)$$

$$T^\perp = \frac{2n_1 \cos \theta_1}{n_1 \cos \theta_1 - j \sqrt{n_1^2 \sin^2 \theta_1 - n_2^2}}. \quad (3.158b)$$

The totally reflected wave penetrates exponentially decaying into the forbidden region 2. This is the origin of the *Goos-Hänchen shift* [4,13]. Due to the imaginary wave impedance of medium 2 the reflected wave experiences a phase shift, the so called Goos-Hänchen shift. For the totally reflected TE wave the Goos-Hänchen shift is

$$\phi_{\perp r} = 2 \tan^{-1} \frac{\sqrt{n_1^2 \sin^2 \theta_1 - n_2^2}}{n_2 \cos \theta_1}. \quad (3.159)$$

For a TM wave the field in region 1 also is represented by (3.137a) and (3.137b). For the field in region 2 we obtain by substituting α_{tz} for $j k_{tz}$ in (3.139a) and (3.139b)

$$\underline{H}^{(t)} = -\omega \epsilon_2 k_x \underline{C}^{(2)} e^{-(j k_x x + \alpha_{tz} z)} dy, \quad (3.160a)$$

$$\underline{E}^{(t)} = -j k_x \alpha_{tz} \underline{C}^{(2)} e^{-(j k_x x + \alpha_{tz} z)} dx + k_x^2 \underline{C}^{(2)} e^{-(j k_x x + \alpha_{tz} z)} dz. \quad (3.160b)$$

Expressing all field components by the electric field amplitude \underline{E}_{y0} of the incident wave we obtain again (3.140a) and (3.140c), where the wave impedance in region 1, Z_1^{\parallel} , is given by (3.113) and (3.141a). The wave impedance of the *evanescent field* in region 2, Z_2^{\parallel} , following from (3.141b) by replacing k_{tz} by $-j \alpha_{tz}$ is purely imaginary, hence

$$Z_1^{\parallel} = \frac{k_{iz}}{\omega \epsilon_1} = \frac{\omega \mu_1}{k_0 \cos \theta_1}, \quad (3.161a)$$

$$Z_2^{\parallel} = \frac{-j \alpha_{tz}}{\omega \epsilon_2} = \frac{j \omega \mu_2}{k_0 \sqrt{n_1^2 \sin^2 \theta_1 - n_2^2}}. \quad (3.161b)$$

For $\mu_1 = \mu_2$ the Fresnel formula (3.145a) and (3.145b) now become

$$R^{\parallel} = -\frac{n_2^2 \cos \theta_1 - j n_1 \sqrt{n_1^2 \sin^2 \theta_1 - n_2^2}}{\cos \theta_1 + j \sqrt{n_1^2 \sin^2 \theta_1 - n_2^2}}, \quad (3.162a)$$

$$T^{\parallel} = \frac{2 n_1 n_2 \cos \theta_1}{n_2^2 \cos \theta_1 + j n_1 \sqrt{n_1^2 \sin^2 \theta_1 - n_2^2}}. \quad (3.162b)$$

In the case of total reflection the reflection coefficient $|R^{\parallel}| = 1$ and the amplitude of the reflected wave has the same amplitude as the incident wave. For the TM wave the Goos-Hänchen shift is given by

$$\phi_{\parallel r} = 2 \tan^{-1} \frac{\sqrt{n_1^2 \sin^2 \theta_1 - n_2^2}}{n_1 \cos \theta_1}. \quad (3.163)$$

Figure 3.7 shows the dependence of the Goos-Hänchen shift $\phi_{\perp r}$ and $\phi_{\parallel r}$ on the angle of incidence θ_1 for $n_1 = 1.5 n_2$. For $n_1 = 1.5 n_2$ the critical angle is $\theta_c = 41.81^\circ$.

3.6 WAVES IN PLANAR LAYERED MEDIA

A *layered medium* consists of a number of layers of homogeneous material. In a *planar layered medium* the layers are bounded by parallel planes. Consider a wave incident on a layered medium from the left-hand side as shown in Figure 3.8. Due to the reflection

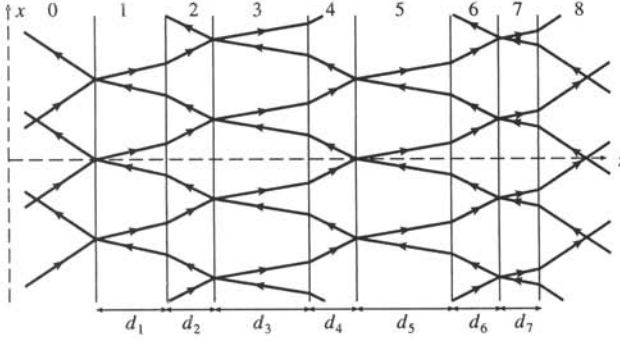


Figure 3.8: Multilayer structure.

and transmission at every boundary surface waves are incident on every boundary surface except on the rightmost surface. Therefore in all layers with exception of the last one waves propagate in positive as well as in negative z -direction.

Planar layered media occur in multifarious forms of technological significance. From the books referring to this subject we mention [4, 12]. Planar layered media are the simplest inhomogeneous media. Planar waves incident on a planar layered medium under an angle θ_1 may be decomposed into a TE wave, polarized normal to the plane of incidence and a TM wave polarized parallel to the plane of incidence.

Consider the m th layer of thickness d_m , shown in Figure 3.9. Assuming wave propagation in positive and negative z -direction, we obtain for TE waves from (3.127a) and (3.127b)

$$\underline{\mathcal{E}}^{\perp(m)} = \underline{\tilde{V}}^{\perp(m)}(z) e^{-j k_x x} dy, \quad (3.164a)$$

$$\underline{\mathcal{H}}^{\perp(m)} = \underline{\tilde{I}}^{\perp(m)}(z) e^{-j k_x x} dx + \frac{\sin \theta_m}{Z_F^{(m)}} \underline{\tilde{V}}^{\perp(m)}(z) e^{-j k_x x} dz \quad (3.164b)$$

with the amplitudes coefficients $\underline{\tilde{V}}^{\perp(m)}(z)$ and $\underline{\tilde{I}}^{\perp(m)}(z)$ describing the z -dependence of the field:

$$\underline{\tilde{V}}^{\perp(m)}(z) = \underline{E}_{y0}^{(m+)} e^{-j k_{mz} z} + \underline{E}_{y0}^{(m-)} e^{j k_{mz} z}, \quad (3.165a)$$

$$\underline{\tilde{I}}^{\perp(m)}(z) = \frac{1}{Z_{\perp}^{(m)}} \left(\underline{E}_{y0}^{(m+)} e^{-j k_{mz} z} - \underline{E}_{y0}^{(m-)} e^{j k_{mz} z} \right). \quad (3.165b)$$

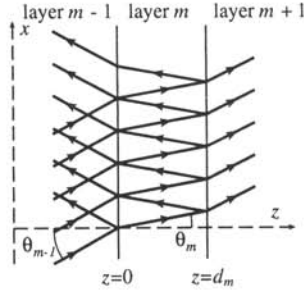


Figure 3.9: Propagation through one layer.

The wave impedance of the TE wave follows from (3.114) and (3.116) as

$$Z^{\perp(m)} = \frac{Z_F^{(m)}}{\cos \theta_m} = \frac{Z_F^{(m)}}{\sqrt{1 - \frac{n_j^2}{n_m^2} \sin^2 \theta_j}}, \quad (3.166)$$

where the index j refers to either to regions 1 or $n+1$ or to any layer from 2 to n . This allows to relate the impedance $Z^{\parallel(m)}$ to the angle θ_j in any other layer. From (3.113) and (3.114) we obtain the z -component of the wave vector

$$k_{mz} = k_m \cos \theta_m = k_m \sqrt{1 - \frac{n_j^2}{n_m^2} \sin^2 \theta_j}. \quad (3.167)$$

The coefficients $\underline{\tilde{V}}(z)$ and $\underline{\tilde{I}}(z)$ may be considered as generalized transverse voltages and currents per unit of length. These equations are in analogy to the transmission-line equations treated in Sections 7.4 and 8.3. From these equations we can express the transverse field amplitudes at the left surface of the l th $\underline{\tilde{V}}(0)$ and $\underline{\tilde{I}}(0)$ as functions of the transverse field amplitudes $\underline{\tilde{V}}(d_m)$ and $\underline{\tilde{I}}(d_m)$ at the right surface of this layer by

$$\underline{\tilde{V}}^{\perp(m)}(0) = \underline{\tilde{V}}^{\perp(m)}(d_m) \cos k_{mz} d_m + j Z^{\perp(m)} \underline{\tilde{I}}^{\perp(m)}(d_m) \sin k_{mz} d_m, \quad (3.168a)$$

$$\underline{\tilde{I}}^{\perp(m)}(0) = \frac{j}{Z^{\perp(m)}} \underline{\tilde{V}}^{\perp(m)}(d_m) \sin k_{mz} d_m + \underline{\tilde{I}}^{\perp(m)}(d_m) \cos k_{mz} d_m. \quad (3.168b)$$

We can express this equation in matrix form by

$$\begin{bmatrix} \underline{\tilde{V}}^{\perp(m)}(0) \\ \underline{\tilde{I}}^{\perp(m)}(0) \end{bmatrix} = \underline{A}^{\perp(m)} \begin{bmatrix} \underline{\tilde{V}}^{\perp(m)}(d_m) \\ \underline{\tilde{I}}^{\perp(m)}(d_m) \end{bmatrix}, \quad (3.169)$$

where the matrix $A^{\perp(m)}$ is given by

$$A^{\perp(m)} = \begin{bmatrix} \cos k_{mz} d_m & j Z^{\perp(m)} \sin k_{mz} d_m \\ \frac{j}{Z^{\perp(m)}} \sin k_{mz} d_m & \cos k_{mz} d_m \end{bmatrix}. \quad (3.170)$$

The matrix $A^{\perp(m)}$ is called the *chain matrix*, also treated in Section 10.2.2. In a multilayer structure as depicted in Figure 3.8 n layers, numbered from 1 to n are embedded between regions 0 and $n + 1$. The amplitudes $\underline{V}(z = 0)$, $\underline{I}(z = 0)$ can be expressed as functions of the amplitudes $\underline{V}(z = d)$, $\underline{I}(z = d)$ with $d = d_1 + d_2 + \dots + d_n$ by

$$\begin{bmatrix} \underline{V}^{\perp}(0) \\ \underline{I}^{\perp}(0) \end{bmatrix} = A^{\perp} \begin{bmatrix} \underline{V}^{\perp}(d) \\ \underline{I}^{\perp}(d) \end{bmatrix}. \quad (3.171)$$

with

$$A^{\perp} = A^{(1)\perp} A^{(2)\perp} \dots A^{(n)\perp}. \quad (3.172)$$

If region $n + 1$ terminates the structure with the wave impedance $Z^{\perp(n+1)}$, then

$$\underline{V}^{\perp}(d) = Z^{\perp(n+1)} \underline{I}^{\perp}(d). \quad (3.173)$$

Together with (3.172) this yields

$$\underline{V}^{\perp}(0) = \frac{A_{11}^{\perp} Z^{\perp(n+1)} + A_{12}^{\perp}}{A_{21}^{\perp} Z^{\perp(n+1)} + A_{22}^{\perp}} \underline{I}^{\perp}(0). \quad (3.174)$$

For TM waves we obtain from (3.143a) and (3.143b)

$$\underline{\mathcal{E}}^{\parallel(m)} = \underline{\tilde{V}}^{\parallel(m)}(z) e^{-j k_x x} dx + Z_F^{(m)} \sin \theta_m \underline{\tilde{I}}^{\parallel(i)}(z) e^{-j k_x x} dz, \quad (3.175a)$$

$$\underline{\mathcal{H}}^{\parallel(m)} = \underline{\tilde{I}}^{\parallel(m)}(z) e^{-j k_x x} dy \quad (3.175b)$$

with the amplitudes coefficients $\underline{\tilde{V}}(z)$ and $\underline{\tilde{I}}(z)$ describing the z -dependence of the field.

$$\underline{\tilde{V}}^{\parallel(m)}(z) = \underline{E}_{x0}^{(m+)} e^{-j k_{mz} z} + \underline{E}_{x0}^{(m-)} e^{j k_{mz} z}, \quad (3.176a)$$

$$\underline{\tilde{I}}^{\parallel(m)}(z) = \frac{1}{Z^{\parallel(m)}} \left(\underline{E}_{x0}^{(m+)} e^{-j k_{mz} z} - \underline{E}_{x0}^{(m-)} e^{j k_{mz} z} \right). \quad (3.176b)$$

The wave impedance of the TE wave follows from (3.114) and (3.142b) as

$$Z^{\perp(m)} = Z_F^{(m)} \cos \theta_m = Z_F^{(m)} \sqrt{1 - \frac{n_j^2}{n_m^2} \sin^2 \theta_j}, \quad (3.177)$$

where the index j may refer to any region. In matrix form we obtain

$$\begin{bmatrix} V^{\parallel(m)}(0) \\ I^{\parallel(m)}(0) \end{bmatrix} = A^{\parallel(m)} \begin{bmatrix} V^{\parallel(m)}(d_m) \\ I^{\parallel(m)}(d_m) \end{bmatrix}. \quad (3.178)$$

where the matrix $A^{\parallel(m)}$ is given by

$$A^{\parallel(m)} = \begin{bmatrix} \cos k_{mz} d_m & j Z^{\parallel(m)} \sin k_{mz} d_m \\ \frac{j}{Z^{\parallel(m)}} \sin k_{mz} d_m & \cos k_{mz} d_m \end{bmatrix}. \quad (3.179)$$

3.7 THIN CONDUCTING SHEETS

Consider the wave propagation through a thin metallic layer of conductivity σ . In the metal we can neglect the displacement current since $\omega\epsilon \ll \sigma$. For a TEM wave in the metal the propagation coefficient γ and the field impedance Z_F are given by

$$\gamma = \sqrt{j\omega\mu_0\sigma} = \sqrt{\frac{\omega\mu_0\sigma}{2}}(1+j), \quad (3.180a)$$

$$Z_F = \sqrt{\frac{j\omega\mu_0}{\sigma}} = \sqrt{\frac{j\omega\mu_0}{2\sigma}}(1+j). \quad (3.180b)$$

In a metal the electric field is rapidly decaying under the surface with the so-called *skin penetration depth* d_0 , given by

$$d_0 = \frac{1}{\Re\{\gamma\}} = \sqrt{\frac{2}{\omega\mu_0\sigma}}. \quad (3.181)$$

The skin effect penetration depth is inversely proportional to the square root of the frequency. For copper with a conductivity of $\sigma = 5.8 \cdot 10^7 \text{ Sm}^{-1}$ we obtain at a frequency of 10 GHz a penetration depth $d_0 = 0.66 \mu\text{m}$. The skin effect will be discussed in Chapter 6.

We assume the plane metallic surfaces of the conducting sheet oriented normally to the z -axis at $z = 0$ and $z = d$. For a uniform plane wave incident under an angle of incidence θ_1 and with the xz -plane as the plane of incidence let k_{ix} be the x -component of the wave vector. Inside the metallic sheet the propagation coefficient of the wave in z -direction is

$$\gamma_z = \sqrt{\gamma^2 + k_{ix}^2}. \quad (3.182)$$

For metallic sheets due to $k_{ix} \ll |\gamma|$ we can set

$$\gamma_z \cong \gamma. \quad (3.183)$$

This means that inside the metallic sheet the electromagnetic wave propagates as a TEM wave in the direction normal to the sheet. This allows to describe the wave propagation through the sheet by the *surface admittance matrix* Y_s or *surface impedance matrix* Z_s as introduced in [14],

$$Y_s = \frac{1}{Z_s} \begin{bmatrix} \coth \gamma d & -\operatorname{csch} \gamma d \\ -\operatorname{csch} \gamma d & \coth \gamma d \end{bmatrix}, \quad (3.184a)$$

$$Z_s = Z_s \begin{bmatrix} \coth \gamma d & -\operatorname{csch} \gamma d \\ -\operatorname{csch} \gamma d & \coth \gamma d \end{bmatrix} \quad (3.184b)$$

with $\operatorname{csch} \gamma d = 1/\sinh \gamma d$. We don't need to distinguish between the TE- and TM cases. Furthermore these relations hold for any values of k_x, k_y as long as $k_x, k_y \ll |\gamma|$ or $k_x d, k_y d \ll 1$. Assuming that the tangential electric and magnetic field components are $\underline{\mathcal{E}}_{t1}, \underline{\mathcal{H}}_{t1}$ at $z = 0$ and $\underline{\mathcal{E}}_{t2}, \underline{\mathcal{H}}_{t2}$ at $z = d$ we obtain

$$\begin{bmatrix} \underline{\mathcal{H}}_{t1} \\ -\underline{\mathcal{H}}_{t2} \end{bmatrix} = \star \, dz \wedge Y_s \begin{bmatrix} \underline{\mathcal{E}}_{t1} \\ \underline{\mathcal{E}}_{t2} \end{bmatrix}, \quad (3.185a)$$

$$\begin{bmatrix} \underline{\mathcal{E}}_{t1} \\ \underline{\mathcal{E}}_{t2} \end{bmatrix} = \star \, dz \wedge Z_s \begin{bmatrix} -\underline{\mathcal{H}}_{t1} \\ \underline{\mathcal{H}}_{t2} \end{bmatrix}. \quad (3.185b)$$

When the material conductivity σ or the thickness d of the sheet is large enough, so that $\gamma d \rightarrow \infty$ the surface impedance matrix becomes

$$Z_s = Z_s \begin{bmatrix} 1 & 0 \\ 0 & 1 \end{bmatrix} \quad \text{for } \gamma d \rightarrow \infty. \quad (3.186)$$

In this case the field does not reach through the conductive sheet and the fields satisfy on both sides of the sheet the boundary conditions

$$\underline{\mathcal{E}}_{t1} = -\star \, dz \wedge Z_s \underline{\mathcal{H}}_{t1}, \quad \underline{\mathcal{E}}_{t2} = \star \, dz \wedge Z_s \underline{\mathcal{H}}_{t2} \quad \text{for } \gamma d \rightarrow \infty. \quad (3.187)$$

These boundary conditions will be treated in detail in Section 6.2. In the limit $\gamma d \rightarrow 0$ no current is flowing in the boundary and we obtain from (2.171a)

$$\mathcal{H}_t^{(2)} - \mathcal{H}_t^{(1)} = 0 \quad \text{for } \gamma d \rightarrow 0. \quad (3.188)$$

3.8 THE VECTOR WAVE EQUATION

In the previous sections we have shown that TE and TM fields can be derived from scalar fields. A general electromagnetic field can be obtained by superposition of TE

and TM field components. In this section we revisit the *vector wave equation* and the *vector Helmholtz equation* to show that in cylindrical and spherical coordinate systems the field can be decomposed in partial fields that can be derived from scalar potentials. Within any closed domain of a homogeneous isotropic and source-free medium the electric and magnetic field forms \mathcal{E} and \mathcal{H} as well as the vector potentials \mathcal{A} , \mathcal{I}_e and \mathcal{I}_m . For \mathcal{C} denoting any of these one-forms the vector wave equation

$$\Delta \mathcal{C} - \mu\epsilon \frac{\partial^2 \mathcal{C}}{\partial t^2} = 0 \quad (3.189)$$

must be fulfilled. Due to the linearity of this equation, field solutions always can be represented by superposition of time-harmonic solutions and without loss in generality we can restrict our considerations to the solutions of the vector Helmholtz equation

$$\Delta \mathcal{C} + k^2 \mathcal{C} = 0 \quad (3.190)$$

with the wave number k defined in (3.42). With (3.14) we obtain from this for one-forms \mathcal{C} the Helmholtz equation in the form

$$d \star d \star \mathcal{C} - \star d \star d \mathcal{C} + k^2 \mathcal{C} = 0. \quad (3.191)$$

We can derive solutions of this vector Helmholtz equation from a scalar field ψ satisfying the scalar Helmholtz equation

$$\Delta \psi + k^2 \psi = 0. \quad (3.192)$$

With (3.13) this can be written as

$$\star d \star d \psi + k^2 \psi = 0. \quad (3.193)$$

From the scalar field ψ and the one-form

$$\mathbf{a} = a_x dx + a_y dy + a_z dz \quad (3.194)$$

describing a constant vector $\mathbf{a} = [a_x, a_y, a_z]^T$ we can derive a set of vector fields described by the one-forms \mathcal{L} , \mathcal{U} and \mathcal{V} as

$$\mathcal{L} = d\psi, \quad (3.195a)$$

$$\mathcal{U} = \star d(a\psi), \quad (3.195b)$$

$$\mathcal{V} = \frac{1}{k} \star d\mathcal{U}. \quad (3.195c)$$

These differential forms \mathcal{L} , \mathcal{U} , and \mathcal{V} correspond to the vector fields introduced by W.W. Hansen [2, 15–17] and therefore are called *Hansen forms*. By insertion into the vector Helmholtz equation (3.191) it can be verified easily that \mathcal{L} , \mathcal{U} , and \mathcal{V} are solutions of this equation.

From (3.195a) it follows

$$d\mathcal{L} = 0. \quad (3.196)$$

Therefore the vector field described by \mathcal{L} is irrotational. From (3.195b) and (3.195c) we obtain

$$d\star\mathcal{U} = 0, \quad d\star\mathcal{V} = 0 \quad (3.197)$$

and therefore the vector fields described by \mathcal{U} and \mathcal{V} are solenoidal. From (3.191) and (3.195b) we obtain the useful relation

$$\mathcal{U} = \frac{1}{k} \star d\mathcal{V} \quad (3.198)$$

and from (3.193) and (3.195a) it follows

$$\star d\star\mathcal{L} = -k^2\psi. \quad (3.199)$$

From (3.29a), (3.29b), (3.36a), and (3.36b) we obtain for source-free regions the electric and magnetic field forms

$$\underline{\mathcal{E}} = \star d\star d\underline{\Pi}_e - j\omega\mu\star d\underline{\Pi}_m, \quad (3.200)$$

$$\underline{\mathcal{H}} = j\omega\epsilon\star d\underline{\Pi}_e + \star d\star d\underline{\Pi}_m. \quad (3.201)$$

Suppose that the solutions of (3.28) and (3.35) for given boundary conditions may be expanded in series

$$\underline{\Pi}_e = \sum_n \underline{A}_n a \psi_{e,n}, \quad (3.202a)$$

$$\underline{\Pi}_m = \sum_n \underline{B}_n a \psi_{m,n} \quad (3.202b)$$

with the expansion coefficients A_n and B_n . In this case the electric and magnetic field forms are

$$\underline{\mathcal{E}} = \sum_n \underline{A}_n k \mathcal{V}_{e,n} - j\omega\mu \underline{B}_n \mathcal{U}_{m,n}, \quad (3.203a)$$

$$\underline{\mathcal{H}} = \sum_n j\omega\epsilon \underline{A}_n \mathcal{U}_{e,n} + \underline{B}_n k \mathcal{V}_{m,n}. \quad (3.203b)$$

with

$$\mathcal{U}_{e,n} = \star d(a\psi_{e,n}), \quad \mathcal{U}_{m,n} = \star d(a\psi_{m,n}), \quad (3.204a)$$

$$\mathcal{V}_{e,n} = \frac{1}{k} \star d\mathcal{U}_{e,n}, \quad \mathcal{V}_{m,n} = \frac{1}{k} \star d\mathcal{U}_{m,n}. \quad (3.204b)$$

The solutions with the amplitudes \underline{A}_n are transverse magnetic with respect to the direction of the vector \mathbf{a} , whereas the solutions with the amplitudes \underline{B}_n are transverse electric with respect to \mathbf{a} . The Hansen forms allow to formulate the field solutions in cylindrical and spherical coordinate systems in a systematic way.

To derive the vector field solutions from a scalar field in spherical coordinates a method described by R.F. Harrington and R.S. Elliott may be more appropriate [3, 18]. Consider the one-form

$$\mathcal{K} = \star r dr \wedge d\psi, \quad (3.205)$$

where ψ is a scalar potential satisfying the scalar Helmholtz equation (3.192). We show that in this case \mathcal{K} is a solution of the vector Helmholtz equation (3.190). From (3.205), (A.165), and (A.168) we obtain

$$\mathcal{K} = -\frac{1}{\sin\theta} \frac{\partial\psi}{\partial\phi} r d\theta + \frac{\partial\psi}{\partial\theta} r \sin\theta d\phi. \quad (3.206)$$

With the Laplace operator for a one-form in spherical coordinates (A.175) we obtain

$$\begin{aligned} \Delta\mathcal{K} = & \left[-\Delta \left(\frac{1}{\sin\theta} \frac{\partial\psi}{\partial\phi} \right) + \frac{1}{r^2 \sin^3\theta} \frac{\partial\psi}{\partial\phi} - \frac{2 \cos\theta}{r^2 \sin\theta} \frac{\partial^2\psi}{\partial\phi\partial\theta} \right] r d\theta \\ & + \left[-\frac{2 \cos\theta}{r^2 \sin^3\theta} \frac{\partial^2\psi}{\partial\phi^2} + \Delta \left(\frac{\partial\psi}{\partial\theta} \right) - \frac{1}{r^2 \sin^2\theta} \frac{\partial\psi}{\partial\theta} \right] r \sin\theta d\phi. \end{aligned} \quad (3.207)$$

With

$$\Delta \left(\frac{1}{\sin\theta} \frac{\partial\psi}{\partial\phi} \right) = \frac{1}{\sin\theta} \frac{\partial}{\partial\phi} (\Delta\psi) - \frac{2 \cos\theta}{r^2 \sin^2\theta} \frac{\partial^2\psi}{\partial\phi\partial\theta} + \frac{1}{r^2 \sin^3\theta} \frac{\partial\psi}{\partial\phi}, \quad (3.208)$$

$$\Delta \left(\frac{\partial\psi}{\partial\theta} \right) = \frac{\partial}{\partial\theta} (\Delta\psi) + \frac{1}{r^2 \sin^2\theta} \frac{\partial\psi}{\partial\theta} + \frac{2 \cos\theta}{r^2 \sin^3\theta} \frac{\partial^2\psi}{\partial\phi^2} \quad (3.209)$$

we obtain from (3.192) and (3.207)

$$\begin{aligned} \Delta\mathcal{K} = & -\frac{1}{\sin\theta} \frac{\partial}{\partial\phi} (\Delta\psi) r d\theta + \frac{\partial}{\partial\theta} (\Delta\psi) r \sin\theta d\phi \\ = & \frac{1}{\sin\theta} k^2 \frac{\partial\psi}{\partial\phi} r d\theta - k^2 \frac{\partial\psi}{\partial\theta} r \sin\theta d\phi = -k^2 \mathcal{K}, \end{aligned} \quad (3.210)$$

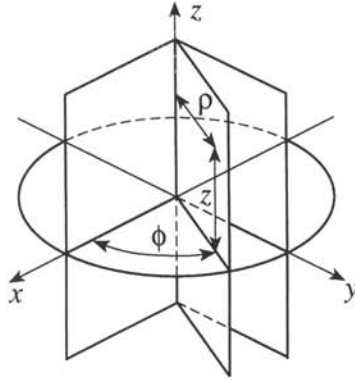


Figure 3.10: Circular cylindric coordinates.

which proves that \mathcal{K} is a solution of the vector Helmholtz equation (3.190). We can show that the field \mathcal{N} related to \mathcal{K} via

$$\mathcal{N} = \frac{1}{k} \star d\mathcal{K}, \quad \mathcal{K} = -\frac{1}{k} \star d\mathcal{N} \quad (3.211)$$

is also a solution of the the vector Helmholtz equation (3.190). The field described by \mathcal{K} is transverse with respect to dr . With \mathcal{K} we can construct independent TE and TM field solutions.

3.9 CIRCULAR CYLINDRICAL WAVES

For the analysis of *circular cylindrical electromagnetic waves* we use circular cylindrical coordinates shown in Figure 3.10. Formulae for circular cylindrical waveguides are summarized in Appendix A.4.2. We consider fields that are either transverse electric or transverse magnetic with respect to the z -axis. In these cases the solution of the Helmholtz equation (3.37) can be derived from the solutions of the scalar Helmholtz equation for the z -component of the magnetic or electric Hertz vector respectively. Fields that are neither transverse electric nor transverse magnetic may be obtained by superposition of transverse electric and transverse magnetic fields.

Due to (A.158) for an electric or magnetic Hertz form $\underline{\Pi}_e$ or $\underline{\Pi}_m$ that exhibits a z -component only,

$$\underline{\Pi}_i = \underline{\Pi}_{iz} dz \quad \text{with } i = e, m, \quad (3.212)$$

the application of the vector Laplace operator (A.158) to the $\underline{\Pi}$ reduces to the application

of the scalar Laplace operator (A.157) to the z -component only,

$$\Delta \Pi = \Delta \Pi_{iz} \, dz. \quad (3.213)$$

Thus inserting Π_i into the homogeneous Helmholtz equation (3.37) yields

$$\frac{\partial^2 \Pi_{iz}}{\partial \rho^2} + \frac{1}{\rho} \frac{\partial \Pi_{iz}}{\partial \rho} + \frac{1}{\rho^2} \frac{\partial^2 \Pi_{iz}}{\partial \phi^2} + \frac{\partial^2 \Pi_{iz}}{\partial z^2} + k_0^2 \Pi_{iz} = 0. \quad (3.214)$$

Applying the method of separation of variables we choose

$$\Pi_{iz} = R(\rho) f(\phi) Z(z). \quad (3.215)$$

Inserting this into (3.214) yields

$$\rho^2 \frac{1}{R} \frac{d^2 R}{d\rho^2} + \rho \frac{1}{R} \frac{dR}{d\rho} + \frac{1}{f} \frac{d^2 f}{d\phi^2} + \rho^2 \left(\frac{1}{Z} \frac{d^2 Z}{dz^2} + k_0^2 \right) = 0. \quad (3.216)$$

This equation can be completely separated into terms depending on one variable only. In order to fulfill the equation, each of these parts must be constant. Introducing the constant separation parameters k_ρ , n and k_z , where k_ρ and k_z fulfill the relation

$$k_\rho^2 + k_z^2 = k_0^2 \quad (3.217)$$

we obtain the separated ordinary differential equations

$$\rho^2 \frac{d^2 R}{d\rho^2} + \rho \frac{dR}{d\rho} + (\rho^2 k_\rho^2 - n^2) R = 0. \quad (3.218a)$$

$$\frac{d^2 f}{d\phi^2} + n^2 f = 0, \quad (3.218b)$$

$$\frac{d^2 Z}{dz^2} + k_z^2 Z = 0, \quad (3.218c)$$

where (3.218a) is the *Bessel's differential equation* of order n . In Appendix B.1 a detailed discussion of the Bessel's differential equation is given. The solutions are the *Bessel function* of the first kind $J_n(k_\rho \rho)$, the *Neumann function* or *Bessel function of the second kind* $Y_n(k_\rho \rho)$, and the *Hankel functions* of the first kind $H_n^{(1)}(k_\rho \rho)$ and of the second kind $H_n^{(2)}(k_\rho \rho)$. The general solution usually is expressed by a linear combination of two of these functions. The index n depends on the order of the differential equation and denotes the order of the function. The Bessel functions of first and second kind, $J_n(k_\rho \rho)$

and $Y_n(k_\rho \rho)$ respectively describe standing wave solutions with respect to ρ -direction as occurring in hollow pipes. The Hankel functions of the first kind $H_n^{(1)}(k_\rho \rho)$ describe waves propagating in negative ρ -direction and the Hankel functions of the second kind $H_n^{(2)}(k_\rho \rho)$ describe waves propagating in positive ρ -direction. The solutions of (3.218b) are $\cos n\phi$, $\sin n\phi$, $e^{-jn\phi}$ and $e^{jn\phi}$, where the solutions $\cos n\phi$ and $\sin n\phi$ describe waves standing in ϕ -direction, and the solutions $e^{-jn\phi}$ and $e^{jn\phi}$ describe fields rotating clockwise and counter-clockwise around the z axis. The z -dependence of the field is given by (3.218c). Here the solutions $\cos k_z z$ and $\sin k_z z$ describe waves standing in z -direction, and the solutions $e^{-jk_z z}$ and $e^{jk_z z}$ describe waves propagating in positive or negative z -direction, respectively.

From (3.29a), (3.29b), (3.36a), and (3.36b) we obtain the transverse magnetic and transverse electric field solutions:

TE_z modes:

$$\underline{\Pi}_m(\rho, \phi, z) = AC_n(k_\rho \rho) \cos n\phi e^{-jk_z z} dz, \quad (3.219a)$$

$$\underline{\mathcal{H}} = d\tilde{d}\underline{\Pi}_m + k_0^2 \underline{\Pi}_m, \quad (3.219b)$$

$$\underline{\mathcal{E}} = -j\omega\mu * d\underline{\Pi}_m. \quad (3.219c)$$

TM_z modes:

$$\underline{\Pi}_e(\rho, \phi, z) = BC_n(k_\rho \rho) \cos n\phi e^{-jk_z z} dz, \quad (3.220a)$$

$$\underline{\mathcal{E}} = d\tilde{d}\underline{\Pi}_e + k_0^2 \underline{\Pi}_e, \quad (3.220b)$$

$$\underline{\mathcal{H}} = j\omega\epsilon * d\underline{\Pi}_e. \quad (3.220c)$$

The TE_z and TM_z modes are transverse electric and transverse magnetic with respect to the z -direction. A and B are arbitrary complex amplitudes. The function $C_n(k_\rho \rho)$ stands for one of the solutions $J_n(k_\rho \rho)$, $Y_n(k_\rho \rho)$, $H_n^{(1)}(k_\rho \rho)$ or $H_n^{(2)}(k_\rho \rho)$. From (3.219a) to (3.220c) we obtain the field components listed in the following.

TE_z modes:

$$\underline{H}_\rho = -jk_z k_\rho AC'_n(k_\rho \rho) \cos n\phi e^{-jk_z z}, \quad (3.221a)$$

$$\underline{H}_\phi = jk_z \frac{n}{\rho} AC_n(k_\rho \rho) \sin n\phi e^{-jk_z z}, \quad (3.221b)$$

$$\underline{H}_z = k_c^2 AC_n(k_\rho \rho) \cos n\phi e^{-jk_z z}, \quad (3.221c)$$

$$\underline{E}_\rho = j\omega\mu_0 \frac{n}{\rho} AC_n(k_\rho \rho) \sin n\phi e^{-jk_z z}, \quad (3.221d)$$

$$\underline{E}_\phi = j\omega\mu_0 k_\rho AC'_n(k_\rho \rho) \cos n\phi e^{-jk_z z}, \quad (3.221e)$$

$$\underline{E}_z = 0. \quad (3.221f)$$

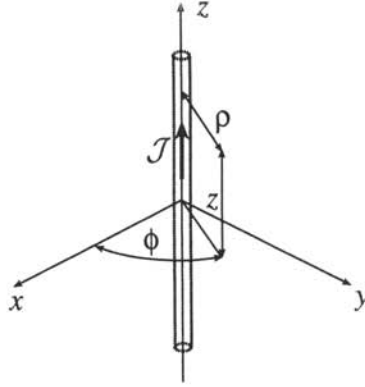


Figure 3.11: Excitation of an electromagnetic field by a current filament.

TM_z modes:

$$\underline{E}_\rho = -j k_z k_\rho B C'_n(k_\rho \rho) \cos n\phi e^{-j k_z z}, \quad (3.222a)$$

$$\underline{E}_\phi = j k_z \frac{n}{\rho} B C_n(k_\rho \rho) \sin n\phi e^{-j k_z z}, \quad (3.222b)$$

$$\underline{E}_z = k_c^2 B C_n(k_\rho \rho) \cos n\phi e^{-j k_z z}, \quad (3.222c)$$

$$\underline{H}_\rho = -j \omega \epsilon_0 \frac{n}{\rho} B C_n(k_\rho \rho) \sin n\phi e^{-j k_z z}, \quad (3.222d)$$

$$\underline{H}_\phi = -j \omega \epsilon_0 k_\rho B C'_n(k_\rho \rho) \cos n\phi e^{-j k_z z}, \quad (3.222e)$$

$$\underline{H}_z = 0. \quad (3.222f)$$

With C'_n we denote the derivative of the Bessel function C_n with respect to the argument,

$$C'_n(x) = \frac{dC_n(x)}{dx}. \quad (3.223)$$

3.9.1 Excitation of a Cylindric Wave by a Uniform Current Filament

Consider a current filament impressed at $\rho = 0$ in z -direction as shown in Figure 3.11. Let the current be time-harmonic with the complex amplitude \underline{I} and frequency ω and uniform in z -direction. If the current flows in the wall of a tube with radius a the current distribution can be described by the differential form

$$\mathcal{J} = \frac{\underline{I}}{\pi a} \delta(\rho - a) r d\rho \wedge d\phi. \quad (3.224)$$

For symmetry reasons the wave excited by this filamentary current will be transverse magnetic with respect to the z -axis and independent from the coordinates ϕ and z . From (3.222a) to (3.222f) we obtain for this case

$$\underline{E}_z = k_\rho^2 B H_0^{(2)}(k_\rho \rho), \quad (3.225a)$$

$$\underline{H}_\phi = -j \omega \epsilon_0 k_\rho B H_0^{(2)'}(k_\rho \rho). \quad (3.225b)$$

All other field components vanish. Assuming a wave propagating in positive ρ direction only we have chosen the Hankel function of the second kind, $H_0^{(2)}(k_\rho \rho)$ for the radial dependence of the wave. For $\rho \rightarrow 0$ the derivative of the Hankel function of the second kind can be approximated by

$$\lim_{\rho \rightarrow 0} H_0^{(2)'}(x) = -\frac{j}{\pi x}. \quad (3.226)$$

Applying Ampère's law (2.57a) to (3.225b) under consideration of (3.226) for $k_\rho \rho \ll 1$ yields

$$\underline{E}_z = -\frac{k_\rho^2 I}{4\omega \epsilon} H_0^{(2)}(k_\rho \rho), \quad (3.227a)$$

$$\underline{H}_\phi = \frac{j k_\rho I}{4} H_0^{(2)'}(k_\rho \rho). \quad (3.227b)$$

For the *far-field* (i.e., for $k_\rho \rho \gg 1$), we obtain the asymptotic solution

$$\underline{E}_z = -Z_F k_\rho I \sqrt{\frac{j}{8\pi}} \frac{e^{-j k_\rho \rho}}{\sqrt{k_\rho \rho}}, \quad (3.228a)$$

$$\underline{H}_\phi = k_\rho I \sqrt{\frac{j}{8\pi}} \frac{e^{-j k_\rho \rho}}{\sqrt{k_\rho \rho}}. \quad (3.228b)$$

In the far-field the ratio of the transverse electric and magnetic field is given by the characteristic impedance of the TEM wave. The field amplitudes decrease as $1/\sqrt{\rho}$ in contrast to the $1/r$ dependence of spherical waves.

3.10 SPHERICAL WAVES

Waves emitted from point-like sources are called *spherical waves* since surfaces of constant phases are spheres. Spherical waves occur in radiation problems [2–4,19]. The Helmholtz equation in spherical coordinates has a *complete set of spherical solutions*.

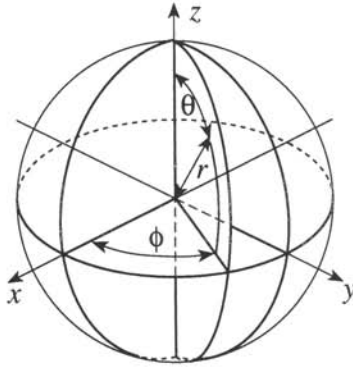


Figure 3.12: Spherical coordinates.

Waves emitted from a closed volume of limited spatial extension usually are represented by a superposition of spherical waves.

We use spherical coordinates shown in Figure 3.12. Formulae for spherical coordinates are summarized in Appendix A.4.3. The solution of the Helmholtz equation (3.28) in spherical coordinates is a difficult task since in spherical coordinates all three coordinates of the Hertz form are mixed in the Laplace operator (A.174). However, also in the case of spherical solutions the TE- and TM-wave solutions may be derived from the solution of the *scalar Helmholtz equation* in spherical coordinates. The homogeneous scalar Helmholtz equation in spherical coordinates is given by

$$\frac{1}{r^2} \frac{\partial}{\partial r} \left(r^2 \frac{\partial \Psi}{\partial r} \right) + \frac{1}{r^2 \sin \theta} \frac{\partial}{\partial \theta} \left(\sin \theta \frac{\partial \Psi}{\partial \theta} \right) + \frac{1}{r^2 \sin^2 \theta} \frac{\partial^2 \Psi}{\partial \phi^2} + k^2 \Psi = 0. \quad (3.229)$$

Introducing

$$\Psi_{nm}(r, \theta, \phi) = z_n(kr) Y_n^m(\theta, \phi) \quad (3.230)$$

the homogeneous scalar Helmholtz equation in spherical coordinates (3.229) is separated into the two differential equations (B.49) and (B.29)

$$r^2 \frac{d^2 z_n(kr)}{dr^2} + 2r \frac{dz_n(kr)}{dr} + (k^2 r^2 - n^2) z_n(kr) = 0, \quad (3.231a)$$

$$\frac{1}{\sin \theta} \frac{d}{d\theta} \left(\sin \theta \frac{dY_n^m(\theta, \phi)}{d\theta} \right) + \frac{1}{\sin^2 \theta} \frac{d^2 Y_n^m(\theta, \phi)}{d\phi^2} + n(n+1) Y_n^m(\theta, \phi) = 0, \quad (3.231b)$$

where $z_n(kr)$ is a *spherical Bessel function* $j_n(kr)$, $y_n(kr)$, $h_n^{(1)}(kr)$, or $h_n^{(2)}(kr)$ as defined in (B.32a) to (B.32d), and $Y_n^m(\theta, \phi)$ is the *spherical harmonic*, defined in (B.52).

The indices m and n can assume the values $n = 1, 2, 3, 4, \dots$ and $m = -n, -(n-1), \dots, -2, -1, 0, 1, 2, \dots, n-1, n$. For real k the solutions $j_n(kr)$ and $y_n(kr)$ represent standing waves with respect to radial direction, $h_n^{(2)}(kr)$ represents outward traveling waves and $h_n^{(1)}(kr)$ represents inward traveling waves.

If both $\Psi_{mn}^{\text{TE}}(r, \theta, \phi)$ and $\Psi_{mn}^{\text{TM}}(r, \theta, \phi)$ are two independent solutions of the scalar Helmholtz equation (3.229), we can use (3.205) to construct solutions of the vector Helmholtz equation by

$$\underline{\mathcal{E}}_{mn}^{\text{TE}} = \star (r \, dr \wedge d\Psi_{mn}^{\text{TE}}), \quad (3.232a)$$

$$\underline{\mathcal{H}}_{mn}^{\text{TE}} = -\frac{1}{j\omega\mu} \star d\underline{\mathcal{E}}_{mn}^{\text{TE}} \quad (3.232b)$$

and

$$\underline{\mathcal{H}}_{mn}^{\text{TM}} = \star (r \, dr \wedge d\Psi_{mn}^{\text{TM}}), \quad (3.233a)$$

$$\underline{\mathcal{E}}_{mn}^{\text{TM}} = \frac{1}{j\omega\epsilon} \star d\underline{\mathcal{H}}_{mn}^{\text{TM}}. \quad (3.233b)$$

From (3.232a) and (3.233a) we can see that $\underline{\mathcal{E}}_{mn}^{\text{TE}}$ and $\underline{\mathcal{H}}_{mn}^{\text{TM}}$ exhibit no longitudinal components. Therefore the solutions with the superscript TE represent the *transverse electric spherical waves* and the solutions with the superscript TM represent the *transverse magnetic waves*. In the case of spherical waves the classifications transverse electric and transverse magnetic refer to the r -direction.

Field solutions exhibiting longitudinal electric and magnetic components may be constructed by superposition of transverse electric and transverse magnetic solutions,

$$\underline{\mathcal{E}}_{mn} = \underline{\mathcal{E}}_{mn}^{\text{TE}} + \underline{\mathcal{E}}_{mn}^{\text{TM}}, \quad (3.234a)$$

$$\underline{\mathcal{H}}_{mn} = \underline{\mathcal{H}}_{mn}^{\text{TE}} + \underline{\mathcal{H}}_{mn}^{\text{TM}}. \quad (3.234b)$$

From this we obtain

$$\underline{E}_r = -\frac{n(n+1)}{j\omega\epsilon r} \Psi_{mn}^{\text{TM}}, \quad (3.235a)$$

$$\underline{E}_\theta = -\frac{1}{\sin\theta} \frac{\partial \Psi_{mn}^{\text{TE}}}{\partial \phi} - \frac{1}{j\omega\epsilon r} \frac{\partial}{\partial r} \left(r \frac{\partial \Psi_{mn}^{\text{TM}}}{\partial \theta} \right), \quad (3.235b)$$

$$\underline{E}_\phi = \frac{\partial \Psi_{mn}^{\text{TE}}}{\partial \theta} - \frac{1}{j\omega\epsilon r \sin\theta} \frac{\partial}{\partial r} \left(r \frac{\partial \Psi_{mn}^{\text{TM}}}{\partial \phi} \right), \quad (3.235c)$$

$$\underline{H}_r = \frac{n(n+1)}{j\omega\mu r} \Psi_{mn}^{\text{TE}}, \quad (3.235d)$$

$$\underline{H}_\theta = \frac{1}{j\omega\mu r} \frac{\partial}{\partial r} \left(r \frac{\partial \Psi_{mn}^{\text{TE}}}{\partial \theta} \right) - \frac{1}{\sin \theta} \frac{\partial \Psi_{mn}^{\text{TM}}}{\partial \phi}, \quad (3.235e)$$

$$\underline{H}_\phi = \frac{1}{j\omega\mu r \sin \theta} \frac{\partial}{\partial r} \left(r \frac{\partial \Psi_{mn}^{\text{TE}}}{\partial \phi} \right) + \frac{\partial \Psi_{mn}^{\text{TM}}}{\partial \theta}. \quad (3.235f)$$

Solutions containing only Ψ_{mn}^{TE} represent the TE waves and solutions containing only Ψ_{mn}^{TM} represent the TM waves.

If all sources of the electromagnetic field are located within a sphere of radius R outside this sphere only outward traveling waves exist. The outward traveling waves may be described by a superposition of waves with the radial dependence given by $h_n^{(2)}(kr)$. The operator $\partial/\partial r$ when applied to e^{-jkr} gives $-jk$. Application of the $\partial/\partial r$ to all other terms gives rise to terms of the order $(1/r)^2$ or higher. In the *far-field approximation* $kr \gg 1$ we keep only the terms of the order $1/r$. Therefore, we can replace the operator $\partial/\partial r$ by jk and obtain the far-field approximation

$$\underline{E}_r = 0, \quad (3.236a)$$

$$\underline{E}_\theta = -\frac{1}{\sin \theta} \frac{\partial \Psi_{mn}^{\text{TE}}}{\partial \phi} + Z_F \frac{\partial \Psi_{mn}^{\text{TM}}}{\partial \theta}, \quad (3.236b)$$

$$\underline{E}_\phi = \frac{\partial \Psi_{mn}^{\text{TE}}}{\partial \theta} + \frac{Z_F}{\sin \theta} \frac{\partial \Psi_{mn}^{\text{TM}}}{\partial \phi}, \quad (3.236c)$$

$$\underline{H}_r = 0, \quad (3.236d)$$

$$\underline{H}_\theta = -\frac{1}{Z_F} \frac{\partial \Psi_{mn}^{\text{TE}}}{\partial \theta} - \frac{1}{\sin \theta} \frac{\partial \Psi_{mn}^{\text{TM}}}{\partial \phi}, \quad (3.236e)$$

$$\underline{H}_\phi = -\frac{1}{Z_F \sin \theta} \frac{\partial \Psi_{mn}^{\text{TE}}}{\partial \phi} + \frac{\partial \Psi_{mn}^{\text{TM}}}{\partial \theta}. \quad (3.236f)$$

From these equations we obtain in the far-field

$$\underline{E}_\theta \cong Z_F \underline{H}_\phi \quad \underline{E}_\phi \cong -Z_F \underline{H}_\theta. \quad (3.237)$$

We can summarize (3.237) in the *Sommerfeld radiation condition*

$$\lim_{r \rightarrow \infty} (\underline{\mathcal{E}} + Z_F \star d\mathbf{r} \wedge \underline{\mathcal{H}}) = 0. \quad (3.238a)$$

The Sommerfeld radiation condition may also be written in the form

$$\lim_{r \rightarrow \infty} (\underline{\mathcal{H}} - Z_F^{-1} \star d\mathbf{r} \wedge \underline{\mathcal{E}}) = 0. \quad (3.238b)$$

It can be shown that the Sommerfeld radiation condition holds for an electromagnetic field generated by any source distribution confined in a volume V of finite extension around $r = 0$. The proof may be given by expanding the field outside V into spherical waves. A general proof of the Sommerfeld radiation condition is given for example in [18]. The radiation condition requires that the electric and magnetic fields bear the relation to each other found in wave propagation in regions remote from the sources.

3.11 PROBLEMS

1. Besides the Lorenz gauge another useful gauge for the potentials is the so-called *Coulomb, radiation, or transverse* gauge for which $d \star \mathcal{A} = 0$. Derive the second-order partial differential equations for \mathcal{A} and Φ in the Coulomb gauge.
2. Show that the Laplace operator applied to a zero-form, (3.13), in conventional vector notation corresponds to $\Delta\Phi = \text{div grad } \Phi$, where Φ is a scalar function.
3. Show that the Laplace operator applied to a one-form, (3.14), in conventional vector notation corresponds to $\Delta\mathbf{A} = \text{grad div } \mathbf{A} - \text{curl curl } \mathbf{A}$, where \mathbf{A} is a vector function.
4. Assume that the impressed current \mathcal{J} can be expressed as the superposition $\mathcal{J} = \mathcal{J}_l + \mathcal{J}_t$ of a *longitudinal* or *irrotational* current \mathcal{J}_l with the property $d \star \mathcal{J}_l = 0$ and a *transverse* or *solenoidal* current \mathcal{J}_t with the property $d\mathcal{J}_t = 0$. Show that in the Coulomb gauge the transverse current is the source of the vector field \mathcal{A} and the longitudinal current is the source of the scalar field Φ .
5. For an electromagnetic wave propagating in a lossless homogeneous isotropic medium the electric Hertz form is given by $\Pi_e = (Ax + By) \cos(\omega t - kz + \phi) dz$.
 - a) Show that the Hertz vector satisfies the wave equation.
 - b) Compute the electric and magnetic fields.
6. Show that (3.20a) and (3.20b) correspond to

$$E = \text{grad div } \Pi_e - \mu\epsilon \frac{\partial^2}{\partial t^2} \Pi_e - \mu\sigma \frac{\partial}{\partial t} \Pi_e,$$

$$H = \text{curl} \left(\epsilon \frac{\partial}{\partial t} \Pi_e + \sigma \Pi_e \right),$$

where Π_e is the electric Hertz vector and E and H are the electric and magnetic field vectors.

7. Consider a perfectly conducting circular cylinder of radius a in free-space. Let the electromagnetic field outside the cylinder be described by the magnetic Hertz form $\underline{\Pi}_m = [f(r) + g(\phi)] e^{jkz} dz$.
 - a) Determine $f(r)$, $g(\phi)$, and k so that $\underline{\Pi}_m$ is a solution of the homogeneous Helmholtz equation.

- b) Compute the electromagnetic field satisfying the boundary condition at the surface of the perfectly conducting cylinder.
8. In the plane $z = 0$ at time $t = 0$ an electric surface polarization \mathcal{M}_{eA} is turned on. This is described by $\mathcal{M}_{eA} = \begin{cases} J_0 t \, dy & \text{for } t \geq 0 \\ 0 & \text{for } t < 0 \end{cases}$. The region $z \neq 0$ is free-space.
 - a) Compute the electric Hertz vector field due to this polarization.
 - b) Compute the electromagnetic wave excited by this polarization.
9. In the plane $z = 0$ a magnetic surface polarization $\underline{\mathcal{M}}_{mA}$ is impressed. This is described by $\underline{\mathcal{M}}_{mA} = \underline{M}_{0Ax} \, dx e^{jky}$. The region $z \neq 0$ is free-space.
 - a) Compute the magnetic Hertz vector field due to this polarization.
 - b) Compute the electromagnetic wave excited by this polarization.
10. Express the solutions of transverse electromagnetic plane waves propagating in free-space in $\pm z$ -direction in terms of the components of the vector potentials \underline{A} and \underline{I}_e .
11. Express the solutions of TE and TM plane waves propagating in free-space in z -direction in terms of the components of the vector potentials \underline{I}_e and \underline{I}_m . Consider all four cases.
12. Consider a plane dielectric plate with thickness d and material parameters $\epsilon_r = 9$, $\mu_r = 1$. The incident plane wave is right-hand circularly polarized with electric field amplitude \underline{E}_0 .
 - a) Compute the electric and magnetic field amplitudes of the reflected and transmitted waves.
 - b) Determine the angle of incidence θ_0 and the thickness d to obtain linear polarization of incident and reflected waves.
13. Consider a plane wave incident on a dielectric plate of thickness d with $\epsilon_r = 2.25$ and $\mu_r = 1$.
 - a) Determine d such that a normally incident wave is not reflected.
 - b) Compute reflection and transmission factors for the same thickness d and arbitrary polarization of the incident wave for skew incidence.

REFERENCES

- [1] A. Sommerfeld, *Elektrodynamik*. Leipzig: Akademische Verlagsgesellschaft Geest & Portig, 1947.
- [2] J. A. Stratton, *Electromagnetic Theory*. New York: McGraw-Hill, 1941.
- [3] R. F. Harrington, *Time Harmonic Electromagnetic Fields*. New York: McGraw-Hill, 1961.
- [4] J. A. Kong, *Electromagnetic Wave Theory*. New York: John Wiley & Sons, 1986.
- [5] L. Lorenz, "On the identity of the vibrations of light with electrical currents," *Philosophical Magazine and Journal of Science*, vol. 34, pp. 287–301, July–December 1867.
- [6] R. Nevels and C.-S. Shin, "Lorenz, Lorentz, and the gauge," *IEEE Trans. Antennas Propagat. Magazine*, vol. 43, pp. 69–70, June 2001.
- [7] H. Hertz, "Die Kräfte electrischer Schwingungen behandelt nach der Maxwell'schen Theorie," *Ann. Phys. Chem.*, vol. 3. Folge 36, no. 1, pp. 1–22, 1889.

- [8] H. Hertz, "Über Strahlen electrischer Kraft," *Ann. Phys. Chem.*, vol. 3. Folge 36, no. 4, pp. 769–783, 1889.
- [9] H. J. Carlin and A. B. Giordano, *Network Theory*. Englewood Cliffs, NJ: Prentice Hall, 1964.
- [10] C. A. Balanis, *Advanced Engineering Electromagnetics*. New York: John Wiley & Sons, 1989.
- [11] P. C. Clemmow, *The Plane Wave Spectrum Representation of Electromagnetic Fields*. New York: Pergamon Press, 1966.
- [12] A. Ishimaru, *Electromagnetic Wave Propagation, Radiation, and Scattering*. Englewood Cliffs, NJ: Prentice Hall, 1991.
- [13] F. Goos and H. Hänchen, "A new and fundamental experiment on total reflection," *Annalen der Physik*, vol. 6, no. 1, pp. 333–346, 1947.
- [14] J. Kessler, R. Dill, P. Russer, and A. A. Valenzuela, "Property calculations of a superconducting coplanar waveguide resonator," *Proc. 20th European Microwave Conference, Budapest*, pp. 798–903, Sept. 1990.
- [15] W. W. Hansen, "A new type of expansion in radiation problems," *Phys. Rev.*, vol. 47, pp. 139–143, Jan. 1935.
- [16] W. W. Hansen and J. G. Beckerley, "Radiation from an antenna over a plane earth of arbitrary characteristics," *Physics*, vol. 7, pp. 220–224, June 1936.
- [17] W. W. Hansen, "Transformations useful in certain antenna calculations," *J. Appl. Physics*, vol. 8, pp. 282–286, Sept. 1937.
- [18] R. S. Elliott, *Electromagnetics – History, Theory, and Applications*. New York: IEEE Press, 1991.
- [19] L. B. Felsen and N. Marcuvitz, *Radiation and Scattering of Waves*. Englewood Cliffs, NJ: Prentice Hall, 1972.

Chapter 4

Concepts, Methods, and Theorems

4.1 ENERGY AND POWER

The field concept is based upon the hypothesis that electromagnetic energy is distributed over the space. The electric and magnetic fields carry energy and changing electric and magnetic energy densities are related to power flow in space [1–6]. We introduce the *electric energy density* $w_e(\mathbf{x}, t)$ and the *magnetic energy density* $w_m(\mathbf{x}, t)$ with the corresponding three-forms

$$\mathcal{W}_e = w_e(\mathbf{x}, t) \, dx \wedge dy \wedge dz , \quad (4.1a)$$

$$\mathcal{W}_m = w_m(\mathbf{x}, t) \, dx \wedge dy \wedge dz . \quad (4.1b)$$

The energy densities are given by

$$\mathcal{W}_e = \frac{1}{2} \mathcal{E} \wedge \mathcal{D} = \frac{1}{2} (E_x D_x + E_y D_y + E_z D_z) \, dx \wedge dy \wedge dz , \quad (4.2a)$$

$$\mathcal{W}_m = \frac{1}{2} \mathcal{H} \wedge \mathcal{B} = \frac{1}{2} (H_x B_x + H_y B_y + H_z B_z) \, dx \wedge dy \wedge dz . \quad (4.2b)$$

Figure 4.1 visualizes the exterior product of the field one-form \mathcal{E} and the flux density two-form \mathcal{D} . The resulting three-form is visualized by the subdivision of the space into cells. The number of cells per unit of volume is proportional to the electric energy density.

In order to investigate energy storage and power flow in the electromagnetic field, we start again with Maxwell's equations (2.114a) and (2.114b). Exterior multiplication of Ampère's law from the left with $-\mathcal{E}$ and of Faraday's law from the right with \mathcal{H} yields

$$-\mathcal{E} \wedge \left| \quad \quad \quad d\mathcal{H} = \dot{\mathcal{D}} + \mathcal{J} , \quad (4.3)$$

$$d\mathcal{E} = -\dot{\mathcal{B}} \quad \left| \quad \quad \wedge \mathcal{H} , \quad (4.4)$$

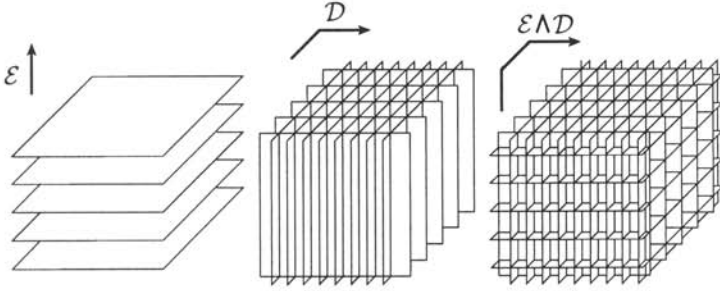


Figure 4.1: The exterior product of the field form \mathcal{E} and the flux density form \mathcal{D} .

where the dot means the partial derivative with respect to t , that is, $\dot{\mathcal{D}} = (\partial/\partial t)\mathcal{D}$. This yields

$$d(\mathcal{E} \wedge \mathcal{H}) = -\mathcal{E} \wedge \dot{\mathcal{D}} - \mathcal{H} \wedge \dot{\mathcal{B}} - \mathcal{E} \wedge \mathcal{J}. \quad (4.5)$$

This equation can be brought into the form

$$d(\mathcal{E} \wedge \mathcal{H}) = -\frac{\partial}{\partial t} \left(\frac{1}{2} \mathcal{E} \wedge \mathcal{D} + \frac{1}{2} \mathcal{H} \wedge \mathcal{B} \right) - \mathcal{E} \wedge \mathcal{J}. \quad (4.6)$$

The *power loss density* $p_L(\mathbf{x}, t)$ with the corresponding differential form

$$\mathcal{P}_L(\mathbf{x}, t) = p_L(\mathbf{x}, t) dx \wedge dy \wedge dz \quad (4.7)$$

is given by

$$\mathcal{P}_L = \mathcal{E} \wedge \sigma \star \mathcal{E}. \quad (4.8)$$

Due to the impressed current density \mathbf{J}_0 , a power per unit of volume $p_0(\mathbf{x}, t)$ is added to the electromagnetic field. With the differential form

$$\mathcal{P}_0(\mathbf{x}, t) = p_0(\mathbf{x}, t) dx \wedge dy \wedge dz \quad (4.9)$$

the power added to the field by the impressed current \mathcal{J}_0 is given by

$$\mathcal{P}_0 = -\mathcal{E} \wedge \mathcal{J}_0. \quad (4.10)$$

We introduce the *Poynting vector* $\mathbf{S}(\mathbf{x}, t)$ with the corresponding *Poynting differential form*

$$\mathcal{S}(\mathbf{x}, t) = S_x dy \wedge dz + S_y dz \wedge dx + S_z dx \wedge dy, \quad (4.11)$$

given by

$$\mathcal{S} = \mathcal{E} \wedge \mathcal{H}. \quad (4.12)$$

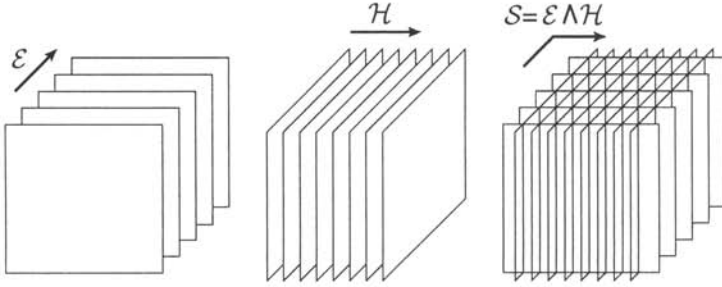


Figure 4.2: The Poynting form S as the product of the field forms E and H .

Figure 4.2 visualizes the Poynting two-form as the exterior product of the electric and magnetic field one-forms E and H . The potential planes of the electric and magnetic fields together form the tubes of the Poynting form. The distance of the electric and magnetic potential planes exhibit the dimensions V and A , respectively. The cross-sectional areas of the flux tubes have the dimension VA . This yields the assumption that the Poynting form describes a power flow through these flux tubes. The proof for this assumption will be given in the following.

Inserting (4.2a), (4.2b), (4.8), and (4.10) into (4.6) yields the local form of *Poynting's theorem*:

$$dS = -\frac{\partial}{\partial t} \mathcal{W}_e - \frac{\partial}{\partial t} \mathcal{W}_m - \mathcal{P}_L + \mathcal{P}_0. \quad (4.13)$$

Integrating (4.13) over a volume V and transforming the integral over S into a surface integral over the boundary ∂V , we obtain the integral form of *Poynting's theorem*:

$$\oint_{\partial V} S = \int_V \mathcal{P}_0 - \frac{d}{dt} \int_V \mathcal{W}_e - \frac{d}{dt} \int_V \mathcal{W}_m - \int_V \mathcal{P}_L. \quad (4.14)$$

The first term on the right side of (4.14) describes the power added into the volume V via impressed currents. The second and third term describe the time variation of the electric and magnetic energy stored in the volume. The last term describes the conductive losses occurring inside the volume V . The right side of the equation comprises the total electromagnetic power generated within the volume V minus the power losses in the volume minus the increase of electric and magnetic energy stored in the volume. This net power must be equal to the power, which is flowing out from the volume V through the boundary ∂V . Therefore we may interpret the surface integral over the Poynting vector on the left side of (4.14) as the total power flowing from inside the volume V to the outside. Since this is valid for an arbitrary choice of volume V , it follows that the Poynting vector describes the energy flowing per units of time through a unit area oriented perpendicular to S .

For time-harmonic electromagnetic fields, the introduction of a *complex Poynting vector* is useful. For this we multiply the complex conjugate of (2.123a) from the left with $(-\underline{\mathcal{E}})$ and (2.123b) from the right with $\underline{\mathcal{H}}^*$ and obtain

$$-\underline{\mathcal{E}} \wedge \left| \quad d\underline{\mathcal{H}}^* = -j\omega \underline{\epsilon}^* \star \underline{\mathcal{E}}^* + \underline{\mathcal{J}}_0^* \right. , \quad (4.15a)$$

$$\left. d\underline{\mathcal{E}} = -j\omega \underline{\mu} \star \underline{\mathcal{H}} \right| \wedge \underline{\mathcal{H}}^* . \quad (4.15b)$$

Forming the sum of both equations, we obtain

$$d\left(\frac{1}{2} \underline{\mathcal{E}} \wedge \underline{\mathcal{H}}^*\right) = -2j\omega \left(\frac{1}{4} \underline{\mu} \underline{\mathcal{H}}^* \wedge \star \underline{\mathcal{H}} - \frac{1}{4} \underline{\epsilon}^* \underline{\mathcal{E}} \wedge \star \underline{\mathcal{E}}^*\right) - \frac{1}{2} \underline{\mathcal{E}} \wedge \underline{\mathcal{J}}_0^* . \quad (4.16)$$

We now introduce the *complex Poynting vector*

$$\underline{T} = [T_x, T_y, T_z]^T \quad (4.17)$$

with the corresponding differential form

$$\underline{\mathcal{T}} = T_x dy \wedge dz + T_y dz \wedge dx + T_z dx \wedge dy , \quad (4.18)$$

given by

$$\underline{\mathcal{T}} = \frac{1}{2} \underline{\mathcal{E}} \wedge \underline{\mathcal{H}}^* . \quad (4.19)$$

We have to note that $\underline{\mathcal{T}}$ is not the phasor corresponding to \underline{S} . Therefore we have used a different character to distinguish between the complex Poynting vector and the real Poynting vector. In order to give an interpretation of the complex Poynting vector \underline{T} , we compute first the time-dependent Poynting vector form \underline{S} for a time-harmonic electromagnetic field

$$\underline{\mathcal{E}}(\underline{x}, t) = \Re \{ \underline{\mathcal{E}}(\underline{x}) e^{j\omega t} \} = \frac{1}{2} \left(\underline{\mathcal{E}}(\underline{x}) e^{j\omega t} + \underline{\mathcal{E}}^*(\underline{x}) e^{-j\omega t} \right) , \quad (4.20a)$$

$$\underline{\mathcal{H}}(\underline{x}, t) = \Re \{ \underline{\mathcal{H}}(\underline{x}) e^{j\omega t} \} = \frac{1}{2} \left(\underline{\mathcal{H}}(\underline{x}) e^{j\omega t} + \underline{\mathcal{H}}^*(\underline{x}) e^{-j\omega t} \right) . \quad (4.20b)$$

Inserting into (4.12) we obtain

$$\underline{S}(\underline{x}, t) = \frac{1}{2} \Re \{ \underline{\mathcal{E}}(\underline{x}) \wedge \underline{\mathcal{H}}^*(\underline{x}) \} + \frac{1}{2} \Re \{ \underline{\mathcal{E}}(\underline{x}) \wedge \underline{\mathcal{H}}(\underline{x}) e^{2j\omega t} \} . \quad (4.21)$$

The first term on the right side of (4.21) is equal to the real part of the complex Poynting form $\underline{\mathcal{T}}$ according to (4.19). This term is independent of time. The second term on the

right side of (4.21) oscillates with the double frequency of the alternating electromagnetic field. The time average of this part vanishes. Therefore the real part of the complex Poynting vector form \mathcal{T} is the time average of the Poynting form \mathcal{S} .

$$\overline{\mathcal{S}(\mathbf{x}, t)} = \Re \{ \mathcal{T}(\mathbf{x}) \}. \quad (4.22)$$

The real part of the complex Poynting form \mathcal{T} denotes the power flowing through a unit area surface element oriented perpendicular to the Poynting vector.

For time-harmonic fields the time averages of the electric and magnetic energy densities \overline{w}_e and \overline{w}_m and the corresponding differential forms are related via

$$\overline{\mathcal{W}}_e = \overline{w}_e \, dx \wedge dy \wedge dz, \quad (4.23)$$

$$\overline{\mathcal{W}}_m = \overline{w}_m \, dx \wedge dy \wedge dz. \quad (4.24)$$

The *time-average electric and magnetic energy density forms* are given by

$$\overline{\mathcal{W}}_e = \frac{1}{4} \epsilon' \underline{\mathcal{E}} \wedge \star \underline{\mathcal{E}}^* = \frac{1}{4} \epsilon' (|\underline{\mathcal{E}}_x|^2 + |\underline{\mathcal{E}}_y|^2 + |\underline{\mathcal{E}}_z|^2) \, dx \wedge dy \wedge dz, \quad (4.25)$$

$$\overline{\mathcal{W}}_m = \frac{1}{4} \mu' \underline{\mathcal{H}} \wedge \star \underline{\mathcal{H}}^* = \frac{1}{4} \mu' (|\underline{\mathcal{H}}_x|^2 + |\underline{\mathcal{H}}_y|^2 + |\underline{\mathcal{H}}_z|^2) \, dx \wedge dy \wedge dz. \quad (4.26)$$

We have to consider that the quantities ϵ' and μ' in the complex representation correspond to the quantities ϵ and μ in the time-dependent formulation. The *time-average electric power dissipation density* \overline{p}_{Le} with the differential form

$$\overline{\mathcal{P}}_{Le} = \overline{p}_{Le} \, dx \wedge dy \wedge dz \quad (4.27)$$

is given by the differential form

$$\overline{\mathcal{P}}_{Le} = \frac{1}{2} \sigma \underline{\mathcal{E}} \wedge \star \underline{\mathcal{E}}^* = \frac{1}{2} \omega \epsilon'' \underline{\mathcal{E}} \wedge \star \underline{\mathcal{E}}^*. \quad (4.28)$$

The introduction of the complex permittivity $\underline{\mu}$ allows also to consider the magnetic losses with the average magnetic power dissipation density \overline{p}_{Lm} with the differential form

$$\overline{\mathcal{P}}_{Lm} = \overline{p}_{Lm} \, dx \wedge dy \wedge dz \quad (4.29)$$

given by

$$\overline{\mathcal{P}}_{Lm} = \frac{1}{2} \omega \mu'' \underline{\mathcal{H}} \wedge \star \underline{\mathcal{H}}^*. \quad (4.30)$$

The total average power dissipation density is described by the differential form

$$\overline{\mathcal{P}}_L = \frac{1}{2} \omega \epsilon'' \underline{\mathcal{E}} \wedge \star \underline{\mathcal{E}}^* + \frac{1}{2} \omega \mu'' \underline{\mathcal{H}} \wedge \star \underline{\mathcal{H}}^*. \quad (4.31)$$

The complex power added to the field per unit volume, $P_{c0}(\mathbf{x})$ due to the impressed current density \mathbf{J}_0 is described by the differential form

$$\mathcal{P}_{c0} = P_{c0} \, d\mathbf{x} \wedge d\mathbf{y} \wedge d\mathbf{z}. \quad (4.32)$$

The differential form describing the complex power added via the impressed current $\underline{\mathcal{J}}_0$ is

$$\mathcal{P}_{c0} = -\frac{1}{2} \underline{\mathcal{E}} \wedge \underline{\mathcal{J}}_0^*. \quad (4.33)$$

The real part of P_{c0} equals the time average \bar{P}_0 according to equation (4.22).

$$\bar{P}_0 = \Re \{ P_{c0} \}. \quad (4.34)$$

The proof is similar to equation (4.22).

After inserting of (4.19), (4.25), (4.26), (4.31), and (4.33) into (4.16), we obtain the local form of the *complex Poynting's theorem*:

$$d\mathcal{T} = -2j\omega(\overline{\mathcal{W}}_m - \overline{\mathcal{W}}_e) - \overline{\mathcal{P}}_L + \mathcal{P}_{c0}. \quad (4.35)$$

By integration over a volume V , we obtain the *integral form of the complex Poynting's theorem*

$$\oint_{\partial V} \mathcal{T} = \int_V \mathcal{P}_{c0} - 2j\omega \int_V (\overline{\mathcal{W}}_m - \overline{\mathcal{W}}_e) - \int_V \overline{\mathcal{P}}_L. \quad (4.36)$$

We consider first the real part of (4.36):

$$\Re \left\{ \oint_{\partial V} \mathcal{T} \right\} = \Re \left\{ \int_V \mathcal{P}_{c0} \right\} - \int_V \overline{\mathcal{P}}_L. \quad (4.37)$$

The left side of (4.37) equals the active power radiated from inside the volume V through the boundary ∂V . On the right side of this equation, the first term denotes the power added via the impressed current density \mathbf{J}_0 ; the second term describes the conductive losses, the dielectric losses and the magnetic losses inside the volume V . The imaginary part of (4.37) is

$$\Im \left\{ \oint_{\partial V} \mathcal{T} \right\} = \Im \left\{ \int_V \mathcal{P}_{c0} \right\} - 2\omega \int_V (\overline{\mathcal{W}}_m - \overline{\mathcal{W}}_e). \quad (4.38)$$

The first term on the right side gives the reactive power added into the volume V via the impressed current density \mathbf{J}_0 . Let us first consider the case where the second term on the right side is vanishing. In this case we see that the left side of (4.38) denotes the reactive power radiated from volume V . Since the volume V can be chosen arbitrarily, it follows that the imaginary part of the complex Poynting vector \mathbf{T} describes the reactive power radiated through a unit area normally oriented to the vector \mathbf{T} . The second term

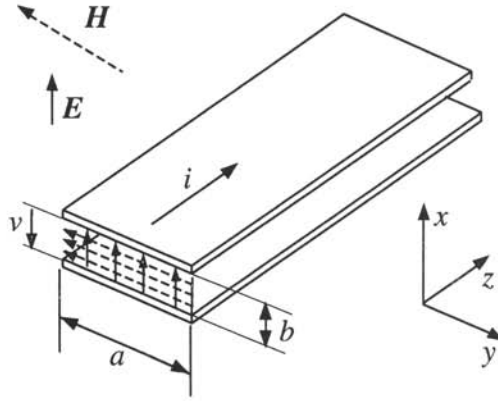


Figure 4.3: Power flow in a stripline.

on the right side of (4.38) contains the product of the double angular frequency with the difference of the average stored magnetic and electric energies. This term yields no contribution, if the magnetic energy stored in the volume V equals the average electric energy stored in V . The magnetic energy as well as electric energy oscillate with an angular frequency 2ω .

The field energy is permanently converted between electric energy and magnetic energy. If the averages \bar{w}_e and \bar{w}_m are equal, electric and magnetic energies may be mutually converted completely. In this case the energy oscillates between electric and magnetic fields inside the volume V . If the average electric and magnetic energies are not equal, energy as well oscillates between volume V and the space outside V . In this case there is a reactive power flow between V and the outer region. For $\bar{w}_m > \bar{w}_e$ the reactive power flowing into volume V is positive, whereas for $\bar{w}_m < \bar{w}_e$ the reactive power flowing into V is negative.

To give an example for the relation between the description by voltages and currents and the electromagnetic field description let us consider the *stripline* depicted in Figure 4.3. We assume a transverse electromagnetic wave to propagate in positive z -direction. In the case of a transverse electromagnetic wave neither the electric field nor the magnetic field exhibits a z -component. Let us furthermore assume the distance b between both conductor strips to be small compared with the width a of the strips. The electric power P transported via the line in the positive z -direction is given by

$$P = v i. \quad (4.39)$$

The voltage v and the current i are given by

$$v = - \int_{x=0}^b \mathcal{E} = - \int_{x=0}^b E_x \, dx = b E_x, \quad (4.40a)$$

$$i = \int_{y=0}^a \mathcal{H} = \int_{y=0}^a H_y \, dy = a H_y. \quad (4.40b)$$

In the *network concept* the electric power is considered to be carried by voltage and current. In the *field concept*, the electric power is considered to be transported via the electromagnetic field. The electromagnetic power flux density is represented by the *Poynting form* S given by

$$S = E_x H_y \, dx \wedge dy. \quad (4.41)$$

If E and H are orthogonal, the vectors E , H and S form a positive-oriented orthogonal trihedron. In Figure 4.3 the Poynting vector $S(\mathbf{x}, t)$ is directed in the positive z -direction, with z -component S_z .

$$P = \int_A S = \int_A E_x H_y \, dx \wedge dy. \quad (4.42)$$

We obtain the power P flowing through the stripline by multiplying the power density S with the cross-sectional area $a b$ of the stripline and obtain

$$P = a b E_x H_y. \quad (4.43)$$

Inserting (4.40a) and (4.40b) into this equation yields (4.39). The network concept and the field concept give the same result.

4.2 FIELD THEORETIC FORMULATION OF TELLEGEN'S THEOREM

Complex electromagnetic structures may be subdivided into several spatial subdomains. Comparing a distributed circuit represented by an electromagnetic structure with a lumped element circuit represented by a network, the spatial subdomains may be considered as the circuit elements whereas the complete set of boundary surfaces separating the subdomains corresponds to the connection circuit [7]. Figure 4.4 shows the segmentation of an electromagnetic structure into different regions \mathcal{R}_l separated by boundaries B_{lk} . The dashed curves denote the boundaries. The regions \mathcal{R}_l may contain any electromagnetic substructure. In our network analogy the two-dimensional manifold of all boundary surfaces B_{lk} represents the connection circuit whereas the

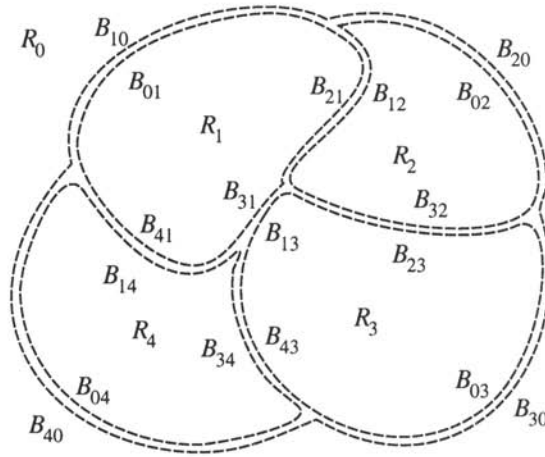


Figure 4.4: Segmentation of an electromagnetic structure.

subdomains R_l are representing the circuit elements. We can establish a field representation of *Tellegen's theorem* relating the tangential electric and magnetic fields on the two-dimensional manifolds of boundaries B_{lk} [8].

Tellegen's theorem states fundamental relations between voltages and currents in a network and is of considerable versatility and generality in network theory [8–10]. A noticeable property of this theorem is that it is only based on Kirchhoff's current and voltage laws (i.e., on topological relationships) and that it is independent from the constitutive laws of the network. The same reasoning that yields from Kirchhoff's laws to Tellegen's theorem allows us to directly derive a field form of Tellegen's theorem from Maxwell's equations [8].

In order to derive Tellegen's theorem for partitioned electromagnetic structures let us consider two electromagnetic structures based on the same partition by equal boundary surfaces. The subdomains of either electromagnetic structure, however, may be filled with different materials. The connection network is established via the relations of the tangential field components on both sides of the boundaries. Since the connection network exhibits zero volume no field energy is stored therein and no power loss occurs therein.

Starting directly from Maxwell's equations we may derive for a closed volume V

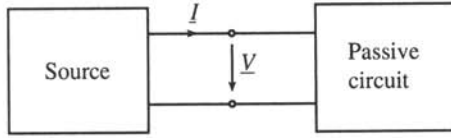


Figure 4.5: Connection of a passive circuit with a source.

with boundary surface ∂V the following relation:

$$\oint_{\partial V} \mathcal{E}'(\mathbf{x}, t') \wedge \mathcal{H}''(\mathbf{x}, t'') = - \int_V \mathcal{E}'(\mathbf{x}, t') \wedge \mathcal{J}''(\mathbf{x}, t'') - \int_V \mathcal{E}'(\mathbf{x}, t') \wedge \frac{\partial \mathcal{D}''(\mathbf{x}, t'')}{\partial t''} - \int_V \mathcal{H}'(\mathbf{x}, t') \wedge \frac{\partial \mathcal{B}''(\mathbf{x}, t'')}{\partial t''}. \quad (4.44)$$

The prime ' and double prime '' denote the case of a different choice of sources and a different choice of materials filling the subdomains. Furthermore the time argument may be different in both cases.

For volumes V of zero measure or free of field the right side of this equation vanishes. Considering an electromagnetic structure as shown in Figure 4.4, we perform the integration over the boundaries of all subregions not filled with ideal electric or magnetic conductors, respectively. The integration over both sides of a boundary yields zero contribution to the integrals on the right side of (4.44). Also the integration over finite volumes filled with ideal electric or magnetic conductors gives no contribution to these integrals. We obtain the *field form of Tellegen's theorem*:

$$\oint_{\partial V} \mathcal{E}'(\mathbf{x}, t') \wedge \mathcal{H}''(\mathbf{x}, t'') = 0. \quad (4.45)$$

Tellegen's theorem is a very powerful theorem yielding important applications in the segmentation of electromagnetic structures and in circuit theory. In Section 10.3 Tellegen's theorem will be treated from the network point of view.

4.3 SOURCES OF THE ELECTROMAGNETIC FIELD

In the network concept, electric sources are modeled using ideal current sources or ideal voltage sources, respectively. Ideal current sources or voltage sources impress a current or a voltage, respectively, into the network. Sources may be modeled by parallel circuiting an ideal current source and an admittance or series circuiting an ideal voltage source and an impedance. In this fashion, we obtain a simple phenomenological description of sources without having to consider the complicated structure

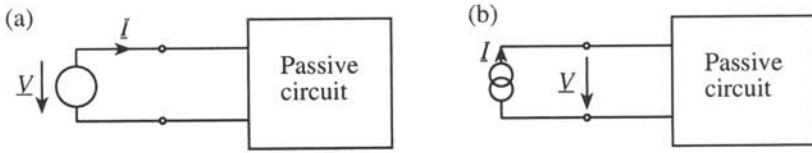


Figure 4.6: Introduction of (a) an equivalent voltage source \underline{V} , and (b) an equivalent current source \underline{I} .

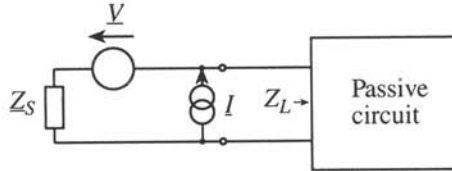


Figure 4.7: Introduction of an equivalent voltage source \underline{V} and an equivalent current source \underline{I} together.

of real sources in detail. In the same way we can establish a simple phenomenological description of electromagnetic field sources [3].

Figure 4.5 shows the connection of a network source with a passive network. The network source and the passive network are connected via one pair of nodes. From the network source a current \underline{I} is flowing into the passive network. At the pair of nodes a voltage \underline{V} is occurring. The node current \underline{I} and node voltage \underline{V} are related via

$$\underline{V} = Z_L \underline{I}, \quad (4.46)$$

where Z_L is the impedance of the passive network. If the node current \underline{I} and the node voltage \underline{V} are known, it is possible to replace the source with a voltage source \underline{V} or a current source \underline{I} . Figure 4.6(a) shows the introduction of an equivalent voltage source \underline{V} , and Figure 4.6(b) shows the introduction of an equivalent current source \underline{I} . It is also possible to introduce an equivalent current source \underline{I} and an equivalent voltage source \underline{V} together as shown in Figure 4.7. Whereas in Figure 4.6(a) the impedance of the source is replaced with a short circuit, and in Figure 4.6(b) the impedance of the source is replaced by an open circuit, we can insert a source impedance Z_S in Figure 4.7. Due to (4.46) in Figure 4.7, no current is flowing through Z_S and no voltage is applied to Z_S . This means that we can replace Z_S by an arbitrary impedance also including a short circuit and an open circuit. Replacing Z_S with a short circuit, we can omit the current source in Figure 4.7 and we have reduced the source to an impressed voltage source as in Figure 4.6(a). If, however, Z_S is replaced by an open circuit, we can omit the impressed voltage source \underline{V} , and we obtain an equivalent circuit as shown in Figure 4.6(b).

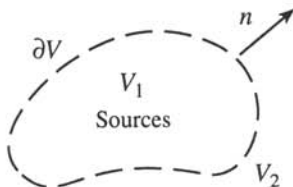


Figure 4.8: Field sources in a volume V_1 .

4.4 THE UNIQUENESS THEOREM

Figure 4.8 shows a number of field sources within a volume V_1 . The volume V_1 is bounded by the virtual boundary ∂V_1 . In our network model of the source we only were interested in investigating the passive circuit and decided not to investigate the source in detail. Therefore we have chosen a simple model for the source. We have an analogous situation in our field model, where we are only interested in the field outside V_1 , which is generated by the sources located within the volume V_1 . We will try to replace the field sources inside volume V_1 by impressed equivalent polarizations at the boundary surface ∂V_1 . To do this, we first prove the so-called *uniqueness theorem* [3, 5], which states:

The electromagnetic field in the source-free outer region V_2 is determined in a unique way, if the tangential component of either the electric field intensity or the magnetic field intensity is known on the boundary surface ∂V_1 .

To prove the uniqueness theorem, we will show that the opposite assumption will yield a wrong result. Let us assume that in the outer region V_2 there exist two different field solutions \underline{E}_a and \underline{H}_a on the one hand, and \underline{E}_b and \underline{H}_b on the other hand. Both exhibit the same tangential electric and magnetic field components on ∂V . The difference between field solutions $\delta \underline{E} = \underline{E}_a - \underline{E}_b$, $\delta \underline{H} = \underline{H}_a - \underline{H}_b$ due to the linearity of the field equations must also be a field solution. In this case, however, either $\delta \underline{E}$ or $\delta \underline{H}$ has no tangential field component on ∂V . Consequently the complex Poynting differential form \mathcal{T} due to (4.19) has no component normal to ∂V , and the surface integral of \mathcal{T} over ∂V vanishes. We now apply the real part of (4.36) to the outer region V_2 . Since the left side of (4.37) vanishes, and since V_2 is free of sources, also the first term on the right side vanishes, and the integral of the average power loss density p_v over V_2 also must vanish. Due to (4.31) the integrand is positive definite and can in the case of arbitrarily small electric and magnetic losses only vanish, if in the complete outer region V_2 , $\delta \underline{E} = \mathbf{0}$ as well as $\delta \underline{H} = \mathbf{0}$ are fulfilled. This means that in V_2 the identities $\underline{E}_a = \underline{E}_b$ as well as $\underline{H}_a = \underline{H}_b$ are fulfilled and consequently the definition of the tangential components of either \underline{E}_a or \underline{H}_a on ∂V determines the electromagnetic

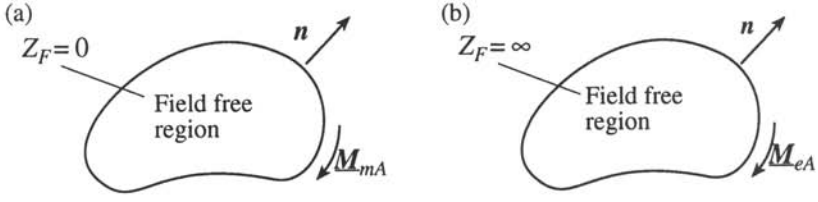


Figure 4.9: (a) Magnetic surface polarization \underline{M}_{mA} impressed on an ideal electric conductor, and (b) electric surface polarization \underline{M}_{eA} impressed on an ideal magnetic conductor.

field in the outer space in a unique way. This proves the uniqueness theorem.

4.5 THE EQUIVALENCE PRINCIPLE

Many source distributions outside a certain region may yield the same field distribution inside that region. Two source distributions outside a region producing the same field distribution inside this region are said to be *equivalent* within that region. This is called the *equivalence principle* [3]. The equivalence principle follows directly from the uniqueness theorem and is an expression of the *Huygens' principle*. Due to the uniqueness theorem different source distributions inside a volume V that produce the same tangential electric or magnetic field distribution on the boundary ∂V will produce the same electromagnetic field outside the volume V .

The uniqueness theorem makes it possible to replace the sources in the volume V_1 by surface polarizations impressed into the boundary surface ∂V . In the same way we have replaced the source in Figure 4.5 by a current source in series with a short circuit in Figure 4.6(b), now we may replace the virtual boundary surface ∂V in Figure 4.8 by a real boundary surface ∂V formed by an ideal conductor as shown in Figure 4.9(a). We impress a magnetic surface polarization \underline{M}_{mA} given by

$$\underline{M}_{mA}(\mathbf{x}') = -\frac{1}{j\omega} n \lrcorner (n \wedge \underline{\mathcal{E}}) = -\frac{1}{j\omega} \underline{\mathcal{E}}_t \quad (4.47)$$

on this conductor, where $\underline{\mathcal{E}}$ is the electric field intensity on ∂V as specified in Figure 4.8. Since we assumed an ideal conductor inside the boundary, now the electric field within V_1 is vanishing. This means that due to (2.175c), the tangential component of the electric field outside ∂V is determined in a unique way. We have assumed that there is no source in the outer region V_2 . Therefore due to the uniqueness theorem on the boundary ∂V the tangential component of the electric field also determines its normal component. The replacement of the source by an equivalent current source in the network model in Figure 4.6(b) corresponds to the insertion of an ideal magnetic conductor ($Z_F = \infty$)

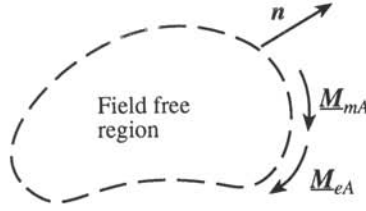


Figure 4.10: Electric surface polarization \underline{M}_{eA} and magnetic area polarization \underline{M}_{mA} impressed in a virtual boundary surface.

in the boundary surface ∂V and replacement of the sources in the volume V_1 by an electric surface polarization \underline{M}_{eA} on ∂V . The electric area polarization is given by

$$\underline{M}_{eA}(\mathbf{x}') = \frac{1}{j\omega} \mathbf{n} \cdot (\mathbf{n} \wedge \underline{\mathcal{H}}) = \frac{1}{j\omega} \underline{\mathcal{H}}_t. \quad (4.48)$$

Since the magnetic field inside the boundary ∂V vanishes, due to (2.175b) for an electric surface polarization \underline{M}_{eA} impressed on the boundary ∂V the tangential magnetic field on the outer surface of ∂V is determined in a unique way. Figure 4.9(b) illustrates the impression of electric surface polarization sources on an ideal magnetic conductor. The ideal conductor in support of the impressed magnetic polarization as shown in Figure 4.9(a) corresponds to the short-circuit in series to the ideal voltage source in Figure 4.6(a) and the ideal magnetic conductor in support of the impressed electric polarization according to Figure 4.9(b) corresponds to the open-circuit in series to the ideal voltage source in Figure 4.6(b).

The combination of impressed voltage sources and impressed current sources due to Figure 4.7 yields an analogous field model. We remove in Figure 4.8 the field sources in the inner region V_1 and impress in ∂V magnetic as well as electric surface polarizations \underline{M}_{mA} and \underline{M}_{eA} , respectively, such that in the inner region V_1 the electromagnetic field vanishes completely, and in the outer region V_2 the electromagnetic field corresponds to the electromagnetic field as generated before by the sources in V_1 . Figure 4.10 illustrates this arrangement. The replacement of the inner field sources by the impressed surface polarizations \underline{M}_{mA} and \underline{M}_{eA} is accomplished by choosing the impressed surface polarizations according to (4.47) and (4.48). Due to (2.175b) and (2.175c) this choice of the equivalent polarizations is compatible with a vanishing field in the inner region V_1 and the field produced by the original field sources in the outer region V_2 . Since in Figure 4.10 both regions V_1 as well as V_2 contain no sources due to the uniqueness theorem this solution also is the only existing solution. Since V_2 is free of field, any medium without sources introduced into the region V_1 does not influence the field in V_2 . This case corresponds to the introduction of a voltage source and a current source in the network model according to Figure 4.7.

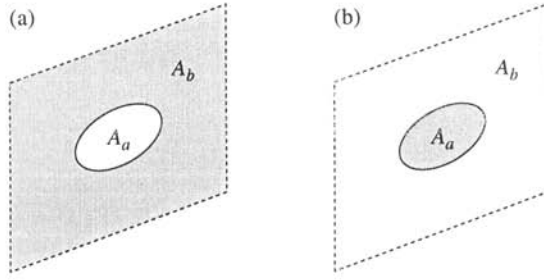


Figure 4.11: Complementary screens: (a) aperture in a conducting screen, and (b) complementary screen.

4.6 BABINET'S PRINCIPLE

Consider a screen with an aperture and its complementary screen as depicted in Figure 4.11. We compare a primary field scattered by the aperture with the field scattered by the complementary screen. There exists an interesting relation between the fields scattered by the aperture and its complementary screen expressed by *Babinet's principle* [11–15]. It states:

The sum of a field behind a plane screen and the field behind the complementary screen is equal to the field if there were no screen present.

Let $\underline{\mathcal{E}}^i, \underline{\mathcal{H}}^i$ be the primary electromagnetic field without a screen, $\underline{\mathcal{E}}^s, \underline{\mathcal{H}}^s$ the scattered field when the screen with an aperture is present, as shown in Figure 4.11(a). In Figure 4.11(a) the aperture surface is denominated with A_a and the surface of the surrounding screen with A_b . The total field $\underline{\mathcal{E}}_1, \underline{\mathcal{H}}_1$ in this case is

$$\underline{\mathcal{E}}_1 = \underline{\mathcal{E}}^i + \underline{\mathcal{E}}^s, \quad (4.49a)$$

$$\underline{\mathcal{H}}_1 = \underline{\mathcal{H}}^i + \underline{\mathcal{H}}^s. \quad (4.49b)$$

In the aperture plane the fields $\underline{\mathcal{E}}_1$ and $\underline{\mathcal{H}}_1$ fulfill the boundary conditions (2.168a) and (2.168c), hence

$$n \wedge \underline{\mathcal{E}}_1 = 0 \quad \text{on } A_b, \quad (4.50a)$$

$$n \wedge \underline{\mathcal{H}}_1 = n \wedge \underline{\mathcal{H}}^i \quad \text{on } A_a, \quad (4.50b)$$

where n is the unit normal form of the screen. Let us now replace the aperture by a thin perfectly magnetic conducting sheet and remove the screen. This yields the complementary structure shown in Figure 4.11(b). Let $\underline{\mathcal{E}}^i, \underline{\mathcal{H}}^i$ be the same primary

electromagnetic field as above, $\underline{\mathcal{E}}^c$, $\underline{\mathcal{H}}^c$ the scattered field when the magnetic conductor screen is present, as shown in Figure 4.11(b). In this case the total field $\underline{\mathcal{E}}_2$, $\underline{\mathcal{H}}_2$ is

$$\underline{\mathcal{E}}_2 = \underline{\mathcal{E}}^i + \underline{\mathcal{E}}^c, \quad (4.51a)$$

$$\underline{\mathcal{H}}_2 = \underline{\mathcal{H}}^i + \underline{\mathcal{H}}^c. \quad (4.51b)$$

This field satisfies the boundary conditions

$$n \wedge \underline{\mathcal{E}}_2 = n \wedge \underline{\mathcal{E}}^i \quad \text{on } A_b, \quad (4.52a)$$

$$n \wedge \underline{\mathcal{H}}_2 = 0 \quad \text{on } A_a. \quad (4.52b)$$

Now consider the superposition of the fields $\underline{\mathcal{E}}_1 + \underline{\mathcal{E}}_2$, $\underline{\mathcal{H}}_1 + \underline{\mathcal{H}}_2$. From (4.50a), (4.50b), (4.52a), and (4.52b) we obtain

$$n \wedge (\underline{\mathcal{E}}_1 + \underline{\mathcal{E}}_2) = n \wedge \underline{\mathcal{E}}^i \quad \text{on } A_b, \quad (4.53a)$$

$$n \wedge (\underline{\mathcal{H}}_1 + \underline{\mathcal{H}}_2) = n \wedge \underline{\mathcal{H}}^i \quad \text{on } A_a. \quad (4.53b)$$

Since the sum of the tangential fields on the infinitely extended surface $A_a \cup A_b$ is equal to the primary field $\underline{\mathcal{E}}^i$, $\underline{\mathcal{H}}^i$ we conclude from the uniqueness theorem presented in Section 4.4 that the sum of the fields $\underline{\mathcal{E}}_1 + \underline{\mathcal{E}}_2$, $\underline{\mathcal{H}}_1 + \underline{\mathcal{H}}_2$ is identical to the primary field, hence

$$\underline{\mathcal{E}}_1 + \underline{\mathcal{E}}_2 = \underline{\mathcal{E}}^i, \quad (4.54a)$$

$$\underline{\mathcal{H}}_1 + \underline{\mathcal{H}}_2 = \underline{\mathcal{H}}^i. \quad (4.54b)$$

Since we have related the field scattered by a perfectly electric conducting (PEC) screen to the field scattered by the complementary perfectly magnetic conducting (PMC) screen, we can apply the principle of duality discussed in Section 3.2 to determine the electromagnetic field scattered by the complementary PEC screen. Let the surface A_a be covered by a PEC. Furthermore let us replace the primary field $\underline{\mathcal{E}}^i$, $\underline{\mathcal{H}}^i$ according to (3.31a) and (3.31b) by the dual primary field $\underline{\mathcal{E}}^{id}$, $\underline{\mathcal{H}}^{id}$

$$\underline{\mathcal{E}}^{id} = -Z_F \underline{\mathcal{H}}^i, \quad (4.55a)$$

$$\underline{\mathcal{H}}^{id} = \frac{1}{Z_F} \underline{\mathcal{E}}^i. \quad (4.55b)$$

That means we have to replace the primary field sources by the dual field sources as described in Section 3.2. Then the total field $\underline{\mathcal{E}}_2^d$, $\underline{\mathcal{H}}_2^d$ also is dual to $\underline{\mathcal{E}}_2$, $\underline{\mathcal{H}}_2$, hence

$$\underline{\mathcal{E}}_2^d = -Z_F \underline{\mathcal{H}}_2, \quad (4.56a)$$

$$\underline{\mathcal{H}}_2^d = \frac{1}{Z_F} \underline{\mathcal{E}}_2. \quad (4.56b)$$

Inserting (4.54a) and (4.54b), this yields

$$\underline{\mathcal{E}}_2^d = -Z_F(\underline{\mathcal{H}}^i - \underline{\mathcal{H}}_1), \quad (4.57a)$$

$$\underline{\mathcal{H}}_2^d = \frac{1}{Z_F}(\underline{\mathcal{E}}^i - \underline{\mathcal{E}}_1). \quad (4.57b)$$

This is the form of Babinet's principle relating the fields scattered by an aperture and a complementary screen provided that the screen and complementary screen both are PECs and the incident electromagnetic field in both cases is dual to each other.

4.7 RECIPROCITY

4.7.1 The Lorentz Reciprocity Theorem

We consider the electromagnetic field excited by various field sources. We combine these field sources into sets of field sources. Each of these sets of field sources may contain an arbitrary distribution of impressed electric polarization sources $\underline{M}_{e0i}(\mathbf{x})$ and an arbitrary distribution of impressed magnetic polarizations $\underline{M}_{m0i}(\mathbf{x})$ with $i = 1, 2, \dots, n$. Let $\underline{E}_i(\mathbf{x})$ and $\underline{H}_i(\mathbf{x})$ be the electromagnetic field excited by the polarization distributions \underline{M}_{e0i} and \underline{M}_{m0i} . From (3.27a) and (3.30b) it follows

$$d\underline{\mathcal{H}}_i = j\omega (\underline{\epsilon} \star \underline{\mathcal{E}}_i + \underline{M}_{e0i}), \quad (4.58a)$$

$$d\underline{\mathcal{E}}_i = -j\omega (\underline{\mu} \star \underline{\mathcal{H}}_i + \underline{M}_{m0i}). \quad (4.58b)$$

Let us now compute the expression

$$\begin{aligned} d(\underline{\mathcal{E}}_i \wedge \underline{\mathcal{H}}_j) &= d\underline{\mathcal{E}}_i \wedge \underline{\mathcal{H}}_j - \underline{\mathcal{E}}_i \wedge d\underline{\mathcal{H}}_j \\ &= -j\omega \left[\underline{\epsilon} \underline{\mathcal{E}}_i \wedge (\star \underline{\mathcal{E}}_j) + \underline{\mu} (\star \underline{\mathcal{H}}_i) \wedge \underline{\mathcal{H}}_j + \underline{M}_{m0i} \wedge \underline{\mathcal{H}}_j + \underline{\mathcal{E}}_i \wedge \underline{M}_{e0j} \right]. \end{aligned} \quad (4.59)$$

After interchanging i and j and forming the difference of both equations, we obtain

$$\begin{aligned} &- d(\underline{\mathcal{E}}_i \wedge \underline{\mathcal{H}}_j - \underline{\mathcal{E}}_j \wedge \underline{\mathcal{H}}_i) \\ &= j\omega \left[\underline{\mathcal{E}}_i \wedge \underline{M}_{e0j} - \underline{\mathcal{H}}_i \wedge \underline{M}_{m0j} - \underline{\mathcal{E}}_j \wedge \underline{M}_{e0i} + \underline{\mathcal{H}}_j \wedge \underline{M}_{m0i} \right]. \end{aligned} \quad (4.60)$$

In a source-free subregion of the space the right side of (4.60) disappears and we obtain the so-called *Lorentz reciprocity theorem*, which states the following: In source-free regions and for isotropic materials the electromagnetic fields $\underline{E}_i, \underline{H}_i$ and $\underline{E}_j, \underline{H}_j$, respectively, excited from different sets of sources $\underline{M}_{e0i}, \underline{M}_{m0i}$ and $\underline{M}_{e0j}, \underline{M}_{m0j}$, respectively, satisfy the equation

$$d(\underline{\mathcal{E}}_i \wedge \underline{\mathcal{H}}_j - \underline{\mathcal{E}}_j \wedge \underline{\mathcal{H}}_i) = 0. \quad (4.61)$$

Integrating this equation over a source-free subdomain V of the space and converting the volume integral into a surface integral by using Stokes' law we obtain the integral form of the *Lorentz reciprocity theorem*

$$\oint_{\partial V} (\underline{\mathcal{E}}_i \wedge \underline{\mathcal{H}}_j - \underline{\mathcal{E}}_j \wedge \underline{\mathcal{H}}_i) = 0. \quad (4.62)$$

4.7.2 The Reciprocity Theorem for Impressed Sources

We now derive from (4.60) another useful form of the theorem of reciprocity. For this purpose we integrate (4.60) over a volume V , where we are transforming the left-hand side into a surface integral over the boundary ∂V .

$$\begin{aligned} - \oint_{\partial V} (\underline{\mathcal{E}}_i \wedge \underline{\mathcal{H}}_j - \underline{\mathcal{E}}_j \wedge \underline{\mathcal{H}}_i) \\ = j\omega \int_V [\underline{\mathcal{E}}_i \wedge \underline{\mathcal{M}}_{e0j} - \underline{\mathcal{H}}_i \wedge \underline{\mathcal{M}}_{m0j} - \underline{\mathcal{E}}_j \wedge \underline{\mathcal{M}}_{e0i} + \underline{\mathcal{H}}_j \wedge \underline{\mathcal{M}}_{m0i}] . \end{aligned} \quad (4.63)$$

$\underline{\mathcal{M}}_{e0i}$, $\underline{\mathcal{M}}_{m0i}$ and $\underline{\mathcal{M}}_{e0j}$, $\underline{\mathcal{M}}_{m0j}$, respectively, are mutually independent distributions of impressed field sources of the source sets i and j . $\underline{\mathcal{E}}_i$, $\underline{\mathcal{H}}_i$, and $\underline{\mathcal{E}}_j$, $\underline{\mathcal{H}}_j$, respectively, are the fields excited by the sets of field source sets i and j . We now are choosing a volume of integration V such that all field sources of the i th group as well as the field sources of the j th group are located in the volume V and choose the boundary ∂V sufficiently far in the far-field so that all the field sources of the i th and the j th set form together a point-like source, if they are observed from any point on the boundary ∂V . Since we may choose the volume V arbitrarily this condition may be fulfilled with an arbitrary accuracy.

We now embed our electromagnetic structure in a spherical volume V with radius r_V and let $r_V \rightarrow \infty$. From the Sommerfeld radiation condition (3.238b) we obtain on the boundary ∂V of the volume V

$$\underline{\mathcal{E}}_i \wedge \underline{\mathcal{H}}_j = \underline{\mathcal{E}}_j \wedge \underline{\mathcal{H}}_i = \frac{1}{Z_{F0}} (\underline{E}_{\theta i} \underline{E}_{\theta j} + \underline{E}_{\phi i} \underline{E}_{\phi j}) r^2 \sin \theta d\theta \wedge d\phi. \quad (4.64)$$

Since the field components are of order $(1/r)$ this expression remains finite for $r \rightarrow \infty$. Therefore the left-hand side of (4.63) vanishes, if we are expanding the volume V into infinity. Integrating over the complete space, the following relation is fulfilled exactly

$$j\omega \int_V [\underline{\mathcal{E}}_i \wedge \underline{\mathcal{M}}_{e0j} - \underline{\mathcal{H}}_i \wedge \underline{\mathcal{M}}_{m0j}] = j\omega \int_V [\underline{\mathcal{E}}_j \wedge \underline{\mathcal{M}}_{e0i} - \underline{\mathcal{H}}_j \wedge \underline{\mathcal{M}}_{m0i}] . \quad (4.65)$$

The integral on the left side describes the *reaction* [3, 16] of the field $\underline{\mathcal{E}}_i$, $\underline{\mathcal{H}}_i$ on the sources $\underline{\mathcal{M}}_{e0j}$, $\underline{\mathcal{M}}_{m0j}$. This is another useful formulation of the reciprocity theorem. We

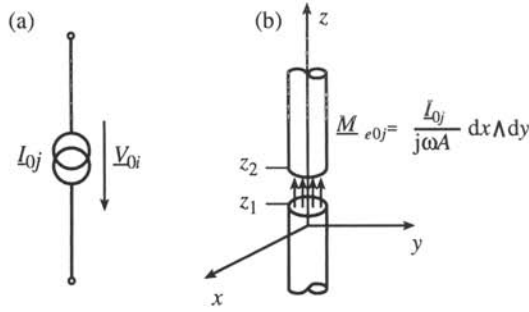


Figure 4.12: Impressed current source (a) in the network concept, and (b) in the field concept.

define the so-called *reaction* R_{ij} of a field $\underline{E}_i, \underline{H}_i$ on the sources $\underline{M}_{e0j}, \underline{M}_{m0j}$ by

$$R_{ij} = j\omega \int_V [\underline{\mathcal{E}}_i \wedge \underline{M}_{e0j} - \underline{\mathcal{H}}_i \wedge \underline{M}_{m0j}] . \quad (4.66)$$

The *reciprocity theorem* according to (4.65) now can be written in the form

$$R_{ij} = R_{ji} . \quad (4.67)$$

The reaction of a field $\underline{E}_i, \underline{H}_i$ on the sources $\underline{M}_{e0j}, \underline{M}_{m0j}$ is equal to the reaction of a field $\underline{E}_j, \underline{H}_j$ on the sources $\underline{M}_{e0i}, \underline{M}_{m0i}$. As an example we compute the reaction of a voltage \underline{V}_i on a current source \underline{I}_{0j} according to Figure 4.12(a). In a field an impressed current source \underline{I}_{0j} can be represented, for example, by a polarization density impressed into a gap of a conductor. Let us impress a polarization

$$\underline{M}_{e0j} = \frac{\underline{I}_{0j}}{j\omega A} dx \wedge dy \quad (4.68)$$

into the gap between the two conductors in Figure 4.12(b). Inserting (3.23) and integrating over the cross-sectional area A verifies this relation. According to (4.66) the reaction of the field \underline{E}_i on the network-source \underline{I}_{0j} is given by

$$R_{ij} = \frac{\underline{I}_{0j}}{A} \int_{V_{0j}} \underline{E}_{iz} dx \wedge dy \wedge dz . \quad (4.69)$$

Performing the integration over the gap region where the impressed polarization \underline{M}_{e0j} exhibits a nonzero value yields

$$\int_{z_1}^{z_2} \underline{E}_{iz} dz = -\underline{V}_i . \quad (4.70)$$

From this we obtain

$$R_{ij} = -\underline{V}_i \underline{I}_{0j}, \quad (4.71)$$

where \underline{V}_i is the node voltage due to the field \underline{E}_i across the nodes of the current source \underline{I}_{0j} . From this and from (4.67) we obtain

$$\underline{V}_i \underline{I}_{0j} = \underline{V}_j \underline{I}_{0i}. \quad (4.72)$$

The port voltages of source-free linear multiports may be represented by the system of equations

$$\underline{V}_i = \sum_j Z_{ij} \underline{I}_{0j}, \quad (4.73)$$

if the \underline{I}_{0j} are the impressed port currents. With (4.67) we obtain from this the condition

$$Z_{ij} = Z_{ji}. \quad (4.74)$$

This is the *network form of the reciprocity theorem*.

4.8 GREEN'S FUNCTION

The reciprocity theorem reveals the relationships between two sets of sources and fields. The mathematical structures constituting these relationships are represented by *Green's theorems* and *Green's functions*. In his work *An Essay on the Application of Mathematical Analysis to the Theories of Electricity and Magnetism* published in 1828, George Green presented a method to solve Poisson's equation in electrostatic potential theory [17, 18]. The method is based on the superposition of functions representing the potentials of point or line sources of unit magnitude. A three-dimensional Green's function $G(\mathbf{x}, \mathbf{x}')$ describes the field at point \mathbf{x} due to a unit point source at \mathbf{x}' . Since any source distribution may be considered a continuous superposition of unit point sources, the field generated by arbitrary source distributions is obtained by superposition of the field contributions of point sources with the source distribution as the weighting function. Green's function technique has been very widely applied to equations arising in field theory and is a fundamental method for solving problems in electromagnetics [2, 19–24]. Reciprocity is expressed by the symmetry of Green's function $G(\mathbf{x}, \mathbf{x}')$ in \mathbf{x} and \mathbf{x}' .

A point-like excitation by an impressed electric or magnetic polarization yields a spherical electromagnetic wave. The computation of the electromagnetic wave due to a point-like excitation is of fundamental importance for the computation of electromagnetic waves excited by arbitrary source distributions since the field generated by arbitrary distributions may be computed by superimposing the fields originating from point-like sources. This follows from the application of the superposition principle and

from the circumstance that every source distribution may be considered as a continuous superposition of point-like sources. The mathematical formulation of this problem yields *Green's function*.

To compute the electromagnetic field generated by electric or magnetic polarizations impressed in space we have to solve the inhomogeneous Helmholtz' equations (3.28) or (3.35), respectively, for arbitrary spatial distribution of the impressed electric polarization \underline{M}_{e0} or the impressed magnetic polarization \underline{M}_{m0} , respectively. Using (3.42), we obtain the Helmholtz' equations

$$\Delta \underline{\Pi}_e + k^2 \underline{\Pi}_e = -\frac{1}{\epsilon} * \underline{M}_{e0}, \quad (4.75a)$$

$$\Delta \underline{\Pi}_m + k^2 \underline{\Pi}_m = -\frac{1}{\mu} * \underline{M}_{m0}. \quad (4.75b)$$

Since we can make use of the principle of duality in the following, it will be sufficient to solve (4.75a). To compute the field at a point \mathbf{x} excited by a point-like source located at \mathbf{x}' we use *Green's double one-form* [25, 26], also called *dyadic Green's form*, defined by

$$\begin{aligned} \underline{G} = & \underline{G}_{11} dx dx' + \underline{G}_{12} dx dy' + \underline{G}_{13} dx dz' \\ & + \underline{G}_{21} dy dx' + \underline{G}_{22} dy dy' + \underline{G}_{23} dy dz' \\ & + \underline{G}_{31} dz dx' + \underline{G}_{32} dz dy' + \underline{G}_{33} dz dz'. \end{aligned} \quad (4.76)$$

We introduce the so-called *identity kernel*

$$\mathcal{I}(\mathbf{x}, \mathbf{x}') = \delta(\mathbf{x} - \mathbf{x}') (dx dx' + dy dy' + dz dz') \quad (4.77)$$

and the *three-dimensional Dirac delta distribution*

$$\delta(\mathbf{x} - \mathbf{x}') = \delta(x - x') \delta(y - y') \delta(z - z'). \quad (4.78)$$

From (D.45) we obtain

$$\int_V \delta(\mathbf{x} - \mathbf{x}') dx \wedge dy \wedge dz = \begin{cases} 1 & \text{for } \mathbf{x}' \in V \\ 0 & \text{for } \mathbf{x}' \notin V \end{cases}. \quad (4.79)$$

For an arbitrary smooth scalar function $f(\mathbf{x})$ we obtain as the three-dimensional generalization of (D.47) the relation

$$\int f(\mathbf{x}) \delta(\mathbf{x} - \mathbf{x}') dx \wedge dy \wedge dz = \begin{cases} f(\mathbf{x}') & \text{for } \mathbf{x}' \in V \\ 0 & \text{for } \mathbf{x}' \notin V \end{cases}. \quad (4.80)$$

With the identity kernel we can map any one-form \mathcal{U} and any two-form \mathcal{V} from the source space to the observation space (i.e., the respective form is mapped in itself and the primed differentials are replaced by unprimed differentials). We obtain

$$\int' \mathcal{I}(\mathbf{x}, \mathbf{x}') \wedge \star \mathcal{U}(\mathbf{x}') = \mathcal{U}(\mathbf{x}) , \quad (4.81a)$$

$$\star \int' \mathcal{I}(\mathbf{x}, \mathbf{x}') \wedge \mathcal{V}(\mathbf{x}') = \mathcal{V}(\mathbf{x}) . \quad (4.81b)$$

The primed integration symbol denotes that the integration is performed over the primed variables. For the integration the unprimed differentials are treated as constants.

Using Green's double one-form we can express the Helmholtz equation (4.75a) for a point-like unit source at \mathbf{x}' by

$$\Delta \underline{\mathcal{G}}(\mathbf{x}, \mathbf{x}') + k^2 \underline{\mathcal{G}}(\mathbf{x}, \mathbf{x}') = -\frac{1}{\epsilon} \mathcal{I}(\mathbf{x}, \mathbf{x}') , \quad (4.82)$$

where $\mathcal{I}(\mathbf{x}, \mathbf{x}')$ is the identity kernel, introduced in (4.77). In the above equation the Laplace operator acts on the unprimed differentials whereas the primed differentials are treated as constants. Forming the exterior product with $\underline{\mathcal{M}}_{e0}(\mathbf{x}')$ integrating over the primed variables and using (4.81b) yields

$$\int' [\Delta \underline{\mathcal{G}}(\mathbf{x}, \mathbf{x}') \wedge \underline{\mathcal{M}}_{e0}(\mathbf{x}') + k^2 \underline{\mathcal{G}}(\mathbf{x}, \mathbf{x}') \wedge \underline{\mathcal{M}}_{e0}(\mathbf{x}')] = -\frac{1}{\epsilon} \star \underline{\mathcal{M}}_{e0}(\mathbf{x}) . \quad (4.83)$$

Since the sequence of partial derivation with respect to the unprimed coordinates and integration over the primed coordinates may be interchanged, under very general conditions we obtain

$$\Delta \left[\int' \underline{\mathcal{G}}(\mathbf{x}, \mathbf{x}') \wedge \underline{\mathcal{M}}_{e0}(\mathbf{x}') \right] + k^2 \left[\int' \underline{\mathcal{G}}(\mathbf{x}, \mathbf{x}') \wedge \underline{\mathcal{M}}_{e0}(\mathbf{x}') \right] = -\frac{1}{\epsilon} \star \underline{\mathcal{M}}_{e0}(\mathbf{x}) . \quad (4.84)$$

Comparing this equation with (4.75a) yields

$$\underline{\Pi}_e(\mathbf{x}) = \int' \underline{\mathcal{G}}(\mathbf{x}, \mathbf{x}') \wedge \underline{\mathcal{M}}_{e0}(\mathbf{x}') . \quad (4.85)$$

In Cartesian coordinates the Laplace operator for one-forms (A.73) is symmetric in its three components and leaves the three components uncoupled. Therefore (4.84) may be solved with

$$\underline{\mathcal{G}}(\mathbf{x}, \mathbf{x}') = \underline{G}(\mathbf{x}, \mathbf{x}') (dx dx' + dy dy' + dz dz') . \quad (4.86)$$

where $\underline{G}(\mathbf{x}, \mathbf{x}')$ is a *scalar Green's function*, obtained by solving the scalar Helmholtz equation

$$(\Delta + k^2)\underline{G}(\mathbf{x}, \mathbf{x}') = -\frac{1}{\epsilon} \delta(\mathbf{x} - \mathbf{x}') . \quad (4.87)$$

In the infinitely extended homogeneous isotropic space the scalar Green's function $\underline{G}(\mathbf{x}, \mathbf{x}')$ must exhibit spherical symmetry and therefore can only depend on the magnitude $r = |\mathbf{r}|$ of the distance vector $\mathbf{r} = \mathbf{x} - \mathbf{x}'$ between the points \mathbf{x} and \mathbf{x}' . We introduce spherical coordinates at the origin $r = 0$. With the scalar Laplace operator in spherical coordinates (A.174) we obtain from (4.87) considering the spherical symmetry

$$\frac{1}{r} \frac{d^2}{dr^2} (r \underline{G}(r)) + k^2 \underline{G}(r) = -\frac{1}{\epsilon} \delta(r) . \quad (4.88)$$

With the exception of the origin $r = 0$, $\underline{G}(r)$ satisfies the homogeneous differential equation

$$\frac{d^2}{dr^2} (r \underline{G}(r)) + k^2 (r \underline{G}(r)) = 0 . \quad (4.89)$$

The solution is given by

$$r \underline{G}(r) = \underline{A} e^{-jkr} + \underline{B} e^{jkr} , \quad (4.90)$$

where \underline{A} and \underline{B} are complex coefficients not yet determined. The first term on the right side of (4.90) describes a wave propagating from the origin $r = 0$ into the space, whereas the second term describes a wave propagating into the origin. The second solution does not occur for physical reasons; therefore we set $\underline{B} = 0$ in the following. To determine \underline{A} we consider the field in a small neighborhood of the point source. We assume the extension of this neighborhood to be much smaller than the wavelength λ . Therefore $|kr| \ll 1$, and k may be neglected in (4.87) and (4.89). Within this approximation we obtain

$$\underline{G}_0(r) = \lim_{k \rightarrow 0} \underline{G}(r) = \frac{\underline{A}}{r} . \quad (4.91)$$

From (4.87) it follows that

$$\Delta \underline{G}_0(\mathbf{x}, \mathbf{x}') = -\frac{1}{\epsilon} \delta(\mathbf{x} - \mathbf{x}') . \quad (4.92)$$

This equation corresponds to the *Poisson equation* from electrostatics,

$$d \star d \underline{G}_0(\mathbf{x}, \mathbf{x}') = -\frac{1}{\epsilon} \delta(\mathbf{x} - \mathbf{x}') dx \wedge dy \wedge dz . \quad (4.93)$$

We integrate both sides of (4.92) over a spherical volume of radius r around the center point \mathbf{x}' . On the left side we can transform the volume integral into a surface integral.

Considering

$$\star d\underline{G}_0(\mathbf{x}, \mathbf{x}') = r^2 \sin \theta \frac{\partial \underline{G}_0}{\partial r} d\theta \wedge d\phi + \sin \theta \frac{\partial \underline{G}_0}{\partial \theta} d\phi \wedge dr + \frac{1}{\sin \theta} \frac{\partial \underline{G}_0}{\partial \phi} dr \wedge d\theta, \quad (4.94)$$

we obtain

$$\oint_{\partial V} r^2 \sin \theta \frac{\partial \underline{G}_0}{\partial r} d\theta \wedge d\phi = -\frac{1}{\epsilon} \int_V \delta(\mathbf{x} - \mathbf{x}') d\mathbf{x} \wedge d\mathbf{y} \wedge d\mathbf{z}. \quad (4.95)$$

Since \underline{G}_0 is uniform over the surface of the sphere, we obtain

$$4\pi r^2 \frac{\partial \underline{G}_0}{\partial r} = -\frac{1}{\epsilon}. \quad (4.96)$$

From this we obtain

$$\underline{G}_0(r) = \frac{1}{4\pi\epsilon r}. \quad (4.97)$$

Comparing with (4.91) yields

$$\underline{A} = \frac{1}{4\pi\epsilon} \quad (4.98)$$

and therewith from (4.90)

$$\underline{G}(r) = \frac{e^{-jk r}}{4\pi\epsilon r}. \quad (4.99)$$

Inserting (4.99) into (4.86) we obtain Green's double one-form

$$\underline{G}(\mathbf{x}, \mathbf{x}') = \frac{e^{-jk|\mathbf{x}-\mathbf{x}'|}}{4\pi\epsilon|\mathbf{x}-\mathbf{x}'|} (d\mathbf{x} d\mathbf{x}' + d\mathbf{y} d\mathbf{y}' + d\mathbf{z} d\mathbf{z}') \quad (4.100)$$

and with this the *retarded electric Hertz differential form*

$$\underline{\Pi}_e(\mathbf{x}) = \int' \frac{e^{-jk|\mathbf{x}-\mathbf{x}'|}}{4\pi\epsilon|\mathbf{x}-\mathbf{x}'|} (d\mathbf{x} d\mathbf{x}' + d\mathbf{y} d\mathbf{y}' + d\mathbf{z} d\mathbf{z}') \wedge \underline{\mathcal{M}}_{e0}(\mathbf{x}'). \quad (4.101)$$

In the same way we obtain for the impressed magnetic polarization $\underline{\mathcal{M}}_{m0}(\mathbf{x}')$ from (4.75b) the *retarded magnetic Hertz differential form* is

$$\underline{\Pi}_m(\mathbf{x}) = \int' \frac{e^{-jk|\mathbf{x}-\mathbf{x}'|}}{4\pi\mu|\mathbf{x}-\mathbf{x}'|} (d\mathbf{x} d\mathbf{x}' + d\mathbf{y} d\mathbf{y}' + d\mathbf{z} d\mathbf{z}') \wedge \underline{\mathcal{M}}_{m0}(\mathbf{x}'). \quad (4.102)$$

By inserting $\underline{M}_{e0}(\mathbf{x}')$ and $\underline{M}_{m0}(\mathbf{x}')$, respectively, in component form into (4.101) and (4.102) we obtain

$$\underline{\Pi}_e(\mathbf{x}) = \int' \frac{e^{-j k |\mathbf{x} - \mathbf{x}'|}}{4\pi\epsilon |\mathbf{x} - \mathbf{x}'|} (\underline{M}_{e0x}(\mathbf{x}') dx + \underline{M}_{e0y}(\mathbf{x}') dy + \underline{M}_{e0z}(\mathbf{x}') dz) \\ dx' \wedge dy' \wedge dz', \quad (4.103a)$$

$$\underline{\Pi}_m(\mathbf{x}) = \int' \frac{e^{-j k |\mathbf{x} - \mathbf{x}'|}}{4\pi\mu |\mathbf{x} - \mathbf{x}'|} (\underline{M}_{m0x}(\mathbf{x}') dx + \underline{M}_{m0y}(\mathbf{x}') dy + \underline{M}_{m0z}(\mathbf{x}') dz) \\ dx' \wedge dy' \wedge dz'. \quad (4.103b)$$

The computation of the field quantities \underline{E} and \underline{H} from \underline{M}_{e0} or \underline{M}_{m0} , respectively, is performed using (3.17a) and (3.17b) or (3.20a) and (3.20b). If impressed electric polarization as well as impressed magnetic polarization exist, the electromagnetic field is obtained by superposition of the electromagnetic fields computed from \underline{M}_{e0} and \underline{M}_{m0} , respectively.

4.9 THE INTEGRAL EQUATION METHOD

The electromagnetic field of a three-dimensional structure can be computed from unknown quantities over certain boundary surfaces that are obtained by the integral equation method [21, 27–30]. If the distribution of the sources of the electromagnetic field is known, the field may be computed in a straightforward way by computing the Hertz vector fields via (4.103a) and (4.103b) and from these the electric and magnetic fields. However, in electromagnetic field computation the source current or polarization distribution is not known initially – its determination is part of the problem. To show this we consider the scattering of the electromagnetic field by a conducting sphere, illustrated in Figure 4.13. Let $\underline{\mathcal{E}}^{(i)}$ be the incident or primary field, existing without the conducting sphere (Figure 4.13(a)). At the surface of the conducting sphere the primary field $\underline{\mathcal{E}}^{(i)}$ will not satisfy the boundary conditions. Therefore in the conducting sphere currents will be induced, creating a secondary or scattered field $\underline{\mathcal{E}}^{(s)}$, so that the total field has no tangential electric field component on the surface of the scattering body. The complete field $\underline{\mathcal{E}}$ on the surface S of the conductive body in Figure 4.13(c) results from the superposition of the incident field $\underline{\mathcal{E}}^{(i)}$ and the scattered field $\underline{\mathcal{E}}^{(s)}$,

$$\underline{\mathcal{E}} = \underline{\mathcal{E}}^{(i)} + \underline{\mathcal{E}}^{(s)}. \quad (4.104)$$

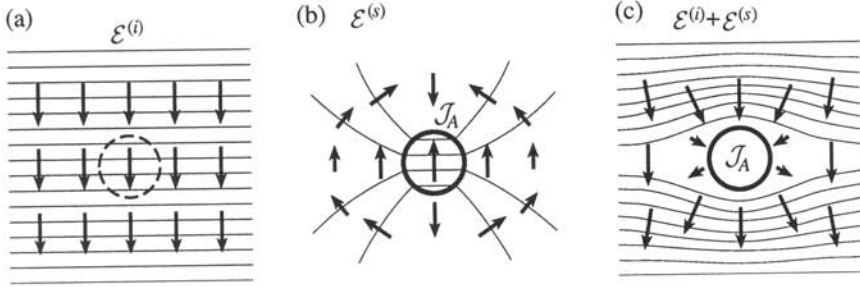


Figure 4.13: Scattering: (a) incident field, (b) scattered field, and (c) total field.

The source of the scattered field is the electric surface current, described by the surface current density form $\underline{\mathcal{J}}_A(\mathbf{x})$. Inserting

$$\frac{\partial}{\partial t} \mathcal{M}_{e0} = \mathcal{J}_0 \quad (4.105)$$

into (4.85) leads to

$$\underline{\Pi}_e(\mathbf{x}) = \frac{1}{j\omega} \int \underline{\mathcal{G}}_{e0}(\mathbf{x}, \mathbf{x}') \wedge \underline{\mathcal{J}}(\mathbf{x}'), \quad (4.106)$$

where the integration is performed over the surface S of the sphere. The free-space Green's dyadic form $\underline{\mathcal{G}}_{e0}$ is given by (4.100),

$$\underline{\mathcal{G}}_{e0}(\mathbf{x}, \mathbf{x}') = \underline{\mathcal{G}}_{e0}(\mathbf{x}, \mathbf{x}')(\mathrm{d}x \mathrm{d}x' + \mathrm{d}y \mathrm{d}y' + \mathrm{d}z \mathrm{d}z') \quad (4.107)$$

with

$$\underline{\mathcal{G}}_{e0}(\mathbf{x}, \mathbf{x}') = \frac{e^{-j k |\mathbf{x} - \mathbf{x}'|}}{4\pi\epsilon |\mathbf{x} - \mathbf{x}'|}. \quad (4.108)$$

With (3.29a) and (3.29b) we obtain the scattered electric field form

$$\underline{\mathcal{E}}^{(s)} = \mathrm{d} \tilde{\mathrm{d}} \underline{\Pi}_e + k^2 \underline{\Pi}_e \quad (4.109)$$

with $k^2 = \omega^2 \epsilon \mu$. We introduce the dyadic Green's function

$$\underline{\mathcal{G}}_{e1}(\mathbf{x}, \mathbf{x}') = \frac{1}{j\omega} (\mathrm{d} \tilde{\mathrm{d}} + k^2) (\underline{\mathcal{G}}_{e0}(\mathbf{x}, \mathbf{x}')(\mathrm{d}x \mathrm{d}x' + \mathrm{d}y \mathrm{d}y' + \mathrm{d}z \mathrm{d}z')), \quad (4.110)$$

where the exterior differential operators d and $\tilde{\mathrm{d}}$ act on the variable \mathbf{x} only and not on \mathbf{x}' , and obtain

$$\underline{\mathcal{E}}^{(s)} = \int' \underline{\mathcal{G}}_{e1}(\mathbf{x}, \mathbf{x}') \wedge \underline{\mathcal{J}}(\mathbf{x}'). \quad (4.111)$$

The integration is performed over x' . In a more explicit notation (4.110) may be written as

$$\begin{aligned} \underline{\mathcal{G}}_{e1}(\mathbf{x}, \mathbf{x}') = \frac{1}{j\omega} \left[\left(\frac{\partial^2 \underline{G}_{e0}}{\partial x^2} + k^2 \underline{G}_{e0} \right) dx dx' + \frac{\partial^2 \underline{G}_{e0}}{\partial x \partial y} dx dy' + \frac{\partial^2 \underline{G}_{e0}}{\partial z \partial x} dx dz' \right. \\ \left. + \frac{\partial^2 \underline{G}_{e0}}{\partial x \partial y} dy dx' + \left(\frac{\partial^2 \underline{G}_{e0}}{\partial y^2} + k^2 \underline{G}_{e0} \right) dy dy' + \frac{\partial^2 \underline{G}_{e0}}{\partial y \partial z} dy dz' \right. \\ \left. + \frac{\partial^2 \underline{G}_{e0}}{\partial z \partial x} dz dx' + \frac{\partial^2 \underline{G}_{e0}}{\partial y \partial z} dz dy' + \left(\frac{\partial^2 \underline{G}_{e0}}{\partial z^2} + k^2 \underline{G}_{e0} \right) dz dz' \right]. \quad (4.112) \end{aligned}$$

Using

$$\mathcal{J}(u, v, n) = \delta(n) n \wedge \mathcal{J}_A(u, v) \quad (4.113)$$

to express the current on the sphere by the surface current density we obtain from (4.111) after integration over the direction normal to the surface the relation between the surface current density on the scatterer $\underline{\mathcal{J}}_A(\mathbf{x}')$ and the scattered electric field

$$\underline{\mathcal{E}}^{(s)} = \int_S' \underline{\mathcal{G}}_{e1}(\mathbf{x}, \mathbf{x}') \wedge \underline{\mathcal{J}}_A(\mathbf{x}'). \quad (4.114)$$

The integral is performed over the surface S with \mathbf{x}' as the variable of integration.

On the surface of the scatterer the tangential electric field component must vanish. With

$$\begin{aligned} \mathcal{E}_t &= n \lrcorner (n \wedge \mathcal{E}) = n \lrcorner [n \wedge (E_u s_1 + E_v s_2 + E_n n)] \\ &= E_u s_1 + E_v s_2, \end{aligned} \quad (4.115a)$$

$$\begin{aligned} \mathcal{D}_n &= n \lrcorner (n \wedge \mathcal{D}) = n \lrcorner [n \wedge (D_u s_2 \wedge n + D_v n \wedge s_1 + D_n s_1 \wedge s_2)] \\ &= D_n s_1 \wedge s_2. \end{aligned} \quad (4.115b)$$

This yields

$$\underline{\mathcal{E}}_t = \underline{\mathcal{E}}_t^{(i)} + \underline{\mathcal{E}}_t^{(s)} = n \lrcorner \left(n \wedge (\underline{\mathcal{E}}^{(i)} + \underline{\mathcal{E}}^{(s)}) \right) = 0 \quad \text{for } \mathbf{x} \in S. \quad (4.116)$$

We obtain the *integral equation*

$$\underline{\mathcal{E}}_t^{(i)} = -n \lrcorner \left(n \wedge \int_S' \underline{\mathcal{G}}_{e1}(\mathbf{x}, \mathbf{x}') \wedge \underline{\mathcal{J}}_A(\mathbf{x}') \right) \quad \text{for } \mathbf{x}, \mathbf{x}' \in S. \quad (4.117)$$

This integral equation can be written as a functional equation

$$\mathcal{L}_{op}(\underline{\mathcal{J}}_A) = \underline{\mathcal{E}}^{(i)} \Big|_t. \quad (4.118)$$

This functional equation is called the *electric field integral equation* (EFIE). It may be solved numerically using the method of moments (see Section 14.2).

4.10 THE FREE-SPACE GREEN'S DYADIC FORM

From (4.106), (3.29a), and (4.116) we obtain for free-space regions with $\underline{M}_{e0} = 0$ the integral equation for the electromagnetic scattering problem in free-space

$$\underline{\mathcal{E}}_t^{(i)}(\mathbf{x}) = \underline{\mathcal{E}}_t^{(s)}(\mathbf{x}) = -\frac{1}{j\omega} \mathbf{n} \cdot \left[\mathbf{n} \wedge \left(\oint_S \underline{\mathcal{G}}_{e0}(\mathbf{x}, \mathbf{x}') \wedge \underline{\mathcal{J}}_A(\mathbf{x}') \right) \right]. \quad (4.119)$$

We introduce the *dyadic Green's form* $\underline{\mathcal{G}}_1(\mathbf{x}, \mathbf{x}')$

$$\underline{\mathcal{G}}_1(\mathbf{x}, \mathbf{x}') = -\frac{1}{j\omega} \mathbf{n} \cdot \left[\mathbf{n} \wedge \left(\oint_S \underline{\mathcal{G}}_{e0}(\mathbf{x}, \mathbf{x}') \right) \right]. \quad (4.120)$$

In the following we derive the *Green's dyadic form* for the free-space in Cartesian coordinates for a plane scatterer with surface S oriented normal to the z -axis. The electric surface area current density exhibits x - and y -components only. The dyadic Green's function $\underline{\mathcal{G}}_1(\mathbf{x}, \mathbf{x}')$ is given by

$$\underline{\mathcal{G}}_1(\mathbf{x}, \mathbf{x}') = G_{xx} dx dx' + G_{xy} dx dy' + G_{yx} dy dx' + G_{yy} dy dy' \quad (4.121)$$

with

$$G_{xx} = \frac{1}{j\omega\epsilon_0} \left[-\frac{jk_0}{r} - \frac{1+k_0^2x^2}{r^2} + \frac{3jk_0x^2}{r^3} + \frac{3x^2}{r^4} \right] \frac{\exp(-jk_0r)}{4\pi r}, \quad (4.122a)$$

$$G_{yy} = \frac{1}{j\omega\epsilon_0} \left[-\frac{jk_0}{r} - \frac{1+k_0^2y^2}{r^2} + \frac{3jk_0y^2}{r^3} + \frac{3y^2}{r^4} \right] \frac{\exp(-jk_0r)}{4\pi r}, \quad (4.122b)$$

$$G_{xy} = G_{yx} = \frac{xy}{j\omega\epsilon_0} \left[-\frac{k_0^2}{r^2} + \frac{3jk_0}{r^3} + \frac{3}{r^4} \right] \frac{\exp(-jk_0r)}{4\pi r} \quad (4.122c)$$

and

$$r = \sqrt{(x-x')^2 + (y-y')^2}. \quad (4.123)$$

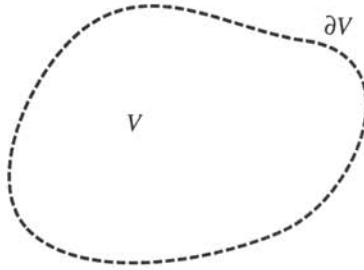
It can be seen that G_{xx} and G_{yy} are even functions in all three space coordinates. The components G_{xy} and G_{yx} are odd functions in x and y and even functions in z . With the dyadic Green's function of free-space we obtain the integral equation

$$\underline{\mathcal{E}}_t^{(i)}(\mathbf{x}) = -\underline{\mathcal{E}}_t^{(s)}(\mathbf{x}) = \int_S \underline{\mathcal{G}}_1(\mathbf{x}, \mathbf{x}') \wedge \underline{\mathcal{J}}_A(\mathbf{x}'). \quad (4.124)$$

4.11 GREEN'S THEOREMS

4.11.1 The Scalar Green's Theorems

Consider a volume V with boundary ∂V as depicted in Figure 4.14. The two scalar functions $\phi(\mathbf{x})$, $\psi(\mathbf{x})$ are assumed to be continuous together with their first and second


 Figure 4.14: Volume V with boundary ∂V .

derivatives in the volume V and on the boundary ∂V . With Stokes' theorem (2.112) we obtain

$$\int_V d \star (\psi d\phi) = \oint_{\partial V} \star (\psi d\phi). \quad (4.125)$$

Expanding the exterior derivation at the left-hand side as

$$d \star (\psi d\phi) = d(\psi \star d\phi) = d\psi \wedge \star d\phi + \psi d \star d\phi = \star d\psi \wedge d\phi + \psi d \star d\phi \quad (4.126)$$

yields *Green's first scalar theorem*

$$\int_V d\psi \wedge \star d\phi + \int_V \psi d \star d\phi = \oint_{\partial V} \star (\psi d\phi). \quad (4.127)$$

Introducing coordinates u, v, n such that u and v are tangential to the surface ∂V and n is normal to ∂V , the surface integral is performed over $du \wedge dv$. With

$$\star (\psi d\phi) = \psi \frac{\partial \phi}{\partial u} \frac{g_v g_n}{g_u} dv \wedge dn + \psi \frac{\partial \phi}{\partial v} \frac{g_n g_u}{g_v} dn \wedge du + \psi \frac{\partial \phi}{\partial n} \frac{g_u g_v}{g_n} du \wedge dv \quad (4.128)$$

we obtain from (4.127) the representation of Green's first scalar theorem,

$$\int_V (d\psi \wedge \star d\phi + \psi d \star d\phi) = \oint_{\partial V} \psi \frac{\partial \phi}{\partial n} \frac{g_u g_v}{g_n} du \wedge dv. \quad (4.129)$$

Inserting

$$d \star d\phi = \star \Delta \phi = \Delta \phi g_u g_v g_n du \wedge dv \wedge dn \quad (4.130)$$

yields another representation of Green's first scalar theorem,

$$\int_V (d\psi \wedge \star d\phi + \star (\psi \Delta \phi)) = \oint_{\partial V} \psi \frac{\partial \phi}{\partial n} \frac{g_u g_v}{g_n} du \wedge dv. \quad (4.131)$$

Interchanging $\phi(\mathbf{x})$ and $\psi(\mathbf{x})$ in (4.127) yields

$$\int_V d\phi \wedge \star d\psi + \int_V \phi d\star d\psi = \oint_{\partial V} \star(\phi d\psi). \quad (4.132)$$

Subtracting (4.132) from (4.127) and considering that $d\psi \wedge \star d\phi = d\phi \wedge \star d\psi$ yields *Green's second scalar theorem*

$$\int_V (\psi d\star d\phi - \phi d\star d\psi) = \oint_{\partial V} [\star(\psi d\phi) - \star(\phi d\psi)]. \quad (4.133)$$

For the coordinates u and v defining the surface ∂V and the coordinate n normal to ∂V , Green's second scalar theorem is expressed by

$$\int_V (\psi d\star d\phi - \phi d\star d\psi) = \oint_{\partial V} \left(\psi \frac{\partial \phi}{\partial n} - \phi \frac{\partial \psi}{\partial n} \right) \frac{g_u g_v}{g_n} du \wedge dv. \quad (4.134)$$

Inserting (4.130) at the right-hand side of (4.134) yields another useful representation of Green's second scalar theorem,

$$\int_V \star(\psi \Delta \phi - \phi \Delta \psi) = \oint_{\partial V} \left(\psi \frac{\partial \phi}{\partial n} - \phi \frac{\partial \psi}{\partial n} \right) \frac{g_u g_v}{g_n} du \wedge dv. \quad (4.135)$$

4.11.2 Green's Theorems in Two Dimensions

For the analysis of two-dimensional structures the scalar Green's theorems in two dimensions are useful. Such two-dimensional problems arise if the properties of transverse modes in electromagnetic structures exhibiting cylindrical symmetry are investigated. Consider a structure with general cylindric symmetry. In a Cartesian coordinate system x, y, z let the z -axis be the axis of the cylindric structure and let x and y be the transverse coordinates. The cylindric structure under investigation exhibits translational invariance in z -direction. We introduce the *transverse exterior derivative*

$$d_t \mathcal{U} = dx \frac{\partial \mathcal{U}}{\partial x} + dy \frac{\partial \mathcal{U}}{\partial y}. \quad (4.136)$$

For a two-form \mathcal{U} exhibiting only transverse components,

$$\mathcal{U}(x, y) = U_x(x, y) dy \wedge dz + U_y(x, y) dz \wedge dx \quad (4.137)$$

Stokes' theorem (2.112) becomes

$$\oint_{\partial V} \mathcal{U} = \int_V d_t \mathcal{U}. \quad (4.138)$$

In component notation this is

$$\begin{aligned} \oint_{\partial V} (U_x(x, y) dy - U_y(x, y) dx) \wedge dz \\ = \int_V \left(\frac{\partial U_x(x, y)}{\partial x} + \frac{\partial U_x(x, y)}{\partial y} \right) dx \wedge dy \wedge dz. \end{aligned} \quad (4.139)$$

Since the integrands in both sides of the equation do not depend on z we can omit the integration over z , hence

$$\begin{aligned} \oint_{\partial A} (U_x(x, y) dy - U_y(x, y) dx) \\ = \int_A \left(\frac{\partial U_x(x, y)}{\partial x} + \frac{\partial U_x(x, y)}{\partial y} \right) dx \wedge dy. \end{aligned} \quad (4.140)$$

On the right-hand side of this equation the integration is performed over a cross-sectional area A of the cylindric structure and the integral on the left-hand side of the equation is performed over the boundary curve ∂A of the area A . We can write this *two-dimensional Stokes' theorem* as

$$\oint_{\partial A} \mathcal{U} \lrcorner dz = \int_A (d_t \mathcal{U}) \lrcorner dz. \quad (4.141)$$

Consider a cross-sectional area A of a cylindric structure, bounded by the closed curve ∂A . Let $\phi(x, y)$ and $\psi(x, y)$ be two-dimensional scalar functions continuous together with their first and second derivatives in the area A and on the boundary ∂A . With the two-dimensional Stokes' theorem (4.141) we obtain

$$\int_A d_t (\star(\psi d_t \phi)) \lrcorner dz = \oint_{\partial A} (\star(\psi d_t \phi)) \lrcorner dz. \quad (4.142)$$

Proceeding as in Section 4.11.1 we obtain the *two-dimensional form of Green's first scalar theorem*

$$\int_A (d_t \psi \wedge \star d_t \phi) \lrcorner dz + \int_A (\psi d_t \star d_t \phi) \lrcorner dz = \oint_{\partial A} (\star(\psi d_t \phi)) \lrcorner dz. \quad (4.143)$$

Choose a coordinate system u, n, z such that u and n are the transverse coordinates and z is the longitudinal coordinate. Furthermore u is tangential and n is normal to the boundary curve ∂A . This yields

$$(\star(\psi d_t \phi)) \lrcorner dz = \psi \frac{\partial \phi}{\partial u} \frac{g_n}{g_u} dn - \psi \frac{\partial \phi}{\partial n} \frac{g_u}{g_n} du. \quad (4.144)$$

Inserting this into (4.143) and using

$$d_t \star d_t \phi = \star \Delta_t \phi = \Delta_t \phi g_u g_n du \wedge dn \wedge dz \quad (4.145)$$

yields an alternative two-dimensional form of Green's first scalar theorem,

$$\int_A \left(\frac{\partial \phi}{\partial u} \frac{\partial \psi}{\partial u} \frac{g_n}{g_u} + \frac{\partial \phi}{\partial n} \frac{\partial \psi}{\partial n} \frac{g_u}{g_n} \right) du \wedge dn + \int_A \psi \Delta_t \phi g_u g_n du \wedge dn = - \oint_{\partial A} \psi \frac{\partial \phi}{\partial n} \frac{g_u}{g_n} du. \quad (4.146)$$

Interchanging ϕ and ψ in (4.143) and forming the difference between both equations considering that $d\psi \wedge \star d\phi = d\phi \wedge \star d\psi$ yields the *two-dimensional form of Green's second scalar theorem*

$$\int_A (\psi d_t \star d_t \phi - \phi d_t \star d_t \psi) \lrcorner dz = \int_{\partial A} [\star(\psi d_t \phi) - \star(\phi d_t \psi)] \lrcorner dz. \quad (4.147)$$

Inserting (4.144) yields an alternative two-dimensional form of Green's second scalar theorem,

$$\int_A (\psi d_t \star d_t \phi - \phi d_t \star d_t \psi) \lrcorner dz = - \int_{\partial A} \left(\psi \frac{\partial \phi}{\partial n} - \phi \frac{\partial \psi}{\partial n} \right) \frac{g_u}{g_n} du. \quad (4.148)$$

With (4.130) we obtain from this

$$\int_A (\psi \Delta_t \phi - \phi \Delta_t \psi) g_u g_n du \wedge dn = - \int_{\partial A} \left(\psi \frac{\partial \phi}{\partial n} - \phi \frac{\partial \psi}{\partial n} \right) \frac{g_u}{g_n} du. \quad (4.149)$$

4.11.3 The Vector Green's Theorems

Let \mathcal{U} and \mathcal{V} be one-forms that are continuous together with their first and second derivatives in the volume V and on the boundary ∂V . With Stokes' theorem (2.112) in analogy to (4.125) we obtain

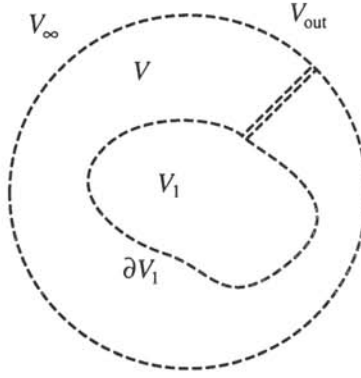
$$\int_V d(\mathcal{U} \wedge \star d\mathcal{V}) = \int_{\partial V} \mathcal{U} \wedge \star d\mathcal{V}. \quad (4.150)$$

Expanding the differential form on the left-hand side into

$$d(\mathcal{U} \wedge \star d\mathcal{V}) = d\mathcal{U} \wedge \star d\mathcal{V} - \mathcal{U} \wedge d \star d\mathcal{V} \quad (4.151)$$

yields *Green's first vector theorem*

$$\int_V (d\mathcal{U} \wedge \star d\mathcal{V} - \mathcal{U} \wedge d \star d\mathcal{V}) = \int_{\partial V} \mathcal{U} \wedge \star d\mathcal{V}. \quad (4.152)$$

Figure 4.15: Volume V with embedded volume V_1 .

Interchanging \mathcal{U} and \mathcal{V} yields

$$\int_V (\mathrm{d}\mathcal{U} \wedge \star \mathrm{d}\mathcal{V} - \mathcal{V} \wedge \star \mathrm{d}\mathcal{U}) = \int_{\partial V} \mathcal{V} \wedge \star \mathrm{d}\mathcal{U}. \quad (4.153)$$

Subtracting (4.153) from (4.152) we obtain *Green's second vector theorem*

$$\int_V (\mathcal{V} \wedge \star \mathrm{d}\mathcal{U} - \mathcal{U} \wedge \star \mathrm{d}\mathcal{V}) = \int_{\partial V} (\mathcal{U} \wedge \star \mathrm{d}\mathcal{V} - \mathcal{V} \wedge \star \mathrm{d}\mathcal{U}). \quad (4.154)$$

4.12 INTEGRAL FORMULATION OF THE EQUIVALENCE PRINCIPLE

Consider a volume V_1 with boundary ∂V_1 enclosed by a volume V with an outer boundary ∂V_{out} against V_∞ and the inner boundary ∂V_1 against V_1 , as shown in Figure 4.15. Now let V_1 be connected with V_∞ via a tube of infinitesimal diameter. The introduction of this tube connecting the inner and outer boundaries of V demonstrates that inner and outer boundaries may be considered as parts of one simply connected boundary surface. Hence V is bounded by a single surface $-\partial V_1 + \partial V_{\text{out}}$. The negative sign of $-\partial V_1$ indicates that the orientation of this part of the boundary of V is opposite to the orientation of the boundary ∂V_1 of V_1 . The surface integral over $-\partial V_1$ is the negative surface integral over ∂V_1 . The complete boundary ∂V of V is $-\partial V_1 + \partial V_{\text{out}}$. The volume V_∞ outside V is extended into infinite space. We assume all sources to be concentrated in volume V_1 . In the following we assume the media in V and V_∞ also to be lossless. For lossless and source-free regions Ampère's law (2.124a) and Faraday's law (2.124b)

are

$$\underline{d} \underline{\mathcal{H}} = j \omega \epsilon \star \underline{\mathcal{E}}, \quad (4.155a)$$

$$\underline{d} \underline{\mathcal{E}} = -j \omega \mu \star \underline{\mathcal{H}} \quad (4.155b)$$

with real ϵ and μ . Under the above assumptions we obtain for the source-free and lossless regions V and V_∞

$$\star \underline{d} \star \underline{d} \underline{\mathcal{E}}(\mathbf{x}) + k^2 \underline{\mathcal{E}}(\mathbf{x}) = 0. \quad (4.156)$$

We consider a dyadic Green's form $\underline{\mathcal{G}}_e(\mathbf{x}, \mathbf{x}')$ as defined in (4.76), fulfilling

$$\star \underline{d} \star \underline{d} \underline{\mathcal{G}}_e(\mathbf{x}, \mathbf{x}') + k^2 \underline{\mathcal{G}}_e(\mathbf{x}, \mathbf{x}') = -\frac{1}{\epsilon} \underline{\mathcal{I}}(\mathbf{x}, \mathbf{x}'), \quad (4.157)$$

where $\underline{\mathcal{I}}(\mathbf{x}, \mathbf{x}')$ is the identity kernel, introduced in (4.77). The exterior derivatives are performed with respect to \mathbf{x} whereas the coordinate \mathbf{x}' is considered to be constant. In the volume V the homogeneous Helmholtz equation (4.156) is valid. The source is embedded in V_1 . Substituting in (4.154) $\underline{\mathcal{E}}$ for \mathcal{V} and $\underline{\mathcal{G}}_e$ for \mathcal{U} yields

$$\begin{aligned} & \int_V [\underline{\mathcal{E}}(\mathbf{x}) \wedge \underline{d} \star \underline{d} \underline{\mathcal{G}}_e(\mathbf{x}, \mathbf{x}') - \underline{\mathcal{G}}_e \wedge \underline{d} \star \underline{d} \underline{\mathcal{E}}(\mathbf{x})] \\ &= \int_{-\partial V_1 + \partial V_{\text{out}}} [\underline{\mathcal{G}}_e(\mathbf{x}, \mathbf{x}') \wedge \star \underline{d} \underline{\mathcal{E}}(\mathbf{x}) - \underline{\mathcal{E}}(\mathbf{x}) \wedge \star \underline{d} \underline{\mathcal{G}}_e(\mathbf{x}, \mathbf{x}')] . \end{aligned} \quad (4.158)$$

The volume V is embedded between the inner volume V_1 and the outer volume V_∞ . Therefore the boundary of V is given by $\partial V = \partial V_{\text{out}} - \partial V_1$, where ∂V_{out} is the outer boundary. The inner boundary $-\partial V_1$ is identical with the boundary ∂V_1 of V_1 but has opposite orientation. The negative sign indicates that the negative contribution of the integral over ∂V_1 has to be taken. Connecting the inner boundary and the outer boundary by a wormhole of infinitesimal cross-section we can consider ∂V_{out} and $-\partial V_1$ as parts of a single boundary surface ∂V .

Inserting (4.156) and (4.157) in the left-hand side of (4.158), we obtain

$$\begin{aligned} & \int_V [\underline{\mathcal{E}}(\mathbf{x}) \wedge \underline{d} \star \underline{d} \underline{\mathcal{G}}_e(\mathbf{x}, \mathbf{x}') - \underline{\mathcal{G}}_e(\mathbf{x}, \mathbf{x}') \wedge \underline{d} \star \underline{d} \underline{\mathcal{E}}(\mathbf{x})] \\ &= -\frac{1}{\epsilon} \int_V \underline{\mathcal{E}}(\mathbf{x}) \wedge \star \underline{\mathcal{I}}(\mathbf{x}, \mathbf{x}') = \begin{cases} -\frac{1}{\epsilon} \underline{\mathcal{E}}(\mathbf{x}') & \text{for } \mathbf{x}' \in V \\ 0 & \text{for } \mathbf{x}' \notin V \end{cases} . \end{aligned} \quad (4.159)$$

Let the boundary ∂V_{out} be spherical and let its radius go to infinity. Assuming that $\underline{\mathcal{E}}$ as well as $\underline{\mathcal{G}}_e$ satisfy the Sommerfeld radiation condition (3.238b), the contribution of

the surface integral over ∂V_{out} vanishes in (4.158) and we obtain

$$\underline{\mathcal{E}}(\mathbf{x}') = \begin{cases} \epsilon \int_{\partial V_1} \underline{\mathcal{E}}(\mathbf{x}) \wedge \star d\underline{\mathcal{G}}_e(\mathbf{x}, \mathbf{x}') - \epsilon \int_{\partial V_1} \underline{\mathcal{G}}_e(\mathbf{x}, \mathbf{x}') \wedge \star d\underline{\mathcal{E}}(\mathbf{x}) & \text{for } \mathbf{x}' \notin V_1 \\ 0 & \text{for } \mathbf{x}' \in V_1 \end{cases} \quad (4.160)$$

This expression is a formulation of the *Huygens' principle*, already discussed in Section 4.5. Inserting Ampère's law (4.155a) into the second integral yields

$$\underline{\mathcal{E}}(\mathbf{x}') = \epsilon \int_{\partial V_1} \underline{\mathcal{E}}(\mathbf{x}) \wedge \star d\underline{\mathcal{G}}_e(\mathbf{x}, \mathbf{x}') + j \frac{\omega}{c^2} \int_{\partial V_1} \underline{\mathcal{G}}_e(\mathbf{x}, \mathbf{x}') \wedge \underline{\mathcal{H}}(\mathbf{x}) \quad \text{for } \mathbf{x}' \notin V_1. \quad (4.161)$$

Following the principle of duality we can derive an equation for the magnetic field:

$$\underline{\mathcal{H}}(\mathbf{x}') = \mu \int_{\partial V_1} \underline{\mathcal{H}}(\mathbf{x}) \wedge \star d\underline{\mathcal{G}}_m(\mathbf{x}, \mathbf{x}') - j \frac{\omega}{c^2} \int_{\partial V_1} \underline{\mathcal{G}}_m(\mathbf{x}, \mathbf{x}') \wedge \underline{\mathcal{E}}(\mathbf{x}) \quad \text{for } \mathbf{x}' \notin V_1. \quad (4.162)$$

4.13 THE STURM-LIOUVILLE EQUATION

The treatment of many boundary value problems in electromagnetics yields to the *Sturm-Liouville differential equation* [21, 31]. The homogeneous Sturm-Liouville differential equation has the general form

$$\frac{d}{dx} \left[p(x) \frac{d\psi(x)}{dx} \right] + [q(x) + \lambda \sigma(x)] \psi(x) = 0, \quad (4.163)$$

where $\psi(x)$ is the unknown function whereas $p(x)$, $q(x)$, and $\sigma(x)$ are real and continuous functions within the considered domain of x . Furthermore, in general $p(x)$ and $\sigma(x)$ are considered to be positive. The constant λ in general may also be complex. In the following we investigate the solutions of the Sturm-Liouville differential equation in the interval $[a, b]$ for the boundary conditions

$$\psi_i + c_a \frac{d\psi_i}{dx} = 0 \quad \text{for } x = a, \quad (4.164a)$$

$$\psi_i + c_b \frac{d\psi_i}{dx} = 0 \quad \text{for } x = b, \quad (4.164b)$$

where c_a and c_b are real. The solutions of the differential equation (4.163) exist for certain *eigenvalues* λ_n of λ . For chosen boundary conditions at $x = a$ and $x = b$, we obtain an infinite number of solutions ψ_n of the differential equation (4.163) with the corresponding eigenvalues λ_n .

If the complex function $f(x)$ and the real positive function $\sigma(x)$ are defined in the interval $[a, b]$ and the integral

$$\langle f|f \rangle = \int_a^b \sigma(x) |f(x)|^2 dx < \infty \quad (4.165)$$

exists, the function $f(x)$ is called *square integrable* with the *kernel function* $\sigma(x)$. The collection of all functions, square integrable in a given interval $[a, b]$, forms an infinite-dimensional complex linear vector space. An infinite-dimensional complex linear vector space is called a *Hilbert space* [32, 33]. In the Hilbert space an inner product and a metric upon this are defined. The expression

$$\langle f(x)|g(x) \rangle = \int_a^b \sigma(x) f^*(x) g(x) dx \quad (4.166)$$

is the *inner product* of the functions $f(x)$ and $g(x)$. The expression

$$\|f\| = \sqrt{\langle f|f \rangle} \quad (4.167)$$

is called the *norm* of $f(x)$.

We show that in the case of fulfilled boundary conditions (4.164a) and (4.164b) the eigenvalues λ_n are real and that the eigenfunctions $\psi_m(x)$ and $\psi_n(x)$ belonging to different eigenvalues λ_m and λ_n are orthogonal with respect to the weighting function $\sigma(x)$, in other words

$$\langle \psi_n | \psi_m \rangle = 0 \quad \text{for } \lambda_m \neq \lambda_n. \quad (4.168)$$

To prove the above assumption we insert ψ_m and λ_m into (4.163) and multiply the equation from the left with ψ_n^* . Then we form the same expression with interchanged indices m and n . The difference of these expressions is integrated over the interval $[a, b]$ and we obtain

$$\int_a^b \left[\psi_n^* \frac{d}{dx} \left(p \frac{d\psi_m}{dx} \right) - \psi_m \frac{d}{dx} \left(p \frac{d\psi_n^*}{dx} \right) \right] dx = \int_a^b (\lambda_n^* - \lambda_m) \sigma \psi_n^* \psi_m dx. \quad (4.169)$$

By partial integration of the left side we obtain

$$\begin{aligned} & p \left[\psi_n^* \frac{d\psi_m}{dx} - \psi_m \frac{d\psi_n^*}{dx} \right] \Big|_a^b - \int_a^b p \left[\frac{d\psi_n^*}{dx} \frac{d\psi_m}{dx} - \frac{d\psi_n^*}{dx} \frac{d\psi_m}{dx} \right] dx \\ &= p \left[\psi_n^* \frac{d\psi_m}{dx} - \psi_m \frac{d\psi_n^*}{dx} \right] \Big|_a^b = (\lambda_n^* - \lambda_m) \int_a^b \sigma \psi_n^* \psi_m dx. \end{aligned} \quad (4.170)$$

If $\psi_m(x)$ and $\psi_n(x)$ fulfill the same boundary conditions (4.164a) and (4.164b) it follows that

$$\psi_n^* \frac{d\psi_m}{dx} - \psi_m \frac{d\psi_n^*}{dx} = 0 \quad \text{for } x = a = b. \quad (4.171)$$

From (4.170) and (4.171) it follows for $n \neq m$ that

$$(\lambda_n^* - \lambda_m) \langle \psi_n | \psi_m \rangle = 0. \quad (4.172)$$

For $m = n$, due to

$$\langle \psi_n | \psi_n \rangle = \int_a^b \sigma |\psi_n|^2 dx \quad (4.173)$$

(4.172) may only be fulfilled for $(\lambda_n^* - \lambda_n) = 0$ (i.e., the eigenvalues λ_n must be real). With this it follows from (4.172) that

$$(\lambda_n - \lambda_m) \langle \psi_n | \psi_m \rangle = 0. \quad (4.174)$$

and from this we obtain (4.168).

The functions ψ_n are orthogonal in the interval $[a, b]$ with respect to the integration kernel $\sigma(x)$. For *degenerate eigenvalues* $\lambda_i = \lambda_j$ the corresponding eigenfunctions $\psi_i(x)$ and $\psi_j(x)$ need not be orthogonal. In this case we may introduce the new eigenfunctions ψ_i^1 and ψ_j^1 by a linear transformation

$$\psi_i^1 = \psi_i, \quad \psi_j^1 = \psi_j + \alpha \psi_i, \quad (4.175)$$

where the coefficient α is given by

$$\alpha = -\frac{\langle \psi_i, \psi_j \rangle}{\langle \psi_i, \psi_i \rangle}. \quad (4.176)$$

This method can be extended to an arbitrary number of degenerate eigenvalues and is called the *Gram-Schmidt orthogonalization method*.

In the following we assume an *orthonormal system of eigenfunctions* (i.e., that all eigenfunctions are normalized and mutually orthogonal), so that

$$\langle \psi_m | \psi_n \rangle = \delta_{mn}. \quad (4.177)$$

The eigenfunctions ψ_n form a *complete set of functions* and allow the expansion of an arbitrary piecewise continuous function $f(x)$ into a series

$$f(x) = \sum_{n=1}^{\infty} a_n \psi_n(x). \quad (4.178)$$

To determine the coefficients a_n we multiply both sides of the equation with $\sigma(x)\psi_m^*(x)$ and integrate from a to b , to obtain

$$\int_a^b \sigma(x)\psi_m^*(x)f(x) dx = \sum_{n=1}^{\infty} a_n \int_a^b \sigma(x)\psi_m^*(x)\psi_n(x) dx = \sum_{n=1}^{\infty} a_n \delta_{mn}. \quad (4.179)$$

From this it follows that

$$a_m = \int_a^b \sigma(x)\psi_m^*(x)f(x) dx. \quad (4.180)$$

The function $f(x)$ is assumed to be square integrable with the kernel function $\sigma(x) > 0$ for $x \in [a, b]$. We investigate the convergence of the series expansion of $f(x)$ into $\psi_n(x)$ and consider the series truncated after the N th term,

$$f_N(x) = \sum_{n=1}^N a_n \psi_n(x), \quad (4.181)$$

where the coefficients a_n are given by (4.180). The $\psi_n(x)$ form a complete set of functions if for every function $f(x)$, square integrable in the interval $[a, b]$, the relation

$$\lim_{N \rightarrow \infty} \int_a^b |f(x) - f_N(x)|^2 \sigma(x) dx = 0 \quad (4.182)$$

is valid. After inserting (4.181), we obtain from this

$$\lim_{N \rightarrow \infty} \int_a^b \left| f(x) - \sum_{n=1}^N a_n \psi_n(x) \right|^2 \sigma(x) dx = 0. \quad (4.183)$$

For $N \rightarrow \infty$ we obtain *Parseval's theorem*

$$\int_a^b |f(x)|^2 \sigma(x) dx = \sum_{n=1}^{\infty} |a_n|^2. \quad (4.184)$$

If (4.182) is fulfilled in the interval (a, b) for any piecewise continuous function $f(x)$, the set of functions $\psi_n(x)$ is complete.

4.14 SPECTRAL REPRESENTATION OF GREEN'S FUNCTIONS

The *inhomogeneous Sturm-Liouville differential equation* for a perturbation $g(x)$ is given by

$$\frac{d}{dx} p(x) \frac{d\psi}{dx} + [q(x) + \lambda \sigma(x)] \psi(x) = g(x). \quad (4.185)$$

The inhomogeneous Sturm-Liouville differential equation for a point-like perturbation at x' described by the delta distribution $\delta(x - x')$ is

$$\frac{d}{dx} p(x) \frac{dG(x, x')}{dx} + [q(x) + \lambda \sigma(x)] G(x, x') = \delta(x - x'). \quad (4.186)$$

Green's function $G(x, x')$ is the solution at x for the point-like perturbation at x' . We expand Green's function $G(x, x')$ into eigenfunctions $\psi_n(x)$ with the eigenvalues λ_n . If the same boundary conditions (4.164a) and (4.164b) are assumed in (4.185) and (4.186), the solution of (4.185) is given by

$$\psi(x) = \int_a^b G(x, x') g(x') dx'. \quad (4.187)$$

Green's function $G(x, x')$ may be considered as a function of the variable x with the parameter x' denoting the position of the point-like source. Since the solutions $\psi_n(x)$ of the homogeneous Sturm-Liouville differential equation (4.163) form a *complete set of basis functions*, we can expand $G(x, x')$ into a series

$$G(x, x') = \sum_{n=-\infty}^{\infty} a_n(x') \psi_n(x), \quad (4.188)$$

where the expansion coefficients $a_n(x')$ depend on the location x' of the source. After inserting into (4.186), it follows with (4.163) that

$$\sum_{n=-\infty}^{\infty} a_n(x') (\lambda - \lambda_n) \sigma(x) \psi_n(x) = \delta(x - x'). \quad (4.189)$$

Multiplying both sides with $\psi_m^*(x)$ and integrating over the interval $[a, b]$, we obtain

$$\begin{aligned} \sum_{n=-\infty}^{\infty} a_n(x') (\lambda - \lambda_n) \int_a^b \sigma(x) \psi_m^*(x) \psi_n(x) dx &= a_m(x') (\lambda - \lambda_m) \\ &= \int_a^b \psi_m^*(x) \delta(x - x') dx = \psi_m^*(x'). \end{aligned} \quad (4.190)$$

With this it follows from (4.188) that

$$G(x, x') = \sum_{n=-\infty}^{\infty} \frac{\psi_n^*(x') \psi_n(x)}{\lambda - \lambda_n}. \quad (4.191)$$

Green's function $G(x, x')$ exhibits poles at $\lambda = \lambda_n$. We note that Green's function is symmetric in x and x' . This expresses the property of reciprocity since we may interchange the point of source with the point of observation.

4.15 PROBLEMS

1. Consider the superposition of two plane waves described by the electric Hertz form

$$\underline{\Pi}_e = (\underline{A}e^{j(k_x x - k_z z)} + \underline{B}e^{j(-k_x x - k_z z)}) dz.$$

- a) Compute the electric and magnetic field of this wave.
 - b) Compute the time-dependent Poynting vector $\mathbf{S}(\mathbf{x}, t)$.
 - c) Compute the complex Poynting vector $\mathbf{T}(\mathbf{x})$.
 - d) Compute the complex power per unit of area flowing in x -, y -, and z -direction.
2. Show that the Poynting vector $\mathbf{S}(\mathbf{x}, t)$ in conventional vector notation is given by

$$\mathbf{S}(\mathbf{x}, t) = \mathbf{E}(\mathbf{x}, t) \times \mathbf{H}(\mathbf{x}, t)$$

and that this equation corresponds to (4.12).

3. Consider a plane dielectric plate depicted in Figure 4.16 with thickness $d = 1$ cm and material parameters $\epsilon_r = 25$, $\mu_r = 1$. The incident harmonic plane wave with frequency 1 GHz is linearly polarized with electric field amplitude $\underline{E}_0 = 10^{-6}$ V/m.
 - a) Compute the electric and magnetic field amplitudes of the waves propagating in positive and negative z -direction in regions 1, 2, and 3.
 - b) Compute the active and reactive power densities in W/m^2 of the waves in regions 1, 2, and 3 as a function of z .
 - c) Compute the electric and magnetic energy stored per m^2 in region 2.
 - d) For which frequencies exhibits the amplitude of the transmitted wave maximum or minimum magnitude?
4. Consider a plane wave incident on a dielectric plate of thickness d with $\epsilon_r = 2.25$ and $\mu_r = 1$ (Figure 4.16).
 - a) Determine d such that a normally incident wave is not reflected.
 - b) Compute reflection and transmission factors for the same thickness d and arbitrary polarization of the incident wave for skew incidence.
 - c) Compute the Poynting form $\mathbf{S}(\mathbf{x}, t)$ for $x < 0$, $0 < x < d$ and $x > d$.
 - d) Compute the complex Poynting form $\mathbf{T}(\mathbf{x})$ for $x < 0$, $0 < x < d$ and $x > d$.

REFERENCES

- [1] A. Sommerfeld, *Elektrodynamik*. Leipzig: Akademische Verlagsgesellschaft Geest & Portig, 1947.
- [2] J. A. Stratton, *Electromagnetic Theory*. New York: McGraw-Hill, 1941.
- [3] R. F. Harrington, *Time Harmonic Electromagnetic Fields*. New York: McGraw-Hill, 1961.
- [4] J. D. Jackson, *Classical Electrodynamics*. New York: John Wiley & Sons, 1975.
- [5] J. A. Kong, *Electromagnetic Wave Theory*. New York: John Wiley & Sons, 1986.
- [6] H. A. Haus and J. R. Melcher, *Electromagnetic Fields and Energy*. Englewood Cliffs, NJ: Prentice Hall, 1989.

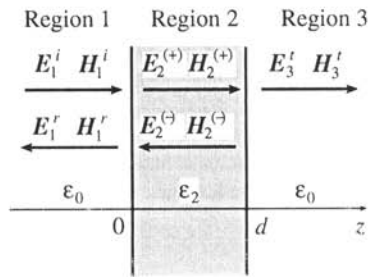


Figure 4.16: Wave incident normally on dielectric plate.

- [7] P. Russer, M. Mongiardo, and L. Felsen, "Electromagnetic field representations and computations in complex structures III: Network representations of the connection and subdomain circuits," *Int. J. Numer. Modeling*, vol. 15, pp. 127–145, 2002.
- [8] P. Penfield, R. Spence, and S. Duinker, *Tellegen's Theorem and Electrical Networks*. Cambridge, Massachusetts: MIT Press, 1970.
- [9] B. D. H. Tellegen, "A general network theorem with applications," *Philips Research Reports*, vol. 7, pp. 259–269, 1952.
- [10] B. D. H. Tellegen, "A general network theorem with applications," *Proc. Inst. Radio Engineers*, vol. 14, pp. 265–270, 1953.
- [11] M. Born and E. Wolf, *Principles of Optics*. Oxford: Pergamon Press, 1975.
- [12] E. A. Wolff, *Antenna Analysis*. Boston: Artech House, 1988.
- [13] J. D. Kraus, *Antennas*. New York: McGraw Hill, 1988.
- [14] T. Rozzi and M. Mongiardo, *Open Electromagnetic Waveguides*. London: IEE, 1997.
- [15] R. S. Elliott, *Antenna Theory and Design*. New York: IEEE Press, 2003.
- [16] V. H. Rumsey, "The reaction concept in electromagnetic theory," *Phys. Rev., ser. 2*, vol. 94, pp. 1483–1491, June 1954.
- [17] D. M. Cannel, *George Green Miller and Mathematician 1793–1841*. Nottingham: City of Nottingham Arts Department, 1988.
- [18] G. Green, "An essay on the application of mathematical analysis to the theories of electricity and magnetism (1828)," in *The Scientific Papers of George Green*, Nottingham: The George Green Memorial Committee, 1995.
- [19] A. Sommerfeld, *Partielle Differentialgleichungen der Physik*. Leipzig: Akademische Verlagsgesellschaft Geest & Portig, 1947.
- [20] L. B. Felsen and N. Marcuvitz, *Radiation and Scattering of Waves*. Englewood Cliffs, NJ: Prentice Hall, 1972.
- [21] R. E. Collin, *Field Theory of Guided Waves*. New York: IEEE Press, 1991.
- [22] A. Ishimaru, *Electromagnetic Wave Propagation, Radiation, and Scattering*. Englewood Cliffs, NJ: Prentice Hall, 1991.
- [23] C.-T. Tai, *Generalized Vector and Dyadic Analysis*. New York: IEEE Press, 1992.
- [24] C.-T. Tai, *Dyadic Green Functions in Electromagnetic Theory*. New York: IEEE Press, 1993.
- [25] G. de Rham, *Differentiable Manifolds*. New York: Springer, 1984.
- [26] K. F. Warnick and D. V. Arnold, "Electromagnetic Green functions using differential forms," *J. Electromagn. Waves and Appl.*, vol. 10, no. 3, pp. 427–438, 1996.
- [27] J. J. Wang, *Generalized Moment Methods in Electromagnetics*. New York: John Wiley & Sons, 1991.

- [28] J. R. Mosig, "Integral equation technique," in *Numerical Techniques for Microwave and Millimeter Wave Passive Structures* (T. Itoh, ed.), pp. 133–213, New York: John Wiley & Sons, 1989.
- [29] C. A. Balanis, *Advanced Engineering Electromagnetics*. New York: John Wiley & Sons, 1989.
- [30] N. Morita, *Integral Equation Methods for Electromagnetics*. Dedham, MA: Artech House, 1990.
- [31] D. G. Dudley, *Mathematic Foundations for Electromagnetic Theory*. New York: IEEE Press, 1994.
- [32] B. Friedman, *Lectures on Applications-Oriented Mathematics*. New York: John Wiley & Sons, 1969.
- [33] S. Hassani, *Mathematical Physics*. Berlin: Springer, 2002.

Chapter 5

Static and Quasistatic Fields

5.1 CONDITIONS FOR STATIC AND QUASISTATIC FIELDS

A field invariant with time is called a *static field*. For static fields the time derivatives in Maxwell's equations (2.114a) to (2.114d) vanish and we obtain

$$d\mathcal{H} = \mathcal{J}, \quad (5.1a) \quad d\mathcal{B} = 0, \quad (5.1b)$$

$$d\mathcal{E} = 0, \quad (5.2a) \quad d\mathcal{D} = \mathcal{Q}. \quad (5.2b)$$

In the static case electric and magnetic fields are not coupled with each other. The source of the electric field is the electric charge and the source of the magnetic field is the electric current. Since in the static case electric and magnetic fields are not coupled with each other the *electrostatic field* and the *magnetostatic field* may be treated independently. Electrostatic phenomena involve time-independent distributions of electric charge and electric field. On the other hand, there are no free magnetic charges. Therefore magnetic phenomena are quite different from electric phenomena. Magnetostatic phenomena involve time-independent distribution of electric current and magnetic field. A detailed treatment of electrostatic and magnetostatic fields is given in [1–5].

An example of an electrostatic problem is an arrangement of two or more conductors insulated from each other at different time-constant potential levels and with no impressed currents. In this case an electric field, but no magnetic field exists. Figure 5.1(a) shows an arrangement of two narrowly spaced conducting plates. The electric field and the stored electric energy are mainly concentrated in the space between the conducting plates. A structure optimized for storing electric energy is called a *capacitor*. An example for a magnetostatic problem is a conductor coil or solenoid with an impressed time-constant current. The current flowing through the conductor gives rise to a static magnetic field only. Figure 5.1(b) shows a solenoid. A current impressed into

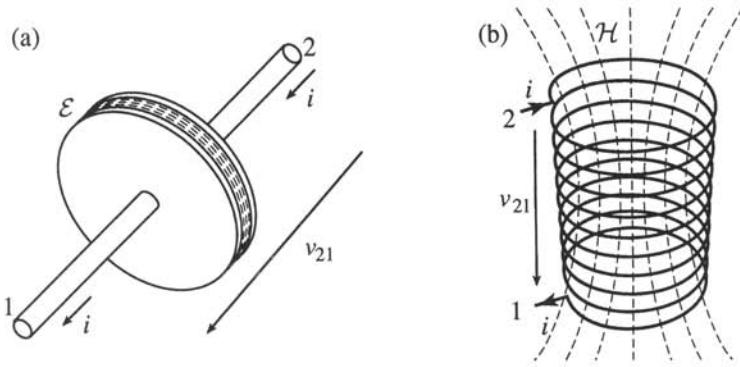


Figure 5.1: (a) Capacitor, and (b) inductor.

the solenoid gives rise to a magnetic field mainly concentrated inside the solenoid. A structure designed for storing magnetic energy when a current is impressed is called an *inductor*.

Maxwell's equations describe the most complex electromagnetic wave phenomena occurring at short time scales or at high frequencies. For problems dealing with relatively long time scales and low frequencies truncated versions of Maxwell's equations may be applied. To establish a measure for the vague characterization "slow," we consider the time an electromagnetic wave needs to propagate through a typical dimension of the system of interest. If this time is small compared with the time scale of field evolution in the system, we may consider the field as a so-called *quasistatic field*.

Slowly varying fields in many cases may be treated as *quasistatic fields* [3, 6]. The quasistatic laws are obtained by neglecting either the time derivative of the magnetic induction or the electric displacement current. The first approximation is called the *electroquasistatic approximation*, the second one the *magnetoquasistatic approximation*. From Maxwell's equations (2.114a)–(2.114d) we obtain

Electroquasistatic approximation

$$d\mathcal{H} = \frac{\partial}{\partial t} \mathcal{D} + \mathcal{J}, \quad (5.3a)$$

$$d\mathcal{E} \cong 0, \quad (5.4a)$$

$$d\mathcal{B} = 0, \quad (5.5a)$$

$$d\mathcal{D} = \mathcal{Q}, \quad (5.6a)$$

Magnetoquasistatic approximation

$$d\mathcal{H} \cong \mathcal{J}, \quad (5.3b)$$

$$d\mathcal{E} = -\frac{\partial}{\partial t} \mathcal{B}, \quad (5.4b)$$

$$d\mathcal{B} = 0, \quad (5.5b)$$

$$d\mathcal{D} = \mathcal{Q}. \quad (5.6b)$$

Due to (5.4a) the electroquasistatic field is essentially irrotational whereas (5.5b) requires the magnetoquasistatic field to be solenoidal.

To give an example of an electroquasistatic field we consider again the capacitor

depicted in Figure 5.1(a). Impressing a slowly time-varying voltage gives rise to a time-varying electric flux between the capacitor plates and by that way to a displacement current flowing between the plates. To describe the capacitor in the case of an applied time-varying voltage we have to consider the time variation of the electric flux density \mathcal{D} . However, in the low-frequency case we usually can neglect the time variation of the magnetic induction \mathcal{B} due to the current flowing through the capacitor. Capacitors may be treated within the electroquasistatic approximation specified by (5.3a) and (5.4a).

The inductor in Figure 5.1(b) may be considered within the magnetoquasistatic approximation specified by (5.3b) and (5.4b). The time variation of the current creates a time variation of the magnetic induction \mathcal{B} in the solenoid and this time-varying flux induces a voltage in the solenoid. In the case of the inductor at low frequencies the displacement current may be neglected.

5.2 STATIC AND QUASISTATIC ELECTRIC FIELDS

5.2.1 Green's Function for the Static Electric Field

In 1828 George Green published *An Essay on the Application of Mathematical Analysis to the Theories of Electricity and Magnetism* [7]. In this work Green developed a technique to solve Poisson's equation of potential theory. Green's function gives the potential of a point or line source of unit strength. Since arbitrary source distributions may be considered as superpositions of point or line sources Green's function is a powerful tool for solving field problems [8, 9].

Due to (5.2a) and (5.4a) in the electrostatic or quasielectrostatic case, the electric field is irrotational and may be derived from the scalar potential Φ as discussed in Section 3.1 from

$$\mathcal{E} = -d\Phi. \quad (5.7)$$

We obtain this equation also from (3.3) for the static case. From (5.6a), (5.7), and the constitutive relation (2.23a) we obtain the *Poisson equation*

$$\Delta\Phi = -\frac{1}{\epsilon} * \mathcal{Q} = -\frac{1}{\epsilon} q. \quad (5.8)$$

We note that the Poisson equation also follows from (3.15b) for the static case.

We calculate the scalar potential field due to a point-like unit charge located at the point \mathbf{x}' . A point-like source may be described by a *three-dimensional Dirac delta distribution*

$$\delta(\mathbf{x} - \mathbf{x}') = \delta(x - x') \delta(y - y') \delta(z - z') \quad (5.9)$$

already introduced in (4.78). The electric field form $\mathcal{Q}(\mathbf{x})$ describing a point-like unit charge located at the point \mathbf{x}' is given by

$$\mathcal{Q}(\mathbf{x}) = \delta(\mathbf{x} - \mathbf{x}') dx \wedge dy \wedge dz. \quad (5.10)$$

Inserting this into (5.8) yields

$$\Delta G_0(\mathbf{x}, \mathbf{x}') = -\frac{1}{\epsilon} \delta(\mathbf{x} - \mathbf{x}') . \quad (5.11)$$

We have renamed the unknown function $\Phi(\mathbf{x})$ by $G_0(\mathbf{x}, \mathbf{x}')$, where \mathbf{x} is the variable, and \mathbf{x}' is the constant coordinate vector denoting the location of the unit source. The function $G_0(\mathbf{x}, \mathbf{x}')$ is called *Green's function*. It relates the *source space* \mathbf{x}' to the *observation space* \mathbf{x} and gives the potential at point \mathbf{x} created by a unit source at point \mathbf{x}' . Multiplying this equation with $Q(\mathbf{x}')$ and integrating over the primed coordinates yields

$$\Delta \int_V' G_0(\mathbf{x}, \mathbf{x}') Q(\mathbf{x}') = -\frac{1}{\epsilon} q(\mathbf{x}) . \quad (5.12)$$

Comparing this with (5.8) yields

$$\Phi(\mathbf{x}) = \int_V' G_0(\mathbf{x}, \mathbf{x}') Q(\mathbf{x}') . \quad (5.13)$$

We apply the Hodge operator on both sides of (5.11) and integrate over a spherical volume of radius r and center point \mathbf{x}' . On the left side we apply Stokes' theorem (A.90) to transform the volume integral into a surface integral.

$$\oint_{\partial V} \star dG_0(\mathbf{x}, \mathbf{x}') = -\frac{1}{\epsilon} \int_V \delta(\mathbf{x} - \mathbf{x}') d\mathbf{x} \wedge d\mathbf{y} \wedge d\mathbf{z} = -\frac{1}{\epsilon} . \quad (5.14)$$

We now introduce spherical coordinates (r, θ, ϕ) around the center point \mathbf{x}' . Due to the spherical symmetry of the problem, $G(\mathbf{x}, \mathbf{x}')$ only depends on $r = |\mathbf{x} - \mathbf{x}'|$ and we can write $G(r)$ instead of $G(\mathbf{x}, \mathbf{x}')$. Since G_0 is constant over the surface of the sphere, performing the integration on the left side of (5.14) yields

$$\oint_{\partial V} \star dG_0(\mathbf{x}, \mathbf{x}') = \oint_{\partial V} \frac{\partial G_0}{\partial r} r^2 \sin \theta d\theta \wedge d\phi = 4\pi r^2 \frac{\partial G_0}{\partial r} . \quad (5.15)$$

From (5.14) and (5.15) we obtain

$$\frac{\partial G_0}{\partial r} = -\frac{1}{4\pi\epsilon r^2} \quad (5.16)$$

and after integration the *scalar Green's function* for the electrostatic problem

$$G_0(r) = \frac{1}{4\pi\epsilon r} . \quad (5.17)$$

Green's function relates the observation space \mathbf{x} to the source space \mathbf{x}' .

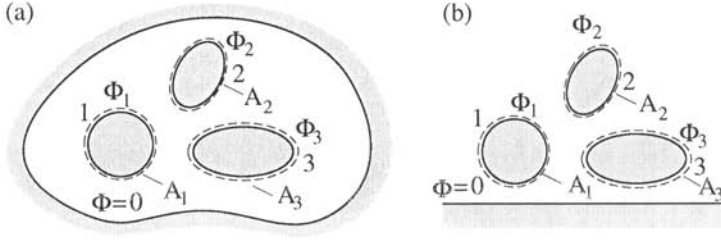


Figure 5.2: (a) Closed multiconductor structure, and (b) open multiconductor structure.

5.2.2 Capacitance

Applying an electric voltage between two conductors yields an electric field and an associated electric flux density between these conductors. The flux density induces positive and negative charges of same magnitude in both conductors. The ratio of the induced charge to the applied voltage is called *capacitance*.

Figure 5.2 shows closed and open multiconductor structures. We consider a multiconductor structure with $N + 1$ conductors. The conductor 0 is assumed to exhibit the potential $\Phi_0 = 0$. Let the voltage between conductor k and conductor 0 be v_k . The potential field for the case when the k th conductor exhibits voltage v_k and all other conductors exhibit voltage $v_l = 0$ for $l \neq k$ is named $\Phi_k(\mathbf{x})$. Applying the superposition principle yields the total potential

$$\Phi(\mathbf{x}) = \sum_{k=1}^N \Phi_k(\mathbf{x}). \quad (5.18)$$

We introduce the normalized potential ϕ_k by

$$\phi_k(\mathbf{x}) = \frac{\Phi_k(\mathbf{x})}{v_k}. \quad (5.19)$$

With this we obtain from (5.18)

$$\Phi(\mathbf{x}) = \sum_{k=1}^N v_k \phi_k(\mathbf{x}). \quad (5.20)$$

The charge of conductor l is given by the integral of the electric flux density over the surface A_l enclosing conductor l .

$$q_l = \oint_{A_l} \mathcal{D} = -\epsilon \oint_{A_l} \star d\Phi = -\sum_{k=1}^N v_k \epsilon \oint_{A_l} \star d\phi_k. \quad (5.21)$$

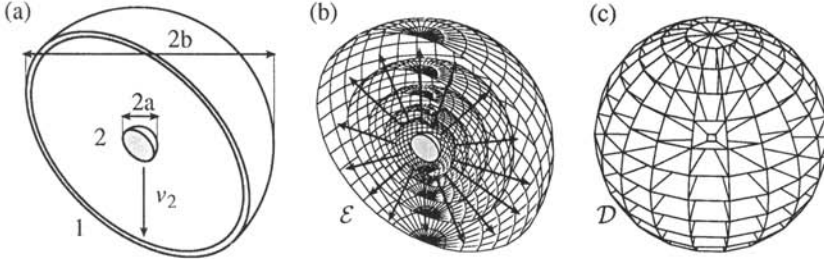


Figure 5.3: (a) Spherical capacitor, (b) electric field, and (c) electric flux density.

The charges induced on conductor l due to the voltages v_k on conductors k is given by

$$q_l = \sum_{k=1}^N C_{lk} v_k, \quad (5.22)$$

where the *partial capacitance* C_{lk} is given by

$$C_{lk} = -\epsilon \oint_{A_l} \star d\phi_k. \quad (5.23)$$

The current i_l flowing into the l th conductor is given by

$$i_l = \frac{dq_l}{dt} = \sum_{k=1}^N C_{lk} \frac{dv_k}{dt}. \quad (5.24)$$

Let us now explicitly calculate the capacitance of some geometrically simple conductor structures. We compute the electric field of an electrically charged spherical conductor of radius a depicted in Figure 5.3(b). We assume spherically symmetric charge distribution over the surface of the spherical conductor. Due to the spherical symmetry of the problem the electric field as well as the electric flux density will only exhibit radial components $E_r(r)$ and $D_r(r)$, where r is the distance from the center of the sphere. In spherical coordinates the electric flux form is given by

$$\mathcal{D}(r) = D_r(r) r^2 \sin \theta d\theta \wedge d\phi. \quad (5.25)$$

Applying Gauss' law (2.57d) and integrating the flux density over a sphere with radius $r \geq a$ yields the charge q

$$q = \int_V \mathcal{Q} = \oint_{\partial V} \mathcal{D} = r^2 D_r(r) \oint_{\partial V} d\theta \wedge d\phi = 4\pi r^2 D_r(r). \quad (5.26)$$

From this we obtain the radial component of the flux density

$$D_r(r) = \frac{q}{4\pi r^2} \quad (5.27)$$

and the flux differential form

$$\mathcal{D}(r) = \frac{q}{4\pi} \sin \theta \, d\theta \wedge d\phi. \quad (5.28)$$

Figure 5.3(c) visualizes the flux differential form \mathcal{D} by cones originating at the center of the sphere. The cross-section of the cones are proportional to $1/r^2$. We consider that it is impossible to give a spherically symmetric tessellation of the surface of a sphere. Therefore the picture in Figure 5.3(c) is not spherically symmetric. However, the shape of the flux tubes is of no account. If all flux tubes have the same cross-section at a given distance r from the center of the sphere, the dielectric flux density exhibits spherical symmetry. With (2.32a) we obtain

$$\mathcal{E}(r) = \frac{1}{\epsilon} \star \mathcal{D}(r) = \frac{q}{4\pi\epsilon r^2} dr \quad (5.29)$$

and the corresponding radial component electric field component

$$E_r(r) = \frac{q}{4\pi\epsilon r^2}. \quad (5.30)$$

Using (2.63) we compute the potential difference $\Phi_2 - \Phi_1$ between the two points 2 and 1 with distance r_2 and r_1 from the origin

$$\Phi(r_2) - \Phi(r_1) = - \int_1^2 \mathcal{E} = \frac{q}{4\pi\epsilon} \left(\frac{1}{r_2} - \frac{1}{r_1} \right). \quad (5.31)$$

Choosing the potential of reference at $\Phi(\infty) = 0$, the potential $\Phi(r)$ is given by

$$\Phi(r) = \frac{q}{4\pi\epsilon r}. \quad (5.32)$$

Figure 5.3(b) shows the equipotential spheres. For an equal potential difference between neighboring spheres the distance between the spheres must be proportional to $1/r$. Drawing the electric field lines normal to the equipotential spheres, the number of field lines piercing an equipotential sphere per unit of area is proportional to $1/r^2$.

The potential of the surface of a metallic sphere with radius a and charge q is $\Phi(a)$. The *capacitance* is defined as the ratio of the charge and the potential,

$$C = \frac{q}{\Phi}. \quad (5.33)$$

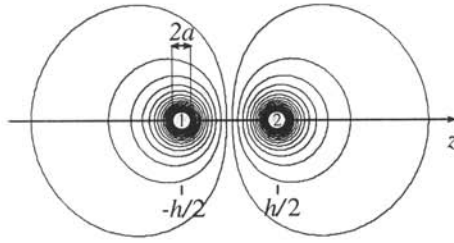


Figure 5.4: Electrostatic field of a dipole.

A sphere with radius a has a capacitance

$$C = 4\pi\epsilon a. \quad (5.34)$$

A *spherical capacitor* is formed by two concentric conducting spheres as depicted in Figure 5.3(a). The inner sphere 2 has a radius a and the inner radius of the outer spherical conductor 1 is b . For a charge q on sphere 2 we obtain from (5.31) the voltage

$$v_{21} = \frac{q}{4\pi\epsilon} \left(\frac{1}{a} - \frac{1}{b} \right) \quad (5.35)$$

and from this with (5.33) the capacitance of the spherical capacitor

$$C = 4\pi\epsilon \frac{ab}{b-a}. \quad (5.36)$$

The charge q on the inner sphere 2 induces a charge $-q$ on the outer sphere 1.

Figure 5.4 shows an electric *dipole* consisting of two spherical conductors of radius a in a distance h . We assume $h \gg a$. This means that we can neglect the perturbation of the field of sphere 1 when bringing the uncharged sphere 2 into the field created by sphere 1. In this case the potentials Φ_1 and Φ_2 on spheres 1 and 2 are approximately given by

$$\Phi_1 = \frac{1}{4\pi\epsilon} \left(\frac{q_1}{a} + \frac{q_2}{h} \right), \quad \Phi_2 = \frac{1}{4\pi\epsilon} \left(\frac{q_2}{a} + \frac{q_1}{h} \right), \quad (5.37)$$

where q_1 and q_2 are the charges of sphere 1 and sphere 2. If both spheres contain charge of equal magnitude and opposite sign, $q = q_1 = -q_2$, the potential difference between the spheres is

$$v_{21} = \Phi_2 - \Phi_1 = \frac{q}{2\pi\epsilon} \left(\frac{1}{a} - \frac{1}{h} \right). \quad (5.38)$$

With (5.33) we obtain the capacitance

$$C = 2\pi\epsilon \frac{a}{1 - a/h}. \quad (5.39)$$

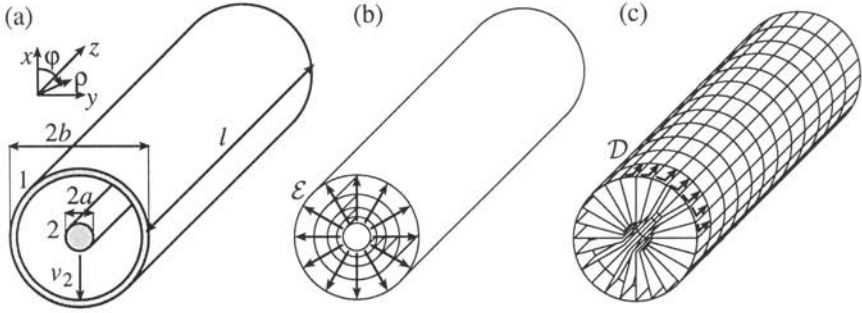


Figure 5.5: (a) Coaxial line segment, (b) electric field, and (c) electric flux density.

For $h \gg a$ the capacitance C becomes independent of h and is half the capacitance of a single sphere. This means the dipole structure of Figure 5.4 in this case behaves like two spheres connected in series.

The coaxial circular cylindric structure shown in Figure 5.5(a) is formed by an inner conductor with outer radius a and an outer conductor with inner radius b . We consider a segment of this structure of length l . Let q be the charge on a segment of length l of the inner conductor. Due to the cylindric symmetry of the structure, the electric field exhibits only an r -component in a cylindric coordinate system. The electric flux form \mathcal{D} is given by

$$\mathcal{D}(\mathbf{r}) = D_r(r) r d\phi \wedge dz. \quad (5.40)$$

Using (2.57d) and integrating the flux density over a cylinder of length l and radius r $a \leq r \leq b$ yields the charge q on the inner conductor segment of length l ,

$$q = \oint_{\partial V} \mathcal{D} = r D_r(r) \oint_{\partial V} d\phi \wedge dz = 2\pi r l D_r(r). \quad (5.41)$$

The charge per unit of length q' is given by

$$q' = \frac{q}{l} = 2\pi r D_r(r). \quad (5.42)$$

From this we obtain the radial component of the flux density

$$D_r(r) = \frac{q'}{2\pi r}. \quad (5.43)$$

and the flux differential form

$$\mathcal{D}(\mathbf{r}) = \frac{q'}{2\pi r} r d\phi \wedge dz. \quad (5.44)$$

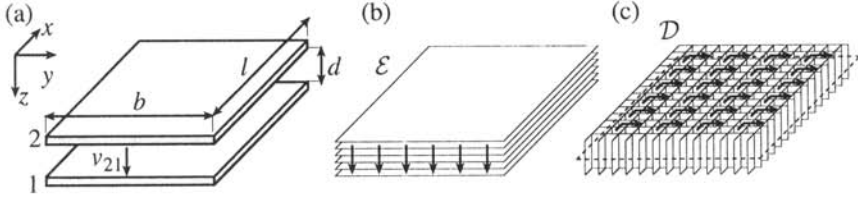


Figure 5.6: (a) Plate capacitor, (b) electric field, and (c) electric flux density.

With (2.32a) we obtain

$$\mathcal{E}(r) = \frac{1}{\epsilon} \star \mathcal{D}(r) = \frac{q'}{2\pi\epsilon r} dr. \quad (5.45)$$

and the corresponding radial component E_r of the electric field,

$$E_r(r) = \frac{q'}{2\pi\epsilon r}. \quad (5.46)$$

The voltage v_{21} between inner conductor 2 and outer conductor 1 is given by

$$v_{21} = \Phi_2 - \Phi_1 = - \int_a^b \mathcal{E} = \frac{q'}{2\pi\epsilon} \ln \frac{b}{a}. \quad (5.47)$$

From this we obtain the *capacitance per unit of length*

$$C' = \frac{2\pi\epsilon}{\ln \frac{b}{a}}. \quad (5.48)$$

The capacitance per unit of length computed in the quasistatic approach is related to the inductance per unit of length and the characteristic impedance of a transverse electromagnetic wave propagating in the cylindric structure (see Table 7.2).

Figure 5.6 shows two parallel plates with distance d . In case of infinite extension of these plates we obtain a homogeneous electric field between the two plates if a voltage v_{21} is applied between both plates. The field solution for infinite extension will also give a good approximation for plates of finite transverse extension if $b, l \gg d$. For symmetry reasons the electric field is homogeneous and only exhibits a component normal to the plates. The plates 1 and 2 exhibit uniform surface charge densities Q_{A1} and Q_{A2} . With (2.170b) we obtain

$$\mathcal{D} = -Q_{A1} = Q_{A2} = q_A dx \wedge dy. \quad (5.49)$$

From (2.32a) we obtain

$$\mathcal{E} = \frac{1}{\epsilon} \star \mathcal{D} = \frac{q_A}{\epsilon} dz. \quad (5.50)$$

With (2.63) we compute the potential difference v_{21} between the top plate 2 and the bottom plate 1.

$$v_{21} = - \int_1^2 \mathcal{E} = - \frac{q_A}{\epsilon} \int_1^2 dz = \frac{q_A d}{\epsilon}. \quad (5.51)$$

From this we obtain the *capacitance per unit of area*

$$C'' = \frac{q_A}{v_{21}} = \frac{\epsilon}{d}. \quad (5.52)$$

5.3 STATIC AND QUASISTATIC MAGNETIC FIELDS

5.3.1 Green's Function for the Static Magnetic Field

Following (3.1) we obtain the magnetic induction form \mathcal{B} from the magnetic vector potential form \mathcal{A} via

$$\mathcal{B} = d\mathcal{A}. \quad (5.53)$$

For static magnetic fields excited by a steady current

$$\mathcal{J}_0 = J_{0x} dy \wedge dz + J_{0y} dz \wedge dx + J_{0z} dx \wedge dy \quad (5.54)$$

we obtain from (3.15a) the *vectorial Poisson equation*

$$\Delta \mathcal{A} = - * \mu \mathcal{J}_0. \quad (5.55)$$

The solution of the vector field problem with unit point-like vectorial source is given by a *dyadic Green's function* with the components G_{ij} relating the i th component of the field vector to the j th component of the source vector [8, 9]. In differential form calculus dyadics may be represented by *double forms*. To compute the field at a point \mathbf{x} excited by a point-like source located at \mathbf{x}' we use *Green's double one-form* [10, 11]. A *double one-form* \mathcal{G} is defined by

$$\begin{aligned} \mathcal{G}(\mathbf{x}, \mathbf{x}') = & G_{11} dx dx' + G_{12} dx dy' + G_{13} dx dz' \\ & + G_{21} dy dx' + G_{22} dy dy' + G_{23} dy dz' \\ & + G_{31} dz dx' + G_{32} dz dy' + G_{33} dz dz'. \end{aligned} \quad (5.56)$$

Green's double form relates the observation space \mathbf{x} to the source space \mathbf{x}' . Primed and unprimed differentials dx'_i and dx_j commute (i.e., in products they may be interchanged without changing the sign). The rules are

$$dx_i dx'_j = dx'_i dx_j \quad \text{with } dx_i = dx, dy, dz. \quad (5.57)$$

With the *identity kernel* already introduced in (4.77)

$$\mathcal{I}(\mathbf{x}, \mathbf{x}') = \delta(\mathbf{x} - \mathbf{x}') (dx dx' + dy dy' + dz dz') \quad (5.58)$$

we can express the vectorial Poisson equation (5.55) for a point-like unit source at \mathbf{x}' by

$$\Delta \mathcal{G}(\mathbf{x}, \mathbf{x}') = -\mu \mathcal{I}(\mathbf{x}, \mathbf{x}') . \quad (5.59)$$

In (5.59) the Laplace operator acts on the unprimed coordinate variables whereas the primed coordinate variables are treated as constants. Forming the exterior product with $\mathcal{J}_0(\mathbf{x}')$, integrating over the primed variables and using (4.81b) yields

$$\star \int' \Delta \mathcal{G}(\mathbf{x}, \mathbf{x}') \wedge \mathcal{J}_0(\mathbf{x}') = -\mu \mathcal{J}_0(\mathbf{x}) . \quad (5.60)$$

Since the sequence of partial derivation with respect to the unprimed coordinates and integration over the primed coordinates may be interchanged under very general conditions, and considering (A.64), we obtain

$$\Delta \int' \mathcal{G}(\mathbf{x}, \mathbf{x}') \wedge \mathcal{J}_0(\mathbf{x}') = -\star \mu \mathcal{J}_0(\mathbf{x}) . \quad (5.61)$$

Comparing this equation with (5.55) yields

$$\mathcal{A}(\mathbf{x}) = \int' \mathcal{G}(\mathbf{x}, \mathbf{x}') \wedge \mathcal{J}_0(\mathbf{x}') . \quad (5.62)$$

In Cartesian coordinates the Laplace operator for one-forms (A.73) is symmetric in its three components and leaves the three components uncoupled. Therefore (5.61) may be solved by

$$\mathcal{G}(\mathbf{x}, \mathbf{x}') = G(\mathbf{x}, \mathbf{x}') (dx dx' + dy dy' + dz dz') , \quad (5.63)$$

where $G(\mathbf{x}, \mathbf{x}')$ is a *scalar Green's function*, obtained by solving the scalar Poisson equation

$$\Delta G(\mathbf{x}, \mathbf{x}') = -\mu \delta(\mathbf{x} - \mathbf{x}') . \quad (5.64)$$

This problem has already been treated in Section 5.2.1. In analogy to the solution (5.17) of (5.8) we obtain

$$G(r) = \frac{\mu}{4\pi r} . \quad (5.65)$$

Inserting (5.54), (5.63) and (5.65) in (5.62) yields

$$\mathcal{A}(\mathbf{x}) = \frac{\mu}{4\pi} \int' \frac{J_{0x}(\mathbf{x}') dx + J_{0y}(\mathbf{x}') dy + J_{0z}(\mathbf{x}') dz}{|\mathbf{x} - \mathbf{x}'|} dx' \wedge dy' \wedge dz' . \quad (5.66)$$

To compute the vector potential \mathcal{A} excited by a thin wire carrying a current I_0 we have to perform the volume integration in (5.62) over the volume of the wire. The integral may be performed first over the cross-sectional area of the wire, which is transverse to the curve followed by the wire and then in the direction tangential to the wire. After the integration over the cross-sectional area we obtain

$$\mathcal{A}(\mathbf{x}) = I_0 \int_{C_1}' \mathcal{G}(\mathbf{x}, \mathbf{x}') . \quad (5.67)$$

With (5.53) we obtain from (5.62) the dependence of the magnetic induction from the current as

$$\mathcal{B}(\mathbf{x}) = d \int_{C_1}' \mathcal{G}(\mathbf{x}, \mathbf{x}') \wedge \mathcal{J}_0(\mathbf{x}') , \quad (5.68)$$

where the exterior derivation is applied to \mathbf{x} and integration is performed over \mathbf{x}' . We introduce Green's form

$$\mathcal{G}_{BS}(\mathbf{x}, \mathbf{x}') = d\mathcal{G}(\mathbf{x}, \mathbf{x}') , \quad (5.69)$$

and obtain the *Biot-Savart law* [3]

$$\mathcal{B}(\mathbf{x}) = \int_{C_1}' \mathcal{G}_{BS}(\mathbf{x}, \mathbf{x}') \wedge \mathcal{J}_0(\mathbf{x}') . \quad (5.70)$$

Biot-Savart's law is often considered as the experimental postulate on which magnetostatics is based [8]. Green's form $\mathcal{G}_{BS}(\mathbf{x}, \mathbf{x}')$ is a *one-two double form* since it is a product of a two-form in \mathbf{x} and a one-form in \mathbf{x}' . From (5.63), (5.65), and (5.69) we obtain

$$\mathcal{G}_{BS}(\mathbf{x}, \mathbf{x}') = -\frac{\mu}{4\pi r^3} (x dx + y dy + z dz) \wedge (dx dx' + dy dy' + dz dz') . \quad (5.71)$$

The magnetic induction \mathcal{B} excited by a thin wire along a curve C_1 carrying a current I_0 is given, similar to (5.67) by

$$\mathcal{B}(\mathbf{x}) = I_0 \int_{C_1}' \mathcal{G}_{BS}(\mathbf{x}, \mathbf{x}') , \quad (5.72)$$

where the integral is performed over the curve C_1 .

5.3.2 Inductance

A current flowing through a conductor creates a magnetic field. The magnetic induction or flux density associated with this field yields a magnetic flux through a coil formed by the conductor. The ratio of this magnetic flux to the current creating the flux is called the *inductance* of the conductor. If the magnetic field that is created by the current in

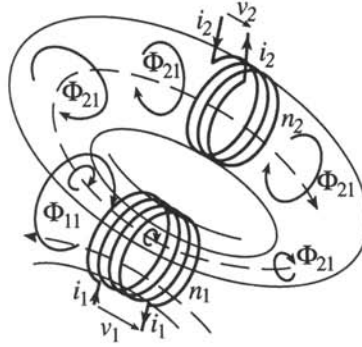


Figure 5.7: Transformer.

one conductor induces a magnetic flux through a coil formed by another conductor, the ratio of the flux through this coil formed by the other conductor to the current through the first conductor is called the *mutual inductance* between both conductors.

Figure 5.7 illustrates the inductive coupling of two coils 1 and 2. The current i_1 flowing through coil 1 creates a magnetic field and a total flux Φ_{11} . The part of the magnetic flux flowing through the coil 2 is denominated with Φ_{21} . If current i_1 changes with time, the corresponding time variations of Φ_{11} and Φ_{21} , respectively, induce voltages u_1 and u_2 across the poles of coil 1 and 2, respectively. The arrangement of two inductive coupled coils is called a *transformer*.

We consider two wire coils 1 and 2 following the closed curves ∂A_1 and ∂A_2 , respectively. These closed curves may be interpreted as the boundaries of the surfaces A_1 and A_2 . The vector potential due to a current i_{01} flowing in coil 1 is given by

$$\mathcal{A}(\mathbf{x}) = i_1 \int'_{\partial A_1} \mathcal{G}(\mathbf{x}, \mathbf{x}') . \quad (5.73)$$

The magnetic flux Φ_{21} through coil 2 due to the current i_1 flowing in coil 1 is

$$\Phi_{21} = \int_{A_2} \mathcal{B}(\mathbf{x}) = \oint_{\partial A_2} \mathcal{A}(\mathbf{x}) . \quad (5.74)$$

Inserting (5.73) into (5.74) yields

$$\Phi_{21} = i_1 \oint_{\partial A_2} \oint'_{\partial A_1} \mathcal{G}(\mathbf{x}, \mathbf{x}') . \quad (5.75)$$

The ratio M_{21} of flux Φ_{21} through coil 2 to the exciting current i_1 through coil 1 is called

the *mutual inductance* between coils 1 and 2.

$$M_{21} = \frac{\Phi_{21}}{i_1} = \oint_{\partial A_2} \oint'_{\partial A_1} \mathcal{G}(\mathbf{x}, \mathbf{x}') . \quad (5.76)$$

We note that the expression for the mutual inductance is symmetric with respect to coils 1 and 2. From this it follows

$$M_{21} = M_{12} . \quad (5.77)$$

If both coils exhibit the same orientation with respect to the flux flow, the mutual inductance is positive; otherwise it is negative. Interchanging the poles of one coil changes the sign of the mutual inductance. The ratio of flux and current through the same coil is called *self-inductance* or simply *inductance*. The inductance of coil 1 is given by

$$L_1 = \oint_{\partial A_1} \oint'_{\partial A_1} \mathcal{G}(\mathbf{x}, \mathbf{x}') . \quad (5.78)$$

If two coils k and l are coupled magnetically, the magnetic flux Φ_l through coil l , excited by a current i_k through coil k is given by

$$\Phi_l = M_{lk} i_k . \quad (5.79)$$

The voltage v_l induced in coil l is given by

$$v_l = \frac{d\Phi_l}{dt} = M_{lk} \frac{di_k}{dt} . \quad (5.80)$$

In the following we will discuss the inductance of some simple conductor structures. Figure 5.8 shows a solenoid of length l and diameter $2a$ and n turns. It is composed of a thin, perfectly conducting wire, wound in a helix. We assume $l \gg 2a$. From Ampère's law (5.3b) we obtain for magnetoquasistatic fields

$$\oint_{\partial A} \mathcal{H} = \int_A \mathcal{J} . \quad (5.81)$$

The area A enclosed by the closed path of integration in Figure 5.8(b) is pierced n times by the conductor of the solenoid. Therefore the path of integration encloses the total current ni . Due to the assumption $l \gg 2a$ the magnetic field created by the current is mainly concentrated inside the solenoid. For this reason we only need to integrate \mathcal{H} over the part of the path inside the solenoid from the bottom 1 to the top 2. We obtain the relation

$$\int_1^2 \mathcal{H} = ni \quad (5.82)$$

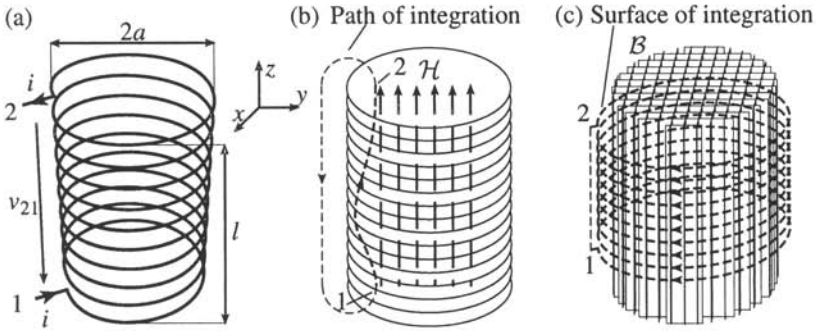


Figure 5.8: (a) Solenoid, (b) magnetic field, and (c) magnetic flux density.

and since the field is homogeneous inside the solenoid

$$\mathcal{H} = \frac{ni}{l} dz. \quad (5.83)$$

With (2.32a) we obtain

$$B = \mu * \mathcal{H} = B_z dx \wedge dy = \frac{n\mu i}{l} dx \wedge dy. \quad (5.84)$$

The coil and therewith the path of integration is linked n times with the flux. Therefore the area of integration A in the above integral is n times the cross-sectional area of the solenoid. The flux Φ through the solenoid is given by

$$\Phi = \int_A B = a^2 \pi B_z = \mu \frac{na^2 \pi}{l} i. \quad (5.85)$$

The surface A_L bounded by the solenoid exhibits n layers as depicted in Figure 5.8(c). Therefore the magnetic flux flows n times through cross-sectional area A and we obtain the *flux linkage*

$$\Phi_L = \int_{A_L} B = n \int_A B = na^2 \pi B_z = \mu \frac{n^2 a^2 \pi}{l} i \quad (5.86)$$

by summing the flux contributions of all the turns of the coil. The flux linked by the coil is due to the current i itself. Since the flux linkage Φ_L is proportional to the current i the ratio of the flux linkage to the current characterizes the solenoid. The *inductance* L is defined as

$$L = \frac{\Phi_L}{i}. \quad (5.87)$$

The inductance of the solenoid is

$$L = \mu \frac{n^2 a^2 \pi}{l}. \quad (5.88)$$

We apply Faraday's law (2.57b)

$$\oint_{\partial A_L} \mathcal{E} = -\frac{d}{dt} \int_{A_L} \mathcal{B}. \quad (5.89)$$

The boundary ∂A_L follows the conductor solenoid and is closed via the path marked by the thin dashed line outside the conductor. Since the electric field component tangential to the solenoid conductor vanishes, only the part of the path outside the conductor region from node 1 to node 2 contributes to the path integral over \mathcal{E} and gives the voltage between nodes 2 and 1:

$$\oint_{\partial A_L} \mathcal{E} = \int_1^2 \mathcal{E} = -v_{21}. \quad (5.90)$$

The voltage v_{21} is independent of the path of integration as long as this path is not wound around the solenoid.

The inductance L is the ratio between the voltage v and the time derivative di/dt of the current:

$$v_{21} = L \frac{di}{dt}. \quad (5.91)$$

A coaxial line structure also exhibits an *inductance per unit of length*. We assume a current i_2 flowing in the z -direction in the inner conductor 2 of the coaxial line depicted in Figure 5.9(a). The magnetic field must exhibit cylindrical symmetry and therefore depend only on r . Due to (5.5b) the r - and z -component of the flux density and the magnetic field vanish and we obtain

$$\mathcal{H} = H_\phi(r) r d\phi. \quad (5.92)$$

From Ampère's law (5.1a) we obtain by integrating over the path C in Figure 5.9(b)

$$\oint_C \mathcal{H} = 2\pi r H_\phi(r) = i_2 \quad (5.93)$$

and from this

$$\mathcal{H} = \frac{i_2}{2\pi r} r d\phi. \quad (5.94)$$

With (2.32a) we obtain the magnetic flux density form

$$\mathcal{B} = \mu * \mathcal{H} = \frac{\mu i_2}{2\pi r} dz \wedge dr. \quad (5.95)$$

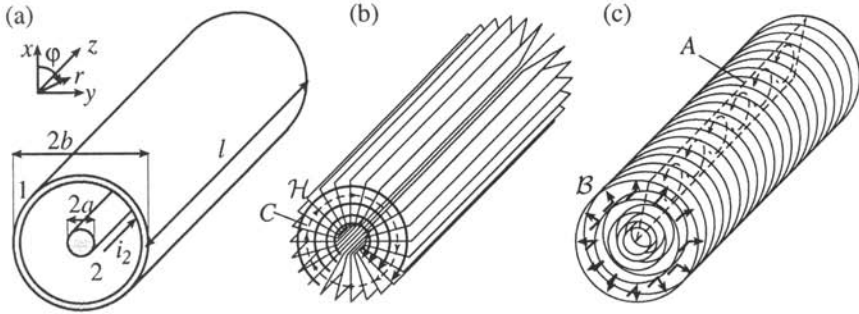


Figure 5.9: (a) Coaxial line segment, (b) magnetic field, and (c) magnetic flux density.

The flux Φ between the inner conductor 2 and the outer conductor 1 over a length l of the coaxial line is given by

$$\Phi = \int_A \mathcal{B} = \frac{\mu l i_2}{2\pi} \int_2^1 \frac{dr}{r} = \frac{\mu l i_2}{2\pi} \ln \frac{b}{a}. \quad (5.96)$$

The flux per unit of length Φ' is given by

$$\Phi' = \Phi/l = \frac{\mu i_2}{2\pi} \ln \frac{b}{a} \quad (5.97)$$

and the *inductance per unit of length* L' of the coaxial line is

$$L' = \Phi'/i_2 = \frac{\mu}{2\pi} \ln \frac{b}{a}. \quad (5.98)$$

We now consider the parallel plate structure shown in Figure 5.10. On the inner surface of both plates surface currents with surface current densities \mathcal{J}_{A1} and \mathcal{J}_{A2} are impressed. We assume the surface current to flow in the positive or negative x -direction. In this case the surface current differential forms are given by

$$\mathcal{J}_{A1} = -\mathcal{J}_{A1x} dy, \quad \mathcal{J}_{A2} = \mathcal{J}_{A2x} dy. \quad (5.99)$$

We make the point that the direction of the surface current flow, the orientation of the twisted one-form, and the orientation of the surface normal direction form a positive oriented orthogonal trihedron. This explains the different signs in the equations above. Due to the symmetry of the structure and also due to (5.5b) between the parallel plates only a tangential magnetic field exists and from (2.168a) it follows

$$\mathcal{H} = \mathcal{J}_{A1} = \mathcal{J}_{A2} \quad (5.100)$$

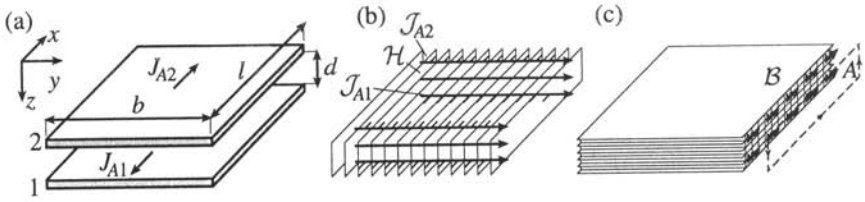


Figure 5.10: (a) Parallel plate structure, (b) magnetic field, and (c) magnetic flux density.

and from this $J_{A1x} = -J_{A2x}$. With (2.32a) we obtain the magnetic flux density form

$$B = \mu * \mathcal{H} = \mu J_{A2x} dz \wedge dx. \quad (5.101)$$

The magnetic flux Φ through the area element A of length l and height d (Figure 5.10(c)) is given by

$$\Phi = \int_A B = \mu d l J_{A2x}. \quad (5.102)$$

The current i_2 flowing on conductor 2 in the positive x -direction within a strip of width b is

$$i_2 = \int_1^2 \mathcal{J}_{A2} = b J_{A2x}. \quad (5.103)$$

From this we obtain the inductance $L_{l/b}$ of a parallel plate segment of width b and length l

$$L_{l/b} = \Phi / i_2 = \mu \frac{d l}{b}. \quad (5.104)$$

Introducing the inductance L_{\square} of a quadratic parallel plate element

$$L_{\square} = \mu d \quad (5.105)$$

we obtain

$$L_{l/b} = \frac{\Phi}{i_2} = \frac{l}{b} L_{\square}. \quad (5.106)$$

5.4 THE LAPLACE EQUATION

Electrostatic and magnetostatic problems involve the solution of the *Laplace equation*. For regions free of charge (i.e., $\mathcal{Q} = 0$), the Poisson's equation (5.8) becomes the Laplace equation

$$\Delta \Phi_e = 0. \quad (5.107)$$

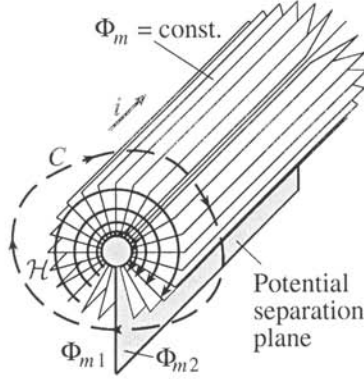


Figure 5.11: Potential separation plane.

In the following sections of this chapter we will denominate the electrostatic potential with Φ_e in order to distinguish it from the magnetic potential introduced below. The electric field is given by

$$\mathcal{E} = -d\Phi_e. \quad (5.108)$$

In the magnetostatic case the magnetic field also may be derived from a scalar potential. For regions where $\mathcal{E} = 0$ from (5.3b) follows $d\mathcal{H} = 0$. Due to Poincaré's lemma (A.61), the magnetic field form can be represented as the exterior derivative of a scalar potential Φ_m :

$$\mathcal{H} = -d\Phi_m. \quad (5.109)$$

With (5.5b), (2.32b), and (3.13)

$$\Delta\Phi_m = 0. \quad (5.110)$$

A solution of the Laplace equation is called a *harmonic function*.

In structures containing perfect electrical conductors the surface of the conductors are equipotential surfaces (i.e., surfaces of constant Φ_e). The exterior derivative $d\Phi_e$ is normal to the surface of a perfect conductor. The magnetic field exhibits no normal component at the surface of a perfect conductor. Therefore, equipotential surfaces of the scalar magnetic potential Φ_m are normal to the surface of a perfect conductor and $d\Phi_m$ is tangential to the surface.

5.4.1 Potential Separation Planes

Consider a wire carrying a current i depicted in Figure 5.11. Due to Ampère's law (2.57a), the integral of \mathcal{H} over the closed curve c enclosing the current i is

$$\oint_C \mathcal{H} = 2\pi i. \quad (5.111)$$

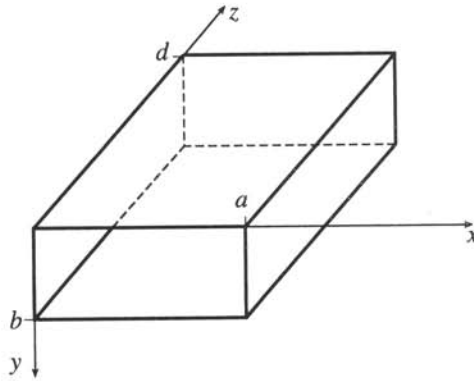


Figure 5.12: Open metallic box.

Note that the potential is multiple valued if the current carrying line is encircled more than once. The Laplace equation is not valid in the conductor. A path of integration encircling the current is not allowed. We can introduce a potential separation surface as shown in Figure 5.11 to make the scalar magnetic potential single-valued [3, 12]. If potential separation planes are introduced in such a way that the complete space region under consideration remains connected but no current can be encircled by a closed path, the static magnetic field can be derived from a scalar magnetic potential ψ . The integral from side 1 of the current separation plane around the current i to the opposite side 2 of the current separation plane is given by

$$\oint_C \mathcal{H} = \oint_1^2 \mathcal{H} = 2\pi i = -(\Phi_{m2} - \Phi_{m1}). \quad (5.112)$$

This expression is valid for any path of integration from side 1 to side 2 of the potential separation plane.

5.4.2 Three-Dimensional Laplace Equation in Cartesian Coordinates

In this section we investigate the scalar field solutions of the Laplace equation when boundary conditions are specified in orthogonal Cartesian coordinates [3]. Consider the three-dimensional solution in Cartesian coordinates. With (A.69) we obtain

$$\frac{\partial^2 \Phi}{\partial x^2} + \frac{\partial^2 \Phi}{\partial y^2} + \frac{\partial^2 \Phi}{\partial z^2} = 0. \quad (5.113)$$

The function

$$\Phi(\mathbf{x}) = e^{j\mathbf{y} \cdot \mathbf{x}} = e^{j(\gamma_x x + \gamma_y y + \gamma_z z)} \quad (5.114)$$

is a solution of the Laplace equation (5.113) for

$$\mathbf{y} \cdot \mathbf{y} = \gamma_x^2 + \gamma_y^2 + \gamma_z^2 = 0. \quad (5.115)$$

Separating the γ_i into real and imaginary parts α_i and β_i by

$$\gamma_i = \alpha_i + j\beta_i \quad \text{for } i = x, y, z \quad (5.116)$$

and inserting this into (5.115) yields

$$\boldsymbol{\alpha} \cdot \boldsymbol{\alpha} - \boldsymbol{\beta} \cdot \boldsymbol{\beta} = \alpha_x^2 - \beta_x^2 + \alpha_y^2 - \beta_y^2 + \alpha_z^2 - \beta_z^2 = 0, \quad (5.117a)$$

$$\boldsymbol{\alpha} \cdot \boldsymbol{\beta} = \alpha_x \beta_x + \alpha_y \beta_y + \alpha_z \beta_z = 0. \quad (5.117b)$$

The field exhibits an exponential behavior in direction of vector $\boldsymbol{\alpha}$ and an oscillatory behavior in direction of vector $\boldsymbol{\beta}$, where $\boldsymbol{\beta}$ is normal to $\boldsymbol{\alpha}$.

Consider a metallic box as depicted in Figure 5.12. The box is open at $z = 0$. All other planes are perfectly electric conducting. Assume the metallic walls at potential $\Phi_e = 0$, the solutions fulfilling the boundary conditions are

$$\Phi_{emn}(x, y, z) = A_{mn} \sin\left(\frac{m\pi x}{a}\right) \sin\left(\frac{n\pi y}{b}\right) \sinh[\alpha_{mn}(d - z)] \quad (5.118)$$

with

$$\alpha_{mn} = \sqrt{\left(\frac{m\pi x}{a}\right)^2 + \left(\frac{n\pi y}{b}\right)^2}. \quad (5.119)$$

We have an infinite number of solutions, parameterized with m and n . The fields belonging to these solutions are called *modes*. Since the solutions are electrostatic ones the modes are *electrostatic modes*. The higher the order mn of the mode is, the steeper is the decay of the static field in z -direction. Any linear combination

$$\Phi_e(x, y, z) = \sum_{m=1}^{\infty} \sum_{n=1}^{\infty} A_{mn} \sin\left(\frac{m\pi x}{a}\right) \sin\left(\frac{n\pi y}{b}\right) \sinh[\alpha_{mn}(d - z)] \quad (5.120)$$

is a solution of the Laplace equation. The contour plot of the solution Φ_{e10} is depicted in Figure 5.13.

For $z = 0$ the modal functions $\Phi_{emn}(x, y, 0)$ are complete in the two-dimensional interval $x \in (0, a)$, $y \in (0, b)$. This allows to expand any potential distribution in the plane $z = 0$ into a two-dimensional Fourier series. If this Fourier series expansion is known, the complete field solution inside the metallic box is also determined. Assume an arbitrary field distribution $\Phi_{e0}(x, y)$ impressed at the surface $z = 0$, satisfying the

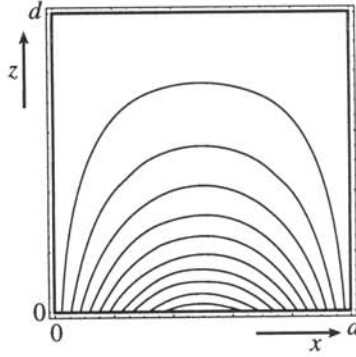


Figure 5.13: Contour plot of electrostatic field in open metallic box.

boundary conditions $\Phi_{e0}(0, y) = \Phi_{e0}(a, y) = \Phi_{e0}(x, 0) = \Phi_{e0}(x, b) = 0$. We can expand $\Phi_{e0}(x, y)$ into a two-dimensional Fourier series

$$\Phi_{e0}(x, y) = \sum_{m=1}^{\infty} \sum_{n=1}^{\infty} B_{mn} \sin\left(\frac{m\pi x}{a}\right) \sin\left(\frac{n\pi y}{b}\right). \quad (5.121)$$

The Fourier coefficients B_{mn} are given by

$$B_{mn} = \frac{4}{ab} \int_{y=0}^b \left[\int_{x=0}^a \Phi_{e0}(x, y) \sin\left(\frac{m\pi x}{a}\right) \sin\left(\frac{n\pi y}{b}\right) dx \right] dy. \quad (5.122)$$

Superimposing the partial solutions of (5.120) in such a way that the obtained expression is equal to $\Phi_{e0}(x, y)$ at $z = 0$ yields the complete field solution inside the box. Comparing (5.121) with (5.120)

$$B_{mn} = A_{mn} \sinh(\alpha_{mn}d). \quad (5.123)$$

With this we obtain the electrostatic potential field $\Phi_e(\mathbf{x})$ in the whole box expressed by the Fourier expansion coefficients of the potential field impressed in the boundary surface at

$$\Phi_e(x, y, z) = \sum_{m=1}^{\infty} \sum_{n=1}^{\infty} \frac{B_{mn}}{\sinh(\alpha_{mn}d)} \sin\left(\frac{m\pi x}{a}\right) \sin\left(\frac{n\pi y}{b}\right) \sinh[\alpha_{mn}(d - z)] \quad (5.124)$$

with B_{mn} given by (5.122) and α_{mn} from (5.119).

As an example we consider the closed metallic box shown in Figure 5.14. All walls are assumed to be ideally conducting. With exception of a patch of width s and height

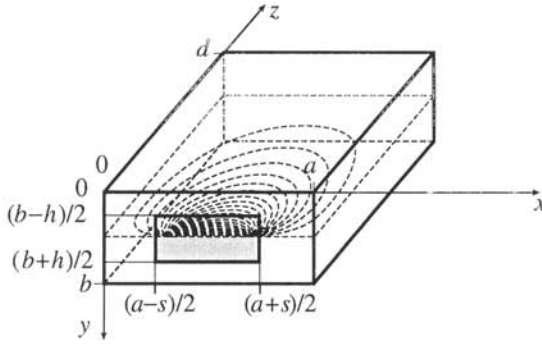


Figure 5.14: Metallic box with patch electrode.

h in the center of the wall at $z = 0$ all walls exhibit potential $\Phi_e = 0$. The patch is ideally conducting, however isolated from the other parts of the wall and at a potential Φ_{e0}

$$\Phi_e(x, z)|_{z=0} = \begin{cases} \Phi_{e0} & \text{for } \frac{1}{2}(a-s) \leq x \leq \frac{1}{2}(a+s) \wedge \frac{1}{2}(b-h) \leq y \leq \frac{1}{2}(b+h) \\ 0 & \text{elsewhere} \end{cases} \quad (5.125)$$

Inserting this into (5.122) yields the Fourier coefficients

$$\begin{aligned} B_{mn} &= \frac{4\Phi_{e0}}{ab} \left[\int_{x=\frac{1}{2}(a-s)}^{x=\frac{1}{2}(a+s)} \sin\left(\frac{m\pi x}{a}\right) dx \right] \left[\int_{y=\frac{1}{2}(b-h)}^{y=\frac{1}{2}(b+h)} \sin\left(\frac{n\pi y}{b}\right) dy \right] \\ &= \frac{16\Phi_{e0}}{mn\pi^2} \sin \frac{1}{2} m\pi \sin \frac{m\pi s}{2a} \sin \frac{1}{2} n\pi \sin \frac{n\pi h}{2b}. \end{aligned} \quad (5.126)$$

This can be simplified to

$$\begin{aligned} B_{2m+1, 2n+1} &= \frac{16\Phi_{e0}}{mn\pi^2} (-1)^{m+n} \sin \frac{(2m+1)\pi s}{2a} \sin \frac{(2n+1)\pi h}{2b}, \\ B_{2m, 2n} &= B_{2m+1, 2n} = B_{2m, 2n+1} = 0. \end{aligned} \quad (5.127)$$

Figure 5.15 shows the equipotential lines in the plane $y = \frac{1}{2}b$ for $s = \frac{1}{2}a$.

5.5 CONFORMAL MAPPING

Two-dimensional electrostatic and magnetostatic field problems can be solved in an efficient way by *conformal mapping* [13–15]. Conformal mapping is based on the theory of complex functions. The method is general for two-dimensional potential problems.

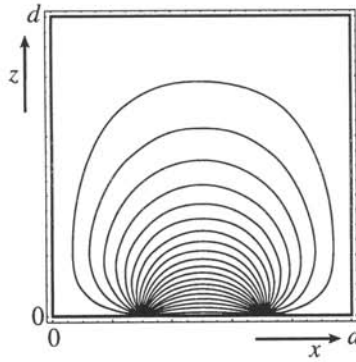


Figure 5.15: Contour plot of electrostatic field in a metallic box excited by an electrode.

In the two-dimensional case, where in the Cartesian coordinate system the field depends only on the two coordinates x and y , the Laplace equation (5.113) reduces to

$$\frac{\partial^2 \Phi_e}{\partial x^2} + \frac{\partial^2 \Phi_e}{\partial y^2} = 0. \quad (5.128)$$

The theory of complex function [16–19] supplies efficient methods to solve the two-dimensional Laplace equation. Let us interpret x and y as real and imaginary parts of a complex number \underline{z}

$$\underline{z} = x + jy. \quad (5.129)$$

We have underlined the complex number \underline{z} in order to distinguish it from the coordinate z in three-dimensional coordinate systems. We define a *complex function* $f(\underline{z})$ to have the form

$$\underline{w} = f(\underline{z}) = u(x, y) + jv(x, y). \quad (5.130)$$

In the following we will discuss some general aspects of field computation by conformal mapping. Figure 5.16(a) shows the contour plot of a conformal mapping. The full curves represent the lines of constant u whereas the dashed curves correspond to constant v .

In analogy to the derivative of a real function the derivative of a complex function $f(\underline{z})$ is defined as

$$\frac{df(\underline{z})}{d\underline{z}} = \lim_{\delta \underline{z} \rightarrow 0} \frac{f(\underline{z} + \delta \underline{z}) - f(\underline{z})}{\delta \underline{z}}. \quad (5.131)$$

Inserting (5.130) yields

$$\frac{df(\underline{z})}{d\underline{z}} = \lim_{\delta x, \delta y \rightarrow 0} \frac{u(x + \delta x, y + \delta y) - u(x, y) + jv(x + \delta x, y + \delta y) - jv(x, y)}{\delta x + j\delta y}. \quad (5.132)$$

We require that the limit is path-independent (i.e., independent on the path in the complex plane over which $\delta \underline{z}$ goes to zero). The result has to be identical if we let first $\delta y \rightarrow 0$ and then $\delta x \rightarrow 0$ or first $\delta x \rightarrow 0$ and then $\delta y \rightarrow 0$. In the following two expressions, the first one describes the case where first the transition $\delta y \rightarrow 0$ has been made and then the $\delta x \rightarrow 0$ is made. The second equation corresponds to the opposite sequence of the limit processes.

$$\frac{df(\underline{z})}{d\underline{z}} = \lim_{\delta x \rightarrow 0} \frac{u(x + \delta x, y) - u(x, y) + jv(x + \delta x, y) - jv(x, y)}{\delta x}, \quad (5.133a)$$

$$\frac{df(\underline{z})}{d\underline{z}} = \lim_{\delta y \rightarrow 0} \frac{u(x, y + \delta y) - u(x, y) + jv(x, y + \delta y) - jv(x, y)}{j\delta y}. \quad (5.133b)$$

This gives for the two cases of limit processes

$$\frac{df(\underline{z})}{d\underline{z}} = \frac{\partial u(x, y)}{\partial x} + j \frac{\partial v(x, y)}{\partial x}, \quad (5.134a)$$

$$\frac{df(\underline{z})}{d\underline{z}} = \frac{\partial v(x, y)}{\partial y} - j \frac{\partial u(x, y)}{\partial y}. \quad (5.134b)$$

If the derivatives have to be path-independent, both expressions must be identical, hence

$$\frac{\partial u(x, y)}{\partial x} = \frac{\partial v(x, y)}{\partial y}, \quad (5.135a)$$

$$\frac{\partial v(x, y)}{\partial x} = -\frac{\partial u(x, y)}{\partial y}. \quad (5.135b)$$

These equations are called the *Cauchy-Riemann equations* and are the necessary conditions for a unique, path-independent derivative of a complex function. A complex function for which the Cauchy-Riemann equations are fulfilled is called an *analytic function*. An analytic function is conformal at any point where it has a nonzero derivative. Conversely, any conformal mapping of a complex variable that has continuous partial derivatives is analytic [17, 20–22].

A *conformal mapping* or *conformal transformation* is a transformation in the complex number plane that preserves local angles [20–22]. The proof of angle preservation can be given as follows. Consider a variation from \underline{z}_0 to \underline{z} by an infinitesimal distance $\delta \underline{z}$, where δr and ϕ are magnitude and phase of this variation, so

$$\underline{z} = \underline{z}_0 + \delta \underline{z} = \underline{z}_0 + e^{j\phi} \delta r. \quad (5.136)$$

Let $\underline{w} = f(\underline{z})$ be an analytic function of \underline{z} . The variation $\delta \underline{z}$ will be mapped into the variation $\delta \underline{w}$, given by

$$\delta \underline{w} = f(\underline{z}) - f(\underline{z}_0) = f'(\underline{z})|_{\underline{z}=\underline{z}_0} \delta \underline{z} = f'(\underline{z})|_{\underline{z}=\underline{z}_0} e^{j\phi} \delta r. \quad (5.137)$$

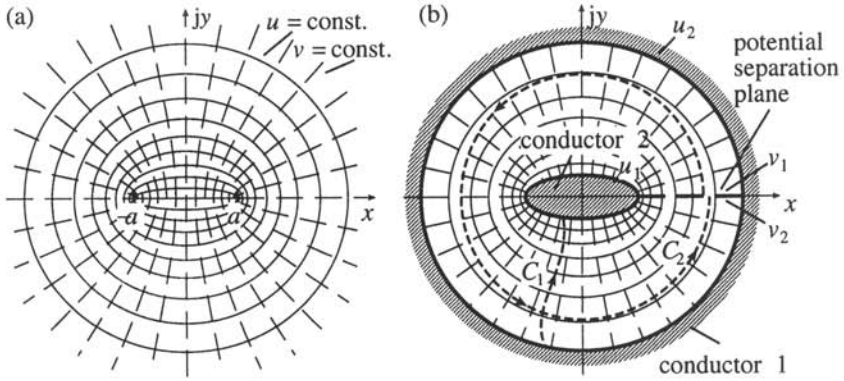


Figure 5.16: (a) Conformal mapping $w = \text{arccosh } \frac{z}{a}$, and (b) confocal elliptic cylinder structure.

This shows that any change of the angle ϕ of $\delta \underline{z}$ yields the same variation of $\delta \underline{w}$. Therefore the conformal mapping is angle preserving. Since the lines of constant u and v respectively constitute an orthogonal grid in the w -plane and the conformal mapping is angle-preserving, both sets of curves with either constant u or constant v are mutually orthogonal.

The angle-preserving property of the conformal mapping has an interesting implication on the metric coefficients defined in (A.104). Inserting the Cauchy-Riemann equations of the inverse mapping,

$$\frac{\partial x(u, v)}{\partial u} = \frac{\partial y(u, v)}{\partial v}, \quad (5.138a)$$

$$\frac{\partial y(u, v)}{\partial u} = -\frac{\partial x(u, v)}{\partial v} \quad (5.138b)$$

into (A.104) yields

$$g_1^2 = \left(\frac{\partial x}{\partial u} \right)^2 + \left(\frac{\partial y}{\partial u} \right)^2 = \left(\frac{\partial y}{\partial v} \right)^2 + \left(\frac{\partial x}{\partial v} \right)^2 = g_2^2. \quad (5.139)$$

The identity of g_1 and g_2 means that in a conformal mapping from z -plane to w -plane, where \underline{z}_0 is mapped to \underline{w}_0 a circle with infinitesimal radius δr and center \underline{z}_0 is mapped into a circle with radius $g \delta r$ and center \underline{w}_0 . We set $g_1 = g_2 = g$. In the three-dimensional cylindric coordinate system with coordinates u, v, z , the metric coefficients are

$$g_1 = g_2 = g, \quad g_3 = 1, \quad (5.140)$$

hence the Hodge operator (A.III) for the three-dimensional cylindric coordinate system u, v, z is

$$\star f = g^2 f \, du \wedge dv \wedge dz, \quad (5.141a)$$

$$\star (A_u du + A_v dv + A_z dz) = (A_u dv \wedge dz + A_v dz \wedge du + g^2 A_z du \wedge dv). \quad (5.141b)$$

Note that z in the above equation is the coordinate normal to x and y in the three-dimensional Cartesian coordinate system, and has to be distinguished from the complex variable \underline{z} .

From the Cauchy-Riemann equations it follows directly

$$\frac{\partial^2 u(x, y)}{\partial x^2} + \frac{\partial^2 u(x, y)}{\partial y^2} = 0, \quad (5.142a)$$

$$\frac{\partial^2 v(x, y)}{\partial x^2} + \frac{\partial^2 v(x, y)}{\partial y^2} = 0. \quad (5.142b)$$

That means that if a function $w(z)$ is analytic, its real part $u(x, y)$ as well as its imaginary part $v(x, y)$ fulfill the two-dimensional Laplace equation.

Consider the exterior derivatives of the scalar fields u and v . With the Cauchy-Riemann equations (5.135a) and (5.135b), we obtain

$$du = \frac{\partial u(x, y)}{\partial x} dx + \frac{\partial u(x, y)}{\partial y} dy = \frac{\partial v(x, y)}{\partial y} dx - \frac{\partial v(x, y)}{\partial x} dy, \quad (5.143a)$$

$$dv = \frac{\partial v(x, y)}{\partial x} dx + \frac{\partial v(x, y)}{\partial y} dy = -\frac{\partial u(x, y)}{\partial y} dx + \frac{\partial u(x, y)}{\partial x} dy. \quad (5.143b)$$

This yields with the twist operator introduced in (2.155):

$$du = -\star (dz \wedge dv) = -\perp_z dv, \quad (5.144a)$$

$$dv = \star (dz \wedge du) = \perp_z du. \quad (5.144b)$$

We obtain the vector field dv by rotating the vector field du locally in every point of space by an angle $\frac{1}{2}\pi$ around the z -axis. Vice versa, local rotation of dv in every point of space by an angle $-\frac{1}{2}\pi$ around the z yields the field du .

The one-forms du and dv also are related by

$$du = dz \lrcorner \star dv, \quad (5.145a)$$

$$dv = -dz \lrcorner \star du. \quad (5.145b)$$

Let the electrostatic potential $\Phi_e(x, y)$ be proportional to $u(x, y)$, hence

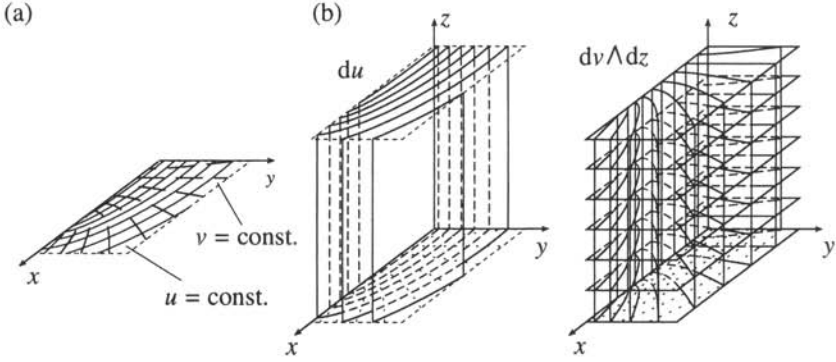


Figure 5.17: (a) Conformal mapping $\underline{w} = f(\underline{z})$, (b) one-form du , and (c) two-form $dv \wedge dz$.

$$\Phi_e(x, y) = A_{e1}u(x, y) + A_{e0}, \quad (5.146)$$

where A_{e1} and A_{e0} are constants to be determined. The equipotential lines are given by setting $u(x, y)$ constant. The choice of the two parameters A_{e1} and A_{e0} allows to match the solution to given potentials at two equipotential lines. If we consider only potential differences we can skip A_{e0} and let $A_{e1} = A_e$. With (5.7) we obtain the electric field form

$$\mathcal{E}(x, y) = -A_e du. \quad (5.147)$$

Figure 5.17(a) shows the equipotential lines of u and v for a conformal mapping and Figure 5.17(b) represents the potential surfaces of the one-form du . With the constitutive relation (2.32a) and the Hodge operator given by (5.141b) we obtain the electric displacement form

$$\mathcal{D}(x, y) = -\epsilon A_e \star du = -\epsilon A_e dv \wedge dz. \quad (5.148)$$

The flux tubes of the two-form $dv \wedge dz$ are shown in Figure 5.17(c).

For the two-dimensional problem it is useful to introduce the *two-dimensional electric displacement form* $\mathcal{D}_A(x, y)$ by integrating over dz over unit length. This means removing dz after bringing it to the left side. This operation can be performed by contracting dz with \mathcal{D} , hence

$$\mathcal{D}_A(x, y) = dz \lrcorner \mathcal{D}(x, y) = \epsilon A_e dv. \quad (5.149)$$

The two-dimensional electric displacement form is a twisted one-form. Integrating $\mathcal{D}_A(x, y)$ over a curve C in the xy -plane yields the electric flux through the side walls

of a cylinder generated by C and of unit height. So the integral of $\mathcal{D}_A(x, y)$ over a curve gives an electric displacement per unit of length.

Consider the cross-section through a structure of two ideally conducting generalized cylinders in Figure 5.16(b). The ideally conducting cylinders are defined by the equipotential planes of constant values v_1 and v_2 . The voltage between conductor 2 and conductor 1 is given by

$$V = A_e(u_2 - u_1). \quad (5.150)$$

We obtain the charge per unit of length Q' by integrating the electric flux density per unit of length \mathcal{D}_A over the closed curve C_2 . Due to the insertion of the potential separation plane, the curve C_2 in Figure 5.16(b) is equivalent to a closed curve. With (5.149) we obtain

$$Q' = \oint \mathcal{D}_A = \int_{C_2} \mathcal{D}_A = \epsilon A_e(v_2 - v_1). \quad (5.151)$$

The *capacitance per unit of length* is given by the ratio of charge per unit of length Q' to voltage V :

$$C' = \frac{Q'}{V} = \epsilon \frac{v_2 - v_1}{u_2 - u_1}. \quad (5.152)$$

Consider now the magnetic field in this structure. At the surface of a perfect electric conductor the magnetic field is tangential. Let the magnetostatic potential $\Phi_m(x, y)$ be proportional to $v(x, y)$:

$$\Phi_m(x, y) = A_m v(x, y). \quad (5.153)$$

From (5.109) we obtain the magnetic field form

$$\mathcal{H} = -d\Phi_m = -A_m dv. \quad (5.154)$$

With (2.32b) and (5.141b) we obtain the magnetic flux density form

$$\mathcal{B} = \mu * \mathcal{H} = -\mu A_m dz \wedge du. \quad (5.155)$$

For the two-dimensional problem we introduce the *two-dimensional magnetic flux density form* $\mathcal{B}_A(x, y)$ by integrating over dz over unit length. By contracting dz with \mathcal{B} we obtain

$$\mathcal{B}_A = -\mu A_m du. \quad (5.156)$$

The current flowing through conductor 2 in positive z -direction is related to \mathcal{H} via Ampère's law (2.57a). Integrating over the path C_2 in Figure 5.16(b) yields

$$I = A_m \int_{C_2} dv = A_m(v_2 - v_1). \quad (5.157)$$

The *magnetic flux per unit of length* Φ' is obtained by integrating \mathcal{B}_A over the curve C_1 in Figure 5.16(b). We obtain

$$\Phi' = \int_{C_1} \mathcal{B}_A = \mu A_m (u_2 - u_1). \quad (5.158)$$

The *inductance per unit of length* L' is the ratio of magnetic flux per unit of length Φ' to the current I :

$$L' = \frac{\Phi'}{I} = \mu \frac{u_2 - u_1}{v_2 - v_1}. \quad (5.159)$$

From (5.152), (5.159), and (2.75) we obtain

$$L' C' = \epsilon \mu = \frac{1}{c^2}. \quad (5.160)$$

This means that the product of the inductance per unit of length L' and the capacitance per unit of length C' is independent from the geometry structure as long as the non-conducting regions are either free-space or filled with homogeneous dielectric. The speed of light c is the speed of a transverse electromagnetic wave in the medium with permittivity ϵ and permeability μ . The propagation of transverse electromagnetic waves in cylindric structures will be discussed in Section 7.4.

A cylindric structure with two unconnected conductors may be characterized by its *characteristic impedance* Z_0 given by

$$Z_0 = \sqrt{\frac{L'}{C'}} = \sqrt{\frac{\mu}{\epsilon} \frac{u_2 - u_1}{v_2 - v_1}}. \quad (5.161)$$

The characteristic impedance describes the ratio of voltage to current of a transverse electromagnetic wave propagating in the cylindric structure with speed c in one direction. This will be discussed in detail in Section 7.4.

Interchanging u and v yields a dual field solution with interchanged electric and magnetic field. Replacing $f(\underline{z})$ by $j f(\underline{z})$ yields

$$f(\underline{z}) \rightarrow j f(\underline{z}) : u(x, y) \rightarrow -v(x, y); v(x, y) \rightarrow u(x, y). \quad (5.162)$$

To every field solution we can find a dual field solution with interchanged electric and magnetic field potential lines. In the dual field solution ideal electric conductors have to be replaced by ideal magnetic conductors and vice versa.

5.5.1 Field of an Elliptic Cylindric Line

Consider the conformal mapping represented in Figure 5.16(a). This mapping is described by the *inverse hyperbolic cosine-transformation*,

$$\underline{w} = \operatorname{arccosh} \frac{\underline{z}}{a}. \quad (5.163)$$

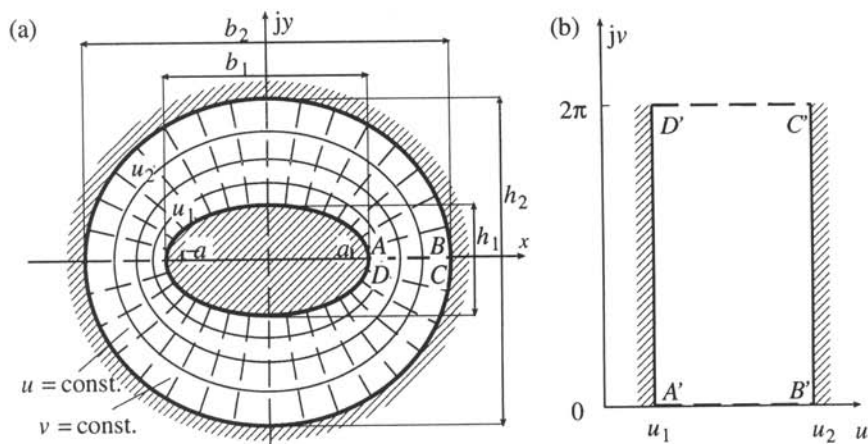


Figure 5.18: (a) Conformal mapping $w = \text{arccosh } \frac{z}{a}$, and (b) confocal elliptic cylinder structure.

The transformation from the w -plane into the z -plane is the *hyperbolic cosine-transformation*

$$(x + jy) = a \cosh(u + jv). \quad (5.164)$$

Splitting this transformation into real and imaginary parts yields

$$x = a \cosh u \cos v, \quad (5.165a)$$

$$y = a \sinh u \sin v. \quad (5.165b)$$

From these equations we obtain the equations for the equipotential lines

$$\frac{x^2}{\cosh^2 u} + \frac{y^2}{\sinh^2 u} = a^2, \quad (5.166a)$$

$$\frac{x^2}{\cos^2 v} - \frac{y^2}{\sin^2 v} = a^2, \quad (5.166b)$$

where (5.166a) describes a set of confocal ellipses and (5.166b) represents a set of confocal hyperbolas. In both cases the focal points are $z = \pm a$.

A confocal elliptic cylindric line with the cross-section depicted in Figure 5.18(a) exhibits an inner conductor at u_1 and an outer conductor at u_2 . The outer dimensions of the inner conductor and the inner dimensions of the outer conductor are given by the widths and heights of the ellipses, b_1 , b_2 , h_1 , and h_2 , respectively. To make v single-valued in the interval $(0, 2\pi)$, the complex z -plane is cut by the line from A to D and C to D , respectively, where the points A and D are located on the upper side of the cut at $v = 0$ and the points C and D are located below the cut at $v = 2\pi$.

The ellipses defined by constant u_1 and u_2 , respectively, in Figure 5.18(a) are mapped into the lines $A'D'$ and $B'C'$ in the w -plane in Figure 5.18(b). Since both ellipses are confocal with the focal points at $z = \pm a$, only three of these four parameters may be chosen independently. From (5.166a) and (5.166b) we obtain for $i = 1, 2$:

$$b_i = 2a \cosh u_i, \quad (5.167a)$$

$$h_i = 2a \sinh u_i. \quad (5.167b)$$

Considering $v_2 - v_1 = 2\pi$ we obtain from (5.152) the capacitance per unit of length

$$C' = \frac{Q'}{V} = \epsilon \frac{v_2 - v_1}{u_2 - u_1} = \frac{2\pi\epsilon}{\operatorname{arctanh} \frac{h_2}{b_2} - \operatorname{arctanh} \frac{h_1}{b_1}} \quad (5.168)$$

with the constraint

$$b_1^2 - h_1^2 = b_2^2 - h_2^2. \quad (5.169)$$

From (5.159) we obtain the inductance per unit of length

$$L' = \frac{\Phi'}{I} = \frac{\mu}{2\pi} \left(\operatorname{arctanh} \frac{h_2}{b_2} - \operatorname{arctanh} \frac{h_1}{b_1} \right). \quad (5.170)$$

Also in this equation the constraint (5.169) has to be considered.

5.5.2 Field of a Coaxial Line

To investigate the field of a coaxial circular cylindric structure shown in Figure 5.5(a) we consider the *logarithmic transformation* [14, 23]

$$w = f(z) = \ln z. \quad (5.171)$$

This function is analytic in the complete z -plane with exception at $z = 0$. Expressing the complex number z by its magnitude r and its phase ϕ ,

$$z = re^{j\phi}, \quad (5.172)$$

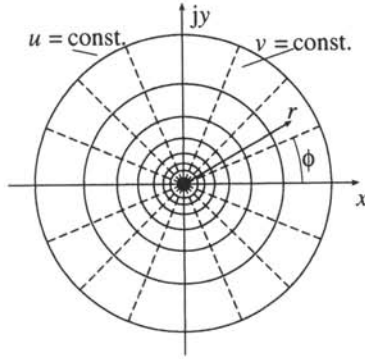
yields

$$w = u + jv = \ln r + j\phi. \quad (5.173)$$

Figure 5.19 illustrates this mapping. Real part u and imaginary part v of w are

$$u = \ln r, \quad (5.174a)$$

$$v = \phi. \quad (5.174b)$$

Figure 5.19: Conformal mapping $\underline{w} = A \ln \underline{z}$.

We choose the electric potential

$$\Phi_e = A_e u = A_e \ln r, \quad (5.175)$$

where A_e is a constant. From (5.146) and (5.149) we obtain with (A.151) the electric field form \mathcal{E} and the electric displacement form \mathcal{D}_A :

$$\mathcal{E} = -d\Phi_e = -A_e du = -A_e \frac{\partial u}{\partial r} dr = -\frac{A_e}{r} dr, \quad (5.176a)$$

$$\mathcal{D}_A = \epsilon A_e dv = \epsilon A_e \frac{\partial v}{\partial \phi} d\phi = \epsilon A_e d\phi. \quad (5.176b)$$

The coaxial line with the cross-section shown in Figure 5.20 exhibits an inner conductor of diameter $2a$ and an outer conductor with inner diameter $2b$. According to (5.150) the voltage V between the conductor 2 and the inner conductor 1 is

$$V = A_e(u(b) - u(a)) = A_e \ln \frac{b}{a}. \quad (5.177)$$

From (5.151) and (5.174b) we obtain the charge per unit of length Q' :

$$Q' = \oint \mathcal{D}_A = 2\pi\epsilon A_e. \quad (5.178)$$

The capacitance per unit of length C' is given by

$$C' = \frac{Q'}{V} = \frac{2\pi\epsilon}{\ln \frac{b}{a}}. \quad (5.179)$$

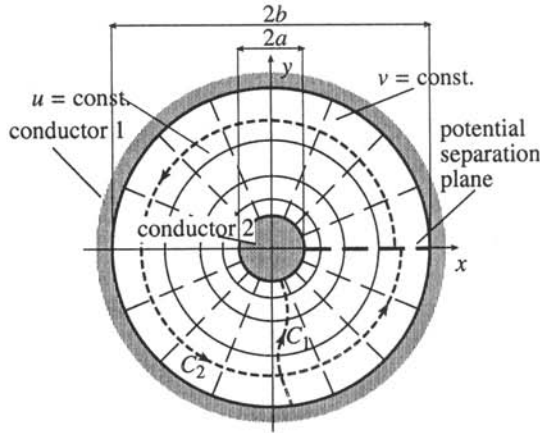


Figure 5.20: Field of a coaxial line.

According to (5.149) and (5.156) we derive the magnetic field \mathcal{H} dual to the electric field \mathcal{E} from the magnetic scalar potential $A_m v(x, y)$ and the magnetic flux per unit of length \mathcal{B}_A from the potential function $\mu A_m u(x, y)$. The constant A_m depends on the current impressed in the conductors,

$$\mathcal{H} = A_m dv = A_m \frac{\partial v}{\partial \phi} d\phi = A_m d\phi, \quad (5.180a)$$

$$\mathcal{B}_A = \mu A_m du = \mu A_m \frac{\partial u}{\partial r} dr = -\mu \frac{A_m}{r} dr. \quad (5.180b)$$

The current I through conductor 2 in positive z -direction is given by the integral (5.157) over the path C_2 in Figure 5.20, hence

$$I = A_m (v(2\pi) - v(0)) = 2\pi A_m. \quad (5.181)$$

The magnetic flux per unit of length Φ'

$$\Phi' = \int_a^b \mathcal{B}_A = \mu A_m \ln \frac{b}{a}. \quad (5.182)$$

The inductance per unit of length L' is

$$L' = \frac{\Phi'}{I} = \frac{\mu \ln \frac{b}{a}}{2\pi}. \quad (5.183)$$

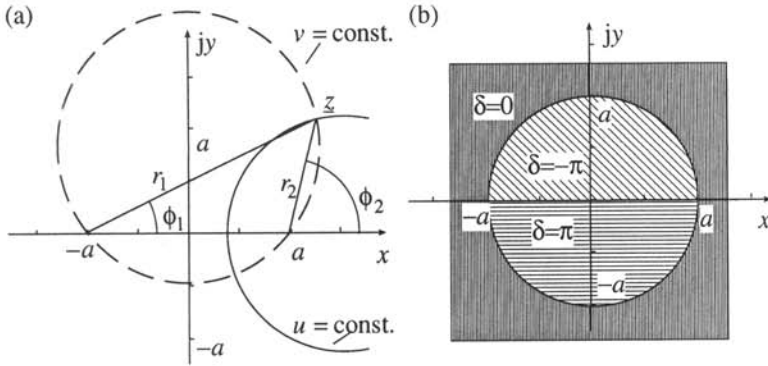


Figure 5.21: (a) Construction of the mapping $\underline{w} = A \ln \frac{z+a}{z-a}$, and (b) region map of δ .

5.5.3 Parallel Wire Line

A *parallel wire line* is formed by two parallel wires [14, 24]. Usually the wires are assumed to be of circular cylindric shape and we will consider only this case here. In the *symmetric parallel wire line* both wires exhibit the same diameter. Considering the mapping

$$\underline{w} = f(\underline{z}) = \ln \frac{\underline{z} + a}{\underline{z} - a} \quad (5.184)$$

as shown in Figure 5.21(a) and representing the complex numbers $\underline{z} + a$ and $\underline{z} - a$ by the real distances r_2 , r_1 and the phase angles ϕ_2 and ϕ_1 , hence

$$\underline{z} - a = r_2 e^{j\phi_2}, \quad (5.185a)$$

$$\underline{z} + a = r_1 e^{j\phi_1}. \quad (5.185b)$$

Inserting these equations into (5.184) yields

$$\underline{w} = \ln \frac{r_1}{r_2} + j(\phi_1 - \phi_2). \quad (5.186)$$

Separating \underline{w} into the real part u and imaginary part v gives

$$u = \ln \frac{r_1}{r_2}, \quad (5.187a)$$

$$v = \phi_1 - \phi_2. \quad (5.187b)$$

We obtain the equipotential lines by setting u constant. This yields

$$r_2 = cr_1 \quad (5.188)$$

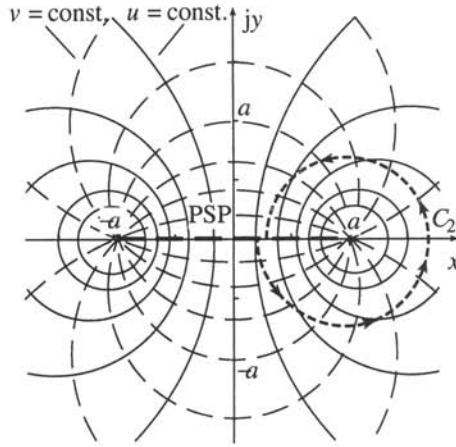


Figure 5.22: Plot of the mapping $w = A \ln \frac{z+a}{z-a}$

where c is a constant. From Figure 5.21 and the equations (5.185a) and (5.185b) we obtain

$$r_2^2 = (x - a)^2 + y^2, \quad (5.189a)$$

$$r_1^2 = (x + a)^2 + y^2. \quad (5.189b)$$

From (5.188) to (5.189b) we obtain

$$(x - x_0)^2 + y^2 = \rho_u^2. \quad (5.190)$$

This equation defines circles with centers on the x -axis, given by

$$x_0 = \pm a \frac{(1 + c^2)}{(1 - c^2)} \quad (5.191)$$

and radius ρ_u given by

$$\rho_u = \frac{2ac}{1 - c^2}. \quad (5.192)$$

Figure 5.22 shows the contour plot of this conformal mapping. The full circles represent constant u . The field exhibits singularities at $z = \pm a$.

To compute the potential lines for constant v we have to set (5.187b) constant. The

angles ϕ_2 and ϕ_1 are given by

$$\phi_1 = \arctan \frac{y}{x+a}, \quad (5.193a)$$

$$\phi_2 = \arctan \frac{y}{x-a}. \quad (5.193b)$$

Using the relation given in [25]

$$\arctan \xi_2 - \arctan \xi_1 = \arctan \left(\frac{\xi_2 - \xi_1}{1 + \xi_2 \xi_1} \right) + \begin{cases} 0 & \text{for } \xi_1 \xi_2 > -1 \\ \pi & \text{for } \xi_2 > 0, \xi_1 \xi_2 < -1 \\ -\pi & \text{for } \xi_2 < 0, \xi_1 \xi_2 < -1 \end{cases} \quad (5.194)$$

we obtain from (5.187b), (5.193a) and (5.193b) by setting $v = v_0$ constant

$$\frac{2ay}{x^2 + y^2 - a^2} = \tan(\phi_2 - \phi_1 - \delta) = \tan(v_0 - \delta), \quad (5.195)$$

where the angle δ is

$$\delta = \begin{cases} 0 & \text{for } x^2 + y^2 > a^2 \\ \pi & \text{for } y < 0, x^2 + y^2 < a^2 \\ -\pi & \text{for } y > 0, x^2 + y^2 < a^2 \end{cases}. \quad (5.196)$$

Figure 5.21(b) shows the region map of the angle δ . We can rewrite (5.195) in the form

$$x^2 + (y - y_0)^2 = \rho_v^2, \quad (5.197)$$

describing circles with centers on the y -axis and going through the points $x = \pm a$. The center of a circle is given by

$$y_0 = a \cot(v_0 - \delta) \quad (5.198)$$

and its radius is

$$\rho_v = \sqrt{a^2 + c^2}. \quad (5.199)$$

In Figure 5.22 the dashed circles represent constant v . These circles exhibit constant values of v inside as well as outside the circle $|z| = a$. However due to (5.187b) the value of v undergoes a change of $\pm\pi$ when the circle passes a singularity at $\underline{z} = \pm a$.

Let the electric equipotential lines be defined by constant u and the magnetic ones be given by constant v . We chose electric and magnetic potentials Φ_e and Φ_m , respectively

$$\Phi_e = A_e u = A_e \ln \frac{r_1}{r_2}, \quad (5.200a)$$

$$\Phi_m = A_m v = A_m (\phi_1 - \phi_2). \quad (5.200b)$$

The constants A_e and A_m will be determined below.

With (5.147) and (5.149) we obtain the electric field \mathcal{E} from the electric scalar potential Φ_e and the electric displacement per unit of length $\mathcal{D}_A(x, y)$ from the potential function $A_e v$:

$$\mathcal{E}(x, y) = -A_e du = -A_e \left(\frac{1}{r_1} dr_1 - \frac{1}{r_2} dr_2 \right), \quad (5.201a)$$

$$\mathcal{D}_A(x, y) = \epsilon A_e dv = \epsilon A_e (d\phi_1 - d\phi_2). \quad (5.201b)$$

The constant A_e depends on elementary charges at the singularities $\underline{z} = \pm a$. We obtain the charge per unit of length Q' at $x = a, y = 0$ with (5.151) by integrating the electric displacement per unit of length $\mathcal{D}_A(x, y)$ over the path C_2 as

$$Q' = \int_{C_2} \mathcal{D}_A = \epsilon A_e \int_{-\pi}^{\pi} d\phi_1 = 2\pi\epsilon A_e. \quad (5.202)$$

In Figure 5.22 we have introduced the potential separation plane PSP between the singularities at $\underline{z} = -a$ and $\underline{z} = a$. This can be done, since the chosen conformal mapping describes a field where the elementary charges at $\underline{z} = -a$ and $\underline{z} = a$ exhibit equal magnitude and opposite sign. The integral over a closed contour not intersecting the potential separation plane yields zero. Such a path of integration encircles either none of the singular points $\underline{z} = \pm a$ or both of them.

Following (5.154) and (5.156), we derive the magnetic field \mathcal{H} dual to the electric field \mathcal{E} from the magnetic scalar potential Φ_m and the magnetic flux per unit of length \mathcal{B}_A from the potential function $\mu A_m u(x, y)$. This yields

$$\mathcal{H} = -d\Phi_m = -A_m dv = -A_m (d\phi_1 - d\phi_2), \quad (5.203a)$$

$$\mathcal{B}_A = -\mu A_m du = -\mu A_m \left(\frac{1}{r_1} dr_1 - \frac{1}{r_2} dr_2 \right). \quad (5.203b)$$

The constant A_m depends on elementary currents impressed at $\underline{z} = \pm a$. The elementary current I at $\underline{z} = a$ is obtained from Ampère's law (2.57a) by integration over the path C_2 in Figure 5.23. This yields

$$I = \oint_{C_2} \mathcal{H} = -A_m \oint_{C_2} d\phi_1 + A_m \oint_{C_1} d\phi_2. \quad (5.204)$$

The path of integration C_2 encircles the singular point at $\underline{z} = a$ but not that at $\underline{z} = -a$. Only the function ϕ_2 exhibits a singular point inside the contour of integration C_2 . Therefore only the second integral on the right-hand gives a contribution, hence

$$I = A_m \int_{-\pi}^{\pi} d\phi_2 = 2\pi A_m. \quad (5.205)$$

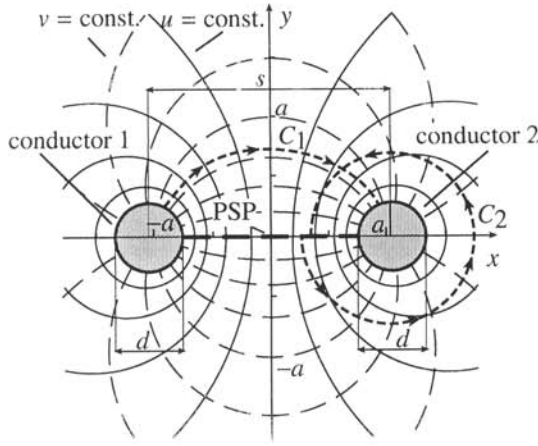


Figure 5.23: Field of a parallel wire line.

Consider the symmetric parallel wire line with the cross-section shown in Figure 5.23. The axes of the wires are separated by a distance s and their diameters are d . Since the boundaries of the wire cross-sections are equipotential circles we obtain from (5.191) and (5.192) the following relations to determine the parameters a and c

$$a = 2\sqrt{s^2 - d^2}, \quad (5.206a)$$

$$c = \frac{s}{d} \pm \sqrt{\frac{s^2}{d^2} - 1}. \quad (5.206b)$$

The negative sign in (5.206b) refers to conductor 1 and the positive sign to conductor 2. From (5.187b), (5.188), and (5.200a) we obtain the voltage V from conductor 2 to conductor 1 as

$$V = \Phi_{e2} - \Phi_{e1} = A_e(u_2 - u_1) = 2A_e \ln c = 2A_e \ln \left(\frac{s}{d} \pm \sqrt{\frac{s^2}{d^2} - 1} \right) = 2A_e \operatorname{arccosh} \frac{s}{d}. \quad (5.207)$$

Inserting (5.202) and (5.207) into (5.152), we obtain the capacitance per unit of length

$$C' = \frac{Q'}{V} = \frac{\pi\epsilon}{\operatorname{arccosh} \frac{s}{d}}. \quad (5.208)$$

We compute the magnetic flux per unit of length Φ' using (5.158) and (5.207),

$$\Phi' = \int_{C_1} B_A = \mu A_m(u_2 - u_1) = 2\mu A_e \operatorname{arccosh} \frac{s}{d}. \quad (5.209)$$

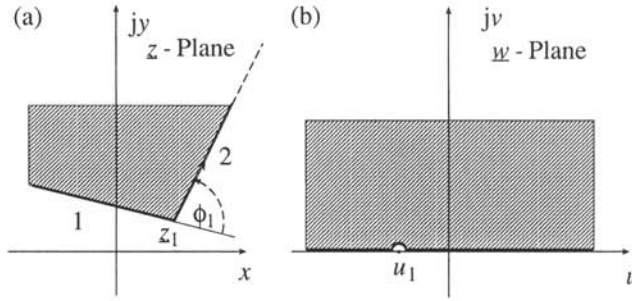


Figure 5.24: Conformal mapping of (a) a polygonal line in the \underline{z} -plane into (b) the u -axis of the \underline{w} -plane.

From this we obtain with (5.159) and (5.158) the inductance per unit of length L' as

$$L' = \frac{\Phi'}{I} = \frac{\mu}{\pi} \operatorname{arccosh} \frac{s}{d}. \quad (5.210)$$

5.6 THE SCHWARZ-CHRISTOFFEL TRANSFORMATION

The *Schwarz-Christoffel transformation* is a general method for conformal mapping of a polygon in the complex \underline{z} -plane into the real axis u of the complex \underline{w} -plane [20, 22, 26]. Consider the polygonal line with vertex \underline{z}_1 depicted in Figure 5.24(a). On a straight line the argument $\arg d\underline{z}$ of the interval $d\underline{z}$ is constant. Now, let the polygonal line be mapped onto the real axis u of the \underline{w} -plane in Figure 5.24(b), such that the vertex \underline{z}_1 is mapped into u_1 . To construct this mapping, we consider

$$\frac{d\underline{z}}{d\underline{w}} = A(u - u_1)^a \quad (5.211)$$

with complex A and real a , u , and u_1 . The derivative $d\underline{z}/d\underline{w}$ undergoes a discontinuous phase change at \underline{z}_1

$$\frac{d\underline{z}}{d\underline{w}} = \begin{cases} |A(u - u_1)^a| e^{j a(\alpha + \pi)} & \text{for } u < u_1 \\ |A(u - u_1)^a| e^{j a\alpha} & \text{for } u > u_1 \end{cases}. \quad (5.212)$$

For the change of the phase angle of $d\underline{z}/d\underline{w}$, we obtain

$$\arg \left(\frac{d\underline{z}}{d\underline{w}} \right) = \begin{cases} a(\alpha + \pi) & \text{for } u < u_1 \\ a\alpha & \text{for } u > u_1 \end{cases}. \quad (5.213)$$

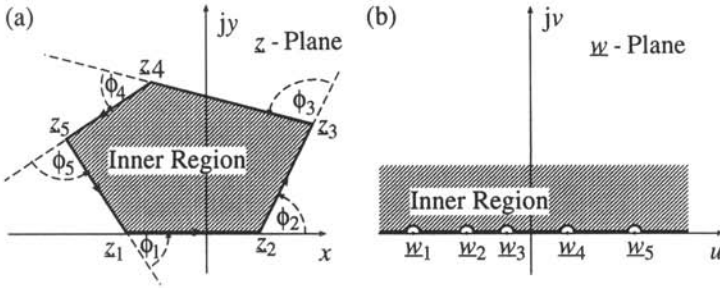


Figure 5.25: Schwarz-Christoffel transformation of (a) a polygon in the \underline{z} -plane into (b) the u -axis of the \underline{w} -plane.

Since the phase angle of $d\underline{z}/d\underline{w}$ remains constant in both regions 1 and 2 for $u < u_1$ and $u > u_1$, respectively, the integration of $d\underline{z}/d\underline{w}$ over du yields straight lines in every region 1 and 2. However at the vortex \underline{z}_1 undergoes a discontinuous change by the angle

$$\phi_1 = -a\pi. \quad (5.214)$$

Inserting this into (5.211) we see that the mapping of the real axis u of the \underline{w} -plane into the polygonal line in the \underline{z} -plane shown in Figure 5.24 has the form

$$\frac{d\underline{z}}{d\underline{w}} = A(u - u_1)^{-\phi_1/\pi}. \quad (5.215)$$

If the argument of $d\underline{z}/d\underline{w}$ is constant the integration of $d\underline{z}/d\underline{w}$ over u yields a straight line. Due to (5.212) the argument of $d\underline{z}/d\underline{w}$ exhibits a discontinuous change when u passes u_1 . Therefore the mapping $\underline{z}(u)$ consists of two straight line segments that are maps of $u < u_1$ and $u > u_1$, respectively. These line segments are connected in the vortex u_1 . We now can construct a function that maps the real axis u of the \underline{w} -plane into a polygon in the \underline{z} -plane as depicted in Figure 5.25. For $\underline{w} = u$ the expression

$$\frac{d\underline{z}}{d\underline{w}} = A(\underline{w} - u_1)e^{-\phi_1}(\underline{w} - u_2)e^{-\phi_2}(\underline{w} - u_3)e^{-\phi_3} \dots (\underline{w} - u_n)e^{-\phi_n} \quad (5.216)$$

changes the argument by ϕ_i whenever u passes u_i . A necessary condition for mapping the u -axis of the complex \underline{w} -plane into a closed polygonal curve in the \underline{z} -plane is

$$\phi_1 + \phi_2 + \phi_3 + \dots + \phi_n = 2\pi. \quad (5.217)$$

This yields the transformation

$$\underline{z} = \underline{z}_0 + A \int (\underline{w} - \underline{w}_1)e^{-\phi_1}(\underline{w} - \underline{w}_2)e^{-\phi_2}(\underline{w} - \underline{w}_3)e^{-\phi_3} \dots (\underline{w} - \underline{w}_n)e^{-\phi_n} d\underline{w}. \quad (5.218)$$

The Schwarz-Christoffel transformation is of great utility for the solution of two-dimensional potential problems for structures with polygonal boundaries [14, 15, 23, 27].

5.6.1 The Coplanar Line

A *coplanar line* consists of a strip of thin metallic film with two ground electrodes in the same plane as the strip and adjacent and parallel to the strip. Consider a coplanar line with negligible thickness of strip and ground electrodes as depicted in Figure 5.26(a). The strip width is $2a$ and the width of each gap is $(b-a)$. The electrostatic field solution can be obtained by application of the Schwarz-Christoffel transformation [28–31].

The upper half-plane $\Im\{z\} \geq 0$ -plane is mapped onto the rectangle in the w -plane shown in Figure 5.26(b) by means of the transformation

$$\underline{w}(\underline{z}) = A \int_0^{\underline{z}} \frac{d\underline{z}}{\sqrt{(\underline{z} - x_1)(\underline{z} - x_2)(\underline{z} - x_3)(\underline{z} - x_4)}}. \quad (5.219)$$

With $x_1 = -b$, $x_2 = -a$, $x_3 = a$, $x_4 = b$ the appropriate transformation is given by [32]

$$\underline{w}(\underline{z}) = A \int_0^{\underline{z}} \frac{d\underline{z}}{\sqrt{(\underline{z}^2 - a^2)(\underline{z}^2 - b^2)}}. \quad (5.220)$$

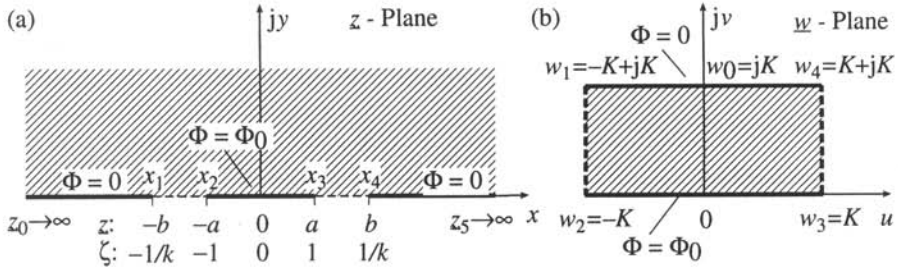
The mapping of the x -axis of the \underline{z} -plane into the boundary of the rectangle in the \underline{w} -plane can be understood as follows. For the mapping of the x -axis the path of integration is along the x -axis. According to Section 5.6 in the map $\underline{w}_1, \underline{w}_2, \underline{w}_3, \underline{w}_4$ of the x_1, x_2, x_3, x_4 a sharp 90° bend is introduced. Furthermore, we consider that for $x_1 < x_2 < x_3 < x_4$ the integrand is real for x between $-\infty$ and x_1 , between x_2 and x_3 and between x_4 and ∞ . The integrand is imaginary for x between x_1 and x_2 and x between x_3 and x_4 . Therefore, the line segments $-\infty < x < x_1$, $x_2 < x < x_3$ and $x_4 < x < \infty$ are mapped into lines with constant v , that means horizontal lines in the z -plane and the segments $x_1 < x < x_2$ and $x_3 < x < x_4$ are mapped into lines with constant u (i.e., vertical lines in the \underline{z} -plane).

The change of variables $\zeta = \underline{z}/a$ and $k = a/b$ yields the normalized representation

$$\underline{w}(\underline{z}) = \frac{A}{b} \int_0^{\underline{z}/a} \frac{d\zeta}{\sqrt{(1 - \zeta^2)(1 - k^2\zeta^2)}}. \quad (5.221)$$

This integral can be expressed by the *inverse elliptic function* [20, 33–35], defined by

$$\text{sn}^{-1}(\zeta, k) = \int_0^{\zeta} \frac{d\zeta_1}{\sqrt{(1 - \zeta_1^2)(1 - k^2\zeta_1^2)}}. \quad (5.222)$$

Figure 5.26: (a) Coplanar line, and (b) mapping into w -plane.

We obtain

$$\underline{w}(z) = \frac{A}{b} \operatorname{sn}^{-1} \left(\frac{z}{a}, k \right). \quad (5.223)$$

The elliptic function $\operatorname{sn}(\xi + j\eta, k)$, where ξ and η are the real and imaginary part of the complex argument ζ is double-periodic with period $4K(k)$ in ξ and period $2K'(k)$ in η . The functions $K(k)$ and $K'(k)$ are given by

$$K(k) = \int_0^1 \frac{d\xi}{\sqrt{(1-\xi^2)(1-k^2\xi^2)}}, \quad (5.224a)$$

$$jK'(k) = \int_1^{k^{-1}} \frac{d\xi}{\sqrt{(1-\xi^2)(1-k^2\xi^2)}}. \quad (5.224b)$$

The function $K(k)$ is called the *complete elliptic integral of the first kind*, and $K'(k)$ is called the *complete elliptic integral of the second kind* [20, 34, 35]. The complete elliptic integral of the second kind also may be expressed by

$$K'(k) = \int_0^1 \frac{d\xi}{\sqrt{(1-\xi^2)(1-\xi^2+k^2\xi^2)}} = K(k') \quad (5.225)$$

with

$$k' = \sqrt{1-k^2}. \quad (5.226)$$

The mapping from the z -plane to the w -plane is performed such that the points listed in Table 5.1 correspond to each other. Applying (5.152) to compute the capacitance per unit of length C' it has to be considered that only the upper half-space of the z -plane has been mapped into the rectangle in the w -plane. The capacitance computed from this formula therefore has to be doubled. This yields

$$C' = 2\epsilon \frac{v_2 - v_1}{u_2 - u_1} = \epsilon \frac{K'(k)}{K(k)}. \quad (5.227)$$

Table 5.1: The Elliptic Function $\text{sn}(\zeta)$

\underline{w}	$-K + jK'$	$-K$	0	K	$K + jK'$	jK'
$\zeta = \text{sn}(\underline{w}, k)$	$-k^{-1}$	-1	0	1	k^{-1}	∞
$\underline{z} = a \text{sn}(\underline{w}, k)$	$-b$	$-a$	0	a	b	∞

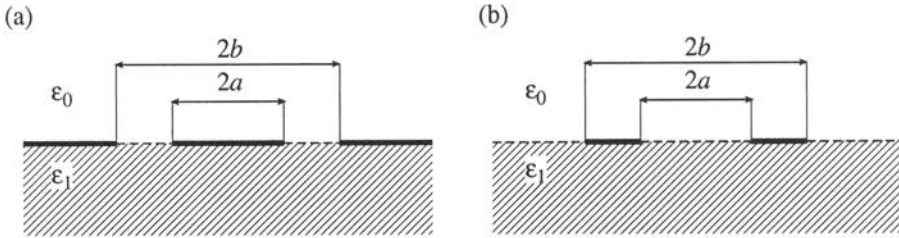


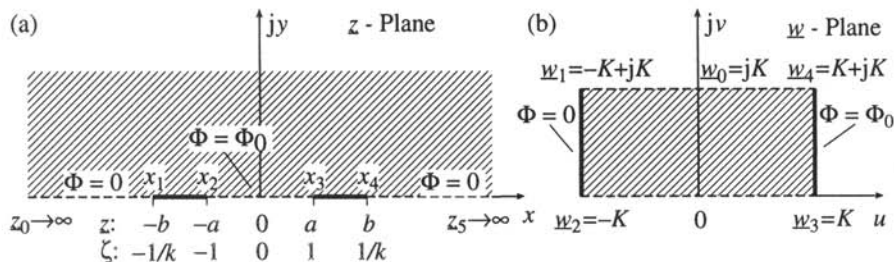
Figure 5.27: (a) Inhomogeneous coplanar line, and (b) inhomogeneous coplanar stripline.

Figure 5.27(a) shows the cross-section of an *inhomogeneous coplanar line* where the dielectric is not uniform in transverse direction. If the lower half-space is filled with a homogeneous isotropic dielectric with permittivity ϵ_1 and the upper half-space is free-space, the partial capacitance of the lower half-space has to be multiplied with ϵ_{r1} . The partial field solutions for the lower and upper half-plane fulfill the boundary conditions, since for $a < |x| < b$ the tangential electric boundary conditions are fulfilled at $y = 0$. Therefore we obtain the capacitance per unit of length as the sum of half the capacitance per unit of length computed with ϵ_0 and half the capacitance per unit of length computed with ϵ_1 ,

$$C' = (\epsilon_0 + \epsilon_1) \frac{v_2 - v_1}{u_2 - u_1} = \epsilon_0 \frac{1 + \epsilon_{r1}}{2} \frac{K'(k)}{K(k)}. \quad (5.228)$$

In computing the inductance per unit of length L' it has to be considered that only the part in the upper part of the path of integration of (5.157) is considered by the conformal mapping in Figure 5.26. Therefore the difference $u_2 - u_1$ has to be multiplied by 2 and we obtain

$$L' = 2\mu \frac{u_2 - u_1}{v_2 - v_1} = 4\mu \frac{K(k)}{K'(k)}. \quad (5.229)$$

Figure 5.28: (a) Coplanar line, and (b) mapping into w -plane.

5.6.2 The Coplanar Stripline

The *coplanar stripline* consists of two parallel conductor strips in the same plan. Figure 5.28(a) shows the cross-section of the coplanar stripline. The strips are of width $b - a$ and are separated by a gap of width $2a$. The thickness of the strips is assumed negligible. The coplanar stripline in Figure 5.28(a) is obtained from the coplanar line in Figure 5.26(a) by replacing at $y = 0$ the metallized regions by nonmetallized ones and vice versa. Both structures are dual to each other. The electric equipotential lines of the coplanar line correspond to the magnetic equipotential lines of the coplanar stripline and vice versa. This allows to use the same conformal mapping for the coplanar stripline as for the coplanar line in the previous section. The mappings in Figure 5.26(b) and Figure 5.28(b) are related by interchanging electric and magnetic walls.

Since in our mapping now the lines of constant v are the electric equipotential lines and the lines of constant u define the electric flux tubes, we have to interchange u and v in (5.152). Furthermore we have, as discussed in the previous section, to multiply this expression by 2 in order to consider the contributions of the lower and the upper half-space to the capacitance. This yields

$$C' = 2\epsilon \frac{u_2 - u_1}{v_2 - v_1} = 4\epsilon \frac{K(k)}{K'(k)}, \quad (5.230)$$

Consider the *inhomogeneous coplanar stripline* with the cross-section depicted in Figure 5.27(b). If the lower half-space is filled with a homogeneous isotropic dielectric with permittivity ϵ_1 and the upper half-space is free-space, the capacitance per unit of length is the mean value of the capacitances per unit of length computed with ϵ_0 and ϵ_1 , hence

$$C' = (\epsilon_0 + \epsilon_1) \frac{v_2 - v_1}{u_2 - u_1} = \epsilon_0 \frac{1 + \epsilon_{r1}}{2} \frac{K'(k)}{K(k)}. \quad (5.231)$$

For the inductance per unit of length L' we obtain from (5.159) by interchanging u and

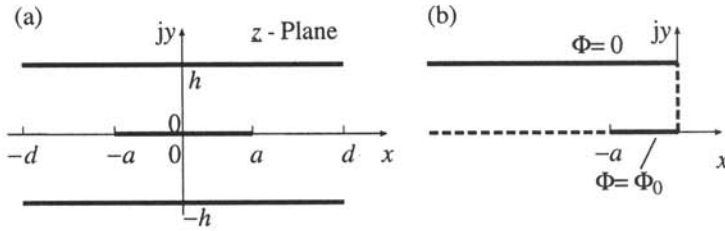


Figure 5.29: Cross-section of (a) a stripline, and (b) one quarter of a stripline.

v and considering a factor 2 for both half-spaces

$$L' = 2\mu \frac{u_2 - u_1}{v_2 - v_1} = 2\mu \frac{K'(k)}{K(k)}. \quad (5.232)$$

5.6.3 The Stripline

Consider the cross-section of a stripline shown in Figure 5.29(a). A conducting strip of width $2a$ and negligible thickness is embedded in the middle between two conducting plates spaced by a distance $2h$. The width $2d$ of the stripline is assumed to be much larger than the distance $2h$. For this reason the field at $x = \pm a$ will be negligible and we can assume $d \rightarrow \infty$. The structure is symmetric with respect to the planes $x = 0$ and $y = 0$. This simplifies the computational task, since it is only necessary to analyze the quarter of the structure depicted in Figure 5.29(b). The full lines represent the conducting planes, whereas the dashed lines indicate the symmetry planes. The electric field is normal and the magnetic field is tangential to the conducting planes. For symmetry reasons the electric field is tangential and the magnetic field is normal to the dashed regions of the symmetry planes. We can assume the dashed lines to be magnetic conductors.

The analysis of the stripline structure by conformal mapping has been treated in literature [9, 36–41]. The usual procedure is based on two consecutive Schwarz-Christoffel transformations, first from the \underline{z} -plane into the \underline{w}' -plane and then from the \underline{w}' -plane into the \underline{w} -plane as illustrated in Figure 5.30. With a first Schwarz-Christoffel transformation the quarter cross-section of the stripline in Figure 5.30(a) is transformed into the plane $v' = 0$ of the \underline{w} -plane. The vortices $\underline{z}_1, \underline{z}_2, \underline{z}_3, \underline{z}_4$ are transformed into the points u'_1, u'_2, u'_3, u'_4 on the u' -axis. With a second Schwarz-Christoffel transformation the structure of Figure 5.30(b) is transformed into the structure shown in Figure 5.30(c). The field in this structure is homogeneous and isotropic with equipotential lines given by constant v .

For the first mapping we can represent the inverse mapping by a Schwarz-Christoffel transformation. The mapping from the \underline{w} -plane into the \underline{z} -plane is performed by the

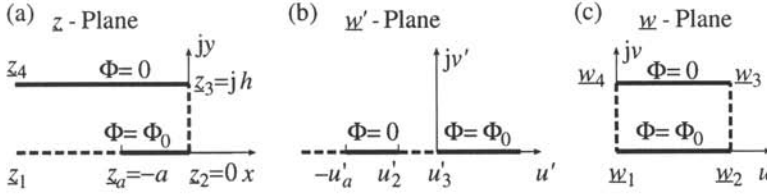


Figure 5.30: (a) Quarter of a stripline, mapping into (b) w' -plane, and (c) w -plane.

Schwarz-Christoffel transformation

$$z(\underline{w}') = A\sqrt{u'_1u'_4} \int \frac{1}{\sqrt{(\underline{w}' - u'_1)(\underline{w}' - u'_2)(\underline{w}' - u'_3)(\underline{w}' - u'_4)}} d\underline{w}' + B. \quad (5.233)$$

The constants A and B will be determined below. The factor $\sqrt{u'_1u'_4}$ may be considered to be a part of the arbitrary constant A . It has been introduced to get a finite limit of this expression if we let u'_1 and u'_4 go to the point at infinity. Note that the complex number plane exhibits a single infinite point, irrespective in which direction we move to infinity. For $u'_1, u'_4 \rightarrow \infty$ we obtain

$$z(\underline{w}') = A \int \frac{1}{\sqrt{(\underline{w}' - u'_2)(\underline{w}' - u'_3)}} d\underline{w}' + B. \quad (5.234)$$

We note that in the complex plane there is only one point at infinity. The transformation to the point at infinity does not occur in the Schwarz-Christoffel transformation. We now choose $u'_2 = -1$ and $u'_3 = 0$ and obtain

$$z(\underline{w}') = A \int \frac{1}{\sqrt{(\underline{w}' + 1)\underline{w}'}} d\underline{w}' + B = 2A \ln \left(\sqrt{\underline{w}'} + \sqrt{\underline{w}' + 1} \right) + B. \quad (5.235)$$

We determine A and B such that $z(-1) = 0$ and $z(0) = jh$ and obtain

$$2A \ln \sqrt{-1} + B = j\pi A + B = 0, \quad (5.236a)$$

$$jh = B. \quad (5.236b)$$

This yields

$$z(\underline{w}') = -\frac{2h}{\pi} \ln \left(\sqrt{\underline{w}'} + \sqrt{\underline{w}' + 1} \right) + jh. \quad (5.237)$$

The point $\underline{w}' = -u'_a$ in the w' -plane is mapped into $z = -a$ in the z -plane, hence

$$\sqrt{u'_a} + \sqrt{u'_a - 1} = \exp \left(\frac{\pi a}{2h} \right). \quad (5.238)$$

This can be expressed as

$$u'_a = \cosh^2 \left(\frac{\pi a}{2h} \right). \quad (5.239)$$

We now perform a second Schwarz-Christoffel transformation from the \underline{w}' -plane shown in Figure 5.30(b) to the \underline{w} -plane depicted in Figure 5.30(c). We require this transformation to map $\underline{w}' = -u'_a \rightarrow \underline{w}_1 = 0$, $\underline{w}' = u'_2 = -1 \rightarrow \underline{w}_2 = 1$, $\underline{w}' = u'_3 = 0 \rightarrow \underline{w}_3 = 1 + j\nu_0$, $\underline{w}' = u'_4 = \infty \rightarrow \underline{w} = j\nu_0$, where ν_0 is a real constant to be determined. Considering that the transformation of the infinite point does not occur explicitly in the Schwarz-Christoffel transformation, we obtain

$$\underline{w}(\underline{w}') = C \int_0^{\underline{w}'} \frac{d\underline{w}'}{\sqrt{(\underline{w}' + u'_a)(\underline{w}' + 1)\underline{w}'}} + D. \quad (5.240)$$

With the change of variables $\underline{w}' = -\zeta^2$ we put the integral into the form

$$\underline{w}(\underline{w}') = \frac{2jC}{\sqrt{u'_a}} \int_0^{\sqrt{-\underline{w}'}} \frac{d\zeta}{\sqrt{(1 - \zeta^2/u'_a)(1 - \zeta^2)}} + D, \quad (5.241)$$

where ζ is a complex variable and k is the *modulus* of the elliptic function (5.222). Elliptic functions are treated in [20, 34]. Using the inverse elliptic function we represent (5.241) by

$$\underline{w}(\underline{w}') = \frac{2jC}{\sqrt{u'_a}} \operatorname{sn}^{-1}((- \underline{w}')^{1/2}, u'_a{}^{-1/2}) + D. \quad (5.242)$$

Fulfilling the above formulated requirements for the mapping of the points $-u'_a$, -1 , 0 of the \underline{w}' -plane into the points 0 , 1 , $1 + j\nu_0$ of the \underline{w} -plane and considering $\operatorname{sn}^{-1}(0, k) = 0$, we obtain the equations

$$\frac{2jC}{\sqrt{u'_a}} \operatorname{sn}^{-1}(u'_a{}^{1/2}, u'_a{}^{-1/2}) + D = 0, \quad (5.243a)$$

$$\frac{2jC}{\sqrt{u'_a}} \operatorname{sn}^{-1}(1, u'_a{}^{-1/2}) + D = 1, \quad (5.243b)$$

$$D = 1 + j\nu_0. \quad (5.243c)$$

From these equations we can determine C , D , and ν_0 as follows:

Table 5.2: Stripline Parameters

$2a/h$	u'_a	$K(u'^{-1/2}_a)$	$K((1 - u'_a)^{-1/2})$	v_0
0.5	1.162	2.731	1.760	1.552
0.7	1.334	2.441	1.854	1.316
1.0	1.755	2.161	2.015	1.075
1.4	2.782	1.949	2.258	0.8632
2.0	6.296	1.775	2.667	0.6661
3.0	28.33	1.654	3.411	0.4848
4.0	134.4	1.606	4.185	0.3838
5.0	644.5	1.587	4.968	0.3194
6.0	$3.098 \cdot 10^3$	1.578	5.752	0.2743
7.0	$1.490 \cdot 10^4$	1.574	6.538	0.2408
8.0	$7.169 \cdot 10^4$	1.572	7.323	0.2147
9.0	$3.449 \cdot 10^5$	1.572	8.108	0.1938
10.0	$1.659 \cdot 10^6$	1.571	8.894	0.1767

$$C = \frac{1}{2} \frac{j u'^{-1/2}_a}{\operatorname{sn}^{-j u'^{-1/2}_a}(u'^{1/2}_a, u'^{-1/2}_a) - \operatorname{sn}^{-1}(1, u'^{-1/2}_a)}, \quad (5.244a)$$

$$D = \frac{\operatorname{sn}^{-1}(u'^{1/2}_a, u'^{-1/2}_a)}{\operatorname{sn}^{-1}(u'^{1/2}_a, u'^{-1/2}_a) - \operatorname{sn}^{-1}(1, u'^{-1/2}_a)}, \quad (5.244b)$$

$$v_0 = \frac{-j \operatorname{sn}^{-1}(1, u'^{-1/2}_a)}{\operatorname{sn}^{-1}(u'^{1/2}_a, u'^{-1/2}_a) - \operatorname{sn}^{-1}(1, u'^{-1/2}_a)}. \quad (5.244c)$$

From

$$\operatorname{sn}(K) = 1, \quad (5.245a)$$

$$\operatorname{sn}(K - j K') = 1/k \quad (5.245b)$$

we obtain

$$\operatorname{sn}^{-1}(1, k) = K, \quad (5.246a)$$

$$\operatorname{sn}^{-1}(1/k, k) = K - j K'. \quad (5.246b)$$

With this we obtain from (5.244c)

$$v_0 = \frac{K(k)}{K'(k)} = \frac{K(k)}{K(\sqrt{1 - k^2})}. \quad (5.247)$$

With (5.239) we obtain k as

$$k = \frac{1}{\sqrt{u'_a}} = \frac{1}{\cosh \frac{\pi a}{2h}}. \quad (5.248)$$

Inserting this into (5.247) we obtain

$$\nu_0 = \frac{K \left(\left(\cosh \frac{\pi a}{2h} \right)^{-1} \right)}{K \left(\tanh \frac{\pi a}{2h} \right)}. \quad (5.249)$$

To compute the capacitance per unit of length we apply (5.152). However, we have to consider that compared with (5.152) the roles of u and v are interchanged in Figure 5.30(c). The equipotential lines now are the lines of constant v . Furthermore, we have considered only a quarter of the cross-section of the complete stripline shown in Figure 5.29(a). Therefore we have to multiply the capacitance per unit of length computed for the quarter cross-section by a factor of 4 and obtain by this way the capacitance per unit of length for the complete stripline:

$$C' = \frac{4\epsilon}{\nu_0} = 4\epsilon \frac{K \left(\tanh \frac{\pi a}{2h} \right)}{K \left(\left(\cosh \frac{\pi a}{2h} \right)^{-1} \right)}. \quad (5.250)$$

Table 5.2 summarizes the stripline parameters for several values of the ratio $2a/h$.

5.7 PROBLEMS

1. A spherical capacitor consists of two concentric metallic spherical surfaces. The inner sphere exhibits a diameter of 5 mm and the outer spherical shell has an inner diameter of 6 mm. The space between the spheres is filled with a dielectric with $\epsilon_r = 20$. Compute the capacitance.
2. Two spheres of 1 cm diameter are arranged in a distance of 10 cm. Compute the capacitance between these two spheres and derive the electric field.
3. Three spheres of 1 cm diameter are arranged in a line every 15 cm.
 - a) Compute the mutual capacitances between these three spheres.
 - b) Compute \mathcal{E} as a function of the potential of the three spheres. (Give an approximate solution that does not exactly match the boundary conditions.)
4. In a box defined by $0 < x < a$, $0 < y < b$, $0 < z < d$, an electrostatic potential

$$\Phi_e(x, y, z) = \Pi_0 \sin \alpha x \sin \beta y \sinh \gamma z$$

is given. The boundary conditions are $\Phi_e = 0$ at $x = 0$, $x = a$, $y = 0$, $y = b$.

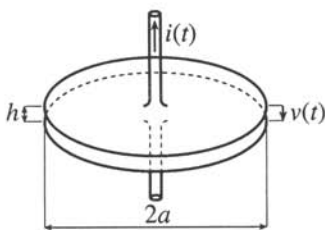


Figure 5.31: Disk capacitor.

- a) Determine α , β and γ .
 - b) Compute \mathcal{E} .
5. Discuss the discharge of the disk capacitor with diameter $2a$ and plate distance h , depicted in Figure 5.31 on the basis of Poynting's theorem. At the time t_0 the voltage across the capacitor is $v(t_0)$.
 - a) Compute the capacitance of the capacitor.
 - b) Compute the electric energy stored in the capacitor.
 - c) Connect a resistor R in parallel to the capacitor. Compute the decay of the voltage across the capacitor with time.
 - d) Apply Poynting's theorem to compute the power flowing out from the capacitor. Where is the power going?
6. Consider a coaxial line. The diameter of the inner conductor is 0.5 mm. The inner diameter of the outer conductor is 1.25 mm. The space between inner and outer conductor is filled with a dielectric with $\epsilon_r = 2.25$. Compute the capacitance per meter and the inductance per meter.
7. Consider a symmetric stripline. The distance between the top and bottom electrodes is 2 mm. The conducting strip of 1 mm width is located in the middle between the top and bottom electrode. The stripline is filled with a dielectric with $\epsilon_r = 4$. The transverse extension of top and bottom electrodes can be assumed to be infinite.
 - a) Compute the capacitance per unit of length and the inductance per unit of length.
 - b) Compute the characteristic impedance of the stripline.
8. Consider the coaxial line of the previous example. Let the inner conductor be biased with a DC voltage of 1 V with respect to the outer conductor and let a DC current of 20 mA flow in positive direction through the inner conductor.
 - a) Compute the electric energy stored per unit of length by integration of the electric energy density.
 - b) Compute the electric energy stored per unit of length from the capacitance per unit of length.

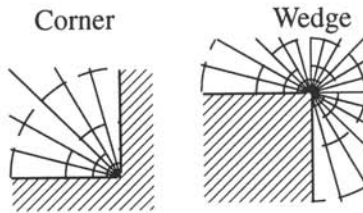


Figure 5.32: Corner and wedge.

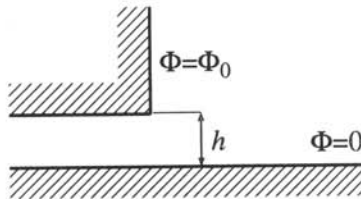


Figure 5.33: Wedge above ground electrode.

- c) Compute the magnetic energy stored per unit of length by integration of the magnetic energy density.
 - d) Compute the magnetic energy stored per unit of length from the inductance per unit of length.
 - e) Compute the dc power flowing through the coaxial line from the electric and the magnetic field using Poynting's theorem and compare the result with the power computed from voltage and current.
9. Show that Biot-Savart's law in conventional vector notation

$$\mathbf{B}(\mathbf{x}) = -\frac{\mu}{4\pi} \int' \frac{(\mathbf{x} - \mathbf{x}') \times \mathbf{J}(\mathbf{x}')}{|\mathbf{x} - \mathbf{x}'|^3} d^3 x'$$

is equivalent to (5.70).

10. Figure 5.32 shows a corner and a wedge formed by two not quite touching half-planes. Assume in both cases that one half-plane is grounded and the other is on potential Φ_0 . Compute the charge distributions on the half-planes.
11. Consider the two-dimensional electrode configuration depicted in Figure 5.33. The ground electrode is on potential $\Phi = 0$ and the wedge electrode is on a dc potential Φ_0 . Use the Schwarz-Christoffel transformation to compute the electric potential field..

REFERENCES

- [1] J. A. Stratton, *Electromagnetic Theory*. New York: McGraw-Hill, 1941.
- [2] J. D. Jackson, *Classical Electrodynamics*. New York: John Wiley & Sons, 1975.
- [3] H. A. Haus and J. R. Melcher, *Electromagnetic Fields and Energy*. Englewood Cliffs, NJ: Prentice Hall, 1989.
- [4] M. N. O. Sadiku, *Elements of Electromagnetics*. Orlando: Saunders, 1989.
- [5] Z. Popović and B. D. Popović, *Introductory Electromagnetics*. Englewood Cliffs, NJ: Prentice Hall, 2000.
- [6] H. A. Haus and J. R. Melcher, "Fields are always dynamic," *IEEE Trans. Education*, pp. 35–46, Feb. 1990.
- [7] G. Green, "An essay on the application of mathematical analysis to the theories of electricity and magnetism (1828)," in *The Scientific Papers of George Green*, Nottingham: The George Green Memorial Committee, 1995.
- [8] R. S. Elliott, *Electromagnetics – History, Theory, and Applications*. New York: IEEE Press, 1991.
- [9] R. E. Collin, *Field Theory of Guided Waves*. New York: IEEE Press, 1991.
- [10] G. de Rham, *Differentiable Manifolds*. New York: Springer, 1984.
- [11] K. F. Warnick and D. V. Arnold, "Electromagnetic Green functions using differential forms," *J. Electromagn. Waves and Appl.*, vol. 10, no. 3, pp. 427–438, 1996.
- [12] A. Sommerfeld, *Elektrodynamik*. Leipzig: Akademische Verlagsgesellschaft Geest & Portig, 1947.
- [13] R. Plonsey and R. E. Collin, *Principles and Applications of Electromagnetic Fields*. New York: McGraw-Hill, 1961.
- [14] S. Ramo, J. R. Whinnery, and T. van Duzer, *Fields and Waves in Communication Electronics*. New York: John Wiley & Sons, 1965.
- [15] R. E. Collin, *Foundations of Microwave Engineering*. New York: McGraw-Hill, 1992.
- [16] B. Friedman, *Lectures on Applications-Oriented Mathematics*. New York: John Wiley & Sons, 1969.
- [17] R. V. Churchill and J. W. Brown, *Complex Variables and Applications*. New York: McGraw Hill, 1990.
- [18] C. W. Wong, *Introduction to Mathematical Physics*. Oxford: Oxford University Press, 1991.
- [19] G. Stephenson and P. M. Radmore, *Advanced Mathematical Methods for Engineering and Science Students*. Cambridge: Cambridge University Press, 1990.
- [20] P. Morse and H. Feshbach, *Methods of Theoretical Physics, Part 1*. New York: McGraw-Hill, 1953.
- [21] S. Hassani, *Mathematical Physics*. Berlin: Springer, 2002.
- [22] W. Appel, *Mathématiques pour la Physique*. Paris: H & K Éditions, 2002.
- [23] E. Philippow, *Grundlagen der Elektrotechnik*. Berlin: VEB Verlag Technik, 1988.
- [24] B. C. Wadell, *Transmission Line Design Handbook*. Boston: Artech House, 1991.
- [25] I. S. Gradshteyn and I. M. Ryzhik, *Tables of Integrals, Series, and Products*. New York: Academic Press, 1965.
- [26] R. E. Collins, *Mathematical Methods for Physicists and Engineers*. New York: Reinhold Book Corporation, 1968.
- [27] E. Costamagna, "On the Numerical Inversion of the Schwarz-Christoffel Conformal Transformation," *IEEE Trans. Microwave Theory Techn.*, vol. 35, pp. 35–40, Jan. 1987.
- [28] W. R. Smythe, *Static and Dynamic Electricity*. New York: Hemisphere Publishing Corporation, 1989.
- [29] C. P. Wen, "Coplanar waveguide: A surface strip transmission line suitable for nonreciprocal gyromagnetic device applications," *IEEE Trans. Microwave Theory Techn.*, vol. 17, pp. 1087–1090, Dec. 1969.
- [30] S. Rawal and D. R. Jackson, "An exact TEM calculation of loss in a stripline of arbitrary dimensions," *IEEE Trans. Microwave Theory Techn.*, vol. 39, pp. 694–699, Apr. 1991.

- [31] M. Gillick, I. D. Robertson, and J. S. Joshi, "Direct analytical solution for the electric field distribution at the conductor surfaces of coplanar waveguides," *IEEE Trans. Microwave Theory Techn.*, vol. 41, pp. 129–135, Jan. 1993.
- [32] Z. Nehari, *Conformal Mapping*. New York: Dover, 1975.
- [33] W. Magnus, F. Oberhettinger, and R. P. Soni, *Formulas and Theorems for the Special Functions of Mathematical Physics*. Berlin: Springer, 1966.
- [34] H. Hancock, *Lectures on the Theory of Elliptic Functions*. New York: Peter Peregrinus, 1958.
- [35] M. Abramowitz and I. Stegun, *Handbook of Mathematical Functions with Formulas, Graphs and Mathematical Tables*. New York: Dover, 1965.
- [36] S. B. Cohn, "Characteristic impedance of the shielded-strip transmission line," *IRE Transactions - Microwave Theory and Techniques*, vol. 2, pp. 52–57, July 1954.
- [37] S. B. Cohn, "Problems in strip transmission lines," *IRE Transactions - Microwave Theory and Techniques*, vol. 3, pp. 119–126, Mar. 1955.
- [38] R. Hayt, "The mutual and input impedance of strips between parallel planes," *IRE Transactions - Microwave Theory and Techniques*, vol. 3, pp. 114–118, Mar. 1955.
- [39] R. H. T. Hayt, "Potential solution of a homogeneous strip-line of finite width," *IRE Transactions - Microwave Theory and Techniques*, vol. 3, pp. 16–18, July 1955.
- [40] R. H. T. Bates, "The characteristic impedance of the shielded slab line," *IRE Transactions - Microwave Theory and Techniques*, vol. 4, pp. 28–33, Jan. 1956.
- [41] B. Bhat and S. K. Koul, *Stripline-Like Transmission Lines for Microwave Integrated Circuits*. New York: John Wiley & Sons, 1989.

Chapter 6

Waves at the Surface of Conducting Media

We consider the propagation of an electromagnetic wave along a plane conducting surface. To simplify our considerations we assume the conducting plane to be infinitely extended in the yz -plane. According to Figure 6.1 the space is subdivided into two half-spaces 1 and 2 by a plane surface at $x = 0$. The half-spaces 1 and 2 each are filled with homogeneous and isotropic media. This problem is encountered when the propagation of electromagnetic waves along the Earth's surface or the propagation of electromagnetic waves along metallic surfaces is considered. Assuming region 1 to be filled with an ideal conductor a TEM wave with electric field perpendicular to the plane $z = 0$ and magnetic field parallel to this plane fulfills the boundary conditions. In the conductor surface the tangential magnetic field induces a surface current, shielding region 1 from the magnetic field. The tangential magnetic field is directed perpendicular to the direction of wave propagation, whereas the surface current is flowing in the direction of wave propagation.

If, however the region 1 is filled with a conductor of finite conductivity, the electromagnetic field and the shielding current are penetrating into the conductor. Due to the finite conductivity, the current flowing in the direction of propagation gives rise to a

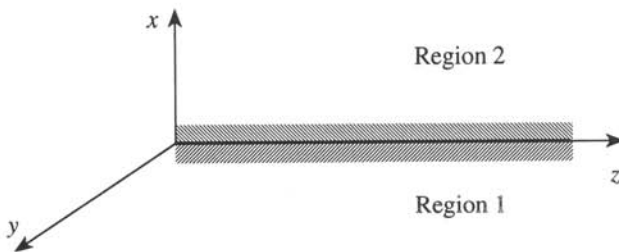


Figure 6.1: The plane surface.

longitudinal electric field component. The field in both regions 1 and 2 is transverse magnetic. Due to the conductor losses, the electromagnetic wave is attenuated in the direction of propagation. In transverse direction, the field is strongly decaying in the conductor region 1 and weakly decaying in region 2 if region 2 is free-space or filled by a dielectric. We call such a wave a *surface wave*. Zenneck was the first to give a solution of Maxwell's equations describing a surface wave guided by a plane interface separating any two media [1]. Therefore this type of wave also is called *Zenneck wave*. Treatment of surface waves is also given in [2–5].

6.1 TRANSVERSE MAGNETIC SURFACE WAVES

We seek solutions of the field equations that describe a plane wave propagating parallel to the surface. Without any restriction in general we assume the z -direction to be the direction of propagation of the electromagnetic wave. According to (3.84) a transverse magnetic wave can be derived from a Hertz form that has a z -component only. Therefore we make the ansatz

$$\underline{\Pi}_{ei}(\mathbf{x}) = \underline{\Pi}_{ezi}(\mathbf{x}) \, dz \quad (6.1)$$

for the Hertz form in either half-spaces $i = 1, 2$. We are only considering a wave propagating in positive z -direction and can therefore describe the z -dependence of the Hertz vector by a factor $e^{-\gamma z}$. This assumption corresponds with an electromagnetic field generated from a source at $z = -\infty$. Thereby we obtain the following ansatz for the z -component of the Hertz vector for both half-spaces 1 and 2:

$$\underline{\Pi}_{ei}(x, z) = \underline{\Pi}_{ez0i}(x) e^{-\gamma z} \, dz. \quad (6.2)$$

The propagation coefficient in the z -direction must be equal in either regions 1 and 2, since only in this way the solution in both half-spaces can be matched along the boundary at $x = 0$. From (3.40) and (6.2) we obtain the Helmholtz equation for the z -component of the Hertz vector for both half-spaces 1 and 2:

$$\frac{\partial^2 \underline{\Pi}_{ezi}}{\partial x^2} + \frac{\partial^2 \underline{\Pi}_{ezi}}{\partial z^2} - \gamma_{0i}^2 \underline{\Pi}_{ezi} = 0. \quad (6.3)$$

In this equation γ_{01} and γ_{02} are the complex propagation coefficients of the plane wave in medium 1 and 2, respectively. According to (3.42) and (3.49) we obtain

$$\gamma_{0i}^2 = -\omega^2 \mu_i \epsilon_i. \quad (6.4)$$

The sign of the γ_{0i} is determined by (3.50). We now solve (6.3) for either half-spaces 1 and 2. Afterwards we match these partial solutions along the boundary surface $x = 0$.

Inserting (6.2) into (6.3) yields

$$\frac{d^2 \underline{\Pi}_{e0i}}{dx^2} + (\gamma^2 - \gamma_{0i}^2) \underline{\Pi}_{e0i} = 0. \quad (6.5)$$

Introducing the propagation coefficient in the x -direction χ_i defined by

$$\chi_i^2 = \gamma_{0i}^2 - \gamma^2 \quad (6.6)$$

we obtain

$$\frac{d^2 \underline{\Pi}_{e0i}}{dx^2} - \chi_i^2 \underline{\Pi}_{e0i} = 0. \quad (6.7)$$

The solution of this equation is given by

$$\underline{\Pi}_{e0i} = \underline{A}_i e^{\chi_i x} + \underline{B}_i e^{-\chi_i x}, \quad (6.8)$$

where \underline{A}_i and \underline{B}_i are complex amplitudes not yet determined. The sign of χ_i is determined via the condition

$$\Re\{\chi_i\} \geq 0. \quad (6.9)$$

The solutions exponentially decaying for $|x| \rightarrow \infty$ are given by

$$\underline{\Pi}_{ez1} = \underline{A}_1 \exp(\chi_1 x - \gamma z), \quad (6.10a)$$

$$\underline{\Pi}_{ez2} = \underline{B}_2 \exp(-\chi_2 x - \gamma z). \quad (6.10b)$$

With (3.85) and (3.86) we obtain the following relations for the field intensities \underline{E} and \underline{H} in both subspaces:

$$\underline{E}_{xi} = \frac{\partial^2 \underline{\Pi}_{ezi}}{\partial x \partial z}, \quad (6.11a)$$

$$\underline{E}_{yi} = 0, \quad (6.11b)$$

$$\underline{E}_{zi} = -\frac{\partial^2 \underline{\Pi}_{ezi}}{\partial x^2}, \quad (6.11c)$$

$$\underline{H}_{xi} = 0, \quad (6.11d)$$

$$\underline{H}_{yi} = -j\omega\epsilon_i \frac{\partial \underline{\Pi}_{ezi}}{\partial x}, \quad (6.11e)$$

$$\underline{H}_{zi} = 0. \quad (6.11f)$$

Inserting (6.10a) and (6.10b), we obtain the field quantities

$$\underline{E}_{x1} = -\chi_1 \gamma \underline{A}_1 \exp(\chi_1 x - \gamma z), \quad (6.12a)$$

$$\underline{E}_{z1} = -\chi_1^2 \underline{A}_1 \exp(\chi_1 x - \gamma z), \quad (6.12b)$$

$$\underline{H}_{y1} = -j \omega \epsilon_1 \chi_1 \underline{A}_1 \exp(\chi_1 x - \gamma z), \quad (6.12c)$$

$$\underline{E}_{x2} = \chi_2 \gamma \underline{B}_2 \exp(-\chi_2 x - \gamma z), \quad (6.12d)$$

$$\underline{E}_{z2} = -\chi_2^2 \underline{B}_2 \exp(-\chi_2 x - \gamma z), \quad (6.12e)$$

$$\underline{H}_{y2} = j \omega \epsilon_2 \chi_2 \underline{B}_2 \exp(-\chi_2 x - \gamma z) \quad (6.12f)$$

in both subspaces. Due to the continuity of the tangential components of the electric field intensity at the boundary surface,

$$\underline{E}_{z1} \Big|_{x=0} = \underline{E}_{z2} \Big|_{x=0}, \quad (6.13)$$

we obtain

$$\chi_1^2 \underline{A}_1 = \chi_2^2 \underline{B}_2. \quad (6.14)$$

In the same way from the continuity of the tangential components of the magnetic field intensities at the boundary surface,

$$\underline{H}_{y1} \Big|_{x=0} = \underline{H}_{y2} \Big|_{x=0}, \quad (6.15)$$

we obtain

$$\epsilon_1 \chi_1 \underline{A}_1 = -\epsilon_2 \chi_2 \underline{B}_2. \quad (6.16)$$

From (6.4), (6.6), (6.14), and (6.16) we obtain the equation for the propagation coefficient γ of the wave propagating along the boundary surface:

$$\gamma^2 = \gamma_{02}^2 \frac{1 - \frac{\gamma_{02}^2 \mu_1^2}{\gamma_{01}^2 \mu_2^2}}{1 - \frac{\gamma_{02}^4 \mu_1^2}{\gamma_{01}^4 \mu_2^2}}. \quad (6.17)$$

From γ and from (6.6), we also may determine the transverse propagation coefficients χ_1 and χ_2 . In the important special case, where both half-spaces exhibit the same permeability, (6.17) reduces to

$$\gamma^2 = \frac{\gamma_{01}^2 \gamma_{02}^2}{\gamma_{01}^2 + \gamma_{02}^2}, \quad \text{for } \mu_1 = \mu_2. \quad (6.18)$$

Before discussing the solution we will make further simplifying assumptions. We consider the case where half-space 1 is filled by a nonmagnetic conductor and half-space 2 is free-space. For this case we obtain

$$\omega\epsilon'_1 \ll \sigma_1, \quad \mu_1 = \mu_0, \quad \epsilon_2 = \epsilon_0, \quad \mu_2 = \mu_0. \quad (6.19)$$

In half-space 1 we can neglect $\omega\epsilon'_1$ compared with σ_1 , and with

$$\sqrt{j} = e^{j\frac{1}{2}\pi} = \frac{1}{\sqrt{2}}(1 + j) \quad (6.20)$$

we obtain

$$\gamma_{01} = \sqrt{j\omega\mu_0\sigma_1} = \sqrt{\frac{1}{2}\omega\mu_0\sigma_1}(1 + j). \quad (6.21)$$

For the free-space region 2 we obtain

$$\gamma_{02} = j\omega\sqrt{\mu_0\epsilon_0} = j\beta_0 = j\frac{\omega}{c_0}, \quad (6.22)$$

where β_0 is the phase coefficient of the free-space and c_0 is the propagation velocity of the plane electromagnetic wave in free-space. Inserting (6.21) and (6.22) into (6.18) yields

$$\gamma = j\beta_0 \frac{1}{\sqrt{1 + j\frac{\omega\epsilon_0}{\sigma_1}}}. \quad (6.23)$$

Under the assumption $\omega\epsilon_0 \ll \sigma_1$, we obtain the following approximation

$$\gamma = \alpha + j\beta = \beta_0 \left(\frac{\omega\epsilon_0}{2\sigma_1} + j \right). \quad (6.24)$$

The transverse propagation coefficient in the quasi-conductor χ_1 can be computed from (6.6). Due to $\omega\epsilon_0 \ll \sigma_1$ we can neglect γ^2 compared with γ_{01}^2 in (6.6) and with $\chi_1^2 = \gamma_{01}^2$ we obtain from (6.21)

$$\chi_1 = \sqrt{\frac{1}{2}\omega\mu_0\sigma_1}(1 + j). \quad (6.25)$$

To compute the transverse propagation coefficient in the free-space, χ_2 , we eliminate from (6.4), (6.14), and (6.16) the ϵ_i as well as the \underline{B}_i and \underline{A}_i and obtain

$$\chi_2 = -\chi_1 \frac{\gamma_{02}^2}{\gamma_{01}^2}. \quad (6.26)$$

After inserting (6.21), (6.22), and (6.26) we obtain

$$\chi_2 = \beta_0 \sqrt{\frac{\omega\epsilon_0}{2\sigma_1}}(1 - j). \quad (6.27)$$

The field is decaying with increasing distance from the boundary surface in the free-space as well as in the conductor. Inside the conductor the field decays with

$$d_0 = \frac{1}{\Re\{\chi_1\}} \quad (6.28)$$

by a factor $1/e$. This effect is called the *skin effect*, and d_0 is called the *skin penetration depth*. Within the chosen approximation we obtain from (6.25) and (6.28)

$$d_0 = \sqrt{\frac{2}{\omega\mu_0\sigma_1}}. \quad (6.29)$$

Also in the free-space the field intensity decays with increasing distance from the boundary surface. Within the *transverse extending height* h_0 , given by

$$h_0 = \frac{1}{\Re\{\chi_2\}}, \quad (6.30)$$

the field intensity decays by a factor $1/e$. From (6.27) and (6.30) we obtain within our approximation

$$h_0 = \frac{1}{\beta_0} \sqrt{\frac{2\sigma_1}{\omega\epsilon_0}}. \quad (6.31)$$

In Figure 6.2 the frequency dependence of the skin penetration depth d_0 and the transverse extending height h_0 are shown for copper and wet soil. For the frequency dependence of the skin penetration depth in copper, we obtain

$$d_0 = \frac{66 \text{ mm}}{\sqrt{f/\text{Hz}}}, \quad \text{for copper.} \quad (6.32)$$

We now compute the field intensities \underline{E} and \underline{H} by inserting (6.24), (6.25), and (6.27) into (6.12a) to (6.12f). Furthermore we use (6.15) and express the complex amplitudes \underline{A}_1 and \underline{B}_2 by the complex magnetic field amplitude \underline{H}_{y0} at $x = 0, z = 0$, given by

$$\underline{H}_{y0} = \underline{H}_{y1}(x = 0, z = 0) = \underline{H}_{y2}(x = 0, z = 0). \quad (6.33)$$

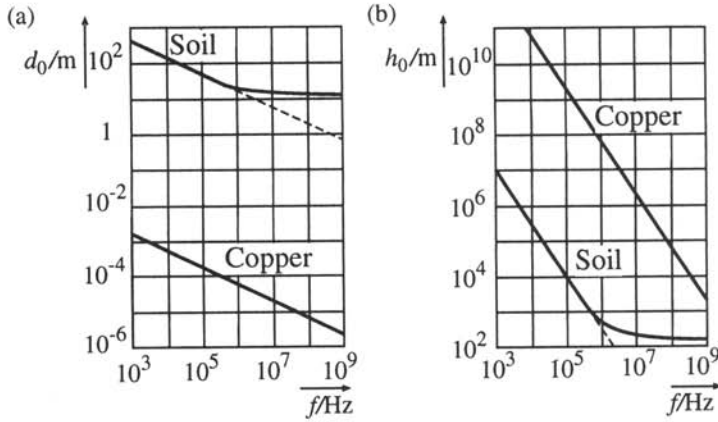


Figure 6.2: (a) Skin depth d_0 , and (b) transverse characteristic height h_0 depending on frequency f for copper ($\sigma = 5.8 \cdot 10^7 \text{ Sm}^{-1}$) and wet soil ($\sigma = 10^{-3} \text{ Sm}^{-1}$, $\epsilon_r = 10$).

We obtain

$$\underline{E}_{x1} = \frac{Z_{F1}^2}{Z_{F0}} \underline{H}_{y0} \exp(\chi_1 x - \gamma z), \quad (6.34a)$$

$$\underline{E}_{z1} = Z_{F1} \underline{H}_{y0} \exp(\chi_1 x - \gamma z), \quad (6.34b)$$

$$\underline{H}_{y1} = \underline{H}_{y0} \exp(\chi_1 x - \gamma z), \quad (6.34c)$$

$$\underline{E}_{x2} = Z_{F0} \underline{H}_{y0} \exp(-\chi_2 x - \gamma z), \quad (6.34d)$$

$$\underline{E}_{z2} = Z_{F1} \underline{H}_{y0} \exp(-\chi_2 x - \gamma z), \quad (6.34e)$$

$$\underline{H}_{y2} = \underline{H}_{y0} \exp(-\chi_2 x - \gamma z). \quad (6.34f)$$

Within our approximation, $\omega\epsilon_1 \ll \sigma_1$, the wave impedance Z_{F1} of the quasi-conductor is given by

$$Z_{F1} = \sqrt{\frac{\omega\mu_0}{2\sigma_1}} (1 + j) = \sqrt{\frac{\omega\mu_0}{\sigma_1}} \exp(j\frac{1}{4}\pi). \quad (6.35)$$

The wave impedance of the free-space, Z_{F0} , is given by

$$Z_{F0} = \sqrt{\frac{\mu_0}{\epsilon_0}}. \quad (6.36)$$

Figure 6.3 shows the time dependence of the electric field intensity at the boundary in the free-space as well as in the conductor. The longitudinal component \underline{E}_z of the electric field intensity is continuous at the boundary plane, whereas the normal component of

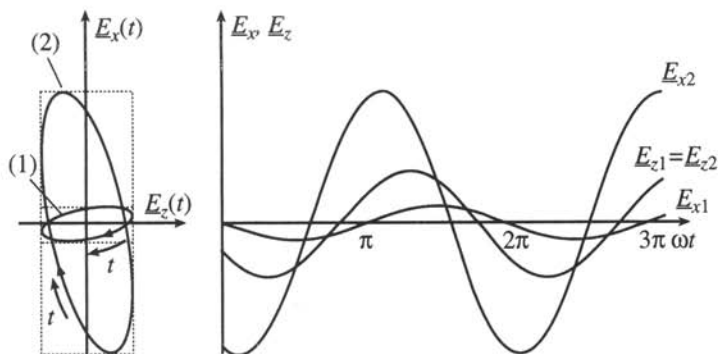


Figure 6.3: Time dependence of electric field intensity in the quasi-conductor and in free-space.

the electric field \underline{E}_x is discontinuous. Usually the magnitude of the wave impedance Z_{F1} of the quasi-conductor is by order of magnitudes smaller than the wave impedance Z_{F0} of free-space. From (6.34a), (6.34b), (6.34d) and (6.34e) it follows that the magnitude $|\underline{E}_{x2}|$ of the transverse component of the electric field in free-space is considerably larger than the magnitude $|\underline{E}_{z2}|$ of the longitudinal component, whereas in the quasi-conductor the magnitude of the transverse component of the electric field $|\underline{E}_{x1}|$ is by orders of magnitude smaller than the magnitude $|\underline{E}_{z1}|$ of the longitudinal component of the electric field. Furthermore longitudinal and transverse components of the electric fields are – neither in free-space nor in the quasi-conductor – in phase with transverse component of the electric field. In free-space the transverse component of the electric field is delayed by 45° with respect to the longitudinal component, whereas in the quasi-conductor the transverse component advances the longitudinal component of the electric field by 45° . In the vector picture the tip of the arrow of the electric field vector moves on an elliptic trace.

We now consider the surfaces of constant phase and constant amplitude of the surface wave. From (6.24) and (6.25), we obtain

$$\exp(\chi_1 x - \gamma z) = \exp\left(\sqrt{\frac{1}{2}\omega\mu_0\sigma_1}x - \frac{\omega^2\epsilon_0}{2\sigma_1 c_0}z\right) \exp\left[j\left(\sqrt{\frac{1}{2}\omega\mu_0\sigma_1}x - \frac{\omega}{c_0}z\right)\right]. \quad (6.37)$$

The first exponential term at the right side of (6.37) gives the space dependence of the amplitude, whereas the second exponential term describes the space dependence of the phase. From (6.24) and (6.26) we obtain for region 2

$$\exp(-\chi_2 x - \gamma z) = \exp\left[-\frac{\omega}{c_0}\sqrt{\frac{\omega\epsilon_0}{2\sigma_1}}\left(x + \sqrt{\frac{\omega\epsilon_0}{2\sigma_1}}z\right)\right] \exp\left[j\frac{\omega}{c_0}\left(\sqrt{\frac{\omega\epsilon_0}{2\sigma_1}}x - z\right)\right]. \quad (6.38)$$

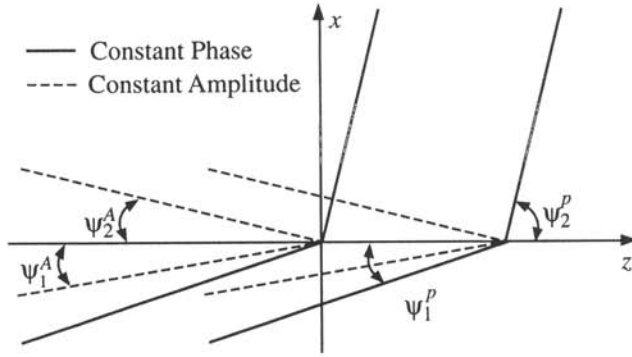


Figure 6.4: Planes of constant amplitude and constant phase.

We obtain the areas of constant amplitude in both regions by setting the first exponential factor on the right side of (6.37) or (6.38), respectively, constant. We obtain the surfaces of constant phase by setting the second exponential factor constant in either equation. The surfaces of constant amplitude as well as constant phase are all planes parallel to the y -axis. Figure 6.4 depicts the planes of constant amplitude and constant phase for either half-space. The planes of constant amplitude enclose angles Ψ_1^A and Ψ_2^A , respectively, with the plane $x = 0$. The planes of constant phase enclose the angles Ψ_1^P and Ψ_2^P with the plane $x = 0$. From (6.37) and (6.38) by setting constant either constant exponential terms we obtain

$$\tan \Psi_1^A = \sqrt{\frac{1}{2} \left(\frac{\omega \epsilon_0}{\sigma_1} \right)^3}, \quad (6.39a) \quad \tan \Psi_1^P = \sqrt{\frac{2\epsilon_0 \omega}{\sigma_1}}, \quad (6.39b)$$

$$\tan \Psi_2^A = \sqrt{\frac{\omega \epsilon_0}{2\sigma_1}}, \quad (6.40a) \quad \tan \Psi_2^P = \sqrt{\frac{2\sigma_1}{\omega \epsilon_0}}. \quad (6.40b)$$

For soil with $\sigma_1 = 10^{-2}$ S/m we obtain at a frequency $f = 1$ MHz the angles $\Psi_2^A = 3^\circ$, $\Psi_2^P = 87^\circ$, $\Psi_1^A = 1'$, $\Psi_1^P = 6^\circ$, where the superscript prime denotes the arc minute. In the case of a good conductor with $\sigma_1 \gg \omega \epsilon_1'$, the planes of constant phase in free-space are nearly perpendicular to the boundary surface, whereas the planes of constant phase in the conductor are nearly parallel to the boundary plane. The planes of constant amplitude are nearly parallel to the boundary plane in either subspaces.

The electric field lines are depicted in Figure 6.5. In metallic conductors the depth of penetration is very small. The transverse extending height exceeds the dimensions of circuit elements or systems considerably and may be considered to be infinite. In free-space the electromagnetic field distribution is not considerably influenced by a finite conductivity of the conductors. Therefore in the electromagnetic modeling of transmission-lines and distributed circuits in a first step, for the computation of the

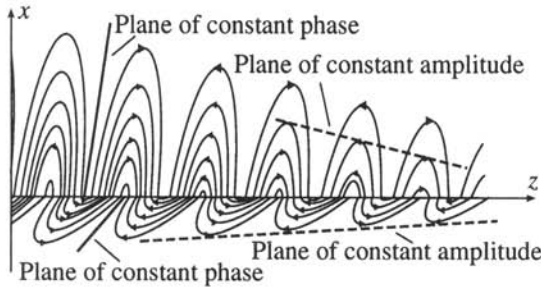


Figure 6.5: Electric field lines of the surface wave.

electromagnetic field in the free-space and dielectric regions, the metallic surface may be considered to be perfectly conducting. In a further step of the analysis the power losses may be computed from the surface current distribution and the finite surface conductivity due to the skin effect. The surface current distribution for the power loss computation is directly obtained from the tangential magnetic field distribution at the metallic surfaces.

The behavior of electromagnetic surface waves also is important for the understanding of wave propagation phenomena along the Earth's surface. The surface wave may be considerably attenuated by losses in the Earth's surface. In this case the transverse extending height cannot be neglected. Surface waves can only be used up to the medium frequency ranges for radio transmission. Below about 10 m wavelength the surface wave will be attenuated within a short distance. In the short-wave range long-distance propagation is achieved by making use of the ionospheric reflection of the wave radiated into space, whereas in the wavelength region down from meter-wave range only line-of-sight propagation is possible.

6.2 SURFACE CURRENTS

We now consider the case of metallic conductors in which σ exceeds $\omega\epsilon'$ by orders of magnitude. In this case the electric field in free-space is nearly normal to the conductor surface, whereas the electric field in the conductor is nearly parallel to the conductor surface. Using (6.24), (6.25), (6.29), and (6.34b) we obtain the longitudinal component of the electric field in the conductor,

$$\begin{aligned} E_{z1}(x, z, t) &= \Re \{ \underline{E}_{z1}(x, z) e^{j\omega t} \} \\ &= |Z_{F1} \underline{H}_{y0}| \exp \left(-\alpha z + \frac{x}{d_0} \right) \cos \left(\omega t + \phi_0 - \beta z + \frac{x}{d_0} \right), \end{aligned} \quad (6.41)$$

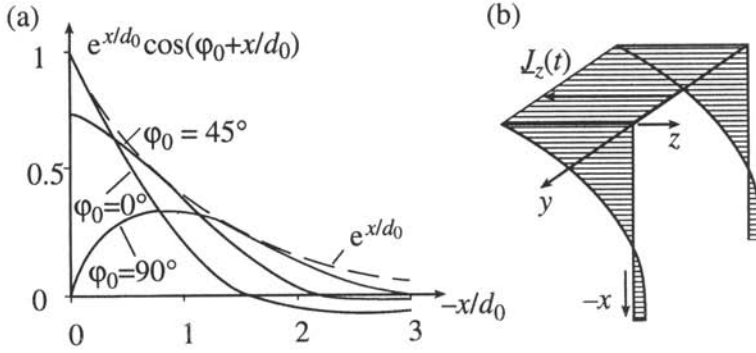


Figure 6.6: Skin effect: (a) The x -dependence of $E_{z1}(x, 0, 0)$ for $\phi = \omega t + \phi_0$, and (b) current distribution in the conductor.

where ϕ_0 is the phase of $Z_{F1}\underline{H}_{y0}$. The x dependence of E_{z1} is shown in Figure 6.6(a). Since the field as well as the current penetrates into the metal only to a depth of the order d_0 we can describe the current by a surface current. From (6.34a), (6.34b) and (6.34c), we obtain

$$\underline{\mathcal{E}} = Z_{F1}\underline{H}_{y0} \exp(\chi_1 x - \gamma z) \left(\frac{Z_{F1}}{Z_{F0}} dx + dz \right), \quad (6.42a)$$

$$\underline{\mathcal{H}} = \underline{H}_{y0} \exp(\chi_1 x - \gamma z) dy. \quad (6.42b)$$

Corresponding to (2.61) we obtain for the conductor region $x \geq 0$ the relation between the current density $\underline{\mathcal{J}}$ and the electric field intensity $\underline{\mathcal{E}}$,

$$\underline{\mathcal{J}} = \sigma_1 \star \underline{\mathcal{E}}. \quad (6.43)$$

Inserting (6.42a) into (6.43), considering $|Z_{F1}| \ll Z_{F0}$ and integrating $\underline{\mathcal{J}}$ over x over the interval $(-\infty, 0)$, we obtain the surface current density form

$$\underline{\mathcal{J}}_A(u, v) = \int_{-\infty}^0 \underline{\mathcal{J}}(u, v, n) = \frac{\sigma_1 Z_{F1}}{\chi_1} \underline{\mathcal{H}}_t \Big|_{x=0} = \underline{\mathcal{H}}_t \Big|_{x=0}. \quad (6.44)$$

At the surface the magnetic field only exhibits a tangential component. Therefore we have set $\underline{\mathcal{H}}|_{x=0} = \underline{\mathcal{H}}_t|_{x=0}$. Since in a metallic conductor $|Z_{F1}| \ll Z_{F0}$ is fulfilled we may neglect inside the conductor the electric field component normal to its surface and obtain from (6.42a) the approximation

$$\underline{\mathcal{E}} \cong \underline{\mathcal{E}}_t = Z_{F1}\underline{H}_{y0} \exp(\chi_1 x - \gamma z) dz. \quad (6.45)$$

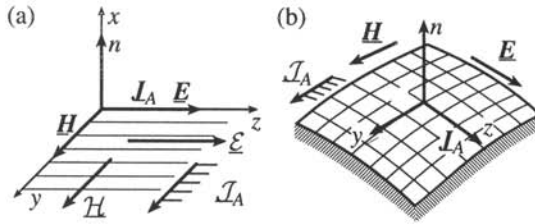


Figure 6.7: Orientation of H , J_A , E : (a) Wave propagation in z -direction, and (b) arbitrary orientation.

Figure 6.6(b) shows the current distribution under the surface of the metal. Using the twist operator (2.155) we can express the relation between the tangential electric and magnetic fields (6.42b), (6.45) on the conductor surface by

$$\begin{aligned}\underline{\mathcal{E}}_t &= Z_{F1} \perp_n \underline{\mathcal{H}}_t, \\ \underline{\mathcal{H}}_t &= -Z_{F1}^{-1} \perp_n \underline{\mathcal{E}}_t.\end{aligned}\quad (6.46)$$

The magnitude of the surface current density is equal to the magnitude of the tangential magnetic field at the surface. The surface current field is orthogonal to the tangential magnetic field at the surface. As we can see from Figure 6.7, the surface normal vector \mathbf{n} , the magnetic field \mathbf{H} , and the surface current density \mathbf{J}_A form a positive-oriented orthogonal trihedron.

We now consider the relation between the surface current density and the electric field in the conductor. The vectors \mathbf{n} , \mathbf{H} , and \mathbf{E} form the positive-oriented orthogonal trihedron depicted in Figure 6.7. Equation (6.46) gives the so-called *practical boundary condition*. We can apply this practical boundary condition also to curved surfaces, if the radius of curvature is large compared to the skin depth. In this case we assume the surface to be replaced in every point by its tangential plane. From (6.44) and (6.46) we obtain

$$\begin{aligned}\underline{\mathcal{E}}_t &= Z_{F1} \perp_n \underline{\mathcal{J}}_A, \\ \underline{\mathcal{J}}_A &= -Z_{F1}^{-1} \perp_n \underline{\mathcal{E}}_t.\end{aligned}\quad (6.47)$$

The relation between the surface current density \mathbf{J}_A and the tangential electric field \mathbf{E}_t on the surface is given by the wave impedance Z_{F1} of the conductor. On a conductor surface the tangential magnetic field and the surface current density have equal amplitude and are mutually orthogonal. The surface current field lines are obtained by rotating the magnetic field lines counterclockwise by 90° .

Consider the rectangular surface element shown in Figure 6.8. Let the longer side l of this rectangular surface element be parallel to the direction of the surface current

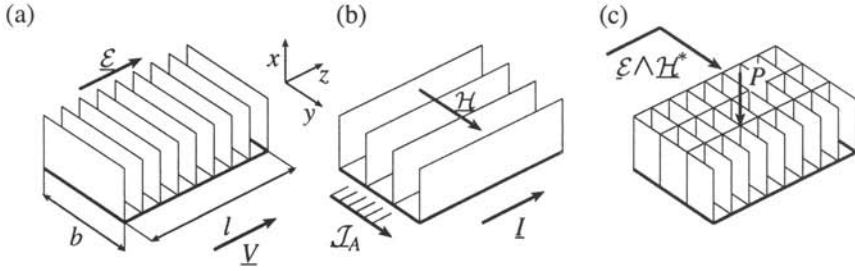


Figure 6.8: Conductor surface element: (a) electric field, (b) magnetic field, and (c) Poynting field.

and assume a surface current flowing in z -direction. The surface current form $\underline{\mathcal{J}}_A$ and the tangential electric and magnetic field forms $\underline{\mathcal{E}}_t$ and $\underline{\mathcal{H}}_t$ are given by

$$\underline{\mathcal{J}}_A = \underline{J}_{Az} dy, \quad \underline{\mathcal{E}}_t = \underline{E}_z dz, \quad \underline{\mathcal{H}}_t = \underline{H}_y dy. \quad (6.48)$$

With (6.46) and (6.47) we obtain

$$\underline{\mathcal{E}}_t = Z_{F1} \underline{J}_{Az} dz, \quad \underline{\mathcal{H}}_t = \underline{J}_{Ay} dy. \quad (6.49)$$

The surface current flowing through this area element in the z -direction is given by

$$\underline{I} = \int_{y_1}^{y_2} \underline{\mathcal{J}}_A = b \underline{J}_{Az}. \quad (6.50)$$

The voltage across the longer side of the area element is

$$\underline{V} = \int_{z_1}^{z_2} \underline{\mathcal{E}}_t = l \underline{E}_{z1} = l Z_{F1} \underline{J}_{Az}. \quad (6.51)$$

From this we obtain the impedance Z of the rectangular area element of length l and width b . The impedance of the rectangular area element oriented in parallel to the surface currents only depends on the ratio side lengths l and b and the wave impedance Z_{F1} of the material,

$$Z = \frac{\underline{V}}{\underline{I}} = \frac{l}{b} Z_{F1}. \quad (6.52)$$

A square area element exhibits an area impedance equal to the wave impedance Z_{F1} independently from its size. At low frequencies we may define for any thin conducting layer with a thickness d a *surface impedance* $Z_A = 1/\sigma d$. If the skin effect occurs, also

for thick conductive layers the current is only flowing within a thin layer under the surface of the conductor. Due to (6.35) the skin effect surface impedance Z_A is given by

$$Z_A = Z_{F1} = \sqrt{\frac{\omega\mu_0}{2\sigma_1}} (1 + j). \quad (6.53)$$

The real part of the surface impedance is the *surface resistance* R_A given by

$$R_A = \Re\{Z_A\} = \sqrt{\frac{\omega\mu_0}{2\sigma_1}} = \frac{1}{\sigma_1 d_0}. \quad (6.54)$$

The surface resistance $\frac{1}{\sigma_1 d_0}$ is equal to the surface resistance of a conducting layer with thickness d_0 and the conductivity σ_1 . The imaginary part of the surface X_A of the surface impedance is equal to its real part. The imaginary part of the surface impedance corresponds to a surface inductance originating from the penetration of the magnetic field into the metal,

$$X_A = R_A. \quad (6.55)$$

If we are only interested in the electromagnetic field in the free-space or in the dielectric material, but not in the field distribution inside the conductor, the practical boundary condition (6.46) allows us to simplify the field computation considerably. We solve the field equations in free-space or in the dielectric material, respectively, and match the electric and magnetic field intensities together at the surface of the conductor using the practical boundary conditions. Let us consider for example the surface wave along a plane. From (6.12d) to (6.12f) we obtain

$$\frac{E_{x2}}{H_{y2}} = \frac{\gamma}{j\omega\epsilon_2}, \quad (6.56a)$$

$$\frac{E_{z2}}{H_{y2}} = -\frac{\chi_2}{j\omega\epsilon_2}. \quad (6.56b)$$

From the practical boundary conditions (6.46) we obtain

$$\frac{E_{x2}}{H_{y2}} = Z_{F1}. \quad (6.57)$$

From (6.4), (6.6), and (6.56a) to (6.57) we obtain γ and χ_2 , which coincide with the values obtained from (6.24) and (6.27). Thereby we have determined the electromagnetic field in region 2 completely without computing the field in region 1.

The results of this section may also be applied to a wire with a circular cross-section, if the cross-sectional radius is considerably larger than d_0 . In this case small surface

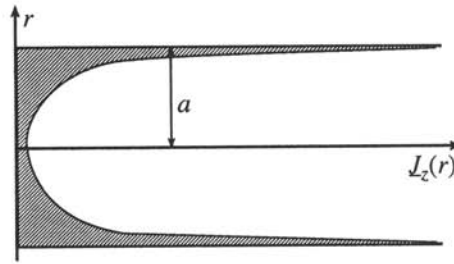


Figure 6.9: Current distribution in conductor with circular cross-section.

elements of the wire can be approximated by their tangential plane and the practical boundary conditions may be applied. Due to the symmetry of a conductor with circular cross-section, the current distribution over the circumference of the conductor is uniform. In Figure 6.9 the current distribution of the current in the circular conductor for $d_0 \ll a$ is shown [6]. With the surface impedance Z_A according to (6.53), we obtain the impedance of a conductor of length l ,

$$Z = R + jX = \frac{l}{2\pi\sigma_1 d_0 a} (1 + j). \quad (6.58)$$

The impedance Z exhibits an inductive imaginary part X , which is due to the penetration of the magnetic field under the conductor surface. This inductive part, however, in general can be neglected in comparison with the inductance due to the magnetic field outside the conductor. At high frequencies due to the small penetration depths, the real part of the impedance Z may be much larger than the DC resistance

$$R_0 = \frac{l}{a^2\pi} \frac{1}{\sigma_1}. \quad (6.59)$$

Figure 6.10 shows the results of an exact computation of R and X for the conductor with a circular cross-section.

6.3 SURFACE CURRENT LOSSES

Surface currents in a conductor yield power loss by conversion of electromagnetic energy into thermal energy. This power loss is the reason for the attenuation of the electromagnetic surface wave. Let us now compute the surface current losses per unit of area. Since the electromagnetic field under the conductor surface decays exponentially with a very small penetration depth d_0 , we can assume that the electromagnetic energy

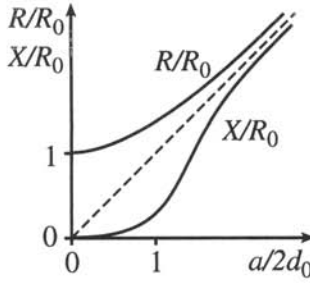


Figure 6.10: Exact values of R and X for a conductor with a circular cross-section.

flowing through the surface into the conductor is converted there directly into heat. The power loss P_L in the conductor consequently is equal to the active power flowing into the conductor through the surface. From (4.37) we obtain

$$P_L = -\Re \left\{ \int_A \mathcal{T} \right\} . \quad (6.60)$$

The negative sign in (6.60) occurs since the area normal vector \mathbf{n} is directed towards the conductor outside, whereas we are computing the power flowing into the conductor. From (4.19) and (6.46) we obtain

$$P_L = -\frac{1}{2} \Re \left\{ \int_A \underline{\mathcal{E}}_t \wedge \underline{\mathcal{H}}_t^* \right\} = \frac{1}{2} \Re \left\{ \int_A \underline{\mathcal{H}}_t^* \wedge (Z_{F1} \perp_n \underline{\mathcal{H}}_t) \right\} . \quad (6.61)$$

Introducing the *surface impedance operator*

$$Z_{F1} = Z_{F1} \perp_n . \quad (6.62)$$

with (C.172) we can express (6.61) as

$$P_L = \frac{1}{2} \Re \left\{ \langle \underline{\mathcal{H}}_t | Z_{F1} \underline{\mathcal{H}}_t \rangle_A \right\} . \quad (6.63)$$

In an orthogonal coordinate system (u, v, n) with the coordinates u and v tangential to the surface and n normal to the surface and the corresponding basis forms s_1, s_2 , and n , the magnetic field form is

$$\underline{\mathcal{H}} = \underline{H}_u s_1 + \underline{H}_v s_2 , \quad (6.64)$$

and we obtain

$$\underline{\mathcal{H}}_t^* \wedge (\perp_n \underline{\mathcal{H}}_t) = (|\underline{H}_u|^2 + |\underline{H}_v|^2) s_1 \wedge s_2 = |\underline{\mathcal{H}}_t|^2 s_1 \wedge s_2 \quad (6.65)$$

and from this

$$P_L = \frac{1}{2} \int_A R_A |\underline{H}_t|^2 s_1 \wedge s_2. \quad (6.66)$$

Since the magnetic field due to (2.114c) is free of divergence and since the magnetic field disappears inside the conductor, the magnetic field exhibits only a tangential component at the conductor surface. We therefore may set $\underline{H} = \underline{H}_t$. If the magnetic field at the conductor surface is known, (6.63) and (6.66) respectively allow us to compute the conductor losses. This allows a further simplification of the field computation, which we will apply in the following as far as possible. The field distribution in the free-space or in the quasi-dielectric, respectively, does not change considerably, if a metallic conductor is replaced by an ideal conductor. Therefore we can proceed in the field computation in two steps:

1. The field is computed for an ideal conductor ($\sigma = \infty$).
2. From the tangential component of the magnetic field at the conductor surface, the losses are computed using (6.66).

If we are using this method, we have to consider the following: If we let $\sigma \rightarrow \infty$, this does not influence the normal components of the electric field and the tangential component of the magnetic field considerably, whereas the tangential component of the electric field at the conductor surface is going to zero. However, this does not cause essential changes in the field distribution, since the tangential component of the electric field in the case of metallic conductors is by orders of magnitude smaller than the normal component.

Let us now consider as an example the power loss in the area element according to Figure 6.8. Inserting (6.48) in (4.19), we obtain the complex Poynting's form

$$\mathcal{T} = -\frac{1}{2} \underline{E}_z \underline{H}_y^* dy \wedge dz. \quad (6.67)$$

With (6.49) it follows that

$$\mathcal{T}_x \Big|_{x=0} = -\frac{1}{2} Z_A |J_{Az}^2| dy \wedge dz. \quad (6.68)$$

The loss of power flowing into the conductor per unit of area is given by

$$\Re \left\{ \mathcal{T}_x \Big|_{x=0} \right\} = -\frac{1}{2} R_A |J_{Az}^2|. \quad (6.69)$$

With (6.60) the power loss flowing into the area element according to Figure 6.8 is given by

$$P_L = \frac{1}{2} b l R_A |J_{Az}^2|. \quad (6.70)$$

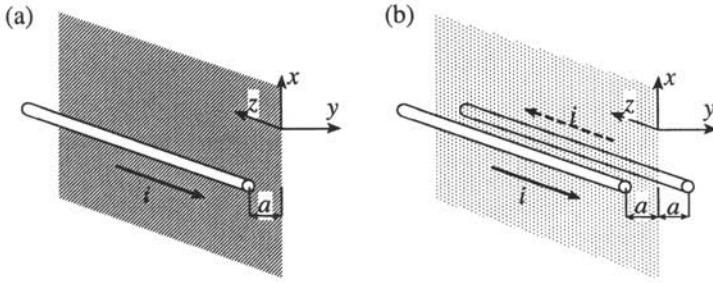


Figure 6.11: (a) Wire in distance a parallel to a conducting wall, and (b) mirror wire.

Similar to (6.52), the real part of the impedance of the area element is

$$R = \frac{l}{b} R_A. \quad (6.71)$$

With (6.50) we obtain from (6.70) the power loss

$$P_L = \frac{1}{2} R |I|^2 \quad (6.72)$$

as the electromagnetic active power flowing into the surface element and being dissipated there. This is exactly the power loss occurring in a resistor R , if a current I is impressed.

6.4 INDUCED SURFACE CURRENTS

A static magnetic field can penetrate a nonmagnetic conductor without any perturbation. Contrary to this a high-frequency electromagnetic field induces surface currents on the conductor, which shield the electromagnetic field from inside the conductor. If the skin penetration depth d_0 is small in comparison with the linear dimensions of the conductor, we can assume the electromagnetic field, to be completely shielded from inside the conductor. If the alternating magnetic field is known at the conductor surface, the surface current density may be computed from (6.46). However, we have to consider that the *induced surface currents* contribute to the electromagnetic field too.

In the following example we consider a straight circular conductor in parallel to a plane conducting surface, as depicted in Figure 6.11(a). We assume the circular conductor as well as the conducting plane to have infinite extension. The distance between the circular conductor and the conducting plane is a . The plane conducting surface is positioned at $y = 0$. The circular conductor is oriented in parallel to the z -axis.

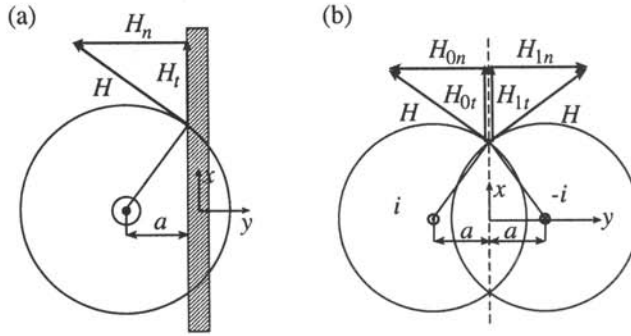


Figure 6.12: (a) Magnetic field around a straight wire in free-space, and (b) introduction of a mirror conductor.

We assume that the radius of the circular conductor may be neglected in comparison to the distance a . We first compute the magnetic field generated by a current I flowing through the conductor in the negative z -direction without assuming the presence of the conducting plane. Due to the symmetry, the magnetic field lines in this case are concentric circles with the circular conductor in the center.

We compute the magnetic field due to the current i flowing through a straight wire in free-space. From Ampère's law we obtain the magnitude of the magnetic field H_0 at a distance r from the axis of the wire given by

$$H_0 = \frac{i}{2r\pi}. \quad (6.73)$$

At the plane $y = 0$ the tangential component of the magnetic field, H_{0t} is given by

$$H_{0t} = \frac{a}{r} H_0 = \frac{i}{2\pi} \frac{a}{a^2 + x^2}, \quad (6.74)$$

as can be concluded directly from the similarity of the two triangles $\{r, a, x\}$ and $\{H, H_t, H_n\}$ in Figure 6.12(a). If we now insert the conducting plane at $y = 0$, the magnetic field H_0 induces a current in the conducting wall, shielding the magnetic field from inside the conductor. For symmetry reasons all the induced wall current flows parallel to the z -axis. The magnetic field H_1 generated by the induced wall current exhibits tangential components that are antisymmetric with respect to the plane $y = 0$. Since the magnetic field H_1 , which is generated by the wall currents, is compensating the primary field H_0 inside the conductor, it follows that outside the conductor the tangential components of H_1 and H_0 exhibit equal magnitude and equal sign. From

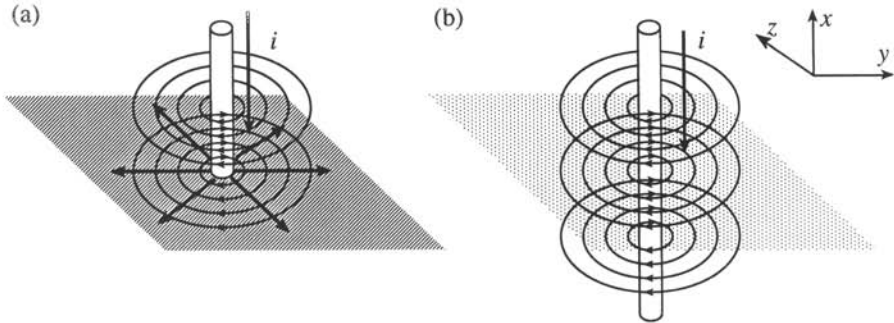


Figure 6.13: (a) Wire normal to a conducting plane, and (b) mirror wire.

this we obtain the surface current density

$$J_{Az} = \underline{H}_t = 2\underline{H}_{0t} = \frac{i}{\pi} \frac{a}{a^2 + x^2}. \quad (6.75)$$

In Figure 6.12(b) a mirror conductor is introduced. The wall at $y = 0$ is removed and an image conductor at $y = a$ is inserted. In the image conductor a current $-i$ with the same magnitude and opposite direction is flowing. In the half-space $y < 0$ this image conductor produces the same magnetic field as the shielding currents in $y = 0$. Figure 6.11 illustrates the *mirror principle*.

We obtain the total current induced in the wall, i_{ind} by integrating the area current density induced in the wall over x :

$$i_{\text{ind}} = \int_{-\infty}^{+\infty} J_{Az} dx = i. \quad (6.76)$$

The total current induced in the wall has the same magnitude as the current flowing in the wire and exhibits opposite direction. We also can use the mirror principle to compute the total magnetic field due to the current in the wire and the current in the wall. If we remove again the wall in the plane $y = 0$ and arrange a mirror wire at $y = a$ with a current $-i$ impressed, the total magnetic field can be computed as the superposition of the field contributions from both wires.

Figure 6.13 illustrates the application of the mirror principle to a wire normal to a conducting plane. In the arrangement of a conducting plane and a straight wire shown in Figure 6.13(a), positioned normal to the conducting plane according to Figure 6.13(b), the conducting plane is replaced by the mirror image of the line in the region $x < 0$. In the case of the wire normal to the plane, the direction of the current in the mirror wire is the same as in the original wire.

We may further generalize the mirror principle to wires of arbitrary shape. We can replace any arrangement of conductors and an infinitely extended wall by the original arrangement of conductors plus the mirror image of this arrangement. The mirror plane is the plane of symmetry. The currents in the mirror conductor arrangement have opposite components in parallel to the symmetry plane and identical components normal to the symmetry plane. If charges are mirrored at a conducting wall the mirror charges have the opposite sign. The mirror currents and the mirror charges are the sources of mirror electromagnetic fields. With respect to the plane of symmetry the tangential components of the magnetic field and the normal component of the electric field are keeping their sign, whereas the tangential components of the electric field and the normal component of the magnetic field are changing their sign.

If we use a perfectly magnetic conducting wall as the mirror, the mirror currents have the same tangential components and opposite normal components, and the mirror charges have the same sign as the original charges. Furthermore the tangential components of the electric field and the normal component of the magnetic field are keeping their sign, whereas the tangential components of the magnetic field and the normal component of the electric field are changing their sign.

6.5 PROBLEMS

1. A linearly polarized time-harmonic plane electromagnetic wave with electric field amplitude E_0 is normally incident from free-space on a plane copper surface ($\sigma = 5.8 \cdot 10^7 \text{ Sm}^{-1}$).
 - a) Compute the electric and magnetic field components of the incident and reflected waves in free-space and the electric and magnetic fields in the metal.
 - b) Compute the complex Poynting vector in the metal and give an interpretation of the meaning of its real and imaginary parts.
 - c) Compute the reflection coefficient for the frequencies 1 GHz, 100 GHz and 10 THz.
2. At 2.5 GHz the biological tissue has the following material properties: Fat: $\epsilon_r = 13$, $\sigma = 0.4 \text{ S/m}$; cartilage $\epsilon_r = 21$, $\sigma = 0.13 \text{ S/m}$; muscle: $\epsilon_r = 50$, $\sigma = 2.2 \text{ S/m}$. Compute for these three cases for an incident power density of 1 mW/cm^2 the specific absorption rate in watts/kg as a function of depth. The specific absorption rate is the absorbed power per unit of mass of the medium. For this calculation we assume that the media exhibit the same mass density as water.
3. The y - z -plane is the boundary surface between the two half-spaces 1 and 2. Half-space 1, $x \leq 0$ is filled with a homogeneous isotropic material, and half-space 2, $x > 0$ is free-space. A transverse magnetic surface wave propagates along the boundary surface in positive z -direction.

- a) Half-space 1 is filled with iron ($\mu_r = 300$, $\sigma = 8.0 \cdot 10^6 \text{ Sm}^{-1}$). Compute the longitudinal propagation coefficient γ , and the transversal propagation coefficient κ_1 and κ_2 , the penetration depth d_0 , the height h_0 , and the surface impedance of the iron surface Z_A for the frequencies 50 Hz, 1 kHz, and 1 MHz.
- b) Half-space 1 is filled with dry earth ($\epsilon'_r = 5$, $\mu_r = 1$, $\sigma = 10^{-5} \text{ Sm}^{-1}$). Compute the longitudinal propagation coefficient γ and the transversal propagation coefficient κ_1 and κ_2 for the frequency 10 MHz.

REFERENCES

- [1] J. Zenneck, "Über die Fortpflanzung ebener elektromagnetischer Wellen längs einer ebenen Leiterfläche und ihre Beziehung zur Drahtlosen Telegraphie," *Annalen der Physik*, vol. 23, pp. 846–866, 1907.
- [2] J. A. Stratton, *Electromagnetic Theory*. New York: McGraw-Hill, 1941.
- [3] R. F. Harrington, *Time Harmonic Electromagnetic Fields*. New York: McGraw-Hill, 1961.
- [4] L. B. Felsen and N. Marcuvitz, *Radiation and Scattering of Waves*. Englewood Cliffs, NJ: Prentice Hall, 1972.
- [5] C. A. Balanis, *Advanced Engineering Electromagnetics*. New York: John Wiley & Sons, 1989.
- [6] A. Sommerfeld, *Elektrodynamik*. Leipzig: Akademische Verlagsgesellschaft Geest & Portig, 1947.

Chapter 7

Transmission-Lines and Waveguides

7.1 INTRODUCTION

A *transmission-line* or *waveguide* allows the guidance of electromagnetic energy along a certain path. Usually the radiation of energy from the line into the environment and also the excitation of waves on the line by environmental fields should be avoided. The transmission-line concept is based on the description of the guided wave by voltages and currents, whereas the term waveguide is related to the field description of the guided wave. In its narrower sense the term transmission-line applies to structures of two or more unconnected conductors between which voltages can be applied. The introduction of generalized voltages and currents, however, allows the application of the transmission-line concept to other types of waveguides. Particularly with regard to the generality of the field concept, transmission-lines may also be considered as waveguides. Therefore the decision whether the term transmission-line or waveguide is more appropriate is also related to the methodology we apply for the investigation of the respective structure. Waveguides and transmission-lines are treated in detail in [1–5].

We use the expression *waveguide* to denote various structures that have the purpose to guide electromagnetic energy. We therefore introduce the following definition: *A waveguide is a structure consisting of various materials that can guide electromagnetic waves along a given curve in space.* A homogeneous cylindrical waveguide has the shape of a generalized homogeneous cylinder. A generalized cylinder is a surface that is generated by moving a closed curve in parallel to a line. A homogeneous cylinder is invariant with respect to translations in the direction of the generating line.

Figure 7.1 shows examples of various types of homogeneous cylindric waveguides. The *parallel wire line*, Figure 7.1(a), and the *coaxial line*, Figure 7.1(b), exhibit a two-fold connected cross-section. These lines have no cutoff frequency and can be used for all frequencies from DC upwards. The *cutoff frequency* of a certain type of a guided wave

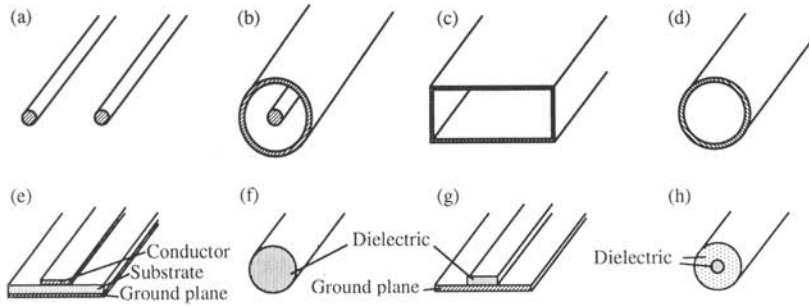


Figure 7.1: (a) Parallel wire line, (b) coaxial line, (c) rectangular waveguide, (d) circular waveguide, (e) microstrip line, (f) circular dielectric waveguide, (g) image line, and (h) optical fiber.

is the frequency below which this type of wave cannot propagate. In the coaxial line the electromagnetic field is confined within the region between the inner conductor and the outer conductor. Therefore the coaxial line is completely shielded. In the parallel wire line the electromagnetic field is not confined within a transverse cross-section of finite extension. Therefore from the parallel wire line and other open waveguide structures, radiation may occur as a leakage effect yielding *radiation loss* and *electromagnetic interference*. At higher frequencies therefore the coaxial line is preferred compared to the parallel wire line, since the coaxial line exhibits no radiation losses. Hollow-pipe waveguides simply are called *hollow waveguides* as the *rectangular waveguide* shown in Figure 7.1(c) and the *circular waveguide* shown in Figure 7.1(d) exhibit only a single connected metallic boundary. The region inside the waveguide is either empty or filled with dielectric material. Hollow-pipe waveguides exhibit a lower cutoff frequency, since there is no electrostatic field solution for the region inside the hollow waveguide. In a hollow waveguide waves can only propagate if half the wavelength of a plane wave is smaller than the largest cross-sectional dimension of the hollow waveguide. By filling the hollow waveguide with the dielectric material, the lower cutoff frequency can be moved to lower values. This, however, will increase the waveguide losses. In comparison with coaxial lines, hollow waveguides exhibit lower conductive losses and are preferred at frequencies above 10 GHz compared with coaxial lines. In order to transmit high power, hollow waveguides are also used at lower frequencies below 1 GHz. At millimeter-wave frequencies and higher frequencies, hollow waveguides also exhibit considerable conductor losses. Therefore, for submillimeter waves, infrared waves and in the optical wavelength region, dielectric waveguides are preferred. Figure 7.1(e) shows a *microstrip line*, consisting of a metallic strip on an insulating substrate with metallic ground plane. The microstrip line is a planar structure and can be fabricated using printed-circuit techniques. Figure 7.1(f) shows a *circular dielectric waveguide*. The *dielectric waveguide* exhibits a higher permittivity than the surrounding dielectric material or free-space,

Table 7.1: Classification of Waveguide Modes

Mode Type	Longitudinal Electric Field	Longitudinal Magnetic Field
TEM or L modes (Lecher modes, transverse electromagnetic modes)	$\underline{E}_z = 0$	$\underline{H}_z = 0$
TE or H modes (transverse electric modes)	$\underline{E}_z = 0$	$\underline{H}_z \neq 0$
TM or E modes (transverse magnetic modes)	$\underline{E}_z \neq 0$	$\underline{H}_z = 0$
Hybrid modes	$\underline{E}_z \neq 0$	$\underline{H}_z \neq 0$

respectively. The electromagnetic field is not strictly confined within the dielectric waveguide, but decays exponentially in a transverse direction outside the core region of the dielectric waveguide. The *image line* depicted in Figure 7.1(g) is a dielectric waveguide mounted on conducting substrate. The electromagnetic field is mirrored on the substrate. Compared with the dielectric waveguide in Figure 7.1(f), the image line provides a mounting of the waveguide without perturbing the electromagnetic field. For very short wavelengths, especially in the optical region, a dielectric waveguide as depicted in Figure 7.1(h) is advantageous. The core of this waveguide with higher permittivity is embedded in a dielectric material with lower permittivity. In the outer region of the waveguide, the electromagnetic field is rapidly decaying, and at the boundary of the outer region the electromagnetic field has decayed sufficiently so that the field is not perturbed by the mounting of the waveguide. Also a cladding deposited onto the outer region will not increase the attenuation of the electromagnetic wave. Circular dielectric waveguides with core and cladding are realized as *optical fibers*.

We now consider a homogeneous cylindric waveguide. We assume that the waveguide is oriented along the z -axis of our cylindric coordinate system. We seek a solution of Maxwell's equations exhibiting the form

$$\underline{\mathcal{E}}(\mathbf{x}) = \underline{\mathcal{E}}_0(x, y) e^{\pm \gamma z}, \quad (7.1a)$$

$$\underline{\mathcal{H}}(\mathbf{x}) = \underline{\mathcal{H}}_0(x, y) e^{\pm \gamma z}. \quad (7.1b)$$

Due to the translational invariance of the waveguide geometry in the z -direction, we can decompose the expressions for the field intensities into the exponential factor $e^{\pm \gamma z}$ and the forms depending only on the transverse coordinates, $\underline{\mathcal{E}}_0(x, y)$ and $\underline{\mathcal{H}}_0(x, y)$, respectively. We will see that there is an infinite number of solutions existing with distinct transverse field structures $\underline{\mathcal{E}}_0(x, y)$ and $\underline{\mathcal{H}}_0(x, y)$, respectively. Each of these solutions is called *mode*. We can subdivide the modes into *propagating modes* and

evanescent modes. In the case of a lossless waveguide, the propagating mode exhibits an imaginary propagation coefficient $\gamma = j\beta$, whereas the evanescent mode exhibits a real propagation coefficient $\gamma = \alpha$. If a mode exhibits a cutoff frequency, below this cutoff frequency the mode will be an evanescent mode, and above the cutoff frequency the mode will be a propagating mode. The number of existing propagating modes increases with increasing frequency. If below some cutoff frequency there exists only one propagating mode, this propagating mode is called the *fundamental mode* of the waveguide. We also may classify the modes with respect to the occurring field components. Table 7.1 summarizes the classification scheme of waveguides. The *transverse electromagnetic modes* or *Lecher modes* exhibit only transverse field components. The *transverse electric modes* (TE modes) exhibit no electric field components in the longitudinal direction, whereas the *transverse magnetic mode* (TM modes) exhibit no magnetic field components in the longitudinal direction. The *hybrid modes* have electric longitudinal field components as well as magnetic longitudinal field components.

7.2 PHASE AND GROUP VELOCITY

For a propagating mode we obtain from (7.1a) for a wave propagating in the positive z -direction the electric field intensity

$$E(\mathbf{x}, t) = \Re\{\underline{E}_0(x, y) e^{j(\omega t - \beta z)}\}. \quad (7.2)$$

The velocity by which a plane of constant phase is propagating is called the *phase velocity*. We obtain the phase velocity by setting the exponential term in (7.2) constant

$$c = \frac{\omega}{\beta}. \quad (7.3)$$

A harmonic electromagnetic wave exhibits a phase velocity, which in general depends on frequency. The frequency dependence of the phase velocity may be caused by the geometric properties of the waveguides as well as by the frequency dependence of the permittivity and permeability of the material filling the waveguide. A wave packet as depicted in Figure 7.2 may be considered a superposition of harmonic waves. The electric field of such a wave packet may be described by

$$E(\mathbf{x}, t) = \Re\left\{\int_{\omega_0 - \Delta\omega}^{\omega_0 + \Delta\omega} \underline{E}_0(x, y, \omega) e^{j(\omega t - \beta(\omega)z)} d\omega\right\}. \quad (7.4)$$

We assume the *phase coefficient* $\beta(\omega)$ to be frequency-dependent. Considering a narrow-band wave packet, the phase term $\omega t - \beta(\omega)z$ may be expanded in a certain frequency

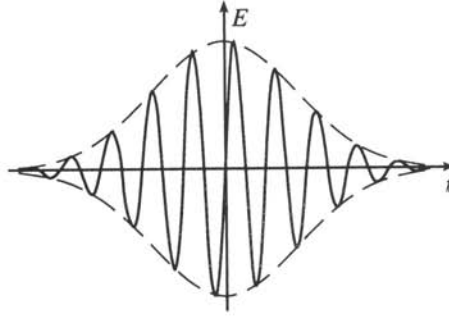


Figure 7.2: A periodic wave train.

interval around the center frequency ω_0 into a Taylor series,

$$\omega t - \beta(\omega)z = \omega_0 t - \beta(\omega_0)z + (\omega - \omega_0) \left(t - \frac{d\beta}{d\omega} \Big|_{\omega_0} z \right). \quad (7.5)$$

After inserting (7.5) into (7.4), we obtain

$$E(x, t) = \Re \left\{ e^{j(\omega_0 t - \beta(\omega_0)z)} \int_{\omega_0 - \Delta\omega}^{\omega_0 + \Delta\omega} \underline{E}_0(x, y, \omega) e^{j(\omega - \omega_0) \left(t - \frac{d\beta}{d\omega} \Big|_{\omega_0} z \right)} d\omega \right\}. \quad (7.6)$$

The exponential term describes a harmonic wave propagating in the z -direction with an angular frequency ω_0 . This harmonic wave propagates according to (7.3) with a phase velocity c . The integral in (7.6) describes the envelope of the wave. Setting $t - (d\beta/d\omega)z$ constant we obtain the velocity v_g of propagation of the envelope,

$$v_g = \left(\frac{d\beta}{d\omega} \right)^{-1}. \quad (7.7)$$

This velocity v_g is called the *group velocity*. Energy and information propagate with the group velocity. The phase velocity is only a virtual velocity of the phase planes and does not determine the velocity of transmission of energy or information, respectively.

7.3 THE FIELD COMPONENTS

In this section we discuss the way to evaluate the electromagnetic field components in linear waveguides. Without any restriction in general we assume the waveguides to be oriented in the z -direction. Furthermore, we assume that the cross-section of

the waveguide may be subdivided into subsections and that each of these subsections is either empty or filled by conducting material or homogeneous isotropic lossless dielectric material. One strategy to solve Maxwell's equations for such structures is to seek the partial solutions for every subsection and to match the solution along the boundaries. If the metallic conductors are considered to be perfectly conducting, we do not need to solve the field equation inside the metallic regions. By superposition of partial solutions the boundary conditions may be fulfilled. The mathematical effort may be reduced considerably, if we can choose a cylindric coordinate system in which boundary surfaces of the waveguide may be defined by setting constant one coordinate. In this case a single partial solution may already represent the field distribution of a mode.

We may derive transverse magnetic modes from the electric Hertz form $\underline{\Pi}_e$ and the transverse electric modes from the magnetic Hertz form $\underline{\Pi}_m$. We can choose an electric Hertz form $\underline{\Pi}_e$ or a magnetic Hertz form $\underline{\Pi}_m$, which exhibits only a longitudinal field component $\underline{\Pi}_{ez}$ or $\underline{\Pi}_{mz}$, respectively. The electric and magnetic Hertz forms and the scalar wave equation for the longitudinal components of the Hertz forms are given by

Transverse Magnetic Field

$$\underline{H}_z = 0$$

$$\underline{\Pi}_e(\mathbf{x}) = \underline{\Pi}_{ez}(\mathbf{x}) \, dz, \quad (7.8a)$$

$$\Delta \underline{\Pi}_{ez} - \gamma_{M0}^2 \underline{\Pi}_{ez} = 0, \quad (7.9a)$$

$$\gamma_{M0}^2 = -\omega^2 \underline{\mu} \underline{\epsilon}, \quad (7.10)$$

$$\underline{\mathcal{E}} = -\tilde{\mathbf{d}} \, d \underline{\Pi}_e = \star \, \mathbf{d} \star \, d \underline{\Pi}_e, \quad (7.11a)$$

$$\underline{\mathcal{H}} = j \omega \underline{\epsilon} \star \, d \underline{\Pi}_e, \quad (7.12a)$$

Transverse Electric Field

$$\underline{E}_z = 0$$

$$\underline{\Pi}_m(\mathbf{x}) = \underline{\Pi}_{mz}(\mathbf{x}) \, dz, \quad (7.8b)$$

$$\Delta \underline{\Pi}_{mz} - \gamma_{M0}^2 \underline{\Pi}_{mz} = 0, \quad (7.9b)$$

$$\gamma_{M0}^2 = -\omega^2 \underline{\mu} \underline{\epsilon}, \quad (7.10)$$

$$\underline{\mathcal{H}} = -\tilde{\mathbf{d}} \, d \underline{\Pi}_m = \star \, \mathbf{d} \star \, d \underline{\Pi}_m, \quad (7.11b)$$

$$\underline{\mathcal{E}} = -j \omega \underline{\mu} \star \, d \underline{\Pi}_m. \quad (7.12b)$$

The field components in Cartesian coordinates are

Transverse Magnetic Field

$$\underline{H}_z = 0$$

$$\underline{E}_x = \frac{\partial^2 \underline{\Pi}_{ez}}{\partial x \partial z}, \quad (7.13a)$$

$$\underline{E}_y = \frac{\partial^2 \underline{\Pi}_{ez}}{\partial y \partial z}, \quad (7.14a)$$

$$\underline{E}_z = \frac{\partial^2 \underline{\Pi}_{ez}}{\partial z^2} - \gamma_{M0}^2 \underline{\Pi}_{ez}, \quad (7.15a)$$

$$\underline{H}_x = j \omega \underline{\epsilon} \frac{\partial \underline{\Pi}_{ez}}{\partial y}, \quad (7.16a)$$

$$\underline{H}_y = -j \omega \underline{\epsilon} \frac{\partial \underline{\Pi}_{ez}}{\partial x}, \quad (7.17a)$$

$$\underline{H}_z = 0, \quad (7.18a)$$

Transverse Electric Field

$$\underline{E}_z = 0$$

$$\underline{H}_x = \frac{\partial^2 \underline{\Pi}_{mz}}{\partial x \partial z}, \quad (7.13b)$$

$$\underline{H}_y = \frac{\partial^2 \underline{\Pi}_{mz}}{\partial y \partial z}, \quad (7.14b)$$

$$\underline{H}_z = \frac{\partial^2 \underline{\Pi}_{mz}}{\partial z^2} - \gamma_{M0}^2 \underline{\Pi}_{mz}, \quad (7.15b)$$

$$\underline{E}_x = -j \omega \underline{\mu} \frac{\partial \underline{\Pi}_{mz}}{\partial y}, \quad (7.16b)$$

$$\underline{E}_y = j \omega \underline{\mu} \frac{\partial \underline{\Pi}_{mz}}{\partial x}, \quad (7.17b)$$

$$\underline{E}_z = 0. \quad (7.18b)$$

For hybrid modes, a linear combination of a longitudinal electric Hertz vector according to (7.8a) and a magnetic Hertz vector according to (7.8b) may be chosen.

7.4 WAVEGUIDES FOR TRANSVERSE ELECTROMAGNETIC WAVES

Transverse electromagnetic or TEM waves exhibit no field components in the direction of propagation [2–5]. Choosing the z -direction as the direction of propagation, we obtain $\underline{E}_z = 0$ and $\underline{H}_z = 0$. Therefore we can derive the transverse electromagnetic wave from (7.8a) as well from (7.8b). We are choosing the formulation (7.8a). In this case the Helmholtz equation (7.9a) is valid and the field components in the Cartesian coordinate system are given by (7.13a)–(7.18a). With $\underline{E}_z = 0$ we obtain from (7.15a)

$$\frac{\partial^2 \underline{\Pi}_{ez}}{\partial z^2} - \gamma_{M0}^2 \underline{\Pi}_{ez} = 0. \quad (7.19)$$

This equation is satisfied by

$$\underline{\Pi}_{ez}(\mathbf{x}) = \underline{\Pi}_{e0}^{(+)}(x, y) e^{-\gamma_{M0} z} + \underline{\Pi}_{e0}^{(-)}(x, y) e^{\gamma_{M0} z}. \quad (7.20)$$

For lossless lines we obtain $\gamma_{M0} = j\beta_{M0}$. Due to (7.10) the phase velocity of the TEM wave is equal to the phase velocity of the plane electromagnetic wave. In the following we assume ideal conductors in lossless media. From (7.9a) and (7.19), we obtain

$$\frac{\partial^2 \underline{\Pi}_{e0}}{\partial x^2} + \frac{\partial^2 \underline{\Pi}_{e0}}{\partial y^2} = 0, \quad (7.21)$$

which holds for $\underline{\Pi}_{e0}^{(+)}(x, y)$ as well as $\underline{\Pi}_{e0}^{(-)}(x, y)$. This equation is the two-dimensional Laplace equation known from electrostatics. Due to (7.13a), (7.14a), (7.16a), and (7.17a) the two-dimensional Laplace equation must also be satisfied by the components \underline{E}_x , \underline{E}_y , \underline{H}_x , and \underline{H}_y . The transverse field distribution therefore corresponds to the field distribution of the static two-dimensional problem. Furthermore, from the validity of the two-dimensional Laplace equation for the transverse field components it follows that in a waveguide bounded by a connected conductor a transverse electromagnetic wave cannot occur. Transverse electromagnetic waves only may occur if the waveguide cross-section exhibits at least two unconnected conductors. Figure 7.3 shows schematically the cross-sections of two transverse electromagnetic waveguides. Figure 7.3(a) generalizes the parallel wire line according to Figure 7.1(a). The transverse electromagnetic field is infinitely extended. In the waveguide cross-section depicted in Figure 7.3(b), the outer conductor 1 completely surrounds the inner conductor 2. The electromagnetic

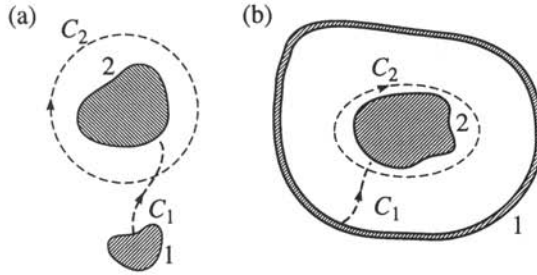


Figure 7.3: Paths of integration C_1 and C_2 for (a) parallel wire line, and (b) shielded line.

field therefore is bounded to the region between the inner conductor and the outer conductor and is shielded from the outside region by the outer conductor.

Using (2.63) we now compute the voltage between conductor 2 and conductor 1 in a transverse plane (i.e., in a plane normal to the z -axis). The integration is performed along a path of integration C_1 . We obtain

$$\underline{V}_{21}(z) = - \int_{C_1} \underline{\mathcal{E}}. \quad (7.22)$$

For any transverse plane (i.e., for a certain z), we obtain a voltage $\underline{V}_{21}(z)$, which is independent from the choice of the path of integration. The independence from the path of integration is due to the circumstance that in the transverse electromagnetic mode, no longitudinal magnetic field occurs and any closed contour of integration yields a zero contribution to the path integral (7.22). We therefore may define for a certain transverse plane a voltage between the two conductors 2 and 1. The voltage $\underline{V}_{21}(z)$, however, depends on the longitudinal coordinate z . Figure 7.4 shows the arrow for the voltage $\underline{V}_{21}(z)$. In the following we shall use the simplified notation $\underline{V}(z)$ instead of $\underline{V}_{21}(z)$. We now determine the current \underline{I}_2 flowing through conductor 2. To do this we insert (2.65c) into (2.57a) and integrate over the closed path C_2 surrounding the conductor 2. Since the transverse electromagnetic mode exhibits no longitudinal electric flux, the integral of the magnetic field over the closed path C_2 is equal to the current flowing through the inner conductor in positive z -direction. We obtain

$$\underline{I}_2(z) = \oint_{C_2} \underline{\mathcal{H}}. \quad (7.23)$$

The arrow for the current $\underline{I}_2(z)$ is shown in Figure 7.4. In the following we write $\underline{I}(z)$ instead of $\underline{I}_2(z)$. If the waveguide cross-section exhibits only two unconnected conductors, the currents flowing into these conductors are of equal magnitude and opposite direction. $\underline{E}_z = 0$ is only valid for ideal conductors with $\sigma = \infty$. In the case of

finite conductivity there also occurs a small z -component of the electric field. However, in most cases we do not need to consider the finite conductivity σ of the metallic surfaces for computing the electromagnetic field distribution of the modes. Electric losses and conductor losses may be calculated on the base of field distributions of lossless lines. Furthermore we restrict our considerations to electromagnetic waves propagating in the positive z -direction. From (7.13a), (7.14a), (7.16a), and (7.17a) we obtain for the transverse field components in the lossless medium

$$\underline{E}_x = -j\beta_{M0} \frac{\partial \Pi_{ez}}{\partial x}, \quad \underline{H}_x = j\omega\epsilon \frac{\partial \Pi_{ez}}{\partial y}, \quad (7.24a)$$

$$\underline{E}_y = -j\beta_{M0} \frac{\partial \Pi_{ez}}{\partial y}, \quad \underline{H}_y = -j\omega\epsilon \frac{\partial \Pi_{ez}}{\partial x}. \quad (7.24b)$$

From (2.79) and (7.10) it follows that

$$\underline{E}_x = Z_F \underline{H}_y, \quad \underline{E}_y = -Z_F \underline{H}_x. \quad (7.25)$$

These equations may be generalized in differential form notation as follows

$$\underline{\mathcal{E}} = -Z_F \star (dz \wedge \underline{\mathcal{H}}), \quad (7.26a)$$

$$\underline{\mathcal{H}} = \frac{1}{Z_F} \star (dz \wedge \underline{\mathcal{E}}). \quad (7.26b)$$

The electromagnetic field distribution is completely described by specifying $\underline{I}(z)$ and $\underline{V}(z)$. We can express the complex field intensities $\underline{E}(\mathbf{x})$ and $\underline{H}(\mathbf{x})$ as a product of the complex scalar amplitudes $\underline{V}(z)$ and $\underline{I}(z)$ with normalized real field vectors $\mathbf{e}(x, y)$ and $\mathbf{h}(x, y)$,

$$\underline{E}(\mathbf{x}) = \underline{V}(z) \mathbf{e}(x, y), \quad (7.27a)$$

$$\underline{H}(\mathbf{x}) = \underline{I}(z) \mathbf{h}(x, y). \quad (7.27b)$$

We call $\mathbf{e}(x, y)$ the *electric structure function* and $\mathbf{h}(x, y)$ the *magnetic structure function* of the TEM mode. The structure functions are given by

$$\mathbf{e}(x, y) = [e_x(x, y), e_y(x, y)]^T, \quad (7.28a)$$

$$\mathbf{h}(x, y) = [h_x(x, y), h_y(x, y)]^T, \quad (7.28b)$$

where $e_x(x, y)$, $e_y(x, y)$, $h_x(x, y)$ and $h_y(x, y)$ are the components of the structure functions. The corresponding differential forms are the *electric structure form* $e(x, y)$ and the *magnetic structure form* $h(x, y)$, given by

$$e(x, y) = e_x(x, y) dx + e_y(x, y) dy, \quad (7.29a)$$

$$h(x, y) = h_x(x, y) dx + h_y(x, y) dy. \quad (7.29b)$$

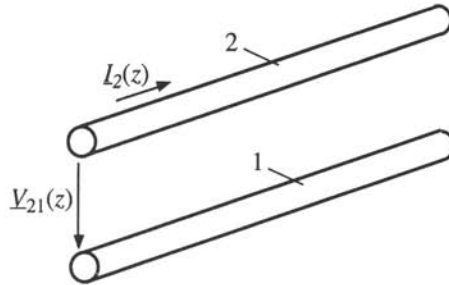


Figure 7.4: Arrows for $\underline{V}(z)$ and $\underline{I}(z)$ in the TEM line.

With this we can express the electric and magnetic field forms by

$$\underline{\mathcal{E}}(\mathbf{x}) = \underline{V}(z) \mathbf{e}(x, y), \quad (7.30a)$$

$$\underline{\mathcal{H}}(\mathbf{x}) = \underline{I}(z) \mathbf{h}(x, y). \quad (7.30b)$$

From (7.22), (7.23), (7.30a), and (7.30b) we obtain

$$-\int_{C_1} \mathbf{e}(x, y) \cdot d\mathbf{C}_1 = 1, \quad (7.31a)$$

$$\oint_{C_2} \mathbf{h}(x, y) \cdot d\mathbf{C}_2 = 1. \quad (7.31b)$$

Due to the uniqueness of the solution of the two-dimensional Laplace equation (7.21) the field vectors in distinct transverse planes only differ by a factor independent from x and y . The structure forms \mathbf{e} and \mathbf{h} are independent from z . The lossless TEM waveguide may be characterized by the *capacitance per unit of length* C' and *inductance per unit of length* L' . Let us consider the *charge per unit of length* Q' on conductor 2. We determine the charge $Q' \Delta z$ stored within a section of length Δz by

$$Q' \Delta z = \epsilon \int_{A_2} \star \underline{\mathcal{E}}. \quad (7.32)$$

The volume of integration V is the cylinder shown in Figure 7.5. The side surface of the cylinder is generated by the curve C_2 . Due to the transverse character of the electric field we only have to integrate over the side surface of the cylinder.

Inserting (7.26a) into (7.32) yields

$$\underline{Q'} \Delta z = -\epsilon Z_F \int_{A_2} d\mathbf{z} \wedge \underline{\mathcal{H}} = \epsilon Z_F \int_{A_2} \underline{\mathcal{H}} \wedge d\mathbf{z}, \quad (7.33a)$$

$$\underline{Q'} = \epsilon Z_F \oint_{C_2} \underline{\mathcal{H}} = \epsilon Z_F \underline{I}. \quad (7.33b)$$

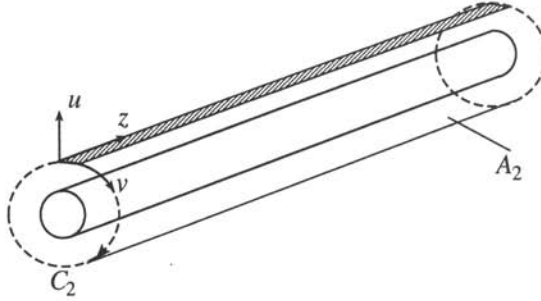


Figure 7.5: Volume for integration to determine the charge.

Inserting (7.27a) into (7.32) we obtain

$$Q' \Delta z = \underline{V} \epsilon \int_{A_2} \star \mathbf{e}. \quad (7.34)$$

Inserting (7.29a) yields

$$\begin{aligned} \underline{Q'} \Delta z &= \underline{V} \epsilon \int_{A_2} (e_x dy \wedge dz + e_y dz \wedge dx) \\ &= \underline{V} \epsilon \int_{A_2} (e_x dy - e_y dx) \wedge dz. \end{aligned} \quad (7.35)$$

The capacitance per unit of length, C' , is given by

$$C' = \frac{Q'}{\underline{V}} = \epsilon \oint_{C_2} (e_x dy - e_y dx). \quad (7.36)$$

If the electromagnetic wave is propagating only in the positive z -direction, the ratio of voltage and current due to (7.33b) and (7.36) is given by

$$Z_0 = \frac{V}{I} = \frac{Q'}{C' I} = \frac{Z_F \epsilon}{C'}. \quad (7.37)$$

Z_0 is the *characteristic impedance* of the transmission-line. The characteristic impedance is the impedance of a line with infinite length. With (2.75) and (2.79) we obtain

$$Z_0 = \frac{1}{c C'}. \quad (7.38)$$

The characteristic impedance depends on the phase velocity and on the capacity per unit of length. The phase velocity c of the transverse electromagnetic wave is equal to

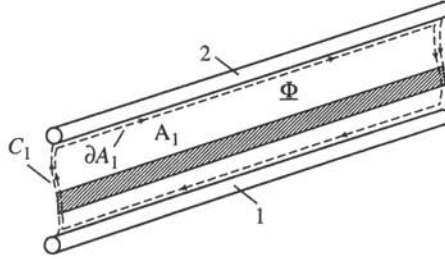


Figure 7.6: Area of integration to determine the magnetic flux $\underline{\Phi}' \Delta z$.

the phase velocity of the plane electromagnetic wave propagating in the same dielectric medium that is filling the space between the conductors in the transverse electromagnetic waveguide. The capacitance C' per unit of length is identical with the electrostatic capacitance per unit of length.

To determine the inductance per unit of length, we consider the line segment of length Δz . Between both conductors a magnetic flux per unit of length $\underline{\Phi}'$ is flowing. From (2.130b) we obtain

$$\underline{\Phi}' \Delta z = \mu \int_{A_1} \star \underline{H}. \quad (7.39)$$

The integration is performed over the area A_1 , which is obtained by parallel translation of the curve C_1 in z -direction by a distance Δz (Figure 7.6). With (7.26b) we obtain

$$\underline{\Phi}' \Delta z = \frac{\mu}{Z_F} \int_{A_1} dz \wedge \underline{\mathcal{E}} = -\frac{\mu}{Z_F} \int_{A_1} \underline{\mathcal{E}} \wedge dz. \quad (7.40)$$

This yields directly

$$\underline{\Phi}' = -\frac{\mu}{Z_F} \int_{C_1} \underline{\mathcal{E}}. \quad (7.41)$$

With (7.22) we obtain

$$\underline{\Phi}' = \frac{\mu}{Z_F} \underline{V}. \quad (7.42)$$

The inductance L' per unit of length is defined by

$$L' = \frac{\underline{\Phi}'}{\underline{I}}. \quad (7.43)$$

From (7.27b) and (7.39) we obtain

$$\begin{aligned} \underline{\Phi}' \Delta z &= \underline{I} \mu \int_{A_1} (h_x dy \wedge dz + h_y dz \wedge dx) \\ &= \underline{I} \mu \int_{A_1} (h_x dy - h_y dx) \wedge dz. \end{aligned} \quad (7.44)$$

This yields directly

$$\underline{\Phi}' = \underline{I} \mu \int_{C_1} (h_x dy - h_y dx) . \quad (7.45)$$

With (7.43) we obtain

$$L' = \mu \int_{C_1} (h_x dy - h_y dx) . \quad (7.46)$$

Using (7.37), (7.42), (7.43), (2.75), and (2.79) we can express the characteristic impedance Z_0 of the transmission-line by the phase velocity c of the electromagnetic wave and the inductance per unit of length L' ,

$$Z_0 = \frac{V}{\underline{\Phi}'} L' = \frac{Z_F}{\mu} L' = c L' . \quad (7.47)$$

Furthermore, we obtain from (2.75), (7.38) and (7.47)

$$Z_0 = \sqrt{\frac{L'}{C'}} , \quad (7.48a)$$

$$c = \frac{1}{\sqrt{L' C'}} = \frac{1}{\sqrt{\epsilon \mu}} . \quad (7.48b)$$

We now consider wave propagation in positive z -direction and in negative z -direction as well, and derive the transmission-line equations for \underline{V} and \underline{I} . To investigate the variation of $\underline{V}(z)$ with z we evaluate the difference of the voltages $\underline{V}(z)$ and $\underline{V}(z + \Delta z)$ drawn in Figure 7.7(a). Since the tangential component of the electric field vanishes at the conductor surface, the difference of the voltages $\underline{V}(z)$ and $\underline{V}(z + \Delta z)$ is given by

$$\underline{V}(z + \Delta z) - \underline{V}(z) = \oint_{\partial A_1} \underline{\mathcal{E}} = \int_{A_1} d\underline{\mathcal{E}} . \quad (7.49)$$

Using Faraday's law (2.123b), (7.39), and (7.43) we obtain

$$\underline{V}(z + \Delta z) - \underline{V}(z) = -j \omega \mu \int_{A_1} \star \underline{\mathcal{H}} = -j \omega \underline{\Phi}' \Delta z = -j \omega L' I \Delta z . \quad (7.50)$$

After performing the transition $\Delta z \rightarrow 0$,

$$\frac{dV}{dz} = \lim_{\Delta z \rightarrow 0} \frac{1}{\Delta z} [\underline{V}(z + \Delta z) - \underline{V}(z)] , \quad (7.51)$$

we obtain the differential equation for the variation of $\underline{V}(z)$,

$$\frac{dV}{dz} = -j \omega L' \underline{I} . \quad (7.52)$$

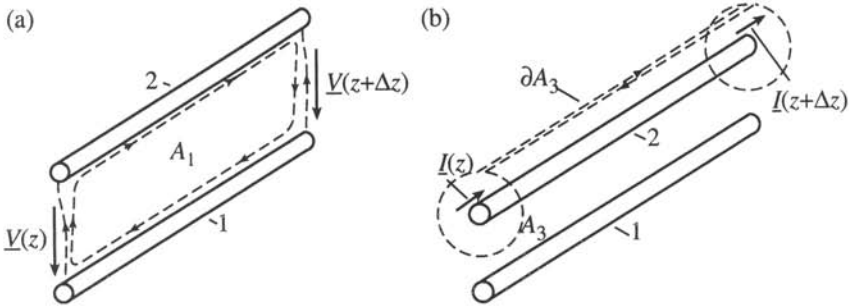


Figure 7.7: (a) Application of Faraday's law, and (b) application of Ampère's law.

We can compute the difference of currents $\underline{I}(z + \Delta z)$ and $\underline{I}(z)$ applying Ampère's law (2.57a), and integrating over the cut cylindric surface in Figure 7.7(b). The circulation integral along ∂A_3 is composed of the circulation integrals in the transverse planes at z and at $z + \Delta z$. These circulation integrals yield the current contributions $\underline{I}(z)$ and $-\underline{I}(z + \Delta z)$. The contributions of the path integrals parallel to the z -axis from z to $z + \Delta z$ compensate each other and therefore give no contribution to the circulation. Therefore we obtain

$$\underline{I}(z + \Delta z) - \underline{I}(z) = - \oint_{\partial A_3} \underline{\mathcal{H}} = - \int_{A_3} d\underline{\mathcal{H}}. \quad (7.53)$$

In the area integral we can replace the cut surface A_3 by the uncut surface A_2 according to Figure 7.5. Since the area A_2 is not penetrated by a conduction current, Ampère's law (2.123a), together with (2.130a) and (7.32) yields

$$\underline{I}(z + \Delta z) - \underline{I}(z) = -j\omega\epsilon \int_{A_3} \star \underline{\mathcal{E}} = -j\omega Q' \Delta z = -j\omega C' \underline{V} \Delta z. \quad (7.54)$$

With the transition $\Delta z \rightarrow 0$ we obtain

$$\frac{d\underline{I}}{dz} = \lim_{\Delta z \rightarrow 0} \frac{1}{\Delta z} [\underline{I}(z + \Delta z) - \underline{I}(z)], \quad (7.55)$$

and therewith it follows from (7.54) that

$$\frac{d\underline{I}}{dz} = -j\omega C' \underline{V}. \quad (7.56)$$

Equations (7.52) and (7.56) are the *first-order transmission-line equations*. We can eliminate \underline{V} or \underline{I} , respectively, and we obtain the *second-order transmission-line equations*,

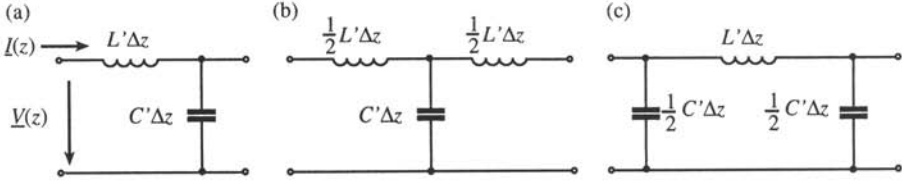


Figure 7.8: Equivalent circuits for a lossless TEM line of length Δz : (a) elementary equivalent circuit, (b) T -equivalent circuit, and (c) Π -equivalent circuit.

also called *telegrapher's equation*

$$\frac{d^2 \underline{I}}{dz^2} + \beta^2 \underline{I} = 0, \quad (7.57a)$$

$$\frac{d^2 \underline{V}}{dz^2} + \beta^2 \underline{V} = 0, \quad (7.57b)$$

with

$$\beta = \beta_{M0} = \omega \sqrt{L' C'}. \quad (7.58)$$

The *transmission-line equations* for the lossless TEM line are (7.51), (7.56), (7.57a) and (7.57b) and describe the z -dependence of \underline{V} and \underline{I} . The phase coefficient β of the TEM mode is identical with the phase coefficient β_{M0} of the plane wave propagating in the same dielectric material. For short line segments we can use equivalent circuits with lumped elements. Figure 7.8 shows three of these equivalent circuits for lossless TEM lines of length Δz . The equivalent circuits provide a good approximation, if Δz is very small in comparison with the wavelength. Let us consider the equivalent circuit according to Figure 7.8(a). As we can see easily, the relation of the four amplitudes and both pairs of nodes of the equivalent circuit is given by

$$\underline{V}(z + \Delta z) = \underline{V}(z) - j \omega L' \Delta z \underline{I}(z), \quad (7.59a)$$

$$\underline{I}(z + \Delta z) = \underline{I}(z) - j \omega C' \Delta z \underline{V}(z). \quad (7.59b)$$

Taking the limit $\Delta z \rightarrow 0$, we obtain (7.52) and (7.56). This means that we can approximate a line segment with arbitrary accuracy, if we are choosing a sufficiently small Δz . If we have to model longer line segments by this equivalent circuit with high accuracy, we can cascade several of these equivalent circuits. The T -equivalent circuit according to Figure 7.8(b) and the Π -equivalent circuit in Figure 7.8(c) are obtained by connecting two equivalent circuits according to Figure 7.8(a).

We can improve the equivalent circuit for the line segment by replacing (7.59a) and

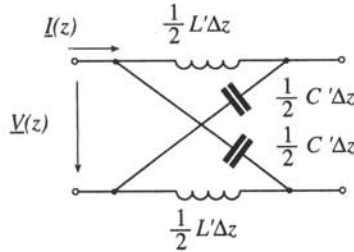


Figure 7.9: Equivalent circuit for a lossless TEM line of length Δz .

(7.59b) by a more accurate integration scheme,

$$\underline{V}(z + \Delta z) = \underline{V}(z) - j \omega L' \Delta z \frac{1}{2} [\underline{I}(z) + \underline{I}(z + \Delta z)], \quad (7.60a)$$

$$\underline{I}(z + \Delta z) = \underline{I}(z) - j \omega C' \Delta z \frac{1}{2} [\underline{V}(z) + \underline{V}(z + \Delta z)]. \quad (7.60b)$$

From these equations we obtain the admittance representation

$$\begin{pmatrix} \underline{I}(z) \\ -\underline{I}(z + \Delta z) \end{pmatrix} = \begin{pmatrix} Y_1 & Y_2 \\ Y_2 & Y_1 \end{pmatrix} \begin{pmatrix} \underline{V}(z) \\ \underline{V}(z + \Delta z) \end{pmatrix} \quad (7.61)$$

with

$$\underline{Y}_1 = \frac{1}{4} j \omega \Delta z C' + \frac{1}{j \omega \Delta z L'}, \quad \underline{Y}_2 = \frac{1}{4} j \omega \Delta z C' - \frac{1}{j \omega \Delta z L'}. \quad (7.62)$$

The corresponding *all-pass equivalent circuit* is shown in Figure 7.9.

Up to now we have considered lossless TEM waveguides only. In the real waveguide, however, losses occur due to the finite conductivity of the metallic conductors. Due to the skin effect these losses are increasing with frequency. If the line is filled with a dielectric, we also have to consider the dielectric losses. The *skin effect losses* as well as the *dielectric loss* increase with increasing frequency. In the case of unshielded transmission-lines at higher frequencies also *radiation loss* has to be considered. Radiation loss occurs if the longitudinal homogeneity of the transmission-line is perturbed. Also longitudinally homogeneous transmission-lines may radiate in the case of improper excitation when the sum of the currents through the conductors does not vanish. In that case the transmission-line is said to be excited in an *antenna mode*. If an antenna mode is excited the radiation can be computed by the methods discussed in Chapter 13.

Let us first compute the losses in the dielectric material. If the dielectric material has an ohmic conductivity $\sigma \neq 0$, due to (2.61) a conduction current is flowing in the

dielectric material. The conductive current $\underline{I}'_L \Delta z$ flowing within the length interval Δz from conductor 2 to conductor 1 is given by

$$\underline{I}'_L \Delta z = \sigma \int_{A_2} \star \underline{\mathcal{E}}. \quad (7.63)$$

\underline{I}'_L is the dielectric loss current per unit of length. The integration is performed over the area A_2 in Figure 7.5. Inserting (7.32) and (7.36) we obtain the conductive loss current \underline{I}'_L per unit of length,

$$\underline{I}'_L = \frac{\sigma}{\epsilon} \underline{Q}' = \frac{\sigma}{\epsilon} C' \underline{V}. \quad (7.64)$$

We define the *conductance per unit of length* G' as the ratio of the current flowing per unit of length from conductor 2 to conductor 1 and the voltage between conductor 2 and conductor 1,

$$G' = \frac{\sigma}{\epsilon} C' = \omega C' \tan \delta_e. \quad (7.65)$$

If a loss current \underline{I}'_L is flowing from conductor 2 to conductor 1 per unit of length, we have to modify (7.56) as follows:

$$\frac{d\underline{I}}{dz} = -j\omega C' \underline{V} - \underline{I}'_L. \quad (7.66)$$

With (7.64) and (7.65) we obtain

$$\frac{d\underline{I}}{dz} = -(j\omega C' + G') \underline{V}. \quad (7.67)$$

The dielectric losses are considered by the loss conductance per unit of length G' .

To compute the skin effect losses in conductors 1 and 2 we use (6.66) and integrate over the areas A' and A'' in Figure 7.10. We introduce a cylindrical coordinate system (n, v, z) with the transverse coordinates n and v and the longitudinal coordinate z . The coordinates v and z are tangential to the conductor surface and the coordinate n is normal to the conductor surface. The corresponding basis differentials are n, s_1, dz . With (6.66) we obtain the skin effect losses $\Delta z P'_L$ within a line segment of length Δz

$$P'_L \Delta z = \frac{1}{2} \int_{A'+A''} R_A |\underline{H}_t|^2 dz \wedge s_1 = \frac{1}{2} \Delta z \oint_{C'+C''} R_A |\underline{H}_t|^2 s_1, \quad (7.68)$$

where R_A is the skin effect surface resistance defined in (6.54). This yields

$$P'_L = \frac{1}{2} \oint_{C'+C''} R_A |\underline{H}_t|^2 s_1. \quad (7.69)$$

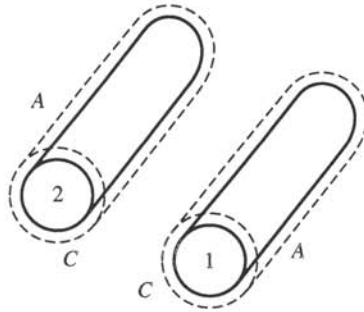


Figure 7.10: Area of integration to determine the skin effect losses.

The skin effect losses per unit of length are proportional to the square of the line current (i.e., the skin effect losses may be expressed by a *resistance per unit of length* R'). The power loss due to the skin effect surface resistance is given by

$$P'_L = \frac{1}{2} R' |I|^2. \quad (7.70)$$

Using (7.23), (7.69), and (7.70) we can express the skin effect resistance per unit of length, R' , by

$$R' = \frac{\oint_{C'+C''} R_A |\underline{H}_t|^2 s_1}{(\oint_{C''} |\underline{H}_t| s_1)^2}. \quad (7.71)$$

Due to the resistance per unit of length, R' , the voltage decreases per unit of length by $R' \underline{I}$. Therefore we have to modify (7.52) as follows:

$$\frac{dV}{dz} = -(j\omega L' + R') \underline{I}. \quad (7.72)$$

For a line segment of length Δz of a lossy TEM waveguide, we obtain the equivalent circuit Figure 7.11. We note that due to the conductor losses also a very small longitudinal electric field component occurs. Nevertheless, we still call this waveguide mode transverse electromagnetic. We can again eliminate $\underline{V}(z)$ or $\underline{I}(z)$, respectively, from (7.67) and (7.72) and obtain the *telegrapher's equation for the lossy transmission-line*.

$$\frac{d^2}{dz^2} \underline{V} - \gamma^2 \underline{V} = 0, \quad (7.73a)$$

$$\frac{d^2}{dz^2} \underline{I} - \gamma^2 \underline{I} = 0. \quad (7.73b)$$

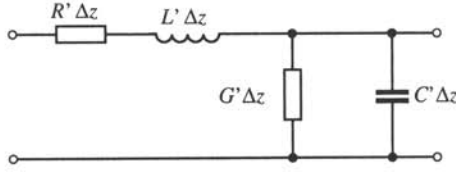
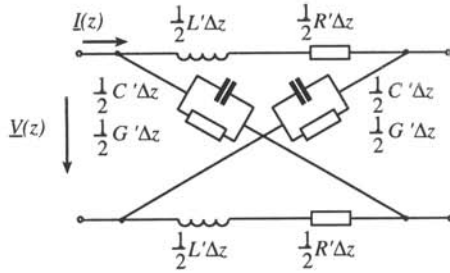
Figure 7.11: Equivalent circuit for a lossy TEM line of length Δz .Figure 7.12: Modified equivalent circuit for a lossy TEM line of length Δz .

Figure 7.12 shows the modification of the equivalent circuit depicted in Figure 7.9 for the lossy transmission-line. The admittances \underline{Y}_1 and \underline{Y}_2 in (7.61) are given by

$$\underline{Y}_1 = \frac{1}{4}\Delta z \underline{Y}' + \frac{1}{\Delta z \underline{Z}'}, \quad \underline{Y}_2 = \frac{1}{4}\Delta z \underline{Y}' - \frac{1}{\Delta z \underline{Z}'} \quad (7.74)$$

with

$$\underline{Z}' = j\omega L' + R', \quad \underline{Y}' = j\omega C' + G'. \quad (7.75)$$

The complex propagation coefficient γ is given by

$$\gamma = \sqrt{(j\omega C' + G')(j\omega L' + R')}. \quad (7.76)$$

The solution of (7.73a) and (7.73b) is given by

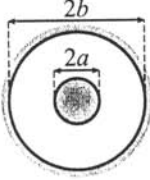
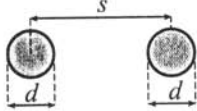
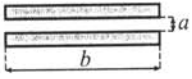
$$\underline{V}(z) = \underline{V}_0^{(+)} e^{-\gamma z} + \underline{V}_0^{(-)} e^{+\gamma z}, \quad (7.77a)$$

$$\underline{I}(z) = \underline{I}_0^{(+)} e^{-\gamma z} + \underline{I}_0^{(-)} e^{+\gamma z}. \quad (7.77b)$$

If the electromagnetic wave propagates only in one direction, the ratio of current and voltage due to (7.67) and (7.72) is given by

$$\underline{V}(z) = \pm Z_0 \underline{I}(z), \quad (7.78)$$

Table 7.2: Data of Some Important TEM Waveguide Structures.

	Coaxial Line	Parallel Wire Line	Parallel Plate Line $a \ll b$
			
Capacitance per unit of length C'	$\frac{2\pi\epsilon}{\ln \frac{b}{a}}$	$\frac{\pi\epsilon}{\operatorname{arcosh} \frac{s}{d}}$	$\frac{\epsilon b}{a}$
Inductance per unit of length L'	$\frac{\mu}{2\pi} \ln \frac{b}{a}$	$\frac{\mu}{\pi} \operatorname{arcosh} \frac{s}{d}$	$\frac{\mu a}{b}$
Conductance per unit of length G'	$\frac{2\pi\sigma}{\ln \frac{b}{a}}$	$\frac{\pi\sigma}{\operatorname{arcosh} \frac{s}{d}}$	$\frac{\sigma b}{a}$
Resistance per unit of length R'	$\frac{R_A}{2\pi} \left(\frac{1}{a} + \frac{1}{b} \right)$	$\frac{2R_A}{\pi d} \frac{s}{\sqrt{s^2 - d^2}}$	$\frac{2R_A}{d}$
Characteristic impedance Z_0 (lossless case)	$\frac{Z_F}{2\pi} \ln \frac{b}{a}$	$\frac{Z_F}{\pi} \operatorname{arcosh} \frac{s}{d}$	$Z_F \frac{a}{b}$

where the complex characteristic impedance Z_0 is given by

$$Z_0 = \sqrt{\frac{j\omega L' + R'}{j\omega C' + G'}}. \quad (7.79)$$

The positive sign in (7.78) is valid if the electromagnetic wave is propagating in the positive z -direction, whereas the negative sign corresponds to a wave propagating in the negative z -direction. For small losses, i.e., $G' \ll \omega C'$ and $R' \ll \omega L'$, we obtain the following approximation for the propagation coefficient and the characteristic impedance,

$$\gamma \cong \omega \sqrt{L'C'} \left[j + \frac{1}{2\omega} \left(\frac{G'}{C'} + \frac{R'}{L'} \right) \right], \quad (7.80a)$$

$$Z_0 \cong \sqrt{\frac{L'}{C'}} \left[1 - \frac{j}{2\omega} \left(\frac{R'}{L'} - \frac{G'}{C'} \right) \right]. \quad (7.80b)$$

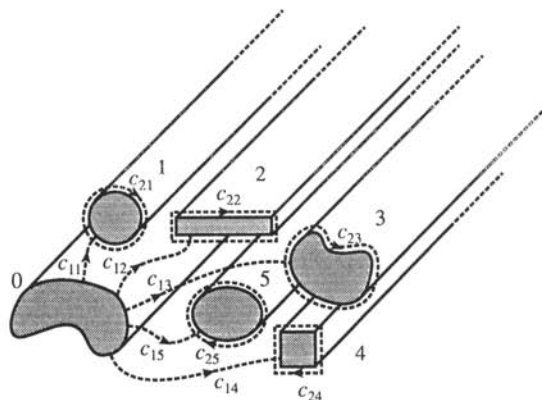


Figure 7.13: Multiconductor transmission-line.

Table 7.2 summarizes the data of some important TEM waveguide structures.

7.5 MULTICONDUCTOR TRANSMISSION-LINES

A *multiconductor transmission-line* is a transmission-line with more than two parallel cylindric conductors as shown in Figure 7.13. In a multiconductor transmission-line all conductors are mutually coupled and signals are coupled from one conductor to the other. If the coupling is unintended this effect is referred to as *crosstalk*. Multiconductor transmission-lines play a role in flat cables for high-speed data transfer, in printed circuit boards, and in monolithic integrated circuits. Multiconductor transmission-lines are treated in detail in [6–10].

In this section the TEM modes of multiconductor transmission-lines filled with homogeneous isotropic dielectric are treated. It will be shown that in the homogeneous multiconductor transmission-line with $n + 1$ conductors n TEM modes can propagate. All these modes propagate with the same velocity, that is, the TEM plane wave velocity c for the dielectric material given in (2.75).

Figure 7.13 gives a schematic view of the general cylindric multiconductor transmission-line. The current flowing in the k th conductor in positive z -direction is $i_k(z, t)$ and the voltage from conductor k to conductor l is $v_{kl}(z, t)$. Usually a transmission-line is operated in such a way that the sum of the currents through all conductors vanishes. Therefore, for a multiconductor transmission-line with $n + 1$ conductors only n currents can be chosen independently. Also from the $\frac{1}{2}(n + 1)n$ voltages $v_{kl}(z, t)$ only n voltages may be chosen independently. Consequently we can choose one conductor as the reference conductor and describe the state of the multiconductor transmission-line by

the currents in the other conductors and the voltages between every conductor and the reference conductor. We number the conductors of a multiconductor transmission-line with $n + 1$ conductors from 0 to n with conductor 0 as the reference conductor. The voltages v_1, v_2, \dots, v_n between conductors 1, 2, \dots , n and the reference conductor 0 and the currents i_1, i_2, \dots, i_n through the conductors 1 to n are summarized in the vectors

$$\mathbf{v}^T(z, t) = [v_1(z, t), v_2(z, t), \dots, v_n(z, t)] , \quad (7.81a)$$

$$\mathbf{i}^T(z, t) = [i_1(z, t), i_2(z, t), \dots, i_n(z, t)] . \quad (7.81b)$$

Let $\mathcal{E}_k(\mathbf{x}, t)$ be the electric field form describing the electric field for the k th conductor at potential $v_k(z)$ and all other conductors at potential zero. Furthermore, let $\mathcal{H}_k(\mathbf{x}, t)$ be the magnetic field created by the current through conductor k when through all other conductors (with the exception of conductor 0) no current is flowing. This partial field is given by

$$\mathcal{E}_k(\mathbf{x}, t) = v_k(z, t) \mathbf{e}_k(x, y) , \quad (7.82a)$$

$$\mathcal{H}_k(\mathbf{x}, t) = i_k(z, t) \mathbf{h}_k(x, y) , \quad (7.82b)$$

where $\mathbf{e}_k(x, y)$ and $\mathbf{h}_k(x, y)$ are electric and magnetic structure forms as defined in (7.29a) and (7.29b). Since we are seeking TEM wave solutions the structure forms are transverse (i.e., they exhibit no dz -components). Consider that the cases where only one of the conductors 1 \dots n exhibits a voltage unequal to zero and where only one of these conductors is carrying a current are different in the following sense. In the first case all conductors apart from the k th one are grounded, whereas in the second case all conductors except from the k th one are open at their ends. Generalizing (7.31a) and (7.31b) for the multiconductor case we obtain

$$\oint_{c_{2l}} \mathbf{h}_k(x, y) = \delta_{kl} , \quad (7.83a)$$

$$\int_{c_{1l}} \mathbf{e}_k(x, y) = -\delta_{kl} . \quad (7.83b)$$

The total electric and magnetic field of the multiconductor transmission-line is represented by the differential forms

$$\mathcal{E}(\mathbf{x}, t) = \sum_{k=1}^n \mathcal{E}_k(\mathbf{x}, t) , \quad (7.84a)$$

$$\mathcal{H}(\mathbf{x}, t) = \sum_{k=1}^n \mathcal{H}_k(\mathbf{x}, t) . \quad (7.84b)$$

For a TEM field the structure functions must satisfy the two-dimensional Laplace equation (7.21) and correspond to the two-dimensional electrostatic and magnetostatic

fields. According to Section 5.4 the structure functions may be derived from normalized scalar electric and magnetic potentials $\phi_{ek}(x, y)$ and $\phi_{mk}(x, y)$, respectively, hence

$$e_k(x, y) = d\phi_{ek}(x, y), \quad (7.85a)$$

$$h_k(x, y) = d\phi_{mk}(x, y). \quad (7.85b)$$

From Poincaré's lemma (A.61) follows

$$de_k(x, y) = 0, \quad (7.86a)$$

$$dh_k(x, y) = 0. \quad (7.86b)$$

With this we obtain from (7.82a) and (7.82b) the exterior derivatives of the partial electric and magnetic field forms,

$$d\mathcal{E}_k(x, t) = \frac{\partial v_k(z, t)}{\partial z} dz \wedge e_k(x, y), \quad (7.87a)$$

$$d\mathcal{H}_k(x, t) = \frac{\partial i_k(z, t)}{\partial z} dz \wedge h_k(x, y). \quad (7.87b)$$

Inserting (7.82a), (7.82b), (7.84a), (7.84b), (7.87b), and the constitutive relation (2.32a) into Ampère's law (2.114a) yields

$$\sum_{k=1}^n \frac{\partial i_k(z, t)}{\partial z} dz \wedge h_k(x, y) = \epsilon \sum_{k=1}^n \frac{\partial v_k(z, t)}{\partial t} * e_k(x, y). \quad (7.88)$$

Contracting this with dz and inserting (2.165b), we obtain

$$\sum_{k=1}^n \frac{\partial i_k(z, t)}{\partial z} h_k(x, y) = \epsilon \sum_{k=1}^n \frac{\partial v_k(z, t)}{\partial t} dz \lrcorner * e_k(x, y). \quad (7.89)$$

Integration over the closed curve c_{2l} yields

$$\sum_{k=1}^n \frac{\partial i_k(z, t)}{\partial z} \oint_{c_{2l}} h_k(x, y) = \epsilon \sum_{k=1}^n \frac{\partial v_k(z, t)}{\partial t} \oint_{c_{2l}} dz \lrcorner * e_k(x, y). \quad (7.90)$$

Inserting (7.83a) for the integral in the left-hand side of this equation and defining

$$C'_{lk} = -\epsilon \oint_{c_{2l}} dz \lrcorner * e_k(x, y) = \epsilon \int [e_{kx}(x, y) dy - e_{ky}(x, y) dx] \quad (7.91)$$

yield the first set of multiconductor transmission-line equations

$$\frac{\partial i_l(z, t)}{\partial z} = - \sum_{k=1}^n C'_{lk} \frac{\partial v_k(z, t)}{\partial t}. \quad (7.92)$$

The coefficients C'_{lk} are the *mutual capacitances per unit of length*.

To obtain the second transmission-line equation we insert (7.82a) (7.82b), (7.84a), (7.84b), (7.87a), and the constitutive relation (2.32b) into Faraday's law (2.114b). This yields

$$\sum_{k=1}^n \frac{\partial v_k(z, t)}{\partial z} dz \wedge e_k(x, y) = -\mu \sum_{k=1}^n \frac{\partial i_k(z, t)}{\partial t} * h_k(x, y). \quad (7.93)$$

Contracting this with dz yields

$$\sum_{k=1}^n \frac{\partial v_k(z, t)}{\partial z} e_k(x, y) = -\mu \sum_{k=1}^n \frac{\partial i_k(z, t)}{\partial t} dz \lrcorner * h_k(x, y). \quad (7.94)$$

We integrate this over the curve c_{ll} and obtain

$$\sum_{k=1}^n \frac{\partial v_k(z, t)}{\partial z} \int_{c_{ll}} e_k(x, y) = -\mu \sum_{k=1}^n \frac{\partial i_k(z, t)}{\partial t} \int_{c_{ll}} dz \lrcorner * h_k(x, y). \quad (7.95)$$

We insert (7.83b) in the left-hand side of this equation and define the inductances per unit of length

$$L'_{lk} = -\mu \int_{c_{ll}} dz \lrcorner * h_k(x, y). \quad (7.96)$$

This yields the second set of the multiconductor transmission-line equations

$$\frac{\partial v_l(z, t)}{\partial z} = - \sum_{k=1}^n L'_{lk} \frac{\partial i_k(z, t)}{\partial t}. \quad (7.97)$$

Summarizing the voltages and currents in the vectors (7.81a) and (7.81b) and the elements C'_{lk} and L'_{lk} in the matrices C' and L' we can write both sets of first-order *multiconductor transmission-line equations* in matrix form as

$$\frac{\partial i(z, t)}{\partial z} = -C' \frac{\partial v(z, t)}{\partial t}, \quad (7.98a)$$

$$\frac{\partial v(z, t)}{\partial z} = -L' \frac{\partial i(z, t)}{\partial t}. \quad (7.98b)$$

From this we obtain the second-order multiconductor transmission-line equations

$$\frac{\partial^2 v(z, t)}{\partial z^2} = L' C' \frac{\partial^2 v(z, t)}{\partial t^2}, \quad (7.99a)$$

$$\frac{\partial^2 i(z, t)}{\partial z^2} = C' L' \frac{\partial^2 i(z, t)}{\partial t^2}. \quad (7.99b)$$

Due to reciprocity the capacitance and inductance matrices satisfy

$$\mathbf{C}' = \mathbf{C}'^T, \quad (7.100a)$$

$$\mathbf{L}' = \mathbf{L}'^T. \quad (7.100b)$$

To derive an important relation between \mathbf{L}' and \mathbf{C}' we insert Ampère's law (2.114a) into Faraday's law (2.114b) and obtain

$$\star d \star d \mathcal{E} = -\mu\epsilon \frac{\partial^2 \mathcal{E}}{\partial t^2}. \quad (7.101)$$

With (7.82a), (7.84a), and (7.87a) this yields

$$\sum_{k=1}^n \frac{\partial^2 v_k(z, t)}{\partial z^2} \star dz \wedge \star dz \wedge e_k(x, y) = -\mu\epsilon \sum_{k=1}^n \frac{\partial^2 v_k(z, t)}{\partial t^2} e_k(x, y). \quad (7.102)$$

With (A.176) and (A.179) we obtain

$$\star dz \wedge \star dz \wedge e_k(x, y) = \perp_z^2 e_k(x, y) = -e_k(x, y), \quad (7.103)$$

and with this

$$\sum_{k=1}^n \frac{\partial^2 v_k(z, t)}{\partial z^2} e_k(x, y) = \mu\epsilon \sum_{k=1}^n \frac{\partial^2 v_k(z, t)}{\partial t^2} e_k(x, y). \quad (7.104)$$

We integrate this equation over the curve c_{1l} ,

$$\sum_{k=1}^n \frac{\partial^2 v_k(z, t)}{\partial z^2} \int_{c_{1l}} e_k(x, y) = \mu\epsilon \sum_{k=1}^n \frac{\partial^2 v_k(z, t)}{\partial t^2} \int_{c_{1l}} e_k(x, y) \quad (7.105)$$

and obtain a second-order transmission-line equation for v_l ,

$$\frac{\partial^2 v_l(z, t)}{\partial z^2} = \frac{1}{c^2} \frac{\partial^2 v_l(z, t)}{\partial t^2}. \quad (7.106)$$

In a similar way we can derive a second-order transmission-line equation for the i_l . We can write these equations in matrix form as

$$\frac{\partial^2 \mathbf{v}(z, t)}{\partial z^2} = \frac{1}{c^2} \frac{\partial^2 \mathbf{v}(z, t)}{\partial t^2}, \quad (7.107a)$$

$$\frac{\partial^2 \mathbf{i}(z, t)}{\partial z^2} = \frac{1}{c^2} \frac{\partial^2 \mathbf{i}(z, t)}{\partial t^2}. \quad (7.107b)$$

Comparing this result with (7.99a) and (7.99b) yields

$$\mathbf{L}'\mathbf{C}' = \mathbf{C}'\mathbf{L}' = \frac{1}{c^2}\mathbf{1}, \quad (7.108)$$

where $\mathbf{1}$ is the unit matrix. This means that all TEM modes of the multiconductor transmission-line exhibit the same velocity c , which is phase and group velocity as well. Such modes are called *degenerate modes*.

7.6 QUASI-TEM MODES OF TRANSMISSION-LINES

7.6.1 Quasi-TEM Modes of Two-Conductor Transmission-Lines

Inhomogeneous transmission-lines (i.e., transmission-lines with transversely inhomogeneous dielectric) are important components in microwave technology. The fundamental mode of a two-conductor inhomogeneous transmission-line exhibits no lower cutoff frequency, and it also exhibits longitudinal electric field components. Examples of inhomogeneous transmission-lines are the *microstrip line* and the *coplanar waveguide*. In these cases the cross-section exhibits metallic, dielectric, and free-space regions. The longitudinal field components are required to satisfy the boundary conditions at the interfaces between dielectric and free-space regions or between dielectric regions of different permittivity. If the longitudinal field components are very much smaller than the transverse ones, these fundamental modes are called quasi-TEM modes. For static field also an inhomogeneous two-conductor transmission exhibits transverse electric and transverse magnetic field solutions. From these transverse static field solutions we can compute capacitance and inductance per unit of length. However, as we have shown in Section 7.4 a TEM wave exhibits the same velocity as a plane wave in the same medium. In an inhomogeneous waveguide the guided wave propagates with an average velocity, deviating from the TEM velocities corresponding to the material in the various parts of the waveguide cross-section.

Consider a coaxial waveguide, partially filled with a dielectric with permittivity ϵ_1 and partially empty with the cross-section depicted in Figure 7.14. From (5.176a), (5.177), (5.180a), and (5.181) we obtain the static electric and magnetic fields for applied DC voltage V and DC current I ,

$$\mathcal{E} = -A_e dr = \frac{V}{r \ln \frac{b}{a}} dr, \quad \mathcal{H} = A_m dv = \frac{I}{2\pi} d\phi. \quad (7.109)$$

This field is not influenced by the dielectric. However, the electric displacement \mathcal{D} is increased by a factor ϵ_{1r} in the dielectric region. Capacitance and inductance per unit

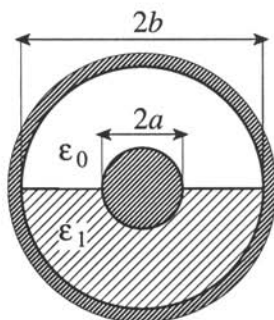


Figure 7.14: Inhomogeneously filled coaxial line.

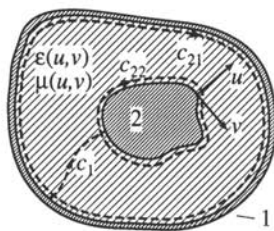


Figure 7.15: Inhomogeneous transmission-line.

of length follow from (5.179) and (5.183) as

$$C' = \frac{\pi \epsilon_0 (1 + \epsilon_{1r})}{\ln \frac{b}{a}}, \quad L' = \frac{\mu_0 \ln \frac{b}{a}}{2\pi}. \quad (7.110)$$

From this and (7.48b) we obtain the wave velocity

$$c = \frac{1}{\sqrt{L'C'}} = \sqrt{\frac{2}{1 + \epsilon_{1r}}} c_0 \quad (7.111)$$

and from (7.48a) the characteristic impedance

$$Z_0 = \sqrt{\frac{L'}{C'}} = \sqrt{\frac{2}{1 + \epsilon_{1r}}} \frac{Z_{F0}}{2\pi} \ln \frac{b}{a}. \quad (7.112)$$

Consider the inhomogeneous transmission-line with the cross-section shown in Figure 7.15. Let the permittivity ϵ and the permeability μ of the material between the

conductors depend on the transverse coordinates u and v . To verify the accuracy of the quasi-TEM approximation of inhomogeneous transmission-lines we expand the field and the phase coefficients into power series of the frequency [11,12]. At first we decompose the field forms \mathcal{E} , \mathcal{H} into transverse parts \mathcal{E}_t , \mathcal{H}_t and longitudinal parts \mathcal{E}_z , \mathcal{H}_z ,

$$\underline{\mathcal{E}} = \underline{\mathcal{E}}_t + \underline{\mathcal{E}}_z. \quad (7.113)$$

In a general cylindric coordinate system with transverse orthogonal curvilinear coordinates u , v and the longitudinal coordinate z this decomposition is done by

$$\underline{\mathcal{E}}_z = dz(dz \lrcorner \underline{\mathcal{E}}) = \underline{E}_z dz, \quad (7.114a)$$

$$\underline{\mathcal{E}}_t = \underline{\mathcal{E}} - \underline{\mathcal{E}}_z = \underline{E}_u du + \underline{E}_v dv. \quad (7.114b)$$

The electric and magnetic field of wave propagating in positive z -direction with a phase coefficient β is described by

$$\underline{\mathcal{E}}(u, v, z) = \tilde{\underline{\mathcal{E}}}(u, v) e^{-j\beta z}, \quad (7.115a)$$

$$\underline{\mathcal{H}}(u, v, z) = \tilde{\underline{\mathcal{H}}}(u, v) e^{-j\beta z}. \quad (7.115b)$$

Exterior derivation of $\underline{\mathcal{E}}$ and $\underline{\mathcal{H}}$ yields

$$d\underline{\mathcal{E}} = d\underline{\mathcal{E}}_z e^{-j\beta z} + d\underline{\mathcal{E}}_t e^{-j\beta z} - j\beta dz \wedge \tilde{\underline{\mathcal{E}}}_t e^{-j\beta z}, \quad (7.116a)$$

$$d\underline{\mathcal{H}} = d\underline{\mathcal{H}}_z e^{-j\beta z} + d\underline{\mathcal{H}}_t e^{-j\beta z} - j\beta dz \wedge \tilde{\underline{\mathcal{H}}}_t e^{-j\beta z}. \quad (7.116b)$$

Inserting (7.113) to (7.116b) in the complex Maxwell's equations (2.124a) and (2.124b) and separating transverse and longitudinal parts yields

$$d\tilde{\underline{\mathcal{E}}}_t = -j\omega\mu(u, v) * \tilde{\underline{\mathcal{H}}}_z, \quad (7.117a)$$

$$d\tilde{\underline{\mathcal{E}}}_z = -j\omega\mu(u, v) * \tilde{\underline{\mathcal{H}}}_t + j\beta dz \wedge \tilde{\underline{\mathcal{E}}}_t, \quad (7.117b)$$

$$d\tilde{\underline{\mathcal{H}}}_t = j\omega\epsilon(u, v) * \tilde{\underline{\mathcal{E}}}_z, \quad (7.117c)$$

$$d\tilde{\underline{\mathcal{H}}}_z = j\omega\epsilon(u, v) * \tilde{\underline{\mathcal{E}}}_t + j\beta dz \wedge \tilde{\underline{\mathcal{H}}}_t. \quad (7.117d)$$

Choosing a coordinate system where at the metallic surfaces du is normal to the surface and dv is tangential to the surface the boundary conditions are

$$du \wedge \tilde{\underline{\mathcal{E}}} = 0, \quad (7.118a)$$

$$dv \wedge \tilde{\underline{\mathcal{H}}} = 0. \quad (7.118b)$$

We seek an asymptotic series solution for equations (7.117a) to (7.118b) represented by a power series with the normalized frequency

$$\Omega = \omega/\omega_0, \quad (7.119)$$

where ω_0 is a frequency of reference which may be chosen arbitrarily. Considering that the complex field forms $\tilde{\mathcal{E}}_t(\omega)$, $\tilde{\mathcal{E}}_z(\omega)$, $\tilde{\mathcal{H}}_t(\omega)$, $\tilde{\mathcal{H}}_z(\omega)$, in (7.117a) to (7.117d) are related to the real time-dependent field forms $\underline{\mathcal{E}}_t(t)$, $\underline{\mathcal{E}}_z(t)$, $\underline{\mathcal{H}}_t(t)$, $\underline{\mathcal{H}}_z(t)$ via Fourier transform, as

$$\tilde{\mathcal{E}}_t(\omega) = \int_{-\infty}^{\infty} \underline{\mathcal{E}}_t(t) e^{-j\omega t} d\omega. \quad (7.120)$$

From this it follows

$$\tilde{\mathcal{E}}_t(-\omega) = \tilde{\mathcal{E}}_t^*(\omega). \quad (7.121)$$

Hence the real part of a field function is an even function and the imaginary part is an odd function of ω . In the static limit the transverse field forms $\tilde{\mathcal{E}}_t(\omega)$ and $\tilde{\mathcal{H}}_t(\omega)$ become real. Therefore we can assume the transverse field forms to be even functions of ω and therefore to be real. Due to (7.117a) and (7.117c) in this case the longitudinal field forms $\tilde{\mathcal{E}}_z(\omega)$ and $\tilde{\mathcal{H}}_z(\omega)$ are odd functions of ω . Also the phase coefficient β is an odd function of ω . This becomes obvious when considering its linear approximation. Therefore the power series expansion of the field forms and the phase coefficient is given by

$$\tilde{\mathcal{E}}_t = \tilde{\mathcal{E}}_{t0} + \Omega^2 d_t \tilde{\mathcal{E}}_{t2} + \dots, \quad (7.122a)$$

$$\tilde{\mathcal{E}}_z = \Omega \tilde{\mathcal{E}}_{z1} + \Omega^3 d_t \tilde{\mathcal{E}}_{z3} + \dots, \quad (7.122b)$$

$$\tilde{\mathcal{H}}_t = \tilde{\mathcal{H}}_{t0} + \Omega^2 d_t \tilde{\mathcal{H}}_{t2} + \dots, \quad (7.122c)$$

$$\tilde{\mathcal{H}}_z = \Omega \tilde{\mathcal{H}}_{z1} + \Omega^3 d_t \tilde{\mathcal{H}}_{z3} + \dots, \quad (7.122d)$$

$$\beta = \Omega b_0 + \Omega^3 b_0 + \dots. \quad (7.122e)$$

Inserting these expansions into (7.117a) to (7.117d) and separating the equations by order of Ω we obtain the zero and first-order equations

$$d \tilde{\mathcal{E}}_{t0} = 0, \quad (7.123a)$$

$$d \tilde{\mathcal{E}}_{z1} = -j\omega\mu(u, v) * \tilde{\mathcal{H}}_{t0} + j\beta dz \wedge \tilde{\mathcal{E}}_{t0}, \quad (7.123b)$$

$$d \tilde{\mathcal{H}}_{t0} = 0, \quad (7.123c)$$

$$d \tilde{\mathcal{H}}_{z1} = j\omega\epsilon(u, v) * \tilde{\mathcal{E}}_{t0} + j\beta dz \wedge \tilde{\mathcal{H}}_{t0}. \quad (7.123d)$$

The higher-order equations are given by

$$d \tilde{\mathcal{E}}_{t,2k} = -j\omega\mu(u, v) * \tilde{\mathcal{H}}_{z,2k-1}, \quad (7.124a)$$

$$d \tilde{\mathcal{E}}_{z,2k+1} = -j\omega\mu(u, v) * \tilde{\mathcal{H}}_{t,2k} + j\beta dz \wedge \tilde{\mathcal{E}}_{t,2k}, \quad (7.124b)$$

$$d \tilde{\mathcal{H}}_{t,2k} = j\omega\epsilon(u, v) * \tilde{\mathcal{E}}_{z,2k-1}, \quad (7.124c)$$

$$d \tilde{\mathcal{H}}_{z,2k+1} = j\omega\epsilon(u, v) * \tilde{\mathcal{E}}_{t,2k} + j\beta dz \wedge \tilde{\mathcal{H}}_{t,2k}. \quad (7.124d)$$

The electrostatic and magnetostatic field approximations for the multiconductor transmission-line must satisfy (7.123a) and (7.123b). However, these equations are not sufficient to determine the electrostatic field solutions. Also the divergence relations (5.1b) and (5.2b) have to be considered. To obtain the electrostatic and magnetostatic field approximations of the multiconductor transmission-line we derive the electric and magnetic fields from the scalar potential Φ and the magnetic vector potential \underline{A} . From (5.2b), (5.7), and the constitutive relation (2.23a) for the electric potential $\Phi(u, v)$ we obtain

$$d[\epsilon(u, v) d\Phi(u, v)] = 0, \quad (7.125)$$

and for the magnetic vector potential \underline{A} from (5.1b), (5.7) and the constitutive relation (5.53) for the magnetic vector potential form $\underline{A}(u, v)$ we obtain

$$d\left[\frac{1}{\mu(u, v)} d\underline{A}(u, v)\right] = 0. \quad (7.126)$$

From (7.118a) and (7.118b) we obtain the boundary conditions for Φ and \underline{A} as

$$du \wedge \epsilon(u, v) d\Phi(u, v) = 0, \quad (7.127a)$$

$$dv \wedge \frac{1}{\mu(u, v)} \underline{A}(u, v) = 0. \quad (7.127b)$$

Equations (7.125) to (7.127b) contain all the information necessary to compute the electric and magnetic fields in the static zero-order approximation. Different from the homogeneous transmission-line, electric and magnetic field functions are now independent from each other. There exists no simple relation between L' and C' and both values have to be computed independently.

Similar to (7.91) and (7.96), we can derive the capacitance per unit of length C' and the inductance per unit of length L' as

$$C' = - \oint_{c_2} \epsilon(u, v) dz_{\perp} \star e_k(u, v), \quad (7.128a)$$

$$L' = - \int_{c_1} \mu(u, v) dz_{\perp} \star h_k(u, v). \quad (7.128b)$$

The integrations are performed over the paths c_1 and c_{22} shown in Figure 7.15. Since in the static approximation no longitudinal field components exist, the integrals in both equations are independent from the paths as long as c_1 is going from conductor 1 to conductor 2, and c_{22} is encircling conductor 2.

The first-order approximation of the longitudinal fields may be computed from (7.123b) and (7.123d) whereas (7.124b) and (7.124d) yield the higher-order field approximations.

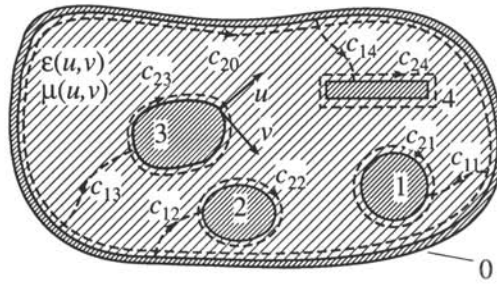


Figure 7.16: Inhomogeneous multiconductor transmission-line.

7.6.2 Quasi-TEM Modes of Multiconductor Transmission-Lines

The quasi-TEM modes have been investigated for *inhomogeneous multiconductor transmission-lines* in [12,13]. Figure 7.16 shows the cross-section of a general multiconductor transmission-line. The above treatment of the field components also holds for the multiconductor transmission-line case. We derive the capacitance per unit of length matrix elements C'_{lk} and the inductance per unit of length matrix elements L'_{lk} as

$$C'_{lk} = - \oint_{c_{2l}} \epsilon(u, v) dz_{\perp} * e_k(u, v), \quad (7.129a)$$

$$L'_{lk} = - \int_{c_{1l}} \mu(u, v) dz_{\perp} * h_k(u, v). \quad (7.129b)$$

The paths of integration are shown in Figure 7.16. Considering the longitudinal field components the degeneration of the modes is canceled and the modes exhibit different velocities. The transmission-line equations (7.98a) and (7.98b) remain valid also for the *quasi-TEM multiconductor transmission-line* but not so (7.107a) and (7.107b). We obtain

$$\frac{dI(z)}{dz} = -j\omega C' V(z), \quad (7.130a)$$

$$\frac{dV(z)}{dz} = -j\omega L' I(z). \quad (7.130b)$$

The modes of the multiconductor transmission-line must be determined by diagonalization of (7.99a) and (7.99b) via solution of the eigenvalue equation

$$\omega^2 L' C' V(z) = \beta^2 V(z), \quad (7.131a)$$

$$\omega^2 C' L' I(z) = \beta^2 I(z). \quad (7.131b)$$

Different from the TEM case for the quasi-TEM modes, the voltages and current vectors describing modal solutions are not be chosen arbitrarily but must be eigenvectors of the

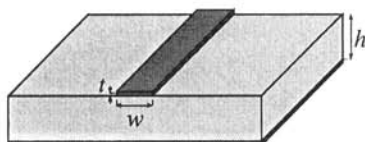


Figure 7.17: Microstrip line.

matrix $L'C'$ and $C'L'$, respectively. The solution of the multiconductor transmission-line equations will be discussed in Section 8.6.

7.7 PLANAR TRANSMISSION-LINES

Planar transmission-lines are formed by metallized plane dielectric plates [14–17]. Planar transmission-lines play an important role as the basic line structures in hybrid and monolithic integrated circuits.

7.7.1 The Microstrip Line

The *microstrip line* is depicted in Figure 7.17. In the microstrip line the electromagnetic field is not confined to the substrate, but spreads over the free-space. The microstrip line is an *inhomogeneous waveguide* since the transverse dielectric region is nonhomogeneous. Due to this circumstance the fundamental mode is not a TEM mode, but a *quasi-TEM mode*. The quasi-TEM mode approaches a TEM mode if the frequency goes to zero.

The analysis of microstrip lines only can be performed using numerical methods. Accurate methods of modeling (integral equation method, spectral domain method, partial wave synthesis, finite difference method, transmission-line matrix method) in some cases may require a high numerical effort. The easiest approximation is the *quasistatic approximation*. In the quasistatic approximation the transmission-line wave is approximated by a TEM wave and the transmission-line properties are calculated from the electrostatic capacitance. This approximation can be used if the transmission-line width as well as the thickness of the substrate are very small in comparison with the wavelength. In the following we give simple formulae for the quasistatic approximation.

Let C_a be the capacitance per unit of length of the microstrip line for the case in which the dielectric is replaced by free-space and let C be the capacitance per unit of length with dielectric. The wave impedance Z_0 and the phase coefficient β are given by

$$Z_0 = 1/c\sqrt{CC_a}, \quad (7.132a)$$

$$\beta = k_0(C/C_a)^{1/2} = k_0\sqrt{\epsilon_{r,\text{eff}}} \quad (7.132b)$$

with

$$\epsilon_{r,\text{eff}} = (\lambda_0/\lambda_c)^2 = C/C_a, \quad (7.133)$$

where λ_0 is the free-space wavelength and λ_c is the wavelength of the guided wave. Closed-form expressions for Z_0 and $\epsilon_{r,\text{eff}}$ have been given by Wheeler [18, 19], Schneider [20] and Hammerstad [21].

The maximum frequency up to which a microstrip line may be used is limited by the losses that increase with frequency. This is in particular due to the excitation of substrate waves. The cutoff frequency f_{cs} , beyond which a strong coupling between the quasi-TEM mode of the microstrip line and the surface wave of lowest-order occurs, is given by

$$f_{cs} = \frac{150}{\pi h} \sqrt{\frac{2}{\epsilon_{r,\text{eff}} - 1}} \tan^{-1} \epsilon_r \text{ GHz mm} \quad (7.134)$$

with the cutoff frequency f_{cs} in GHz and the height h in millimeters. From this it follows for a GaAs substrate with $\epsilon_r=12.9$ that for a frequency of 100 GHz the maximum thickness of the substrate should not exceed 0.3 mm.

Furthermore, the maximum substrate thickness is limited by the radiation losses excited at transmission-line discontinuities. For a $\frac{1}{2}\lambda$ resonator the Q -factor due to radiation approximately is given by

$$Q_r = \frac{3\epsilon_r Z_0 \lambda_0^2}{32 \eta_0 h^2}. \quad (7.135)$$

At 100 GHz a GaAs substrate therefore must be thinner than 0.125 mm to achieve a $Q > 100$.

In the following the approximate formulae for the computation of the parameters of a microstrip line are summarized [16]. The approximation formula for the characteristic impedance is given by

$$Z_0 = \begin{cases} \frac{\eta_0}{2\pi\sqrt{\epsilon_{r,\text{eff}}}} \ln \left(\frac{8h}{w'} + 0.25 \frac{w'}{h} \right) & \text{for } w/h \leq 1, \\ \frac{\eta_0}{\sqrt{\epsilon_{r,\text{eff}}}} \left[\frac{w'}{h} + 1.393 + 0.667 \ln \left(\frac{w'}{h} + 1.444 \right) \right]^{-1} & \text{for } w/h \geq 1, \end{cases} \quad (7.136)$$

with

$$\frac{w'}{h} = \begin{cases} \frac{w}{h} + \frac{1.25}{\pi} \frac{t}{h} \left(1 + \ln \frac{4\pi w}{t} \right) & \text{for } w/h \leq 1, \\ \frac{w}{h} + \frac{1.25}{\pi} \frac{t}{h} \left(1 + \ln \frac{2h}{t} \right) & \text{for } w/h \geq 1. \end{cases} \quad (7.137)$$

The approximation formula for the effective permittivity is given by

$$\epsilon_{r,\text{eff}} = \frac{\epsilon_r + 1}{2} + \frac{\epsilon_r - 1}{2} F(w/h) - \frac{\epsilon_r - 1}{4.6} - \frac{t/h}{\sqrt{w/h}} \quad (7.138)$$

with

$$F(w/h) = \begin{cases} (1 + 12h/w)^{-1/2} + 0.04(1 - w/h)^2 & \text{for } w/h \leq 1, \\ (1 + 12h/w)^{-1/2} & \text{for } w/h \geq 1. \end{cases} \quad (7.139)$$

The attenuation coefficient is given by

$$\alpha_c = \begin{cases} 1.38 \frac{R_s}{hZ_0} \frac{32 - (w'/h)^2}{32 + (w'/h)^2} \Lambda & \text{for } w/h \leq 1, \\ 6.1 \times 10^{-5} \frac{R_s Z_0 \epsilon_{r, \text{eff}}}{h} \left[w'/h + \frac{0.667 w'/h}{w'/h + 1.444} \right] \Lambda & \text{for } w/h \geq 1, \end{cases} \quad (7.140)$$

with

$$\Lambda = \begin{cases} 1 + \frac{h}{w'} \left(1 + \frac{1.25t}{\pi w'} + \frac{1.25}{\pi} \ln \frac{4\pi w}{t} \right) & \text{for } w/h \leq 1, \\ 1 + \frac{h}{w'} \left(1 - \frac{1.25t}{\pi h} + \frac{1.25}{\pi} \ln \frac{2h}{t} \right) & \text{for } w/h \geq 1. \end{cases} \quad (7.141)$$

The microstrip line is the most common planar transmission-line structure. The full metallization of the bottom side of the substrate facilitates the mounting. The insertion of circuit elements in series can be done without difficulty; however, parallel circuiting of circuit elements requires either wire holes or the realization of short circuits via $\frac{1}{4}\lambda$ lines. The latter solution is possible within a narrow-band only.

7.7.2 Quasistatic Approximation for the Microstrip Line

Figure 7.18 shows a cross-sectional view of the shielded microstrip line. The microstrip line exhibits a conductor strip of width w on a dielectric substrate of height h . The permittivity of the substrate is ϵ_1 . The ground plane of the substrate of a microstrip line usually is fully metallized. The thickness of the strip conductor is neglected. For computational reasons we have embedded the microstrip line in a waveguide of width a and height h . We assume a and h to be sufficiently large, so that the influence of the embedding on the characteristics of the microstrip line may be neglected.

We apply a *quasistatic approximation* [22] to analyze the shielded microstrip line where we assume that in subregions with constant ϵ the transverse electric field is governed by the two-dimensional *Laplace equation*

$$\frac{\partial^2 \Phi}{\partial x^2} + \frac{\partial^2 \Phi}{\partial y^2} = 0. \quad (7.142)$$

The boundary conditions for the electric potential $\Phi(x, y)$ are

$$\Phi(-\tfrac{1}{2}a, y) = \Phi(\tfrac{1}{2}a, y) = \Phi(x, 0) = \Phi(x, b). \quad (7.143)$$

We expand $\Phi(x, y)$ into products of the basis functions $\phi_n(x)$ and $\psi_n(y)$

$$\Phi(x, y) = \sum_n c_n \phi_n(x) \psi_n(y). \quad (7.144)$$

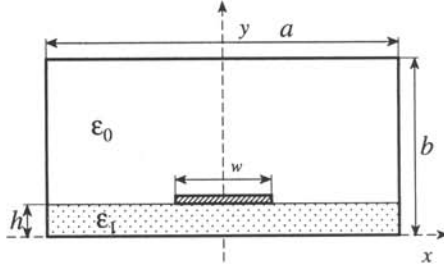


Figure 7.18: Cross-section of the shielded microstrip line.

As the basis functions $\phi_n(x)$ we choose

$$\phi_n(x) = \cos \frac{n\pi x}{a} \quad \text{with } n = 1, 3, 5, \dots \quad (7.145)$$

Presupposing that each term in the sum at the right-hand side of (7.144) fulfills the Laplace equation (7.142), it follows that

$$\psi_n(y) = \sinh \frac{n\pi y}{a} \quad \text{for } 0 \leq y \leq h \quad (7.146)$$

and we obtain for the region $0 \leq y \leq h$ the series expansion

$$\Phi_1(x, y) = \sum_{n=1,3,5,\dots} c_n \cos \frac{n\pi x}{a} \sinh \frac{n\pi y}{a} \quad \text{for } 0 \leq y \leq h. \quad (7.147)$$

In a similar way we obtain for $h \leq y \leq b$ the series expansion

$$\Phi_0(x, y) = \sum_{n=1,3,5,\dots} d_n \cos \frac{n\pi x}{a} \sinh \frac{n\pi(y-b)}{a} \quad \text{for } h \leq y \leq b. \quad (7.148)$$

On the boundary surface $y = h$ the area charge density ρ_A is given by

$$\rho_A = \sum_{n=1,3,5,\dots} r_n \cos \frac{n\pi x}{a}. \quad (7.149)$$

A surface charge density $\rho_A \neq 0$ only exists on the conductor, that means in the region $|x| \leq \frac{1}{2}w$. This condition is enforced by extending the Fourier integral for determination of the coefficients r_n only over the interval $[-\frac{1}{2}w, \frac{1}{2}w]$:

$$r_n = \frac{2}{a} \int_{-w/2}^{w/2} \rho_A(x) \cos \frac{n\pi x}{a} dx. \quad (7.150)$$

On the boundary surface $x = h$ the continuity condition

$$\Phi_1(x, h) = \Phi_0(x, h) \quad (7.151)$$

must be fulfilled. From this it follows that

$$d_n \sinh \frac{n\pi(h-b)}{a} = c_n \sinh \frac{n\pi h}{a}. \quad (7.152)$$

From the boundary condition for the electric flux density it follows that

$$-\epsilon_0 \frac{\partial}{\partial y} \Phi_0(x, y) + \epsilon_1 \frac{\partial}{\partial y} \Phi_1(x, y) = \rho_A \Big|_{y=h} \quad (7.153)$$

and from this

$$\frac{n\pi}{a} \left(-\epsilon_0 d_n \cosh \frac{n\pi(h-b)}{a} + \epsilon_1 c_n \cosh \frac{n\pi h}{a} \right) = r_n. \quad (7.154)$$

From (7.148), (7.150), (7.152), and (7.154) we finally obtain

$$\Phi(x, h) = \sum_{n=1,3,5,\dots} g_n \cos \frac{n\pi x}{a} \int_{-w/2}^{w/2} \rho_A(x') \cos \frac{n\pi x'}{a} dx' \quad (7.155)$$

with

$$g_n = \frac{2}{n\pi} \frac{1}{\epsilon_1 \coth \frac{n\pi h}{a} - \epsilon_0 \coth \frac{n\pi(h-b)}{a}}. \quad (7.156)$$

In (7.155) the integration is only performed over the interval $[-\frac{1}{2}w, \frac{1}{2}w]$ since the integrand vanishes outside this interval. We put this equation into the form

$$V_0 = \Phi(x, h) = \int_{-w/2}^{w/2} G(x, x') \rho_A(x') dx' \quad \text{for } |x| \leq \frac{1}{2}w, \quad (7.157)$$

where V_0 is the potential of the conductor strip and the *Green's function* for this problem $G(x, x')$ is given by

$$G(x, x') = \sum_{n=1,3,5,\dots} g_n \cos \frac{n\pi x}{a} \cos \frac{n\pi x'}{a}. \quad (7.158)$$

For $b \rightarrow \infty$ we obtain from (7.156)

$$g_n = \frac{2}{n\pi} \frac{1}{\epsilon_1 \coth \frac{n\pi h}{a} + \epsilon_0}. \quad (7.159)$$

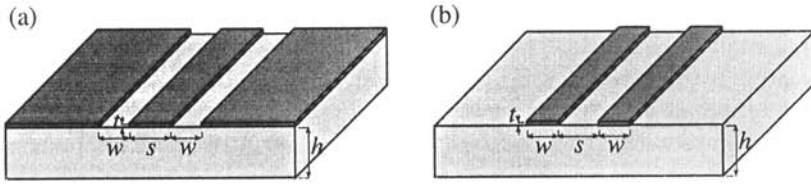


Figure 7.19: (a) Coplanar waveguide, and (b) coplanar stripline.

The charge per unit of length q' is

$$q' = \int_{-w/2}^{w/2} \rho_A(x) dx. \quad (7.160)$$

The capacitance per unit of lengths C' of the microstrip line is

$$C' = \frac{q'}{V_0}. \quad (7.161)$$

7.7.3 Coplanar Waveguide and Coplanar Stripline

Figure 7.19 shows the *coplanar waveguide* and the *coplanar stripline*. On coplanar waveguides and coplanar striplines, quasi-TEM modes may propagate. The approximation formula for the characteristic impedance of a coplanar waveguide is

$$Z_0 = \frac{Z_{F0}}{4\sqrt{\epsilon_{r,\text{eff}}}} \frac{K(k')}{K(k)} \quad (7.162)$$

and the approximation formula for the effective relative permittivity of a coplanar waveguide is

$$\epsilon_{r,\text{eff}} = 1 + \frac{\epsilon_r - 1}{2} \frac{K(k')K(k_1)}{K(k)K(k'_1)} \quad (7.163)$$

with $k = a/b$, $a = \frac{1}{2}s$, $b = \frac{1}{2}s + w$, and $k_1 = \sinh(\pi a/2h)/\sinh(\pi b/2h)$. The functions $K(k)$ and $K'(k) = K(k')$ are the complete elliptic integrals defined in (5.224a), (5.224b), and (5.225). The function $K(k)$ is called the *complete elliptic integral of the first kind*, and $K'(k)$ is called the *complete elliptic integral of the second kind* [23–25]. The ratio $K(k)/K'(k)$ is given by the following approximation formula

$$\frac{K(k)}{K'(k)} = \begin{cases} \left[\frac{1}{\pi} \ln \left(2 \frac{1+\sqrt{k}}{1-\sqrt{k}} \right) \right]^{-1} & \text{for } 0 \leq k \leq 0.7 \\ \frac{1}{\pi} \ln \left(2 \frac{1+\sqrt{k}}{1-\sqrt{k}} \right) & \text{for } 0.7 \leq k \leq 1 \end{cases} \quad (7.164)$$

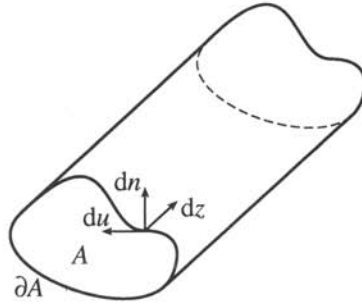


Figure 7.20: Hollow waveguide.

The approximation formula for the characteristic impedance of a coplanar stripline is

$$Z_0 = \frac{Z_{F0}}{\sqrt{\epsilon_{r,\text{eff}}}} \frac{K(k)}{K(k')} . \quad (7.165)$$

The approximation formula for the effective permittivity of a coplanar stripline is also given by (7.163).

7.8 HOLLOW WAVEGUIDES

In 1897 Lord Rayleigh in his paper “On the passage of electric waves through tubes, or the vibrations of dielectric cylinders” suggested that electromagnetic waves could propagate through metallic tubes or dielectric cylinders [26]. A *hollow waveguide* exhibits a single connected metallic boundary. Figure 7.20 shows the schematic drawing of a cylindric hollow waveguide. Since electrostatic fields cannot occur inside closed hollow tubes TEM modes will not exist. However, electromagnetic wave solutions with either a longitudinal electric field or a longitudinal magnetic field exist. Hollow waveguides play an important role in microwave technology, especially for low attenuation and high power applications and as basic elements of microwave circuits. In the following we discuss the general properties of TE-, and TM modes. For a first reading the reader may directly proceed to Section 7.9.

7.8.1 TE Modes

Consider a closed uniform general cylindric *hollow waveguide* with cross-section A and bounded by perfectly conducting walls at ∂A as depicted in Figure 7.20. Let the waveguide be filled with a lossless dielectric. To represent the electromagnetic field in the waveguide we choose a general cylindric coordinate system with the coordinates

u, v, z where z is a linear coordinate and u, v are orthogonal curvilinear coordinates transverse to z . Furthermore, we choose the transverse coordinates such that the wall of the waveguide is a boundary surface (i.e., a surface defined by setting one of the transverse coordinates constant). In Figure 7.20 the boundary is defined by setting v constant. In this case du is tangential and dv is normal to the waveguide wall. If the waveguide wall exhibits wedges (e.g., in the case of the rectangular waveguide) the coordinates u and v may change their role of being tangential or normal. We denote the coordinate normal to the waveguide boundary with n . In Figure 7.20 we have $v = n$ since we usually denote the coordinate normal to the boundary surface with n .

Following (7.8b) we can derive all components of a TE field propagating or decaying in positive or negative z -direction from a magnetic Hertz form $\underline{\Pi}_m(\mathbf{x})$ exhibiting a z -component $\underline{\Pi}_{mz}(\mathbf{x})$ only. We set

$$\underline{\Pi}_m(\mathbf{x}) = \underline{\Pi}_{mz}(\mathbf{x}) dz = \Psi^{\text{TE}}(u, v) e^{\mp \gamma z} dz, \quad (7.166)$$

where $\Psi^{\text{TE}}(u, v)$ is a scalar potential defining the transverse field distribution and γ is the *propagation coefficient of the TE mode*.

The negative sign in the exponent of the above equation corresponds to a wave propagating or decaying in positive z -direction whereas the positive sign occurs when the wave is propagating in negative z -direction. The following formulae are given for waves propagating or fields decaying in either positive and or negative z -direction. The upper sign of \pm and \mp always corresponds to propagation or decay in positive z -direction case whereas the lower sign corresponds to propagation or decay in negative z -direction. The real part α and the imaginary part β of γ are the attenuation and phase coefficients,

$$\gamma = \alpha + j\beta. \quad (7.167)$$

From (7.9b) and (7.10), we obtain the Helmholtz equation for the z -component of the magnetic Hertz vector describing the TE waveguide modes,

$$\Delta \underline{\Pi}_z^{\text{TE}} + \beta_{M0}^2 \underline{\Pi}_z^{\text{TE}} = 0. \quad (7.168)$$

According to (7.10), the plane wave phase coefficient β_{M0} of the plane wave in lossless media is

$$\beta_{M0} = \omega \sqrt{\mu \epsilon}. \quad (7.169)$$

This yields the *two-dimensional scalar Helmholtz equation* for $\Psi^{\text{TE}}(u, v)$

$$\Delta_t \Psi^{\text{TE}}(u, v) + \beta_{c, \text{TE}}^2 \Psi^{\text{TE}}(u, v) = 0 \quad (7.170)$$

with the *two-dimensional Laplace operator* Δ_t defined in (A.138). For a bounded waveguide cross-section of finite extension, this two-dimensional elliptic partial differential

equation usually exhibits an infinite number of solutions belonging to a discrete eigenvalue spectrum of $\beta_{c,TE}$. In the lossless case the propagation coefficient γ either is purely real or purely imaginary. The waveguide propagation coefficient γ is related to the plane wave phase coefficient β_{M0}

$$\gamma = \alpha = \sqrt{\beta_{c,TE}^2 - \beta_{M0}^2} \quad \text{for } \beta_{M0} < \beta_{c,TE}, \quad (7.171a)$$

$$\gamma = j\beta = j\sqrt{\beta_{M0}^2 - \beta_{c,TE}^2} \quad \text{for } \beta_{M0} > \beta_{c,TE}, \quad (7.171b)$$

where $\beta_{c,TE}$ is the *cutoff phase coefficient*. For $\beta_{M0} < \beta_{c,TE}$, the TE mode is evanescent whereas for $\beta_{M0} > \beta_{c,TE}$ the TE mode is a propagating wave. Inserting (7.166) into (7.8b), (7.11b), (7.12b), and using (7.170), we obtain

$$\underline{\mathcal{E}}^{TE} = \underline{\mathcal{E}}_t^{TE} = -j\omega\mu \star d \underline{\Pi}_m^{TE} = j\omega\mu \star (dz \wedge d_t \Psi^{TE}(u, v)) e^{\mp \gamma z}, \quad (7.172a)$$

$$\underline{\mathcal{H}}^{TE} = \star d \star d \underline{\Pi}_m^{TE} = \underline{\mathcal{H}}_t^{TE} + \underline{\mathcal{H}}_l^{TE}, \quad (7.172b)$$

$$\underline{\mathcal{H}}_t^{TE} = \mp \gamma d_t \Psi^{TE}(u, v) e^{\mp \gamma z}, \quad (7.172c)$$

$$\underline{\mathcal{H}}_l^{TE} = -\Delta_t \Psi^{TE}(u, v) dz e^{\mp \gamma z} = \beta_{c,TE}^2 \Psi^{TE}(u, v) dz e^{\mp \gamma z}, \quad (7.172d)$$

where $\underline{\mathcal{E}}_t^{TE}$ and $\underline{\mathcal{H}}_t^{TE}$ are the transverse electric and magnetic fields and $\underline{\mathcal{H}}_l^{TE}$ is the longitudinal magnetic field. In Cartesian coordinate notation the TE field components are

$$\underline{\mathcal{E}}_t^{TE}(x) = -j\omega\mu \left(\frac{\partial \Psi^{TE}(x, y)}{\partial y} dx - \frac{\partial \Psi^{TE}(x, y)}{\partial x} dy \right) e^{\mp \gamma z}, \quad (7.173a)$$

$$\underline{\mathcal{H}}_t^{TE}(x) = \mp \gamma \left(\frac{\partial \Psi^{TE}(x, y)}{\partial x} dx + \frac{\partial \Psi^{TE}(x, y)}{\partial y} dy \right) e^{\mp \gamma z}, \quad (7.173b)$$

$$\underline{\mathcal{H}}_l^{TE}(x) = \beta_{c,TE}^2 \Psi^{TE}(x, y) dz e^{\mp \gamma z}. \quad (7.173c)$$

From (7.172a), (7.172c) and (2.155) we obtain

$$\underline{\mathcal{E}}_t^{TE} = \mp Z_{TE} \star (dz \wedge \underline{\mathcal{H}}_t) = \mp Z_{TE} \perp_z \underline{\mathcal{H}}_t, \quad (7.174a)$$

$$\underline{\mathcal{H}}_t^{TE} = \pm \frac{1}{Z_{TE}} \star (dz \wedge \underline{\mathcal{E}}_t) = \pm \frac{1}{Z_{TE}} \perp_z \underline{\mathcal{E}}_t \quad (7.174b)$$

with the *wave impedance of the TE mode*

$$Z_{TE} = \frac{j\omega\mu}{\gamma}. \quad (7.175)$$

This means that the transverse electric and magnetic fields are orthogonal and their ratio is independent from the transverse coordinates and given by the wave impedance

of the TE mode. The wave impedance is imaginary below the cutoff frequency and real above the cutoff frequency. With (7.171a) and (7.171b) we obtain

$$Z_{TE} = \frac{j\omega\mu}{\alpha} = \frac{j\omega\mu}{\sqrt{\beta_{c,TE}^2 - \beta_{M0}^2}} = jZ_F \frac{\omega}{\sqrt{\omega_c^2 - \omega^2}} \quad \text{for } \omega < \omega_c, \quad (7.176a)$$

$$Z_{TE} = \frac{\omega\mu}{\beta} = \frac{\omega\mu}{\sqrt{\beta_{M0}^2 - \beta_{c,TE}^2}} = Z_F \frac{\omega}{\sqrt{\omega^2 - \omega_c^2}} \quad \text{for } \omega > \omega_c \quad (7.176b)$$

with the wave impedance of the homogeneous isotropic medium filling the waveguide given by

$$Z_F = \sqrt{\frac{\mu}{\epsilon}} \quad (7.177)$$

and the angular cutoff frequency $\omega_{c,TE}$,

$$\omega_{c,TE} = \frac{\beta_{c,TE}}{\sqrt{\epsilon\mu}}. \quad (7.178)$$

On ∂A the tangential component of the electric field must vanish. In accordance with (2.173c) this yields

$$n \wedge \underline{\mathcal{E}} = 0. \quad (7.179)$$

With (7.172a) we obtain for the potential Ψ^{TE} the boundary condition

$$n \wedge (\star d \underline{\Pi}_m^{TE}) = n \wedge [\star d (\Psi^{TE}(u, v) e^{-j\beta z} dz)] = 0, \quad (7.180)$$

where $n = g_n dn$ is the unit differential form normal to the boundary ∂A . From this we obtain

$$dn \wedge \left(\frac{\partial \Psi^{TE}(u, v)}{\partial v} du - \frac{\partial \Psi^{TE}(u, v)}{\partial u} dv \right) = 0. \quad (7.181)$$

Introducing a local coordinate system where either du or dv is identical with dn yields

$$\frac{\partial \Psi^{TE}}{\partial n} = 0. \quad (7.182)$$

This condition is called the *Neumann boundary condition*. It can be applied if a coordinate system can be chosen, where the boundary of the waveguide cross-section is defined by setting u constant and v is the normal coordinate and vice versa. In cases where the waveguide cross-section boundary exhibits 90° edges for parts of the boundary u and for other parts v may be the normal coordinate.

The partial differential equation (7.168) together with the boundary condition (7.182) define an eigenvalue problem. Since the field is bounded in transverse directions the two-dimensional Helmholtz equation (7.170) exhibits a *discrete eigenvalue spectrum* of $\beta_{c,TE}^2$.

The *eigenfunctions* $\Psi^{\text{TE}}(u, v)$ belonging to the *eigenvalues* $\beta_{c, \text{TE}}$ define the waveguide modes. The set of eigenfunctions and eigenvalues usually are numbered with two indices m and n as Ψ_{mn} and $\beta_{c, \text{TE}mn}$. Eigenvalues are usually distinct. Eigenvalues that coincide are said to be *degenerate*.

7.8.2 TM Modes

To investigate the TM modes in a closed uniform cylindric hollow waveguide with cross-section A and bounded by perfectly conducting walls at ∂A shown in Figure 7.20, we essentially proceed as in the previous section. Let the waveguide be filled with a lossless dielectric. According to (7.8a), for a TM field propagating or decaying in positive or negative z -direction, choose an electric Hertz form exhibiting a z -component only.

$$\underline{\Pi}_e^{\text{TM}}(\mathbf{x}) = \underline{\Pi}_z^{\text{TM}}(\mathbf{x}) dz = \Psi^{\text{TM}}(u, v) e^{\mp \gamma z} dz, \quad (7.183)$$

where $\Psi^{\text{TM}}(u, v)$ is a scalar potential defining the transverse field distribution, u, v are orthogonal curvilinear coordinates, and γ is the *propagation coefficient of the TM mode*. The negative sign in the exponent of the above equation corresponds to a field propagating or decaying in positive z -direction, whereas the positive sign occurs when the field is propagating or decaying in negative z -direction. From (7.9b) and (7.10) we obtain the Helmholtz equation for the z -component of the magnetic Hertz vector describing the TM waveguide modes,

$$\Delta \underline{\Pi}_z^{\text{TM}} + \beta_{M0}^2 \underline{\Pi}_z^{\text{TM}} = 0, \quad (7.184)$$

with β_{M0} given in (7.169). This yields the *two-dimensional scalar Helmholtz equation* for $\Psi^{\text{TM}}(u, v)$

$$\Delta_t \Psi^{\text{TM}}(u, v) + \beta_{c, \text{TM}}^2 \Psi^{\text{TM}}(u, v) = 0 \quad (7.185)$$

with the two-dimensional Laplace operator Δ_t defined in (A.138). For a bounded waveguide cross-section of finite extension, this two-dimensional elliptic partial differential equation usually exhibits an infinite number of solutions belonging to a discrete eigenvalue spectrum of $\beta_{c, \text{TM}}^2$. In the lossless case the propagation coefficient γ either is purely real or purely imaginary. The waveguide propagation coefficient $\gamma = \alpha + j\beta$ is given in (7.171a) and (7.171b). For $\beta_{M0} < \beta_{c, \text{TM}}$ the TM mode is an evanescent mode $\beta_{M0} > \beta_{c, \text{TM}}$, and the TM mode is a propagating wave. With (7.183), (7.8a), (7.11a), (7.12a), and (7.185) we obtain

$$\underline{\mathcal{E}}^{\text{TM}} = \star d \star d \underline{\Pi}_e^{\text{TM}} = \underline{\mathcal{E}}_t^{\text{TM}} + \underline{\mathcal{E}}_l^{\text{TM}}, \quad (7.186a)$$

$$\underline{\mathcal{E}}_t^{\text{TM}} = \mp \gamma d_t \Psi^{\text{TM}}(u, v) e^{\mp \gamma z}, \quad (7.186b)$$

$$\underline{\mathcal{E}}_l^{\text{TM}} = -\Delta_t \Psi^{\text{TM}}(u, v) dz e^{\mp \gamma z} = \beta_{c, \text{TM}}^2 \Psi^{\text{TM}}(u, v) dz e^{\mp \gamma z}, \quad (7.186c)$$

$$\underline{\mathcal{H}}^{\text{TM}} = \underline{\mathcal{H}}_t^{\text{TM}} = j\omega\epsilon \star d \underline{\Pi}_e^{\text{TM}} = -j\omega\epsilon \star (dz \wedge d_t \Psi^{\text{TM}}(u, v)) e^{\mp \gamma z}, \quad (7.186d)$$

where $\underline{\mathcal{E}}_t^{\text{TM}}$ and $\underline{\mathcal{H}}_t^{\text{TM}}$ are the transverse electric and magnetic fields and $\underline{\mathcal{E}}_l^{\text{TM}}$ is the longitudinal magnetic field. In Cartesian coordinate notation the TM field components are

$$\underline{\mathcal{E}}_t^{\text{TM}}(\mathbf{x}) = \mp \gamma \left(\frac{\partial \Psi^{\text{TM}}(x, y)}{\partial x} dx + \frac{\partial \Psi^{\text{TM}}(x, y)}{\partial y} dy \right) e^{\mp \gamma z}, \quad (7.187a)$$

$$\underline{\mathcal{E}}_l^{\text{TM}}(\mathbf{x}) = \beta_{c, \text{TM}}^2 \Psi^{\text{TM}}(x, y) dz e^{\mp \gamma z}, \quad (7.187b)$$

$$\underline{\mathcal{H}}_t^{\text{TM}}(\mathbf{x}) = j\omega\epsilon \left(\frac{\partial \Psi^{\text{TM}}(x, y)}{\partial y} dx - \frac{\partial \Psi^{\text{TM}}(x, y)}{\partial x} dy \right) e^{\mp \gamma z}. \quad (7.187c)$$

From (7.186d), (7.186b) and (2.155), we obtain

$$\underline{\mathcal{E}}_t^{\text{TM}} = \mp Z_{\text{TM}} \star (dz \wedge \underline{\mathcal{H}}_t) = \mp Z_{\text{TM}} \perp_z \underline{\mathcal{H}}_t, \quad (7.188a)$$

$$\underline{\mathcal{H}}_t^{\text{TM}} = \pm \frac{1}{Z_{\text{TM}}} \star (dz \wedge \underline{\mathcal{E}}_t) = \pm \frac{1}{Z_{\text{TM}}} \perp_z \underline{\mathcal{E}}_t \quad (7.188b)$$

with the *wave impedance of the TM mode*

$$Z_{\text{TM}} = \frac{\gamma}{j\omega\epsilon}. \quad (7.189)$$

This means that the transverse electric and magnetic fields are orthogonal and their ratio is independent from the transverse coordinates and given by the wave impedance of the TM mode. The wave impedance is imaginary below the cutoff frequency and real above the cutoff frequency. With (7.171a) and (7.171b) we obtain

$$Z_{\text{TM}} = \frac{\alpha}{j\omega\epsilon} = \frac{\sqrt{\beta_{c, \text{TM}}^2 - \beta_{M0}^2}}{j\omega\epsilon} = -j Z_F \frac{\sqrt{\omega_c^2 - \omega^2}}{\omega} \quad \text{for } \omega < \omega_c, \quad (7.190a)$$

$$Z_{\text{TM}} = \frac{\beta}{\omega\epsilon} = \frac{\sqrt{\beta_{M0}^2 - \beta_{c, \text{TM}}^2}}{\omega\epsilon} = Z_F \frac{\sqrt{\omega^2 - \omega_c^2}}{\omega} \quad \text{for } \omega > \omega_c \quad (7.190b)$$

with the wave impedance of the homogeneous isotropic medium filling the waveguide Z_F given in (7.177) and the angular cutoff frequency ω_c defined in (7.178).

On ∂A the tangential component of the electric field must vanish. In accordance with (2.173c) this yields

$$n \wedge \underline{\mathcal{E}} = 0, \quad (7.191)$$

where $n = g_n dn$ is the unit differential form normal to the boundary ∂A . With (7.186b) and (7.186c) we obtain for the potential Ψ^{TM} the boundary condition

$$dn \wedge d_t \Psi^{\text{TM}}(u, v) = 0, \quad (7.192a)$$

$$dn \wedge dz \Psi^{\text{TM}}(u, v) = 0. \quad (7.192b)$$

From (7.192a) we obtain

$$dn \wedge \left(\frac{\partial \Psi^{\text{TM}}(u, v)}{\partial u} du + \frac{\partial \Psi^{\text{TM}}(u, v)}{\partial v} dv \right) = 0. \quad (7.193)$$

We can introduce a local coordinate system where the boundary is ∂A defined by either constant u or constant v . Let us introduce a local coordinate system where u is tangential to ∂A and $n = v$ is normal to ∂A . Let the boundary be defined by $v = v_0$. For

$$\Psi^{\text{TM}}(u, v_0) = 0 \quad (7.194)$$

the equation (7.192b) is fulfilled. From (7.194) follows

$$\frac{\partial \Psi^{\text{TM}}(u, v_0)}{\partial u} = 0 \quad (7.195)$$

and therefore also (7.192a) and (7.193) are fulfilled. That means that the tangential electric field component at ∂A vanishes if and only if (7.194) is fulfilled. This condition is called the *Dirichlet boundary condition*. If a coordinate system can be chosen, where the boundary of the waveguide cross-section is defined by setting u constant, then v is the normal coordinate and vice versa. In cases where the waveguide cross-section boundary exhibits 90° edges for parts of the boundary u and for other parts v may be the normal coordinate.

The partial differential equation (7.184) together with the boundary condition (7.194) define an eigenvalue problem. Since the field is bounded in transverse directions the two-dimensional Helmholtz equation (7.185) exhibits a *discrete eigenvalue spectrum* of $\beta_{c, \text{TM}}^2$. The *eigenfunctions* $\Psi^{\text{TM}}(u, v)$ belonging to the *eigenvalues* β_c^{TM} define the waveguide modes. The set of eigenfunctions and eigenvalues usually are numbered with two indices m and n as Ψ_{mn} and $\beta_{c, \text{TM}mn}$. Eigenvalues are usually distinct.

7.8.3 Modal Expansions in Waveguides

Any electromagnetic field in a waveguide can be expanded in a series of all possible TE and TM modes. We first prove that in the non-degenerate case each waveguide mode is orthogonal to all others. We consider TE and TM modes numbered with k with associated scalar potential functions $\Psi_k^{\text{TE}}(u, v)$ and $\Psi_k^{\text{TM}}(u, v)$, fulfilling the Helmholtz equation (7.170) for the eigenvalues $\beta_{c, k}$, respectively. In this section we number the modes with one index. The TE mode belonging to the eigenvalue $\beta_{c, k}$ is called the TE_k mode. Dealing with specific waveguide structures it will be reasonable to denominate every mode with two indices.

From (7.172a), (7.172c), (7.186b), and (7.186d) we obtain the transverse electric field and the transverse part of the magnetic field of the TE_k and TM_k modes,

$$\underline{\mathcal{E}}_{k,t}^{\text{TE}} = j\omega\mu \star (dz \wedge d_t \Psi_k^{\text{TE}}(u, v)) e^{\mp \gamma_k z}, \quad (7.196a)$$

$$\underline{\mathcal{H}}_{k,t}^{\text{TE}} = \mp \gamma_k d_t \Psi_k^{\text{TE}}(u, v) e^{\mp \gamma_k z}, \quad (7.196b)$$

$$\underline{\mathcal{E}}_{k,t}^{\text{TM}} = \mp \gamma_k d_t \Psi_k^{\text{TM}}(u, v) e^{\mp \gamma_k z}, \quad (7.196c)$$

$$\underline{\mathcal{H}}_{k,t}^{\text{TM}} = -j\omega\epsilon \star (dz \wedge d_t \Psi_k^{\text{TM}}(u, v)) e^{\mp \gamma_k z}. \quad (7.196d)$$

We can express the transverse field forms as products of electric and magnetic structure forms $e_k^{\text{TE}}(u, v)$ and $h_k^{\text{TE}}(u, v)$ with complex amplitudes depending on the z -coordinate only, such that

$$\underline{\mathcal{E}}_{k,t}^{\text{P}} = \left(V_k^{\text{P}(+)} e^{-\gamma_k z} + V_k^{\text{P}(-)} e^{\gamma_k z} \right) e_k^{\text{P}}(u, v), \quad (7.197a)$$

$$\underline{\mathcal{H}}_{k,t}^{\text{P}} = \frac{1}{Z_{\text{P},k}} \left(V_k^{\text{P}(+)} e^{-\gamma_k z} - V_k^{\text{P}(-)} e^{\gamma_k z} \right) h_k^{\text{P}}(u, v) \quad (7.197b)$$

where P stands for TE or TM. The structure forms are given by

$$e_k^{\text{TE}}(u, v) = \star (dz \wedge d_t \Psi_k^{\text{TE}}(u, v)) = -\star (dz \wedge h_k^{\text{TE}}(u, v)), \quad (7.198a)$$

$$h_k^{\text{TE}}(u, v) = -d_t \Psi_k^{\text{TE}}(u, v) = \star (dz \wedge e_k^{\text{TE}}(u, v)), \quad (7.198b)$$

$$e_k^{\text{TM}}(u, v) = -d_t \Psi_k^{\text{TM}}(u, v) = \star (dz \wedge h_k^{\text{TM}}(u, v)), \quad (7.198c)$$

$$h_k^{\text{TM}}(u, v) = -\star (dz \wedge d_t \Psi_k^{\text{TM}}(u, v)) = -\star (dz \wedge e_k^{\text{TM}}(u, v)). \quad (7.198d)$$

Inserting $\Psi_k^{\text{TE}*}(u, v)$ and $\Psi_l^{\text{TE}}(u, v)$ or $\Psi_k^{\text{TM}*}(u, v)$ and $\Psi_l^{\text{TM}}(u, v)$ into the two-dimensional form of Green's second scalar theorem (4.149) yields

$$\begin{aligned} & \int_A (\Psi_k^{\text{P}*}(u, v) \Delta_t \Psi_l^{\text{P}}(u, v) - \Psi_l^{\text{P}}(u, v) \Delta_t \Psi_k^{\text{P}*}(u, v)) g_u g_n du \wedge dn \\ &= - \oint_{\partial A} \left(\Psi_k^{\text{P}*}(u, v) \frac{\partial \Psi_l^{\text{P}}(u, v)}{\partial n} - \Psi_l^{\text{P}}(u, v) \frac{\partial \Psi_k^{\text{P}*}(u, v)}{\partial n} \right) \frac{g_u}{g_n} du, \end{aligned} \quad (7.199)$$

where P stands for either TE or TM. In the TE case $\Psi_k^{\text{TE}}(u, v)$ and $\Psi_l^{\text{TE}}(u, v)$ fulfill the Neumann boundary condition (7.182) on ∂A and the right-hand side of (7.199) vanishes. In the TE case $\Psi_k^{\text{TE}}(u, v)$ and $\Psi_l^{\text{TE}}(u, v)$ satisfy the Dirichlet boundary condition (7.195) on ∂A . Therefore, also in this case the right-hand side of (7.199) becomes zero. Inserting (7.170) on the left-hand side yields

$$(\beta_{c,k}^2 - \beta_{c,l}^2) \int_A \Psi_k^{\text{P}*}(u, v) \Psi_l^{\text{P}}(u, v) g_u g_n du \wedge dn = 0. \quad (7.200)$$

From this it follows

$$\int_A \Psi_k^{p*}(u, v) \Psi_l^p(u, v) g_u g_n du \wedge dn = 0 \quad \text{for } \beta_{c,k} \neq \beta_{c,l}. \quad (7.201)$$

The scalar potentials $\Psi_k^p(u, v)$ and $\Psi_l^p(u, v)$ are orthogonal for $\beta_{c,k} \neq \beta_{c,l}$. For $k = l$ the integral assumes a positive and real value. We normalize the potential functions $\Psi_k^{\text{TE}}(u, v)$ so that

$$\int_A \Psi_k^{p*}(u, v) \Psi_l^p(u, v) g_u g_n du \wedge dn = a_l \delta_{kl} \quad (7.202)$$

is fulfilled, where a_l is a positive real quantity to be determined in an appropriate way. Now we insert $\Psi_k^{p*}(u, v)$ and $\Psi_l^p(u, v)$, Green's first identity in two dimensions (4.143) and obtain

$$\int_A (d_t \Psi_k^{p*}(u, v) \wedge \star d_t \Psi_l^p(u, v)) \lrcorner dz + \int_A (\Psi_k^{p*}(u, v) d_t \star d_t \Psi_l^p(u, v)) \lrcorner dz = 0. \quad (7.203)$$

For $p = \text{TE}$ as well as for $p = \text{TM}$ the right-hand side of this equation vanishes since in the TE case the $\Psi_l^{\text{TE}}(u, v)$ fulfills the Neumann boundary condition (7.182) on ∂A , and in the TM case $\Psi_l^{\text{TM}}(u, v)$ fulfills the Dirichlet boundary condition (7.195) on ∂A . Transforming the second term of the left-hand side of this equation in the form of (4.146) and considering the Helmholtz equation (7.170), we obtain

$$\int_A (d_t \Psi_k^{p*}(u, v) \wedge \star d_t \Psi_l^p(u, v)) \lrcorner dz = \beta_{c,l}^2 \int_A (\Psi_k^{p*}(u, v) \Psi_l^p(u, v)) g_u g_n du \wedge dn. \quad (7.204)$$

Inserting (7.202) and choosing $a_l = \beta_{c,l}^{-2}$ we obtain

$$\int_A (d_t \Psi_k^{p*}(u, v) \wedge \star d_t \Psi_l^p(u, v)) \lrcorner dz = \delta_{kl}. \quad (7.205)$$

At first we prove the orthogonality of the TE and TM modes. Inserting (7.198a) and (7.198b) into (7.205) yields

$$\int_A e_k^{\text{TE}*}(u, v) \wedge h_l^{\text{TE}}(u, v) = \beta_{c,l}^2 \int_A (\Psi_k^{\text{TE}*}(u, v) \Psi_l^{\text{TE}}(u, v)) g_u g_n du \wedge dn, \quad (7.206)$$

where we have considered that $e_k^{\text{TE}}(u, v)$ and $e_l^{\text{TM}}(u, v)$ both exhibit no z -component. We obtain the *orthonormality relations for the exterior product of electric and magnetic structure forms*,

$$\int_A e_k^{\text{TE}*}(u, v) \wedge h_l^{\text{TE}}(u, v) = \delta_{kl}. \quad (7.207)$$

The dual set of structure forms $e_k^{\text{TE}}(u, v)$ and $h_k^{\text{TE}}(u, v)$ is called a *biorthonormal set of structure forms*. We can write this in Dirac notation (C.173) as

$$\langle e_k^{\text{TE}} | h_l^{\text{TE}} \rangle_A = - \langle h_k^{\text{TE}} | e_l^{\text{TE}} \rangle_A = \delta_{kl}. \quad (7.208)$$

In a similar way we can derive the orthonormality relations for the electric and magnetic structure forms of the TE modes. Inserting (7.198c) and (7.198d) into (7.205) yields the orthonormality relations for the product of electric and magnetic structure functions

$$\int_A e_k^{\text{TM}*}(u, v) \wedge h_l^{\text{TM}}(u, v) = \langle e_k^{\text{TM}} | h_l^{\text{TM}} \rangle_A = - \langle h_k^{\text{TM}} | e_l^{\text{TM}} \rangle_A = \delta_{kl}. \quad (7.209)$$

We now show that every TE mode is orthogonal to any TM mode. With (7.198a) and (7.198c) we obtain

$$\int_A (e_k^{\text{TE}}(u, v) \wedge * e_l^{\text{TM}}(u, v)) \lrcorner dz = \int_A (dz \wedge d_t \Psi_k^{\text{TE}}(u, v) \wedge d_t \Psi_l^{\text{TM}}(u, v)) \lrcorner dz. \quad (7.210)$$

Using (A.59) and Poincaré's lemma (A.61) we obtain

$$dz \wedge d_t \Psi_k^{\text{TE}}(u, v) \wedge d_t \Psi_l^{\text{TM}}(u, v) = - d_t (dz \wedge \Psi_k^{\text{TE}}(u, v) \wedge d_t \Psi_l^{\text{TM}}(u, v)). \quad (7.211)$$

This yields

$$\begin{aligned} & \int_A (dz \wedge d_t \Psi_k^{\text{TE}}(u, v) \wedge d_t \Psi_l^{\text{TM}}(u, v)) \lrcorner dz \\ &= - \oint_{\partial A} (dz \wedge \Psi_k^{\text{TE}}(u, v) \wedge d_t \Psi_l^{\text{TM}}(u, v)) \lrcorner dz = 0. \end{aligned} \quad (7.212)$$

The right-hand side of this integral vanishes since $\Psi_k^{\text{TE}}(u, v)$ fulfills the Dirichlet boundary condition and $\Psi_l^{\text{TM}}(u, v)$ fulfills the Neumann boundary condition, both on ∂A . From (7.205) and (7.198a) to (7.198d) we obtain the orthogonality relations for the product of TE electric with TM magnetic structure functions and the product of TM electric with TE magnetic structure functions,

$$\int_A e_k^{\text{TE}}(u, v) \wedge h_l^{\text{TM}}(u, v) = \langle e_k^{\text{TE}} | h_l^{\text{TM}} \rangle_A = 0, \quad (7.213a)$$

$$\int_A e_k^{\text{TM}}(u, v) \wedge h_l^{\text{TE}}(u, v) = \langle e_k^{\text{TM}} | h_l^{\text{TE}} \rangle_A = 0. \quad (7.213b)$$

From (7.198a), (7.198b), (7.198c), and (7.198d) we derive further useful relations between the structure forms,

$$* d_t * e_k^{\text{TE}}(u, v) = * d_t (dz \wedge d_t \Psi_k^{\text{TE}}(u, v)) = 0, \quad (7.214a)$$

$$* d_t * h_k^{\text{TE}}(u, v) = - \Delta_t \Psi_k^{\text{TE}}(u, v) = \beta_{c,k}^{\text{TE}2} \Psi_k^{\text{TE}}(u, v), \quad (7.214b)$$

$$* d_t * e_k^{\text{TM}}(u, v) = - \Delta_t \Psi_k^{\text{TM}}(u, v) = \beta_{c,k}^{\text{TM}2} \Psi_k^{\text{TM}}(u, v), \quad (7.214c)$$

$$* d_t * h_k^{\text{TM}}(u, v) = - * d_t (dz \wedge d_t \Psi_k^{\text{TM}}(u, v)) = 0. \quad (7.214d)$$

This yields

$$\mathbf{d}_t \star \mathbf{d}_t \star \mathbf{e}_k^{\text{TE}}(u, v) = 0, \quad (7.215a)$$

$$\mathbf{d}_t \star \mathbf{d}_t \star h_k^{\text{TE}}(u, v) = -\beta_{c,k}^{\text{TE}2} h_k^{\text{TE}}(u, v), \quad (7.215b)$$

$$\mathbf{d}_t \star \mathbf{d}_t \star \mathbf{e}_k^{\text{TM}}(u, v) = -\beta_{c,k}^{\text{TM}2} \mathbf{e}_k^{\text{TM}}(u, v), \quad (7.215c)$$

$$\mathbf{d}_t \star \mathbf{d}_t \star h_k^{\text{TM}}(u, v) = 0. \quad (7.215d)$$

In a similar way we obtain

$$\star \mathbf{d}_t \star \mathbf{d}_t \mathbf{e}_k^{\text{TE}}(u, v) = \beta_{c,k}^{\text{TE}2} \mathbf{e}_k^{\text{TE}}(u, v), \quad (7.216a)$$

$$\star \mathbf{d}_t \star \mathbf{d}_t h_k^{\text{TE}}(u, v) = 0, \quad (7.216b)$$

$$\star \mathbf{d}_t \star \mathbf{d}_t \mathbf{e}_k^{\text{TM}}(u, v) = 0, \quad (7.216c)$$

$$\star \mathbf{d}_t \star \mathbf{d}_t h_k^{\text{TM}}(u, v) = \beta_{c,k}^{\text{TM}2} h_k^{\text{TM}}(u, v). \quad (7.216d)$$

Inserting (7.215a) to (7.215d) into (3.14) yields

$$\Delta \mathbf{e}_k^{\text{TE}}(u, v) = -\beta_{c,k}^{\text{TE}2} \mathbf{e}_k^{\text{TE}}(u, v), \quad (7.217a)$$

$$\Delta h_k^{\text{TE}}(u, v) = -\beta_{c,k}^{\text{TE}2} h_k^{\text{TE}}(u, v), \quad (7.217b)$$

$$\Delta \mathbf{e}_k^{\text{TM}}(u, v) = -\beta_{c,k}^{\text{TM}2} \mathbf{e}_k^{\text{TM}}(u, v), \quad (7.217c)$$

$$\Delta h_k^{\text{TM}}(u, v) = -\beta_{c,k}^{\text{TM}2} h_k^{\text{TM}}(u, v). \quad (7.217d)$$

7.9 RECTANGULAR WAVEGUIDES

Figure 7.21 shows a *rectangular waveguide* (i.e., a waveguide with a rectangular cross-section and the inner dimensions a and b). The waveguide may be empty inside or filled with dielectric material. We first consider the lossless case and assume the waveguide walls to be perfectly conductive and the inner region to be either empty or filled with a homogeneous isotropic lossless dielectric.

7.9.1 Transverse Electric Modes

The electromagnetic field transverse electric (TE) or H modes can be derived from a magnetic Hertz form $\underline{\Pi}_m$ exhibiting only a longitudinal component $\underline{\Pi}_{mz}$ as introduced in (7.8b). In the lossless case the Helmholtz equation (7.9b) is given by

$$\Delta \underline{\Pi}_{mz} + \beta_{M0}^2 \underline{\Pi}_{mz} = 0, \quad (7.218)$$

where the phase coefficient β_{M0} is given by

$$\beta_{M0} = \omega \sqrt{\epsilon \mu} = \beta_0 \sqrt{\epsilon_r \mu_r}. \quad (7.219)$$

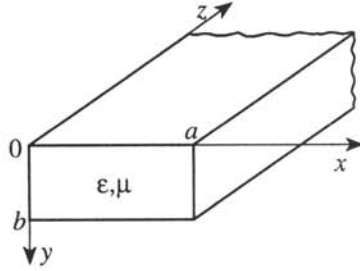


Figure 7.21: Waveguide with rectangular cross-section.

For a wave propagating in the positive z -direction we choose

$$\underline{\Pi}_{mz}(\mathbf{x}) = \underline{\Pi}_{m0}(x, y) e^{-j\beta z}. \quad (7.220)$$

Furthermore for $\underline{\Pi}_{m0}(x, y)$ we choose

$$\underline{\Pi}_{m0}(x, y) = \underline{X}(x) \underline{Y}(y) \quad (7.221)$$

and obtain from (7.218), (7.219), and (7.220)

$$\frac{1}{\underline{X}} \frac{d^2 \underline{X}}{dx^2} + \frac{1}{\underline{Y}} \frac{d^2 \underline{Y}}{dy^2} + (\beta_{M0}^2 - \beta^2) = 0. \quad (7.222)$$

Since the first term in (7.222) depends on x only and the second term on y only, this equation can be satisfied only if both terms are constant. Therefore the equations

$$\frac{1}{\underline{X}} \frac{d^2 \underline{X}}{dx^2} = -\beta_x^2, \quad (7.223a)$$

$$\frac{1}{\underline{Y}} \frac{d^2 \underline{Y}}{dy^2} = -\beta_y^2 \quad (7.223b)$$

must be satisfied and β_x and β_y have to fulfill the condition

$$\beta_x^2 + \beta_y^2 = \beta_{M0}^2 - \beta^2. \quad (7.224)$$

The general solutions for $\underline{X}(x)$ and $\underline{Y}(y)$ are given by

$$\underline{X}(x) = \underline{A}' \sin \beta_x x + \underline{B}' \cos \beta_x x, \quad (7.225a)$$

$$\underline{Y}(y) = \underline{C}' \sin \beta_y y + \underline{D}' \cos \beta_y y. \quad (7.225b)$$

Since we have assumed perfectly conducting waveguide walls, the tangential electric field components must vanish at the waveguide walls. From (7.16b), (7.221), (7.225a), and (7.225b) we obtain $\underline{C}' = 0$, if \underline{E}_x has to vanish at $y = 0$. Furthermore it follows

$$\beta_y = \frac{n\pi}{b} \quad \text{for } n = 0, 1, 2, \dots, \quad (7.226a)$$

if $\underline{E}_x|_{y=b} = 0$ has to be satisfied. In the same way we obtain from (7.17b) $\underline{A}' = 0$ and

$$\beta_x = \frac{m\pi}{a} \quad \text{for } m = 0, 1, 2, \dots, \quad (7.226b)$$

if \underline{E}_y has to vanish at $y = 0$ and $y = a$. From (7.221) and (7.225a) to (7.226b) we obtain therefore

$$\underline{\Pi}_{m0}(x, y) = \underline{A} \cos \frac{m\pi x}{a} \cos \frac{n\pi y}{b}, \quad (7.227)$$

where \underline{A} is a complex wave amplitude. The quantities β_x and β_y are determined by the cross-sectional dimensions a and b of the rectangular waveguide and by the positive integer numbers m and n . The waveguide modes are indicated by m and n . The transverse electric mode belonging to the indices m and n is called TE_{mn} mode or H_{mn} mode, respectively. From (7.227) and (7.220) we obtain for the wave propagating in the positive z -direction

$$\underline{\Pi}_{mz}(\mathbf{x}) = \underline{A} \cos \frac{m\pi x}{a} \cos \frac{n\pi y}{b} e^{-j\beta z}. \quad (7.228)$$

After inserting into (7.218) we obtain

$$\beta^2 = \beta_{M0}^2 - \beta_{Mc}^2 \quad (7.229)$$

with

$$\beta_{Mc} = \sqrt{\beta_x^2 + \beta_y^2} = \sqrt{\left(\frac{m\pi}{a}\right)^2 + \left(\frac{n\pi}{b}\right)^2}. \quad (7.230)$$

The relation between the wavelength of the plane wave in free-space λ_0 and the phase coefficient β_{M0} of the plane wave in the medium is given by

$$\lambda_0 = \frac{2\pi}{\beta_0} = \sqrt{\epsilon_r \mu_r} \frac{2\pi}{\beta_{M0}}. \quad (7.231)$$

The *guide wavelength* λ_g is given by

$$\lambda_g = \frac{2\pi}{\beta}. \quad (7.232)$$

We define the so-called *cutoff wavelength* λ_c by

$$\lambda_c = \sqrt{\epsilon_r \mu_r} \frac{2\pi}{\beta_{Mc}} = \frac{2\sqrt{\epsilon_r \mu_r}}{\sqrt{\left(\frac{m}{a}\right)^2 + \left(\frac{n}{b}\right)^2}}. \quad (7.233)$$

From (7.229) to (7.233) it follows

$$\lambda_g = \frac{1}{\sqrt{\epsilon_r \mu_r}} \frac{\lambda_0}{\sqrt{1 - \left(\frac{\lambda_0}{\lambda_c}\right)^2}}. \quad (7.234)$$

A waveguide mode can only propagate if the free-space wavelength λ_0 is smaller than the cutoff wavelength λ_c . The cutoff wavelength λ_c depends on the mode and decreases for increasing m and n . The *cutoff frequency*

$$f_c = \frac{c_0}{\lambda_c} \quad (7.235)$$

is the frequency corresponding to the cutoff wavelength. For $a > b$ the fundamental mode (i.e., the mode with the largest cutoff wavelength), is the TE_{10} mode. For the TE_{10} mode we obtain

$$\lambda_c = 2a\sqrt{\epsilon_r \mu_r}. \quad (7.236)$$

If in a rectangular waveguide a side ratio $a/b = 2$ is chosen in the frequency interval between the cutoff frequency and the double cutoff frequency, only the fundamental TE_{10} mode can propagate. The modes TE_{20} and TE_{01} have twice the cutoff frequency of the fundamental mode and all other modes have higher cutoff frequencies. From (7.3), (7.231), (7.232) and (7.234) we obtain with $c_0 = \omega/\beta_0$ the phase velocity c of the guided wave

$$c_H = \frac{1}{\sqrt{\epsilon_r \mu_r}} \frac{c_0}{\sqrt{1 - \left(\frac{\lambda_0}{\lambda_c}\right)^2}}. \quad (7.237)$$

The group velocity of the waveguide wave is computed from (7.7) under the assumption that the permittivity of the dielectric material filling the waveguide is frequency-independent. From (7.229) we obtain

$$2\beta \frac{d\beta}{d\omega} = 2\epsilon_r \mu_r \beta_0 \frac{d\beta_0}{d\omega} = 2\epsilon_r \mu_r \frac{\omega}{c_0^2} \quad (7.238)$$

and from that using (7.7) and (7.237) the group velocity v_g of the waveguide wave

$$v_g = \left(\frac{d\beta}{d\omega}\right)^{-1} = \frac{c_0^2}{\epsilon_r \mu_r} \frac{\beta}{\omega} = \frac{c_0}{\sqrt{\epsilon_r \mu_r}} \sqrt{1 - \left(\frac{\lambda_0}{\lambda_c}\right)^2}. \quad (7.239)$$

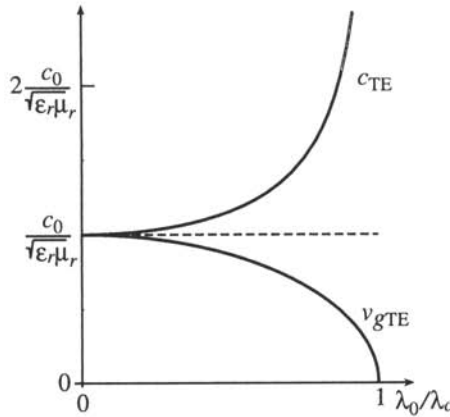


Figure 7.22: Wavelength dependence of c_{TE} and v_{gTE} .

Figure 7.22 shows the wavelength dependence of the phase velocity and the group velocity of the waveguide wave. For small wavelengths the phase and group velocities approach the velocity of the TEM wave propagating in the waveguide medium. If the wavelength approaches the cutoff wavelength, the waveguide group velocity approaches zero, and the waveguide phase velocity goes to infinity. The group velocity in the waveguide never can exceed the propagation velocity of the plane wave in the waveguide medium. If two or more modes exhibit the same cutoff frequency these modes are called *degenerate modes*. Degenerate modes exhibit same frequency dependence of phase and group velocity.

We obtain the field components of the TE_{mn} mode from (7.13b) to (7.18b) and (7.228) as follows

$$\underline{E}_x = j\omega\mu \left(\frac{n\pi}{b} \right) \underline{A} \cos \frac{m\pi x}{a} \sin \frac{n\pi y}{b} e^{-j\beta z}, \quad (7.240a)$$

$$\underline{E}_y = -j\omega\mu \left(\frac{m\pi}{a} \right) \underline{A} \sin \frac{m\pi x}{a} \cos \frac{n\pi y}{b} e^{-j\beta z}, \quad (7.240b)$$

$$\underline{E}_z = 0, \quad (7.240c)$$

$$\underline{H}_x = j\beta \left(\frac{m\pi}{a} \right) \underline{A} \sin \frac{m\pi x}{a} \cos \frac{n\pi y}{b} e^{-j\beta z}, \quad (7.240d)$$

$$\underline{H}_y = j\beta \left(\frac{n\pi}{b} \right) \underline{A} \cos \frac{m\pi x}{a} \sin \frac{n\pi y}{b} e^{-j\beta z}, \quad (7.240e)$$

$$\underline{H}_z = \beta_{Mc}^2 \underline{A} \cos \frac{m\pi x}{a} \cos \frac{n\pi y}{b} e^{-j\beta z}. \quad (7.240f)$$

For the wave propagating in the negative z -direction we have to replace $e^{-j\beta z}$ by $e^{j\beta z}$

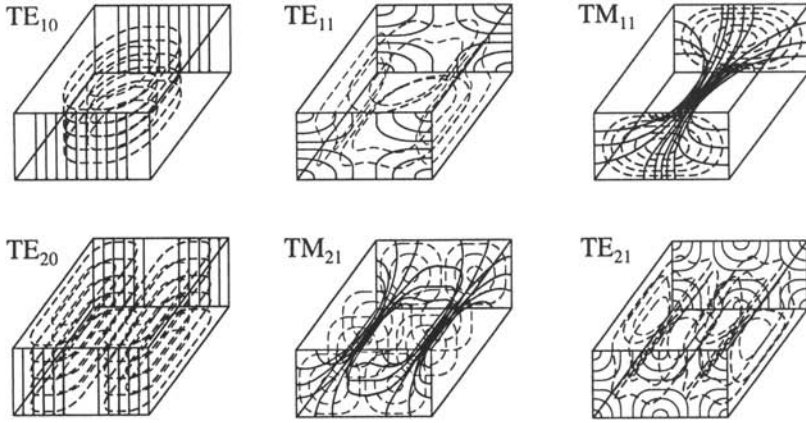


Figure 7.23: Field distribution of some waveguide modes of waveguides with a rectangular cross-section.

and due to the partial derivation with respect to z in (7.13b) and (7.14b) the sign of (7.240d) and (7.240e) must be changed. Figure 7.23 shows the field distribution of some waveguide modes of waveguides with a rectangular cross-section. From (7.240a), (7.240b), (7.240d) and (7.240e) and using (2.79), (7.231), (7.232) and (7.234) we obtain for the wave propagating in the positive z -direction

$$\frac{\underline{E}_x}{\underline{H}_y} = -\frac{\underline{E}_y}{\underline{H}_x} = \frac{\omega\mu}{\beta} = \frac{Z_F}{\sqrt{1 - \left(\frac{\lambda_0}{\lambda_c}\right)^2}}. \quad (7.241)$$

We define the *wave impedance* Z_{TE} of the TE mode by

$$Z_{TE} = \frac{Z_F}{\sqrt{1 - \left(\frac{\lambda_0}{\lambda_c}\right)^2}}. \quad (7.242)$$

In the general notation of (7.241) we obtain with (2.155) for the waveguide wave propagating in the positive z -direction

$$\underline{\mathcal{E}}_{tr} = -Z_{TE} \perp_z \underline{\mathcal{H}}_{tr}. \quad (7.243)$$

$\underline{\mathcal{E}}_{tr}$ and $\underline{\mathcal{H}}_{tr}$ are the transverse electric and the magnetic field forms

$$\underline{\mathcal{E}}_{tr} = \underline{E}_x dx + \underline{E}_y dy, \quad (7.244a)$$

$$\underline{\mathcal{H}}_{tr} = \underline{H}_x dx + \underline{H}_y dy. \quad (7.244b)$$

For the wave propagating in the negative z -direction we have to replace Z_{TE} in (7.243) by minus $-Z_{TE}$. For the TE_{10} mode we obtain from (7.240a) to (7.240f):

$$\underline{E}_x = 0, \quad (7.245a)$$

$$\underline{E}_y = -j\omega\mu\frac{\pi}{a}\underline{A}\sin\frac{\pi x}{a}e^{-j\beta z}, \quad (7.245b)$$

$$\underline{E}_z = 0, \quad (7.245c)$$

$$\underline{H}_x = j\beta\frac{\pi}{a}\underline{A}\sin\frac{\pi x}{a}e^{-j\beta z}, \quad (7.245d)$$

$$\underline{H}_y = 0, \quad (7.245e)$$

$$\underline{H}_z = \beta_{Mc}^2\underline{A}\cos\frac{\pi x}{a}e^{-j\beta z}. \quad (7.245f)$$

Waveguides with the side ratio $a/b = 2$ have a maximum monomode frequency range from f_c to $2f_c$ and are in general used in a frequency region from $1.25f_c$ to $1.9f_c$. For frequencies below $1.25f_c$ the dispersion and the attenuation become too large. For frequencies above $1.9f_c$ the attenuation coefficient of the higher modes becomes too small so that evanescent modes with cutoff at $2f_c$ can reach too far into the waveguide. In Table 7.3 the data of standardized waveguides with a rectangular cross-section are summarized. The frequency regions of standardized waveguides are overlapping.

7.9.2 Transverse Magnetic Modes

To investigate transverse magnetic TM- or E-field types we start with an electric Hertz form $\underline{\mathcal{E}}$ with a longitudinal component $\underline{\Pi}_{ez}$ as given in (7.8a). The derivation is performed as in the preceding section. Equations (7.229)–(7.235) and (7.237)–(7.239) are also valid for TM modes. These modes are named TM_{mn} or E_{mn} modes. Instead of (7.228) we obtain using (7.13a) and (7.14a) for the waveguide wave propagating in the positive z -direction

$$\underline{\Pi}_{ez}(x) = \underline{B}\sin\frac{m\pi x}{a}\sin\frac{n\pi y}{b}e^{-j\beta z}. \quad (7.246)$$

Using (7.13a) to (7.18a) we obtain the field components of the TM_{mn} modes:

$$\underline{E}_x = -j\beta\left(\frac{m\pi}{a}\right)\underline{B}\cos\frac{m\pi x}{a}\sin\frac{n\pi y}{b}e^{-j\beta z}, \quad (7.247a)$$

$$\underline{E}_y = -j\beta\left(\frac{n\pi}{b}\right)\underline{B}\sin\frac{m\pi x}{a}\cos\frac{n\pi y}{b}e^{-j\beta z}, \quad (7.247b)$$

$$\underline{E}_z = \beta_{Mc}^2\underline{B}\sin\frac{m\pi x}{a}\sin\frac{n\pi y}{b}e^{-j\beta z}, \quad (7.247c)$$

Table 7.3: Data of Standardized Rectangular Waveguides for the TE_{10} Mode. (Frequency range given by $1.25f_c \leq f \leq 1.9f_c$, attenuation α for copper metallization with $\sigma_{Cu} = 5.8 \cdot 10^7$ S/m at $1.5f_c$.)

EIA	Type DIN	Frequency Range	Dimensions		Attenuation at $1.5f_c$		
		(GHz)	a (mm)	b (mm)	$1.5f_c$ (GHz)	theor. (dB/m)	max accept. (dB/m)
WR 2300	R 3	0.32 – 0.49	584.2	292.1	0.385	0.00078	0.001
WR 2100	R 4	0.35 – 0.53	533.4	266.7	0.422	0.00090	0.0012
WR 1800	R 5	0.41 – 0.62	457.2	228.6	0.49	0.00113	0.0015
WR 1500	R 6	0.49 – 0.75	381.0	190.5	0.59	0.00149	0.002
WR 1150	R 8	0.64 – 0.98	292.1	146.05	0.77	0.00221	0.003
WR 975	R 9	0.76 – 1.15	247.65	123.82	0.91	0.00283	0.004
WR 770	R 12	0.96 – 1.46	195.58	97.79	1.15	0.00405	0.005
WR 650	R 14	1.13 – 1.73	165.1	82.55	1.36	0.00522	0.007
WR 510	R 18	1.45 – 2.2	129.54	64.77	1.74	0.00748	0.01
WR 430	R 22	1.72 – 2.61	109.22	54.61	2.06	0.00967	0.013
WR 340	R 26	2.17 – 3.3	86.36	43.18	2.6	0.0138	0.018
WR 284	R 32	2.6 – 3.95	72.14	34.04	3.12	0.0188	0.024
WR 229	R 40	3.22 – 4.90	58.17	29.08	3.87	0.0249	0.032
WR 187	R 48	3.94 – 5.99	47.549	22.149	4.73	0.0354	0.046
WR 159	R 58	4.64 – 7.05	40.386	20.193	5.57	0.0430	0.056
WR 137	R 70	5.38 – 8.17	34.849	15.799	6.45	0.0575	0.075
WR 112	R 84	6.57 – 9.99	28.499	12.624	7.89	0.0791	0.103
WR 90	R 100	8.2 – 12.5	22.860	10.160	9.84	0.110	0.143
WR 75	R 120	9.84 – 15.0	19.050	9.525	11.8	0.133	
WR 62	R 140	11.9 – 18.0	15.799	7.899	14.2	0.176	
WR 51	R 180	14.5 – 22.0	12.954	6.477	17.4	0.236	
WR 42	R 220	17.6 – 26.7	10.668	4.318	21.1	0.368	
WR 34	R 260	21.7 – 33.0	8.636	4.318	26.0	0.436	
WR 28	R 320	26.3 – 40.0	7.112	3.556	31.6	0.538	
WR 22	R 400	32.9 – 50.1	5.690	2.845	39.5	0.815	
WR 19	R 500	39.2 – 59.6	4.775	2.388	47.1	1.058	
WR 15	R 620	49.8 – 75.8	3.759	1.880	59.8	1.52	
WR 12	R 740	60.5 – 91.9	3.0998	1.5494	72.6	2.02	
WR 10	R 900	73.8 – 112	2.5400	1.2700	88.5	2.73	
WR 08	R 1200	92.2 – 140	2.0320	1.0160	110.7	3.81	
WR 06	R 1400	113 – 173	1.651	0.8255	136.2	5.21	
WR 05	R 1800	145 – 220	1.2954	0.6477	173.6	7.49	
WR 04	R 2200	172 – 261	1.0922	0.5461	205.9	9.68	
WR 03	R 26001	217 – 330	0.8636	0.4318	260.2	13.76	

$$\underline{H}_x = j \omega \epsilon \left(\frac{n\pi}{b} \right) \underline{B} \sin \frac{m\pi x}{a} \cos \frac{n\pi y}{b} e^{-j\beta z}, \quad (7.247d)$$

$$\underline{H}_y = -j \omega \epsilon \left(\frac{m\pi}{a} \right) \underline{B} \cos \frac{m\pi x}{a} \sin \frac{n\pi y}{b} e^{-j\beta z}, \quad (7.247e)$$

$$\underline{H}_z = 0. \quad (7.247f)$$

The field distribution of the TM_{11} and TM_{21} modes are shown in Figure 7.23. From (7.247a), (7.247b), (7.247d) and (7.247e) we obtain with (2.79), (7.231), (7.232) and (7.234) for the wave propagating in the positive z -direction:

$$\frac{\underline{E}_x}{\underline{H}_y} = -\frac{\underline{E}_y}{\underline{H}_x} = \frac{\beta}{\omega \mu} = Z_F \sqrt{1 - \left(\frac{\lambda_0}{\lambda_c} \right)^2}. \quad (7.248)$$

We introduce the *wave impedance* Z_{TM} for the transverse magnetic modes as

$$Z_{\text{TM}} = Z_F \sqrt{1 - \left(\frac{\lambda_0}{\lambda_c} \right)^2}. \quad (7.249)$$

In the general notation of (7.248) we obtain with (2.155) for the transverse magnetic wave propagating in the positive z -direction

$$\underline{\mathcal{E}}_{\text{tr}} = -Z_{\text{TM}} \perp_z \underline{\mathcal{H}}_{\text{tr}}. \quad (7.250)$$

7.9.3 Power Flow in the Waveguide

The active power P flowing through the waveguide is obtained from (4.37) as the real part of the integral of the complex Poynting form \mathcal{T} over the waveguide cross-section $A|_z$ at the longitudinal coordinate z ,

$$P(z) = \Re \left\{ \int_{A|_z} \mathcal{T}(\mathbf{x}) \right\} = \Re \left\{ \int_{A|_z} T_z(\mathbf{x}) \, dx \wedge dy \right\} = \Re \left\{ \int_0^b \left(\int_0^a T_z(\mathbf{x}) \, dx \right) dy \right\}. \quad (7.251)$$

In the lossless waveguide the active power is independent from the longitudinal coordinate z .

Let us first compute the power transmitted by the TE_{mn} mode. From (4.19) and (7.243) we obtain for the electromagnetic wave propagating in the positive z -direction

$$\underline{T}_z = \frac{1}{2} (\underline{E}_x \underline{H}_y^* - \underline{E}_y \underline{H}_x^*) = \frac{1}{2} Z_{\text{TE}} (|\underline{H}_y|^2 + |\underline{H}_x|^2). \quad (7.252)$$

We now insert (7.240d), (7.240e) and (7.252) into (7.251). Using

$$\int_0^a \int_0^b \sin^2 \frac{m\pi x}{a} \cos^2 \frac{n\pi y}{b} \, dx \, dy = \frac{1}{4} ab (1 - \delta_{m0})(1 + \delta_{n0}), \quad (7.253)$$

where δ_{mn} is the Kronecker symbol defined in (A.8), we obtain the power P transmitted through the waveguide

$$P = \frac{1}{8} ab Z_{TE, mn} \beta^2 |A|^2 \left[\left(\frac{m\pi}{a} \right)^2 (1 - \delta_{m0})(1 + \delta_{n0}) + \left(\frac{n\pi}{b} \right)^2 (1 + \delta_{m0})(1 - \delta_{n0}) \right]. \quad (7.254)$$

From this we obtain

$$P_{mn}^{TE} = \begin{cases} \frac{1}{8} ab Z_{TE, mn} \beta^2 \beta_{Mc}^2 |A_{mn}|^2 & \text{for } m \neq 0, n \neq 0 \\ \frac{1}{4} ab Z_{TE, mn} \beta^2 \beta_{Mc}^2 |A_{mn}|^2 & \text{for } n = 0 \text{ or } m = 0 \end{cases}. \quad (7.255)$$

Transverse magnetic modes only exist for $m \neq 0, n \neq 0$. For the TM modes evaluation of the integral (7.251) under consideration of (7.247a), (7.247b), (7.248) and (7.249) yields

$$P_{mn}^{TM} = \frac{ab}{8 Z_{TM, mn}} \beta^2 \beta_{Mc}^2 |B_{mn}|^2. \quad (7.256)$$

7.9.4 Orthogonality of the Waveguide Modes

Under general excitation conditions several modes may propagate in a waveguide. The electromagnetic field is represented by

$$\underline{\mathcal{E}}(\mathbf{x}) = \sum_{m,n} [\underline{\mathcal{E}}_{mn}^{TE}(\mathbf{x}) + \underline{\mathcal{E}}_{mn}^{TM}(\mathbf{x})], \quad (7.257a)$$

$$\underline{\mathcal{H}}(\mathbf{x}) = \sum_{m,n} [\underline{\mathcal{H}}_{mn}^{TE}(\mathbf{x}) + \underline{\mathcal{H}}_{mn}^{TM}(\mathbf{x})]. \quad (7.257b)$$

The summation is performed over all propagating modes. Inserting these modal expansions of $\underline{\mathcal{E}}(\mathbf{x})$ and $\underline{\mathcal{H}}(\mathbf{x})$ into (4.19) and (4.37) we obtain the active power P flowing through the waveguide cross-section $A|_z$ at the longitudinal coordinate z as

$$\begin{aligned} P(z) &= \frac{1}{2} \Re \left\{ \int_{A|_z} \underline{\mathcal{E}}(\mathbf{x}) \wedge \underline{\mathcal{H}}^*(\mathbf{x}) \right\} \\ &= \frac{1}{2} \sum_{\substack{m,n,M \\ m',n',M'}} \Re \left\{ \int_{A|_z} \underline{\mathcal{E}}_{mn}^M(\mathbf{x}) \wedge \underline{\mathcal{H}}_{m'n'}^{M'*}(\mathbf{x}) \right\}, \end{aligned} \quad (7.258)$$

where the superscript M may assume TE or TM. With (7.240a), (7.240b), (7.240d), (7.240e), (7.247a), (7.247b), (7.247d), (7.247e), (7.255) and (7.256) we obtain the *orthogo-*

nality relationships

$$\frac{1}{2}\Re \left\{ \int_{A|z} \underline{\mathcal{E}}_{mn}^{\text{TE}}(\mathbf{x}) \wedge \underline{\mathcal{H}}_{m'n'}^{\text{TE}}(\mathbf{x}) \right\} = \delta_{mm'} \delta_{nn'} P_{mn}^{\text{TE}}, \quad (7.259a)$$

$$\frac{1}{2}\Re \left\{ \int_{A|z} \underline{\mathcal{E}}_{mn}^{\text{TM}}(\mathbf{x}) \wedge \underline{\mathcal{H}}_{m'n'}^{\text{TM}}(\mathbf{x}) \right\} = \delta_{mm'} \delta_{nn'} P_{mn}^{\text{TM}}, \quad (7.259b)$$

$$\frac{1}{2}\Re \left\{ \int_{A|z} \underline{\mathcal{E}}_{mn}^{\text{TE}}(\mathbf{x}) \wedge \underline{\mathcal{H}}_{m'n'}^{\text{TM}}(\mathbf{x}) \right\} = 0, \quad (7.259c)$$

$$\frac{1}{2}\Re \left\{ \int_{A|z} \underline{\mathcal{E}}_{mn}^{\text{TM}}(\mathbf{x}) \wedge \underline{\mathcal{H}}_{m'n'}^{\text{TE}}(\mathbf{x}) \right\} = 0, \quad (7.259d)$$

where δ_{mn} is the Kronecker delta function, defined in (A.8). The orthogonality of functions is discussed in Section 4.13. Inserting these equations into (7.258) yields

$$P(z) = \frac{1}{2} \sum_{m,n} \Re \left\{ \int_{A|z} \underline{\mathcal{E}}_{mn}^{\text{TE}}(\mathbf{x}) \wedge \underline{\mathcal{H}}_{mn}^{\text{TE}}(\mathbf{x}) \right\} + \frac{1}{2} \sum_{m,n} \Re \left\{ \int_{A|z} \underline{\mathcal{E}}_{mn}^{\text{TM}}(\mathbf{x}) \wedge \underline{\mathcal{H}}_{mn}^{\text{TM}}(\mathbf{x}) \right\}. \quad (7.260)$$

7.9.5 Generalized Currents and Voltages in Waveguides

Section 7.4 has shown that for TEM waves the transverse complex field vectors \underline{E} and \underline{H} may be represented as products of scalar *complex amplitudes* and real vector *structure functions*. The complex scalar amplitudes only depend on the longitudinal coordinate z , whereas the structure function only depends on the transverse coordinates x and y . This decomposition of the transverse electric and magnetic field functions into a real structure function and a scalar complex amplitude has been very useful, since the vector structure function only depends on the mode, and hence is independent of the excitation of the waveguide. The excitation of the waveguide only determines the scalar amplitude. Since in the waveguide longitudinal field components also exist, the integrals defining voltage and currents now are dependent on the paths of integration. It is, however, also possible to introduce complex scalar amplitudes for hollow waveguides. One possibility may be to introduce scalar amplitudes as path integrals of the complex field intensities \underline{E} and \underline{H} over specified paths of integration. Another way to introduce integral field quantities is to define complex amplitudes via area integrals of the field quantities. We demonstrate this method for the TE_{10} mode. We introduce a generalized complex current $\underline{I}(z)$ and a generalized complex voltage $\underline{V}(z)$ for the electromagnetic wave propagating in the positive z -direction. We impose the condition that the generalized voltage $\underline{V}(z)$ and the generalized current $\underline{I}(z)$ are related in analogy to (7.37) via the wave impedance Z_{TE} of the waveguide

$$\underline{V}(z) = Z_{\text{TE}} \underline{I}(z). \quad (7.261)$$

Furthermore, we want to introduce the generalized voltage $\underline{V}(z)$ and the generalized current $\underline{I}(z)$ such that the transmitted active power can be described in the usual way by

$$P(z) = \frac{1}{2} \Re \{ \underline{V}(z) \underline{I}(z)^* \}. \quad (7.262)$$

With (7.261) it follows that the wave propagating in the positive z -direction is carrying the active power

$$P(z) = \frac{1}{2} Z_{TE} |\underline{I}(z)|^2. \quad (7.263)$$

Using (7.255) and (7.263) we now can express the complex amplitude \underline{A} by the generalized current $\underline{I}(z)$, and we obtain

$$\underline{A} = \frac{j}{\beta_{Mc}} \sqrt{\frac{2}{ab}} \underline{I}(z=0), \quad (7.264)$$

where we have to impose a condition for the choice of the phase of $\underline{I}(z)$. Using (7.261) and (7.264) we can express the transverse field components of the TE_{10} mode in (7.245b) and (7.245d) by the generalized voltage $\underline{V}(z)$ and the generalized current $\underline{I}(z)$. The phase of $\underline{I}(z)$ in (7.263) has been chosen such that $\underline{V}(z)$ and $\underline{E}(x, y, z)$ both are in phase. For the wave propagating in positive z -direction, the z -dependence of $\underline{V}(z)$ and $\underline{I}(z)$ is given by an exponential factor $e^{-j\beta z}$, and for a wave propagating in the negative z -direction the z -dependence of $\underline{V}(z)$ and $\underline{I}(z)$ is given by the exponential factor $e^{j\beta z}$. In this case (7.261) has to be replaced by

$$\underline{V}(z) = -Z_{TE} \underline{I}(z). \quad (7.265)$$

Now we allow wave propagation in both directions and use the equations

$$\underline{E}_y = \sqrt{\frac{2}{ab}} \underline{V}(z) \sin \frac{\pi x}{a}, \quad (7.266a)$$

$$\underline{H}_x = -\sqrt{\frac{2}{ab}} \underline{I}(z) \sin \frac{\pi x}{a}, \quad (7.266b)$$

with not yet determined $\underline{V}(z)$ and $\underline{I}(z)$. From Faraday's law (2.57b) it follows that

$$\frac{\partial \underline{E}_y}{\partial x} = -j\omega\mu \underline{H}_x. \quad (7.267)$$

We now can express the longitudinal component \underline{H}_z of the magnetic field by the generalized voltage $\underline{V}(z)$

$$\underline{H}_z = \frac{j}{\omega\mu} \frac{\pi}{a} \sqrt{\frac{2}{ab}} \underline{V}(z) \cos \frac{\pi x}{a}. \quad (7.268)$$

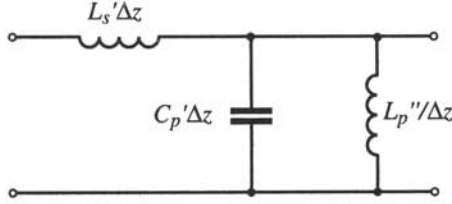


Figure 7.24: Equivalent circuit of a waveguide segment of length Δz excited in the TE_{10} mode.

Furthermore it follows from (2.57b)

$$\frac{\partial \underline{E}_y}{\partial z} = +j\omega\mu \underline{H}_x. \quad (7.269)$$

Inserting (7.266a) and (7.266b) we obtain

$$\frac{dV}{dz} = -j\omega\mu \underline{I}. \quad (7.270)$$

From Ampère's law (2.57a), it follows that

$$\frac{\partial \underline{H}_x}{\partial z} - \frac{\partial \underline{H}_z}{\partial x} = j\omega\epsilon \underline{E}_y. \quad (7.271)$$

After inserting (7.266a), (7.266b) and (7.268) we obtain

$$\frac{d\underline{I}}{dz} = -j \left[\omega\epsilon - \frac{1}{\omega\mu} \left(\frac{\pi}{a} \right)^2 \right] \underline{V}. \quad (7.272)$$

Equations (7.270) and (7.272) correspond with the transmission-line equations

$$\frac{dV}{dz} = -j\omega L'_s \underline{I}, \quad (7.273a)$$

$$\frac{d\underline{I}}{dz} = -j \left(\omega C'_p - \frac{1}{\omega L''_p} \right) \underline{V}. \quad (7.273b)$$

The series inductance per unit of length L'_s , the parallel inductance per unit of length C'_p , and the parallel capacitance per unit of length L''_p are defined in the following way

$$L'_s = \mu = \frac{Z_F}{c}, \quad (7.274a)$$

$$C'_p = \epsilon = \frac{1}{Z_F c}, \quad (7.274b)$$

$$L''_p = \mu \left(\frac{a}{\pi} \right)^2 = \frac{Z_F}{c \beta_{Mc}^2}. \quad (7.274c)$$

From the transmission-line equations (7.273a) and (7.273b) we obtain for a short line segment of length Δz the equivalent circuit as depicted in Figure 7.24. Due to the parallel inductance $L''_p/\Delta z$ the equivalent circuit exhibits high-pass behavior. This corresponds to the high-pass property of the waveguide.

7.9.6 Attenuation Due to Conductor Losses

Due to *conductor losses* the guided wave is attenuated. In this case the propagation coefficient $\gamma = \alpha + j\beta$ is complex. For small losses $\alpha \ll \beta$ the field distribution and the phase coefficient β can be calculated disregarding the losses. The conductor losses then are computed from the current distribution in the waveguide walls and the surface resistance. Considering that the transmitted active power P_z is proportional to the absolute square of the amplitude of the guided wave, for an attenuated wave propagating in the positive z -direction the relation

$$P(z) = P_0 e^{-2\alpha z} \quad (7.275)$$

must hold. From this it follows that

$$\frac{dP}{dz} = -2\alpha P, \quad (7.276)$$

and therefrom we obtain

$$\alpha = -\frac{1}{2P} \frac{dP}{dz}. \quad (7.277)$$

Therefore we can calculate the attenuation coefficients α , if we know the transmitted power $P(z)$ and the power loss per unit of length $P'_v = -\frac{dP}{dz}$. Initially we consider the field solution for the lossless waveguide and compute the power losses due to the wall currents using (6.66). We integrate (6.66) over an infinitesimal wall surface element of length dz according to Figure 7.25. The power loss in this area element is equal to $-dP$, and we obtain

$$P'_L = -\frac{dP}{dz} = \frac{1}{2} \oint_{\partial A} R_A |H_t|^2 ds. \quad (7.278)$$

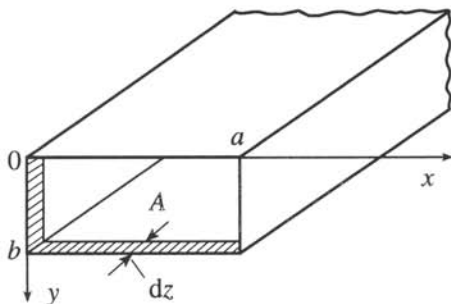


Figure 7.25: The wall currents in the rectangular waveguide.

We compute the power losses due to the wall currents for the TE_{mn} mode of the rectangular waveguide. From (7.278) we obtain

$$P'_L = R_A \int_0^a [|\underline{H}_x|^2 + |\underline{H}_z|^2] dx \Big|_{y=0} + R_A \int_0^b [|\underline{H}_y|^2 + |\underline{H}_z|^2] dy \Big|_{x=0}. \quad (7.279)$$

With (7.240d) to (7.240f) we obtain

$$[|\underline{H}_x|^2 + |\underline{H}_z|^2] \Big|_{y=0} = \beta^2 \left(\frac{m\pi}{a} \right)^2 |A|^2 \sin^2 \frac{m\pi x}{a} + \beta_{Mc}^4 |A|^2 \cos^2 \frac{m\pi x}{a}, \quad (7.280)$$

$$[|\underline{H}_y|^2 + |\underline{H}_z|^2] \Big|_{x=0} = \beta^2 \left(\frac{n\pi}{b} \right)^2 |A|^2 \sin^2 \frac{n\pi y}{b} + \beta_{Mc}^4 |A|^2 \cos^2 \frac{n\pi y}{b}. \quad (7.281)$$

From this it follows with (7.279) for the power losses due to the wall currents per unit of length

$$P'_L = \frac{1}{2} R_A |A|^2 \left[\beta^2 \left(\frac{m\pi}{a} \right)^2 (1 - \delta_{m0}) a + \beta_{Mc}^4 (1 + \delta_{m0}) a + \beta^2 \left(\frac{n\pi}{b} \right)^2 (1 - \delta_{n0}) b + \beta_{Mc}^4 (1 + \delta_{n0}) b \right]. \quad (7.282)$$

Inserting (7.254) and (7.282) into (7.277) we obtain the attenuation coefficient

$$\frac{P'_L}{2P} = \frac{2R_A}{abZ_{TE}\beta^2} \cdot \frac{\beta^2 \left[\left(\frac{m\pi}{a} \right)^2 a(1 - \delta_{m0}) + \left(\frac{n\pi}{b} \right)^2 b(1 - \delta_{n0}) \right] + \beta_{Mc}^4 [(1 + \delta_{m0})a + (1 + \delta_{n0})b]}{\left[\left(\frac{m\pi}{a} \right)^2 (1 - \delta_{m0})(1 + \delta_{n0}) + \left(\frac{n\pi}{b} \right)^2 (1 + \delta_{m0})(1 - \delta_{n0}) \right]}. \quad (7.283)$$

Using (7.229)–(7.234) and (7.242) we obtain

$$\alpha = \frac{2R_A}{abZ_F} \cdot \frac{\left(\frac{m^2}{a^2}(1-\delta_{m0}) + \frac{n^2}{b^2}(1-\delta_{n0})\right) \left(1 - \frac{\lambda_0^2}{\lambda_c^2}\right) + \left(\frac{m^2}{a^2} + \frac{n^2}{b^2}\right) [(1+\delta_{m0})a + (1+\delta_{n0})b] \frac{\lambda_0^2}{\lambda_c^2}}{\sqrt{1 - \left(\frac{\lambda_0}{\lambda_c}\right)^2} \left[\left(\frac{m}{a}\right)^2 (1-\delta_{m0})(1+\delta_{n0}) + \left(\frac{n}{b}\right)^2 (1+\delta_{m0})(1-\delta_{n0})\right]} \quad (7.284)$$

For the TE_{10} mode it follows with $\delta_{m0} = 0$, $\delta_{n0} = 1$,

$$\alpha = \frac{2R_A}{bZ_F \sqrt{1 - \left(\frac{\lambda_0}{\lambda_c}\right)^2}} \left(\frac{1}{2} + \frac{b}{a} \frac{\lambda_0^2}{\lambda_c^2} \right). \quad (7.285)$$

For the TE_{10} mode the theoretic losses and the maximum losses allowed due to the DIN standard are summarized in Table 7.3. To compute the wall current losses for the TM_{10} modes we obtain from (7.278)

$$P'_L = R_A \int_0^a |\underline{H}_x|^2 dx \Big|_{y=0} + R_A \int_0^b |\underline{H}_y|^2 dy \Big|_{x=0}. \quad (7.286)$$

After inserting (7.247d) and (7.247e) and applying (7.230), (7.248) and (7.249) we obtain

$$-\frac{dP}{dz} = \frac{1}{2} R_A |B|^2 \left[\left(\frac{n\pi}{b} \right)^2 a + \left(\frac{m\pi}{a} \right)^2 b \right] \frac{\beta^2}{Z_{TM}^2}. \quad (7.287)$$

With (7.256) we obtain the attenuation coefficient of the TM_{mn} mode

$$\alpha = \frac{2R_A}{abZ_{TM}} \frac{\left(\frac{m}{a}\right)^2 b + \left(\frac{n}{b}\right)^2 a}{\left(\frac{m}{a}\right)^2 + \left(\frac{n}{b}\right)^2}. \quad (7.288)$$

7.9.7 Attenuation Due to Dielectric Losses

If a waveguide is filled with lossy dielectric material in addition to the conductor losses *dielectric losses* will also occur. In case of dielectric losses the free-space TEM wave propagation coefficient γ_{M0} becomes complex. With the complex permittivity introduced in (2.125) we obtain

$$\gamma_{M0} = \alpha_{M0} + j\beta_{M0} = j\omega \sqrt{(\epsilon' - j\epsilon'')\mu_0}. \quad (7.289)$$

We generalize (7.229) to

$$\gamma^2 = \gamma_{M0}^2 + \beta_{Mc}^2. \quad (7.290)$$

Inserting (7.289) yields

$$\gamma = j \sqrt{\omega^2(\epsilon' - j\epsilon'')\mu_0 - \beta_{Mc}^2} = j\beta \sqrt{1 - j \frac{\omega^2\epsilon''\mu}{\beta^2}} \quad (7.291)$$

with

$$\beta = \sqrt{\omega^2\epsilon'\mu_0 - \beta_{Mc}^2}. \quad (7.292)$$

For weak dielectric losses characterized by $\epsilon'' \ll \epsilon'$ we can approximate

$$\sqrt{1 - j \frac{\omega^2\epsilon''\mu}{\beta^2}} \simeq 1 - j \frac{\omega^2\epsilon''\mu}{2\beta^2}, \quad (7.293a)$$

$$\beta_{M0} \simeq \omega \sqrt{\epsilon'\mu_0} \quad (7.293b)$$

and the attenuation coefficient α and the phase coefficient β are

$$\alpha = \frac{\omega^2\epsilon''\mu}{2\beta} = \frac{\omega^2\epsilon''\mu}{2\sqrt{\beta_{M0}^2 - \beta_{Mc}^2}}, \quad (7.294a)$$

$$\beta = \sqrt{\beta_{M0}^2 - \beta_{Mc}^2}. \quad (7.294b)$$

With the dielectric loss angle δ_e introduced in (2.126) we can put (7.294a) in the form

$$\alpha = \frac{\beta_{M0} \tan \delta_e}{2\sqrt{1 - \left(\frac{\beta_{Mc}}{\beta_{M0}}\right)^2}} = \frac{\pi \sqrt{\epsilon'_r} \tan \delta_e}{\lambda_0 \sqrt{1 - \left(\frac{\lambda_0}{\lambda_c}\right)^2}}. \quad (7.295)$$

If the waveguide exhibits conductor losses as well as dielectric losses, the total attenuation coefficient α_{total} is the sum of the attenuation coefficient $\alpha_{\text{cond.}}$ due to the conductor losses and the attenuation coefficient $\alpha_{\text{diel.}}$ due to the dielectric losses,

$$\alpha_{\text{total}} = \alpha_{\text{cond.}} + \alpha_{\text{diel.}} \quad (7.296)$$

7.10 CIRCULAR CYLINDRIC WAVEGUIDES

7.10.1 The Circular Waveguide Modes

Figure 7.26 shows a circular waveguide with inner diameter $2a$. We investigate the lossless circular waveguide with a perfectly conducting wall and free-space inner region.

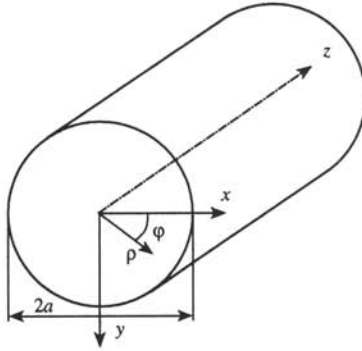


Figure 7.26: Circular cylindric waveguide.

To investigate the TM and TE modes of the circular cylindric waveguide we derive the fields either from an electric Hertz form $\underline{\Pi}_e$ or a magnetic Hertz form $\underline{\Pi}_m$ exhibiting only a z -component

$$\underline{\Pi}_e = \underline{\Pi}_{ez} \, dz, \quad (7.297a)$$

$$\underline{\Pi}_m = \underline{\Pi}_{mz} \, dz. \quad (7.297b)$$

For both cases the Helmholtz equation (3.28) has the following form:

$$\Delta \underline{\Pi}_{iz} + \beta_0^2 \underline{\Pi}_{iz} = 0 \quad i = e, m \quad (7.298)$$

with $\beta_0^2 = \omega^2 \epsilon_0 \mu_0$. With (A.157) we obtain for circular cylindric coordinates

$$\frac{\partial^2 \underline{\Pi}_{iz}}{\partial r^2} + \frac{1}{r} \frac{\partial \underline{\Pi}_{iz}}{\partial r} + \frac{1}{r^2} \frac{\partial^2 \underline{\Pi}_{iz}}{\partial \phi^2} + \frac{\partial^2 \underline{\Pi}_{iz}}{\partial z^2} + \beta_0^2 \underline{\Pi}_{iz} = 0. \quad (7.299)$$

We seek solutions for waves propagating in the positive z -direction and choose the separation formulation

$$\underline{\Pi}_{iz}(r, \phi, z) = R(r) f(\phi) e^{-j\beta z}. \quad (7.300)$$

From this it follows that

$$f \frac{d^2 R}{dr^2} + f \frac{1}{r} \frac{dR}{dr} + \frac{R}{r^2} \frac{d^2 f}{d\phi^2} + (\beta_0^2 - \beta^2) R f = 0. \quad (7.301)$$

We introduce the parameter k_c given by

$$k_c^2 = \beta_0^2 - \beta^2 \quad (7.302)$$

and obtain

$$r^2 \frac{1}{R} \frac{d^2 R}{dr^2} + r \frac{1}{R} \frac{dR}{dr} + \frac{1}{f} \frac{d^2 f}{d\phi^2} + r^2 k_c^2 = 0. \quad (7.303)$$

The first two terms of this equation are dependent on r only, whereas the third term only depends on ϕ . This equation therefore can be fulfilled only if the sum of the first two terms and the last term as well as the third term each are independently constant. Therefore we set the third term equal to $-n^2$ and obtain

$$\frac{d^2 f}{d\phi^2} + n^2 f = 0. \quad (7.304)$$

The solution of this equation is

$$f(\phi) = \underline{A}' \sin n\phi + \underline{B}' \cos n\phi. \quad (7.305)$$

Since $f(\phi)$ is periodic with 2π , the parameter n must be an integer. Furthermore $\underline{A}' = 0$ without loss of generality, since both solutions in (7.305) only are distinguished by a rotation of the field distribution around the z -axis by 90° . For $R(r)$ we obtain from (7.303) Bessel's differential equation

$$r^2 \frac{d^2 R}{dr^2} + r \frac{dR}{dr} + (r^2 k_c^2 - n^2) R = 0. \quad (7.306)$$

The solution is given by

$$R(r) = \underline{C}' J_n(k_c r) + \underline{D}' Y_n(k_c r), \quad (7.307)$$

where $J_n(x)$ and $Y_n(x)$ are the ordinary Bessel functions of the n th-order and first and second kind. Since $Y_n(x)$ for $x = 0$ exhibits a singularity, $\underline{D}' = 0$ must be valid in (7.307). Up to now the treatment of the Helmholtz equation is the same for the electric and magnetic Hertz forms $\underline{\Pi}_e$ and $\underline{\Pi}_m$. From (3.29a), (3.29b), (3.36a), (3.36b) and (7.300), (7.305), (7.307) we obtain

$$\text{TM modes: } \underline{\Pi}_e(r, \phi, z) = \underline{B} J_n(k_c r) \cos n\phi e^{-j\beta z} dz, \quad (7.308a)$$

$$\underline{\mathcal{E}} = d\tilde{d} \underline{\Pi}_e + \beta_0^2 \underline{\Pi}_e, \quad (7.308b)$$

$$\underline{\mathcal{H}} = j\omega \underline{\epsilon} \star d \underline{\Pi}_e. \quad (7.308c)$$

$$\text{TE modes: } \underline{\Pi}_m(r, \phi, z) = \underline{A} J_n(k_c r) \cos n\phi e^{-j\beta z} dz, \quad (7.309a)$$

$$\underline{\mathcal{H}} = d\tilde{d} \underline{\Pi}_m + \beta_0^2 \underline{\Pi}_m, \quad (7.309b)$$

$$\underline{\mathcal{E}} = -j\omega \underline{\mu} \star d \underline{\Pi}_m. \quad (7.309c)$$

\underline{A} and \underline{B} are arbitrary complex amplitudes. For circular cylindric coordinates we obtain for the Hertz form (7.297a)

$$d\underline{\Pi}_e = \frac{1}{r} \frac{\partial \underline{\Pi}_{ez}}{\partial \phi} dr - \frac{\partial \underline{\Pi}_{ez}}{\partial r} r d\phi, \quad (7.310)$$

$$d\tilde{d}\underline{\Pi}_e = \frac{\partial^2 \underline{\Pi}_{ez}}{\partial r \partial z} dr + \frac{1}{r} \frac{\partial^2 \underline{\Pi}_{ez}}{\partial \phi \partial z} r d\phi + \frac{\partial^2 \underline{\Pi}_{ez}}{\partial z^2} dz. \quad (7.311)$$

With (7.302) we obtain

$$d\tilde{d}\underline{\Pi}_e + \beta_0^2 \underline{\Pi}_e = \frac{\partial^2 \underline{\Pi}_{ez}}{\partial r \partial z} dr + \frac{1}{r} \frac{\partial^2 \underline{\Pi}_{ez}}{\partial \phi \partial z} r d\phi + k_c^2 \underline{\Pi}_{ez} dz. \quad (7.312)$$

With this we obtain from (7.308a) to (7.309c) the field components

$$\text{TM modes: } \underline{E}_r = -j\beta k_c \underline{B} J'_n(k_c r) \cos n\phi e^{-j\beta z}, \quad (7.313a)$$

$$\underline{E}_\phi = j\beta \frac{n}{r} \underline{B} J_n(k_c r) \sin n\phi e^{-j\beta z}, \quad (7.313b)$$

$$\underline{E}_z = k_c^2 \underline{B} J_n(k_c r) \cos n\phi e^{-j\beta z}, \quad (7.313c)$$

$$\underline{H}_r = -j\omega\epsilon_0 \frac{n}{r} \underline{B} J_n(k_c r) \sin n\phi e^{-j\beta z}, \quad (7.313d)$$

$$\underline{H}_\phi = -j\omega\epsilon_0 k_c \underline{B} J'_n(k_c r) \cos n\phi e^{-j\beta z}, \quad (7.313e)$$

$$\underline{H}_z = 0, \quad (7.313f)$$

$$\text{TE modes: } \underline{H}_r = -j\beta k_c \underline{A} J'_n(k_c r) \cos n\phi e^{-j\beta z}, \quad (7.314a)$$

$$\underline{H}_\phi = j\beta \frac{n}{r} \underline{A} J_n(k_c r) \sin n\phi e^{-j\beta z}, \quad (7.314b)$$

$$\underline{H}_z = k_c^2 \underline{A} J_n(k_c r) \cos n\phi e^{-j\beta z}, \quad (7.314c)$$

$$\underline{E}_r = j\omega\mu_0 \frac{n}{r} \underline{A} J_n(k_c r) \sin n\phi e^{-j\beta z}, \quad (7.314d)$$

$$\underline{E}_\phi = j\omega\mu_0 k_c \underline{A} J'_n(k_c r) \cos n\phi e^{-j\beta z}, \quad (7.314e)$$

$$\underline{E}_z = 0. \quad (7.314f)$$

With J'_n we denote the derivative of the ordinary Bessel function of the first kind with respect to the argument. At the perfectly conducting waveguide wall the tangential component of the electric field must vanish at $r = a$ (i.e., $\underline{E}_\phi|_{r=a} = 0$ and $\underline{E}_z|_{r=a} = 0$). From this it follows for the TM and TE modes:

Table 7.4: The m th Roots for $J_n(x)$ and m th Roots for $J'_n(x)$

ξ_{nm} :				ξ'_{nm} :			
n	$m = 1$	$m = 2$	$m = 3$	n	$m = 1$	$m = 2$	$m = 3$
0	2.405	5.520	8.654	0	3.832	7.016	10.173
1	3.832	7.016	10.173	1	1.840	5.330	8.540
2	5.135	8.417	11.620	2	3.054	6.706	9.969

TM modes

$$J_n(k_c a) = 0, \quad (7.315a)$$

$$J'_n(k_c a) = 0, \quad (7.316a)$$

TE modes

$$(k_c)_{nm} = \xi_{nm} a^{-1}, \quad (7.315b)$$

$$(k_c)_{nm} = \xi'_{nm} a^{-1}. \quad (7.316b)$$

For the transverse magnetic modes the Bessel function J_n for $r = a$ must be zero, whereas for transverse electric modes the derivative of the Bessel function J'_n must be zero at $r = a$. The m th zero of J_n is denoted with ξ_{nm} , and the m th zero of J'_n is denoted with ξ'_{nm} . The lowest-order zeros ξ_{nm} and ξ'_{nm} are listed in Table 7.4.

The k_c are determined by the conditions (7.315a) and (7.316a), respectively. According to (7.302) we obtain the phase coefficient β of the waveguide wave.

$$\beta = \sqrt{\beta_0^2 - k_c^2}. \quad (7.317)$$

With the free-space wavelength $\lambda_0 = 2\pi/\beta_0$, the guide wavelength $\lambda_g = 2\pi/\beta$ and the cutoff wavelength $\lambda_c = 2\pi/k_c$ it follows that

$$\lambda_g = \frac{\lambda_0}{\sqrt{1 - \left(\frac{\lambda_0}{\lambda_c}\right)^2}}. \quad (7.318)$$

This equation is identical with (7.234) for the guide with rectangular cross-section. A waveguide mode only can propagate, if $\lambda_0 < \lambda_c$. From (7.315b), (7.316b) and $\lambda_c = 2\pi/k_c$ we obtain the cutoff wavelength

$$\text{TM modes: } (\lambda_c)_{mn} = \frac{2\pi a}{\xi_{nm}}, \quad (7.319a)$$

$$\text{TE modes: } (\lambda_c)_{mn} = \frac{2\pi a}{\xi'_{nm}}. \quad (7.319b)$$

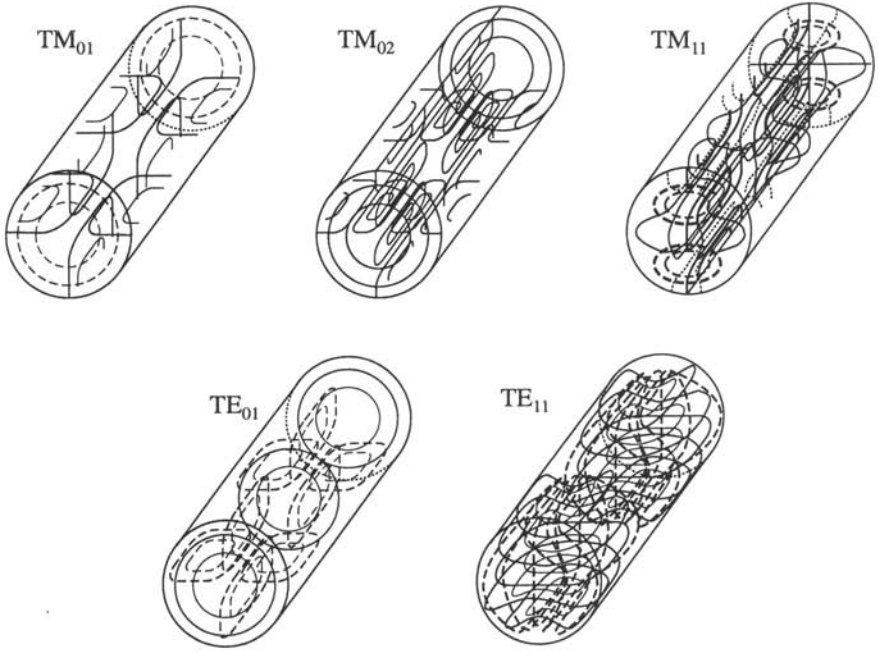


Figure 7.27: Field distribution of some waveguide modes of waveguides with a circular cross-section.

The wave impedances Z_{TM} and Z_{TE} follow from (7.313a) to (7.314e) and (7.317) to (7.318)

$$\text{TM modes: } Z_{\text{TM}} = \frac{E_r}{H_\phi} = -\frac{E_\phi}{H_r} = \frac{\beta}{\omega\epsilon_0} = Z_{F0} \sqrt{1 - \left(\frac{\lambda_0}{\lambda_c}\right)^2}, \quad (7.320a)$$

$$\text{TE modes: } Z_{\text{TE}} = \frac{E_r}{H_\phi} = -\frac{E_\phi}{H_r} = \frac{\omega\mu_0}{\beta} = \frac{Z_{F0}}{\sqrt{1 - \left(\frac{\lambda_0}{\lambda_c}\right)^2}}. \quad (7.320b)$$

Therefore (7.242) and (7.249) are valid also for circular waveguides. Furthermore the generalization (7.243) and (7.250) is valid, since \mathbf{e}_r , \mathbf{e}_ϕ and \mathbf{e}_z form a right-handed orthonormal frame.

The field lines of the most important modes are shown in Figure 7.27. The data of some standardized waveguides is presented in Table 7.5. A relative frequency range for single-mode operation in the case of cylindric waveguides is smaller than that for rectangular waveguides. For circular waveguides the TE_{0m} modes are of special interest since the attenuation of these modes decreases with increasing frequency. From (7.314a) to (7.314f) we obtain for the TE_{0m} modes the following field distribution:

Table 7.5: Data of Standardized Circular Waveguides.

Type	Cutoff Frequencies		Dimension $2a$ [mm]	Attenuation of TE_{11} mode		
	TE_{11} f_c [GHz]	TM_{01} f_c [GHz]		$1.2 \cdot f_c$ [GHz]	$\sigma_{cu} = 5.8 \cdot 10^7$ S/m	α [dB/m]
					Theor.	max accept.
C 3.3	0.27	0.35	647.9	0.325	0.00067	0.0009
C 6.2	0.51	0.66	345.1	0.611	0.00174	0.0023
C 12	0.96	1.25	183.77	1.147	0.00447	0.0058
C 25	2.1	2.74	83.6	2.521	0.014	0.018
C 48	3.95	5.16	44.45	4.74	0.0375	0.049
C 104	8.68	11.3	20.244	10.42	0.122	0.15
C 255	21.1	27.5	8.33	25.31	0.462	–
C 495	40.2	52.5	4.369	48.26	1.211	–
C 890	73.6	96.1	2.388	88.3	3.011	–

$$\underline{E}_r = 0, \quad (7.321a)$$

$$\underline{E}_\phi = j\omega\mu_0 k_c A J'_0(k_c r) e^{-j\beta z}, \quad (7.321b)$$

$$\underline{E}_z = 0, \quad (7.321c)$$

$$\underline{H}_r = -j\beta k_c A J'_0(k_c r) e^{-j\beta z}, \quad (7.321d)$$

$$\underline{H}_\phi = 0, \quad (7.321e)$$

$$\underline{H}_z = k_c^2 A J_0(k_c r) e^{-j\beta z}. \quad (7.321f)$$

Figure 7.27 shows the field distribution of some waveguide modes of waveguides with circular cross-section.

7.10.2 Power Flow and Attenuation in the TE_{01} Mode

We determine the active power flowing through the waveguide as the real part of the integral of the complex Poynting differential form over the waveguide cross-section. For the TE_{01} mode it follows from (4.19), (7.320b) and (7.321a)–(7.321d):

$$T_z = -\frac{1}{2} \underline{E}_\phi \underline{H}_r^* = \frac{1}{2} Z_{\text{TE}} |\underline{H}_r|^2 = \frac{1}{2} Z_{\text{TE}} \beta^2 k_c^2 |A|^2 J_0'^2(k_c r). \quad (7.322)$$

Since the z -component of the complex Poynting vector only depends on r , the active power P flowing through the waveguide is given by

$$P = 2\pi \Re \left\{ \int_0^a r T_z(r) dr \right\}. \quad (7.323)$$

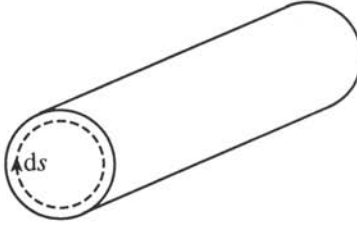


Figure 7.28: Path of integration.

After insertion of (7.322) we obtain

$$P = \pi Z_{\text{TE}} \beta^2 k_c^2 |A|^2 \int_0^a r J_0'^2(k_c r) dr. \quad (7.324)$$

With (B.27) we obtain from this

$$P = \frac{1}{2} \pi Z_{\text{TE}} \beta^2 |A|^2 (k_c a)^2 J_0^2(k_c a). \quad (7.325)$$

With $\xi'_{01} = 3.83$ it follows that

$$\frac{1}{2} \pi (k_c a)^2 J_0^2(k_c a) = 3.74 \quad (7.326)$$

and with this

$$P = 3.74 Z_{\text{TE}} \beta^2 |A|^2. \quad (7.327)$$

The conductor losses per unit of length P'_L are calculated with (7.278). The integration is performed over the boundary ∂A of the waveguide cross-section A according to Figure 7.28. Since \underline{H}_z is independent from ϕ it follows that

$$P'_L = \frac{1}{2} R_A \oint_{\partial A} |\underline{H}_z|^2 ds = \pi a R_A |\underline{H}_z|^2 \Big|_{r=a}. \quad (7.328)$$

After inserting (7.321f) we obtain the current losses per unit of length

$$P'_L = \pi a R_A k_c^4 |A|^2 J_0^2(k_c a). \quad (7.329)$$

The attenuation coefficient alpha follows from (7.277):

$$\alpha = \frac{-1}{2P} \frac{dP}{dz} = \frac{P'_L}{2P} = \frac{R_A k_c^2}{Z_{\text{TE}} \beta^2 a}. \quad (7.330)$$

Using (7.302), (7.318), (7.320b), $\lambda_c = 2\pi/k_c$ and $\lambda_0 = 2\pi/\beta_0$ we obtain from this

$$\alpha = \frac{R_A}{Z_{F0} a} \frac{\left(\frac{\lambda_0}{\lambda_c}\right)^2}{\sqrt{1 - \left(\frac{\lambda_0}{\lambda_c}\right)^2}}. \quad (7.331)$$

We see that for $\lambda_0 \ll \lambda_c$ the attenuation coefficient α is proportional to $\lambda_0^{3/2}$. The decrease of attenuation with increasing frequency in the TE_{01} mode has the following reason. Since according to (7.321e) the ϕ -component of the magnetic field vanishes, the wall currents and therewith the wall current losses are only due to the longitudinal magnetic field component H_z . The ratio of the longitudinal magnetic field component H_z to the transverse magnetic field decreases according to $1/f$. The transmitted power is proportional to the square of the magnitude of the transverse field. The wall current losses are proportional to the square of the magnitude longitudinal field. For a frequency-independent surface resistance R_A , therefore the losses would decrease with increasing frequency according to $1/f^2$. Taking into consideration the skin effect, according to (6.54) the surface resistance R_A increases with $f^{1/2}$, and considering both effects we obtain a total frequency dependence of the losses proportional to $1/f^{3/2}$.

This holds for all TE_{0n} modes of the circular waveguide, since in these cases according to (7.321e) we obtain $H_\phi = 0$. The TE_{01} mode is the most interesting mode here, since it exhibits the lowest cutoff frequency of all TE_{0n} modes. However, if this mode will be used for low-attenuation signal transmission it has to be considered that the TE_{01} mode is not the fundamental mode. Also, if the mode is used at higher frequencies, a number of higher-order modes may also be excited at these frequencies in principle, and therefore it is necessary to take care that only the TE_{01} mode will be excited. Inhomogeneities and perturbations in the waveguide have to be avoided in order to obtain mode conversion. It has to be considered that the TM_{11} mode exhibits the same cutoff frequency as the TE_{01} mode. Therefore both modes have the same guide wavelength at the same frequency. This is called *mode degeneration*. Mode degeneration may yield to mode coupling even in the case of small inhomogeneities of the waveguide.

7.11 RADIAL WAVEGUIDES

7.11.1 Radial Parallel Plate Waveguide

In a *radial waveguide* electromagnetic waves propagate in $\pm\rho$ -direction. Figure 7.29 shows a *radial parallel plate waveguide* formed by two circular disks with inner diameter ρ_1 and outer diameter ρ_2 . The disks are in distance h . In Section 3.9 we have calculated the circular cylindric TE^z modes and TM^z that are transverse electric and transverse magnetic with respect to the z -direction. We will obtain the modal field functions of the

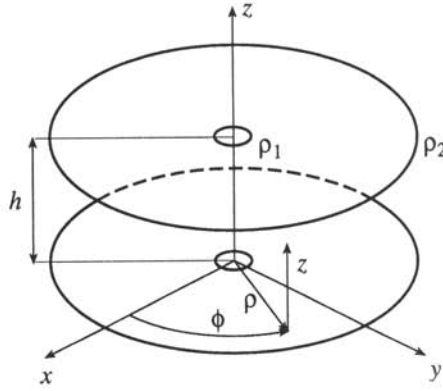


Figure 7.29: Radial parallel plate waveguide.

radial parallel plate waveguide by matching these solutions to the boundary conditions of this waveguide. In this way we will obtain two sets of solutions that are transverse electric or transverse magnetic with respect to the z -direction.

The TE^z modes we obtain from (3.221a) to (3.221f) considering also the waves propagating in negative z -direction. Deriving the wave components for the wave propagating in negative z -direction k_z must be substituted by $-k_z$. In this case (3.221a) and (3.221b) change the sign and we obtain

$$\text{TE}^z: \quad \underline{H}_\rho = -j k_z k_\rho C'_m(k_\rho \rho) \cos m\phi \left(\underline{A}^{(+z)} e^{-j k_z z} - \underline{A}^{(-z)} e^{j k_z z} \right), \quad (7.332a)$$

$$\underline{H}_\phi = j k_z \frac{m}{\rho} C_m(k_\rho \rho) \sin m\phi \left(\underline{A}^{(+z)} e^{-j k_z z} - \underline{A}^{(-z)} e^{j k_z z} \right), \quad (7.332b)$$

$$\underline{H}_z = k_\rho^2 C_m(k_\rho \rho) \cos m\phi \left(\underline{A}^{(+z)} e^{-j k_z z} + \underline{A}^{(-z)} e^{j k_z z} \right), \quad (7.332c)$$

$$\underline{E}_\rho = j \omega \mu_0 \frac{m}{\rho} C_m(k_\rho \rho) \sin m\phi \left(\underline{A}^{(+z)} e^{-j k_z z} + \underline{A}^{(-z)} e^{j k_z z} \right), \quad (7.332d)$$

$$\underline{E}_\phi = j \omega \mu_0 k_\rho C'_m(k_\rho \rho) \cos m\phi \left(\underline{A}^{(+z)} e^{-j k_z z} + \underline{A}^{(-z)} e^{j k_z z} \right), \quad (7.332e)$$

$$\underline{E}_z = 0. \quad (7.332f)$$

With C'_n we denote the derivative of the Bessel function C_n with respect to the argument. To satisfy the boundary conditions at the metallic plates \underline{E}_ρ and \underline{E}_ϕ must vanish at $z = 0$ and at $z = h$. The first condition yields $\underline{A}^{(-z)} = -\underline{A}^{(+z)}$ and the second condition requires $k_z = n\pi/h$ with integer n . We replace $\frac{1}{2}\underline{A}^{(+z)} = -\frac{1}{2}\underline{A}^{(-z)}$ by the amplitudes $\underline{A}^{(+)}$ and $\underline{A}^{(-)}$ of the wave propagating in positive and negative ρ -direction. For a wave propagating in positive ρ -direction $C_m(k_\rho \rho)$ is given by $H_m^{(2)}(k_\rho \rho)$ and for a

wave propagating in negative ρ -direction the radial dependence of the wave is given by $H_m^{(1)}(k_\rho \rho)$. Hence we obtain for a wave propagating in positive and negative ρ -directions

$$\text{TE}^z : \underline{H}_\rho = -j k_z k_\rho \left(\underline{A}^{(+)} H_m^{(2)'}(k_\rho \rho) + \underline{A}^{(-)} H_m^{(1)'}(k_\rho \rho) \right) \cos m\phi \cos \frac{n\pi z}{h}, \quad (7.333a)$$

$$\underline{H}_\phi = j k_z \frac{m}{\rho} \left(\underline{A}^{(+)} H_m^{(2)}(k_\rho \rho) + \underline{A}^{(-)} H_m^{(1)}(k_\rho \rho) \right) \sin m\phi \cos \frac{n\pi z}{h}, \quad (7.333b)$$

$$\underline{H}_z = -j k_\rho^2 \left(\underline{A}^{(+)} H_m^{(2)}(k_\rho \rho) - \underline{A}^{(-)} H_m^{(1)}(k_\rho \rho) \right) \cos m\phi \sin \frac{n\pi z}{h}, \quad (7.333c)$$

$$\underline{E}_\rho = \omega \mu_0 \frac{m}{\rho} \left(\underline{A}^{(+)} H_m^{(2)}(k_\rho \rho) - \underline{A}^{(-)} H_m^{(1)}(k_\rho \rho) \right) \sin m\phi \sin \frac{n\pi z}{h}, \quad (7.333d)$$

$$\underline{E}_\phi = \omega \mu_0 k_\rho \left(\underline{A}^{(+)} H_m^{(2)'}(k_\rho \rho) - \underline{A}^{(-)} H_m^{(1)'}(k_\rho \rho) \right) \cos m\phi \sin \frac{n\pi z}{h}, \quad (7.333e)$$

$$\underline{E}_z = 0. \quad (7.333f)$$

From (3.217) we obtain the radial wave number

$$k_\rho = \sqrt{k_0^2 - k_{c,n}^2} \quad (7.334)$$

with

$$k_{c,n} = \frac{n\pi}{h}. \quad (7.335)$$

The corresponding cutoff frequency is

$$f_{c,n} = \frac{n}{2h\sqrt{\epsilon_r \mu}}. \quad (7.336)$$

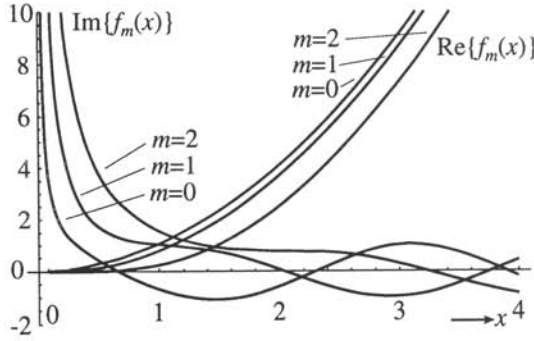
The guide wavelength λ_g of the radial waveguide as in (7.232) is given by

$$\lambda_g = \frac{1}{\sqrt{\epsilon_r \mu_r}} \frac{\lambda_0}{\sqrt{1 - \left(\frac{\lambda_0}{\lambda_{c,n}} \right)^2}} \quad (7.337)$$

with the cutoff wavelength for the TM^z modes given by

$$\lambda_{c,n} = \frac{2h}{n} \sqrt{\epsilon_r \mu_r}. \quad (7.338)$$

For the radial transmission the wave impedance is defined as the ratio of electric and magnetic field components transverse to the direction of propagation. The wave impedance of the radial transmission-line depends on ρ and also is different for the

Figure 7.30: The function $f_m(x)$ for $m = 0, 1, 2$.

waves propagating in positive and negative ρ -directions. The wave impedance $Z_{\text{TE}}^{(+)}(\rho)$ of the wave propagating in positive ρ -direction is given by

$$Z_{\text{TE}}^{(+)}(\rho) = \frac{\underline{E}_{\phi}^{(+)}}{\underline{H}_z^{(+)}} = j Z_{F0} \frac{k_0}{k_{\rho}} \frac{H_m^{(2)'}(k_{\rho}\rho)}{H_m^{(2)}(k_{\rho}\rho)} = j \frac{H_m^{(2)'}(k_{\rho}\rho)}{H_m^{(2)}(k_{\rho}\rho)} \frac{Z_{F0}}{\sqrt{1 - \left(\frac{\lambda_0}{\lambda_c}\right)^2}}. \quad (7.339)$$

With $\underline{E}_{\phi}^{(+)}, \underline{H}_z^{(+)}$ and $\underline{E}_{\phi}^{(-)}, \underline{H}_z^{(-)}$ we denote the electric and magnetic field components of the waves propagating in positive or negative ρ -direction only. The wave impedance $Z_{\text{TE}}^{(-)}(\rho)$ of the wave propagating in negative ρ -direction is

$$Z_{\text{TE}}^{(-)}(\rho) = -\frac{\underline{E}_{\phi}^{(-)}}{\underline{H}_z^{(-)}} = -j Z_{F0} \frac{k_0}{k_{\rho}} \frac{H_m^{(1)'}(k_{\rho}\rho)}{H_m^{(1)}(k_{\rho}\rho)} = -j \frac{H_m^{(1)'}(k_{\rho}\rho)}{H_m^{(1)}(k_{\rho}\rho)} \frac{Z_{F0}}{\sqrt{1 - \left(\frac{\lambda_0}{\lambda_c}\right)^2}}. \quad (7.340)$$

With (B.7a) and (B.8b) we obtain from (7.339) and (7.340)

$$Z_{\text{TE}}^{(-)}(\rho) = Z_{\text{TE}}^{(+)*}(\rho). \quad (7.341)$$

This result is not surprising and reveals that the segments in a chain of radial waveguides with equal h are matched to each other if both ends of the chain are terminated reflection-free.

Inserting (B.6a) and (B.6b) into (7.339) and considering (B.12b) we can separate $Z_{\text{TE}}^{(+)}(\rho)$ into real and imaginary parts, hence

$$Z_{\text{TE}}^{(+)}(\rho) = Z_{F0} \frac{k_0}{k_{\rho}} f_m(k_{\rho}\rho) \quad (7.342)$$

with $f_m(x)$ given by

$$f_m(x) = \frac{\frac{2}{\pi x} + j [J_m(x)J'_m(x) + Y_m(x)Y'_m(x)]}{J_m(x)^2 + Y_m(x)^2}. \quad (7.343)$$

The function $f_m(x)$ is plotted in Figure 7.30 for $m = 0, 1, 2$ and in Figure 7.31 for $m = 0, 10, 20, 30$. The cutoff frequency does not depend on the azimuthal wave number $f_{c,v}$ defined in (7.336). For $k_\rho \rho \ll n$ the electromagnetic field's behaviour is evanescent with a predominant imaginary part of the wave impedance, whereas the wave for $k_\rho \rho > n$ is oscillatory with predominantly real wave impedance.

The TE_{0n}^z modes exhibit rotational symmetry with respect to the z -axis. Using (B.10) we obtain

$$\text{TE}_{0n}^z: \quad \underline{H}_\rho = j k_z k_\rho \left(\underline{A}^{(+)} H_1^{(2)}(k_\rho \rho) + \underline{A}^{(-)} H_1^{(1)}(k_\rho \rho) \right) \cos \frac{n\pi z}{h}, \quad (7.344a)$$

$$\underline{H}_z = -j k_\rho^2 \left(\underline{A}^{(+)} H_0^{(2)}(k_\rho \rho) - \underline{A}^{(-)} H_0^{(1)}(k_\rho \rho) \right) \sin \frac{n\pi z}{h}, \quad (7.344b)$$

$$\underline{E}_\phi = -\omega \mu_0 k_\rho \left(\underline{A}^{(+)} H_1^{(2)}(k_\rho \rho) - \underline{A}^{(-)} H_1^{(1)}(k_\rho \rho) \right) \sin \frac{n\pi z}{h}. \quad (7.344c)$$

The TE_{0n}^z modes exhibit no \underline{H}_ϕ -, \underline{E}_ρ - or \underline{E}_z -components.

The TM^z modes are transverse magnetic with respect to the z -direction. We obtain these modes from (3.222a) to (3.222f), hence

$$\text{TM}^z: \quad \underline{E}_\rho = -j k_z k_\rho C'_m(k_\rho \rho) \cos m\phi \left(B^{(+z)} e^{-j k_z z} - B^{(-z)} e^{j k_z z} \right), \quad (7.345a)$$

$$\underline{E}_\phi = j k_z \frac{m}{\rho} C_m(k_\rho \rho) \sin m\phi \left(B^{(+z)} e^{-j k_z z} - B^{(-z)} e^{j k_z z} \right), \quad (7.345b)$$

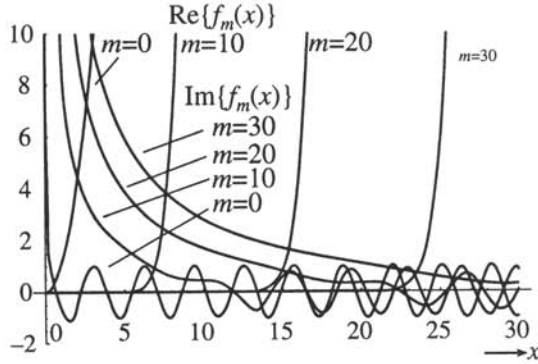
$$\underline{E}_z = k_\rho^2 C_m(k_\rho \rho) \cos m\phi \left(B^{(+z)} e^{-j k_z z} + B^{(-z)} e^{j k_z z} \right), \quad (7.345c)$$

$$\underline{H}_\rho = -j \omega \epsilon_0 \frac{m}{\rho} C_m(k_\rho \rho) \sin m\phi \left(B^{(+z)} e^{-j k_z z} + B^{(-z)} e^{j k_z z} \right), \quad (7.345d)$$

$$\underline{H}_\phi = -j \omega \epsilon_0 k_\rho C'_m(k_\rho \rho) \cos m\phi \left(B^{(+z)} e^{-j k_z z} + B^{(-z)} e^{j k_z z} \right), \quad (7.345e)$$

$$\underline{H}_z = 0. \quad (7.345f)$$

The boundary conditions at the metallic discs require that \underline{E}_ρ and \underline{E}_ϕ vanish at $z = 0$ and at $z = h$, hence yield $B^{(-z)} = B^{(+z)}$ and $k_z = n\pi/h$ with integer h . Replacing $\frac{1}{2}B^{(+z)} = \frac{1}{2}B^{(-z)}$ by the amplitudes $B^{(+)}$ and $B^{(-)}$ of the wave propagating in positive and negative ρ -directions and taking $H_m^{(2)}(k_\rho \rho)$ and $H_m^{(1)}(k_\rho \rho)$ for the waves propagating in positive

Figure 7.31: The function $f_m(x)$ for $m = 0, 10, 20, 30$.

and negative ρ -directions yields

TM_{mn}^z :

$$\underline{E}_\rho = -k_z k_\rho \left(\underline{B}^{(+)} H_m^{(2)'}(k_\rho \rho) + \underline{B}^{(-)} H_m^{(1)'}(k_\rho \rho) \right) \cos m\phi \sin \frac{n\pi z}{h}, \quad (7.346a)$$

$$\underline{E}_\phi = k_z \frac{m}{\rho} \left(\underline{B}^{(+)} H_m^{(2)}(k_\rho \rho) + \underline{B}^{(-)} H_m^{(1)}(k_\rho \rho) \right) \sin m\phi \sin \frac{n\pi z}{h}, \quad (7.346b)$$

$$\underline{E}_z = k_\rho^2 \left(\underline{B}^{(+)} H_m^{(2)}(k_\rho \rho) + \underline{B}^{(-)} H_m^{(1)}(k_\rho \rho) \right) \cos m\phi \cos \frac{n\pi z}{h}, \quad (7.346c)$$

$$\underline{H}_\rho = -j\omega\epsilon_0 \frac{m}{\rho} \left(\underline{B}^{(+)} H_m^{(2)}(k_\rho \rho) + \underline{B}^{(-)} H_m^{(1)}(k_\rho \rho) \right) \sin m\phi \cos \frac{n\pi z}{h}, \quad (7.346d)$$

$$\underline{H}_\phi = -j\omega\epsilon_0 k_\rho \left(\underline{B}^{(+)} H_m^{(2)'}(k_\rho \rho) + \underline{B}^{(-)} H_m^{(1)'}(k_\rho \rho) \right) \cos m\phi \cos \frac{n\pi z}{h}, \quad (7.346e)$$

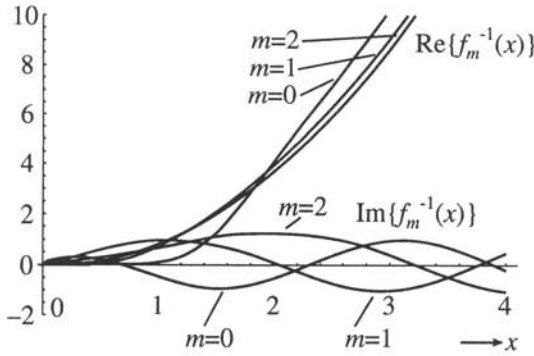
$$\underline{H}_z = 0. \quad (7.346f)$$

The wave impedance $Z_{\text{TM}}^{(+)}$ is given by

$$Z_{\text{TM}}^{(+)} = -\frac{\underline{E}_z}{\underline{H}_\phi} = -jZ_{F0} \frac{k_\rho}{k_0} \frac{H_m^{(2)}(k_\rho \rho)}{H_m^{(2)'}(k_\rho \rho)} = -jZ_{F0} \frac{H_m^{(2)}(k_\rho \rho)}{H_m^{(2)'}(k_\rho \rho)} \sqrt{1 - \left(\frac{\lambda_0}{\lambda_c}\right)^2}. \quad (7.347)$$

Inserting (B.6a) and (B.6b) into (7.347) and considering (B.12b) we obtain

$$Z_{\text{TM}}^{(+)}(\rho) = Z_{F0} \frac{k_\rho}{k_0} f_m^{-1}(k_\rho \rho) \quad (7.348)$$

Figure 7.32: The function $f_m^{-1}(x)$.

with $f_m^{-1}(x)$ given by

$$f_m^{-1}(x) = \frac{\frac{2}{\pi x} - j [J_m(x)J'_m(x) + Y_m(x)Y'_m(x)]}{J_m(x)^2 + Y_m(x)^2}. \quad (7.349)$$

Figure 7.32 shows plots of $f_m^{-1}(x)$ for $m = 0, 1, 2$. The rotationally symmetric modes TE_{0n}^z exhibit no \underline{E}_ϕ -, \underline{H}_ρ -, and \underline{H}_z -components. Their field components are given by

$$\text{TM}_{0n}^z: \quad \underline{E}_\rho = k_z k_\rho \left(\underline{B}^{(+)} H_1^{(2)}(k_\rho \rho) + \underline{B}^{(-)} H_1^{(1)}(k_\rho \rho) \right) \sin \frac{n\pi z}{h}, \quad (7.350a)$$

$$\underline{E}_z = k_\rho^2 \left(\underline{B}^{(+)} H_0^{(2)}(k_\rho \rho) + \underline{B}^{(-)} H_0^{(1)}(k_\rho \rho) \right) \cos \frac{n\pi z}{h}, \quad (7.350b)$$

$$\underline{H}_\phi = j \omega \epsilon_0 k_\rho \left(\underline{B}^{(+)} H_1^{(2)}(k_\rho \rho) + \underline{B}^{(-)} H_1^{(1)}(k_\rho \rho) \right) \cos \frac{n\pi z}{h}. \quad (7.350c)$$

The TM_{m0}^z modes are uniform in z -direction and exhibit no lower cutoff frequency. Their field components are

$$\text{TM}_{m0}^z: \quad \underline{E}_z = k_\rho^2 \left(\underline{B}^{(+)} H_m^{(2)}(k_\rho \rho) + \underline{B}^{(-)} H_m^{(1)}(k_\rho \rho) \right) \cos m\phi, \quad (7.351a)$$

$$\underline{H}_\rho = -j \omega \epsilon_0 \frac{m}{\rho} \left(\underline{B}^{(+)} H_m^{(2)}(k_\rho \rho) + \underline{B}^{(-)} H_m^{(1)}(k_\rho \rho) \right) \sin m\phi, \quad (7.351b)$$

$$\underline{H}_\phi = -j \omega \epsilon_0 k_\rho \left(\underline{B}^{(+)} H_m^{(2)'}(k_\rho \rho) + \underline{B}^{(-)} H_m^{(1)'}(k_\rho \rho) \right) \cos m\phi. \quad (7.351c)$$

The TM_{m0}^z modes exhibit no cutoff frequency. The wave impedance is given by

$$Z_{\text{TM}}^{(+)} = -\frac{\underline{E}_z}{\underline{H}_\phi} = -j Z_{F0} \frac{H_m^{(2)}(k_\rho \rho)}{H_m^{(2)'}(k_\rho \rho)}. \quad (7.352)$$

The TM_{00}^z mode is transverse electromagnetic with respect to the ρ -direction (i.e., TEM_{00}^p).

$$\text{TM}_{00}^z : \quad \underline{E}_z = k_\rho^2 \underline{B} H_0^{(2)}(k_\rho \rho), \quad (7.353a)$$

$$\underline{H}_\phi = j \omega \epsilon_0 k_\rho \underline{B} H_1^{(2)}(k_\rho \rho). \quad (7.353b)$$

The wave impedance is

$$Z_{\text{TM}}^{(+)} = -\frac{\underline{E}_z}{\underline{H}_\phi} = -j Z_{F0} \frac{H_0^{(2)}(k_\rho \rho)}{H_1^{(2)}(k_\rho \rho)}. \quad (7.354)$$

7.11.2 Wedged Radial Parallel Plate Waveguide

The *wedged radial waveguide* as depicted in Figure 7.33 is bounded by conducting surfaces at $z = 0$, $z = h$, $\phi = 0$ and $\phi = \phi_0$. Following the procedure as for deriving (7.332a) to (7.332f) in the previous section we obtain for the field $\text{TE}_{\nu_m n}^z$ modes the field components

$\text{TE}_{\nu_m n}^z :$

$$\underline{H}_\rho = -j k_z k_\rho \left(\underline{A}^{(+)} H_{\nu_m}^{(2)'}(k_\rho \rho) + \underline{A}^{(-)} H_{\nu_m}^{(1)'}(k_\rho \rho) \right) \cos \nu_m \phi \cos \frac{n\pi z}{h}, \quad (7.355a)$$

$$\underline{H}_\phi = j k_z \frac{\nu_m}{\rho} \left(\underline{A}^{(+)} H_{\nu_m}^{(2)}(k_\rho \rho) + \underline{A}^{(-)} H_{\nu_m}^{(1)}(k_\rho \rho) \right) \sin \nu_m \phi \cos \frac{n\pi z}{h}, \quad (7.355b)$$

$$\underline{H}_z = -j k_\rho^2 \left(\underline{A}^{(+)} H_{\nu_m}^{(2)}(k_\rho \rho) - \underline{A}^{(-)} H_{\nu_m}^{(1)}(k_\rho \rho) \right) \cos \nu_m \phi \sin \frac{n\pi z}{h}, \quad (7.355c)$$

$$\underline{E}_\rho = \omega \mu_0 \frac{\nu_m}{\rho} \left(\underline{A}^{(+)} H_{\nu_m}^{(2)}(k_\rho \rho) - \underline{A}^{(-)} H_{\nu_m}^{(1)}(k_\rho \rho) \right) \sin \nu_m \phi \sin \frac{n\pi z}{h}, \quad (7.355d)$$

$$\underline{E}_\phi = \omega \mu_0 k_\rho \left(\underline{A}^{(+)} H_{\nu_m}^{(2)'}(k_\rho \rho) - \underline{A}^{(-)} H_{\nu_m}^{(1)'}(k_\rho \rho) \right) \cos \nu_m \phi \sin \frac{n\pi z}{h}, \quad (7.355e)$$

$$\underline{E}_z = 0. \quad (7.355f)$$

In order to satisfy the boundary conditions, fractional order Hankel functions $H_{\nu_m}^{(2)}(k_\rho \rho)$ and $H_{\nu_m}^{(1)}(k_\rho \rho)$ are used here. The order ν_m of the Hankel functions is given by

$$\nu_m = \frac{m\pi}{\phi_0}. \quad (7.356)$$

Using (3.217) we obtain the radial wave number

$$k_\rho = \sqrt{k_0^2 - k_{c,n}^2} \quad (7.357)$$

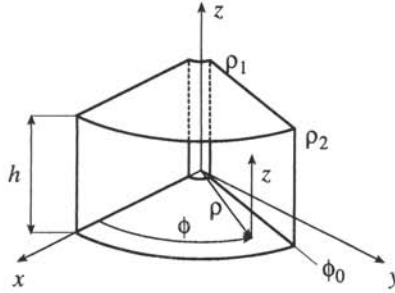


Figure 7.33: Wedged radial parallel plate waveguide.

with the cutoff wave number

$$k_{c,n} = \frac{n\pi}{h}. \quad (7.358)$$

From this we get the cutoff frequency

$$f_{c,n} = \frac{n}{2h\sqrt{\epsilon\mu}}. \quad (7.359)$$

The characteristic impedances $Z_{TE}^{(+)}(\rho)$ and $Z_{TE}^{(-)}(\rho)$ are derived in the same way as (7.339) and (7.340). We only have to replace m by ν_m , hence

$$Z_{TE}^{(+)}(\rho) = Z_{TE}^{(-)*}(\rho) = jZ_{F0} \frac{k_0}{k_\rho} \frac{H_{\nu_m}^{(2)'}(k_\rho \rho)}{H_{\nu_m}^{(2)}(k_\rho \rho)}. \quad (7.360)$$

In analogy to (7.342) we find

$$Z_{TE}^{(+)}(\rho) = Z_{F0} \frac{k_0}{k_\rho} f_{\nu_m}(k_\rho \rho) \quad (7.361)$$

with $f_{\nu_m}(x)$ given by

$$f_{\nu_m}(x) = \frac{2}{\pi x} + j \frac{[J_{\nu_m}(x)J'_{\nu_m}(x) + Y_{\nu_m}(x)Y'_{\nu_m}(x)]}{J_{\nu_m}(x)^2 + Y_{\nu_m}(x)^2}. \quad (7.362)$$

To obtain the $TM_{\nu_m n}^z$ modes of the wedged radial waveguide we rotate the radial modes (7.346a) to (7.346f) by $\frac{1}{2}\pi$ around the z -axis in order to satisfy the boundary conditions at $\phi = 0$. This is done by the substitutions $\sin \nu_m \phi \rightarrow \cos \nu_m \phi$ and $\cos \nu_m \phi \rightarrow -\sin \nu_m \phi$.

Furthermore, to fulfill the boundary conditions at $\phi = \phi_0$ we use fractional order Hankel functions with order ν_m given by (7.356). This yields

$\text{TM}_{\nu_m n}^z :$

$$\underline{E}_\rho = k_z k_\rho \left(\underline{B}^{(+)} H_{\nu_m}^{(2)'}(k_\rho \rho) + \underline{B}^{(-)} H_{\nu_m}^{(1)'}(k_\rho \rho) \right) \sin \nu_m \phi \sin \frac{n\pi z}{h}, \quad (7.363a)$$

$$\underline{E}_\phi = k_z \frac{\nu_m}{\rho} \left(\underline{B}^{(+)} H_{\nu_m}^{(2)}(k_\rho \rho) + \underline{B}^{(-)} H_{\nu_m}^{(1)}(k_\rho \rho) \right) \cos \nu_m \phi \sin \frac{n\pi z}{h}, \quad (7.363b)$$

$$\underline{E}_z = -k_\rho^2 \left(\underline{B}^{(+)} H_{\nu_m}^{(2)}(k_\rho \rho) + \underline{B}^{(-)} H_{\nu_m}^{(1)}(k_\rho \rho) \right) \sin \nu_m \phi \cos \frac{n\pi z}{h}, \quad (7.363c)$$

$$\underline{H}_\rho = -j \omega \epsilon_0 \frac{\nu_m}{\rho} \left(\underline{B}^{(+)} H_{\nu_m}^{(2)}(k_\rho \rho) + \underline{B}^{(-)} H_{\nu_m}^{(1)}(k_\rho \rho) \right) \cos \nu_m \phi \cos \frac{n\pi z}{h}, \quad (7.363d)$$

$$\underline{H}_\phi = j \omega \epsilon_0 k_\rho \left(\underline{B}^{(+)} H_{\nu_m}^{(2)'}(k_\rho \rho) + \underline{B}^{(-)} H_{\nu_m}^{(1)'}(k_\rho \rho) \right) \sin \nu_m \phi \cos \frac{n\pi z}{h}, \quad (7.363e)$$

$$\underline{H}_z = 0. \quad (7.363f)$$

Similar to (7.347) the wave impedance is given by

$$Z_{\text{TM}}^{(+)}(\rho) = Z_{\text{TM}}^{(-)*}(\rho) = -j Z_{F0} \frac{k_\rho}{k_0} \frac{H_{\nu_m}^{(2)}(k_\rho \rho)}{H_{\nu_m}^{(2)'}(k_\rho \rho)}. \quad (7.364)$$

As in (7.348) we obtain the wave impedance

$$Z_{\text{TM}}^{(+)}(\rho) = Z_{F0} \frac{k_\rho}{k_0} f_{\nu_m}^{-1}(k_\rho \rho) \quad (7.365)$$

with $f_{\nu_m}^{-1}(x)$ given by

$$f_{\nu_m}^{-1}(x) = \frac{\frac{2}{\pi x} - j [J_{\nu_m}(x) J_{\nu_m}'(x) + Y_{\nu_m}(x) Y_{\nu_m}'(x)]}{J_{\nu_m}'(x)^2 + Y_{\nu_m}'(x)^2}. \quad (7.366)$$

7.12 SPHERICAL WAVEGUIDES

If the walls of a waveguide conform to the spherical coordinate system the waveguide is called a *spherical waveguide*. If the waveguide wall is a cone specified by constant θ these waveguides are *conical waveguides*. Waveguides formed by two cones with the same axis such that the wave is guided between these cones are called *biconical waveguides*. To satisfy the boundary conditions at the conducting walls *fractional degree associated Legendre functions* can be used. For fractional order ν the associated Legendre function $P_\nu^m(x)$ exhibits a pole at $x = -1$. Therefore $P_\nu^m(\cos \theta)$ becomes infinite at $\theta = \pi$ and

$P_v^m(-\cos \theta)$ becomes infinite at $\theta = 0$. Inserting (B.59a) and (B.59b) into the scalar potential $\Psi(r, \theta, \phi)$ introduced in (3.230) and allowing also fractional degree associated Legendre functions we obtain the potential

$$\Psi(r, \theta, \phi) = \underline{A} \begin{Bmatrix} h_v^{(2)}(kr) \\ h_v^{(1)}(kr) \end{Bmatrix} \begin{Bmatrix} \cos m\phi \\ \sin m\phi \end{Bmatrix} \begin{Bmatrix} P_v^m(\cos \theta) \\ P_v^m(-\cos \theta) \end{Bmatrix} \quad (7.367)$$

from which the field components of conical and biconical waveguides may be derived. The *spherical Hankel functions* $h_v^{(1)}(x)$ and $h_v^{(2)}(x)$ are solutions of the differential equation (B.29). The spherical Hankel function of the first kind $h_v^{(1)}(x)$ describes a wave propagating in negative r -direction, whereas the spherical Hankel function of the second kind $h_v^{(2)}(x)$ describes a wave propagating in positive r -direction. Since in the spherical wave solution the order v of the spherical Hankel functions corresponds to the degree of the associated Legendre functions the Hankel functions are of fractional order.

Inserting (7.367) for $\Psi_1(r, \theta, \phi)$ into (3.235a) to (3.235f) yields the TE_{mn} field components

TE_{mn} :

$$\underline{E}_r = 0, \quad (7.368a)$$

$$\underline{E}_\theta = -\underline{A} \frac{m}{\sin \theta} \begin{Bmatrix} h_v^{(2)}(kr) \\ h_v^{(1)}(kr) \end{Bmatrix} \begin{Bmatrix} -\sin m\phi \\ \cos m\phi \end{Bmatrix} \begin{Bmatrix} P_v^m(\cos \theta) \\ P_v^m(-\cos \theta) \end{Bmatrix}, \quad (7.368b)$$

$$\underline{E}_\phi = \underline{A} \begin{Bmatrix} h_v^{(2)}(kr) \\ h_v^{(1)}(kr) \end{Bmatrix} \begin{Bmatrix} \cos m\phi \\ \sin m\phi \end{Bmatrix} \begin{Bmatrix} \frac{dP_v^m(\cos \theta)}{d\theta} \\ \frac{dP_v^m(-\cos \theta)}{d\theta} \end{Bmatrix}, \quad (7.368c)$$

$$\underline{H}_r = \underline{A} \frac{v(v+1)}{j\omega\mu r} \begin{Bmatrix} h_v^{(2)}(kr) \\ h_v^{(1)}(kr) \end{Bmatrix} \begin{Bmatrix} \cos m\phi \\ \sin m\phi \end{Bmatrix} \begin{Bmatrix} P_v^m(\cos \theta) \\ P_v^m(-\cos \theta) \end{Bmatrix}, \quad (7.368d)$$

$$\underline{H}_\theta = \underline{A} \frac{1}{j\omega\mu r} \begin{Bmatrix} \frac{d}{dr}(rh_v^{(2)}(kr)) \\ \frac{d}{dr}(rh_v^{(1)}(kr)) \end{Bmatrix} \begin{Bmatrix} \cos m\phi \\ \sin m\phi \end{Bmatrix} \begin{Bmatrix} \frac{dP_v^m(\cos \theta)}{d\theta} \\ \frac{dP_v^m(-\cos \theta)}{d\theta} \end{Bmatrix}, \quad (7.368e)$$

$$\underline{H}_\phi = \underline{A} \frac{m}{j\omega\mu r \sin \theta} \begin{Bmatrix} \frac{d}{dr}(rh_v^{(2)}(kr)) \\ \frac{d}{dr}(rh_v^{(1)}(kr)) \end{Bmatrix} \begin{Bmatrix} -\sin m\phi \\ \cos m\phi \end{Bmatrix} \begin{Bmatrix} P_v^m(\cos \theta) \\ P_v^m(-\cos \theta) \end{Bmatrix}. \quad (7.368f)$$

Inserting (7.367) for $\Psi_2(r, \theta, \phi)$ into (3.235a) to (3.235f) yields the TM_{mn} field compo-

nents

TM_{mn} :

$$\underline{E}_r = -B \frac{\nu(\nu+1)}{j\omega\epsilon r} \left\{ h_\nu^{(2)}(kr) \right\} \left\{ \cos m\phi \right\} \left\{ \begin{matrix} P_\nu^m(\cos\theta) \\ P_\nu^m(-\cos\theta) \end{matrix} \right\}, \quad (7.369a)$$

$$\underline{E}_\theta = -B \frac{1}{j\omega\epsilon r} \left\{ \frac{d}{dr}(rh_\nu^{(2)}(kr)) \right\} \left\{ \cos m\phi \right\} \left\{ \begin{matrix} \frac{dP_\nu^m(\cos\theta)}{d\theta} \\ \frac{dP_\nu^m(-\cos\theta)}{d\theta} \end{matrix} \right\}, \quad (7.369b)$$

$$\underline{E}_\phi = -B \frac{m}{j\omega\epsilon r \sin\theta} \left\{ \frac{d}{dr}(rh_\nu^{(2)}(kr)) \right\} \left\{ \begin{matrix} -\sin m\phi \\ \cos m\phi \end{matrix} \right\} \left\{ \begin{matrix} P_\nu^m(\cos\theta) \\ P_\nu^m(-\cos\theta) \end{matrix} \right\}, \quad (7.369c)$$

$$\underline{H}_r = 0, \quad (7.369d)$$

$$\underline{H}_\theta = -B \frac{m}{\sin\theta} \left\{ h_\nu^{(2)}(kr) \right\} \left\{ \begin{matrix} -\sin m\phi \\ \cos m\phi \end{matrix} \right\} \left\{ \begin{matrix} P_\nu^m(\cos\theta) \\ P_\nu^m(-\cos\theta) \end{matrix} \right\}, \quad (7.369e)$$

$$\underline{H}_\phi = B \left\{ h_\nu^{(2)}(kr) \right\} \left\{ \cos m\phi \right\} \left\{ \begin{matrix} \frac{dP_\nu^m(\cos\theta)}{d\theta} \\ \frac{dP_\nu^m(-\cos\theta)}{d\theta} \end{matrix} \right\}. \quad (7.369f)$$

Superimposing these field components such that the boundary conditions are fulfilled we can construct the TE_{mn} and TM_{mn} modes of radial waveguides. The partial waves containing $P_\nu^m(\cos\theta)$ and $P_\nu^m(-\cos\theta)$ become infinite for $\theta = 0$ and $\theta = \pi$, respectively. These singularities must be located outside the field region, (i.e., covered by the ideal conductor). For conical waveguides only one of these solutions is used. For biconical waveguides in general both solutions have to be superimposed to satisfy the boundary conditions at both cone surfaces.

7.12.1 Conical Waveguide

The *conical waveguide* is formed by one cone as depicted in Figure 7.34. The TE_{mn} modes and the TM_{mn} modes of the conical waveguide we obtain from (7.368a) to (7.368f) and (7.369a) to (7.369f), respectively, considering the partial waves depending on $P_\nu^m(\cos\theta)$ but omitting the partial waves $P_\nu^m(-\cos\theta)$. At the cone surface the tangential electric field components \underline{E}_r and \underline{E}_θ must vanish. For the TE_{mn} modes together with (7.368b) this yields

$$\left. \frac{dP_\nu^m(\cos\theta)}{d\theta} \right|_{\theta_1} = 0 \quad \text{for } \text{TE}_{mn} \text{ modes}. \quad (7.370)$$

For the TE_{mn} mode the fractional degree ν must be chosen such that the n th zero of the derivative of the associated Legendre function fulfills (7.370). This n th solution of the equation we name ν'_{nm} . For the TM_{mn} modes the boundary conditions $\underline{E}_r = 0$ and

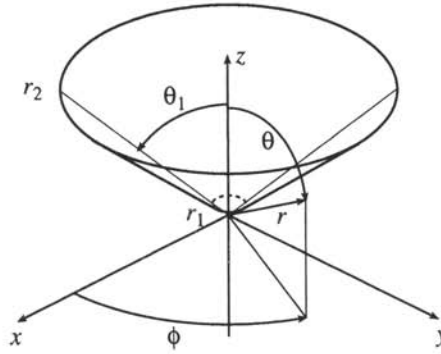


Figure 7.34: Conical waveguide.

$\underline{E}_\phi = 0$ on the cone surface yield

$$P_\nu^m(\cos \theta_1) = 0 \quad \text{for TM}_{mn} \text{ modes.} \quad (7.371)$$

For the TM_{mn} mode the n th zero ν_{nm} of the fractional degree ν of the associated Legendre function fulfills (7.371). In general the zeros of (7.370) and (7.371) with respect to ν'_{nm} and ν_{nm} have to be computed numerically. The conical waveguide modes exhibit no cutoff frequency. However, for small values of $kr < 1$ the modes exhibit evanescent character and show wave character for larger $kr > 1$.

The wave impedance $Z_{\text{TE}}^{(+)}(r)$ of the wave propagating in positive r -direction and $Z_{\text{TE}}^{(-)}(r)$ of the wave propagating in negative r -direction follow from (7.368b), (7.368c), (7.368e) and (7.368f) as

$$Z_{\text{TE}}^{(+)}(r) = -\frac{\underline{E}_\phi^{(+)}}{\underline{H}_\theta^{(+)}} = -\frac{\underline{E}_\theta^{(+)}}{\underline{H}_\phi^{(+)}} = -jkZ_{F0} \frac{r h_{\nu_{mn}}^{(2)}(kr)}{\frac{d}{dr} (r h_{\nu_{mn}}^{(2)}(kr))}, \quad (7.372a)$$

$$Z_{\text{TE}}^{(-)}(r) = \frac{\underline{E}_\phi^{(-)}}{\underline{H}_\theta^{(-)}} = -\frac{\underline{E}_\theta^{(-)}}{\underline{H}_\phi^{(-)}} = jkZ_{F0} \frac{r h_{\nu_{mn}}^{(1)}(kr)}{\frac{d}{dr} (r h_{\nu_{mn}}^{(1)}(kr))}. \quad (7.372b)$$

The wave impedance $Z_{\text{TM}}^{(+)}(r)$ of the wave propagating in positive r -direction and $Z_{\text{TM}}^{(-)}(r)$ of the wave propagating in negative r -direction follow from (7.369b), (7.369c),

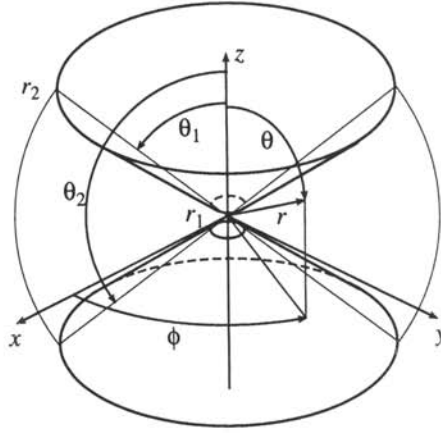


Figure 7.35: Biconical waveguide.

(7.369e) and (7.369f) as

$$Z_{\text{TM}}^{(+)}(r) = -\frac{\underline{E}_{\phi}^{(+)}}{\underline{H}_{\theta}^{(+)}} = \frac{\underline{E}_{\theta}^{(+)}}{\underline{H}_{\phi}^{(+)}} = j \frac{Z_{F0}}{k} \frac{\frac{d}{dr} \left(r h_{v_{mn}}^{(2)}(kr) \right)}{r h_{v_{mn}}^{(2)}(kr)}, \quad (7.373a)$$

$$Z_{\text{TM}}^{(-)}(r) = \frac{\underline{E}_{\phi}^{(-)}}{\underline{H}_{\theta}^{(-)}} = -\frac{\underline{E}_{\theta}^{(-)}}{\underline{H}_{\phi}^{(-)}} = -j \frac{Z_{F0}}{k} \frac{\frac{d}{dr} \left(r h_{v_{mn}}^{(1)}(kr) \right)}{r h_{v_{mn}}^{(1)}(kr)}. \quad (7.373b)$$

Since the spherical Hankel functions of first and second kind are mutually complex conjugate it follows

$$Z_{\text{TE}}^{(-)}(r) = Z_{\text{TE}}^{(+)*}(r), \quad (7.374a)$$

$$Z_{\text{TM}}^{(-)}(r) = Z_{\text{TM}}^{(+)*}(r). \quad (7.374b)$$

7.12.2 Biconical Waveguide

The *biconical waveguide* is formed by two cones $\theta = \theta_1$ and $\theta = \theta_2$ as depicted in Figure 7.35. Since in the biconical waveguide $\theta = 0$ as well as $\theta = \pi$ are outside the region of the field we can use both associated Legendre function solutions $P_v^m(\cos \theta)$ and $P_v^m(-\cos \theta)$. This allows to fulfill the boundary conditions at the cone surfaces at θ_1 and θ_2 . To obtain the field components of the TE_{mn} modes of the biconical waveguides, we superimpose solutions $P_v^m(\cos \theta)$ and $P_v^m(-\cos \theta)$ in (7.368a) to (7.368f),

TE_{mn} modes:

$$\underline{E}_r = 0, \quad (7.375a)$$

$$\underline{E}_\theta = -\frac{m}{\sin \theta} \left\{ \frac{h_{v_{mn}}^{(2)}(kr)}{h_{v_{mn}}^{(1)}(kr)} \right\} \left\{ \begin{matrix} -\sin m\phi \\ \cos m\phi \end{matrix} \right\} (\underline{A}_1 P_{v_{mn}}^m(\cos \theta) + \underline{A}_2 P_{v_{mn}}^m(-\cos \theta)), \quad (7.375b)$$

$$\underline{E}_\phi = \left\{ \frac{h_{v_{mn}}^{(2)}(kr)}{h_{v_{mn}}^{(1)}(kr)} \right\} \left\{ \begin{matrix} \cos m\phi \\ \sin m\phi \end{matrix} \right\} \left(\underline{A}_1 \frac{dP_{v_{mn}}^m(\cos \theta)}{d\theta} + \underline{A}_2 \frac{dP_{v_{mn}}^m(-\cos \theta)}{d\theta} \right), \quad (7.375c)$$

$$\underline{H}_r = \frac{v_{mn}(v_{mn}+1)}{j\omega\mu r} \left\{ \frac{h_{v_{mn}}^{(2)}(kr)}{h_{v_{mn}}^{(1)}(kr)} \right\} \left\{ \begin{matrix} \cos m\phi \\ \sin m\phi \end{matrix} \right\} (\underline{A}_1 P_{v_{mn}}^m(\cos \theta) + \underline{A}_2 P_{v_{mn}}^m(-\cos \theta)), \quad (7.375d)$$

$$\underline{H}_\theta = \frac{1}{j\omega\mu r} \left\{ \frac{\frac{d}{dr} (rh_{v_{mn}}^{(2)}(kr))}{\frac{d}{dr} (rh_{v_{mn}}^{(1)}(kr))} \right\} \left\{ \begin{matrix} \cos m\phi \\ \sin m\phi \end{matrix} \right\} \left(\underline{A}_1 \frac{dP_{v_{mn}}^m(\cos \theta)}{d\theta} + \underline{A}_2 \frac{dP_{v_{mn}}^m(-\cos \theta)}{d\theta} \right), \quad (7.375e)$$

$$\underline{H}_\phi = \frac{m}{j\omega\mu r \sin \theta} \left\{ \frac{\frac{d}{dr} (rh_{v_{mn}}^{(2)}(kr))}{\frac{d}{dr} (rh_{v_{mn}}^{(1)}(kr))} \right\} \left\{ \begin{matrix} -\sin m\phi \\ \cos m\phi \end{matrix} \right\} (\underline{A}_1 P_{v_{mn}}^m(\cos \theta) + \underline{A}_2 P_{v_{mn}}^m(-\cos \theta)). \quad (7.375f)$$

Denoting with $P_v^{m'}(\cos \theta)$ the derivative of $P_v^m(\cos \theta)$ to its argument we can write

$$\frac{dP_v^m(\pm \cos \theta)}{d\theta} = \mp P_v^{m'}(\pm \cos \theta) \sin \theta. \quad (7.376)$$

The boundary condition $\underline{E}_\phi = 0$ at the cone surface yields

$$\underline{A}_1 P_v^{m'}(\cos \theta_1) - \underline{A}_2 P_v^{m'}(-\cos \theta_1) = 0 \quad \text{for TE}_{mn} \text{ modes}, \quad (7.377a)$$

$$\underline{A}_1 P_v^{m'}(\cos \theta_2) - \underline{A}_2 P_v^{m'}(-\cos \theta_2) = 0. \quad (7.377b)$$

The v_{mn} are determined as the roots of the characteristic equation

$$P_v^{m'}(\cos \theta_1) P_v^{m'}(-\cos \theta_2) - P_v^{m'}(-\cos \theta_1) P_v^{m'}(\cos \theta_2) = 0, \quad (7.378)$$

where n refers to the n th root for given m . The biconical waveguide modes exhibit no cutoff frequency but are evanescent for $kr \ll v$ and wavelike for $kr \gg v$.

The wave impedances $Z_{TE}^{(+)}(r)$ and r -direction and $Z_{TE}^{(-)}(r)$ of the waves propagating in positive and negative r -direction, respectively, follow from (7.375b), (7.375c), (7.375e),

and (7.375f) as

$$Z_{TE}^{(+)}(r) = -\frac{\underline{E}_\phi^{(+)}}{\underline{H}_\theta^{(+)}} = \frac{\underline{E}_\theta^{(+)}}{\underline{H}_\phi^{(+)}} = -jkZ_{F0} \frac{r h_{v_{mn}}^{(2)}(kr)}{\frac{d}{dr} \left(r h_{v_{mn}}^{(2)}(kr) \right)}. \quad (7.379)$$

This expression is identical with those obtained for the conical waveguide in (7.372a) and (7.373a).

The field components of the TM_{mn} modes of the biconical waveguides are obtained by superposition of the solutions $P_v^m(\cos \theta)$ and $P_v^m(-\cos \theta)$ given in (7.369a) to (7.369f),

TM_{mn} modes:

$$\underline{E}_r = -\frac{n(n+1)}{j\omega\epsilon r} \left\{ \frac{h_{v_{mn}}^{(2)}(kr)}{h_{v_{mn}}^{(1)}(kr)} \right\} \begin{Bmatrix} \cos m\phi \\ \sin m\phi \end{Bmatrix} (\underline{B}_1 P_{v_{mn}}^m(\cos \theta) + \underline{B}_2 P_{v_{mn}}^m(-\cos \theta)), \quad (7.380a)$$

$$\underline{E}_\theta = -\frac{1}{j\omega\epsilon r} \left\{ \frac{d}{dr} \left(r h_{v_{mn}}^{(2)}(kr) \right) \right\} \begin{Bmatrix} \cos m\phi \\ \sin m\phi \end{Bmatrix} \left(\underline{B}_1 \frac{dP_{v_{mn}}^m(\cos \theta)}{d\theta} + \underline{B}_2 \frac{dP_{v_{mn}}^m(-\cos \theta)}{d\theta} \right), \quad (7.380b)$$

$$\underline{E}_\phi = -\frac{m}{j\omega\epsilon r \sin \theta} \left\{ \frac{d}{dr} \left(r h_{v_{mn}}^{(2)}(kr) \right) \right\} \begin{Bmatrix} -\sin m\phi \\ \cos m\phi \end{Bmatrix} (\underline{B}_1 P_{v_{mn}}^m(\cos \theta) + \underline{B}_2 P_{v_{mn}}^m(-\cos \theta)), \quad (7.380c)$$

$$\underline{H}_r = 0, \quad (7.380d)$$

$$\underline{H}_\theta = -\frac{m}{\sin \theta} \left\{ \frac{h_{v_{mn}}^{(2)}(kr)}{h_{v_{mn}}^{(1)}(kr)} \right\} \begin{Bmatrix} -\sin m\phi \\ \cos m\phi \end{Bmatrix} (\underline{B}_1 P_{v_{mn}}^m(\cos \theta) + \underline{B}_2 P_{v_{mn}}^m(-\cos \theta)), \quad (7.380e)$$

$$\underline{H}_\phi = \left\{ \frac{h_{v_{mn}}^{(2)}(kr)}{h_{v_{mn}}^{(1)}(kr)} \right\} \begin{Bmatrix} \cos m\phi \\ \sin m\phi \end{Bmatrix} \left(\underline{B}_1 \frac{dP_{v_{mn}}^m(\cos \theta)}{d\theta} + \underline{B}_2 \frac{dP_{v_{mn}}^m(-\cos \theta)}{d\theta} \right). \quad (7.380f)$$

The boundary conditions $\underline{E}_r = 0$ and $\underline{E}_\phi = 0$ at the cone surface yield

$$\underline{B}_1 P_v^m(\cos \theta_1) + \underline{B}_2 P_v^m(-\cos \theta_1) = 0 \quad \text{for } TE_{mn} \text{ modes}, \quad (7.381a)$$

$$\underline{B}_1 P_v^m(\cos \theta_2) + \underline{B}_2 P_v^m(-\cos \theta_2) = 0. \quad (7.381b)$$

The v_{mn} are determined as the n th roots of the characteristic equation

$$P_v^m(\cos \theta_1) P_v^m(-\cos \theta_2) - P_v^m(-\cos \theta_1) P_v^m(\cos \theta_2) = 0. \quad (7.382)$$

The wave impedances $Z_{TE}^{(+)}(r)$ and $Z_{TE}^{(-)}(r)$ of the waves propagating in positive and negative r -direction, respectively, we calculate from (7.380b), (7.380c), (7.380e) and (7.380f), hence

$$Z_{TE}^{(+)}(r) = Z_{TE}^{(-)*}(r) = j \frac{Z_{F0}}{k} \frac{\frac{d}{dr} \left(r h_{v_{mn}}^{(2)}(kr) \right)}{r h_{v_{mn}}^{(2)}(kr)}. \quad (7.383)$$

This result is in coincidence with that obtained for the conical waveguide in (7.373a) and (7.373b).

7.13 DIELECTRIC WAVEGUIDES AND OPTICAL FIBERS

7.13.1 Homogeneous Planar Dielectric Waveguides

The simplest dielectric waveguide is the *planar dielectric waveguide* depicted in Figure 7.36. The planar dielectric waveguide consists of a dielectric slab of thickness h and permittivity ϵ_2 enclosed by two regions with lower permittivities ϵ_1 and ϵ_3 , respectively [3, 5, 27]. In Figure 7.36 the slab region is called region 2. Regions 1 and 3 either are filled by a dielectric or are free-space regions. For $\epsilon_2 > \epsilon_1, \epsilon_3$ the slab can guide electromagnetic waves. In the following we assume a symmetric dielectric waveguide with the same permittivity ϵ_1 in regions 1 and 3. We assume in all regions nonmagnetic media with permittivity μ_0 . The TM modes may be derived from an electric Hertz form exhibiting only a z -component $\underline{\Pi}_{ez} dz$ whereas the TE modes may be derived using a magnetic Hertz form $\underline{\Pi}_{mz} dz$, that is

$$\underline{\Pi}_{ei} = \underline{\Pi}_{ezi} dz \quad \text{for TM modes,} \quad (7.384a)$$

$$\underline{\Pi}_{mi} = \underline{\Pi}_{mzi} dz \quad \text{for TE modes.} \quad (7.384b)$$

For the TM modes the Helmholtz equation in medium i is given by

$$\Delta \underline{\Pi}_{ei} + \beta_{0i}^2 \underline{\Pi}_{ei} = 0 \quad \text{for } i = 1, 2, \quad (7.385)$$

where the phase coefficients β_{01} and β_{02} for transverse electromagnetic waves in media 1 and 2 are

$$\beta_{0i} = \omega \sqrt{\epsilon_i \mu_i} \quad \text{for } i = 1, 2. \quad (7.386)$$

Regions 1 and 3 are filled by medium 1, whereas region 2 is filled by medium 2. We look for solutions of the Helmholtz equation guiding waves propagating in the z -direction. We assume uniform field distribution in y -direction and therefore $\partial/\partial y = 0$. This yields the two-dimensional Helmholtz equation,

$$\frac{\partial^2 \underline{\Pi}_{ezi}}{\partial x^2} + \frac{\partial^2 \underline{\Pi}_{ezi}}{\partial z^2} + \beta_{0i}^2 \underline{\Pi}_{ezi} = 0. \quad (7.387)$$

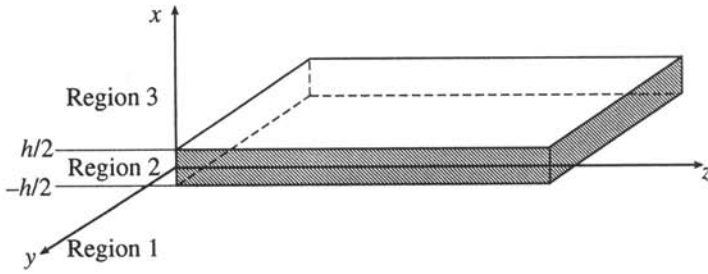


Figure 7.36: The planar dielectric waveguide.

Assuming wave propagation in the positive z -direction we choose

$$\underline{\Pi}_{ezi} = X_i(x) e^{-j\beta z}.$$

Inserting this into (7.387) gives

$$\frac{d^2 X_i}{dx^2} + (\beta_{0i}^2 - \beta^2) X_i = 0. \quad (7.388)$$

Guided waves with a phase coefficient β exist for

$$\beta_{01} < \beta < \beta_{02}. \quad (7.389)$$

This condition yields solutions that are oscillatory in the transverse direction in the slab region and are varying exponentially in the transverse direction outside the slab region.

The transverse components of the Hertz vector are even or odd functions of x . The odd function $\underline{\Pi}_{zi}^{(o)}$ yields symmetric transverse field distribution whereas the even function $\underline{\Pi}_{zi}^{(e)}$ yields anti-symmetric transverse field distribution. With the transverse phase coefficient β_{x2} for region 2 and the transverse attenuation coefficient for regions 1 and 3, given by

$$\beta_{x2} = \sqrt{\beta_{02}^2 - \beta^2}, \quad (7.390a)$$

$$\alpha_{x1} = \sqrt{\beta^2 - \beta_{01}^2} \quad (7.390b)$$

we obtain the odd solutions

$$\underline{X}_1^{(o)}(x) = \underline{B} \sin \beta_x x \quad \text{for } |x| \leq \frac{1}{2}h, \quad (7.391a)$$

$$\underline{X}_1^{(o)}(x) = \text{sign}(x) \underline{D} e^{-\alpha_x |x|} \quad \text{for } |x| \geq \frac{1}{2}h \quad (7.391b)$$

and the even solutions

$$X_1^{(e)}(x) = \underline{B} \cos \beta_x x \quad \text{for } |x| \leq \frac{1}{2}h, \quad (7.392a)$$

$$X_1^{(e)}(x) = \underline{D} e^{-\alpha_x |x|} \quad \text{for } |x| \geq \frac{1}{2}h. \quad (7.392b)$$

The expression for the TM-mode therefore is

$$\Pi_z^{(ez)} = \begin{cases} \underline{\Pi}_{ez1}^{(o)} = \underline{D} e^{\alpha_x x} e^{-j\beta z} & \text{for } x \leq -\frac{1}{2}h \\ \underline{\Pi}_{ez2}^{(o)} = \underline{B} \sin \beta_x x e^{-j\beta z} & \text{for } |x| \leq \frac{1}{2}h, \\ \underline{\Pi}_{ez3}^{(o)} = -\underline{D} e^{-\alpha_x x} e^{-j\beta z} & \text{for } x \geq \frac{1}{2}h \end{cases} \quad (7.393a)$$

$$\Pi_z^{(ez)} = \begin{cases} \underline{\Pi}_{ez1}^{(e)} = \underline{D} e^{\alpha_x x} e^{-j\beta z} & \text{for } x \leq -\frac{1}{2}h \\ \underline{\Pi}_{ez2}^{(e)} = \underline{B} \cos \beta_x x e^{-j\beta z} & \text{for } |x| \leq \frac{1}{2}h. \\ \underline{\Pi}_{ez3}^{(e)} = \underline{D} e^{-\alpha_x x} e^{-j\beta z} & \text{for } x \geq \frac{1}{2}h \end{cases} \quad (7.393b)$$

Inserting (7.393a) into (6.11a) to (6.11f) we obtain the field components

$$\underline{E}_x = \begin{cases} j\alpha_x \beta \underline{D} e^{\alpha_x x} e^{-j\beta z} & \text{for } x < -\frac{1}{2}h \\ -j\beta_x \beta \underline{B} \cos \beta_x x e^{-j\beta z} & \text{for } |x| < \frac{1}{2}h, \\ j\alpha_x \beta \underline{D} e^{-\alpha_x x} e^{-j\beta z} & \text{for } x > \frac{1}{2}h \end{cases} \quad (7.394a)$$

$$\underline{E}_z = \begin{cases} \alpha_x^2 \underline{D} e^{\alpha_x x} e^{-j\beta z} & \text{for } x < -\frac{1}{2}h \\ \beta_x^2 \underline{B} \sin \beta_x x e^{-j\beta z} & \text{for } |x| < \frac{1}{2}h, \\ -\alpha_x^2 \underline{D} e^{-\alpha_x x} e^{-j\beta z} & \text{for } x > \frac{1}{2}h \end{cases} \quad (7.394b)$$

$$\underline{H}_y = \begin{cases} j\omega\epsilon_1 \alpha_x \underline{D} e^{\alpha_x x} e^{-j\beta z} & \text{for } x < -\frac{1}{2}h \\ -j\omega\epsilon_2 \beta_x \underline{B} \cos \beta_x x e^{-j\beta z} & \text{for } |x| < \frac{1}{2}h. \\ j\omega\epsilon_1 \alpha_x \underline{D} e^{-\alpha_x x} e^{-j\beta z} & \text{for } x > \frac{1}{2}h \end{cases} \quad (7.394c)$$

For simplicity of notation we choose

$$u = \frac{1}{2}\beta_x h, \quad v = \frac{1}{2}\alpha_x h. \quad (7.395)$$

Continuity of \underline{E}_z and \underline{H}_y at $x \pm \frac{1}{2}h$ requires

$$v^2 e^{-v} \underline{D} + u^2 \sin u \underline{B} = 0, \quad (7.396a)$$

$$\epsilon_1 v e^{-v} \underline{D} + \epsilon_2 u \cos u \underline{B} = 0. \quad (7.396b)$$

This set of homogenous equations only has solutions with non-vanishing B and D if the determinant of the coefficients is zero. This condition yields

$$v = \frac{\epsilon_1}{\epsilon_2} u \tan u \quad \text{for odd TM mode}. \quad (7.397)$$

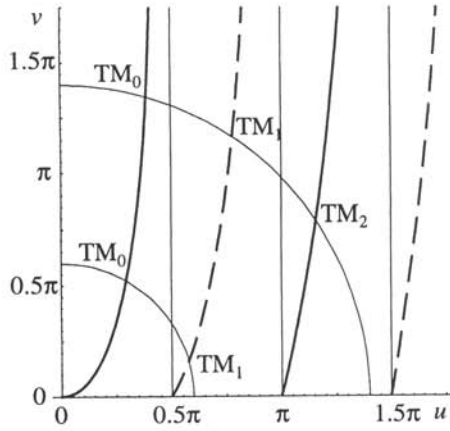


Figure 7.37: Graphical solution for eigenvalues for TM modes.

From (7.390a), (7.390b) and (7.395) we obtain

$$u^2 + v^2 = w^2 \quad (7.398)$$

with the *normalized frequency* w defined by

$$w = \frac{1}{2}h\sqrt{\beta_{02}^2 - \beta_{01}^2} = \frac{\omega h}{2c_0}\sqrt{\epsilon_{r2} - \epsilon_{r1}} = \frac{\omega h}{2c_0}\sqrt{n_2^2 - n_1^2}, \quad (7.399)$$

where n_2 is the refractive index of the slab medium and n_1 is the refractive index of the medium in regions 1 and 3. This, coupled with (7.397), is the *characteristic equation* for determining the phase coefficient β and the cutoff frequency of the odd TM modes of the symmetric planar waveguide.

Even TM modes are obtained by inserting (7.393b) into (6.11a) to (6.11f) and following the same procedure as above. The characteristic equation for even TM modes is

$$v = -\frac{\epsilon_1}{\epsilon_2} u \cot u \quad \text{for even TM mode}, \quad (7.400)$$

together with (7.398).

The characteristic equations for even and odd TM modes can be solved graphically. This is accomplished by the diagram shown in Figure 7.37 where the abscissa represents u and the ordinate v . The full curves are the plot of (7.397) and the dashed curves represent (7.400). Both plots are drawn for $\epsilon_2/\epsilon_1 = 2.5$. The plots of (7.398) are circles with the radius w . The intersections of the circles with the curves representing (7.397)

and (7.400) determine the modes that propagate unattenuated in the dielectric slab waveguide.

TE modes of the planar dielectric waveguide may be derived using (7.384b). There is a complete duality between TM and TE modes. In the coordinate system of Figure 7.36 the TE mode propagating in the z -direction will exhibit an electric field in the y -direction and magnetic field components in the x - and z -direction. Applying the principle of duality to (7.397) and (7.400) we obtain the characteristic equations for the TE modes given by

$$v = \frac{\mu_1}{\mu_2} u \tan u \quad \text{for odd TE mode ,} \quad (7.401a)$$

$$v = -\frac{\mu_1}{\mu_2} u \cot u \quad \text{for even TE mode} \quad (7.401b)$$

together with (7.398). For nonmagnetic media we obtain $\mu_1/\mu_2 = 1$.

The cutoff frequencies for TE_{*n*} and TM_{*n*} modes are identical for the same n . The cutoff frequency TE₀ mode as well as the TM₀ mode is zero. This means the TE₀ and TM₀ propagate unattenuated no matter how thin the slab is. However, if the slab is very thin the field extends wide into the regions 1 and 3 and becomes the TEM wave with infinite extension in x -direction when the frequency becomes zero. In this limiting case the wave is not guided any more by the slab.

The normalized cutoff frequency $w_{c,n}$ of the TE_{*n*} and TM_{*n*} modes is given by

$$w_{c,n} = \frac{1}{2} n \pi . \quad (7.402)$$

With (7.359) we obtain the cutoff frequency

$$f_{c,n} = \frac{nc_0}{2h\sqrt{\epsilon_{r2} - \epsilon_{r1}}} . \quad (7.403)$$

In the design of planar circuits for higher frequencies one has to take care that higher-order surface waves cannot propagate. The lowest higher-order modes are the TE₁ and TM₁ modes. In case of a silicon substrate with $\epsilon_r = 12.6$ the cutoff frequency of TE₁ and TM₁ modes is

$$f_{c,1} = \frac{c_0}{2h\sqrt{\epsilon_{r1} - 1}} = \frac{42.1 \text{ GHz}}{h/[\text{mm}]} . \quad (7.404)$$

7.13.2 Dielectric Slab with Single-Sided Metallization

Figure 7.38 shows the dielectric slab of thickness h with single-sided metallization. The slab has the permittivity ϵ_{r2} . The region above the slab ($x > h$) exhibits a permittivity ϵ_{r1} . The dielectric plate with metallization on one side carries surface waves of TM

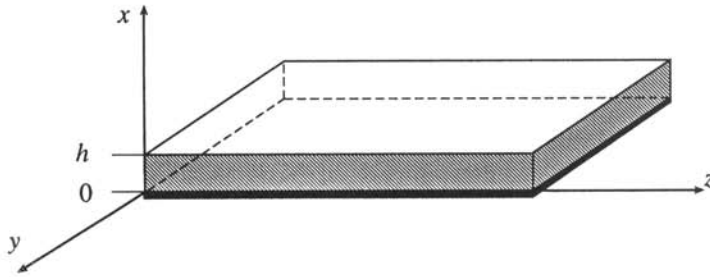


Figure 7.38: The planar dielectric waveguide.

type as well as of TE type. We can obtain the field solutions for the dielectric slab with single-sided metallization directly from the solutions for the slab without metallization by application of the mirror principle. At the plane $x = 0$ odd TM modes and even TE modes of the dielectric slab waveguide without metallization exhibit an electric field normal to this plane and a magnetic field tangential to this plane. Therefore, these field solutions remain valid in either half-space $x \geq 0$ or $x \leq 0$ if a perfectly conducting sheet is inserted in the plane $x = 0$.

In the case of the TE wave the current lines are normal to the direction of propagation, whereas the TM wave exhibits current lines in direction of propagation. The phase coefficients for the TM waves and TE waves, respectively, are determined via the eigenvalue equations

$$v = \frac{\epsilon_{r1}}{\epsilon_{r2}} u \tan u \quad \text{for TM modes,} \quad (7.405a)$$

$$v = -u \cot u \quad \text{for TE modes,} \quad (7.405b)$$

where the parameters u and v are given by

$$\begin{aligned} u &= h \sqrt{\beta_{02}^2 - \beta^2}, \\ v &= h \sqrt{\beta^2 - \beta_{01}^2}. \end{aligned} \quad (7.406)$$

The normalized frequency w is given by

$$w = \sqrt{u^2 + v^2} = h \sqrt{\beta_{02}^2 - \beta_{01}^2}. \quad (7.407)$$

The TM_0 mode has no lower cutoff frequency. For the higher modes the normalized

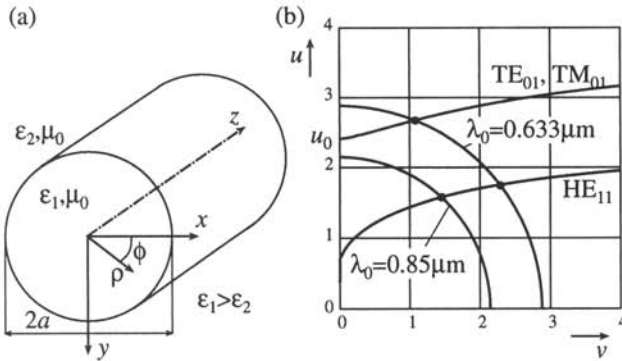


Figure 7.39: (a) Dielectric waveguide and (b) graphic solution of the eigenvalue equation.

cutoff frequencies are given by

$$\nu_{c, TMn} = n\pi \quad \text{for TM modes,} \quad (7.408)$$

$$\nu_{c, TE n} = \left(n + \frac{1}{2}\right)\pi \quad \text{for TE modes.} \quad (7.409)$$

The lowest higher-order mode is the TE_0 mode for which the cutoff frequency on silicon substrate is given by

$$f_{c, TE0} = \frac{c_0}{4h\sqrt{\epsilon_{r1} - 1}} = \frac{21.0 \text{ GHz}}{h/[\text{mm}]} \quad (7.410)$$

7.13.3 Circular Dielectric Waveguides with Step Index Profile

The circular cylindric dielectric waveguide plays an important role as optical fibers [28–31]. Figure 7.39(a) shows the circular cylindric dielectric waveguide. The core region $r \leq a$ (region 1) is filled with a homogeneous isotropic dielectric with a permittivity ϵ_1 . The outer region $r > a$ (region 2) also is homogeneous and isotropic and has a permittivity ϵ_2 . The outer region either is free-space ($\epsilon_2 = \epsilon_0$) or filled with a dielectric. In order to guide a wave $\epsilon_2 < \epsilon_1$ must be valid. The dielectric waveguide is an open waveguide. This means that the electromagnetic field is not confined within the waveguide, but is extended also in the outer region. Therefore we have to solve the field equations in both regions $r \leq a$ and $r > a$. This is done by seeking the general solutions in both regions assuming either region to be infinitely extended and then by matching these partial solutions along the boundary. Since the boundary surface between the core region and outer region is a circular cylinder, the circular cylindric coordinate system is most suitable to solve the problem. The circular cylindric dielectric waveguide also exhibits hybrid modes. These are modes exhibiting electric as well as magnetic longitudinal

components. Therefore, in general we have to superimpose solutions derived from a longitudinal electric Hertz vector field $\underline{\Pi}_{ez}$ and solutions derived from a longitudinal magnetic Hertz vector field $\underline{\Pi}_{mz}$ if we want to use Hertz vector fields exhibiting z -components only. For the core region 1 with $r \leq a$ the solutions (7.313a)–(7.314f) of the field equations are valid. We now have to consider that the core region is filled with a dielectric and therefore (7.302) has to be replaced with

$$k_c^2 = \beta_{01}^2 - \beta^2 \quad (7.411)$$

with the phase coefficient β_{01} of the plane wave in a medium with permittivity ϵ_1 given by

$$\beta_{01} = \omega \sqrt{\mu_0 \epsilon_1} = \sqrt{\epsilon_{r1}} \beta_0. \quad (7.412)$$

The occurrence of hybrid modes follows from the circumstance that the boundary conditions at $r = a$ can be generally fulfilled only if transverse electric *and* transverse magnetic partial solutions are superimposed. Comparing the field components of the transverse magnetic partial solutions (7.313a)–(7.313f) with the field components of the transverse electric partial solutions (7.314a)–(7.314f) we see that we have to rotate one of the two partial solutions by 90° around the z -axis in order to match the TE partial solutions and TM partial solutions. We rotate the TM partial solutions by 90° using the solution $\sin n\phi$ instead of the solution $\cos n\phi$ of (7.305). The corresponding solutions are obtained by the substitutions $\cos n\phi \rightarrow \sin n\phi$ and $\sin n\phi \rightarrow -\cos n\phi$ in (7.308a) and (7.313a)–(7.313f). Instead of (7.308a) and (7.309a) we use the following z -components of the electric and magnetic Hertz vectors

$$\underline{\Pi}_e(r, \phi, z) = \underline{B}J_n(k_c r) \sin n\phi e^{-j\beta z} dz, \quad (7.413a)$$

$$\underline{\Pi}_m(r, \phi, z) = \underline{A}J_n(k_c r) \cos n\phi e^{-j\beta z} dz. \quad (7.413b)$$

By superposition of TE partial solution and the rotated TM partial solution (7.313a)–(7.313f) we obtain

$$\underline{E}_r = j \left[\omega \mu_0 \frac{n}{r} \underline{A}J_n(k_c r) - \beta k_c \underline{B}J'_n(k_c r) \right] \sin n\phi e^{-j\beta z}, \quad (7.414a)$$

$$\underline{E}_\phi = j \left[\omega \mu_0 k_c \underline{A}J'_n(k_c r) - \beta \frac{n}{r} \underline{B}J_n(k_c r) \right] \cos n\phi e^{-j\beta z}, \quad (7.414b)$$

$$\underline{E}_z = k_c^2 \underline{B}J_n(k_c r) \sin n\phi e^{-j\beta z}, \quad (7.414c)$$

$$\underline{H}_r = -j \left[\beta k_c \underline{A}J'_n(k_c r) - \omega \epsilon_1 \frac{n}{r} \underline{B}J_n(k_c r) \right] \cos n\phi e^{-j\beta z}, \quad (7.414d)$$

$$\underline{H}_\phi = j \left[\beta \frac{n}{r} \underline{A}J_n(k_c r) - \omega \epsilon_1 k_c \underline{B}J'_n(k_c r) \right] \sin n\phi e^{-j\beta z}, \quad (7.414e)$$

$$\underline{H}_z = k_c^2 \underline{A}J_n(k_c r) \cos n\phi e^{-j\beta z}. \quad (7.414f)$$

For region 2 we are seeking solutions decaying stronger than exponentially with $r \rightarrow \infty$. Such solutions describe guided waves. It exists for $\beta_{02} < \beta$, where β_{02} is the phase coefficient for a plane wave in the medium of region 2, given by

$$\beta_{02} = \omega \sqrt{\mu_0 \epsilon_2} = \sqrt{\epsilon_{r2}} \beta_0. \quad (7.415)$$

We introduce the parameter κ_c , given by

$$\kappa_c^2 = \beta^2 - \beta_{02}^2 \quad (7.416)$$

and obtain for the subregion 2 instead of (7.306) the Bessel differential equation

$$r^2 \frac{d^2 R}{dr^2} + r \frac{dR}{dr} - (r^2 \kappa_c^2 + n^2) R = 0. \quad (7.417)$$

The solutions are the modified Bessel functions $K_n(x)$ and $I_n(x)$. The solution $K_n(x)$ for $x \rightarrow \infty$ goes to 0 stronger than exponentially, whereas the solution $I_n(x)$ is not bounded for $x \rightarrow \infty$. We obtain the solutions for subregion 2 from the solutions for subregion (7.414a)–(7.414f) by performing the following substitutions

$$J_n(k_c r) \rightarrow K_n(\kappa_c r), \quad (7.418a)$$

$$k_c J'_n(k_c r) \rightarrow \kappa_c K'_n(\kappa_c r), \quad (7.418b)$$

$$\epsilon_1 \rightarrow \epsilon_2, \quad (7.418c)$$

$$k_c^2 \rightarrow -\kappa_c^2 \quad (7.418d)$$

and obtain

$$E_r = j \left[\omega \mu_0 \frac{n}{r} \underline{C} K_n(\kappa_c r) - \beta \kappa_c \underline{D} K'_n(\kappa_c r) \right] \sin n\phi e^{-j\beta z}, \quad (7.419a)$$

$$E_\phi = j \left[\omega \mu_0 \kappa_c \underline{C} K'_n(\kappa_c r) - \beta \frac{n}{r} \underline{D} K_n(\kappa_c r) \right] \cos n\phi e^{-j\beta z}, \quad (7.419b)$$

$$E_z = -\kappa_c^2 \underline{D} K_n(\kappa_c r) \sin n\phi e^{-j\beta z}, \quad (7.419c)$$

$$\underline{H}_r = -j \left[\beta \kappa_c \underline{C} K'_n(\kappa_c r) - \omega \epsilon_2 \frac{n}{r} \underline{D} K_n(\kappa_c r) \right] \cos n\phi e^{-j\beta z}, \quad (7.419d)$$

$$\underline{H}_\phi = j \left[\beta \frac{n}{r} \underline{C} K_n(\kappa_c r) - \omega \epsilon_2 \kappa_c \underline{D} K'_n(\kappa_c r) \right] \sin n\phi e^{-j\beta z}, \quad (7.419e)$$

$$\underline{H}_z = -\kappa_c^2 \underline{C} K_n(\kappa_c r) \cos n\phi e^{-j\beta z}. \quad (7.419f)$$

We now introduce the normalized parameters u and v by

$$u = k_c a = a \sqrt{\beta_{01}^2 - \beta^2}, \quad (7.420a)$$

$$v = \kappa_c a = a \sqrt{\beta^2 - \beta_{02}^2}. \quad (7.420b)$$

With (7.411) and (7.416) we obtain therefrom

$$u^2 + v^2 = a^2(\beta_{01}^2 - \beta_{02}^2), \quad (7.421a)$$

$$u^2 + v^2 = a^2\beta_0^2(\epsilon_{r1} - \epsilon_{r2}). \quad (7.421b)$$

The partial solutions for subregions 1 and 2 must fulfill the boundary conditions (2.160) and (2.164) at $r = a$. The tangential components E_ϕ , E_z , H_ϕ and H_z of the fields at the boundary surface must be continuous at $r = a$. From (7.414b), (7.414c), (7.414e), (7.414f), (7.419b), (7.419c), (7.419e) and (7.419f) we obtain therewith

$$\omega\mu_0 u J'_n(u) \underline{A} - \beta n J_n(u) \underline{B} = \omega\mu_0 v K'_n(v) \underline{C} - \beta n K_n(v) \underline{D}, \quad (7.422a)$$

$$u^2 J_n(u) \underline{B} = -v^2 K_n(v) \underline{D}, \quad (7.422b)$$

$$\beta n J_n(u) \underline{A} - \omega\epsilon_1 u J'_n(u) \underline{B} = \beta n K_n(v) \underline{C} - \omega\epsilon_2 v K'_n(v) \underline{D}, \quad (7.422c)$$

$$u^2 J_n(u) \underline{A} = -v^2 K_n(v) \underline{C}. \quad (7.422d)$$

Using (7.422b) and (7.422d) we can express the complex amplitudes \underline{C} and \underline{D} by \underline{A} and \underline{B} , and after inserting into (7.422a) and (7.422c) we obtain

$$\omega\mu_0 \left(\frac{1}{u} \frac{J'_n(u)}{J_n(u)} + \frac{1}{v} \frac{K'_n(v)}{K_n(v)} \right) \underline{A} - \beta n \left(\frac{1}{u^2} + \frac{1}{v^2} \right) \underline{B} = 0, \quad (7.423a)$$

$$\beta n \left(\frac{1}{u^2} + \frac{1}{v^2} \right) \underline{A} - \omega\epsilon_0 \left(\frac{\epsilon_{r1}}{u} \frac{J'_n(u)}{J_n(u)} + \frac{\epsilon_{r2}}{v} \frac{K'_n(v)}{K_n(v)} \right) \underline{B} = 0. \quad (7.423b)$$

This homogeneous system of equations for \underline{A} and \underline{B} only has a solution if the coefficient determinant vanishes. This yields the eigenvalue equation

$$\frac{\omega^2}{c_0^2} \left[\frac{1}{u} \frac{J'_n(u)}{J_n(u)} + \frac{1}{v} \frac{K'_n(v)}{K_n(v)} \right] \left[\frac{\epsilon_{r1}}{u} \frac{J'_n(u)}{J_n(u)} + \frac{\epsilon_{r2}}{v} \frac{K'_n(v)}{K_n(v)} \right] - \beta^2 n^2 \left(\frac{1}{u^2} + \frac{1}{v^2} \right)^2 = 0. \quad (7.424)$$

We eliminate the unknown phase coefficient β . From (7.420a) and (7.420b) we obtain

$$\beta^2 \left[\frac{1}{u^2} + \frac{1}{v^2} \right] = \left[\frac{\beta_{01}^2}{u^2} + \frac{\beta_{02}^2}{v^2} \right] = \frac{\omega^2}{c_0^2} \left[\frac{\epsilon_{r1}}{u^2} + \frac{\epsilon_{r2}}{v^2} \right] \quad (7.425)$$

and with this from (7.424) the eigenvalue equation in the following form

$$\left[\frac{1}{u} \frac{J'_n(u)}{J_n(u)} + \frac{1}{v} \frac{K'_n(v)}{K_n(v)} \right] \left[\frac{\epsilon_{r1}}{u} \frac{J'_n(u)}{J_n(u)} + \frac{\epsilon_{r2}}{v} \frac{K'_n(v)}{K_n(v)} \right] = n^2 \left[\frac{\epsilon_{r1}}{u^2} + \frac{\epsilon_{r2}}{v^2} \right] \left[\frac{1}{u^2} + \frac{1}{v^2} \right]. \quad (7.426)$$

From (7.421b) and (7.426) the normalized parameters u and v and from this the quantities β , k_c and κ_c may be determined. The solution of the eigenvalue equation only may be obtained by numeric or graphic methods. To obtain the graphic solution we introduce the functions

$$\xi_n(u) = \frac{1}{u} \frac{J'_n(u)}{J_n(u)}, \quad (7.427)$$

$$\eta_n(v) = \frac{1}{v} \frac{K'_n(v)}{K_n(v)} \quad (7.428)$$

and obtain the eigenvalue equations

$$(\xi_n(u) + \eta_n(v))(\epsilon_{r1}\xi_n(u) + \epsilon_{r2}\eta_n(v)) = n^2 \left(\frac{\epsilon_{r1}}{u^2} + \frac{\epsilon_{r2}}{v^2} \right) \left(\frac{1}{u^2} + \frac{1}{v^2} \right), \quad (7.429)$$

$$u^2 + v^2 = a^2 \beta_0^2 (\epsilon_{r1} - \epsilon_{r2}). \quad (7.430)$$

These equations are solved graphically by drawing the curves given by both equations in the uv -plane. The solutions are given by the intersections of the curves. The curve given by (7.429) only depends on the parameter n and the geometric parameters of the waveguide. By (7.430) circles in the uv -plane are defined, the radius of which is proportional to the frequency. The graphic solution is depicted in Figure 7.39(b). In (7.429) a family of curves belongs to each n . According to (7.414a) to (7.414f) the ϕ -dependence of the field components is given by $\sin n\phi$ and $\cos n\phi$, respectively. The parameter n therefore determines the number of node planes in the field. Furthermore the circular cylindric dielectric waveguide exhibits a number of node cylinder surfaces. Modes are marked with indices n and m where n is the number of node planes and m is the number of node cylinders for a certain mode. To each pair of indices two field types are assigned. For $n = 0$ these two field types are transverse electric modes and the transverse magnetic modes. For $n \neq 0$ the modes are of hybrid type exhibiting longitudinal electric as well longitudinal magnetic field components. These field types are HE_{nm} and EH_{nm} modes, respectively, depending on whether the transverse field structure is similar to the TE_{nm} modes or the TM_{nm} modes of the circular cylindric hollow waveguide.

Let us first consider the modes with $n = 0$. These modes exhibit rotational symmetry. For $n = 0$ the right side of the eigenvalue equations (7.426) and (7.429), respectively, vanish. These equations are fulfilled if one of the expressions in brackets on the left side vanishes. For the TE_{0m} waves we obtain

$$\xi_0(u) + \eta_0(v) = 0, \quad (7.431)$$

whereas for the TM_{0m} waves

$$\epsilon_{r1}\xi_0(u) + \epsilon_{r2}\eta_0(v) = 0 \quad (7.432)$$

Table 7.6: Parameter u_0 at the Cutoff Wavelength λ_c

	HE _{nm} – Modes (TM _{0m} for $n = 0$)	EH _{nm} – Modes (TE _{0m} for $n = 0$)
$n = 0$	$J_0(u_0) = 0$	$J_0(u_0) = 0$
$n = 1$	$J_1(u_0) = 0, (u_0 \neq 0)$	$J_1(u_0) = 0, (u_0 \neq 0)$
$n \geq 2$	$\frac{J_{n-2}(u_0)}{J_{n-1}(u_0)} = \frac{\epsilon_{r1} - \epsilon_{r2}}{\epsilon_{r1} + \epsilon_{r2}}$	$J_n(u_0) = 0, (u_0 \neq 0)$

is valid. The assignment of these equations for $n = 0$ to the transverse electric and transverse magnetic fields, respectively, becomes obvious by comparison with (7.423a) and (7.423b). For $n = 0$ both equations are uncoupled. The transverse electric field with amplitude \underline{A} and the transverse magnetic field with amplitude \underline{B} therefore are not coupled.

In Figure 7.39(b) solution curves of (7.429) are drawn for the HE₁₁ mode, the H₀₁ mode and the E₀₁ mode. The solution curve for the HE₁₁ mode originates at $u = 0$, $v = 0$. Therefore for circles according to (7.430) with an arbitrarily small radius, a point of intersection exists (i.e., the HE₁₁ mode exhibits no lower cutoff frequency and can propagate for arbitrarily small frequencies). The field distribution of the HE₁₁ mode is depicted in Figure 7.40(a). For all other modes the curves of solution of (7.429) exhibit $v = 0$ for $u > 0$. The values u_0 of u for which the curve of solution of the specific modes are going through $v = 0$ are summarized in Table 7.6. These values u_0 determine the lowest values of β_0 according to (7.430) and the largest values of the free-space wavelength λ_0 for which the mode can propagate. The cutoff wavelengths λ_c of the modes are given by

$$\lambda_c = \frac{2\pi a}{u_0} \sqrt{\epsilon_{r1} - \epsilon_{r2}}. \quad (7.433)$$

With the exception of the HE₁₁ mode, which has no cutoff frequency, the TE₀₁ mode exhibits the lowest cutoff frequency. According to Table 7.6 and (7.433) it is given by

$$\lambda_c^{(\text{TE}_{01})} = \frac{2\pi a}{2.405} \sqrt{\epsilon_{r1} - \epsilon_{r2}}. \quad (7.434)$$

Figure 7.39(b) shows the solution curves for the HE₁₁, TM₀₁ and the TE₀₁ modes for $\sqrt{\epsilon_{r1}} = 1.5$ and $\sqrt{\epsilon_{r2}} = 1.4955$. The square roots of the relative permittivities are equal to the refractive indices. For optical fibers such small differences of the refractive indices between the core and cladding region are usual. Such small differences may be realized by different doping of the quartz material. Small differences between core and cladding

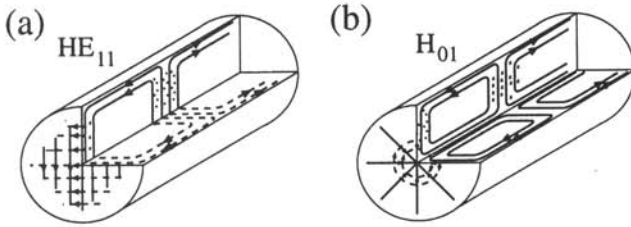


Figure 7.40: Field lines of the (a) HE_{11} mode and (b) the TE_{01} mode.

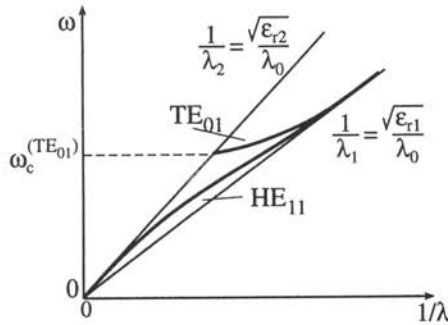


Figure 7.41: Dispersion diagram for the HE_{11} and TE_{01} modes.

refractive indices allow for the realization of optical fibers with a core diameter of up to $10\text{ }\mu\text{m}$, in single-mode operation for less than $1\text{ }\mu\text{m}$ wavelength. Figure 7.39(b) shows the graphic solution of the eigenvalue equations for a circular cylindric dielectric waveguide with a core diameter of $2a = 5\text{ }\mu\text{m}$ and core and cladding refractive indices of 1.5 and 1.4955, respectively. From (7.434) we obtain a cutoff wavelength $\lambda_c = 0.758\text{ }\mu\text{m}$.

Figure 7.40 depicts the field distribution of the TE_{01} mode. For the small difference between ϵ_{r1} and ϵ_{r2} , (7.431) and (7.432) are nearly identical. Therefore the solution curves for the TE_{01} and the TM_{01} modes cannot be distinguished. Figure 7.41 shows the dispersion diagram of the TE_{01} mode. The HE_{11} mode exhibits no lower cutoff frequency; however, it is not suitable to guide waves of an arbitrarily low frequency. The lower the frequency becomes, the less the electromagnetic field is guided by the core of the fiber and the more it is spread in the cladding of the fiber or in free-space in the case of small perturbations of the waveguide or even small bending. The optical waveguide has to be designed such that the electromagnetic field is rapidly decaying in the cladding region. Otherwise the electromagnetic energy will be attenuated by lossy material on the surface of the cladding or it will be scattered.

7.14 PROBLEMS

1. Consider the electric and magnetic Hertz forms given by

$$\underline{\Pi}_e = \frac{1}{\rho} \left(\underline{A}^{(+)} e^{-j\beta z} + \underline{A}^{(-)} e^{j\beta z} \right) d\rho,$$

$$\underline{\Pi}_m = \left(\underline{B}^{(+)} e^{-j\beta z} + \underline{B}^{(-)} e^{j\beta z} \right) d\phi.$$

- Show that each of these Hertz forms allows to compute the field of the time-harmonic waves TEM mode of the coaxial circular cylindric waveguide.
 - Compute electric and magnetic field forms for the coaxial circular cylindric waveguide with inner conductor diameter $2a$ and inner diameter of the outer conductor $2b$.
 - Find the normalized electric and magnetic field structure functions and express the field forms by voltages $\underline{V}^{(+)}(z)$, $\underline{V}^{(-)}(z)$ and currents $\underline{I}^{(+)}(z)$, $\underline{I}^{(-)}(z)$ describing the waves propagating in positive and negative z -direction and the structure functions.
 - Compute the characteristic impedance of the coaxial circular cylindric waveguide.
 - Compute the complex Poynting vector for the general case of waves propagating through the waveguide in both directions.
 - Compute the complex power $P_c(z)$ flowing through the waveguide for the general case of waves propagating in both directions by integrating the complex Poynting vector over the cross-section of the waveguide. Compare this result with the complex power computed from the voltages $\underline{V}^{(+)}(z)$, $\underline{V}^{(-)}(z)$ and currents $\underline{I}^{(+)}(z)$, $\underline{I}^{(-)}(z)$.
 - Give the conditions for $P_c(z)$ being either real or imaginary over the whole length of the waveguide.
2. Show that the electromagnetic wave propagating in a coaxial circular cylindric waveguide can be derived from the magnetic Hertz form

$$\underline{\Pi}_m = \left(f^{(+)}(z - ct) + f^{(-)}(z + ct) \right) d\phi.$$

- Compute electric and magnetic field forms for the coaxial circular cylindric waveguide with inner conductor diameter $2a$ and inner diameter of the outer conductor $2b$.
- Find the normalized electric and magnetic field structure functions and express the field forms by voltages $v^{(+)}(z - ct)$, $v^{(-)}(z + ct)$ and currents $i^{(+)}(z - ct)$, $i^{(-)}(z + ct)$ describing the waves propagating in positive and negative z -direction and the structure functions.
- Compute the characteristic impedance of the coaxial circular cylindric waveguide.

- d) Compute the time-dependent Poynting vector for the general case of waves propagating through the waveguide in both directions.
 - e) Compute the power $P(z, t)$ flowing through the waveguide for the general case of waves propagating in both directions by integrating the complex Poynting vector over the cross-section of the waveguide. Compare this result with the complex power computed from the voltages $v^{(+)}(z - ct)$, $v^{(-)}(z + ct)$ and currents $i^{(+)}(z - ct)$, $i^{(-)}(z + ct)$.
3. Consider a circular cylindric coaxial transmission-line with copper conductors ($\sigma_K = 5.8 \cdot 10^7 \text{ Sm}^{-1}$). The diameter of the inner conductor is $2a = 0.9 \text{ mm}$ and the inner diameter of the outer conductor is $2b = 2.95 \text{ mm}$. The coaxial cable is filled with polyethylene (μ_0 , $\epsilon'_r = 2.1$, $\tan \delta_e = 2 \cdot 10^{-4}$ at 1 GHz).
- a) Compute the parameters C' , L' , G' and R' .
 - b) Compute the propagation coefficient γ and characteristic impedance Z_0 .
 - c) Draw the T -, Π - and allpass lumped element equivalent circuits for a line segment of length Δz and compute the lumped element parameters for $\Delta z = 2 \text{ cm}$.
4. A multiconductor transmission-line exhibits three conductors 1, 2, 3 shielded by a conductor 0. The space between the conductors is filled with a homogeneous isotropic dielectric material of $\epsilon_r = 2.25$. The capacitance per unit of length matrix is

$$\mathbf{C}' = \begin{bmatrix} 60 & 20 & 20 \\ 20 & 60 & 20 \\ 20 & 20 & 60 \end{bmatrix} \text{ pF}.$$

- a) Compute the wave velocity.
 - b) Compute the inductance per unit of length matrix \mathbf{L}' .
5. Show that the TE_{m0} modes of the rectangular waveguide can be derived from a magnetic Hertz form

$$\underline{\Pi}_m = \underline{A} \sin \beta_x x e^{-j\beta_z z} dy$$

and compute the field components.

6. Consider a lossless rectangular waveguide with given height to width ratios $b/a = 1, 0.5$ and 0.2 .
- a) Compute the cutoff frequency f_c of the fundamental mode TE_{10} .
 - b) Compute the cutoff frequencies of the next four higher modes.
 - c) Give the single-mode frequency range.
7. Consider a rectangular waveguide with copper walls ($\sigma = 5.8 \cdot 10^7 \text{ Sm}^{-1}$) and inner dimensions $a = 1 \text{ cm}$, $b = 0.5 \text{ cm}$ is filled with air. Let the waveguide be excited in the TE_{10} mode.
- a) Compute the cutoff frequency f_c and the cutoff wavelength λ_c of the fundamental mode.
 - b) Compute the cutoff frequencies and the cutoff wavelengths of the next four higher modes.

- c) Compute the free-space wavelengths and the TE_{10} guide wavelengths for the frequencies $f = 1.1 f_c, 1.5 f_c, 1.9 f_c$.
 - d) Compute the amplitude attenuation coefficient α due to the skin effect losses for the TE_{10} mode at the frequencies $f = 1.1 f_c, 1.5 f_c, 1.9 f_c$.
 - e) Compute the amplitude attenuation coefficient α for the evanescent fields of the next four higher modes at the frequencies $f = 1.1 f_c, 1.5 f_c, 1.9 f_c$. For these computations the skin effect losses may be neglected.
8. Consider an empty rectangular hollow R 320 waveguide (inner dimensions $a = 7.112$ mm, $b = 3.556$ mm).
- a) Compute the cutoff frequencies for the TE_{10} and TE_{11} modes.
 - b) Compute the guide wavelengths at 60 GHz for the TE_{10} and TE_{11} modes.
 - c) Compute the attenuation coefficients due to skin effect losses in copper walls ($\sigma = 5.8 \cdot 10^7$ Sm $^{-1}$) at 60 GHz for the TE_{10} and TE_{11} modes.
 - d) Let waveguide now be filled with a homogeneous isotropic dielectric with permittivity ($\epsilon_r = 2.25$) and loss tangent $\tan \delta_e = 0.001$. Compute the cutoff frequencies for the TE_{10} and TE_{11} modes.
 - e) Compute the guide wavelengths for the filled waveguide at 60 GHz for the TE_{10} and TE_{11} modes.
 - f) Compute the attenuation coefficients due to skin effect losses in copper walls for the filled waveguide at 60 GHz for the TE_{10} and TE_{11} modes.
 - g) Compute the attenuation coefficients due to the dielectric losses in the filled waveguide at 60 GHz for the TE_{10} and TE_{11} modes.
9. Consider the empty rectangular hollow R 100 waveguide with copper ($\sigma = 5.8 \cdot 10^7$ Sm $^{-1}$) walls of inner dimension $a = 22.86$ mm, $b = 10.16$ mm. The waveguide is excited in the TE_{10} mode at a frequency of 10 GHz. The power of 1 mW is fed into the waveguide.
- a) Compute the guide wavelength, the phase coefficient, the attenuation coefficient, the phase velocity and the wave impedance.
 - b) Compute the amplitudes of the transverse electric and magnetic fields and of the longitudinal magnetic field.
 - c) Compare the calculated waveguide attenuation with the attenuation of a coaxial line with diameter of the inner conductor $2a = 0.9$ mm and inner diameter of the outer conductor $2b = 2.85$ mm, filled with a dielectric with permittivity ($\epsilon_r = 2.25$) and loss tangent $\tan \delta_e = 0.001$ at 10 GHz. Consider skin effect losses as well as dielectric losses.
10. Consider the standardized circular cylindric waveguide C 48 with an inner diameter $2a = 44.45$ mm. The waveguide consists of copper ($\sigma = 5.8 \cdot 10^7$ Sm $^{-1}$).
- a) Compute the cutoff frequencies TE_{01} , TE_{11} , TM_{01} and TM_{11} modes.
 - b) Assuming a perfectly conducting waveguide wall, compute for the TE_{01} mode the wave impedance, the guide wavelength and the phase and group velocities of the guided wave at the frequencies 10 GHz, 12 GHz, 15 GHz,

20 GHz, 40 GHz and 60 GHz.

- c) For the waveguide consisting of copper ($\sigma = 5.8 \cdot 10^7 \text{ Sm}^{-1}$), compute the attenuation coefficient of the TE_{01} at the frequencies 10 GHz, 12 GHz, 15 GHz, 20 GHz, 40 GHz and 60 GHz.
11. An empty circular cylindric hollow waveguide of inner diameter $2a = 2 \text{ mm}$ guides an optical wave with a free-space wavelength $\lambda_0 = 1.3 \mu\text{m}$. The waveguide is excited in the TE_{01} mode. The waveguide is made from copper ($\sigma = 5.8 \cdot 10^7 \text{ Sm}^{-1}$). Compute the attenuation coefficient.
12. Consider the radial waveguide excited in the TE_{00} mode.
 - a) Show that this mode is a TEM mode.
 - b) Show that in a surface $\rho = \text{const.}$ a voltage $\underline{V}(\rho)$ and a current $\underline{I}(\rho)$ can be defined by $\underline{V}(\rho) = -h\underline{E}_z(\rho)$, $\underline{I}(\rho) = 2\pi\rho\underline{H}_\phi(\rho)$.
 - c) Express electric and magnetic field forms by generalized voltage and current amplitudes and the electric and magnetic structure forms.
 - d) Show that $\underline{V}(\rho)$ and $\underline{I}(\rho)$ satisfy the differential equations $\frac{d\underline{V}(\rho)}{d\rho} = -j\omega L'(\rho)\underline{I}(\rho)$ and $\frac{d\underline{I}(\rho)}{d\rho} = -j\omega C'(\rho)\underline{V}(\rho)$ with $L'(\rho) = \frac{\mu h}{2\pi\rho}$, $C'(\rho) = \frac{2\pi\epsilon\rho}{h}$.
 - e) Compute the wave impedance $Z_F(\rho)$ and the characteristic impedance $Z_0(\rho)$.
 - f) Compute the complex Poynting form $\mathcal{T}(\rho)$ for a superposition of harmonic waves flowing in positive and negative ρ -directions.
13. Using the asymptotic expansions of the spherical Hankel functions, show that the wave impedances of the conical and biconical waveguide modes satisfy $\lim_{r \rightarrow \infty} Z_{\text{TE}}^{(+)}(r) = \lim_{r \rightarrow \infty} Z_{\text{TM}}^{(+)}(r) = Z_{F0}$, $\lim_{r \rightarrow 0} Z_{\text{TE}}^{(+)}(r) = j \frac{k r}{v} Z_{F0}$, $\lim_{r \rightarrow 0} Z_{\text{TM}}^{(+)}(r) = -j \frac{v}{k r} Z_{F0}$.
14. Consider a dielectric slab of 1 mm thickness and relative permittivity $\epsilon_r = 12$. Give the cutoff frequency of the eight lowest surface wave modes.
15. Consider a perfectly conducting metallic plate clad by a dielectric layer of 0.5 mm thickness and relative permittivity $\epsilon_r = 12$. Give the cutoff frequencies of the eight lowest surface wave modes.
16. Design an optical fiber for monomode transmission of light with a free-space wavelength $\lambda_0 = 1.6 \mu\text{m}$. Let the refractive index of the core be $n_1 = 1.5$ and the refractive index of the cladding $n_2 = 1.497$.
 - a) Determine the core diameter such that the normalized frequency is $w = 2$.
 - b) Give the cutoff wavelength of the next two modes.
17. Consider the shielded microstrip line with cross-section depicted in Figure 7.18. The dimensions are $a = 4 \text{ mm}$, $b = 2 \text{ mm}$, $w = 0.6 \text{ mm}$ and $h = 0.6 \text{ mm}$. The region $0 \leq y \leq h$ is filled with a dielectric with relative permittivity $\epsilon_r = 12$. Use the quasistatic approximation in the following computations.
 - a) Compute the capacitance per unit of length.

- b) Compute the inductance per unit of length.
- c) Compute the wave velocity.
- d) Compute the characteristic impedance.

Hint: The numerical computations require some numerical effort. Using a high-level programming tool like Mathematica or Matlab will be helpful.

REFERENCES

- [1] J. A. Stratton, *Electromagnetic Theory*. New York: McGraw-Hill, 1941.
- [2] R. E. Collin, *Field Theory of Guided Waves*. New York: IEEE Press, 1991.
- [3] R. F. Harrington, *Time Harmonic Electromagnetic Fields*. New York: McGraw-Hill, 1961.
- [4] S. Ramo, J. R. Whinnery, and T. van Duzer, *Fields and Waves in Communication Electronics*. New York: John Wiley & Sons, 1965.
- [5] C. A. Balanis, *Advanced Engineering Electromagnetics*. New York: John Wiley & Sons, 1989.
- [6] P. I. Kuznetsov and R. L. Stratonovich, *The Propagation of Electromagnetic Waves in Multiconductor Transmission Lines*. Oxford: Pergamon Press, 1964.
- [7] S. Frankel, *Multiconductor Transmission Line Analysis*. Boston: Artech House, 1977.
- [8] J. A. Brandão Faria, *Multiconductor Transmission-Line Structures*. New York: John Wiley & Sons, 1993.
- [9] N. Fäché, F. Olyslager, and D. De Zutter, *Electromagnetic Circuit Modelling of Multiconductor Transmission Lines*. Oxford: Clarendon Press, 1993.
- [10] C. R. Paul, *Analysis of Multiconductor Transmission Lines*. New York: John Wiley & Sons, 1994.
- [11] A. F. D. Santos and J. P. Figanier, "The method of series expansion in the frequency domain applied to multidielectric transmission lines," *IEEE Trans. Microwave Theory Techn.*, vol. 23, pp. 753–756, Sept. 1975.
- [12] I. V. Lindell, "On the quasi-TEM modes in inhomogeneous multiconductor transmission lines," *IEEE Trans. Microwave Theory Techn.*, vol. 29, pp. 812–817, Aug. 1981.
- [13] I. V. Lindell and Q. Gu, "Theory of Time-Domain Quasi-TEM Modes Multiconductor Lines in Inhomogeneous Multiconductor Lines," *IEEE Trans. Microwave Theory Techn.*, vol. 35, pp. 893–897, Oct. 1987.
- [14] K. C. Gupta, R. Garg, I. Bahl, and P. Bhartia, *Microstrip Lines and Slotlines*. Boston: Artech House, 1996.
- [15] B. C. Wadell, *Transmission Line Design Handbook*. Boston: Artech House, 1991.
- [16] K. Chang, *Handbook of Microwave and Optical Components, Vol. 1, Microwave Passive and Antenna Components*. New York: John Wiley & Sons, 1989.
- [17] R. K. Hoffmann, *Integrierte Mikrowellenschaltungen*. Berlin: Springer, 1983.
- [18] H. A. Wheeler, "Transmission line properties of parallel strips separated by a dielectric sheet," *IEEE Trans. Microwave Theory Techn.*, vol. 13, pp. 172–185, Mar. 1965.
- [19] H. A. Wheeler, "Transmission line properties of a strip on a dielectric sheet on a plane," *IEEE Trans. Microwave Theory Techn.*, vol. 25, pp. 631–647, Aug. 1977.
- [20] M. V. Schneider, "Microstrip lines for microwave integrated circuits," *Bell System Tech. J.*, vol. 1969, pp. 1422–1444, 1969.
- [21] E. O. Hammerstad, "Accurate models for microstrip computer-aided design," *1980 Int. Microwave Symposium Digest*, pp. 407–409, June 1980.
- [22] R. C. Booton, *Computational Methods for Electromagnetics and Microwaves*. New York: John Wiley & Sons, 1992.
- [23] P. Morse and H. Feshbach, *Methods of Theoretical Physics, Part 1*. New York: McGraw-Hill, 1953.

- [24] H. Hancock, *Lectures on the Theory of Elliptic Functions*. New York: Peter Peregrinus, 1958.
- [25] M. Abramowitz and I. Stegun, *Handbook of Mathematical Functions with Formulas, Graphs and Mathematical Tables*. New York: Dover, 1965.
- [26] J. Rayleigh, "On the passage of electric waves through tubes, or the vibrations of dielectric cylinders," *Phil. Mag.*, vol. 43, pp. 125–132, Feb. 1897.
- [27] H. Kogelnik, "Theory of dielectric waveguides," in *Integrated Optics* (T. Tamir, ed.), no. 7 in Topics in Applied Optics, pp. 13–81, Berlin Heidelberg New York: Springer, 1979.
- [28] H. G. Unger, *Planar Optical Waveguides and Fibers*. Oxford: Clarendon Press, 1977.
- [29] D. Marcuse, *Light Transmission Optics*. New York: Van Nostrand Reinhold, 1982.
- [30] J. A. Buck, *Fundamentals of Optical Fibers*. New York: John Wiley & Sons, 1995.
- [31] K. Chang, *Handbook of Microwave and Optical Components, Vol. 3, Optical Components*. New York: John Wiley & Sons, 1990.

Chapter 8

The Transmission-Line Equations

8.1 THE TRANSMISSION-LINE CONCEPT

In this chapter we are concerned with the longitudinal variations of the wave amplitudes on a transmission-line. We assume the transmission-line to be excited in a certain mode. The transverse field distribution is determined by the excited mode. In the longitudinal direction the spatial variation of the field is governed by the *transmission-line equations* (7.57a) and (7.57b). Transmission-line theory is presented in [1–4].

In our treatment of the TEM waveguide we have observed that the transverse field distribution is only determined by the geometry of the waveguide. The state of a transmission-line is described completely by the scalar quantities $\underline{V}(z)$ and $\underline{I}(z)$, respectively. Current and voltage are governed by the line equations (7.67) and (7.72). In the same way we can describe the TE_{10} mode of a rectangular waveguide by the transmission-line equations (7.273a) and (7.273b), if we are introducing *generalized currents* and *generalized voltages* to describe the electromagnetic wave in the waveguide. If we are choosing a certain mode in a waveguide, the specific state of excitation also is given by the generalized voltage and the generalized current, which depend on the longitudinal coordinate z only. We can now formulate the transmission-line equations in a more general form, which is valid for TEM modes in two-conductor waveguides as

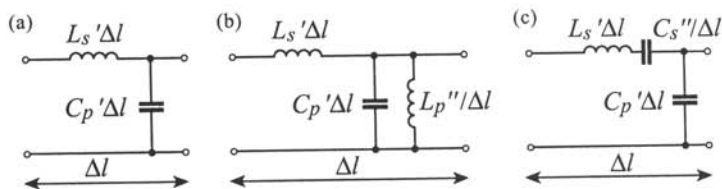


Figure 8.1: Equivalent circuits for (a) the TEM waveguide, (b) the TE waveguide, and (c) the TM waveguide.

Table 8.1: Transmission-Line Parameters of Lossless Waveguides

Mode	Impedance per unit of length Z'	Admittance per unit of length Y'	Characteristic impedance Z_0	Phase coefficient β
TEM	$j\omega L'_s$	$j\omega C'_p$	$\sqrt{\frac{L'_s}{C'_p}}$	$\omega\sqrt{L'_s C'_p}$
TE	$j\omega L'_s$	$j\left(\omega C'_p - \frac{1}{\omega L'_p}\right)$	$Z_H = \frac{Z_F}{\sqrt{1 - \left(\frac{\lambda_0}{\lambda_c}\right)^2}}$	$\frac{\omega}{c}\sqrt{1 - \left(\frac{\lambda_0}{\lambda_c}\right)^2}$
	$j\frac{\omega Z_F}{c}$	$j\frac{\omega}{cZ_F}\left(1 - \frac{\omega^2}{\omega_c^2}\right)$		
TM	$j\left(\omega L'_s - \frac{1}{\omega C'_s}\right)$	$j\omega C'_p$	$Z_E = Z_F\sqrt{1 - \left(\frac{\lambda_0}{\lambda_c}\right)^2}$	$\frac{\omega}{c}\sqrt{1 - \left(\frac{\lambda_0}{\lambda_c}\right)^2}$
	$j\frac{\omega Z_F}{c}\left(1 - \frac{\omega^2}{\omega_c^2}\right)$	$j\frac{\omega}{cZ_F}$		

well as for TE and TM modes,

$$\frac{dV}{dz} = -Z' \underline{I}, \quad \frac{dI}{dz} = -Y' \underline{V}. \quad (8.1)$$

The characteristic impedance Z_0 is given by

$$Z_0 = \sqrt{\frac{Z'}{Y'}}. \quad (8.2)$$

The propagation coefficient $\underline{\gamma}$ is given by

$$\gamma = \alpha + j\beta = \sqrt{Z'Y'}. \quad (8.3)$$

For the TEM wave and for the TE₁₀ waveguide mode we know the impedance per unit of length Z' and the admittance per unit of length Y' . If we now assume that transmission-line equations of the type of (8.1) also are valid for other waveguide modes, we can derive the impedance per unit of length Z' and the admittance per unit of length Y' from the characteristic impedance Z_0 and the propagation coefficient γ of these modes using (8.2) and (8.3),

$$Z' = \gamma Z_0, \quad Y' = \frac{\gamma}{Z_0}. \quad (8.4)$$

These quantities are summarized in Table 8.1 for the lossless line. Using the impedance per unit of length Z' and the admittance per unit of length Y' we can specify the equivalent circuits according to Figure 8.1 for short line segments of length Δl . The equivalent circuits according to Figure 8.1(a) and 8.1(b) are the equivalent circuits already derived for the TEM waveguide mode and for the rectangular waveguide mode. The equivalent circuits according to Figure 8.1(b) and 8.1(c) are valid in general for the TE_{mn} modes and TM_{mn} modes of waveguides, respectively. In Figure 8.1(b) and 8.1(c) we have applied for the first time the network concept to a waveguide segment where current and voltage are not defined as usual by line integrals over magnetic and electric fields, respectively. This extension of the network concept will be very useful in the following. It allows not only a simple description of waveguide circuits, but also the application of network theory to waveguide circuits.

8.2 GENERALIZED VOLTAGES AND CURRENTS

Like voltages and currents generalized voltages and generalized currents are integral field quantities. For these integral field quantities different definitions are used in literature. For transverse electromagnetic waves the definition of current and voltage as usual by line integrals makes sense. We also want to introduce for waveguide modes definitions of generalized voltages and generalized currents, which are independent from the waveguide modes. For the TE_{10} mode of the rectangular waveguide we have introduced the generalized voltage \underline{V} and the generalized current \underline{I} such that they are interrelated with the transmitted active power according to (7.262). We want to keep this definition in the following. Since the transmitted active power depends on the transverse components of the electromagnetic field, it makes sense to define the generalized currents and voltages as integrals of the transverse field intensities of the waveguide modes.

We subdivide the field in the waveguide into transverse and longitudinal components. The transverse field components are described by the differential forms $\underline{\mathcal{E}}_{tr}$ and $\underline{\mathcal{H}}_{tr}$, respectively, and the longitudinal components are described by the differential forms $\underline{\mathcal{E}}_l$ and $\underline{\mathcal{H}}_l$, respectively. For the xy -plane as the transverse plane and z -direction as the longitudinal direction, we obtain

$$\underline{\mathcal{E}}(\mathbf{x}) = \underline{\mathcal{E}}_{tr}(\mathbf{x}) + \underline{\mathcal{E}}_l(\mathbf{x}), \quad (8.5a)$$

$$\underline{\mathcal{H}}(\mathbf{x}) = \underline{\mathcal{H}}_{tr}(\mathbf{x}) + \underline{\mathcal{H}}_l(\mathbf{x}) \quad (8.5b)$$

with

$$\underline{\mathcal{E}}_{tr}(\mathbf{x}) = \underline{E}_x(\mathbf{x}) dx + \underline{E}_y(\mathbf{x}) dy, \quad (8.6a)$$

$$\underline{\mathcal{E}}_l(\mathbf{x}) = \underline{E}_z(\mathbf{x}) dz, \quad (8.6b)$$

$$\underline{\mathcal{H}}_{\text{tr}}(\mathbf{x}) = \underline{H}_x(\mathbf{x}) dx + \underline{H}_y(\mathbf{x}) dy, \quad (8.6c)$$

$$\underline{\mathcal{H}}_l(\mathbf{x}) = \underline{H}_z(\mathbf{x}) dz. \quad (8.6d)$$

We now split up the transverse field intensities as in (7.27a) and (7.27b) into the *complex amplitudes* $\underline{V}(z)$ and $\underline{I}(z)$ and the real normalized *structure functions* $\mathbf{e}(x, y)$ and $\mathbf{h}(x, y)$. For the TEM mode $\mathbf{e}(x, y)$ and $\mathbf{h}(x, y)$ have been normalized in Section 4.4 such that $\underline{V}(z)$ and $\underline{I}(z)$ are defined via the path integral from conductor 1 to conductor 2 and the circulation integral around conductor 2.

In (7.27a) and (7.27b) we introduced the structure functions \mathbf{e} and \mathbf{h} . Introducing structure functions for the transverse field components we generalize the definition of the *structure functions* for TEM, TE, and TM waves,

$$\underline{E}_{\text{tr}}(\mathbf{x}) = \underline{V}(z)\mathbf{e}(x, y), \quad (8.7a)$$

$$\underline{H}_{\text{tr}}(\mathbf{x}) = \underline{I}(z)\mathbf{h}(x, y). \quad (8.7b)$$

In (7.27a) and (7.27b) the differential forms e and h were introduced:

$$e(x, y) = e_x(x, y) dx + e_y(x, y) dy, \quad (8.8a)$$

$$h(x, y) = h_x(x, y) dx + h_y(x, y) dy. \quad (8.8b)$$

From (8.7a) and (8.7b) we obtain the corresponding relation for the differential forms:

$$\underline{\mathcal{E}}_{\text{tr}}(\mathbf{x}) = \underline{V}(z)e(x, y), \quad (8.9a)$$

$$\underline{\mathcal{H}}_{\text{tr}}(\mathbf{x}) = \underline{I}(z)h(x, y). \quad (8.9b)$$

Let us first consider the TEM modes. For the TEM mode the field intensities are coincident with the transverse field intensities. We can normalize the structure functions via path integrals with the normalization already given in (7.31a) and (7.31b).

Figure 8.2 shows the relation of the direction of the arrows for current and voltage and the direction of field lines and the Poynting vector. For the waveguide the introduction of integral field quantities can only be performed if the path of integration is specified. The disadvantage of this method, however, is that we have to specify a path of integration for every waveguide mode, and a definition of a path of integration independent from the mode is not possible. We therefore will perform the normalization on the basis of the area integral over the absolute squares of the transverse field quantities. The active power transmitted by the waveguide is given by

$$P = \frac{1}{2}\Re \left\{ \int_A \underline{\mathcal{E}}_{\text{tr}}(x, y) \wedge \underline{\mathcal{H}}_{\text{tr}}^*(x, y) \right\}. \quad (8.10)$$

The area integral is performed over the cross-sectional area A of the waveguide. Inserting (8.9a) and (8.9b) yields

$$P = \frac{1}{2}\Re \{ \underline{V}(z) \underline{I}^*(z) \} \int_A e(x, y) \wedge h(x, y). \quad (8.11)$$

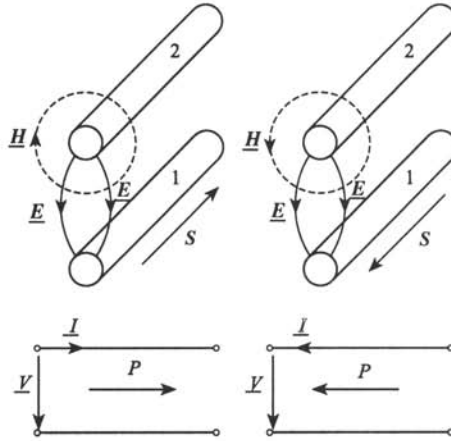


Figure 8.2: Relation of arrows and field orientation in the TEM waveguide.

From (7.31a) and (7.31b) we obtain

$$\int_A \underline{e}(x, y) \wedge h(x, y) = - \int_{C_1} \underline{e}(x, y) \oint_{C_2} h(x, y) = 1 \quad (8.12)$$

and with this from (8.11)

$$P = \frac{1}{2} \Re \{ \underline{V}(z) \underline{I}(z)^* \} . \quad (8.13)$$

To consider rectangular and circular hollow waveguides we summarize (7.241), (7.242), (7.248) and (7.249), which have been derived for waveguides with a rectangular cross-section in

$$\frac{\underline{E}_x}{\underline{H}_y} = - \frac{\underline{E}_y}{\underline{H}_x} = Z_0 . \quad (8.14)$$

Furthermore

$$Z_0 = \begin{cases} Z_{TE} & \text{for TE modes} \\ Z_{TM} & \text{for TM modes} \end{cases} \quad (8.15)$$

is valid. Since (7.243) and (7.250) also have to be considered for waveguides with a rectangular cross-section as well as for waveguides with a circular cross-section, we obtain

$$\underline{\mathcal{H}}_{tr} = \frac{1}{Z_0} * dz \wedge \underline{\mathcal{E}}_{tr} , \quad (8.16a)$$

$$\underline{\mathcal{E}}_{tr} = -Z_0 * dz \wedge \underline{\mathcal{H}}_{tr} . \quad (8.16b)$$

We now are inserting (8.9a) and (8.16a) into (8.10) and obtain for the guided wave propagating in positive z -direction the transmitted active power

$$P = \frac{1}{2Z_0} |\underline{V}|^2 \int_A \mathbf{e} \wedge \star (\mathrm{d}z \wedge \mathbf{e}). \quad (8.17)$$

This yields

$$P = \frac{1}{2Z_0} |\underline{V}|^2 \int_A (e_x^2 + e_y^2) \mathrm{d}x \wedge \mathrm{d}y. \quad (8.18)$$

We now specify the structure function \mathbf{e} to be real and normalize it according to

$$\int_A (e_x^2 + e_y^2) \mathrm{d}x \wedge \mathrm{d}y = 1. \quad (8.19)$$

Inserting (8.8b) and (8.16b) into (8.10) we obtain for the active power P transmitted in the positive z -direction

$$P = \frac{1}{2} Z_0 |\underline{I}|^2 \int_A (h_x^2 + h_y^2) \mathrm{d}x \wedge \mathrm{d}y. \quad (8.20)$$

We now normalize the real structure function \mathbf{h} according to

$$\int_A (h_x^2 + h_y^2) \mathrm{d}x \wedge \mathrm{d}y = 1. \quad (8.21)$$

The differential forms of the electric and magnetic structure functions are related via

$$\mathbf{h} = \star (\mathrm{d}z \wedge \mathbf{e}), \quad (8.22a)$$

$$\mathbf{e} = -\star (\mathrm{d}z \wedge \mathbf{h}). \quad (8.22b)$$

From (8.22a), (8.22b) and (8.20) it follows that

$$\int_A \mathbf{e} \wedge \mathbf{h} = 1. \quad (8.23)$$

Application of this normalization to the TE_{10} mode of the rectangular waveguide yields

$$\underline{\mathcal{E}}_{\mathrm{tr}} = \sqrt{\frac{2}{ab}} \underline{V} \sin \frac{\pi x}{a} \mathrm{d}y, \quad (8.24a)$$

$$\underline{\mathcal{H}}_{\mathrm{tr}} = \frac{1}{Z_0} \star \mathrm{d}z \wedge \underline{\mathcal{E}}_{\mathrm{tr}} = -\sqrt{\frac{2}{ab}} \underline{I} \sin \frac{\pi x}{a} \mathrm{d}x. \quad (8.24b)$$

Concerning the structure functions we have only decided that they are real and that their absolute square is normalized. We may choose the sign of \underline{V} and \underline{I} , and we have

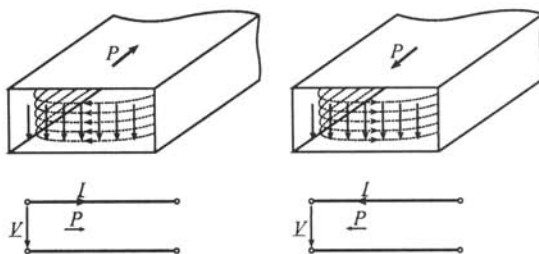


Figure 8.3: Relation of arrows and field orientation in a hollow waveguide.

to decide how the signs of \underline{V} and \underline{I} shall be related to the direction of the electric and magnetic fields. Figure 8.3 shows the assignment chosen in the following for the relation between the arrow of the generalized voltage \underline{V} and the generalized current \underline{I} , respectively, and the direction of the field quantities in the TE_{10} mode.

We note that for TEM modes the currents and voltages are defined in the conventional way via the line integrals over \mathcal{H} and \mathcal{E} . Therefore, the ratio of voltage and current differs from the ratio of transverse electric and magnetic fields. The characteristic impedance for a TEM transmission-line wave therefore is not identical with the wave impedance of the corresponding field. For TE and TM modes, however, we have defined generalized voltages and currents in such a way that the ratio of generalized voltage and generalized current is identical with the ratio of the transverse electric and magnetic fields. For the modes of hollow waveguides the characteristic impedance therefore is identical with the wave impedance.

8.3 SOLUTION OF THE TRANSMISSION-LINE EQUATIONS

Eliminating \underline{V} and \underline{I} in (8.1), we obtain again the transmission-line equation, see (7.73a) and (7.73b), respectively. This second-order ordinary differential equation has the two independent solutions $e^{-\gamma z}$ and $e^{\gamma z}$ or $\cosh \gamma z$ and $\sinh \gamma z$, respectively. Let us consider the first pair of solutions. The solution $e^{-\gamma z}$ describes a wave propagating in the positive z -direction, whereas $e^{\gamma z}$ describes a wave propagating in the negative z -direction. The generalized voltage V may be represented by

$$\underline{V}(z) = \underline{V}^{(+)} e^{-\gamma z} + \underline{V}^{(-)} e^{\gamma z}, \quad (8.25)$$

where $\underline{V}^{(+)}$ and $\underline{V}^{(-)}$ are the complex amplitudes of the wave propagating in the positive and negative z -direction, respectively. Introducing (8.25) into (8.1) we obtain

$$\underline{I}(z) = \frac{1}{Z_0} (\underline{V}^{(+)} e^{-\gamma z} - \underline{V}^{(-)} e^{\gamma z}). \quad (8.26)$$

In the same way as \underline{V} , the generalized current \underline{I} may be represented by

$$\underline{I}(z) = \underline{I}^{(+)} e^{-\gamma z} + \underline{I}^{(-)} e^{\gamma z}, \quad (8.27)$$

where $\underline{I}^{(+)}$ and $\underline{I}^{(-)}$ are the complex amplitudes of the electromagnetic waves propagating in the positive and negative direction respectively. Comparing (8.26) and (8.27) we obtain

$$\underline{I}^{(+)} = \frac{\underline{V}^{(+)}}{Z_0}, \quad \underline{I}^{(-)} = -\frac{\underline{V}^{(-)}}{Z_0}. \quad (8.28)$$

If an electromagnetic wave is propagating only in one direction the ratio between voltage and current is given by Z_0 and is independent from z . If we know voltage and current at a certain point of the line (e.g., at $z = 0$), and want to compute voltage and current at any other point of the line, it is useful to represent the solution of the transmission-line equation in terms of $\cosh \gamma z$ and $\sinh \gamma z$. For the voltage \underline{V} we obtain the general solution

$$\underline{V}(z) = \underline{A} \cosh \gamma z + \underline{B} \sinh \gamma z, \quad (8.29)$$

where \underline{A} and \underline{B} are complex amplitudes. With (8.1) we obtain

$$\underline{I}(z) = -\frac{1}{Z_0} (\underline{A} \sinh \gamma z + \underline{B} \cosh \gamma z). \quad (8.30)$$

At $z = 0$ voltage and current are given by

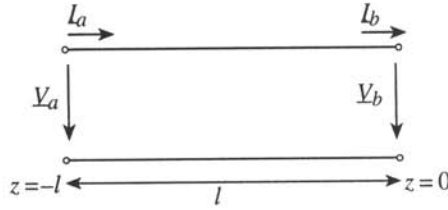
$$\underline{V}(z=0) = \underline{A}, \quad \underline{I}(z=0) = -\frac{\underline{B}}{Z_0}. \quad (8.31)$$

We therefore can express \underline{A} and \underline{B} by \underline{V} and \underline{I} and obtain

$$\underline{V}(z) = \underline{V}(z=0) \cosh \gamma z - Z_0 \underline{I}(z=0) \sinh \gamma z, \quad (8.32a)$$

$$\underline{I}(z) = -\frac{\underline{V}(z=0)}{Z_0} \sinh \gamma z + \underline{I}(z=0) \cosh \gamma z. \quad (8.32b)$$

Since we may choose the point $z = 0$ at any position of the line we may calculate from $\underline{V}(0)$ and $\underline{I}(0)$ the voltage $\underline{V}(z)$ and the current $\underline{I}(z)$ at any other position z on the line. Let us consider a line segment of length l as depicted in Figure 8.4. Let \underline{V}_a and \underline{I}_a

Figure 8.4: Line segment of length l .

be voltage and current at the input of the line segment and \underline{V}_b and \underline{I}_b the voltage and the current at the output of the line segment. We can compute \underline{V}_a and \underline{I}_a as a function of \underline{V}_b and \underline{I}_b . From (8.32a) and (8.32b) choosing $z = 0$ at the output, at the line input we then obtain $z = -l$.

$$\underline{V}_a = \underline{V}_b \cosh \gamma l + Z_0 \underline{I}_b \sinh \gamma l, \quad (8.33a)$$

$$\underline{I}_a = \frac{\underline{V}_b}{Z_0} \sinh \gamma l + \underline{I}_b \cosh \gamma l. \quad (8.33b)$$

The hyperbolic functions with the complex argument γl may be represented by

$$\sinh \gamma l = \sinh \alpha l \cos \beta l + j \cosh \alpha l \sin \beta l, \quad (8.34a)$$

$$\cosh \gamma l = \cosh \alpha l \cos \beta l + j \sinh \alpha l \sin \beta l. \quad (8.34b)$$

For the lossless line with the characteristic impedance Z_0 and the phase coefficient β we obtain

$$\underline{V}_a = \underline{V}_b \cos \beta l + j Z_0 \underline{I}_b \sin \beta l, \quad (8.35a)$$

$$\underline{I}_a = j \frac{\underline{V}_b}{Z_0} \sin \beta l + \underline{I}_b \cos \beta l. \quad (8.35b)$$

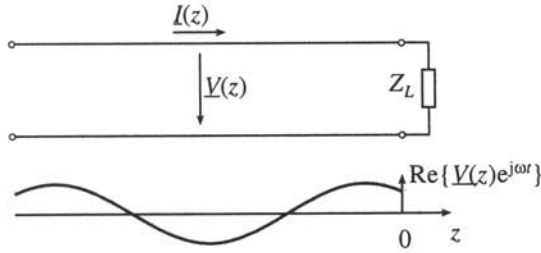
Considering a line terminated with an impedance Z_L at the end of the line at $z = 0$, according to Figure 8.5 we obtain the relation

$$\underline{V}_b = Z_L \underline{I}_b, \quad (8.36a)$$

$$Z_a = \frac{\underline{V}_a}{\underline{I}_a}. \quad (8.36b)$$

After inserting (8.33a) and (8.33b) we obtain

$$\frac{Z_a}{Z_0} = \frac{Z_L + Z_0 \tanh \gamma l}{Z_0 + Z_L \tanh \gamma l}. \quad (8.37)$$

Figure 8.5: Line terminated with Z_L .

For complex γ we use

$$\tanh \gamma l = \frac{\tanh \alpha l + j \tan \beta l}{1 + j \tanh \alpha l \tan \beta l}. \quad (8.38)$$

For the lossless line we therefore obtain

$$\frac{Z_a}{Z_0} = \frac{Z_L + j Z_0 \tan \beta l}{Z_0 + j Z_L \tan \beta l}. \quad (8.39)$$

8.4 WAVE AMPLITUDES

We already have shown that a transmission-line wave of a certain mode may be described by two complex amplitudes $\underline{V}(z)$ and $\underline{I}(z)$. If the wave is propagating in one direction only, it may be completely described either by the voltage amplitude $\underline{V}(z)$ or the current amplitude $\underline{I}(z)$, since for a wave propagating in the positive z -direction the voltage to current ratio is given by $\underline{V}(z)/\underline{I}(z) = Z_0$ and for a wave propagating in the negative z -direction the voltage to current ratio is given by $\underline{V}(z)/\underline{I}(z) = -Z_0$. Instead of voltage $\underline{V}(z)$ and current $\underline{I}(z)$ we may also use the amplitudes of the electromagnetic waves propagating in the positive and negative z -direction, respectively. In the following we assume the line to be lossless and the characteristic impedance to be real and define the *wave amplitudes* $\underline{a}(z)$ and $\underline{b}(z)$ via

$$\underline{a}(z) = \frac{1}{2\sqrt{Z_0}} [\underline{V}(z) + Z_0 \underline{I}(z)], \quad (8.40a)$$

$$\underline{b}(z) = \frac{1}{2\sqrt{Z_0}} [\underline{V}(z) - Z_0 \underline{I}(z)]. \quad (8.40b)$$

After inserting (8.25) and (8.26), we obtain

$$\underline{a}(z) = \frac{1}{\sqrt{Z_0}} \underline{V}^{(+)} e^{-j\beta z}, \quad (8.41a)$$

$$\underline{b}(z) = \frac{1}{\sqrt{Z_0}} \underline{V}^{(-)} e^{j\beta z}. \quad (8.41b)$$

These equations show that $\underline{a}(z)$ describes the wave propagating in the positive z -direction, whereas $\underline{b}(z)$ describes a wave propagating in the negative z -direction. The voltage $\underline{V}(z)$ and the current $\underline{I}(z)$ may be expressed by the wave amplitudes $\underline{a}(z)$ and $\underline{b}(z)$ as follows

$$\underline{V}(z) = \sqrt{Z_0} [\underline{a}(z) + \underline{b}(z)], \quad (8.42a)$$

$$\underline{I}(z) = \frac{1}{\sqrt{Z_0}} [\underline{a}(z) - \underline{b}(z)]. \quad (8.42b)$$

From (8.1), (8.4), (8.40a), and (8.40b) we obtain the transmission-line equations for the wave amplitudes $\underline{a}(z)$ and $\underline{b}(z)$

$$\frac{d\underline{a}}{dz} = -j\beta \underline{a}, \quad (8.43a)$$

$$\frac{d\underline{b}}{dz} = j\beta \underline{b}. \quad (8.43b)$$

The transmission-line equations for the wave amplitudes $\underline{a}(z)$ and $\underline{b}(z)$ are not coupled. The waves propagating in the positive and negative z -directions are propagating independently. The solutions of (8.43a) and (8.43b) are given by

$$\underline{a}(z) = \underline{a}(z=0) e^{-j\beta z}, \quad (8.44a)$$

$$\underline{b}(z) = \underline{b}(z=0) e^{j\beta z}. \quad (8.44b)$$

The active power transmitted through the line in the positive z -direction is given by

$$P(z) = \frac{1}{2} \Re \{ \underline{V}(z) \underline{I}^*(z) \} = \frac{1}{2} \Re \{ |\underline{a}(z)|^2 - |\underline{b}(z)|^2 + \underline{a}^*(z) \underline{b}(z) - \underline{a}(z) \underline{b}^*(z) \}. \quad (8.45)$$

From this it follows

$$P(z) = \frac{1}{2} (|\underline{a}(z)|^2 - |\underline{b}(z)|^2). \quad (8.46)$$

The first term $|\underline{a}(z)|^2$ describes the power transmitted by the wave $\underline{a}(z)$ in the positive z -direction, whereas the second term $|\underline{b}(z)|^2$ describes the power transmitted by the wave $\underline{b}(z)$ in the negative z -direction. We have defined the wave amplitudes only for

lossless lines. This definition may also be used for lines with small losses where the complex characteristic impedance of the transmission-line can be approximated by a real characteristic impedance Z_0 . In (8.41a), (8.41b), and (8.43a)–(8.44b) we have to replace $j\beta$ with γ . This approximation is justified since the characteristic impedance of a transmission-line with weak losses only differs slightly from the characteristic impedance of a lossless line. In the treatment of waveguides and waveguide circuits, the use of wave amplitudes $\underline{a}(z)$ and $\underline{b}(z)$ is more common than the use of generalized voltages and generalized currents, the reason being that for waveguides wave amplitudes are physically descriptive and, furthermore, may be measured directly. Numerous simple design methods for microwave circuits are based on the wave amplitude description. The introduction of generalized voltages and currents, however, allows the application of common network theoretic design methods. Therefore, one always will choose the representations of the integral field quantities, which are better suited for either measurement or analysis and change the representation, if necessary.

8.5 REFLECTION COEFFICIENT AND SMITH CHART

The lossless line terminated at the end exhibits an input impedance as described by (8.39). The input impedance gives the ratio of generalized voltage \underline{V} and generalized current \underline{I} at the input of the line. We also may describe the impedance by the ratio of the complex amplitudes of the incident wave and the reflected wave. We name this ratio the *reflection coefficient* ρ defined by

$$\rho(z) = \frac{\underline{b}(z)}{\underline{a}(z)}. \quad (8.47)$$

Let us assume the reflection coefficient ρ at $z = 0$ is given by

$$\rho_0 = \frac{\underline{b}(0)}{\underline{a}(0)}. \quad (8.48)$$

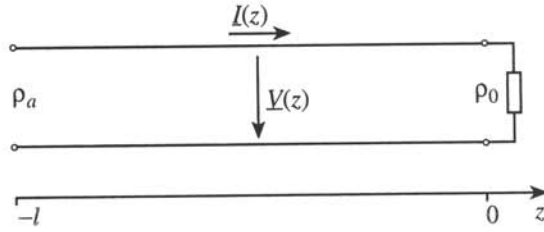
With (8.44a) and (8.44b) we obtain

$$\rho(z) = \rho_0 e^{2j\beta z}. \quad (8.49)$$

For a line segment of length l according to Figure 8.6 that is terminated at the end with ρ_0 , we obtain from (8.49) the reflection coefficient ρ at the line input

$$\rho_a = \rho(z = -l) = \rho_0 e^{-2j\beta l}. \quad (8.50)$$

From (8.42a) and (8.42b) we obtain the input impedance Z_a of the terminated line

Figure 8.6: Line terminated with ρ_0 .

$$Z_a = \frac{V_a}{I_a} = Z_0 \frac{1 + \rho_a}{1 - \rho_a}. \quad (8.51)$$

From this we obtain the following relations between impedance Z and reflection coefficient ρ ,

$$\frac{Z}{Z_0} = \frac{1 + \rho}{1 - \rho}, \quad (8.52a)$$

$$\rho = \frac{Z - Z_0}{Z + Z_0}. \quad (8.52b)$$

The description of the terminated lines by that reflection coefficient at the input is equivalent to the description by the input impedance. Comparing (8.39) and (8.49) we see that the relation between the reflection coefficient and length of the line has a much simpler form than the relation between line impedance and line length. If the reflection coefficient ρ is given at a certain point of the line, and if we propagate along the line in the positive or negative z -direction, the reflection coefficient ρ is moving on a circle with center zero in the complex ρ -plane. The graphical representation of the impedance transformation properties of a line is given by the *Smith chart* [5], depicted in Figure 8.7. The point with

$$\rho_0 = |\rho_0| e^{j\delta_0} \quad (8.53)$$

is marked in the diagram. Increasing the distance from the line termination means to move in the negative z -direction. According to (8.49) and (8.50) in this case we move clockwise on a circle $\rho = \text{const.}$ Moving by half the line wavelength $\frac{1}{2}\lambda$ corresponds to a complete rotation of 360° in the Smith chart. Mapping the coordinate grid of the Z -plane into the ρ -plane yields a circular coordinate grid as depicted in Figure 8.7. Any *linear fractional transformation* in the complex plane is mapping circles into circles [6]. Straight lines also belong to the set of circles, since a straight line may be considered as a circle through the infinite point. It is useful to normalize the mapping between the impedance and reflection coefficient with respect to the characteristic impedance Z_0 . We obtain the orthogonal circular coordinate grid for $X = \text{const.}$ and $R = \text{const.}$, respectively. This diagram with the Z -coordinate grid drawn in the ρ -plane is called the *Smith chart*. The Smith chart provides an easy way to determine the input impedance

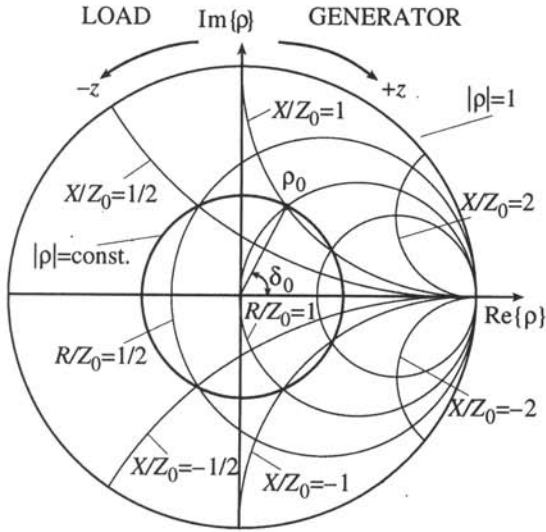


Figure 8.7: The Smith chart.

of a line terminated at the end and shows the graphic solution of impedance matching problems. It provides information regarding the impedance, reflection coefficient, and the standing wave ratio of a microwave circuit. Figure 8.8 shows the complete Smith chart with scaled curves of constant R/Z_0 and constant X/Z_0 . On the periphery of the Smith chart the phase angle βl and the normalized line length l/λ are scaled. This scaled Smith chart is a powerful tool for the graphical design of microwave circuits within a reasonable degree of accuracy. The scales of the Smith chart allow us to determine the position of a normalized impedance directly. As shown in Figure 8.7 we can determine magnitude and phase of the corresponding reflection coefficient ρ .

If a transmission-line is terminated with the wave impedance Z_0 (i.e., $Z_L = Z_0$), we obtain from (8.52b) the input reflection coefficient $\rho = 0$. If the line is terminated with its characteristic impedance no wave will be reflected from its end. Due to (8.49) we have $\rho = 0$ over the whole line length and therefore also at the input of the line no wave is reflected. In the case of a non-reflecting terminated line we have power matching. For $\rho_0 \neq 0$ the magnitudes $|\underline{V}(z)|$ and $|\underline{I}(z)|$ depend on z . To determine the z dependence of the magnitude of the voltage, we insert (8.49) and (8.53) into (8.42a) and obtain

$$|\underline{V}(z)| = |\underline{a}(0)| \sqrt{Z_0 [1 + |\rho_0|^2 + 2|\rho_0| \cos(2\beta z + \delta_0)]}. \quad (8.54)$$

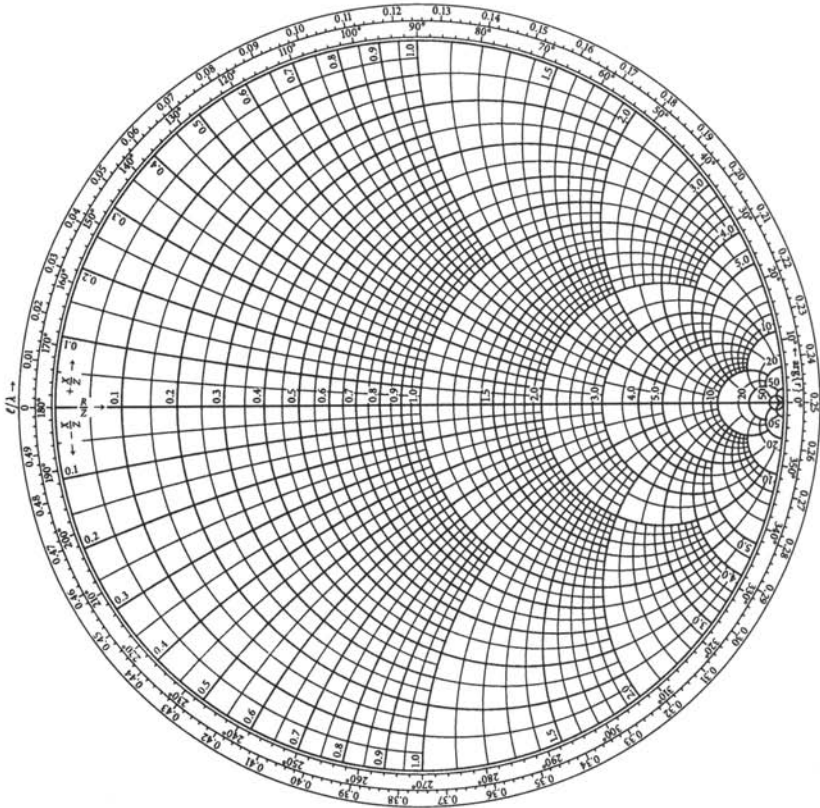


Figure 8.8: The complete Smith chart.

In the same way we obtain from (8.42b) the absolute value of the current

$$|I(z)| = |a(0)| \sqrt{\frac{1}{Z_0} [1 + |\rho_0|^2 - 2|\rho_0| \cos(2\beta z + \delta_0)]}. \quad (8.55)$$

The z dependence of $|V(z)|$ and $|I(z)|$ is demonstrated in Figure 8.9. The magnitude of the voltage $|V(z)|$ assumes its maximum value $|V(z)|_{\max}$ at z_a and its minimum value $|V(z)|_{\min}$ at z_b . From (8.54) and (8.55) we obtain for the maximum and minimum magnitudes of $|V(z)|$ and $|I(z)|$:

$$V_{\max} = Z_0 I_{\max} = \sqrt{Z_0} |a(0)| (1 + |\rho_0|), \quad (8.56a)$$

$$V_{\min} = Z_0 I_{\min} = \sqrt{Z_0} |a(0)| (1 - |\rho_0|). \quad (8.56b)$$

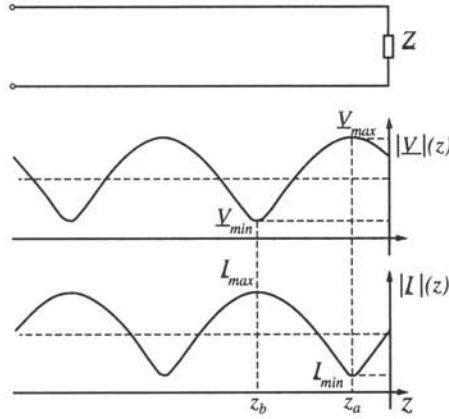


Figure 8.9: Variation of $|V(z)|$ and $|I(z)|$ along the transmission-line.

We define the *standing wave ratio* (SWR) as

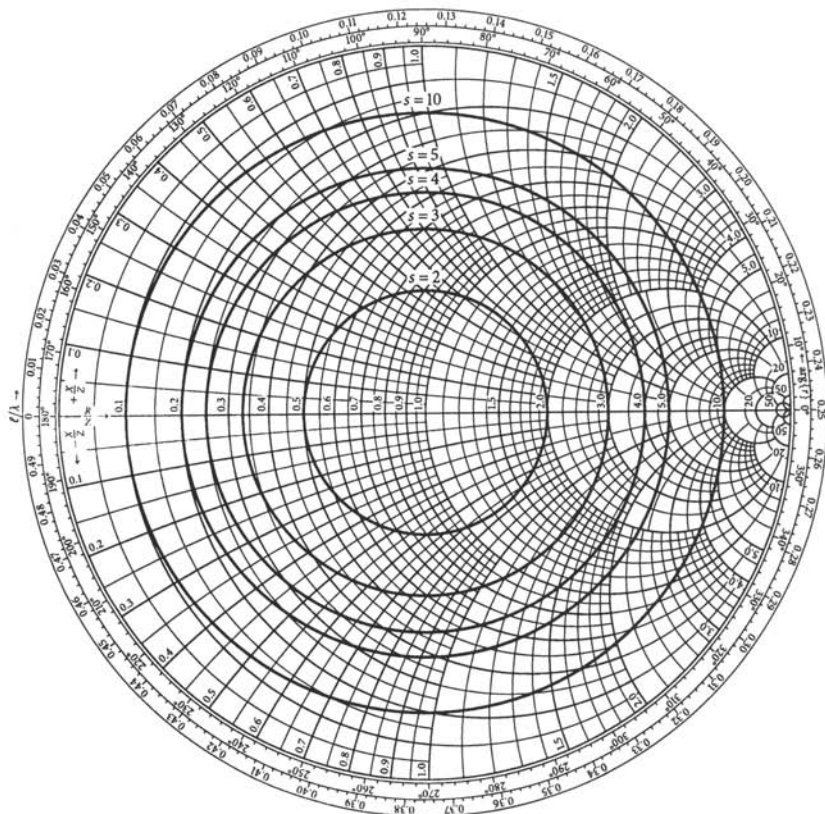
$$s = \frac{V_{\max}}{V_{\min}} = \frac{I_{\max}}{I_{\min}}. \quad (8.57)$$

The standing wave ratio s is a real number such that $1 \leq s \leq \infty$. This quantity also is called *voltage standing wave ratio* (VSWR). With (8.52a), (8.56a), and (8.56b) it follows that

$$s = \frac{Z(z_a)}{Z_0} = \frac{Z_0}{Z(z_b)}. \quad (8.58)$$

The voltage standing wave ratio depends only on the magnitude $|\rho|$ of the reflection coefficient. In the Smith chart the locations of constant s are circles centered around the origin. Figure 8.10 shows the circles of constant s .

From measuring the z dependence of the magnitude of the voltage $|V(z)|$ with a potential probe we can determine the reflection coefficient. From the ratio of the maximum magnitude and the minimum magnitude of the voltage we can determine the magnitude of the reflection coefficient from the position z_a or z_b , respectively. Using (8.54) we can determine δ_0 and thereby the phase ρ_0 . This determination may also be performed using the Smith chart since z_a and z_b are positioned on the $X = 0$ axis of the Smith chart. The right intersection of the circle $\rho = \text{const.}$ with the $X = 0$ axis yields Z_a , whereas the left intersection of the circle $\rho = \text{const.}$ with the $X = 0$ axis yields Z_b . From the Smith chart we may compute not only the complex impedance Z , but also the complex admittance Y . The *normalized impedance* \underline{z} and the *normalized admittance* \underline{y} are given by

Figure 8.10: Circles of constant s in the Smith chart.

$$\underline{z} = \frac{Z}{Z_0}, \quad (8.59a) \quad \underline{y} = Y Z_0. \quad (8.59b)$$

The normalized impedance \underline{z} and the normalized admittance \underline{y} are related by

$$\underline{y} = \underline{z}^{-1}. \quad (8.60)$$

The relation between the reflection coefficient ρ and the normalized impedance \underline{z} and the normalized \underline{y} , respectively, according to (8.52b), (8.59b), and (8.60) is given by

$$\rho = \frac{\underline{z} - 1}{\underline{z} + 1}, \quad (8.61a) \quad -\rho = \frac{\underline{y} - 1}{\underline{y} + 1}. \quad (8.61b)$$

We can use the coordinate grid of the Smith chart for the normalized impedance \underline{z} as well as for the normalized admittance \underline{y} if we consider that transforming from the

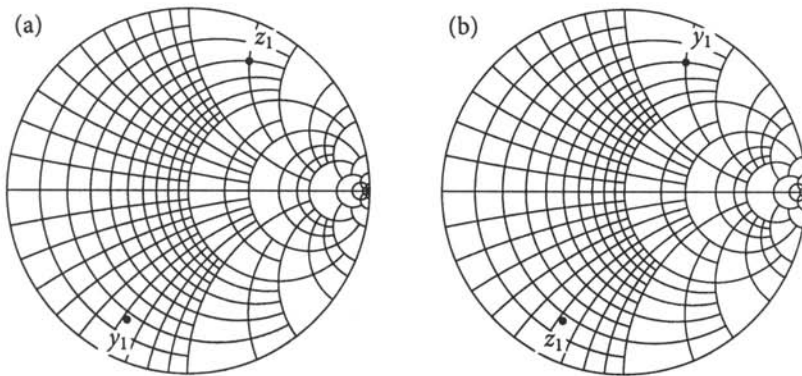


Figure 8.11: Representation of impedances and admittances in the Smith chart.

normalized impedance to the normalized admittance means a change of sign of the reflection coefficient and therefore mirroring ρ at the origin of the Smith chart.

The inversion in the impedance or admittance plane corresponds to a rotation by 180° in the ρ -plane. Figure 8.11(a) shows the Smith chart with the impedance grid. The admittance grid is depicted in Figure 8.11(b). The normalized impedance z_1 and the normalized admittance $y_1 = 1/z_1$ can be determined from the reflection coefficient ρ using the impedance or the admittance grid respectively. Instead of rotating the grid it is more convenient to rotate the ρ -plane by 180° . This means that if we want to determine the normalized admittance y_1 we remain in the impedance grid and mirror the location of the impedance at the origin of the Smith chart.

The Smith chart provides information about circuits containing transmission-line elements and is a valuable tool for microwave circuit design [7, 8]. Up to now we have assumed the transmission-line to be lossless. If the transmission-line is lossy, however, we have to replace (8.50) with

$$\rho_a = \rho_0 e^{-2\gamma l}. \quad (8.62)$$

Propagating on a lossy line from the load towards the generator, we are moving in the Smith chart on a logarithmic spiral instead of a circle (Figure 8.12). For a long lossy line the input impedance also converges to the characteristic impedance of the line if the line is not terminated with its characteristic impedance. With a lossy line we cannot perform extreme impedance transformations, since normalized impedances with very large magnitudes as well as normalized impedances with very small magnitudes are located in the Smith chart close to the point $\rho = \pm 1$. With the spiral we cannot transform to such points. A short circuit, for example, cannot be transformed with a lossy $\frac{1}{4}\lambda$ line

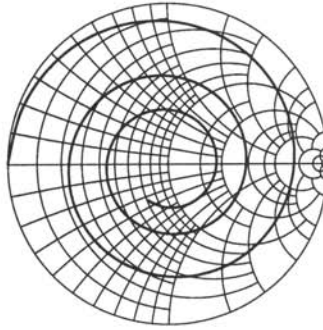


Figure 8.12: Reflection coefficient of a lossy line terminated with $(\rho_0 = -1)$.

into an open circuit with $\rho = 1$, but is transformed due to (8.62) into a finite impedance with $\rho = e^{-\frac{1}{2}\alpha\lambda}$. A detailed treatment of lossy transmission-lines is given in [9].

8.5.1 Impedance Matching with Lumped Elements

Using two lumped reactance elements any complex load Z_L with $\Re\{Z_L\} \geq 0$ can be matched to a real impedance Z_0 . Figure 8.13 shows the matching of a load with a series capacitor and a parallel inductor. Consider a load with normalized impedance $z_L = 0.2 + j2$. The location of this impedance is at the intersection of the circles $r = 0.2$ and $x = 2$. Connecting a series capacitance C_s means to move in negative direction on the circle of constant r . In this way we transform to the point z_1 . The change from the normalized impedance z_1 to the normalized admittance $y_1 = 1/z_1$ is performed by mirroring at the origin. We now are in the normalized admittance representation, where the circles of constant r and x have changed to circles of constant g and b respectively. The parallel connection of the inductor L_p yields a transformation of y_1 into the origin $\rho = 0$. To perform this transformation the real part of y_1 must be $\Re\{y_1\} = 1$. This can be achieved by drawing the auxiliary dashed half-circle that mirrors the half-circle $\Re\{y\} = 1$ at the origin. The location of z_1 is found as the intersection of the $r = \Re\{z_L\}$ circle with the dashed auxiliary circle. In this way we obtain $z_1 = 0.2 - j0.4$ with $1/j\omega C_s Z_0 = -j2.4$. Inverting z_1 yields $y_1 = 1 + j2$. The transformation from y_1 to the origin $y = 1$ is achieved by a parallel inductance L_p with $Z_0/j\omega L_p = -j2$.

Figure 8.14 shows a matching circuit consisting of a series inductor L_s and a parallel capacitor C_p to match the load impedance Z_L to the real impedance Z_0 . With the series inductor we transform z_L moving clockwise on a circle of constant r into a z_1 that can be mirrored into y_1 located on the circle of constant normalized conductivity $g = 1$. To find this point we draw the dashed auxiliary circle. For a given $z_L = 0.2 - j0.6$ we

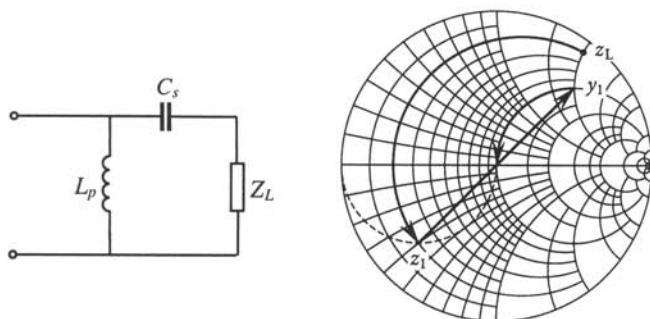


Figure 8.13: Matching of a load with a series capacitor and a parallel inductor.

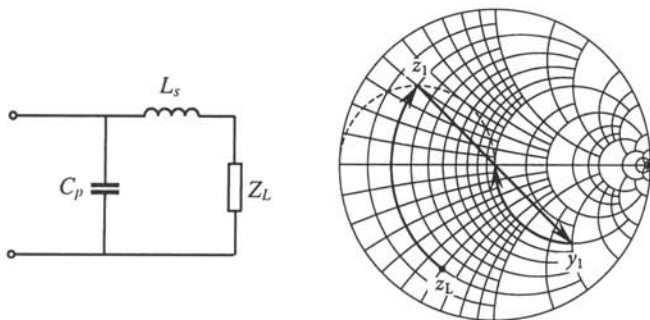


Figure 8.14: Matching of a load with a series inductor and a parallel capacitor.

obtain $z_1 = 0.2 + j0.4$ and from this $j\omega L_s/Z_0 = j$. Mirroring z_1 at the origin of the chart yields $y_1 = 1 - j2$. This normalized admittance can be transformed into the origin by a parallel capacitor with $j\omega C_p Z_0 = j2$.

In the matching circuit depicted in Figure 8.15 first an inductor L_p is connected parallel to the load impedance Z_L and then the capacitance C_s is connected in series to this circuit. Let the normalized load impedance be $z_L = 0.2 - j1.4$. Inversion of z_L by mirroring at the origin of the Smith chart yields $y_L = 0.1 + j0.7$. With the parallel conductor we move on the $g = 0.1$ -circle in negative direction to the intersection with the dashed auxiliary circle. This yields $y_1 = 0.1 - 0.3$ and $Z_0/j\omega L_p = -j$. Mirroring y_1 we obtain $z_1 = 1 + j3$. This can be transformed into the origin with a series capacitance $1/j\omega C_s Z_0 = -j3$.

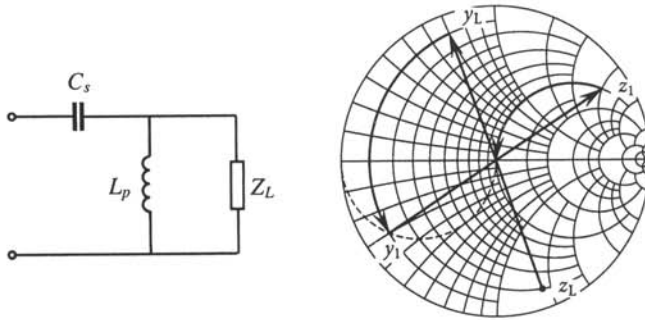


Figure 8.15: Matching of a load with a parallel inductor and a series capacitor.

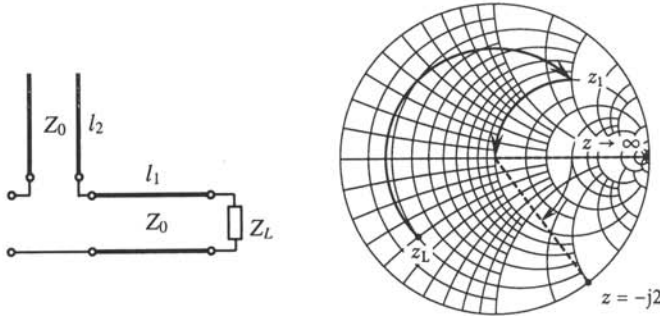


Figure 8.16: Matching of a load with transmission-line and open series stub line.

8.5.2 Impedance Matching with Stubs

At higher frequencies the realization of matching circuits with transmission-line elements becomes advantageous since the required transmission-line elements are of shorter length and allow the realization of compact matching circuits. Furthermore, transmission-line elements exhibit a higher Q -factor than lumped reactances and also can be integrated by the use of planar transmission-line elements. Open or shorted transmission-line elements allow the realization of any reactance. In addition to this the impedance transformation can be used.

Figure 8.16 shows a matching circuit consisting of a transmission-line of length l_1 and an open line stub of length l_2 . On the transmission-line the impedance is transformed on a circle of constant $|\rho|$. We choose the length l_1 of the transmission-line such that z_1 is on the circle $\Re\{z\} = 1$. From the scale on the periphery of the Smith chart we can read $l_1/\lambda = 0.25$. Via the transmission-line the load impedance is transformed into the

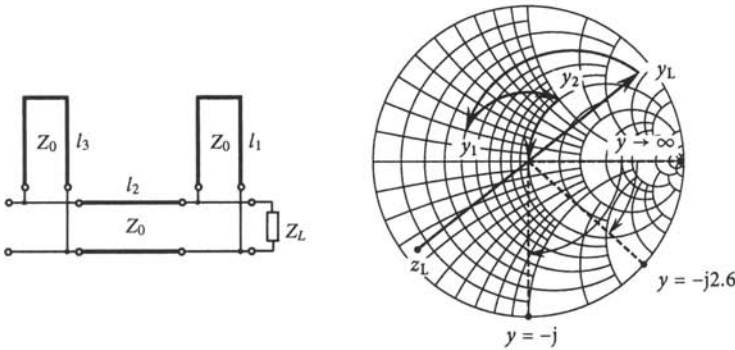


Figure 8.17: Matching of a load with two parallel short-circuited stub lines.

normalized impedance $z_1 = 1 + j2$. This can be transformed with normalized series reactance $z = -j2$ into the origin. This capacitive reactance can be realized via an open stub line. The length of the open stub line also may be determined via the Smith chart. Assume that the open stub line also has a characteristic impedance Z_0 . Then the length of the open stub determined with the Smith chart is $l_2/\lambda = 0.074$.

Figure 8.17 shows the matching of a load by two short-circuited stub lines. Starting from the load with a given normalized impedance $z_L = 0.05 - j0.35$ we obtain by mirroring at the origin $y_L = 0.4 + j2.8$. Parallel circuiting a stub with a normalized admittance $-j2.6$ yields $y_1 = 0.4 + j0.2$. This admittance can be realized with a short-circuited stub line of characteristic impedance Z_0 the length l_1 of which can also be determined with the Smith chart. We obtain an electrical length $\beta l_1 = 42.075^\circ$ which corresponds to $l_1/\lambda = 0.0584$. The next step is to transform the admittance such that its location in the Smith chart is on the circle $\Re\{y\} = 1$. The admittance is moved on a circle of constant $|\rho|$ up to the intersection with the $\Re\{y\} = 1$ -circle. This yields the normalized admittance $y_2 = 1 + j$ and the electrical length of the transmission-line $\beta l_2 = 90^\circ$ corresponding to $l_2/\lambda = 0.125$. The transformation from y_2 to the origin is performed by stub with a normalized admittance $-j$. This admittance can be realized with a short-circuited stub with an electrical length $\beta l_2 = 90^\circ$ corresponding to $l_1/\lambda = 0.125$.

8.6 SOLUTION OF THE MULTICONDUCTOR TRANSMISSION-LINE EQUATIONS

We consider a multiconductor transmission-line with $n + 1$ conductors shown in Figure 8.18. The transmission-line is assumed to be inhomogeneous, therefore the mul-

multiconductor transmission-line will exhibit n quasi-TEM modes. For a detailed treatment of multiconductor transmission-lines, see [10–15]. In the case of a lossy multiconductor transmission-line the conductor losses are described by a per-unit-length resistance matrix \mathbf{R}' and the dielectric losses are represented by a per-unit-length conductance matrix \mathbf{G}' . The first-order time-domain multiconductor transmission-line equations derived in Section 7.5, (7.98a) and (7.98b) are

$$\frac{\partial \mathbf{i}(z, t)}{\partial z} = -\mathbf{G}' \mathbf{v}(z, t) - \mathbf{C}' \frac{\partial \mathbf{v}(z, t)}{\partial t}, \quad (8.63a)$$

$$\frac{\partial \mathbf{v}(z, t)}{\partial z} = -\mathbf{R}' \mathbf{i}(z, t) - \mathbf{L}' \frac{\partial \mathbf{i}(z, t)}{\partial t} \quad (8.63b)$$

with the per-unit-length impedance matrix \mathbf{Z}' and the per-unit-length admittance matrix \mathbf{Y}' , given by

$$\mathbf{Z}' = \mathbf{R}' + j\omega \mathbf{L}', \quad (8.64a)$$

$$\mathbf{Y}' = \mathbf{G}' + j\omega \mathbf{C}'. \quad (8.64b)$$

The frequency-domain first-order transmission-line equations for the lossy multiconductor transmission-line are

$$\frac{d\mathbf{I}(z)}{dz} = -\mathbf{Y}' \mathbf{V}(z), \quad (8.65a)$$

$$\frac{d\mathbf{V}(z)}{dz} = -\mathbf{Z}' \mathbf{I}(z). \quad (8.65b)$$

In frequency-domain the second-order multiconductor transmission-line equations are given by

$$\frac{d^2 \mathbf{V}(z)}{dz^2} = \mathbf{Z}' \mathbf{Y}' \mathbf{V}(z), \quad (8.66a)$$

$$\frac{d^2 \mathbf{I}(z)}{dz^2} = \mathbf{Y}' \mathbf{Z}' \mathbf{I}(z). \quad (8.66b)$$

For a closed form frequency-domain solution of the multiconductor transmission-line equations we diagonalize the per-unit-length impedance and admittance matrices \mathbf{Z}' and \mathbf{Y}' by a similarity transformation (see Section C.2). We seek matrices \mathbf{M}_V and \mathbf{M}_I such that $\mathbf{M}_V^{-1} \mathbf{Z}' \mathbf{M}_I$ and $\mathbf{M}_I^{-1} \mathbf{Y}' \mathbf{M}_V$ are diagonal and given by

$$\mathbf{M}_V^{-1} \mathbf{Z}' \mathbf{M}_I = \tilde{\mathbf{Z}}' = \text{diag}[\tilde{Z}_1, \tilde{Z}_2, \dots, \tilde{Z}_n], \quad (8.67a)$$

$$\mathbf{M}_I^{-1} \mathbf{Y}' \mathbf{M}_V = \tilde{\mathbf{Y}}' = \text{diag}[\tilde{Y}_1, \tilde{Y}_2, \dots, \tilde{Y}_n]. \quad (8.67b)$$

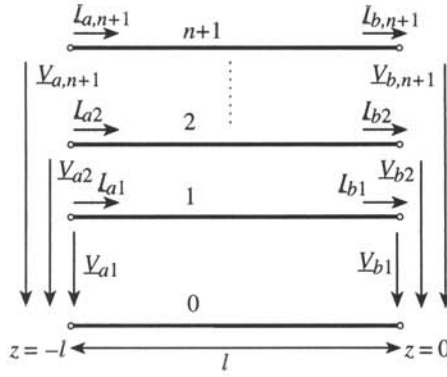


Figure 8.18: Multiconductor transmission-line segment of length l .

The *mode voltages* $\underline{\tilde{V}}(z)$ and *mode currents* $\underline{\tilde{I}}(z)$ are given by

$$\underline{\tilde{V}}(z) = \underline{M}_V^{-1} \underline{V}(z), \quad (8.68a)$$

$$\underline{\tilde{I}}(z) = \underline{M}_I^{-1} \underline{I}(z). \quad (8.68b)$$

Inserting (8.67a) to (8.68b) into (8.65a) and (8.65b) yields

$$\frac{d\underline{\tilde{I}}(z)}{dz} = -\tilde{\mathbf{Y}}' \underline{\tilde{V}}(z), \quad (8.69a)$$

$$\frac{d\underline{\tilde{V}}(z)}{dz} = -\tilde{\mathbf{Z}}' \underline{\tilde{I}}(z), \quad (8.69b)$$

where the modes are uncoupled. From this we obtain the uncoupled second-order multiconductor transmission-line equations

$$\frac{d^2 \underline{\tilde{V}}(z)}{dz^2} = \tilde{\mathbf{Z}}' \tilde{\mathbf{Y}}' \underline{\tilde{V}}(z), \quad (8.70a)$$

$$\frac{d^2 \underline{\tilde{I}}(z)}{dz^2} = \tilde{\mathbf{Y}}' \tilde{\mathbf{Z}}' \underline{\tilde{I}}(z). \quad (8.70b)$$

From (8.67a) and (8.67b) we obtain

$$\tilde{\mathbf{Z}}' \tilde{\mathbf{Y}}' = \underline{M}_V^{-1} \mathbf{Z}' \mathbf{Y}' \underline{M}_V, \quad (8.71a)$$

$$\tilde{\mathbf{Y}}' \tilde{\mathbf{Z}}' = \underline{M}_I^{-1} \mathbf{Y}' \mathbf{Z}' \underline{M}_I. \quad (8.71b)$$

Since \tilde{Z}' and \tilde{Y}' are both diagonal matrices, their product is commutative, that is,

$$\tilde{Z}'\tilde{Y}' = \tilde{Y}'\tilde{Z}' \quad (8.72)$$

and the expressions $M_V^{-1}Z'Y'M_V$ and $M_I^{-1}Z'Y'M_I$ are identical with their transposes. We therefore can write

$$M_V^{-1}Z'Y'M_V = M_V^T Y' Z' (M_V^{-1})^T = M_I^{-1} Y' Z' M_I = M_I^T Y' Z' (M_I^{-1})^T. \quad (8.73)$$

From this it follows $M_V^{-1} = M_I^T$. This means that we only need to diagonalize either the product $Z'Y'$ or the product $Y'Z'$. We introduce

$$M = M_V = (M_I^T)^{-1}. \quad (8.74)$$

Introducing the diagonal matrix

$$\tilde{y}^2 = \tilde{Z}'\tilde{Y}' = \tilde{Y}'\tilde{Z}' = \text{diag}[\tilde{y}_1^2, \tilde{y}_2^2, \dots, \tilde{y}_n^2], \quad (8.75)$$

the uncoupled second-order multiconductor transmission-line equations (8.70a) and (8.70b) can be written as

$$\frac{d^2 \tilde{V}(z)}{dz^2} = \tilde{y}^2 \tilde{V}(z), \quad (8.76a)$$

$$\frac{d^2 \tilde{I}(z)}{dz^2} = \tilde{y}^2 \tilde{I}(z). \quad (8.76b)$$

According to (8.25) and (8.26) the solutions are given by

$$\tilde{V}(z) = e^{-\tilde{y}z} \tilde{V}^{(+)} + e^{\tilde{y}z} \tilde{V}^{(-)}, \quad (8.77a)$$

$$\tilde{I}(z) = e^{-\tilde{y}z} \tilde{I}^{(+)} + e^{\tilde{y}z} \tilde{I}^{(-)} \quad (8.77b)$$

with

$$e^{\pm \tilde{y}z} = \text{diag}[e^{\pm \tilde{y}_1 z}, e^{\pm \tilde{y}_2 z}, \dots, e^{\pm \tilde{y}_n z}]. \quad (8.78)$$

The modal voltage and current amplitudes are summarized in the vectors

$$\tilde{V}^{(\pm)}(z) = [\tilde{V}_1^{(\pm)}, \tilde{V}_2^{(\pm)}, \dots, \tilde{V}_n^{(\pm)}]^T, \quad (8.79a)$$

$$\tilde{I}^{(\pm)}(z) = [\tilde{I}_1^{(\pm)}, \tilde{I}_2^{(\pm)}, \dots, \tilde{I}_n^{(\pm)}]^T. \quad (8.79b)$$

With (8.68a) and (8.68b) we obtain from (8.77a) and (8.77b) the conductor voltages $\underline{V}(z)$ and conductor currents $\underline{I}(z)$ as

$$\underline{V}(z) = \underline{M} \left(e^{-\tilde{\gamma}z} \underline{\tilde{V}}^{(+)} + e^{\tilde{\gamma}z} \underline{\tilde{V}}^{(-)} \right), \quad (8.80a)$$

$$\underline{I}(z) = (\underline{M}^T)^{-1} \left(e^{-\tilde{\gamma}z} \underline{\tilde{I}}^{(+)} + e^{\tilde{\gamma}z} \underline{\tilde{I}}^{(-)} \right). \quad (8.80b)$$

Inserting (8.80a) into (8.69b) yields

$$\underline{I}(z) = \tilde{\underline{Z}}'^{-1} \underline{M} \underline{\gamma} \left(e^{-\tilde{\gamma}z} \underline{\tilde{V}}^{(+)} - e^{\tilde{\gamma}z} \underline{\tilde{V}}^{(-)} \right). \quad (8.81)$$

We define the *characteristic impedance matrix*

$$\underline{Z}_0 = \underline{M} \underline{\gamma}^{-1} \underline{M}^{-1} \tilde{\underline{Z}}. \quad (8.82)$$

With this the current vector (8.81) can be expressed as

$$\underline{I}(z) = \underline{Z}_0^{-1} \underline{M} \left(e^{-\tilde{\gamma}z} \underline{\tilde{V}}^{(+)} - e^{\tilde{\gamma}z} \underline{\tilde{V}}^{(-)} \right). \quad (8.83)$$

We decompose the multiconductor transmission-line waves into waves propagating in positive z -direction described by the voltage and current vectors $\underline{V}^{(+)}(z)$ and $\underline{I}^{(+)}(z)$ and waves propagating in negative z -direction described by the voltage and current vectors $\underline{V}^{(-)}(z)$ and $\underline{I}^{(-)}(z)$,

$$\underline{V}(z) = \underline{V}^{(+)}(z) + \underline{V}^{(-)}(z), \quad (8.84a)$$

$$\underline{I}(z) = \underline{I}^{(+)}(z) + \underline{I}^{(-)}(z). \quad (8.84b)$$

The voltage and current vectors of the unidirectional waves follow from (8.84a) and (8.83) as

$$\underline{V}^{(+)}(z) = \underline{M} e^{-\tilde{\gamma}z} \underline{\tilde{V}}^{(+)}, \quad (8.85a)$$

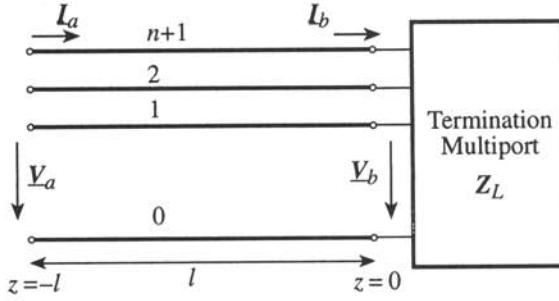
$$\underline{V}^{(-)}(z) = \underline{M} e^{\tilde{\gamma}z} \underline{\tilde{V}}^{(-)}, \quad (8.85b)$$

$$\underline{I}^{(+)}(z) = \underline{Z}_0^{-1} \underline{M} e^{-\tilde{\gamma}z} \underline{\tilde{V}}^{(+)}, \quad (8.85c)$$

$$\underline{I}^{(-)}(z) = -\underline{Z}_0^{-1} \underline{M} e^{\tilde{\gamma}z} \underline{\tilde{V}}^{(-)}. \quad (8.85d)$$

We define the *reflection coefficient matrix* $\underline{\Gamma}(z)$ relating the backward-propagating voltage waves to the forward-propagating voltage waves via

$$\underline{V}^{(-)}(z) = \underline{\Gamma}(z) \underline{V}^{(+)}(z). \quad (8.86)$$

Figure 8.19: Multiconductor transmission-line segment of length l .

Inserting (8.85a) and (8.85b) yields

$$\underline{M}e^{\tilde{\gamma}z} \underline{\tilde{V}}^{(-)} = \underline{\Gamma}(z) \underline{M}e^{-\tilde{\gamma}z} \underline{\tilde{V}}^{(+)} . \quad (8.87)$$

From this we obtain the relation between reflection coefficient matrix values at the two longitudinal coordinates z and z_1 ,

$$\underline{\Gamma}(z) = \underline{M}e^{\tilde{\gamma}(z-z_1)} \underline{M}^{-1} \underline{\Gamma}(z_1) \underline{M}e^{\tilde{\gamma}(z_1-z)} \underline{M}^{-1} . \quad (8.88)$$

With (8.85c) and (8.85d) we obtain from (8.86)

$$\underline{I}^{(-)}(z) = -\underline{Z}_0^{-1} \underline{\Gamma}(z) \underline{Z}_0 \underline{I}^{(+)}(z) . \quad (8.89)$$

From (8.84a) to (8.85d), (8.86), and (8.89) we obtain

$$\underline{V}(z) = (\underline{1} + \underline{\Gamma}(z)) \underline{M}e^{-\tilde{\gamma}z} \underline{\tilde{V}}^{(+)} , \quad (8.90a)$$

$$\underline{I}(z) = \underline{Z}_0^{-1} (\underline{1} - \underline{\Gamma}(z)) \underline{M}e^{-\tilde{\gamma}z} \underline{\tilde{V}}^{(+)} . \quad (8.90b)$$

We define the impedance matrix $\underline{Z}(z)$ relating the voltages and currents at z ,

$$\underline{V}(z) = \underline{Z}(z) \underline{I}(z) . \quad (8.91)$$

From (8.90a) into (8.90b) we determine $\underline{Z}(z)$ as

$$\underline{Z}(z) = (\underline{1} + \underline{\Gamma}(z)) (\underline{1} - \underline{\Gamma}(z))^{-1} \underline{Z}_0 . \quad (8.92)$$

The dependence of the impedance matrix $\underline{Z}(z)$ on the reflection coefficient matrix $\underline{\Gamma}(z)$ is given by

$$\underline{\Gamma}(z) = (\underline{Z}(z) - \underline{Z}_0) (\underline{Z}(z) + \underline{Z}_0)^{-1} . \quad (8.93)$$

Consider the multiconductor transmission-line of length l terminated at $z = 0$ with a load multiport with impedance matrix \mathbf{Z}_L shown in Figure 8.19. At the end of the transmission-line, $z = 0$, the matrix $\mathbf{Z}(z)$ becomes

$$\mathbf{Z}(0) = \mathbf{Z}_L. \quad (8.94)$$

The load may be characterized by the reflection coefficient matrix $\mathbf{\Gamma}_L$,

$$\mathbf{\Gamma}(0) = \mathbf{\Gamma}_L. \quad (8.95)$$

The reflection coefficient matrix at the load is

$$\mathbf{\Gamma}_L = (\mathbf{Z}_L - \mathbf{Z}_0)(\mathbf{Z}_L + \mathbf{Z}_0)^{-1}. \quad (8.96)$$

Terminating the multiconductor transmission-line with a multiport whose impedance matrix \mathbf{Z}_L is equal to the characteristic impedance matrix \mathbf{Z}_0 of the multiconductor transmission-line yields $\mathbf{\Gamma}_L = \mathbf{0}$. Due to (8.88) the reflection coefficient matrix vanishes everywhere, that is, $\mathbf{\Gamma}(z) = \mathbf{0}$ if $\mathbf{\Gamma}(0) = \mathbf{\Gamma}_L = \mathbf{0}$. For a reflection-free termination of a multiconductor transmission-line, a load multiport with the impedance matrix \mathbf{Z}_0 is required. It is not sufficient to connect every conductor via an impedance to ground. All conductors must be mutually connected via impedances corresponding to the matrix elements of \mathbf{Z}_0 .

The total active power flowing in positive z -direction through the multiconductor transmission-line is

$$P(z) = \frac{1}{2} \Re \{ \mathbf{I}^\dagger(z) \mathbf{V}(z) \}, \quad (8.97)$$

where the symbol \dagger denotes the Hermitian conjugate. Inserting (8.84a) and (8.83) into this equation we can express the active power flow in terms of voltage and current amplitudes of forward and backward traveling waves

$$P(z) = \frac{1}{2} \Re \{ \mathbf{I}^{(+)\dagger}(z) \mathbf{V}^{(+)}(z) + \mathbf{I}^{(+)\dagger}(z) \mathbf{V}^{(-)}(z) + \mathbf{I}^{(-)\dagger}(z) \mathbf{V}^{(+)}(z) + \mathbf{I}^{(-)\dagger}(z) \mathbf{V}^{(-)}(z) \}, \quad (8.98)$$

where $\mathbf{I}^{(+)\dagger}(z) \mathbf{V}^{(+)}(z)$ and $\mathbf{I}^{(-)\dagger}(z) \mathbf{V}^{(-)}(z)$ represent the average powers flowing in positive and negative z -directions and $\mathbf{I}^{(+)\dagger}(z) \mathbf{V}^{(-)}(z)$ and $\mathbf{I}^{(-)\dagger}(z) \mathbf{V}^{(+)}(z)$ are cross-coupling terms between waves flowing in positive and negative z -directions.

We can introduce *wave amplitudes* for multiconductor transmission-lines generalizing the wave amplitude concept introduced in Section 8.4,

$$\mathbf{a}(z) = \frac{1}{2} [\mathbf{g}^{-1} \mathbf{V}(z) + \mathbf{g} \mathbf{I}(z)], \quad (8.99a)$$

$$\mathbf{b}(z) = \frac{1}{2} [\mathbf{g}^{-1} \mathbf{V}(z) - \mathbf{g} \mathbf{I}(z)], \quad (8.99b)$$

where the matrix \mathbf{g} has to be determined such that

$$\mathbf{g}^2 = \mathbf{Z}_0. \quad (8.100)$$

The voltage and current vectors expressed by the wave amplitude vectors are

$$\underline{\mathbf{V}}(z) = \mathbf{g}[\underline{\mathbf{a}}(z) + \underline{\mathbf{b}}(z)], \quad (8.101a)$$

$$\underline{\mathbf{I}}(z) = \mathbf{g}^{-1}[\underline{\mathbf{a}}(z) - \underline{\mathbf{b}}(z)]. \quad (8.101b)$$

The wave amplitude vectors $\underline{\mathbf{a}}(z)$ and $\underline{\mathbf{b}}(z)$ are related to the unidirectional voltage and current wave vectors $\underline{\mathbf{V}}^{(\pm)}(z)$ and $\underline{\mathbf{I}}^{(\pm)}(z)$ defined in (8.85a) to (8.85d) via

$$\underline{\mathbf{a}}(z) = \mathbf{g}^{-1}\underline{\mathbf{V}}^{(+)}(z) = \mathbf{g}\underline{\mathbf{I}}^{(+)}(z), \quad (8.102a)$$

$$\underline{\mathbf{b}}(z) = \mathbf{g}^{-1}\underline{\mathbf{V}}^{(-)}(z) = \mathbf{g}\underline{\mathbf{I}}^{(-)}(z). \quad (8.102b)$$

With 8.86 this yields

$$\underline{\mathbf{b}}(z) = \mathbf{g}^{-1}\underline{\mathbf{I}}(z)\mathbf{g}\underline{\mathbf{a}}(z). \quad (8.103)$$

8.7 MULTIMODE EXCITATION OF UNIFORM HOLLOW WAVEGUIDES

Consider a uniform cylindric hollow waveguide with cross-section A and boundary of the cross-section ∂A as depicted in Figure 8.20. Let the waveguide be bounded by an ideal conductor. In Section 7.8 the modal field solutions of a closed uniform cylindric hollow waveguides were already discussed. The modal fields have been derived from scalar potentials fulfilling the two-dimensional scalar Helmholtz equation in A and either the Neumann or the Dirichlet boundary condition on the boundary ∂A of the waveguide cross-section.

In this section we investigate the general excitation of hollow waveguides also including the case of sources inside the waveguide. In addition to the excitation of modes from the ends of the waveguide we also allow excitation by internal sources over the whole length of the waveguide [11]. First-order partial differential equations governing the transverse electric and magnetic field equations are derived. Expanding the transverse electric and magnetic field forms into a series of electric and magnetic structure forms with generalized voltages and currents as the expansion coefficients yields the multimode transmission-line equations for the generalized voltages and currents.

8.7.1 The Transverse Field Equations

Allowing electric and magnetic sources described by the impressed electric and magnetic polarizations $\underline{\mathcal{M}}_{e0}(\mathbf{x})$ and $\underline{\mathcal{M}}_{m0}(\mathbf{x})$ the electromagnetic field in the waveguide

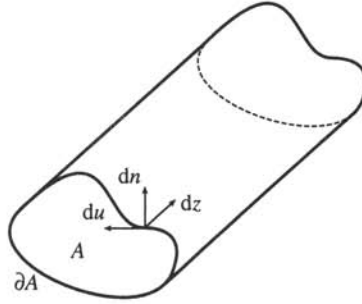


Figure 8.20: Relation of arrows and field orientation in a hollow waveguide.

is governed by Ampère's law (3.27a) and Faraday's law (3.30b),

$$d\mathcal{H} = j\omega(\epsilon \star \mathcal{E} + \underline{M}_{e0}), \quad (8.104a)$$

$$d\mathcal{E} = -j\omega(\mu \star \mathcal{H} + \underline{M}_{m0}). \quad (8.104b)$$

We introduce the general cylindric coordinate system u, n, z with the curvilinear transverse coordinates u, n and the longitudinal coordinate z . We assume that the boundary du is tangential to the boundary whereas dn is normal to the boundary. Hence the boundary conditions are

$$dn \wedge \mathcal{E} = 0 \quad \text{on } \partial A, \quad (8.105a)$$

$$dn \lrcorner \mathcal{H} = 0 \quad \text{on } \partial A. \quad (8.105b)$$

As already shown in Section 7.6 we can separate the electric and magnetic fields \mathcal{E} and \mathcal{H} into transverse parts $\mathcal{E}_t, \mathcal{H}_t$ and longitudinal parts $\mathcal{E}_z, \mathcal{H}_z$,

$$\mathcal{E} = \mathcal{E}_t + \mathcal{E}_z, \quad (8.106a)$$

$$\mathcal{H} = \mathcal{H}_t + \mathcal{H}_z. \quad (8.106b)$$

For transverse orthogonal curvilinear coordinates u, v and the longitudinal coordinate z this is performed by

$$\mathcal{E}_z = dz(dz \lrcorner \mathcal{E}) = \underline{E}_z dz, \quad (8.107a)$$

$$\mathcal{E}_t = \mathcal{E} - \mathcal{E}_z = \underline{E}_u du + \underline{E}_v dv \quad (8.107b)$$

and in a similar way for \mathcal{H} . A two-form, as for example \underline{M}_{e0} , can be subdivided into a transverse part \underline{M}_{e0t} and a longitudinal part \underline{M}_{e0z} by

$$\underline{M}_{e0z} = dz \lrcorner (dz \wedge \underline{M}_{e0}) = \underline{M}_{e0z} du \wedge dv, \quad (8.108a)$$

$$\underline{M}_{e0t} = \underline{M}_{e0} - \underline{M}_{e0z} = \underline{M}_{e0u} dv \wedge dz + \underline{M}_{e0v} dz \wedge du. \quad (8.108b)$$

The exterior differential operator d is split into a *transverse exterior derivative* d_t and a longitudinal derivative,

$$d\underline{\mathcal{E}} = d_t \underline{\mathcal{E}} + dz \wedge \frac{\partial \underline{\mathcal{E}}}{\partial z}, \quad (8.109a)$$

$$d_t \underline{\mathcal{E}} = du \wedge \frac{\partial \underline{\mathcal{E}}}{\partial u} + dv \wedge \frac{\partial \underline{\mathcal{E}}}{\partial v}. \quad (8.109b)$$

Application of the Hodge operator on both sides of Maxwell's equations (8.104a) and (8.104b) and exterior multiplication from the left with dz yields

$$dz \wedge (\star d\underline{\mathcal{E}}) = -j\omega\mu dz \wedge \star \underline{\mathcal{H}} - j\omega dz \wedge \star \underline{\mathcal{M}}_{m0}, \quad (8.110a)$$

$$dz \wedge (\star d\underline{\mathcal{H}}) = j\omega\epsilon dz \wedge \star \underline{\mathcal{E}} + j\omega dz \wedge \star \underline{\mathcal{M}}_{e0}. \quad (8.110b)$$

Considering that the exterior product of dz with any one-form depends only on the transverse part of this one-form and using the identity

$$dz \wedge (\star d\underline{\mathcal{E}}) = \star d\underline{\mathcal{E}}_z - \star \frac{\partial}{\partial z} \underline{\mathcal{E}} = \star d_t \underline{\mathcal{E}}_z - \star \frac{\partial}{\partial z} \underline{\mathcal{E}}_t \quad (8.111)$$

we obtain from above equations

$$-\frac{\partial}{\partial z} \underline{\mathcal{E}}_t = -j\omega \star (\mu dz \wedge \star \underline{\mathcal{H}}_t + dz \wedge \star \underline{\mathcal{M}}_{m0t}) - d_t \underline{\mathcal{E}}_z, \quad (8.112a)$$

$$-\frac{\partial}{\partial z} \underline{\mathcal{H}}_t = j\omega \star (\epsilon dz \wedge \star \underline{\mathcal{E}}_t + dz \wedge \star \underline{\mathcal{M}}_{e0t}) - d_t \underline{\mathcal{H}}_z. \quad (8.112b)$$

Multiplying both sides of Maxwell's equations (8.104a) and (8.104b) from the left with dz we obtain another set of equations,

$$dz \wedge d\underline{\mathcal{H}} = j\omega(\epsilon dz \wedge \star \underline{\mathcal{E}} + dz \wedge \star \underline{\mathcal{M}}_{e0t}), \quad (8.113a)$$

$$dz \wedge d\underline{\mathcal{E}} = -j\omega(\mu dz \wedge \star \underline{\mathcal{H}} + dz \wedge \star \underline{\mathcal{M}}_{m0t}). \quad (8.113b)$$

This yields

$$\underline{\mathcal{E}}_z = \frac{-j}{\omega\epsilon} \star (dz \wedge d_t \underline{\mathcal{H}}) - \frac{1}{\epsilon} \underline{\mathcal{M}}_{e0z}, \quad (8.114a)$$

$$\underline{\mathcal{H}}_z = \frac{j}{\omega\mu} \star (dz \wedge d_t \underline{\mathcal{E}}) - \frac{1}{\mu} \underline{\mathcal{M}}_{m0z}. \quad (8.114b)$$

Eliminating the longitudinal field components \underline{E}_z and \underline{H}_z by inserting (8.114a) into (8.112a) and (8.114b) into (8.112b) yields

$$-\frac{\partial}{\partial z} \underline{\mathcal{E}}_t = j\omega\mu \star \left(1 + \frac{1}{\omega^2\mu\epsilon} \star d_t \star d_t\right) (\underline{\mathcal{H}}_t \wedge dz) + j\omega \star ((\star \underline{\mathcal{M}}_{m0t}^{\text{eff}}) \wedge dz), \quad (8.115a)$$

$$-\frac{\partial}{\partial z} \underline{\mathcal{H}}_t = j\omega\epsilon \star \left(1 + \frac{1}{\omega^2\mu\epsilon} \star d_t \star d_t\right) (dz \wedge \underline{\mathcal{E}}_t) + j\omega \star (dz \wedge (\star \underline{\mathcal{M}}_{e0t}^{\text{eff}})), \quad (8.115b)$$

where we have defined the *effective transverse electric and magnetic polarizations* $\underline{\mathcal{M}}_{e0t}^{\text{eff}}$ and $\underline{\mathcal{M}}_{m0t}^{\text{eff}}$, respectively, by

$$\underline{\mathcal{M}}_{e0t}^{\text{eff}} = \underline{\mathcal{M}}_{e0t} - \frac{1}{j\omega\epsilon} dz \wedge d_t \underline{\mathcal{M}}_{m0z}, \quad (8.116a)$$

$$\underline{\mathcal{M}}_{m0t}^{\text{eff}} = \underline{\mathcal{M}}_{m0t} + \frac{1}{j\omega\epsilon} dz \wedge d_t \underline{\mathcal{M}}_{e0z}. \quad (8.116b)$$

The *transverse field equations* provide a complete description of the electromagnetic field in the hollow waveguide.

8.7.2 Modal Field Representation

As discussed in Section 7.9.4 for a homogeneous waveguide with perfectly conducting walls and filled with lossless dielectric the electromagnetic field can be expanded into orthogonal modal functions. Following (7.257a) and (7.257b) the transverse electromagnetic field can be represented by

$$\underline{\mathcal{E}}_t(\mathbf{x}) = \sum_{m,n} [\underline{\mathcal{E}}_{t,mn}^{\text{TE}}(\mathbf{x}) + \underline{\mathcal{E}}_{t,mn}^{\text{TM}}(\mathbf{x})], \quad (8.117a)$$

$$\underline{\mathcal{H}}_t(\mathbf{x}) = \sum_{m,n} [\underline{\mathcal{H}}_{t,mn}^{\text{TE}}(\mathbf{x}) + \underline{\mathcal{H}}_{t,mn}^{\text{TM}}(\mathbf{x})], \quad (8.117b)$$

where the index t denotes the transverse field component. The summation is performed over all modes, including propagating and evanescent modes. As in (8.9a) and (8.9b) we can represent each modal field form as a product of a normalized structure form $e_{mn}^{\text{TE}}(u, v)$, $e_{mn}^{\text{TM}}(u, v)$, $h_{mn}^{\text{TE}}(u, v)$, and $h_{mn}^{\text{TM}}(u, v)$ depending on the transverse coordinates u, v only and a scalar amplitude. These scalar amplitudes are the generalized voltages $\underline{V}_{mn}^{\text{TE}}(z)$, $\underline{V}_{mn}^{\text{TM}}(z)$ and generalized currents $\underline{I}_{mn}^{\text{TE}}(z)$, $\underline{I}_{mn}^{\text{TM}}(z)$, $\underline{I}_{mn}^{\text{TE}}(z)$ and

$\underline{I}_{mn}^{\text{TM}}(z)$ as introduced in Section 7.9.5

$$\underline{\mathcal{E}}_{t,mn}^{\text{TE}}(\mathbf{x}) = \underline{V}_{mn}^{\text{TE}}(z) e_{mn}^{\text{TE}}(u, v), \quad (8.118a)$$

$$\underline{\mathcal{E}}_{t,mn}^{\text{TM}}(\mathbf{x}) = \underline{V}_{mn}^{\text{TM}}(z) e_{mn}^{\text{TM}}(u, v), \quad (8.118b)$$

$$\underline{\mathcal{H}}_{t,mn}^{\text{TE}}(\mathbf{x}) = \underline{I}_{mn}^{\text{TE}}(z) h_{mn}^{\text{TE}}(u, v), \quad (8.118c)$$

$$\underline{\mathcal{H}}_{t,mn}^{\text{TM}}(\mathbf{x}) = \underline{I}_{mn}^{\text{TM}}(z) h_{mn}^{\text{TM}}(u, v). \quad (8.118d)$$

The generalized voltages and currents representing the transverse electric and magnetic field amplitudes of the waveguide modes also are called the *modal voltages* and *modal currents* respectively. Assuming the set of TE together with TE structure functions to be complete we can expand the transverse component of the electromagnetic field into the structure forms as

$$\underline{\mathcal{E}}_t(\mathbf{x}) = \sum_{mn} [\underline{V}_{mn}^{\text{TE}}(z) e_{mn}^{\text{TE}}(u, v) + \underline{V}_{mn}^{\text{TM}}(z) e_{mn}^{\text{TM}}(u, v)], \quad (8.119a)$$

$$\underline{\mathcal{H}}_t(\mathbf{x}) = \sum_{mn} [\underline{I}_{mn}^{\text{TE}}(z) h_{mn}^{\text{TE}}(u, v) + \underline{I}_{mn}^{\text{TM}}(z) h_{mn}^{\text{TM}}(u, v)]. \quad (8.119b)$$

The effective transverse electric polarization $\underline{\mathcal{M}}_{e0t}^{\text{eff}}$ and the effective transverse magnetic polarization $\underline{\mathcal{M}}_{m0t}^{\text{eff}}$ introduced in (8.116a) and (8.116b) can be expanded into the structure forms. Considering that the structure forms are one-forms and the transverse polarizations are two-forms we have to apply the star operator,

$$\underline{\mathcal{M}}_{e0t}^{\text{eff}}(\mathbf{x}) = \sum_{mn} * [\underline{M}_{e0,mn}^{\text{TE}}(z) e_{mn}^{\text{TE}}(u, v) + \underline{M}_{e0,mn}^{\text{TM}}(z) e_{mn}^{\text{TM}}(u, v)], \quad (8.120a)$$

$$\underline{\mathcal{M}}_{m0t}^{\text{eff}}(\mathbf{x}) = \sum_{mn} * [\underline{M}_{m0,mn}^{\text{TE}}(z) h_{mn}^{\text{TE}}(u, v) + \underline{M}_{m0,mn}^{\text{TM}}(z) h_{mn}^{\text{TM}}(u, v)]. \quad (8.120b)$$

The $\underline{M}_{e0,mn}^{\text{TE}}(z)$, $\underline{M}_{e0,mn}^{\text{TM}}(z)$, $\underline{M}_{m0,mn}^{\text{TE}}(z)$, $\underline{M}_{m0,mn}^{\text{TM}}(z)$ are the *modal amplitudes of the effective transverse electric polarization and magnetic polarizations*. With (7.208), (7.209), (7.213a) and (7.213b) we obtain the orthonormality relations for the structure forms of the waveguide

$$\langle e_{kl}^{\text{TE}} | h_{mn}^{\text{TE}} \rangle_A = - \langle h_{kl}^{\text{TE}} | e_{mn}^{\text{TE}} \rangle_A = \delta_{km} \delta_{ln}, \quad (8.121a)$$

$$\langle e_{kl}^{\text{TM}} | h_{mn}^{\text{TM}} \rangle_A = - \langle h_{kl}^{\text{TM}} | e_{mn}^{\text{TM}} \rangle_A = \delta_{km} \delta_{ln}, \quad (8.121b)$$

$$\langle e_{kl}^{\text{TE}} | h_{mn}^{\text{TM}} \rangle_A = \langle h_{kl}^{\text{TM}} | e_{mn}^{\text{TE}} \rangle_A = 0, \quad (8.121c)$$

$$\langle e_{kl}^{\text{TM}} | h_{mn}^{\text{TE}} \rangle_A = \langle h_{kl}^{\text{TE}} | e_{mn}^{\text{TM}} \rangle_A = 0. \quad (8.121d)$$

Using these orthonormality properties we obtain from (8.117a) to (8.118d) the ampli-

tudes of the modal voltages $\underline{V}_{mn}^{\text{TE}}(z)$, $\underline{V}_{mn}^{\text{TM}}(z)$ and the modal currents $\underline{I}_{mn}^{\text{TE}}(z)$, $\underline{I}_{mn}^{\text{TM}}(z)$,

$$\underline{V}_{mn}^{\text{TE}}(z) = - \langle h_{kl}^{\text{TE}}(u, v) | \underline{\mathcal{E}}_t(\mathbf{x}) \rangle_A \Big|_z, \quad (8.122a)$$

$$\underline{V}_{mn}^{\text{TM}}(z) = - \langle h_{kl}^{\text{TM}}(u, v) | \underline{\mathcal{E}}_t(\mathbf{x}) \rangle_A \Big|_z, \quad (8.122b)$$

$$\underline{I}_{mn}^{\text{TE}}(z) = \langle e_{kl}^{\text{TE}}(u, v) | \underline{\mathcal{H}}_t(\mathbf{x}) \rangle_A \Big|_z, \quad (8.122c)$$

$$\underline{I}_{mn}^{\text{TM}}(z) = \langle e_{kl}^{\text{TM}}(u, v) | \underline{\mathcal{H}}_t(\mathbf{x}) \rangle_A \Big|_z. \quad (8.122d)$$

These inner products are computed by integration over the cross-sectional surface A with the longitudinal coordinate z kept constant. From (8.120a) to (8.121d) we obtain the modal amplitudes of the effective transverse electric and magnetic polarizations

$$\underline{M}_{e0,mn}^{\text{TE}}(z) = - \langle h_{kl}^{\text{TE}}(u, v) | * \underline{\mathcal{M}}_{e0t}^{\text{eff}}(\mathbf{x}) \rangle_A \Big|_z, \quad (8.123a)$$

$$\underline{M}_{e0,mn}^{\text{TM}}(z) = - \langle h_{kl}^{\text{TM}}(u, v) | * \underline{\mathcal{M}}_{e0t}^{\text{eff}}(\mathbf{x}) \rangle_A \Big|_z, \quad (8.123b)$$

$$\underline{M}_{m0,mn}^{\text{TE}}(z) = \langle e_{kl}^{\text{TE}}(u, v) | * \underline{\mathcal{M}}_{m0t}^{\text{eff}}(\mathbf{x}) \rangle_A \Big|_z, \quad (8.123c)$$

$$\underline{M}_{m0,mn}^{\text{TM}}(z) = \langle e_{kl}^{\text{TM}}(u, v) | * \underline{\mathcal{M}}_{m0t}^{\text{eff}}(\mathbf{x}) \rangle_A \Big|_z. \quad (8.123d)$$

According to (7.198a), (7.198b), (7.198c) and (7.198d) the electric and magnetic structure forms are related as

$$e_{kl}^{\text{TE}}(u, v) = * (h_{kl}^{\text{TE}}(u, v) \wedge dz), \quad (8.124a)$$

$$e_{kl}^{\text{TM}}(u, v) = * (h_{kl}^{\text{TM}}(u, v) \wedge dz), \quad (8.124b)$$

$$h_{kl}^{\text{TE}}(u, v) = * (dz \wedge e_{kl}^{\text{TE}}(u, v)), \quad (8.124c)$$

$$h_{kl}^{\text{TM}}(u, v) = * (dz \wedge e_{kl}^{\text{TM}}(u, v)). \quad (8.124d)$$

8.7.3 Multimode Transmission-Line Equations for Hollow Waveguides

To derive the multimode transmission-line equations for hollow waveguides we insert the modal expansions of the transverse field and the effective transverse polarizations into the transverse field equations. Inserting (8.119a), (8.119b) and (8.120b) into (8.115a)

yields

$$\begin{aligned}
 & - \sum_{kl} \frac{dV_{kl}^{\text{TE}}(z)}{dz} e_{kl}^{\text{TE}}(u, v) - \sum_{kl} \frac{dV_{kl}^{\text{TM}}(z)}{dz} e_{kl}^{\text{TM}}(u, v) \\
 & = j\omega\mu \sum_{kl} \underline{I}_{kl}^{\text{TE}}(z) * (1 + \beta_{M0}^{-2} * d_t * d_t) (h_{kl}^{\text{TE}}(u, v) \wedge dz) \\
 & \quad + j\omega\mu \sum_{kl} \underline{I}_{kl}^{\text{TM}}(z) * (1 + \beta_{M0}^{-2} * d_t * d_t) (h_{kl}^{\text{TM}}(u, v) \wedge dz) \\
 & \quad + j\omega \sum_{kl} \underline{M}_{m0,kl}^{\text{TE}}(z) * (h_{kl}^{\text{TE}}(u, v) \wedge dz) \\
 & \quad + j\omega \sum_{kl} \underline{M}_{m0,kl}^{\text{TM}}(z) * (h_{kl}^{\text{TM}}(u, v) \wedge dz) \tag{8.125}
 \end{aligned}$$

with the plane wave phase coefficient

$$\beta_{M0} = \omega \sqrt{\mu\epsilon}. \tag{8.126}$$

Inserting (8.124a) and (8.124b) and using (7.215a) and (7.215c) we obtain

$$\begin{aligned}
 & - \sum_{kl} \frac{dV_{kl}^{\text{TE}}(z)}{dz} e_{kl}^{\text{TE}}(u, v) - \sum_{kl} \frac{dV_{kl}^{\text{TM}}(z)}{dz} e_{kl}^{\text{TM}}(u, v) \\
 & = j\omega\mu \sum_{kl} \underline{I}_{kl}^{\text{TE}}(z) e_{kl}^{\text{TE}}(u, v) + j\omega\mu \sum_{kl} \underline{I}_{kl}^{\text{TM}}(z) (1 - (\beta_{c\text{TM},mn}/\beta_{M0})^2) e_{kl}^{\text{TM}}(u, v) \\
 & \quad + j\omega \sum_{kl} \underline{M}_{m0,kl}^{\text{TE}}(z) e_{kl}^{\text{TE}}(u, v) + j\omega \sum_{kl} \underline{M}_{m0,kl}^{\text{TM}}(z) e_{kl}^{\text{TM}}(u, v). \tag{8.127}
 \end{aligned}$$

Forming the exterior product of this equation with $h_{mn}^{\text{TE}}(u, v)$ and $h_{mn}^{\text{TM}}(u, v)$ respectively, integrating this over the cross-sectional area A of the waveguide, applying the orthonormality cross relations (8.121a) to (8.121d) and considering (7.169) and (7.178) we obtain the transmission-line equations

$$\frac{dV_{mn}^{\text{TE}}(z)}{dz} = -j\omega\mu \underline{I}_{mn}^{\text{TE}}(z) - j\omega \underline{M}_{m0,mn}^{\text{TE}}(z), \tag{8.128a}$$

$$\frac{dV_{mn}^{\text{TM}}(z)}{dz} = -j\omega\mu [1 - (\omega_{c,\text{TM},mn}/\omega)^2] \underline{I}_{mn}^{\text{TM}}(z) - j\omega \underline{M}_{m0,mn}^{\text{TM}}(z) \tag{8.128b}$$

with the cutoff frequency $\omega_{c,\text{TM},mn}$ of the TM_{mn} mode,

$$\omega_{c,\text{TM},mn} = \frac{\beta_{c,\text{TM},mn}}{\sqrt{\epsilon\mu}}. \tag{8.129}$$

In an analogous way we can derive a second set of transmission-line equations by inserting (8.119a), (8.119b) and (8.120a) into (8.115b),

$$\frac{d\underline{I}_{mn}^{\text{TE}}(z)}{dz} = -j\omega\epsilon \left[1 - (\omega_{c,k}^{\text{TE}}/\omega)^2 \right] \underline{V}_{mn}^{\text{TE}}(z) - j\omega \underline{M}_{e0,mn}^{\text{TE}}(z), \quad (8.130a)$$

$$\frac{d\underline{I}_{mn}^{\text{TM}}(z)}{dz} = -j\omega\epsilon \underline{V}_{mn}^{\text{TM}}(z) - j\omega \underline{M}_{e0,mn}^{\text{TM}}(z) \quad (8.130b)$$

with the cutoff frequency $\omega_{c\text{TE},mn}$ of the TE_{mn} mode,

$$\omega_{c\text{TE},mn} = \frac{\beta_{c,\text{TE},mn}}{\sqrt{\epsilon\mu}}. \quad (8.131)$$

The propagation coefficient as introduced in (7.171a) and (7.171b) is given by

$$\gamma_{\text{TE/TM},mn} = \alpha_{\text{TE/TM},mn} = \sqrt{\epsilon\mu} \sqrt{\omega_{c\text{TE/TM},mn}^2 - \omega^2} \quad \text{for } \omega < \omega_{c\text{TE/TM}}, \quad (8.132a)$$

$$\gamma_{\text{TE/TM},mn} = j\beta_{\text{TE/TM},mn} = j\sqrt{\epsilon\mu} \sqrt{\omega^2 - \omega_{c\text{TE/TM},mn}^2} \quad \text{for } \omega > \omega_{c\text{TE/TM}}. \quad (8.132b)$$

The characteristic impedances introduced in (7.176a), (7.176b), (7.190a) and (7.190b) are

$$Z_{0\text{TE},mn} = \frac{j\omega\mu}{\alpha_{\text{TE},mn}} = Z_F \frac{j\omega}{\sqrt{\omega_{c\text{TE},mn}^2 - \omega^2}} \quad \text{for } \omega < \omega_{c\text{TE},mn}, \quad (8.133a)$$

$$Z_{0\text{TE},mn} = \frac{\omega\mu}{\beta_{\text{TE},mn}} = Z_F \frac{\omega}{\sqrt{\omega^2 - \omega_{c\text{TE},mn}^2}} \quad \text{for } \omega > \omega_{c\text{TE},mn}, \quad (8.133b)$$

$$Z_{0\text{TM},mn} = \frac{\alpha_{\text{TM},mn}}{j\omega\epsilon} = Z_F \frac{\sqrt{\omega_{c\text{TM},mn}^2 - \omega^2}}{j\omega} \quad \text{for } \omega < \omega_{c\text{TM},mn}, \quad (8.133c)$$

$$Z_{0\text{TM},mn} = \frac{\beta_{\text{TM},mn}}{\omega\epsilon} = Z_F \frac{\sqrt{\omega^2 - \omega_{c\text{TM},mn}^2}}{\omega} \quad \text{for } \omega > \omega_{c\text{TM},mn}. \quad (8.133d)$$

Above the cutoff frequency $\omega_{c\text{TE/TM},mn}$ the characteristic impedance $Z_{0\text{TE/TE},mn}$ is real and positive. Below the cutoff frequency the characteristic impedance $Z_{0\text{TE/TE},mn}$ is purely imaginary. The imaginary part of $Z_{0\text{TE},mn}$ is positive (i.e., below cutoff the characteristic impedance of a TE mode is inductive, whereas the imaginary part of $Z_{0\text{TM},mn}$ is negative and therefore below cutoff the characteristic impedance of a TM mode is capacitive).

With (8.132a) to (8.133d) we can write the transmission-line equations (8.128a) and (8.130a) for the TE modes as

$$\frac{d\underline{V}_{mn}^{\text{TE}}(z)}{dz} = -\gamma_{\text{TE},mn} Z_{0\text{TE},mn} \underline{I}_{mn}^{\text{TE}}(z) - j\omega \underline{M}_{m0,mn}^{\text{TE}}(z), \quad (8.134a)$$

$$\frac{d\underline{I}_{mn}^{\text{TE}}(z)}{dz} = -\frac{\gamma_{\text{TE},mn}}{Z_{0\text{TE},mn}} \underline{V}_{mn}^{\text{TE}}(z) - j\omega \underline{M}_{e0,mn}^{\text{TE}}(z) \quad (8.134b)$$

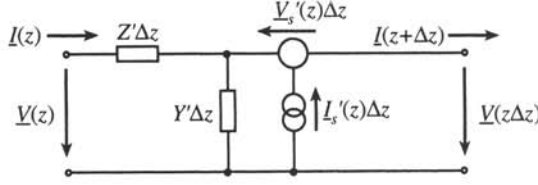


Figure 8.21: Equivalent circuit for a mode in a waveguide segment with impressed voltage and current sources.

and the transmission-line equations (8.128b) and (8.130b) for the TM modes as

$$\frac{dV_{mn}^{\text{TM}}(z)}{dz} = -\gamma_{\text{TM},mn} Z_{0\text{TM},mn} I_{mn}^{\text{TM}}(z) - j\omega \underline{M}_{m0,mn}^{\text{TM}}(z), \quad (8.135a)$$

$$\frac{dI_{mn}^{\text{TM}}(z)}{dz} = -\frac{\gamma_{\text{TM},mn}}{Z_{0\text{TM},mn}} V_{mn}^{\text{TM}}(z) - j\omega \underline{M}_{e0,mn}^{\text{TM}}(z). \quad (8.135b)$$

For the TE_{mn} modes the impedances per unit of length $Z'_{\text{TE},mn}$ and the admittances per unit of length $Y'_{\text{TE},mn}$ are

$$Z'_{\text{TE},mn} = \gamma_{\text{TE},mn} Z_{0\text{TE},mn} = j\omega\mu, \quad (8.136a)$$

$$Y'_{\text{TE},mn} = \frac{\gamma_{\text{TE},mn}}{Z_{0\text{TE},mn}} = j\omega\epsilon \frac{\omega^2 - \omega_{c\text{TE},mn}^2}{\omega^2} \quad (8.136b)$$

and for the TM_{mn} modes the impedances per unit of length $Z'_{\text{TM},mn}$ and the admittances per unit of length $Y'_{\text{TM},mn}$ are

$$Z'_{\text{TM},mn} = \gamma_{\text{TM},mn} Z_{0\text{TM},mn} = j\omega\mu \frac{\omega^2 - \omega_{c\text{TE},mn}^2}{\omega^2}, \quad (8.137a)$$

$$Y'_{\text{TM},mn} = \frac{\gamma_{\text{TE},mn}}{Z_{0\text{TE},mn}} = j\omega\epsilon. \quad (8.137b)$$

We introduce the modal amplitudes of the *impressed voltage* $\underline{V}'_{s,mn}{}^{\text{TE/TM}}(z)$ and the *impressed current* $\underline{I}'_{s,mn}{}^{\text{TE/TM}}(z)$ as

$$\underline{V}'_{s,mn}{}^{\text{TE/TM}}(z) = -j\omega \underline{M}_{m0,mn}^{\text{TE/TM}}(z), \quad (8.138a)$$

$$\underline{I}'_{s,mn}{}^{\text{TE/TM}}(z) = -j\omega \underline{M}_{e0,mn}^{\text{TE/TM}}(z). \quad (8.138b)$$

Figure 8.21 shows the equivalent circuit for a mode in a waveguide segment of length Δz with the impedance and admittance per unit of length Z' and Y' , and the impressed

voltage and current sources per unit of length $\underline{V}'(z)$ and $\underline{I}'(z)$ respectively. For the *two-port current-voltage source* the symmetric representation discussed in Section 10.6 is used. With the above definitions the transmission-line equations (8.134a), (8.134b), (8.135a) and (8.135b), can be written as

$$\frac{d\underline{V}_{mn}^{\text{TE/TM}}(z)}{dz} = -Z'_{\text{TE/TM},mn} \underline{I}_{mn}^{\text{TE/TM}}(z) + \underline{V}'_{s,mn}(z), \quad (8.139a)$$

$$\frac{d\underline{I}_{mn}^{\text{TE/TM}}(z)}{dz} = -Y'_{\text{TE/TM},mn} \underline{V}_{mn}^{\text{TE/TM}}(z) + \underline{I}'_{s,mn}(z). \quad (8.139b)$$

In the homogeneous waveguide the modal transmission-line equations are uncoupled and can be solved independently as in the single mode case. Sources in the waveguide may be expanded into modal amplitudes and contribute to the excitation of the waveguide modes according to their modal amplitudes. Figure 8.21 shows the equivalent circuit of a section of infinitesimal length Δz of one waveguide mode. Since this equivalent circuit is the same for all TE and TM waveguide modes, we have omitted all indices. For any source distribution in the waveguide the impressed electric polarization \underline{M}_{e0} of (8.104a) and the impressed magnetic polarization \underline{M}_{m0} of (8.104b) can be expanded into modal amplitudes. To do this we have at first to compute the effective transverse electric and magnetic polarizations introduced in (8.116a) and (8.116b). From their modal amplitudes the modal amplitudes of the impressed voltage and the impressed current can be computed. From (8.116a) and (8.116b) we see that the modal amplitudes of the effective transverse electric polarization and the impressed current depend on the transverse component of the impressed electric polarization \underline{M}_{e0} and the longitudinal component of the impressed magnetic polarization \underline{M}_{m0} . The modal amplitudes of the effective transverse magnetic polarization and the impressed voltage depend on the transverse component of the impressed magnetic polarization \underline{M}_{m0} and the longitudinal component of the impressed electric polarization \underline{M}_{e0} .

Since in the homogeneous waveguide the transmission-line equations for different modes are uncoupled we can solve them for every mode independently. For arbitrary source distributions, we can do this by applying Green's function methods [11, 16]. From (8.139a) and (8.139b) it follows that for every mode we have to solve the pair of *inhomogeneous first-order transmission-line equations*

$$\frac{d\underline{V}(z)}{dz} = -jX'(\omega)\underline{I}(z) + \underline{V}'_s(z), \quad (8.140a)$$

$$\frac{d\underline{I}(z)}{dz} = -jB'(\omega)\underline{V}(z) + \underline{I}'_s(z), \quad (8.140b)$$

where $\underline{V}(z)$ and $\underline{I}(z)$ are the modal transmission-line voltage and current, $\underline{V}'_s(z)$ and $\underline{I}'_s(z)$ are the impressed modal voltages and currents per unit of length, $X'(\omega)$ is the

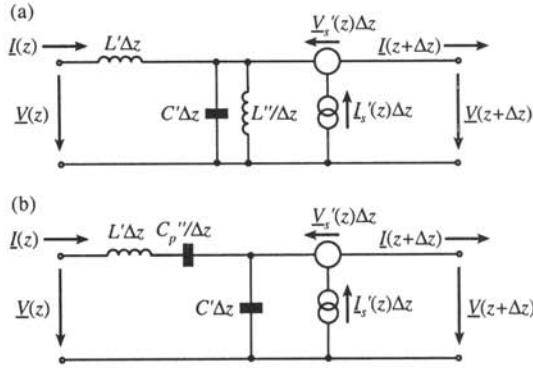


Figure 8.22: Equivalent circuit for a mode in a waveguide segment with impressed voltage and current sources, (a) for a TE mode, and (b) for a TM mode.

series reactance per unit of length and $B'(\omega)$ is the parallel susceptance per unit of length. For the TE modes we obtain from (8.136a) and (8.136b)

$$X'_{\text{TE}} = \omega\mu = \omega L', \quad (8.141a)$$

$$B'_{\text{TE}} = \omega\epsilon - \frac{\omega^2 \epsilon_{\text{TE}}}{\omega} = \omega C' - \frac{1}{\omega L_p''}. \quad (8.141b)$$

Figure 8.22(a) shows the equivalent circuit for the TE modes in a waveguide segment of length Δz with internal sources.

The equivalent circuit for a waveguide segment excited in a TE mode is shown in Figure 8.1(b). The parallel capacitance per unit of length C' and the series inductance per unit of length L' are related to the modal electric and magnetic energies of the transverse electric and magnetic fields. The parallel inductance is inversely proportional to the energy stored in the longitudinal component of the magnetic field. For the TM modes we obtain from (8.137a) and (8.137b)

$$X'_{\text{TM}} = \omega\mu - \frac{\omega^2 \epsilon_{\text{TM}}\mu}{\omega} = \omega L' - \frac{1}{\omega C_s'}, \quad (8.142a)$$

$$B'_{\text{TM}} = \omega\epsilon = \omega C'. \quad (8.142b)$$

In this case the inverse series capacitance per unit of length is related to the longitudinal electric field component. Figure 8.22(b) shows the equivalent circuits for the TM modes in a waveguide segment of length Δz with internal sources.

8.7.4 Multimode Transmission-Line Equations of Lossless Waveguides without Internal Sources

Let us consider the waveguide without internal sources. This means $\underline{V}'_s(z) = 0$ and $\underline{I}'_s(z) = 0$ and we obtain from (8.140a) and (8.140b) the *homogeneous first-order transmission-line equations*

$$\frac{d\underline{V}(z)}{dz} = -jX'(\omega)\underline{I}(z), \quad (8.143a)$$

$$\frac{d\underline{I}(z)}{dz} = -jB'(\omega)\underline{V}(z). \quad (8.143b)$$

Eliminating either $\underline{I}(z)$ or $\underline{V}(z)$ in these equations yields the *second-order homogeneous transmission-line equations*

$$\frac{d^2\underline{V}(z)}{dz^2} + \beta^2\underline{V}(z) = 0, \quad (8.144a)$$

$$\frac{d^2\underline{I}(z)}{dz^2} + \beta^2\underline{I}(z) = 0 \quad (8.144b)$$

with the phase coefficient

$$\beta = \sqrt{X'(\omega)B'(\omega)}. \quad (8.145)$$

Below the cutoff frequency of the respective mode $\omega_{\text{cte/TM}}$ either $X'(\omega)$ or $B'(\omega)$ is negative and therefore $\gamma = \alpha$ is real. The field of a mode below its cutoff frequency is evanescent. Above the cutoff frequency $\omega_{\text{cte/TM}}$ the series reactance per unit of length $X'(\omega)$ as well as the parallel susceptance per unit of length $B'(\omega)$ are positive and therefore $\gamma = j\beta$ is imaginary. In this case the modal field is a space-harmonic wave.

Above the cutoff frequency $\omega_{\text{cte/TM}}$ we obtain solutions representing space-harmonic waves propagating in positive and negative z -directions.

$$\underline{V}(z) = \underline{V}^{(+)}e^{-j\beta z} + \underline{V}^{(-)}e^{j\beta z}, \quad (8.146a)$$

$$\underline{I}(z) = \underline{I}^{(+)}e^{-j\beta z} + \underline{I}^{(-)}e^{j\beta z}, \quad (8.146b)$$

where $\underline{V}^{(+)}$ and $\underline{I}^{(+)}$ are the voltage and current amplitudes of the waves propagating in positive z -direction and $\underline{V}^{(-)}$ and $\underline{I}^{(-)}$ are the voltage and current amplitudes of the waves propagating in negative z -direction. Below the cutoff frequency $\omega_{\text{cte/TM}}$ we obtain the evanescent field solution

$$\underline{V}(z) = \underline{V}^{(+)}e^{-\alpha z} + \underline{V}^{(-)}e^{\alpha z}, \quad (8.147a)$$

$$\underline{I}(z) = \underline{I}^{(+)}e^{-\alpha z} + \underline{I}^{(-)}e^{\alpha z}, \quad (8.147b)$$

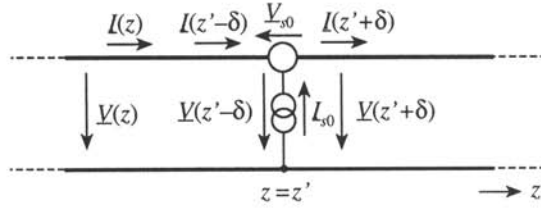


Figure 8.23: Line with impressed voltage and current sources.

where $\underline{V}^{(+)}$ and $\underline{I}^{(+)}$ are the voltage and current amplitudes of the evanescent mode decaying in positive z -direction and $\underline{V}^{(-)}$ and $\underline{I}^{(-)}$ are the voltage and current amplitudes of the evanescent mode decaying in negative z -direction. From (8.143a) and (8.143b) we obtain for $\omega_{c, \text{TE/TM}}$ modes

$$\underline{V}^{(+)} = Z_{0\text{TE/TM}} \underline{I}^{(+)}, \quad (8.148a)$$

$$\underline{V}^{(-)} = -Z_{0\text{TE/TM}} \underline{I}^{(-)}. \quad (8.148b)$$

The characteristic impedance $Z_{0\text{TE/TM}}$ is given by (8.133a) to (8.133d). Above the cutoff $\omega_{c\text{TE/TM}}$ the characteristic impedance is real and positive. Below cutoff the characteristic impedance is imaginary with a positive imaginary part for TE modes and a negative imaginary part for TM modes.

8.8 GREEN'S FUNCTIONS FOR TRANSMISSION-LINES

To solve the transmission-line equations for arbitrary distributions of voltage sources and current sources along the line, we can apply the superposition principle and consider any distribution of sources as a continuous superposition of point-like sources. Consider a transmission-line with a point-like combined voltage and current source at z' as shown in Figure 8.23. The first-order transmission-line equations (8.140a) and (8.140b) yield

$$\frac{d\underline{V}(z)}{dz} = -jX'(\omega)\underline{I}(z) + \underline{V}_{s0}\delta(z - z'), \quad (8.149a)$$

$$\frac{d\underline{I}(z)}{dz} = -jY'(\omega)\underline{V}(z) + \underline{I}_{s0}\delta(z - z') \quad (8.149b)$$

with the voltage \underline{V}_{s0} and the current \underline{I}_{s0} impressed at z' . Integrating (8.149a) and (8.149b) from $z' - \delta$ to $z' + \delta$ yields

$$\underline{V}(z' + \delta) = \underline{V}(z' - \delta) + \underline{V}_{s0}, \quad (8.150a)$$

$$\underline{I}(z' + \delta) = \underline{I}(z' - \delta) + \underline{I}_{s0}. \quad (8.150b)$$

From (8.149a) and (8.149b) we obtain

$$\frac{d^2 \underline{V}(z)}{dz^2} - \gamma^2 \underline{V}(z) = -\underline{V}_{s0} \delta'(z - z') - jX'(\omega) \underline{I}_{s0} \delta(z - z') \quad (8.151)$$

with the propagation coefficient γ given by

$$\gamma^2 = -X'(\omega)Y'(\omega). \quad (8.152)$$

The distribution $\delta'(z)$ represents the derivative of the delta distribution $\delta(z)$. It can be defined via partial integration. For a smooth function $f(x)$ the distribution $\delta'(x)$ is defined by

$$\int \delta'(x - x') f(x) dx = - \int \delta(x - x') \frac{df(x)}{dx} dx = - \left. \frac{df(x)}{dx} \right|_{x=x'}. \quad (8.153)$$

For $z \neq z'$ we have to solve the homogeneous transmission-line equation

$$\frac{d^2 \underline{V}(z)}{dz^2} - \gamma^2 \underline{V}(z) = 0. \quad (8.154)$$

Due to the impressed current and voltage at $z = z'$, the line voltage and the line current exhibit a discontinuous change at this point. We therefore obtain partial solutions for $z < z'$ and $z > z'$, hence

$$\underline{V}(z) = \begin{cases} \underline{V}_1^{(+)} e^{-\gamma(z-z')} + \underline{V}_1^{(-)} e^{\gamma(z-z')} & \text{for } z < z', \\ \underline{V}_2^{(+)} e^{-\gamma(z-z')} + \underline{V}_2^{(-)} e^{\gamma(z-z')} & \text{for } z > z', \end{cases} \quad (8.155a)$$

$$\underline{I}(z) = \begin{cases} Y_0 \underline{V}_1^{(+)} e^{-\gamma(z-z')} - Y_0 \underline{V}_1^{(-)} e^{\gamma(z-z')} & \text{for } z < z', \\ Y_0 \underline{V}_2^{(+)} e^{-\gamma(z-z')} - Y_0 \underline{V}_2^{(-)} e^{\gamma(z-z')} & \text{for } z > z' \end{cases} \quad (8.155b)$$

with the characteristic admittance Y_0 (i.e., the reciprocal characteristic impedance Z_0) given by

$$Y_0^{-1} = Z_0 = \sqrt{\frac{X'}{Y'}}. \quad (8.156)$$

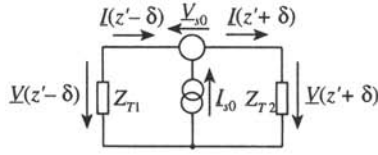


Figure 8.24: Voltage and current sources with terminations.

The line voltage and current at the left-hand side of the point sources are $V(z' - \delta)$ and $I(z' - \delta)$ at the right-hand side of the point sources the line voltage and current are $V(z' + \delta)$ and $I(z' + \delta)$,

$$\underline{V}(z' - \delta) = \underline{V}_1^{(+)} + \underline{V}_1^{(-)}, \quad (8.157a)$$

$$\underline{V}(z' + \delta) = \underline{V}_2^{(+)} + \underline{V}_2^{(-)}, \quad (8.157b)$$

$$\underline{I}(z' - \delta) = Y_0 \underline{V}_1^{(+)} - Y_0 \underline{V}_1^{(-)}, \quad (8.157c)$$

$$\underline{I}(z' + \delta) = Y_0 \underline{V}_2^{(+)} - Y_0 \underline{V}_2^{(-)}, \quad (8.157d)$$

where δ is an infinitesimal distance. From this we obtain

$$\underline{V}_1^{(+)} = \frac{1}{2} [\underline{V}(z' - \delta) + Z_0 \underline{I}(z' - \delta)], \quad (8.158a)$$

$$\underline{V}_1^{(-)} = \frac{1}{2} [\underline{V}(z' - \delta) - Z_0 \underline{I}(z' - \delta)], \quad (8.158b)$$

$$\underline{V}_2^{(+)} = \frac{1}{2} [\underline{V}(z' + \delta) + Z_0 \underline{I}(z' + \delta)], \quad (8.158c)$$

$$\underline{V}_2^{(-)} = \frac{1}{2} [\underline{V}(z' + \delta) - Z_0 \underline{I}(z' + \delta)]. \quad (8.158d)$$

To determine the voltage and current amplitudes we consider the combined voltage and current source terminated with the impedances Z_{T1} and Z_{T2} as shown in Figure 8.24. The impedances Z_{T1} and Z_{T2} are the impedances of the waveguide connected with the sources on the left and on the right. For an infinitely extended waveguide we will set $Z_{T1} = Z_{T2} = Z_0$. However, for a waveguide of finite length Z_{T1} and Z_{T2} will depend on the waveguide termination on both ends. We compute the voltage and current amplitudes as

$$\underline{V}(z' - \delta) = -\frac{Z_{T1}}{Z_{T1} + Z_{T2}} \underline{V}_{s0} + \frac{Z_{T1} Z_{T2}}{Z_{T1} + Z_{T2}} \underline{I}_{s0}, \quad (8.159a)$$

$$\underline{V}(z' + \delta) = \frac{Z_{T2}}{Z_{T1} + Z_{T2}} \underline{V}_{s0} + \frac{Z_{T1} Z_{T2}}{Z_{T1} + Z_{T2}} \underline{I}_{s0}, \quad (8.159b)$$

$$\underline{I}(z' - \delta) = \frac{1}{Z_{T1} + Z_{T2}} \underline{V}_{s0} - \frac{Z_{T2}}{Z_{T1} + Z_{T2}} \underline{I}_{s0}, \quad (8.159c)$$

$$\underline{I}(z' + \delta) = \frac{1}{Z_{T1} + Z_{T2}} \underline{V}_{s0} + \frac{Z_{T1}}{Z_{T1} + Z_{T2}} \underline{I}_{s0}. \quad (8.159d)$$

8.8.1 Green's Function for the Transmission-Line with Matched Terminations

Let us solve the transmission-line equations for the transmission-line infinitely extended in both directions. For the transmission-line terminated with its characteristic impedance Z_0

$$Z_{T1} = Z_{T2} = Z_0. \quad (8.160)$$

For $z > z'$ only waves propagating or decaying in positive z -direction occur and for $z < z'$ only waves propagating or decaying in negative z -direction occur. Therefore, (8.155a) and (8.155b) reduce to

$$\underline{V}(z) = \begin{cases} \underline{V}_2^{(+)} e^{-\gamma(z-z')} & \text{for } z > z', \\ \underline{V}_1^{(-)} e^{\gamma(z-z')} & \text{for } z < z', \end{cases} \quad (8.161a)$$

$$\underline{I}(z) = \begin{cases} \underline{I}_2^{(+)} e^{-\gamma(z-z')} & \text{for } z > z', \\ \underline{I}_1^{(-)} e^{\gamma(z-z')} & \text{for } z < z'. \end{cases} \quad (8.161b)$$

We obtain from (8.159a) to (8.159d)

$$\underline{V}_1^{(-)} = -Z_0 \underline{I}_1^{(-)} = \frac{1}{2} (-\underline{V}_{s0} + Z_0 \underline{I}_{s0}), \quad (8.162a)$$

$$\underline{V}_2^{(+)} = Z_0 \underline{I}_2^{(+)} = \frac{1}{2} (\underline{V}_{s0} + Z_0 \underline{I}_{s0}). \quad (8.162b)$$

Inserting this into (8.161a) and (8.161b) yields

$$\underline{V}(z) = \frac{1}{2} [\xi(z - z') \underline{V}_{s0} + Z_0 \underline{I}_{s0}] e^{-\gamma|z-z'|}, \quad (8.163a)$$

$$\underline{I}(z) = \frac{1}{2} [Z_0^{-1} \underline{V}_{s0} + \xi(z - z') \underline{I}_{s0}] e^{-\gamma|z-z'|} \quad (8.163b)$$

where the function $\xi(x)$ is defined as

$$\xi(x) = \begin{cases} -1 & \text{for } x < 0 \\ 0 & \text{for } x = 0 \\ 1 & \text{for } x > 0 \end{cases}. \quad (8.164)$$

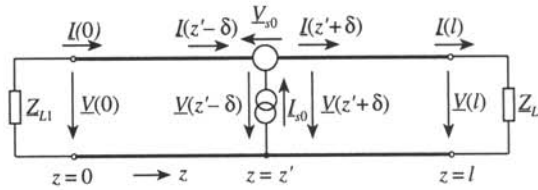


Figure 8.25: Terminated line with impressed current source.

From this we obtain the *dyadic Green's function* $G(z, z')$ for the transmission-line terminated at both ends with its wave impedance Z_0

$$G(z, z') = \frac{1}{2} \begin{bmatrix} \xi(z - z') & Z_0 \\ Z_0^{-1} & \xi(z - z') \end{bmatrix} e^{-\gamma|z - z'|}. \quad (8.165)$$

For a transmission-line with distributed voltage and current sources where $V'_s(z)$ is the impressed voltage per unit of length and $I'_s(z)$ is the impressed current per unit of length, the transmission-line voltage $V(z)$ and the transmission-line current $I(z)$ can be computed by

$$\begin{bmatrix} V(z) \\ I(z) \end{bmatrix} = \int_0^l G(z, z') \begin{bmatrix} V'_s(z') \\ I'_s(z') \end{bmatrix} dz'. \quad (8.166)$$

The integration is performed over the length l of the transmission-line.

8.8.2 Green's Function for the Transmission-Line with Arbitrary Linear Passive Terminations

Consider a transmission-line of length l terminated with the linear impedances Z_{L1} at $z = 0$ and Z_{L2} at $z = l$ and the combined voltage and current source at $z = z'$, as shown in Figure 8.25. If the impedances Z_{L1} and Z_{L2} deviate from the characteristic impedance Z_L of the transmission-line, the wave is reflected at the respective end. To determine the transmission-line voltages and currents we use the equivalent circuit shown in Figure 8.25. Using (8.37), we determine the impedances Z_{T1} and Z_{T2} as

$$Z_{T1}(z) = Z_0 \frac{Z_{L1} + Z_0 \tanh \gamma z}{Z_0 + Z_{L1} \tanh \gamma z}, \quad (8.167a)$$

$$Z_{T2}(z) = Z_0 \frac{Z_{L2} + Z_0 \tanh \gamma(l - z)}{Z_0 + Z_{L2} \tanh \gamma(l - z)}. \quad (8.167b)$$

From (8.158a) to (8.158d) and (8.159a) to (8.159d) we obtain

$$\underline{V}_1^{(\pm)}(z') = \frac{1}{2} \left[\frac{-Z_{T1}(z') \pm Z_0}{Z_{T1}(z') + Z_{T2}(z')} \underline{V}_{s0} + \frac{(Z_{T1}(z') \mp Z_0)Z_{T2}}{Z_{T1}(z') + Z_{T2}(z')} \underline{I}_{s0} \right], \quad (8.168a)$$

$$\underline{V}_2^{(\pm)}(z') = \frac{1}{2} \left[\frac{Z_{T2}(z') \pm Z_0}{Z_{T1}(z') + Z_{T2}(z')} \underline{V}_{s0} + \frac{(Z_{T2}(z') \pm Z_0)Z_{T1}}{Z_{T1}(z') + Z_{T2}(z')} \underline{I}_{s0} \right]. \quad (8.168b)$$

We can express this relation as

$$\begin{bmatrix} \underline{V}(z) \\ \underline{I}(z) \end{bmatrix} = \mathbf{G}(z, z') \begin{bmatrix} \underline{V}_{s0} \\ \underline{I}_{s0} \end{bmatrix} dz'. \quad (8.169)$$

The *dyadic Green's function* of the terminated transmission-line $\mathbf{G}(z, z')$ is given by

$$\mathbf{G}(z, z') = \frac{1}{2} \begin{bmatrix} G_{VV}(z, z') & G_{VI}(z, z') \\ G_{IV}(z, z') & G_{II}(z, z') \end{bmatrix} e^{-\gamma|z-z'|}. \quad (8.170)$$

with the matrix elements

$$G_{VV}(z, z') = \frac{\xi(z, z')Z_T(z, z') \cosh \gamma(z - z') - Z_0 \sinh \gamma(z - z')}{Z_{T1}(z') + Z_{T2}(z')}, \quad (8.171a)$$

$$G_{VI}(z, z') = \frac{Z_{T1}(z')Z_{T2}(z') \cosh \gamma(z - z') - \xi(z, z')Z_0Z_T(z', z) \sinh \gamma(z - z')}{Z_{T1}(z') + Z_{T2}(z')}, \quad (8.171b)$$

$$G_{IV}(z, z') = \frac{-\xi(z, z')Z_{T1}(z')Z_{T2}(z') \sinh \gamma(z - z') + Z_0 \cosh \gamma(z - z')}{Z_0(Z_{T1}(z') + Z_{T2}(z'))}, \quad (8.171c)$$

$$G_{II}(z, z') = \frac{-Z_{T1}(z')Z_{T2}(z') \sinh \gamma(z - z') + \xi(z, z')Z_0Z_T(z', z) \cosh \gamma(z - z')}{Z_0(Z_{T1}(z') + Z_{T2}(z'))}. \quad (8.171d)$$

The function $\xi(z, z')$ given by (8.164) and $Z_T(z, z')$ is given by

$$Z_T(z, z') = \begin{cases} Z_{T1} & \text{for } z < z', \\ Z_{T2} & \text{for } z > z'. \end{cases} \quad (8.172)$$

For voltage and current sources distributed over the transmission-line with the impressed voltage per unit of length $\underline{V}'_s(z)$ and the impressed current per unit of length $\underline{I}'_s(z)$ we obtain

$$\begin{bmatrix} \underline{V}(z) \\ \underline{I}(z) \end{bmatrix} = \int_0^l \mathbf{G}(z, z') \begin{bmatrix} \underline{V}'_s(z') \\ \underline{I}'_s(z') \end{bmatrix} dz'. \quad (8.173)$$

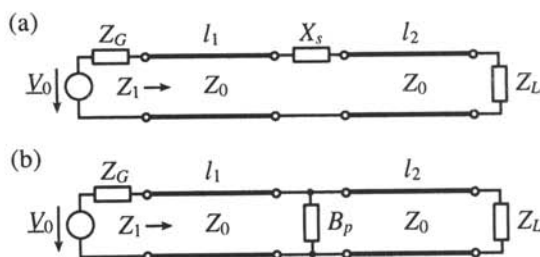


Figure 8.26: Matching circuits.

8.9 PROBLEMS

- Consider an R 320 rectangular waveguide with inner dimensions $a = 7.112$ mm and $b = 3.556$ mm. Determine the equivalent circuits according to Figure 8.1 for a waveguide section of length $\Delta l = 0.5$ mm for the TE_{10} , TE_{01} , TE_{20} , TE_{11} and TM_{11} modes.
- Consider the matching circuits shown in Figure 8.26. The matching circuit consists of two coaxial cable segments ($Z_0 = 60 \Omega$, $c = 2 \cdot 10^8$ ms $^{-1}$) with lengths l_1 and l_2 and either a series reactance X_s or a shunt susceptance B_p between. The generator provides a harmonic signal of frequency $f = 100$ MHz and has an impedance $Z_G = 50 \Omega$ and is terminated with an RL series circuit with an impedance $Z_L = (35 + j14) \Omega$.
 - Determine the parameters X_s , l_1 and l_2 of the matching circuit shown in Figure 8.26(a) for matching Z_L to Z_G for minimum lengths of l_1 and l_2 and either an inductor or a capacitor as the series reactance X_s .
 - Realize the series inductance with a short-circuited stub of a shielded parallel wire line ($Z_0 = 60 \Omega$, $c = 2 \cdot 10^8$ ms $^{-1}$). Determine the minimum length l_{s1} of this stub.
 - Determine the parameters B_p , l_1 and l_2 of the matching circuit shown in Figure 8.26(b) for matching Z_L to Z_G for minimum lengths of l_1 and l_2 and either an inductor or a capacitor as the series susceptance B_p .
 - Realize the series admittance B_p with a short-circuited stub of a coaxial line ($Z_0 = 60 \Omega$, $c = 2 \cdot 10^8$ ms $^{-1}$). Determine the minimum length l_{s2} of this stub.
 - Compare the frequency behavior of both matching circuits (a) and (b) in the frequency interval from 90 GHz to 110 GHz by drawing real and imaginary parts of Z_1 for the above matching circuits.
- For the load and the generator given in Problem 2 determine lumped element matching circuits as shown in Figures 8.13, 8.14 and 8.15. Determine the L - and

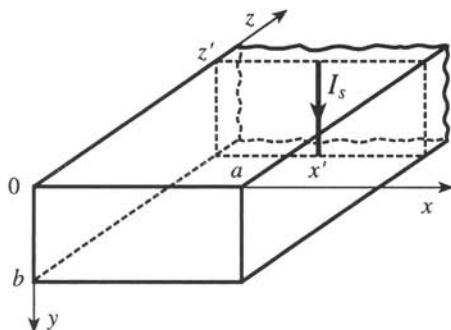


Figure 8.27: Excitation of a waveguide by a current filament.

C-values of the four possible circuits and compare the frequency behavior of these matching circuits in the frequency interval from 90 GHz to 110 GHz by drawing real and imaginary parts of Z_1 .

4. An X-band rectangular waveguide ($a = 22.86$ mm, $b = 10.16$ mm) of 9 cm length is excited in the TE_{10} mode at the frequency $f = 10$ GHz. At its end the waveguide is filled over a length $d = 7$ mm with a dielectric material ($\epsilon_r = 2.5$) and then short-circuited. Determine the input impedance of the line.
5. A four-conductor transmission-line with the conductors embedded in free-space has the per unit of length inductance matrix $L = \begin{pmatrix} 10 & 5 & 3 \\ 5 & 10 & 5 \\ 3 & 5 & 10 \end{pmatrix}$ nH/m.
 - a) Determine the per unit of length capacitance matrix.
 - b) Determine the characteristic impedance matrix Z_0 .
 - c) Determine the load impedance matrix Z_L for reflection-free termination of the four-conductor transmission-line.
6. A four-conductor transmission-line has the per unit of length inductance and capacitance matrices $L' = \begin{pmatrix} 10 & 1 & 3 \\ 1 & 4 & 1 \\ 3 & 1 & 6 \end{pmatrix}$ nH/m and $C' = \begin{pmatrix} 5 & 2.5 & 1.5 \\ 2.5 & 4 & 1 \\ 1.5 & 1 & 3 \end{pmatrix}$ pF/m.
 - a) Give the multiconductor transmission-line equations.
 - b) Derive the diagonal form of the multiconductor transmission-line equations.
 - c) Determine the load impedance matrix Z_L for reflection-free termination of the four-conductor transmission-line.
7. A rectangular waveguide of width a , height $b = \frac{1}{2}a$, and infinite extension in positive and negative z -directions is excited by a current filament $I(y)$ in y -direction placed at x' , z' (see Figure 8.27). Compute the modal amplitudes of the excited electric and magnetic fields.
 - a) Assume uniform current distribution $I(y) = I_0$ over the interval $0 \leq y \leq b$ and excitation at a frequency $f = 1.4f_{cTE10}$.

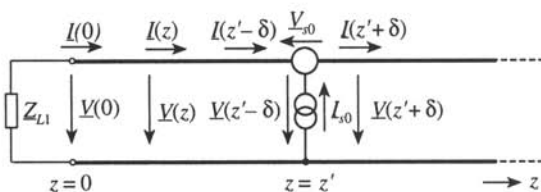


Figure 8.28: Transmission-line with impressed sources terminated at one side.

- b) Assume a current distribution $\underline{I}(y) = \underline{I}_0 \sin \frac{\pi y}{b}$ over the interval $0 \leq y \leq b$ and excitation at a frequency $f = 1.4 f_{\text{TE10}}$.
8. A rectangular waveguide of width a height $b = \frac{1}{2}a$ and infinite extension in positive and negative z -directions is excited by two current filaments directed in y -direction and uniform over their whole length. One filament is placed at z' and $x' = \frac{1}{4}a$ and excited with the current \underline{I} . The other current filament is placed at z' and $x' = \frac{3}{4}a$ and excited with the current $-\underline{I}$ in the opposite direction. The frequency is $f = 2.4 f_{\text{TE10}}$. Compute the modal amplitudes of the excited electric and magnetic fields.
9. Compute Green's function for the transmission-line terminated at the left-hand side with the impedance Z_{L1} and infinitely extended on its right-hand side, as shown in Figure 8.28.
10. Consider a lossless two-conductor transmission-line of length l with characteristic impedance Z_0 and phase coefficient $\beta = \omega/c$. Let the transmission-line be terminated at $z = 0$ and $z = l$ with Z_0 .
- a) Impress a current per unit of length $\underline{I}'_s(z)$ given by

$$\underline{I}'_s(z) = \begin{cases} \underline{I}'_{s0} e^{-j\beta z} & \text{for } \frac{1}{3}l \leq z \leq \frac{2}{3}l \\ 0 & \text{elsewhere} \end{cases}$$

and compute the voltage and current distribution over the whole transmission-line.

- b) Impress a voltage per unit of length $\underline{V}'_s(z)$ given by

$$\underline{V}'_s(z) = \begin{cases} \underline{V}'_{s0} e^{-j\beta z} & \text{for } \frac{1}{3}l \leq z \leq \frac{2}{3}l \\ 0 & \text{elsewhere} \end{cases}$$

and compute the voltage and current distribution over the whole transmission-line.

- c) Impress a current per unit of length $\underline{I}'_s(z)$ together with a voltage per unit of length $\underline{V}'_s(z)$ with the distributions given in the two previous paragraphs. Discuss the case $\underline{V}'_s(z) = \pm Z_0 \underline{I}'_s(z)$.

REFERENCES

- [1] R. W. P. King, *Transmission-Line Theory*. New York: McGraw Hill, 1955.
- [2] S. Ramo, J. R. Whinnery, and T. van Duzer, *Fields and Waves in Communication Electronics*. New York: John Wiley & Sons, 1965.
- [3] R. E. Collin, *Foundations of Microwave Engineering*. New York: McGraw-Hill, 1992.
- [4] P. C. Magnusson, G. C. Alexander, V. Tripathi, and A. Weisshaar, *Transmission Lines and Wave Propagation*. Boca Raton: CRC Press, 2001.
- [5] P. H. Smith, *Electronic Applications of the Smith Chart in Waveguide, Circuit and Components Analysis*. New York: McGraw-Hill, 1969.
- [6] R. V. Churchill and J. W. Brown, *Complex Variables and Applications*. New York: McGraw Hill, 1990.
- [7] D. K. Misra, *Radio-Frequency and Microwave Communication Circuits*. New York: John Wiley & Sons, 2001.
- [8] M. M. Radmanesh, *Microwave Electronics*. Upper Saddle River, NJ: Prentice Hall PTR, 2001.
- [9] F. E. Gardiol, *Lossy Transmission Lines*. Boston: Artech House, 1987.
- [10] P. I. Kuznetsov and R. L. Stratonovich, *The Propagation of Electromagnetic Waves in Multiconductor Transmission Lines*. Oxford: Pergamon Press, 1964.
- [11] L. B. Felsen and N. Marcuvitz, *Radiation and Scattering of Waves*. Englewood Cliffs, NJ: Prentice Hall, 1972.
- [12] S. Frankel, *Multiconductor Transmission Line Analysis*. Boston: Artech House, 1977.
- [13] J. A. Brandão Faria, *Multiconductor Transmission-Line Structures*. New York: John Wiley & Sons, 1993.
- [14] N. Faché, F. Olyslager, and D. De Zutter, *Electromagnetic Circuit Modelling of Multiconductor Transmission Lines*. Oxford: Clarendon Press, 1993.
- [15] C. R. Paul, *Analysis of Multiconductor Transmission Lines*. New York: John Wiley & Sons, 1994.
- [16] C.-T. Tai, *Dyadic Green Functions in Electromagnetic Theory*. New York: IEEE Press, 1993.

Chapter 9

Resonant Circuits and Resonators

Resonant circuits and resonators are important circuit elements in radio-frequency engineering. A resonant circuit is formed by a capacitor and an inductor connected in parallel or in series. As components in active and passive circuits, resonant circuits and resonators allow a selective transmission or blocking of signals. In oscillators these components serve as the frequency-determining elements.

9.1 THE LINEAR PASSIVE ONE-PORT

A circuit element with a single port is called a *one-port*. Figure 9.1 shows the schematic drawing and the equivalent circuit of a one-port. Incident and reflected waves are related to a given transverse plane of reference. The signal at the port is described either by the complex amplitudes \underline{a} and \underline{b} of the incident and scattered waves or by the voltage \underline{V} and current \underline{I} . If the relation between \underline{V} and \underline{I} or \underline{a} and \underline{b} , respectively, is known, the one-port is defined as a circuit element. If the relation between \underline{V} and \underline{I} or \underline{a} and \underline{b} , respectively, is linear, the one-port is called a linear one-port. The complex power P_c flowing into the one-port is given by

$$P_c = - \int_A \mathcal{T} . \quad (9.1)$$

The integration is performed over the cross-sectional area A of the waveguide port in the plane of reference. With (4.19), (8.9a), (8.9b) and (8.22a) we obtain a complex power P_c flowing into the one-port:

$$P_c = \frac{1}{2} \underline{V} \underline{I}^* . \quad (9.2)$$

The real part of the complex power P_c is the active power P . The imaginary part is the reactive power P_r :

$$P_c = P + j P_r . \quad (9.3)$$

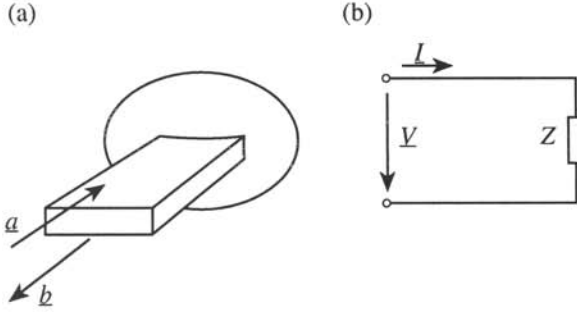


Figure 9.1: One-port: (a) schematic drawing, and (b) equivalent circuit.

Using (8.42a) and (8.42b) we express the complex power P_c by wave amplitudes,

$$P_c = \frac{1}{2} (|a|^2 - |b|^2 + a^* b - a b^*) . \quad (9.4)$$

For $P = 0$ the one-port is lossless. A lossless one-port also is called a reactive one-port. For the passive one-port we obtain $|\rho| \leq 1$. For the reactive one-port $|\rho| = 1$ is valid. For the source-free one-port we obtain from (4.36) and (9.1)

$$P_c = P + 2j\omega(W_m - W_e) , \quad (9.5)$$

where W_m is the average stored magnetic energy and W_e is the average stored electric energy. The momentary values of W_e and W_m oscillate between zero and their maximum value with the double oscillation frequency. For $W_e = W_m$ within a quarter of the period of oscillation the stored magnetic energy is completely transformed in electric energy and vice versa. For $W_m \neq W_e$ a periodical energy exchange also occurs with an external circuit driving the resonant circuit. In this case the reactive power is flowing through the port. The ratio of voltage and current or generalized voltage and generalized current is given by the complex impedance Z or the complex admittance Y , respectively. It follows from (9.2) that

$$P_c = \frac{1}{2} Z |I|^2 = \frac{1}{2} Y^* |V|^2 . \quad (9.6)$$

With (9.5) we obtain

$$Z = \frac{P + 2j\omega(W_m - W_e)}{\frac{1}{2}|I|^2} , \quad (9.7a)$$

$$Y = \frac{P + 2j\omega(W_e - W_m)}{\frac{1}{2}|V|^2} . \quad (9.7b)$$

The reactance X and the susceptance B are

$$X = \frac{4\omega}{|I|^2} (W_m - W_e) , \quad (9.8a)$$

$$B = \frac{4\omega}{|V|^2} (W_e - W_m) . \quad (9.8b)$$

9.2 THE REACTANCE THEOREM

Foster's reactance theorem [1–3] imposes a condition on the frequency dependence of a reactance. From the complex Maxwell equations (2.130a) and (2.130b) we obtain for real permittivity, real permeability, and no sources

$$d\underline{\mathcal{H}} = j\omega\epsilon \star \underline{\mathcal{E}}, \quad (9.9a)$$

$$d\underline{\mathcal{E}} = -j\omega\mu \star \underline{\mathcal{H}}. \quad (9.9b)$$

The partial derivative of these equations with respect to ω is given by

$$d\frac{\partial\underline{\mathcal{H}}}{\partial\omega} = j\epsilon \star \underline{\mathcal{E}} + j\omega\epsilon \star \frac{\partial\underline{\mathcal{E}}}{\partial\omega}, \quad (9.10a)$$

$$d\frac{\partial\underline{\mathcal{E}}}{\partial\omega} = -j\mu \star \underline{\mathcal{H}} - j\omega\mu \star \frac{\partial\underline{\mathcal{H}}}{\partial\omega}. \quad (9.10b)$$

We now compute the following expressions

$$d\left(\frac{\partial\underline{\mathcal{H}}}{\partial\omega} \wedge \underline{\mathcal{E}}^*\right) = j\epsilon (\star \underline{\mathcal{E}}) \wedge \underline{\mathcal{E}}^* + j\omega\epsilon \left(\star \frac{\partial\underline{\mathcal{E}}}{\partial\omega}\right) \wedge \underline{\mathcal{E}}^* - j\omega\mu \frac{\partial\underline{\mathcal{H}}}{\partial\omega} \wedge (\star \underline{\mathcal{H}}^*), \quad (9.11a)$$

$$d\left(\frac{\partial\underline{\mathcal{E}}}{\partial\omega} \wedge \underline{\mathcal{H}}^*\right) = -j\mu (\star \underline{\mathcal{H}}) \wedge \underline{\mathcal{H}}^* - j\omega\mu \left(\star \frac{\partial\underline{\mathcal{H}}}{\partial\omega}\right) \wedge \underline{\mathcal{H}}^* + j\omega\epsilon \frac{\partial\underline{\mathcal{E}}}{\partial\omega} \wedge (\star \underline{\mathcal{E}}^*). \quad (9.11b)$$

From these equations and (4.25) and (4.26) we obtain

$$d\left(\frac{\partial\underline{\mathcal{E}}}{\partial\omega} \wedge \underline{\mathcal{H}}^*\right) - d\left(\frac{\partial\underline{\mathcal{H}}}{\partial\omega} \wedge \underline{\mathcal{E}}^*\right) = -8j (\overline{\mathcal{W}}_e + \overline{\mathcal{W}}_m). \quad (9.12)$$

Integrating this equation over a volume V with the boundary ∂V and applying Stokes' theorem (A.90) yields

$$\oint_{\partial V} \left(\frac{\partial\underline{\mathcal{E}}}{\partial\omega} \wedge \underline{\mathcal{H}}^* - \frac{\partial\underline{\mathcal{H}}}{\partial\omega} \wedge \underline{\mathcal{E}}^*\right) = -8j \int_V (\overline{\mathcal{W}}_e + \overline{\mathcal{W}}_m). \quad (9.13)$$

We apply this relation to the one-port depicted in Figure 9.1(a). The boundary surface ∂V is assumed to enclose the complete one-port. The reference plane A of the waveguide defining the port is assumed to be a part of the boundary ∂V . Therefore on the left-hand side of (9.13) we only need to perform the integration over the cross-sectional area A of the waveguide. We consider that the orientation of the boundary surface ∂V of the volume V is outwards, whereas the cross-sectional area A of the waveguides is oriented inwards. Therefore we have to change the sign on the left-hand side of (9.13) when we

are replacing ∂V by A . Since A is a transverse plane, $\underline{\mathcal{E}}$ and $\underline{\mathcal{H}}$ may be replaced by their transverse components $\underline{\mathcal{E}}_{\text{tr}}$ and $\underline{\mathcal{H}}_{\text{tr}}$ as introduced in (8.6a) and (8.6c). From (8.9a) and (8.9b) we obtain

$$\underline{\mathcal{E}}_{\text{tr}}(\mathbf{x}) = \underline{V} e(u, v), \quad (9.14a) \quad \underline{\mathcal{H}}_{\text{tr}}(\mathbf{x}) = \underline{I} h(u, v), \quad (9.14b)$$

$$\frac{\partial}{\partial \omega} \underline{\mathcal{E}}_{\text{tr}}(\mathbf{x}) = \frac{dV}{d\omega} e(u, v), \quad (9.15a) \quad \frac{\partial}{\partial \omega} \underline{\mathcal{H}}_{\text{tr}}(\mathbf{x}) = \frac{dI}{d\omega} h(u, v), \quad (9.15b)$$

where u, v are the transverse coordinates in the port plane. From (9.14a) to (9.15b) and (8.23) it follows that

$$\oint_{\partial V} \frac{\partial \underline{\mathcal{E}}}{\partial \omega} \wedge \underline{\mathcal{H}}^* = - \oint_A \frac{\partial \underline{\mathcal{E}}_{\text{tr}}}{\partial \omega} \wedge \underline{\mathcal{H}}_{\text{tr}}^* = - \frac{dV}{d\omega} \underline{I}^*, \quad (9.16a)$$

$$\oint_{\partial V} \frac{\partial \underline{\mathcal{H}}}{\partial \omega} \wedge \underline{\mathcal{E}}^* = - \oint_A \frac{\partial \underline{\mathcal{H}}_{\text{tr}}}{\partial \omega} \wedge \underline{\mathcal{E}}_{\text{tr}}^* = \frac{dI}{d\omega} \underline{V}^*. \quad (9.16b)$$

Inserting this into (9.13) we obtain

$$\frac{dV}{d\omega} \underline{I}^* + \frac{dI}{d\omega} \underline{V}^* = 8j \int_V (\overline{W}_e + \overline{W}_m) = 8j (W_e + W_m). \quad (9.17)$$

From

$$\underline{V} = j X \underline{I}, \quad (9.18a) \quad \underline{I} = j B \underline{V} \quad (9.18b)$$

we obtain

$$\frac{dV}{d\omega} = j \frac{dX}{d\omega} \underline{I} \Big|_{\underline{I}=\text{const.}}, \quad \frac{dI}{d\omega} = j \frac{dB}{d\omega} \underline{V} \Big|_{\underline{V}=\text{const.}}. \quad (9.19)$$

and

$$\frac{dX}{d\omega} |\underline{I}|^2 = \frac{dB}{d\omega} |\underline{V}|^2. \quad (9.20)$$

Inserting (9.19) and (9.20) into (9.17) yields

$$\frac{dX}{d\omega} |\underline{I}|^2 = 4 (W_e + W_m), \quad (9.21a) \quad \frac{dB}{d\omega} |\underline{V}|^2 = 4 (W_e + W_m). \quad (9.21b)$$

Together with (9.8a) and (9.8b) this yields

$$W_e = \frac{1}{8} \left(\frac{dX}{d\omega} - \frac{X}{\omega} \right) |\underline{I}|^2 = \frac{1}{8} \left(\frac{dB}{d\omega} + \frac{B}{\omega} \right) |\underline{V}|^2, \quad (9.22a)$$

$$W_m = \frac{1}{8} \left(\frac{dX}{d\omega} + \frac{X}{\omega} \right) |\underline{I}|^2 = \frac{1}{8} \left(\frac{dB}{d\omega} - \frac{B}{\omega} \right) |\underline{V}|^2. \quad (9.22b)$$

Since W_e and W_m are non negative it follows for passive lossless one-ports

$$\frac{dX}{d\omega} > \left| \frac{X}{\omega} \right|, \quad (9.23a) \quad \frac{dB}{d\omega} > \left| \frac{B}{\omega} \right|. \quad (9.23b)$$

This is called *Foster's reactance theorem*.

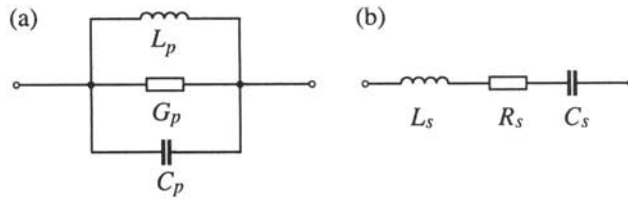


Figure 9.2: Resonant circuit: (a) parallel circuit, and (b) series circuit.

9.3 RESONANT CIRCUITS

In Figure 9.2 the *parallel resonant circuit* and the *series resonant circuit* are depicted. Parallel and serial resonant circuits are mutually dual. Therefore we will treat them in the following in parallel. The admittance Y_p of the parallel resonant circuit and the impedance Z_s of the series resonant circuit are given by

Parallel resonant circuit

$$Y_p = G_p + j\left(\omega C_p - \frac{1}{\omega L_p}\right), \quad (9.24a)$$

Series resonant circuit

$$Z_s = R_s + j\left(\omega L_s - \frac{1}{\omega C_s}\right). \quad (9.24b)$$

At the resonant frequency ω_0 given by

Parallel resonant circuit

$$\omega_0 = \frac{1}{\sqrt{L_p C_p}}, \quad (9.25a)$$

Series resonant circuit

$$\omega_0 = \frac{1}{\sqrt{L_s C_s}} \quad (9.25b)$$

the admittance Y_p and Z_s , respectively, are real.

Parallel resonant circuit

For constant impressed current the parallel resonant circuit exhibits a voltage maximum at the resonant frequency.

Series resonant circuit

For impressed voltage a series resonant circuit exhibits a current maximum at the resonant frequency.

The complex power P_c flowing into the resonant circuit and the active power P are given by

Parallel resonant circuit

$$P_c = \frac{1}{2} Y_p^* |V|^2, \quad (9.26a)$$

$$P = \frac{1}{2} G_p |V|^2, \quad (9.27a)$$

Series resonant circuit

$$P_c = \frac{1}{2} Z_s |I|^2, \quad (9.26b)$$

$$P = \frac{1}{2} R_s |I|^2, \quad (9.27b)$$

The average electric energy W_e stored in the capacitor and the average magnetic energy W_m stored in the inductor for both cases are given by

$$W_e = \frac{1}{4} C |V|^2, \quad (9.28)$$

$$W_m = \frac{1}{4} L |I|^2. \quad (9.29)$$

For resonance we obtain in both cases

$$W_e = W_m. \quad (9.30)$$

The total stored energy W_{tot} is given by

$$W_{\text{tot}} = W_e + W_m = \frac{1}{2} C |V|^2 = \frac{1}{2} L |I|^2. \quad (9.31)$$

The quality Q of a resonant circuit is defined by

$$Q = 2\pi \frac{\text{Stored energy}}{\text{Energy dissipated per period}}. \quad (9.32)$$

The energy dissipated per period is given by

$$\frac{2\pi P}{\omega_0} = \text{Energy dissipated per period}. \quad (9.33)$$

With this we obtain

Parallel resonant circuit

$$Q = \frac{\omega_0 C_p}{G_p} = \frac{1}{\omega_0 L_p G_p}, \quad (9.34a)$$

Series resonant circuit

$$Q = \frac{\omega_0 L_s}{R_s} = \frac{1}{\omega_0 C_s R_s}. \quad (9.34b)$$

In many cases it is useful to introduce the so-called detuning parameter ν

$$\nu = \left(\frac{\omega}{\omega_0} - \frac{\omega_0}{\omega} \right). \quad (9.35)$$

For small detuning ν the following approximate formula

$$\nu = 2 \frac{\omega - \omega_0}{\omega_0} \quad \text{for} \quad \frac{\omega - \omega_0}{\omega_0} \ll 1. \quad (9.36)$$

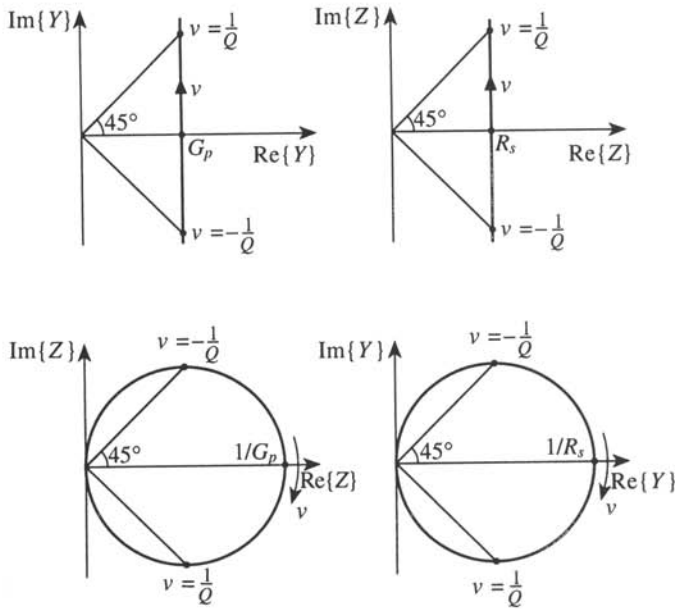


Figure 9.3: Impedance and admittance plots of series and parallel resonant circuits in the Y -plane and Z -plane.

is valid. With (9.25a), (9.25b), (9.34a), (9.34b), and (9.35) we obtain the normalized representation

Parallel resonant circuit

$$Y_p = G_p(1 + jQv), \quad (9.37a)$$

Series resonant circuit

$$Z_s = R_s(1 + jQv). \quad (9.37b)$$

In Figure 9.3 the admittance and impedance curves of the parallel and series resonant circuits are depicted in the Y -plane as well as in the Z -plane. The 3 dB cutoff frequencies ω_+ and ω_- are the frequencies for which the voltage across the parallel resonant circuit for the impressed current of constant amplitude decreases by a factor $1/\sqrt{2}$ compared with the resonant case. For the series resonant circuit with impressed voltage of constant amplitude the current is reduced by a factor $1/\sqrt{2}$ compared with the resonant case. The 3 dB cutoff frequency ω_+ is given by $v = 1/Q$ and the cutoff frequency ω_- is given by $v = -1/Q$. With (9.35) it follows that

$$\frac{\omega_+}{\omega_0} = \frac{1}{2Q} + \sqrt{\left(\frac{1}{2Q}\right)^2 + 1}, \quad (9.38a)$$

$$\frac{\omega_-}{\omega_0} = -\frac{1}{2Q} + \sqrt{\left(\frac{1}{2Q}\right)^2 + 1}. \quad (9.38b)$$

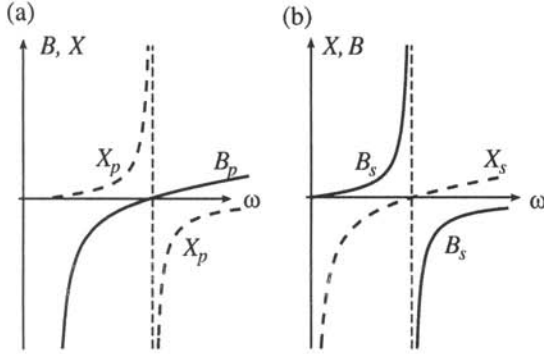


Figure 9.4: Reactance X and susceptance B of the lossless (a) parallel and (b) series resonant circuits.

The 3 dB bandwidth $\Delta\omega$ is given by the difference

$$\Delta\omega = \omega_+ - \omega_- . \quad (9.39)$$

With (9.38a) and (9.38b) we obtain

$$\Delta\omega = \frac{\omega_0}{Q} . \quad (9.40)$$

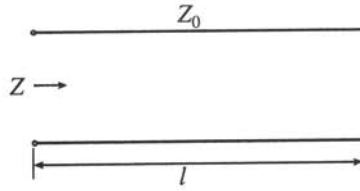
The *relative bandwidth* $\Delta\omega/\omega_0$ is equal to the reciprocal quality factor. In some cases in literature the parameter *damping* d also is used

$$\frac{\Delta\omega}{\omega_0} = \frac{1}{Q} = d . \quad (9.41)$$

For lossless resonant circuits $G_p = 0$ and $R_s = 0$, respectively, are valid. In Figure 9.4 the frequency dependence of reactance X and the susceptance B according to (9.24a) and (9.24b) is depicted.

9.4 THE TRANSMISSION-LINE RESONATOR

A segment of a transmission-line at one or both ends, either open or short-circuited, is a resonant structure. Such a circuit element is called a *transmission-line resonator*. We consider a lossless transmission-line of length l with characteristic impedance Z_0 , which is short-circuited at one end as depicted in Figure 9.5. This short-circuited transmission-line is a reactive one-port. From (8.39) we obtain the input impedance Z and the input admittance Y ,

Figure 9.5: Transmission-line of length l short-circuited at one end.

$$Z = jX = jZ_0 \tan \frac{\omega l}{c}, \quad (9.42a) \quad Y = jB = -\frac{j}{Z_0} \cot \frac{\omega l}{c}. \quad (9.42b)$$

We introduce the angular frequency $\omega_1 = \pi \frac{c}{l}$ and obtain

$$Z = jX = jZ_0 \tan \pi \frac{\omega}{\omega_1}, \quad (9.43a) \quad Y = jB = -\frac{j}{Z_0} \cot \pi \frac{\omega}{\omega_1}. \quad (9.43b)$$

The frequency dependence of the reactance X and the susceptance B are depicted in Figure 9.6. In order to obtain the equivalent circuit for the short-circuited transmission-line we perform a *Mittag-Leffler expansion* [4] of $\tan \pi \frac{\omega}{\omega_1}$ and $\cot \pi \frac{\omega}{\omega_1}$, respectively, and obtain

$$\tan \pi x = \frac{2x}{\pi} \sum_{n=1}^{\infty} \frac{1}{(n - \frac{1}{2})^2 - x^2}, \quad \cot \pi x = \frac{1}{\pi x} + \frac{2x}{\pi} \sum_{n=1}^{\infty} \frac{1}{x^2 - n^2}. \quad (9.44a) \quad (9.44b)$$

After inserting into (9.43a) and (9.43b), respectively, it follows that

$$Z = jZ_0 \frac{2\omega}{\pi\omega_1} \sum_{n=1}^{\infty} \frac{1}{(n - \frac{1}{2})^2 - \left(\frac{\omega}{\omega_1}\right)^2}, \quad (9.45a)$$

$$Y = -\frac{j}{Z_0} \left[\frac{\omega_1}{\pi\omega} + \frac{2\omega}{\pi\omega_1} \sum_{n=1}^{\infty} \frac{1}{\left(\frac{\omega}{\omega_1}\right)^2 - n^2} \right], \quad (9.45b)$$

and from this that

$$Z = \sum_{n=1}^{\infty} \frac{1}{j \left[\omega \frac{\pi}{2\omega_1 Z_0} - \frac{1}{\omega} \frac{(n - \frac{1}{2})^2 \pi \omega_1}{2Z_0} \right]}, \quad (9.46a)$$

$$Y = \frac{1}{j\omega \frac{\pi Z_0}{\omega_1}} + \sum_{n=1}^{\infty} \frac{1}{j \left[\omega \frac{\pi Z_0}{2\omega_1} - \frac{1}{\omega} \frac{n^2 \pi \omega_1 Z_0}{2} \right]}. \quad (9.46b)$$

We now introduce the following quantities

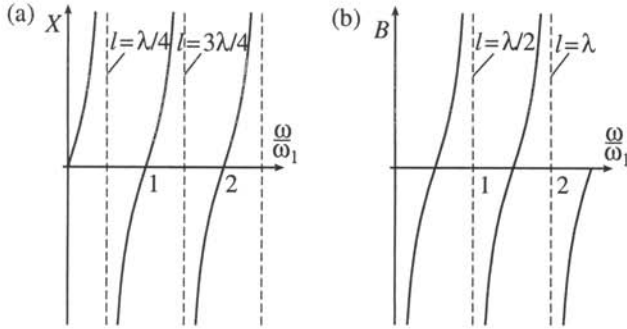


Figure 9.6: (a) Reactance $X(\omega)$, and (b) susceptance $B(\omega)$ of the short-circuited transmission-line.

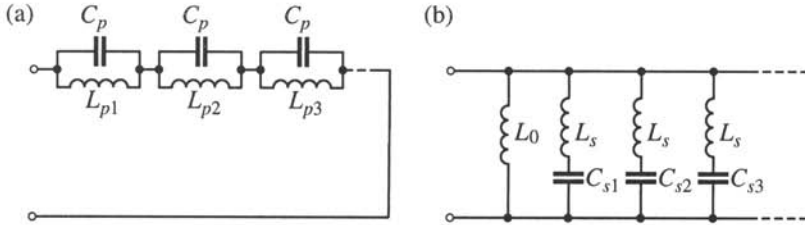


Figure 9.7: Equivalent circuits of the lossless transmission-line resonator (a) according to (9.50a) and (b) according to (9.50b).

$$C_p = \frac{\pi}{2\omega_1 Z_0}, \quad (9.47a)$$

$$L_{pn} = \frac{2Z_0}{(n - \frac{1}{2})^2 \pi \omega_1}, \quad (9.48a)$$

$$\omega_{0pn} = \frac{1}{\sqrt{C_p L_{pn}}} = (n - \frac{1}{2}) \omega_1, \quad (9.49a)$$

$$L_0 = \frac{\pi Z_0}{\omega_1}, \quad L_s = \frac{\pi Z_0}{2\omega_1}, \quad (9.47b)$$

$$C_{sn} = \frac{2}{n^2 \pi \omega_1 Z_0}, \quad (9.48b)$$

$$\omega_{0sn} = \frac{1}{\sqrt{L_s C_{sn}}} = n \omega_1 \quad (9.49b)$$

and obtain with this

$$Z = \sum_{n=1}^{\infty} \frac{1}{j \left(\omega C_p - \frac{1}{\omega L_{pn}} \right)}, \quad (9.50a)$$

$$Y = \frac{1}{j \omega L_0} + \sum_{n=1}^{\infty} \frac{1}{j \left(\omega L_s - \frac{1}{\omega C_{sn}} \right)}. \quad (9.50b)$$

These fractional expansion representations are called the *Foster representations* [3, 5]. The *Foster representation of the first kind*, given by (9.50a), describes the series connection of an infinite number of parallel resonant circuits with resonance frequencies given by (9.49a), whereas the *Foster representation of the second kind*, (9.50b), describes the parallel connection of an infinite number of series resonant circuits and one inductance

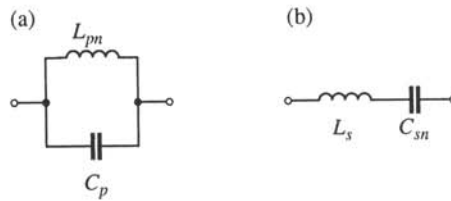


Figure 9.8: Equivalent circuits of the lossless transmission-line resonator (a) near a parallel resonance and (b) near a series resonance.

L_0 where the resonant frequencies of the series resonant circuits are given by (9.49b). The corresponding *equivalent circuits* are the *Foster equivalent circuit of the first kind* shown in Figure 9.7(a) and the *Foster equivalent circuit of the second kind* shown in Figure 9.7(b).

For lossy transmission-lines we have to add loss resistors in the equivalent circuits. In the case of Figure 9.7(b) we have to add a loss conductor in parallel to each parallel resonant circuit, and in the case of Figure 9.7(a) we have to add a loss resistor in series to each series resonant circuit. Considering a transmission-line resonator at frequencies ω_{0pn} or ω_{0sn} in the neighborhood of one pole of the reactance function allows us to neglect all poles with the exception of the pole under consideration. In this way the equivalent circuit may be reduced to a single resonant circuit describing the pole under consideration. Figure 9.8 shows the corresponding equivalent circuits consisting of a single parallel or series resonant circuit, respectively. The short-circuited transmission-line allows for the replacement of series resonant circuits as well as parallel resonant circuits. A short-circuited transmission-line exhibits an infinite number of resonances; however, in general it is possible to design a circuit with transmission-line resonators in such a way that only one dominant pole plays a role. Compared with lumped element resonant circuits realized with lumped elements, a resonator in general exhibits a much higher quality factor.

9.5 CAVITY RESONATORS

9.5.1 The Rectangular Cavity Resonator

We have seen that a transmission-line short-circuited at the end is a *resonator*. The transmission-line may be either a TEM transmission-line or another type of transmission-line (e.g., a waveguide). Such a transmission-line segment terminated by short circuit or open circuit is a resonator. Resonators formed by segments of hollow waveguides are called *cavity resonators*.

Figure 9.9 shows a rectangular cavity resonator with side-lengths a , b , and d . This

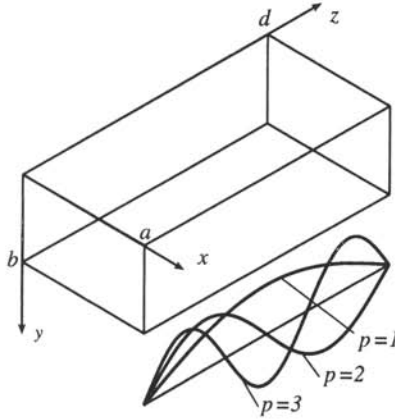


Figure 9.9: Rectangular cavity resonator.

cavity resonator consists of a waveguide segment of length d , terminated at both ends by conducting planes. The electromagnetic field in the resonator consists of a superposition of waves traveling in the positive and negative set direction exhibiting node planes at $z = 0$ and $z = d$. We obtain the boundary conditions $E_{tr}|_{z=0} = 0$, $E_{tr}|_{z=d} = 0$. To fulfill these boundary conditions the distance d must be an integer multiple of $\frac{1}{2}\lambda_g$.

$$d = \frac{1}{2}p\lambda_g, \quad \text{for } p = 0, 1, 2, \dots \quad (9.51)$$

Superimposing waves in the forward and backward direction yields nodes in distances $\frac{1}{2}\lambda_g$. With (7.229) to (7.232) it follows that the phase coefficient $\beta = \beta_{mnp}$ is given by

$$\beta_{mnp}^2 = \left(\frac{m\pi}{a}\right)^2 + \left(\frac{n\pi}{b}\right)^2 + \left(\frac{p\pi}{d}\right)^2. \quad (9.52)$$

The resonant frequency ω_{mnp} and the corresponding free-space wavelength λ_{mnp} are given by

$$\omega_{mnp} = \frac{c_0}{\sqrt{\epsilon_r \mu_r}} \sqrt{\left(\frac{m\pi}{a}\right)^2 + \left(\frac{n\pi}{b}\right)^2 + \left(\frac{p\pi}{d}\right)^2}, \quad (9.53)$$

$$\lambda_{mnp} = \frac{\sqrt{\epsilon_r \mu_r}}{\sqrt{\left(\frac{m}{2a}\right)^2 + \left(\frac{n}{2b}\right)^2 + \left(\frac{p}{2d}\right)^2}}. \quad (9.54)$$

If the resonant mode originates from the TE_{mn} mode of the waveguide, the resonator mode is called the TE_{mnp} mode. If the resonator mode originates from the TM_{mn} mode of the waveguide, the resonator mode is called the TM_{mnp} mode.

9.5.1.1 The TE_{mnp} Modes of the Rectangular Cavity Resonator

To determine the field components of the TE_{mnp} modes of the rectangular cavity resonator we consider the field components of the TE_{mn} waveguide modes of the waveguide with a rectangular cross-section according to (7.240a)–(7.240f). We superimpose a waveguide wave of amplitude $\underline{A}^{(+)}$ propagating in the positive z -direction with a waveguide mode with amplitude $\underline{A}^{(-)}$ propagating in the negative z -direction. We take into consideration that the wave propagating in the negative z -direction exhibits the inverse sign of the transverse magnetic field components. This change of sign is due to the replacement of $e^{-j\beta z}$ by $e^{+j\beta z}$ and follows from (7.13b) and (7.14b) due to the partial derivation with respect to z . Therefore we obtain

$$\underline{E}_x = j\omega\mu \frac{n\pi}{b} \cos \frac{m\pi x}{a} \sin \frac{n\pi y}{b} (\underline{A}^{(+)} e^{-j\beta z} + \underline{A}^{(-)} e^{j\beta z}), \quad (9.55a)$$

$$\underline{E}_y = -j\omega\mu \frac{m\pi}{a} \sin \frac{m\pi x}{a} \cos \frac{n\pi y}{b} (\underline{A}^{(+)} e^{-j\beta z} + \underline{A}^{(-)} e^{j\beta z}), \quad (9.55b)$$

$$\underline{E}_z = 0, \quad (9.55c)$$

$$\underline{H}_x = j\beta \frac{m\pi}{a} \sin \frac{m\pi x}{a} \cos \frac{n\pi y}{b} (\underline{A}^{(+)} e^{-j\beta z} - \underline{A}^{(-)} e^{j\beta z}), \quad (9.55d)$$

$$\underline{H}_y = j\beta \frac{n\pi}{b} \cos \frac{m\pi x}{a} \sin \frac{n\pi y}{b} (\underline{A}^{(+)} e^{-j\beta z} - \underline{A}^{(-)} e^{j\beta z}), \quad (9.55e)$$

$$\underline{H}_z = \beta_{Mc}^2 \cos \frac{m\pi x}{a} \cos \frac{n\pi y}{b} (\underline{A}^{(+)} e^{-j\beta z} + \underline{A}^{(-)} e^{j\beta z}). \quad (9.55f)$$

At $z = 0$ the transverse components of the electric field vanish (i.e., in this transverse plane $\underline{E}_x = 0$ and $\underline{E}_y = 0$ must be valid). From this we obtain

$$\underline{A}^{(-)} = -\underline{A}^{(+)}. \quad (9.56)$$

From this condition (9.51) follows. With (9.56) we obtain from (9.55a) to (9.55f)

$$\underline{E}_x = 2\beta Z_{\text{TE}} \frac{n\pi}{b} \underline{A} \cos \frac{m\pi x}{a} \sin \frac{n\pi y}{b} \sin \frac{p\pi z}{d}, \quad (9.57a)$$

$$\underline{E}_y = -2\beta Z_{\text{TE}} \frac{m\pi}{a} \underline{A} \sin \frac{m\pi x}{a} \cos \frac{n\pi y}{b} \sin \frac{p\pi z}{d}, \quad (9.57b)$$

$$\underline{E}_z = 0, \quad (9.57c)$$

$$\underline{H}_x = 2j\beta \frac{m\pi}{a} \underline{A} \sin \frac{m\pi x}{a} \cos \frac{n\pi y}{b} \cos \frac{p\pi z}{d}, \quad (9.57d)$$

$$\underline{H}_y = 2j\beta \frac{n\pi}{b} \underline{A} \cos \frac{m\pi x}{a} \sin \frac{n\pi y}{b} \cos \frac{p\pi z}{d}, \quad (9.57e)$$

$$\underline{H}_z = -2j\beta_{Mc}^2 \underline{A} \cos \frac{m\pi x}{a} \cos \frac{n\pi y}{b} \sin \frac{p\pi z}{d}. \quad (9.57f)$$

9.5.1.2 The TM_{mnp} Modes of the Rectangular Cavity Resonator

We obtain the TM_{mnp} modes of the rectangular cavity resonator from the TM_{mn} modes of the rectangular waveguide. Starting with (7.247a)–(7.247f) and considering that replacing $e^{-j\beta z}$ by $e^{+j\beta z}$ due to (7.13a) and (7.14a) yields a change of sign of \underline{E}_x and \underline{E}_y , we obtain

$$\underline{E}_x = -j\beta \frac{m\pi}{a} \cos \frac{m\pi x}{a} \sin \frac{n\pi y}{b} (\underline{B}^{(+)} e^{-j\beta z} - \underline{B}^{(-)} e^{j\beta z}), \quad (9.58a)$$

$$\underline{E}_y = -j\beta \frac{n\pi}{b} \sin \frac{m\pi x}{a} \cos \frac{n\pi y}{b} (\underline{B}^{(+)} e^{-j\beta z} - \underline{B}^{(-)} e^{j\beta z}), \quad (9.58b)$$

$$\underline{E}_z = \beta_{Mc}^2 \sin \frac{m\pi x}{a} \sin \frac{n\pi y}{b} (\underline{B}^{(+)} e^{-j\beta z} + \underline{B}^{(-)} e^{j\beta z}), \quad (9.58c)$$

$$\underline{H}_x = j \frac{\beta}{Z_{\text{TM}}} \frac{n\pi}{b} \sin \frac{m\pi x}{a} \cos \frac{n\pi y}{b} (\underline{B}^{(+)} e^{-j\beta z} + \underline{B}^{(-)} e^{j\beta z}), \quad (9.58d)$$

$$\underline{H}_y = -j \frac{\beta}{Z_{\text{TM}}} \frac{m\pi}{a} \cos \frac{m\pi x}{a} \sin \frac{n\pi y}{b} (\underline{B}^{(+)} e^{-j\beta z} + \underline{B}^{(-)} e^{j\beta z}), \quad (9.58e)$$

$$\underline{H}_z = 0. \quad (9.58f)$$

From the boundary conditions $\underline{E}_x|_{z=0} = 0$, $\underline{E}_y|_{z=0} = 0$ it follows that

$$\underline{B}^{(+)} = \underline{B}^{(-)} = \underline{B}. \quad (9.59)$$

With this we obtain the field components of the TM_{mnp} mode

$$\underline{E}_x = -2\beta \frac{m\pi}{a} \underline{B} \cos \frac{m\pi x}{a} \sin \frac{n\pi y}{b} \sin \frac{p\pi z}{d}, \quad (9.60a)$$

$$\underline{E}_y = -2\beta \frac{n\pi}{b} \underline{B} \sin \frac{m\pi x}{a} \cos \frac{n\pi y}{b} \sin \frac{p\pi z}{d}, \quad (9.60b)$$

$$\underline{E}_z = 2\beta_{Mc}^2 \underline{B} \sin \frac{m\pi x}{a} \sin \frac{n\pi y}{b} \cos \frac{p\pi z}{d}, \quad (9.60c)$$

$$\underline{H}_x = 2j \frac{\beta}{Z_{\text{TM}}} \frac{n\pi}{b} \underline{B} \sin \frac{m\pi x}{a} \cos \frac{n\pi y}{b} \cos \frac{p\pi z}{d}, \quad (9.60d)$$

$$\underline{H}_y = -2j \frac{\beta}{Z_{\text{TM}}} \frac{m\pi}{a} \underline{B} \cos \frac{m\pi x}{a} \sin \frac{n\pi y}{b} \cos \frac{p\pi z}{d}, \quad (9.60e)$$

$$\underline{H}_z = 0. \quad (9.60f)$$

9.5.1.3 The Quality of Rectangular Cavity Resonators

The definition of the quality factor Q according to (9.32) has been so general that it may also be applied to the resonator. To every mode a quality factor Q_{mnp} may be assigned

by

$$Q_{mnp} = \frac{\omega_{mnp} W_{mnp}}{P_{l mnp}}, \quad (9.61)$$

where W_{mnp} is the average energy stored in mode mnp and $P_{l mnp}$ is the energy of the mode dissipated per unit of time. Furthermore, the quantities marked with mnp depend on whether we are considering the TM mode or the TE mode. With (2.32a), (2.32b), (4.2a), and (4.2b) the average stored energy W_{mnp} is given by

$$W_{mnp} = \frac{1}{4} \int_V (\epsilon' \mathcal{E}^* \wedge \star \mathcal{E} + \mu' \mathcal{H}^* \wedge \star \mathcal{H}) . \quad (9.62)$$

The integration is performed over the resonator volume V . According to (6.66), the power loss $P_{l mnp}$ is given by

$$P_{l mnp} = \frac{1}{2} \oint_{\partial V} R_A |\mathbf{H}_t|^2 s_1 \wedge s_2 . \quad (9.63)$$

The integration is performed over the boundary ∂V (i.e., the walls of the resonator). For the TE₁₀₁ mode with the field components following from (9.57a) to (9.57f) we obtain

$$\underline{E}_y = -2\beta Z_{TE} \frac{\pi}{a} \underline{A} \sin \frac{\pi x}{a} \sin \frac{\pi z}{d}, \quad (9.64a)$$

$$\underline{H}_x = 2j\beta \frac{\pi}{a} \underline{A} \sin \frac{\pi x}{a} \cos \frac{\pi z}{d}, \quad (9.64b)$$

$$\underline{H}_z = -2j\beta_{Mc}^2 \underline{A} \cos \frac{\pi x}{a} \sin \frac{\pi z}{d}. \quad (9.64c)$$

The quality is given by

$$Q_{101} = \frac{\pi Z_F}{2R_A} \frac{b(a^2 + d^2)^{\frac{1}{2}}}{ad(a^2 + d^2) + 2b(a^3 + d^3)}. \quad (9.65)$$

The field lines of the TE₁₀₁ mode of the rectangular resonator are depicted in Figure 9.10.

9.5.2 The Circular Cylindric Cavity Resonator

The circular cylindric cavity resonator is formed by a segment of a circular cylindric waveguide terminated at both ends by a conducting plane. The resonator modes originate from the circular cylindric waveguide modes. The waveguide wavelength λ_g has to fulfill the condition (9.51). From the TE_{*nm*} modes and the TM_{*nm*} modes, respectively, of the circular cylindric waveguide we obtain the TE_{*nmp*} modes and the TM_{*nmp*} modes of

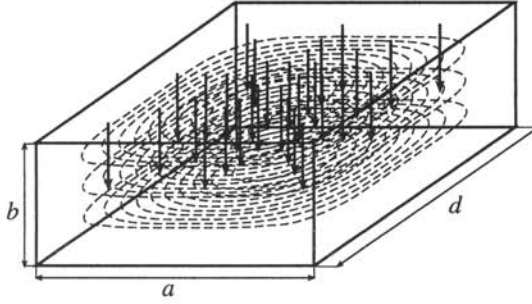


Figure 9.10: Field lines of the TE_{101} mode of the rectangular cavity resonator.

the circular cylindric cavity resonator. The resonant frequencies following from (7.317), (7.318), (7.319a) and (7.319b) are

$$\omega_{mnp}^{TM} = \frac{c_0}{\epsilon_r \mu_r} \sqrt{\xi_{nm}^2 + \left(\frac{p\pi}{d}\right)^2}, \quad (9.66a)$$

$$\omega_{mnp}^{TE} = \frac{c_0}{\epsilon_r \mu_r} \sqrt{\xi_{nm}^2 + \left(\frac{p\pi}{d}\right)^2}. \quad (9.66b)$$

As an example we calculate the field of the TM_{010} mode of the circular cavity resonator. From (7.313a)–(7.313e) it follows that

$$\underline{E}_r = -j\beta k_c J'_0(k_c r) \left(\underline{B}^{(+)} e^{-j\beta z} - \underline{B}^{(-)} e^{j\beta z} \right), \quad (9.67a)$$

$$\underline{E}_z = k_c^2 J_0(k_c r) \left(\underline{B}^{(+)} e^{-j\beta z} + \underline{B}^{(-)} e^{j\beta z} \right), \quad (9.67b)$$

$$\underline{H}_\phi = -j\omega\epsilon_0 k_c J'_0(k_c r) \left(\underline{B}^{(+)} e^{-j\beta z} + \underline{B}^{(-)} e^{j\beta z} \right). \quad (9.67c)$$

The negative sign in (9.67a) originates from the partial derivative with respect to z in the first term on the right side of (7.312). For the TM_{010} mode we obtain $\beta = 0$. This corresponds to the operation of the waveguide at the cutoff wavelength. The radial electric field component \underline{E}_r must vanish at $z = 0$ and $z = d$, and due to $\beta = 0$ vanishes everywhere. We obtain

$$\underline{B}^{(+)} = \underline{B}^{(-)} = \underline{B}. \quad (9.68)$$

From (7.317) we obtain with $\beta = 0$ and (7.315b)

$$\beta_0 = \frac{2.405}{a}, \quad \lambda_0 = \frac{2\pi}{\beta_0} = 2.61a. \quad (9.69)$$

From (9.67a) to (9.67c) we obtain the two remaining field components \underline{E}_z and \underline{H}_ϕ :

$$\underline{E}_z = 2\underline{B}\beta_0^2 J_0(\beta_0 r), \quad (9.70a)$$

$$\underline{H}_\phi = 2j\underline{B} \frac{\beta_0^2}{Z_{F0}} J_1(\beta_0 r). \quad (9.70b)$$

9.5.2.1 The Quality of the Circular Cylindric Cavity Resonators

The quality of a circular cylindric resonator excited in the TM_{010} mode is computed in the following using (9.61)–(9.63). At the resonant frequency we obtain

$$W = 2W_e = \frac{1}{2}\epsilon_0 \int_V |\underline{E}_z|^2 r \, dr \wedge d\phi \wedge dz. \quad (9.71)$$

With (9.70a) it follows that

$$W = 4\pi\epsilon_0 |\underline{B}|^2 \beta_0^4 d \int_0^a r J_0^2(\beta_0 r) dr. \quad (9.72)$$

With (B.28) we obtain

$$W = 2\pi\epsilon_0 |\underline{B}|^2 \beta_0^4 a^2 d J_1^2(\beta_0 a). \quad (9.73)$$

The power loss follows from (9.63):

$$P_l = \frac{1}{2} R_A \oint_{\partial V} |\underline{H}_\phi|^2 r (d\phi \wedge dz + dr \wedge d\phi). \quad (9.74)$$

The integral has to be performed over the side wall and the top and bottom walls of the circular cavity resonator. We obtain

$$P_l = 2R_A |\underline{B}|^2 \frac{\beta_0^4}{Z_{F0}^2} \left[2\pi a d J_1^2(\beta_0 a) + 4\pi \int_0^a r J_1^2(\beta_0 r) dr \right], \quad (9.75)$$

where the first term corresponds to the integral over the side wall and the second term is the integral over the top and bottom walls. With (B.27) it follows that

$$P_l = 4\pi a (d + a) R_A |\underline{B}|^2 \frac{\beta_0^4}{Z_{F0}^2} J_1^2(\beta_0 a). \quad (9.76)$$

From (9.61), (9.73) and (9.76) we finally obtain

$$Q_0 = \frac{\epsilon_0 \omega_0 a d}{2(d + a)} \frac{Z_{F0}^2}{R_A}. \quad (9.77)$$

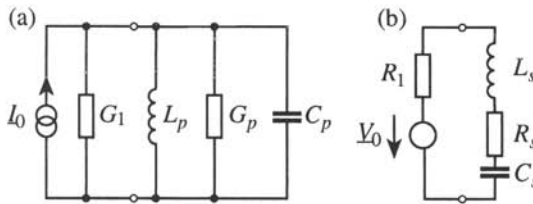


Figure 9.11: Resonant circuit connected with generator.

With (7.315b) it follows that

$$\beta_0 a = \xi_{01} = 2.405 \quad (9.78)$$

and with $\epsilon_0 \omega_0 Z_{F0} = \beta_0$ we obtain the quality factor

$$Q_0 = \frac{Z_{F0}}{R_A} \frac{\xi_{01}}{2 \left(1 + \frac{a}{d}\right)}. \quad (9.79)$$

9.6 COUPLING OF RESONANT CIRCUITS AND RESONATORS

9.6.1 The Loaded Quality Factor

If a resonant circuit or a resonator is coupled to an external circuit, energy stored in the resonant circuit or the resonator will be exchanged with the external circuit. Figure 9.11 depicts the connection of a parallel resonant circuit and a series resonant circuit, respectively, with a generator. The generator consists of an impressed current source I_0 and an inner conductance G_1 or of an impressed voltage source V_0 and the inner resistance R_1 . We have assumed the impedance of the generator to be real. This simplifies the following considerations; however, it does not impose restrictions since in the case of a reactive component of the generator impedance this can be easily compensated by detuning of the resonant circuit.

According to (9.34a) and (9.34b) the quality factor Q_0 of the resonant circuit not connected with the generator is given by

Parallel resonant circuit

$$Q_0 = \frac{\omega_0 C_p}{G_p}, \quad (9.80a)$$

Series resonant circuit

$$Q_0 = \frac{\omega_0 L_s}{R_s}. \quad (9.80b)$$

If the resonant circuit is connected with the generator, the resonant circuit also is damped by the external conductance G_1 or the external resistance R_1 , respectively.

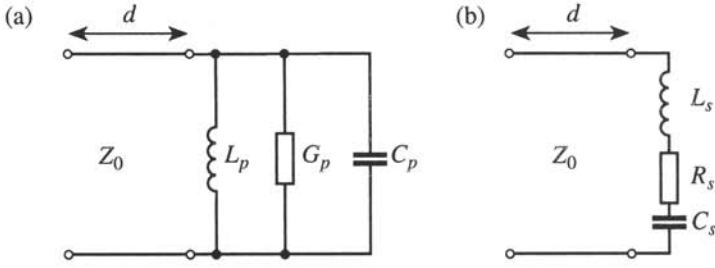


Figure 9.12: Transmission-line terminated with resonant circuit.

Considering the generator as ideal current source or ideal voltage source, respectively, and G_1 or R_1 to be part of the lossy resonant circuit, we can introduce a loaded quality factor Q_L given by

Parallel resonant circuit

$$Q_L = \frac{\omega_0 C_p}{G_1 + G_p}, \quad (9.81a)$$

Series resonant circuit

$$Q_L = \frac{\omega_0 L_s}{R_1 + R_s}. \quad (9.81b)$$

We name Q_0 as the *unloaded quality factor* or *unloaded Q* and Q_L as the *loaded quality factor* or *loaded Q*. It is useful to introduce also a so-called *external quality factor* Q_{ext} given by

Parallel resonant circuit

$$Q_{\text{ext}} = \frac{\omega_0 C_p}{G_1}, \quad (9.82a)$$

Series resonant circuit

$$Q_{\text{ext}} = \frac{\omega_0 L_s}{R_1}. \quad (9.82b)$$

The external quality factor Q_{ext} is a measure for the damping resonant circuit by the external circuit. From (9.80a)–(9.82a) and (9.80b) – (9.82b), respectively, it follows that

$$\frac{1}{Q_L} = \frac{1}{Q_0} + \frac{1}{Q_{\text{ext}}}. \quad (9.83)$$

The smaller Q_{ext} is, the larger the damping due to the coupling of the resonant circuit to an external circuit. For $Q_{\text{ext}} > Q_0$ the resonant circuit is *undercoupled*, for $Q_{\text{ext}} = Q_0$ we obtain *critical coupling*, and for $Q_{\text{ext}} < Q_0$ the resonant circuit is *overcoupled*.

9.6.2 Termination of a Transmission-Line with a Resonant Circuit

We now consider a transmission-line terminated either with a parallel resonant circuit or a series resonant circuit as depicted in Figure 9.12. The transmission-line input is connected to a generator with an internal impedance equal to the wave impedance

Z_0 of the transmission-line. Therefore the resonant circuit also is terminated with the characteristic impedance Z_0 . According to (9.82a) and (9.82b) we obtain

Parallel resonant circuit

$$Q_{\text{ext}} = \omega_0 C_p Z_0, \quad (9.84a)$$

Series resonant circuit

$$Q_{\text{ext}} = \frac{\omega_0 L_s}{Z_0}. \quad (9.84b)$$

Using (8.59a), (8.59b), (9.24a), (9.24b), (9.80a), (9.80b), (9.82a) and (9.82b) we normalize the admittance of the parallel resonant circuit and the impedance of the series resonant circuit with respect to the wave impedance and obtain

Parallel resonant circuit

$$y_p = \frac{Q_{\text{ext}}}{Q_0} (1 + j Q_0 v), \quad (9.85a)$$

Series resonant circuit

$$z_s = \frac{Q_{\text{ext}}}{Q_0} (1 + j Q_0 v). \quad (9.85b)$$

With (8.61a) and (8.61b) we obtain the reflection coefficient

Parallel resonant circuit

$$\underline{\rho}_p = \frac{1 - \frac{Q_{\text{ext}}}{Q_0} (1 + j Q_0 v)}{1 + \frac{Q_{\text{ext}}}{Q_0} (1 + j Q_0 v)}, \quad (9.86a)$$

Series resonant circuit

$$\underline{\rho}_s = - \frac{1 - \frac{Q_{\text{ext}}}{Q_0} (1 + j Q_0 v)}{1 + \frac{Q_{\text{ext}}}{Q_0} (1 + j Q_0 v)}. \quad (9.86b)$$

The rational functions (9.86a) and (9.86b) define circles in the $\underline{\rho}$ -plane. In Figure 9.13 the curves of the parallel resonant circuit and the series resonant circuit are given for undercritical coupling, critical coupling and overcritical coupling.

In the case of critical coupling the impedance curve passes $\underline{\rho} = 0$ at resonance. In the case of overcritical coupling the origin $\underline{\rho} = 0$ is enclosed by the reflection factor curve, whereas for undercritical coupling $\underline{\rho} = 0$ is not enclosed by the reflection factor curve. The 3 dB cutoff frequencies ω_- and ω_+ correspond to points on the reflection factor curve with $X = R$ and $X = -R$ of the Smith chart. We obtain these curves by drawing a circle with center at $\underline{\rho} = -j$ or $\underline{\rho} = j$, respectively, and passing through $\underline{\rho} = -1$ and $\underline{\rho} = 1$.

To determine the input impedance of a transmission-line of length d and characteristic impedance Z_0 terminated with a parallel resonant circuit we have to rotate the points of the $\underline{\rho}$ curve of the parallel resonant circuit according to Figure 9.12(a) in the Smith chart by $\pi d/\lambda$. Strictly speaking we have to rotate every point of the $\underline{\rho}$ curve by another angle since each point belongs to another frequency. If, however, the resonant circuit exhibits sufficiently high quality the essential part of the $\underline{\rho}$ curve belongs to a very small frequency interval. In this case by approximation we may rotate the $\underline{\rho}$ curve by an angle corresponding to the waveguide length d and the waveguide wavelength λ or λ_g , respectively, at the center frequency of the resonant circuit.

Comparing Figure 9.13(a) and 9.13(b) we see that the reflection factor curves of the parallel resonant circuit are transformed in the Smith chart by a rotation over 180° into

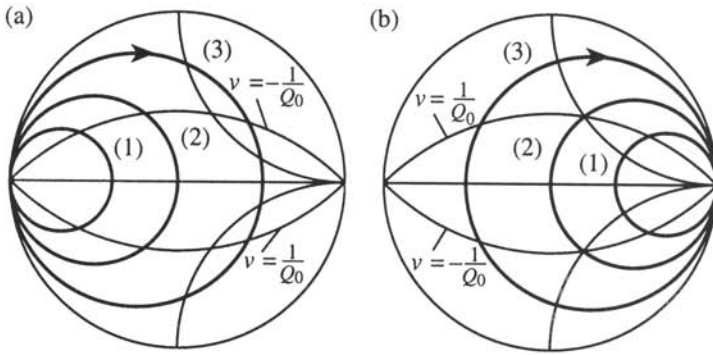


Figure 9.13: Curves (a) of the parallel resonant circuit and (b) of the series resonant circuit for (1) under-critical, (2) critical, and (3) overcritical coupling.

the reflection factor curves of the series resonant circuit. Therefore a $\frac{1}{4}\lambda$ transmission-line terminated with a series resonant circuit behaves like a parallel resonant circuit and vice versa.

9.6.3 Inductive Coupling of Cavity Resonators

Resonators may be coupled to external circuits, via coaxial lines, waveguides or other kinds of transmission-lines. The coupling may be performed inductively over a loop or capacitively over a pin or by some combination of these methods. In Figure 9.14 various examples for the coupling of resonators to waveguides are depicted.

As an example we treat the inductive coupling of a coaxial line to the TM_{010} mode of the circular cylindric resonator. Figure 9.15 shows the inductive coupling of a coaxial line to a circular cylindric resonator. The inner conductor of the coaxial line inside the resonator forms a coupling loop enclosing an area A . The magnetic field in ϕ -direction intersects the loop normally. If at the resonant frequency of the TM_{010} mode a current with amplitude \underline{I} is impressed, a magnetic field in the resonator is induced. On the other hand the alternating magnetic field of the excited TM_{010} mode induces a voltage in the loop. This voltage will assume a maximum value at the resonant frequency of the TM_{010} mode. Therefore we expect that the equivalent circuit of the cavity resonator excited in the TM_{010} mode via an inductive loop will be a parallel resonant circuit, if we assume that the transverse plane of reference is positioned in the side wall of the resonator. The voltage \underline{V} induced in the inductive loop is given by

$$\underline{V} = j\omega\mu_0 A \underline{H}_\phi + j\omega L \underline{I}, \quad (9.87)$$

where the first term at the right side of (9.87) describes the voltage induced due to Faraday's law (2.57b) by the magnetic field of the TM_{010} mode in the coupling loop.

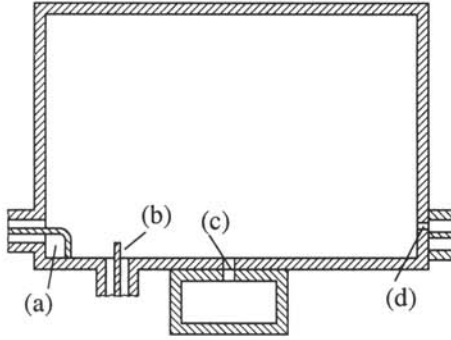


Figure 9.14: Coupling of a resonator to a waveguide with (a) inductive loop coupling, (b) capacitive pin coupling, (c) hole coupling, and (d) inductive hole coupling.

The second term in (9.87) is due to the self-induction due to the inductance L of the coupling loop. The computation of L is more complicated since we have to consider all resonator modes for this. However, it is not necessary to know the value of L since in the case of a high resonator Q factor the inductance L will cause only a minor detuning of the resonator. We can compensate the influence of L by a small change of frequency. The complex power P_c flowing into the resonator is given by

$$P_c = \frac{1}{2} V I^* = \frac{1}{2} j \omega \mu_0 A \underline{H}_\phi(a) \underline{I}^* + \frac{1}{2} j \omega L |\underline{I}|^2. \quad (9.88)$$

In the resonant case the complex power P_c is real and equal to the loss power P_l ,

$$P_c = P_l = \frac{1}{2} j \omega \mu_0 A \underline{H}_\phi(a) \underline{I}^*, \quad (9.89)$$

where the resonant case is defined by tuning for real input impedance. The contribution of the loop inductance L in this case is compensated by a small detuning of the resonator. Assuming that the power loss flowing into the cavity resonator only is due to the resonator wall losses, we obtain from (9.70b) and (9.76):

$$P_l = \pi a(d+a) R_A |\underline{H}_\phi(a)|^2 \quad \text{for } \omega = \omega_0. \quad (9.90)$$

From (9.89) and (9.90), it follows that

$$P_l = \frac{(\omega \mu_0 A)^2 |\underline{I}|^2}{4\pi a(d+a) R_A}. \quad (9.91)$$

On the other hand according to Figure 9.2(a) we obtain for the parallel resonant circuit

$$P_l = \frac{|\underline{I}|^2}{2G_p}. \quad (9.92)$$

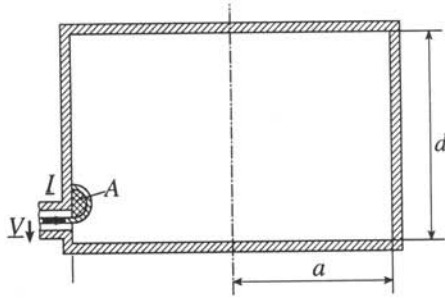


Figure 9.15: Inductive coupling of a coaxial line to a circular cylindric resonator.

From (9.91) and (9.92) we obtain the loss conductance G_p of the parallel resonant circuit according to Figure 9.2(a):

$$G_p = \frac{2\pi a(d+a)R_A}{(\omega\mu_0 A)^2}. \quad (9.93)$$

Since we already have computed the quality Q_0 for the TM_{010} mode of the circular cylindric resonator in (9.79) according to (9.37a), we obtain

$$\underline{Y} = G_p(1 + jQ_0\nu). \quad (9.94)$$

This is the admittance of the cavity resonator of excitation in the TM_{010} mode and refers to the plane of reference in the resonator wall. According to the made assumptions this admittance is only correct within a neighborhood of the resonant frequency of the TM_{010} mode, since only in this case the magnetic field contribution of the TM_{010} mode is the dominating magnetic flux contribution in the coupling loop.

9.7 ORTHOGONALITY OF THE RESONATOR MODES

For a resonator filled with homogeneous isotropic material, with perfectly electrically conducting walls and without source we obtain from Ampère's law (3.27a) and Faraday's law (3.30b) the equations

$$\star d \star d \underline{\mathcal{E}}_k - \omega_k^2 \epsilon \mu \underline{\mathcal{E}}_k = 0, \quad (9.95a)$$

$$\star d \star d \underline{\mathcal{H}}_k - \omega_k^2 \epsilon \mu \underline{\mathcal{H}}_k = 0, \quad (9.95b)$$

where k is the mode index, ω_k is the resonant frequency or eigenfrequency of the k th mode, and $\underline{\mathcal{E}}$ and $\underline{\mathcal{H}}$ are the electric and magnetic modal fields. Let n be the unit differential form normal to the ideally conducting boundary ∂V . Then the boundary conditions for the electric and magnetic fields are

$$n \wedge \underline{\mathcal{E}} = 0 \quad \text{on } \partial V, \quad (9.96a) \quad n \underline{\mathcal{H}} = 0 \quad \text{on } \partial V. \quad (9.96b)$$

Equations (9.95a) or (9.95b) together with the boundary conditions (9.96a) and (9.96b) define an *eigenvalue problem*. For a finite resonator volume solutions exist for a discrete eigenvalue spectrum ω_k . We need to solve the eigenvalue problem either for the electric or the magnetic field only. The complementary field can be determined from (3.27a) or (3.30b). According to Section C.4.1 solutions of (9.95a) and (9.95b) belonging to different eigenvalues are orthogonal. The modal functions of the electric and magnetic fields form a complete set of functions that can be used as a basis to expand any electromagnetic field distribution in the resonator. We introduce the electric and magnetic *structure forms* E_k and H_k satisfying (9.95a) and (9.95b). With the inner product defined in (C.157) the orthonormalization relations are written as

$$\int_V (\star E_k^\star) \wedge E_l = \langle \underline{\mathcal{E}}_k | \underline{\mathcal{E}}_l \rangle = \delta_{kl}, \quad (9.97a)$$

$$\int_V (\star H_k^\star) \wedge H_l = \langle \underline{\mathcal{H}}_k | \underline{\mathcal{H}}_l \rangle = \delta_{kl}. \quad (9.97b)$$

For cylindric cavity resonators the orthogonality of the modal functions also follows from the orthogonality of the transverse structure functions and the orthogonality of the longitudinal sinusoidal functions. For resonators of more general shape the reader is referred to the literature [6–9].

The cavity modes usually are characterized by three indices m, n, p and the property TE or TM. To abbreviate the notation in the following a single index is used to mark the mode. An initially excited cavity can oscillate at one or more of its resonant frequencies at the resonant frequencies without being connected to an external source. Since the resonator modal functions constitute a complete set of orthogonal basis functions we can expand any field in a driven resonator into modal basis functions.

For an arbitrary field distribution $\underline{\mathcal{E}}$ and $\underline{\mathcal{H}}$ in the cavity satisfying (9.103a) and (9.103b) may be expanded into series

$$\underline{\mathcal{E}}(\mathbf{x}) = \sum_k \underline{V}_k \sqrt{\frac{c}{\omega_k}} E_k(\mathbf{x}), \quad (9.98a)$$

$$\underline{\mathcal{H}}(\mathbf{x}) = \sum_k \underline{I}_k \sqrt{\frac{c}{\omega_k}} H_k(\mathbf{x}), \quad (9.98b)$$

where the coefficients \underline{V}_k and \underline{I}_k may be considered as *generalized resonator voltages and currents* with dimensions V and A respectively, and c is the speed of light in the resonator medium. The factor $(c/\omega_k)^{1/2}$ has been introduced to obtain generalized voltages and currents as the expansion coefficients.

To represent the resonator modes by equivalent lumped element resonant circuits, we introduce equivalent capacitances C_k and equivalent inductances L_k , imposing

their relationship to the resonant frequency ω_r and the wave impedance Z_F given by

$$\frac{1}{\sqrt{L_k C_k}} = \omega_k, \quad \sqrt{\frac{L_k}{C_k}} = \sqrt{\frac{\mu}{\epsilon}} = Z_F. \quad (9.99)$$

This yields

$$C_k = \frac{1}{\omega_k} \sqrt{\frac{\epsilon}{\mu}}, \quad L_k = \frac{1}{\omega_k} \sqrt{\frac{\mu}{\epsilon}}. \quad (9.100)$$

With (4.25) and (4.26) and the inner product defined in (C.157) we obtain the mean values of the electric and magnetic energy stored in the cavity \overline{W}_e and \overline{W}_m as

$$\overline{W}_e = \int_V \overline{W}_e = \frac{1}{4} \epsilon \langle \underline{\mathcal{E}} | \underline{\mathcal{E}} \rangle, \quad (9.101a)$$

$$\overline{W}_m = \int_V \overline{W}_m = \frac{1}{4} \mu \langle \underline{\mathcal{H}} | \underline{\mathcal{H}} \rangle. \quad (9.101b)$$

Inserting (9.98a) and (9.98b), considering the orthonormality relations (9.97a), (9.97b) and also (9.100) we can express the stored electric and magnetic energies as

$$\overline{W}_e = \frac{1}{4} \sum_k C_k |\underline{V}_k|^2, \quad (9.102a)$$

$$\overline{W}_m = \frac{1}{4} \sum_k L_k |\underline{I}_k|^2. \quad (9.102b)$$

9.8 EXCITATION OF RESONATORS BY INTERNAL SOURCES

Allowing electric and magnetic sources described by the impressed polarizations $\underline{M}_{e0}(\mathbf{x})$ and $\underline{M}_{m0}(\mathbf{x})$ the electromagnetic field in the waveguide is governed by Ampère's law (3.27a) and Faraday's law (3.30b),

$$d\underline{\mathcal{H}} = j\omega(\epsilon \star \underline{\mathcal{E}} + \underline{M}_{e0}), \quad (9.103a)$$

$$d\underline{\mathcal{E}} = -j\omega(\mu \star \underline{\mathcal{H}} + \underline{M}_{m0}). \quad (9.103b)$$

Consider the electromagnetic field in a resonator excited by an electric polarization \underline{M}_{e0} only. For $\underline{M}_{m0} = 0$ we obtain from (9.103a) and (9.103b)

$$\sum_k \sqrt{\frac{c}{\omega_k}} \underline{V}_k (\star d \star d E_k - \omega^2 \epsilon \mu E_k) = \omega^2 \star \mu \underline{M}_{e0}. \quad (9.104)$$

The structure form E_k is a solution of (9.95a) for the eigenfrequency ω_k ,

$$\star \mathbf{d} \star \mathbf{d} E_k - \omega_k^2 \epsilon \mu E_k = 0. \quad (9.105)$$

Subtracting (9.105) from every term in the sum of (9.104) yields

$$\sum_k \epsilon \sqrt{\frac{c}{\omega_k}} V_k (\omega_k^2 - \omega^2) E_k = \omega^2 \star \underline{\mathcal{M}}_{e0}. \quad (9.106)$$

Forming the inner product with E_k on both sides over the whole cavity volume V and considering the orthonormality relation (9.97a) we obtain

$$(\omega_k^2 - \omega^2) \sqrt{\frac{c}{\omega_k}} V_k = 4\omega^2 \langle E_k | \star \underline{\mathcal{M}}_{e0} \rangle. \quad (9.107)$$

Inserting this into (9.98a) gives the electric resonator field \mathcal{E} due to the excitation by the electric polarization $\underline{\mathcal{M}}_{e0}$ as

$$\underline{\mathcal{E}} = \sum_k \frac{4\omega^2}{\omega_k^2 - \omega^2} E_k \langle E_k | \star \underline{\mathcal{M}}_{e0} \rangle. \quad (9.108)$$

The magnetic field form is given by

$$\underline{\mathcal{H}} = \sum_k \frac{4\omega\omega_k}{\omega_k^2 - \omega^2} H_k \langle E_k | \star \underline{\mathcal{M}}_{e0} \rangle. \quad (9.109)$$

At the resonance frequencies ω_k the field becomes infinite. This is true for a lossless driven resonator. However, in reality any resonator exhibits losses and therefore a finite Q -factor. Therefore the field also remains finite in the lossless case.

For a field excited by a magnetic polarization $\underline{\mathcal{M}}_{m0}$ only with $\underline{\mathcal{M}}_{e0} = 0$ we obtain from (9.103a) and (9.103b)

$$\sum_k \sqrt{\frac{c}{\omega_k}} I_k (\star \mathbf{d} \star \mathbf{d} H_k - \omega^2 \epsilon \mu H_k) = \omega^2 \star \epsilon \underline{\mathcal{M}}_{m0}. \quad (9.110)$$

The structure function H_k is a solution of (9.95b) for the eigenfrequency ω_k ,

$$\star \mathbf{d} \star \mathbf{d} H_k - \omega_k^2 \epsilon \mu H_k = 0. \quad (9.111)$$

Subtracting (9.111) from every term in the sum of (9.110) yields

$$\sum_k \mu \sqrt{\frac{c}{\omega_k}} I_k (\omega_k^2 - \omega^2) H_k = j \omega \star \underline{\mathcal{M}}_{m0}. \quad (9.112)$$

We form on both sides of the equation the inner product with H_k over the whole cavity volume V . With the orthonormality relation (9.97b) we get

$$(\omega_k^2 - \omega^2) \sqrt{\frac{c}{\omega_k}} I_k = 4\omega^2 \langle H_k | * \underline{M}_{m0} \rangle. \quad (9.113)$$

Inserting this into (9.98b) gives the magnetic resonator field \mathcal{H} due to the excitation by the magnetic polarization \underline{M}_{m0} as

$$\underline{\mathcal{H}} = \sum_k \frac{4\omega^2}{\omega_k^2 - \omega^2} H_k \langle H_k | * \underline{M}_{m0} \rangle. \quad (9.114)$$

The electric field form is given by

$$\underline{\mathcal{E}} = \sum_k \frac{4\omega\omega_k}{\omega_k^2 - \omega^2} E_k \langle H_k | * \underline{M}_{m0} \rangle. \quad (9.115)$$

9.9 PROBLEMS

1. A rectangular hollow (ϵ_0, μ_0) cavity resonator, made of copper ($\sigma = 5.8 \cdot 10^7 \text{ Sm}^{-1}$), and with inner dimensions $a = 5 \text{ cm}$, $b = 2 \text{ cm}$, and $d = 6 \text{ cm}$, is excited in the TE_{101} mode with an electric field amplitude $|E_x(\frac{1}{2}a, y, \frac{1}{2}d)| = 1 \text{ Vm}^{-1}$.
 - a) Determine the resonance frequency.
 - b) Compute the energy dissipation P_V due to the finite conductivity of the resonator walls.
 - c) Determine the time average stored energy \overline{W} .
 - d) Compute the unloaded quality factor Q_0 .
2. A coaxial resonator of length $l = 20 \text{ mm}$ is formed of a coaxial line with inner diameter $2a = 2 \text{ mm}$ and outer diameter $2b = 5 \text{ mm}$. The resonator is made of copper ($\sigma = 5.8 \cdot 10^7 \text{ Sm}^{-1}$) and filled with a dielectric with $\epsilon_r = 2.25$. The dielectric can be considered as lossless.
 - a) Compute the 3 lowest parallel resonance frequencies and determine the equivalent circuit of the resonator considering these resonance frequencies only.
 - b) Compute the 3 lowest series resonance frequencies and determine the equivalent circuit of the resonator considering these resonance frequencies only.
 - c) Considering the skin effect compute the ratio of power loss per period of oscillation to the stored energy and from this the quality factors for the three lowest parallel resonance modes.

- d) Determine the equivalent circuit for the three lowest parallel resonance modes also including the parallel loss conductance.
- e) Considering the skin effect compute the ratio of power loss per period of oscillation to the stored energy and from this the quality factors for the three lowest series resonance modes.
- f) Determine the equivalent circuit for the three lowest series resonance modes also including the series loss resistance.

REFERENCES

- [1] R. M. Foster, "A reactance theorem," *Bell System Tech. J.*, vol. 3, pp. 259–267, 1924.
- [2] H. J. Carlin and A. B. Giordano, *Network Theory*. Englewood Cliffs, NJ: Prentice Hall, 1964.
- [3] R. F. Harrington, *Time Harmonic Electromagnetic Fields*. New York: McGraw-Hill, 1961.
- [4] S. Hassani, *Mathematical Physics*. Berlin: Springer, 2002.
- [5] V. Belevitch, *Classical Network Theory*. San Francisco, California: Holden-Day, 1968.
- [6] T. Teichmann and E. P. Wigner, "Electromagnetic field expansions in loss-free cavities excited through holes," *J. Appl. Phys.*, vol. 24, pp. 262–267, Mar. 1953.
- [7] S. A. Schelkunoff, "On representation of electromagnetic fields in cavities in terms of natural modes of oscillation," *J. Appl. Phys.*, vol. 26, pp. 1231–1234, Oct. 1955.
- [8] K. Kurokawa, "The expansions of electromagnetic fields in cavities," *IEEE Trans. Microwave Theory Techn.*, vol. 6, pp. 178–187, Apr. 1958.
- [9] R. E. Collin, *Field Theory of Guided Waves*. New York: IEEE Press, 1991.

Chapter 10

Passive Microwave Circuits

10.1 LINEAR MULTIPORTS

A general microwave circuit is a *multiport* (i.e., a circuit with a number of *ports*) [1–4]. In the network picture, a port is constituted by a pair of external nodes where the currents flowing into the two nodes of a port have equal amplitude and opposite signs. In microwave circuits a multiport usually exhibits waveguide ports. The port is defined by the junction plane of the waveguide. If more than one mode is excited in the junction plane of the waveguide, we have to assign one port to every mode. In the following we assume that in every waveguide only a single transverse waveguide mode is excited. In this case the number of physical ports is identical with the number of ports in the abstract multiport scheme.

Figure 10.1 shows the schematic drawing of a multiport. The port either may be of

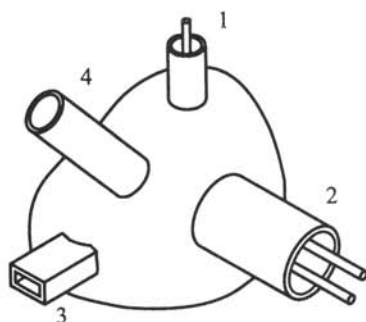


Figure 10.1: Multiport.

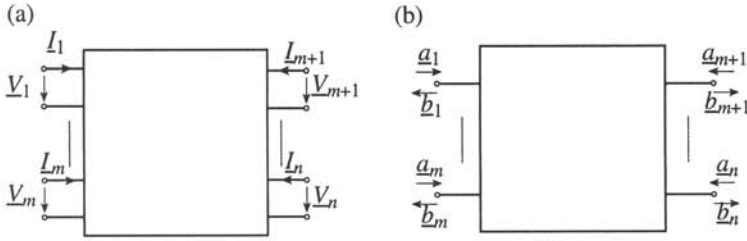


Figure 10.2: Multiport described by the amplitudes (a) $\underline{V}_k, \underline{I}_k$ and (b) $\underline{a}_k, \underline{b}_k$.

a coaxial type, a waveguide type, or any other type. To each port a pair of complex amplitudes is assigned; these describe the incident and scattered electromagnetic waves completely. The complex amplitudes are defined for a certain plane of reference in the waveguide termination. To describe the state of the k th port ($k = 1 \dots n$) we may take the incident and scattered wave amplitudes \underline{a}_k and \underline{b}_k or the current \underline{I}_k and the voltage \underline{V}_k . Current and voltage may be defined in a conventional way for TEM ports. For non-TEM waveguide ports, currents and voltages may be considered as generalized currents and voltages.

Figure 10.2 shows the schematic representations of a multiport. In Figure 10.2(a), a pair of nodes is assigned to each port. The arrows for the voltages \underline{V}_k and currents \underline{I}_k are drawn for every port. Voltages are only defined between the two nodes of the same port, but are undefined between nodes of different ports. The currents flowing into the nodes of one port have the same amplitude, but opposite sign. If the signals are characterized by the wave amplitudes of incident and scattered electromagnetic waves \underline{a}_k and \underline{b}_k respectively, an assignment of arrows according to Figure 10.2(b) is possible. The multiport may be completely described by specifying the relations between incident and scattered amplitudes.

10.2 SOURCE-FREE LINEAR MULTIPORTS

10.2.1 Impedance and Admittance Representations

Source-free linear multiports are described by a linear system of equations [2, 3, 5]. In a multiport with n ports, also called an n -port, the n port voltages $\underline{V}_1 \dots \underline{V}_n$ are related to the n port currents $\underline{I}_1 \dots \underline{I}_n$ via an n -dimensional linear systems of equations:

$$\begin{aligned} \underline{V}_1 &= Z_{11}\underline{I}_1 + Z_{12}\underline{I}_2 + \dots + Z_{1n}\underline{I}_n, \\ \underline{V}_2 &= Z_{21}\underline{I}_1 + Z_{22}\underline{I}_2 + \dots + Z_{2n}\underline{I}_n, \\ &\vdots \\ \underline{V}_n &= Z_{n1}\underline{I}_1 + Z_{n2}\underline{I}_2 + \dots + Z_{nn}\underline{I}_n, \end{aligned} \quad (10.1)$$

where Z_{mn} are impedances. These equations may be written in the following form

$$\underline{V}_i = \sum_{k=1}^n Z_{ik} \underline{I}_k \quad \text{for} \quad i = 1 \dots n. \quad (10.2)$$

Port voltages and port currents are described by n -dimensional vectors. An n -dimensional column vector is a matrix of type $\langle n \times 1 \rangle$,

$$\underline{V}_{\langle n \times 1 \rangle} = \begin{bmatrix} \underline{V}_1 \\ \vdots \\ \underline{V}_n \end{bmatrix}, \quad (10.3a) \quad \underline{I}_{\langle n \times 1 \rangle} = \begin{bmatrix} \underline{I}_1 \\ \vdots \\ \underline{I}_n \end{bmatrix}. \quad (10.3b)$$

The impedances Z_{ik} may be summarized in a matrix of type $\langle n \times n \rangle$ (i.e., an n th order quadratic matrix)

$$\underline{Z}_{\langle n \times n \rangle} = (Z_{ik}) = \begin{bmatrix} Z_{11} & \dots & Z_{1n} \\ \vdots & \ddots & \vdots \\ Z_{n1} & \dots & Z_{nn} \end{bmatrix}. \quad (10.4)$$

The circuit equations (10.1) and (10.2), respectively, can be written in matrix notation,

$$\underline{V} = \underline{Z} \underline{I}. \quad (10.5)$$

\underline{Z} is called the *impedance matrix* of the multiport. The description of the multiport by (10.1), (10.2) and (10.5) is the \underline{Z} -representation or *impedance representation* of the multiport equations. On the other hand, the *admittance matrix* \underline{Y} and the \underline{Y} -representation or *admittance representation* represent the port currents as a function of the port voltages,

$$\underline{I} = \underline{Y} \underline{V}. \quad (10.6)$$

From (10.6) and (10.5), it follows that

$$\underline{V} = \underline{Z} \underline{I} = \underline{Z} \underline{Y} \underline{V} \quad (10.7)$$

and we obtain

$$\underline{Y} = \underline{Z}^{-1}. \quad (10.8)$$

10.2.2 The Chain Matrix

The multiport in Figure 10.3 is *port-number symmetric*, i.e., it has the same number $m = \frac{1}{2}n$ of input ports and output ports. In the *chain representation* of the circuit equations, the currents and voltages of the m input ports are represented as functions of currents and voltages of the m output ports. The input ports are numbered from 1 to

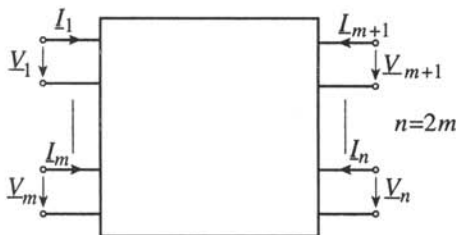


Figure 10.3: Port-number symmetric multiport.

m and the output ports are numbered from $m + 1$ to n . The input amplitudes may be summarized in the m -dimensional vectors

$$\underline{V}_{1(m \times 1)} = [\underline{V}_1, \underline{V}_2, \dots, \underline{V}_m]^T, \quad (10.9a)$$

$$\underline{I}_{1(m \times 1)} = [\underline{I}_1, \underline{I}_2, \dots, \underline{I}_m]^T. \quad (10.9b)$$

To save space in the book we sometimes write column vectors as transposed row vectors. The output quantities are summarized in

$$\underline{V}_{2(m \times 1)} = [\underline{V}_{m+1}, \underline{V}_{m+2}, \dots, \underline{V}_n]^T, \quad (10.9c)$$

$$\underline{I}_{2(m \times 1)} = [\underline{I}_{m+1}, \underline{I}_{m+2}, \dots, \underline{I}_n]^T. \quad (10.9d)$$

The input quantities are represented in dependence of the output quantities by

$$\begin{aligned} \underline{V}_1 &= A_{11} \underline{V}_2 + A_{12} (-\underline{I}_2), \\ \underline{I}_1 &= A_{21} \underline{V}_2 + A_{22} (-\underline{I}_2). \end{aligned} \quad (10.10)$$

where $A_{11(m \times m)}, \dots, A_{22(m \times m)}$ are quadratic m th order submatrices. These may be summarized in a supermatrix $A_{(n \times n)}$, given by

$$A = \begin{bmatrix} A_{11} & A_{12} \\ A_{21} & A_{22} \end{bmatrix}. \quad (10.11)$$

Summarizing the input quantities and the output quantities in n -dimensional vectors, we obtain

$$\begin{bmatrix} \underline{V}_1 \\ \underline{I}_1 \end{bmatrix} = A \begin{bmatrix} \underline{V}_2 \\ -\underline{I}_2 \end{bmatrix}. \quad (10.12)$$

The matrix A is called *chain matrix*. The chain representation is useful for the analysis of cascaded multiports. Figure 10.4 shows the cascading of two port-number symmetric

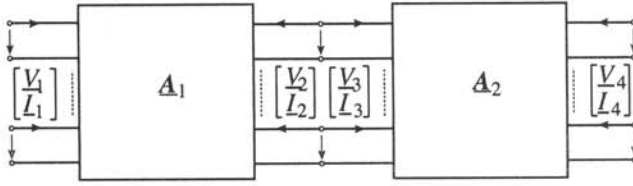


Figure 10.4: Cascading of two multiports.

multiports. The first multiport is described by the chain matrix A_1 , the second multiport by the chain matrix A_2 . The m output ports of the first multiport are connected with the m input ports of the second multiport. Both multiports are described in chain representation by

$$\begin{bmatrix} \frac{V_1}{I_1} \end{bmatrix} = A_1 \begin{bmatrix} \frac{V_2}{-I_2} \end{bmatrix}, \quad (10.13)$$

$$\begin{bmatrix} \frac{V_3}{I_3} \end{bmatrix} = A_2 \begin{bmatrix} \frac{V_4}{-I_4} \end{bmatrix}. \quad (10.14)$$

For appropriate numbering of the output ports of the first multiport and the input ports of the second multiport we obtain

$$\begin{bmatrix} \frac{V_2}{-I_2} \end{bmatrix} = \begin{bmatrix} \frac{V_3}{I_3} \end{bmatrix}. \quad (10.15)$$

From (10.13) to (10.15) it follows that

$$\begin{bmatrix} \frac{V_1}{I_1} \end{bmatrix} = A_1 A_2 \begin{bmatrix} \frac{V_4}{-I_4} \end{bmatrix}. \quad (10.16)$$

The chain matrix

$$A = A_1 A_2 \quad (10.17)$$

describes a multiport obtained by cascading of the multiports 1 and 2 in Figure 10.4. We obtain

$$\begin{bmatrix} \frac{V_1}{I_1} \end{bmatrix} = A \begin{bmatrix} \frac{V_4}{-I_4} \end{bmatrix}. \quad (10.18)$$

To convert the Z -representation into the A -representation we first write (10.5) in the form

$$\begin{aligned} V_1 &= Z_{11} I_1 + Z_{12} I_2, \\ V_2 &= Z_{21} I_1 + Z_{22} I_2, \end{aligned} \quad (10.19)$$

where $\underline{V}_1, \underline{I}_1$ are the input quantities and $\underline{V}_2, \underline{I}_2$ are the output quantities. The $\underline{Z}_{11} \dots \underline{Z}_{22}$ are the four m th order quadratic submatrices of the matrix \underline{Z} . To compute \underline{A}_{11} we set $\underline{I}_2 = 0$ in (10.10) and obtain

$$\underline{V}_1 = \underline{A}_{11} \underline{V}_2 \quad \text{for } \underline{I}_2 = 0 . \quad (10.20)$$

From (10.19) it follows that

$$\underline{V}_1 = \underline{Z}_{11} \underline{I}_1 = \underline{Z}_{11} \underline{Z}_{21}^{-1} \underline{V}_2 \quad \text{for } \underline{I}_2 = 0 . \quad (10.21)$$

From this we obtain

$$\underline{A}_{11} = \underline{Z}_{11} \underline{Z}_{21}^{-1} \quad \text{for } \underline{I}_2 = 0 . \quad (10.22)$$

For \underline{A}_{21} we obtain from (10.10)

$$\underline{I}_1 = \underline{A}_{21} \underline{V}_2 \quad \text{for } \underline{I}_2 = 0 . \quad (10.23)$$

In the same way we obtain for $\underline{I}_2 = 0$ the submatrix

$$\underline{A}_{21} = \underline{Z}_{21}^{-1} . \quad (10.24)$$

To determine \underline{A}_{12} and \underline{A}_{22} we set $\underline{V}_2 = 0$ and obtain from (10.10) and (10.19)

$$\underline{I}_1 = -\underline{Z}_{21}^{-1} \underline{Z}_{22} \underline{I}_2 \quad \text{for } \underline{V}_2 = 0 . \quad (10.25)$$

By comparison with (10.10) we obtain

$$\underline{A}_{22} = \underline{Z}_{21}^{-1} \underline{Z}_{22} . \quad (10.26)$$

From (10.19) it follows that

$$\underline{V}_1 = (-\underline{Z}_{11} \underline{Z}_{21}^{-1} \underline{Z}_{22} + \underline{Z}_{12}) \underline{I}_2 \quad (10.27)$$

and therewith under comparison with (10.10) we obtain

$$\underline{A}_{12} = -\underline{Z}_{12} + \underline{Z}_{11} \underline{Z}_{21}^{-1} \underline{Z}_{22} \quad \text{for } \underline{V}_2 = 0 . \quad (10.28)$$

With this we can express the \underline{A} matrix by the \underline{Z} matrix in the following form:

$$\underline{A} = \begin{bmatrix} \underline{Z}_{11} \underline{Z}_{21}^{-1} & -\underline{Z}_{12} + \underline{Z}_{11} \underline{Z}_{21}^{-1} \underline{Z}_{22} \\ \underline{Z}_{21}^{-1} & \underline{Z}_{21}^{-1} \underline{Z}_{22} \end{bmatrix} . \quad (10.29)$$

The so-called *inverse chain matrix* \mathbf{B} represents the output signals as a function of the input signals

$$\begin{bmatrix} \underline{V}_2 \\ \underline{I}_2 \end{bmatrix} = \mathbf{B} \begin{bmatrix} \underline{V}_1 \\ -\underline{I}_1 \end{bmatrix}. \quad (10.30)$$

For the cascading of two multiports according to Figure 10.4 we obtain

$$\mathbf{B} = \mathbf{B}_2 \mathbf{B}_1. \quad (10.31)$$

We consider that in spite of the name inverse chain matrix $\mathbf{B} \neq \mathbf{A}^{-1}$. Conversion formulae between the \mathbf{Y} -, \mathbf{Z} -, \mathbf{A} -, and \mathbf{B} -representation are given in Table 10.1.

10.2.3 The Scattering Matrix

The multiport according to Figure 10.2(b) is described by the wave amplitudes of the waves incident through the ports and scattered through the ports. The wave amplitudes \underline{a}_k and \underline{b}_k are related to the (generalized) voltages \underline{V}_k and (generalized) currents \underline{I}_k according to (8.40a) and (8.40b) via

$$\underline{a}_k = \frac{1}{2} \left(\frac{\underline{V}_k}{\sqrt{Z_{0k}}} + \sqrt{Z_{0k}} \underline{I}_k \right), \quad (10.32a)$$

$$\underline{b}_k = \frac{1}{2} \left(\frac{\underline{V}_k}{\sqrt{Z_{0k}}} - \sqrt{Z_{0k}} \underline{I}_k \right). \quad (10.32b)$$

We allow at various ports different kinds of waveguide types (e.g., a multiport may contain coaxial ports as well as waveguide ports). We also have to consider that the wave impedances of the transmission-lines of the various ports may be different. We summarize the wave amplitudes of the n incident waves $\underline{a}_1 \dots \underline{a}_n$ and the n scattered waves $\underline{b}_1 \dots \underline{b}_n$ in n -dimensional column vector

$$\underline{\mathbf{a}} = [\underline{a}_1, \underline{a}_2, \dots, \underline{a}_n]^T, \quad (10.33a)$$

$$\underline{\mathbf{b}} = [\underline{b}_1, \underline{b}_2, \dots, \underline{b}_n]^T. \quad (10.33b)$$

With the diagonal matrix \mathbf{g} summarizing the square roots of the characteristic impedances,

$$\mathbf{g} = \text{diag} \left[\sqrt{Z_{01}}, \sqrt{Z_{02}}, \dots, \sqrt{Z_{0n}} \right], \quad (10.34)$$

we can write (10.32a) and (10.32b) in matrix notation:

$$\underline{\mathbf{a}} = \frac{1}{2} (\mathbf{g}^{-1} \underline{\mathbf{V}} + \mathbf{g} \underline{\mathbf{I}}), \quad (10.35a)$$

$$\underline{\mathbf{b}} = \frac{1}{2} (\mathbf{g}^{-1} \underline{\mathbf{V}} - \mathbf{g} \underline{\mathbf{I}}). \quad (10.35b)$$

Table 10.1: Transformation of Signal Transmission Matrices

	Y	Z	A
Y	Y	Z^{-1}	$\begin{bmatrix} 0 & A_{12} \\ 1 & A_{22} \end{bmatrix}^{-1} \begin{bmatrix} -1 & A_{11} \\ 0 & A_{21} \end{bmatrix}$
Z	Y^{-1}	Z	$\begin{bmatrix} -1 & A_{11} \\ 0 & A_{21} \end{bmatrix}^{-1} \begin{bmatrix} 0 & A_{12} \\ 1 & A_{22} \end{bmatrix}$
A	$\begin{bmatrix} Y_{11} & -1 \\ -Y_{21} & 0 \end{bmatrix}^{-1} \begin{bmatrix} Y_{12} & 0 \\ -Y_{22} & -1 \end{bmatrix}$	$\begin{bmatrix} -1 & Z_{11} \\ 0 & Z_{21} \end{bmatrix}^{-1} \begin{bmatrix} 0 & Z_{12} \\ 1 & Z_{22} \end{bmatrix}$	A
B	$\begin{bmatrix} -Y_{12} & 0 \\ -Y_{22} & 1 \end{bmatrix}^{-1} \begin{bmatrix} Y_{11} & 1 \\ Y_{21} & -0 \end{bmatrix}$	$\begin{bmatrix} 0 & Z_{12} \\ -1 & Z_{22} \end{bmatrix}^{-1} \begin{bmatrix} 1 & Z_{11} \\ 0 & Z_{21} \end{bmatrix}$	$\begin{bmatrix} A_{11} & -A_{12} \\ A_{21} & -A_{22} \end{bmatrix}^{-1} \begin{bmatrix} 1 & 0 \\ 0 & -1 \end{bmatrix}$
S	$\begin{bmatrix} g^{-1} + Yg \end{bmatrix}^{-1} \begin{bmatrix} g^{-1} - Yg \end{bmatrix}$	$\begin{bmatrix} Zg^{-1} + g \end{bmatrix}^{-1} \begin{bmatrix} Zg^{-1} - g \end{bmatrix}$	$-\begin{bmatrix} g_1 & -A_{11}g_2 - A_{12}g_2^{-1} \\ -g_1^{-1} & -A_{21}g_2 - A_{22}g_2^{-1} \end{bmatrix}^{-1} \begin{bmatrix} g_1 & -A_{11}g_2 + A_{12}g_2^{-1} \\ g_1^{-1} & -A_{21}g_2 + A_{22}g_2^{-1} \end{bmatrix}$
T	$\begin{bmatrix} Y_{11}g_1 + g_1^{-1} & Y_{11}g_1 - g_1^{-1} \\ Y_{21}g_1 & Y_{21}g_1 \end{bmatrix}^{-1} \begin{bmatrix} -Y_{12}g_2 & -Y_{12}g_2 \\ -Y_{22}g_2 + g_2^{-1} & -Y_{22}g_2 - g_2^{-1} \end{bmatrix}$	$-\begin{bmatrix} Z_{11}g_1^{-1} + g_1 & -Z_{11}g_1^{-1} + g_1 \\ Z_{21}g_1^{-1} & -Z_{21}g_1^{-1} \end{bmatrix}^{-1} \begin{bmatrix} -Z_{12}g_2^{-1} & Z_{12}g_2^{-1} \\ -Z_{22}g_2^{-1} + g_2 & Z_{22}g_2^{-1} + g_2 \end{bmatrix}$	$-\begin{bmatrix} g_1 & g_1 \\ -g_1^{-1} & g_1^{-1} \end{bmatrix}^{-1} \begin{bmatrix} -A_{11}g_2 + A_{12}g_2^{-1} & -A_{11}g_2 - A_{12}g_2^{-1} \\ -A_{21}g_2 + A_{22}g_2^{-1} & -A_{21}g_2 - A_{22}g_2^{-1} \end{bmatrix}$

If all ports exhibit the same characteristic impedance Z_0 , we obtain

$$g = \sqrt{Z_0} \mathbf{1}. \quad (10.36)$$

Table 10.2: Continued: Transformation of Signal Transmission Matrices

B	S	T
$\begin{bmatrix} B_{12} & 0 \\ B_{22} & 1 \end{bmatrix}^{-1} \begin{bmatrix} B_{11} & -1 \\ B_{21} & 0 \end{bmatrix}$	$\begin{bmatrix} g+Sg \end{bmatrix}^{-1} \begin{bmatrix} g^{-1}-Sg^{-1} \end{bmatrix}$	$\begin{bmatrix} g_1 & (T_{11}-T_{12})g_2 \\ -g_1 & (T_{21}-T_{22})g_2 \end{bmatrix}^{-1} \begin{bmatrix} g_1^{-1} & -(T_{11}+T_{12})g_2^{-1} \\ g_1^{-1} & -(T_{21}+T_{22})g_2^{-1} \end{bmatrix}$
$\begin{bmatrix} B_{11} & -1 \\ B_{21} & 0 \end{bmatrix}^{-1} \begin{bmatrix} B_{12} & 0 \\ B_{22} & -1 \end{bmatrix}$	$\begin{bmatrix} g^{-1}-Sg^{-1} \end{bmatrix}^{-1} \begin{bmatrix} g+Sg \end{bmatrix}$	$-\begin{bmatrix} g_1^{-1} & -(T_{11}+T_{12})g_2^{-1} \\ g_1^{-1} & -(T_{21}+T_{22})g_2^{-1} \end{bmatrix}^{-1} \begin{bmatrix} -g_1 & (-T_{11}+T_{12})g_2 \\ g_1 & (-T_{21}+T_{22})g_2 \end{bmatrix}$
$\begin{bmatrix} B_{11} & -B_{12} \\ B_{21} & -B_{22} \end{bmatrix}^{-1} \begin{bmatrix} 1 & 0 \\ 0 & -1 \end{bmatrix}$	$-\begin{bmatrix} (1-S_{11})g_1^{-1} & -(1+S_{11})g_1 \\ -S_{21}g_1 & -S_{21}g_1 \end{bmatrix}^{-1} \begin{bmatrix} -S_{12}g_2^{-1} & S_{12}g_2 \\ (1-S_{22})g_2^{-1} & (1+S_{22})g_2 \end{bmatrix}$	$-\begin{bmatrix} g_1^{-1} & -g_1 \\ g_1^{-1} & g_1 \end{bmatrix}^{-1} \begin{bmatrix} -(T_{11}+T_{12})g_2^{-1} & (T_{11}-T_{12})g_2 \\ -(T_{21}+T_{22})g_2^{-1} & (T_{21}-T_{22})g_2 \end{bmatrix}$
B	$-\begin{bmatrix} -S_{12}g_2^{-1} & -S_{12}g_2 \\ (1-S_{22})g_2^{-1} & -(1+S_{22})g_2 \end{bmatrix}^{-1} \begin{bmatrix} (1-S_{11})g_1^{-1} & (1+S_{11})g_1 \\ -S_{21}g_1^{-1} & S_{21}g_1 \end{bmatrix}$	$\begin{bmatrix} (T_{11}+T_{12})g_2^{-1} & (T_{11}-T_{12})g_2 \\ (T_{21}+T_{22})g_2^{-1} & (T_{21}-T_{22})g_2 \end{bmatrix}^{-1} \begin{bmatrix} g_1^{-1} & g_1 \\ g_1^{-1} & -g_1 \end{bmatrix}$
$\begin{bmatrix} -B_{11}g_1-B_{12}g_1^{-1} & g_2 \\ -B_{21}g_1-B_{22}g_1^{-1} & -g_2^{-1} \end{bmatrix}^{-1} \begin{bmatrix} -B_{11}g_1+B_{12}g_1^{-1} & g_2 \\ -B_{21}g_1+B_{22}g_1^{-1} & g_2^{-1} \end{bmatrix}$	S	$\begin{bmatrix} -1 & T_{12} \\ 0 & T_{22} \end{bmatrix}^{-1} \begin{bmatrix} 0 & T_{11} \\ 1 & T_{21} \end{bmatrix}$
$\begin{bmatrix} B_{11}g_1+B_{12}g_1^{-1} & B_{11}g_1-B_{12}g_1^{-1} \\ B_{21}g_1+B_{22}g_1^{-1} & -B_{21}g_1-B_{22}g_1^{-1} \end{bmatrix}^{-1} \begin{bmatrix} g_2 & g_2 \\ g_2^{-1} & -g_2^{-1} \end{bmatrix}$	$\begin{bmatrix} -1 & S_{11} \\ 0 & S_{21} \end{bmatrix}^{-1} \begin{bmatrix} -S_{12} & 0 \\ -S_{22} & 1 \end{bmatrix}$	T

Multiplying (10.35a) and (10.35b) from the left with g and g^{-1} , respectively, and forming the sum and the difference, we obtain in analogy to (8.42a) and (8.42b)

$$\underline{V} = g(\underline{a} + \underline{b}), \quad (10.37a)$$

$$\underline{I} = g^{-1}(\underline{a} - \underline{b}). \quad (10.37b)$$

The linear system of equations

$$\underline{b} = \underline{S} \underline{a} \quad (10.38)$$

gives the dependence of \underline{b} on \underline{a} . The matrix \underline{S} is called the \underline{S} matrix or *scattering matrix*. The representation of a multiport by the scattering matrix is the *scattering representation*. This name originates from the picture that the waves incident into the multiport leave the multiport as scattered waves through the ports.

Conversion formulae between the \underline{Y} , \underline{Z} , and \underline{S} representations are given in Table 10.1. We show how the scattering matrix may be represented in terms of the impedance matrix. To do this we insert (10.37a) and (10.37b) into (10.5) and obtain

$$\underline{g} (\underline{a} + \underline{b}) = \underline{Z} \underline{g}^{-1} (\underline{a} - \underline{b}). \quad (10.39)$$

Multiplying this equation from the left with \underline{g}^{-1} we obtain

$$(\underline{g}^{-1} \underline{Z} \underline{g}^{-1} + \underline{1}) \underline{b} = (\underline{g}^{-1} \underline{Z} \underline{g}^{-1} - \underline{1}) \underline{a}. \quad (10.40)$$

Multiplying from the left with the inverse of the bracketed expression on the right we obtain

$$\underline{b} = (\underline{g}^{-1} \underline{Z} \underline{g}^{-1} + \underline{1})^{-1} (\underline{g}^{-1} \underline{Z} \underline{g}^{-1} - \underline{1}) \underline{a}. \quad (10.41)$$

Comparing this with (10.38) yields the representation of the scattering matrix via the \underline{Z} matrix

$$\underline{S} = (\underline{g}^{-1} \underline{Z} \underline{g}^{-1} + \underline{1})^{-1} (\underline{g}^{-1} \underline{Z} \underline{g}^{-1} - \underline{1}). \quad (10.42)$$

We note that the bracketed expressions in (10.42) may be interchanged. The proof for this is as follows: The matrix $\underline{1}$ may be interchanged with every matrix, and therefore also with $\underline{g}^{-1} \underline{Z} \underline{g}^{-1}$. If two matrices may be interchanged, the sum of both matrices may also be interchanged with the difference of both matrices. Furthermore, the two matrices \underline{A} and \underline{B}^{-1} may be interchanged, if \underline{A} and \underline{B} are interchangeable. This may be demonstrated by multiplying the equation $\underline{A} \underline{B} = \underline{B} \underline{A}$ on both sides from the left and from the right with \underline{B}^{-1} .

We now consider the connection of two multiports according to Figure 10.5. The first multiport has a port number n_1 ; the second multiport has a port number $n_2 < n_1$. Every port of the second multiport is connected with a port of the first multiport. Therefore at the first multiport

$$n = n_1 - n_2 \quad (10.43)$$

ports remain unconnected. We number the ports of the first multiport such that the ports remaining unconnected have the numbers 1 to n . The multiports 1 and 2 are described by the scattering matrices $\underline{S}^{(1)}$ and $\underline{S}^{(2)}$. We summarize the wave amplitudes of the ports 1 to n of the first multiport in the vectors \underline{a}_1 and \underline{b}_1 . The wave amplitudes of ports $n+1$ to n_1 are summarized in the column vectors \underline{a}_2 and \underline{b}_2 . The waves incident

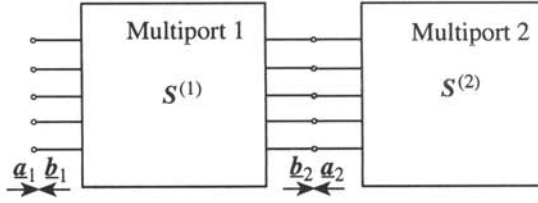


Figure 10.5: Connection of two multiports.

into the second multiport are summarized in \underline{b}_2 ; the waves flowing out from the ports of the second multiport are described by \underline{a}_2 . We assume that the connected ports of both multiports are of the same type. The circuit equations of both multiports are

$$\begin{bmatrix} \underline{b}_1 \\ \underline{b}_2 \end{bmatrix} = S^{(1)} \begin{bmatrix} \underline{a}_1 \\ \underline{a}_2 \end{bmatrix}, \quad (10.44a)$$

$$\underline{a}_2 = S^{(2)} \underline{b}_2. \quad (10.44b)$$

Subdividing the scattering matrix of the first multiport into submatrices S_{11} , S_{12} , S_{21} and S_{22} , we obtain from (10.44a)

$$\underline{b}_1 = S_{11}^{(1)} \underline{a}_1 + S_{12}^{(1)} \underline{a}_2, \quad (10.45a)$$

$$\underline{b}_2 = S_{21}^{(1)} \underline{a}_1 + S_{22}^{(1)} \underline{a}_2. \quad (10.45b)$$

Inserting (10.45b) into (10.44b) yields

$$\underline{a}_2 = S^{(2)} S_{21}^{(1)} \underline{a}_1 + S^{(2)} S_{22}^{(1)} \underline{a}_2. \quad (10.46)$$

We bring this expression into the following form:

$$\underline{a}_2 = (1 - S^{(2)} S_{22}^{(1)})^{-1} S^{(2)} S_{21}^{(1)} \underline{a}_1. \quad (10.47)$$

After inserting into (10.45a), we obtain

$$\underline{b}_1 = \left[S_{11}^{(1)} + S_{12}^{(1)} (1 - S^{(2)} S_{22}^{(1)})^{-1} S^{(2)} S_{21}^{(1)} \right] \underline{a}_1. \quad (10.48)$$

For the scattering matrix $S_{<n \times n>}$, which relates incident and scattered waves of the first n ports of the first multiport according to

$$\underline{b}_1 = S_{<n \times n>} \underline{a}_1 \quad (10.49)$$

we obtain

$$S = S_{11}^{(1)} + S_{12}^{(1)} (1 - S^{(2)} S_{22}^{(1)})^{-1} S^{(2)} S_{21}^{(1)}. \quad (10.50)$$

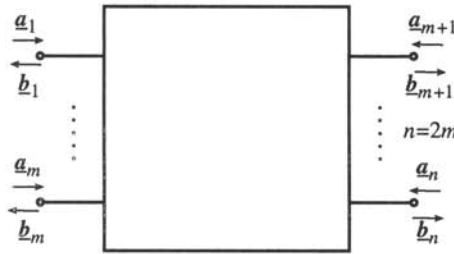


Figure 10.6: Portnumber symmetric multiport.

10.2.4 The Transmission Matrix

The *transmission matrix* may be defined for port-number symmetric multiports according to Figure 10.6. It represents the incident and scattered wave amplitudes of the input ports in dependence from the incident and scattered wave amplitudes of the output ports. This representation of a multiport is called the *transmission representation*,

$$\begin{bmatrix} \underline{b}_1 \\ \underline{a}_1 \end{bmatrix} = T \begin{bmatrix} \underline{a}_2 \\ \underline{b}_2 \end{bmatrix}. \quad (10.51)$$

The transmission matrix for the wave amplitudes therefore corresponds to the chain matrix for (generalized) voltages and (generalized) currents. In the column vectors \underline{a}_1 and \underline{b}_1 , the wave amplitudes of the m input ports and in the vectors \underline{a}_2 and \underline{b}_2 the wave amplitudes of the m output ports are summarized. The total number of ports is $n = 2m$. The transmission matrix allows one to compute easily the cascading of two port-number symmetric multiports. For two cascaded multiports according to Figure 10.7 we obtain

$$\begin{bmatrix} \underline{b}_1 \\ \underline{a}_1 \end{bmatrix} = T^{(1)} \begin{bmatrix} \underline{a}_2 \\ \underline{b}_2 \end{bmatrix}, \quad (10.52)$$

$$\begin{bmatrix} \underline{b}_3 \\ \underline{a}_3 \end{bmatrix} = T^{(2)} \begin{bmatrix} \underline{a}_4 \\ \underline{b}_4 \end{bmatrix}, \quad (10.53)$$

where $T^{(1)}$ and $T^{(2)}$ are the transmission matrices of the multiports 1 and 2. By appropriately numbering the output ports of the first multiport and the input ports of the second multiport we obtain

$$\begin{bmatrix} \underline{a}_2 \\ \underline{b}_2 \end{bmatrix} = \begin{bmatrix} \underline{b}_3 \\ \underline{a}_3 \end{bmatrix}. \quad (10.54)$$

From (10.52) to (10.54) it follows that

$$\begin{bmatrix} \underline{b}_1 \\ \underline{a}_1 \end{bmatrix} = T \begin{bmatrix} \underline{a}_4 \\ \underline{b}_4 \end{bmatrix}, \quad (10.55)$$

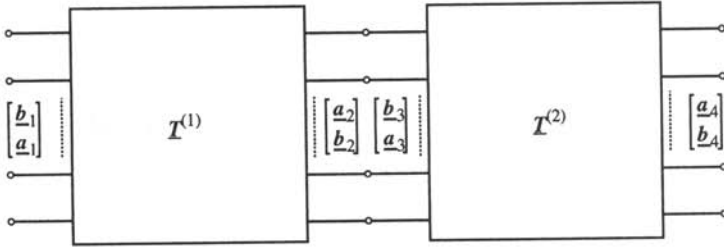


Figure 10.7: Cascading of two multiports.

where the transmission matrix T of the multiport obtained by cascading multiport 1 and multiport 2 is given by

$$T = T^{(1)} T^{(2)}. \quad (10.56)$$

The transformation between the scattering representation and the transmission representation is performed by the formulae summarized in Table 10.1.

10.3 TELLEGEN'S THEOREM

We have already discussed the field form (4.45) of *Tellegen's theorem* in Section 4.2. Tellegen's theorem states fundamental relations between voltages and currents in a circuit. It is only based on topological relationships and is independent from the constitutive laws of the network [6–9]. In network theory Tellegen's theorem gives a fundamental relation between voltages and currents in the connection network of a circuit. The connection network consists only of connections and ideal transformers. Stressing the analogy between an electromagnetic structure and an electric network, we can partition an electromagnetic structure by separating surfaces into substructures. These substructures can be set in analogy to the circuit elements of an electric network and the set of separating surfaces plays the role of the connection network.

To derive the *network form of Tellegen's theorem* from field form (4.45) of Tellegen's theorem we consider the set V_B of all boundary surfaces of the electromagnetic structure. The set of boundary surfaces is of zero volume. In the integral we can substitute the fields by the transverse field components since the normal field components give no contribution,

$$\oint_{\partial V_B} \mathcal{E}'_{tr}(\mathbf{x}, t') \wedge \mathcal{H}''_{tr}(\mathbf{x}, t'') = 0, \quad (10.57)$$

where $\mathcal{E}_{tr}(\mathbf{x}, t)$ and $\mathcal{H}_{tr}(\mathbf{x}, t)$ are field forms representing the transverse electric and magnetic field components (i.e., the field components tangential to the boundary surfaces). Each surface of V_B has two sides and the integral over the boundary ∂V_B is

performed over both sides of every boundary surface. We mark each side of every part of the set of boundary surfaces by α or β .

We now expand the fields \mathcal{E}_{tr} and \mathcal{H}_{tr} at the boundary surfaces into a *biorthonormal set of basis forms* e_m^ξ and h_m^ξ as introduced in (7.197a), (7.197b) and (C.174) with $\xi = \alpha, \beta$, where α and β denote the side of the boundary surface. If we choose structure forms as (7.197a) and (7.197b) as the basis forms, these forms are already solutions of Maxwell's equations and we have only to satisfy the boundary conditions. Since the field functions in time domain are real we have to choose a real basis of structure forms. The numbers of structure forms are N_α on side α and N_β on side β . The expansion coefficients are the generalized voltages V_m^ξ and the generalized currents I_m^ξ . Inserting (8.9a) and (8.9b) we obtain

$$\mathcal{E}_{\text{tr}}^\xi = \sum_m^{N_\xi} V_m^\xi e_m^\xi, \quad (10.58a)$$

$$\mathcal{H}_{\text{tr}}^\xi = \sum_m^{N_\xi} I_m^\xi h_m^\xi. \quad (10.58b)$$

Inserting this expansions into (10.57) yields

$$\begin{aligned} \oint_{\partial V_B} \mathcal{E}'(\mathbf{x}, t') \wedge \mathcal{H}''(\mathbf{x}, t'') &= \sum_n^{N_\alpha} \sum_m^{N_\alpha} V_m^{\alpha'}(t') I_n^{\alpha''}(t'') \oint_{\partial V_B} e_m^\alpha \wedge h_n^\alpha \\ &+ \sum_n^{N_\beta} \sum_m^{N_\beta} V_m^{\beta'}(t') I_n^{\beta''}(t'') \oint_{\partial V_B} e_m^\beta \wedge h_n^\beta = 0. \end{aligned} \quad (10.59)$$

We assume *biorthonormal structure forms* as introduced in (7.197a) and (7.197b), however, for the expansion of time-domain field forms we require the structure forms to be real. As in (7.206) the structure forms are *biorthogonal*,

$$\oint_{\partial V_B} e_m^\xi \wedge h_n^\xi = \delta_{mn} \quad (10.60)$$

and obtain

$$\sum_n^{N_\alpha} V_n^{\alpha'}(t') I_n^{\alpha''}(t'') + \sum_n^{N_\beta} V_n^{\beta'}(t') I_n^{\beta''}(t'') = 0. \quad (10.61)$$

We summarize all voltages and currents in the vectors

$$\mathbf{V}(t) = \left[V_1^\alpha(t), \dots, V_{N_\alpha}^\alpha(t), V_1^\beta(t), \dots, V_{N_\beta}^\beta(t) \right]^T, \quad (10.62a)$$

$$\mathbf{I}(t) = \left[I_1^\alpha(t), \dots, I_{N_\alpha}^\alpha(t), I_1^\beta(t), \dots, I_{N_\beta}^\beta(t) \right]^T \quad (10.62b)$$

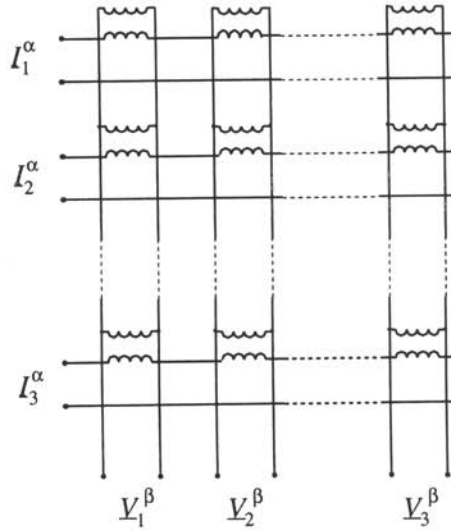


Figure 10.8: Canonical form of the connection network.

and obtain the *general network form of Tellegen's theorem* [6–8, 10]

$$\mathbf{V}'^T(t') \mathbf{I}''(t'') = 0, \quad (10.63)$$

where $\mathbf{V}(t)$ and $\mathbf{I}(t)$ denote the voltage and current vectors of the connection circuit. The prime ' and double prime '' again denote different circuit elements and different times in both cases. It is only required that the topological structure of the connection circuit remains unchanged.

Taking (10.63) and

$$\mathbf{I}'^T(t') \mathbf{V}''(t'') = 0, \quad (10.64)$$

which follows directly from (10.63) by interchanging the primed with the double primed variables and considering the symmetry of the inner product and inserting (10.37a) and (10.37b) in both equations we obtain, after forming the sum and the difference of the resulting equations, *Tellegen's Theorem in wave amplitude representation* [11, 12]

$$\mathbf{a}'^T(t') \mathbf{b}''(t'') = \mathbf{b}'^T(t') \mathbf{a}''(t''), \quad (10.65a)$$

$$\mathbf{a}'^T(t') \mathbf{a}''(t'') = \mathbf{b}'^T(t') \mathbf{b}''(t''). \quad (10.65b)$$

In a *network representation* of a circuit the *connection circuit* contains all connections but no energy storing or dissipating circuit elements [5]. Ideal transformers may be

considered as parts of the connection circuit and not as circuit elements. Expanding the tangential electric and magnetic fields on the boundaries again into basis functions allows us to give an equivalent circuit representation for the boundary surfaces. The equivalent circuit of the boundary surfaces is a connection circuit exhibiting only connections and ideal transformers.

Consistent choices of independent and dependent fields do not violate Tellegen's theorem and allow to draw canonical networks, which are based only on connections and ideal transformers. Figure 10.8 shows the canonical form of the connection network when using as independent fields the vectors \mathbf{V}^β (dimension N_β) and \mathbf{I}^α (dimension N_α). In this case the dependent fields are \mathbf{V}^α (dimension N_α) and \mathbf{I}^β (dimension N_β). In all cases we have $N_\beta + N_\alpha$ independent quantities and the same number of dependent quantities. Note that scattering representations are also allowed and that the connection network is frequency-independent. It is apparent from the canonical network representations that the scattering matrix is symmetric (i.e., $\mathbf{S}^T = \mathbf{S}$), orthogonal, (i.e., $\mathbf{S}^T \mathbf{S} = \mathbf{I}$) and unitary (i.e., $\mathbf{S} \mathbf{S}^\dagger = \mathbf{I}$). The † denotes the hermitian conjugate matrix.

10.3.1 Connection Networks

We now consider the fields as expanded on finite orthonormal basis function sets; the assumption of orthonormal basis is not necessary, and is introduced to simplify the notation. We consider a set of expansion functions of dimension N_α on side α and a basis of dimension N_β on side β .

Subject to the above assumption, we may write the transverse field expansions as

$$\tilde{\mathcal{E}}_t^\alpha = \sum_n^{N_\alpha} V_n^\alpha e_n^\alpha(\mathbf{x}), \quad \tilde{\mathcal{E}}_t^\beta = \sum_m^{N_\beta} V_m^\beta e_m^\beta(\mathbf{x}), \quad (10.66)$$

$$\tilde{\mathcal{H}}_t^\alpha = \sum_n^{N_\alpha} I_n^\alpha h_n^\alpha(\mathbf{x}), \quad \tilde{\mathcal{H}}_t^\beta = \sum_m^{N_\beta} I_m^\beta h_m^\beta(\mathbf{x}) \quad (10.67)$$

where we have used the tilde, as in [13], in order to denote fields expressed by finite expansions. The vector fields $e_n^\xi(\mathbf{x})$ and $h_n^\xi(\mathbf{x})$, $\xi = \alpha, \beta$, are the selected basis functions for electric and magnetic fields. Moreover, V_n^ξ and I_n^ξ , $\xi = \alpha, \beta$, denote the field amplitudes of the electric and magnetic fields, respectively. They are conveniently grouped into the following arrays for the expansion coefficients of the electric field, which are *generalized voltages*,

$$\underline{\mathbf{V}}^\alpha = [V_1^\alpha \quad V_2^\alpha \quad \dots \quad V_{N_\alpha}^\alpha]^T, \quad \underline{\mathbf{V}}^\beta = [V_1^\beta \quad V_2^\beta \quad \dots \quad V_{N_\beta}^\beta]^T \quad (10.68)$$

and the expansion coefficients of the magnetic fields, which are *generalized currents*,

$$\underline{I}^\alpha = [I_1^\alpha \quad I_2^\alpha \quad \dots \quad I_{N_\alpha}^\alpha]^T, \quad \underline{I}^\beta = [I_1^\beta \quad I_2^\beta \quad \dots \quad I_{N_\beta}^\beta]^T, \quad (10.69)$$

leading compactly to

$$\underline{V} = \begin{bmatrix} \underline{V}^\alpha \\ \underline{V}^\beta \end{bmatrix}, \quad \underline{I} = \begin{bmatrix} \underline{I}^\alpha \\ \underline{I}^\beta \end{bmatrix}. \quad (10.70)$$

10.3.2 Tellegen's Theorem for Discretized Fields

We start by expanding the fields in (10.57) into basis functions:

$$\begin{aligned} \oint_{\partial V_B} \mathcal{E}'(\mathbf{x}, t') \wedge \mathcal{H}''(\mathbf{x}, t'') &= \sum_n^{N_\alpha} \sum_m^{N_\alpha} V_m^{\alpha'}(t') I_n^{\alpha''}(t'') \oint_{\partial \mathcal{R}} e_m^\alpha \wedge h_n^\alpha \\ &\quad + \sum_n^{N_\beta} \sum_m^{N_\beta} V_m^{\beta'}(t') I_n^{\beta''}(t'') \oint_{\partial \mathcal{R}} e_m^\beta \wedge h_n^\beta. \end{aligned} \quad (10.71)$$

By introducing the matrix Λ with elements

$$\Lambda_{mn}^\xi = \oint_{\partial \mathcal{R}} e_m^\xi \wedge h_n^\xi, \quad (10.72)$$

with ξ standing either for α or β , the general form of Tellegen's theorem is

$$\underline{V}'^T(t') \Lambda \underline{I}''(t'') = 0. \quad (10.73)$$

In general it is convenient to consider orthogonal electric and magnetic field expansions; when this is not the case a suitable orthogonalization process can be carried out providing an orthogonalized basis. In that case Tellegen's theorem takes the standard form

$$\underline{V}'^T(t') \underline{I}''(t'') = 0 \quad (10.74)$$

where $\underline{V}(t)$ and $\underline{I}(t)$ denote the voltage and current vectors of the connection circuit. The prime ' and double prime '' again denote different circuit elements and different times in both cases. It is only required that the topological structure of the connection circuit remains unchanged.

10.4 THE POWER PROPERTIES

The total active power P flowing into a multiport is equal to the sum of the active power flowing into every port. We obtain from (8.46)

$$P = \sum_{i=1}^n |\underline{a}_i|^2 - |\underline{b}_i|^2 = \underline{\mathbf{a}}^\dagger \underline{\mathbf{a}} - \underline{\mathbf{b}}^\dagger \underline{\mathbf{b}}. \quad (10.75)$$

The superscript † denotes the *Hermitian conjugate* of a vector or matrix, respectively, as defined in (C.38). The term $\underline{\mathbf{a}}^\dagger \underline{\mathbf{a}}$ represents the power carried by the waves incident into the multiport and $\underline{\mathbf{b}}^\dagger \underline{\mathbf{b}}$ is the power carried by the waves scattered from the multiport. The difference is the power P absorbed in the multiport. Inserting (10.38) and its Hermitian conjugate

$$\underline{\mathbf{b}}^\dagger = \underline{\mathbf{a}}^\dagger \mathbf{S}^\dagger \quad (10.76)$$

we can represent this equation by

$$P = \underline{\mathbf{a}}^\dagger (\mathbf{1} - \mathbf{S}^\dagger \mathbf{S}) \underline{\mathbf{a}}. \quad (10.77)$$

For a *passive multiport* for an arbitrary choice of the incident waves $\underline{\mathbf{a}}$ $P \geq 0$ must always be valid, i.e., the right-hand side of (10.77) must be a *positive semidefinite Hermitian form* in $\underline{\mathbf{a}}$. This is fulfilled if and only if

$$\det_k (\mathbf{1} - \mathbf{S}^\dagger \mathbf{S}) \geq 0 \quad \text{for } k = 1 \dots n \quad (10.78)$$

is valid, where the symbol \det_k denotes the *leading principal minor* of order k of a matrix as defined in (C.53).

If the multiport is *lossless*, the total absorbed active power is $P = 0$. A lossless multiport is called a *reactance multiport*. With (10.77) we obtain

$$\mathbf{S}^\dagger = \mathbf{S}^{-1} \quad \text{for lossless multiports.} \quad (10.79)$$

A matrix fulfilling (10.79) is called *unitary*. The scattering matrix describing a *lossless multiport* is unitary. In impedance and admittance representation we obtain from (10.42) and (10.79) for *reactance multiports*

$$\mathbf{Z}(\omega) + \mathbf{Z}^\dagger(\omega) = \mathbf{0}, \quad \mathbf{Y}(\omega) + \mathbf{Y}^\dagger(\omega) = \mathbf{0}. \quad (10.80)$$

A *lossless one-port* is called a *reactance one-port*. It has the property

$$\Re\{Z(\omega)\} = 0, \quad \Re\{Y(\omega)\} = 0, \quad |\rho(\omega)| = 1. \quad (10.81)$$

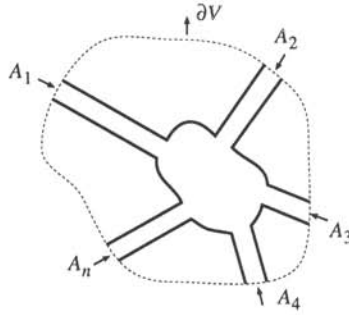


Figure 10.9: Embedding of a multiport into the domain of integration V .

10.5 RECIPROCAL MULTIPORTS

We already have treated reciprocity in Section 4.7 from a field point of view. We now derive the reciprocity theorem for source-free multiports. To do this we consider the multiport depicted schematically in Figure 10.9 and apply the integral form of the Lorentz reciprocity theorem to this structure.

The planes of reference of the m ports are part of the boundary ∂V of the volume V . From (8.9a) and (8.9b) we obtain the transverse components of the field quantities in the plane of reference of the k th port, ($k = 1 \dots n$):

$$\underline{\mathcal{E}}_{tr,k}^{(i)} = \underline{V}_k^{(i)} \underline{e}_k, \quad (10.82)$$

$$\underline{\mathcal{H}}_{tr,k}^{(i)} = \underline{I}_k^{(i)} \underline{h}_k. \quad (10.83)$$

The index i refers to the excitation of field by the i th group, ($i = 1 \dots n$), of impressed field sources where the impressed field sources all are located outside the volume V and may be represented by sources connected to the ports of the multiport. The voltages $\underline{V}_k^{(i)}$ and the currents $\underline{I}_k^{(i)}$ are the (generalized) port voltages and (generalized) port currents of the k th port in the case of excitation of the i th group of sources. The one-forms \underline{e}_k and \underline{h}_k are the normalized structure forms according to (8.8a) and (8.8b).

We compute the area integral of $\underline{\mathcal{E}}_i \wedge \underline{\mathcal{H}}_j$ over the boundary ∂V . Since an electromagnetic field only occurs inside the waveguides, the integral only needs to be performed over the cross-sectional areas $A_1 \dots A_n$ of the n waveguides. Since $A_1 \dots A_n$ are transverse cross-sectional areas, only the transverse field components in the waveguide cross-section give contributions to the area integral. We follow the usual conventions that the orientation of the boundary surface ∂V of the volume V is outwards whereas the cross-sectional areas of the waveguides are oriented inwards. Therefore the integrals

over ∂V and over all A_i have opposite sign. With (10.82) and (10.83) we obtain

$$\oint_{\partial V} \underline{\mathcal{E}}_i \wedge \underline{\mathcal{H}}_j = - \sum_{k=1}^n \int_{A_k} \underline{\mathcal{E}}_{tr,k}^{(i)} \wedge \underline{\mathcal{H}}_{tr,k}^{(i)} = - \sum_{k=1}^n \underline{V}_k^{(i)} \underline{I}_k^{(j)} \int_{A_k} \mathbf{e}_k \wedge \mathbf{h}_k. \quad (10.84)$$

From (8.24a) it follows that

$$\int_{A_k} \mathbf{e}_k \wedge \mathbf{h}_k = 1 \quad (10.85)$$

and therewith

$$\oint_{\partial V} \underline{\mathcal{E}}_i \wedge \underline{\mathcal{H}}_j = - \sum_{k=1}^n \underline{V}_k^{(i)} \underline{I}_k^{(j)}. \quad (10.86)$$

Inserting (10.86) into (4.62), we obtain

$$\sum_{k=1}^n \underline{V}_k^{(i)} \underline{I}_k^{(j)} = \sum_{k=1}^n \underline{V}_k^{(j)} \underline{I}_k^{(i)}. \quad (10.87)$$

We summarize the $\underline{V}_k^{(i)}$ and $\underline{I}_k^{(i)}$ into the n -dimensional column vectors $\underline{V}^{(i)}$ and $\underline{I}^{(i)}$. With the transposed vectors $\underline{V}^{T(i)}$ and $\underline{I}^{T(i)}$, we obtain according to

$$\mathbf{a}^T \mathbf{b} = a_1 b_1 + a_2 b_2 + \dots + a_n b_n \quad (10.88)$$

from (10.87)

$$\underline{V}^{T(i)} \underline{I}^{(j)} = \underline{I}^{T(i)} \underline{V}^{(j)}. \quad (10.89)$$

With (10.5) and the transposed equation

$$\underline{V}^T = \underline{I}^T \mathbf{Z}^T \quad (10.90)$$

we obtain

$$\underline{I}^{T(i)} \mathbf{Z}^T \underline{I}^{(j)} = \underline{I}^{T(i)} \mathbf{Z} \underline{I}^{(j)}. \quad (10.91)$$

This equation is valid for connection of arbitrary groups of external sources i and j . This is only possible for

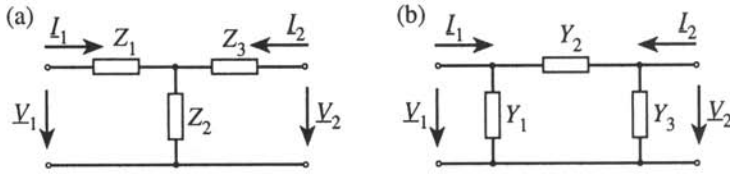
$$\mathbf{Z} = \mathbf{Z}^T. \quad (10.92)$$

For a *reciprocal multiport* the \mathbf{Z} matrix is symmetric. In component notation this means $Z_{ik} = Z_{ki}$. With (10.8) it follows that

$$\mathbf{Y} = \mathbf{Y}^T. \quad (10.93)$$

The \mathbf{A} matrix of a reciprocal multiport fulfills

$$\mathbf{A}_{11} \mathbf{A}_{22} - \mathbf{A}_{12} \mathbf{A}_{21} = \mathbf{1}. \quad (10.94)$$

Figure 10.10: Reciprocal two-ports: (a) T-circuit, and (b) π -circuit.

From this we obtain for reciprocal multiports

$$\det \mathbf{A} = 1. \quad (10.95)$$

Inserting (10.92) into (10.42) and considering that the bracketed expressions in (10.42) are commuting and that $\mathbf{g} = \mathbf{g}^T$ we obtain

$$\mathbf{S} = \mathbf{S}^T. \quad (10.96)$$

10.6 ELEMENTARY TWO-PORTS

In the following we discuss some important elementary two-ports. We confine the treatment of this topic to the basics required for the modeling of passive microwave circuits and sources. From (10.92), (10.93), and (10.94) we obtain for a *reciprocal two-port*

$$Z_{12} = Z_{21}, \quad Y_{12} = Y_{21}, \quad A_{11}A_{22} - A_{12}A_{21} = 1. \quad (10.97)$$

A reciprocal two-port can be represented by the *T*-equivalent circuit shown in Figure 10.10(a) or the π -equivalent circuit shown in Figure 10.10(b). The impedance and admittance matrices for these equivalent circuits are given by

$$\begin{bmatrix} V_1 \\ V_2 \end{bmatrix} = \begin{bmatrix} Z_1 + Z_2 & Z_2 \\ Z_2 & Z_3 + Z_2 \end{bmatrix} \begin{bmatrix} I_1 \\ I_2 \end{bmatrix}, \quad (10.98a)$$

$$\begin{bmatrix} I_1 \\ I_2 \end{bmatrix} = \begin{bmatrix} Y_1 + Y_2 & -Y_2 \\ -Y_2 & Y_3 + Y_2 \end{bmatrix} \begin{bmatrix} V_1 \\ V_2 \end{bmatrix}. \quad (10.98b)$$

A two-port which is invariant under exchange of ports 1 and 2 is called a *symmetrical two-port*. The symmetrical two-port is a special case of the reciprocal two-port. For the symmetrical two-port in addition to (10.97) we obtain also

$$Z_{11} = Z_{22}, \quad Y_{11} = Y_{22}, \quad A_{11} = A_{22}. \quad (10.99)$$

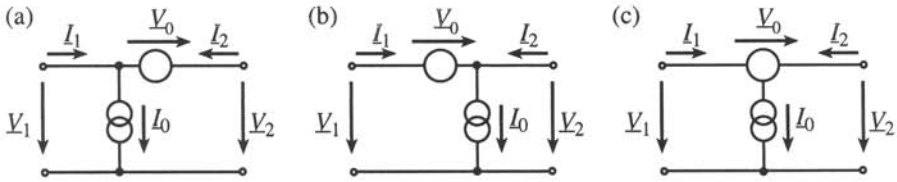


Figure 10.11: Two-port source.

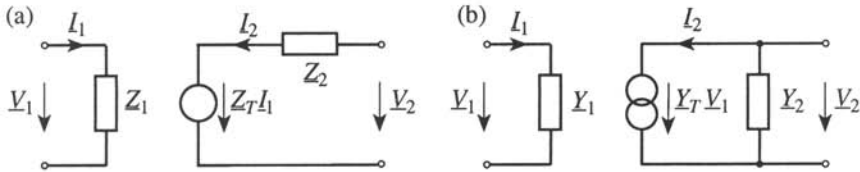


Figure 10.12: General controlled sources with arbitrary input and output impedance: (a) current controlled voltage source, and (b) voltage controlled current source.

Figure 10.11 shows a *two-port current-voltage source*. The two circuits in Figure 10.11(a) and (b) are electrically equivalent. We therefore use the symmetrical symbol depicted in Figure 10.11(c). The impressed voltage \underline{V}_0 enforces a difference between \underline{V}_1 and \underline{V}_2 and the impressed current \underline{I}_0 causes a difference between \underline{I}_1 and $-\underline{I}_2$. This yields

$$\underline{V}_1 = \underline{V}_2 + \underline{V}_0, \quad (10.100a) \quad \underline{I}_1 = -\underline{I}_2 + \underline{I}_0. \quad (10.100b)$$

Controlled sources, the ideal transformer and the gyrator are two-port circuit elements that are very useful in circuit modeling. Some of these two-port circuit elements cannot be described in the Y- or Z-matrix representation or in both of them. However, there are no restrictions in the S-matrix representation of these circuit elements.

Figure 10.12 shows the *general controlled source* with arbitrary input and output reflection factors. Figure 10.12(a) shows a *current controlled voltage source* with *transimpedance* Z_T . Figure 10.12(a) and Figure 10.12(b) show a *voltage controlled current source* with *transadmittance* Y_T . The general controlled source is described by the scattering matrix

$$\underline{S} = \begin{bmatrix} \rho_1 & 0 \\ \tau & \rho_2 \end{bmatrix}, \quad (10.101)$$

where for the voltage controlled current source the *reflection coefficients* ρ_1 , ρ_2 and the *transmission coefficient* τ are

$$\rho_1 = \frac{Z_{11} - Z_{01}}{Z_{11} + Z_{01}}, \quad \rho_2 = \frac{Z_{22} - Z_{02}}{Z_{22} + Z_{02}}, \quad \tau = \frac{2Z_T \sqrt{Z_{01}Z_{02}}}{(Z_{11} + Z_{01})(Z_{22} + Z_{02})} \quad (10.102)$$

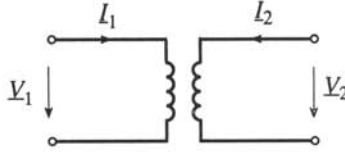


Figure 10.13: The ideal transformer.

whereas for the current controlled voltage source these coefficients are

$$\rho_1 = \frac{1 - Y_{11}Z_{01}}{1 + Y_{11}Z_{01}}, \quad \rho_2 = \frac{1 - Y_{22}Z_{02}}{1 + Y_{22}Z_{02}}, \quad \tau = \frac{2Y_T\sqrt{Z_{01}Z_{02}}}{(1 + Y_{11}Z_{01})(1 + Y_{22}Z_{02})}. \quad (10.103)$$

For $\rho_1 = 0$ and $\rho_2 = 0$ we obtain the matched controlled source. The ideal transformer (Figure 10.13) relates the voltages and currents V_1 , V_2 and I_1 , I_2 , respectively, of two branches 1 and 2 via

$$V_1 - nV_2 = 0, \quad (10.104a) \quad nI_1 - I_2 = 0, \quad (10.104b)$$

where n is a real number, called the turns ratio. With

$$\xi = n\sqrt{\frac{Z_{02}}{Z_{01}}}, \quad (10.105)$$

where Z_{02} and Z_{01} are the characteristic impedances of reference for the ports 1 and 2 we obtain the S matrix \underline{S}_{tr} of the ideal transformer

$$\underline{S}_{tr} = \begin{bmatrix} \frac{\xi^2 - 1}{\xi^2 + 1} & \frac{2\xi}{\xi^2 + 1} \\ \frac{2\xi}{\xi^2 + 1} & \frac{1 - \xi^2}{\xi^2 + 1} \end{bmatrix}. \quad (10.106)$$

If the turns ratio is given by the square root of the ratio of the characteristic impedances Z_{01} and Z_{02} , the ideal transformer is matched and we obtain

$$\underline{S}_{tr} = \begin{bmatrix} 0 & 1 \\ 1 & 0 \end{bmatrix} \quad \text{for} \quad n = \sqrt{\frac{Z_{01}}{Z_{02}}}. \quad (10.107)$$

Choosing the characteristic impedances Z_{01} and Z_{02} according to (10.107) shows that the ideal transformer may also be interpreted as part of the connection circuit instead of a circuit element.

The *gyrator* with the circuit symbol shown in Figure 10.14 relates the voltages and currents V_1 , V_2 and I_1 , I_2 , respectively, of two branches 1 and 2 via

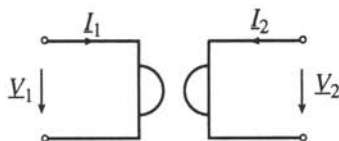


Figure 10.14: The gyrator.

$$\underline{I}_1 - G_g \underline{V}_2 = 0, \quad (10.108a) \quad \underline{I}_2 + G_g \underline{V}_1 = 0. \quad (10.108b)$$

The real conductance G_g is called the *gyration conductance*. With

$$\eta = \sqrt{\underline{Z}_{01} \underline{Z}_{02}} G_g \quad (10.109)$$

we obtain the S matrix $\underline{S}_{\text{gyr}}$ of the gyrator

$$\underline{S}_{\text{gyr}} = \begin{bmatrix} \frac{1-\eta^2}{1+\eta^2} & \frac{-2\eta}{1+\eta^2} \\ \frac{2\eta}{1+\eta^2} & \frac{1-\eta^2}{1+\eta^2} \end{bmatrix}. \quad (10.110)$$

Choosing the appropriate characteristic impedances \underline{Z}_{01} and \underline{Z}_{02} we obtain the matched gyrator.

$$\underline{S}_{\text{gyr}} = \begin{bmatrix} 0 & -1 \\ 1 & 0 \end{bmatrix} \quad \text{for} \quad G_g = \frac{1}{\sqrt{\underline{Z}_{01} \underline{Z}_{02}}}. \quad (10.111)$$

10.7 SIGNAL FLOW GRAPHS

We can represent the relations between the wave amplitudes established by the scattering parameters in a graphic format. The corresponding graphs are called *signal flow graphs* [14–16]. A microwave circuit can be analyzed by investigation of the structure of the signal flow graph. The description of a circuit by its signal flow graph is equivalent to its description by the circuit system of equations. This way of solving the network equations is very efficient. The *signal flow graph* is specified as a set of nodes together with a set of directed branches. It represents incident and reflected waves as nodes and the scattering parameters as directed branches. The rules for the construction of the signal flow graph are: 1. Draw a node for every \underline{a}_i and every \underline{b}_i . 2. Draw a directed line from \underline{a}_j to \underline{b}_i for every S_{ij} . Figure 10.15 shows the flow graphs for some common circuit elements.

Consider a two-port connected at port 1 to a generator and at port 2 to a load as shown in Figure 10.16(a). The *open-circuit voltage* is \underline{V}_G of the generator and the *generator*

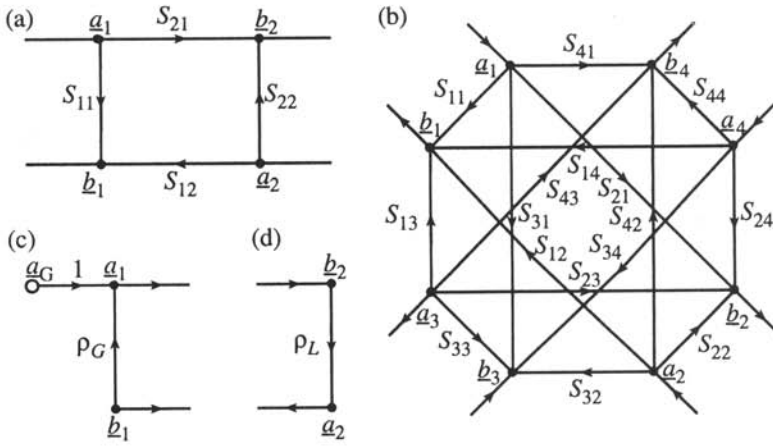


Figure 10.15: Signal flow graph of common circuit elements, (a) two-port, (b) four-port, (c) generator, (d) load.

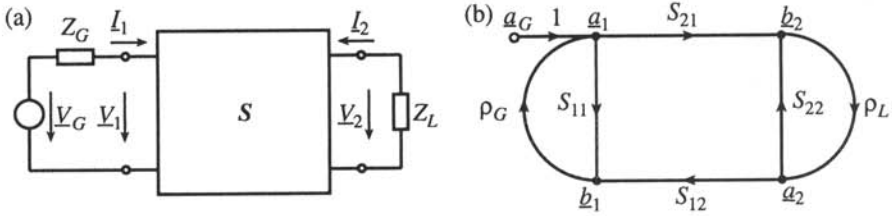


Figure 10.16: (a) Two-port with source and load, (b) corresponding signal flow graph.

impedance is Z_G . The load impedance is Z_L . The S matrix of the two-port is

$$\begin{bmatrix} \underline{b}_1 \\ \underline{b}_2 \end{bmatrix} = \begin{bmatrix} S_{11} & S_{12} \\ S_{21} & S_{22} \end{bmatrix} \begin{bmatrix} \underline{a}_1 \\ \underline{a}_2 \end{bmatrix} \quad (10.112)$$

and the flow graph of the two-port is represented in Figure 10.15(a). The generator and the load are described by

$$\underline{a}_1 = \underline{a}_G + \rho_G \underline{b}_1, \quad (10.113a)$$

$$\underline{a}_2 = \rho_L \underline{b}_2, \quad (10.113b)$$

with the generator wave amplitude \underline{a}_G given by

$$\underline{a}_G = \frac{\sqrt{Z_{01}}}{Z_G + Z_{01}}. \quad (10.114)$$

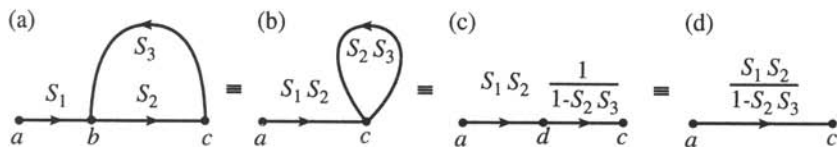


Figure 10.17: Transformation: (a) a graph with loop into (b) equivalent graph with loop, (c) equivalent graph without loop, (d) equivalent branch.

The flow graph of the generator and the load are drawn in Figure 10.15(c) and (d).

When circuits are connected it is only necessary to connect the corresponding flow graphs since the outgoing wave of one circuit is the incoming wave to the circuit connected with it. Connecting the flow graphs of generator, two-port, and load yields the flow graph shown in Figure 10.16(b). The system described by the signal flow graph has only one independent variable, the generator wave amplitude a_G . The signal flow graph contains *paths* and *loops*. A path is a sequence of branches directed in the same direction such that no node is touched more than once by one branch. The value of the path is the product of all the values assigned to its branches. Two parallel paths in the same direction can be replaced by one path that is the sum of these two paths. There is one path from the node a_G to the node b_2 . Its value is S_{12} . A *first-order loop* is a closed sequence of branches in the same direction such that no node is touched more than once by one branch. The value of the loop is the product of all the values of its branches.

If a graph contains a loop we can replace this graph by an equivalent graph without loop, as shown in Figure 10.17. In a first step the graph with loop (a) is transformed into a graph with a loop beginning and ending in the same node. A loop with the value S can be expanded into a branch with the value

$$\sum_{n=0}^{\infty} S^n = \frac{1}{1-S}. \quad (10.115)$$

After combining the two branches in the path (c) we can represent the graph by a single branch (d). We apply this rule to the computation of the ratios $\underline{b}_1/\underline{a}_1$ and $\underline{b}_2/\underline{a}_G$ in Figure 10.16(b) and obtain

$$\frac{\underline{b}_1}{\underline{a}_1} = S_{11} + S_{21} \frac{\rho_L}{1 - S_{22}\rho_L} S_{12}, \quad (10.116a)$$

$$\frac{\underline{b}_2}{\underline{a}_G} = \frac{S_{21}}{1 - S_{11}\rho_G - S_{22}\rho_L + \rho_G\rho_L(S_{11}S_{22} - S_{12}S_{21})}. \quad (10.116b)$$

10.8 LUMPED ELEMENT EQUIVALENT CIRCUITS

The application of network-oriented methods to electromagnetic field problems can contribute significantly to the problem formulation and solution methodology. The field problem can be systematically treated by the segmentation technique and by specifying canonical Foster representations for the subcircuits. Connection between different subdomains is obtained by selecting the appropriate independent field quantities via Tellegen's theorem. For each subdomain, as well as for the entire circuit, an equivalent circuit extraction procedure is feasible, either in closed form for subdomains amenable to analytical description or via the relevant pole structure description when a numerical solution is available.

10.8.1 Foster Representation of Reactance Multiports

The field solution $\underline{\mathcal{E}}(\mathbf{x}, \omega)$ may be expressed in integral form [17, 18] as

$$\underline{\mathcal{E}}(\mathbf{x}, \omega) = \int_{R_I}' \mathcal{G}_e^I(\mathbf{x}, \mathbf{x}', \omega) \wedge \underline{\mathcal{J}}(\mathbf{x}', \omega), \quad (10.117)$$

where $\underline{\mathcal{J}}(\mathbf{x}', \omega)$ is the excitation electric density current distribution within the region R_I and $\mathcal{G}_e^I(\mathbf{x}, \mathbf{x}', \omega)$ is the electric dyadic Green's form (4.76)

$$\begin{aligned} \mathcal{G}_e^I = & G_{11} dx dx' + G_{12} dx dy' + G_{13} dx dz' \\ & + G_{21} dy dx' + G_{22} dy dy' + G_{23} dy dz' \\ & + G_{31} dz dx' + G_{32} dz dy' + G_{33} dz dz'. \end{aligned} \quad (10.118)$$

The prime in the integral denotes that this operation is carried out with respect to the source point \mathbf{x}' . The current density can be expressed by means of a surface density current $\underline{\mathcal{J}}_{eA}(\mathbf{x}', \omega)$ flowing on the surface $\partial R_I' = (u', v', w' = w_0)$ and related to $\underline{\mathcal{J}}(\mathbf{x}', \omega)$ as follows

$$\underline{\mathcal{J}}(\mathbf{x}', \omega) = \delta(w' - w_0) n' \wedge \underline{\mathcal{J}}_{eA}(\mathbf{x}', \omega) \quad \text{for } \mathbf{x}' \in \partial R_I, \quad (10.119)$$

where the n is the unit differential form corresponding to the vertical coordinate w and whose orientation is normal outward with respect to ∂R_I . Inserting (10.119) in (10.117) yields

$$\underline{\mathcal{E}}(\mathbf{x}, \omega) = \oint_{\partial R_I}' \mathcal{G}_e^I(\mathbf{x}, \mathbf{x}', \omega) \wedge \underline{\mathcal{J}}_{eA}(\mathbf{x}', \omega). \quad (10.120)$$

Now by imposing the continuity condition of the tangential components, and applying the equivalence principle, the surface ∂R_I is replaced by a perfect magnetic conductor and the equivalent electric surface current defined as

$$\underline{\mathcal{J}}_{eA}(\mathbf{x}', \omega) = \underline{\mathcal{H}}_t^I(\mathbf{x}', \omega). \quad (10.121)$$

Also the tangential component of the electric field can be obtained by recognizing that

$$\underline{\mathcal{E}}_t^l = n \lrcorner n \wedge \underline{\mathcal{E}}, \quad (10.122)$$

where the contraction $s_i \lrcorner s_j$ of two unit differential forms s_i and s_j is defined by

$$s_i \lrcorner s_j = \delta_{ij}. \quad (10.123)$$

Applying this relationship together with (10.121), (10.120) results in

$$\underline{\mathcal{E}}_t^l(\mathbf{x}, \omega) = \oint_{\partial R_l}' n \lrcorner (n \wedge \mathcal{G}_e^l(\mathbf{x}, \mathbf{x}', \omega)) \wedge \underline{\mathcal{H}}_t^l(\mathbf{x}', \omega). \quad (10.124)$$

The superscript l in (10.124) implies that the corresponding quantity belongs to the region R_l , so that $\underline{\mathcal{E}}_t^l$ and $\underline{\mathcal{H}}_t^l$, for instance, represent the electric and magnetic field components tangential to ∂R_l , transferred into the region R_l . The operation $n \lrcorner n \wedge$ applies only to the observation point \mathbf{x} while the integral is over \mathbf{x}' . This allows to define

$$\mathcal{Z}^l(\mathbf{x}, \mathbf{x}', \omega) = n \lrcorner (n \wedge \mathcal{G}_e^l(\mathbf{x}, \mathbf{x}', \omega)) \quad (10.125)$$

as the double differential form for the impedance representation of the *dyadic Green's form*. The substitution of (10.125) into (10.124) yields

$$\underline{\mathcal{E}}_t^l(\mathbf{x}, s) = \oint_{\partial R_l}' \mathcal{Z}^l(\mathbf{x}, \mathbf{x}', \omega) \wedge \underline{\mathcal{H}}_t^l(\mathbf{x}', \omega), \quad (10.126)$$

which provides an integral relationship between the tangential electric and magnetic components on the considered subdomain surface ∂R_l . In the same way we can derive

$$\underline{\mathcal{H}}_t^l(\mathbf{x}, s) = \oint_{\partial R_l}' \mathcal{Y}^l(\mathbf{x}, \mathbf{x}', \omega) \wedge \underline{\mathcal{E}}_t^l(\mathbf{x}', \omega), \quad (10.127)$$

where $\mathcal{Z}(\mathbf{x}, \mathbf{x}', \omega)$ and $\mathcal{Y}(\mathbf{x}, \mathbf{x}', \omega)$ are the dyadic Green's forms in the impedance representation or admittance representation, respectively. Green's forms $\mathcal{Z}(\mathbf{x}, \mathbf{x}', \omega)$ and $\mathcal{Y}(\mathbf{x}, \mathbf{x}', \omega)$ are given by [9]

$$\mathcal{Z}^l(\mathbf{x}, \mathbf{x}', \omega) = \frac{1}{j\omega} \mathcal{L}_0^l(\mathbf{x}, \mathbf{x}') + \sum_p \frac{\mathcal{L}_p^l(\mathbf{x}, \mathbf{x}')}{j(\omega - \omega_p)} \quad (10.128)$$

and

$$\mathcal{Y}^l(\mathbf{x}, \mathbf{x}', \omega) = \frac{1}{j\omega} \mathcal{C}_0^l(\mathbf{x}, \mathbf{x}') + \sum_q \frac{\mathcal{C}_q^l(\mathbf{x}, \mathbf{x}')}{j(\omega - \omega_q)}. \quad (10.129)$$

The dyadic forms $\mathcal{L}_0^l(\mathbf{x}, \mathbf{x}')$ and $\mathcal{C}_0^l(\mathbf{x}, \mathbf{x}')$ represent the static parts of Green's functions, whereas every term $\mathcal{L}_p^l(\mathbf{x}, \mathbf{x}')$ and $\mathcal{C}_p^l(\mathbf{x}, \mathbf{x}')$, respectively, corresponds to a pole at the frequency ω_p or ω_q , respectively.

We discretize (10.126) and (10.127) by expanding the tangential fields on ∂R_l into a complete set of vector orthonormal basis functions. These expansions need only to be valid on ∂R_l ,

$$\underline{\mathcal{E}}_t^l(\mathbf{x}, \omega) = \sum_{n=1}^{N_l} \underline{V}_n^l(\omega) \mathbf{e}_n^l(\mathbf{x}), \quad (10.130a)$$

$$\underline{\mathcal{H}}_t^l(\mathbf{x}, \omega) = \sum_{n=1}^{N_l} \underline{I}_n^l(\omega) \mathbf{h}_n^l(\mathbf{x}). \quad (10.130b)$$

The electric and magnetic basis forms are related via

$$\mathbf{h}_n^l = \star (\mathbf{n}^l \wedge \mathbf{e}_n^l), \quad (10.131a) \quad \mathbf{e}_n^l = -\star (\mathbf{n}^l \wedge \mathbf{h}_n^l) \quad (10.131b)$$

and satisfy the orthogonality relation

$$\int_{\partial R_l} \mathbf{e}_m^{l*} \wedge \mathbf{h}_n^l = \langle \mathbf{e}_m^l | \mathbf{h}_n^l \rangle_{\partial R_l} = \delta_{mn}, \quad (10.132)$$

where $\mathbf{n}^l(\mathbf{x})$ is the unit differential form normal to ∂R_l . The expansion coefficients \underline{V}_n and \underline{I}_n may be considered as generalized voltages and currents. From (10.130a) and (10.130b) and the orthogonality relation (10.132) we obtain

$$\underline{V}_n(\omega) = \int_{\partial R_l} \mathbf{h}_n^{l*}(\mathbf{x}) \wedge \underline{\mathcal{E}}_t(\mathbf{x}, \omega) = -\langle \mathbf{h}_n^l | \underline{\mathcal{E}}_t(\mathbf{x}, \omega) \rangle_{\partial R_l}, \quad (10.133a)$$

$$\underline{I}_n(\omega) = \int_{\partial R_l} \mathbf{e}_n^{l*}(\mathbf{x}) \wedge \underline{\mathcal{H}}_t(\mathbf{x}, \omega) = \langle \mathbf{e}_n^l | \underline{\mathcal{H}}_t(\mathbf{x}, \omega) \rangle_{\partial R_l}. \quad (10.133b)$$

If the domain R_l is partially bounded by an ideal electric or magnetic wall $\underline{\mathcal{E}}_t$ or $\underline{\mathcal{H}}_t$, respectively, vanish on these walls. If the independent field variable vanishes on the boundary, this part of the boundary does not need to be represented by the basis functions. If only electric walls are involved, the admittance representation of Green's function will be appropriate, and if only magnetic walls are involved, the impedance representation will be appropriate. Consider for example the case where the main part of the boundary ∂R_l is formed by an electric wall and only the ports are left open. Choosing the admittance representation, we only need to expand the field on the port surfaces into basis functions. Applying the method of moments, we obtain

$$\mathbf{Z}_{m,n}^l(\omega) = \iint_{\partial R_l} \mathbf{e}_m^{l*}(\mathbf{x}) \wedge \mathcal{Z}^l(\mathbf{x}, \mathbf{x}', \omega) \wedge \mathbf{h}_n^l(\mathbf{x}'), \quad (10.134a)$$

$$\mathbf{Y}_{m,n}^l(\omega) = \iint_{\partial R_l} \mathbf{h}_m^{l*}(\mathbf{x}) \wedge \mathcal{Y}^l(\mathbf{x}, \mathbf{x}', \omega) \wedge \mathbf{e}_n^l(\mathbf{x}'). \quad (10.134b)$$

Then from (10.128) and (10.129), the impedance matrix $Z_{m,n}(\omega)$ and the admittance matrix $Y_{m,n}(\omega)$ may be represented by

$$Z_{m,n}(\omega) = \frac{1}{j\omega} z_{0m,n}^l + \sum_p \frac{1}{j\omega} \frac{\omega^2}{\omega^2 - \omega_p^2} z_{pm,n}^l, \quad (10.135a)$$

$$Y_{m,n}(\omega) = \frac{1}{j\omega} y_{0m,n}^l + \sum_q \frac{1}{j\omega} \frac{\omega^2}{\omega^2 - \omega_q^2} y_{qm,n}^l. \quad (10.135b)$$

For a linear reciprocal lossless multiport an equivalent circuit model may be specified by the canonical Foster representation [19, 20]. Figure 10.18(a) shows a *compact reactance multiport* describing a pole at the frequency ω_λ . This compact multiport consists of one series resonant circuit and M ideal transformers. The admittance matrix of this compact multiport is given by

$$Y_\lambda(\omega) = \frac{1}{j\omega L_\lambda} \frac{\omega^2}{\omega^2 - \omega_\lambda^2} A_\lambda \quad (10.136)$$

with the real frequency-independent rank 1 matrix A_λ given by

$$A_\lambda = \begin{bmatrix} n_{\lambda 1}^2 & n_{\lambda 1} n_{\lambda 2} & \cdots & n_{\lambda 1} n_{\lambda M} \\ n_{\lambda 2} n_{\lambda 1} & n_{\lambda 2}^2 & \cdots & n_{\lambda 2} n_{\lambda M} \\ \vdots & \vdots & \ddots & \vdots \\ n_{\lambda M} n_{\lambda 1} & n_{\lambda M} n_{\lambda 2} & \cdots & n_{\lambda M}^2 \end{bmatrix}. \quad (10.137)$$

The $n_{\lambda i}$ are the turns ratios of the ideal transformers in Figure 10.18(a). A *compact reactance multiport* describing a pole at the frequency $\omega = 0$ is shown in Figure 10.18(b). The admittance matrix of this compact multiport is given by

$$Y_0 = \frac{1}{j\omega L_0} A_0, \quad (10.138)$$

where A_0 is a real frequency-independent rank 1 matrix as defined in (10.137). If the admittance matrix is of rank higher than 1 it has to be decomposed into a sum of rank 1 matrices. Each rank 1 matrix corresponds to a compact multiport.

The complete admittance matrix describing a circuit with a finite number of poles is obtained by parallel connecting the circuits describing the individual poles. In the *canonical Foster admittance representation*, the admittance matrix $Y(p)$ is given by

$$Y_\lambda(\omega) = \frac{1}{j\omega L_0} A_0 + \sum_{\lambda=1}^N \frac{1}{j\omega L_\lambda} \frac{\omega^2}{\omega^2 - \omega_\lambda^2} A_\lambda. \quad (10.139)$$

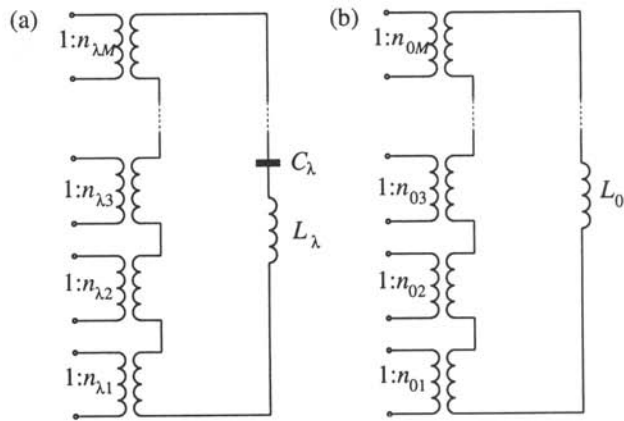


Figure 10.18: A compact series multiport element representing a pole, a) at $\omega = \omega_{\lambda}$, and, b) at $\omega = 0$.

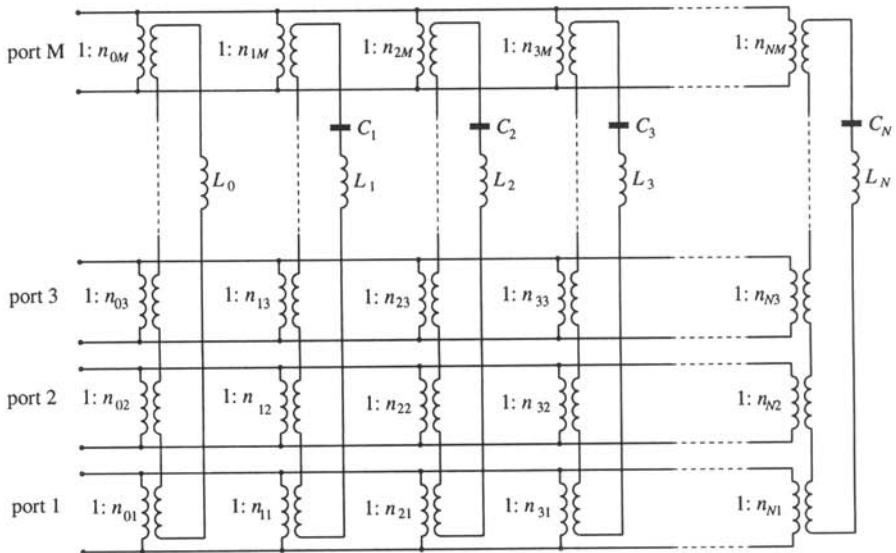


Figure 10.19: Foster admittance representation of a multiport.

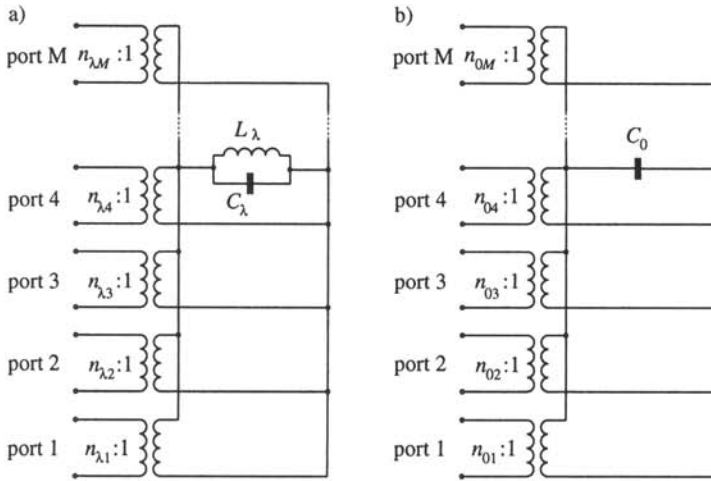


Figure 10.20: A compact parallel multiport element representing a pole, a) at $\omega = \omega_\lambda$, and, b) at $\omega = 0$.

This admittance matrix describes a parallel connection of elementary multiports, each of which consists of a series resonant circuit and an ideal transformer. Figure 10.19 shows the complete circuit of the canonical Foster admittance representation. There exists also a dual impedance representation where elementary circuits consisting of parallel resonant circuits and ideal transformers are connected in series. Figure 10.20(a) shows a *compact reactance multiport* describing a pole at the frequency ω_λ . This compact multiport consists of one parallel circuit and M ideal transformers. The impedance matrix of this compact multiport is given by

$$\mathbf{Z}_\lambda(\omega) = \frac{1}{j\omega C_\lambda} \frac{\omega^2}{\omega^2 - \omega_\lambda^2} \mathbf{B}_\lambda \quad (10.140)$$

with the real frequency independent rank 1 matrix \mathbf{B}_λ given by

$$\mathbf{B}_\lambda = \begin{bmatrix} n_{\lambda 1}^2 & n_{\lambda 1}n_{\lambda 2} & \cdots & n_{\lambda 1}n_{\lambda M} \\ n_{\lambda 2}n_{\lambda 1} & n_{\lambda 2}^2 & \cdots & n_{\lambda 2}n_{\lambda M} \\ \vdots & \vdots & \ddots & \vdots \\ n_{\lambda M}n_{\lambda 1} & n_{\lambda M}n_{\lambda 2} & \cdots & n_{\lambda M}^2 \end{bmatrix}. \quad (10.141)$$

Figure 10.20(b) shows a *compact reactance multiport* describing a pole at the frequency $\omega = 0$. The impedance matrix of this compact multiport is given by

$$\mathbf{Z}_0 = \frac{1}{j\omega C_0} \mathbf{B}_0, \quad (10.142)$$

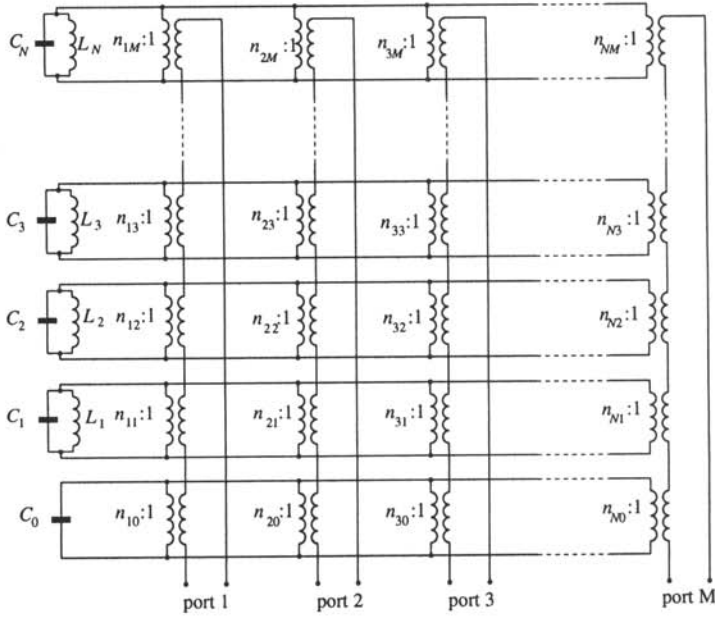


Figure 10.21: Foster impedance representation of a multiport.

where \mathbf{B}_0 is a real frequency independent rank 1 matrix as defined in (10.137). The complete impedance matrix describing a circuit with a finite number of poles is obtained by parallel connecting the circuits describing the individual poles. In the canonical Foster representation, the impedance matrix $\mathbf{Z}(\omega)$ is given by

$$\mathbf{Z}_\lambda(\omega) = \frac{1}{j\omega C_0} \mathbf{B}_0 + \sum_{\lambda=1}^N \frac{1}{j\omega C_\lambda} \frac{\omega^2}{\omega^2 - \omega_\lambda^2} \mathbf{B}_\lambda. \quad (10.143)$$

The equivalent Foster admittance multiport representation or Foster impedance representation may be computed analytically from Green's function. However, it is also possible to find an equivalent Foster representation from admittance parameters calculated by numerical field analysis by methods of system identification.

10.8.2 Cauer Representation of Radiating Structures

Let us assume the complete electromagnetic structure under consideration embedded in a virtual sphere S as shown in Figure 10.22. Outside the sphere free-space is assumed. The complete electromagnetic field outside the sphere may be expanded into a set of TM and TE spherical waves propagating in outward direction. In 1948 L.J. Chu in his

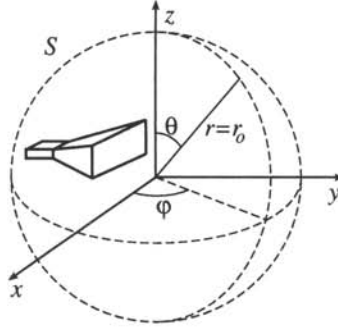


Figure 10.22: Embedding of an electromagnetic structure into a sphere.

paper on physical limitations of omni-directional antennas investigated the orthogonal mode expansion of the radiated field [21]. Using the recurrence formula for spherical Bessel functions, he gave the Caier representation [19, 20] of the equivalent circuits of the TM_n and the TE_n spherical waves. The equivalent circuit expansion of spherical waves also is treated in [22, 23].

We derive the TM spherical wave solutions from the potential introduced in (3.230). Superimposing the solutions (3.230) with positive and negative n we obtain waves standing in ϕ -direction described by the potentials

$$\Psi_{mn}^{\text{TM},c} = A_{mn}^c P_n^m(\cos \theta) \cos m\phi h_n^{(2)}(kr), \quad (10.144a)$$

$$\Psi_{mn}^{\text{TM},s} = A_{mn}^s P_n^m(\cos \theta) \sin m\phi h_n^{(2)}(kr), \quad (10.144b)$$

where the $P_n^m(\cos \theta)$ are the associated Legendre polynomials and $h_n^{(2)}(kr)$ are the Hankel functions. The A_{mn}^c and A_{mn}^s are coefficients. Inward propagating waves are represented by $h_n^{(1)}(kr)$ and outward propagating waves are represented by $h_n^{(2)}(kr)$. Since outside the sphere, for $r > r_0$ no sources exist, only outward propagating waves occur and we have only to consider the spherical Hankel functions $h_n^{(2)}(kr)$. The coefficients n and m can assume the values $n = 1, 2, 3, 4, \dots, \infty$ and $m = 0, 1, 2, \dots, n-1$, n and $i = c, s$. The superscripts c and s denote waves mutually rotated around the z -axis by an angle of $\frac{1}{2}\pi$. With (3.233a) and (3.233b) we compute the magnetic and electric fields of the TM modes as

$$\underline{\mathcal{H}}_{mn}^{\text{TM},i} = \star (r \, dr \wedge d\Psi_{mn}^{\text{TM},i}), \quad (10.145a)$$

$$\underline{\mathcal{E}}_{mn}^{\text{TM},i} = \frac{1}{j\omega\epsilon} \star d\underline{\mathcal{H}}_{mn}^{\text{TM},i}. \quad (10.145b)$$

The TE modes are dual with respect to the TM . Superimposing the solutions (3.230)

with positive and negative n we obtain the potentials

$$\Psi_{mn}^{\text{TE},c} = B_{mn}^c P_n^m(\cos \theta) \cos m\phi h_n^{(2)}(kr), \quad (10.146a)$$

$$\Psi_{mn}^{\text{TE},s} = B_{mn}^s P_n^m(\cos \theta) \sin m\phi h_n^{(2)}(kr), \quad (10.146b)$$

from which we can derive the electromagnetic field of the TE spherical waves. The B_{mn}^c and B_{mn}^s are coefficients. From (3.232a) and (3.232b) we obtain

$$\underline{\mathcal{E}}_{mn}^{\text{TE},i} = * (dr \wedge d\Psi_{mn}^{\text{TE},i}), \quad (10.147a) \quad \underline{\mathcal{H}}_{mn}^{\text{TE},i} = -\frac{1}{j\omega\mu} * d\underline{\mathcal{E}}_{mn}^{\text{TE},i} \quad (10.147b)$$

where $n = 1, 2, 3, 4, \dots, \infty$, $m = 1, 2, 3, 4, \dots, n$, and $i = c, s$.

The wave impedances for the outward propagating TM and TE modes are

$$Z_{mn}^+ = \frac{E_{mn\theta}^+}{H_{mn\phi}^+} = -\frac{E_{mn\phi}^+}{H_{mn\theta}^+}. \quad (10.148)$$

The superscript + denotes the outward propagating wave. With (3.235b), (3.235c), (3.235e), and (3.235f) we obtain the wave impedances for the TM and TE modes

$$Z_{mn}^{\text{TM}} = jZ_{F0} \frac{\frac{d}{dr}(rh_n^{(2)'}(kr))}{rh_n^{(2)}(kr)}, \quad (10.149a)$$

$$Z_{mn}^{\text{TE}} = -jZ_{F0} \frac{rh_n^{(2)}(kr)}{\frac{d}{dr}(rh_n^{(2)'}(kr))}, \quad (10.149b)$$

where $Z_{F0} = \sqrt{\mu/\epsilon}$ is the wave impedance of the plane wave. The prime ' denotes the derivation of the function with respect to its argument. We note that the characteristic wave impedances only depend on the index n and the radius r_0 of the sphere.

Using the recurrence formulae (B.8a) and (B.8b) we perform a continued fraction expansions of the wave impedances of the TM modes

$$Z_{mn}^{\text{TM}} = Z_{F0} \left[\frac{\frac{n}{jkr} + \frac{1}{\frac{2n-1}{jkr} + \frac{1}{\frac{2n-3}{jkr} + \dots + \frac{1}{\frac{3}{jkr} + \frac{1}{jkr+1}}}}}{\dots} \right] \quad (10.150)$$

and the TE modes

$$Z_{mn}^{\text{TE}} = Z_{F0} \left[\frac{1}{\frac{\frac{n}{jkr} + \frac{2n-1}{jkr} + \frac{1}{\frac{2n-3}{jkr} + \frac{1}{\frac{2n-5}{jkr} + \dots + \frac{1}{\frac{3}{jkr} + \frac{1}{jkr+1}}}}}{\dots} \right]. \quad (10.151)$$

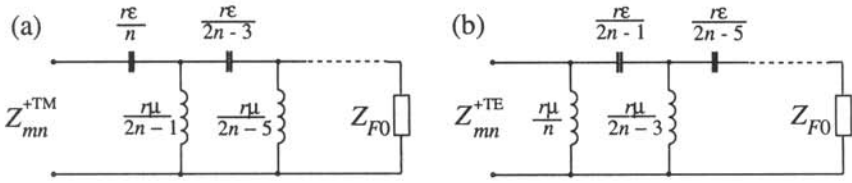


Figure 10.23: Equivalent circuit of (a) TM_{mn} , (b) TE_{mn} spherical wave.

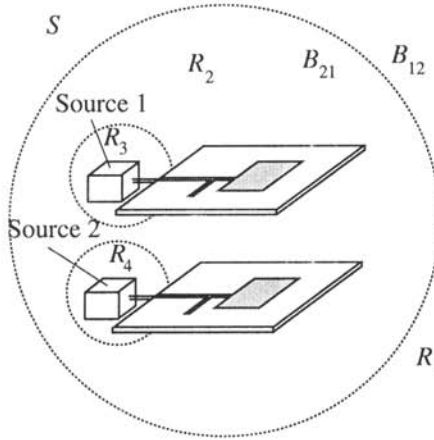


Figure 10.24: The complete radiating electromagnetic structure.

These continued fraction expansions represent the *Cauer canonic realizations* of the outward propagating TM_{mn} modes shown in Figure 10.23(a) and TE_{mn} modes shown in Figure 10.23(b). We note that the equivalent circuit representing the TE_{mn} mode is dual to the equivalent circuit representing the TM_{mn} mode. The equivalent circuits for the radiation modes exhibit highpass character. For very low frequencies the wave impedance of the TM_{mn} mode is represented by a capacitor $C_{0n} = \epsilon r/n$ and the wave impedance of the TE_{mn} mode is represented by an inductor $L_{0n} = \mu r/n$. For $f \rightarrow \infty$ we obtain $Z_{mn}^{+\text{TM}}, Z_{mn}^{+\text{TE}} \rightarrow Z_{F0}$.

In order to establish the equivalent circuit of a reciprocal linear lossless radiating electromagnetic structure, we embed the structure in a sphere S according to Figure 10.24. The internal sources 1 and 2 are enclosed in regions R_3 and R_4 . Region R_2 only contains the reciprocal passive linear electromagnetic structure. Region R_1 is the infinite free-space region outside the sphere S . R_2 may be either considered as a whole or may be subdivided into subregions. If the electromagnetic structure embedded in

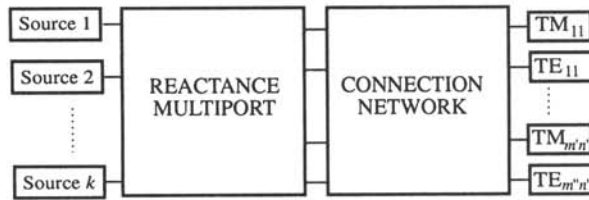


Figure 10.25: Equivalent circuit of the complete radiating electromagnetic structure.

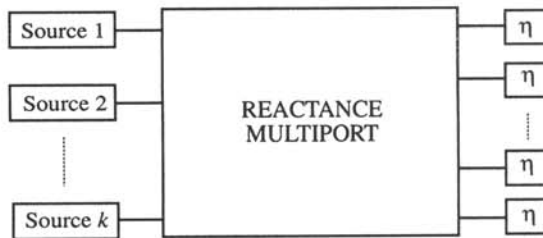


Figure 10.26: Equivalent circuit of the modified complete radiating electromagnetic structure.

R_2 is considered as a whole it may be modeled either by a canonical Foster admittance representation according to Figure 10.19 or a canonical Foster impedance representation according to Figure 10.21. If the internal sources are coupled via a single transverse mode with the electromagnetic structure, one-port per source is required to model the coupling between the source and the electromagnetic structure. The radiating modes in R_1 are represented by one-ports modeled by canonical Cauer representations according to Figure 10.23. The external ports of the canonical Foster equivalent circuit (i.e., the ports representing the tangential field on the surface of S) are connected via a connection network as shown in Figure 10.8.

From the above considerations, we obtain for a reciprocal linear lossless radiating electromagnetic structure with internal sources an equivalent circuit described by a block diagram as shown in Figure 10.25. This block structure can be further simplified by contracting the equivalent circuit describing the electromagnetic structure R_2 , the connection circuit and the reactive parts of the equivalent circuits of the radiation modes into a reactance multiport. This reactance multiport again may be represented by canonical Foster representations. Now the remaining resistors Z_{F0} are connected to the external ports of the modified reactance multiport and we obtain the equivalent circuit shown in Figure 10.26. We summarize the result of the above considerations:

Any reciprocal linear lossless radiating electromagnetic structure may be described by a reactance multiport, terminated by the sources and by one

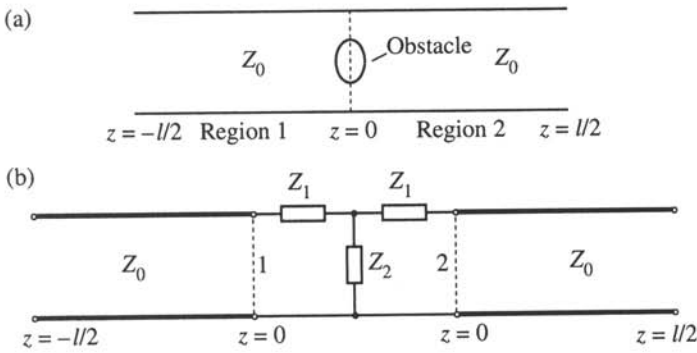


Figure 10.27: (a) Symmetrical obstacle in a waveguide, and (b) equivalent circuit.

resistor for every considered radiation mode.

For electromagnetic structures amenable of analytical description equivalent circuits may be computed directly. However, topology as well as parameters of the equivalent circuit may be obtained from the relevant pole spectrum computation when a numerical solution is available [24, 25]. A heuristic approach also allows to model lossy electromagnetic structures [24, 25]. System identification and spectral analysis methods allow an efficient determination of generation of topology as well as parameters of the lumped element equivalent circuit [17, 26]. This approach produces topology as well as parameters of a model conserving basic properties such as reciprocity and passivity.

10.9 OBSTACLES IN WAVEGUIDES

An object inserted in a homogeneous cylindrical waveguide scatters waves incident on it. An incident wave is scattered in forward and backward directions. The scattered field can be expanded in propagating and evanescent modes. If only the fundamental mode can propagate and the distance of the waveguide ports from the object are sufficiently large, at the ports besides the incident wave only the fundamental mode of the forward and backscattered waves occur. The waveguide with obstacle can be described by a *two-port*. The higher-order evanescent parts of the scattered fields in the environment of the scattering object store electric and magnetic energy and therefore contribute to reactance elements describing the two-port.

Consider a cylindrical waveguide with an embedded obstacle, symmetrical with respect to mirroring at a transverse plane at $z = 0$ as shown in Figure 10.27(a). We assume that at the considered frequency only the fundamental mode can propagate in the waveguide and that the evanescent higher-order modes excited by scattering of

incident waves are sufficiently decayed at the ports at $z = \pm \frac{1}{2}l$. In this case the waveguide with obstacle can be represented as a *symmetrical two-port* with a *T-equivalent circuit*, shown in Figure 10.27(b),

$$\mathbf{Z} = \begin{bmatrix} Z_1 + Z_2 & Z_2 \\ Z_2 & Z_1 + Z_2 \end{bmatrix}. \quad (10.152)$$

In case of even excitation of the symmetrical two-port with $\underline{I}_2 = \underline{I}_1$ we obtain for symmetry reasons $\underline{V}_2 = \underline{V}_1$ with

$$\underline{V}_i = Z_e \underline{I}_i = (Z_1 + 2Z_2) \underline{I}_i \quad \text{for } i = 1, 2. \quad (10.153)$$

For odd excitation of the symmetrical two-port with $\underline{I}_2 = -\underline{I}_1$ for symmetry reasons $\underline{V}_2 = -\underline{V}_1$ and

$$\underline{V}_i = Z_o \underline{I}_i = Z_1 \underline{I}_i \quad \text{for } i = 1, 2. \quad (10.154)$$

The equivalent circuit impedances Z_1 and Z_2 can be determined from the port impedances for even and odd excitation, Z_e and Z_v as

$$Z_1 = Z_o, \quad (10.155a) \quad Z_2 = \frac{1}{2}(Z_e - Z_o). \quad (10.155b)$$

For even excitation due to symmetry the transverse magnetic field must vanish in the symmetry plane and we can introduce a magnetic wall at $z = 0$. This divides the two-port into two identical one-ports. Figure 10.28(a) shows the equivalent one-port for even excitation. The corresponding equivalent circuit is shown in Figure 10.28(b). For odd excitation for symmetry reasons the transverse electric field must vanish at $z = 0$. Therefore we can insert an electric wall at $z = 0$ and the two-port again is split up into two identical one-ports. Figure 10.28(c) shows the equivalent one-port for odd excitation, and Figure 10.28(d) presents the corresponding equivalent circuit. To excite these one-ports we use *fundamental mode polarization sheets* at $z = -\frac{1}{2}l$. A fundamental mode polarization sheet is a surface polarization sheet in a transverse plane with a transverse field distribution given by the electric or magnetic field structure form of the fundamental mode $e_0(u, v)$ or $h_0(u, v)$, respectively. From (8.120a) and (8.120b) we obtain the effective transverse electric and magnetic polarizations as

$$\underline{\mathcal{M}}_{e0t}^{\text{eff}}(\mathbf{x}) = \star \underline{M}_{e01}(z) e_0(u, v), \quad (10.156a)$$

$$\underline{\mathcal{M}}_{m0t}^{\text{eff}}(\mathbf{x}) = \star \underline{M}_{m01}(z) h_0(u, v), \quad (10.156b)$$

where $\underline{M}_{e01}(z)$ and $\underline{M}_{m01}(z)$ are the modal amplitudes of the effective transverse electric and magnetic polarizations. With the modal amplitudes of the impressed current $\underline{I}_{s0} \delta(z + \frac{1}{2}l)$ and the impressed voltage $\underline{V}_{s0} \delta(z + \frac{1}{2}l)$ for polarization sheets at

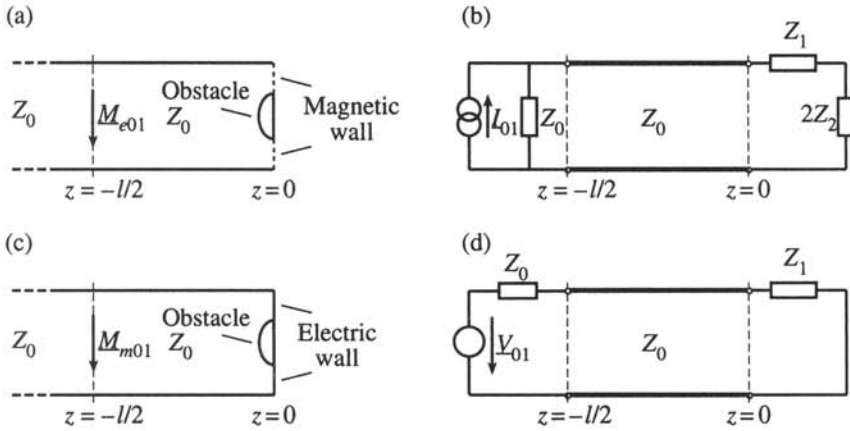


Figure 10.28: (a) Even excitation of waveguide with obstacle, (b) equivalent circuit for even excitation of waveguide with obstacle, (c) odd excitation of waveguide with obstacle, and (d) equivalent circuit for odd excitation of waveguide with obstacle.

$z = -\frac{1}{2}l$ as defined in (8.138a) and (8.138b) we obtain

$$\underline{M}_{e01}(z) = \frac{1}{j\omega} \underline{I}_{s0} \delta(z + \frac{1}{2}l), \quad (10.157a)$$

$$\underline{M}_{m01}(z) = \frac{1}{j\omega} \underline{V}_{s0} \delta(z + \frac{1}{2}l), \quad (10.157b)$$

where $\delta(z)$ is the delta distribution. With (10.156a) and (10.156b) this yields

$$\underline{\mathcal{M}}_{e0t}^{\text{eff}}(\underline{x}) = \frac{1}{j\omega} * \underline{I}_{s0} \delta(z + \frac{1}{2}l) \underline{e}_0(u, v), \quad (10.158a)$$

$$\underline{\mathcal{M}}_{m0t}^{\text{eff}}(\underline{x}) = \frac{1}{j\omega} * \underline{V}_{s0} \delta(z + \frac{1}{2}l) \underline{h}_0(u, v). \quad (10.158b)$$

The fundamental mode polarization sheets excite fundamental mode waves propagating in negative z -direction for $z < -\frac{1}{2}l$ and in positive z -direction for $z > \frac{1}{2}l$. At $z = 0$ the waveguide is terminated with half the obstacle which is modeled by either an electric wall or a magnetic wall. The back-scattered field due to the obstacle is composed of a fundamental mode wave propagating in negative z -direction and higher-order evanescent fields decaying in negative z -direction. The length $\frac{1}{2}l$ is assumed to be sufficiently large that the field contribution of the higher-order modes can be neglected at $z = -\frac{1}{2}l$.

So far we have reduced the analysis of a symmetrical two-port to the analysis of the two equivalent one-ports describing even and odd excitation of the two-port. To

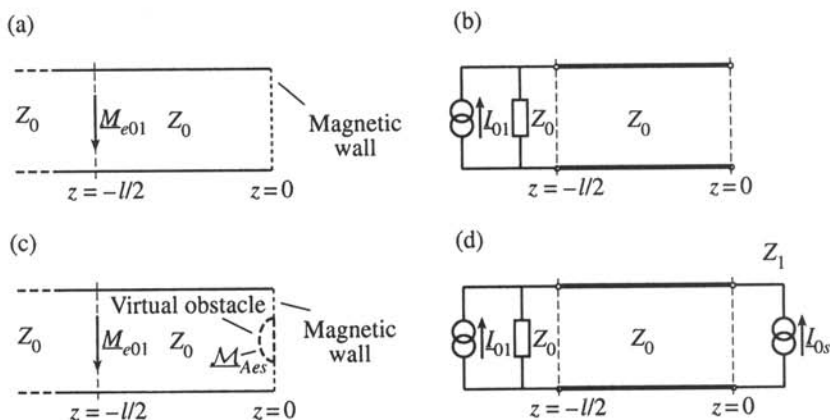


Figure 10.29: (a) Even excitation of waveguide without obstacle, (b) equivalent circuit for even excitation without obstacle, (c) even excitation of waveguide with virtual obstacle, and (d) equivalent circuit for even excitation of waveguide with virtual obstacle.

further simplify the analysis of the problem we split the task into parts. For even excitation in a first step we omit the obstacle and consider the waveguide terminated by a magnetic wall only, as shown in Figure 10.29(a). For this arrangement we compute the primary field $\underline{\mathcal{E}}_p$. In the absence of an obstacle from the magnetic wall at $z=0$ only the fundamental mode will be backscattered. Assuming infinite extension of the waveguide in negative z -direction or termination of the waveguide with its characteristic impedance at $z < -\frac{1}{2}l$, we obtain a fundamental mode wave propagating in negative z -direction and for $-\frac{1}{2}l < z < 0$ a fundamental mode standing wave. From (8.119a) and (8.119b) we obtain

$$\underline{\mathcal{E}}_t(\mathbf{x}) = \underline{V}(z) \mathbf{e}_0(u, v), \quad (10.159a)$$

$$\underline{\mathcal{H}}_t(\mathbf{x}) = \underline{I}(z) \mathbf{h}_0(u, v). \quad (10.159b)$$

Due to (8.149a) and (8.149b) the transmission-line equations in the case of excitation by fundamental mode electric and magnetic polarization sheets at $z = -\frac{1}{2}l$ are

$$\frac{d\underline{V}(z)}{dz} = -jX'(\omega)\underline{I}(z) + \underline{V}_{s0}\delta(z + \tfrac{1}{2}l), \quad (10.160a)$$

$$\frac{d\underline{I}(z)}{dz} = -jY'(\omega)\underline{V}(z) + \underline{I}_{s0}\delta(z + \tfrac{1}{2}l). \quad (10.160b)$$

For the transmission-line terminated at $z=0$ with a magnetic wall we obtain $\underline{I}(0) = 0$.

Considering this boundary condition we obtain for $z \neq -\frac{1}{2}l$ the solutions

$$\underline{V}(z) = \begin{cases} \underline{A}e^{j\beta z} & \text{for } z < -\frac{1}{2}l \\ \underline{B}\cos(\beta z) & \text{for } -\frac{1}{2}l < z \leq 0 \end{cases}, \quad (10.161a)$$

$$\underline{I}(z) = \begin{cases} -\underline{A}Z_0^{-1}e^{j\beta z} & \text{for } z < -\frac{1}{2}l \\ -j\underline{B}Z_0^{-1}\sin(\beta z) & \text{for } -\frac{1}{2}l < z \leq 0 \end{cases} \quad (10.161b)$$

with the phase coefficient β and the characteristic impedance Z_0 given by

$$\beta = \sqrt{X'B'}, \quad (10.162a) \quad Z_0 = \sqrt{\frac{X'}{B'}}. \quad (10.162b)$$

At $z = -\frac{1}{2}l$ continuity demands

$$\underline{A}e^{-j\frac{1}{2}\beta l} = \underline{B}\cos\frac{1}{2}\beta l, \quad (10.163a)$$

$$\underline{A}Z_0^{-1}e^{-j\frac{1}{2}\beta l} = \underline{I}_{s0} + j\underline{B}Z_0^{-1}\sin\frac{1}{2}\beta l. \quad (10.163b)$$

From these equations we obtain

$$\underline{I}_{s0} = \underline{B}Z_0^{-1}e^{-j\frac{1}{2}\beta l}. \quad (10.164)$$

With (10.159a), (10.159b), (10.161a), and (10.161b) we obtain the transverse electric and magnetic fields,

$$\underline{\mathcal{E}}_t(\mathbf{x}) = \begin{cases} \underline{A}e^{j\beta z}\mathbf{e}_0(u, v) & \text{for } z < -\frac{1}{2}l \\ \underline{B}\cos(\beta z)\mathbf{e}_0(u, v) & \text{for } -\frac{1}{2}l < z \leq 0 \end{cases}, \quad (10.165a)$$

$$\underline{\mathcal{H}}_t(\mathbf{x}) = \begin{cases} -\underline{A}Z_0^{-1}e^{j\beta z}\mathbf{e}_0(u, v) & \text{for } z < -\frac{1}{2}l \\ -j\underline{B}Z_0^{-1}\sin(\beta z)\mathbf{e}_0(u, v) & \text{for } -\frac{1}{2}l < z \leq 0 \end{cases}. \quad (10.165b)$$

Inserting (10.158a) and (10.165a) into (4.66) we compute the self-reaction of the current sheet as

$$\begin{aligned} R_{11} &= j\omega \int_V \underline{\mathcal{E}}_t \wedge \underline{\mathcal{M}}_{e0t}^{\text{eff}} = \underline{B}I_{s0} \int_V \cos(\beta z)\delta(z + \frac{1}{2}l)\mathbf{e}_0(u, v) \wedge \star \mathbf{e}_0(u, v) \\ &= \underline{B}I_{s0} \cos\frac{1}{2}\beta l. \end{aligned} \quad (10.166)$$

Inserting (10.164) we obtain

$$R_{11} = \frac{B^2}{2Z_0} (1 + e^{-j\beta l}). \quad (10.167)$$

Assuming \underline{B} to be real, this yields

$$\frac{\Im\{R_{sp}\}}{\Re\{R_{sp}\}} = \frac{-\sin \beta l}{1 + \cos \beta l} = -\tan \frac{1}{2}\beta l. \quad (10.168)$$

In a second step we consider a virtual obstacle (i.e., an immaterial obstacle consisting only of a surface polarization $\underline{\mathcal{M}}_{Aes}$ impressed on a surface corresponding to the surface of the obstacle). This virtual obstacle excites a secondary field $\underline{\mathcal{E}}_p$. The total electric field $\underline{\mathcal{E}}$ is given by

$$\underline{\mathcal{E}} = \underline{\mathcal{E}}_p + \underline{\mathcal{E}}_s. \quad (10.169)$$

As discussed in Section 4.9 the surface polarization $\underline{\mathcal{M}}_{Aes}$ has to be determined such that the tangential component of the electrical field vanishes on the surface A_{ob} of the obstacle. With the unit form n_{ob} normal to the surface A_{ob} , this condition is written as

$$n_{ob} \wedge \underline{\mathcal{E}} = n_{ob} \wedge (\underline{\mathcal{E}}_p + \underline{\mathcal{E}}_s) = 0. \quad (10.170)$$

The complete electromagnetic field can be determined by solving the integral equation for this problem.

Choosing l such that the transverse electric field vanishes at $z = -\frac{1}{2}l$, we obtain from (8.39)

$$X_1 + 2X_2 = -Z_0 \tan \beta l. \quad (10.171)$$

From (10.168) and (10.171) we get

$$\frac{X_1 + 2X_2}{Z_0} = -\frac{\Im\{R_{sp}\}}{\Re\{R_{sp}\}}. \quad (10.172)$$

The reaction R_{11} can be decomposed as follows

$$R_{11} = j\omega \int_V \underline{\mathcal{E}} \wedge \underline{\mathcal{M}}_{e0t}^{\text{eff}} = j\omega \int_V (\underline{\mathcal{E}}_p + \underline{\mathcal{E}}_s) \wedge \underline{\mathcal{M}}_{e0t}^{\text{eff}} = R_{pp} + R_{sp}. \quad (10.173)$$

Since the total transverse electric field vanishes at $z = -\frac{1}{2}l$, we obtain $R_{11} = 0$, hence

$$R_{pp} = -R_{sp}. \quad (10.174)$$

Due to reciprocity we obtain

$$R_{sp} = R_{ps} = j\omega \int_{V_{ob}} \underline{\mathcal{E}}_p \wedge \underline{\mathcal{M}}_{eob}, \quad (10.175)$$

where the integration is performed over the obstacle. From (10.170) and (10.175) it follows

$$R_{ps} = -R_{ss} = -j\omega \int_{V_{ob}} \underline{\mathcal{E}}_s \wedge \underline{\mathcal{M}}_{eob}. \quad (10.176)$$

This yields with (10.172)

$$\frac{X_1 + 2X_2}{Z_0} = -\frac{\Im\{R_{ss}\}}{\Re\{R_{ss}\}}. \quad (10.177)$$

10.10 THE SYMMETRY PROPERTIES OF WAVEGUIDE JUNCTIONS

The complete analysis of distributed circuits by solving Maxwell's equations requires a considerable mathematical effort also in the case of simple structures. For waveguide circuits exhibiting geometric symmetries from the symmetry properties of the circuits, symmetry properties of the scattering matrices also follow. Also from general considerations we can get important information about the scattering matrix of a multiport. For example, we know that the scattering matrix of a reciprocal passive lossless multiport must be symmetric and unitary.

We will show in the following that from geometric symmetry considerations we can get additional information about the scattering matrix and the scattering matrix from this may be determined with the exception of only a few unknown parameters. If, for example, only a single parameter may not be determined from computation, in many cases the experimental determination of this parameter may be a good solution.

We consider multiports exhibiting certain geometric symmetries. If, for example, the geometric structure of a multiport exhibits symmetry with respect to the rotation around an axis or with respect to mirroring at a symmetry plane, this rotation and this mirroring are *symmetry operations* for that multiport. The multiport is said to be invariant with respect to these symmetry operations. In that case the field solution remains unchanged if the symmetry operation is performed to the multiport. If the arrows indicating the direction of the field remain unchanged when the symmetry operation is performed, the scattering matrix remains unchanged under this symmetry operation.

The mirroring of the multiport structure may yield a change of sign of field components. Considering the mirroring in the yz -plane, we obtain

$$x \rightarrow -x, \quad y \rightarrow y, \quad z \rightarrow z. \quad (10.178)$$

Making this substitution in Maxwell's equation, this will yield the following changes in the field components:

$$\begin{aligned} \underline{E}_x(x, y, z) &\rightarrow -\underline{E}_x(-x, y, z), & \underline{E}_y(x, y, z) &\rightarrow \underline{E}_y(-x, y, z), \\ \underline{E}_z(x, y, z) &\rightarrow \underline{E}_z(-x, y, z), & \underline{H}_x(x, y, z) &\rightarrow \underline{H}_x(-x, y, z), \\ \underline{H}_y(x, y, z) &\rightarrow -\underline{H}_y(-x, y, z), & \underline{H}_z(x, y, z) &\rightarrow -\underline{H}_z(-x, y, z). \end{aligned} \quad (10.179)$$

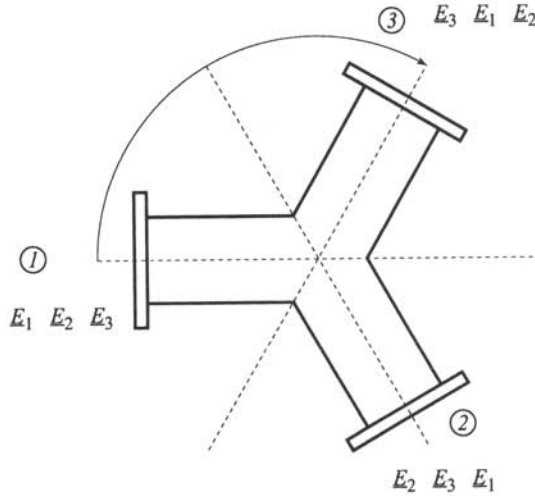


Figure 10.30: Fully symmetric three-port parallel waveguide junction.

Let $\underline{E}_{tr,i}$ be the transverse component of the electric field intensity in a certain point of the reference plane of the i th multiport. We assume that by a certain symmetry operation ports i and j are transformed into ports k and l , respectively. From this it follows that

$$\underline{E}_{tr,i} \rightarrow \delta_1 \underline{E}_{tr,k} \quad \underline{E}_{tr,j} \rightarrow \delta_2 \underline{E}_{tr,l} \quad \delta_1, \delta_2 = \pm 1. \quad (10.180)$$

Depending on the change of sign of the transverse electric fields in ports j and k , the matrix element S_{kl} remains unchanged or changes its sign when the symmetry operation is performed, following the rule

$$S_{ij} = \delta_1 \delta_2 S_{kl}. \quad (10.181)$$

10.10.1 Symmetric Three-Port Waveguide Junctions

We consider the fully symmetric three-port *parallel waveguide junction* according to Figure 10.30. The three waveguide segments are long enough that any perturbation of the field distribution occurring in the center region where all three waveguides are connected already has decayed in the port plane. We can assume that in the port plane the transverse field distribution corresponds to the TE_{10} mode. We assume the waveguide three-port parallel waveguide junction to be reciprocal and lossless. In the case of the parallel waveguide junction the broader side of the rectangular waveguide

is in parallel to the plane of the drawing. The electric field is normal to the plane of the drawing. This corresponds to the case of parallel circuited transmission-lines. Therefore, this junction is called a parallel junction. The circuit is invariant with respect to rotation by 120° around an axis normal to the plane of the drawing. Furthermore, the structure exhibits three symmetry planes normal to the plane of the drawing. We allow a lossless scattering object in the center of the waveguide junction and we make the general assumption that the symmetry properties of the waveguide junction are not disturbed by this scatterer. The rotation of the waveguide branch by 120° affects the following interchange of field quantities:

$$\underline{E}_1 \rightarrow \underline{E}_2, \quad \underline{E}_2 \rightarrow \underline{E}_3, \quad \underline{E}_3 \rightarrow \underline{E}_1. \quad (10.182)$$

With (10.181) we obtain from this

$$S_{11} = S_{22} = S_{33}, \quad S_{12} = S_{23} = S_{31}. \quad (10.183)$$

The mirroring in the symmetry plane parallel to the axis of waveguide branch 1 affects the following interchanges of electric field components

$$\underline{E}_1 \rightarrow \underline{E}_1, \quad \underline{E}_2 \rightarrow \underline{E}_3, \quad \underline{E}_3 \rightarrow \underline{E}_2. \quad (10.184)$$

From this it follows that

$$S_{23} = S_{32}. \quad (10.185)$$

Due to the reciprocity, this relation also follows from (10.96). Due to (10.183) and (10.185) the scattering matrix now is determined with the exception of the two complex parameters ρ and τ :

$$S = \begin{bmatrix} \rho & \tau & \tau \\ \tau & \rho & \tau \\ \tau & \tau & \rho \end{bmatrix}. \quad (10.186)$$

Assuming the junction to be lossless, we obtain from (10.79)

$$|\rho|^2 + 2|\tau|^2 = 1, \quad (10.187a)$$

$$\rho^* \tau + \rho \tau^* = -|\tau|^2. \quad (10.187b)$$

Expressing the left side of (10.187b) by magnitude $2|\rho||\tau|$ and phase ϕ ,

$$\rho^* \tau + \rho \tau^* = 2|\rho||\tau| \cos \phi \quad (10.188)$$

we obtain with (10.187b)

$$2|\rho| \cos \phi = -|\tau|. \quad (10.189)$$

After inserting (10.187a), we obtain

$$|\rho|^2(1 + 8 \cos^2 \phi) = 1. \quad (10.190)$$

We see that the fully symmetric parallel junction with three terminations cannot simultaneously be realized as a matched multiport (i.e., with $\rho = 0$). The minimum value of ρ is obtained for $\cos^2 \phi = 1$. In this case we obtain

$$|\rho| = \frac{1}{3}, \quad |\tau| = \frac{2}{3}. \quad (10.191)$$

Furthermore, it follows from (10.189) that $\cos \phi$ must be negative. With $\cos \phi = -1$, we obtain from (10.188)

$$\Re\{\rho\tau^*\} = -|\rho||\tau| \quad (10.192)$$

and from this with (10.191)

$$\rho = -\frac{1}{3}e^{-j\phi_1}, \quad \tau = \frac{2}{3}e^{-j\phi_1}, \quad (10.193)$$

where $e^{-j\phi_1}$ is a parameter depending on the length of the waveguide arms. Using symmetry and power considerations we could determine the scattering matrix of the completely symmetric parallel junction with three arms with the exception of a remaining scalar parameter ϕ_1 . The optimization of the parameter ϕ_1 may be accomplished empirically by variation of the scatterer introduced in the center of the parallel junction.

We have seen that a matched completely symmetric lossless three-port parallel junction cannot be realized. It can be shown in general that a matched lossless reciprocal three-port cannot be realized. A matched three-port must be characterized by the scattering matrix

$$\mathbf{S} = \begin{bmatrix} 0 & S_{12} & S_{13} \\ S_{12} & 0 & S_{23} \\ S_{13} & S_{23} & 0 \end{bmatrix}. \quad (10.194)$$

If the three-port is lossless, the scattering matrix must be unitary. With (10.79) we obtain from (10.194)

$$\begin{aligned} S_{13}S_{23}^* &= 0, \\ S_{12}S_{13}^* &= 0, \\ S_{12}S_{23}^* &= 0. \end{aligned} \quad (10.195)$$

These equations may only be fulfilled if at least two of the S_{ik} are vanishing.

10.10.2 Symmetric Four-Port Waveguide Junctions

The so-called *directional coupler* according to Figure 10.31 exhibits two symmetry planes normal to the plane of the drawing. Mirroring in symmetry plane 1 yields the following interchanges of field components

$$\underline{E}_1 \rightarrow \underline{E}_3, \quad \underline{E}_2 \rightarrow \underline{E}_4, \quad \underline{E}_3 \rightarrow \underline{E}_1, \quad \underline{E}_4 \rightarrow \underline{E}_2. \quad (10.196)$$

From this it follows for the scattering matrix

$$\begin{aligned} S_{11} &= S_{33}, & S_{22} &= S_{44}, \\ S_{12} &= S_{34}, & (S_{13} &= S_{31}), \\ S_{14} &= S_{32}, & (S_{24} &= S_{42}). \end{aligned} \quad (10.197)$$

The bracketed conditions already followed from reciprocity. From the mirroring in the second symmetry plane we obtain the following exchanges

$$\underline{E}_1 \rightarrow \underline{E}_2, \quad \underline{E}_2 \rightarrow \underline{E}_1, \quad \underline{E}_3 \rightarrow \underline{E}_4, \quad \underline{E}_4 \rightarrow \underline{E}_3 \quad (10.198)$$

and from this the following additional conditions for the scattering matrix

$$S_{11} = S_{22}, \quad S_{33} = S_{44}, \quad S_{13} = S_{24}. \quad (10.199)$$

With this the scattering matrix is determined with the exception of four complex parameters ρ , τ_1 , τ_2 , and τ_3 .

$$S = \begin{bmatrix} \rho & \tau_1 & \tau_2 & \tau_3 \\ \tau_1 & \rho & \tau_3 & \tau_2 \\ \tau_2 & \tau_3 & \rho & \tau_1 \\ \tau_3 & \tau_2 & \tau_1 & \rho \end{bmatrix}. \quad (10.200)$$

We now assume the multiport to be matched so that $\rho = 0$ is valid. This may be achieved, for example, if both waveguides in Figure 10.31 are only weakly coupled over small holes or if the coupling region of both waveguides is long enough so that a coupling of waves in the forward and backward directions will not occur. Assuming the directional coupler to be lossless, we obtain from (10.79)

$$\Re\{\tau_2^* \tau_3\} = 0, \quad \Re\{\tau_1^* \tau_3\} = 0, \quad \Re\{\tau_2^* \tau_1\} = 0. \quad (10.201)$$

These three equations mean that the three complex quantities τ_1 , τ_2 and τ_3 are mutually orthogonal in the complex number plane. Hence one of these quantities must vanish. Without restriction of generality we assume $\tau_1 = 0$ and obtain the scattering matrix

$$S = \begin{bmatrix} 0 & S_{12} \\ S_{12}^T & 0 \end{bmatrix}, \quad (10.202)$$

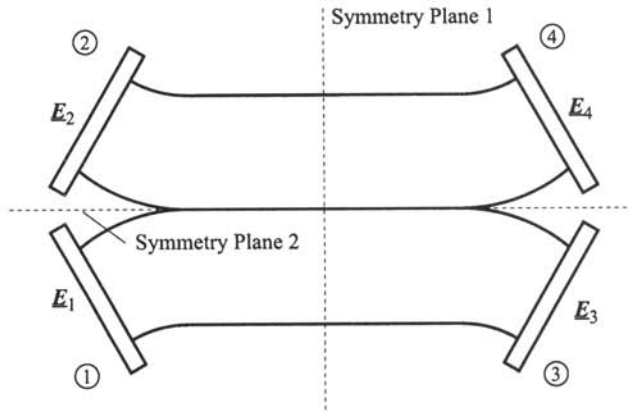


Figure 10.31: Directional coupler.

where the submatrix S_{12} is given by

$$S_{12} = S_{12}^T = \begin{bmatrix} \tau_2 & \tau_3 \\ \tau_3 & \tau_2 \end{bmatrix}. \quad (10.203)$$

Due to (10.79), S_{12} also must be unitary and we obtain

$$|\tau_2|^2 + |\tau_3|^2 = 1. \quad (10.204)$$

The scattering matrix of the matched lossless directional coupler only depends on a parameter τ_3 and with the exception of a phase factor it is given by

$$\begin{bmatrix} 0 & 0 & \sqrt{1-k^2} & \pm jk \\ 0 & 0 & \pm jk & \sqrt{1-k^2} \\ \sqrt{1-k^2} & \pm jk & 0 & 0 \\ \pm jk & \sqrt{1-k^2} & 0 & 0 \end{bmatrix}. \quad (10.205)$$

For the 3 dB coupler we obtain

$$k = \frac{1}{\sqrt{2}}. \quad (10.206)$$

The *hybrid junction* or *magic T*, respectively, according to Figure 10.32 exhibits only a symmetry plane $z = 0$. In the ports 1 to 3 the electric field lines are parallel to the symmetry plane, whereas in port 4 the electric field is normal to the symmetry

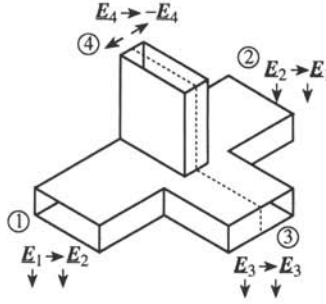


Figure 10.32: Hybrid junction.

plane. According to (10.179) the mirroring in the symmetry plane yields the following interchange of the electric field components

$$\underline{E}_1 \rightarrow \underline{E}_2, \quad \underline{E}_2 \rightarrow \underline{E}_1, \quad \underline{E}_3 \rightarrow \underline{E}_3, \quad \underline{E}_4 \rightarrow -\underline{E}_4. \quad (10.207)$$

Ports 1 and 2 are interchanged in the mirroring, whereas ports 3 and 4 are transformed into themselves. Since the electric field in port 4 is normal to the symmetry plane, the sign of \underline{E}_4 is changed in the case of the mirroring. With (10.180) and (10.181) we obtain the following relations for the scattering parameters:

$$S_{11} = S_{22}, \quad S_{13} = S_{23}, \quad S_{14} = -S_{24}, \quad S_{34} = -S_{34} = 0. \quad (10.208)$$

From this it follows that ports 3 and 4 are not directly coupled with each other. Therefore it must be possible to insert independently matching elements in arms 3 and 4 of the hybrid junction and to tune S_{33} and S_{44} independently such that

$$S_{33} = S_{44} = 0 \quad (10.209)$$

is valid. The tuning elements must be inserted in such a way that the symmetry is maintained. If ports 3 and 4 are tuned to be free of reflection, the scattering matrix assumes the following form:

$$\begin{bmatrix} \alpha & \beta & \gamma & \delta \\ \beta & \alpha & \gamma & -\delta \\ \gamma & \gamma & 0 & 0 \\ \delta & -\delta & 0 & 0 \end{bmatrix}. \quad (10.210)$$

Assuming the circuit to be lossless, we obtain from (10.79)

$$|\alpha|^2 + |\beta|^2 + |\gamma|^2 + |\delta|^2 = 1, \quad 2|\gamma|^2 = 1, \quad 2|\delta|^2 = 1. \quad (10.211)$$

From this we obtain

$$\alpha = \beta = 0, \quad |\gamma| = |\delta| = \frac{1}{\sqrt{2}}. \quad (10.212)$$

Therefore ports 1 and 2 are not coupled directly with each other. The scattering matrix according to (10.210) again describes a directional coupler. It may be shown in general that every matched lossless reciprocal four-port is a directional coupler. We can determine the lengths of arms 3 and 4 independently and therefore we may choose independently the phases of γ and δ . Without loss of generality we are choosing γ and δ to be positive and real and obtain

$$S = \frac{1}{\sqrt{2}} \begin{bmatrix} 0 & 0 & 1 & 1 \\ 0 & 0 & 1 & -1 \\ 1 & 1 & 0 & 0 \\ 1 & -1 & 0 & 0 \end{bmatrix}. \quad (10.213)$$

10.11 PROBLEMS

- Consider the two-port described by the admittance matrix $S = j \begin{pmatrix} B_1+B_3 & -B_3 \\ -B_3 & B_2+B_3 \end{pmatrix}$ with $B_i = G_i \left(\frac{\omega}{\omega_i} - \frac{\omega_i}{\omega} \right)$ for $i = 1, 2, 3$.
 - Draw the Foster admittance representation of this three-port and determine the circuit elements.
 - Compute the impedance matrix of this three-port.
 - Draw the Foster impedance representation of this three-port and determine the circuit elements.
- Consider a hybrid T-junction (magic T) terminated at ports 1 and 2 with loads with reflection factors ρ_1 and ρ_2 . The TE branch (port 3) is terminated with an RF source and the TM branch (port 4) with a detector.
 - Give the scattering matrix for the ports 3 and 4 as a function of the parameters ρ_1 and ρ_2 .
 - Which amount of energy is detected when the source is supplying a wave amplitude a_0 and the detector exhibits no reflection?
- Consider the four-port depicted in Figure 10.33.
 - Give the Z , Y and S matrices of this four-port.
 - Which representations exist for $Z_1 \rightarrow 0$?
 - Which representations exist for $Z_2 \rightarrow \infty$?
 - Which representations exist for $Z_1 \rightarrow 0$ and $Z_2 \rightarrow \infty$?
- A circulator is a nonreciprocal circuit, usually realized with unsymmetrically anisotropic magnetic material. The scattering matrix of a circulator four-port

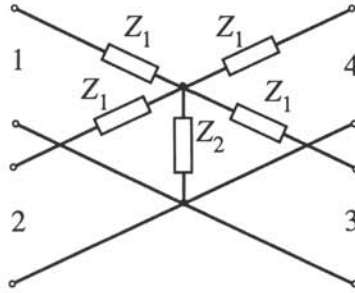


Figure 10.33: Multiport.

is given by $S = \begin{pmatrix} 0 & 0 & 0 & 1 \\ 1 & 0 & 0 & 0 \\ 0 & 1 & 0 & 0 \\ 0 & 0 & 1 & 0 \end{pmatrix}$. Terminate port 2 with a reflection factor ρ and port 4 reflection free. Give the scattering matrix of the resulting two-port.

5. An optical ring-interferometer can be easily described as a trunk of optical fiber, a laser, a detector, and a 3 dB directional coupler. For the optical fiber the condition of monomode propagation will be assumed. The scattering matrix for this trunk of line is $S = \begin{pmatrix} 0 & \exp(j(\phi + \frac{1}{2}\Delta\phi)) \\ \exp(j(\phi - \frac{1}{2}\Delta\phi)) & 0 \end{pmatrix}$. For $\Delta\phi \neq 0$ (due to an external static magnetic field), the optical fiber is nonreciprocal. The optical fiber is connected to ports 3 and 4 of the 3 dB directional coupler, the detector to port 2, and the laser to port 1. How much power P_1 and P_2 flows out from ports 1 and 2 of the 3 dB directional coupler in case of matched detector?
6. Compare a lossless transmission-line of characteristic impedance Z_0 and length $\frac{1}{4}\lambda$ with a gyrator with the gyration conductance $G_g = 1/Z_0$.
 - a) Compare the input impedance for the $\frac{1}{4}\lambda$ -line and the gyrator terminated with ρ .
 - b) Compute the signal transmission behavior in both cases.
7. Consider the fully symmetric three-port waveguide junction ($\rho = -\frac{1}{3}$, $\tau = \frac{2}{3}$), which is terminated at port 3 by various types of load. Give the scattering matrix for the remaining two-port in the case of
 - a) port 3 terminated reflection-free,
 - b) port 3 short-circuited,
 - c) port 3 left open.
8. Consider a sphere of radius $r = 10$ cm.
 - a) Compute the wave impedances Z_{mn}^{+TE} and Z_{mn}^{+TM} characterizing the tangential field at the sphere for $n = 1, 2, 3$ and the frequencies 1 GHz, 10 GHz, and 100 GHz.
 - b) Draw the Cauer equivalent circuits for the wave impedances Z_{mn}^{+TE} and Z_{mn}^{+TM} for $n = 1, 2, 3$ and determine the values of the circuit elements.

- c) Determine the complex power flowing through the sphere in the above cases.
- d) How does the complex power flowing through the surface of the sphere change when the radius of the sphere is changed to $r = 20$ cm?

REFERENCES

- [1] C. G. Montgomery, R. H. Dicke, and E. M. Purcell, *Principles of Microwave Circuits*. New York: McGraw-Hill, 1948.
- [2] H. Brand, *Schaltungslehre linearer Mikrowellennetze*. Stuttgart: Hirzel, 1970.
- [3] R. E. Collin, *Foundations of Microwave Engineering*. New York: McGraw-Hill, 1992.
- [4] G. H. Owyang, *Foundations for Microwave Circuits*. Berlin: Springer, 1989.
- [5] H. J. Carlin and A. B. Giordano, *Network Theory*. Englewood Cliffs, NJ: Prentice Hall, 1964.
- [6] B. D. H. Tellegen, "A general network theorem with applications," *Philips Research Reports*, vol. 7, pp. 259–269, 1952.
- [7] B. D. H. Tellegen, "A general network theorem with applications," *Proc. Inst. Radio Engineers*, vol. 14, pp. 265–270, 1953.
- [8] P. Penfield, R. Spence, and S. Duinker, *Tellegen's Theorem and Electrical Networks*. Cambridge, Massachusetts: MIT Press, 1970.
- [9] P. Russer, M. Mongiardo, and L. Felsen, "Electromagnetic field representations and computations in complex structures III: Network representations of the connection and subdomain circuits," *Int. J. Numer. Modeling*, vol. 15, pp. 127–145, 2002.
- [10] C. A. Desoer and E. S. Kuh, *Basic Circuit Theory*. New York: Mc Graw Hill, 1969.
- [11] K. C. Gupta, R. Garg, and R. Chadha, *Computer-Aided Design of Microwave Circuits*. Boston: Artech House, 1981.
- [12] J. A. Dobrowolski, *Introduction to Computer Methods for Microwave Circuit Analysis and Design*. Boston: Artech House, 1991.
- [13] L. B. Felsen, M. Mongiardo, and P. Russer, "Electromagnetic field representations and computations in complex structures I: Complexity architecture and generalized network formulation," *Int. J. Numer. Modeling*, vol. 15, pp. 93–107, 2002.
- [14] J. K. Hunton, "Analysis of microwave measurement techniques by means of signal flow graphs," *IEEE Trans. Microwave Theory Techn.*, vol. 8, pp. 206–212, Mar. 1960.
- [15] H. J. Michel, *Zweitor-Analyse mit Leistungswellen*. Stuttgart: Teubner, 1981.
- [16] E. A. Wolff and R. Kaul, *Microwave Engineering and Systems Applications*. Boston: Wiley, 1988.
- [17] P. Russer and A. C. Cangellaris, "Network-oriented modeling, complexity reduction and system identification techniques for electromagnetic systems," *Proc. 4th Int. Workshop on Computational Electromagnetics in the Time-Domain: TLM/FDTD and Related Techniques, 17–19 September 2001 Nottingham*, pp. 105–122, Sept. 2001.
- [18] R. E. Collin, *Field Theory of Guided Waves*. New York: IEEE Press, 1991.
- [19] W. Cauer, *Theorie der linearen Wechselstromschaltungen*. Berlin: Akademie-Verlag, 1954.
- [20] V. Belevitch, *Classical Network Theory*. San Francisco, California: Holden-Day, 1968.
- [21] L. Chu, "Physical limitations of omni-directional antennas," *J. Appl. Physics*, vol. 19, pp. 1163–1175, Dec. 1948.
- [22] R. F. Harrington, *Time Harmonic Electromagnetic Fields*. New York: McGraw-Hill, 1961.
- [23] L. B. Felsen and N. Marcuvitz, *Radiation and Scattering of Waves*. Englewood Cliffs, NJ: Prentice Hall, 1972.
- [24] T. Mangold and P. Russer, "Modeling of multichip module interconnections by the TLM method and system identification," *Proc. 27th European Microwave Conference, Jerusalem*, pp. 538–543, Sept. 1997.
- [25] T. Mangold and P. Russer, "Full-wave modeling and automatic equivalent-circuit generation of millimeter-wave planar and multilayer structures," *IEEE Trans. Microwave Theory Techn.*, vol. 47, pp. 851–858, June 1999.
- [26] V. Chitchekatourov, W. Fisch, F. Coccetti, and P. Russer, "Full-wave analysis and model-based parameter estimation approaches for s- and y- matrix computation of microwave distributed circuits," in *2001 Int. Microwave Symposium Digest, Phoenix*, pp. 1037–1040, 2001.

Chapter 11

Periodic Structures and Filters

11.1 PERIODIC ELECTROMAGNETIC STRUCTURES

Periodic electromagnetic structures exhibit numerous applications as frequency-selective structures and slow-wave structures [1–4].

With the space-dependent real permittivity $\epsilon(\mathbf{x})$ and the space-dependent real permeability $\mu(\mathbf{x})$ for source-free regions Maxwell's equations (2.124a) and (2.124b) become

$$\mathbf{d} \underline{\mathcal{H}}(\mathbf{x}) = \mathbf{j} \omega \epsilon(\mathbf{x}) * \underline{\mathcal{E}}(\mathbf{x}), \quad (11.1a)$$

$$\mathbf{d} \underline{\mathcal{E}}(\mathbf{x}) = -\mathbf{j} \omega \mu(\mathbf{x}) * \underline{\mathcal{H}}(\mathbf{x}). \quad (11.1b)$$

Eliminating either $\underline{\mathcal{E}}(\mathbf{x})$ or $\underline{\mathcal{H}}(\mathbf{x})$ yields the second-order equations for an inhomogeneous isotropic medium

$$\epsilon^{-1}(\mathbf{x}) * \mathbf{d} \mu^{-1}(\mathbf{x}) * \mathbf{d} \underline{\mathcal{E}}(\mathbf{x}) + \omega^2 \underline{\mathcal{E}}(\mathbf{x}) = 0, \quad (11.2a)$$

$$\mu^{-1}(\mathbf{x}) * \mathbf{d} \epsilon^{-1}(\mathbf{x}) * \mathbf{d} \underline{\mathcal{H}}(\mathbf{x}) + \omega^2 \underline{\mathcal{H}}(\mathbf{x}) = 0. \quad (11.2b)$$

Either one of the above equations is self-contained. We can derive the solution for the complete electromagnetic field by solving just one of them. If only $\epsilon(\mathbf{x})$ depends on space and μ is uniform we obtain from (11.2a)

$$* \mathbf{d} * \mathbf{d} \underline{\mathcal{E}}(\mathbf{x}) + \omega^2 \epsilon(\mathbf{x}) \mu \underline{\mathcal{E}}(\mathbf{x}) = 0. \quad (11.3)$$

11.1.1 TE Modes in Rectangular Periodic Waveguides

Consider a rectangular waveguide filled with a dielectric having a permittivity varying periodically in z -direction as shown in Figure 11.1. For the electric field form $\underline{\mathcal{E}}(\mathbf{x})$ of

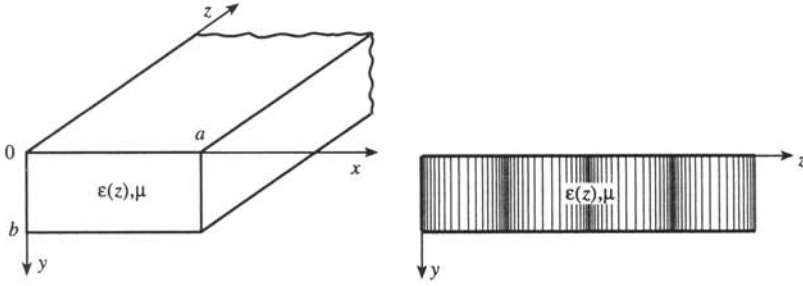


Figure 11.1: Waveguide with rectangular cross-section.

the transverse electric TE_{mn} mode we make the ansatz

$$\underline{\mathcal{E}}_{mn}^{TE}(\mathbf{x}) = \underline{V}_{mn}^{TE} e_{mn}^{TE}(x, y) f_{mn}^{TE}(z), \quad (11.4)$$

where \underline{V}_{mn}^{TE} is a complex voltage amplitude, $e_{mn}^{TE}(x, y)$ is the electric structure form introduced in (7.198a), and $f_{mn}^{TE}(z)$ describes the longitudinal variation of the field. To solve (11.3) we first consider the first term on its left-hand side,

$$\begin{aligned} \star d \star d [f_{mn}^{TE}(z) e_{mn}^{TE}(x, y)] &= f_{mn}^{TE}(z) \star d_t \star d_t e_{mn}^{TE}(x, y) \\ &\quad + \frac{df_{mn}^{TE}(z)}{dz} \star dz \wedge \star [d_t e_{mn}^{TE}(x, y)] \\ &\quad - \frac{d^2 f_{mn}^{TE}(z)}{dz^2} \star dz \wedge \star [dz \wedge e_{mn}^{TE}(x, y)]. \end{aligned} \quad (11.5)$$

On the right-hand side of this equation the second term vanishes and in the third term the two-fold application of the operator $\star dz \wedge (\cdot)$ means a rotation of $e(x, y)$ by 180° . Therefore we obtain

$$\star d \star d [f_{mn}^{TE}(z) e_{mn}^{TE}(x, y)] = f_{mn}^{TE}(z) \star d_t \star d_t e_{mn}^{TE}(x, y) + \frac{d^2 f_{mn}^{TE}(z)}{dz^2} e_{mn}^{TE}(x, y). \quad (11.6)$$

Due to (7.216a) the structure function of the TE_{mn} mode fulfills

$$\star d_t \star d_t e_{mn}^{TE}(x, y) = -\beta_{c, TE_{mn}}^2 e_{mn}^{TE}(x, y), \quad (11.7)$$

where $\beta_{c, TE_{mn}}$ is the cutoff phase coefficient of the TE_{mn} mode. Inserting this into (11.6) yields

$$\star d \star d [f_{mn}^{TE}(z) e_{mn}^{TE}(x, y)] = \left[\beta_{c, TE_{mn}}^2 f_{mn}^{TE}(z) - \frac{d^2 f_{mn}^{TE}(z)}{dz^2} \right] e_{mn}^{TE}(x, y). \quad (11.8)$$

Let the permittivity $\epsilon(z)$ depend on the longitudinal coordinate z only. We insert (11.4) and (11.7) into (11.3) and obtain

$$\left[\frac{d^2 f_{mn}^{\text{TE}}(z)}{dz^2} + (\omega^2 \epsilon(z) \mu - \beta_{c, \text{TE}mn}^2) f_{mn}^{\text{TE}}(z) \right] e_{mn}^{\text{TE}}(x, y) = 0. \quad (11.9)$$

The TE_{mn} mode for the longitudinally inhomogeneous rectangular waveguide has the same transverse field distribution as the TE_{mn} mode of the longitudinally homogeneous waveguide. The longitudinal field variation is described by $f_{mn}^{\text{TE}}(z)$, which is a solution of the ordinary differential equation

$$\frac{d^2 f(z)}{dz^2} + (\omega^2 \epsilon(z) \mu - \beta_c^2) f(z) = 0. \quad (11.10)$$

In this equation and in the following equations we omit the indices TE , m and n in order to simplify the notation.

Let the period of the longitudinal variation of the permittivity be p . In this case we have

$$\epsilon(z + p) = \epsilon(z). \quad (11.11)$$

Introducing κ as

$$\kappa(z) = \omega^2 \epsilon(z) \mu - \beta_{c, \text{TE}mn}^2 \quad (11.12)$$

the differential equation (11.10) assumes the form

$$\frac{d^2 f(z)}{dz^2} + \kappa(z) f(z) = 0. \quad (11.13)$$

This second order differential equation has two fundamental solutions. Let us call these solutions $f_1(z)$ and $f_2(z)$. Furthermore the differential equation is invariant under transformations $z \rightarrow z + np$, where n is an arbitrary integer. Therefore at any $z + np$ the solutions of the differential equations must be linear combinations of the two fundamental solutions, hence

$$f_1(z + p) = \xi_{11} f_1(z) + \xi_{12} f_2(z), \quad (11.14a)$$

$$f_2(z + p) = \xi_{21} f_1(z) + \xi_{22} f_2(z), \quad (11.14b)$$

where the ξ_{ij} are coefficients to be determined. The general solution of the differential equation (11.13) is a linear combination of the particular solutions f_1 and f_2 , therefore

$$f(z) = c_1 f_1(z) + c_2 f_2(z), \quad (11.15)$$

where c_1 and c_2 are suitably determined coefficients. From (11.14a), (11.14b) and (11.15) we obtain

$$f(z + p) = (c_1 \xi_{11} + c_2 \xi_{21}) f_1(z) + (c_1 \xi_{12} + c_2 \xi_{22}) f_2(z). \quad (11.16)$$

If $f(z)$ represents a wave propagating in positive z -direction it must fulfill the relation

$$f(z+p) = e^{-\gamma p} f(z), \quad (11.17)$$

hence, (11.15) multiplied by $e^{-\gamma p}$ must be equal (11.16). This yields

$$c_1(\xi_{11} - e^{-\gamma p}) + c_2\xi_{21} = 0, \quad (11.18a)$$

$$c_1\xi_{12} + c_2(\xi_{22} - e^{-\gamma p}) = 0. \quad (11.18b)$$

We obtain a nontrivial solution for these equations only if

$$e^{-2\gamma p} - (\xi_{11} + \xi_{22})e^{-\gamma p} + \xi_{11}\xi_{22} - \xi_{12}\xi_{21} = 0 \quad (11.19)$$

is fulfilled. The solution of this quadratic equation is

$$e^{-\gamma p} = \frac{1}{2}(\xi_{11} + \xi_{22}) \pm \sqrt{\frac{1}{4}(\xi_{11} + \xi_{22})^2 - (\xi_{11}\xi_{22} - \xi_{12}\xi_{21})}. \quad (11.20)$$

Now consider the Wronsky determinant

$$W(f_1(z), f_2(z)) = \begin{vmatrix} f_1(z) & f_2(z) \\ \frac{df_1(z)}{dz} & \frac{df_2(z)}{dz} \end{vmatrix} = f_1(z) \frac{df_2(z)}{dz} - f_2(z) \frac{df_1(z)}{dz}. \quad (11.21)$$

With (11.13) we obtain for the derivative of the Wronsky determinant

$$\frac{dW(f_1(z), f_2(z))}{dz} = f_1(z) \frac{d^2 f_2(z)}{dz^2} - f_2(z) \frac{d^2 f_1(z)}{dz^2} = 0. \quad (11.22)$$

Therefore the Wronsky determinant $W(f_1(z), f_2(z)) = W$ is constant. From this and (11.14a) and (11.14b) it follows

$$\xi_{11}\xi_{22} - \xi_{12}\xi_{21} = 1. \quad (11.23)$$

We may substitute

$$\cosh \theta = \frac{1}{2}(\xi_{11} + \xi_{22}), \quad (11.24a)$$

$$\sinh \theta = \sqrt{\frac{1}{4}(\xi_{11} + \xi_{22})^2 - 1}. \quad (11.24b)$$

Inserting these equations into (11.19) yields

$$e^{-\gamma p} = e^{\pm \theta}. \quad (11.25)$$

Let us introduce the function $u(z)$ as

$$u(z) = e^{-\gamma p} f(z). \quad (11.26)$$

From (11.17) we obtain

$$u(z + p) = u(z). \quad (11.27)$$

The function $u(z)$ is periodic in z with a period p . We therefore come to the conclusion that $f(z)$ can be expressed as the product of $e^{\mp \gamma z}$ with a function $u(z)$ periodic in z with a period p ,

$$f(z) = e^{\pm \gamma z} u(z). \quad (11.28)$$

In this equation γ is a propagation constant. This proposition is known as *Floquet's theorem* [4–7].

The periodic function $u(z)$ may be expanded in a Fourier series as

$$u(z) = \sum_{n=-\infty}^{\infty} u_n e^{-j 2\pi n z / p}. \quad (11.29)$$

In the lossless case there will be propagating solutions with $\gamma = j\beta$ and evanescent solutions with $\gamma = \alpha$. The wave propagating in positive z -direction is described by

$$f(z) = \sum_{n=-\infty}^{\infty} u_n e^{-j(\beta + 2\pi n/p)z} = \sum_{n=-\infty}^{\infty} u_n e^{-j\beta_n z} \quad (11.30)$$

with

$$\beta_n = \beta + \frac{2n\pi}{p}. \quad (11.31)$$

Considering (11.29) describing a superposition of partial waves, every harmonic exhibits a different phase velocity

$$c_n = \frac{\omega}{\beta_n} = \frac{\omega}{\beta + \frac{2n\pi}{p}}. \quad (11.32)$$

The group velocity v_g , however, is the same for all harmonics,

$$v_g = \left(\frac{d\beta_n}{d\omega} \right)^{-1} = \left(\frac{d\beta}{d\omega} \right)^{-1}. \quad (11.33)$$

With (11.4) we obtain the field solution for the TE_{mn} modes for both directions of propagation

$$\underline{\mathcal{E}}_{mn}^{\text{TE}}(x) = \left(\underline{V}_{mn}^{\text{TE}(+)} e^{-\gamma_{\text{TE},mn} z} u_{mn}^{\text{TE}}(z) + \underline{V}_{mn}^{\text{TE}(-)} e^{\gamma_{\text{TE},mn} z} u_{mn}^{\text{TE}}(z) \right) e_{mn}^{\text{TE}}(x, y). \quad (11.34)$$

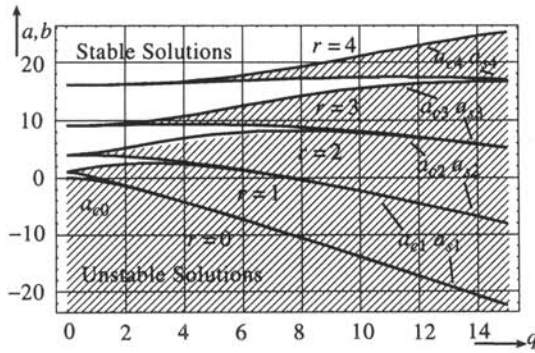


Figure 11.2: The characteristic values a_c of $\phi_c(\zeta)$ and a_s of $\phi_s(\zeta)$ as functions of q .

11.1.2 Sinusoidal Variation of the Permittivity

Consider a waveguide as depicted in Figure 11.1 filled with a dielectric medium with periodic variation in z -direction and homogeneous in transverse direction. Let $\epsilon(\mathbf{x})$ be given by

$$\epsilon(\mathbf{x}) = \epsilon_m - \Delta\epsilon \cos \kappa z, \quad (11.35)$$

where κ depends on the period p via

$$\kappa = \frac{2\pi}{p}, \quad (11.36)$$

and $\Delta\epsilon$ is the amplitude of the variation of the permittivity. Inserting this into (11.3) yields

$$\star d \star d \underline{\mathcal{E}}(\mathbf{x}) + \omega^2 \mu [\epsilon_m - \Delta\epsilon \cos(\kappa z)] \underline{\mathcal{E}}(\mathbf{x}) = 0. \quad (11.37)$$

For this case the differential equation (11.10) becomes

$$\frac{d^2 f(z)}{dz^2} + \{\omega^2 \mu [\epsilon_m - \Delta\epsilon \cos(\kappa z)] - \beta_c^2\} f(z) = 0. \quad (11.38)$$

Introducing the variable ζ , the constants a and q and the function $\eta(\zeta)$,

$$\zeta = \frac{1}{2} \kappa z, \quad (11.39a)$$

$$\eta(\zeta) = f(z), \quad (11.39b)$$

$$a = \frac{4}{\kappa^2} (\omega^2 \mu \epsilon_m - \beta_c^2), \quad (11.39c)$$

$$q = \frac{2}{\kappa^2} \omega^2 \mu \Delta\epsilon \quad (11.39d)$$

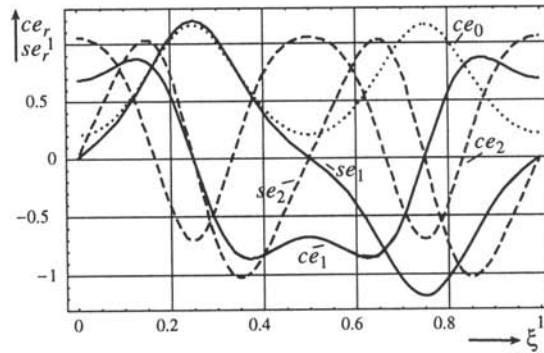


Figure 11.3: The Mathieu functions ce_0 , ce_1 , se_1 , ce_2 , se_2 for $q = 2$.

we can transform the differential equation (11.38) into the normalized form

$$\frac{d^2 \eta(\zeta)}{d\zeta^2} + (a - 2q \cos(2\zeta))\eta(\zeta) = 0. \quad (11.40)$$

This differential equation is called the *Mathieu differential equation*. The *Mathieu functions* $C(a, q, \zeta)$ and $S(a, q, \zeta)$ are solutions of this differential equation. The function $C(a, q, \zeta)$ is called the even Mathieu function and the function $S(a, q, \zeta)$ is called the odd Mathieu function, both of r th order [5, 8, 9]. For $q = 0$ the Mathieu functions are simply the harmonic functions,

$$C(a, 0, \zeta) = \cos(\sqrt{a}\zeta), \quad (11.41a)$$

$$S(a, 0, \zeta) = \sin(\sqrt{a}\zeta). \quad (11.41b)$$

For $q \neq 0$, the Mathieu functions are only periodic for the *Mathieu characteristic values* of a . The even and odd Mathieu functions with characteristic values a_{cr} and a_{sr} , respectively, are denoted $ce_r(\zeta, q)$ and $se_r(\zeta, q)$. The characteristic values a_c of $ce_r(\zeta, q)$ and a_s of $se_r(\zeta, q)$ are plotted as functions of q in Figure 11.2. The curves for the characteristic values separate the regions with stable solutions from the regions with unstable solutions. In the regions with $a_{cr} < a < a_{s,r+1}$ the solutions of the Mathieu equation are stable and describe propagating waves. For $a_{sr} < a < a_{cr}$ the solutions are unstable and describe evanescent waves. In Figure 11.2 the unstable regions are hatched.

Figure 11.3 shows the even and odd Mathieu functions $ce_r(\zeta, q)$ and $se_r(\zeta, q)$ up to second order for $q = 2$. For the even Mathieu functions the lowest order is 0, whereas for the odd Mathieu functions the lowest order is 1.

Since the coefficient of the Mathieu differential equation is periodic in ζ with a period π , it follows from Floquet's theorem that the Mathieu functions can be written

in the form

$$C(a, q, \zeta) = e^{j\nu\zeta} \phi_c(\zeta), \quad (11.42a)$$

$$S(a, q, \zeta) = e^{j\nu\zeta} \phi_s(\zeta), \quad (11.42b)$$

where $\phi_c(\zeta)$ and $\phi_s(\zeta)$ are periodic in ζ with a period π and the *Mathieu characteristic exponent* ν depends on a and q . When a belongs to the set of characteristic values a_{sr}, a_{cr} , then ν is zero or an integer. If ν is not an integer then the Floquet solutions $C(a, q, \zeta)$ and $S(a, q, \zeta)$ are linearly independent.

With the solutions (11.42a) and (11.42b) and considering (11.39a) and (11.39b) we obtain

$$f(z) = \underline{A}C(a, q, \tfrac{1}{2}\kappa z) + \underline{B}S(a, q, \tfrac{1}{2}\kappa z), \quad (11.43)$$

where a and q are given by (11.39c) and (11.39d) and \underline{A} and \underline{B} are the complex amplitudes of the even and odd waves. With (11.4) we obtain for the TE_{mn} modes of the rectangular waveguide

$$\underline{\mathcal{E}}_{mn}^{\text{TE}}(\mathbf{x}) = [\underline{V}_c(a, q, \tfrac{1}{2}\kappa z) + \underline{V}_s(a, q, \tfrac{1}{2}\kappa z)] e_{mn}^{\text{TE}}(x, y) \quad (11.44)$$

with

$$a_{mn} = \frac{4}{\kappa^2} (\omega^2 \epsilon_m \mu - \beta_{c, \text{TE}mn}^2), \quad (11.45a)$$

$$q = \frac{2}{\kappa^2} \omega^2 \mu \Delta \epsilon. \quad (11.45b)$$

These equations hold also for a TEM wave propagating in a medium with a permittivity of sinusoidal variation in the direction of propagation only. In that case $\beta_{c, \text{TE}mn}^2$ becomes zero.

11.2 WAVE PARAMETER THEORY OF TWO-PORTS

One-dimensional periodic structures also can be realized by a periodic sequence of chain-connected two-ports. In Section 3.6 we already treated planar layered media as cascaded two-ports. Multiport methods are powerful tools for the investigation of periodic electromagnetic structures.

The characteristic impedance of a transmission-line is defined as the impedance of a transmission-line of infinite length. Consider the transmission-line of infinite extension in one direction, schematically drawn in Figure 11.4(a). Let the characteristic impedance of the transmission-line be Z_0 . If the transmission-line is cut into two parts at distance l from its end and both parts are connected, this has no influence on the impedance Z_0 measured at the open end of the resulting circuit. However, we also can consider the circuit as a transmission-line segment of length l terminated by its characteristic



Figure 11.4: Termination with characteristic impedance, (a) transmission-line segment, and (b) two-port.

impedance. Considering the transmission-line segment as a symmetric two-port, we can generalize the definition of the characteristic impedance of a symmetric two-port as follows:

The characteristic impedance of a symmetric two-port is that specific impedance with which we have to terminate the two-port at one of its ports to obtain the same impedance as the input impedance at the other port.

Figure 11.4(b) shows a symmetric two-port terminated with its *characteristic impedance* Z_0 . The wave impedance of a symmetric two-port is the input impedance of an infinite chain of such two-ports. Let the symmetric two-port in Figure 11.4(b) be described by a wave impedance A . The input voltage and current $\underline{V}_1, \underline{I}_1$ are related to the output voltage and current $\underline{V}_2, \underline{I}_2$ by

$$\begin{bmatrix} \underline{V}_1 \\ \underline{I}_1 \end{bmatrix} = A \begin{bmatrix} \underline{V}_2 \\ -\underline{I}_2 \end{bmatrix}. \quad (11.46)$$

Interchanging input and output yields

$$\begin{bmatrix} \underline{V}_2 \\ \underline{I}_2 \end{bmatrix} = B \begin{bmatrix} \underline{V}_1 \\ -\underline{I}_1 \end{bmatrix}. \quad (11.47)$$

The chain matrix A and the inverse chain matrix B are related via

$$B = \begin{bmatrix} A_{11} & -A_{12} \\ A_{21} & -A_{22} \end{bmatrix}^{-1} \begin{bmatrix} 1 & 0 \\ 0 & -1 \end{bmatrix} = \frac{1}{\det A} \begin{bmatrix} A_{22} & A_{12} \\ A_{21} & A_{11} \end{bmatrix}. \quad (11.48)$$

In the chain matrix of the inverted two-port A_{11} and A_{22} are interchanged. For a symmetric two-port $A_{11} = A_{22}$ holds.

Terminating a nonsymmetric two-port A at its port 2 with a load impedance Z_{L2} as shown in Figure 11.5(a) yields an input impedance

$$Z_1 = \frac{A_{11}Z_{L2} + A_{12}}{A_{21}Z_{L2} + A_{22}}. \quad (11.49)$$

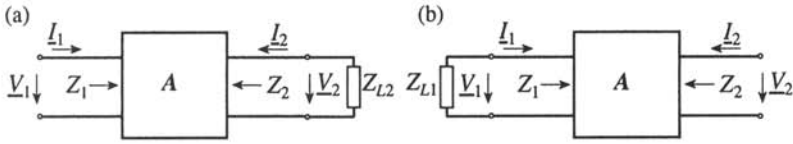


Figure 11.5: Termination of two-ports with characteristic impedance.

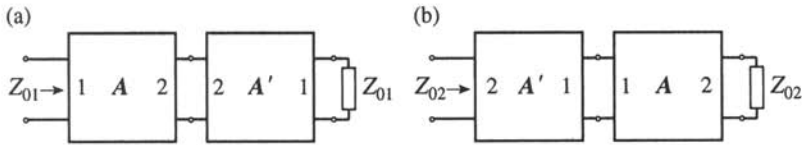


Figure 11.6: Cascading of a two-port with its inverted two-port.

For a symmetric two-port the characteristic impedance must be mapped into itself. With $Z_1 = Z_{L2} = Z_0$ and $A_{11} = A_{22}$ we obtain from the above equation

$$Z_0 = \frac{A_{11}Z_0 + A_{12}}{A_{21}Z_0 + A_{11}}. \quad (11.50)$$

This yields

$$Z_0 = \sqrt{\frac{A_{12}}{A_{21}}}. \quad (11.51)$$

To generalize the characteristic impedance concept for the case of nonsymmetric two-ports as depicted in Figure 11.5 we consider the chain connection of a nonsymmetric two-port with its inverted two-port (i.e., the two-port we obtain by exchanging the two ports). In this way we can form two different symmetric two-ports, as shown in Figure 11.6. For each of these two symmetric two-ports we can define a wave impedance. The wave impedance of the two-port shown in Figure 11.6(a) is Z_{01} and characteristic impedance of the two-port in Figure 11.6(b) is Z_{02} . The wave impedance Z_{01} is the input impedance of an infinite chain of cascaded pairs A, A' and the wave impedance Z_{02} is the input impedance of an infinite chain of cascaded pairs A', A . With the exception of the first two-port, both infinite chains are identical. If A is the first two-port in the infinite chain, the input impedance will be Z_{01} . Removing the first two-port of the infinite chain yields an infinite chain beginning with the inverted two-port A' . The input impedance of this chain now is Z_{02} . We now can define two *characteristic*

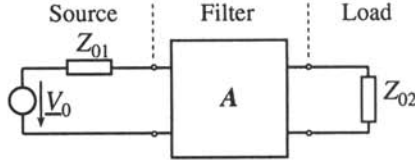


Figure 11.7: Filter two-port terminated with its image impedances.

impedances of the nonsymmetric two-port, such that

$$Z_{01} = \frac{A_{11}Z_{02} + A_{12}}{A_{21}Z_{02} + A_{22}}, \quad (11.52a)$$

$$Z_{02} = \frac{A_{22}Z_{01} + A_{12}}{A_{21}Z_{01} + A_{11}}. \quad (11.52b)$$

From these equations we obtain the characteristic impedances

$$Z_{01} = \sqrt{\frac{A_{11}A_{12}}{A_{21}A_{22}}}, \quad (11.53a)$$

$$Z_{02} = \sqrt{\frac{A_{22}A_{12}}{A_{21}A_{11}}}. \quad (11.53b)$$

Consider a filter two-port A terminated with its image impedances Z_{01} and Z_{02} as shown in Figure 11.7. The forward voltage transfer ratio A_V and the forward current transfer ratio A_I are given by

$$A_V = \frac{V_2}{V_1} = \frac{Z_{02}}{Z_{02}A_{11} + A_{12}}, \quad (11.54a)$$

$$A_I = \frac{-I_2}{I_1} = \frac{1}{Z_{02}A_{21} + A_{22}}. \quad (11.54b)$$

Inserting (11.53a) and (11.53b) yields

$$A_V = \sqrt{\frac{A_{22}}{A_{11}}} \frac{1}{\sqrt{A_{11}A_{22}} + \sqrt{A_{12}A_{21}}}, \quad (11.55a)$$

$$A_I = \sqrt{\frac{A_{11}}{A_{22}}} \frac{1}{\sqrt{A_{11}A_{22}} + \sqrt{A_{12}A_{21}}}. \quad (11.55b)$$

We define a *propagation factor* for the filter two-port by

$$e^{-g} = \frac{1}{\sqrt{A_{11}A_{22}} + \sqrt{A_{12}A_{21}}}, \quad (11.56)$$

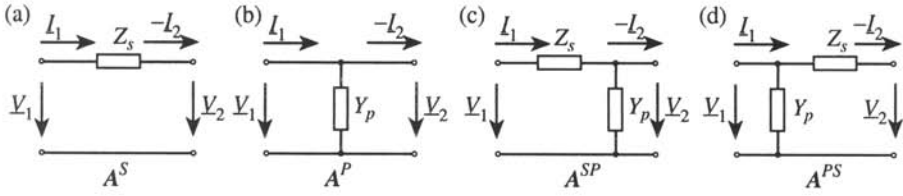


Figure 11.8: (a) Series element, (b) parallel element, (c) SP element, and (d) PS element.

where the g is a logarithmic attenuation measure. Since the determinant of reciprocal multiports is 1, as shown in (10.95), we obtain from (11.56)

$$e^{-g} = \sqrt{A_{11}A_{22}} - \sqrt{A_{12}A_{21}}. \quad (11.57)$$

We can synthesize ladder networks by cascading series- and shunt two-ports. The chain matrix of the series element depicted in Figure 11.8(a) is

$$A^S = \begin{bmatrix} 1 & Z_s \\ 0 & 1 \end{bmatrix}. \quad (11.58)$$

The parallel element of Figure 11.8(b) has the chain matrix

$$A^P = \begin{bmatrix} 1 & 0 \\ Y_p & 1 \end{bmatrix}. \quad (11.59)$$

Cascading a series and a parallel element as shown in Figure 11.8(c) yields

$$A^{(SP)} = A^S A^P = \begin{bmatrix} 1 + Y_p Z_s & Z_s \\ Y_p & 1 \end{bmatrix}, \quad (11.60)$$

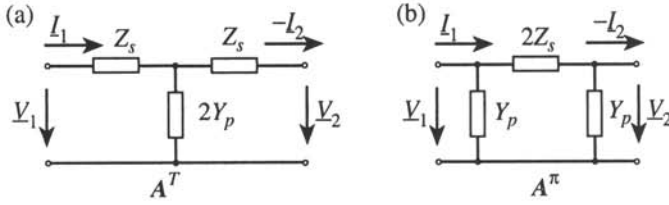
and for the circuit shown in Figure 11.8(d) we obtain

$$A^{(PS)} = A^P A^S = \begin{bmatrix} 1 & Z_s \\ Y_p & 1 + Y_p Z_s \end{bmatrix}. \quad (11.61)$$

The characteristic impedances as defined in (11.52a) and (11.52b) of the SP and PS circuits are

$$Z_{01}^{(SP)} = Z_{02}^{(PS)} = \sqrt{\frac{Z_s}{Y_p}} \sqrt{1 + Y_p Z_s}, \quad (11.62a)$$

$$Z_{02}^{(SP)} = Z_{01}^{(PS)} = \sqrt{\frac{Z_s}{Y_p}} \frac{1}{\sqrt{1 + Y_p Z_s}}. \quad (11.62b)$$


 Figure 11.9: (a) T element, and (b) π element.

The propagation factor according to (11.57) is

$$e_{(SP)}^{-g} = e_{(PS)}^{-g} = \sqrt{1 + Y_p Z_s} - \sqrt{Y_p Z_s}. \quad (11.63)$$

The T circuit according to Figure 11.9(a) is described by the chain matrix

$$A^{(T)} = A^{(SP)} A^{(PS)} = \begin{bmatrix} 1 + 2Y_p Z_s & 2Z_s(1 + Y_p Z_s) \\ 2Y_p & 1 + 2Y_p Z_s \end{bmatrix}. \quad (11.64)$$

The impedance matrix of the T circuit is

$$Z_s^{(T)} = \begin{bmatrix} Z_s + \frac{1}{2Y_p} & \frac{1}{2Y_p} \\ \frac{1}{2Y_p} & Z_s + \frac{1}{2Y_p} \end{bmatrix}. \quad (11.65)$$

Since the T circuit is symmetric (i.e., $A_{11} = A_{22}$), the characteristic impedances $Z_{01}^{(T)}$ and $Z_{02}^{(T)}$ are identical,

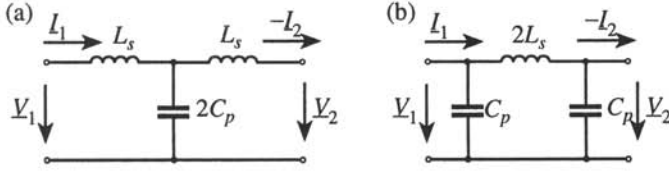
$$Z_0^{(T)} = Z_{01}^{(T)} = Z_{02}^{(T)} = \sqrt{\frac{A_{12}}{A_{21}}} = \sqrt{\frac{Z_s}{Y_p} \sqrt{1 + Y_p Z_s}}. \quad (11.66)$$

The propagation factor of the T circuit is

$$e_{(T)}^{-g} = 1 + 2Y_p Z_s - 2\sqrt{Y_p Z_s} \sqrt{1 + Y_p Z_s}. \quad (11.67)$$

For the π circuit shown in Figure 11.9(b), the chain matrix is given by

$$A^{(\pi)} = A^{(PS)} A^{(SP)} = \begin{bmatrix} 1 + 2Y_p Z_s & 2Z_s \\ 2Y_p(1 + Y_p Z_s) & 1 + 2Y_p Z_s \end{bmatrix}. \quad (11.68)$$

Figure 11.10: Low-pass filter, (a) T element, and (b) π element.

The admittance matrix of the π circuit is

$$Y^{(\pi)} = \begin{bmatrix} Y_p + \frac{1}{2Z_s} & -\frac{1}{2Z_s} \\ -\frac{1}{2Z_s} & Y_p + \frac{1}{2Z_s} \end{bmatrix}. \quad (11.69)$$

The characteristic impedance $Z_0^{(\pi)}$ of the π circuit is

$$Z_0^{(\pi)} = \sqrt{\frac{A_{12}}{A_{21}}} = \sqrt{\frac{Z_s}{Y_p} \frac{1}{\sqrt{1 + Y_p Z_s}}}. \quad (11.70)$$

The propagation factor of the π circuit is the same as the propagation factor of the T circuit,

$$e_{(\pi)}^{-g} = 1 + 2Y_p Z_s - 2\sqrt{Y_p Z_s} \sqrt{1 + Y_p Z_s}. \quad (11.71)$$

Consider a low-pass filter shown in Figure 11.10. The characteristic impedances are given by

$$Z_0^{(T)} = \sqrt{\frac{L_s}{C_p} \sqrt{1 - \omega^2 L_s C_p}}, \quad (11.72a)$$

$$Z_0^{(\pi)} = \sqrt{\frac{L_s}{C_p} \frac{1}{\sqrt{1 - \omega^2 L_s C_p}}}. \quad (11.72b)$$

The propagation factor is

$$e_{(T)}^{-g} = e_{(\pi)}^{-g} = 1 - 2\omega^2 L_s C_p - 2j\omega\sqrt{L_s C_p} \sqrt{1 - \omega^2 L_s C_p}. \quad (11.73)$$

We introduce the cutoff frequency ω_c , the normalized frequency Ω , and \tilde{Z}_0 by

$$\omega_c = \frac{1}{\sqrt{L_s C_p}}, \quad \tilde{Z}_0 = \sqrt{\frac{L_s}{C_p}}, \quad \Omega = \frac{\omega}{\omega_c}. \quad (11.74)$$

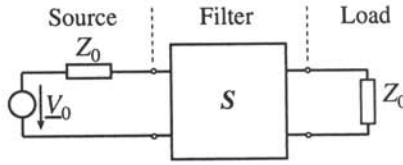


Figure 11.11: Filter two-port connected to source and load.

With this we can put (11.72a) to (11.73) in the normalized form

$$Z_0^{(T)} = \tilde{Z}_0 \sqrt{1 - \Omega^2}, \quad (11.75a)$$

$$Z_0^{(\pi)} = \tilde{Z}_0 \frac{1}{\sqrt{1 - \Omega^2}}. \quad (11.75b)$$

From (11.73) and (11.74) we obtain the propagation factor

$$e_{(T)}^{-g} = e_{(\pi)}^{-g} = 1 - \Omega^2 - 2j\Omega\sqrt{1 - \Omega^2}. \quad (11.76)$$

11.3 LUMPED LOW-PASS FILTER PROTOTYPES

A low-pass filter prototype is a passive, reciprocal reactance two-port that is designed for insertion between a generator and a load, both with a real impedance Z_0 [10, 11]. Consider the filter two-port connected to source and load as depicted in Figure 11.11. We define the *return loss* L_R and the *insertion loss* L_A as

$$L_R = \frac{\text{Power available from the source}}{\text{Power reflected to the source}}, \quad (11.77a)$$

$$L_A = \frac{\text{Power available from the source}}{\text{Power delivered to the load}}. \quad (11.77b)$$

For the S -parameters referred to Z_0 , the reflection factor of the load is 0 and the reflection factor at the input of the terminated two-port is S_{11} . From this it follows

$$L_R = |S_{11}|^{-2} \quad L_A = |S_{21}|^{-2}. \quad (11.78)$$

Since the filter two-port is assumed to be lossless, according to (10.79) the scattering matrix is unitary and therefore

$$|S_{11}|^2 + |S_{21}|^2 = 1. \quad (11.79)$$

This allows to determine L_A from the magnitude of the reflection coefficient of the one-port resulting when the filter is terminated with Z_0 ,

$$L_A = \frac{1}{1 - |S_{11}|^2}. \quad (11.80)$$

11.3.1 The Butterworth Prototype

A maximally flat filter characteristic will be given by a loss characteristic

$$L_A(\Omega) = 1 + \Omega^{2n}, \quad (11.81)$$

where the *normalized frequency* Ω is defined as

$$\Omega = \frac{\omega}{\omega_c} \quad (11.82)$$

with the angular cutoff frequency ω_c . Since the first $n - 1$ derivatives of $L_A(\Omega)$ vanish at $\Omega = 0$, the insertion loss characteristic exhibits maximum flatness. For $\Omega = 1$ (i.e., at the cutoff angular frequency ω_c) the insertion loss L_A is 3 dB, and for $\Omega > 1$ the insertion loss rapidly increases with Ω . From (11.78), (11.79), and (11.81) we obtain

$$|S_{21}(\Omega)|^2 = \frac{1}{1 + \Omega^{2n}}, \quad (11.83a)$$

$$|S_{11}(\Omega)|^2 = \frac{\Omega^{2n}}{1 + \Omega^{2n}}. \quad (11.83b)$$

The maximally flat filter response according to (11.83a) is called the *Butterworth response*. Figure 11.12 shows the Butterworth response for $n = 4, 6, 8$. For real Ω the magnitude $|S_{11}(\Omega)|$ is given by

$$|S_{11}(\Omega)| = \frac{\Omega^n}{\sqrt{1 + \Omega^{2n}}}. \quad (11.84)$$

For real Ω the relation between $S_{11}(\Omega)$ and its complex conjugate $S_{11}^*(\Omega)$ is given by

$$S_{11}^*(\Omega) = S_{11}(-\Omega). \quad (11.85)$$

The complex conjugate of an expression is not an analytic function of this expression. The function $S_{11}(-\Omega)$ is the analytic continuation of $S_{11}^*(\Omega)$. We introduce the normalized complex frequency

$$p = \sigma + j\Omega \quad (11.86)$$

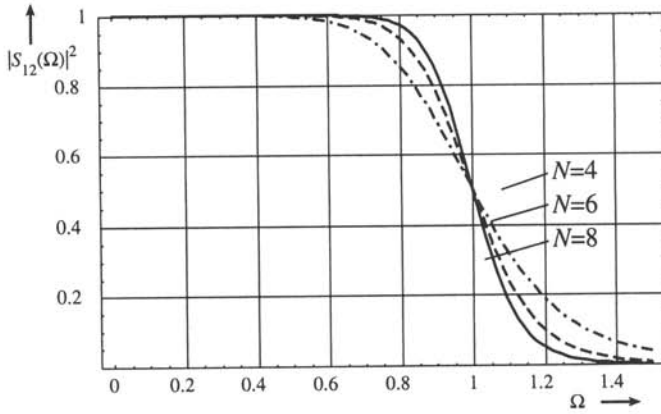


Figure 11.12: Butterworth low-pass characteristic.

with the real part σ and the imaginary part Ω . Replacing Ω by $-jp$ yields $S_{11}(\Omega) \rightarrow S_{11}(-jp)$ and $S_{11}(-\Omega) \rightarrow S_{11}(jp)$. For $p = j\Omega$ we obtain from (11.83b)

$$S_{11}(\Omega)S_{11}(-\Omega) = \frac{\Omega^{2n}}{1 + \Omega^{2n}}. \quad (11.87)$$

The analytic continuation $f(p)$ of this function for complex frequencies p is

$$f(p) = S_{11}(-jp)S_{11}(jp) = \frac{(-jp)^{2n}}{1 + (-jp)^{2n}}. \quad (11.88)$$

For $p = j\Omega$ this analytic continuation coincides with $|S_{11}(\Omega)|^2$. The poles of $f(p)$ are given by the zeros of the denominator,

$$1 + (-jp_k)^{2n} = 0. \quad (11.89)$$

From this we obtain

$$p_k = j \sqrt[2n]{-1}. \quad (11.90)$$

This equation exhibits $2n$ solutions located on the unit circle in the complex number plane,

$$p_k = j \exp\left(j \frac{2k-1}{2n} \pi\right) \quad \text{with } k = 1 \dots n. \quad (11.91)$$

Figure 11.13 shows the location of the poles p_k in the complex p -plane for the cases $n = 4$ and $n = 5$. From the $2n$ poles of $f(\Omega)$ the poles numbered from 1 to n exhibit negative

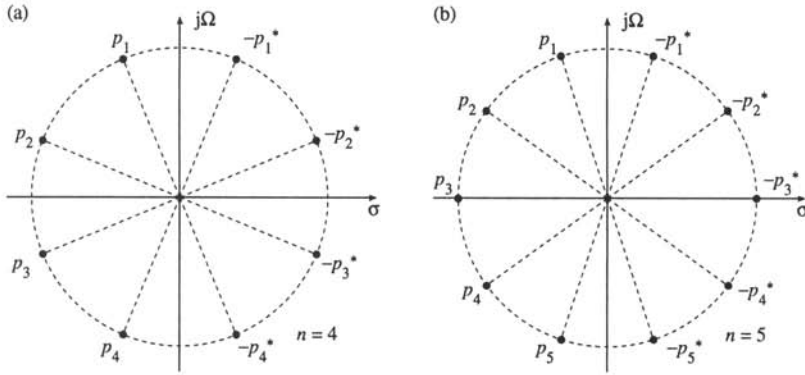


Figure 11.13: Location of the poles for (a) $n = 4$, (b) $n = 5$.

real part. We design $S_{11}(\Omega)$ such that the negative real half-plane poles are assigned to $S_{11}(\Omega)$. This ensures the stability of the corresponding two-port. The positive real half-plane poles are contained in $S_{11}(-\Omega)$, which is the analytic continuation of the complex conjugate of $S_{11}(\Omega)$ and has only been used as an auxiliary function. From (11.90) we obtain

$$p_k = j \cos \frac{(2k-1)\pi}{2n} - \sin \frac{(2k-1)\pi}{2n}. \quad (11.92)$$

With this we obtain the scattering parameters of the filter two-port

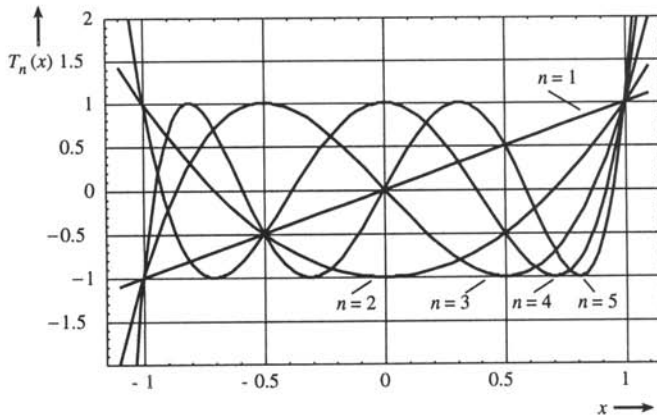
$$S_{12}(\Omega) = \frac{\pm 1}{\prod_{k=1}^n \left(\Omega - e^{j\frac{2k-1}{2n}\pi} \right)}, \quad (11.93a)$$

$$S_{11}(\Omega) = \frac{\pm \Omega^{2n}}{\prod_{k=1}^n \left(\Omega - e^{j\frac{2k-1}{2n}\pi} \right)}. \quad (11.93b)$$

If the filter two-port is terminated with Z_0 , the reflection coefficient at the input is S_{11} and the input impedance of the terminated filter two-port is

$$Z(\Omega) = Z_0 \frac{1 + S_{11}(\Omega)}{1 - S_{11}(\Omega)}. \quad (11.94)$$

The filter design task is to synthesize a reactance two-port that exhibits the input impedance $Z(\Omega)$ when terminated by the real impedance Z_0 . This means to synthesize a one-port. This problem can be solved in various ways [10–13].

Figure 11.14: Chebyshev polynomials $T_n(x)$.

11.3.2 The Chebyshev Prototype

An interesting filter characteristic for many practical applications is one where the loss ripples in the pass-band is bounded between two given values and beyond the cutoff frequency the loss rapidly increases. The *Chebyshev filter characteristic* exhibits this property. The insertion loss characteristic of the Chebyshev filter prototype is given by

$$L_A(\Omega) = 1 + \eta^2 T_n^2(\Omega), \quad (11.95)$$

where the *normalized frequency* Ω is defined by (11.82), $T_n(\Omega)$ is the *Chebyshev polynomial* of the first kind and n th degree [9,14], and η is a parameter determining the ripple of the filter characteristics in the pass-band. The Chebyshev polynomial $T_n(x)$ is defined as

$$T_n(x) = \cos(n \arccos x). \quad (11.96)$$

The explicit form of the Chebyshev polynomials of the first kind and degrees 1 to 8 are

$$T_1(x) = x, \quad (11.97a)$$

$$T_2(x) = -1 + 2x^2, \quad (11.97b)$$

$$T_3(x) = -3x + 4x^3, \quad (11.97c)$$

$$T_4(x) = 1 - 8x^2 + 8x^4, \quad (11.97d)$$

$$T_5(x) = 5x - 20x^3 + 16x^5, \quad (11.97e)$$

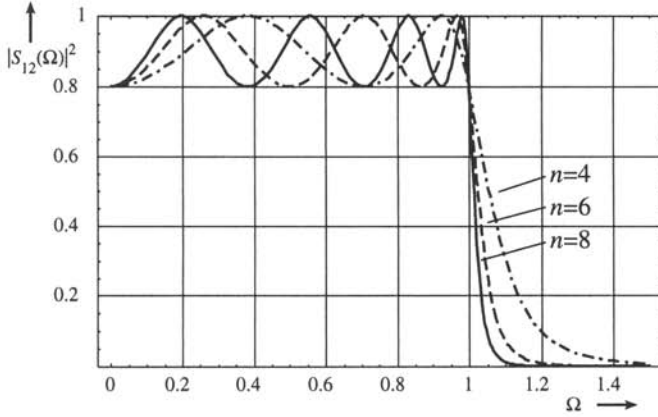


Figure 11.15: Chebyshev low-pass characteristics for $\eta = 0.5$ and $n = 4, 6, 8$.

$$T_6(x) = -1 + 18x^2 - 48x^4 + 32x^6, \quad (11.97f)$$

$$T_7(x) = -7x + 56x^3 - 112x^5 + 64x^7, \quad (11.97g)$$

$$T_8(x) = 1 - 32x^2 + 160x^4 - 256x^6 + 128x^8. \quad (11.97h)$$

Figure 11.14 shows plots of the Chebyshev polynomials $T_n(x)$ of degrees $n = 1 \dots 5$.

For $|\Omega| \leq 1$ the Chebyshev polynomials are bounded in the interval ± 1 and assume the values ± 1 for $|\Omega| = 1$. Therefore in the pass-band, specified by $|\Omega| \leq 1$ the insertion loss $L_A(\Omega)$ satisfies

$$1 \leq L_A(\Omega) \leq 1 + \eta^2. \quad (11.98)$$

For $|\Omega| > 1$ the magnitude $|T_n(\Omega)|$ exhibits a steep increase with $|\Omega|$. Choosing a higher value of $|\Omega|$ yields a steeper increase of the attenuation in the stop-band but also a higher ripple in the pass-band.

For $\Omega = 1$ i.e. at the cutoff angular frequency ω_c , the insertion loss L_A is

$$L_A(\Omega = 1) = 1 + \eta^2. \quad (11.99)$$

From (11.78), (11.79), and (11.95) we obtain

$$|S_{12}(\Omega)|^2 = \frac{1}{1 + \eta^2 T_n^2(\Omega)}, \quad (11.100a)$$

$$|S_{11}(\Omega)|^2 = \frac{\eta^2 T_n^2(\Omega)}{1 + \eta^2 T_n^2(\Omega)}. \quad (11.100b)$$

Figure 11.15 shows the plots of the Chebyshev low-pass $|S_{12}(\Omega)|^2$ for $\eta = 0.5$ and $n = 4, 6, 8$. With the complex frequency $p = \sigma + j\Omega$ introduced in (11.86), poles occur for

$$T_n(-jp)^2 = -\frac{1}{\eta^2}. \quad (11.101)$$

With (11.96), this yields

$$\cos^2 [n \arccos(-jp)] = -\frac{1}{\eta^2}. \quad (11.102)$$

To proceed in the determination of the poles we introduce the parameter κ as

$$\kappa = \sinh \left[\frac{1}{n} \operatorname{arcsinh} \left(\frac{1}{\eta} \right) \right]. \quad (11.103)$$

This yields

$$\frac{1}{\eta} = \sinh [n \operatorname{arcsinh}(\kappa)]. \quad (11.104)$$

From (11.102) and (11.104) we obtain

$$\cos^2 [n \arccos(-jp)] = -\sinh^2 [n \operatorname{arcsinh}(\kappa)] = \sin^2 [n \arcsin(j\kappa)]. \quad (11.105)$$

This yields

$$\cos^2 [n \arccos(-jp)] = \cos^2 [n \arcsin(j\kappa) + (2k-1)\frac{1}{2}\pi] \quad (11.106)$$

with integer k . From there we obtain

$$\arccos(-jp_k) = \arcsin(j\kappa) + \frac{(2k-1)\pi}{2n} \quad (11.107)$$

with $2n$ solutions for $k = 1 \dots 2n$ given by

$$p_k = \sigma_k p j \Omega_k = j \cos \left[\arcsin(j\kappa) + \frac{(2k-1)\pi}{2n} \right]. \quad (11.108)$$

The real part σ_k and the imaginary part Ω_k of the poles p_k are given by

$$\sigma_k = \kappa \sin \left(\frac{(2k-1)\pi}{2n} \right), \quad (11.109a)$$

$$\Omega_k = \sqrt{1 - \kappa^2} \cos \left(\frac{(2k-1)\pi}{2n} \right). \quad (11.109b)$$

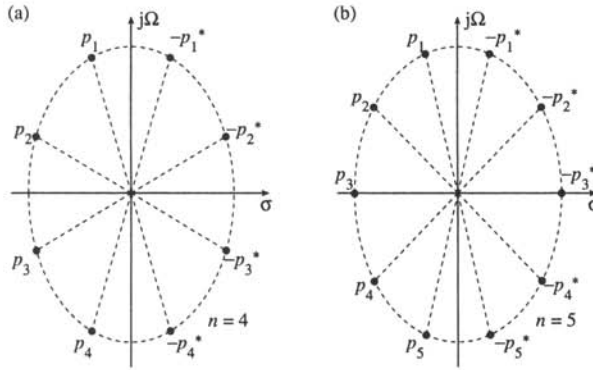


Figure 11.16: Location of the poles for (a) $n = 4$, and (b) $n = 5$.

From

$$\frac{\sigma_k^2}{\kappa^2} + \frac{\Omega_k^2}{1 - \kappa^2} = 1 \quad (11.110)$$

it follows that the poles are located on an ellipse in the $\sigma - \Omega$ -plane. Figure 11.16 shows the location of the poles p_k .

11.4 LADDER FILTER NETWORKS

A common realization of filter two-ports is the ladder network [10, 11]. Figure 11.17 shows ladder network realizations of low-pass filters. The four cases shown in that figure differ in whether they are beginning or ending either with shunt capacitors or series resistors. For an LC ladder two-port beginning with a shunt capacitor C_1 , ending with a shunt capacitor C_n , and terminated with an ohmic resistor Z_0 , as shown in Figure 11.17(a), the input impedance is given by the continued fraction expansion

$$Z_1^{-1} = pC_1 + \frac{1}{pL_2 + \frac{1}{pC_3 + \ddots + \frac{1}{pL_{n-1} + \frac{1}{pC_n + \frac{1}{Z_0}}}}} \quad (11.111)$$

In this case the number of capacitors is one larger than the number of inductors, the shunt capacitors exhibit odd indices, the series inductors exhibit even indices and the total number n of elements of the ladder two-port is odd.

For the ladder two-port beginning with series inductances and terminating with Z_0

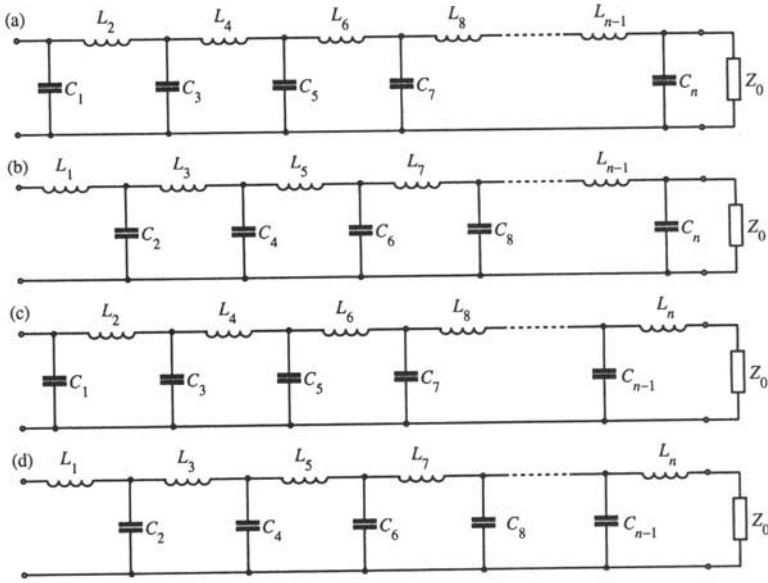


Figure 11.17: Low-pass filter prototype ladder networks, (a) beginning and ending with a shunt capacitor, (b) beginning with a series inductor and ending with a shunt capacitor, (c) beginning with a shunt capacitor and ending with a series inductor, and (d) beginning and ending with a series inductor.

as depicted in Figure 11.17(b), the continued fraction expansion is

$$Z_1 = pL_1 + \frac{1}{pC_2 + \frac{1}{pL_3 + \ddots + \frac{1}{pC_{n-1} + \frac{1}{pL_n + Z_0}}}}. \quad (11.112)$$

The reader may easily write down the corresponding expressions for the circuits depicted in Figures 11.17(c) and (d).

11.4.1 Butterworth Ladder Networks

Orchard has given formulae for the elements of Butterworth ladder filters [10, 15]. For ladder filters of order n and cutoff frequency ω_c beginning with a shunt capacitor as in Figures 11.17(a,c) the element values C_{2k-1} and L_{2k} can be determined from

$$C_{2k-1} = \frac{g_{2k-1}}{\omega_c Z_0}, \quad (11.113a)$$

$$L_{2k} = \frac{g_{2k} Z_0}{\omega_c}. \quad (11.113b)$$

Table 11.1: Element Values for the Butterworth Ladder Filter

n	g_1	g_2	g_3	g_4	g_5	g_6	g_7	g_8
1	1.00000							
2	0.707107	1.41421						
3	0.50000	1.33333	1.50000					
4	0.382683	1.08239	1.57716	1.53073				
5	0.309017	0.894427	1.38197	1.69443	1.54508			
6	0.258819	0.757875	1.20163	1.55291	1.75931	1.55291		
7	0.222521	0.655971	1.05496	1.39717	1.65883	1.79883	1.55765	
8	0.195090	0.577552	0.937052	1.25882	1.52832	1.72874	1.82464	1.56072

For ladder filters beginning with a series inductor as in Figures 11.17(b,d) the element values C_{2k} and L_{2k-1} are given by

$$L_{2k-1} = \frac{g_{2k-1}Z_0}{\omega_c}, \quad (11.114a)$$

$$C_{2k} = \frac{g_{2k}}{\omega_c Z_0}. \quad (11.114b)$$

The values g_k are given by

$$a_k = \sin \frac{(2k-1)\pi}{2n}, \quad (11.115a)$$

$$b_k = \cos^2 \frac{k\pi}{2n}, \quad (11.115b)$$

$$g_1 = a_1, \quad (11.115c)$$

$$g_k = \frac{a_k a_{k-1}}{c_{k-1} g_{k-1}} \quad \text{for } k = 2, 3, \dots, n. \quad (11.115d)$$

Table 11.1 summarizes the element values for Butterworth ladder filters of order 1 to 8.

11.4.2 Chebyshev Ladder Networks

For Chebyshev ladder filters Orchard's equations [10, 15, 16] for the parameters g_k are

$$a_k = \sin \frac{(2k-1)\pi}{2n}, \quad (11.116a)$$

$$d_k = \left[\sinh^2 \left(\frac{\xi}{2n} \right) + \sin^2 \left(\frac{k\pi}{2n} \right) \right] \cos^2 \frac{k\pi}{2n}, \quad (11.116b)$$

Table 11.2: Element Values for the Chebyshev Ladder Filter with 0.1 dB Ripple

n	g_1	g_2	g_3	g_4	g_5	g_6	g_7	g_8
1	0.152628							
2	0.421534	0.715866						
3	0.515793	1.08641	1.08949					
4	0.554406	1.19943	1.45758	1.24534				
5	0.573419	1.24903	1.55624	1.59238	1.3759			
6	0.584068	1.27524	1.59987	1.67493	1.72359	1.40351		
7	0.590601	1.29079	1.62357	1.71067	1.79872	1.73947	1.4745	
8	0.594888	1.30079	1.63804	1.7302	1.83022	1.80698	1.81628	1.46603

Table 11.3: Element Values for the Chebyshev Ladder Filter with 0.2 dB Ripple

n	g_1	g_2	g_3	g_4	g_5	g_6	g_7	g_8
1	0.217102							
2	0.518935	0.817675						
3	0.613789	1.18888	1.19006					
4	0.651438	1.29358	1.56157	1.2898				
5	0.669739	1.33824	1.65416	1.63202	1.43563			
6	0.679923	1.36153	1.69376	1.70833	1.78707	1.41828		
7	0.686148	1.37524	1.7149	1.74018	1.85901	1.75057	1.51619	
8	0.690223	1.38401	1.72767	1.7572	1.88804	1.81446	1.86239	1.46769

$$g_1 = \frac{a_1}{\sinh\left(\frac{\xi}{2n}\right)}, \quad (11.116c)$$

$$g_k = \frac{a_k a_{k-1}}{d_{k-1} g_{k-1}} \quad \text{for } k = 2, 3, \dots, n, \quad (11.116d)$$

where the parameter ξ is given by

$$\xi = \ln \left[\coth \frac{\Delta_{\text{ripple}}/\text{dB}}{17.37} \right] \quad (11.117)$$

and Δ_{ripple} is the specified pass-band ripple in dB. Tables 11.2 and 11.3 summarize the element values for Chebyshev ladder filters with 0.1 dB and 0.2 dB ripple.

11.5 FREQUENCY TRANSFORMATION

So far we have treated low-pass filters in this section. We may also require high-pass, band-pass and band-stop filters. It is possible to derive these filter characteristics from the low-pass characteristics via *frequency transformation*. Since the frequency transformation may also be applied to the circuit elements, high-pass, band-pass, and band-stop filters can be derived from the low-pass filter prototypes. The low-pass filter prototypes are normalized to unit cutoff frequency of the normalized frequency Ω and unit wave impedance. To transform the normalized *low-pass prototype filter* to a low-pass filter with arbitrary cutoff frequency ω_c low-pass transformation, we substitute the normalized frequency Ω by ω/ω_c . The normalized prototype filter uses normalized inductances l_k and capacitances c_k ,

$$l_k = \frac{\omega_c L_k}{Z_0}, \quad (11.118a)$$

$$c_k = \omega_c C_k Z_0. \quad (11.118b)$$

The normalized inductances l_k and capacitances c_k are normalized with respect to the low-pass cutoff frequency ω_c and the characteristic impedance Z_0 which is equal to the terminating resistor of the filter two-port. The l_k and c_k are the inductance and capacitance values for unit cutoff frequency and unit load impedance. If we have determined these normalized circuit element values for a prototype low-pass filter we can easily determine the element values for arbitrary cutoff frequency ω_c and characteristic impedance Z_0 . Furthermore frequency transformation allows to derive high-pass, band-pass and band-stop filters from the low-pass filter prototype.

11.5.1 Low-Pass to High-Pass Transformation

For a given normalized low-pass prototype filter the *low-pass to high-pass transformation* is performed by

$$\Omega = \frac{\omega_c}{\omega}. \quad (11.119)$$

Figure 11.18 shows the Chebyshev high-pass characteristic we obtain by applying this transformation to the prototype Butterworth low-pass characteristic. Applying this transformation to inductors L_k and capacitors C_l yields

$$\omega L_k = \Omega Z_0 l_k \rightarrow \frac{1}{\omega} \omega_c Z_0 l_k = \frac{1}{\omega C_k}, \quad (11.120a)$$

$$\omega C_l = \Omega \frac{c_l}{Z_0} \rightarrow \frac{1}{\omega} \frac{\omega_c C_l}{Z_0} = \frac{1}{\omega L_l}. \quad (11.120b)$$

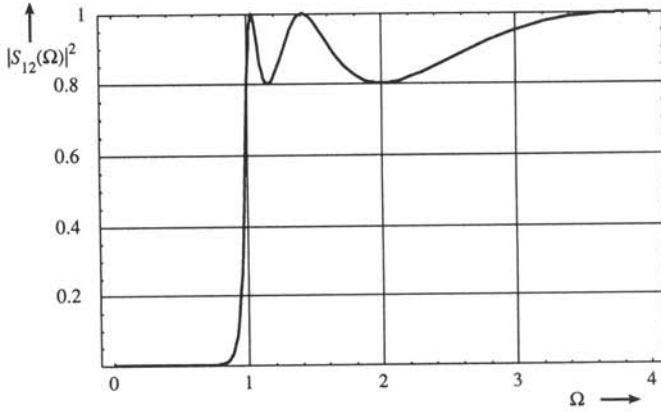


Figure 11.18: Chebyshev high-pass characteristics.

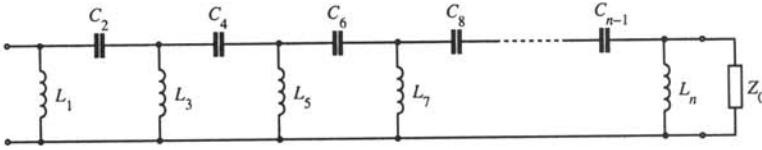


Figure 11.19: High-pass filter ladder network beginning and ending with a shunt inductor.

This means we have to replace inductors L_k by capacitors C_k and capacitors C_l by inductors L_l according to

$$C_k = \frac{1}{\omega_c c_k Z_0}, \quad (11.121a)$$

$$L_l = \frac{Z_0}{\omega_c c_l}. \quad (11.121b)$$

Figure 11.19 shows the high-pass ladder network we obtain in that way.

11.5.2 Low-Pass to Band-Pass Transformation

The *low-pass to band-pass transformation* converts the low-pass prototype filter into a band-pass filter with a lower cutoff frequency ω_{c1} and an upper cutoff frequency ω_{c2} . The low-pass to band-pass frequency transformation is given by

$$\Omega(\omega) = \kappa \left(\frac{\omega}{\omega_0} - \frac{\omega_0}{\omega} \right). \quad (11.122)$$

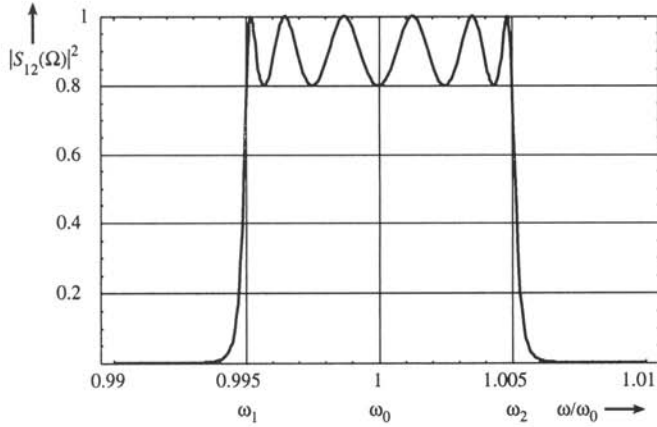


Figure 11.20: Chebyshev band-pass characteristics.

Choosing ω_0 and κ such that the cutoff frequencies ω_{c1} and ω_{c2} are mapped into $\Omega = \mp 1$ yields

$$\omega_0 = \sqrt{\omega_{c1}\omega_{c2}}, \quad (11.123a)$$

$$\kappa = \frac{\omega_0}{\omega_{c2} - \omega_{c1}}. \quad (11.123b)$$

Figure 11.20 shows the characteristics of a Chebyshev band-pass filter of order $n = 6$ with $\eta = 0.5$ and a relative bandwidth $(\omega_{c2} - \omega_{c1})/\omega_0 = 0.01$. Applying this low-pass to band-pass transformation to the normalized inductors l_k and capacitors c_l yields

$$X_k(\omega) = \Omega(\omega)Z_0 l_k = \frac{\omega_0}{\omega_{c2} - \omega_{c1}} \left(\frac{\omega}{\omega_0} - \frac{\omega_0}{\omega} \right) Z_0 l_k, \quad (11.124a)$$

$$B_l(\omega) = \Omega(\omega) \frac{c_l}{Z_0} = \frac{\omega_0}{\omega_{c2} - \omega_{c1}} \left(\frac{\omega}{\omega_0} - \frac{\omega_0}{\omega} \right) \frac{c_l}{Z_0}. \quad (11.124b)$$

We have to replace inductors l_k by series resonant circuits with L_k , C_k and the capacitors c_l by parallel resonant circuits with L_l , C_l according to

$$X_k(\omega) = \omega L_k - \frac{1}{\omega C_k}, \quad (11.125a)$$

$$B_l(\omega) = \omega C_l - \frac{1}{\omega L_l} \quad (11.125b)$$

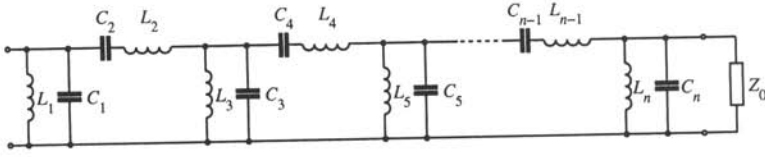


Figure 11.21: Band-pass filter ladder network beginning and ending with a shunt inductor.

with

$$L_k = \frac{Z_0 l_k}{\omega_{c2} - \omega_{c1}}, \quad (11.126a)$$

$$C_k = \frac{\omega_{c2} - \omega_{c1}}{\omega_0^2 Z_0 l_k}, \quad (11.126b)$$

$$L_l = \frac{(\omega_{c2} - \omega_{c1}) Z_0}{\omega_0^2 c_l}, \quad (11.126c)$$

$$C_l = \frac{c_l}{(\omega_{c2} - \omega_{c1}) Z_0}. \quad (11.126d)$$

Figure 11.21 shows the band-pass ladder network we obtain by replacing in the low-pass ladder network of Figure 11.17(a) the series inductors with series resonant circuits and the shunt capacitors with parallel resonant circuits.

11.5.3 Low-Pass to Band-Stop Transformation

The *low-pass to band-stop transformation* transforms the low-pass prototype filter into a band-stop filter with a lower cutoff frequency ω_{c1} and an upper cutoff frequency ω_{c2} . The low-pass to band-stop frequency transformation is performed by

$$\Omega(\omega) = \frac{1}{\kappa \left(\frac{\omega}{\omega_0} - \frac{\omega_0}{\omega} \right)}. \quad (11.127)$$

Choosing ω_0 and κ such that the cutoff frequencies ω_{c1} and ω_{c2} are mapped into $\Omega = \mp 1$ yields

$$\omega_0 = \sqrt{\omega_{c1} \omega_{c2}}, \quad (11.128a)$$

$$\kappa = \frac{\omega_0}{\omega_{c2} - \omega_{c1}}. \quad (11.128b)$$

Figure 11.22 shows the characteristics of a Chebychev band-stop filter of order $n = 6$ with $\eta = 0.5$ and a relative bandwidth $(\omega_{c2} - \omega_{c1})/\omega_0 = 0.01$. Applying this low-pass

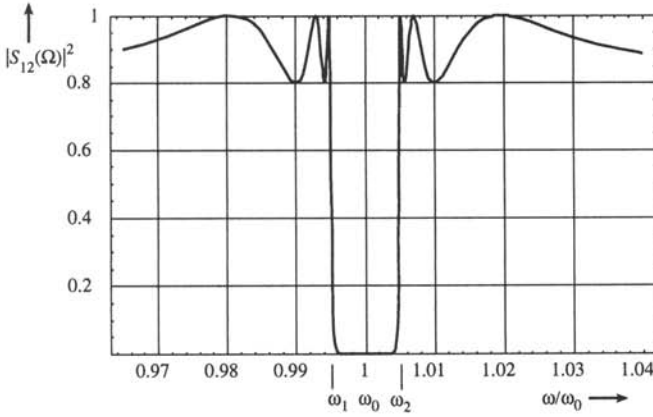


Figure 11.22: Chebyshev band-stop characteristics.

to band-stop transformation to the normalized inductors l_k and capacitors c_l yields

$$X_k(\omega) = \Omega(\omega) Z_0 l_k = \frac{\omega_{c2} - \omega_{c1}}{\omega_0} \frac{1}{\frac{\omega}{\omega_0} - \frac{\omega_0}{\omega}} Z_0 l_k, \quad (11.129a)$$

$$B_l(\omega) = \Omega(\omega) \frac{c_l}{Z_0} = \frac{\omega_{c2} - \omega_{c1}}{\omega_0} \frac{1}{\frac{\omega}{\omega_0} - \frac{\omega_0}{\omega}} \frac{c_l}{Z_0}. \quad (11.129b)$$

We have to replace inductors l_k by series resonant circuits consisting of L_k , C_k and the capacitors c_l by parallel resonant circuits consisting of L_l , C_l according to

$$X_k(\omega) = -\frac{1}{\omega C_k - \frac{1}{\omega L_k}}, \quad (11.130a)$$

$$B_l(\omega) = -\frac{1}{\omega L_l - \frac{1}{\omega C_l}} \quad (11.130b)$$

with

$$C_k = \frac{l_k}{(\omega_{c2} - \omega_{c1}) Z_0}, \quad (11.131a)$$

$$L_k = \frac{(\omega_{c2} - \omega_{c1}) Z_0}{\omega_0^2 l_k}, \quad (11.131b)$$

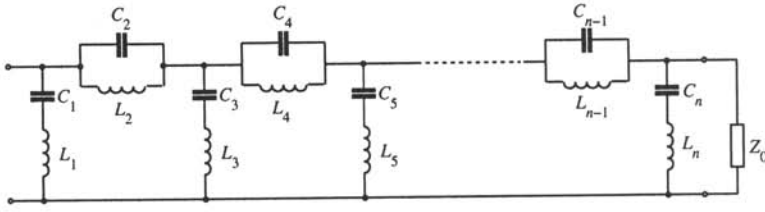
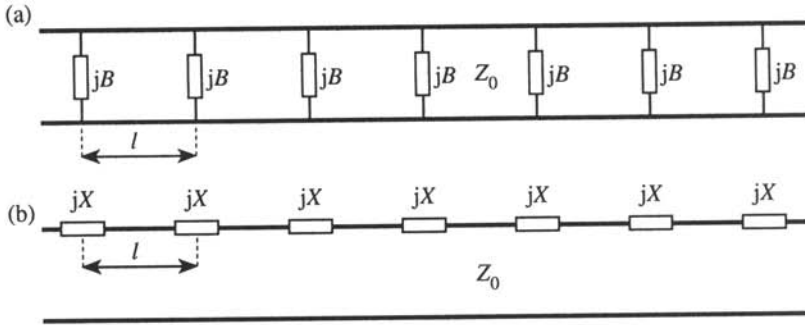


Figure 11.23: Band-stop filter ladder network beginning and ending with a shunt inductor.


 Figure 11.24: Transmission-line periodically loaded with (a) the parallel susceptance B , and (b) the series reactance X .

$$C_l = \frac{\omega_{c2} - \omega_{c1}}{\omega_0^2 c_l Z_0}, \quad (11.131c)$$

$$L_l = \frac{c_l Z_0}{\omega_{c2} - \omega_{c1}}. \quad (11.131d)$$

Figure 11.23 shows a band-stop ladder filter network.

11.6 TRANSMISSION-LINE WITH PERIODIC LOAD

Consider a transmission-line of characteristic impedance Z_0 , periodically loaded with either parallel susceptances B or series reactances X , as shown in Figure 11.24(a) and (b), respectively. Such a periodically loaded transmission-line may be considered as a chain connection of two-ports as shown in Figure 11.25(a) and (b). These two-ports represent loaded transmission-line segments of length l . To make these segments symmetric the loads are embedded between two transmission-line segments $\frac{1}{2}l$. The voltage and current at the left-hand port of the k th segment are called $\underline{V}_k, \underline{I}_k$. Voltage and current at the input of the k th segment are related to voltage and current at the input of the

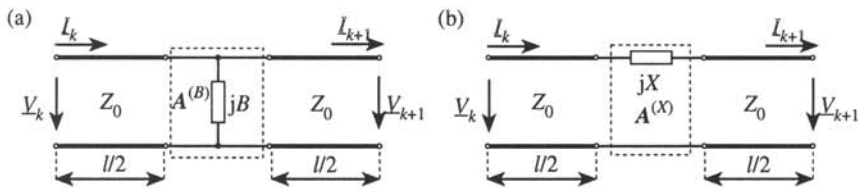


Figure 11.25: Transmission-line periodically loaded with (a) parallel susceptance, (b) series reactance.

$(k + 1)$ th segment by

$$\begin{bmatrix} V_k \\ I_k \end{bmatrix} = A \begin{bmatrix} V_{k+1} \\ I_{k+1} \end{bmatrix}. \quad (11.132)$$

The chain matrix $A^{(ls)}$ of a line segment of length $\frac{1}{2}l$, the characteristic impedance Z_0 , and the phase coefficient β_l is

$$A^{(ls)} = \begin{bmatrix} \cos \frac{1}{2}\beta_l l & jZ_0 \sin \frac{1}{2}\beta_l l \\ jZ_0^{-1} \sin \frac{1}{2}\beta_l l & \cos \frac{1}{2}\beta_l l \end{bmatrix}. \quad (11.133)$$

The embedded two-port consisting of the parallel susceptance B only is described by the chain matrix

$$A^{(B)} = \begin{bmatrix} 1 & 0 \\ jB & 1 \end{bmatrix}. \quad (11.134)$$

The complete segment according to Figure 11.25(a) is represented by the chain matrix

$$A^{(segB)} = A^{(ls)} A^{(B)} A^{(ls)}. \quad (11.135)$$

Inserting (11.133) and (11.134) into this equation yields

$$A^{(segB)} = \begin{bmatrix} \cos \beta_l l - \frac{1}{2}BZ_0 \sin \beta_l l & jZ_0 [\frac{1}{2}BZ_0 (-1 + \cos \beta_l l) + \sin \beta_l l] \\ jZ_0^{-1} [\frac{1}{2}BZ_0 (1 + \cos \beta_l l) + \sin \beta_l l] & \cos \beta_l l - \frac{1}{2}BZ_0 \sin \beta_l l \end{bmatrix}. \quad (11.136)$$

The determinant of the chain matrix is

$$|A^{(segB)}| = 1. \quad (11.137)$$

Consider the transmission-line periodically loaded with reactances X . The embedded two-port exhibiting the series reactance X only is described by the chain matrix

$$A^{(X)} = \begin{bmatrix} 1 & jX \\ 0 & 1 \end{bmatrix}. \quad (11.138)$$

The loaded transmission-line segment according to Figure 11.25(b) is described by

$$\mathbf{A}^{(\text{seg}X)} = \mathbf{A}^{(ls)} \mathbf{A}^{(X)} \mathbf{A}^{(ls)} . \quad (11.139)$$

Inserting (11.133) and (11.138) into this equation yields

$$\mathbf{A}^{(\text{seg}X)} = \begin{bmatrix} \cos \beta_l l - \frac{1}{2} X Z_0^{-1} \sin \beta_l l & j Z_0 \left[\frac{1}{2} X Z_0^{-1} (1 + \cos \beta_l l) + \sin \beta_l l \right] \\ j Z_0^{-1} \left[\frac{1}{2} X Z_0^{-1} (-1 + \cos \beta_l l) + \sin \beta_l l \right] & \cos \beta_l l - \frac{1}{2} X Z_0^{-1} \sin \beta_l l \end{bmatrix} . \quad (11.140)$$

The determinant of the chain matrix again is

$$|\mathbf{A}^{(\text{seg}X)}| = 1 . \quad (11.141)$$

For a wave propagating along the loaded transmission-line with a propagation coefficient γ voltages and currents at the inputs of the k th and $(k+1)$ th segments must be related by

$$\underline{V}_{n+1} = e^{-\gamma l} \underline{V}_n , \quad \underline{I}_{n+1} = e^{-\gamma l} \underline{I}_n . \quad (11.142)$$

Together with (11.132) this yields

$$\begin{bmatrix} A_{11} - e^{\gamma l} & A_{12} \\ A_{21} & A_{22} - e^{\gamma l} \end{bmatrix} \begin{bmatrix} \underline{V}_{n+1} \\ \underline{I}_{n+1} \end{bmatrix} = \mathbf{0} . \quad (11.143)$$

This homogeneous system of equation only exhibits a nontrivial solution if the coefficient determinant vanishes. This yields the quadratic equation

$$e^{2\gamma l} - (A_{11} + A_{22})e^{\gamma l} + A_{11}A_{22} - A_{12}A_{21} = 0 . \quad (11.144)$$

With (11.137) or (11.141), respectively, we obtain

$$e^{2\gamma l} - (A_{11} + A_{22})e^{\gamma l} + 1 = 0 . \quad (11.145)$$

The solutions of this equation are

$$e^{\gamma l} = \frac{A_{11} + A_{22}}{2} \pm \sqrt{\left(\frac{A_{11} + A_{22}}{2}\right)^2 - 1} . \quad (11.146)$$

This yields

$$\cosh \gamma l = \frac{A_{11} + A_{22}}{2} . \quad (11.147)$$

Expanding the left-hand side of this equation into real and imaginary parts and inserting A_{11} and A_{22} from (11.133) we obtain

$$\cosh \gamma l = \cosh \alpha l \cos \beta l + j \sinh \alpha l \sin \beta l = \cos \beta l - \frac{1}{2}x \sin \beta l \quad (11.148)$$

with

$$x = \begin{cases} XZ_0^{-1} & \text{for series reactance} \\ BZ_0 & \text{for parallel susceptance} \end{cases} \quad (11.149)$$

Since both sides of (11.148) must be real either α or β must vanish. We therefore have to distinguish two cases,

$$\cos \beta l = \cos \beta l - \frac{1}{2}x \sin \beta l \quad \text{for } |\cos \beta l - \frac{1}{2}x \sin \beta l| < 1, \quad (11.150a)$$

$$\cosh \alpha l = \cos \beta l - \frac{1}{2}x \sin \beta l \quad \text{for } |\cos \beta l - \frac{1}{2}x \sin \beta l| \geq 1. \quad (11.150b)$$

The first case with $\alpha = 0$ and $\beta \neq 0$ corresponds to a propagating wave, whereas the unstable solution $\alpha \neq 0$ and $\beta = 0$ describes evanescent waves.

The cutoff frequencies between both regimes are determined by

$$\cos \beta l - \frac{1}{2}x \sin \beta l = 1. \quad (11.151)$$

From this we obtain

$$\cos^2 \beta l = \frac{1}{4}x^2 \sin^2 \beta l + x \sin \beta l + 1 \quad (11.152)$$

and

$$(1 + \frac{1}{4}x^2) \sin^2 \beta l + x \sin \beta l = 0. \quad (11.153)$$

Finally, this yields the equation for the determination of the cutoff frequencies ω_c ,

$$\sin \beta l = \frac{-4x}{4 + x^2}. \quad (11.154)$$

For the transmission-line loaded with parallel susceptances the characteristic impedance Z_{p0} follows from (11.51) and (11.136) as

$$Z_{p0}^B = \sqrt{\frac{A_{12}^{(\text{seg}B)}}{A_{21}^{(\text{seg}B)}}} = Z_0 \sqrt{\frac{BZ_0 (\cos \beta l - 1) + 2 \sin \beta l}{BZ_0 (1 + \cos \beta l) + 2 \sin \beta l}}, \quad (11.155)$$

where Z_0 is the characteristic impedance of the unloaded transmission-line. For the transmission-line loaded with series reactances the characteristic impedance Z_{p0} follows from (11.51) and (11.140) as

$$Z_{p0}^X = \sqrt{\frac{A_{12}^{(\text{seg}X)}}{A_{21}^{(\text{seg}X)}}} = Z_0 \sqrt{\frac{XZ_0^{-1} (1 + \cos \beta l) + 2 \sin \beta l}{XZ_0^{-1} (\cos \beta l - 1) + 2 \sin \beta l}}. \quad (11.156)$$

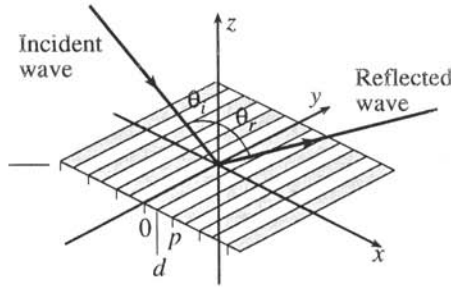


Figure 11.26: TEM wave incident on a plane periodic surface.

11.7 PLANE WAVE SCATTERING BY PERIODIC STRUCTURES

11.7.1 Scattering of TE Waves by Periodic Structures

Consider a time-harmonic TEM wave incident on a plane periodic structure as depicted in Figure 11.26. Assume TE polarization with respect to the plane of incidence. The field of the incident wave can be derived from the magnetic Hertz form

$$\underline{\Pi}_m^{(i)} = \underline{A}^{(i)} e^{-j(k_x x - k_{iz} z)} dz \quad (11.157)$$

with

$$k_x^2 + k_{iz}^2 = k_0^2 = \frac{\omega^2}{c^2}. \quad (11.158)$$

With (3.36a) and (3.36b) we obtain the field of the incident wave as

$$\underline{\mathcal{E}}^{(i)} = -j\omega\mu_0 * d\underline{\Pi}_m = \omega\mu_0 k_x \underline{A}^{(i)} e^{-j(k_x x - k_{iz} z)} dy, \quad (11.159a)$$

$$\underline{\mathcal{H}}^{(i)} = -\tilde{d} d\underline{\Pi}_m = k_x k_{iz} \underline{A}^{(i)} e^{-j(k_x x - k_{iz} z)} dx + k_x^2 \underline{A}^{(i)} e^{-j(k_x x - k_{iz} z)} dz. \quad (11.159b)$$

The planar structure at $z = 0$ is a *surface impedance plane* with a surface impedance $Z_s(\omega, x)$ dependent on frequency periodic in x -direction with a period p , hence

$$Z_s(\omega, x) = Z_s(\omega, x + p). \quad (11.160)$$

The surface impedance can be expanded in a Fourier series,

$$Z_s(\omega, x) = \sum_{m=-\infty}^{\infty} Z_{s,m}(\omega) e^{-jm\kappa x} \quad (11.161)$$

with

$$\kappa = \frac{2\pi}{p} . \quad (11.162)$$

The total field $\underline{\mathcal{E}}, \underline{\mathcal{H}}$ is the superposition of the incident field and the scattered field $\underline{\mathcal{E}}^{(sc)}, \underline{\mathcal{H}}^{(sc)}$,

$$\underline{\mathcal{E}} = \underline{\mathcal{E}}^{(i)} + \underline{\mathcal{E}}^{(sc)} , \quad (11.163a)$$

$$\underline{\mathcal{H}} = \underline{\mathcal{H}}^{(i)} + \underline{\mathcal{H}}^{(sc)} . \quad (11.163b)$$

On the plane periodic surface at $z = 0$ incident and reflected waves satisfy the boundary condition as introduced in (6.46),

$$\underline{\mathcal{E}}_t(\omega, x)|_{z=0} = Z_s(\omega, x) \perp_z \underline{\mathcal{H}}_t(\omega, x)|_{z=0} . \quad (11.164)$$

With (A.176) this can be written as

$$\underline{\mathcal{E}}_t(\omega, x)|_{z=0} = * Z_s(\omega, x) \, dz \wedge \underline{\mathcal{H}}_t(\omega, x)|_{z=0} . \quad (11.165)$$

Considering Floquet's theorem (11.28) the scattered field must be of the form

$$\underline{\mathcal{E}}^{(sc)} = \omega \mu_0 k_x \sum_{n=-\infty}^{\infty} \underline{a}_n^{(sc)}(z) e^{-j\beta_n x} dy \quad (11.166)$$

with

$$\beta_n = k_x + n\kappa . \quad (11.167)$$

The scattered field must satisfy the Helmholtz equation,

$$\Delta \underline{\mathcal{E}}^{(sc)} + k_0^2 \underline{\mathcal{E}}^{(sc)} = 0 . \quad (11.168)$$

Inserting (11.166) yields

$$\frac{d^2 \underline{a}_n^{(sc)}(z)}{dz^2} + q_n^2 \underline{a}_n^{(sc)}(z) = 0 \quad (11.169)$$

with

$$q_n = \sqrt{k_0^2 - (k_x + n\kappa)^2} . \quad (11.170)$$

The solutions of (11.169) are

$$\underline{a}_n^{(sc)}(z) = \underline{A}_n^{(sc)} e^{-j q_n z} . \quad (11.171)$$

For

$$k_0^2 > (k_x + n\kappa)^2 \quad (11.172)$$

the corresponding field term in the series expansion describes a plane wave scattered away from the impedance boundary. Otherwise the field component is evanescent in z -direction and oscillating in x -direction. The evanescent solutions contribute to the energy stored in the field. Since the scattered wave propagates in positive z -direction q_n must be positive and only the positive roots of (11.170), $q_n = q_{-n} = |q_n|$ have to be taken. For the evanescent solutions the negative imaginary values of q_n have to be considered.

Inserting (11.171) into (11.166) yields

$$\underline{\mathcal{E}}^{(sc)} = \omega\mu_0 k_x \sum_{n=-\infty}^{\infty} \underline{A}_n^{(sc)} e^{-j(\beta_n x + q_n z)} dy. \quad (11.173)$$

With Faraday's law (2.124b) we obtain the scattered magnetic field

$$\underline{\mathcal{H}}^{(sc)} = \frac{j}{\omega\mu_0} * d\underline{\mathcal{E}}^{(sc)} = - \sum_{n=-\infty}^{\infty} [k_x q_n dx - k_x \beta_n dz] \underline{A}_n^{(sc)} e^{-j(\beta_n x + q_n z)}. \quad (11.174)$$

From (11.159a), (11.159b), (11.163a), (11.163b), (11.166) and (11.174) we obtain the total field

$$\underline{\mathcal{E}} = \omega\mu_0 k_x \underline{A}^{(i)} e^{-j(k_x x - k_{iz} z)} dy + \omega\mu_0 k_x \sum_{n=-\infty}^{\infty} \underline{A}_n^{(sc)} e^{-j(\beta_n x + q_n z)} dy, \quad (11.175a)$$

$$\begin{aligned} \underline{\mathcal{H}} = & \left[k_x k_{iz} \underline{A}^{(i)} e^{-j(k_x x - k_{iz} z)} - \sum_{n=-\infty}^{\infty} k_x q_n \underline{A}_n^{(sc)} e^{-j(\beta_n x + q_n z)} \right] dx \\ & + \left[k_x^2 \underline{A}^{(i)} e^{-j(k_x x - k_{iz} z)} + \sum_{n=-\infty}^{\infty} k_x \beta_n \underline{A}_n^{(sc)} e^{-j(\beta_n x + q_n z)} \right] dz. \end{aligned} \quad (11.175b)$$

Rotating $\underline{\mathcal{H}}_t$ at $z = 0$ counterclockwise by 90° around the z -axis yields

$$* (dz \wedge \underline{\mathcal{H}}_t)|_{z=0} = \left[k_x k_{iz} \underline{A}^{(i)} e^{-j(k_x x - k_{iz} z)} - \sum_{n=-\infty}^{\infty} k_x q_n \underline{A}_n^{(sc)} e^{-j(\beta_n x + q_n z)} \right] dy. \quad (11.176)$$

Inserting (11.161), (11.175a) and (11.176) into (11.165) yields

$$\begin{aligned} \omega\mu_0 \underline{A}^{(i)} e^{-j k_x x} + \omega\mu_0 \sum_{n=-\infty}^{\infty} \underline{A}_n^{(sc)} e^{-j(k_x + n\kappa)x} = \\ \sum_{m=-\infty}^{\infty} k_{iz} Z_{s,m} \underline{A}^{(i)} e^{-j(k_x + m\kappa)x} - \sum_{m=-\infty}^{\infty} \sum_{n=-\infty}^{\infty} q_n Z_{s,m} \underline{A}_n^{(sc)} e^{-j(k_x + (n+m)\kappa)x}. \end{aligned} \quad (11.177)$$

Dividing this equation by $e^{-j k_x x}$ and replacing in the first term of the right-hand side the index m by n and in the second term n by $n - m$ yield

$$\underline{A}^{(i)} + \sum_{n=-\infty}^{\infty} \underline{A}_n^{(sc)} e^{-j n \kappa x} = \sum_{n=-\infty}^{\infty} \frac{\cos \theta_i}{Z_{F0}} Z_{s,n} \underline{A}^{(i)} e^{-j n \kappa x} - \sum_{n=-\infty}^{\infty} \sum_{m=-\infty}^{\infty} \frac{q_{n-m}}{\omega \mu_0} Z_{s,m} \underline{A}_{n-m}^{(sc)} e^{-j n \kappa x}, \quad (11.178)$$

where we have used

$$k_{iz} = k_0 \cos \theta_i \quad (11.179)$$

with the angle of incidence is θ_i and the free-space wave impedance $Z_{F0} = \sqrt{\frac{\mu_0}{\epsilon_0}}$. Multiplying (11.178) with $e^{j l \kappa x}$ and integrating over the interval $[0, p]$ and using the orthogonality relations

$$\frac{1}{p} \int_0^p e^{j(m-n)\kappa x} dx = \delta_{mn} \quad (11.180)$$

we obtain

$$\underline{A}_0^{(sc)} + \sum_{m=-\infty}^{\infty} \underline{A}_{-m}^{(sc)} \frac{q_{-m}}{\omega \mu_0} Z_{s,m} = \underline{A}^{(i)} \left(\frac{\cos \theta_i}{Z_{F0}} Z_{s,0} - 1 \right) \quad \text{for } n = 0, \quad (11.181a)$$

$$\underline{A}_n^{(sc)} + \sum_{m=-\infty}^{\infty} \underline{A}_{n-m}^{(sc)} \frac{q_{n-m}}{\omega \mu_0} Z_{s,m} = \underline{A}^{(i)} \frac{\cos \theta_i}{Z_{F0}} Z_{s,n} \quad \text{for } n \neq 0. \quad (11.181b)$$

The solution of this system of equations yields the expansion coefficients $\underline{A}_n^{(sc)}$ for the series expansions (11.173) and (11.174) of the scattered field. The plane waves constituting the scattered field are called *Floquet modes*, *Bloch waves*, or *space harmonics*. If (11.172) is fulfilled and q_n is real, the corresponding Floquet mode describes a plane wave scattered away from the impedance surface. Otherwise the Floquet mode describes a surface wave propagating along the impedance surface and decaying exponentially in z -direction. Considering

$$k_x = k_0 \sin \theta_i \quad (11.182)$$

we obtain from (11.172)

$$k_0^2 - (k_0 \sin \theta_i + n \kappa)^2 > 0. \quad (11.183)$$

With the free-space wavelength λ_0 defined in (2.88) this can be put into the form

$$\left[\frac{1}{\lambda_0} (1 - \sin \theta_i) - \frac{n}{p} \right] \left[\frac{1}{\lambda_0} (1 + \sin \theta_i) + \frac{n}{p} \right] > 0. \quad (11.184)$$

This yields the condition

$$-\frac{p}{\lambda_0} (1 + \sin \theta_i) \leq n \leq \frac{p}{\lambda_0} (1 - \sin \theta_i) \quad (11.185)$$

for the existence a propagating Floquet mode of order n .

Consider the surface with an impedance grating as shown in Figure 11.26 with a period $p = \frac{1}{2}\lambda$. An incident uniform plane wave exhibits an angle of incidence $\theta_i = 60^\circ$ and is polarized transverse to the plane of incidence. In this case (11.185) yields

$$-\frac{\sqrt{3}+2}{4} \leq n \leq \frac{\sqrt{3}-2}{4}. \quad (11.186)$$

This condition is only fulfilled for $n = 0$ and the reflected plane wave exhibits an angle of reflection that is identical with the angle of incidence. For $p = \lambda$ and $\theta_i = 60^\circ$ we obtain from (11.185)

$$-\frac{\sqrt{3}+2}{2} \leq n \leq \frac{\sqrt{3}-2}{2}. \quad (11.187)$$

In this case we obtain two propagating Floquet modes with $n = -1$. From (11.170) we obtain with $\kappa = k_0$

$$q_{-1} = k_0 \sqrt{1 - (1 - \sin \theta_i)^2} = \frac{1}{2}k\sqrt{4\sqrt{3}-3}. \quad (11.188)$$

The angle θ_n under which the n th order Floquet mode is radiated is given by

$$\theta_n = \arccos\left(\frac{q_{-1}}{k_0}\right). \quad (11.189)$$

In the above example we obtain $\theta_{-1} = 7.7^\circ$.

11.7.2 Scattering of TM Waves by Periodic Structures

Consider now a time-harmonic TEM wave incident on a plane periodic structure shown in Figure 11.26 and TM polarization with respect to the plane of incidence. That means that the magnetic field of incident and scattered waves is in y -direction and normal to the plane of incidence and the electric field is in the plane of incidence. The field of the incident wave can be derived from the electric Hertz form

$$\underline{\Pi}_e^{(i)} = \underline{B}^{(i)} e^{-j(k_x x - k_{iz} z)} dz \quad (11.190)$$

with k_x , k_y and k_0 related by (11.158). With (3.29a) and (3.29b) we obtain the field of the incident wave

$$\underline{\mathcal{H}}^{(i)} = j\omega\epsilon_0 * d\underline{\Pi}_e = \omega\mu_0 k_x \underline{B}^{(i)} e^{-j(k_x x - k_{iz} z)} dy, \quad (11.191a)$$

$$\underline{\mathcal{E}}^{(i)} = -\tilde{d} d\underline{\Pi}_e = k_x k_{iz} \underline{B}^{(i)} e^{-j(k_x x - k_{iz} z)} dx + k_x^2 \underline{B}^{(i)} e^{-j(k_x x - k_{iz} z)} dz. \quad (11.191b)$$

Applying the principle of duality introduced in Section 3.2 we obtain the formulae describing the scattering of TM waves from the equations derived in Section 11.7.1 by the substitutions (3.31a) and (3.31c). In this way we obtain the total field

$$\underline{\mathcal{H}} = -\omega\epsilon_0 k_x \underline{B}^{(i)} e^{-j(k_x x - k_{iz} z)} dy - \omega\epsilon_0 k_x \sum_{n=-\infty}^{\infty} \underline{B}_n^{(sc)} e^{-j(\beta_n x + q_n z)} dy, \quad (11.192a)$$

$$\begin{aligned} \underline{\mathcal{E}} = & \left[k_x k_{iz} \underline{B}^{(i)} e^{-j(k_x x - k_{iz} z)} - \sum_{n=-\infty}^{\infty} k_x q_n \underline{B}_n^{(sc)} e^{-j(\beta_n x + q_n z)} \right] dx \\ & + \left[k_x^2 \underline{B}^{(i)} e^{-j(k_x x - k_{iz} z)} + \sum_{n=-\infty}^{\infty} k_x \beta_n \underline{B}_n^{(sc)} e^{-j(\beta_n x + q_n z)} \right] dz. \end{aligned} \quad (11.192b)$$

Imposing the impedance boundary condition (11.165) at $z = 0$ and imposing the Fourier series expansion (11.161) of the surface impedance $Z_s(\omega, x)$ we obtain from (11.192a) and (11.192b)

$$\begin{aligned} \omega\epsilon_0 \sum_{m=-\infty}^{\infty} k_{iz} Z_{s,m} \underline{B}^{(i)} e^{-j(k_x + m\kappa)x} + \omega\epsilon_0 \sum_{m=-\infty}^{\infty} \sum_{n=-\infty}^{\infty} Z_{s,m} \underline{B}_n^{(sc)} e^{-j(k_x + (n+m)\kappa)x} = \\ - \underline{B}^{(i)} e^{-j k_x x} + \sum_{n=-\infty}^{\infty} q_n \underline{B}_n^{(sc)} e^{-j(k_x + n\kappa)x}. \end{aligned} \quad (11.193)$$

We proceed as in Section 11.7.1 and obtain

$$\underline{B}_0^{(sc)} \frac{q_0}{k_0} - \sum_{m=-\infty}^{\infty} \underline{B}_{-m}^{(sc)} \frac{Z_{s,m}}{Z_{F0}} = \underline{B}^{(i)} \left(\frac{Z_{s,0}}{Z_{F0}} + \cos \theta_i \right) \quad \text{for } n = 0, \quad (11.194a)$$

$$\underline{B}_n^{(sc)} \frac{q_n}{k_0} - \sum_{m=-\infty}^{\infty} \underline{B}_{n-m}^{(sc)} \frac{Z_{s,m}}{Z_{F0}} = \underline{B}^{(i)} \frac{Z_{s,n}}{Z_{F0}} \quad \text{for } n \neq 0 \quad (11.194b)$$

for determination of the amplitudes $\underline{B}_n^{(sc)}$ of the Floquet modes. The condition for the existence of a propagating Floquet mode of order n is given by (11.185).

One method to realize an impedance grating is a *corrugated surface* [17] as shown in Figure 11.27. The corrugated plane exhibits grooves of width w and depth h with a period $p = d + w$ and is assumed perfectly conducting and infinite in extent. We assume a uniform incident plane wave polarized in y -direction. If the width w of the groove is small compared to the wavelength then the incident wave excites TEM waves in the grooves with the electric field directed in x -direction and the magnetic field directed in y -direction. Figure 11.28(a) shows schematically the electric field potential planes in the groove. A groove can be modeled by a short-circuited transmission-line of length h as shown in Figure 11.28(b). Since we want to model the field impedance, we take the field impedance of the free-space Z_{F0} as the characteristic impedance of the transmission-line. With (8.39) we obtain for the surface impedance $Z_s(\omega, x)$

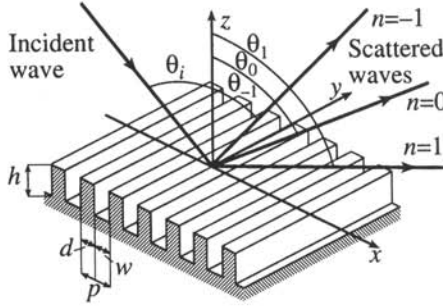


Figure 11.27: TEM wave incident on a periodic corrugated surface.

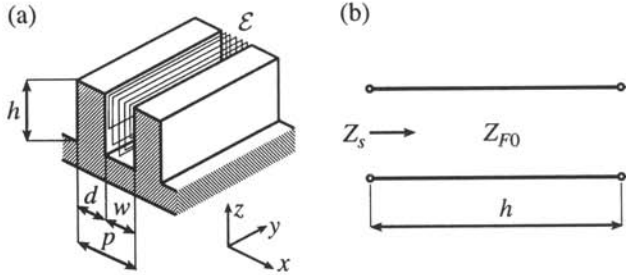


Figure 11.28: Excitation of a periodic corrugated surface, (a) TEM field in a groove, (b) transmission-line model of a groove.

$$Z_s(\omega, x) = \begin{cases} Z_{F0} \tan k_0 h & \text{for } np - w \leq x < np \\ 0 & \text{for } np \leq x < np + w \end{cases}, \quad (11.195)$$

where n is an integer. The Fourier coefficients for the series expansion (11.161) are

$$Z_{s,m}(\omega) = \frac{1}{p} Z_{F0} \tan k_0 h \int_{-w}^0 e^{j \frac{m 2\pi x}{p}} dx = \frac{w}{p} Z_{F0} \tan k_0 h \left[1 - \exp\left(j \frac{m 2\pi w}{p}\right) \right]. \quad (11.196)$$

11.8 METAMATERIALS

A *metamaterial* is an electromagnetic structure designed to exhibit special material properties like negative permeability, negative permittivity or negative refractive index [18, 19]. Veselago in his 1968 paper investigated materials with negative real parts of permittivity and permeability [20]. Veselago showed that in negative refractive index materials for an electromagnetic plane wave the directions of the electric field, the

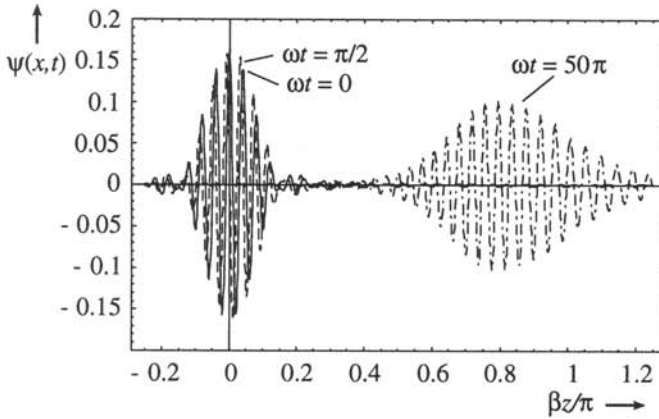


Figure 11.29: Propagation of a wave packet.

magnetic field, and the wave vector form a left-handed orthogonal trihedron. This means that for a plane wave the wave vector and the Poynting vector exhibit opposite directions. Metamaterials also are referred to as *left-handed materials*. A wave with opposite group and phase velocity was already discussed by Pocklington [21]. Waves in which phase- and group velocity exhibit opposite signs are called *backward waves* [22]. A fundamental property of metamaterials is that they cannot be realized by homogeneous materials. Metamaterials so far are composite materials exhibiting an internal structure [19, 23]. Early examples of composite structures are given in [24]. Composite materials with simultaneously negative permittivity and permeability are investigated experimentally [25, 26]. The singular properties of metamaterials allow a multitude of interesting applications in microwave circuits, transmission-lines and antennas. Pendry has suggested the application of negative refraction material to realize a perfect optical lens [27]. Experimental verification of negative index of refraction has been given in [28].

In 1905 Pocklington published a short letter "Growth of a wave-group when the group velocity is negative," which may be considered as the first treatment of negative index material [21]. Pocklington already stated that in the considered case a wave would move towards a perturbation. To establish an elementary model of a negative refractive index material we examine whether there is the possibility for a material for which group velocity and phase velocity are of equal magnitude but opposite signs. With (7.3) and (7.7) we obtain

$$\frac{d\beta}{d\omega} = -\frac{\beta}{\omega}. \quad (11.197)$$

Integration of this equation yields the dispersion relation

$$\beta = \frac{\kappa}{\omega}, \quad (11.198)$$

where κ is a constant with the dimension $\text{m}^{-1}\text{s}^{-1}$. According to (7.3) and (7.7) the phase velocity c_n and the group velocity v_{gn} are

$$c_n = \frac{\omega}{\beta} = \mp \frac{\omega^2}{\kappa}, \quad (11.199a)$$

$$v_{gn} = \left(\frac{d\beta}{d\omega} \right)^{-1} = \pm \frac{\omega^2}{\kappa}. \quad (11.199b)$$

Phase and group velocities exhibit opposite sign. A partial differential equation describing a one-dimensional scalar field $\psi(z, t)$ and satisfying the dispersion relation (11.197) is

$$\frac{\partial^4 \psi(z, t)}{\partial z^2 \partial t^2} = \kappa^2 \psi(z, t). \quad (11.200)$$

This equation exhibits the time and frequency harmonic solution

$$\psi(z, t) = A^{(+)} \cos(\omega t - \beta z + \phi^{(+)}) + A^{(-)} \cos(\omega t - \beta z + \phi^{(-)}), \quad (11.201)$$

where $A^{(+)}$, $A^{(-)}$, are the amplitudes and $\phi^{(+)}$ and $\phi^{(-)}$ are the amplitudes and phases of the waves with the phase planes moving positive and negative z -directions. Figure 11.29 shows the propagation of a wave packet formed by superposition of harmonic waves,

$$\psi(z, t) = \frac{2}{\pi} \sum_{n=N_1}^{N_2} \frac{1}{n} \sin \frac{n\pi}{20} \cos \left(\frac{n}{N_0} \beta_0 x + \frac{N_0}{n} \omega_0 t \right) \quad (11.202)$$

for $N_0 = 40$, $N_1 = 20$, and $N_2 = 60$. For small time increments ($\omega_0 t = \frac{1}{2}\pi$) we see that the phase is moving in negative z -direction. The envelope of the wave, however, is propagating in positive z -direction as we can see for larger times ($\omega_0 t = 50\pi$). The wave is highly dispersive.

Figure 11.30 shows the transmission-line equivalent circuit model for a plane wave in material with positive and negative refractive index, where Δz is the length of the modeled longitudinal section of the transmission-line, and L'_R and C'_R are the series inductance and the parallel capacitance *per unit of length*. For the *left-handed transmission-line* we have the series capacitances and parallel inductances C'_L and L'_L *times unit of length*. In the limit $\Delta z \rightarrow 0$ the element values of $L'_R \Delta z$ and $C'_R \Delta z$ go to zero. The elements values of $L'_L / \Delta z$ and $C'_R / \Delta z$, however, go to infinity for $\Delta z \rightarrow 0$. This indicates that a left-handed transmission-line or a left-handed material cannot be realized as a homogeneous structure.

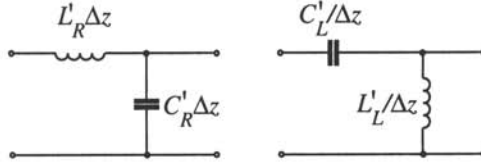


Figure 11.30: Transmission-line equivalent circuit model: (a) positive refractive index, and (b) negative refractive index.

The magnitude of the phase and group velocities grows in proportion to ω^2 . Therefore it becomes unphysical when the magnitude of the group velocity exceeds the free-space speed of light. Physically it is not possible to realize a transmission-line with a series capacitor and a parallel inductor only. A more realistic transmission-line model shown in Figure 11.31 contains also a series inductance and a parallel capacitance. The reactance per unit of length $X'(\omega)$ and the susceptance per unit of length $B'(\omega)$ are given by

$$X'(\omega) = \left(\omega L'_R - \frac{1}{\omega C'_L} \right), \quad B'(\omega) = \left(\omega C'_R - \frac{1}{\omega L'_L} \right). \quad (11.203)$$

The series resonance frequency ω_{rs} of $X'(\omega)$ and the parallel resonance frequency ω_{rp} of $B'(\omega)$ are given by

$$\omega_{rs} = \frac{1}{\sqrt{L'_R C'_L}}, \quad \omega_{rp} = \frac{1}{\sqrt{L'_L C'_R}}. \quad (11.204)$$

Below both resonance frequencies ω_{rs} and ω_{rp} and the reactance per unit of length $X'(\omega)$ as well as the susceptance per unit of length $B'(\omega)$ are negative. This yields a real negative refractive index. Between both resonance frequencies ω_{rs} and ω_{rp} the reactance per unit of length $X'(\omega)$ as well as the susceptance per unit of length $B'(\omega)$ exhibit opposite signs and the refractive index becomes imaginary. The frequency band between ω_{rs} and ω_{rp} therefore is a stop-band. Above both resonance frequencies $X'(\omega)$ as well as $B'(\omega)$ are positive and the refractive index is real and positive.

With (8.3) we obtain the *dispersion characteristics* for the pass-bands $\omega < \omega_{c1}$ and $\omega > \omega_{c2}$,

$$\beta(\omega) = s(\omega) \sqrt{\omega^2 L'_R C'_R + \frac{1}{\omega^2 L'_L C'_L} - \frac{L'_R}{L'_L} - \frac{C'_R}{C'_L}} \quad (11.205)$$

with

$$s(\omega) = \begin{cases} -1 & \text{if } \omega < \omega_{c1} \\ 1 & \text{if } \omega > \omega_{c2} \end{cases} \quad (11.206)$$

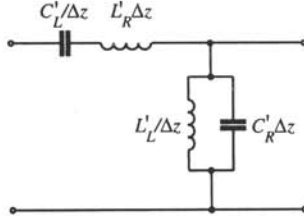


Figure 11.31: One-dimensional equivalent circuit model.

and the lower cutoff frequency ω_{c1} and the upper cutoff frequency ω_{c2} are given by

$$\omega_{c1} = \min(\omega_{rs}, \omega_{rp}), \quad \omega_{c2} = \max(\omega_{rs}, \omega_{rp}). \quad (11.207)$$

In the stop-band $\omega_{c1} < \omega < \omega_{c2}$ the attenuation coefficient is given by

$$\alpha(\omega) = \sqrt{\frac{L'_R}{L'_L} + \frac{C'_R}{C'_L} - \omega^2 L'_R C'_R - \frac{1}{\omega^2 L'_L C'_L}}. \quad (11.208)$$

The dispersion diagram is shown in Figure 11.32(a). This case, where series and parallel resonances differ from each other, is called unbalanced. When the series and parallel resonances are equal (i.e., $\omega_{rs} = \omega_{rp}$) no stop-band occurs. At the transition frequency ω_0 given by

$$\omega_0 = \frac{1}{\sqrt{L'_R C'_L}} = \frac{1}{\sqrt{L'_L C'_R}} \quad (11.209)$$

the phase coefficient changes the sign. The phase coefficient β can now be expressed by

$$\beta = \beta_L + \beta_R \quad (11.210)$$

with

$$\beta_L = -\frac{1}{\omega \sqrt{L'_L C'_L}}, \quad \beta_R = \omega \sqrt{L'_R C'_R}. \quad (11.211)$$

The dispersion diagram for the balanced left-handed transmission-line is shown in Figure 11.32(b).

Left-handed structures may be composed only by connection of segments of finite size or by embedding finite-size structures in the material. Left-handed materials can be of periodic or random structure. Periodic metamaterials differ from periodic structures as treated in Section 11.1 particularly with respect to the size of the period. In periodic

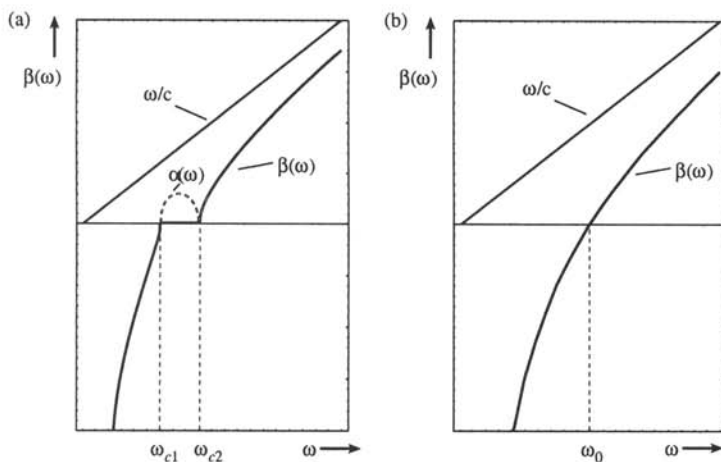


Figure 11.32: Dispersion diagrams: (a) unbalanced case, and (b) balanced case.

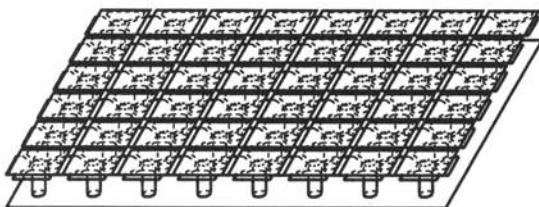


Figure 11.33: Two-dimensional metamaterial structure.

structures where the frequency selective properties are utilized the period is in the order of the wavelength. Periodic metamaterials are designed such that the period is small compared with the wavelength in order to keep the dispersion as small as possible. A two-dimensional metamaterial structure can be realized by a mushroom structure [29] as depicted in Figure 11.33. The mushroom structure consists of a two-dimensional periodic array of small conducting plates mounted on the top of thin conducting posts. The posts are mounted on a conducting ground plate. The posts act as inductors between the mushroom caps and the ground plate. The gaps between the plates are narrow so that each mushroom cap is capacitively coupled with its neighbors. However, it is inevitable that every mushroom cap also exhibits a capacitive coupling to the ground in parallel to the post inductance and an inductive coupling in series to the capacitive coupling to the neighboring cell. This can be seen easily when trying to increase the parallel inductance as well as the series capacitances of a cell. In the limit, when parallel inductance and series capacitances are going to infinity, the post

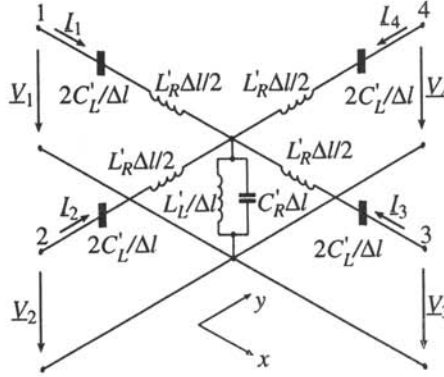


Figure 11.34: Two-dimensional equivalent circuit model.

diameter as well as the width of the gap between the cells are going to zero. In this limit the structure becomes a parallel plate structure with only parallel capacitance and series inductance.

The equivalent circuit of a cell of two-dimensional mushroom structure is presented in Figure 11.34. This circuit has been investigated in [30]. From the definition of the impedance matrix (10.3b), it follows that the matrix element Z_{ij} of the impedance matrix is the ratio of port voltage V_i to port current I_j when all ports with exception of the j th one are open. This allows us to write down the impedance matrix of the four-port depicted in Figure 11.34 directly as

$$\mathbf{Z} = \mathbf{Z}_1(\omega) \begin{bmatrix} 1 & 0 & 0 & 0 \\ 0 & 1 & 0 & 0 \\ 0 & 0 & 1 & 0 \\ 0 & 0 & 0 & 1 \end{bmatrix} + \mathbf{Z}_2(\omega) \begin{bmatrix} 1 & 1 & 1 & 1 \\ 1 & 1 & 1 & 1 \\ 1 & 1 & 1 & 1 \\ 1 & 1 & 1 & 1 \end{bmatrix} \quad (11.212)$$

with

$$Z_1(\omega) = \frac{1}{2} \Delta l \left(\frac{1}{j\omega C'_L} + j\omega L'_R \right) \quad Z_2^{-1}(\omega) = \Delta l \left(\frac{1}{j\omega L'_L} + j\omega C'_R \right). \quad (11.213)$$

Consider a plane wave with wave vector components k_x and k_y propagating through a two-dimensional array of cells. To simplify the model we assume infinite extension of the structure in the xy -plane. Applying Floquet's theorem we imply the boundary

conditions

$$\underline{V} = \begin{bmatrix} V_1(\omega) \\ V_2(\omega) \\ V_3(\omega) \\ V_4(\omega) \end{bmatrix} = \begin{bmatrix} \underline{V}_x \exp(\frac{1}{2}j k_x \Delta l) \\ \underline{V}_y \exp(\frac{1}{2}j k_y \Delta l) \\ \underline{V}_x \exp(-\frac{1}{2}j k_x \Delta l) \\ \underline{V}_y \exp(-\frac{1}{2}j k_y \Delta l) \end{bmatrix}, \quad (11.214a)$$

$$\underline{I} = \begin{bmatrix} I_1(\omega) \\ I_2(\omega) \\ I_3(\omega) \\ I_4(\omega) \end{bmatrix} = \begin{bmatrix} \underline{I}_x \exp(\frac{1}{2}j k_x \Delta l) \\ \underline{I}_y \exp(\frac{1}{2}j k_y \Delta l) \\ -\underline{I}_x \exp(-\frac{1}{2}j k_x \Delta l) \\ -\underline{I}_y \exp(-\frac{1}{2}j k_y \Delta l) \end{bmatrix}. \quad (11.214b)$$

With the transformation matrix

$$\underline{M} = \frac{1}{\sqrt{2}} \begin{bmatrix} -1 & 0 & 0 & 1 \\ -1 & 0 & 1 & 0 \\ -1 & 1 & 0 & 0 \\ 1 & 1 & 1 & 1 \end{bmatrix} \quad (11.215)$$

we can diagonalize the matrix \underline{Z} and obtain

$$\tilde{\underline{Z}} = \underline{M} \underline{Z} \underline{M}^{-1} = \begin{bmatrix} Z_1 & 0 & 0 & 0 \\ 0 & Z_1 & 0 & 0 \\ 0 & 0 & Z_1 & 0 \\ 0 & 0 & 0 & Z_1 + 4Z_2 \end{bmatrix}. \quad (11.216)$$

The transformed voltages and currents are

$$\tilde{\underline{V}} = \underline{M} \underline{V} = \frac{1}{\sqrt{2}} \begin{bmatrix} -\underline{V}_x \exp(\frac{1}{2}j k_x \Delta l) + \underline{V}_y \exp(-\frac{1}{2}j k_y \Delta l) \\ -\underline{V}_x \exp(\frac{1}{2}j k_x \Delta l) + \underline{V}_x \exp(-\frac{1}{2}j k_x \Delta l) \\ -\underline{V}_x \exp(\frac{1}{2}j k_x \Delta l) + \underline{V}_y \exp(\frac{1}{2}j k_y \Delta l) \\ 2\underline{V}_x \cos(\frac{1}{2}j k_x \Delta l) + 2\underline{V}_y \cos(\frac{1}{2}j k_y \Delta l) \end{bmatrix}, \quad (11.217a)$$

$$\tilde{\underline{I}} = \underline{M} \underline{I} = \frac{1}{\sqrt{2}} \begin{bmatrix} -\underline{I}_x \exp(\frac{1}{2}j k_x \Delta l) - \underline{I}_y \exp(-\frac{1}{2}j k_y \Delta l) \\ -\underline{I}_x \exp(\frac{1}{2}j k_x \Delta l) - \underline{I}_x \exp(-\frac{1}{2}j k_x \Delta l) \\ -\underline{I}_x \exp(\frac{1}{2}j k_x \Delta l) + \underline{I}_y \exp(\frac{1}{2}j k_y \Delta l) \\ 2\underline{I}_x \cos(\frac{1}{2}j k_x \Delta l) + 2\underline{I}_y \cos(\frac{1}{2}j k_y \Delta l) \end{bmatrix}. \quad (11.217b)$$

The transformed variables are related by

$$\tilde{\underline{V}} = \tilde{\underline{Z}} \tilde{\underline{I}}. \quad (11.218)$$

Inserting (11.217a) and (11.217b) yields a homogeneous system of equations with the four amplitudes V_x , I_x , V_y and I_y . The determinant of the coefficient of the system of equations yields the characteristic equation

$$\sin^2\left(\frac{1}{2}k_x\Delta l\right) + \sin^2\left(\frac{1}{2}k_y\Delta l\right) = -\frac{1}{2}\frac{Z_1(\omega)}{Z_2(\omega)}. \quad (11.219)$$

Inserting (11.213) we obtain the *dispersion relation*

$$\sin^2\left(\frac{1}{2}k_x\Delta l\right) + \sin^2\left(\frac{1}{2}k_y\Delta l\right) = \frac{\omega_L^2}{\omega^2}\left(1 - \frac{\omega^2}{\omega_{rp}^2}\right)\left(1 - \frac{\omega^2}{\omega_{rs}^2}\right) \quad (11.220)$$

with

$$\omega_L = \frac{\Delta l}{2\sqrt{L'_L C'_L}}, \quad \omega_{rp} = \frac{1}{\sqrt{L'_L C'_R}}, \quad \omega_{rs} = \frac{1}{\sqrt{L'_R C'_L}}. \quad (11.221)$$

The dispersion characteristics is anisotropic. Comparing the dispersion characteristics for propagation in the x - or y -direction with the dispersion characteristics in the diagonal direction yields

$$\sin^2\left(\frac{1}{2}k\Delta l\right) = \frac{\omega_L^2}{\omega^2}\left(1 - \frac{\omega^2}{\omega_{rp}^2}\right)\left(1 - \frac{\omega^2}{\omega_{rs}^2}\right) \quad \text{for } k = k_x, k_y, \quad (11.222a)$$

$$2\sin^2\left(\frac{1}{4}\sqrt{2}k\Delta l\right) = \frac{\omega_L^2}{\omega^2}\left(1 - \frac{\omega^2}{\omega_{rp}^2}\right)\left(1 - \frac{\omega^2}{\omega_{rs}^2}\right) \quad \text{for } k_x = k_y = \frac{1}{\sqrt{2}}\sqrt{2}k, \quad (11.222b)$$

For small wave numbers k in the limit $k \rightarrow 0$ we can approximate the dispersion relation by

$$k = \sqrt{k_x^2 + k_y^2} = \frac{\Delta l}{\omega\sqrt{L'_L C'_L}} \quad \text{for } k \rightarrow 0. \quad (11.223)$$

11.9 PROBLEMS

- Consider a time-harmonic TEM wave propagating in z -direction in an isotropic medium with a permittivity $\epsilon(z)$ varying in z -direction sinusoidally according to (11.35) and (11.36). The parameters are $\epsilon_m = 12$, $\Delta\epsilon = 9.2$ and $p = 5$ mm.
 - Compute the cutoff frequencies of the three lowest pass-bands.
 - Draw the dispersion characteristics for the three lowest pass-bands.
- Consider a waveguide WR28 (see Table 7.3) filled with the material specified in the previous example with permittivity varying in longitudinal direction of the waveguide.

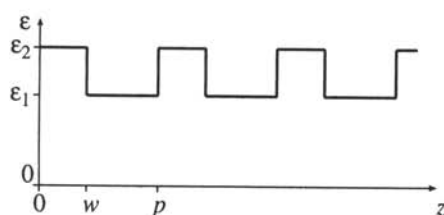


Figure 11.35: Variation of the permittivity.

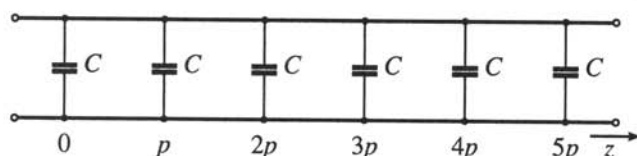


Figure 11.36: Transmission line with periodic capacitive load.

- a) Compute the edge frequencies of the three lowest pass-bands for the TE_{10} mode.
 - b) Compute the edge frequencies of the three lowest pass-bands for the TE_{20} mode.
3. Consider an isotropic dielectric with periodic permittivity variation in z -direction with period p as shown in Figure 11.35. The parameters are $\epsilon_m = 1.5$, $\Delta\epsilon = 0.1$, $p = 5$ mm, and $w = 2$ mm. Consider a time-harmonic TEM wave propagating in z -direction in an isotropic medium with a permittivity $\epsilon(z)$ varying in z -direction sinusoidally according to (11.35) and (11.36).
 - a) Compute the cutoff frequencies of the three lowest pass-bands.
 - b) Draw the dispersion characteristics for the three lowest pass-bands.
 - c) Compute the field impedances when looking at $z = 0$ and $z = w$ into the right half-space.
4. Consider a transmission-line periodically loaded with a capacitance C as shown schematically in Figure 11.36. The transmission-line is excited in the TEM mode. The unloaded transmission-line is characterized by the wave impedance Z_0 and the wave velocity c .
 - a) Compute the dispersion characteristics of the loaded transmission-line.
 - b) Compute the characteristic impedance of the loaded transmission-line for the plane of reference at $z = 0$.
 - c) Compute the frequency dependence of the dispersion characteristics and the characteristic impedance for $Z_0 = 50 \Omega$, $c = 2 \cdot 10^8 \text{ ms}^{-1}$, $p = 3$ cm, $C = 0.1$ pF.

5. Design a Butterworth band-pass filter with a center frequency of 1 GHz and a bandwidth of 10 MHz and $n = 5$.
6. Design a Chebyshev band-pass filter with a mid frequency of 1 GHz and a bandwidth of 10 MHz, 0.1 dB ripple and $n = 5$.
7. Consider a harmonic TEM wave of frequency $f = 60$ GHz normally incident on the corrugated surface depicted in Figure 11.27 and polarized in y -direction. Let $d = 10$ mm and $w = 2$ mm.
 - a) Determine h for maximum variation of the surface impedance.
 - b) Identify all propagating Floquet modes and their angle of scattering.
 - c) Discuss the power flow.
8. Consider a left-handed transmission-line. The equivalent circuit model is given by Figure 11.31. Realize this left-handed transmission-line by periodically cascading this two-port and its inverted two-port.
 - a) Compute and draw the dispersion diagram and frequency dependence of the group velocity and the characteristic impedances for $\Delta z = 1$ mm, $L'_R \Delta z = 0.25$ nH, $C'_R \Delta z = 0.1$ pF, $L'_L / \Delta z = 1$ nH, and $C'_L / \Delta z = 1$ pF.
 - b) Compute and draw the dispersion diagram and frequency dependence of the group velocity and the characteristic impedances for $\Delta z = 1$ mm, $L'_R \Delta z = 0.25$ nH, $C'_R \Delta z = 0.1$ pF, $L'_L / \Delta z = 1$ nH, and $C'_L / \Delta z = 0.8$ pF.
 - c) Change the electrical length of the transmission-line segment to $\Delta z = 0.2$ mm and keep the parameters L'_R , C'_R , L'_L , and C'_L unchanged. How does this affect the circuit elements in Figure 11.31 and the dispersion characteristics in both cases?
9. Consider the equivalent circuit of a two-dimensional metamaterial structure shown in Figure 11.34. The parameters are $L'_R \Delta l = 0.5$ nH, $C'_R \Delta l = 0.1$ pF, $L'_L / \Delta l = 1$ nH, and $C'_L / \Delta l = 1$ pF. Compute the dispersion characteristics and the frequency dependence for wave propagation in the axial direction and for wave propagation in the diagonal direction.

REFERENCES

- [1] L. Brillouin, *Wave Propagation in Periodic Structures*. New York: Dover, 1953.
- [2] E. L. Chu and W. Hansen, "The theory of disk-loaded waveguides," *J. Appl. Physics*, vol. 18, pp. 996–1008, July 1947.
- [3] L. Brillouin, "Plane wave coupling to multiple conductor transmission-lines above a lossy earth," *J. Appl. Physics*, vol. 19, pp. 1023–1041, Nov. 1948.
- [4] R. E. Collin, *Field Theory of Guided Waves*. New York: IEEE Press, 1991.
- [5] E. L. Ince, *Ordinary Differential Equations*. New York: Dover, 1956.
- [6] H. Reinhard, *Differential Equations - Foundations and Applications*. London: North Oxford Academic Publishers, 1986.
- [7] D. Zwillinger, *Handbook of Differential Equations*. New York: Academic Press, 1989.
- [8] P. Morse and H. Feshbach, *Methods of Theoretical Physics, Part I*. New York: McGraw-Hill, 1953.

- [9] M. Abramowitz and I. Stegun, *Handbook of Mathematical Functions with Formulas, Graphs and Mathematical Tables*. New York: Dover, 1965.
- [10] G. Matthaei, L. Young, and E. M. T. Jones, *Microwave Filters, Impedance Matching Networks, and Coupling Structures*. Boston: Artech House, 1980.
- [11] I. Hunter, *Theory and Design of Microwave Filters*. London: IEE, 2001.
- [12] R. Saal and W. Entenmann, *Handbuch zum Filterentwurf - Handbook of Filter Design*. Heidelberg: Hüthig, 1988.
- [13] A. I. Zverev, *Handbook of Filter Synthesis*. New York: John Wiley & Sons, 1967.
- [14] G. Arfken, *Mathematical Methods for Physicists*. New York: Academic Press, 1985.
- [15] H. J. Orchard, "Formula for ladder filters," *Wireless Engineer*, vol. 30, pp. 3–5, Jan. 1953.
- [16] L. Weinberg, "Explicit formulas for Tscheybscheff and Butterworth ladder networks," *J. Appl. Physics*, vol. 28, pp. 1155–1160, Oct. 1957.
- [17] R. S. Elliott, "On the theory of corrugated plane surfaces," *IRE Trans. Antennas Propagat.*, vol. 2, pp. 71–81, Apr. 1954.
- [18] A. Lai, T. Itoh, and C. Caloz, "Composite right/left-handed transmission-line metamaterials," *IEEE Microwave Magazine*, vol. 5, pp. 34–50, Sept. 2004.
- [19] S. Tretyakov, *Analytical Modeling in Applied Electromagnetics*. Boston: Artech House, 2003.
- [20] V. G. Veselago, "The electrodynamics of substances with simultaneously negative values of ϵ and μ ," *Sov. Phys. Usp.*, pp. 509–514, Jan.-Feb. 1968.
- [21] H. C. Pocklington, "Growth of a wave-group when the group velocity is negative," *Nature*, vol. 71, pp. 607–608, 1905.
- [22] S. Ramo, J. R. Whinnery, and T. van Duzer, *Fields and Waves in Communication Electronics*. New York: John Wiley & Sons, 1965.
- [23] F. Mariotte, B. Sauviac, and S. A. Tretyakov, "Artificial bianisotropic composites," in *Frontiers in Electromagnetics* (D. H. Werner and R. Mittra, eds.), New York: IEEE Press, 2000.
- [24] W. Rotman, "Plasma simulation by artificial dielectrics and parallel-plate media," *IEEE Trans. Antennas Propagat.*, vol. 10, pp. 82–95, Jan. 1962.
- [25] D. R. Smith, W. J. Padilla, D. C. Vier, S. C. Nemat-Nasser, and S. Schultz, "Composite medium with simultaneously negative permeability and permittivity," *Phys. Rev. Lett.*, vol. 84, pp. 4184–4187, May 2000.
- [26] D. R. Smith and N. Kroll, "Negative refractive index in left-handed materials," *Phys. Rev. Lett.*, vol. 85, pp. 2933–2936, Oct. 2000.
- [27] J. B. Pendry, "Negative refraction makes a perfect lens," *Phys. Rev. Lett.*, vol. 85, pp. 3966–3969, Oct. 2000.
- [28] R. A. Shelby, D. R. Smith, and S. Schultz, "Experimental verification of a negative index of refraction," *Nature*, vol. 292, pp. 77–79, Apr. 2001.
- [29] A. Sanada, C. Caloz, and C. Itoh, "Planar distributed structures with negative refractive index," *IEEE Trans. Microwave Theory Techn.*, vol. 52, pp. 1252–1263, Apr. 2004.
- [30] A. Grbic and G. V. Eleftheriades, "Periodic analysis of a 2-d negative refractive index transmission line structure," *IEEE Trans. Microwave Theory Techn.*, vol. 51, pp. 2604–2611, Oct. 2003.

Chapter 12

Radiation from Dipoles

12.1 THE HERTZIAN DIPOLE

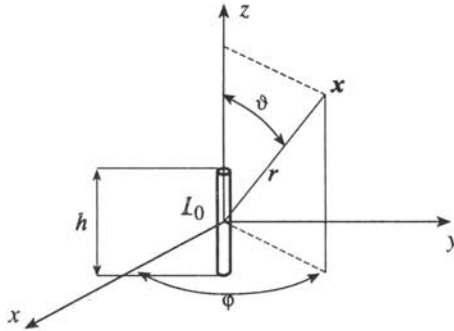
Heinrich Hertz was the first to compute the radiation of an electric dipole and he also published the first diagrams showing the development and outward propagation of the field radiated from the dipole [1–4]. In his derivation of the electromagnetic field excited by a short electric dipole he introduced a vector quantity that is named after him the *Hertz vector*.

We compute the radiation field of a short straight wire segment with impressed harmonic current. The length h of this conductor is assumed to be small compared to the wavelength. Therefore the current \underline{I} may be considered to be uniform over the length h of the wire segment. Such an arrangement is called a short electric dipole or Hertzian dipole. In his early experiments, Heinrich Hertz realized such a dipole by attaching spheres at the end of the line segment. These spheres are storing the charge accumulated at the end of the wire, if a uniformly distributed current is flowing through the wire. Complex wire antennas or other radiating wire structures may be modeled by segments of Hertzian dipoles. The current \underline{I}_0 may be impressed at some intersection introduced into the Hertzian dipole. For r much larger than h we may consider the polarization excited by the current \underline{I} to be concentrated into the origin. From (4.103a) we obtain under this assumption the approximate solution for the Hertz form

$$\underline{\Pi}_e(\mathbf{x}) = \frac{e^{-jkr}}{4\pi\epsilon_0 r} \int_V (\underline{M}_{e0x}(\mathbf{x}') dx' + \underline{M}_{e0y}(\mathbf{x}') dy' + \underline{M}_{e0z}(\mathbf{x}') dz') dx' \wedge dy' \wedge dz'. \quad (12.1)$$

Due to (3.23), the impressed electric polarization \underline{M}_{e0} and the impressed current density $\underline{\mathcal{J}}_0$ are related by

$$\underline{M}_{e0} = \frac{1}{j\omega} \underline{\mathcal{J}}_0. \quad (12.2)$$

Figure 12.1: Conductor of the length h .

According to Figure 12.1, the current density $\underline{J}_0(\mathbf{x})$ exhibits only a z -component. Since the surface integral of \underline{J}_0 over the cross-section of the conductor is equal to the current $I_0(\mathbf{x})$, we obtain

$$\int_V \underline{J}_0 = h I_0. \quad (12.3)$$

The polarization $\underline{M}_{e0}(\mathbf{x}')$ also exhibits a z -component only. From (12.1) and (12.3) it follows that

$$\underline{\Pi}_{ez}(\mathbf{x}) = \frac{h I_0}{4\pi j \omega \epsilon_0} \frac{e^{-jk r}}{r}. \quad (12.4)$$

From (A.160) and (A.163) we obtain

$$\underline{\Pi}_e = \Pi_z dz = \cos \theta \Pi_z s_1 - \sin \theta \Pi_z s_2 = \cos \theta \Pi_z dr - r \sin \theta \Pi_z d\theta. \quad (12.5)$$

Using (3.29a) and (3.29b) and considering that \underline{M}_{e0} vanishes outside the conductor, we can compute $\underline{\mathcal{E}}$ and $\underline{\mathcal{H}}$,

$$\underline{\mathcal{H}} = j \omega \underline{\epsilon} \star d \underline{\Pi}_e, \quad (12.6a)$$

$$\underline{\mathcal{E}} = -\tilde{d} d \underline{\Pi}_e. \quad (12.6b)$$

From (12.5) we obtain

$$d \underline{\Pi}_e = \frac{\partial}{\partial \theta} (\cos \theta \Pi_z) d\theta \wedge dr - \frac{\partial}{\partial r} (r \sin \theta \Pi_z) dr \wedge d\theta. \quad (12.7)$$

Inserting (12.4), it follows that

$$d \underline{\Pi}_e = \frac{h I_0}{4\pi j \omega \epsilon_0} \left(\frac{1}{r^2} + \frac{j k}{r} \right) e^{-jk r} \sin \theta r dr \wedge d\theta. \quad (12.8)$$

Applying the Hodge operator yields

$$\star d \underline{\Pi}_e = \frac{h I_0}{4\pi j \omega \epsilon_0} \left(\frac{1}{r^2} + \frac{j k}{r} \right) e^{-j k r} \sin \theta r \sin \theta d\phi. \quad (12.9)$$

Using (12.6a) yields

$$\underline{\mathcal{H}} = \frac{h I_0}{4\pi} \left(\frac{1}{r^2} + \frac{j k}{r} \right) e^{-j k r} \sin \theta r \sin \theta d\phi. \quad (12.10)$$

Consequently, the magnetic field only exhibits a ϕ -component

$$\underline{H}_\phi = \frac{h I_0}{4\pi} \left(\frac{j k}{r} + \frac{1}{r^2} \right) e^{-j k r} \sin \theta. \quad (12.11)$$

In order to obtain $\underline{\mathcal{E}}$ from (12.6b) we first compute the exterior derivative of (12.9) and obtain

$$\begin{aligned} d \star d \underline{\Pi}_e = \frac{h I_0}{4\pi j \omega \epsilon_0} & \left[\left(-\frac{k^2}{r} + \frac{j k}{r^2} + \frac{1}{r^3} \right) e^{-j k r} \sin \theta r \sin \theta d\phi \wedge dr \right. \\ & \left. + 2 \left(\frac{j k}{r^2} + \frac{1}{r^3} \right) e^{-j k r} \cos \theta r^2 \sin \theta d\theta \wedge d\phi \right]. \end{aligned} \quad (12.12)$$

Applying the Hodge operator yields

$$\begin{aligned} \underline{\mathcal{E}} = \star d \star d \underline{\Pi}_e = \frac{h I_0}{4\pi j \omega \epsilon_0} & \left[\left(-\frac{k^2}{r} + \frac{j k}{r^2} + \frac{1}{r^3} \right) e^{-j k r} \sin \theta r d\theta \right. \\ & \left. + 2 \left(\frac{j k}{r^2} + \frac{1}{r^3} \right) e^{-j k r} \cos \theta dr \right]. \end{aligned} \quad (12.13)$$

The electric field exhibits θ -components and r -components,

$$\underline{E}_\theta = \frac{h I_0}{4\pi j \omega \epsilon_0} \left(-\frac{k^2}{r} + \frac{j k}{r^2} + \frac{1}{r^3} \right) e^{-j k r} \sin \theta, \quad (12.14a)$$

$$\underline{E}_r = \frac{h I_0}{2\pi j \omega \epsilon_0} \left(\frac{j k}{r^2} + \frac{1}{r^3} \right) e^{-j k r} \cos \theta. \quad (12.14b)$$

For $kr \ll 1$ the magnetic field component \underline{H}_ϕ is only determined by the term proportional to $1/r^2$ and \underline{E}_r and \underline{E}_θ are only determined by the terms proportional to $1/r^3$. This region is the *near-field* region. In the near-field the magnetic field is in phase with the current. The magnetic field there corresponds to the magnetic field distribution

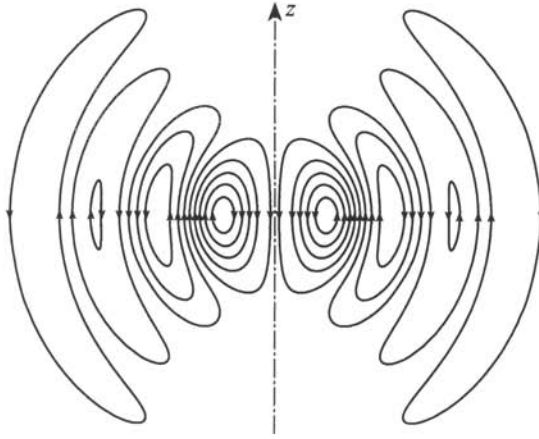


Figure 12.2: Electric flux lines in the near-field of the Hertzian dipole.

generated by the stationary current. The electric near-field also corresponds to the field distribution excited by a static electric dipole.

Figure 12.2 shows the electric field lines in the near-field. The field in the region $kr \gg 1$ is called the *far-field*. With the exception of the electric field in the directions $\theta = 0$ and $\theta = \pi$, respectively, the field quantities proportional to $1/r$ are dominant, and the electric field exhibits a θ -component only. For the far-field region we obtain the approximate differential forms

$$\underline{\mathcal{E}} = \frac{j\omega\mu_0 h \underline{I}_0}{4\pi} \frac{e^{-jkr}}{r} \sin\theta \, r \, d\theta, \quad (12.15a)$$

$$\underline{\mathcal{H}} = \frac{jk h \underline{I}_0}{4\pi} \frac{e^{-jkr}}{r} \sin\theta \, r \, \sin\theta \, d\phi \quad (12.15b)$$

and the corresponding field components

$$\underline{E}_\theta = \frac{j\omega\mu_0 h \underline{I}_0}{4\pi} \frac{e^{-jkr}}{r} \sin\theta, \quad (12.16)$$

$$\underline{H}_\phi = \frac{jk h \underline{I}_0}{4\pi} \frac{e^{-jkr}}{r} \sin\theta. \quad (12.17)$$

In the far-field the electric and magnetic field components are mutually orthogonal and both are orthogonal to the direction of propagation (Figure 12.3). Furthermore the electric field and the magnetic field are proportional to each other and in phase. The *radiation diagram* of an antenna depicts the angular distribution of the radiated field.

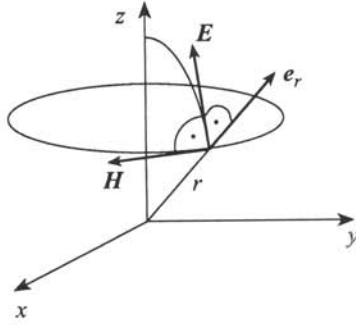


Figure 12.3: Orientation of E , H , and e_r in the far-field of the Hertzian dipole.

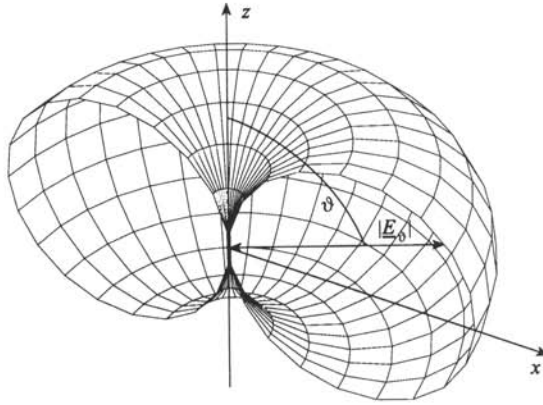


Figure 12.4: Radiation diagram of the Hertzian dipole.

The antenna characteristics of the Hertzian dipole is given by the dependence of the magnitude of the electric field $|\underline{E}_\theta|$ from the angles θ and ϕ (Figure 12.4). From (12.16), (12.17), and (6.36) it follows that the ratio of electric and magnetic field in the far-field is given by

$$\frac{\underline{E}_\theta}{\underline{H}_\phi} = Z_{F0} \cong 377 \Omega. \quad (12.18)$$

From (4.19), (12.15a), and (12.15b) we obtain the complex Poynting form \mathcal{T} for the far-field

$$\mathcal{T} = \frac{1}{2} \underline{\mathcal{E}} \wedge \underline{\mathcal{H}}^* = \frac{1}{2} \underline{E}_\theta \underline{H}_\phi^* r^2 \sin \theta d\theta \wedge d\phi = \frac{Z_{F0} k^2 h^2 |\underline{L}_0|^2}{32\pi^2} \sin^3 \theta d\theta \wedge d\phi. \quad (12.19)$$

In the far-field the complex Poynting vector exhibits only a radial component

$$\underline{T}_r = \frac{Z_{F0} k^2 h^2 |\underline{I}_0|^2}{32\pi^2 r^2} \sin^2 \theta. \quad (12.20)$$

In this case \underline{T}_r is real and the active power P radiated from the Hertzian dipole is obtained by integrating \mathcal{T} over a closed surface surrounding the Hertzian dipole in the far-field,

$$P = \int_{\theta=0}^{\pi} \int_{\phi=0}^{2\pi} \mathcal{T}. \quad (12.21)$$

With

$$\int_0^{\pi} \sin^3 \theta d\theta = \frac{4}{3} \quad (12.22)$$

we obtain from (12.20) and (12.21)

$$P = \frac{1}{12\pi} Z_{F0} k^2 h^2 |\underline{I}_0|^2. \quad (12.23)$$

With $k = 2\pi/\lambda_0$ we obtain from this

$$P = \frac{1}{3}\pi Z_{F0} \left(\frac{h}{\lambda_0} \right)^2 |\underline{I}_0|^2. \quad (12.24)$$

We can introduce formally a radiation resistance R_r in which the active power P is anticipated, if a current I_0 is impressed,

$$P = \frac{1}{2} R_r |\underline{I}_0|^2. \quad (12.25)$$

Therewith we obtain

$$R_r = \frac{2}{3}\pi Z_{F0} \left(\frac{h}{\lambda_0} \right)^2. \quad (12.26)$$

12.2 APERIODIC SPHERICAL WAVES

To investigate the emission of *aperiodic spherical waves* we analyze the Hertzian dipole in the time domain. In the time domain the impressed polarization $m_{e0}(t)$ and the impressed current $i_0(t)$ are related via the inverse Fourier transform of (12.2),

$$\mathcal{M}_{e0}(\mathbf{x}, t) = \int_0^t \mathcal{J}_0(\mathbf{x}, t_1) dt_1. \quad (12.27)$$

Integrating the electric polarization form \mathcal{M}_{e0} over the volume V of the Hertzian dipole yields

$$m_{e0}(t) = \int_V \mathcal{M}_{e0}(\mathbf{x}, t) = h \int_0^t i_0(t_1) dt_1, \quad (12.28)$$

where $i_0(t)$ is the current through the Hertzian dipole, $m_{e0}(t)$ the polarization due to this current, and h the dipole length. This yields

$$\Pi_{ez}(\mathbf{x}, t) = \frac{h}{4\pi\epsilon_0 r} m_{e0} \left(t - \frac{r}{c} \right). \quad (12.29)$$

Using (3.20b) and (3.21) and considering that $\mathcal{M}_{e0}(\mathbf{x}, t)$ vanishes outside the conductor, we can compute $\mathcal{E}(\mathbf{x}, t)$ and $\mathcal{H}(\mathbf{x}, t)$,

$$\mathcal{H}(\mathbf{x}, t) = \star d\epsilon \frac{\partial}{\partial t} \Pi_e(\mathbf{x}, t), \quad (12.30a)$$

$$\mathcal{E}(\mathbf{x}, t) = -\tilde{d} d \Pi_e(\mathbf{x}, t). \quad (12.30b)$$

Using (12.30a) yields

$$\mathcal{H} = \frac{h}{4\pi} \left[\frac{1}{r^2} m'_{e0} \left(t - \frac{r}{c} \right) + \frac{1}{cr} m''_{e0} \left(t - \frac{r}{c} \right) \right] \sin \theta r \sin \theta d\phi. \quad (12.31)$$

The magnetic field only exhibits a ϕ -component

$$H_\phi = \frac{h}{4\pi} \left[\frac{1}{r^2} m'_{e0} \left(t - \frac{r}{c} \right) + \frac{1}{cr} m''_{e0} \left(t - \frac{r}{c} \right) \right] \sin \theta. \quad (12.32)$$

The electric field form is

$$\begin{aligned} \mathcal{E} = \frac{h}{4\pi\epsilon_0} \left\{ \left[\frac{1}{r^3} m_{e0} \left(t - \frac{r}{c} \right) + \frac{1}{cr^2} m'_{e0} \left(t - \frac{r}{c} \right) \right. \right. \\ \left. \left. + \frac{1}{c^2 r} m''_{e0} \left(t - \frac{r}{c} \right) \right] \sin \theta r d\theta \right. \\ \left. + 2 \left[\frac{1}{r^3} m_{e0} \left(t - \frac{r}{c} \right) + \frac{1}{cr^2} m'_{e0} \left(t - \frac{r}{c} \right) \right] \cos \theta dr \right\}. \end{aligned} \quad (12.33)$$

The electric field exhibits the θ - and r -components

$$E_\theta = \frac{h}{4\pi\epsilon_0} \left[\frac{1}{r^3} m_{e0} \left(t - \frac{r}{c} \right) + \frac{1}{cr^2} m'_{e0} \left(t - \frac{r}{c} \right) + \frac{1}{c^2 r} m''_{e0} \left(t - \frac{r}{c} \right) \right] \sin \theta, \quad (12.34a)$$

$$E_r = \frac{h}{2\pi\epsilon_0} \left[\frac{1}{r^3} m_{e0} \left(t - \frac{r}{c} \right) + \frac{1}{cr^2} m'_{e0} \left(t - \frac{r}{c} \right) \right] \cos \theta. \quad (12.34b)$$

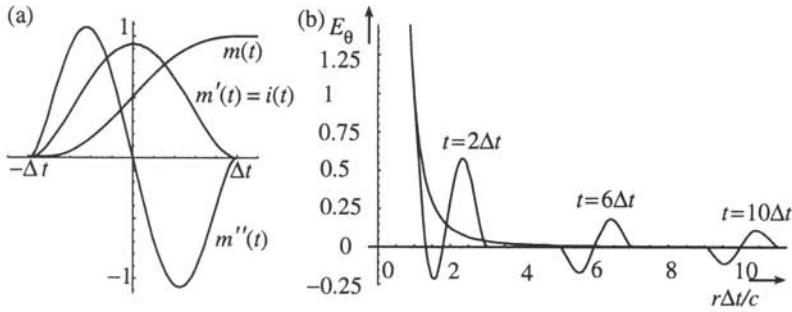


Figure 12.5: Wave pulse: (a) pulse waveforms and (b) radial dependence of the wave pulse.

As an example we consider a wave pulse emitted from a Hertzian dipole excited by a current pulse. In Figure 12.5(a) the dipole current pulse $i(t) = m'(t)$ of width $2\Delta t$, its integral over time $m(t)$ and its time derivative $m''(t)$ are depicted. Figure 12.5(b) shows the time evolution of $E_\theta(r, 0, 0, t)$. The wave front of width $2\Delta t$ mainly depends on $m'(t)$ and $m''(t)$. In the far-field region, defined by $r \gg c\Delta t$, the terms proportional to $1/r$ in E_θ and H_ϕ exhibit the double pulse shape specified by $m''(t)$. The energy connected with this term is constrained within the shell of width $2c\Delta t$ at the wave front and transported into infinity. This is the radiated part of the field. The electric and magnetic far-field time waveforms E_θ and H_ϕ of the wave pulse are proportional to the time derivative of the driving current $i(t)$ of the dipole. The near-field parts of the electric and magnetic field proportional to $m'(t - r/c)/r^2$ also are confined to the wave front in a shell of width $2\Delta t$. This part of the wave front is carrying the electromagnetic energy for building up the near-field. It leaves behind the wave front an electric field proportional to $m(t - r/c)/r^3$. This field behind the wave front corresponds to the electrostatic field excited by a static dipole. Figure 12.6 shows the electric field in a meridional plane.

In the far-field we obtain the approximate differential forms

$$\mathcal{E}(r, \theta, t) = \frac{\mu_0 h}{4\pi} \frac{m''_{e0} \left(t - \frac{r}{c}\right)}{r} \sin \theta r d\theta, \quad (12.35a)$$

$$\mathcal{H}(r, \theta, t) = \frac{h}{4\pi c} \frac{m''_{e0} \left(t - \frac{r}{c}\right)}{r} \sin \theta r \sin \theta d\phi \quad (12.35b)$$

and the corresponding field components

$$E_\theta(r, \theta, t) = \frac{\mu_0 h}{4\pi} \frac{m''_{e0} \left(t - \frac{r}{c}\right)}{r} \sin \theta, \quad (12.36)$$

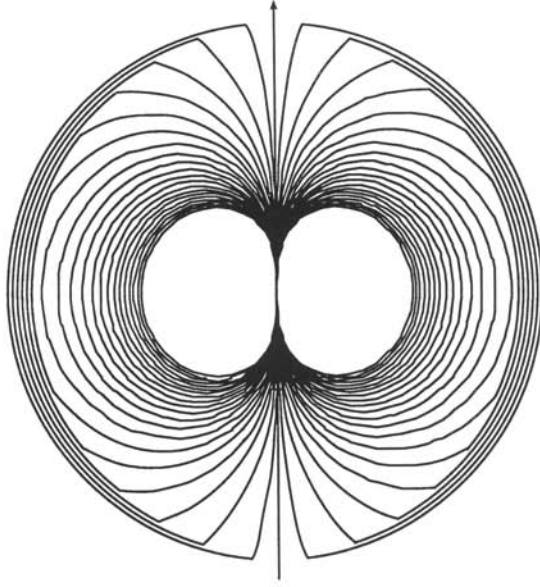


Figure 12.6: Near-field of the Hertzian dipole under pulse excitation.

$$H_{\phi}(r, \theta, t) = \frac{h}{4\pi c} \frac{m''_{e0} \left(t - \frac{r}{c}\right)}{r} \sin \theta. \quad (12.37)$$

The far-field is depicted in Figure 12.7. From (12.36), (12.37) and (6.36) it follows that the ratio of the electric and magnetic fields in the far-field is given by Z_{F0} . From (4.19), (12.35a) and (12.35b) we obtain the time-dependent Poynting form \mathcal{S} for the far-field

$$\mathcal{S}(r, \theta, t) = \frac{1}{2} \mathcal{E} \wedge \mathcal{H} = \frac{Z_{F0} h^2}{32\pi^2 c^2} m''_{e0}{}^2 \left(t - \frac{r}{c}\right) \sin^3 \theta \, d\theta \wedge d\phi. \quad (12.38)$$

In the far-field the complex Poynting vector exhibits only a radial component

$$S_r(r, \theta, t) = \frac{Z_{F0} h^2}{32\pi^2 r^2 c^2} m''_{e0}{}^2 \left(t - \frac{r}{c}\right) \sin^2 \theta. \quad (12.39)$$

The power $P(r, t)$ radiated from the Hertzian dipole through a spherical surface with radius r in the far-field is obtained by integrating \mathcal{S} over this surface.

$$P(r, t) = \int_{\theta=0}^{\pi} \int_{\phi=0}^{2\pi} \mathcal{S}(r, \theta, t). \quad (12.40)$$

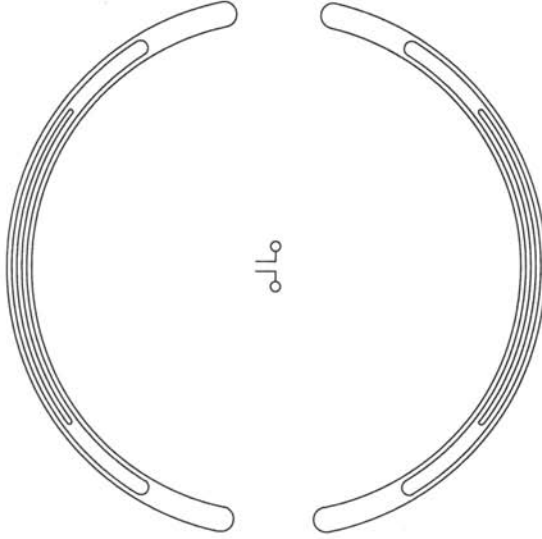


Figure 12.7: Far-field of the Hertzian dipole under pulse excitation..

We obtain from (12.39) and (12.40)

$$P(r, t) = \frac{Z_{F0} h^2}{12\pi c^2} m_{e0}''^2 \left(t - \frac{r}{c} \right). \quad (12.41)$$

12.3 VERTICALLY ORIENTED ELECTRIC DIPOLE OVER LOSSY HALF-SPACE

Radio-wave propagation over flat earth has been a subject of interest from the beginning of the 20th century. Consider a vertically oriented electric dipole above an infinitely extended lossy half-space as depicted in Figure 12.8. Sommerfeld gave a solution to this problem in 1909 [5, 6]. In his analytic treatment Sommerfeld was able to classify and evaluate the wave types excited by a dipole over ground. In addition to the treatment of electromagnetic wave propagation over the earth surface, Sommerfeld's theory became crucial for the computation of electromagnetic fields in planar and layered structures and therefore is fundamental for many advanced computational methods for microwave circuit and antenna design.

Following Sommerfeld's treatment we subdivide the space into three regions. Region 1 is the free-space above the dipole for $z > h$, region 2 is the free-space $0 < z \leq h$ and region 3 is the half-space filled by a lossy dielectric material in $z \leq 0$. The field will be

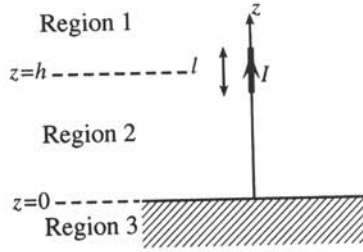


Figure 12.8: Vertically oriented dipole above a lossy half-space.

derived from a Hertz form $\underline{\Pi}_e$. The Hertz form fulfills the Helmholtz equation (3.28)

$$\Delta \underline{\Pi}_e + \omega^2 \underline{\mu} \underline{\epsilon} \underline{\Pi}_e = -\frac{1}{\underline{\epsilon}} * \underline{\mathcal{M}}_{e0}. \quad (12.42)$$

For the Hertzian dipole oriented in z -direction the polarization $\underline{\mathcal{M}}_{e0}$ is given by

$$\underline{\mathcal{M}}_{e0} = \frac{1}{j\omega} J_z \, dx \wedge dy, \quad (12.43a)$$

$$J_z = lI \delta(\mathbf{x} - \mathbf{x}_0) \quad \text{with } \mathbf{x}_0 = [0, 0, h]^T. \quad (12.43b)$$

The Hertz form in this case exhibits only a z -component

$$\underline{\Pi}_e(\mathbf{x}) = \underline{\Pi}_z(\mathbf{x}) \, dz. \quad (12.44)$$

Since the problem exhibits circular cylindric symmetry, we will introduce circular cylindric coordinates to solve this problem. The Hertz form only has a z -component that can be determined in free-space (regions 1 and 2) from the scalar Helmholtz equation

$$\Delta \underline{\Pi}_z + k^2 \underline{\Pi}_z = j \frac{lI}{\omega \epsilon_0} \delta(\mathbf{x} - \mathbf{x}_0) \quad (12.45)$$

and in the lossy medium (region 3) from

$$\Delta \underline{\Pi}_z + k_m^2 \underline{\Pi}_z = 0. \quad (12.46)$$

Since region 3 is assumed to be source-free, (12.46) is homogeneous. The wave numbers k in free-space and k_m in the medium are

$$k^2 = \omega^2 \mu_0 \epsilon_0, \quad (12.47a)$$

$$k_m^2 = \omega^2 \mu_0 \underline{\epsilon}_m. \quad (12.47b)$$

The permittivity $\underline{\epsilon}_m$ in the lossy medium is complex and given by

$$\underline{\epsilon}_m = \epsilon'_m - j \frac{\sigma}{\omega}, \quad (12.48)$$

where ϵ'_m is the real part of the complex permittivity of the medium. In the following we first consider the primary Hertz vector field $\underline{\Pi}_e^{(i)}$ radiated from the Hertzian dipole into free-space. This primary field is scattered at the boundary surface between free-space and medium and yields the scattered field $\underline{\Pi}_e^{(s)}$. The total field $\underline{\Pi}_e$ results from a superposition of the primary field $\underline{\Pi}_e^{(i)}$ and the scattered field $\underline{\Pi}_e^{(s)}$. In our case for symmetry reasons the primary Hertzian field $\underline{\Pi}_e^{(i)}$ as well as the scattered field $\underline{\Pi}_e^{(s)}$ only have z -components $\underline{\Pi}_z^{(i)}$. The solution for the primary field is given by

$$\underline{\Pi}_z^{(i)} = -\frac{jII}{4\pi\omega\epsilon_0} \frac{\exp(-jk|\mathbf{x} - \mathbf{x}_0|)}{|\mathbf{x} - \mathbf{x}_0|}. \quad (12.49)$$

The field components transmitted through the boundary surface and reflected from the boundary surface are computed by matching partial solutions of the Helmholtz equation under consideration of the boundary conditions at the boundary surface $z = 0$. To proceed in that way we represent the Hertzian vector in cylinder coordinates (ρ, ϕ, z) . We obtain from (12.45) and (A.157) the Helmholtz equation in circular cylindric coordinates,

$$\left\{ \frac{1}{\rho} \frac{\partial}{\partial \rho} \left(\rho \frac{\partial}{\partial \rho} \right) + \frac{1}{\rho^2} \frac{\partial^2}{\partial \phi^2} + \frac{\partial^2}{\partial z^2} + k^2 \right\} \underline{\Pi}_z^{(i)} = j \frac{II}{\omega\epsilon_0\rho} \delta(\rho - \rho_0) \delta(\phi - \phi_0) \delta(z - z_0). \quad (12.50)$$

First we expand $\underline{\Pi}_z$ into a Fourier series in ϕ and obtain

$$\underline{\Pi}_z(\rho, \phi, z) = \sum_{m=-\infty}^{m=\infty} \underline{\pi}_m(\rho, z) e^{-jm(\phi - \phi_0)}, \quad (12.51)$$

where $\underline{\pi}_m(\rho, z)$ is given by

$$\underline{\pi}_m(\rho, z) = \frac{1}{2\pi} \int_0^{2\pi} \underline{\Pi}_z(\rho, \phi, z) \exp[jm(\phi - \phi_0)] d\phi. \quad (12.52)$$

With this we obtain

$$\left\{ \frac{1}{\rho} \frac{\partial}{\partial \rho} \left(\rho \frac{\partial}{\partial \rho} \right) - \frac{m^2}{\rho^2} + \frac{\partial^2}{\partial z^2} + k^2 \right\} \underline{\pi}_m = \frac{jII}{2\pi\omega\epsilon_0\rho} \delta(\rho - \rho_0) \delta(z - z_0). \quad (12.53)$$

Now we perform a Bessel transformation with respect to the coordinate ρ and obtain

$$\underline{\pi}_m(\rho, z) = \int_0^\infty g_m(k_\rho, z) J_m(k_\rho \rho) k_\rho dk_\rho, \quad (12.54a)$$

$$g_m(k_\rho, z) = \int_0^\infty \underline{\pi}_m(\rho, z) J_m(k_\rho \rho_0) \rho d\rho. \quad (12.54b)$$

With this we obtain from (12.53)

$$\left\{ \frac{\partial^2}{\partial z^2} + k^2 - k_\rho^2 \right\} g_m(k_\rho, z) = j \frac{II}{2\pi\omega\epsilon_0} \delta(z - z_0) J_m(k_\rho \rho_0). \quad (12.55)$$

The solution of (12.55) is given by

$$g_m(k_\rho, z) = -\frac{II}{4\pi\omega\epsilon_0 k_z} \exp(-j k_z |z - z_0|) J_m(k_\rho \rho_0) \quad (12.56)$$

with

$$k_z^2 = k^2 - k_\rho^2. \quad (12.57)$$

Inserting (12.56) into (12.54a) and then (12.51) and (12.52) yields

$$\underline{\Pi}_z^{(i)}(\rho, \phi, z) = -\frac{II}{4\pi\omega\epsilon_0} \sum_{m=-\infty}^{m=\infty} e^{-jm(\phi-\phi_0)} \int_0^\infty J_m(k_\rho \rho) J_m(k_\rho \rho_0) e^{-j k_z |z-z_0|} \frac{k_\rho}{k_z} dk_\rho. \quad (12.58)$$

The equation (12.58) corresponds to (12.49), if the wave emitted from the Hertzian dipole is expanded into cylindrical functions with the propagation coefficient k_ρ . The boundary conditions at the boundary surface $z = 0$ are fulfilled for all ρ by matching all partial waves with the same k_ρ on both sides of the boundary surface.

For a Hertzian dipole at $\rho_0 = 0$ and $z_0 = h$ we obtain from (12.58)

$$\underline{\Pi}_z^{(i)}(\rho, \phi, z) = -\frac{II}{4\pi\omega\epsilon_0} \int_0^\infty J_0(k_\rho \rho) \exp(-j k_z |z - h|) \frac{k_\rho}{k_z} dk_\rho. \quad (12.59)$$

We solve (12.45) for x_0 given by $\rho_0 = 0$ and $z_0 = h$. The Hertz vector field $\underline{\Pi}_z$ is composed by the primary Hertz vector field $\underline{\Pi}_z^{(i)}$ excited by the Hertzian dipole and the scattered Hertz vector field $\underline{\Pi}_z^{(s)}$. The field $\underline{\Pi}_z^{(s)}$ originates from transmission and reflection of the primary vector field at the boundary surface $z = 0$.

We represent the primary field in region 1 by

$$\underline{\Pi}_z^{(i)}(\rho, \phi, z) = -\frac{II}{4\pi\omega\epsilon} \int_0^\infty J_0(k_\rho \rho) \exp[-j k_z (z - h)] \frac{k_\rho}{k_z} dk_\rho \quad (12.60)$$

and in region 2 by

$$\underline{\Pi}_z^{(i)}(\rho, \phi, z) = -\frac{II}{4\pi\omega\epsilon_0} \int_0^\infty J_0(k_\rho \rho) \exp[jk_z(z-h)] \frac{k_\rho}{k_z} dk_\rho. \quad (12.61)$$

The different exponential terms in (12.60) and (12.61) reflect the singularity of the primary field at $z = h$. The scattered Hertz vector field $\underline{\Pi}_z^{(s)}$ exhibits no singularity at $z_0 = h$ and consequently may be represented in both subspaces 1 and 2 by the same expression

$$\underline{\Pi}_z^{(s)}(\rho, \phi, z) = -\frac{II}{4\pi\omega\epsilon_0} \int_0^\infty R(k_\rho) J_0(k_\rho \rho) \exp[-jk_z(z+h)] \frac{k_\rho}{k_z} dk_\rho. \quad (12.62)$$

In this equation $R(k_\rho)$ is the reflection coefficient that is determined by matching of the partial waves. In the lossy medium of region 3 with $z < 0$ the variables k and k_z must be replaced by k_m and k_{mz} ,

$$k_{mz}^2 = k_m^2 - k_\rho^2. \quad (12.63)$$

In region 3 there exists no primary Hertz vector field and the transmitted vector field fulfills the scalar Helmholtz equation

$$\Delta \underline{\Pi}_z + k_m^2 \underline{\Pi}_z = 0. \quad (12.64)$$

The solution in region 3 is given by

$$\underline{\Pi}_z^{(s)}(\rho, \phi, z) = -\frac{II}{4\pi\omega\epsilon_0} \int_0^\infty T(k_\rho) J_0(k_\rho \rho) \exp[j(k_{mz}z - k_z h)] \frac{k_\rho}{k_z} dk_\rho. \quad (12.65)$$

The variable $T(k_\rho)$ is the transmission coefficient that has to be determined by matching of the partial waves. In region 3 we have to replace (12.57) by

$$k_{mz}^2 = k_m^2 - k_\rho^2. \quad (12.66)$$

In (12.60), (12.61), (12.62), and (12.65) the sign of $jk_z z$ is chosen in such a way that the expression for $|z| \rightarrow \infty$ goes to zero. We determine $R(k_\rho)$ and $T(k_\rho)$ by matching the partial waves at $z = 0$. From

$$\underline{\mathcal{E}} = d \tilde{d} \underline{\Pi}_e + \omega^2 \underline{\mu} \underline{\epsilon} \underline{\Pi}_e = -\tilde{d} d \underline{\Pi}_e - \frac{1}{\underline{\epsilon}} * \underline{\mathcal{M}}_{e0}, \quad (12.67a)$$

$$\underline{\mathcal{H}} = j \omega \underline{\epsilon} * d \underline{\Pi}_e \quad (12.67b)$$

we obtain

$$\underline{E}_\rho = \frac{\partial^2}{\partial \rho \partial z} \underline{\Pi}_z, \quad (12.68a)$$

$$\underline{E}_z = \left(\frac{\partial^2}{\partial z^2} + k^2 \right) \underline{\Pi}_z, \quad (12.68b)$$

$$\underline{H}_\phi = -j \omega \epsilon \frac{\partial}{\partial \rho} \underline{\Pi}_z. \quad (12.68c)$$

For symmetry reasons only these field components exist. At $z = 0$ the tangential field components \underline{E}_ρ and \underline{H}_ϕ have to be matched. The boundary conditions are given by

$$\frac{\partial}{\partial z} \underline{\Pi}_z^{(2)} = \frac{\partial}{\partial z} \underline{\Pi}_z^{(3)}, \quad (12.69a)$$

$$\underline{\Pi}_z^{(2)} = n^2 \underline{\Pi}_z^{(3)}. \quad (12.69b)$$

The complex refractive index n is given by

$$n^2 = \underline{\epsilon}_m / \epsilon_0. \quad (12.70)$$

From (12.61), (12.62), (12.65), (12.69a) and (12.69b) we obtain

$$R(k_\rho) = \frac{n^2 k_z - k_{mz}}{n^2 k_z + k_{mz}}, \quad (12.71a)$$

$$T(k_\rho) = \frac{2k_z}{n^2 k_z + k_{mz}}. \quad (12.71b)$$

With this we obtain for the Hertz vector the solutions

$$\begin{aligned} \underline{\Pi}_z(\rho, \phi, z) = & -\frac{lI}{4\pi\omega\epsilon_0} \left[\int_0^\infty J_0(k_\rho \rho) \exp(-j k_z |z - h|) \frac{k_\rho}{k_z} dk_\rho + \right. \\ & \left. + \int_0^\infty \frac{n^2 k_z - k_{mz}}{n^2 k_z + k_{mz}} J_0(k_\rho \rho) \exp[-j k_z (z + h)] \frac{k_\rho}{k_z} dk_\rho \right] \text{ for } z \geq 0 \end{aligned} \quad (12.72)$$

and

$$\begin{aligned} \underline{\Pi}_z^{(s)}(\rho, \phi, z) = & -\frac{lI}{4\pi\omega\epsilon_0} \int_0^\infty \frac{2k_z}{n^2 k_z + k_{mz}} J_0(k_\rho \rho) \exp[j(k_{mz} z - k_z h)] \frac{k_\rho}{k_z} dk_\rho \text{ for } z < 0. \end{aligned} \quad (12.73)$$

We consider the wave in free-space and start with the superposition of the z -components of the Hertz vector $\underline{\Pi}_z^{(i)}$ and $\underline{\Pi}_z^{(s)}$. In this way we obtain

$$\underline{\Pi}_z = \underline{\Pi}_z^{(i)} + \underline{\Pi}_z^{(s)}. \quad (12.74)$$

The z -component of Hertz vector of the primary wave $\underline{\Pi}_z^{(i)}$ is given by the spherical wave

$$\underline{\Pi}_z^{(i)}(\rho, \phi, z) = -j \frac{II}{4\pi\omega\epsilon_0} \frac{\exp(-jk|\mathbf{x} - \mathbf{x}_0|)}{4\pi|\mathbf{x} - \mathbf{x}_0|}. \quad (12.75)$$

The scattered wave in free-space is described by

$$\underline{\Pi}_z^{(s)}(\rho, \phi, z) = -\frac{II}{4\pi\omega\epsilon} \int_0^\infty \frac{n^2 k_z - k_{mz}}{n^2 k_z + k_{mz}} J_0(k_\rho \rho) \exp[-jk_z(z+h)] \frac{k_\rho}{k_z} dk_\rho. \quad (12.76)$$

To compute the integral we enlarge the integration interval from $[0, \infty)$ to $(-\infty, \infty)$. This simplifies the evaluation of the integral using methods of theory of functions. For this purpose we express the Bessel function $J_0(z)$ through the Hankel function $H_0^{(1)}(z)$ and $H_0^{(2)}(z)$. The Hankel functions are related to the Bessel functions $J_m(z)$ and $Y_m(z)$ in the following way

$$H_m^{(1)}(z) = J_m(z) + j Y_m(z), \quad (12.77a)$$

$$H_m^{(2)}(z) = J_m(z) - j Y_m(z). \quad (12.77b)$$

With

$$J_0(k_\rho \rho) = \frac{1}{2} H_0^{(1)}(k_\rho \rho) + \frac{1}{2} H_0^{(2)}(k_\rho \rho) \quad (12.78)$$

the contour integral over C_1 can be decomposed in the following way

$$\int_{C_1} f(k_\rho) J_0(k_\rho \rho) dk_\rho = \frac{1}{2} \int_{C_1} f(k_\rho) H_0^{(1)}(k_\rho \rho) dk_\rho + \frac{1}{2} \int_{C_1} f(k_\rho) H_0^{(2)}(k_\rho \rho) dk_\rho. \quad (12.79)$$

With the substitution $k_{\rho 1} = -k_\rho$ and using the identity

$$H_m^{(1)}(z \exp j\pi) = -\exp(-jm\pi) H_m^{(2)}(z) \quad (12.80)$$

we obtain

$$\begin{aligned} \int_{C_1} f(k_\rho) H_0^{(1)}(k_\rho \rho) dk_\rho &= - \int_{C_2} f(-k_{\rho 1}) H_0^{(1)}(-k_{\rho 1} \rho) dk_{\rho 1} \\ &= \int_{-C_2} f(-k_{\rho 1}) H_0^{(2)}(k_{\rho 1} \rho) dk_{\rho 1}. \end{aligned} \quad (12.81)$$

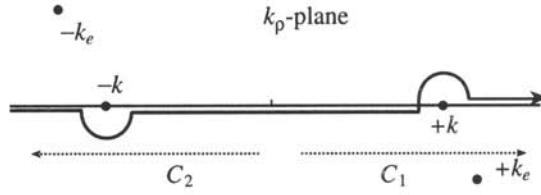


Figure 12.9: Path of integration for the integral (12.83).

The path of integration (Figure 12.9) C_2 goes from 0 to $-\infty$. The reverse path of integration from $-\infty$ to 0 is denoted by $-C_2$. Under the assumption $f(k_\rho) = f(-k_\rho)$, we obtain from (12.79) finally

$$\begin{aligned} \int_{C_1} f(k_\rho) J_0(k_\rho \rho) dk_\rho &= \int_{-C_2} f(k_{\rho 1}) H_0^{(2)}(k_{\rho 1} \rho) dk_{\rho 1} + \int_{C_1} f(k_\rho) H_0^{(2)}(k_\rho \rho) dk_\rho \\ &= \int_C f(k_\rho) H_0^{(2)}(k_\rho \rho) dk_\rho. \end{aligned} \quad (12.82)$$

where the path of integration C is extended from $-\infty$ to ∞ . Using (12.82), we can write down (12.76) in the form

$$\underline{\Pi}_z^{(s)}(\rho, \phi, z) = -\frac{II}{8\pi\omega\epsilon} \int_C \frac{n^2 k_z - k_{mz}}{n^2 k_z + k_{mz}} H_0^{(2)}(k_\rho \rho) e^{-j k_z(z+h)} \frac{k_\rho}{k_z} dk_\rho. \quad (12.83)$$

This integral cannot be represented by elementary functions in a closed form, but the solution by approximation methods is possible.

Since Sommerfeld's first publication from 1909 [5], literature dealing with the evaluation of Sommerfeld's integrals has grown extensively. Detailed treatments are given in Sommerfeld's textbook on partial differential equations of physics [6] and in a number of other textbooks [7–9] and in [10–12]. There have been numerous controversies in the literature concerning the existence of certain solutions, particularly the Zenneck surface wave. A comprehensive overview of the literature on ground-wave propagation has been given by Wait [13]. In 2004, Collin revisited the electromagnetic field radiated by an infinitesimal electrical dipole over a lossy homogeneous half-space [14, 15]. He demonstrated that Sommerfeld's original work was correct and that there was no sign error in Sommerfeld's work as had been claimed in parts of the literature.

Moving the singular points at $-k$ and k by an infinitesimal imaginary distance $j\delta$ to $-k + j\delta$ and $k - j\delta$ can replace the path of integration in Figure 12.9 by an integration along the real axis of the k_ρ -plane from $-\infty$ to ∞ , as shown in Figure 12.10.

Due to (12.57) and (12.63) the denominator of the integrand in (12.83) contains the

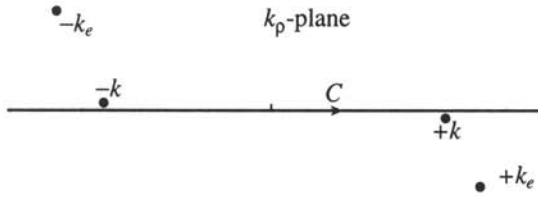


Figure 12.10: Modified path of integration for the integral (12.83).

square roots

$$k_z = \sqrt{k^2 - k_\rho^2}, \quad (12.84a)$$

$$k_{mz} = \sqrt{k_m^2 - k_\rho^2}. \quad (12.84b)$$

The integrand in (12.83) therefore contains four branch points at $k_r = \pm k$ and $k_r = \pm k_m$. This follows from the property of the integrand to change its sign when k_ρ follows a path around a branch point. Due to the four possible combinations of signs in (12.84a) and (12.84b) the integrand is a multiple-valued function containing four branches. A branch of a multiple-valued complex function $f(z)$ is any single-valued function $f_i(z)$ so that the value of $f_i(z)$ is identical with one of the possible values of $f(z)$ and which is analytic in some domain of z [16, 17]. To make the integrand single-valued, we introduce branch cuts in the complex plane from every branch point to the point at infinity as shown in Figure 12.11. Across the branch cut the single-valued function is discontinuous. The branch cut may be chosen in an appropriate way to make the computations simple. In performing the integration the path of integration must not cross the branch cut. We decide to use that branch, which exhibits positive real parts of k_z and k_{mz} .

There is a further singularity in the integrand at the point $k_\rho = k_p$ of the k_ρ -plane where the denominator vanishes. The value of k_p is determined by

$$n^2 k_z + k_{mz} = 0. \quad (12.85)$$

The pole k_p is called the *Sommerfeld pole*. From (12.84a), (12.84b), and (12.85) we obtain

$$\sqrt{\frac{k_p^2 - k^2}{k_p^2 - k_m^2}} = -\frac{k^2}{k_m^2} \quad (12.86)$$

and from this

$$k_p^2 = \frac{k^2 k_m^2}{k^2 + k_m^2}. \quad (12.87)$$

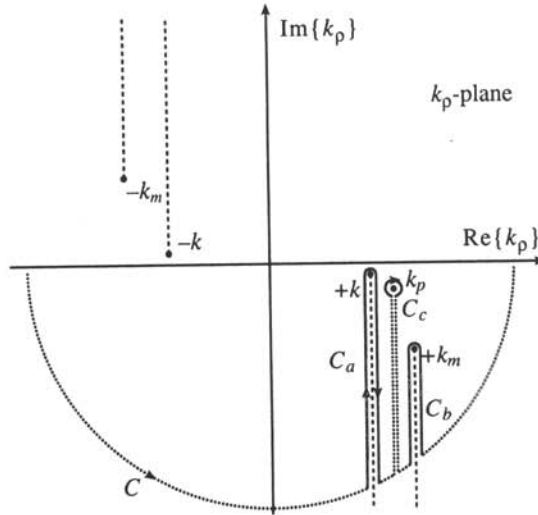


Figure 12.11: Branch cuts for the integration of (12.83).

Since we have chosen the real parts of k_z and k_{mz} as positive, this yields

$$\sqrt{k_p^2 - k^2} = \frac{j k^2}{\sqrt{k^2 + k_m^2}}, \quad (12.88a)$$

$$\sqrt{k_p^2 - k_m^2} = \frac{-j k_m^2}{\sqrt{k^2 + k_m^2}}. \quad (12.88b)$$

For $|k_m| \gg k$ we can use the approximation

$$k_p \cong k \left(1 - \frac{k^2}{2k_m^2} \right). \quad (12.89)$$

However, we note that the exact value of k_p is symmetrical in k^2 and k_m^2 .

We now can replace the integration over the real axis from $-\infty$ to ∞ by an integral over a complex contour C , shown in Figure 12.11. For $\mathcal{I}\{k_p\} \rightarrow -\infty$, the integrand goes sufficiently strong to zero so that the dotted parts of the contour C give no contribution to the integral. The only contributions arise from the parts C_a , C_b , and C_c , where C_a and C_b contribute the integrals over a path from the point at infinity to one of the branch points k or k_m along one side of the branch cut and from the respective branch point back to the point at infinity. Since the integrand is discontinuous along the branch cut, the contributions to the integral from both sides of the branch cut do not cancel

each other. The contribution to the integral along the contour C_c is given by the residue of the integrand at k_ρ .

12.3.1 The Far-Field of the Vertical Dipole over Ground

Consider the far-field of the dipole over ground for $k_\rho \rho \gg 1$. In the far-field case we can approximate the Hankel function in (12.83) by its asymptotic form

$$H_0^{(2)}(k_\rho \rho) \cong \sqrt{\frac{2}{\pi k_\rho \rho}} e^{-j k_\rho \rho + j \pi/4} \quad \text{for } k_\rho \rho \gg 1. \quad (12.90)$$

This yields

$$\underline{\Pi}_z^{(s)}(\rho, \phi, z) = -\frac{II}{8\pi\omega\epsilon} \int_C \frac{n^2 k_z - k_{mz}}{n^2 k_z + k_{mz}} \sqrt{\frac{2}{\pi k_\rho \rho}} e^{-j k_z(z+h) - j k_\rho \rho + j \pi/4} \frac{k_\rho}{k_z} dk_\rho. \quad (12.91)$$

To evaluate the integral we use the saddle point method described in Section E.3. From (E.16) and (E.29) we obtain

$$\int_C f(\zeta) e^{ug(\zeta)} d\zeta = \sqrt{\frac{2\pi}{up}} f(\zeta_s) e^{ug(\zeta_s) + j\psi}. \quad (12.92)$$

Applying this to (12.90) yields

$$\int_C f(k_\rho) e^{-j k_z(z+h) - j k_\rho \rho + j \pi/4} dk_\rho = \sqrt{\frac{2\pi}{kr_2}} k f(k \sin \theta) \cos \theta e^{-j k r_2 + j \pi/4} \quad (12.93)$$

with

$$r_2 = \sqrt{\rho^2 + (z+h)^2}, \quad (12.94a)$$

$$z = r_2 \cos \theta - h, \quad (12.94b)$$

$$\rho = r_2 \sin \theta. \quad (12.94c)$$

From this we obtain

$$\underline{\Pi}_z^{(s)}(\rho, \phi, z) = -\frac{jII}{4\pi\omega\epsilon_0} R(\theta) \frac{e^{-j k r_2}}{4\pi r_2} \quad (12.95)$$

with

$$R(\theta) = \frac{n^2 \cos \theta - \sqrt{n^2 - \sin^2 \theta}}{n^2 \cos \theta + \sqrt{n^2 - \sin^2 \theta}}. \quad (12.96)$$

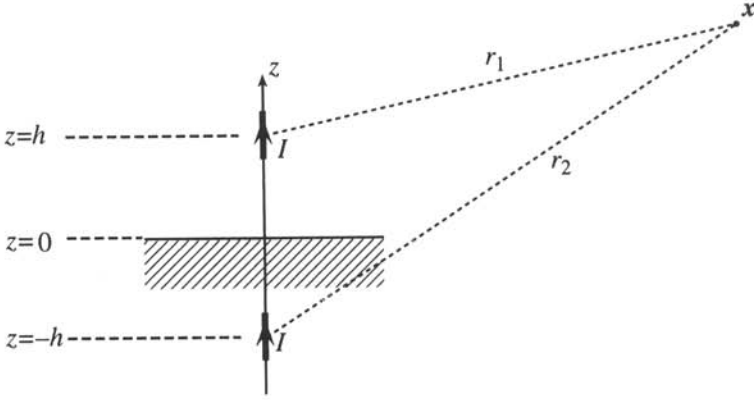


Figure 12.12: Vertical dipole with mirror dipole.

This solution corresponds to the integration over C_a in Figure 12.11. For $|k_m| \gg k$ the contribution of the integration C_b can be neglected. Together with the Hertz form for the primary field (12.49), the total field is represented by

$$\underline{\Pi}_z(\rho, \phi, z) = \underline{\Pi}_z^{(i)}(\rho, \phi, z) + \underline{\Pi}_z^{(s)}(\rho, \phi, z) = -\frac{jII}{4\pi\omega\epsilon_0} \left[\frac{e^{-jkr_1}}{4\pi r_1} + R(\theta) \frac{e^{-jkr_2}}{4\pi r_2} \right] \quad (12.97)$$

with

$$r_1 = \sqrt{\rho^2 + (z-h)^2}. \quad (12.98)$$

The electric and magnetic field components can be computed from (12.68a) to (12.68c). The second term in (12.97) can be interpreted as originating from a mirror dipole as depicted in Figure 12.12.

12.3.2 The Surface Wave

We now show that the integration of (12.83) over C_c around the Sommerfeld pole at k_p in Figure 12.11 yields a surface wave, the so-called *Zenneck surface wave* [18] already discussed in Chapter 6. To apply the method of residues for computing the integral along C_c , we replace in all terms of the integrand with the exception of the denominator the variable k_p by the location of the pole k_p [6]. Since due to (12.86) the denominator in the integrand in (12.83) vanishes for $k_p = k_p$, we use (E.13). We have to set

$$\frac{d}{dk_p}(n^2 k_z + k_{mz}) = k_p \left(\frac{n^2}{\sqrt{k_p^2 - k^2}} + \frac{1}{\sqrt{k_p^2 - k_m^2}} \right) \quad \text{for } k_p = k_p. \quad (12.99)$$

This yields the expression

$$\left. \frac{d}{dk_p} (n^2 k_z + k_{mz}) \right|_{k_p=k_p} = \frac{k_p}{k_m^2} K, \quad (12.100)$$

where K is given by

$$K = \left(\frac{n^2 k_m^2}{\sqrt{k_p^2 - k^2}} + \frac{k_m^2}{\sqrt{k_p^2 - k_m^2}} \right) = -j \left(\frac{k_m^2}{k^2} - \frac{k^2}{k_m^2} \right). \quad (12.101)$$

The quantity K is antisymmetric in k and k_m . For the free-space region $z \geq 0$ the contribution to the integral (12.83) is

$$\underline{\Pi}_z^{(s)}(\rho, \phi, z) = -j \frac{II}{4\omega\epsilon} \frac{k_m^2}{K} H_0^{(2)}(k_p \rho) \exp\left(-\sqrt{k_p^2 - k^2} z\right) \quad \text{for } z \geq 0. \quad (12.102a)$$

For $z < 0$ we obtain by interchanging k and k_m and reversing the sign of z

$$\underline{\Pi}_z^{(s)}(\rho, \phi, z) = -j \frac{II}{4\omega\epsilon} \frac{k^2}{K} H_0^{(2)}(k_p \rho) \exp\left(\sqrt{k_p^2 - k_m^2} z\right) \quad \text{for } z < 0. \quad (12.102b)$$

For regions with $k_p \rho \gg 1$ we can use the asymptotic approximation (12.90) for the Hankel function and obtain

$$\underline{\Pi}_z^{(s)}(\rho, \phi, z) = -j \frac{II}{4\omega\epsilon} \sqrt{\frac{2}{\pi k_p \rho}} \frac{k_m^2}{K} e^{-j k_p \rho + j \pi/4} \exp\left(-\sqrt{k_p^2 - k^2} z\right) \quad \text{for } z \geq 0, \quad (12.103a)$$

$$\underline{\Pi}_z^{(s)}(\rho, \phi, z) = -j \frac{II}{4\omega\epsilon} \sqrt{\frac{2}{\pi k_p \rho}} \frac{k^2}{K} e^{-j k_p \rho + j \pi/4} \exp\left(\sqrt{k_p^2 - k_m^2} z\right) \quad \text{for } z < 0. \quad (12.103b)$$

This wave is a *surface wave* since it decays exponentially with the distance $|z|$ from the surface. For $|k_m| \gg k$ the wave decays in the medium more rapidly with the distance from the surface than in free-space above the surface. Besides the exponential attenuation due to the losses the surface wave depends on the distance from the origin like $1/\sqrt{\rho}$. This is characteristic of two-dimensional wave propagation.

12.4 HORIZONTALLY ORIENTED ELECTRIC DIPOLE OVER LOSSY HALF-SPACE

We consider a dipole oriented horizontally in the x -direction in free-space over lossy half-space as depicted in Figure 12.13. As in the case of the vertical dipole the space

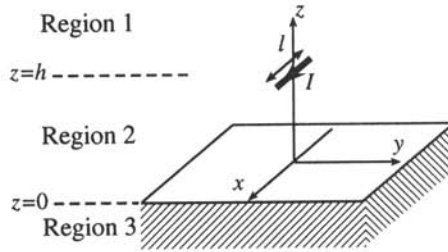


Figure 12.13: Horizontally oriented dipole above a lossy half-space.

is subdivided into three regions. Region 1 is the free-space region above the dipole with $z < h$. Region 2 is given by $0 < z \leq h$, and region 3 is the region filled with a lossy medium in the lower half-space, $z < 0$. We recall the derivation of the electric field from the electric Hertz form $\underline{\Pi}_e$ satisfying the Helmholtz equation

$$\Delta \underline{\Pi}_e^{(i)} + \omega^2 \underline{\mu} \underline{\Pi}_e^{(i)} = -\frac{1}{\underline{\epsilon}} * \underline{\mathcal{M}}_{e0}. \quad (12.104)$$

For the Hertzian dipole oriented in x -direction the polarization $\underline{\mathcal{M}}_{e0}$ is given by

$$\underline{\mathcal{M}}_{e0} = \frac{1}{j\omega} J_x \, dy \wedge dz, \quad (12.105a)$$

$$J_x = II \delta(\mathbf{x} - \mathbf{x}_0) \quad \text{with } \mathbf{x}_0 = [0, 0, h]^T. \quad (12.105b)$$

The primary wave can be derived from a Hertz form exhibiting an x -component only,

$$\underline{\Pi}_e^{(i)}(\mathbf{x}) = \underline{\Pi}_x^{(i)}(\mathbf{x}) \, dx. \quad (12.106)$$

For the primary wave the x -component of the Hertz vector in free-space (regions 1 and 2) can be determined from the scalar Helmholtz equation

$$\Delta \underline{\Pi}_x + k^2 \underline{\Pi}_x = j \frac{II}{\omega \epsilon_0} \delta(\mathbf{x} - \mathbf{x}_0). \quad (12.107)$$

Since the problem of the horizontal dipole over ground exhibits no rotational symmetry, we also introduce a z -component of the Hertz vector. This will allow to satisfy the boundary conditions for the tangential electric and magnetic field components at the $z = 0$ -plane. Therefore for the secondary field we make the ansatz

$$\underline{\Pi}_e^{(s)}(\mathbf{x}) = \underline{\Pi}_x^{(s)}(\mathbf{x}) \, dx + \underline{\Pi}_z^{(s)}(\mathbf{x}) \, dz. \quad (12.108)$$

Inserting this into (12.104) yields the scalar Laplace equations for the x - and z -components $\underline{\Pi}_x$ and $\underline{\Pi}_z$ of the electric Hertz vector,

$$\Delta \underline{\Pi}_i + k^2 \underline{\Pi}_i = 0 \quad \text{for } i = x, z \quad z \geq 0, \quad (12.109a)$$

$$\Delta \underline{\Pi}_i + k_m^2 \underline{\Pi}_i = 0, \quad \text{for } i = x, z \quad z < 0 \quad (12.109b)$$

with

$$k^2 = \omega^2 \mu_0 \epsilon_0, \quad (12.110a)$$

$$k_m^2 = \omega^2 \mu_0 \underline{\epsilon}_m. \quad (12.110b)$$

The permittivity $\underline{\epsilon}_m$ in the lossy medium is complex and given by

$$\underline{\epsilon}_m = \epsilon'_m - j \frac{\sigma}{\omega}. \quad (12.111)$$

The solution for the primary field is given by

$$\underline{\Pi}_x^{(i)} = -\frac{j I l}{4 \pi \omega \epsilon_0} \frac{\exp(-j k |\mathbf{x} - \mathbf{x}_0|)}{|\mathbf{x} - \mathbf{x}_0|}. \quad (12.112)$$

From (2.173b) and (2.173c), we obtain the boundary conditions

$$dz \wedge \left(\underline{\mathcal{H}}^{(2)} - \underline{\mathcal{H}}^{(3)} \right) \Big|_{z=0} = 0, \quad (12.113a)$$

$$dz \wedge \left(\underline{\mathcal{E}}^{(2)} - \underline{\mathcal{E}}^{(3)} \right) \Big|_{z=0} = 0. \quad (12.113b)$$

With (3.29a), (3.29b), (12.110a) and (12.110b) this yields

$$dz \wedge \left(\epsilon_0 \star d \underline{\Pi}_e^{(2)} - \underline{\epsilon}_m \star d \underline{\Pi}_e^{(3)} \right) \Big|_{z=0} = 0, \quad (12.114a)$$

$$dz \wedge \left(\star d \star d \underline{\Pi}_e^{(2)} - \star d \star d \underline{\Pi}_e^{(3)} \right) \Big|_{z=0} = 0. \quad (12.114b)$$

From the boundary condition for the magnetic field (12.114a) and using (12.110a) and (12.110b) we obtain the boundary conditions for the components of the Hertz vector,

$$k^2 \partial \underline{\Pi}_z^{(2)} = k_m^2 \partial \underline{\Pi}_z^{(3)}, \quad (12.115a)$$

$$k^2 \left(\frac{\partial \underline{\Pi}_x^{(2)}}{\partial z} + \frac{\partial \underline{\Pi}_z^{(2)}}{\partial x} \right) = k_m^2 \left(\frac{\partial \underline{\Pi}_x^{(3)}}{\partial z} + \frac{\partial \underline{\Pi}_z^{(3)}}{\partial x} \right). \quad (12.115b)$$

The boundary condition for the electric field (12.114b) together with (12.113a) and (12.113b) yields

$$\frac{\partial \underline{\Pi}_x^{(2)}}{\partial x} + \frac{\partial \underline{\Pi}_z^{(2)}}{\partial z} = \frac{\partial \underline{\Pi}_x^{(3)}}{\partial x} + \frac{\partial \underline{\Pi}_z^{(3)}}{\partial z}, \quad (12.115c)$$

$$k^2 \underline{\Pi}_x^{(2)} = k_m^2 \underline{\Pi}_x^{(3)}. \quad (12.115d)$$

Solving the Helmholtz equation in circular cylindrical coordinates,

$$\left\{ \frac{1}{\rho} \frac{\partial}{\partial \rho} \left(\rho \frac{\partial}{\partial \rho} \right) - \frac{m^2}{\rho^2} + \frac{\partial^2}{\partial z^2} + k^2 \right\} \underline{\Pi}_m = \frac{jI}{2\pi\omega\epsilon_0\rho} \delta(\rho - \rho_0) \delta(z - z_0) \quad (12.116)$$

we obtain for the x -components of the Hertz vector expressions similar to (12.62) and (12.65),

$$\underline{\Pi}_x^{(s)}(\rho, z) = -\frac{II}{4\pi\omega\epsilon_0} \int_0^\infty R_x(k_\rho) J_0(k_\rho\rho) \exp[-jk_z(z+h)] \frac{k_\rho}{k_z} dk_\rho \quad \text{for } z \geq 0, \quad (12.117a)$$

$$\underline{\Pi}_x^{(s)}(\rho, z) = -\frac{II}{4\pi\omega\epsilon_0} \int_0^\infty T_x(k_\rho) J_0(k_\rho\rho) \exp[j(k_{mz}z - k_zh)] \frac{k_\rho}{k_z} dk_\rho \quad \text{for } z < 0 \quad (12.117b)$$

with the reflection coefficient $R(k_\rho)$ and the transmission coefficient $T(k_\rho)$ computed from (12.115a) and (12.115d) as

$$R_x(k_\rho) = \frac{k_z - k_{mz}}{2k_z + k_{mz}}, \quad (12.118a)$$

$$T_x(k_\rho) = \frac{1}{n^2} \frac{2k_z}{2k_z + k_{mz}}. \quad (12.118b)$$

To compute the z -component of the Hertz vector we use (12.115b) and (12.115c). First we consider that

$$\frac{\partial}{\partial x} = \frac{\partial \rho}{\partial x} \frac{\partial}{\partial \rho} + \frac{\partial \phi}{\partial x} \frac{\partial}{\partial \phi} = \cos \phi \frac{\partial}{\partial \rho} - \rho \sin \phi \frac{\partial}{\partial \phi}. \quad (12.119)$$

Since the z -components of the Hertz vector are independent from ϕ we obtain from (12.115c)

$$\frac{\partial}{\partial z} (\underline{\Pi}_z^{(3)} - \underline{\Pi}_z^{(2)}) = \frac{\partial}{\partial x} (\underline{\Pi}_x^{(3)} - \underline{\Pi}_x^{(2)}) = \frac{\partial}{\partial \rho} (\underline{\Pi}_x^{(3)} - \underline{\Pi}_x^{(2)}) \cos \phi. \quad (12.120)$$

With (B.10) this yields

$$\underline{\Pi}_z^{(s)}(\rho, \phi, z) = -\frac{lI \cos \phi}{4\pi\omega\epsilon_0} \int_0^\infty R_z(k_\rho) J_1(k_\rho \rho) \exp[-jk_z(z+h)] k_\rho^2 dk_\rho \quad \text{for } z \geq 0, \quad (12.121a)$$

$$\underline{\Pi}_z^{(s)}(\rho, \phi, z) = -\frac{lI \cos \phi}{4\pi\omega\epsilon_0} \int_0^\infty T_z(k_\rho) J_1(k_\rho \rho) \exp[j(k_{mz}z - k_z h)] k_\rho^2 dk_\rho \quad \text{for } z < 0 \quad (12.121b)$$

with

$$R_x(k_\rho) = -\frac{2}{k^2} \frac{k_z - k_{mz}}{n^2 k_z + k_{mz}}, \quad (12.122a)$$

$$T_x(k_\rho) = -\frac{2}{n^2 k^2} \frac{k_z - k_{mz}}{n^2 k_z + k_{mz}}. \quad (12.122b)$$

The horizontal dipole over ground primarily radiates in directions perpendicular to its axis. Also, in the case of the horizontal dipole, the secondary field consists of a field radiated from the mirror image of the dipole into space and a surface wave. In this case the field from the image dipole has the tendency to cancel the primary field.

12.5 PROBLEMS

- Consider a short electric dipole of length $l = 2$ cm. A sinusoidal current of 1 mA amplitude and 900 MHz frequency is impressed into the dipole.
 - Compute for $\theta = 0$ and $\theta = \frac{1}{2}\pi$ the electric and magnetic field components at distances of $r = 10$ cm, 1 m, 10 m, 100 m and 1 km from the origin.
 - Compute the same for θ and r the complex Poynting vector.
- Consider a short electric dipole of length $l = 2$ cm. Let the dipole be excited by a current pulse

$$i(t) = \begin{cases} I_0 \sin^2\left(\frac{t}{T}\pi\right) & \text{for } 0 \leq t \leq T \\ 0 & \text{for } t < 0 \text{ and } t > T \end{cases}$$

- Compute for $\theta = 0$ and $\theta = \frac{1}{2}\pi$ the electric and magnetic field components at distances of $r = 10$ cm, 1 m, 10 m, 100 m and 1 km from the origin.
 - Compute the same for θ and r the complex Poynting vector.
- Consider a vertically oriented electrical dipole in height h over ground as depicted in Figure 12.8.

- a) Show that for a perfectly conducting ground the electromagnetic field in regions 1 and 2 can be derived from a Hertz form

$$\underline{\Pi}_e(\mathbf{x}) = -\frac{jII}{4\pi\omega\epsilon_0} \left(\frac{\exp(-jk|\mathbf{x} - \mathbf{x}_0|)}{|\mathbf{x} - \mathbf{x}_0|} + \frac{\exp(-jk|\mathbf{x} + \mathbf{x}_0|)}{|\mathbf{x} + \mathbf{x}_0|} \right) dz.$$

- b) Compute the electric and magnetic field components for this case.
4. Consider a horizontally oriented electrical dipole in height h over ground as depicted in Figure 12.13.

- a) Show that for a perfectly conducting ground the electromagnetic field in regions 1 and 2 can be derived from a Hertz form

$$\underline{\Pi}_e(\mathbf{x}) = -\frac{jII}{4\pi\omega\epsilon_0} \left(\frac{\exp(-jk|\mathbf{x} - \mathbf{x}_0|)}{|\mathbf{x} - \mathbf{x}_0|} - \frac{\exp(-jk|\mathbf{x} + \mathbf{x}_0|)}{|\mathbf{x} + \mathbf{x}_0|} \right) d\mathbf{x}.$$

- b) Compute the electric and magnetic field components for this case.
5. Derive the formulae for the field of a vertically oriented magnetic dipole over ground.
6. Derive the formulae for the electric and magnetic fields of a horizontally oriented magnetic dipole over ground.
7. A vertical electric dipole of length $l = 2$ cm is located in height $h = 2$ m over ground. A sinusoidal current of 1 mA amplitude and 900 MHz frequency is impressed into the dipole. The conductivity of the ground is $\sigma = 10^{-2}$ S/m and its relative permittivity is $\epsilon_r = 10$.
- a) Compute the values of k and k_m .
- b) Find the location of the Sommerfeld pole k_p in the k_ρ -plane.
- c) Compute the attenuation factor of the surface wave.

REFERENCES

- [1] H. Hertz, "Die Kräfte electrischer Schwingungen behandelt nach der Maxwell'schen Theorie," *Ann. Phys. Chem.*, vol. 3. Folge 36, no. 1, pp. 1–22, 1889.
- [2] H. Hertz, "Über Strahlen electrischer Kraft," *Ann. Phys. Chem.*, vol. 3. Folge 36, no. 4, pp. 769–783, 1889.
- [3] H. Hertz, *Gesammelte Werke, Untersuchungen über die Ausbreitung der elektrischen Kraft*, vol. 2. Leipzig: Johann Ambrosius Barth, 1894.
- [4] J. D. Kraus, "Heinrich Hertz - theorist and experimenter," *IEEE Trans. Microwave Theory Techn.*, pp. 824–829, May 1988.
- [5] A. Sommerfeld, "Über die Ausbreitung der Wellen in der Drahtlosen Telegraphie," *Ann. Physik*, vol. 28, pp. 665–737, 1909.
- [6] A. Sommerfeld, *Partielle Differentialgleichungen der Physik*. Leipzig: Akademische Verlagsgesellschaft Geest & Portig, 1947.
- [7] R. E. Collin, *Field Theory of Guided Waves*. New York: IEEE Press, 1991.

- [8] W. C. Chew, *Fields in Inhomogeneous Media*. New York: Van Nostrand Reinhold, 1990.
- [9] A. Ishimaru, *Electromagnetic Wave Propagation, Radiation, and Scattering*. Englewood Cliffs, NJ: Prentice Hall, 1991.
- [10] I. V. Lindell and E. Alanen, "Exact image theory for the Sommerfeld half-space problem, part I: Vertical magnetic dipole," *IEEE Trans. Antennas Propagat.*, vol. 32, pp. 126–133, Feb. 1984.
- [11] I. V. Lindell and E. Alanen, "Exact image theory for the Sommerfeld half-space problem, part II: Vertical electrical dipole," *IEEE Trans. Antennas Propagat.*, vol. 32, pp. 841–847, Aug. 1984.
- [12] I. V. Lindell and E. Alanen, "Exact image theory for the Sommerfeld half-space problem, part III: General formulation," *IEEE Trans. Antennas Propagat.*, vol. 32, pp. 1027–1032, Sept. 1984.
- [13] J. R. Wait, "The ancient and modern history of EM ground-wave propagation," *IEEE Trans. Antennas Propagat. Magazine*, vol. 40, pp. 7–24, Oct. 1998.
- [14] R. E. Collin, "Hertzian dipole radiating over a lossy earth or sea: some early and late 20th-century controversies," *IEEE Trans. Antennas Propagat. Magazine*, vol. 46, pp. 64–79, Apr. 2004.
- [15] R. E. Collin, "Some observations about the near zone electric field of a Hertzian dipole above a lossy earth," *IEEE Trans. Antennas Propagat.*, vol. 52, pp. 3133–3137, Nov. 2004.
- [16] R. V. Churchill and J. W. Brown, *Complex Variables and Applications*. New York: McGraw Hill, 1990.
- [17] B. Friedman, *Lectures on Applications-Oriented Mathematics*. New York: John Wiley & Sons, 1969.
- [18] J. Zenneck, "Über die Fortpflanzung ebener elektromagnetischer Wellen längs einer ebenen Leiterfläche und ihre Beziehung zur Drahtlosen Telegraphie," *Annalen der Physik*, vol. 23, pp. 846–866, 1907.

Chapter 13

Antennas

13.1 INTRODUCTION

An antenna is any structure or device used to collect or radiate electromagnetic waves. Antennas allow the transformation of electromagnetic waves propagating along a transmission-line into electromagnetic waves propagating in free-space. This transformation may be performed in both directions. A transmitting antenna transforms a transmission-line wave into a free-space wave, whereas a receiving antenna converts part of the free-space wave into a transmission-line wave. An antenna usually is a reciprocal device and, in principle, each antenna may be used for receiving as well as for transmitting electromagnetic waves. However, the choice of the type of antenna and details in their construction depend on the special application of the antenna. An antenna is designed to achieve a certain *radiation pattern* (i.e., angular distribution of the radiated power). Furthermore, volume, weight and mechanical stability play a role. In the case of transmitting antennas, the power of the transmitted signal also has to be considered. With decreasing wavelength the antenna dimensions decrease as well. Due to this circumstance the scope for antenna design at higher frequencies is larger. Figure 13.1 shows some antenna types. One of the most common antenna types is the dipole antenna shown in Figure 13.1(b). The dipole antenna usually is formed by two straight wire segments and excited by a source inserted between these segments. Using the mirror principle, we can put one wire segment in a position normal to a conducting plane. This yields the *monopole antenna* according to Figure 13.1(a). This antenna type is used frequently in the medium-wave and short-wave range. In this case the conducting plane is formed by Earth's surface. The loop antenna depicted in Figure 13.1(c) excites a field that is dual to the field excited by the dipole antenna. The loop is formed by one or several turns of a wire. Figure 13.1(e) depicts a horn antenna. The horn antenna is formed by conically expanding a waveguide. If the aperture of the horn is large compared to the wavelength, the radiated power may be concentrated

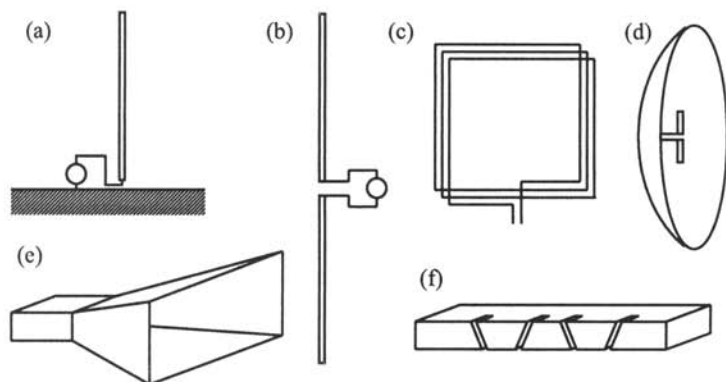


Figure 13.1: Different antenna types: (a) monopole antenna, (b) dipole antenna, (c) loop antenna, (d) parabolic reflector antenna, (e) horn antenna, and (f) slot antenna.

in a certain direction. We say then that this antenna has a high *directivity* compared with an imagined isotropic radiator. If in a waveguide wall currents are interrupted by slots, from these slots electromagnetic energy can also be radiated. Figure 13.1(f) shows a slot antenna. The directivity of antennas may be increased by combining several antennas into antenna arrays or by the usage of reflectors. Figure 13.1(d) shows as an example the combination of a dipole with a parabolic reflector. The dipole that excites a primary wave is positioned into the focal point of the parabolic reflector. By the parabolic reflector the spherical wave excited by the dipole is transformed into an almost plane wave.

A fundamental problem in computing the electromagnetic field excited by an antenna is to compute the electromagnetic field excited by the surface currents flowing in the metallic conductors forming the antenna. In general the current distribution on the antenna surface is also completely unknown. We may consider the antenna to be excited by some primary field or by currents or voltages impressed at certain points. Our task then will be first to compute the current distribution on the antenna and then the electromagnetic field generated by this current distribution. An exact treatment of this problem requires us also to consider the influence of the radiation field on the current distribution in the antenna. This usually requires a solution of integral equations as discussed in Section 13.3. However, the treatment of the problem may be simplified considerably if the current distribution on the antenna is already known. For simple antenna structures the current distribution may be computed with satisfactory accuracy without taking into account the radiation. In this case the problem of computing the field radiated by the antenna may be done in two steps. In the first step the current distribution in the antenna is computed, and in the second step the field radiated by the antenna is computed by superimposing the contributions of the infinitesimally

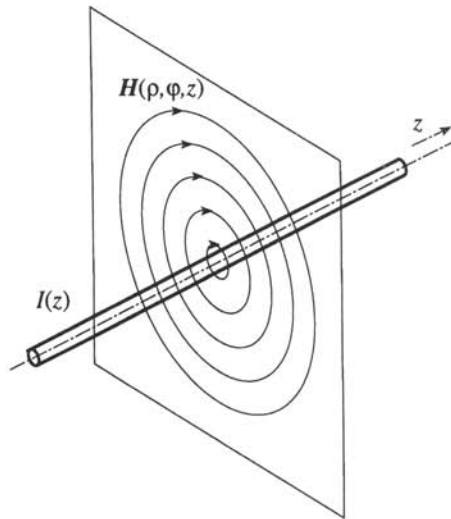


Figure 13.2: Magnetic field of the linear conductor.

small antenna elements. For a detailed treatment of antennas the reader is referred to [1–6].

13.2 LINEAR ANTENNAS

Linear antennas are formed by segments of straight cylindric conductors. The linear antenna according to Figure 13.1(a) and the dipole antenna according to Figure 13.1(b) are examples of linear antennas. The excitation of the linear antenna is performed in a gap between two wire segments or across the gap between the wire segment and the conducting plane in Figure 13.1(a). We assume the cross-sectional dimensions of the conductor are small; furthermore we can assume that short segments of the linear conductor act as Hertzian dipoles. To compute the field produced by the linear antenna we can superimpose the field contributions of small wire segments, which may be considered as Hertzian dipoles. In general the current will be varying over the length of a linear antenna. Therefore at first we will investigate the spatial variation of a current along a linear conductor. For an exact analysis of a linear antenna, the current distribution must be computed by taking into consideration the electromagnetic field radiated by the antenna. In many cases, however, we can obtain a good approximation by splitting up the problem into first computing the current distribution over the linear wire without considering the radiated field, and then, in the second step of our analysis,

by computing the radiated field from the given current distribution. In this section we will proceed in that way. Consider an infinitely extended straight wire with a circular cross-section. Figure 13.2 shows the magnetic field lines in a transverse plane of the infinitely extended straight wire.

For symmetry reasons the magnetic field lines are concentric circles in the transverse planes with the center in the wire axis. Assuming no longitudinal electric field, we obtain from Ampère's law

$$\underline{\mathcal{H}}(r, z) = \underline{H}_\phi(r, z) r d\phi = \frac{1}{2\pi} I(z) d\phi. \quad (13.1)$$

Due to (3.28), and (3.29b) the magnetic field must fulfill the Helmholtz equation in free-space.

$$\Delta \underline{\mathcal{H}} + k^2 \underline{\mathcal{H}} = 0. \quad (13.2)$$

From (3.14) we obtain for the cylindric coordinate system (r, ϕ, z) defined by

$$x = r \cos \phi, \quad y = r \sin \phi, \quad z = z, \quad (13.3)$$

and with

$$g_1 = 1, \quad g_2 = r, \quad g_3 = 1, \quad (13.4)$$

the Laplace operator for one-forms,

$$\begin{aligned} \Delta \underline{\mathcal{H}} = & \left(\frac{\partial^2 \underline{H}_r}{\partial r^2} + \frac{1}{r} \frac{\partial \underline{H}_r}{\partial r} + \frac{1}{r^2} \frac{\partial^2 \underline{H}_r}{\partial \phi^2} + \frac{\partial^2 \underline{H}_r}{\partial z^2} - \frac{1}{r^2} \underline{H}_r - \frac{2}{r^2} \frac{\partial \underline{H}_\phi}{\partial \phi} \right) dr \\ & + \left(\frac{\partial^2 \underline{H}_\phi}{\partial r^2} + \frac{1}{r} \frac{\partial \underline{H}_\phi}{\partial r} + \frac{1}{r^2} \frac{\partial^2 \underline{H}_\phi}{\partial \phi^2} + \frac{\partial^2 \underline{H}_\phi}{\partial z^2} - \frac{1}{r^2} \underline{H}_\phi + \frac{2}{r^2} \frac{\partial \underline{H}_r}{\partial \phi} \right) r d\phi \\ & + \left(\frac{\partial^2 \underline{H}_z}{\partial r^2} + \frac{1}{r} \frac{\partial \underline{H}_z}{\partial r} + \frac{1}{r^2} \frac{\partial^2 \underline{H}_z}{\partial \phi^2} + \frac{\partial^2 \underline{H}_z}{\partial z^2} \right) dz. \end{aligned}$$

If $\underline{\mathcal{H}}$ exhibits only a ϕ -component depending only on r and z the Laplace operator reduces to

$$\Delta \underline{\mathcal{H}} = \left(\frac{\partial^2 \underline{H}_\phi}{\partial r^2} + \frac{1}{r} \frac{\partial \underline{H}_\phi}{\partial r} - \frac{1}{r^2} \underline{H}_\phi + \frac{\partial^2 \underline{H}_\phi}{\partial z^2} \right) r d\phi. \quad (13.5)$$

Inserting into (13.2) yields

$$\frac{\partial^2 \underline{H}_\phi}{\partial r^2} + \frac{1}{r} \frac{\partial \underline{H}_\phi}{\partial r} - \frac{1}{r^2} \underline{H}_\phi + \frac{\partial^2 \underline{H}_\phi}{\partial z^2} + k^2 \underline{H}_\phi = 0. \quad (13.6)$$

Inserting (13.1) into (13.6) the first three terms on the left side of (13.6) vanish, and we

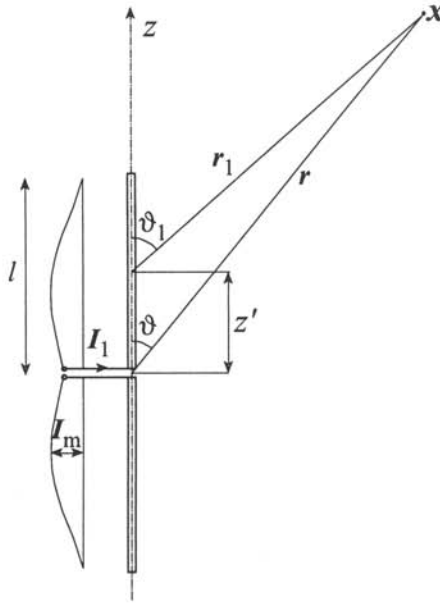


Figure 13.3: Dipole antenna.

obtain

$$\frac{d^2 \underline{I}}{dz^2} + k^2 \underline{I} = 0. \quad (13.7)$$

This is the well-known transmission-line equation for the TEM wave with the solution

$$\underline{I}(z) = \underline{I}^{(+)} e^{-jkz} + \underline{I}^{(-)} e^{jkz}, \quad (13.8)$$

where $\underline{I}^{(+)}$ and $\underline{I}^{(-)}$ are the amplitudes of current waves propagating in positive and negative z -directions, respectively. A current wave propagates on the straight wire with the velocity c_0 of the plane wave in free-space. Let us consider the symmetric dipole antenna according to Figure 13.3. Both segments of the dipole antenna have a length l . With $\underline{I}(\pm l) = 0$ we obtain from (13.8) the current distribution

$$\underline{I}(z) = \begin{cases} \underline{I}_m \sin[k(l - z)] & z > 0 \\ \underline{I}_m \sin[k(l + z)] & z < 0 \end{cases} \quad (13.9)$$

on the dipole. According to (12.16), the contribution of the current flowing through a

line segment of length dz to the electric far-field in point \mathbf{x} is given by

$$d\mathbf{E}_\theta = \frac{j\omega\mu_0\mathbf{I}(z)}{4\pi} \frac{e^{-jkr_1}}{r_1} \sin\theta_1 dz. \quad (13.10)$$

To determine \mathbf{E} we have to integrate $d\mathbf{E}_\theta$ from $z = -l$ to $z = l$. For points \mathbf{x} in the far-field all lines drawn from a certain point of the far-field to any point of the linear antenna may be considered to be parallel. Assuming $\theta_1 = \theta$, we obtain

$$r_1 = r - z \cos\theta. \quad (13.11)$$

The exponential factor e^{-jkr_1} is strongly varying with r_1 , whereas in the denominator of (13.10) the variable r_1 may be substituted by r . By that way we obtain from (13.10) and (13.11) the approximate formula

$$\mathbf{E}_\theta \cong \frac{j\omega\mu_0\mathbf{I}_m}{4\pi} \frac{e^{-jkr}}{r} \sin\theta \int_{-l}^{+l} \mathbf{I}(z) e^{jkz \cos\theta} dz. \quad (13.12)$$

With (13.9) it follows

$$\begin{aligned} \mathbf{E}_\theta = \frac{j\omega\mu_0\mathbf{I}_m}{4\pi} \frac{e^{-jkr}}{r} \sin\theta \left\{ \int_{-l}^0 e^{jkz \cos\theta} \sin[k(l+z)] dz \right. \\ \left. + \int_0^{+l} e^{jkz \cos\theta} \sin[k(l-z)] dz \right\}. \end{aligned} \quad (13.13)$$

With

$$\int e^{ax} \sin(bx+c) dx = \frac{e^{ax}}{a^2+b^2} [a \sin(bx+c) - b \cos(bx+c)] \quad (13.14)$$

and

$$\frac{\omega\mu_0}{k} = Z_{F0} \quad (13.15)$$

we obtain

$$\mathbf{E}_\theta = \frac{jZ_{F0}\mathbf{I}_m}{2\pi} \frac{e^{-jkr}}{r} \frac{\cos(kl \cos\theta) - \cos kl}{\sin\theta}. \quad (13.16)$$

For a *half-wave dipole* with a length $2l = \frac{1}{2}\lambda$ we obtain $kl = \frac{1}{2}\pi$ and from this

$$\mathbf{E}_\theta = \frac{jZ_{F0}\mathbf{I}_m}{2\pi} \frac{e^{-jkr}}{r} \frac{\cos(\frac{1}{2}\pi \cos\theta)}{\sin\theta}. \quad (13.17)$$

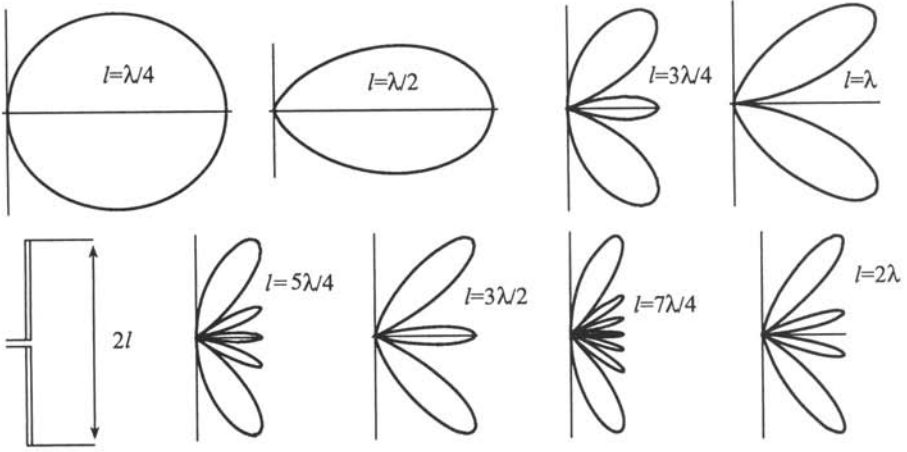


Figure 13.4: Radiation pattern of linear dipole antennas with various lengths.

Since in the far-field (12.18) is valid for the contributions of all differential current elements, we obtain for the total far-field of the linear dipole antenna also

$$\underline{H}_\phi = \frac{\underline{E}_\theta}{Z_{F0}}. \quad (13.18)$$

Figure 13.4 shows the radiation patterns of linear dipole antennas with a half-length l , which is an integer multiple of $\frac{1}{4}\lambda_0$. If l is an odd integer multiple of $\frac{1}{4}\lambda_0$, the number of the maxima of the radiation pattern is equal to $4l/\lambda_0$. If l is an integer multiple of $\frac{1}{2}\lambda_0$, the number of the maxima in the radiation pattern is equal to $2l/\lambda_0$. With (12.19) we obtain the radial component T_r of the complex Poynting vector

$$\underline{T}_r = \frac{Z_{F0}|\underline{I}_m|^2}{8\pi^2 r^2} \left[\frac{\cos(kl \cos \theta) - \cos kl}{\sin \theta} \right]^2. \quad (13.19)$$

In the far-field \underline{T}_r is real (i.e., there is only an active power flow). The active power radiated by the antenna is obtained by integrating \underline{T}_r over a closed surface surrounding the antenna in the far-field. Integrating over the surface of a sphere, we obtain from (12.21)

$$P = \frac{Z_{F0}|\underline{I}_m|^2}{4\pi} f(kl) \quad (13.20)$$

with

$$f(kl) = \int_0^\pi \frac{[\cos(kl \cos \theta) - \cos kl]^2}{\sin \theta} d\theta. \quad (13.21)$$

The evaluation of the integral yields

$$f(kl) = C + \ln 2kl - Ci(2kl) + \frac{1}{2}[Si(4kl) - 2Si(2kl)] \sin 2kl \\ + \frac{1}{2}[C + \ln kl + Ci(4kl) - 2Ci(2kl)] \cos 2kl \quad (13.22)$$

where $C = 0.5772157 \dots$ is known as the *Euler constant* and the integral sine Si and the integral cosine Ci are given by

$$Si(x) = \int_0^x \frac{\sin x}{x} dx, \quad (13.23a)$$

$$Ci(x) = - \int_x^\infty \frac{\cos x}{x} dx. \quad (13.23b)$$

With reference to the current maximum I_m we may define the *radiation resistance* R_{rm} by

$$P = \frac{1}{2} R_{rm} |I_m|^2. \quad (13.24)$$

With (13.20) we obtain

$$R_{rm} = \frac{1}{2\pi} Z_{F0} f(kl) = 60 f(kl) \Omega. \quad (13.25)$$

In Figure 13.5, R_{rm} is represented as a function of $kl = 2\pi l/\lambda_0$. The current I_1 at the excitation point $z = 0$ of the antenna is given by

$$I_1 = I_m \sin kl \quad \text{for } kl \neq n\pi. \quad (13.26)$$

In the derivation of (13.8) we did not consider the attenuation of the current wave by the radiation of electromagnetic energy. Due to the radiation the wave is attenuated exponentially. Therefore the wave on the antenna wire is not really a standing wave, and also in the case $kl = n\pi$ we have no current nodes at $z = 0$. With this restriction we obtain the radiation resistance R_r with respect to the current impressed at the excitation point of the antenna,

$$R_r = \frac{2P}{|I_1|^2}. \quad (13.27)$$

Inserting (13.24) and (13.26) yields

$$R_r = \frac{R_{rm}}{\sin^2 kl}. \quad (13.28)$$

For the $\frac{1}{2}\lambda$ dipole with $l = \frac{1}{4}\lambda$ we obtain

$$R_r = R_{rm} = 73.4 \Omega \quad \text{for } l = \frac{1}{4}\lambda. \quad (13.29)$$

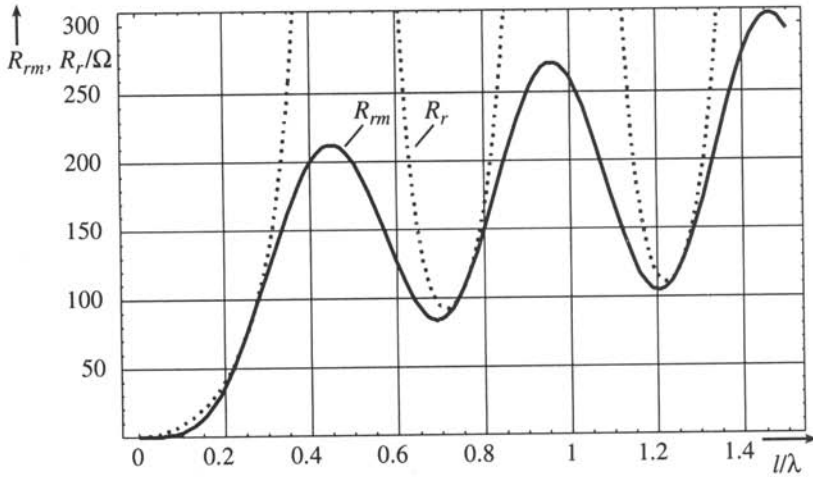


Figure 13.5: Radiation resistances R_{rm} and R_r of the dipole antenna referred to the maximum current I_m and the feed current I_1 , respectively, in dependence of l/λ_0 .

The radiation resistance of the dipole antenna R_r according to (13.28) has been computed from the power radiated by the antenna into the far-field. Since the free-space is lossless, the spherical wave emitted by a dipole propagates without losses, and in the case of time-harmonic excitation of the dipole the active power flowing through a sphere surrounding the dipole does not depend on the radius of that sphere. The reactive power flowing into the antenna feed, however, is related to the electromagnetic energy stored in the near-field of the antenna. Therefore, the computation of the imaginary part of the antenna impedance requires the consideration of the antenna near-field. This will be done in Section 13.4.

13.3 THE INTEGRAL EQUATION FOR THE LINEAR ANTENNA

Up to now we have investigated linear antennas on the basis of a given current distribution on the antenna. This allowed us to determine the radiation pattern of the antenna with satisfactory accuracy; however, we could not determine the antenna impedance in this way. For a more accurate computation of the radiation pattern and for the computation of the antenna impedance, an accurate determination of the current distribution under consideration of the radiation is necessary. In the following we apply the integral equation method in connection with the method of moments (MoM) to determine the

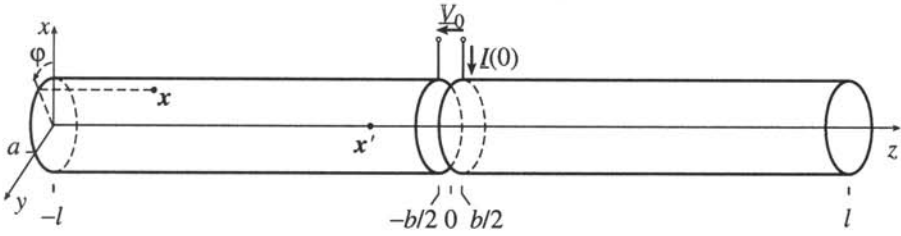


Figure 13.6: Dipole antenna.

current distribution on a linear antenna [2, 3, 7, 8].

We investigate the linear dipole antenna depicted in Figure 13.6. The linear antenna consists of a straight circular cylindric conductor of length $2l$ with diameter $2a$ – much smaller than the wavelength. If a primary wave is incident on an ideally conducting surface, on this surface currents are induced, causing the tangential component of the total electric field to vanish on the surface of the ideal conductor. Assuming an ideal conductor, the surface current density $\underline{\mathcal{I}}_{\mathcal{A}}$ is bounded to an infinitesimally thin surface layer of the antenna. The linear dipole antenna exhibits a current flow in the z -direction only. From (4.111) we obtain

$$\underline{\mathcal{E}}^{(s)} = \int_{V_{\text{ant}}} \underline{\mathcal{G}}_{e1}(\mathbf{x}, \mathbf{x}') \wedge \underline{\mathcal{I}}(\mathbf{x}') . \quad (13.30)$$

The integration is performed over the coordinates \mathbf{x}' over the volume of the antenna wires V_{ant} . The points of observation \mathbf{x} are located on the surface of the antenna wires. If the antenna exhibits infinite conductivity the current is confined to the wire surface. We can simplify the computation by replacing the current on the wire surface by a current line source in the axis of the cylinder. For the field excited by the current on the wire surface and outside the conductor this will be a good approximation. The virtual field excited by the equivalent line source inside the wire will be ignored, since the field vanishes inside an ideal conductor. In this case we can set $\mathbf{x}' = (0, 0, z')$ in $\underline{\mathcal{G}}_{e1}(\mathbf{x}, \mathbf{x}')$. Integrating the current density over the wire cross-section $A_{\text{ant}}(z)$ yields the antenna current

$$\underline{I}(z) = \int_{A_{\text{ant}}(z)} \underline{\mathcal{I}}(\mathbf{x}) . \quad (13.31)$$

Integrating (13.30) over the wire cross-section $A_{\text{ant}}(z)$, we obtain with (4.107) and (4.112) Pocklington's integral equation [9]

$$\underline{E}_z^{(s)}(z) \Big|_{r=a} = \frac{1}{4\pi j \omega \epsilon_0} \int_{z'=-l}^{z'=l} \left(\frac{\partial^2}{\partial z^2} + k^2 \right) \frac{\exp(-jkr)}{r} \underline{I}(z') dz' \quad (13.32)$$

with

$$r = |\mathbf{x} - \mathbf{x}'| = \sqrt{a^2 + (z - z')^2}. \quad (13.33)$$

The kernel of Pocklington's integral equation (13.32) may be written in the more convenient *Richmond form* [10] as

$$\underline{E}_z^{(s)}(z) \Big|_{r=a} = \frac{1}{4\pi j \omega \epsilon_0} \int_{z'=-l}^{z'=l} \frac{e^{-jkr}}{r^5} [(1 + jkr)(2r^2 - 3a^2) + k^2 a^2 r^2] \underline{I}(z') dz'. \quad (13.34)$$

Exciting the dipole in the gap $[-\frac{1}{2}b, \frac{1}{2}b]$ with a voltage \underline{V}_0 yields

$$\underline{E}_{iz}(z) \Big|_{x \in \mathcal{A}} = \begin{cases} \underline{V}_0/b & \text{for } |z| \leq \frac{1}{2}b \\ 0 & \text{for } \frac{1}{2}b < |z| < l \end{cases}. \quad (13.35)$$

The solution of this integral equation (13.34) of type

$$\underline{E}_z^{(s)}(z) \Big|_{r=a} = \int_{z'=-l}^{z'=l} K(z, z') \underline{I}(z') dz' \quad (13.36)$$

is performed using the method of moments. We make the following staircase approximation of the current distribution

$$I(z) = \sum_{n=1}^N I_n P\left(\frac{z - z_n}{\Delta z}\right) \quad (13.37)$$

with

$$\Delta z = \frac{2l}{N+1}, \quad (13.38a)$$

$$z_n = -l + n\Delta z. \quad (13.38b)$$

As the test function we use the delta distributions

$$\psi_n = \delta(z - z_n) \quad (13.39)$$

and obtain

$$\sum_n L_{mn} \alpha_n = \beta_m \quad (13.40)$$

with

$$\beta_m = \Delta z E_{iz}(z_m) \quad (13.41)$$

and

$$L_{mn} = \Delta z \int_{z_n - \frac{1}{2}\Delta z}^{z_n + \frac{1}{2}\Delta z} K(z_m, z') dz'. \quad (13.42)$$

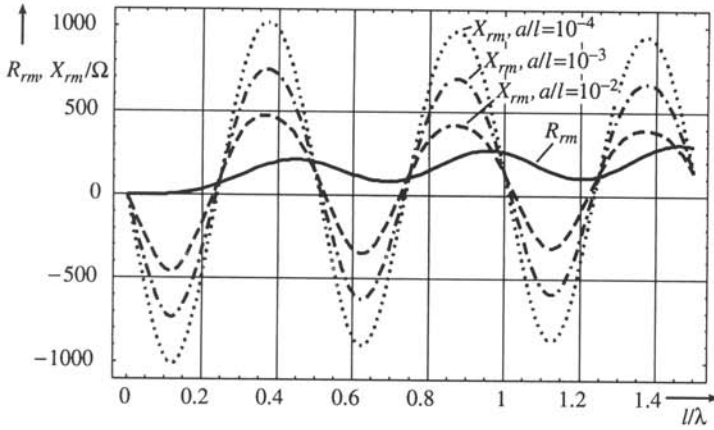


Figure 13.7: Radiation impedance Z_{rm} of the linear dipole for $a/l = 10^{-4}, 10^{-3}, 10^{-2}$.

13.4 THE IMPEDANCE OF THE LINEAR ANTENNA

In the following we show a method to compute the complex antenna impedance by approximation [3, 4, 11]. We consider again the linear antenna depicted in Figure 13.3. The antenna consists of two circular cylindric conductors separated by a gap. We assume the diameter of the conductors to be small compared with the wavelength. The z -component of the electric field is given by (13.36) as

$$\underline{E}_z(z)|_{x \in A} = \int_{-l}^l K(z, z') \underline{I}(z') dz'. \quad (13.43)$$

At the surface of the ideally conducting antenna rod the tangential electric field vanishes. In the gap between the two rods of the dipole the electric field is assumed to be homogeneous. Let the voltage across the gap be \underline{V}_0 . This yields

$$\underline{E}_z(z)|_{x \in A} = \begin{cases} \underline{E}_0 = \frac{\underline{V}_0}{\delta} & \text{for } |z| < \frac{1}{2}\delta \\ 0 & \text{for } \frac{1}{2}\delta < |z| < l \end{cases} \quad (13.44)$$

Multiplying both sides of (13.44) with $\underline{I}(z)$ and integrating over z from $-l$ to l yields

$$\int_{-l}^l \underline{E}_z(z) \underline{I}(z) dz = -\underline{V}_0 \underline{I}_1. \quad (13.45)$$

From this we obtain the antenna impedance Z_{rm} related to the maximum current \underline{I}_m ,

$$Z_r = \frac{\underline{V}_0}{\underline{I}_1} = -\frac{1}{\underline{I}_1^2} \int_{-l}^l \underline{E}_z(z) \underline{I}(z) dz. \quad (13.46)$$

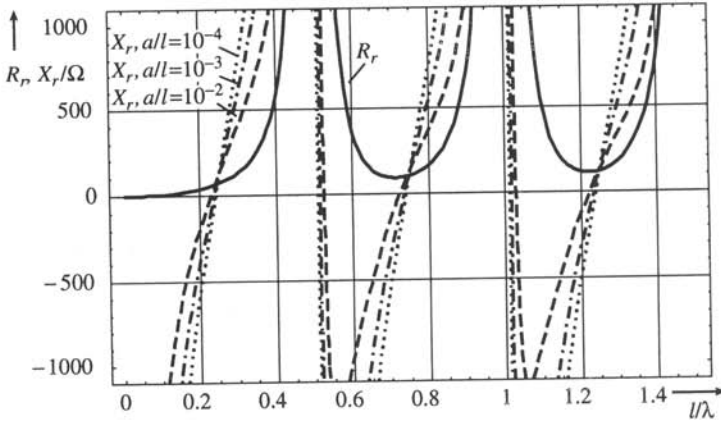


Figure 13.8: Radiation impedance Z_r of the linear dipole for $a/l = 10^{-4}, 10^{-3}, 10^{-2}$.

Inserting (13.43) for $\underline{E}_z(z)$ yields

$$Z_r = -\frac{1}{I_1^2} \int_{-l}^l \int_{-l}^l \underline{I}(z) K(z, z') \underline{I}(z') dz dz'. \quad (13.47)$$

Let us assume the current distribution $\underline{I}(z)$ to be known. We can for example use the approximation of the current distribution used in (13.9), hence

$$\underline{I}(z) = \underline{I}_m \sin k(l - |z|), \quad \underline{I}_1(z) = \underline{I}_m \sin k(l). \quad (13.48)$$

The antenna impedance Z_r exhibits a real part R_r and an imaginary part X_r . The real part is given by (13.27). Inserting (13.48) into (13.46) yields the reactive part of the radiation impedance,

$$X_r = \frac{X_{mr}}{\sin^2 kl} = \frac{Z_{F0}}{4\pi \sin^2 kl} \left\{ 2\text{Si}(2kl) + [2\text{Si}(2kl) - \text{Si}(4kl)] \cos(kl) - [2\text{Ci}(2kl) - \text{Ci}(4kl) - \text{Ci}(4kl)] \sin(ka^2 l^{-1}) \right\}, \quad (13.49)$$

with the integral sine Si and the integral cosine Ci given by (13.23a) and (13.23b). This method for computation of the antenna impedance also gives good results if only an approximation of the current distribution is used. The reason for this is that the expression (13.47) exhibits a quadratic dependence on the current distribution. Therefore it is not sensitive to small errors in the current distribution. Figure 13.8 shows real and imaginary parts of the radiation impedance $Z_{mr} = R_{mr} + jX_{mr}$ referred

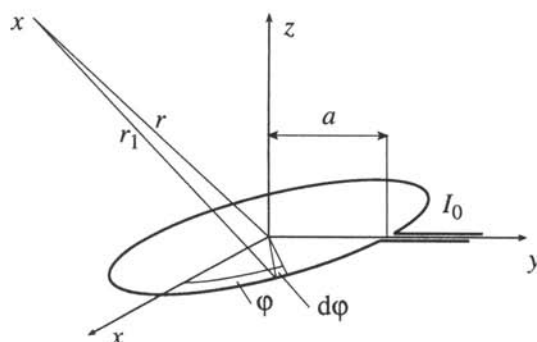
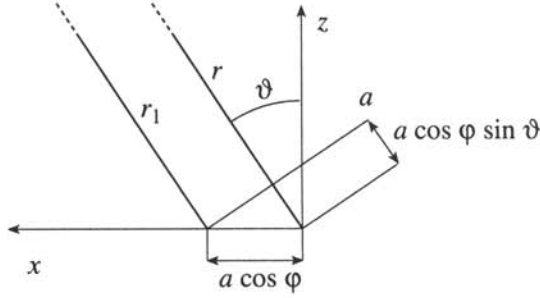


Figure 13.9: Loop antenna.

to the maximum current I_m , and Figure 13.7 shows real and imaginary parts of the radiation impedance $Z_r = R_r + jX_r$ referred to the feed current I_1 for various ratios of a/l . The real part of the radiation impedance is related to the power radiated into the antenna far-field, whereas its imaginary part is connected with the reactive power flowing forth and back between the antenna feed and the near-field. The reactive power is proportional to the difference of the average magnetic and electric energies stored in the near-field. Since the near-field exhibits a singularity in the dipole axis, the stored near-field increases when the dipole diameter is lowered.

13.5 THE LOOP ANTENNA

A loop antenna consists of a wire loop of one or more turns. The loop antenna primarily excites a magnetic dipole moment, which may be considered as the source of the electromagnetic wave. Figure 13.9 shows a circular loop antenna of diameter $2a$ with one turn. We consider the circumference of the loop to be small compared to the wavelength so that we can assume the current flowing through the loop to be spatially uniform. We compute the electric Hertz vector using (4.103a). The loop antenna exhibits rotational symmetry with respect to rotation around the z -axis. The necessary feeding line yields no perturbation of this symmetry since the field contributions of the two wires of the feeding line compensate each other. Due to the symmetry properties of the circular loop antenna the electromagnetic field also exhibits rotational symmetry; therefore it will be sufficient in the following to compute the Hertz vector $\underline{\Pi}_e(\mathbf{x})$ in the plane $y = 0$. The volume integration in (4.103a) needs to be performed over the volume

Figure 13.10: Definition of r_1 .

filled by the conductor only. According to (12.2), we obtain for the region

$$* \underline{\mathcal{M}}_{e0} = \frac{I_0}{j\omega A} r d\phi = \frac{I_0}{j\omega A} (-\sin\phi dx + \cos\phi dy), \quad (13.50)$$

where A is the cross-sectional area of the conductor. The volume element is given by $Aa d\phi$. For $\underline{\Pi}_{e,y}$ we obtain from (4.103a)

$$\underline{\Pi}_{e,y}(x_0) = \frac{aI_0}{4\pi j\omega\epsilon_0} \int_0^{2\pi} \frac{\cos\phi e^{-jk r_1}}{r_1} d\phi, \quad (13.51)$$

where r_1 marks the connection from the point x in the far-field to the conductor. For a point x in the far-field we can assume the lines r and r_1 to be parallel. Since $\underline{\mathcal{M}}_{e0}$ exhibits no z -component, $\underline{\Pi}_{e,z} = 0$ is also valid. Furthermore, it follows from (13.50) that in the plane $y = 0$ the x -component of the Hertz vector disappears, that is, $\underline{\Pi}_{e,x}(x, 0, z) = 0$. According to Figure 13.10, we obtain

$$r_1 = r - a \cos\phi \sin\theta. \quad (13.52)$$

We use this expression in the exponent of the integrand, since the exponential function is strongly varying with r_1 , whereas in the denominator r_1 may be replaced by r . Furthermore, due to the rotational symmetry of the electromagnetic field we obtain

$$\underline{\Pi}_\phi(r, \theta) = \underline{\Pi}_y(r, \theta) \Big|_{\phi=0}. \quad (13.53)$$

This yields

$$\underline{\Pi}_\phi = \frac{aI_0}{4\pi j\omega\epsilon_0} \frac{e^{-jkr}}{r} \int_0^{2\pi} \cos\phi e^{jka \cos\phi \sin\theta} d\phi. \quad (13.54)$$

Since the circumference of the current loop is small compared with the wavelength, $ka \ll 1$ is valid, and we can make the approximation

$$e^{jka \cos \phi \sin \theta} \approx 1 + jka \cos \phi \sin \theta. \quad (13.55)$$

Therewith we obtain from (13.54)

$$\underline{\Pi}_e = \frac{ka^2 \underline{I}_0}{4\omega\epsilon_0} e^{-jkr} \sin^2 \theta d\phi. \quad (13.56)$$

With (12.6a) we obtain

$$\underline{\mathcal{H}} = j\omega\epsilon_0 * d\underline{\Pi}_e = j\frac{1}{4}ka^2 \underline{I}_0 e^{-jkr} \left(\frac{2}{r^2} \cos \theta dr + \frac{jk}{r} \sin \theta r d\theta \right), \quad (13.57)$$

and therewith

$$\underline{H}_\theta = -\frac{1}{4}k^2 a^2 \underline{I}_0 \frac{e^{-jkr}}{r} \sin \theta, \quad (13.58a)$$

$$\underline{H}_r = \frac{1}{2}jka^2 \underline{I}_0 \frac{e^{-jkr}}{r^2} \cos \theta. \quad (13.58b)$$

With (12.6b) and $Z_{F0} = k/\omega\epsilon_0$ we obtain

$$\underline{\mathcal{E}} = * d * d\underline{\Pi}_e = \frac{1}{4}a^2 Z_{F0} \underline{I}_0 e^{-jkr} \left(\frac{k^2}{r} + \frac{2}{r^3} \right) r \sin^2 \theta d\phi, \quad (13.59)$$

and therefrom

$$\underline{E}_\phi = \frac{1}{4}a^2 Z_{F0} \underline{I}_0 \left(\frac{k^2}{r} + \frac{2}{r^3} \right) e^{-jkr} \sin \theta. \quad (13.60)$$

In the far-field $r \rightarrow \infty$ we obtain from (13.57) and (13.59)

$$\underline{\mathcal{H}} = -\frac{1}{4}k^2 a^2 \underline{I}_0 \frac{e^{-jkr}}{r} \sin \theta r d\theta, \quad (13.61a)$$

$$\underline{\mathcal{E}} = \frac{1}{4}Z_{F0} k^2 a^2 \underline{I}_0 \frac{e^{-jkr}}{r} \sin \theta r \sin \theta d\phi \quad (13.61b)$$

and the corresponding field components

$$\underline{H}_\theta = -\frac{1}{4}k^2 a^2 \underline{I}_0 \frac{e^{-jkr}}{r} \sin \theta, \quad (13.62a)$$

$$\underline{E}_\phi = \frac{1}{4}Z_{F0} k^2 a^2 \underline{I}_0 \frac{e^{-jkr}}{r} \sin \theta. \quad (13.62b)$$

The far-field is given by (13.58a) and

$$\underline{E}_\phi = -Z_{F0}\underline{H}_\theta = \frac{1}{4}Z_{F0}k^2a^2\underline{L}_0 \frac{e^{-jkr}}{r} \sin \theta. \quad (13.63)$$

The far-field of the loop antenna with a small diameter is dual to the far-field of the Hertzian dipole. From (4.19), (13.58a), and (13.63) we obtain the complex Poynting form \mathcal{T} for the far-field

$$\mathcal{T} = -\frac{1}{2}\underline{E}_\phi \underline{H}_\theta^* r^2 \sin \theta d\theta \wedge d\phi = \frac{1}{32}Z_{F0}k^4a^4|\underline{L}_0|^2 \sin^3 \theta d\theta \wedge d\phi. \quad (13.64)$$

In the far-field the complex Poynting vector exhibits only a radial component

$$T_r = \frac{Z_{F0}k^4a^4|\underline{L}_0|^2 \sin^2 \theta}{32r^2}. \quad (13.65)$$

The power radiated from the loop antenna follows from this with (12.21) and (12.22)

$$P = \frac{1}{12}\pi Z_{F0}k^4a^4|\underline{L}_0|^2. \quad (13.66)$$

We again introduce the radiation resistance defined in (12.26) and obtain

$$R_r = \frac{2P}{|\underline{L}_0|^2} = \frac{1}{6}\pi Z_{F0}k^4a^4. \quad (13.67)$$

13.6 RECEIVING ANTENNAS

13.6.1 The Hertzian Dipole as Receiving Antenna

We consider the Hertzian dipole as depicted in Figure 13.11 in the field of a plane electromagnetic wave. The magnetic field \underline{H} may be oriented normal to the dipole axis. The direction of the electric field \underline{E} may enclose an angle θ' with the dipole axis. The Hertzian dipole of length l is formed by two wires with spheres attached at the end. The wires are assumed to be thin enough so that only the spheres at the end of the wires are contributing to the capacitance of the antenna. The current flowing in the short linear conductors between the spheres may be considered to be spatially uniform. The circuit loop is closed via the displacement current between the two spheres. The potential difference \underline{V}_0 between both spheres is given by

$$\underline{V}_0 = - \int_{-\frac{1}{2}l}^{+\frac{1}{2}l} \underline{\mathcal{E}} = -l\underline{E} \cos \theta'. \quad (13.68)$$

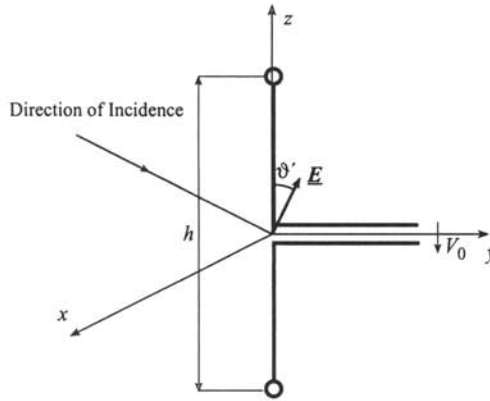


Figure 13.11: The Hertzian dipole as receiving antenna.

This voltage is equal to the open circuit voltage in the feeding point of the antenna. If the antenna is oriented in parallel to the direction of the electric field the node voltage \underline{V}_0 assumes a maximum value $\underline{V}_{0,\max}$. We obtain

$$|\underline{V}_{0,\max}| = h|\underline{E}|. \quad (13.69)$$

The length h of the Hertzian dipole determines the ratio between the open circuit voltage across the antenna port and the electric field intensity. Via (13.69) an *effective antenna length* l_{eff} may be defined for arbitrary antennas.

13.6.2 The Loop Antenna as Receiving Antenna

A plane wave is incident on a loop antenna according to Figure 13.12. We assume that \underline{E} is parallel to the plane of the loop, whereas the direction of the magnetic field \underline{H} encloses with the normal to the loop plane an angle θ' . We assume $a \ll \lambda$. From (2.114b) we obtain the open-circuit node voltage of the loop antenna

$$\underline{V}_0 = j\omega\Phi \quad (13.70)$$

where the magnetic flux according to (2.29) is given by

$$\Phi = \int_A \mathcal{B} = A\mu_0 \underline{H} \cos \theta' \quad (13.71)$$

where A is the surface of the loop antenna. For the circular loop antenna according to Figure 13.12 we obtain

$$A = a^2 \pi. \quad (13.72)$$

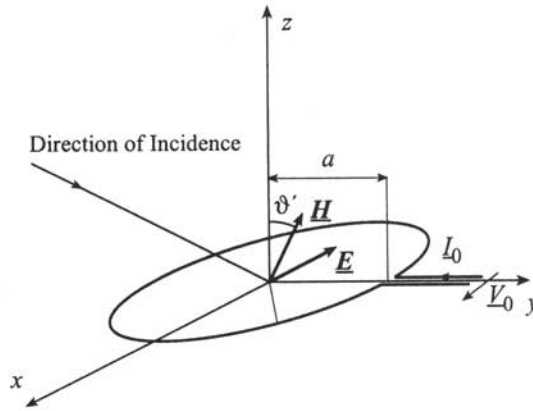


Figure 13.12: The loop antenna as receiving antenna.

We want to represent \underline{V}_0 as a function of the electric field intensity \underline{E} and obtain with

$$\frac{\omega \mu_0}{Z_{F0}} = \frac{2\pi}{\lambda_0} \quad (13.73)$$

from (13.18), (13.70), and (13.71)

$$\underline{V}_0 = \frac{2\pi j A}{\lambda_0} \underline{E} \cos \theta' . \quad (13.74)$$

We now define according to (13.73) an effective antenna length l_{eff} for the case of an incident wave polarized in parallel to the axis of the linear antenna:

$$|\underline{V}_0| = l_{\text{eff}} |\underline{E}| . \quad (13.75)$$

We obtain from (13.73) and (13.75) the effective antenna length of the loop antenna

$$l_{\text{eff}} = \frac{2\pi A}{\lambda_0} . \quad (13.76)$$

13.6.3 The Linear Dipole Antenna as Receiving Antenna

If we are using an antenna as a receiving antenna we want to know the signal obtained at the antenna port if the antenna is irradiated by an electromagnetic field. Usually a receiving antenna is positioned in the far-field of the transmitter and the distance between the transmitter and the receiving antenna is by orders of magnitude larger

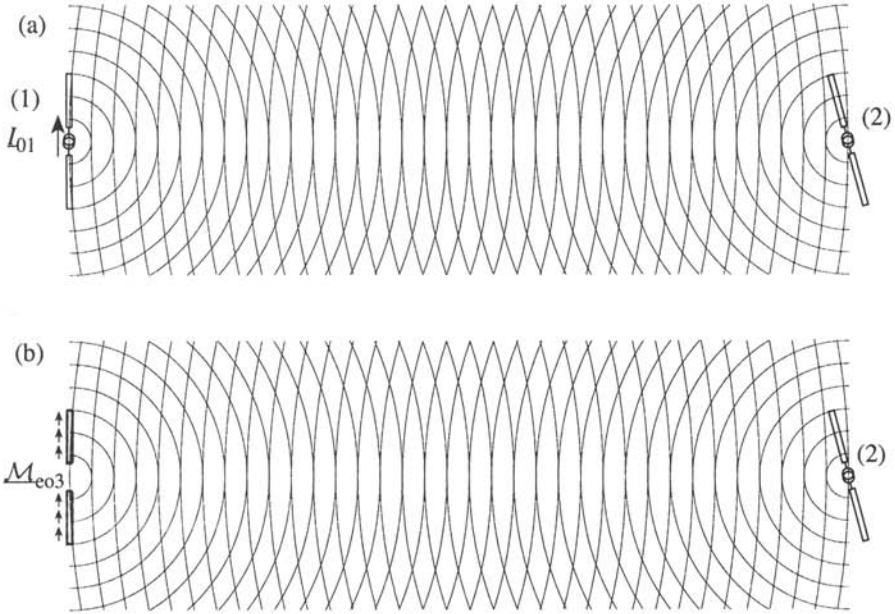


Figure 13.13: Calculating h_{eff} of the dipole antenna.

than the linear dimensions of the antenna. Therefore we can assume the received electromagnetic wave within a spatial region of the size of the antenna to be a plane wave. However, arranging the antenna in the received field will create a considerable perturbation. The primary field will be scattered by the antenna and the resulting electromagnetic field will no longer be a plane wave field. In the following we shall overcome this difficulty by applying the theorem of reciprocity. We will demonstrate a way to analyze the receiving antenna on the basis of the unperturbed primary incident plane wave field.

Let us consider the two antennas, (1) and (2), respectively, depicted in Figure 13.13(a). We assume both antennas to be coupled via the far-field – that means the distance between the antennas is by orders of magnitude larger than their linear dimensions. Let antenna (1) be a linear dipole antenna according to Figure 13.3, whereas antenna (2) may be of an arbitrary type. At the feeding nodes of antenna (1) and antenna (2), respectively, the currents I_{01} and I_{02} may be impressed. The current distribution $I_1(z)$ on the antenna wires of antenna (1) is due to the impression of the node current I_{01} . The reaction of the far-field of antenna (1) on the current I_{02} impressed into antenna (2) is given by R_{12} , whereas the reaction of the far-field of antenna (2) on the current

source \underline{I}_{01} is given by R_{21} . From (4.67) we obtain

$$R_{12} = R_{21} \quad (13.77)$$

and (4.71) yields

$$R_{21} = -\underline{V}_2 \underline{I}_{01}, \quad (13.78)$$

where V_2 is the open circuit voltage excited from the far-field of antenna (2) in the nodes of antenna (1). We now replace the current distribution $\underline{I}_1(z)$ due to the excitation of antenna (1) with the current source \underline{I}_{01} by a polarization $\underline{M}_{e03}(\mathbf{x})$ impressed into free-space. Similar to (4.68), we obtain

$$\underline{M}_{e03}(\mathbf{x}) = \frac{1}{j\omega A} \underline{I}_1(z) d\mathbf{x} \wedge d\mathbf{y} \quad (13.79)$$

where A is the cross-sectional area of the linear dipole antenna (1). The impressed polarization $\underline{M}_{e03}(\mathbf{x})$ excites the same field as antenna (1). Therefore the reaction R_{32} of the far-field excited by $\underline{M}_{e03}(\mathbf{x})$ on the current source \underline{I}_{02} must also be equal to the reaction R_{12} of the far-field excited from antenna (1) on the current source \underline{I}_{02} .

$$R_{32} = R_{12}. \quad (13.80)$$

On the other hand due to the reciprocity of the radio link formed by the two antennas we obtain from (4.67)

$$R_{32} = R_{23}. \quad (13.81)$$

From (13.77), (13.80) and (13.81) it follows that

$$R_{21} = R_{23}. \quad (13.82)$$

The field excited from antenna (2) at the location of the impressed polarization $\underline{M}_{e03}(\mathbf{x})$ is equal to the unperturbed electric field since we have removed antenna (1). This procedure allows us to compute the voltage induced in the receiving antenna without considering the field perturbation by bringing the receiving antenna into the primary field. The reaction R_{23} of the field $\underline{E}(\mathbf{x})$ on $\underline{M}_{e03}(\mathbf{x})$ according to (4.66) is given by

$$R_{23} = j\omega \int_V \underline{\mathcal{E}}_2 \wedge \underline{M}_{e03}, \quad (13.83)$$

where the integration is performed over the volume \mathcal{V}_{03} , where $\underline{M}_{e03}(\mathbf{x})$ is impressed. Since $\underline{E}(\mathbf{x})$ and $\underline{M}_{e03}(\mathbf{x})$ are uniformly distributed over the cross-sectional area, we obtain from (13.79)

$$R_{23} = \int_{-l}^{+l} \underline{I}_1(z) \underline{E}_z(z) dz. \quad (13.84)$$

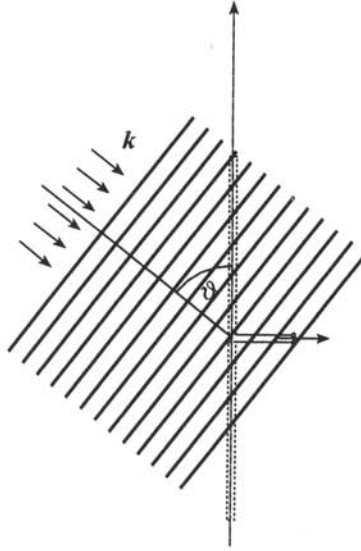


Figure 13.14: Unperturbed plane wave at the position of the linear dipole antenna.

The integration is performed over a length $2l$ of the linear dipole antenna from $z = -l$ to $z = +l$. The current distribution $I_1(z)$ is given by (13.9).

For an electromagnetic wave incident under an angle θ relative to the dipole axis, as shown in Figure 13.14, with the wave number k and the electric field parallel to the plane $x = 0$, we obtain

$$k_z = -k \cos \theta \quad (13.85)$$

for the z -component of the unperturbed electric field

$$\underline{E}_z = \underline{E}_0 \sin \theta e^{jkz \cos \theta}. \quad (13.86)$$

Inserting (13.14) and (13.86) into (13.84) we obtain

$$R_{23} = \frac{2\underline{E}_0 \underline{I}_m}{k \sin \theta} [\cos(kl \cos \theta) - \cos(kl)]. \quad (13.87)$$

With (13.26), we relate R_{23} to the node current \underline{I}_{01} and obtain

$$R_{23} = 2\underline{E}_0 \underline{I}_{01} \frac{\cos(kl \cos \theta) - \cos kl}{k \sin \theta \sin kl}. \quad (13.88)$$

With (13.78) and (13.82) we obtain with $\underline{V}_0 = \underline{V}_2$

$$\underline{V}_0 = -2\underline{E}_0 \frac{\cos(kl \cos \theta) - \cos kl}{k \sin \theta \sin kl}. \quad (13.89)$$

A comparison with (13.16) shows that the antenna pattern of the receiving antenna is the same as the antenna pattern of the transmitting antenna. We will demonstrate the identity of the receiving antenna pattern and transmitting antenna pattern for arbitrary antennas in Section 13.7. This identity is a consequence of the reciprocity theorem.

For the case of an incident wave polarized in parallel to the axis of the linear antenna, we obtain from (13.75) and (13.89) for $\theta = \frac{1}{2}\pi$

$$l_{\text{eff}} = 2 \frac{1 - \cos kl}{k \sin kl} = \frac{\lambda_0}{\pi} \frac{1 - \cos kl}{\sin kl}. \quad (13.90)$$

For the short linear antenna with $kl \ll 1$, we obtain

$$l_{\text{eff}} = l. \quad (13.91)$$

For the half-wave dipole with $2l = \frac{1}{2}\lambda_0$, we obtain

$$l_{\text{eff}} = \frac{\lambda_0}{\pi} \quad \text{for } 2l = \frac{1}{2}\lambda_0. \quad (13.92)$$

For arbitrary directions of incidence $\theta \neq \frac{1}{2}\pi$, we obtain from (13.89) and (13.75) the *general effective antenna length*

$$l_{\text{eff}} = \left| 2 \frac{\cos(kl \cos \theta) - \cos kl}{k \sin \theta \sin kl} \right|. \quad (13.93)$$

13.7 GAIN AND EFFECTIVE ANTENNA APERTURE

The power radiated by an antenna into a certain solid angle depends on the direction. We define an *antenna gain* G as the ratio of the active power density radiated by the antenna to the power density radiated by an antenna of reference. As the reference antenna we use the isotropic spherical radiator, which distributes the radiated power uniformly over all directions. Such a uniform radiator cannot be realized physically. The best approximation to the uniform radiator is the Hertzian dipole which, however, exhibits a non-uniform angular distribution of the radiated power. Let P_r be the active power emitted by a radiator. In this case the power density of an isotropic spherical radiator at a distance r will be $P_r/4\pi r^2$. Using the isotropic spherical radiator as a reference, the antenna gain is given by

$$G = \frac{4\pi r^2 \Re\{T_r(r, \theta, \phi)\}}{P_r}. \quad (13.94)$$

The direction in which the active power radiated by the antenna per unit of solid angle is maximum is called the direction of maximum radiation. The antenna gain in the

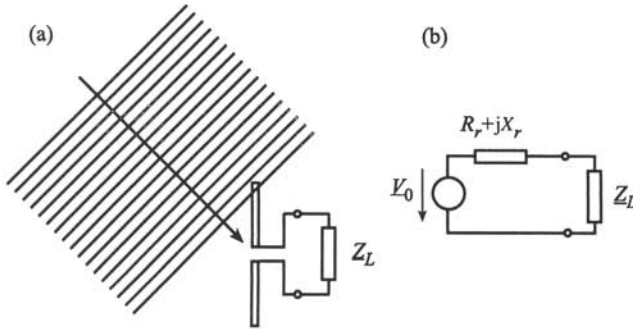


Figure 13.15: (a) Receiving antenna loaded with Z_L and (b) two-port equivalent circuit.

direction of maximum radiation is the maximum antenna gain. For a Hertzian dipole it follows from (12.23), (12.26), and (13.94) that

$$G = \frac{3}{2} \sin^2 \theta. \quad (13.95)$$

We obtain the same result from (13.65) and (13.66) for the small loop antenna according to Figure 13.9. The maximum antenna gain is obtained for $\theta = \frac{1}{2}\pi$

$$G_{\max} = \frac{3}{2}. \quad (13.96)$$

For receiving antennas an effective aperture (or effective area) A_e may be defined. Figure 13.15(a) shows a wave incident on an antenna loaded with in impedance Z_L . The effective aperture is an equivalent area through which the incident wave transports a power equal to the power received by the antenna. Multiplying the power density of the incident wave with the effective antenna aperture yields the power received by the antenna. Let $\Re\{\underline{T}\}$ be the power density of the incident wave and P_r the active power received by the antenna; we obtain the following relation

$$P_r = A_e \Re\{\underline{T}\}. \quad (13.97)$$

Since the received power depends on the orientation of the antenna as well as on matching of the load to the antenna, the effective aperture also depends on these conditions. The receiving antenna may be considered as a one-port source as shown in Figure 13.15(b). The magnitude of the open-circuit node voltage V_0 may be obtained from (13.75). If the antenna exhibits no losses, the real part of the antenna impedance is equal to the radiation resistance R_r . For power matching the load impedance is given by

$$Z_L = R_r - jX_s. \quad (13.98)$$

In this case the antenna delivers the power

$$P_r = \frac{1}{8} \frac{|V_0|^2}{R_r} \quad (13.99)$$

to the load. For an incident plane wave the power density is given by

$$\underline{T} = \frac{1}{2Z_{F0}} |\underline{E}|^2. \quad (13.100)$$

From (13.75), (13.94), (13.99), and (13.100) we obtain the following relation between effective antenna aperture and effective antenna length

$$A_e = \frac{Z_{F0} I_{\text{eff}}^2}{4R_r} \quad \text{for power matching.} \quad (13.101)$$

For the Hertzian dipole oriented parallel to the electric field we obtain from (12.26)

$$A_e = \frac{3\lambda_0^2}{8\pi}. \quad (13.102)$$

The effective aperture of the Hertzian dipole is independent from h . Therefore the power as specified in (13.97) may be received irrespective of how short the antenna may be. This statement, however, is only valid if the conductive losses in the antenna may be neglected and the antenna can be matched to the load. The radiation resistance of short antennas according to (12.26) is proportional to the square of the antenna length. Hence for very short antennas it may not be possible to neglect the ohmic losses in comparison with the radiation resistance. Furthermore, if the radiation resistance is very small, a power matching of the antenna will only be possible in a very narrow frequency band.

Considering the Poynting vector field of power flow we can visualize the meaning of the effective aperture. Figure 13.16 depicts the Poynting vector field in the vicinity of an antenna. If a plane wave is incident on an antenna, this wave will be scattered from the antenna. The scattering of the incident wave also depends on the matching of the antenna to the load. An antenna matched to the load is equivalent to a resonant circuit. If the plane wave is incident at the resonant frequency of this resonant circuit, an oscillation of considerable amplitude may be built up in the resonant circuit. Due to this excitation the antenna will radiate a secondary wave. This scattered field of the antenna now is superimposed to the primary incident wave and the Poynting vector field now depends on the superposition of the primary field and the secondary field. As can be seen in Figure 13.16(a) the antenna is perturbing the power flow in its neighborhood considerably. A part of the power flow lines is now flowing in the

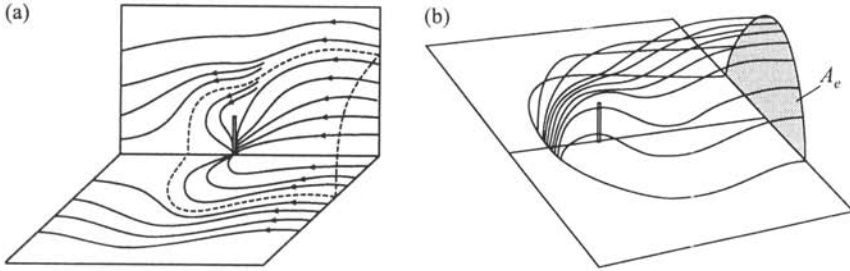


Figure 13.16: (a) Power flow lines $\Re\{T\}$ at a linear receiving antenna and (b) effective aperture A_e of the linear receiving antenna [8, 12].

feed line of the receiving antenna. In Figure 13.16(b) the surface A_1 is shown separating the region where all power flow lines are flowing into the antenna feed line from the outer region, where the power flow lines are passing the antenna. By that way we may construct a tube, which has the property that all the field energy flowing inside is fed into the antenna. We can follow this tube to a region far distant enough from the antenna so that there is no distortion of the plane wave field anymore. At this point the cross-sectional area of the tube corresponds exactly with the effective aperture of the antenna. We now can understand why the effective antenna area may exhibit a much larger dimension than the antenna. When the antenna is very small the radiation resistance becomes small, too. If the antenna exhibits no losses and is terminated by matched load, the equivalent circuit of the terminated antenna is a resonant circuit with very high Q -factor. An incident wave at the resonant frequency will excite an oscillation of high amplitude and in this way also a large scattered field contribution. Such a small antenna will only exhibit a large effective antenna aperture within a very narrow frequency band.

Let us now consider the transmission properties of a radio link formed by two antennas depicted schematically in Figure 13.17(a). We assume the antennas to be sufficiently coupled via their far-field only. We may consider one of the antennas to be the transmitting antenna and the other antenna to be the receiving antenna. Let us first consider antenna (1) to be the transmitting antenna and antenna (2) the receiving antenna. In this case from (13.94) and (13.97) we obtain the following relation between the power P_{t1} emitted from antenna (1) and the power P_{r2} received from antenna (2)

$$P_{r2} = \frac{G_1 A_{e2}}{4\pi r^2} P_{t1}. \quad (13.103)$$

In this equation, G_1 is the gain of antenna (1) and A_{e2} is the effective aperture of antenna (2). If we otherwise use antenna (2) as the transmitting antenna and antenna (1) as the

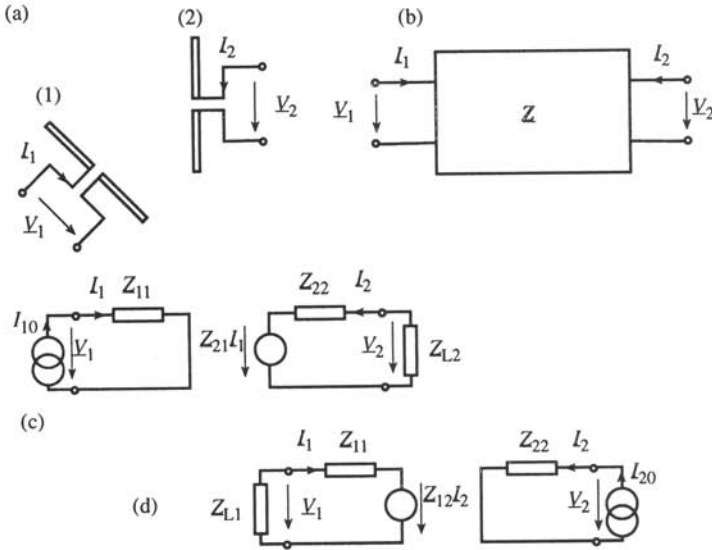


Figure 13.17: Two coupled antennas: (a) schematic presentation, (b) two-port-equivalent circuit, and (c)/(d) approximated equivalent circuit for antenna (1)/(2) as transmitting antenna.

receiving antenna, we obtain

$$P_{r1} = \frac{G_2 A_{e1}}{4\pi r^2} P_{t2}. \quad (13.104)$$

The two antennas coupled via their radiation field are forming a linear transmission link. Let us now assume that both antennas are only separated via free-space and that there are no further radiation sources existing. The geometric arrangement of both antennas and of the surrounding matter may be fixed. If we want to describe the relations between port voltages and port currents of both antennas, we can consider this transmission link as the linear source free two-port. Figure 13.17(b) shows the two-port equivalent circuit of the transmission link according to Figure 13.17(a). The coupling of two antennas usually is very weak. Therefore, in the impedance representation we can assume that $|Z_{12}| \ll |Z_{11}|, |Z_{22}|$. In this case we can neglect the reaction of the receiving antenna on the transmitting antenna and obtain the simplified equivalent circuits according to Figure 13.17(c/d). In this approximation the input impedances of antenna (1) and antenna (2) are independent from the termination of the other antenna by Z_{11} and Z_{22} , respectively, and we obtain

$$\Re\{Z_{ii}\} = R_{ri}, \quad i = 1, 2, \quad (13.105)$$

where R_{ri} is the radiation resistance of antenna (i). We now assume in both cases of

operation according to Figure 13.17(c) and 13.17(d), respectively, power-matching to be fulfilled, in other words

$$Z_{Li} = Z_{ii}^* . \quad (13.106)$$

For antenna (1) as the transmitting antenna and antenna (2) as the receiving antenna, we obtain

$$P_{t1} = \frac{1}{2} R_{r1} |I_{10}|^2 , \quad (13.107a)$$

$$P_{r2} = \frac{1}{2} \Re\{Z_{L2}\} |I_2|^2 . \quad (13.107b)$$

For the equivalent circuit according to Figure 13.17(c), we obtain from (13.105) to (13.107b)

$$\frac{P_{r2}}{P_{t1}} = \frac{|Z_{21}|^2}{4R_{r1}R_{r2}} . \quad (13.108)$$

If antenna (2) is the transmitting antenna and antenna (1) the receiving antenna it follows from Figure 13.17(d) that

$$\frac{P_{r1}}{P_{t2}} = \frac{|Z_{12}|^2}{4R_{r1}R_{r2}} . \quad (13.109)$$

Due to the reciprocity (4.67) is fulfilled and therefore

$$Z_{12} = Z_{21} . \quad (13.110)$$

From this it follows that

$$\frac{P_{r2}}{P_{t1}} = \frac{P_{r1}}{P_{t2}} \quad (13.111)$$

for the case of power matching of the load to the receiving antenna. The ratio of the available active power at the port of the receiving antenna to the input power of the transmitting antenna is called the transmission factor. According to (13.111) the transmission factor of a radio link corresponding to Figure 13.17(a) is of equal size in both directions. From (13.103), (13.104) and (13.111) we obtain

$$\frac{G_1}{A_{e1}} = \frac{G_2}{A_{e2}} . \quad (13.112)$$

We see that the ratio of gain to effective aperture is the same for both antennas. The quantities G_1 , A_{e1} only depend on antenna (1) and the quantities G_2 , A_{e2} only depend on antenna (2), and we also have considered the possibility of using different antenna types (1) and (2). Equation (13.112) only may be satisfied if the ratio of the gain and effective aperture is the same for all types of antennas. For an optimally oriented

Hertzian dipole ($\theta = \frac{1}{2}\pi$), we can compute from (13.96) and (13.102) the following relation between gain and effective antenna aperture

$$A_e = \frac{\lambda_0^2}{4\pi} G. \quad (13.113)$$

This relation also holds for any type of antenna and for any orientation of the antenna. Therefore the transmission ratio may be expressed by the gain of both antennas or by the effective aperture of both antennas or by the gain of one antenna and the effective aperture of the other antenna. The relation

$$\frac{P_{r2}}{P_{t1}} = \frac{P_{r1}}{P_{t2}} = \frac{G_1 A_{e2}}{4\pi r^2} = \frac{G_2 A_{e1}}{4\pi r^2} = \frac{\lambda_0^2 G_1 G_2}{16\pi^2 r^2} = \frac{A_{e1} A_{e2}}{\lambda_0^2 r^2} \quad (13.114)$$

is known as the *Friis transmission formula*.

13.8 ANTENNA ARRAYS

13.8.1 Linear Antenna Arrays

An *antenna array* is an arrangement of antenna elements distributed in space. The waves radiated by these antenna elements have defined amplitudes and phases and are superimposed in space. Antenna arrays allow the formation of antenna patterns of high gain and strong directivity. The pattern of an antenna array depends on the pattern of the antenna elements, the spatial arrangement of the antenna elements and the amplitude and phase of the feeding signals of each antenna element. Figure 13.18 shows a linear antenna array (i.e., a linear array of dipole antennas). The computation of the pattern of the linear antenna array is simplified if all antenna elements exhibit identical shapes and if their arrangement obeys some spatial symmetry.

Let us consider a single linear dipole antenna element radiating a vertically polarized wave. In polar coordinates the far-field of the antenna is given by

$$\underline{E}_\theta = Z_{F0} \underline{H}_\phi = \underline{A} \frac{e^{-jkr}}{2\pi r} F(\theta, \phi) \quad (13.115)$$

where \underline{A} is the complex amplitude and $F(\theta, \phi)$ is the *element pattern*. For the linear dipole antenna according to Figure 13.3 we obtain from (13.16)

$$A = j Z_{F0} I_m, \quad (13.116)$$

$$F(\theta, \phi) = \frac{\cos(kl \cos \theta) - \cos kl}{\sin \theta}. \quad (13.117)$$

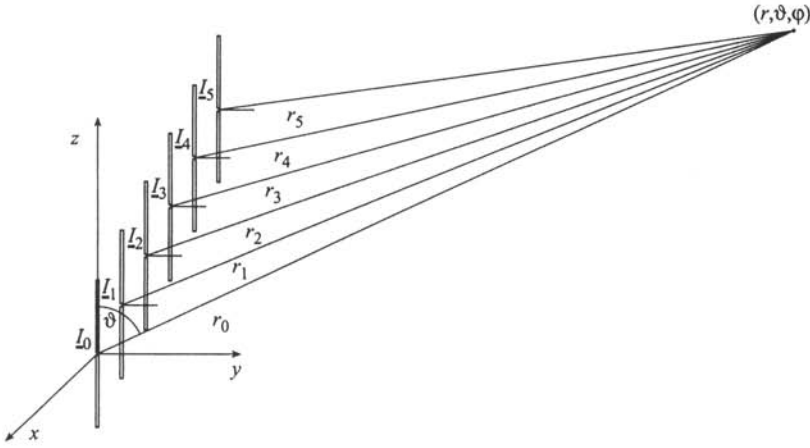


Figure 13.18: Linear antenna array formed by linear dipole antennas.

Let us now consider an arrangement of n parallel antenna elements with an identical element pattern. The contribution of the v th antenna element ($v = 1 \dots n$) to the far-field is given by

$$\underline{E}_{\theta v} = Z_{F0} \underline{H}_{\phi v} = \underline{A}_v \frac{e^{-jkr_v}}{2\pi r_v} F(\theta, \phi), \quad (13.118)$$

where r_v is the distance from the center of the v th dipole element to the point of observation in the far-field. The complex amplitudes \underline{A}_v of the antenna elements are put into relation to the amplitude \underline{A}_0 by

$$\underline{A}_v = p_v \underline{A}_0 e^{-j\delta_v} \quad (13.119)$$

where p_v and δ_v are the corresponding amplitude and phase ratios. We obtain the total far-field of the antenna array by superimposing the contributions of all antenna elements:

$$\underline{E}_{\theta} = Z_{F0} \underline{H}_{\phi} = \underline{A}_0 F(\theta, \phi) \sum_{v=1}^n p_v \frac{e^{-j(kr_v + \delta_v)}}{2\pi r_v}. \quad (13.120)$$

We choose the origin of our coordinate system near to the antenna array. Let r_v be the distance from the far-field point of observation to the center of the v th antenna element. We obtain for the far-field the following approximation:

$$r_v = r_0 - x_v \sin \theta \cos \phi - y_v \sin \theta \sin \phi - z_v \cos \theta. \quad (13.121)$$

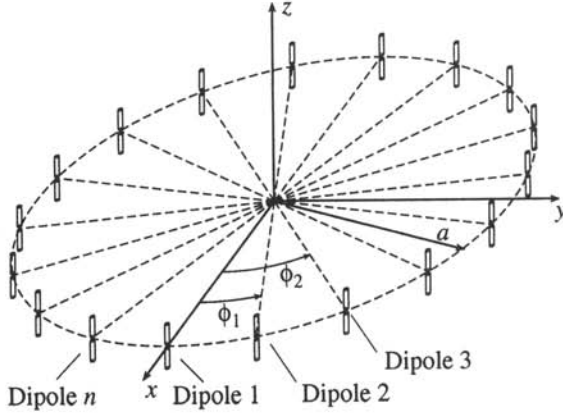


Figure 13.19: Circular antenna array formed by linear dipole antennas.

In (13.120) we can approximate r_v in the denominator by r_0 and obtain

$$\underline{E}_\theta = \underline{A}_0 \frac{e^{-jkr_0}}{2\pi r_0} F(\theta, \phi) M(\theta, \phi), \quad (13.122)$$

where the so-called *array factor* $M(\theta, \phi)$ is given by

$$M(\theta, \phi) = \sum_{v=1}^n p_v \exp\{-j[k(r_v - r_0) + \delta_v]\}. \quad (13.123)$$

We obtain the following simple result: *The pattern of an antenna array with equal, equally oriented, and equidistant antenna elements is the product of the pattern of a single antenna element and the array factor.* This law is called the *multiplicative law*.

13.8.2 Circular Antenna Arrays

Consider a *circular antenna array*, also called a *ring array*, in Figure 13.19. The circular antenna array consists of n antenna elements arranged in angular positions ϕ_v along a circle of radius a . For the circular antenna array the array factor is given by

$$M(\theta, \phi) = \sum_{v=1}^n A_v \exp\{j[k\rho_v \sin \theta \cos(\phi - \phi_v) + \delta_v]\}. \quad (13.124)$$

For maximum radiation in direction (θ_0, ϕ_0) we have to choose

$$\delta_v = j[k\rho_v \sin \theta_0 \cos(\phi_0 - \phi_v)]. \quad (13.125)$$

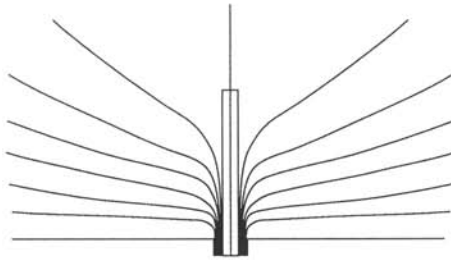


Figure 13.20: Poynting vector field of a vertical antenna.

For half-wave dipoles as antenna elements with an element pattern given by (13.17) the pattern of the antenna array is given by

$$M(\theta, \phi) = \frac{\cos(\frac{1}{2}\pi \cos \theta)}{\sin \theta} \frac{\sum_{v=1}^n A_v \exp\{j[k\rho_v \sin \theta \cos(\phi - \phi_v) + \delta_v]\}}{\sum_{v=1}^n A_v}. \quad (13.126)$$

Usually circular antenna arrays exhibit uniform angular distance between the antenna elements. In this case the ϕ_v are given by

$$\phi_v = 2\pi \frac{v-1}{n}. \quad (13.127)$$

13.9 APERTURE ANTENNAS

13.9.1 Radiating Apertures

The antennas treated so far have been composed of linear conductors. To design antennas we first have computed the current distribution on the linear conductor. Then we have treated this current distribution as an impressed current distribution. In a further step we have computed the radiated field from the impressed current distribution using (4.103a) and (12.2). The subdivision of the design procedure into computation of the current distribution without considering radiation, and subsequently computing the radiation on the basis of a given current distribution, allows a straightforward computation of the radiation pattern of the antenna. However, this method neglects the reaction of the radiation field on the current distribution in the antenna. For example, the attenuation of the current wave on the antenna conductors due to the radiation has not been considered.

Another consequence of this model has been that it has supported a picture in which the current flowing in the conductor at some point is the source of the field. However, at this point we only have changed a model from the network and transmission-line

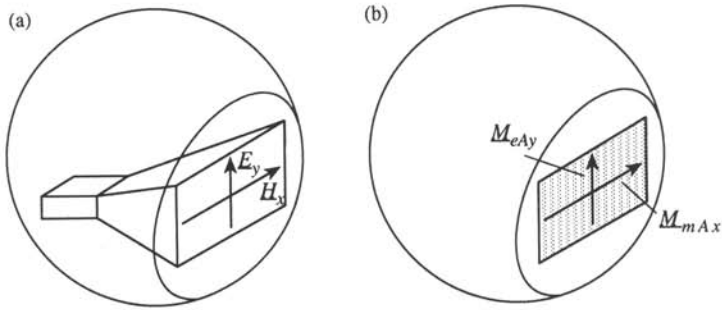


Figure 13.21: (a) Horn antenna and (b) impressed equivalent surface polarizations.

model to the field model. A consequent application of the field picture shows that the electromagnetic energy is carried in the feedline of the antenna as well as in the free-space by the electromagnetic field. Figure 13.20 shows a vertical linear antenna fed by a coaxial line and it illustrates the continuous transition of the field lines of the Poynting vector field from the feed line region into the free-space region. In the coaxial feed line the Poynting vector field lines are oriented in parallel to the axis of the coaxial line, and these Poynting field lines pass through the aperture and then spread into free-space surrounding the antenna. In this field picture the opening from the feed line into free-space (i.e., the aperture is the source of the radiation). In principle also the open end of a coaxial line or any other line will radiate electromagnetic energy into space. As long as the transverse dimensions of a line are small compared with the wavelength, the main part of an electromagnetic wave propagating in the line towards the open end will be reflected and only a very small part will be radiated. This situation changes considerably if the transverse dimensions of a waveguide are in the order of magnitude of the wavelength λ_0 or exceed the wavelength of the electromagnetic wave. In this case the main part of the wave may be radiated into space.

The horn antenna shown in Figure 13.1(e) was obtained by continuously widening a waveguide with a rectangular cross-section such that the transverse dimensions of the aperture are larger than the wavelength λ_0 . If the widening of the waveguide is smooth, the transverse field distribution of the waveguide mode will be scaled up according to the widening of the waveguide. With an increasing widening of the cross-section the cutoff wavelength increases, and according to (7.242) the wave impedance of the waveguide approaches the field impedance of free-space. In this case the waveguide wave is well matched to the free-space and is radiated with only low reflection.

If we know the transverse field distribution in the aperture of the horn antenna or if we know the tangential electric or magnetic field distribution in an arbitrary surface enclosing the antenna we can compute the radiation field of the antenna using Huygens' principle. Figure 13.21 illustrates this procedure for the horn antenna. Knowing the

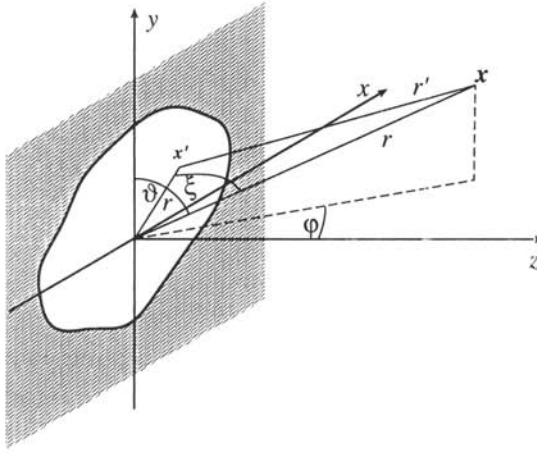


Figure 13.22: Aperture of a surface emitter.

tangential components of $\underline{\mathcal{E}}$ and $\underline{\mathcal{H}}$ we can compute the equivalent magnetic surface polarization $\underline{\mathcal{M}}_{mA}$ and the equivalent electric surface polarization $\underline{\mathcal{M}}_{eA}$ in the aperture plane.

We consider an arbitrarily shaped surface emitter aperture in the xy -plane at $z = 0$ as depicted in Figure 13.22. The electric and magnetic field components tangential to the aperture are described by the differential forms

$$\underline{\mathcal{E}}_t(\mathbf{x}') = \underline{E}_x(\mathbf{x}') dx' + \underline{E}_y(\mathbf{x}') dy', \quad (13.128a)$$

$$\underline{\mathcal{H}}_t(\mathbf{x}') = \underline{H}_x(\mathbf{x}') dx' + \underline{H}_y(\mathbf{x}') dy', \quad (13.128b)$$

where \mathbf{x}' denotes a point in the aperture plane. The area polarizations $\underline{\mathcal{M}}_{eA}(\mathbf{x}')$ and $\underline{\mathcal{M}}_{mA}(\mathbf{x}')$ are represented by the twisted one-forms

$$\underline{\mathcal{M}}_{eA}(\mathbf{x}') = \underline{M}_{eAy}(\mathbf{x}') dx' - \underline{M}_{eAx}(\mathbf{x}') dy', \quad (13.129a)$$

$$\underline{\mathcal{M}}_{mA}(\mathbf{x}') = \underline{M}_{mAy}(\mathbf{x}') dx' - \underline{M}_{mAx}(\mathbf{x}') dy'. \quad (13.129b)$$

In the aperture plane we obtain from (4.47) and (4.48):

$$\underline{\mathcal{M}}_{mA}(\mathbf{x}') = -\frac{1}{j\omega} dz' \lrcorner (dz' \wedge \underline{\mathcal{E}}(\mathbf{x}')), \quad (13.130a)$$

$$\underline{\mathcal{M}}_{eA}(\mathbf{x}') = \frac{1}{j\omega} dz' \lrcorner (dz' \wedge \underline{\mathcal{H}}(\mathbf{x}')). \quad (13.130b)$$

From this we can compute the electric Hertz form $\underline{\Pi}_e$ and the magnetic Hertz form $\underline{\Pi}_m$ using (4.103a) and (12.2). Since \underline{M}_{eA} and \underline{M}_{mA} describe area polarizations, the integrals have to be performed over surfaces, and we obtain

$$\underline{\Pi}_m(\mathbf{x}) = \frac{1}{4\pi\mu_0} \int_A' (dx dx' + dy dy') \wedge \frac{\underline{M}_{mA}(\mathbf{x}') e^{-jk|\mathbf{x}-\mathbf{x}'|}}{|\mathbf{x}-\mathbf{x}'|}, \quad (13.131a)$$

$$\underline{\Pi}_e(\mathbf{x}) = \frac{1}{4\pi\epsilon_0} \int_A' (dx dx' + dy dy') \wedge \frac{\underline{M}_{eA}(\mathbf{x}') e^{-jk|\mathbf{x}-\mathbf{x}'|}}{|\mathbf{x}-\mathbf{x}'|}. \quad (13.131b)$$

If we are interested only in the far-field of the surface emitter, the integrals (13.131a) and (13.131b) may be simplified in a similar way as we have done it for the linear antenna. Let us consider the aperture in a plane surface emitter located in $z = 0$, depicted in Figure 13.22. For a far-field point \mathbf{x} the lines r and r' can be assumed to be parallel so that

$$|\mathbf{x} - \mathbf{x}'| = r - r_0 \cos \xi \quad (13.132)$$

is valid. Applying this approximation in the exponent of the integrand of (13.131a) and (13.131b) and setting $|\mathbf{x} - \mathbf{x}'| = r$ in the denominator only, we obtain

$$\underline{\Pi}_m(\mathbf{x}) = \frac{e^{-jkr}}{4\pi\mu_0 r} \int_A' (dx dx' + dy dy') \wedge \underline{M}_{mA}(\mathbf{x}') e^{jkr_0 \cos \xi}, \quad (13.133a)$$

$$\underline{\Pi}_e(\mathbf{x}) = \frac{e^{-jkr}}{4\pi\epsilon_0 r} \int_A' (dx dx' + dy dy') \wedge \underline{M}_{eA}(\mathbf{x}') e^{jkr_0 \cos \xi}. \quad (13.133b)$$

The forms $\underline{\mathcal{E}}$ and $\underline{\mathcal{H}}$ are computed from $\underline{\Pi}_m$ and $\underline{\Pi}_e$ using (3.29a), (3.29b), (3.36a) and (3.36b). The partial fields computed from $\underline{\Pi}_e$ and $\underline{\Pi}_m$ have to be superimposed. For the computation of the far-field it is useful to represent $\underline{\Pi}_e$ and $\underline{\Pi}_m$ in spherical coordinates. The computations can be simplified by neglecting all terms going to zero stronger than by r^{-1} for $r \rightarrow \infty$. Considering (13.133a) and (13.133b), we see that the r dependence of $\underline{\Pi}_e$ and $\underline{\Pi}_m$ is due to the factor e^{-jkr}/r . Computing the $\underline{\Pi}_e$ and $\underline{\Pi}_m$, we only consider these terms where the negative power of r is not increased. For the far-field computation of a one-form

$$\mathcal{U} = U_r dr + U_\theta r d\theta + U_\phi r \sin \theta d\phi, \quad (13.134)$$

we have to consider that

$$U_i \sim \frac{e^{-jkr}}{r} \quad \text{for } kr \gg 1, \quad i = r, \phi, \theta. \quad (13.135)$$

Therefore we may replace $\partial/\partial r$ with $-jk$ and obtain the following approximation for the far-field computation:

$$d\mathcal{U} \cong -jk dr \wedge \mathcal{U} \quad \text{for } kr \gg 1, \quad (13.136a)$$

$$\star d \star d\mathcal{U} \cong k^2 \mathcal{U}. \quad (13.136b)$$

Using this approximation we obtain from (3.20a), (3.20b), (3.36a) and (3.36b) the far-field components

$$\underline{E}_\theta = Z_{F0} \underline{H}_\phi = k^2 (\underline{\Pi}_{e\theta} + Z_{F0} \underline{\Pi}_{m\phi}) , \quad (13.137a)$$

$$\underline{E}_\phi = -Z_{F0} \underline{H}_\theta = k^2 (\underline{\Pi}_{e\phi} - Z_{F0} \underline{\Pi}_{m\theta}) . \quad (13.137b)$$

13.9.2 Horn Antennas

Let us now compute the far-field of the horn antenna excited in the TE_{10} mode according to Figure 13.23. From (7.261), (7.266a) and (7.266b) we obtain the transverse field components of the rectangular waveguide excited in the TE_{10} mode

$$\underline{E}_y = -Z_{\text{TE}} \underline{H}_x = \sqrt{\frac{2}{ab}} V(z) \cos \frac{\pi x}{a} . \quad (13.138)$$

If the waveguide cross-section is gradually increased in the z -direction, this transverse field distribution will be scaled up correspondingly. According to (7.242), a field impedance of the waveguide $Z_{\text{TE}10}$ approaches the free-space field impedance Z_{F0} . If the wave impedance of the waveguide is smoothly varying with z , only low reflections will occur. We assume that the transverse widening of the aperture plane is sufficiently large that $Z_{\text{TE}10}$ may be approximated by Z_{F0} in the aperture plane. Using (13.129a) and (13.129b) we now can determine the equivalent surface polarizations in the aperture plane A :

$$\underline{M}_{mAx} = \frac{1}{j\omega} \underline{E}_y \Big|_{z=0} = \frac{1}{j\omega} \sqrt{\frac{2}{ab}} V \cos \frac{\pi x}{a} , \quad (13.139a)$$

$$\underline{M}_{eAy} = \frac{1}{j\omega} \underline{H}_x \Big|_{z=0} = -\frac{1}{Z_{F0}} \underline{M}_{mAx} . \quad (13.139b)$$

We now have approximated $Z_{\text{TE}10}$ by Z_{F0} . Inserting (13.139a) into (13.133a) we obtain

$$\underline{\Pi}_{mx}(\mathbf{x}) = \frac{e^{-jkr}}{4\pi\mu_0 r} \int_A \underline{M}_{mAx}(\mathbf{x}') e^{jkr_0 \cos \xi} dA . \quad (13.140)$$

Let us now introduce spherical coordinates with respect to the y -axis (Figure 13.23). With

$$r_0 \cos \xi = x' \sin \phi \sin \theta + y' \cos \theta \quad (13.141)$$

we obtain from (13.139a), (13.140) and (13.141):

$$\underline{\Pi}_{mx}(\mathbf{x}) = \frac{e^{-jkr}}{4\pi j \omega \mu_0 r} \sqrt{\frac{2}{ab}} XY \underline{V} \quad (13.142a)$$

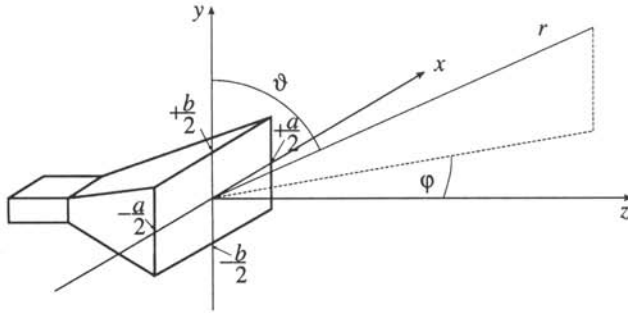


Figure 13.23: Horn antenna.

with

$$X = \int_{-a/2}^{a/2} \cos \frac{\pi x'}{a} e^{j k x' \sin \phi \sin \theta} dx', \quad (13.142b)$$

$$Y = \int_{-b/2}^{b/2} e^{j k y' \cos \theta} dy'. \quad (13.142c)$$

After evaluation of the integrals we obtain

$$X = \frac{2\pi a \cos(\frac{1}{2}ka \sin \phi \sin \theta)}{\pi^2 - k^2 a^2 \sin^2 \phi \sin^2 \theta}, \quad (13.143a)$$

$$Y = \frac{2 \sin(\frac{1}{2}kb \cos \theta)}{k \cos \theta}. \quad (13.143b)$$

From (13.133a), (13.133b), and (13.139b) we obtain

$$\underline{\Pi}_{ey} = -Z_{F0} \underline{\Pi}_{mx}. \quad (13.144)$$

The Hertz vector has the following spherical components

$$\underline{\Pi}_{m\theta} = \underline{\Pi}_{mx} \cos \theta \sin \phi, \quad (13.145a)$$

$$\underline{\Pi}_{m\phi} = \underline{\Pi}_{mx} \cos \phi, \quad (13.145b)$$

$$\underline{\Pi}_{e\theta} = -\underline{\Pi}_{ey} \sin \theta. \quad (13.145c)$$

From (13.137a), (13.137b), (13.144), and (13.145a)–(13.145c) we obtain the far-field of the horn antenna:

$$\underline{E}_{\theta} = Z_{F0} \underline{H}_{\phi} = k^2 Z_{F0} \underline{\Pi}_{mx} (\sin \theta + \cos \phi), \quad (13.146a)$$

$$\underline{E}_\phi = -Z_{F0}\underline{H}_\theta = -k^2 Z_{F0}\underline{\Pi}_{mx} \cos \theta \sin \phi. \quad (13.146b)$$

With (13.142a), (13.143a), and (13.143b) we obtain using $kZ_{F0}/\omega\mu_0 = 1$:

$$\begin{aligned} \underline{E}_\theta(r, \theta, \phi) &= Z_{F0}\underline{H}_\phi(r, \theta, \phi) \\ &= \sqrt{\frac{2}{ab}} k \underline{V} \frac{e^{-jkr}}{4\pi jr} X(\theta, \phi) Y(\theta) (\sin \theta + \cos \phi), \end{aligned} \quad (13.147a)$$

$$\begin{aligned} \underline{E}_\phi(r, \theta, \phi) &= -Z_{F0}\underline{H}_\theta(r, \theta, \phi) \\ &= -\sqrt{\frac{2}{ab}} k \underline{V} \frac{e^{-jkr}}{4\pi jr} X(\theta, \phi) Y(\theta) \cos \theta \sin \phi. \end{aligned} \quad (13.147b)$$

In the *main beam direction* ($\theta = \frac{1}{2}\pi$, $\phi = 0$) we obtain from (13.143a) and (13.143b)

$$X\left(\frac{1}{2}\pi, 0\right) Y\left(\frac{1}{2}\pi\right) = \frac{2}{\pi} ab. \quad (13.148)$$

The field intensity in the main beam direction is

$$\underline{E}_\theta = Z_{F0}\underline{H}_\phi = \frac{-j}{\pi^2} \sqrt{2ab} k \underline{V} \frac{e^{-jkr}}{r}. \quad (13.149)$$

The power density in the main beam direction is

$$T\left(r, \frac{1}{2}\pi, 0\right) = \frac{1}{2} Z_{F0}^{-1} |\underline{E}_\theta|^2 = \frac{ab}{\pi^4 r^2} k^2 Z_{F0}^{-1} |\underline{V}|^2. \quad (13.150)$$

Since we have assumed that the wave traveling in the waveguide towards the aperture is completely radiated, the complete active power radiated from the horn antenna according to (4.139) and (4.141) is given by

$$P_r = \frac{1}{2} Z_{F0}^{-1} |\underline{V}|^2. \quad (13.151)$$

With (13.94) we obtain from this the maximum antenna gain

$$G_{\max} = \frac{8abk^2}{\pi^3} = \frac{32ab}{\pi\lambda_0^2}. \quad (13.152)$$

The maximum antenna gain is proportional to the aperture area $a \cdot b$ of the horn antenna. From (13.113) and (13.152) we obtain the effective antenna area

$$A_e = \frac{8}{\pi^2} ab \cong 0.81ab. \quad (13.153)$$

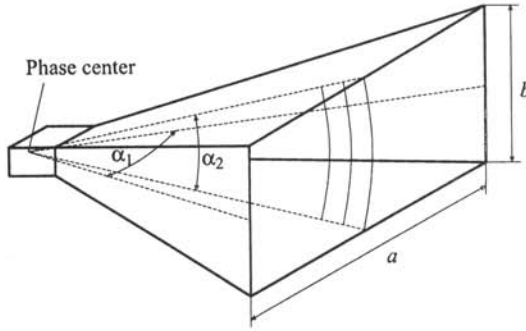


Figure 13.24: Curvature of the phase front.

The effective antenna area is only 81 % of the geometric area. The high gain in the case of large apertures means a high directivity. For $ka \gg 1$ and $kb \gg 1$ the main radiation lobe in the $\phi = 0$ -plane exhibits the angular width

$$\Delta\theta = 2 \frac{\lambda_0}{b}. \quad (13.154)$$

In the $\theta = \frac{1}{2}\pi$ -plane and the angular width of the main radiation lobe is

$$\Delta\phi = 3 \frac{\lambda_0}{a}. \quad (13.155)$$

In our considerations up to now we have neglected the curvature of the phase front in the aperture. This assumption is only justified if the beam angles α_1 and α_2 in Figure 13.24 fulfill the conditions $a\alpha_1 \ll \lambda_0$, $b\alpha_2 \ll \lambda_0$. The real or virtual origin of a spherical wave is called the *phase center*.

13.9.3 Gain and Effective Area of Aperture Antennas

Let us now treat the gain and effective antenna area of the plane surface emitter more generally. According to Figure 13.22 we make no special assumptions about the aperture of the antenna. To achieve a high gain of the surface emitter we assume a plane phase front in the aperture and the electrical field to be vertically polarized in the aperture. In the aperture the electric and magnetic field in (13.139a) and (13.139b) may be replaced by equivalent surface polarizations

$$\underline{M}_{mA x} = \frac{1}{j\omega} \underline{E}_y \Big|_{z=0}, \quad (13.156a)$$

$$\underline{M}_{eAy} = \frac{1}{j\omega} \underline{H}_x \Big|_{z=0} = -\frac{1}{Z_{F0}} \underline{M}_{mA x}. \quad (13.156b)$$

Furthermore, we assume that the field exhibits no node lines in the aperture plane and therefore the direction normal to the aperture plane will be the main radiation direction. From (13.133a), (13.133b) and (13.156b) we obtain for the main radiation direction

$$\underline{\Pi}_{ey} = -Z_{F0} \underline{\Pi}_{mx} = -\frac{c_0}{4\pi} \frac{e^{-jkr}}{r} \int_A \underline{M}_{eAx} dA. \quad (13.157)$$

The integration is performed over the aperture plane. With (13.137a) we obtain the far-field components \underline{E}_θ and \underline{H}_ϕ for $\theta = \frac{1}{2}\pi$, $\phi = 0$ (with $\underline{\Pi}_\theta = -\underline{\Pi}_y$, $\underline{\Pi}_\phi = \underline{\Pi}_x$)

$$\underline{E}_\theta = Z_{F0} \underline{H}_\phi = -k^2 (\underline{\Pi}_{ey} - Z_{F0} \underline{\Pi}_{mx}) = -2k^2 \underline{\Pi}_y \quad \text{for } \theta = \frac{1}{2}\pi, \phi = 0. \quad (13.158)$$

From this we obtain

$$\underline{E}_\theta = -jk \frac{e^{-jkr}}{2\pi r} \int_A \underline{E}_y \Big|_{z=0} dA. \quad (13.159)$$

With (12.16) we obtain the radiation density in the main beam direction

$$T = \frac{k^2}{8\pi^2 r^2 Z_{F0}} \left| \int_A \underline{E}_y \Big|_{z=0} dA \right|^2. \quad (13.160)$$

The total active power radiated from the aperture is obtained by integrating \mathcal{T} over the aperture,

$$P_r = \frac{1}{2Z_{F0}} \int_A |\underline{E}_y|^2 \Big|_{z=0} dA. \quad (13.161)$$

The gain G_{max} in the main beam direction follows from (13.76), (13.160) and (13.161)

$$G_{max} = \frac{4\pi r^2 T}{P_r} = \frac{4\pi}{\lambda_0^2} \frac{\left| \int_A \underline{E}_y \Big|_{z=0} dA \right|^2}{\int_A |\underline{E}_y|^2 \Big|_{z=0} dA}. \quad (13.162)$$

With (13.94) we obtain from this the effective area in the main beam direction

$$A_e = \frac{\left| \int_A \underline{E}_y \Big|_{z=0} dA \right|^2}{\int_A |\underline{E}_y|^2 \Big|_{z=0} dA}. \quad (13.163)$$

If the aperture is uniformly illuminated (i.e., the electromagnetic field is uniform over the aperture), we obtain the maximum value of the effective aperture, given by $A_e = A$, and it follows: *For a plane surface emitter the aperture dimensions of which are large compared with the wavelength λ_0 , the aperture of which is uniformly illuminated and the phase front is plane and parallel to the aperture plane, the effective antenna area is equal to the geometric aperture area.*

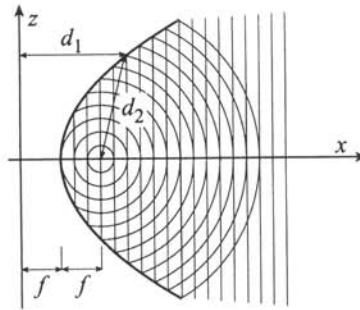


Figure 13.25: Phase surfaces in a parabolic reflector antenna.

13.9.4 Mirror and Lens Antennas

To realize large apertures with plane phase fronts, methods from optics are used to transform a spherical wave radiated by a primary radiator into a plane wave. This can be achieved using lenses or mirrors. Figure 13.25 gives a schematic illustration of a parabolic reflector antenna. A primary radiator in the focal point of a paraboloid emits a spherical wave. The spherical wave is reflected by the conducting paraboloid and in this way transformed into a plane wave. Transformation occurs due to the circumstance that the distances d_1 and d_2 are equal. Removing the paraboloid reflector and bringing the spherical wave originating from the focal point to interfere with a plane wave propagating in the x -direction from the left produces a node surface of paraboloid shape. Inserting a conducting paraboloid this node surface meets with the boundary conditions. Now the plane wave incident from the left is converted into a spherical wave and the spherical wave originating from a source in the focal point of the paraboloid is converted into a plane wave when incident on the reflector. In the next step of our consideration we may omit the plane wave incident from the left.

Figure 13.26 shows various types of reflector antennas. The reflector antenna in Figure 13.26(a) is excited by a small horn antenna or a small dipole antenna positioned in the focal point of the paraboloid. To achieve an effective antenna area coming as close as possible to the geometric antenna area, a uniform irradiation of the paraboloid is required. The primary radiator should only irradiate the paraboloid reflector and not the regions beside the reflector. Therefore, the primary radiator should exhibit an appropriate directivity. These requirements will yield a higher focal length of the parabolic antenna and consequently large antenna dimensions in the longitudinal direction.

The antenna dimension in the longitudinal direction can be reduced by introducing a second mirror as shown in Figure 13.26(b). This antenna type is called a cassegrain antenna. Both antenna types shown in Figure 13.26(a) and Figure 13.26(b) suffer from

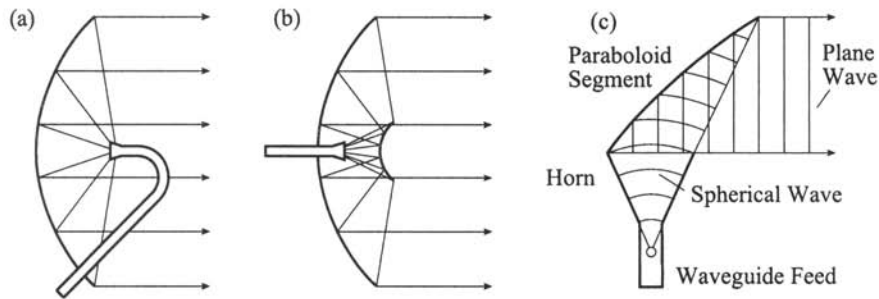


Figure 13.26: Reflector antennas: (a) parabolic reflector antenna, (b) cassegrain antenna, and (c) horn parabolic antenna.

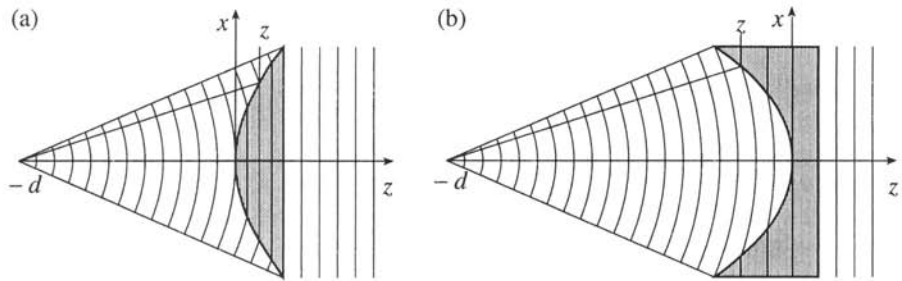


Figure 13.27: Lenses for transformation of spherical waves into plane waves: (a) $n > 1$ and (b) $n < 1$.

the disadvantage that the primary radiator is in the path of the secondary beam. The scattering of the secondary beam by the primary radiator not only degrades the antenna pattern, but also yields a frequency-dependent mismatch of the antenna to the feed line. Both disadvantages can be avoided with the horn paraboloid antenna, shown in Figure 13.26(c). In this antenna for the reflection, only a sector of the paraboloid is used; it is crossed by the axis of the paraboloid. Therefore the reflected secondary beam does not pass the focal point and will not be scattered by the primary radiator. Figure 13.27 illustrates the application of lenses for the transformation of a spherical wave into a wave with a plane phase front. The dimensions of the lens are assumed to be large compared with the wavelength. Therefore we can apply geometric optic methods to compute the shape of the lens. The phase velocity c of a ray corresponds to the phase velocity of a plane wave. In the lens the phase velocity c of the electromagnetic wave deviates from the free-space phase velocity c_0 . The refractive index n is given by

$$n = \frac{c_0}{c} \tag{13.164}$$

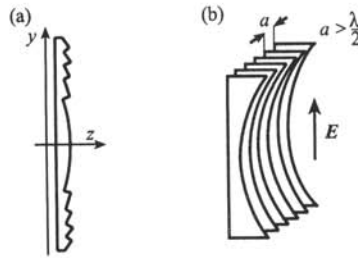


Figure 13.28: (a) Fresnel lens and (b) waveguide lens

The refractive index n may be either larger or smaller than 1. A refractive index $n > 1$ given by (2.77) may be realized using dielectric materials. To transform a spherical wave into a plane wave, the optical length of the path (i.e., the geometrical length weighted with the refractive index), must be equal for the central path C_1 and any path C_2 in Figure 13.27(a). This yields

$$d + nz = \sqrt{(d+z)^2 + x^2}. \quad (13.165)$$

From this it follows that the lens surface is given by a hyperboloid according to

$$z^2(n^2 - 1) + 2dz(n - 1) - x^2 = 0. \quad (13.166)$$

In order to save material and weight a dielectric lens may be designed as a step-lens or Fresnel lens as in Figure 13.28(a). A lens with $n < 1$ can be realized using a stack of equidistant parallel conducting plates as in Figure 13.28(b). If an incident plane wave is polarized parallel to the conducting plates, TE_{10} waveguide modes are excited between every two plates. According to (7.237) the phase velocity of the TE_{10} waves is given by

$$c = \frac{c_0}{\sqrt{1 - \left(\frac{\lambda_0}{2a}\right)^2}}. \quad (13.167)$$

From this we obtain an ellipsoid lens surface given by

$$z^2(1 - n^2) - 2dz(1 - n) + x^2 = 0. \quad (13.168)$$

13.9.5 Slot Antennas

A slot antenna is an aperture antenna with a narrow aperture, extended only in one dimension. The slot width is small compared with the wavelength λ_0 . Figure 13.29 shows a slot antenna excited by a coaxial line, and Figure 13.1(f) shows an array of a

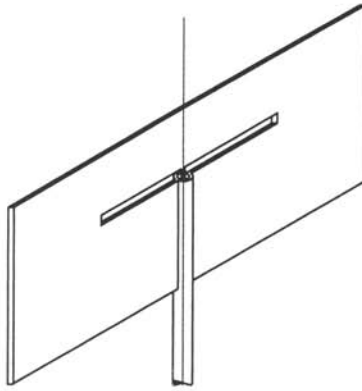


Figure 13.29: Slot antenna fed via coaxial line.

slot antenna excited by a rectangular waveguide. The slot in Figure 13.29 behaves as a line short-circuited on both ends. By the coaxial line a standing wave with voltage nodes at both ends of the slot is excited. The voltage occurring along the slot $\underline{V}(z)$ and the magnetic surface polarization equivalent to the electric aperture field are depicted in Figure 13.30. The magnetic area polarization is given by

$$\underline{M}_{mAz} = \frac{1}{j\omega} \frac{1}{s} \underline{V}(z). \quad (13.169)$$

The slot width is s . Usually a slot antenna is shielded on the rear side so that the slot is radiating only in one half-space. Electric and magnetic surface polarization give the same far-field contribution as shown in (13.158). We therefore can take twice the far-field contribution obtained from the magnetic surface polarization instead of also computing a far-field contribution from the electric area polarization. From (12.5), (13.11), (13.140), (13.146b), and (13.169) we obtain

$$\underline{H}_\theta = -\frac{\underline{E}_\phi}{Z_{F0}} = +\frac{j\omega\epsilon_0}{2\pi} \frac{e^{-jkr}}{r} \sin\theta \int_{-l}^{+l} \underline{V}(z) e^{jkz \cos\theta} dz. \quad (13.170)$$

This equation is dual to the equation derived for the linear dipole (13.12), if one considers that the radiator is radiating only into a half-space, therefore creating twice the field intensity in this half-space. The duality with respect to the linear antenna becomes obvious if we are performing the following substitution:

$$\underline{I}(z) \rightarrow \frac{2}{Z_{F0}} \underline{V}(z), \quad (13.171a)$$

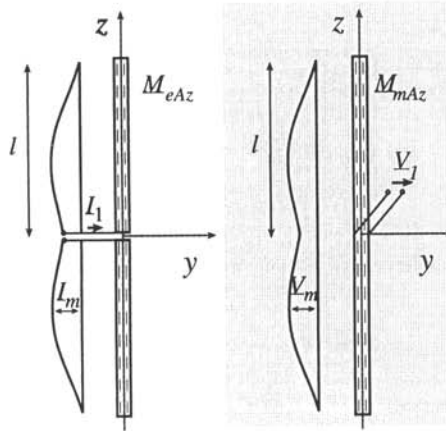


Figure 13.30: Slot antenna.

$$\underline{E}_\theta \rightarrow Z_{F0} \underline{H}_\theta, \quad (13.171b)$$

$$\underline{H}_\phi \rightarrow -\frac{1}{Z_{F0}} \underline{E}_\phi. \quad (13.171c)$$

Since the power P radiated from the slot antenna is proportional to $|\underline{V}_m|^2$, we can define a radiation conductance G_{rm} related to the voltage maximum $|\underline{V}_m|$ via

$$P = \frac{1}{2} G_{rm} |\underline{V}_m|^2. \quad (13.172)$$

In this way we obtain from (13.24) and (13.171a) the following relation between the radiation resistance related to the voltage maximum $|\underline{V}_m|$ of the linear antenna and the radiation conductance G_{rm} of the slot antenna

$$G_{rm} = \frac{4R_{rm}}{Z_{F0}^2}. \quad (13.173)$$

This equation is *Booker's relation* [13,14], which holds not only for the real radiation resistance but also for the complex self-impedance of a slender dipole and the complementary slot dipole. Booker's relation allows to extend the knowledge about center-fed slender dipoles to center-fed slot dipoles. The relationship between wire and slot dipoles is a consequence of *Babinet's principle*.

13.10 MICROSTRIP ANTENNAS

The microstrip antenna is a metallic patch printed on a thin, grounded dielectric substrate [15–19]. Microstrip antennas can be realized using printed circuit technology. The

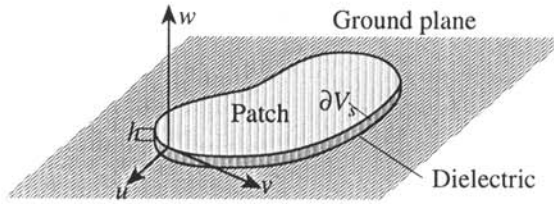


Figure 13.31: Arbitrarily shaped patch antenna.

advantages of printed antennas are small dimensions, light weight, easy manufacturing, and easy integration into arrays. Microstrip antennas can also be printed on curved surfaces to make conformal antennas. Disadvantages of printed antennas are usually a narrow bandwidth and comparatively high losses.

The patches of a microstrip antenna may have various geometries. The most simple type of a microstrip antenna is a radiating metallic patch on one side of a dielectric substrate that has a ground plane on the other side. In Figure 13.31 an arbitrarily shaped patch antenna is depicted. The substrate thickness is h . If the transverse size of the patch is large compared to h , then the electromagnetic field between the patch and the ground plane is uniform in w direction, the electric field being normal to the patch, and the magnetic field being tangential to the patch. Therefore

$$\underline{\mathcal{E}}(u, v) = \underline{E}_w(u, v) s_3, \quad (13.174a)$$

$$\underline{\mathcal{H}}(u, v) = \underline{H}_u(u, v) s_1 + \underline{H}_v(u, v) s_2. \quad (13.174b)$$

The electromagnetic field in the interior region can be described by TM modes, for w being the direction of propagation. It can be computed by solving the Helmholtz equation (3.28) with the ansatz

$$\underline{\Pi}_e(u, v) = \underline{\Pi}_{ew}(u, v) s_3. \quad (13.175)$$

The structure formed by the patch on the grounded dielectric can be understood as a resonator, too. In the cavity model of the patch antenna the field computation is performed in two steps. In the first step the interior field of this region under the patch is modeled as a cavity bounded by electric walls on the top and bottom and a magnetic wall along the periphery ∂V_s . In this first step the radiation from the open periphery of the resonator is neglected. In the second step Huygen's principle is applied to compute from (4.47) the equivalent magnetic surface polarization on the periphery ∂V_s ,

$$\underline{\mathcal{M}}_{mA}(u, v) = -\frac{1}{j\omega} s_1 \lrcorner (s_1 \wedge \underline{\mathcal{E}}(u, v)) = -\frac{1}{j\omega} \underline{E}_w(u, v) s_3, \quad (13.176)$$

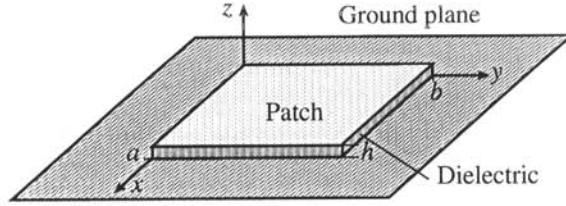


Figure 13.32: Rectangular patch antenna.

and from this the field radiated from the patch antenna.

From (13.133a) we obtain the magnetic Hertz form describing the radiated field. In the far-field the electric and magnetic field components are

$$\underline{\Pi}_m(\mathbf{x}) = \frac{e^{-jkr}}{4\pi\mu_0 r} \int_{\partial V'} (s_2 s'_2 + s_3 s'_3) \wedge \underline{M}_{mA}(u', v') e^{jkr_0 \cos \xi}, \quad (13.177)$$

where the angle ξ is specified in Figure 13.22. In the far-field the electric and magnetic field components may be computed from (13.137a), (13.137b):

$$\underline{E}_\theta = Z_{F0} \underline{H}_\phi = k^2 Z_{F0} \underline{\Pi}_{m\phi}, \quad (13.178a)$$

$$\underline{E}_\phi = -Z_{F0} \underline{H}_\theta = -k^2 Z_{F0} \underline{\Pi}_{m\theta}. \quad (13.178b)$$

The patch antenna either may be fed by a coaxial feed through the ground plane or by a planar feed line [15–19]. Exciting the microstrip antenna by a microstrip line on the same substrate allows to fabricate antenna and feed line simultaneously.

A microstrip antenna fabricated on a plane substrate is called a planar antenna. As in the case of conventional antennas, microstrip antennas may also be combined to form arrays [15–18]. The elements of an array may be spatially distributed to form a linear or a two-dimensional array.

Conformal microstrip antennas and antenna arrays are fabricated on curved substrates [16,17,20,21]. The shape of a conformal antenna is usually defined by the contours of the object on which it is mounted (e.g., a vehicle or an aircraft). This means that the shape of the antenna is not at the disposal of the antenna designer.

13.10.1 Planar Rectangular Patch Antenna

We apply the cavity model to the rectangular patch antenna shown in Figure 13.32 [18]. In the resonator the electromagnetic field is represented by

$$\underline{\mathcal{E}}(\mathbf{x}) = \underline{E}_z(\mathbf{x}) \, dz, \quad (13.179a)$$

$$\underline{\mathcal{H}}(\mathbf{x}) = \underline{H}_x(\mathbf{x}) \, dx + \underline{H}_y(\mathbf{x}) \, dy. \quad (13.179b)$$

For the resonant mode (m, n) , the electric field is given by

$$\underline{E}_z(\mathbf{x}) = \underline{E}_0 \cos \frac{m\pi x}{a} \cos \frac{n\pi y}{b}. \quad (13.180)$$

With (2.130b) we obtain from this

$$\underline{H}_x(\mathbf{x}) = -\frac{j}{\omega\mu} \frac{n\pi}{b} \underline{E}_0 \cos \frac{m\pi x}{a} \sin \frac{n\pi y}{b}, \quad (13.181a)$$

$$\underline{H}_y(\mathbf{x}) = \frac{j}{\omega\mu} \frac{m\pi}{a} \underline{E}_0 \sin \frac{m\pi x}{a} \cos \frac{n\pi y}{b}. \quad (13.181b)$$

From (13.133a) we obtain

$$\underline{\Pi}_m(\mathbf{x}) = \frac{j e^{-jkr}}{4\pi\omega\mu_0 r} \int_{\partial V_s}' (dx dx' + dy dy') \wedge dz' \underline{E}_z(\mathbf{x}) e^{jkr_0 \cos \xi}. \quad (13.182)$$

We choose $a > b$. In this case the mode $(1, 0)$ is the fundamental mode. In this case the field in the resonator is given by

$$\underline{E}_z(\mathbf{x}) = \underline{E}_0 \cos \frac{\pi x}{a}, \quad (13.183a)$$

$$\underline{H}_x(\mathbf{x}) = 0, \quad (13.183b)$$

$$\underline{H}_y(\mathbf{x}) = \frac{j}{\omega\mu} \frac{\pi}{a} \underline{E}_0 \sin \frac{\pi x}{a}. \quad (13.183c)$$

Using (13.182) we can compute $\underline{\Pi}_m(\mathbf{x})$ for the far-field and from this with (13.178a) and (13.178b) the far-field components for the electric field. We give the solution for $\phi = 0$ and $\phi = \frac{1}{2}\pi$. The plane $\phi = 0$ is parallel to the electric field and is called the E -plane whereas the plane $\phi = \frac{1}{2}\pi$ is parallel to the magnetic field and is called the H -plane. For the E -plane we obtain

$$\underline{E}_\theta(r, \theta, 0) = j \frac{bk e^{-jkr}}{r\pi} h \underline{E}_0 \exp\left(\frac{1}{2}jka \sin \theta\right) \cos\left(\frac{1}{2}ka \sin \theta\right), \quad (13.184a)$$

$$\underline{E}_\phi(r, \theta, 0) = 0, \quad (13.184b)$$

and for the H -plane

$$\underline{E}_\theta(r, \theta, \frac{1}{2}\pi) = 0, \quad (13.185a)$$

$$\underline{E}_\phi(r, \theta, \frac{1}{2}\pi) = -j \frac{bk e^{-jkr}}{r\pi} h \underline{E}_0 \exp\left(\frac{1}{2}jkb \sin \theta\right) \frac{\sin\left(\frac{1}{2}kb \sin \theta\right)}{\frac{1}{2}kb \sin \theta}. \quad (13.185b)$$

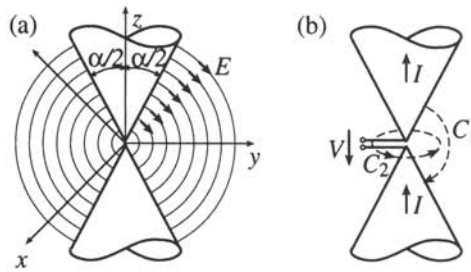


Figure 13.33: Biconical antenna: (a) electric field, (b) voltages and currents.

13.11 BROADBAND ANTENNAS

For applications that require coverage of a wide range of frequencies broadband antennas are required. An antenna may be scaled in wavelength by changing its linear dimensions. Therefore, an antenna structure that is invariant under linear scaling of its dimensions by an arbitrary scale factor must be frequency-independent. A simple antenna structure with broadband characteristics is the biconical antenna [3]. Strictly speaking, a structure invariant under scaling of its dimensions must be of infinite extension. Truncating such a structure to finite extension, however, will yield a broadband antenna structure [22–24].

We analyze the biconical antenna geometry depicted in Figure 13.33. The cone surface is defined by $\theta = \frac{1}{2}\alpha$ where α is the angle enclosed by the cone. For infinite extension of the cones in the r -direction the problem may be easily treated analytically. Furthermore, in the case of infinite extension it is obvious that the electromagnetic properties of the structure are frequency-independent since the structure is invariant under a scaling transformation in radial direction.

For symmetry reasons we expect a field solution with only an \underline{E}_θ and \underline{H}_ϕ -component. We make the ansatz

$$\underline{\mathcal{E}}(r, \theta, \phi) = \underline{E}_\theta(r, \theta, \phi) r d\theta, \quad (13.186a)$$

$$\underline{\mathcal{H}}(r, \theta, \phi) = \underline{H}_\phi(r, \theta, \phi) r \sin \theta d\phi. \quad (13.186b)$$

With (2.124a), (2.124b) and (A.170) we obtain from this the solution

$$\underline{\mathcal{E}}(r, \theta) = Z_{F0} \frac{\underline{H}_0}{\sin \theta} \frac{e^{-jkr}}{r} r d\theta, \quad (13.187a)$$

$$\underline{\mathcal{H}}(r, \theta) = \underline{H}_0 \frac{e^{-jkr}}{r \sin \theta} r \sin \theta d\phi. \quad (13.187b)$$

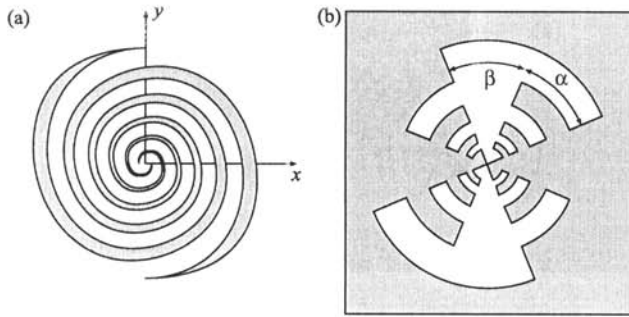


Figure 13.34: Logarithmic-periodic antenna: (a) log-spiral antenna, and (b) log-periodic slot antenna.

A voltage $V(r)$ and a current $I(r)$ may be defined by

$$V(r) = - \int_{C_1} \underline{\mathcal{E}}(r, \theta) = 2Z_{F0} \underline{H}_0 e^{-jkr} \ln [\cot (\tfrac{1}{4} \alpha)] , \quad (13.188a)$$

$$I(r) = \int_{C_2} \underline{\mathcal{H}}(r, \theta) = 2\pi \underline{H}_0 e^{-jkr} . \quad (13.188b)$$

The power P_r radiated by the antenna is

$$P_r = \tfrac{1}{2} \Re \{ \underline{V}(0) \underline{I}^*(0) \} = 2\pi Z_{F0} |\underline{H}_0|^2 \ln [\cot (\tfrac{1}{4} \alpha)] . \quad (13.189)$$

The radiation resistance R_r is given by

$$R_r = \frac{V(0)}{I(0)} = \frac{Z_{F0}}{\pi} \ln [\cot (\tfrac{1}{4} \alpha)] . \quad (13.190)$$

The logarithmic-periodic geometry allows to realize frequency-independent antennas. A logarithmic-periodic antenna is a set of adjoining cells, each cell being scaled in dimensions relative to the adjacent cells by a factor that remains fixed throughout [22–24]. Figure 13.34 shows two examples of planar logarithmic-periodic antennas. Apart from the truncation of the structures the spiral antenna structure (see Figure 13.34(a)) is invariant under arbitrary linear scaling, whereas the structure depicted in Figure 13.34(b) is invariant under scaling by a given factor and its powers, respectively.

Due to Babinet's principle, (13.173) holds for a pair of dual planar antenna structures complementary in the metallized and nonmetallized regions [3, 14]. The structure in Figure 13.34(b) is congruent with its dual structure and therefore the radiation impedance is real and frequency-independent and given by $R_r = \tfrac{1}{2} Z_{F0}$.

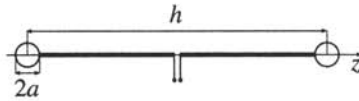


Figure 13.35: Hertzian dipole.

13.12 PROBLEMS

- Consider a Hertzian dipole consisting of two thin rods, each of length $h/2$, capacitively loaded with spheres of radius a as depicted in Figure 13.35. Let $h = 10$ cm and $a = 0.5$ cm. The Hertzian dipole operates at $f = 100$ MHz.
 - Compute the radiation resistance of the Hertzian dipole.
 - Draw the equivalent circuit of the Hertzian dipole.
 - Compute the complex impedance of the Hertzian dipole.
 - Compute the effective antenna area.
- Consider a circular loop antenna with 10 cm diameter exhibiting a single turn of copper wire with 4 mm diameter. The conductivity of copper is $\sigma = 5.8 \cdot 10^7 \text{ Sm}^{-1}$. The antenna is operated at $f = 30$ MHz.
 - Compute the radiation resistance of the antenna.
 - Compute the ohmic resistance of the antenna under consideration of the skin effect.
 - Draw the equivalent circuit of the Hertzian dipole.
 - Compute the maximum efficiency of the antenna under consideration of the skin effect losses.
 - Compute the effective antenna area.
- Consider a plate capacitor as depicted in Figure 13.36 operated as a dipole antenna. The dimensions are $a = 2$ cm, $h = 5$ mm and the operation frequency is 1 GHz. Assume the electric field between the plates to be homogeneous and neglect the fringing effects.
 - Compute the radiation resistance of the antenna.
 - Compute the capacitance of the antenna.
 - Draw the equivalent circuit of the antenna.
 - Compute the complex impedance of the antenna.
- Consider a Hertzian dipole oriented in a z -direction, operated at 1 GHz and radiating a total active power of 100 mW.
 - Compute the complex Poynting vector T at the angular position $\phi = 0$ $\theta = \frac{1}{2}\pi$ for $r = 10$ cm, $r = 1$ m, $r = 10$ m, and $r = 1$ km.
 - Consider a further Hertzian dipole as depicted in Figure 13.35, dimensions $h = 2$ cm and $a = 0.3$ cm, located at $x = 1$ km, $y = 0$, $z = 0$, and oriented in z -direction as the receiving antenna.

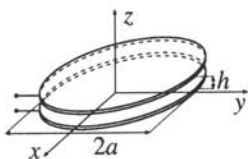


Figure 13.36: Circular plate antenna.

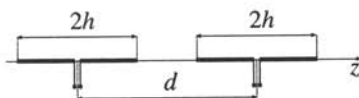


Figure 13.37: Two-antenna array.

- i. Compute the open-circuit voltage of the receiving antenna.
 - ii. Determine the optimum load impedance of the antenna.
 - iii. Compute the received active power.
 - iv. Compute the effective area A_e of the receiving antenna.
5. A transmitting antenna with a gain $G = 1.5$ and transmitted power $P = 2$ W and a receiving antenna are mounted in $d = 1$ km distance. The effective aperture of the receiving antenna is $A_e = 0.4$ m². Compute the received power.
6. Write a computer program to solve (13.40) and to determine in this way the current distribution on a linear dipole antenna in the staircase approximation.
 - a) Compute the current distribution on the antenna for $2h = \frac{1}{2}\lambda_0$ choosing a discretization $N = 100$.
 - b) Compute the vertical far-field pattern and compare the numerical result with the result obtained with (13.16).
7. A colinear array formed by two linear dipoles of length $2h = \frac{1}{2}\lambda$ and $2l = \lambda$ mounted in a distance oriented in the z -direction is shown in Figure 13.37. Compute the array factors and the radiation patterns and give the angular positions of the zeros in the radiation pattern and the number of radiation lobes for
 - a) $2h = \frac{1}{2}\lambda_0$ and $d = \lambda$,
 - b) $2h = \frac{1}{4}\lambda_0$ and $d = \lambda$,
 - c) $2h = \frac{1}{4}\lambda_0$ and $d = \frac{1}{2}\lambda$.
8. An array consisting of six center-fed linear antennas of length $2h$ oriented in z -direction along the y -axis with a spacing d is shown in Figure 13.38. The antennas are fed with a current of amplitude $|I_n|$ and phase ϕ_n .
 - a) Let $h = \frac{1}{4}\lambda$, the antenna spacing $d = \frac{1}{4}\lambda$, and all antenna elements be fed with equal amplitude and phase (i.e. $I_n = I_0$), for $n = 1 \dots 5$. Compute and draw the vertical antenna pattern in the plane $\phi = 0$ and the horizontal

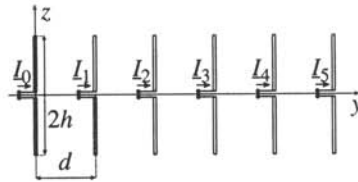


Figure 13.38: Linear antenna array.

- antenna pattern in the plane $\theta = \frac{1}{2}\pi$.
- Let $d = \frac{1}{2}\lambda$ and the other parameters as before. Compute and draw the vertical and horizontal antenna patterns in the planes $\phi = 0$ and $\theta = \frac{1}{2}\pi$, respectively.
 - Let $d = \lambda$ and the other parameters as before. Compute and draw the vertical and horizontal antenna patterns in the planes $\phi = 0$ and $\theta = \frac{1}{2}\pi$, respectively.
 - Let $h = \frac{1}{4}\lambda$ and the antenna spacing $d = \frac{1}{4}\lambda$. Assume all antenna elements to be fed with currents of equal magnitude $|I_n| = |I_0|$ for $n = 1 \dots 5$. Determine the phase differences $\phi_n - \phi_0$ in such a way that the main beam direction is given by $\phi = 30^\circ$. Compute and draw the horizontal antenna pattern.
9. An antenna array consists of 2 by N identical vertically oriented linear dipole antennas of length $2h$ as shown in Figure 13.39. The antenna spacing in x -direction is b and the antenna spacing in y -direction is d .
- Compute the array factor for even and odd N .
 - Compute and draw the horizontal pattern of the antenna array for $N = 6$, $b = d = \frac{1}{2}\lambda$, and excitation of the antenna elements with $I_{n0} = -I_{n1} = I_{00}$.
 - Compute and draw the horizontal pattern of the antenna array for $N = 6$, $b = \frac{1}{4}\lambda$, $d = \frac{1}{2}\lambda$, and excitation of the antenna elements with $I_{n0} = jI_{n1} = I_{00}$.
 - Compute and draw the horizontal pattern of the antenna array for $N = 6$, $b = \frac{1}{2}\lambda$, $d = \frac{1}{4}\lambda$, and excitation of the antenna elements with $I_{n0} = I_{n1} = j^n I_{00}$.
10. A linear antenna array consisting of N vertically oriented equally spaced dipoles is arranged a quarter-wavelength in front of a perfectly electrically conducting plate as shown in Figure 13.40. The conducting plate is assumed to be infinitely extended in the xy -plane.
- Compute the array factor for even and odd N .
 - Compute and draw the horizontal pattern of the antenna array for $N = 8$, $d = \frac{1}{2}\lambda$, and uniform excitation of all antenna elements with $I_n = CPI_0$.
 - Compute and draw the horizontal pattern of the antenna array for $N = 8$, $d = \frac{1}{2}\lambda$ and uniform excitation of all antenna elements with $I_n =$

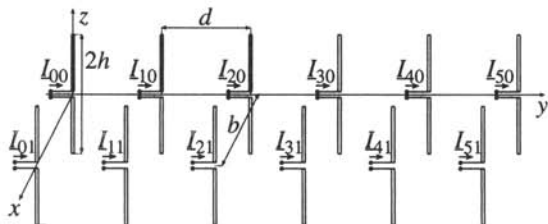


Figure 13.39: Two-dimensional antenna array.

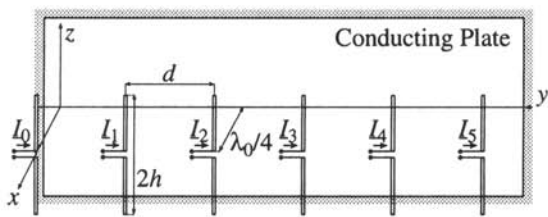


Figure 13.40: Antenna array with reflector plate.

$\exp(\frac{1}{8}j n \pi) I_0.$

- 11. A circular antenna array as depicted in Figure 13.19 consists of 12 vertically oriented dipoles positioned in uniform angular distance on a circle with radius a . Let the antenna elements be excited with currents of uniform magnitude $|I_0|$.
 - a) For $a = 4\lambda$ determine the phases of the excitation currents $|I_0| \dots |I_{11}|$ for main beam direction $\phi = 0^\circ$.
 - b) Compute and draw the radiation pattern for this case.
 - c) For $a = 8\lambda$ determine the phases of the excitation currents $|I_0| \dots |I_{11}|$ for main beam direction $\phi = 0^\circ$.
 - d) Compute and draw the radiation pattern for this case.
- 12. The rectangular horn antenna shown in Figure 13.41 has the aperture dimensions $a = 3\lambda$, $b = 2\lambda$, respectively, in the plane $\theta = \frac{1}{2}\pi$ and in the plane $\phi = 0$.
 - a) Compute and draw the far-field pattern.
 - b) Compute the angular positions of zeros of radiation as well as the side lobe level a_N . ($a_N = 20 \log |E|_{\max 0} / |E|_{\max 1}$, whereas $|E|_{\max 0}$ is the magnitude of the far-field intensity in the main radiation direction and $|E|_{\max 1}$ the magnitude of the far-field intensity in the maximum of the largest radiation side lobe.)

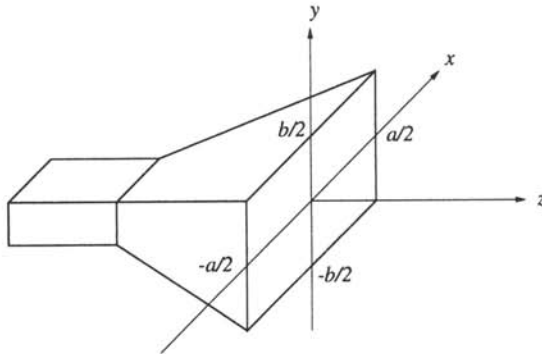


Figure 13.41: Rectangular horn antenna.

REFERENCES

- [1] S. Silver, *Microwave Antenna Theory and Design*. New York: McGraw-Hill, 1949.
- [2] W. Stutzman and G. A. Thiele, *Antenna Theory and Design*. New York: John Wiley & Sons, 1981.
- [3] C. A. Balanis, *Antenna Theory*. New York: John Wiley & Sons, 2005.
- [4] E. A. Wolff, *Antenna Analysis*. Boston: Artech House, 1988.
- [5] E. Roubine and J. C. Bolomey, *Antennas, Volume 1, General Principles*. London: North Oxford Academic, 1987.
- [6] S. Drabowitch and C. Ancona, *Antennas, Volume 1, General Principles*. London: North Oxford Academic, 1987.
- [7] J. D. Kraus, *Antennas*. New York: McGraw Hill, 1988.
- [8] F. M. Landstorfer and R. Sacher, *Optimisation of Wire Antennas*. New York: Letchworth, Research Studies Press Ltd, Wiley, 1990.
- [9] H. C. Pocklington, "Electrical oscillations in wire," *Cambridge Philos. Soc. Proc.*, vol. 9, pp. 324–332, 1897.
- [10] J. H. Richmond, "Digital computer solutions of the rigorous equations for scattering problems," *Proceedings of the IEEE*, vol. 53, pp. 796–804, Aug. 1965.
- [11] J. Richmond, "A reaction theorem and its application to antenna impedance calculations," *IRE Trans. Antennas Propagat.*, vol. 9, pp. 515–520, Nov. 1961.
- [12] F. Landstorfer, H. Liska, H. Meinke, and B. Müller, "Energienströmung in elektromagnetischen Wellenfeldern," *Nachrichtentechn. Z.*, pp. 225–231, May 1972.
- [13] H. Booker, "Slot aeriels and their relation to complementary wire aeriels," *J. IEE, Part IIIA*, pp. 620–626, 1946.
- [14] R. S. Elliott, *Antenna Theory and Design*. New York: IEEE Press, 2003.
- [15] R. Garg, P. Bhartia, I. Bahl, and A. Ittipiboon, *Microstrip Antenna Design Handbook*. Norwood, MA: Artech House, 2000.
- [16] J. R. James and P. S. Hall, *Handbook of Microstrip Antennas, Volume 1*. London: Peter Peregrinus, 1989.
- [17] J. R. James and P. S. Hall, *Handbook of Microstrip Antennas, Volume 2*. London: Peter Peregrinus, 1989.
- [18] S. Drabowitch, A. Papiernik, H. Griffith, J. Encinas, and B. L. Smith, *Modern Antennas*. London: Chapman and Hall, 1998.

- [19] D. M. Pozar, "Microstrip antennas," *Proceedings of the IEEE*, vol. 80, pp. 79–91, Jan. 1992.
- [20] R. E. Munson, "Conformal microstrip antennas and microstrip phased arrays," *IEEE Trans. Antennas Propagat.*, vol. 22, pp. 74–78, Jan. 1974.
- [21] S. V. Sohtell, "Microstrip antennas on a cylindrical surface," in *Handbook of Microstrip Antennas, Volume 2* (J. R. James and P. S. Hall, eds.), pp. 496–591, London: Peter Peregrinus, 1989.
- [22] V. H. Rumsey, *Frequency-Independent Antennas*. New York: Academic Press, 1985.
- [23] E. C. Jordan, G. A. Deschamps, J. D. Dyson, and P. E. Mayes, "Developments in broadband antennas," *IEEE Spectrum*, vol. 1, pp. 58–71, Apr. 1964.
- [24] P. E. Mayes, "Frequency-independent antennas and broad-band derivatives thereof," *Proceedings of the IEEE*, vol. 80, pp. 103–112, Jan. 1992.

Chapter 14

Numerical Electromagnetics

14.1 INTRODUCTION

For many electromagnetic structures, exact analytical solutions cannot be found. It is therefore necessary to consider numerical methods to obtain approximate solutions of field problems. A great variety of methods for electromagnetic field modeling has been developed [1–3]. In order to obtain results of the required accuracy with a minimum of computational effort, a method matched to the problem has to be chosen. The optimum design of radio-frequency devices, circuits and systems strongly depends on the availability of advanced *computer-aided design* (CAD) tools for modeling and optimization.

The *method of moments* (MoM) plays a crucial role in numerical electromagnetics [4–6]. In the MoM the field functions are expanded into series of *basis functions*. The problem of solving partial differential equations or integral equations for the field functions is converted into the problem of solving linear systems of equations for determining the coefficients of the series expansions of the field functions. Within the methods for field computation the MoM holds a special position since most of the methods of field computation – for example the integral equation method, the spectral domain method, the partial wave synthesis, the transmission-line matrix method and the finite difference method – may be considered in connection with the MoM. MoM is a very general scheme for the discretization of the field problem, whereas the other methods specify in detail how the discretization is performed.

Table 14.1 lists some of the most widely used methods for electromagnetic field computation [1]. The *integral equation* (IE) method introduces the far-field interaction via Green's functions and may reduce the dimension of the field problem [6, 7]. Since the interaction with infinite space is included in Green's function, integral equation methods are especially powerful in the case of radiating structures. In the *spectral domain method* the integral equations are transformed into algebraic equations by

Table 14.1: Methods for Numerical Electromagnetic Field Computation

<i>Method</i>	<i>Memory Requirement</i>	<i>CPU Time</i>	<i>Preprocessing</i>	<i>Generality</i>
Integral equation method	<i>SM</i>	<i>SM</i>	<i>M</i>	+
Spectral domain method	<i>S</i>	<i>S</i>	<i>L</i>	–
Partial wave synthesis	<i>M</i>	<i>S/M</i>	<i>M</i>	+
Method of lines	<i>M</i>	<i>S</i>	<i>L</i>	+
Finite difference method	<i>L</i>	<i>L</i>	<i>S</i>	++
Transmission-line matrix method	<i>L</i>	<i>L</i>	<i>S</i>	++
Finite element method	<i>L</i>	<i>M/L</i>	<i>S</i>	++

Notes: *L* ... large, *M* moderate, *S* ... small, ++ ... very good, + ... good, – ... marginal.

Fourier transformation with respect to the space coordinates [8]. Integral equation methods as well as spectral domain methods are computationally efficient but require considerable analytic preprocessing for the specific class of structures to be modeled.

In the *partial wave synthesis* method or *mode-matching* method the space is subdivided into subdomains and within each subdomain the electromagnetic field is expanded into modal solutions of the field equation. The partial wave synthesis method is efficient if boundary surfaces separating the subdomains are coordinate surfaces belonging to coordinate systems for which the analytic field solutions are known [9,10]. The partial wave synthesis method has been applied successfully to coplanar transmission-line structures [11] and to coplanar transmission-line discontinuities [12] with a small transverse dimension where electromagnetic full-wave modeling also inside the conductor is required.

In the *method of lines* (MoL) [13,14], all but one of the independent variables of the field equations are discretized to obtain a system of ordinary differential equations. With respect to the continuous variable analytic solutions are sought. Concerning the treatment of the continuous variables the MoL may be compared with the mode-matching method, whereas the treatment of the discretized variables corresponds to the finite difference method.

The *finite difference* (FD) method [15,16], the *finite integration* (FI) method [17–19], the *finite element* (FE) method [20], and the *transmission-line matrix* (TLM) method [21–24] are suited for modeling general three-dimensional structures without analytic preprocessing of the problem. However, all these space-discretizing methods require a high computational effort and usually need a long time for computation. In principle, the time-discretizing methods may be applied either in the frequency domain or time domain. The FE methods usually are applied in the frequency domain, the FD methods are applied in the frequency domain (FDFD) as well as in the time domain (FDTD), whereas the TLM method mainly is used in the time domain. Frequency domain

modeling is more appropriate for narrow-band simulation of high-Q structures. Time domain modeling allows for the characterization of the electromagnetic properties of the structures under consideration in a broad frequency band by computing the response to a single impulsive excitation [25]. The space-discretizing methods are less suitable to model radiating structures and structures including large free-space regions. For such applications hybrid methods, combining the TLM method with the integral equation method allow for accurate and efficient modeling [26].

In the following we give a short overview of the fundamentals of numerical field modeling. The MoM allows one to convert problems formulated by differential equations or integral equations into a representation by a system of algebraic equations. This corresponds to the transformation of a field problem into a network problem.

The modeling of radiation and of electromagnetic interaction between substructures over larger distances can be treated using the TLM-Integral Equation (TLM-IE) method [26, 27] and the TLM Multipole Expansion (TLMME) [28] method. The hybridization of these methods combines the versatility of the space discretizing methods with the capability of analytic methods to model radiation. An improvement of the efficiency of the methods is obtained by combining the methods of field analysis with spectral analysis and system identification methods [29] and with model order reduction methods [30, 31]. In this way the computational effort and the computation time can be reduced considerably without compromising accuracy. The generation of lumped element circuit models and other compact models links the electromagnetic models to circuit-level models [25]. The combination of various methods of electromagnetic field analysis and their hybridization, and the application of advanced signal processing methods, together with the embedding of the tools in a parallelized grid-computing environment should enhance the potential of an accurate and efficient modeling of complex electromagnetic structures and also their optimization considerably [32, 33]. A comprehensive presentation of fast and efficient algorithms in computational electromagnetics is given in [34].

14.2 THE METHOD OF MOMENTS

The *method of moments* is a general concept allowing the expansion of the field solutions into a set of *basis functions*. In this way the electromagnetic field problem, which is primarily described by partial differential equations or integral equations, is transformed into a problem described by a linear system of algebraic equations [4–6]. The linear system of equations relates the coefficients of the series expansion of the electric field with the coefficients of the series expansions of the magnetic field. Formally the expansion coefficients of electric and magnetic fields can be interpreted as generalized voltages and currents, respectively, and the coefficient matrix of the linear system of equations as a generalized impedance matrix or admittance matrix. We therefore may

interpret the application of the MoM as the transformation of a field problem into a network problem. If the electric and the magnetic fields are expanded into complete sets of basis functions, the series expansions usually will exhibit an infinite number of elements resulting in a system of equations of infinite dimension. Truncating the series expansions after a finite number of elements reduces the system of equations to a finite dimension and allows an approximate numerical solution of the problem. By this reduction the field problem becomes equivalent to a network problem with a finite number of network elements.

We distinguish between basis functions defined on the entire domain under consideration (*entire domain basis functions*) and basis functions, which are only defined on subdomains of the considered domain (*subsectional basis functions*). If the domain of definition of the solution function is within the domain of definition of the basis functions and if the system of basis functions is *complete* within this domain, the representation of the solution by an infinite series of the basis functions is possible under quite general conditions. Representing the solution with a series of basis functions, we obtain from the system of differential or integral equations to be solved a linear system of algebraic equations for the expansion coefficients of the series representing the solution. Truncation of the series expansion after a finite number of series elements yields a finite-dimensional system of algebraic equations, which may be solved numerically.

In the geometrical picture of the Hilbert space the solution function is represented by a vector. We are seeking linear combinations of a finite number of basis functions or basis vectors, respectively, which approximate the exact solution function or solution vector, respectively. The approximation of the solution by a series expansion is found if the components of the corresponding vector in Hilbert space are known. Linear differential equations and linear integral equations are both linear operator equations. In the following we will restrict our considerations to functions of only one variable. We consider the operator equation

$$L_{op} f(x) = g(x), \quad (14.1)$$

where the linear differential operator L_{op} is applied to the unknown function $f(x)$. The function $g(x)$ is known. Examples for linear differential operators are $L_{op} = -d^2/dx^2$ or $L_{op} = d^2/dx^2 + k^2$. The function $g(x)$ is given and $f(x)$ has to be determined. The unknown function $f(x)$ may be represented by a linear combination of a set of functions $\phi_n(x)$, as

$$f(x) = \sum_n \alpha_n \phi_n(x) \quad (14.2)$$

with the unknown expansion coefficients α_n . Inserting (14.2) into (14.1) yields

$$\sum_n \alpha_n L_{op} \phi_n(x) = g(x). \quad (14.3)$$

We choose a test function ψ_m , multiply it with (14.3) and compute the following integral

$$\sum_n \alpha_n \int_a^b \psi_m^* L_{\text{op}} \phi_n dx = \int_a^b \psi_m^*(x) g(x) dx. \quad (14.4)$$

The functions $f(x)$, $g(x)$, $\phi_n(x)$ are defined in the interval $[a, b]$. Introducing the matrix elements

$$L_{mn} = \int_a^b \psi_m^*(x) L_{\text{op}} \phi_n(x) dx \quad (14.5)$$

of the linear operator L_{op} and the expansion coefficients

$$\beta_m = \int_a^b \psi_m^*(x) g(x) dx \quad (14.6)$$

of the function $g(x)$ yields the linear system of equations

$$\sum_n L_{mn} \alpha_n = \beta_m \quad (14.7)$$

for the determination of the unknown expansion coefficients α_n of the function $f(x)$. Truncating the series expansions with $m = 1 \dots M$ and $n = 1 \dots N$ yields a finite-dimensional linear system of equations. With the vectors

$$\beta = [\beta_1 \dots \beta_M]^T, \quad \alpha = [\alpha_1 \dots \alpha_N]^T \quad (14.8)$$

and the matrix

$$L = \begin{bmatrix} L_{11} & \cdots & L_{1N} \\ \vdots & \ddots & \vdots \\ L_{M1} & \cdots & L_{MN} \end{bmatrix} \quad (14.9)$$

we obtain the linear system of equations in matrix notation

$$L\alpha = \beta. \quad (14.10)$$

For $M = N$ we obtain a quadratic matrix L , which may be inverted for nonsingular L . The solution of the linear system of equations (14.10) yields

$$\alpha = L^{-1}\beta. \quad (14.11)$$

As an example we investigate the following boundary value problem. The differential equation

$$\frac{d^2 f}{dx^2} = -1 + 3x - 12x^2 \quad x \in [0, 1] \quad (14.12)$$

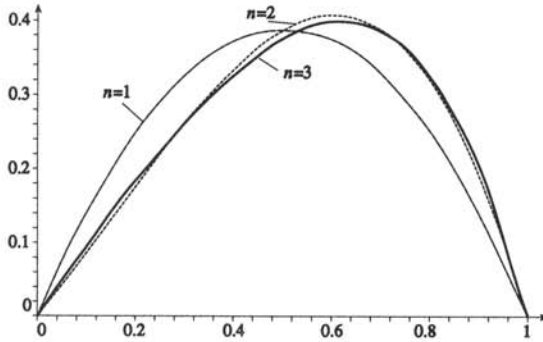


Figure 14.1: The approximations $f_1(x)$, $f_2(x)$ and $f_3(x)$.

has to be solved for the Dirichlet boundary conditions $f(0) = f(1) = 0$. The exact solution of (14.12) is

$$f(x) = x - \frac{1}{2}x^2 + \frac{1}{2}x^3 - x^4. \quad (14.13)$$

To demonstrate the solution using MoM we use the expansion function

$$\phi_n(x) = x^n(1-x). \quad (14.14)$$

The special case of the MoM in which the test function is equal to the expansion function,

$$\phi_n = \psi_n, \quad (14.15)$$

is called *Galerkin's method*. Choosing

$$f = \sum_{n=1}^N \alpha_n \phi_n(x) \quad (14.16)$$

we obtain with $L_{op} = d^2/dx^2$

$$L_{mn} = \frac{-2mn}{[(m+n)^2 - 1](m+n)} \quad (14.17)$$

and

$$\beta_m = \frac{-2(12 + 14m + 5m^2)}{(1+m)(2+m)(3+m)(4+m)}. \quad (14.18)$$

For $N = 3$ we obtain the linear system of equations

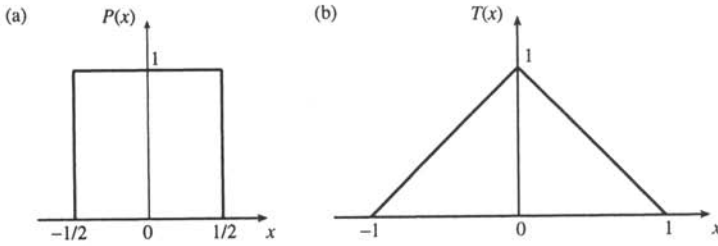


Figure 14.2: (a) Pulse function $P(x)$ and (b) triangle function $T(x)$.

$$\begin{bmatrix} -\frac{1}{3} & -\frac{1}{6} & -\frac{1}{10} \\ -\frac{1}{6} & -\frac{2}{15} & -\frac{1}{10} \\ -\frac{1}{10} & -\frac{1}{10} & -\frac{3}{35} \end{bmatrix} \begin{bmatrix} \alpha_1 \\ \alpha_2 \\ \alpha_3 \end{bmatrix} = \begin{bmatrix} -\frac{31}{60} \\ -\frac{1}{3} \\ -\frac{33}{140} \end{bmatrix}. \quad (14.19)$$

The solution is given by $[\alpha_1, \alpha_2, \alpha_3] = [1, \frac{1}{2}, 1]$. From this we obtain

$$f_3(x) = \phi_1(x) + \frac{1}{2}\phi_2(x) + \phi_3(x) = x - \frac{1}{2}x^2 + \frac{1}{2}x^3 - x^4 = f(x). \quad (14.20)$$

This approximation already agrees with the exact solution. Figure 14.1 shows the approximations $f_1(x)$, $f_2(x)$ and the exact solution $f_3(x) = f(x)$. In many cases for the approximation of functions $f(x)$ *subdomain basis functions* or *subsectional basis functions*, respectively, are useful. For N sampling points in the interval $[a, b]$ we obtain

$$x_n = a + \frac{n(b-a)}{N+1}. \quad (14.21)$$

The pulse function according to Figure 14.2(a) is defined by

$$P(x) = \begin{cases} 1 & \text{for } |x| < \frac{1}{2} \\ 0 & \text{for } |x| > \frac{1}{2}. \end{cases} \quad (14.22)$$

Using pulse functions as basis, a function may be approximated by a staircase function. Triangle functions according to Figure 14.2(b) yield a continuous linear approximation by a polygon curve.

$$T(x) = \begin{cases} 1 - |x| & \text{for } |x| < 1 \\ 0 & \text{for } |x| > 1 \end{cases}. \quad (14.23)$$

As an example we investigate the boundary value problem according to (14.12) for the Dirichlet boundary conditions $f(0) = f(1) = 0$. We subdivide the interval $[0, 1]$ by N

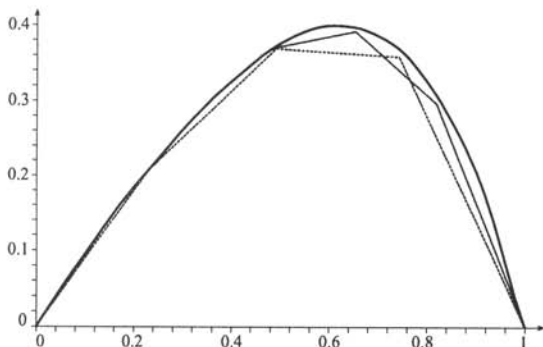


Figure 14.3: The approximation by triangle functions for $N = 3$, $N = 5$ and $N = 10$ in comparison with the exact solution.

sampling points into $N + 1$ intervals and apply triangular functions according to (14.23) as expansion functions. We make the series expansion

$$f_N(x) = \sum_{n=1}^N \alpha_n \phi_n(x) \quad (14.24)$$

with the basis functions

$$\phi_{N,n}(x) = T((N+1)x - n). \quad (14.25)$$

As test functions we apply the pulse functions

$$\psi_{N,n}(x) = P((N+1)x - n). \quad (14.26)$$

We compute the matrix elements of the operator $L_{\text{op}} = d^2/dx^2$:

$$d^2/dx^2 \phi_{N,n}(x) = (N+1) \left[\delta\left(x - \frac{n-1}{N+1}\right) - 2\delta\left(x - \frac{n}{N+1}\right) + \delta\left(x - \frac{n+1}{N+1}\right) \right]. \quad (14.27)$$

From (14.5) we obtain

$$L_{N,mn} = \int_a^b P((N+1)x - m) \frac{d^2 \phi_{N,n}(x)}{dx^2} dx = (N+1) (\delta_{m,n-1} - 2\delta_{m,n} + \delta_{m,n+1}). \quad (14.28)$$

The components of the vector β_N are

$$\beta_{N,m} = \int_a^b \psi_{N,m}^*(x) g(x) dx = \int_{\frac{m-1/2}{N+1}}^{\frac{m+1/2}{N+1}} g(x) dx. \quad (14.29)$$

For $N = 5$ we obtain the linear system of equations

$$\begin{bmatrix} -12 & 6 & 0 & 0 & 0 \\ 6 & -12 & 6 & 0 & 0 \\ 0 & 6 & -12 & 6 & 0 \\ 0 & 0 & 6 & -12 & 6 \\ 0 & 0 & 0 & 6 & -12 \end{bmatrix} \begin{bmatrix} \alpha_1 \\ \alpha_2 \\ \alpha_3 \\ \alpha_4 \\ \alpha_5 \end{bmatrix} = \begin{bmatrix} -\frac{31}{216} \\ -\frac{49}{216} \\ -\frac{91}{216} \\ -\frac{157}{216} \\ -\frac{247}{216} \end{bmatrix}. \quad (14.30)$$

The solution of (14.30) is

$$\alpha_{(5)}^T = \left[\frac{395}{2592} \quad \frac{91}{324} \quad \frac{107}{288} \quad \frac{127}{324} \quad \frac{755}{2592} \right]. \quad (14.31)$$

For $N = 3$ we obtain the solution vector

$$\alpha_{(3)}^T = \left[\frac{111}{512} \quad \frac{47}{128} \quad \frac{183}{512} \right] \quad (14.32)$$

and for $N = 10$ the solution vector

$$\alpha_{(10)}^T = [0.087, 0.167, 0.239, 0.303, 0.355, 0.388, 0.398, 0.375, 0.309, 0.189]. \quad (14.33)$$

Figure 14.3 shows the approximations of $f(x)$ by triangle functions.

14.3 THE TRANSMISSION-LINE MATRIX METHOD

The *transmission-line matrix* (TLM) method introduced by Johns [35] is a space and time discretizing method of electromagnetic field computation. Originally TLM is based on the analogy between the electromagnetic field and a mesh of transmission-lines [36]. The TLM method allows one to model complex electromagnetic structures. Detailed descriptions are given in [21–24, 37, 38]. The TLM scheme has been derived from Maxwell's equations using the finite difference approximation [39], the finite integration approximation [40] and the MoM [41]. In the following we introduce the TLM scheme via finite integration [42, 43].

Figure 14.4 illustrates the principle of TLM. In a first step the space is discretized in TLM cells. Although other discretization geometries are possible, we assume in the following cells with a cube shape. As shown in Figure 14.4(a) on every surface of the TLM cell samples of tangential electric and magnetic fields are taken. This may be done either by taking a probe of the tangential field components in the centers of the surface or by averaging over a certain volume. The first approach is called the finite difference approach, whereas the second one is called the finite integration approach. In both cases we obtain 12 electric field samples and 12 magnetic field samples per TLM cell. The

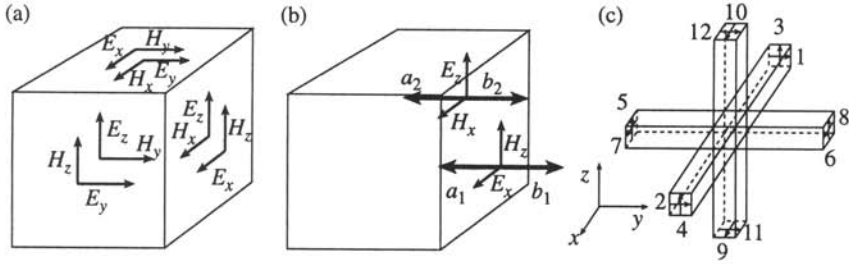


Figure 14.4: (a) The TLM cell, (b) the wave amplitudes and (c) the condensed symmetric TLM node.

sampled electric and magnetic field components are summarized in 12-dimensional vectors

$${}_k \mathbf{E}_{l,m,n} = {}_k [E_1, E_2, E_3, \dots, E_{10}, E_{11}, E_{12}]_{l,m,n}^T, \quad (14.34a)$$

$${}_k \mathbf{H}_{l,m,n} = {}_k [H_1, H_2, H_3, \dots, H_{10}, H_{11}, H_{12}]_{l,m,n}^T. \quad (14.34b)$$

The orientation of electric and magnetic field samples is chosen in such a way that the power flow is directed into the TLM cell if the electric and magnetic field components have the same sign. Assuming a spatial discretization with Δl and a time discretization with Δt and introducing the discrete space coordinates l, m, n and the discrete time coordinate k , the relation between the continuous coordinates x, y, z, t and the discrete coordinates are given by

$$x = l\Delta l, \quad y = m\Delta l, \quad z = n\Delta l, \quad t = k\Delta t. \quad (14.35)$$

We now introduce the wave amplitude vectors

$$\begin{aligned} {}_k \mathbf{a}_{l,m,n} &= {}_k [a_1, a_2, a_3, \dots, a_{10}, a_{11}, a_{12}]_{l,m,n}^T, \\ {}_k \mathbf{b}_{l,m,n} &= {}_k [b_1, b_2, b_3, \dots, b_{10}, b_{11}, b_{12}]_{l,m,n}^T, \end{aligned} \quad (14.36)$$

where ${}_k \mathbf{a}_{l,m,n}$ summarizes the waves incident in the TLM cell and ${}_k \mathbf{b}_{l,m,n}$ contains the amplitudes of the waves scattered by the TLM cell. The incident and the scattered waves propagate normal to the tangential planes. The wave amplitude and the field components are related via

$${}_k \mathbf{a}_{l,m,n} = \frac{1}{2\sqrt{Z_F}} {}_k \mathbf{E}_{l,m,n} + \frac{\sqrt{Z_F}}{2} {}_k \mathbf{H}_{l,m,n}, \quad (14.37a)$$

$${}_k \mathbf{b}_{l,m,n} = \frac{1}{2\sqrt{Z_F}} {}_k \mathbf{E}_{l,m,n} - \frac{\sqrt{Z_F}}{2} {}_k \mathbf{H}_{l,m,n} \quad (14.37b)$$

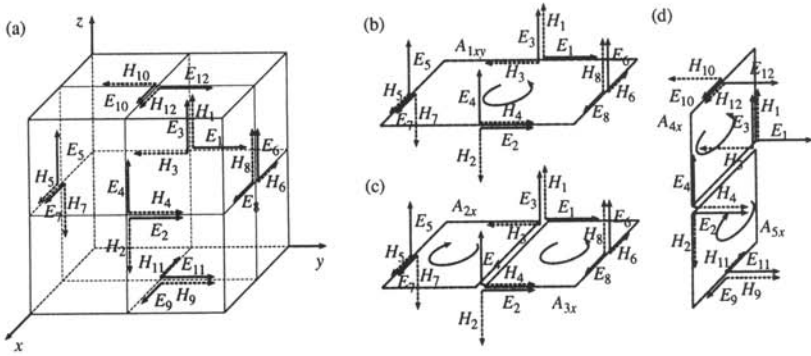


Figure 14.5: (a) The TLM cell, (b) integration path ∂A_{1xy} , (c) integration paths ∂A_{2xz} and ∂A_{3xz} and (d) integration paths ∂A_{4xz} and ∂A_{5xz} .

and

$${}_k \mathbf{E}_{l,m,n} = \sqrt{Z_F} ({}_k \mathbf{a}_{l,m,n} + {}_k \mathbf{b}_{l,m,n}), \quad (14.38a)$$

$${}_k \mathbf{H}_{l,m,n} = \frac{1}{\sqrt{Z_F}} ({}_k \mathbf{a}_{l,m,n} - {}_k \mathbf{b}_{l,m,n}), \quad (14.38b)$$

where $Z_F = \sqrt{\frac{\mu}{\epsilon}}$ is the field impedance. In the network model of TLM, in each sampling point, one port is assigned to each polarization. Now we can replace the geometric model by a network model (i.e., the TLM node depicted in Figure 14.4(c)). In the following, we use the term TLM cell for the geometrical object we have defined in the continuous space, whereas the term TLM node is used for the abstract network model.

To derive relations between the incident waves ${}_k \mathbf{a}_{l,m,n}$ and the scattered waves ${}_k \mathbf{b}_{l,m,n}$ of the cell l, m, n , we apply finite integration to the TLM cell shown in Figure 14.5(a). Ampère's law (2.57a) and Faraday's law (2.57b) yield

$$\oint_{\partial A_{iuv}} \mathcal{H}(\mathbf{x}, t) = \frac{d}{dt} \int_{A_{iuv}} \mathcal{D}(\mathbf{x}, t), \quad (14.39a)$$

$$\oint_{\partial A_{iuv}} \mathcal{E}(\mathbf{x}, t) = -\frac{d}{dt} \int_{A_{iuv}} \mathcal{B}(\mathbf{x}, t). \quad (14.39b)$$

In order to obtain a system of 12 linear equations relating the scattered wave amplitudes \mathbf{b} to the incident wave amplitudes \mathbf{a} we proceed as follows. First we apply both laws to three surfaces of integration A_{1xy} , A_{1yz} and A_{1zx} . The surface A_{1xy} , shown in Figure 14.5(b) is parallel to the xy -plane and goes through the center of the TLM cell. The surfaces A_{1yz} and A_{1zx} , respectively, are parallel to the yz -plane and the zx -plane. This yields six independent equations. For the time discretization we apply a Crank-Nicolson

scheme [44]. That means we replace the time-derivative by forward differences and time-dependent quantities by the arithmetic mean of the two time steps involved. From (14.39a) and (14.39b) we obtain in this way

$$\frac{1}{2} \oint_{\partial A_{iuv}} ({}_k \mathcal{H} + {}_{k-1} \mathcal{H}) = \frac{\epsilon}{\Delta t} \int_{A_{iuv}} \star ({}_k \mathcal{E} - {}_{k-1} \mathcal{E}) , \quad (14.40a)$$

$$\frac{1}{2} \oint_{\partial A_{iuv}} ({}_k \mathcal{E} + {}_{k-1} \mathcal{E}) = -\frac{\mu}{\Delta t} \int_{A_{iuv}} \star ({}_k \mathcal{H} - {}_{k-1} \mathcal{H}) . \quad (14.40b)$$

We compute these integrals for the surface A_{1xy} depicted in Figure 14.5(b). Sampling the electric and magnetic fields in the center points of the TLM cell surfaces, we obtain

$$\oint_{\partial A_{1xy}} \mathcal{H} \cong \Delta l (H_5 + H_4 + H_6 + H_3) , \quad (14.41a)$$

$$\int_{A_{1xy}} \star \mathcal{E} \cong \frac{1}{4} \Delta l^2 (E_5 + E_4 + E_6 + E_3) , \quad (14.41b)$$

$$\oint_{\partial A_{1xy}} \mathcal{E} \cong \Delta l (E_7 + E_2 - E_8 - E_1) , \quad (14.41c)$$

$$\int_{A_{1xy}} \star \mathcal{H} \cong \frac{1}{4} \Delta l^2 (-H_7 - H_2 + H_8 + H_1) . \quad (14.41d)$$

Inserting (14.41a) and (14.41b) into (14.40a) and considering $\epsilon = 1/Z_F c$, we obtain

$$({}_k H_5 + {}_{k-1} H_5 + {}_k H_4 + {}_{k-1} H_4 + {}_k H_6 + {}_{k-1} H_6 + {}_k H_3 + {}_{k-1} H_3) = \frac{\Delta l}{2Z_F c \Delta t} ({}_k E_5 - {}_{k-1} E_5 + {}_k E_4 - {}_{k-1} E_4 + {}_k E_6 - {}_{k-1} E_6 + {}_k E_3 - {}_{k-1} E_3) . \quad (14.42)$$

Choosing the ratio of the space interval Δl and the time interval Δt as $\frac{\Delta l}{\Delta t} = 2c$ we obtain with (14.38a) and (14.38b)

$${}_k (b_5 + b_4 + b_6 + b_3) = {}_{k-1} (a_5 + a_4 + a_6 + a_3) . \quad (14.43)$$

Inserting (14.41c), (14.41d), and $\frac{\Delta l}{\Delta t} = 2c$ into (14.40b) and considering $\mu = Z_F/c$ we obtain

$$({}_k E_7 + {}_{k-1} E_7 + {}_k E_2 + {}_{k-1} E_2 - {}_k E_8 - {}_{k-1} E_8 - {}_k E_1 - {}_{k-1} E_1) = \frac{Z_F \Delta l}{2c \Delta t} ({}_k H_7 - {}_{k-1} H_7 + {}_k H_2 - {}_{k-1} H_2 - {}_k H_8 + {}_{k-1} H_8 - {}_k H_1 + {}_{k-1} H_1) . \quad (14.44)$$

We obtain with (14.38a) and (14.38b)

$${}_k (b_7 + b_2 - b_8 - b_1) = -{}_{k-1} (a_7 + a_2 - a_8 - a_1) . \quad (14.45)$$

Performing these integrations also over the surfaces A_{1yz} and A_{1zx} yields a total of the following six equations

$${}_k(b_5 + b_4 + b_6 + b_3) = {}_{k-1}(a_5 + a_4 + a_6 + a_3), \quad (14.46a)$$

$${}_k(b_9 + b_8 + b_{10} + b_7) = {}_{k-1}(a_9 + a_8 + a_{10} + a_7), \quad (14.46b)$$

$${}_k(b_1 + b_{12} + b_2 + b_{11}) = {}_{k-1}(a_1 + a_{12} + a_2 + a_{11}), \quad (14.46c)$$

$${}_k(b_7 + b_2 - b_8 - b_1) = -{}_{k-1}(a_7 + a_2 - a_8 - a_1), \quad (14.46d)$$

$${}_k(b_{11} + b_6 - b_{12} - b_5) = -{}_{k-1}(a_{11} + a_6 - a_{12} - a_5), \quad (14.46e)$$

$${}_k(b_3 + b_{10} - b_4 - b_9) = -{}_{k-1}(a_3 + a_{10} - a_4 - a_9). \quad (14.46f)$$

A first-order finite difference scheme based on Ampère's law and Faraday's law may only exhibit six equations. However, to relate the 12 scattered waves to the 12 incident waves of a TLM cell we need 12 equations. To obtain six additional independent equations, we perform the integrations of (14.40a) and (14.40b) over the area A_{2x} and A_{3x} depicted in Figure 14.5(c) and over the areas A_{4x} and A_{5x} in Figure 14.5(d). The contributions to the line integrals through the center of the cells in Figures 14.5(c) and 14.5(d) compensate each other. By that way we obtain two further equations, and by performing this procedure for all three spatial orientations we obtain in total the following additional six equations:

$${}_k(b_7 - b_2 - b_8 + b_1) = {}_{k-1}(a_7 - a_2 - a_8 + a_1), \quad (14.47a)$$

$${}_k(b_{11} - b_6 - b_{12} + b_5) = {}_{k-1}(a_{11} - a_6 - a_{12} + a_5), \quad (14.47b)$$

$${}_k(b_3 - b_{10} - b_4 + b_9) = {}_{k-1}(a_3 - a_{10} - a_4 + a_9), \quad (14.47c)$$

$${}_k(b_5 - b_4 + b_6 - b_3) = -{}_{k-1}(a_5 - a_4 + a_6 - a_3), \quad (14.47d)$$

$${}_k(b_9 - b_8 + b_{10} - b_7) = -{}_{k-1}(a_9 - a_8 + a_{10} - a_7), \quad (14.47e)$$

$${}_k(b_1 - b_{12} + b_2 - b_{11}) = -{}_{k-1}(a_1 - a_{12} + a_2 - a_{11}). \quad (14.47f)$$

We put (14.46a) to (14.46f) and (14.47a) to (14.47f) in the form

$$\mathbf{M}_k \mathbf{b} = \mathbf{L} \mathbf{M}_{k-1} \mathbf{a} \quad (14.48)$$

with

$$\mathbf{L} = \text{diag} [1, 1, 1, -1, -1, -1, 1, 1, 1, -1, -1, -1], \quad (14.49)$$

where we have used the notation introduced in (C.20) for the diagonal matrix. \mathbf{L} is a diagonal matrix with the diagonal elements ± 1 and turns out to be the scattering matrix of the *symmetric condensed TLM node* in its eigensystem. The scattering matrix \mathbf{S} of the symmetric condensed TLM node is given by

$$\mathbf{S} = \mathbf{M}^{-1} \mathbf{L} \mathbf{M}. \quad (14.50)$$

The scattering matrix S is given by

$$S = \begin{bmatrix} 0 & S_0 & S_0^T \\ S_0^T & 0 & S_0 \\ S_0 & S_0^T & 0 \end{bmatrix} \quad \text{with } S_0 = \begin{bmatrix} 0 & 0 & \frac{1}{2} & -\frac{1}{2} \\ 0 & 0 & -\frac{1}{2} & \frac{1}{2} \\ \frac{1}{2} & \frac{1}{2} & 0 & 0 \\ \frac{1}{2} & \frac{1}{2} & 0 & 0 \end{bmatrix}. \quad (14.51)$$

The scattering matrix S has the property $S = S^T = S^\dagger = S^{-1}$ (i.e., it is real, symmetric, hermitian and unitary). Consequently the TLM scheme fulfills energy conservation, reciprocity, and invariance with respect to time reversal exactly. We note that the scattering matrix S may also be determined completely by considering only symmetry and energy conservation.

We consider the TLM mesh to be composed of condensed symmetric TLM nodes as shown in Figure 14.4(c), where each of the six arms is of length $\frac{1}{2}\Delta l$. We assume a homogeneous lossless space with no sources. All incident and scattered wave amplitudes at the node (l, m, n) can be summarized in the vectors ${}_k \mathbf{a}_{l,m,n}$ and ${}_k \mathbf{b}_{l,m,n}$.

In order to describe the complete discretized mesh state, we introduce the field state space. To the node with the discrete space coordinate (l, m, n) at the discrete time coordinate k a base vector $|k; l, m, n\rangle$ is assigned. The set of basis vectors $|k_2; l_2, m_2, n_2\rangle$ is orthonormal. The orthogonality relations are given by

$$\langle k_1; l_1, m_1, n_1 | k_2; l_2, m_2, n_2 \rangle = \delta_{k_1, k_2} \delta_{l_1, l_2} \delta_{m_1, m_2} \delta_{n_1, n_2}. \quad (14.52)$$

The electric field vector $|F_E\rangle$ and the magnetic field vector $|F_M\rangle$ combine all tangential field samples of the TLM mesh

$$|F_E\rangle = \frac{1}{\sqrt{Z}} \sum_{k,l,m,n} {}_k \mathbf{E}_{l,m,n} |k; l, m, n\rangle, \quad |F_M\rangle = \sqrt{Z} \sum_{k,l,m,n} {}_k \mathbf{H}_{l,m,n} |k; l, m, n\rangle. \quad (14.53)$$

All incident and scattered wave amplitudes of the TLM mesh can be combined in two vectors $|\mathbf{a}\rangle$ and $|\mathbf{b}\rangle$, respectively

$$|\mathbf{a}\rangle = \sum_{k,l,m,n} {}_k \mathbf{a}_{l,m,n} |k; l, m, n\rangle, \quad |\mathbf{b}\rangle = \sum_{k,l,m,n} {}_k \mathbf{b}_{l,m,n} |k; l, m, n\rangle. \quad (14.54)$$

The cell boundary mapping is a bijective one-to-one mapping between the 24 electric and magnetic field components and the 24 incident and scattered wave amplitudes at one condensed symmetric TLM node. Since all tangential electric and magnetic field components in each cell boundary surface are also specified in the neighboring cell boundary surfaces, only 12 field components per TLM cell are linearly independent. Specifying, for example, all 12 incident wave amplitudes per TLM cell yields a complete description of the field state.

The time shift operator T_s and its hermitian conjugate T_s^\dagger increment or decrement k by 1 (i.e., it shifts the field state by Δt),

$$T_s |k; l, m, n\rangle = |k+1; l, m, n\rangle, \quad T_s^\dagger |k; l, m, n\rangle = |k-1; l, m, n\rangle. \quad (14.55)$$

If we connect a time delay Δt with the scattering, the simultaneous scattering at all TLM mesh nodes can be described by the operator equation

$$|b\rangle = T_s S |a\rangle. \quad (14.56)$$

In order to describe the propagation of the wave amplitudes in the TLM mesh, we define the spatial shift operators X_s, Y_s, Z_s and their hermitian conjugates X_s^\dagger, Y_s^\dagger and Z_s^\dagger , which increment and decrement the three discrete spatial coordinates l, m and n in the same way as the operators T_s and T_s^\dagger do this with the discrete time coordinate k . We introduce the connection operator

$$\begin{aligned} \Gamma = & X_s(\Delta_{1,2} + \Delta_{3,4}) + X_s^\dagger(\Delta_{2,1} + \Delta_{4,3}) + Y_s(\Delta_{5,6} + \Delta_{7,8}) \\ & + Y_s^\dagger(\Delta_{6,5} + \Delta_{8,7}) + Z_s(\Delta_{9,10} + \Delta_{11,12}) + Z_s^\dagger(\Delta_{10,9} + \Delta_{12,11}). \end{aligned} \quad (14.57)$$

with the 12×12 (m, n) -matrix $(\Delta_{i,j})_{m,n} = \delta_{i,m} \delta_{j,n}$. The scattered wave amplitudes are incident into the neighboring TLM cells. If we assume an instantaneous propagation, we may describe the propagation of all wave amplitudes in the TLM mesh by

$$|a\rangle = \Gamma |b\rangle. \quad (14.58)$$

The connection operator has the properties $\Gamma = \Gamma^\dagger = \Gamma^{-1}$ (i.e., it is hermitian and unitary). The two equations (14.56) and (14.58) constitute the complete TLM scheme.

14.4 THE MODE MATCHING METHOD

Mode matching is the superposition of modal field solutions. If an electromagnetic structure is subdivided into substructures and complete sets of modal field solutions are known for the subdomains, these modal solutions form a complete basis and allow to expand the field solutions into these basis functions. Choosing modal functions as the basis functions ensures that these functions are already solutions within the respective regions and we need only to care that the boundary conditions are fulfilled. The mode matching method is potentially exact if we allow infinite series expansions. Considering the modal basis functions as the basis of a function space, Hilbert space methods, in particular MoM [5], can be applied. Baudrand and Bajon introduced Hilbert space methods to transform integral formulations of electromagnetic field

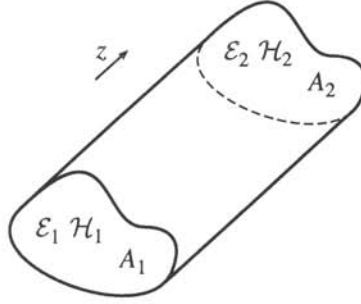


Figure 14.6: Hollow waveguide segment.

problems into algebraic ones [45, 46]. An extension of this method has been given in the *transverse wave formulation* [47–49]. To introduce the basic concepts of the method, consider the waveguide segment depicted in Figure 14.6. The field can be expanded in TE_{mn} and TM_{mn} modes. In (7.197a) and (7.197b) we have expressed the transverse field forms as products of electric and magnetic structure forms $e_k(u, v)$ and $h_k(u, v)$ with complex amplitudes depending on the z -coordinate. The index k is a compact notation for the double index mn and the TE_{mn} and TM_{mn} modes. Summation over k means summation over all TE_{mn} and TM_{mn} modes. The total transverse field is represented by the superposition of the transverse modes, hence

$$\underline{\mathcal{E}}_t(\mathbf{x}) = \sum_k \left(\underline{V}_k^{(+)} e^{-\gamma_k z} + \underline{V}_k^{(-)} e^{\gamma_k z} \right) e_k(u, v), \quad (14.59a)$$

$$\underline{\mathcal{H}}_t(\mathbf{x}) = \sum_k \frac{1}{Z_{W,k}} \left(\underline{V}_k^{(+)} e^{-\gamma_k z} - \underline{V}_k^{(-)} e^{\gamma_k z} \right) h_k(u, v). \quad (14.59b)$$

According to (7.198a) and (7.198b), the electric and magnetic structure vectors are mutually orthogonal in any point and the structure forms $e_k(u, v)$ and $h_k(u, v)$ fulfill

$$e_k(u, v) = - \star [dz \wedge h_k(u, v)], \quad (14.60a)$$

$$h_k(u, v) = \star [dz \wedge e_k(u, v)]. \quad (14.60b)$$

Furthermore, due to (7.208) the structure forms $e_k(u, v)$ and $h_k(u, v)$ form a normalized biorthogonal basis, as discussed in Section C.4.3:

$$\langle e_k | h_l \rangle_A = - \langle h_k | e_l \rangle_A = \delta_{kl}. \quad (14.61)$$

With this we can represent the fields by Hilbert space vectors as

$$|\underline{\mathcal{E}}_t(z)\rangle = \sum_k \left(\underline{V}_k^{(+)} e^{-\gamma_k z} + \underline{V}_k^{(-)} e^{\gamma_k z} \right) |e_k\rangle, \quad (14.62a)$$

$$|\underline{\mathcal{H}}_t(z)\rangle = \sum_k \frac{1}{Z_{W,k}} \left(\underline{V}_k^{(+)} e^{-\gamma_k z} - \underline{V}_k^{(-)} e^{\gamma_k z} \right) |h_k\rangle, \quad (14.62b)$$

where the $|e_k\rangle$ and $|h_k\rangle$ form a biorthogonal set of basis vectors. The electric and magnetic field forms can be computed from the corresponding Hilbert space vectors via

$$\underline{\mathcal{E}}_t(\mathbf{x}) = \sum_k e_k(u, v) \langle h_k | \underline{\mathcal{E}}_t \rangle, \quad (14.63a)$$

$$\underline{\mathcal{H}}_t(\mathbf{x}) = \sum_k \frac{1}{Z_{W,k}} h_k(u, v) \langle e_k | \underline{\mathcal{H}}_t \rangle. \quad (14.63b)$$

We define the *wave impedance operator*

$$\underline{Z}_W = \sum_{n=1}^{\infty} Z_{W,k} (|h_n\rangle \langle e_n| - |e_n\rangle \langle h_n|). \quad (14.64)$$

With this we introduce the *wave amplitude* vectors $|\underline{\tilde{A}}\rangle$ and $|\underline{\tilde{B}}\rangle$ as

$$|\underline{\tilde{A}}\rangle = \frac{1}{2} [|\underline{\mathcal{E}}_t\rangle + \underline{Z}_W |\underline{\mathcal{H}}_t\rangle], \quad (14.65a)$$

$$|\underline{\tilde{B}}\rangle = \frac{1}{2} [|\underline{\mathcal{E}}_t\rangle - \underline{Z}_W |\underline{\mathcal{H}}_t\rangle]. \quad (14.65b)$$

Inserting (14.62a) and (14.62b) yields

$$|\underline{\tilde{A}}(z)\rangle = \sum_k \underline{V}_k^{(+)} e^{-\gamma_k z} |e_k\rangle, \quad (14.66a) \quad |\underline{\tilde{B}}(z)\rangle = \sum_k \underline{V}_k^{(-)} e^{\gamma_k z} |e_k\rangle. \quad (14.66b)$$

We compute the transverse electric and magnetic fields from the wave amplitudes via

$$|\underline{\mathcal{E}}_t\rangle = |\underline{\tilde{A}}\rangle + |\underline{\tilde{B}}\rangle, \quad (14.67a) \quad |\underline{\mathcal{H}}_t\rangle = \underline{Z}_W^{-1} (|\underline{\tilde{A}}\rangle - |\underline{\tilde{B}}\rangle). \quad (14.67b)$$

We introduce the operator $\Gamma(z)$ and its inverse as

$$\Gamma(z) = \sum_{n=1}^{\infty} e^{-\gamma_n z} (|h_n\rangle \langle e_n| - |e_n\rangle \langle h_n|), \quad (14.68a)$$

$$\Gamma^{-1}(z) = \sum_{n=1}^{\infty} e^{\gamma_n z} (|h_n\rangle \langle e_n| - |e_n\rangle \langle h_n|). \quad (14.68b)$$

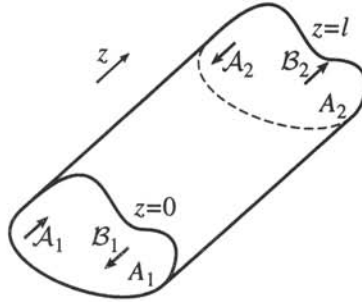


Figure 14.7: Wave amplitudes in the waveguide segment.

With these operators we obtain from (14.66a) and (14.66b)

$$|\underline{\tilde{A}}(z_2)\rangle = \Gamma(z_2 - z_1)|\underline{\tilde{A}}(z_1)\rangle \quad |\underline{\tilde{A}}(z_1)\rangle = \Gamma^{-1}(z_2 - z_1)|\underline{\tilde{A}}(z_2)\rangle, \quad (14.69a)$$

$$|\underline{\tilde{B}}(z_2)\rangle = \Gamma^{-1}(z_2 - z_1)|\underline{\tilde{B}}(z_1)\rangle \quad |\underline{\tilde{B}}(z_1)\rangle = \Gamma(z_2 - z_1)|\underline{\tilde{B}}(z_2)\rangle. \quad (14.69b)$$

Choosing the direction of the wave amplitude vectors at the ports of the waveguide segment according to Figure 14.7 yields

$$|\underline{\tilde{A}}_1\rangle = |\underline{\tilde{A}}(z_1)\rangle, \quad |\underline{\tilde{B}}_1\rangle = |\underline{\tilde{B}}(z_1)\rangle, \quad |\underline{\tilde{A}}_2\rangle = |\underline{\tilde{B}}(z_2)\rangle, \quad |\underline{\tilde{B}}_2\rangle = |\underline{\tilde{A}}(z_2)\rangle. \quad (14.70)$$

With this we can introduce a *transmission matrix* representation in analogy to Section 10.2.4, hence

$$\begin{bmatrix} |\underline{\tilde{B}}_1\rangle \\ |\underline{\tilde{A}}_1\rangle \end{bmatrix} = T \begin{bmatrix} |\underline{\tilde{A}}_2\rangle \\ |\underline{\tilde{B}}_2\rangle \end{bmatrix}. \quad (14.71)$$

For the line segment of length $l = z_2 - z_1$ shown in Figure 14.7 the transmission matrix is given by

$$T = \begin{bmatrix} \Gamma(l) & 0 \\ 0 & \Gamma^{-1}(l) \end{bmatrix}. \quad (14.72)$$

Consider a thin sheet as shown in Figure 14.8 with a surface current distribution $\underline{\mathcal{J}}_A$ on it. According to (2.175a) and (2.175b) the surface currents or electric surface polarizations, respectively, in the sheet yield a magnetic field discontinuity, whereas due to (2.175c) the magnetic surface polarizations yield an electric field discontinuity, hence

$$|\underline{\mathcal{H}}_{t2} - \underline{\mathcal{H}}_{t1}\rangle = j\omega|\underline{\mathcal{M}}_{eA}\rangle = |\underline{\mathcal{J}}_A\rangle, \quad (14.73a)$$

$$|\underline{\mathcal{E}}_{t2} - \underline{\mathcal{E}}_{t1}\rangle = -j\omega|\underline{\mathcal{M}}_{mA}\rangle. \quad (14.73b)$$

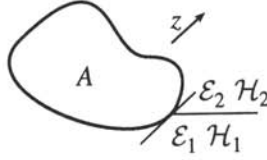


Figure 14.8: Surface current sheet .

Like the tangential magnetic field from the surface current form and the surface polarization forms can be expanded into the magnetic field structure functions:

$$\underline{\mathcal{J}}_A(u, v) = \sum_k \underline{I}_{Ak} h_k(u, v), \quad (14.74a)$$

$$\underline{\mathcal{M}}_{eA}(u, v) = \frac{1}{j\omega} \sum_k \underline{I}_{Ak} h_k(u, v), \quad (14.74b)$$

$$\underline{\mathcal{M}}_{mA}(u, v) = \frac{1}{j\omega} \sum_k \underline{V}_{Ak} e_k(u, v). \quad (14.74c)$$

The surface current $\underline{\mathcal{J}}_A$ also is represented by the Hilbert space vector $|\underline{\mathcal{J}}_A\rangle$ given by

$$|\underline{\mathcal{J}}_A\rangle = \sum_k \underline{I}_{Ak} |h_k(u, v)\rangle, \quad (14.75a)$$

$$\underline{I}_{Ak}(u, v) = \langle e_k(u, v) | \underline{\mathcal{J}}_A \rangle. \quad (14.75b)$$

The surface current $\underline{\mathcal{J}}_A$ may be either an impressed surface current originating from current sources or a current evoked from the electric field due to a surface admittance. With the impressed polarizations we can proceed in an analogous way.

The *surface admittance matrix* description, introduced with (3.184a) for thin conductive sheets, can be extended to sheets structured in the u, v -plane. If the surface is structured the surface admittance in general depends on the transverse coordinates u and v , hence

$$\begin{bmatrix} \underline{\mathcal{H}}_{t1}(u, v) \\ -\underline{\mathcal{H}}_{t2}(u, v) \end{bmatrix} = \star dz \wedge \tilde{Y}(u, v) \begin{bmatrix} \underline{\mathcal{E}}_{t1}(u, v) \\ \underline{\mathcal{E}}_{t2}(u, v) \end{bmatrix} \quad (14.76)$$

with the surface admittance matrix $\tilde{Y}(u, v)$ given by

$$\tilde{Y}(u, v) = \begin{bmatrix} Y_{11}(u, v) & Y_{12}(u, v) \\ Y_{21}(u, v) & Y_{22}(u, v) \end{bmatrix}. \quad (14.77)$$

The surface admittance matrix has been marked with a tilde in order to distinguish it from the surface impedance operator that will be introduced in the following. In

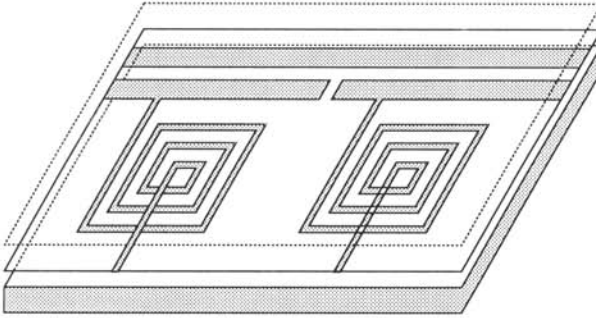


Figure 14.9: Multilayer circuit.

operator notation (14.76) can be written as

$$\begin{bmatrix} |\mathcal{H}_{t1}\rangle \\ -|\mathcal{H}_{t2}\rangle \end{bmatrix} = Y \begin{bmatrix} |\mathcal{E}_{t1}\rangle \\ |\mathcal{E}_{t2}\rangle \end{bmatrix} \quad (14.78)$$

with the *surface admittance operator*

$$Y = \begin{bmatrix} Y_{11} & Y_{12} \\ Y_{21} & Y_{22} \end{bmatrix}, \quad (14.79)$$

the matrix elements of which are operators given by

$$Y_{ij} = |h_k\rangle Y_{ij,kl} \langle e_l| \quad (14.80)$$

with the $Y_{ij,kl}$ given by

$$Y_{ij,kl} = \int_A Y_{ij}(u, v) e(u, v)_k^* \wedge h(u, v)_l. \quad (14.81)$$

In this *generalized transmission-line* (GTL) description for the layered electromagnetic structure, the generalized voltages and currents and the wave amplitudes are summarized in Hilbert space vectors describing the complete transverse field distribution [45, 47, 49]. Using this formalism we can analyze multilayer structures as shown in Figure 14.9, where homogeneous layers of finite extension in z -direction alternate with thin structured layers. The structured layers are described by the surface admittance matrices $Y_{ij}(u, v)$ and the surface admittance operators Y derived from it. The transverse distribution of impressed surface currents is given by (14.74a) or (14.74b), respectively, and voltages varying in transverse direction are described by (14.74c).

Thick homogeneous layers are described by (14.72). Cascading these multiports, we can describe multilayer structures consisting of thin layers, with structured metallization, resistive layers, and impressed voltage and current sources and thick homogeneous material. For a detailed description of the method the reader is referred to [49].

REFERENCES

- [1] T. Itoh, *Numerical Techniques for Microwave and Millimeter-Wave Passive Structures*. New York: John Wiley & Sons, 1989.
- [2] R. Sorrentino, *Numerical Methods for Passive Microwave and Millimeter Wave Structures*. IEEE Press, 1989.
- [3] E. Yamashita, *Analysis Methods for Electromagnetic Wave Problems*. Boston, London: Artech House, 1990.
- [4] R. F. Harrington, "Matrix methods for field problems," *Proceedings of the IEEE*, vol. 55, pp. 136–149, Feb. 1967.
- [5] R. F. Harrington, *Field Computation by Moment Methods*. San Francisco: IEEE Press, 1968.
- [6] J. J. Wang, *Generalized Moment Methods in Electromagnetics*. New York: John Wiley & Sons, 1991.
- [7] J. R. Mosig, "Integral equation technique," in *Numerical Techniques for Microwave and Millimeter Wave Passive Structures* (T. Itoh, ed.), pp. 133–213, New York: John Wiley & Sons, 1989.
- [8] D. Mirshekar-Syahkal, *Spectral Domain Methods for Microwave Integrated Circuits*. Taunton, Somerset, England: Research Studies Press, 1990.
- [9] M. Mongiardo, P. Russer, C. Tomassoni, and L. B. Felsen, "Analysis of N-furcation in elliptical waveguides via the generalized network formulation," *IEEE Trans. Microwave Theory Techn.*, vol. 47, pp. 2473–2478, Dec. 1999.
- [10] G. Conciauro, M. Guglielmi, and R. Sorrentino, *Advanced Modal Analysis*. New York: John Wiley & Sons, 2000.
- [11] J. Kessler, R. Dill, and P. Russer, "Field theory investigation of high- T_c superconducting coplanar wave guide transmission-lines and resonators," *IEEE Trans. Microwave Theory Techn.*, vol. 39, pp. 1566–1574, Sept. 1991.
- [12] R. Schmidt and P. Russer, "Modelling of cascaded coplanar waveguide discontinuities by the mode-matching approach," *1995 Int. Microwave Symposium Digest, Orlando*, pp. 281–284, May 1995.
- [13] U. Schulz and R. Pregla, "A new technique for the analysis of the dispersion characteristics of planar waveguides and its application to microstrips with tunig septums," *Radio Sci.*, vol. 16, pp. 1173–1178, Nov.–Dec. 1981.
- [14] R. Pregla and W. Pascher, "The method of lines," in *Numerical Techniques for Microwave and Millimeter Wave Passive Structures* (T. Itoh, ed.), pp. 381–446, New York: John Wiley & Sons, 1989.
- [15] K. S. Yee, "Numerical solution of initial boundary value problems involving Maxwell's equations in isotropic media," *IEEE Trans. Antennas Propagat.*, vol. 14, pp. 302–307, May 1966.
- [16] A. Taflov, *Computational Electrodynamics - The Finite-Difference Time-Domain Method*. Norwood, MA: Artech House, 1995.
- [17] T. Weiland, "A discretization method for the solution of Maxwell's equations for six-component fields," *Electronics and Communications (AEU)*, vol. 31, pp. 116–120, 1977.
- [18] T. Weiland, "On the Unique Numerical Solution of Maxwellian Eigenvalue Problems in Three Dimensions," *Particle Accelerators*, vol. 17, pp. 227–242, 1985.
- [19] T. Weiland, "Time domain electromagnetic field computation with finite difference methods," *Int. J. Numer. Modeling*, vol. 9, pp. 295–319, 1996.
- [20] J. Jin, *The Finite Element Method in Electromagnetics*. New York: John Wiley & Sons, 1993.

- [21] W. J. R. Hoefer, "The transmission line matrix method-theory and applications," *IEEE Trans. Microwave Theory Techn.*, vol. 33, pp. 882–893, Oct. 1985.
- [22] W. J. R. Hoefer, "The transmission line matrix (TLM) method," in *Numerical Techniques for Microwave and Millimeter Wave Passive Structures* (T. Itoh, ed.), pp. 496–591, New York: John Wiley & Sons, 1989.
- [23] C. Christopoulos, *The Transmission-Line Modeling Method TLM*. New York: IEEE Press, 1995.
- [24] P. Russer, "The transmission line matrix method," in *Applied Computational Electromagnetics*, NATO ASI Series, pp. 243–269, Berlin Heidelberg New York: Springer, 2000.
- [25] T. Mangold and P. Russer, "Full-wave modeling and automatic equivalent-circuit generation of millimeter-wave planar and multilayer structures," *IEEE Trans. Microwave Theory Techn.*, vol. 47, pp. 851–858, June 1999.
- [26] S. Lindenmeier, L. Pierantoni, and P. Russer, "Hybrid space discretizing-integral equation methods for numerical modeling of transient interference," *IEEE Trans. Electromagn. Compatibility*, vol. 41, pp. 425–430, Nov. 1999.
- [27] S. Lindenmeier, L. Pierantoni, and P. Russer, "Time domain modeling of E.M. coupling between microwave circuit structures," *1999 Int. Microwave Symposium Digest, Anaheim*, pp. 1569–1572, June 1999.
- [28] P. Lorenz and P. Russer, "Hybrid transmission line matrix (TLM) and multipole expansion method for time-domain modeling of radiating structures," *2001 Int. Microwave Symposium Digest, Fort Worth*, pp. 1037–1040, June 2004.
- [29] F. Coccetti and P. Russer, "Application of system identification to time-domain modeling of electromagnetic structures," in *Fields, Networks, Methods, and Systems in Modern Electrodynamics* (P. Russer and M. Mongiardo, eds.), pp. 143–156, Berlin: Springer, 2004.
- [30] A. C. Cangellaris, M. Celik, S. Pasha, and L. Zhao, "Electromagnetic model order reduction for system level modeling," *IEEE Trans. Microwave Theory Techn.*, vol. 47, pp. 840–850, June 1999.
- [31] P. R. Lukashevich, A. Cangellaris, "TLM model order reduction," in *Fields, Networks, Methods, and Systems in Modern Electrodynamics* (P. Russer and M. Mongiardo, eds.), pp. 200–205, Berlin: Springer, 2004.
- [32] L. Tarricone and A. Esposito, *Grid Computing for Electromagnetics*. Norwood, MA: Artech House, 2004.
- [33] P. Lorenz, J. V. Vital, B. Bisconti, and P. Russer, "High-throughput transmission line matrix (TLM) system in grid environment for the analysis of complex electromagnetic structures," *Proc. 21th Annual Review of Progress in Applied Computational Electromagnetics, Hawaii*, Apr. 2005.
- [34] W. C. Chew, J. M. Jin, E. Michielssen, and J. M. Song, *Fast and efficient algorithms in computational electromagnetics*. Norwood, MA: Artech House, 2000.
- [35] P. B. Johns and R. L. Beurle, "Numerical solution of 2-dimensional scattering problems using a transmission-line matrix," *Proc. IEE*, vol. 118, pp. 1203–1208, Sept. 1971.
- [36] G. Kron, "Equivalent circuit of the field equations of Maxwell I," *Proc. IRE*, vol. 32, pp. 289–299, May 1944.
- [37] C. Christopoulos and P. Russer, "Application of TLM to microwave circuits," in *Applied Computational Electromagnetics*, NATO ASI Series, pp. 300–323, Berlin Heidelberg New York: Springer, 2000.
- [38] C. Christopoulos and P. Russer, "Application of TLM to EMC problems," in *Applied Computational Electromagnetics*, NATO ASI Series, pp. 324–350, Berlin Heidelberg New York: Springer, 2000.
- [39] S. Hein, "Consistent finite difference modeling of Maxwell's equations with lossy symmetrical condensed TLM node," *Int. J. Numer. Modeling*, vol. 6, pp. 207–220, 1993.
- [40] M. Aidam and P. Russer, "Derivation of the TLM method by finite integration," *AEÜ Int. J. Electron. Commun.*, vol. 51, pp. 35–39, 1997.

- [41] M. Krumpholz and P. Russer, "A field theoretical derivation TLM," *IEEE Trans. Microwave Theory Techn.*, vol. 42, pp. 1660–1668, Sept. 1994.
- [42] N. Peña and M. M. Ney, "A general and complete two-dimensional TLM hybrid node formulation based on Maxwell's integral equations," in *Proc. 12th Annual Review of Progress in Applied Computational Electromagnetics, Monterey*, (Monterey, CA), pp. 254–261, Mar. 1996.
- [43] N. Peña and M. Ney, "A general formulation of a three-dimensional TLM condensed node with the modeling of electric and magnetic losses and current sources," in *Proc. 12th Annual Review of Progress in Applied Computational Electromagnetics, Monterey*, (Monterey, CA), pp. 262–269, Mar. 1996.
- [44] J. Thomas, *Numerical Partial Differential Equations*. New York: Springer, 1995.
- [45] H. Baudrand, *Introduction au Calcul des Elements de Circuits Passifs en Hyperfrequences*. Toulouse: Cépaduès-Éditions, 2001.
- [46] H. Baudrand and D. Bajon, "Equivalent circuit representation for integral formulation of electromagnetic problems," *Int. J. Numer. Modeling*, vol. 15, pp. 23–57, 2002.
- [47] S. Wane, D. Bajon, and H. Baudrand, "Fullwave analysis of stacked structures including inhomogeneous antennas," in *New Trends and Concepts in Microwave Theory and Technics* (H. Baudrand, ed.), pp. 131–166, Trivandrum, India: Research Signpost, 2003.
- [48] D. Bajon, S. Wane, and H. Baudrand, "Multi-scale investigation of global coupling between blocks and sub-blocks including lumped components in rf integrated circuits," *Proc. 34th European Microwave Conference, Amsterdam*, vol. 2, pp. 873–875, Oct. 2004.
- [49] S. Wane, D. Bajon, H. Baudrand, and P. Gamand, "A new full-wave hybrid differential-integral approach for the investigation of multilayer structures including nonuniformly doped diffusions," *IEEE Trans. Microwave Theory Techn.*, vol. 53, pp. 200–214, Jan. 2005.

Appendix A

Vectors and Differential Forms

A.1 VECTORS

This section gives a compact summary of the vector algebra for the linear three-dimensional vector space. For a more detailed treatment see for example [1, 2]. A *vector* is a variable quantity that has both magnitude and direction and can be resolved into components, such as force, electric, and magnetic field. In the *Cartesian coordinate system* (x, y, z) a vector \mathbf{a} is represented by its Cartesian coordinates (a_x, a_y, a_z) . The vector may be visualized by an arrow starting from the origin and terminating at the point (a_x, a_y, a_z) , as depicted in Figure A.1(a). However, we could start from any point in our Cartesian reference frame. The origin only is chosen for simplicity.

Let \mathbf{e}_x be a vector of unit magnitude pointing in the positive x -direction and \mathbf{e}_y and \mathbf{e}_z vectors of unit magnitude pointing in the positive y - and z -directions, respectively. By vector addition we obtain

$$\mathbf{a} = a_x \mathbf{e}_x + a_y \mathbf{e}_y + a_z \mathbf{e}_z = \begin{bmatrix} a_x \\ a_y \\ a_z \end{bmatrix}. \quad (\text{A.1})$$

The vectors \mathbf{e}_x , \mathbf{e}_y , and \mathbf{e}_z form a *basis* of our three-dimensional linear vector space. Figure A.1(a) shows the vector \mathbf{a} in a right-handed Cartesian coordinate system (x, y, z) , whereas in Figure A.1(b) the same vector \mathbf{a} is represented in a left-handed coordinate system $(x', y', z') = (-x, -y, -z)$. In the new coordinate system (x', y', z') , the vector \mathbf{a} exhibits the coordinates $(a'_x, a'_y, a'_z) = (-a_x, -a_y, -a_z)$. The vector \mathbf{a} itself remains unchanged under this coordinate transformation. We have

$$\mathbf{a} = a_x \mathbf{e}_x + a_y \mathbf{e}_y + a_z \mathbf{e}_z = a'_x \mathbf{e}_{x'} + a'_y \mathbf{e}_{y'} + a'_z \mathbf{e}_{z'}. \quad (\text{A.2})$$

The components of the vector are odd functions of the coordinates. A vector with this

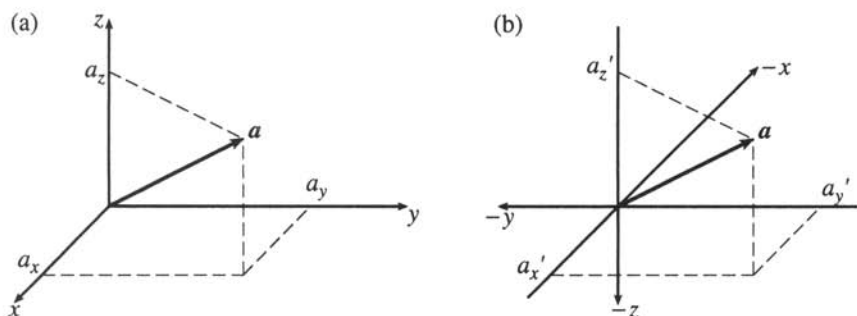


Figure A.1: Cartesian components of a vector (a) in a right-handed coordinate system, and (b) in a left-handed coordinate system.

property is called a *polar vector*. Vectors occurring in curve integrals like the vectors representing the electric or magnetic field are represented by polar vectors.

The sum of two vectors \mathbf{a} and \mathbf{b} is given by

$$\mathbf{a} + \mathbf{b} = \begin{bmatrix} a_x + b_x \\ a_y + b_y \\ a_z + b_z \end{bmatrix}. \quad (\text{A.3})$$

The *magnitude* $|\mathbf{a}|$ of the vector \mathbf{a} is given by

$$|\mathbf{a}| = \sqrt{|a_x|^2 + |a_y|^2 + |a_z|^2}. \quad (\text{A.4})$$

The *inner product* or *scalar product* of two vectors \mathbf{a} and \mathbf{b} is defined as

$$\mathbf{a} \cdot \mathbf{b} = a_x b_x + a_y b_y + a_z b_z. \quad (\text{A.5})$$

For real vectors \mathbf{a} and \mathbf{b} the inner product is given by

$$\mathbf{a} \cdot \mathbf{b} = |\mathbf{a}| |\mathbf{b}| \cos \phi, \quad (\text{A.6})$$

where ϕ is the angle enclosed by \mathbf{a} and \mathbf{b} . The vectors \mathbf{e}_x , \mathbf{e}_y , and \mathbf{e}_z fulfill the relation

$$\mathbf{e}_i \cdot \mathbf{e}_j = \delta_{ij} \quad \text{for } i, j = x, y, z, \quad (\text{A.7})$$

where the *Kronecker delta symbol* δ_{mn} is given by

$$\delta_{mn} = \begin{cases} 0 & \text{for } m \neq n \\ 1 & \text{for } m = n \end{cases}. \quad (\text{A.8})$$

The vectors \mathbf{e}_x , \mathbf{e}_y , and \mathbf{e}_z form a complete set of *orthonormal basis vectors* of our three-dimensional vector space.

The *cross-product* or *vector product*

$$\mathbf{c} = \mathbf{a} \times \mathbf{b} \quad (\text{A.9})$$

of two vectors \mathbf{a} and \mathbf{b} is a vector normal to both vectors \mathbf{a} and \mathbf{b} and with the magnitude

$$|\mathbf{a} \times \mathbf{b}| = |\mathbf{a}||\mathbf{b}| \sin \phi. \quad (\text{A.10})$$

If the two vectors \mathbf{a} and \mathbf{b} define a parallelogram, then the magnitude $|\mathbf{a} \times \mathbf{b}|$ of the cross-product is the area of the parallelogram. The vectors \mathbf{a} , \mathbf{b} and $\mathbf{a} \times \mathbf{b}$ form a right-handed system. We assume the orthonormal basis vectors \mathbf{e}_x , \mathbf{e}_y and \mathbf{e}_z to form a right-handed system according to Figure A.1(a). In this case the relations

$$\begin{aligned} \mathbf{e}_x \times \mathbf{e}_y &= -\mathbf{e}_y \times \mathbf{e}_x = \mathbf{e}_z, \\ \mathbf{e}_y \times \mathbf{e}_z &= -\mathbf{e}_z \times \mathbf{e}_y = \mathbf{e}_x, \\ \mathbf{e}_z \times \mathbf{e}_x &= -\mathbf{e}_x \times \mathbf{e}_z = \mathbf{e}_y \end{aligned} \quad (\text{A.11})$$

are fulfilled. The *Kronecker tensor* is defined as

$$\delta_{ijk} = \begin{cases} +1 & \text{if } (ijk) \text{ is an even permutation of } (xyz) \\ -1 & \text{if } (ijk) \text{ is an odd permutation of } (xyz) \\ 0 & \text{if } (ijk) \text{ is no permutation of } (xyz) \end{cases}. \quad (\text{A.12})$$

Permutations from an original ordered sequence such as ijk can be achieved by successive interchanges of elements. A permutation is said to be *even* or *odd* if an even or odd number of transpositions is required for the rearrangement.

We can express (A.11) in the following form:

$$\mathbf{e}_i \times \mathbf{e}_j = \sum_k \delta_{ijk} \mathbf{e}_k. \quad (\text{A.13})$$

For two vectors \mathbf{a} and \mathbf{b} we obtain

$$\mathbf{a} \times \mathbf{b} = \sum_{i,j,k} a_i b_j \delta_{ijk} \mathbf{e}_k. \quad (\text{A.14})$$

From this we obtain (A.9) in component representation

$$\begin{bmatrix} c_x \\ c_y \\ c_z \end{bmatrix} = \begin{bmatrix} a_y b_z - a_z b_y \\ a_z b_x - a_x b_z \\ a_x b_y - a_y b_x \end{bmatrix}. \quad (\text{A.15})$$

The vector \mathbf{c} defined by the cross-product (A.9) behaves fundamentally different from the polar vectors. If the coordinate axes are inverted we obtain $a_i \rightarrow -a'_i$, $b_i \rightarrow -b'_i$. However, due to (A.15) this yields $c_i \rightarrow c'_i$. Under coordinate inversion the cross-product vector \mathbf{c} does not behave like a polar vector. A vector with these transformation properties is called an *axial vector* or *pseudovector*. Vectors occurring in surface integrals like the vectors representing current or flux densities are represented by axial vectors.

With (C.23) the cross-product may also be represented as determinant:

$$\mathbf{a} \times \mathbf{b} = \begin{vmatrix} \mathbf{e}_x & \mathbf{e}_y & \mathbf{e}_z \\ a_1 & a_2 & a_3 \\ b_1 & b_2 & b_3 \end{vmatrix}. \quad (\text{A.16})$$

The cross-product is anticommutative, in other words,

$$\mathbf{b} \times \mathbf{a} = -\mathbf{a} \times \mathbf{b}. \quad (\text{A.17})$$

The *triple scalar product* of three vectors \mathbf{a} , \mathbf{b} , and \mathbf{c} , defined by

$$[\mathbf{abc}] = \mathbf{a} \cdot (\mathbf{b} \times \mathbf{c}) = (\mathbf{a} \times \mathbf{b}) \cdot \mathbf{c} \quad (\text{A.18})$$

yields the volume of the parallelepiped defined by the vectors \mathbf{a} , \mathbf{b} and \mathbf{c} . The triple scalar product is invariant under cyclic permutation of the factors; however, it changes its sign if two factors are interchanged. From (A.5), (A.14) and (A.18) we obtain

$$[\mathbf{abc}] = \sum_{i,j,k} a_i b_j c_k \delta_{ijk} = \begin{vmatrix} a_1 & a_2 & a_3 \\ b_1 & b_2 & b_3 \\ c_1 & c_2 & c_3 \end{vmatrix}. \quad (\text{A.19})$$

In the case of the inversion of all coordinate axes the triple scalar product changes its sign. A scalar with the transformation properties of a triple scalar product is called a *pseudoscalar*. Scalar quantities occurring in volume integrals, as for example charge densities or energy densities, are represented by pseudoscalars. Pseudoscalars are distinguished from *scalars* describing quantities that are not integrated over space coordinates. Examples for scalars are scalar potential functions.

For the twofold cross-product of three vectors we obtain

$$(\mathbf{a} \times \mathbf{b}) \times \mathbf{c} = (\mathbf{a} \cdot \mathbf{c})\mathbf{b} - (\mathbf{b} \cdot \mathbf{c})\mathbf{a}, \quad (\text{A.20})$$

$$\mathbf{a} \times (\mathbf{b} \times \mathbf{c}) = (\mathbf{a} \cdot \mathbf{c})\mathbf{b} - (\mathbf{a} \cdot \mathbf{b})\mathbf{c}. \quad (\text{A.21})$$

For the threefold products of four vectors the following relations hold:

$$(\mathbf{a} \times \mathbf{b}) \cdot (\mathbf{c} \times \mathbf{d}) = \begin{vmatrix} (\mathbf{a} \cdot \mathbf{c}) & (\mathbf{a} \cdot \mathbf{d}) \\ (\mathbf{b} \cdot \mathbf{c}) & (\mathbf{b} \cdot \mathbf{d}) \end{vmatrix}, \quad (\text{A.22})$$

$$(\mathbf{a} \times \mathbf{b}) \times (\mathbf{c} \times \mathbf{d}) = [\mathbf{abd}]\mathbf{c} - [\mathbf{abc}]\mathbf{d} = [\mathbf{acd}]\mathbf{b} - [\mathbf{bcd}]\mathbf{a}. \quad (\text{A.23})$$

A.2 DIFFERENTIAL FORMS

In this section the framework of differential forms used in this book is presented. For further reading see [3–7]. Scalar and vector fields may be represented by *exterior differential forms*. Differential forms are essentially the expressions under an integration symbol. An exterior differential form of order p is called a p -form. In n -dimensional space the order of a differential form may assume values $1 \dots n$. In this book we only consider the three-dimensional case. The p -forms in three-dimensional space are

$$\text{zero-form:} \quad f(\mathbf{x}), \quad (\text{A.24})$$

$$\text{one-form:} \quad \mathcal{U}(\mathbf{x}) = U_x dx + U_y dy + U_z dz, \quad (\text{A.25})$$

$$\text{two-form:} \quad \mathcal{V}(\mathbf{x}) = V_x dy \wedge dz + V_y dz \wedge dx + V_z dx \wedge dy, \quad (\text{A.26})$$

$$\text{three-form:} \quad \mathcal{Q}(\mathbf{x}) = \rho dx \wedge dy \wedge dz. \quad (\text{A.27})$$

For the exterior differential form $dx \wedge dy$ the following *commutation relation* holds:

$$dx \wedge dy = -dy \wedge dx. \quad (\text{A.28})$$

Deciding

$$dx \wedge dy = dx dy \quad (\text{A.29})$$

assigns to $dx \wedge dy$ the positive orientation and to $dy \wedge dx$ the negative orientation. For a p -form \mathcal{U} and a q -form \mathcal{V} the commutation relation is

$$\mathcal{U} \wedge \mathcal{V} = (-1)^{p+q+1} \mathcal{V} \wedge \mathcal{U}. \quad (\text{A.30})$$

We introduce the bracket symbol $[]^{(p)}$ to express the relation of a scalar field ($p = 0, 3$) or a vector field ($p = 1, 2$) to a p -form. The p -forms are related to scalar and vector fields via

$$f(\mathbf{x}) = [f(\mathbf{x})]^{(0)}, \quad (\text{A.31})$$

$$\mathcal{U}(\mathbf{x}) = [\mathbf{U}(\mathbf{x})]^{(1)} = U_x dx + U_y dy + U_z dz, \quad (\text{A.32})$$

$$\mathcal{V}(\mathbf{x}) = [\mathbf{V}(\mathbf{x})]^{(2)} = V_x dy \wedge dz + V_y dz \wedge dx + V_z dx \wedge dy, \quad (\text{A.33})$$

$$\mathcal{Q}(\mathbf{x}) = [\rho(\mathbf{x})]^{(3)} = \rho dx \wedge dy \wedge dz. \quad (\text{A.34})$$

In these equations f is a scalar, \mathbf{U} is a vector, \mathbf{V} is a pseudovector, and ρ is a pseudoscalar. In differential form notation a clear distinction between scalars, pseudoscalars, vectors and pseudovectors is made. Scalars are represented by zero-forms, pseudoscalars by three-forms, vectors by one-forms and pseudovectors by two-forms. The domains of integration are a curve C for a one-form, an area A for a two-form, and a volume V for a three-form (Figure A.2). The corresponding integrals are

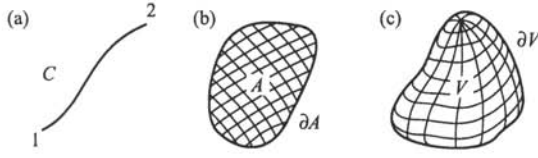


Figure A.2: Domains of integration: (a) curve, (b) surface and (c) volume.

$$\text{one-form:} \quad \int_1^2 \mathcal{U} = \int_1^2 U_x dx + U_y dy + U_z dz, \quad (\text{A.35})$$

$$\text{two-form:} \quad \int_A \mathcal{V} = \int_A V_x dy \wedge dz + V_y dz \wedge dx + V_z dx \wedge dy, \quad (\text{A.36})$$

$$\text{three-form:} \quad \int_V \mathcal{Q} = \int_V \rho dx \wedge dy \wedge dz. \quad (\text{A.37})$$

We introduce the *star operator* or *Hodge operator* \star defined via

$$\begin{aligned} \star f &= f dx \wedge dy \wedge dz, \\ \star (A_x dx + A_y dy + A_z dz) &= A_x dy \wedge dz + A_y dz \wedge dx + A_z dx \wedge dy, \\ \star (A_x dy \wedge dz + A_y dz \wedge dx + A_z dx \wedge dy) &= A_x dx + A_y dy + A_z dz, \\ \star f dx \wedge dy \wedge dz &= f. \end{aligned} \quad (\text{A.38})$$

The star operator has the property

$$\star \star = 1. \quad (\text{A.39})$$

A.2.1 Products of Exterior Differential Forms

The product of a p -form and a q -form is a $(p+q)$ -form. The product of two one-forms \mathcal{A} and \mathcal{B} is

$$\begin{aligned} \mathcal{A} \wedge \mathcal{B} &= (A_x dx + A_y dy + A_z dz) \wedge (B_x dx + B_y dy + B_z dz) \\ &= (A_y B_z - A_z B_y) dy \wedge dz + (A_z B_x - A_x B_z) dz \wedge dx \\ &\quad + (A_x B_y - A_y B_x) dx \wedge dy. \end{aligned} \quad (\text{A.40})$$

The relation to vector notation is given by

$$\mathcal{A} = [\mathbf{A}]^{(1)}, \quad \mathcal{B} = [\mathbf{B}]^{(1)} \quad \rightarrow \quad \mathcal{A} \wedge \mathcal{B} = [\mathbf{A} \times \mathbf{B}]^{(2)}. \quad (\text{A.41})$$

The exterior product of two one-forms corresponds to the cross-product (A.9) of two vectors. The exterior product of a one-form \mathcal{A} and a two-form \mathcal{D} is

$$\begin{aligned}\mathcal{A} \wedge \mathcal{D} &= (A_x dx + A_y dy + A_z dz) \wedge (D_x dy \wedge dz + D_y dz \wedge dx + D_z dx \wedge dy) \\ &= (A_x D_x + A_y D_y + A_z D_z) dx \wedge dy \wedge dz.\end{aligned}\tag{A.42}$$

The relation to vector notation is given by

$$\mathcal{A} = [\mathbf{A}]^{(1)}, \quad \mathcal{D} = [\mathbf{D}]^{(2)} \quad \rightarrow \quad \mathcal{A} \wedge \mathcal{D} = [\mathbf{A} \cdot \mathbf{D}]^{(3)}.\tag{A.43}$$

The exterior product of a one-form with a two-form corresponds to the scalar product (A.5) of two vectors. The exterior product of three one-forms \mathcal{A} , \mathcal{B} , and \mathcal{C} is

$$\begin{aligned}\mathcal{A} \wedge \mathcal{B} \wedge \mathcal{C} &= (A_x dx + A_y dy + A_z dz) \wedge (B_x dx + B_y dy + B_z dz) \\ &\quad \wedge (C_x dx + C_y dy + C_z dz) \\ &= (A_x B_y C_z + A_y B_z C_x + A_z B_x C_y \\ &\quad - A_z B_y C_x - A_x B_z C_y - A_y B_x C_z) dx \wedge dy \wedge dz.\end{aligned}\tag{A.44}$$

The relation to vector notation is given by

$$\mathcal{A} = [\mathbf{A}]^{(1)}, \quad \mathcal{B} = [\mathbf{B}]^{(1)}, \quad \mathcal{C} = [\mathbf{C}]^{(1)} \quad \rightarrow \quad \mathcal{A} \wedge \mathcal{B} \wedge \mathcal{C} = [[\mathbf{A}\mathbf{B}\mathbf{C}]]^{(3)}.\tag{A.45}$$

The exterior product of three one-forms corresponds to the triple scalar product (A.18) of three vectors.

A.2.2 The Contraction

The *contraction* $\mathcal{A} \lrcorner \mathcal{B}$ of two differential forms \mathcal{A} and \mathcal{B} is defined via

$$dx_i \lrcorner dx_j = \delta_{ij} \quad \text{with } dx_i, dx_j = dx, dy, dz,\tag{A.46}$$

$$\mathcal{A} \lrcorner (\mathcal{B} \wedge \mathcal{C}) = (\mathcal{A} \lrcorner \mathcal{B}) \wedge \mathcal{C} + (-1)^{\deg(\mathcal{A})} \mathcal{B} \wedge (\mathcal{A} \lrcorner \mathcal{C}).\tag{A.47}$$

The symbol \lrcorner is named “angle” and the contraction also is called *angle product*. The angle product has been introduced by Burke [4]. We use the modified form given by Warnick [8].

The contraction operator is useful to obtain the tangential component of a one-form or the normal component of a two-form with respect to a surface. For a one-form \mathcal{E} and a two-form \mathcal{D} we obtain

$$dz \lrcorner (dz \wedge \mathcal{E}) = E_x dx + E_y dy,\tag{A.48}$$

$$dz \lrcorner (dz \wedge \mathcal{D}) = D_z dx \wedge dy.\tag{A.49}$$

The contraction may also be expressed via the Hodge operator by

$$\mathcal{A} \lrcorner \mathcal{B} = *(\star \mathcal{B} \wedge \mathcal{A}) . \quad (\text{A.50})$$

This relation vice versa sometimes is used to define the Hodge operator via the contraction [9]

$$\star \mathcal{A} = \mathcal{A} \lrcorner dx \wedge dy \wedge dz . \quad (\text{A.51})$$

A.2.3 The Exterior Derivative

The *exterior derivative* $d\mathcal{U}$ of an exterior differential form \mathcal{U} is defined as

$$d\mathcal{U} = \sum_i dx_i \wedge \frac{\partial \mathcal{U}}{\partial x_i} . \quad (\text{A.52})$$

For the exterior differentiation the following product rules are valid:

$$d(\mathcal{U} + \mathcal{V}) = d\mathcal{U} + d\mathcal{V} , \quad (\text{A.53})$$

$$d(\mathcal{U} \wedge \mathcal{V}) = d\mathcal{U} \wedge \mathcal{V} + (-1)^{(\deg \mathcal{U})} \mathcal{U} \wedge d\mathcal{V} . \quad (\text{A.54})$$

The exterior derivatives of p -forms are

$$\text{zero-form:} \quad df(\mathbf{x}) = \frac{\partial f}{\partial x} dx + \frac{\partial f}{\partial y} dy + \frac{\partial f}{\partial z} dz , \quad (\text{A.55})$$

$$\begin{aligned} \text{one-form:} \quad d\mathcal{U}(\mathbf{x}) = & \left(\frac{\partial U_z}{\partial y} - \frac{\partial U_y}{\partial z} \right) dy \wedge dz + \left(\frac{\partial U_x}{\partial z} - \frac{\partial U_z}{\partial x} \right) dz \wedge dx \\ & + \left(\frac{\partial U_y}{\partial x} - \frac{\partial U_x}{\partial y} \right) dx \wedge dy , \end{aligned} \quad (\text{A.56})$$

$$\text{two-form:} \quad d\mathcal{V}(\mathbf{x}) = \left(\frac{\partial V_x}{\partial x} + \frac{\partial V_y}{\partial y} + \frac{\partial V_z}{\partial z} \right) dx \wedge dy \wedge dz , \quad (\text{A.57})$$

$$\text{three-form:} \quad d\mathcal{Q}(\mathbf{x}) = 0 . \quad (\text{A.58})$$

The exterior derivative of a product of a p -form \mathcal{A} with q -form \mathcal{B} is given by

$$d(\mathcal{A} \wedge \mathcal{B}) = d\mathcal{A} \wedge \mathcal{B} + (-1)^p \mathcal{A} \wedge d\mathcal{B} . \quad (\text{A.59})$$

A form \mathcal{V} for which $d\mathcal{V} = 0$ is said to be *closed*, and a form \mathcal{V} for which $\mathcal{V} = d\mathcal{U}$ is said to be *exact*. The relation

$$d d\mathcal{U} = 0 \quad (\text{A.60})$$

may be verified easily. For differential forms the statement $\mathcal{V} = d\mathcal{U}$ implies $d\mathcal{V} = 0$. In conventional vector notation this corresponds to $\text{curl grad} = \mathbf{0}$ and $\text{div curl} = 0$. All exact forms are closed. However it may also be shown that all closed forms are exact. Poincaré's lemma [3, 4] states

$$d\mathcal{V} = 0 \quad \leftrightarrow \quad \mathcal{V} = d\mathcal{U}. \quad (\text{A.61})$$

A.2.4 The Laplace Operator

We define the *covariant derivative*, expressed by the operator \tilde{d} , by

$$\tilde{d}\mathcal{U} = (-1)^{\deg \mathcal{U} + 1} \star d \star \mathcal{U}. \quad (\text{A.62})$$

The *Laplace operator* Δ is defined by

$$\Delta = \tilde{d}d + d\tilde{d}. \quad (\text{A.63})$$

From this definition it follows that for any p -form \mathcal{U} , the Laplace operator can be interchanged with the Hodge operator:

$$\Delta \star \mathcal{U} = \star \Delta \mathcal{U}. \quad (\text{A.64})$$

Applying the Laplace operator to a zero-form f , a one-form \mathcal{A} , a two-form \mathcal{B} and a three-form \mathcal{Q} yields

$$\text{zero-form:} \quad \Delta f = \star d \star df, \quad (\text{A.65})$$

$$\text{one-form:} \quad \Delta \mathcal{A} = (d \star d \star - \star d \star d) \mathcal{A}, \quad (\text{A.66})$$

$$\text{two-form:} \quad \Delta \mathcal{B} = (\star d \star d - d \star d \star) \mathcal{B}, \quad (\text{A.67})$$

$$\text{three-form:} \quad \Delta \mathcal{Q} = d \star d \star \mathcal{Q}. \quad (\text{A.68})$$

In Cartesian coordinates the application of the Laplace operator to a zero-form f yields

$$\Delta f = \frac{\partial^2 f}{\partial x^2} + \frac{\partial^2 f}{\partial y^2} + \frac{\partial^2 f}{\partial z^2}. \quad (\text{A.69})$$

To apply the Laplace operator to a one-form \mathcal{A} in Cartesian coordinates, we compute

$$\begin{aligned} \star d \star d \mathcal{A} = & \left(\frac{\partial^2 A_y}{\partial x \partial y} + \frac{\partial^2 A_z}{\partial z \partial x} - \frac{\partial^2 A_x}{\partial y^2} - \frac{\partial^2 A_x}{\partial z^2} \right) dx \\ & + \left(\frac{\partial^2 A_z}{\partial y \partial z} + \frac{\partial^2 A_x}{\partial x \partial y} - \frac{\partial^2 A_y}{\partial z^2} - \frac{\partial^2 A_y}{\partial x^2} \right) dy \\ & + \left(\frac{\partial^2 A_x}{\partial z \partial x} + \frac{\partial^2 A_y}{\partial y \partial z} - \frac{\partial^2 A_z}{\partial x^2} - \frac{\partial^2 A_z}{\partial y^2} \right) dz, \end{aligned} \quad (\text{A.70})$$

$$\begin{aligned}
d \star d \star \mathcal{A} = & \left(\frac{\partial^2 A_x}{\partial x^2} + \frac{\partial^2 A_y}{\partial x \partial y} + \frac{\partial^2 A_z}{\partial x \partial z} \right) dx \\
& + \left(\frac{\partial^2 A_x}{\partial x \partial y} + \frac{\partial^2 A_y}{\partial y^2} + \frac{\partial^2 A_z}{\partial z \partial y} \right) dy \\
& + \left(\frac{\partial^2 A_x}{\partial z \partial x} + \frac{\partial^2 A_y}{\partial y \partial z} + \frac{\partial^2 A_z}{\partial z^2} \right) dz
\end{aligned} \tag{A.71}$$

and from this we obtain

$$\begin{aligned}
\Delta \mathcal{A} = & \left(\frac{\partial^2 A_x}{\partial x^2} + \frac{\partial^2 A_x}{\partial y^2} + \frac{\partial^2 A_x}{\partial z^2} \right) dx + \\
& + \left(\frac{\partial^2 A_y}{\partial x^2} + \frac{\partial^2 A_y}{\partial y^2} + \frac{\partial^2 A_y}{\partial z^2} \right) dy + \\
& + \left(\frac{\partial^2 A_z}{\partial x^2} + \frac{\partial^2 A_z}{\partial y^2} + \frac{\partial^2 A_z}{\partial z^2} \right) dz.
\end{aligned} \tag{A.72}$$

Therefore, in Cartesian coordinates the Laplace operator for one-forms is given by

$$\Delta \mathcal{A} = \frac{\partial^2 \mathcal{A}}{\partial x^2} + \frac{\partial^2 \mathcal{A}}{\partial y^2} + \frac{\partial^2 \mathcal{A}}{\partial z^2} = \Delta A_x dx + \Delta A_y dy + \Delta A_z dz. \tag{A.73}$$

A.3 STOKES' THEOREM

Stokes' theorem relates the integration of a p -form \mathcal{U} over the closed p -dimensional boundary ∂V of a $p+1$ -dimensional volume V to the volume integral of the $p+1$ -form $d\mathcal{U}$ over V via

$$\oint_{\partial V} \mathcal{U} = \int_V d\mathcal{U}. \tag{A.74}$$

In the following we give the proof for the two-dimensional area integral and the three-dimensional volume integral. For a more general discussion of Stokes' theorem, the reader is referred to the literature [3-7]. To give the proof of Stokes' theorem for the area integral we consider the one-form

$$\mathcal{U} = U_x dx + U_y dy + U_z dz \tag{A.75}$$

and its exterior derivative

$$d\mathcal{U} = \left(\frac{\partial U_z}{\partial y} - \frac{\partial U_y}{\partial z} \right) dy \wedge dz + \left(\frac{\partial U_x}{\partial z} - \frac{\partial U_z}{\partial x} \right) dz \wedge dx + \left(\frac{\partial U_y}{\partial x} - \frac{\partial U_x}{\partial y} \right) dx \wedge dy. \tag{A.76}$$

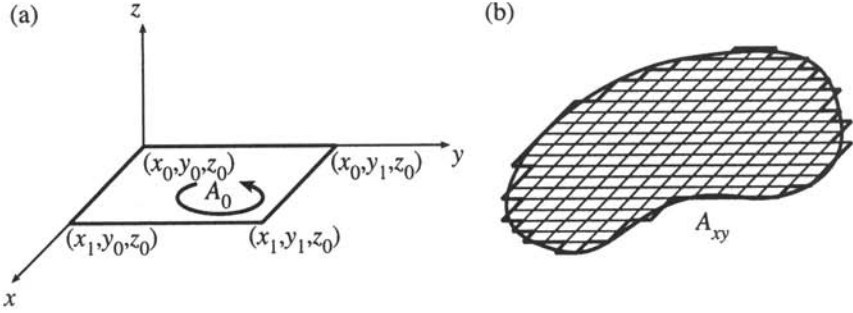


Figure A.3: (a) Surface element, and (b) surface.

Integrating $d\mathcal{U}$ over the rectangular area element A_0 shown in Figure A.3(a) yields

$$\begin{aligned}
 \int_{A_0} d\mathcal{U} &= \int_{A_0} \left(\frac{\partial U_y}{\partial x} - \frac{\partial U_x}{\partial y} \right) dx \wedge dy \\
 &= \int_{y_0}^{y_1} \left(\int_{x_0}^{x_1} \frac{\partial U_y}{\partial x} dx \right) dy - \int_{x_0}^{x_1} \left(\int_{y_0}^{y_1} \frac{\partial U_x}{\partial y} dy \right) dx \\
 &= \int_{y_0}^{y_1} [U_y(x_1, y) - U_y(x_0, y)] dy - \int_{x_0}^{x_1} [U_x(x, y_1) - U_x(x, y_0)] dx \\
 &= \int_{x_0}^{x_1} U_x(x, y_0) dx + \int_{y_0}^{y_1} U_y(x_1, y) dy \\
 &\quad + \int_{x_1}^{x_0} U_x(x, y_1) dx + \int_{y_1}^{y_0} U_y(x_0, y) dy = \oint_{\partial A_0} \mathcal{U}. \tag{A.77}
 \end{aligned}$$

Since the above relation is valid for the rectangular area element in Figure A.3(a), we can approximate an arbitrarily shaped area A_{xy} in the xy -plane by small area elements as shown in Figure A.3(b). The sum of the surface integrals of $d\mathcal{U}$ over the areas of all surface elements is equal to the circulation integrals of \mathcal{U} over the boundaries of all surface elements. We consider that the contributions of the adjacent edges of two neighboring surface elements cancel each other out. Therefore only the path elements through the outer edges contribute to the circulation integral. If we let the side lengths of the area elements go to zero, the approximated area converges to the given area A_{xy} with the smooth boundary ∂A_{xy} and we obtain

$$\int_{A_{xy}} d\mathcal{U} = \oint_{\partial A_{xy}} \mathcal{U}. \tag{A.78}$$

So far we have only considered a plane surface. To derive Stokes' theorem for curved

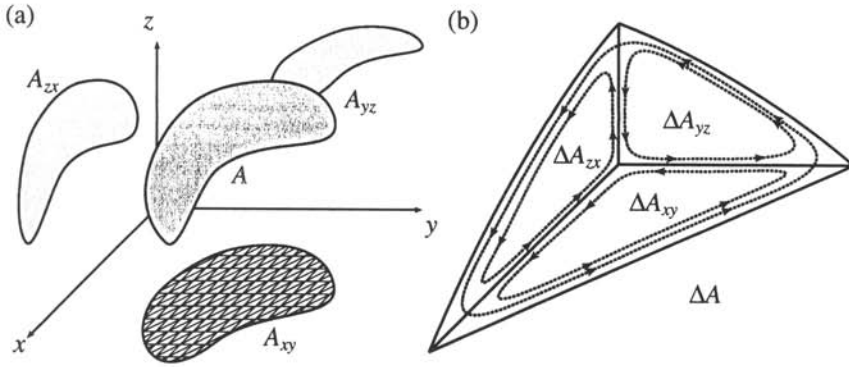


Figure A.4: (a) Curved surface and its projections on the coordinate planes, and (b) triangular surface element.

surfaces in three-dimensional space, we decompose the surface integral into three parts corresponding to the projection of the area A on the three coordinate planes, as shown in Figure A.4(a). We introduce the parametric representation

$$U_i^x(y, z) = U_i(x(y, z), y, z), \quad (\text{A.79})$$

$$U_i^y(z, x) = U_i(x, y(z, x), z), \quad (\text{A.80})$$

$$U_i^z(x, y) = U_i(x, y, z(x, y)). \quad (\text{A.81})$$

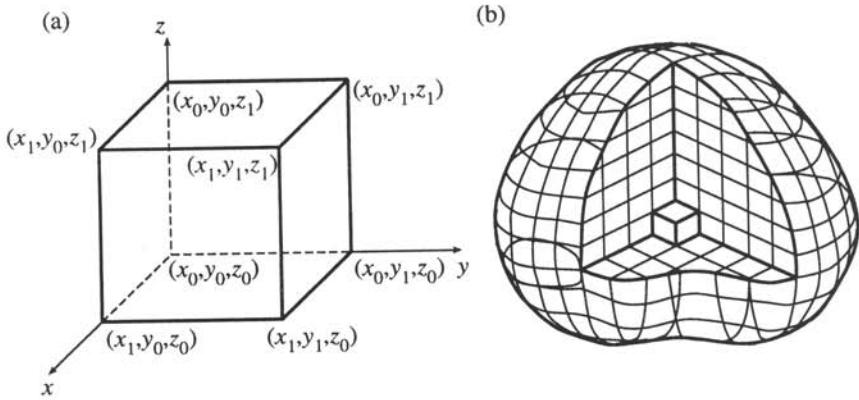
From (A.77) we obtain

$$\int_{A_{xy}} \left(\frac{\partial U_y^z}{\partial x} - \frac{\partial U_x^z}{\partial y} \right) dx \wedge dy = \oint_{\partial A_{xy}} U_x^z dx + U_y^z dy, \quad (\text{A.82})$$

$$\int_{A_{yz}} \left(\frac{\partial U_z^x}{\partial y} - \frac{\partial U_y^x}{\partial z} \right) dy \wedge dz = \oint_{\partial A_{yz}} U_y^x dy + U_z^x dz, \quad (\text{A.83})$$

$$\int_{A_{zx}} \left(\frac{\partial U_x^y}{\partial z} - \frac{\partial U_z^y}{\partial x} \right) dz \wedge dx = \oint_{\partial A_{zx}} U_z^y dz + U_x^y dx. \quad (\text{A.84})$$

We subdivide the area A_{xy} in triangular infinitesimal surface elements as depicted in Figure A.4(a). This generates also a triangular subdivision of the curved surface A . Figure A.4(b) shows one infinitesimal triangular surface element ΔA and its projections on the coordinate planes ΔA_{yz} , ΔA_{zx} , and ΔA_{xy} . The curve integral over the boundary $\partial \Delta A$ is the sum of the curve integrals over the boundaries $\partial \Delta A_{yz}$, $\partial \Delta A_{zx}$ and $\partial \Delta A_{xy}$. In the three coordinate planes the sum over all integrals over the boundaries of the


 Figure A.5: (a) Volume element ΔV and (b) volume V .

area elements $\partial\Delta A_{ij}$ yields the integral over the boundary ∂A_{ij} , and we obtain

$$\oint_{\partial A_{xy}} U_x^z dx + U_y^z dy + \oint_{\partial A_{yz}} U_y^x dy + U_z^x dz + \oint_{\partial A_{zx}} U_z^y dz + U_x^y dx = \oint_{\partial A} U_x dx + U_y dy + U_z dz. \quad (\text{A.85})$$

Inserting (A.82), (A.83) and (A.84) yields Stokes' theorem for curved surfaces

$$\int_A \left[\left(\frac{\partial U_z}{\partial y} - \frac{\partial U_y}{\partial z} \right) dy \wedge dz + \left(\frac{\partial U_x}{\partial z} - \frac{\partial U_z}{\partial x} \right) dz \wedge dx + \left(\frac{\partial U_y}{\partial x} - \frac{\partial U_x}{\partial y} \right) dx \wedge dy \right] = \oint_{\partial A} U_x dx + U_y dy + U_z dz. \quad (\text{A.86})$$

In order to derive Stokes' theorem for three-dimensional volumes we consider an infinitesimal rectangular parallelepiped volume element ΔV as depicted in Figure A.5(a). The integral of the two-form

$$\mathcal{D} = D_x dy \wedge dz + D_y dz \wedge dx + D_z dx \wedge dy \quad (\text{A.87})$$

over the surface $\partial\Delta V$ of the parallelepiped is given by

$$\begin{aligned}\oint_{\partial\Delta V} \mathcal{D} &= \int_{y_0}^{y_1} \int_{z_0}^{z_1} (D_x(x_1, y, z) - D_x(x_0, y, z)) dy \wedge dz \\ &+ \int_{z_0}^{z_1} \int_{x_0}^{x_1} (D_y(x, y_1, z) - D_y(x, y_0, z)) dz \wedge dx \\ &+ \int_{x_0}^{x_1} \int_{y_0}^{y_1} (D_z(x, y, z_1) - D_z(x, y, z_0)) dx \wedge dy .\end{aligned}\quad (\text{A.88})$$

For $\Delta V \rightarrow 0$ this may be approximated by

$$\oint_{\partial\Delta V} \mathcal{D} = \int_{\Delta V} \left(\frac{\partial D_x}{\partial x} + \frac{\partial D_y}{\partial y} + \frac{\partial D_z}{\partial z} \right) dx \wedge dy \wedge dz = \int_{\Delta V} d\mathcal{D} . \quad (\text{A.89})$$

A volume V with boundary ∂V as depicted in Figure A.5(b) may be considered to consist of infinitesimally small rectangular parallelepiped volume elements. The sum of the volume integrals over all volume elements is equal to the volume integral over V . Computing the sum of all surface integrals over the boundaries of the volume cells, we consider that the contributions from adjacent surfaces of neighboring cells cancel each other and only the outer surfaces contribute. The set of the outer surfaces of the volume cells converges to ∂V and we obtain *Stokes' theorem*

$$\oint_{\partial V} \mathcal{D} = \int_V d\mathcal{D} . \quad (\text{A.90})$$

A.4 CURVILINEAR COORDINATES

A three-dimensional *curvilinear coordinate system* with coordinates u, v, w may be defined via embedding in the three-dimensional Cartesian coordinate system x, y, z and specifying the functions

$$\begin{aligned}u &= u(x, y, z) , \\ v &= v(x, y, z) , \\ w &= w(x, y, z) .\end{aligned}\quad (\text{A.91})$$

We can express the differentials dx, dy, dz by the differentials du, dv, dw via

$$dx = \frac{\partial x}{\partial u} du + \frac{\partial x}{\partial v} dv + \frac{\partial x}{\partial w} dw , \quad (\text{A.92})$$

$$dy = \frac{\partial y}{\partial u} du + \frac{\partial y}{\partial v} dv + \frac{\partial y}{\partial w} dw , \quad (\text{A.93})$$

$$dz = \frac{\partial z}{\partial u} du + \frac{\partial z}{\partial v} dv + \frac{\partial z}{\partial w} dw . \quad (\text{A.94})$$

For the exterior product of two differentials we obtain the transformation rule

$$\begin{aligned} dx \wedge dy &= \left(\frac{\partial x}{\partial u} \frac{\partial y}{\partial v} - \frac{\partial x}{\partial v} \frac{\partial y}{\partial u} \right) du \wedge dv \\ &+ \left(\frac{\partial x}{\partial v} \frac{\partial y}{\partial w} - \frac{\partial x}{\partial w} \frac{\partial y}{\partial v} \right) dv \wedge dw \\ &+ \left(\frac{\partial x}{\partial w} \frac{\partial y}{\partial u} - \frac{\partial x}{\partial u} \frac{\partial y}{\partial w} \right) dw \wedge du. \end{aligned} \quad (\text{A.95})$$

This defines the *Jacobian determinant*

$$\frac{\partial(x, y)}{\partial(u, v)} \equiv \begin{vmatrix} \frac{\partial x}{\partial u} & \frac{\partial x}{\partial v} \\ \frac{\partial y}{\partial u} & \frac{\partial y}{\partial v} \end{vmatrix} = \frac{\partial x}{\partial u} \frac{\partial y}{\partial v} - \frac{\partial x}{\partial v} \frac{\partial y}{\partial u}. \quad (\text{A.96})$$

We obtain

$$dx \wedge dy = \frac{\partial(x, y)}{\partial(u, v)} du \wedge dv + \frac{\partial(x, y)}{\partial(v, w)} dv \wedge dw + \frac{\partial(x, y)}{\partial(w, u)} dw \wedge du. \quad (\text{A.97})$$

Analogous equations are obtained for $dy \wedge dz$ and $dz \wedge dx$. To express $du \wedge dv$, $dv \wedge dw$ and $dw \wedge du$ by $dx \wedge dy$, $dy \wedge dz$, and $dz \wedge dx$ insert (A.92)–(A.94) and reorder the terms.

For three-forms we obtain

$$dx \wedge dy \wedge dz = \frac{\partial(x, y, z)}{\partial(u, v, w)} du \wedge dv \wedge dw \quad (\text{A.98})$$

with the Jacobian determinant

$$\frac{\partial(x, y, z)}{\partial(u, v, w)} \equiv \begin{vmatrix} \frac{\partial x}{\partial u} & \frac{\partial x}{\partial v} & \frac{\partial x}{\partial w} \\ \frac{\partial y}{\partial u} & \frac{\partial y}{\partial v} & \frac{\partial y}{\partial w} \\ \frac{\partial z}{\partial u} & \frac{\partial z}{\partial v} & \frac{\partial z}{\partial w} \end{vmatrix}. \quad (\text{A.99})$$

Expanding the Jacobian determinant yields

$$\begin{aligned} \frac{\partial(x, y, z)}{\partial(u, v, w)} &= \frac{\partial x}{\partial u} \frac{\partial y}{\partial v} \frac{\partial z}{\partial w} + \frac{\partial x}{\partial v} \frac{\partial y}{\partial w} \frac{\partial z}{\partial u} + \frac{\partial x}{\partial w} \frac{\partial y}{\partial u} \frac{\partial z}{\partial v} \\ &- \frac{\partial x}{\partial u} \frac{\partial y}{\partial w} \frac{\partial z}{\partial v} - \frac{\partial x}{\partial v} \frac{\partial y}{\partial u} \frac{\partial z}{\partial w} - \frac{\partial x}{\partial w} \frac{\partial y}{\partial v} \frac{\partial z}{\partial u}. \end{aligned} \quad (\text{A.100})$$

Consider the vector $\mathbf{x} = [x, y, z]^T$. The length of a path element is given by

$$ds = \sqrt{d\mathbf{x} \cdot d\mathbf{x}}. \quad (\text{A.101})$$

Using (A.92)–(A.94) we obtain

$$\begin{aligned} d\mathbf{x} \cdot d\mathbf{x} &= dx^2 + dy^2 + dz^2 \\ &= \frac{\partial \mathbf{x}}{\partial u} \cdot \frac{\partial \mathbf{x}}{\partial u} du^2 + \frac{\partial \mathbf{x}}{\partial v} \cdot \frac{\partial \mathbf{x}}{\partial v} dv^2 + \frac{\partial \mathbf{x}}{\partial w} \cdot \frac{\partial \mathbf{x}}{\partial w} dw^2 \\ &\quad + 2 \frac{\partial \mathbf{x}}{\partial u} \cdot \frac{\partial \mathbf{x}}{\partial v} du dv + 2 \frac{\partial \mathbf{x}}{\partial v} \cdot \frac{\partial \mathbf{x}}{\partial w} dv dw + 2 \frac{\partial \mathbf{x}}{\partial w} \cdot \frac{\partial \mathbf{x}}{\partial u} dw du. \end{aligned} \quad (\text{A.102})$$

A coordinate system $u(\mathbf{x}), v(\mathbf{x}), w(\mathbf{x})$ in the three-dimensional Euclidean space with Cartesian coordinates x, y, z is called an *orthogonal coordinate system* if the *tangent vectors* $\partial \mathbf{x} / \partial u, \partial \mathbf{x} / \partial v, \partial \mathbf{x} / \partial w$ are mutually perpendicular. For orthogonal coordinate systems (u, v, w) , the relations

$$\frac{\partial \mathbf{x}}{\partial u} \cdot \frac{\partial \mathbf{x}}{\partial v} = 0, \quad \frac{\partial \mathbf{x}}{\partial v} \cdot \frac{\partial \mathbf{x}}{\partial w} = 0, \quad \frac{\partial \mathbf{x}}{\partial w} \cdot \frac{\partial \mathbf{x}}{\partial u} = 0 \quad (\text{A.103})$$

must be fulfilled. The *metric coefficients* g_1^2, g_2^2 , and g_3^2 defined by

$$g_1^2 = \frac{\partial \mathbf{x}}{\partial u} \cdot \frac{\partial \mathbf{x}}{\partial u}, \quad g_2^2 = \frac{\partial \mathbf{x}}{\partial v} \cdot \frac{\partial \mathbf{x}}{\partial v}, \quad g_3^2 = \frac{\partial \mathbf{x}}{\partial w} \cdot \frac{\partial \mathbf{x}}{\partial w} \quad (\text{A.104})$$

give the lengths of the tangent vectors $\partial \mathbf{x} / \partial u, \partial \mathbf{x} / \partial v$, and $\partial \mathbf{x} / \partial w$ [10]. For suitable functions $g_1(\mathbf{x}), g_2(\mathbf{x}), g_3(\mathbf{x})$ we obtain the *orthonormal basis vectors*

$$\mathbf{e}_1 = \frac{1}{g_1} \frac{\partial \mathbf{x}}{\partial u}, \quad \mathbf{e}_2 = \frac{1}{g_2} \frac{\partial \mathbf{x}}{\partial v}, \quad \mathbf{e}_3 = \frac{1}{g_3} \frac{\partial \mathbf{x}}{\partial w}. \quad (\text{A.105})$$

We attach to each point \mathbf{x} of the three-dimensional Euclidean space a right-handed orthonormal frame $\mathbf{e}_1, \mathbf{e}_2, \mathbf{e}_3$ with

$$\mathbf{e}_i \cdot \mathbf{e}_j = \delta_{ij}, \quad (\text{A.106})$$

where δ_{ij} is the Kronecker delta symbol defined in (A.8).

The orthonormal basis vectors constitute a *moving frame* [3, 4]. Moving frames represent geometric objects in a basis that is tied to intrinsic geometric features of the problem. We presuppose the moving frame $\mathbf{e}_1, \mathbf{e}_2, \mathbf{e}_3$ is right-handed. Otherwise we change the order of the three vectors. We now express $d\mathbf{x}$ by

$$d\mathbf{x} = \frac{\partial \mathbf{x}}{\partial u} du + \frac{\partial \mathbf{x}}{\partial v} dv + \frac{\partial \mathbf{x}}{\partial w} dw. \quad (\text{A.107})$$

Inserting (A.105) yields

$$d\mathbf{x} = g_1 \mathbf{e}_1 du + g_2 \mathbf{e}_2 dv + g_3 \mathbf{e}_3 dw. \quad (\text{A.108})$$

Introducing the *unit one-forms*

$$s_1 = g_1 du, \quad s_2 = g_2 dv, \quad s_3 = g_3 dw \quad (\text{A.109})$$

yields

$$dx = s_1 e_1 + s_2 e_2 + s_3 e_3. \quad (\text{A.110})$$

The *star operator* or *Hodge operator* \star as defined in (A.38) is given by

$$\begin{aligned} \star f &= f s_1 \wedge s_2 \wedge s_3, \\ \star (A_u s_1 + A_v s_2 + A_w s_3) &= A_u s_2 \wedge s_3 + A_v s_3 \wedge s_1 + A_w s_1 \wedge s_2, \\ \star (A_u s_2 \wedge s_3 + A_v s_3 \wedge s_1 + A_w s_1 \wedge s_2) &= A_u s_1 + A_v s_2 + A_w s_3, \\ \star (f s_1 \wedge s_2 \wedge s_3) &= f. \end{aligned} \quad (\text{A.111})$$

Let us now consider the exterior derivative in curvilinear coordinates. The exterior derivative of a zero-form f is given by

$$df = \frac{\partial f}{\partial u} du + \frac{\partial f}{\partial v} dv + \frac{\partial f}{\partial w} dw. \quad (\text{A.112})$$

Inserting (A.109) yields

$$df = \frac{1}{g_1} \frac{\partial f}{\partial u} s_1 + \frac{1}{g_2} \frac{\partial f}{\partial v} s_2 + \frac{1}{g_3} \frac{\partial f}{\partial w} s_3. \quad (\text{A.113})$$

In conventional vector analysis the exterior derivative of a zero-form corresponds to the application of the gradient operator:

$$\text{grad } f = \frac{1}{g_1} \frac{\partial f}{\partial u} e_1 + \frac{1}{g_2} \frac{\partial f}{\partial v} e_2 + \frac{1}{g_3} \frac{\partial f}{\partial w} e_3. \quad (\text{A.114})$$

We compute the exterior derivative of a one-form \mathcal{A} , given by

$$\mathcal{A} = A_u s_1 + A_v s_2 + A_w s_3. \quad (\text{A.115})$$

With (A.109) we obtain

$$\mathcal{A} = g_1 A_u du + g_2 A_v dv + g_3 A_w dw. \quad (\text{A.116})$$

Forming the exterior derivative yields

$$\begin{aligned} d\mathcal{A} = & \left(\frac{\partial(g_2 A_v)}{\partial u} - \frac{\partial(g_1 A_u)}{\partial v} \right) du \wedge dv \\ & + \left(\frac{\partial(g_3 A_w)}{\partial v} - \frac{\partial(g_2 A_v)}{\partial w} \right) dv \wedge dw \\ & + \left(\frac{\partial(g_1 A_u)}{\partial w} - \frac{\partial(g_3 A_w)}{\partial u} \right) dw \wedge du \end{aligned} \quad (\text{A.117})$$

and after again inserting (A.109) we obtain

$$\begin{aligned} d\mathcal{A} = & \frac{1}{g_2 g_3} \left(\frac{\partial(g_3 A_w)}{\partial v} - \frac{\partial(g_2 A_v)}{\partial w} \right) s_2 \wedge s_3 \\ & + \frac{1}{g_3 g_1} \left(\frac{\partial(g_1 A_u)}{\partial w} - \frac{\partial(g_3 A_w)}{\partial u} \right) s_3 \wedge s_1 \\ & + \frac{1}{g_1 g_2} \left(\frac{\partial(g_2 A_v)}{\partial u} - \frac{\partial(g_1 A_u)}{\partial v} \right) s_1 \wedge s_2 . \end{aligned} \quad (\text{A.118})$$

In conventional vector analysis the exterior derivative of a one-form corresponds to the curl operator:

$$\begin{aligned} \text{curl } A = & \frac{1}{g_2 g_3} \left(\frac{\partial(g_3 A_w)}{\partial v} - \frac{\partial(g_2 A_v)}{\partial w} \right) e_1 \\ & + \frac{1}{g_3 g_1} \left(\frac{\partial(g_1 A_u)}{\partial w} - \frac{\partial(g_3 A_w)}{\partial u} \right) e_2 \\ & + \frac{1}{g_1 g_2} \left(\frac{\partial(g_2 A_v)}{\partial u} - \frac{\partial(g_1 A_u)}{\partial v} \right) e_3 . \end{aligned} \quad (\text{A.119})$$

To compute the exterior derivative of a two-form \mathcal{B} , given by

$$\mathcal{B} = B_u s_2 \wedge s_3 + B_v s_3 \wedge s_1 + B_w s_1 \wedge s_2 \quad (\text{A.120})$$

first we insert (A.109) and obtain

$$\mathcal{B} = g_2 g_3 B_u dv \wedge dw + g_3 g_1 B_v dw \wedge du + g_1 g_2 B_w du \wedge dv . \quad (\text{A.121})$$

After applying the exterior derivative and again inserting (A.109), we obtain

$$d\mathcal{B} = \frac{1}{g_1 g_2 g_3} \left[\frac{\partial(g_2 g_3 B_u)}{\partial u} + \frac{\partial(g_3 g_1 B_v)}{\partial v} + \frac{\partial(g_1 g_2 B_w)}{\partial w} \right] s_1 \wedge s_2 \wedge s_3 . \quad (\text{A.122})$$

In conventional vector analysis the exterior derivative of a two-form corresponds to the divergence operator:

$$\operatorname{div} \mathbf{B} = \frac{1}{g_1 g_2 g_3} \left[\frac{\partial(g_2 g_3 B_u)}{\partial u} + \frac{\partial(g_3 g_1 B_v)}{\partial v} + \frac{\partial(g_1 g_2 B_w)}{\partial w} \right]. \quad (\text{A.123})$$

Let us now apply the Laplace operator (3.12) to a scalar field f . From (3.13) we obtain

$$\Delta f = \star d \star df. \quad (\text{A.124})$$

We start with

$$df = \frac{\partial f}{\partial u} du + \frac{\partial f}{\partial v} dv + \frac{\partial f}{\partial w} dw. \quad (\text{A.125})$$

Inserting (A.109) yields

$$df = \frac{1}{g_1} \frac{\partial f}{\partial u} s_1 + \frac{1}{g_2} \frac{\partial f}{\partial v} s_2 + \frac{1}{g_3} \frac{\partial f}{\partial w} s_3. \quad (\text{A.126})$$

Applying the star operator (A.111) gives

$$\star df = \frac{1}{g_1} \frac{\partial f}{\partial u} s_2 \wedge s_3 + \frac{1}{g_2} \frac{\partial f}{\partial v} s_3 \wedge s_1 + \frac{1}{g_3} \frac{\partial f}{\partial w} s_1 \wedge s_2, \quad (\text{A.127})$$

and with (A.109) we obtain

$$\star df = \frac{g_2 g_3}{g_1} \frac{\partial f}{\partial u} dv \wedge dw + \frac{g_3 g_1}{g_2} \frac{\partial f}{\partial v} dw \wedge du + \frac{g_1 g_2}{g_3} \frac{\partial f}{\partial w} du \wedge dv. \quad (\text{A.128})$$

We now compute again the exterior derivative

$$\begin{aligned} d \star df = & \left[\frac{\partial}{\partial u} \left(\frac{g_2 g_3}{g_1} \frac{\partial f}{\partial u} \right) + \frac{\partial}{\partial v} \left(\frac{g_3 g_1}{g_2} \frac{\partial f}{\partial v} \right) \right. \\ & \left. + \frac{\partial}{\partial w} \left(\frac{g_1 g_2}{g_3} \frac{\partial f}{\partial w} \right) \right] du \wedge dv \wedge dw, \quad (\text{A.129}) \end{aligned}$$

and obtain with (A.109)

$$\begin{aligned} d \star df = & \frac{1}{g_1 g_2 g_3} \left[\frac{\partial}{\partial u} \left(\frac{g_2 g_3}{g_1} \frac{\partial f}{\partial u} \right) + \frac{\partial}{\partial v} \left(\frac{g_3 g_1}{g_2} \frac{\partial f}{\partial v} \right) \right. \\ & \left. + \frac{\partial}{\partial w} \left(\frac{g_1 g_2}{g_3} \frac{\partial f}{\partial w} \right) \right] s_1 \wedge s_2 \wedge s_3. \quad (\text{A.130}) \end{aligned}$$

Using (A.124) and (A.111) yields

$$\Delta f = \frac{1}{g_1 g_2 g_3} \left[\frac{\partial}{\partial u} \left(\frac{g_2 g_3}{g_1} \frac{\partial f}{\partial u} \right) + \frac{\partial}{\partial v} \left(\frac{g_3 g_1}{g_2} \frac{\partial f}{\partial v} \right) + \frac{\partial}{\partial w} \left(\frac{g_1 g_2}{g_3} \frac{\partial f}{\partial w} \right) \right]. \quad (\text{A.131})$$

A.4.1 General Cylindrical Coordinates

A *general cylindrical coordinate system* is linear and translationally invariant in one direction (i.e., the longitudinal direction and curvilinear in the transverse directions). Let the z -direction be the longitudinal direction and u and v the transverse coordinates. In this case the coordinates are u, v, z and the unit differential forms are

$$s_1 = g_1 du, \quad s_2 = g_2 dv, \quad s_3 = dz. \quad (\text{A.132})$$

In the treatment of field problems in general curvilinear coordinates it often is useful to separate field functions $\Psi(u, v, z)$ in a transverse part $\psi(u, v)$ and a longitudinal part $f(z)$:

$$\Psi(u, v, z) = \psi(u, v) f(z). \quad (\text{A.133})$$

We can separate the exterior derivative (A.112) in a *transverse exterior derivative* d_t and the longitudinal derivative (i.e., the derivative with respect to the z -coordinate).

$$d = d_t + \frac{\partial}{\partial z} dz \quad (\text{A.134})$$

with the transverse derivative given by

$$d_t = \frac{\partial}{\partial u} du + \frac{\partial}{\partial v} dv. \quad (\text{A.135})$$

The exterior derivative of the three-dimensional scalar function $\Psi(x, y, z)$ given in (A.133) can be expressed as

$$d\Psi(u, v, z) = (d_t \psi(u, v)) f(z) + \psi(u, v) \frac{\partial f(z)}{\partial z} dz. \quad (\text{A.136})$$

The scalar Laplace operator (A.124) becomes

$$\Delta = \Delta_t + \frac{\partial^2}{\partial z^2} \quad (\text{A.137})$$

with the *transverse Laplace operator* or *two-dimensional Laplace operator* Δ_t given by

$$\Delta_t f = \frac{1}{g_1 g_2} \left[\frac{\partial}{\partial u} \left(\frac{g_2}{g_1} \frac{\partial f}{\partial u} \right) + \frac{\partial}{\partial v} \left(\frac{g_1}{g_2} \frac{\partial f}{\partial v} \right) \right]. \quad (\text{A.138})$$

Applying the Laplace operator to $\Psi(x, y, z)$ yields

$$\Delta\Psi(u, v, z) = (\Delta_t\Psi(u, v))f(z) + \psi(u, v)\frac{\partial^2 f(z)}{\partial z^2}. \quad (\text{A.139})$$

In Cartesian coordinates x, y, z with z being the longitudinal coordinate and x, y being the transverse coordinates, the transverse exterior derivative is

$$d_t = \frac{\partial}{\partial x} dx + \frac{\partial}{\partial y} dy \quad (\text{A.140})$$

and the transverse Laplace operator is

$$\Delta_t = \frac{\partial^2}{\partial x^2} + \frac{\partial^2}{\partial y^2}. \quad (\text{A.141})$$

A.4.2 Circular Cylindric Coordinates

To deal with circular cylindrical electromagnetic structures we introduce *circular cylindrical coordinates*. Figure A.6 shows the circular cylindrical coordinates. The coordinates ρ, ϕ, z are defined in the following intervals:

$$\begin{aligned} u &= \rho, & 0 &\leq \rho < \infty, \\ v &= \phi, & 0 &\leq \phi < 2\pi, \\ w &= z, & -\infty &< z < +\infty. \end{aligned} \quad (\text{A.142})$$

The circular cylindric coordinates ρ, ϕ, z are related to the Cartesian coordinates x, y, z via

$$x = \rho \cos \phi \quad y = \rho \sin \phi \quad z = z \quad (\text{A.143})$$

and

$$\rho = \sqrt{x^2 + y^2} \quad \phi = \arctan \frac{y}{x} \quad z = z. \quad (\text{A.144})$$

Inserting (A.143) into (A.104) yields the metric coefficients of the circular cylindrical coordinate system:

$$g_1 = 1 \quad g_2 = \rho \quad g_3 = 1 \quad (\text{A.145})$$

and the unit forms

$$s_1 = d\rho \quad s_2 = \rho d\phi \quad s_3 = dz. \quad (\text{A.146})$$

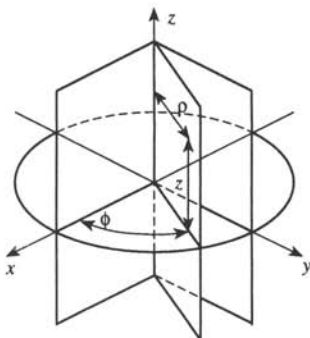


Figure A.6: Circular cylindric coordinates.

The components of the p -forms are referred to the unit forms and given by

$$\begin{aligned}
 \text{zero-form:} & \quad f(\mathbf{x}), \\
 \text{one-form:} & \quad \mathcal{E}(\mathbf{x}) = E_\rho d\rho + E_\phi \rho d\phi + E_z dz, \\
 \text{two-form:} & \quad \mathcal{D}(\mathbf{x}) = D_\rho \rho d\phi \wedge dz + D_\phi dz \wedge d\rho + D_z \rho d\rho \wedge d\phi, \\
 \text{three-form:} & \quad \mathcal{Q}(\mathbf{x}) = \rho_{el} \rho d\rho \wedge d\phi \wedge dz.
 \end{aligned} \tag{A.147}$$

From (A.111) and (A.146) we obtain

$$\begin{aligned}
 *f &= f \rho d\rho \wedge d\phi \wedge dz, \\
 *(A_\rho d\rho + A_\phi \rho d\phi + A_z dz) &= A_\rho \rho d\phi \wedge dz + A_\phi dz \wedge d\rho + A_z \rho d\rho \wedge d\phi.
 \end{aligned} \tag{A.148}$$

The length ds of a path element is given by

$$ds = \sqrt{(d\rho)^2 + \rho^2(d\phi)^2 + (dz)^2}. \tag{A.149}$$

In circular cylindrical coordinates the exterior differential operator is

$$d\mathcal{A} = d\rho \wedge \frac{\partial \mathcal{A}}{\partial \rho} + d\phi \wedge \frac{\partial \mathcal{A}}{\partial \phi} + dz \wedge \frac{\partial \mathcal{A}}{\partial z}. \tag{A.150}$$

From (A.113) and (A.145) we obtain the exterior derivative of a zero-form f

$$df = \frac{\partial f}{\partial \rho} d\rho + \frac{1}{\rho} \frac{\partial f}{\partial \phi} \rho d\phi + \frac{\partial f}{\partial z} dz. \tag{A.151}$$

The corresponding relation in conventional vector notation is

$$\text{grad } f = \mathbf{e}_\rho \frac{\partial f}{\partial \rho} + \mathbf{e}_\phi \frac{1}{\rho} \frac{\partial f}{\partial \phi} + \mathbf{e}_z \frac{\partial f}{\partial z}. \quad (\text{A.152})$$

From (A.118) and (A.145) we obtain the exterior derivative of a one-form

$$\begin{aligned} dA = \frac{1}{\rho} \left(\frac{\partial A_z}{\partial \phi} - \frac{\partial(\rho A_\phi)}{\partial z} \right) \rho d\phi \wedge dz + \left(\frac{\partial A_\rho}{\partial z} - \frac{\partial A_z}{\partial \rho} \right) dz \wedge d\rho \\ + \frac{1}{\rho} \left(\frac{\partial(\rho A_\phi)}{\partial \rho} - \frac{\partial A_\rho}{\partial \phi} \right) \rho d\rho \wedge d\phi. \end{aligned} \quad (\text{A.153})$$

In conventional vector analysis the exterior derivative of a one-form corresponds to the curl operator:

$$\text{curl } A = \frac{1}{\rho} \left(\frac{\partial A_z}{\partial \phi} - \frac{\partial(\rho A_\phi)}{\partial z} \right) \mathbf{e}_\rho + \left(\frac{\partial A_\rho}{\partial z} - \frac{\partial A_z}{\partial \rho} \right) \mathbf{e}_\phi + \frac{1}{\rho} \left(\frac{\partial(\rho A_\phi)}{\partial \rho} - \frac{\partial A_\rho}{\partial \phi} \right) \mathbf{e}_z. \quad (\text{A.154})$$

From (A.122) and (A.145) we obtain the derivative of a two-form \mathcal{D}

$$d\mathcal{D} = \frac{1}{\rho} \left[\frac{\partial(\rho D_\rho)}{\partial \rho} + \frac{\partial D_\phi}{\partial \phi} + \frac{\partial(\rho D_z)}{\partial z} \right] \rho d\rho \wedge d\phi \wedge dz. \quad (\text{A.155})$$

In conventional vector analysis the exterior derivative of a two-form corresponds to the divergence:

$$\text{div } \mathbf{D} = \frac{1}{\rho} \left[\frac{\partial(\rho D_\rho)}{\partial \rho} + \frac{\partial D_\phi}{\partial \phi} + \frac{\partial(\rho D_z)}{\partial z} \right]. \quad (\text{A.156})$$

From (A.124) and (A.145) we determine that the scalar Laplace operator in circular cylindric coordinates

$$\Delta f = \frac{\partial^2 f}{\partial \rho^2} + \frac{1}{\rho} \frac{\partial f}{\partial \rho} + \frac{1}{\rho^2} \frac{\partial^2 f}{\partial \phi^2} + \frac{\partial^2 f}{\partial z^2}. \quad (\text{A.157})$$

In circular cylindric coordinates the Laplace operator applied to a one-form \mathcal{A} yields

$$\begin{aligned} \Delta \mathcal{A} = d\rho \left(\Delta A_\rho - \frac{1}{\rho^2} A_\rho - \frac{2}{\rho^2} \frac{\partial A_\phi}{\partial \phi} \right) \\ + \rho d\phi \left(\Delta A_\phi - \frac{1}{\rho^2} A_\phi + \frac{2}{\rho^2} \frac{\partial A_\rho}{\partial \phi} \right) + dz \Delta A_z. \end{aligned} \quad (\text{A.158})$$

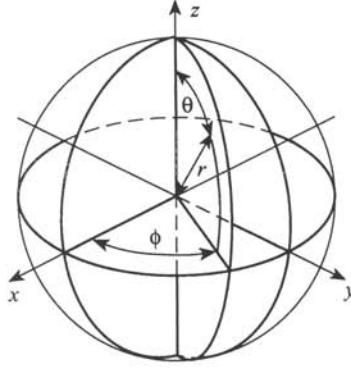


Figure A.7: Spherical coordinates.

The Laplace operator on the right-hand side of this differential equation is the scalar Laplace operator as defined in (A.157). If the one-form \mathcal{A} exhibits only a z -component, the explicit Laplace operator for the one-form reduces to the explicit Laplace operator for the zero-form.

A.4.3 Spherical Coordinates

The analysis of electromagnetic structures with spherical symmetry usually is performed in *spherical coordinates*. Figure A.7 shows the spherical coordinates. The coordinates r, ϕ, θ are defined in the following intervals:

$$\begin{aligned} u &= r, & 0 \leq r < \infty, \\ v &= \theta, & 0 \leq \theta \leq \pi, \\ w &= \phi, & 0 \leq \phi < 2\pi. \end{aligned} \quad (\text{A.159})$$

The spherical coordinates r, θ, ϕ are related to the Cartesian coordinates x, y, z via

$$x = r \sin \theta \cos \phi \quad y = r \sin \theta \sin \phi \quad z = r \cos \theta \quad (\text{A.160})$$

and

$$r = \sqrt{x^2 + y^2 + z^2} \quad \theta = \arctan \frac{\sqrt{x^2 + y^2}}{z} \quad \phi = \arctan \frac{y}{x}. \quad (\text{A.161})$$

Inserting (A.160) into (A.104) yields the metric coefficients of the spherical coordinate system:

$$g_1 = 1 \quad g_2 = r \quad g_3 = r \sin \theta \quad (\text{A.162})$$

and the unit differential forms

$$s_1 = dr \quad s_2 = r d\theta \quad s_3 = r \sin \theta d\phi. \quad (\text{A.163})$$

The components of the p -forms are referred to the unit forms and given by

$$\begin{aligned} \text{zero-form: } & f(x), \\ \text{one-form: } & \mathcal{E}(x) = E_r dr + E_\theta r d\theta + E_\phi r \sin \theta d\phi, \\ \text{two-form: } & \mathcal{D}(x) = D_r r^2 \sin \theta d\theta \wedge d\phi + D_\theta r \sin \theta d\phi \wedge dr + D_\phi r dr \wedge d\theta, \\ \text{three-form: } & \mathcal{Q}(x) = \rho r^2 \sin \theta dr \wedge d\theta \wedge d\phi. \end{aligned} \quad (\text{A.164})$$

From (A.111) and (A.163) we obtain

$$\begin{aligned} *f &= f r^2 \sin \theta dr \wedge d\theta \wedge d\phi, \\ *(A_r dr + A_\theta r d\theta + A_\phi r \sin \theta d\phi) &= A_r r^2 \sin \theta d\theta \wedge d\phi + A_\theta r \sin \theta d\phi \wedge dr \\ &\quad + A_\phi r dr \wedge d\theta. \end{aligned} \quad (\text{A.165})$$

The length ds of a path element is given by

$$ds = \sqrt{(dr)^2 + r^2(d\theta)^2 + r^2 \sin^2 \theta (d\phi)^2}. \quad (\text{A.166})$$

In spherical coordinates the exterior differential operator is

$$d\mathcal{A} = dr \wedge \frac{\partial \mathcal{A}}{\partial r} + d\theta \wedge \frac{\partial \mathcal{A}}{\partial \theta} + d\phi \wedge \frac{\partial \mathcal{A}}{\partial \phi}. \quad (\text{A.167})$$

From (A.113) and (A.163) we obtain the exterior derivative of a zero-form f

$$df = \frac{\partial f}{\partial r} dr + \frac{1}{r} \frac{\partial f}{\partial \theta} r d\theta + \frac{1}{r \sin \theta} \frac{\partial f}{\partial \phi} r \sin \theta d\phi. \quad (\text{A.168})$$

The corresponding relation in conventional vector notation is

$$\text{grad } f = \mathbf{e}_r \frac{\partial f}{\partial r} + \mathbf{e}_\theta \frac{1}{r} \frac{\partial f}{\partial \theta} + \mathbf{e}_\phi \frac{1}{r \sin \theta} \frac{\partial f}{\partial \phi}. \quad (\text{A.169})$$

From (A.117) and (A.163) we obtain the exterior derivative of a one-form

$$\begin{aligned} d\mathcal{A} &= \frac{1}{r^2 \sin \theta} \left(\frac{\partial(r \sin \theta A_\phi)}{\partial \theta} - \frac{\partial(r A_\theta)}{\partial \phi} \right) r^2 \sin \theta d\theta \wedge d\phi \\ &\quad + \frac{1}{r \sin \theta} \left(\frac{\partial A_r}{\partial \phi} - \frac{\partial(r \sin \theta A_\phi)}{\partial r} \right) r \sin \theta d\phi \wedge dr \\ &\quad + \frac{1}{r} \left(\frac{\partial(r A_\theta)}{\partial r} - \frac{\partial A_r}{\partial \theta} \right) r dr \wedge d\theta. \end{aligned} \quad (\text{A.170})$$

In conventional vector analysis the exterior derivative of a one-form corresponds to the curl operator:

$$\begin{aligned}\text{curl } \mathbf{A} &= \frac{1}{r^2 \sin \theta} \left(\frac{\partial(r \sin \theta A_\phi)}{\partial \theta} - \frac{\partial(r A_\theta)}{\partial \phi} \right) \mathbf{e}_r \\ &+ \frac{1}{r \sin \theta} \left(\frac{\partial A_r}{\partial \phi} - \frac{\partial(r \sin \theta A_\phi)}{\partial r} \right) \mathbf{e}_\theta \\ &+ \frac{1}{r} \left(\frac{\partial(r A_\theta)}{\partial r} - \frac{\partial A_r}{\partial \theta} \right) \mathbf{e}_\phi.\end{aligned}\quad (\text{A.171})$$

From (A.118) and (A.163) we obtain the derivative of a two-form \mathcal{B}

$$d\mathcal{B} = \frac{1}{r^2 \sin \theta} \left[\frac{\partial(r^2 \sin \theta B_r)}{\partial r} + \frac{\partial(r \sin \theta B_\theta)}{\partial \theta} + \frac{\partial(r B_\phi)}{\partial \phi} \right] r^2 \sin \theta dr \wedge d\theta \wedge d\phi.\quad (\text{A.172})$$

In conventional vector analysis the exterior derivative of a two-form corresponds to the divergence operator:

$$\text{div } \mathbf{B} = \frac{1}{r^2 \sin \theta} \left[\frac{\partial(r^2 \sin \theta B_r)}{\partial r} + \frac{\partial(r \sin \theta B_\theta)}{\partial \theta} + \frac{\partial(r B_\phi)}{\partial \phi} \right].\quad (\text{A.173})$$

From (A.124) and (A.163) we obtain the scalar Laplace operator for a zero-form f

$$\Delta f = \frac{1}{r^2} \frac{\partial}{\partial r} \left(r^2 \frac{\partial f}{\partial r} \right) + \frac{1}{r^2 \sin \theta} \frac{\partial}{\partial \theta} \left(\sin \theta \frac{\partial f}{\partial \theta} \right) + \frac{1}{r^2 \sin^2 \theta} \frac{\partial^2 f}{\partial \phi^2}.\quad (\text{A.174})$$

The Laplace operator for a one-form \mathcal{A} is given by

$$\begin{aligned}\Delta \mathcal{A} &= dr \left(\Delta A_r - \frac{2}{r^2} A_r - \frac{2}{r^2} \frac{\partial A_\theta}{\partial \theta} - \frac{2 \cot \theta}{r^2} A_\theta - \frac{2}{r^2 \sin \theta} \frac{\partial A_\phi}{\partial \phi} \right) \\ &+ r d\theta \left(\frac{2}{r^2} \frac{\partial A_r}{\partial \theta} + \Delta A_\theta - \frac{1}{r^2 \sin^2 \theta} A_\theta - \frac{2 \cot \theta}{r^2 \sin \theta} \frac{\partial A_\phi}{\partial \phi} \right) \\ &+ r \sin \theta d\phi \left(\frac{2}{r^2 \sin \theta} \frac{\partial A_r}{\partial \phi} + \frac{2 \cot \theta}{r^2 \sin \theta} \frac{\partial A_\theta}{\partial \phi} + \Delta A_\phi - \frac{1}{r^2 \sin^2 \theta} A_\phi \right).\end{aligned}\quad (\text{A.175})$$

The Laplace operator on the right-hand side of this differential equation is the scalar Laplace operator as defined in (A.174).

A.4.4 Twisted Forms

To describe a surface and its neighborhood we introduce a right-handed curvilinear orthogonal coordinate system u, v, n , where u, v are coordinates tangential to the surface and the coordinate n is normal to the surface. The tangential unit one-forms s_1 and s_2 and the normal unit one-form n are defined as in (2.138).

To transform an ordinary one-form into a *twisted one-form* and vice versa we introduce the *twist operator* by

$$\perp_n \mathcal{U} = \star (n \wedge \mathcal{U}), \quad (\text{A.176})$$

where n is a unit normal form (i.e., a unit form as defined in (2.138) that is normal to a coordinate surface). We restrict our consideration to surfaces that are coordinate surfaces in orthogonal coordinate systems. In most cases it is possible to introduce such a coordinate system at least locally. The index n of the twist operator \perp_n denotes the axis of rotation. If u, v are the coordinates tangential to the surface and n is the coordinate normal to the surface, the application of the twist operator \perp_n to a one-form tangential to the surface rotates the one-form around n by 90° in the positive direction,

$$\perp_n (U_u s_1 + U_v s_2) = -U_v s_1 + U_u s_2, \quad (\text{A.177})$$

$$\perp_n (U_v s_1 - U_u s_2) = U_u s_1 + U_v s_2. \quad (\text{A.178})$$

From this it follows that two-fold application of the twist operator \perp_n to a one-form tangential to the surface inverts this one-form,

$$\perp_n^2 \mathcal{U} = -\mathcal{U} \quad \text{for } n \lrcorner \mathcal{U} = 0. \quad (\text{A.179})$$

We note that the use of the term twisted forms is distinct from that given by Burke [11].

A.4.5 Integration of Differential Forms by Pullback

In contrast to the integration of vector fields the integration of differential forms requires no metric. The integration of differentials can be done simply by the *method of pullback* [12]. If a path integral

$$\int_P \mathcal{A} \quad (\text{A.180})$$

over the path P has to be evaluated, and the path P is parametrized by

$$x = p_1(t), \quad y = p_2(t), \quad z = p_3(t) \quad (\text{A.181})$$

for $t_1 \leq t \leq t_2$, we introduce the *pullback* of \mathcal{A} to the path P , defined by

$$\begin{aligned} P^{\triangleleft} \mathcal{A} &= P^{\triangleleft} (A_x dx + A_y dy + A_z dz) \\ &= A_x(p_1, p_2, p_3) dp_1 + A_y(p_1, p_2, p_3) dp_2 + A_z(p_1, p_2, p_3) dp_3 \\ &= \left(A_x(p_1, p_2, p_3) \frac{\partial p_1}{\partial t} + A_y(p_1, p_2, p_3) \frac{\partial p_2}{\partial t} + A_z(p_1, p_2, p_3) \frac{\partial p_3}{\partial t} \right) dt . \end{aligned} \quad (\text{A.182})$$

With the pullback of \mathcal{A} we convert the integral over the path P to an integral in t over the interval $t_1 \leq t \leq t_2$

$$\int_P \mathcal{A} = \int_{t_1}^{t_2} P^{\triangleleft} \mathcal{A} . \quad (\text{A.183})$$

A.5 DOUBLE DIFFERENTIAL FORMS

In vector analysis a *dyadic* defines a linear mapping of vectors [13–15]. In vector calculus a dyadic is the formal sum of a finite number of *dyads*, a dyad being a pair of vectors [16]. In differential form calculus dyadics may be represented by *double forms* [12, 17]. A *double one-form* \mathcal{G} is defined by

$$\begin{aligned} \mathcal{G} &= G_{11} dx dx' + G_{12} dx dy' + G_{13} dx dz' \\ &\quad + G_{21} dy dx' + G_{22} dy dy' + G_{23} dy dz' \\ &\quad + G_{31} dz dx' + G_{32} dz dy' + G_{33} dz dz' . \end{aligned} \quad (\text{A.184})$$

Green's double form relates the observation space \mathbf{x} to the source space \mathbf{x}' . Primed and unprimed differentials dx'_i and dx_j commute (i.e., in products they may be interchanged without changing the sign). The rules are

$$dx_i dx'_j = dx'_j dx_i \quad \text{with} \quad dx_i = dx, dy, dz . \quad (\text{A.185})$$

A one-form \mathcal{A} is mapped into a one-form \mathcal{B} and a two-form \mathcal{C} is mapped into a two-form \mathcal{D} via

$$\mathcal{B}(\mathbf{x}) = \int' \mathcal{G}(\mathbf{x}, \mathbf{x}') \wedge \star \mathcal{A}(\mathbf{x}') , \quad (\text{A.186a})$$

$$\mathcal{D}(\mathbf{x}) = \star \int' \mathcal{G}(\mathbf{x}, \mathbf{x}') \wedge \mathcal{C}(\mathbf{x}') . \quad (\text{A.186b})$$

In these equations $\mathcal{G}(\mathbf{x}, \mathbf{x}')$ is called the *kernel* of integration. The primed integration symbol denotes that the integration is performed over the primed variables. For the integration the unprimed differentials are treated as constants.

Table A.1: Differential Operators

Vector Differential Operator	Exterior Differential Operator
$\text{grad } f$	df
$\text{curl } A$	dA
$\text{div } B$	dB
$\text{curl grad } f = 0$	$ddf = 0$
$\text{div curl } A = 0$	$ddA = 0$
$\text{div grad } f$	$d \star df \text{ or } \star d \star df$
$\text{grad div } A$	$d \star d \star A$
$\text{grad div } B$	$\star d \star dB$
$\text{curl curl } A$	$d \star dA \text{ or } \star d \star dA$
$\Delta f = \text{div grad } f$	$\Delta f = \star d \star df$
$\Delta A = \text{grad div } A - \text{curl curl } A$	$\Delta A = d \star d \star A - \star d \star dA$
$\Delta B = \text{grad div } B - \text{curl curl } B$	$\Delta B = \star d \star dB - d \star d \star B$
$\text{grad}(fg) = g \text{ grad } f + f \text{ grad } g$	$d(fg) = gdf + f dg$
$\text{curl}(fA) = \text{grad } f \times A + f \text{ curl } A$	$d(fA) = df \wedge A + f dA$
$\text{div}(A \times C) = \text{curl } A \cdot C - A \cdot \text{curl } C$	$d(A \wedge B) = dA \wedge B - A \wedge dB$
$\text{div}(fB) = \text{grad } f \cdot B + f \text{ div } B$	$d(f \wedge B) = df \wedge B + f dB$

Notes: $f = [f]^{(0)}$, $g = [g]^{(0)}$, $A = [A]^{(1)}$, $B = [B]^{(2)}$, $C = [C]^{(1)}$.

Table A.2: Maxwell's Equations

Equation	Vector Notation	Differential Form Notation
Ampère's law	$\text{curl } H = \frac{\partial D}{\partial t} + J$	$d\mathcal{H} = \frac{\partial \mathcal{D}}{\partial t} + \mathcal{J}$
Faraday's law	$\text{curl } E = -\frac{\partial B}{\partial t}$	$d\mathcal{E} = -\frac{\partial \mathcal{B}}{\partial t}$
Gauss' law	$\text{div } D = \rho$	$d\mathcal{D} = \mathcal{Q}$
Magnetic flux continuity	$\text{div } B = 0$	$d\mathcal{B} = 0$
Electric constitutive equation	$D = \epsilon E$	$\mathcal{D} = \star \epsilon \mathcal{E}$
Magnetic constitutive equation	$B = \mu H$	$\mathcal{B} = \star \mu \mathcal{H}$
Ampère's law	$\text{curl } \underline{H} = j \omega \underline{\epsilon} E + \underline{I}_0$	$d\mathcal{H} = \star j \omega \underline{\epsilon} \mathcal{E} + \underline{\mathcal{J}}$
Faraday's law	$\text{curl } \underline{E} = -j \omega \underline{\mu} H$	$d\mathcal{E} = -\star j \omega \underline{\mu} \mathcal{H}$

With the *identity kernel*, defined by

$$\mathcal{I}(\mathbf{x}, \mathbf{x}') = \delta(\mathbf{x} - \mathbf{x}') (dx dx' + dy dy' + dz dz'), \quad (\text{A.187})$$

any one-form \mathcal{A} and any two-form \mathcal{C} , respectively, is mapped in itself. We obtain

$$\int' \mathcal{I}(\mathbf{x}, \mathbf{x}') \wedge \star \mathcal{A}(\mathbf{x}') = \mathcal{A}(\mathbf{x}), \quad (\text{A.188a})$$

$$\star \int' \mathcal{I}(\mathbf{x}, \mathbf{x}') \wedge \mathcal{C}(\mathbf{x}') = \mathcal{C}(\mathbf{x}). \quad (\text{A.188b})$$

A.6 RELATIONS BETWEEN EXTERIOR CALCULUS AND CONVENTIONAL VECTOR NOTATION

A.6.1 Differential Operators

In conventional vector notation three differential operators are defined. The *gradient operator* applied to a scalar yields a vector

$$\text{grad } f = \begin{bmatrix} \frac{\partial f}{\partial x} \\ \frac{\partial f}{\partial y} \\ \frac{\partial f}{\partial z} \end{bmatrix}. \quad (\text{A.189})$$

The *curl operator* applied to a vector \mathbf{U} yields the pseudovector

$$\text{curl } \mathbf{U} = \begin{bmatrix} \frac{\partial U_z}{\partial y} - \frac{\partial U_y}{\partial z} \\ \frac{\partial U_x}{\partial z} - \frac{\partial U_z}{\partial x} \\ \frac{\partial U_y}{\partial x} - \frac{\partial U_x}{\partial y} \end{bmatrix}. \quad (\text{A.190})$$

The *divergence operator* applied to a pseudovector \mathbf{V} yields the pseudoscalar

$$\text{div } \mathbf{V} = \frac{\partial V_x}{\partial x} + \frac{\partial V_y}{\partial y} + \frac{\partial V_z}{\partial z}. \quad (\text{A.191})$$

Table A.1 shows the correspondences between the differential operators in conventional vector notation and exterior differential form notation.

A.6.2 Maxwell's Equations

Table A.2 shows the correspondences between Maxwell's equations in vector notation and differential form notation.

REFERENCES

- [1] G. Arfken, *Mathematical Methods for Physicists*. New York: Academic Press, 1985.
- [2] C. W. Wong, *Introduction to Mathematical Physics*. Oxford: Oxford University Press, 1991.
- [3] H. Flanders, *Differential Forms*. New York: Academic Press, 1963.
- [4] W. L. Burke, *Applied Differential Geometry*. Cambridge: Cambridge University Press, 1985.
- [5] P. Bamberg and S. Sternberg, *A Course in Mathematics for Students in Physics 2*. Cambridge: Cambridge University Press, 1990.
- [6] T. Frankel, *The Geometry of Physics*. Cambridge: Cambridge University Press, 1997.
- [7] S. H. Weintraub, *Differential Forms – A Complement to Vector Calculus*. New York: Academic Press, 1997.
- [8] K. F. Warnick, R. H. Selfridge, and D. V. Arnold, "Electromagnetic boundary conditions and differential forms," *IEE Proc., Microw. Antennas Propag.*, vol. 142, pp. 326–332, Aug. 1995.
- [9] W. Thirring, *Lehrbuch der Mathematischen Physik*, vol. 2. Wien: Springer, 1978.
- [10] P. Moon and D. E. Spencer, *Field Theory Handbook*. Berlin: Springer, 1991.
- [11] W. L. Burke, "Manifested parity invariant electromagnetic theory and twisted tensors," *J. Math. Phys.*, vol. 24, pp. 65–69, Jan. 1983.
- [12] K. F. Warnick and D. V. Arnold, "Electromagnetic Green functions using differential forms," *J. Electromagn. Waves and Appl.*, vol. 10, no. 3, pp. 427–438, 1996.
- [13] R. E. Collin, *Field Theory of Guided Waves*. New York: IEEE Press, 1991.
- [14] C.-T. Tai, *Generalized Vector and Dyadic Analysis*. New York: IEEE Press, 1992.
- [15] C.-T. Tai, *Dyadic Green Functions in Electromagnetic Theory*. New York: IEEE Press, 1993.
- [16] R. Abraham, J. E. Marsden, and T. Ratiu, *Manifolds, Tensor Analysis and Applications*. London: Addison-Wesley, 1983.
- [17] G. de Rham, *Differentiable Manifolds*. New York: Springer, 1984.

Appendix B

Special Functions

For a number of coordinate systems the Laplace equation, the Helmholtz equation, and the wave equation may be solved exactly by separation into ordinary differential equations. As the solutions of these ordinary differential equations, special functions occur. In this chapter special functions for circular cylindrical and spherical coordinate systems and some important formulae are summarized. For a detailed presentation of the mathematical background, see for example, [1, 2]. A comprehensive presentation of the coordinate systems for which the partial differential equations mentioned above may be solved exactly, and the methods of solutions are given in [3]. Comprehensive collections of formulae and theorems for the special functions of mathematical physics are provided in [4, 5].

B.1 ORDINARY BESSEL FUNCTIONS

The separation of the Helmholtz or wave equation in circular cylindrical coordinates leads to *Bessel's differential equation*

$$z \frac{d}{dz} \left(z \frac{df}{dz} \right) + (z^2 - n^2)f = 0. \quad (\text{B.1})$$

The variable z and the parameter n can be arbitrarily complex. However, in the following n will be assumed as real and integer or half-integer. The solutions of Bessel's differential equation are the *Bessel function* of the first kind $J_n(z)$, the *Neumann function* or Bessel function of the second kind $Y_n(z)$, and the *Hankel functions* of the first kind $H_n^{(1)}(z)$ and of the second kind $H_n^{(2)}(z)$. The index n denotes the order of the function. The Bessel functions of the first kind $J_n(z)$ [1] are defined by

$$J_n(z) = \sum_{k=0}^{\infty} \frac{(-1)^k \left(\frac{1}{2}z\right)^{2k+n}}{k! \Gamma(n+k+1)}. \quad (\text{B.2})$$

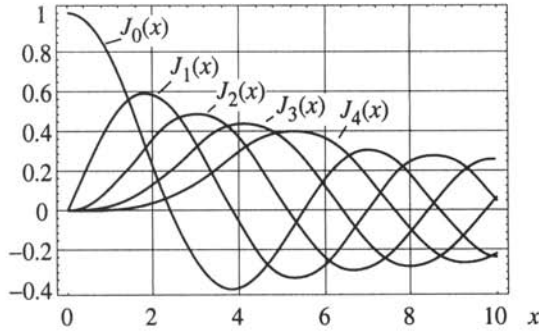


Figure B.1: The Bessel functions of the first kind of order 0, 1, 2, 3, and 4.

For integer n the *factorial* $n!$, the *double factorial* $n!!$, and the *gamma function* $\Gamma(n)$ [6] are given by

$$n! = \begin{cases} n \cdot (n-1) \dots 3 \cdot 2 \cdot 1 & \text{for integer } n \geq 1 \\ 1 & \text{for } n = 0 \end{cases}, \quad (\text{B.3a})$$

$$n!! = \begin{cases} n \cdot (n-2) \dots 5 \cdot 3 \cdot 1 & \text{for } n \text{ odd} \\ n \cdot (n-2) \dots 6 \cdot 4 \cdot 2 & \text{for } n \text{ even} \\ 1 & \text{for } n = -1, 0 \end{cases}, \quad (\text{B.3b})$$

$$\Gamma(n) = (n-1)! \quad \text{for integer } n \geq 1, \quad (\text{B.3c})$$

$$\Gamma(n + \tfrac{1}{2}) = \frac{(2n-1)!!\sqrt{\pi}}{2^n} \quad \text{for integer } n \geq 0. \quad (\text{B.3d})$$

Figure B.1 shows the Bessel functions of the first kind of order 0, 1, 2, 3 and 4. The Neumann function $Y_n(z)$ [1] is defined by

$$Y_n(z) = \frac{J_n(z) \cos(n\pi) - J_{-n}(z)}{\sin(n\pi)}. \quad (\text{B.4})$$

Figure B.2 shows the Neumann functions of order 0, 1, 2, 3 and 4. The Hankel functions $H_n^{(1)}(z)$ and $H_n^{(2)}(z)$ [1] are defined by

$$H_n^{(1)}(z) = j \frac{J_n(z) e^{-jn\pi} - J_{-n}(z)}{\sin(n\pi)}, \quad (\text{B.5a})$$

$$H_n^{(2)}(z) = j \frac{J_{-n}(z) - J_n(z) e^{jn\pi}}{\sin(n\pi)}. \quad (\text{B.5b})$$

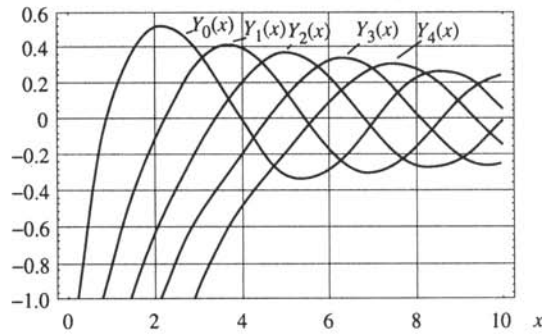


Figure B.2: The Neumann functions of order 0, 1, 2, 3 and 4.

The Hankel functions are related to the Bessel functions of the first and second kind via

$$H_n^{(1)}(z) = J_n(z) + j Y_n(z) , \quad (\text{B.6a})$$

$$H_n^{(2)}(z) = J_n(z) - j Y_n(z) . \quad (\text{B.6b})$$

For real order n the Hankel functions of the first and second kind are related by

$$H_n^{(1)}(z^*) = H_n^{(2)*}(z) , \quad (\text{B.7a})$$

$$H_n^{(2)}(z^*) = H_n^{(1)*}(z) . \quad (\text{B.7b})$$

Denoting by $f_n(z)$ any of the functions $J_n(z)$, $Y_n(z)$, $H_n^{(1)}(z)$, $H_n^{(2)}(z)$, the following recurrence relations are valid:

$$f_{n-1}(z) + f_{n+1}(z) = \frac{2n}{z} f_n(z) , \quad (\text{B.8a})$$

$$f_{n-1}(z) - f_{n+1}(z) = 2f'_n(z) . \quad (\text{B.8b})$$

The expression $f'_n(z)$ denotes the derivation of f_n with respect to z . The functions of positive and negative order are related via

$$f_{-n}(z) = (-1)^n f_n(z) . \quad (\text{B.9})$$

From (B.8b) and (B.9) it follows that

$$f'_0(z) = -f_1(z) . \quad (\text{B.10})$$

The *Wronskian* of two functions $f(z)$ and $g(z)$ is defined as

$$W\{f(z), g(z)\} = \begin{vmatrix} f(z) & g(z) \\ f'(z) & g'(z) \end{vmatrix} = f(z)g'(z) - f'(z)g(z). \quad (\text{B.11})$$

The following Wronskian relations hold for Bessel functions:

$$W\{J_n(z), J_{-n}(z)\} = J_{n+1}(z)J_{-n}(z) + J_n(z)J_{-(n+1)}(z) = -2\frac{\sin n\pi}{\pi z}, \quad (\text{B.12a})$$

$$W\{J_n(z), Y_n(z)\} = J_{n+1}(z)Y_n(z) - J_n(z)Y_{n+1}(z) = \frac{2}{\pi z}, \quad (\text{B.12b})$$

$$W\{H_n^{(1)}(z), H_n^{(2)}(z)\} = H_{n+1}^{(1)}(z)H_n^{(2)}(z) - H_n^{(1)}(z)H_{n+1}^{(2)}(z) = -\frac{4j}{\pi z}. \quad (\text{B.12c})$$

The ordinary Bessel functions of the first kind are the Fourier series expansion coefficients of the *generating function*

$$e^{jz \sin \phi} = \sum_{n=-\infty}^{+\infty} J_n(z) e^{jn\phi}. \quad (\text{B.13})$$

If ξ_{ni} and ξ_{nk} are the i th and k th zero of $J_n(x)$, in other words

$$J_n(\xi_{ni}) = 0, \quad J_n(\xi_{nk}) = 0, \quad (\text{B.14})$$

the following *orthogonality relation* is valid:

$$\int_0^a r J_n\left(\frac{\xi_{ni}r}{a}\right) J_n\left(\frac{\xi_{nk}r}{a}\right) dr = \begin{cases} 0 & \text{for } i \neq k \\ \frac{1}{2}a^2 J_n'^2(\xi_i) & \text{for } i = k \end{cases}. \quad (\text{B.15})$$

B.2 MODIFIED BESSEL FUNCTIONS

Modified Bessel functions are the solutions of the *modified Bessel differential equation*

$$z \frac{d}{dz} \left(z \frac{df}{dz} \right) - (z^2 + n^2)f = 0. \quad (\text{B.16})$$

The modified Bessel differential equation is obtained by replacing z by jz in the Bessel differential equation (B.1). Solutions are the *modified Bessel function of the first kind*

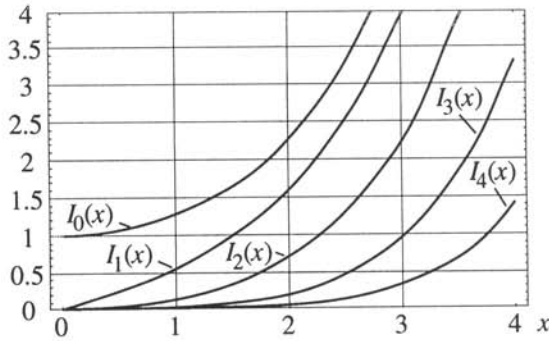


Figure B.3: Modified Bessel functions of the first kind of order 0, 1, 2, 3, and 4.

$I_n(z)$ and the *modified Bessel function of the second kind* $K_n(z)$. The index n denotes the order of the modified Bessel functions. The modified Bessel function of the first kind is defined by the series expansion [4]

$$I_n(z) = \sum_{k=0}^{\infty} \frac{(\frac{1}{2}z)^{2k+n}}{k!(n+k+1)!}. \quad (\text{B.17})$$

Figure B.3 shows modified Bessel functions of the first kind. The modified Bessel function of the second kind is related to the modified Bessel function of the first kind via [4, 7]

$$K_\nu(z) = \frac{1}{2}\pi \frac{I_{-\nu}(z) - I_\nu(z)}{\sin(n\pi)}, \quad (\text{B.18})$$

where the right-hand side of the equation must be replaced by its limiting value if ν is an integer. Modified Bessel functions are related to ordinary Bessel functions via

$$I_n(z) = (-j)^n J_n(jz), \quad (\text{B.19a})$$

$$K_n(z) = \frac{1}{2}\pi(j)^{n+1} [J_n(jz) + jY_n(jz)]. \quad (\text{B.19b})$$

Figure B.4 shows modified Bessel functions of the second kind. For modified Bessel functions the following recurrence relations are valid:

$$I_{n-1}(z) - I_{n+1}(z) = \frac{2n}{z} I_n(z), \quad (\text{B.20a})$$

$$I_{n-1}(z) + I_{n+1}(z) = 2I'_n(z), \quad (\text{B.20b})$$

$$K_{n-1}(z) - K_{n+1}(z) = -\frac{2n}{z} K_n(z), \quad (\text{B.20c})$$

$$K_{n-1}(z) + K_{n+1}(z) = -2K'_n(z). \quad (\text{B.20d})$$

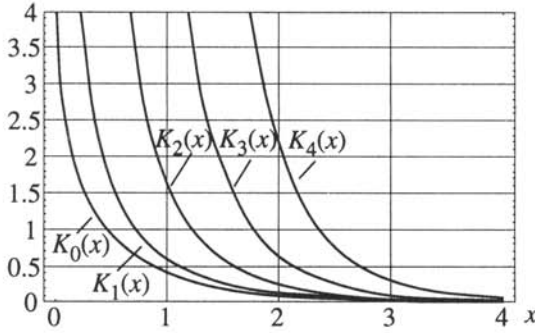


Figure B.4: Modified Bessel functions of the second kind of order 0, 1, 2, 3 and 4.

Modified Bessel functions of positive and negative integer order are related via

$$I_{-n}(z) = I_n(z) , \quad (\text{B.21a})$$

$$K_{-n}(z) = K_n(z) . \quad (\text{B.21b})$$

From (B.20b), (B.21a), (B.20d), and (B.21b) we obtain

$$I'_0(z) = I_1(z) , \quad (\text{B.22a})$$

$$K'_0(z) = -K_1(z) . \quad (\text{B.22b})$$

Modified Bessel functions of the first kind are the Fourier series expansion coefficients of the *generating function*

$$e^{z \cos \phi} = I_0(z) + 2 \sum_{n=1}^{\infty} I_n(z) \cos(n\phi) . \quad (\text{B.23})$$

Now we list some important integrals involving Bessel functions. A large number of integrals involving Bessel functions are contained in [4, 5, 7]. The functions $f_n(z)$, $g_n(z)$ may denote any of the functions $J_n(z)$, $Y_n(z)$, $I_n(z)$, $K_n(z)$.

$$\int x f_n(\alpha x) g_n(\beta x) dx = \frac{\beta x f_n(\alpha x) g_{n-1}(\beta x) - \alpha x f_{n-1}(\alpha x) g_n(\beta x)}{\alpha^2 - \beta^2} , \quad (\text{B.24})$$

$$\int x f_n^2(\alpha x) dx = \frac{1}{2} x^2 [f_n^2(\alpha x) - f_{n-1}(\alpha x) f_{n+1}(\alpha x)] . \quad (\text{B.25})$$

From (B.10) and (B.25) we obtain

$$\int x J_0'^2(\alpha x) dx = \frac{1}{2} x^2 [J_1^2(\alpha x) - J_0(\alpha x) J_2(\alpha x)] . \quad (\text{B.26})$$

From (B.10) and (B.25) it follows that

$$\int_0^{x_0} x J_1^2(\alpha x) dx = \int_0^{x_0} x J_0'^2(\alpha x) dx = \begin{cases} \frac{1}{2} x_0^2 J_1^2(\alpha x_0) & \text{for } J_0(\alpha x_0) = 0 \\ \frac{1}{2} x_0^2 J_0^2(\alpha x_0) & \text{for } J_0'(\alpha x_0) = 0 \\ -\frac{1}{2} x_0^2 J_0(\alpha x_0) J_2(\alpha x_0) & \text{for } J_1(\alpha x_0) = 0 \end{cases} \quad (\text{B.27})$$

From (B.25) we obtain

$$\int_0^{x_0} x J_0^2(\alpha x) dx = \frac{1}{2} x_0^2 [J_0^2(\alpha x_0) + J_1^2(\alpha x_0)] \quad (\text{B.28})$$

B.3 SPHERICAL BESSEL FUNCTIONS

The *spherical Bessel functions* $j_n(x)$, $y_n(x)$ and the *spherical Hankel functions* of first and second kind $h_n^{(1)}(x)$, $h_n^{(2)}(x)$ are solutions of the differential equation

$$x^2 \frac{d^2 z_n(x)}{dx^2} + 2x \frac{dz_n(x)}{dx} + (x^2 - n(n+1))z_n(x) = 0 \quad (\text{B.29})$$

This differential equation is the differential equation (3.231a) normalized to $x = kr$, and describes the radial component of spherical wave functions. With the substitution

$$z_n(x) = \frac{1}{\sqrt{x}} f_{n+1/2} \quad (\text{B.30})$$

we transform (B.29) into

$$x^2 \frac{d^2 f_{n+1/2}(x)}{dx^2} + x \frac{df_{n+1/2}(x)}{dx} + [x^2 - (n+1/2)^2] f_{n+1/2}(x) = 0 \quad (\text{B.31})$$

This is Bessel's differential equation (B.1) for half-odd integer order $n + \frac{1}{2}$. The spherical Bessel functions $j_n(x)$, $y_n(x)$ and spherical Hankel functions of first and second kind $h_n^{(1)}(x)$, $h_n^{(2)}(x)$ are related to the cylindrical Bessel and Hankel functions of order

$n + \frac{1}{2}$ by

$$j_n(x) = \sqrt{\frac{\pi}{2x}} J_{n+1/2}(x), \quad (\text{B.32a})$$

$$y_n(x) = \sqrt{\frac{\pi}{2x}} Y_{n+1/2}(x), \quad (\text{B.32b})$$

$$h_n^{(1)}(x) = \sqrt{\frac{\pi}{2x}} H_{n+1/2}^{(1)}(x), \quad (\text{B.32c})$$

$$h_n^{(2)}(x) = \sqrt{\frac{\pi}{2x}} H_{n+1/2}^{(2)}(x). \quad (\text{B.32d})$$

The spherical Bessel functions of order 0 to 2 are given by

$$j_0(x) = \frac{\sin x}{x}, \quad (\text{B.33a})$$

$$j_1(x) = \frac{\sin x}{x^2} - \frac{\cos x}{x}, \quad (\text{B.33b})$$

$$j_2(x) = \left(\frac{3}{x^3} - \frac{1}{x} \right) \sin x - \frac{3}{x^2} \cos x \quad (\text{B.33c})$$

and

$$y_0(x) = -\frac{\cos x}{x}, \quad (\text{B.34a})$$

$$y_1(x) = -\frac{\sin x}{x} - \frac{\cos x}{x^2}, \quad (\text{B.34b})$$

$$y_2(x) = \left(-\frac{3}{x^3} + \frac{1}{x} \right) \cos x - \frac{3}{x^2} \sin x \quad (\text{B.34c})$$

and the spherical Hankel functions of order 0 to 2 are given by

$$h_0^{(1)}(x) = h_0^{(2)*}(x) = -\frac{j}{x} e^{jx}, \quad (\text{B.35a})$$

$$h_1^{(1)}(x) = h_1^{(2)*}(x) = \left(-\frac{1}{x} - \frac{j}{x^2} \right) e^{jx}, \quad (\text{B.35b})$$

$$h_2^{(1)}(x) = h_2^{(2)*}(x) = \left(\frac{j}{x} - \frac{3}{x^2} - \frac{3j}{x^3} \right) e^{jx}. \quad (\text{B.35c})$$

B.4 LEGENDRE POLYNOMIALS

The separation of the Helmholtz or wave equation in spherical coordinates leads to the following differential equation for the function of the θ coordinate

$$\frac{1}{\sin \theta} \frac{d}{d\theta} \left(\sin \theta \frac{df}{d\theta} \right) + \left[n(n+1) - \frac{m^2}{\sin^2 \theta} \right] f = 0. \quad (\text{B.36})$$

With the substitution

$$x = \cos \theta \quad (\text{B.37})$$

we can bring (B.36) in the form

$$(1-x^2) \frac{d^2 f}{dx^2} - 2x \frac{df}{dx} + \left[n(n+1) - \frac{m^2}{1-x^2} \right] f = 0. \quad (\text{B.38})$$

This is the *Legendre differential equation*. The variable x and the parameters n and m can be arbitrarily complex. However, in the following m and n will be assumed as real and integer. Since in the spherical coordinate system we consider the interval $0 \leq \theta \leq \pi$, this yields $-1 \leq x \leq 1$. The solutions of the Legendre differential equation are the *associated Legendre functions* of the first kind $P_n^m(z)$, and the second kind $Q_n^m(z)$. The subscript n denotes the degree and the superscript m the order of the Legendre function.

For $m = 0$ we obtain the *ordinary Legendre differential equation*

$$(1-x^2) \frac{d^2 f}{dx^2} - 2x \frac{df}{dx} + n(n+1)f = 0. \quad (\text{B.39})$$

The solutions of the ordinary Legendre differential equation are the *ordinary Legendre functions of the first kind* $P_n(x)$, and the second kind $Q_n(x)$. For integer n the ordinary Legendre functions of the first kind are polynomials of degree n and therefore are also called *Legendre polynomials* of degree n . The explicit expression for the Legendre polynomial is

$$P_n(x) = \sum_{m=0}^M (-1)^m \frac{(2n-2m)! x^{n-2m}}{2^n m! (n-m)! (n-2m)!}, \quad (\text{B.40})$$

where $M = \frac{1}{2}n$ for even n and $M = \frac{1}{2}(n-1)$ for odd n . In terms of x and $\cos \theta$ the five Legendre polynomials of lowest order are

$$P_0(x) = 1, \quad (\text{B.41a})$$

$$P_1(x) = x = \cos \theta, \quad (\text{B.41b})$$

$$P_2(x) = \frac{1}{2}(3x^2 - 1) = \frac{1}{4}(1 + 3 \cos 2\theta), \quad (\text{B.41c})$$

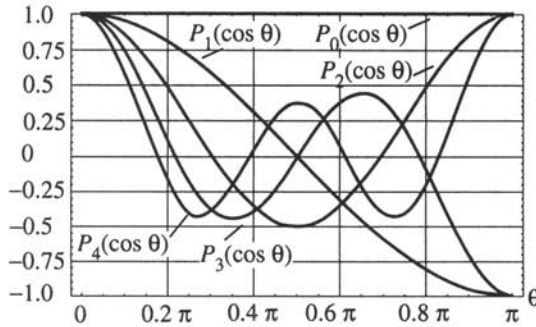


Figure B.5: The Legendre polynomials of the first kind of order 0, 1, 2, 3, and 4.

$$P_3(x) = \frac{1}{2}(5x^3 - 3x) = \frac{1}{8}(3 \cos \theta + 5 \cos 3\theta), \quad (\text{B.41d})$$

$$P_4(x) = \frac{1}{8}(35x^4 - 30x^2 + 3) = \frac{1}{64}(9 + 20 \cos 2\theta + 35 \cos 4\theta). \quad (\text{B.41e})$$

Figure B.5 shows the Legendre polynomials of the first kind of order 0, 1, 2, 3 and 4. The Legendre functions of the second kind $Q_n(x)$ are infinite at $x = \pm 1$, or at $\theta = 0$ and $\theta = \pi$. The lowest order Legendre functions of the second kind are given by

$$Q_0(x) = \frac{1}{2} \ln \frac{1+x}{1-x} = \ln \cot \frac{1}{2} \theta, \quad (\text{B.42a})$$

$$Q_1(x) = \frac{1}{2} x \ln \frac{1+x}{1-x} - 1 = \cos \theta \ln \cot \frac{1}{2} \theta - 1, \quad (\text{B.42b})$$

$$Q_2(x) = \frac{1}{4}(3x^2 - 1) \ln \frac{1+x}{1-x} - \frac{3}{2}x = \frac{1}{2}(3 \cos^2 \theta - 1) \ln \cot \frac{1}{2} \theta - \frac{3}{2} \cos \theta. \quad (\text{B.42c})$$

The n th order Legendre function of the second kind is

$$Q_n(x) = Q_0(x)P_n(x) - \sum_{m=0}^M \frac{2n-4m+3}{(2m-1)(n-m+1)} P_{n-2m+1}(x), \quad (\text{B.43})$$

where $M = \frac{1}{2}n$ for even n and $M = \frac{1}{2}(n+1)$ for odd n . The Legendre functions with positive and negative arguments are related via

$$P_n(-x) = (-1)^n P_n(x), \quad (\text{B.44a})$$

$$Q_n(-x) = (-1)^{n+1} Q_n(x). \quad (\text{B.44b})$$

Figure B.6 shows the Legendre polynomials of the first kind of order 0, 1, 2, 3, and 4. The

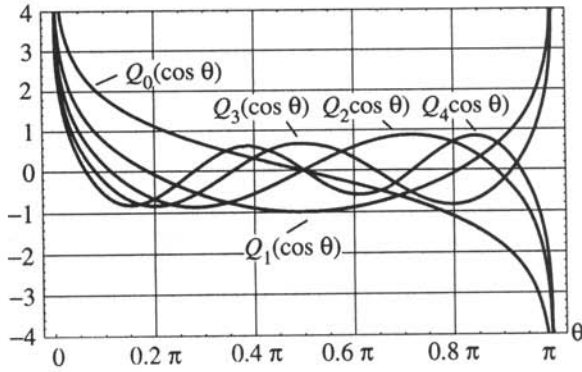


Figure B.6: The Legendre polynomials of the second kind of order 0, 1, 2, 3, and 4.

associated Legendre functions (i.e., the solutions of the associated Legendre differential equation (B.38)) are

$$P_n^m(x) = (-1)^m (1-x^2)^{m/2} \frac{d^m P_n(x)}{dx^m}, \quad (\text{B.45a})$$

$$Q_n^m(x) = (-1)^m (1-x^2)^{m/2} \frac{d^m Q_n(x)}{dx^m}. \quad (\text{B.45b})$$

Some lower-order associated Legendre functions of the first kind are

$$P_1^1(x) = -(1-x^2)^{1/2}, \quad (\text{B.46a})$$

$$P_2^1(x) = -3x(1-x^2)^{1/2}, \quad (\text{B.46b})$$

$$P_2^2(x) = 3(1-x^2), \quad (\text{B.46c})$$

$$P_3^1(x) = \frac{3}{2}(1-x^2)^{1/2}(1-5x^2), \quad (\text{B.46d})$$

$$P_3^2(x) = 15x(1-x^2), \quad (\text{B.46e})$$

$$P_3^3(x) = -15(1-x^2)^{3/2}. \quad (\text{B.46f})$$

Some lower order associated Legendre functions of the second kind are

$$Q_1^1(x) = \frac{1}{2}\sqrt{x^2-1} \ln \frac{x+1}{x-1} - \frac{x}{\sqrt{x^2-1}} \quad (\text{B.47a})$$

$$Q_2^1(x) = \frac{3}{2}x\sqrt{x^2-1} \ln \frac{x+1}{x-1} - \frac{3x^2-2}{\sqrt{x^2-1}} \quad (\text{B.47b})$$

$$Q_2^2(x) = \frac{3}{2}(x^2-1) \ln \frac{x+1}{x-1} + 5\frac{x}{x^2-1} \quad (\text{B.47c})$$

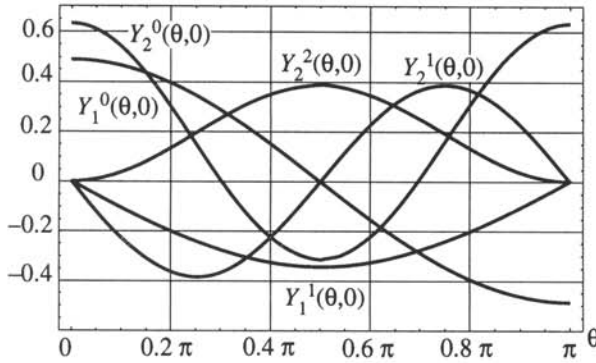


Figure B.7: The spherical harmonics Y_1^0 , Y_1^1 , Y_2^0 , Y_2^1 , Y_2^2 .

The *orthogonality relation* for associated Legendre functions is

$$\int_{-1}^1 P_{n_1}^m(x) P_{n_2}^m(x) dx = \frac{2}{2n_1 + 1} \frac{(n_1 + m)!}{(n_1 - m)!} \delta_{n_1, n_2}. \quad (\text{B.48})$$

B.5 SPHERICAL HARMONICS

Spherical harmonics are solutions of the partial differential equation

$$\frac{1}{\sin \theta} \frac{d}{d\theta} \left(\sin \theta \frac{\partial f(\theta, \phi)}{\partial \theta} \right) + \frac{1}{\sin^2 \theta} \frac{\partial^2 f(\theta, \phi)}{\partial \phi^2} + n(n+1)f = 0. \quad (\text{B.49})$$

Setting

$$f(\theta, \phi) = \Theta(\theta)\Phi(\phi) \quad (\text{B.50})$$

with the integer separation parameter m with $|m| \leq n$ the partial differential equation (B.49) may be separated into (B.36) for $\Theta(\theta)$ and the second order differential equation for $\Phi(\phi)$:

$$\frac{1}{\sin \theta} \frac{d}{d\theta} \left(\sin \theta \frac{d\Theta(\theta)}{d\theta} \right) + \left[n(n+1) - \frac{m^2}{\sin^2 \theta} \right] \Theta(\theta) = 0, \quad (\text{B.51a})$$

$$\frac{d^2 \Phi(\phi)}{d\phi^2} + m^2 \Phi(\phi) = 0. \quad (\text{B.51b})$$

The normalized solution of (B.49) is the spherical harmonic

$$Y_n^m(\theta, \phi) = c_n^m P_n^m(\cos \theta) e^{jm\phi} \quad (\text{B.52})$$

where c_n^m is a normalization constant, given by

$$c_n^m = \sqrt{\frac{1}{4\pi} (2n+1) \frac{(n-m)!}{(n+m)!}}. \quad (\text{B.53})$$

Some lower order spherical harmonics are

$$Y_0^0(\theta, \phi) = \frac{1}{\sqrt{4\pi}}, \quad (\text{B.54a})$$

$$Y_1^1(\theta, \phi) = -\sqrt{\frac{3}{8\pi}} \sin \theta e^{j\phi}, \quad (\text{B.54b})$$

$$Y_1^0(\theta, \phi) = \sqrt{\frac{3}{4\pi}} \cos \theta, \quad (\text{B.54c})$$

$$Y_1^{-1}(\theta, \phi) = \sqrt{\frac{3}{8\pi}} \sin \theta e^{-j\phi}, \quad (\text{B.54d})$$

$$Y_2^2(\theta, \phi) = \sqrt{\frac{5}{96\pi}} 3 \sin^2 \theta e^{2j\phi}, \quad (\text{B.54e})$$

$$Y_2^1(\theta, \phi) = -\sqrt{\frac{5}{24\pi}} 3 \sin \theta \cos \theta e^{j\phi}, \quad (\text{B.54f})$$

$$Y_2^0(\theta, \phi) = \sqrt{\frac{5}{4\pi}} \left(\frac{3}{2} \cos^2 \theta - \frac{1}{2} \right), \quad (\text{B.54g})$$

$$Y_2^{-1}(\theta, \phi) = \sqrt{\frac{5}{24\pi}} 3 \sin \theta \cos \theta e^{-j\phi}, \quad (\text{B.54h})$$

$$Y_2^{-2}(\theta, \phi) = \sqrt{\frac{5}{96\pi}} 3 \sin^2 \theta e^{-2j\phi}. \quad (\text{B.54i})$$

Figure B.7 shows some of the lowest-order spherical harmonics.

The *orthogonality relation* for spherical harmonics is

$$\int_{\phi=0}^{2\pi} \int_{\theta=0}^{\pi} Y_{n_1}^{m_1*}(\theta, \phi) Y_{n_2}^{m_2}(\theta, \phi) \sin \theta d\theta d\phi = \delta_{n_1, n_2} \delta_{m_1, m_2}. \quad (\text{B.55})$$

The spherical harmonics constitute a *complete system of functions* within the interval $0 \leq \theta \leq \pi$, $0 \leq \phi \leq 2\pi$. Any function $f(\theta, \phi)$ with sufficient continuity properties may be expanded in this interval in a series

$$f(\theta, \phi) = \sum_{m, n} a_{m, n} Y_m(\theta, \phi). \quad (\text{B.56})$$

The expansion coefficients $a_{m,n}$ are

$$a_{m,n} = \int_{\phi=0}^{2\pi} \int_{\theta=0}^{\pi} Y_n^{m*}(\theta, \phi) f(\theta, \phi) \sin \theta \, d\theta \, d\phi. \quad (\text{B.57})$$

The spherical harmonics may be separated in their real and imaginary parts

$$Y_n^m(\theta, \phi) = Y_n^{mc}(\theta, \phi) + j Y_n^{ms}(\theta, \phi) \quad (\text{B.58})$$

with

$$Y_n^{mc}(\theta, \phi) = c_n^m P_n^m(\cos \theta) \cos m\phi, \quad (\text{B.59a})$$

$$Y_n^{ms}(\theta, \phi) = c_n^m P_n^m(\cos \theta) \sin m\phi. \quad (\text{B.59b})$$

REFERENCES

- [1] P. Morse and H. Feshbach, *Methods of Theoretical Physics, Part 1*. New York: McGraw-Hill, 1953.
- [2] P. Morse and H. Feshbach, *Methods of Theoretical Physics, Part 2*. New York: McGraw-Hill, 1953.
- [3] P. Moon and D. E. Spencer, *Field Theory Handbook*. Berlin: Springer, 1991.
- [4] M. Abramowitz and I. Stegun, *Handbook of Mathematical Functions with Formulas, Graphs and Mathematical Tables*. New York: Dover, 1965.
- [5] W. Magnus, F. Oberhettinger, and R. P. Soni, *Formulas and Theorems for the Special Functions of Mathematical Physics*. Berlin: Springer, 1966.
- [6] L. Rade and B. Westergren, *Mathematics Handbook for Science and Engineering*. Berlin, Heidelberg, New York: Springer, 1995.
- [7] I. S. Gradshteyn and I. M. Ryzhik, *Tables of Integrals, Series, and Products*. New York: Academic Press, 1965.

Appendix C

Linear Algebra

C.1 UNITARY VECTOR SPACE

This section recalls the basic definitions and the basic formulae of linear algebra. For a more detailed treatment, see for example [1–3].

A *matrix* is a rectangular array of *scalars* (e.g., integer, real, or complex numbers or integer-, real-, or complex-valued functions). The rectangular array

$$\mathbf{A} = \begin{bmatrix} A_{11} & A_{12} & \cdots & A_{1n} \\ A_{21} & A_{22} & \cdots & A_{2n} \\ \vdots & \vdots & \ddots & \vdots \\ A_{m1} & A_{m2} & \cdots & A_{mn} \end{bmatrix}, \quad (\text{C.1})$$

is called a *matrix* of m rows and n columns. We denote matrices with boldface letters. We may use the index $\langle m \times n \rangle$ to indicate the numbers of rows and columns. A matrix of type $\langle m \times n \rangle$ is said to be an m by n matrix. A matrix of type $\langle n \times n \rangle$ is called a square matrix of order n . A matrix of type $\langle m \times 1 \rangle$ is a *column vector*, and a matrix of type $\langle 1 \times n \rangle$ is a *row vector*,

$$\mathbf{x}_{\langle m \times 1 \rangle} = \begin{bmatrix} x_1 \\ x_2 \\ \vdots \\ x_m \end{bmatrix}, \quad (\text{C.2a})$$

$$\mathbf{y}_{\langle 1 \times n \rangle} = [y_1, y_2, \dots, y_n]. \quad (\text{C.2b})$$

For two matrices \mathbf{A} and \mathbf{B} of the same size $\langle m \times n \rangle$ a *matrix sum*

$$\mathbf{C}_{\langle m \times n \rangle} = \mathbf{A}_{\langle m \times n \rangle} + \mathbf{B}_{\langle m \times n \rangle} \quad (\text{C.3})$$

is defined such that

$$C_{ij} = A_{ij} + B_{ij} \quad (\text{C.4})$$

for each i and j . The product of a matrix A and B with a scalar b

$$C_{\langle m \times n \rangle} = b A_{\langle m \times n \rangle} \quad (\text{C.5})$$

is defined by

$$C_{ij} = b \sum_{k=1}^l A_{ik} \quad (\text{C.6})$$

For two matrices A and B of the type $\langle m \times l \rangle$ and $\langle l \times n \rangle$, a *product*

$$C_{\langle m \times n \rangle} = A_{\langle m \times l \rangle} B_{\langle l \times n \rangle} \quad (\text{C.7})$$

is defined. The elements of C are given by

$$C_{ij} = \sum_{k=1}^l A_{ik} B_{kj} \quad (\text{C.8})$$

for each i and j . The matrix product has the following properties:

$$(A B) C = A (B C) = A B C \quad \text{associative,} \quad (\text{C.9})$$

$$(A + B) C = A C + B C \quad \text{distributive,} \quad (\text{C.10})$$

$$C (A + B) = C A + C B \quad \text{distributive,} \quad (\text{C.11})$$

$$A B \neq B A \quad \text{in general noncommutative.} \quad (\text{C.12})$$

If all elements of a matrix are 0, the matrix is called the *null matrix* $\mathbf{0}$:

$$\mathbf{0}_{\langle m \times n \rangle} = \begin{bmatrix} 0 & 0 & \cdots & 0 & 0 \\ 0 & 0 & \cdots & 0 & 0 \\ \vdots & \vdots & \ddots & \vdots & 0 \\ 0 & 0 & \cdots & 0 & 0 \\ 0 & 0 & \cdots & 0 & 0 \end{bmatrix}. \quad (\text{C.13})$$

For any matrix $A_{\langle m \times n \rangle}$ the sum with the null matrix is given by

$$A_{\langle m \times n \rangle} + \mathbf{0}_{\langle m \times n \rangle} = A_{\langle m \times n \rangle} \quad (\text{C.14})$$

and the product with the null matrix is given by

$$\mathbf{0}_{\langle k \times m \rangle} A_{\langle m \times n \rangle} = \mathbf{0}_{\langle k \times n \rangle}, \quad (\text{C.15})$$

$$A_{\langle m \times n \rangle} \mathbf{0}_{\langle n \times k \rangle} = \mathbf{0}_{\langle m \times k \rangle}. \quad (\text{C.16})$$

The *unit matrix* $\mathbf{1}$ is a quadratic matrix with the Konecker delta δ_{ij} as the matrix elements

$$\mathbf{1}_{(m \times m)} = [\delta_{ij}] = \begin{bmatrix} 1 & 0 & \cdots & 0 & 0 \\ 0 & 1 & \cdots & 0 & 0 \\ \vdots & \vdots & \ddots & \vdots & 0 \\ 0 & 0 & \cdots & 1 & 0 \\ 0 & 0 & \cdots & 0 & 1 \end{bmatrix}. \quad (\text{C.17})$$

For any matrix $A_{(n \times n)}$, the product with the unit matrix has the property

$$\mathbf{1}_{(m \times m)} A_{(m \times n)} = A_{(m \times n)} \mathbf{1}_{(n \times n)} = A_{(m \times n)}. \quad (\text{C.18})$$

The *commutator* of two quadratic matrices A and B of same dimension is defined as

$$[A, B] = AB - BA. \quad (\text{C.19})$$

If the commutator is $\mathbf{0}$ the matrices A and B are said to commute. In this case the product AB is invariant under exchange of the factors A and B .

A square matrix in which all nondiagonal elements are zero is a *diagonal matrix*. It can be written in the following abbreviated form:

$$\begin{bmatrix} D_1 & 0 & \cdots & 0 & 0 \\ 0 & D_2 & \cdots & 0 & 0 \\ \vdots & \vdots & \ddots & \vdots & 0 \\ 0 & 0 & \cdots & D_{n-1} & 0 \\ 0 & 0 & \cdots & 0 & D_n \end{bmatrix} = \text{diag}[D_1, D_2, \dots, D_{n-1}, D_n]. \quad (\text{C.20})$$

If two matrices C and D are diagonal these matrices commute and the product CD is also diagonal,

$$CD = DC = \text{diag}[C_1 D_1, C_2 D_2, \dots, C_{n-1} D_{n-1}, C_n D_n]. \quad (\text{C.21})$$

A matrix A may be composed by submatrices A_{11} , A_{12} , A_{21} , A_{22} in the following way:

$$A_{(m \times n)} = \begin{bmatrix} A_{11(p \times q)} & A_{12(p \times (n-q))} \\ A_{21((m-p) \times q)} & A_{22((m-p) \times (n-q))} \end{bmatrix}. \quad (\text{C.22})$$

For a quadratic matrix $A_{(n \times n)}$ a *determinant* of n th order

$$\det A_{(n \times n)} = \begin{vmatrix} A_{11} & \cdots & A_{1n} \\ \vdots & \ddots & \vdots \\ A_{n1} & \cdots & A_{nn} \end{vmatrix} \quad (\text{C.23})$$

is defined by

$$\det A_{(n \times n)} = \sum (-1)^\alpha A_{1,p_1} \dots A_{n,p_n}, \quad (\text{C.24})$$

where the summation has to be performed over all $n!$ permutations of the second indices $p_1 \dots p_n$. The exponent α is the number of exchanges of indices for transforming the sequence $1 \dots n$ into $p_1 \dots p_n$. The determinant of a second order matrix is

$$\det A_{(2 \times 2)} = A_{11}A_{22} - A_{12}A_{21}, \quad (\text{C.25})$$

and the determinant of a third order matrix is

$$\begin{aligned} \det A_{(3 \times 3)} = & A_{11}A_{22}A_{33} + A_{12}A_{23}A_{31} + A_{13}A_{21}A_{32} \\ & - A_{13}A_{22}A_{31} - A_{11}A_{23}A_{32} - A_{12}A_{21}A_{33}. \end{aligned} \quad (\text{C.26})$$

The determinant of the submatrix of a quadratic matrix obtained by deleting the i th row and the j th column is called the *minor* of the element A_{ij} and is given by

$$A_{ij}^m = \begin{vmatrix} A_{11} & \dots & A_{1,j-1} & A_{1,j+1} & \dots & A_{1n} \\ \vdots & \ddots & \vdots & \vdots & \ddots & \vdots \\ A_{l-1,1} & \dots & A_{l-1,j-1} & A_{l-1,j+1} & \dots & A_{l-1,n} \\ A_{l+1,1} & \dots & A_{l+1,j-1} & A_{l+1,j+1} & \dots & A_{l+1,n} \\ \vdots & \ddots & \vdots & \vdots & \ddots & \vdots \\ A_{n1} & \dots & A_{n,j-1} & A_{n,j+1} & \dots & A_{nn} \end{vmatrix}. \quad (\text{C.27})$$

The *cofactor* A_{ij}^a of the element A_{ij} of a quadratic matrix is given by

$$A_{ij}^a = (-1)^{i+j} A_{ij}^m. \quad (\text{C.28})$$

Due to (C.24), an n th-order determinant may be expanded as a sum of the products of the elements of any row or column of the appropriate matrix with their cofactors. This is the *Laplace expansion*

$$\det A_{(n \times n)} = \sum_{i=1}^n A_{ij} A_{ij}^a = \sum_{j=1}^n A_{ij} A_{ij}^a. \quad (\text{C.29})$$

A quadratic matrix is called *singular* if $\det A = 0$. If a quadratic matrix is *nonsingular* (i.e., $\det A \neq 0$), the inverse A^{-1} is defined by its property

$$A^{-1} A = A A^{-1} = \mathbf{1}, \quad (\text{C.30})$$

and may be computed using *Cramer's rule*:

$$A_{(n \times n)}^{-1} = \frac{1}{\det A} \begin{bmatrix} A_{11}^a & A_{21}^a & \dots & A_{n1}^a \\ A_{12}^a & A_{22}^a & \dots & A_{n2}^a \\ \vdots & \vdots & \ddots & \vdots \\ A_{1n}^a & A_{2n}^a & \dots & A_{nn}^a \end{bmatrix}. \quad (\text{C.31})$$

The inverse of the product of two matrices is

$$(AB)^{-1} = B^{-1} A^{-1}. \quad (\text{C.32})$$

The inverse of a diagonal matrix is the diagonal matrix of the inverse elements:

$$(\text{diag}[D_1, D_2, \dots, D_{n-1}, D_n])^{-1} = \text{diag}[D_1^{-1}, D_2^{-1}, \dots, D_{n-1}^{-1}, D_n^{-1}]. \quad (\text{C.33})$$

The *transpose* A^T of a matrix A is obtained by interchanging columns and rows of the matrix A :

$$A^T = \begin{bmatrix} A_{11} & A_{21} & \cdots & A_{m1} \\ A_{12} & A_{22} & \cdots & A_{m2} \\ \vdots & \vdots & \ddots & \vdots \\ A_{1n} & A_{2n} & \cdots & A_{mn} \end{bmatrix}. \quad (\text{C.34})$$

If $A = A^T$ the matrix A is *symmetric*. The transpose of the product of two matrices is

$$(AB)^T = B^T A^T. \quad (\text{C.35})$$

If a matrix has the property $N^T = N^{-1}$ the matrix is called *orthogonal*.

The *complex conjugate* A^* of a matrix A is obtained by taking the complex conjugates of all elements of the matrix A :

$$A^* = \begin{bmatrix} A_{11}^* & A_{12}^* & \cdots & A_{1n}^* \\ A_{21}^* & A_{22}^* & \cdots & A_{2n}^* \\ \vdots & \vdots & \ddots & \vdots \\ A_{m1}^* & A_{m2}^* & \cdots & A_{mn}^* \end{bmatrix}. \quad (\text{C.36})$$

If $A = A^*$ the matrix A is called a *real* matrix. The complex conjugate of the product of two matrices is

$$(AB)^* = A^* B^*. \quad (\text{C.37})$$

The *Hermitian conjugate* A^\dagger of a matrix A is the transpose of the complex conjugate of A . It is obtained by taking the complex conjugates of all elements of the matrix A interchanging columns and rows of the matrix:

$$A^\dagger = (A^*)^T = (A^T)^* = \begin{bmatrix} A_{11}^* & A_{21}^* & \cdots & A_{m1}^* \\ A_{12}^* & A_{22}^* & \cdots & A_{m2}^* \\ \vdots & \vdots & \ddots & \vdots \\ A_{1n}^* & A_{2n}^* & \cdots & A_{mn}^* \end{bmatrix}. \quad (\text{C.38})$$

If $A = A^\dagger$ the matrix A is called a *Hermitian* matrix. The Hermitian conjugate of the product of two matrices is

$$(AB)^\dagger = B^\dagger A^\dagger. \quad (\text{C.39})$$

If a matrix has the property $U^\dagger = U^{-1}$ the matrix is called *unitary*. The inverses of the transpose, the complex conjugate, and the Hermitian conjugate matrix are

$$(A^T)^{-1} = (A^{-1})^T, \quad (\text{C.40})$$

$$(A^*)^{-1} = (A^{-1})^*, \quad (\text{C.41})$$

$$(A^\dagger)^{-1} = (A^{-1})^\dagger. \quad (\text{C.42})$$

Determinants have the following properties:

$$\det A^T = \det A, \quad (\text{C.43})$$

$$\det A^\dagger = \det A^* = (\det A)^*, \quad (\text{C.44})$$

$$\det(kA_{(n \times n)}) = k^n \det A, \quad (\text{C.45})$$

$$\det(AB) = (\det A)(\det B), \quad (\text{C.46})$$

$$\det(A^{-1}) = 1/\det A, \quad (\text{C.47})$$

$$\det(A+B) \neq \det A + \det B. \quad (\text{C.48})$$

The determinant of a Hermitian matrix is real.

The *inner product* of two n -dimensional column vectors $\mathbf{x}_{(n \times 1)}$ and $\mathbf{y}_{(n \times 1)}$ is given by

$$\mathbf{x}^\dagger \mathbf{y} = [x_1^* y_1 + x_2^* y_2 + \dots + x_n^* y_n]. \quad (\text{C.49})$$

The *norm* or *magnitude* of a vector $\mathbf{x}_{(n \times 1)}$ is defined as

$$|\mathbf{x}| = \sqrt{|x_1|^2 + |x_2|^2 + \dots + |x_n|^2}. \quad (\text{C.50})$$

The *dyadic product* of two vectors $\mathbf{x}_{(m \times 1)}$ and $\mathbf{y}_{(1 \times m)}$ is

$$\mathbf{x} \mathbf{y} = \begin{bmatrix} x_1 y_1 & x_1 y_2 & \cdots & x_1 y_n \\ x_2 y_1 & x_2 y_2 & \cdots & x_2 y_n \\ \vdots & \vdots & \ddots & \vdots \\ x_m y_1 & x_m y_2 & \cdots & x_m y_n \end{bmatrix}. \quad (\text{C.51})$$

Let $A_{(n \times n)} = A^\dagger$ be a Hermitian matrix, $\mathbf{x}_{(n \times 1)}$ an n -dimensional column vector, and $\mathbf{x}_{(1 \times n)}^\dagger$ its Hermitian conjugate row vector. The expression

$$\mathbf{x}^\dagger \mathbf{A} \mathbf{x} = \sum_{i,k} A_{ik} x_i^* x_k \quad (\text{C.52})$$

is called a *Hermitian form*. For arbitrary vectors \mathbf{x} the Hermitian form is real. If the Hermitian form is positive for arbitrary \mathbf{x} it is called *positive definite*. If the Hermitian form is positive or zero for arbitrary \mathbf{x} it is called *positive semidefinite*.

The determinant of the submatrix consisting of the first k rows and the first k columns of a matrix A is called its *leading principal minor* $\det_k A$ of order k :

$$\begin{aligned}\det_1 A_{(n \times n)} &= A_{11}, \\ \det_k A_{(n \times n)} &= \det \begin{bmatrix} A_{11} & \cdots & A_{1k} \\ \vdots & \ddots & \vdots \\ A_{k1} & \cdots & A_{kk} \end{bmatrix} \text{ for } 1 < k < n, \\ \det_n A_{(n \times n)} &= \det A.\end{aligned}\tag{C.53}$$

A Hermitian form is positive definite if all its leading principal minors are positive and it is positive semidefinite if all the leading principal minors are nonnegative.

C.2 DIAGONALIZATION OF A MATRIX

Let $A_{(n \times n)}$ be an n -dimensional quadratic matrix, and $\mathbf{x}_{(n \times 1)}$ an n -dimensional column vector. In the equation

$$A\mathbf{x} = \lambda\mathbf{x}\tag{C.54}$$

the scalar λ is called an *eigenvalue* and \mathbf{x} the corresponding *eigenvector*. We prove that if A is Hermitian its eigenvalues are real and its eigenvectors are orthogonal. Consider the eigenvalues λ_i, λ_j and the corresponding eigenvectors $\mathbf{x}_i, \mathbf{x}_j$ fulfilling

$$A\mathbf{x}_i = \lambda_i\mathbf{x}_i,\tag{C.55a}$$

$$A\mathbf{x}_j = \lambda_j\mathbf{x}_j.\tag{C.55b}$$

Multiplying the first equation from the left with Hermitian conjugate vector \mathbf{x}_j^\dagger and the second equation with \mathbf{x}_i^\dagger yields

$$\mathbf{x}_j^\dagger A\mathbf{x}_i = \lambda_i\mathbf{x}_j^\dagger\mathbf{x}_i,\tag{C.56a}$$

$$\mathbf{x}_i^\dagger A\mathbf{x}_j = \lambda_j\mathbf{x}_i^\dagger\mathbf{x}_j.\tag{C.56b}$$

The Hermitian conjugate of the second equation is

$$\mathbf{x}_j^\dagger A^\dagger \mathbf{x}_i = \lambda_j^* \mathbf{x}_j^\dagger \mathbf{x}_i.\tag{C.57}$$

Subtracting (C.57) from (C.56a) yields

$$\mathbf{x}_j^\dagger (A - A^\dagger) \mathbf{x}_i = (\lambda_i - \lambda_j^*) \mathbf{x}_j^\dagger \mathbf{x}_i.\tag{C.58}$$

If A is Hermitian (i.e. $A = A^\dagger$) we obtain

$$(\lambda_i - \lambda_j^*) \mathbf{x}_j^\dagger \mathbf{x}_i = 0.\tag{C.59}$$

This result holds for any combination of i, j . For $i = j$ we obtain

$$(\lambda_i - \lambda_i^*) \mathbf{x}_i^\dagger \mathbf{x}_i = 0. \quad (\text{C.60})$$

Apart from the excluded trivial case where \mathbf{x}_i is the null vector, the product $\mathbf{x}_i^\dagger \mathbf{x}_i$ is real and positive. This yields

$$\lambda_i = \lambda_i^* \quad (\text{C.61})$$

hence *the eigenvalues of a Hermitian matrix are real*.

For $i \neq j$ (C.60) yields

$$\mathbf{x}_i^\dagger \mathbf{x}_j = 0 \quad \text{for } i \neq j. \quad (\text{C.62})$$

This means that *the eigenvectors of distinct eigenvalues are orthogonal*.

To determine the eigenvalues and the eigenvectors of A , we bring (C.54) in the form

$$(A - \lambda \mathbf{1}) \mathbf{x} = \mathbf{0}. \quad (\text{C.63})$$

In component notation this reads

$$\begin{bmatrix} A_{11} - \lambda & A_{12} & \cdots & A_{1n} \\ A_{21} & A_{22} - \lambda & \cdots & A_{2n} \\ \vdots & \vdots & \ddots & \vdots \\ A_{n1} & A_{n2} & \cdots & A_{nn} - \lambda \end{bmatrix} \begin{bmatrix} x_1 \\ x_2 \\ \vdots \\ x_n \end{bmatrix} = \begin{bmatrix} 0 \\ 0 \\ \vdots \\ 0 \end{bmatrix}. \quad (\text{C.64})$$

This homogeneous equation yields nontrivial solutions only if the coefficient determinant vanishes,

$$|A - \lambda \mathbf{1}| = 0. \quad (\text{C.65})$$

This n th order algebraic equation is called the *secular equation* or *eigenvalue equation*.

Let K be a matrix formed by the eigenvectors $\mathbf{x}_1, \mathbf{x}_2, \dots, \mathbf{x}_n$ in any order,

$$K = [\mathbf{x}_1, \mathbf{x}_2, \dots, \mathbf{x}_n]. \quad (\text{C.66})$$

From (C.56a), (C.56b) with the diagonal matrix notation introduced in (C.20), it follows

$$AK = \text{diag}[\lambda_1, \lambda_2, \dots, \lambda_n] K. \quad (\text{C.67})$$

With the diagonal *eigenvalue matrix*

$$\lambda = \text{diag}[\lambda_1, \lambda_2, \dots, \lambda_n] \quad (\text{C.68})$$

this can be written as

$$AK = \lambda K. \quad (\text{C.69})$$

Multiplying this from the left with K^{-1} and considering that a diagonal matrix can be interchanged with any quadratic matrix of the same dimension yields

$$K^{-1}AK = K^{-1}\lambda K = \lambda K^{-1}K = \lambda. \quad (\text{C.70})$$

The similarity transformation

$$K^{-1}AK = \lambda \quad (\text{C.71})$$

is called *diagonalization*. If K is unitary (i.e., $K^\dagger = K^{-1}$), the diagonalization becomes a *unitary transformation*

$$K^\dagger AK = \lambda \quad (\text{C.72})$$

and the matrices A and λ are said to be *unitarily similar*.

If the matrix A is real and symmetric all eigenvalues and eigenvectors are real. If in this case K is orthogonal (i.e., $K^T = K^{-1}$), the diagonalization becomes an *orthogonal transformation*

$$K^T AK = \lambda. \quad (\text{C.73})$$

In this case the matrices A and λ are said to be *orthogonally similar*.

If two matrices A and B can be diagonalized by the same orthogonal transformation K , both matrices commute,

$$K^T AK = \lambda_A, \quad (\text{C.74a})$$

$$K^T BK = \lambda_B. \quad (\text{C.74b})$$

Considering that the diagonal matrices λ_A and λ_B commute, the proof is

$$AB - BA = K\lambda_A K^{-1} K\lambda_B K^{-1} - K\lambda_B K^{-1} K\lambda_A K^{-1} = K(\lambda_A \lambda_B - \lambda_B \lambda_A)K^{-1} = 0. \quad (\text{C.75})$$

C.3 MATRIX FUNCTIONS

The power A^n of a quadratic matrix A for a nonnegative integer n is defined as the matrix product of n copies of A ,

$$A^n = \underbrace{AA \dots A}_n. \quad (\text{C.76})$$

The matrix to the power of zero is defined to be the unit matrix of the same dimension

$$A^0 = 1. \quad (\text{C.77})$$

The matrix to the negative integer power $-n$ is defined as the inverse of the matrix A^n ,

$$A^{-n} = (A^n)^{-1}. \quad (\text{C.78})$$

For a diagonal matrix

$$\mathbf{D} = \text{diag}[D_1, D_2, \dots, D_{m-1}, D_m] \quad (\text{C.79})$$

the power \mathbf{D}^n is given by

$$\mathbf{D}^n = \text{diag}[D_1^n, D_2^n, \dots, D_{m-1}^n, D_m^n]. \quad (\text{C.80})$$

The *exponential of a matrix* \mathbf{A} is defined via the power series representing the exponential function as

$$e^{\mathbf{A}} = \sum_{n=0}^{\infty} \frac{1}{n!} \mathbf{A}^n. \quad (\text{C.81})$$

The exponential of a diagonal matrix \mathbf{D} given in (C.79) is

$$e^{\mathbf{D}} = \text{diag}[e^{D_1}, e^{D_2}, \dots, e^{D_{m-1}}, e^{D_m}]. \quad (\text{C.82})$$

Let $f(z)$ be a function defined for a complex scalar variable. The Maclaurin series expansion of $f(z)$ is given by

$$f(z) = \sum_{n=0}^{\infty} \frac{1}{n!} f^{(n)}(0) z^n \quad (\text{C.83})$$

where $f^{(n)}(0)$ denotes the n th derivative of $f(z)$ at $z = 0$. The *matrix function* $f(\mathbf{A})$ is defined via the Maclaurin series expansion as

$$f(\mathbf{A}) = \sum_{n=0}^{\infty} \frac{1}{n!} f^{(n)}(0) \mathbf{A}^n. \quad (\text{C.84})$$

The function $f(\mathbf{D})$ of a diagonal matrix \mathbf{D} given in (C.79) is

$$f(\mathbf{D}) = \text{diag}[f(D_1), f(D_2), \dots, f(D_{m-1}), f(D_m)]. \quad (\text{C.85})$$

Consider the matrix function $f(z\mathbf{A})$ where z is a complex variable and \mathbf{A} is a constant matrix. The Maclaurin series expansion according to (C.84) is

$$f(z\mathbf{A}) = \sum_{n=0}^{\infty} \frac{1}{n!} f^{(n)}(0) z^n \mathbf{A}^n. \quad (\text{C.86})$$

Differentiation with respect to z yields

$$\frac{d}{dz} f(z\mathbf{A}) = \sum_{n=1}^{\infty} \frac{1}{(n-1)!} f^{(n)}(0) z^{(n-1)} \mathbf{A}^n = \mathbf{A} \sum_{n=0}^{\infty} \frac{1}{n!} f^{(n+1)}(0) z^n \mathbf{A}^n. \quad (\text{C.87})$$

The expression under the sum is the Maclaurin series expansion of the derivative $f'(zA)$, where $f'(z) = df(z)/dz$ denotes the derivative with respect to the argument of the function. This yields

$$\frac{d}{dz}f(zA) = Af'(zA). \quad (\text{C.88})$$

For the exponential function this yields

$$\frac{d}{dz}e^{zA} = Ae^{zA}. \quad (\text{C.89})$$

Consider the n -dimensional vector $\mathbf{x}(t)$ given by

$$\mathbf{x}(t) = e^{tA} \mathbf{x}_0 \quad (\text{C.90})$$

where \mathbf{x}_0 is a constant n -dimensional vector and t is a real scalar variable. Derivation with respect to t yields

$$\frac{d}{dt}\mathbf{x}(t) = Ae^{tA} \mathbf{x}_0. \quad (\text{C.91})$$

Comparing (C.91) with (C.90) shows that $\mathbf{x}(t)$ is a solution of the first-order system of differential equations

$$\frac{d}{dt}\mathbf{x}(t) = A\mathbf{x}(t). \quad (\text{C.92})$$

If two matrices A and B fulfill $[A, [A, B]] = [B, [A, B]] = \mathbf{0}$ the *Baker-Hausdorff formula* holds:

$$e^{tA} e^{tB} e^{-t^2[A, B]} = e^{t(A+B)} \quad \text{for } [A, [A, B]] = [B, [A, B]] = \mathbf{0}. \quad (\text{C.93})$$

In particular we obtain

$$e^{tA} e^{tB} = e^{t(A+B)} \quad \text{for } [A, B] = \mathbf{0}. \quad (\text{C.94})$$

A detailed treatment of matrix analysis including the criteria for convergence is given in [4, 5].

C.4 THE HILBERT SPACE

If a unitary vector space of countable infinite dimension is *complete*, it is called a *Hilbert space* [1, 5–7]. Operators of the Hilbert space define mappings of Hilbert space vectors. P.A.M. Dirac introduced a compact notation of states and operators by interpreting the

expression $\langle \psi_i | \psi_j \rangle$ as the inner product of the vectors $\langle \psi_i |$ and $|\psi_j\rangle$ [8]. Since formally the bracket expression has been subdivided, Dirac has divided the word “*bracket*” also in two parts and has introduced the denomination *bra-vector* for the expression $\langle \psi_i |$ and *ket-vector* for the vector $|\psi_j\rangle$. To any two vectors of a Hilbert space is assigned a complex number as a *scalar product*. In a vector space with a positive definite metric (which we are assuming in the following), a scalar product of a vector with itself is positive and real unless the vector is a null vector.

The sum of two vectors $|\phi\rangle$ and $|\psi\rangle$ of Hilbert space again is a vector of Hilbert space. For this vector we can use the notation $|\phi + \psi\rangle$ and obtain

$$|\phi\rangle + |\psi\rangle = |\phi + \psi\rangle . \quad (\text{C.95})$$

The sum of vectors of Hilbert space is *commutative* and *associative*

$$\text{commutative :} \quad |\phi\rangle + |\psi\rangle = |\psi\rangle + |\phi\rangle , \quad (\text{C.96})$$

$$\text{associative :} \quad |\phi\rangle + |\psi + \chi\rangle = |\phi + \psi\rangle + |\chi\rangle . \quad (\text{C.97})$$

The product of a complex number c with a vector $|\phi\rangle$ again is a vector of the Hilbert space

$$c |\phi\rangle \equiv |c\phi\rangle . \quad (\text{C.98})$$

To distinguish a variable that may be represented by a number from vector and operators, we use the name “*c-number*.” The product of *c-numbers* and vectors of Hilbert space follows the *distributive law*:

$$c |\phi + \psi\rangle = c |\phi\rangle + c |\psi\rangle . \quad (\text{C.99})$$

The *scalar product* of two vectors $|\psi\rangle$ and $|\phi\rangle$ is a complex number a . The corresponding notation is

$$\langle \phi | \psi \rangle = a . \quad (\text{C.100})$$

The scalar product we obtain by interchanging bra- and ket-vectors is assigned the complex conjugate number

$$\langle \psi | \phi \rangle = \langle \phi | \psi \rangle^* = a^* . \quad (\text{C.101})$$

The scalar product is distributive, hence

$$\langle \phi | \psi_1 + \psi_2 \rangle = \langle \phi | \psi_1 \rangle + \langle \phi | \psi_2 \rangle . \quad (\text{C.102})$$

From the scalar product a complex number c may be extracted in the following way

$$\langle \phi | c\psi \rangle = c \langle \phi | \psi \rangle . \quad (\text{C.103})$$

With (C.101) we obtain from this

$$\langle c\psi|\phi\rangle = \langle\phi|c\psi\rangle^* = c^* \langle\psi|\phi\rangle . \quad (\text{C.104})$$

If the complex number c is extracted from the bra-vector, it occurs as the complex conjugate factor outside of the scalar product. The bra-vectors and the ket-vectors are Hermitian conjugate to each other (i.e., adjoint to each other). Adjoint expressions are marked by the superscript † ; we obtain

$$(|\phi\rangle)^\dagger = \langle\phi| , \quad (\text{C.105})$$

$$(|\phi\rangle)^\dagger = |\phi\rangle . \quad (\text{C.106})$$

The vector spaces of bra-vectors and ket-vectors are mutually dual. To obtain the adjoint expression for an arbitrary expression, we have to replace all symbols by the adjoint symbols and to invert their sequence. From (C.101), (C.104), (C.105), and (C.106) we obtain

$$(c|\phi\rangle)^\dagger = c^* \langle\phi| , \quad (\text{C.107})$$

$$(\langle\phi|\psi\rangle)^\dagger = \langle\phi|\psi\rangle^* . \quad (\text{C.108})$$

From (C.101) it follows that the scalar product $\langle\phi|\phi\rangle$ always is real. Furthermore, we set the condition that the scalar product of a vector with itself is nonnegative:

$$\langle\phi|\phi\rangle \geq 0 \quad \text{real} . \quad (\text{C.109})$$

The equal sign only is valid if $|\phi\rangle = 0$, where 0 denotes the *null vector*. The null vector 0 is defined by

$$|\phi\rangle + 0 = |\phi\rangle . \quad (\text{C.110})$$

The use of the symbol "0" for the null vector is possible since the multiplication of bra- or ket-vectors with 0 has the same effect as the forming of the inner product with the null vector. The *length* or *norm* $\|\phi\|$ of a vector $|\phi\rangle$ is given by

$$\|\phi\| = \sqrt{\langle\phi|\phi\rangle} . \quad (\text{C.111})$$

For mutually orthogonal vectors $|\phi\rangle$ and $|\psi\rangle$ we obtain

$$\langle\phi|\psi\rangle = 0 , \quad (\text{C.112})$$

also if none of the vectors $|\phi\rangle$ and $|\psi\rangle$ is the null vector.

The dimension of the Hilbert space is *countable infinite*. Furthermore, the Hilbert space fulfills the following properties:

1. The Hilbert space is *complete*. That is, if a sequence of vectors $|\phi_1\rangle, |\phi_2\rangle, \dots$ satisfies *Cauchy's criterion of convergence* there exists a limit vector $|\phi\rangle$, which is also a vector of Hilbert space. Cauchy's criterion on convergence: For every real number $\epsilon > 0$ an index $N = N(\epsilon)$ exists such that for all $n, m > N(\epsilon)$ the inequality $\| |\phi_n\rangle - |\phi_m\rangle \| < \epsilon$ is satisfied.
2. The Hilbert space is *separable*. That is for each element $|\phi\rangle$ of the Hilbert space there exists a sequence with $|\phi\rangle$ as the limit vector.

The expansion of a vector $|\phi\rangle$ of Hilbert space into a series of basis vectors $|\psi_n\rangle$ in Hilbert space in general yields an infinite series

$$|\phi\rangle = \sum_{n=0}^{\infty} a_n |\psi_n\rangle . \quad (\text{C.113})$$

The components of the vector $|\phi\rangle$ with respect to the basis $|\psi_n\rangle$ are complex numbers that are numbered with the index n . It is useful to introduce *orthonormal basis vectors* for which

$$\langle \psi_m | \psi_n \rangle = \delta_{mn} \quad (\text{C.114})$$

is fulfilled. To determine the components a_n of the vector $|\phi\rangle$ with respect to the basis $|\psi_n\rangle$, we multiply (C.113) from the left with the bra-vector $\langle \psi_n |$ and obtain with (C.114)

$$\langle \psi_m | \phi \rangle = \sum_n a_n \langle \psi_m | \psi_n \rangle = \sum_n a_n \delta_{mn} . \quad (\text{C.115})$$

From this it follows

$$a_m = \langle \psi_m | \phi \rangle . \quad (\text{C.116})$$

From (C.113) and (C.116) we obtain

$$|\phi\rangle = \sum_n |\psi_n\rangle \langle \psi_n | \phi \rangle . \quad (\text{C.117})$$

C.4.1 Linear Operators in Hilbert Space

An *operator* L maps a vector $|\phi\rangle$ into another vector $|\psi\rangle$ of the Hilbert space

$$L|\phi\rangle = |\psi\rangle . \quad (\text{C.118})$$

In the following we consider the properties of linear operators in Hilbert space. By linear operators in Hilbert space, a linear mapping of vectors in Hilbert space is accomplished. Linear operators follow the rules

$$L|\phi_1 + \phi_2\rangle = L|\phi_1\rangle + L|\phi_2\rangle , \quad (\text{C.119a})$$

$$L|a\phi\rangle = aL|\phi\rangle . \quad (\text{C.119b})$$

The sum of two operators L and M is defined by

$$(L + M) |\phi\rangle = L |\phi\rangle + M |\phi\rangle . \quad (\text{C.120})$$

The product of two operators L and M is defined by

$$LM |\phi\rangle = L(M |\phi\rangle) . \quad (\text{C.121})$$

The null element and the one element of the Hilbert space operators are the *null operator* $\mathbf{0}$ and the *unit operator* $\mathbf{1}$. Often these operators are denoted simply by 0 or 1, respectively. This yields no difficulty since the multiplications of vectors and operators with numbers is allowed and the multiplication with 0 or 1, respectively, has the same effect as the multiplication with $\mathbf{0}$ or $\mathbf{1}$. The null operator $\mathbf{0}$ and the unit operator $\mathbf{1}$ are defined by the action upon arbitrary vectors $|\phi\rangle$ of Hilbert space in the following way:

$$\forall |\phi\rangle, |\psi\rangle \Rightarrow \langle \psi | \mathbf{0} | \phi \rangle = 0 , \quad (\text{C.122a})$$

$$\forall |\phi\rangle \Rightarrow \mathbf{1} |\phi\rangle = |\phi\rangle . \quad (\text{C.122b})$$

In general for the multiplication of operators the commutative law is *not* valid:

$$ML \neq LM . \quad (\text{C.123})$$

The expression

$$[M, L] = ML - LM \quad (\text{C.124})$$

is called the *commutator* between M and L . If $[M, L] = 0$ is valid, the operators M and L are said to be *exchangeable* or *commuting*. From two vectors $|\alpha\rangle$ and $|\beta\rangle$ of Hilbert space we can form the so-called *dyadic product*

$$|\alpha\rangle \langle \beta| . \quad (\text{C.125})$$

The dyadic product is an operator. By formal multiplication of a ket-vector from the left side with the dyadic product we obtain

$$\underbrace{(|\alpha\rangle \langle \beta|)}_{\text{operator}} |\psi\rangle = |\alpha\rangle \underbrace{(\langle \beta | \psi \rangle)}_{\text{complex number}} . \quad (\text{C.126})$$

Any Hilbert space operator may be represented as a sum of dyadic products. The proof of this statement is given in the following. According to (C.117) for a complete orthonormal basis system $|\psi_n\rangle$ we obtain

$$\forall |\phi\rangle, |\phi\rangle = \sum_n |\psi_n\rangle \langle \psi_n | \phi \rangle . \quad (\text{C.127})$$

With this we obtain from (C.122b)

$$\mathbf{1} = \sum_n |\psi_n\rangle \langle \psi_n| . \quad (\text{C.128})$$

We can represent an operator L by its components with respect to a complete orthonormal system of basis vectors $|\psi_n\rangle$. To do this we multiply the operator L from the left and from the right with the unity operator $\mathbf{1}$ and obtain with (C.128)

$$L = \mathbf{1}L\mathbf{1} = \sum_{m,n} |\psi_m\rangle \langle \psi_m| L |\psi_n\rangle \langle \psi_n| . \quad (\text{C.129})$$

From the terms in the sum at the right-hand side of the above equation we may extract the terms

$$L_{mn} = \langle \psi_m | L | \psi_n \rangle \quad (\text{C.130})$$

and obtain

$$L = \sum_{m,n} L_{mn} |\psi_m\rangle \langle \psi_n| . \quad (\text{C.131})$$

The complex quantities L_{mn} are called *matrix elements* of the operator L with respect to the basis $|\psi_n\rangle$.

The *inverse operator* L^{-1} of an operator L is defined by

$$\forall |\phi\rangle, |\psi\rangle = L |\phi\rangle \Rightarrow |\phi\rangle = L^{-1} |\psi\rangle . \quad (\text{C.132})$$

From this definition we obtain the relations

$$LL^{-1} = L^{-1}L = \mathbf{1} , \quad (\text{C.133a})$$

$$(aL)^{-1} = \frac{1}{a} L^{-1} , \quad (\text{C.133b})$$

$$(ML)^{-1} = L^{-1}M^{-1} . \quad (\text{C.133c})$$

The proof of (C.133c) follows from

$$(ML)(ML)^{-1} = MLL^{-1}M^{-1} = MM^{-1} = \mathbf{1} . \quad (\text{C.134})$$

The operator L^\dagger is *adjoint* or *Hermitian conjugate*, respectively, to the operator L . The adjoint operator is defined by the property

$$\langle \phi | L^\dagger | \psi \rangle = (\langle \psi | L | \phi \rangle)^\dagger = \langle \psi | L | \phi \rangle^* \quad (\text{C.135})$$

where $|\phi\rangle$ and $|\psi\rangle$ are arbitrary vectors of the Hilbert space. We note that the rule for the forming of adjoint expressions according to (C.101) is obeyed in this definition.

According to this rule every symbol has to be replaced by the adjoint symbol and the sequence of the symbols has to be inverted. From (C.105), (C.106), (C.108) and from (C.135) we obtain

$$(L|\phi\rangle)^\dagger = \langle\phi|L^\dagger, \quad (\text{C.136a})$$

$$(L^\dagger|\phi\rangle)^\dagger = \langle\phi|L. \quad (\text{C.136b})$$

Denoting the vector resulting by application of the operator L on the vector $|\phi\rangle$ with

$$|L\phi\rangle = L|\phi\rangle, \quad (\text{C.137})$$

we obtain

$$\langle L\phi| = \langle\phi|L^\dagger \quad (\text{C.138})$$

and

$$\langle\psi|L|\phi\rangle = \langle\psi|L\phi\rangle = \langle L^\dagger\psi|\phi\rangle. \quad (\text{C.139})$$

Moving in a scalar product an operator L from the right or to the left or vice versa, the operator is replaced by its adjoint operator. According to (C.130) the matrix elements L_{mn}^* are given by

$$L_{mn}^\dagger = \langle\psi_m|L^\dagger|\psi_n\rangle \quad (\text{C.140})$$

From (C.135) it follows

$$L_{mn}^\dagger = \langle\psi_n|L|\psi_m\rangle^* = L_{nm}^*. \quad (\text{C.141})$$

Furthermore, the following relations are valid

$$(L^\dagger)^\dagger = L, \quad (\text{C.142a})$$

$$(aL)^\dagger = a^*L^\dagger, \quad (\text{C.142b})$$

$$(L + M)^\dagger = L^\dagger + M^\dagger, \quad (\text{C.142c})$$

$$(LM)^\dagger = M^\dagger L^\dagger. \quad (\text{C.142d})$$

The proof (C.142d) follows by application of (C.139).

$$\langle\psi|(LM)^\dagger\phi\rangle = \langle LM\psi|\phi\rangle = \langle M\psi|L^\dagger\phi\rangle = \langle\psi|M^\dagger L^\dagger\phi\rangle. \quad (\text{C.143})$$

If an operator L is identical with its adjoint operator L^\dagger (i.e., $L = L^\dagger$), this operator is called an *Hermitian operator* or a *self-adjoint operator*. Hermitian operators exhibit real eigenvalues. Observables are represented by Hermitian operators.

An operator U , the inverse of which U^{-1} is equal to the adjoint operator U^\dagger (i.e., $U^{-1} = U^\dagger$), is called a *unitary operator*. The unitary operator is defined by the property

$$U^\dagger U = 1. \quad (\text{C.144})$$

If the operator U is unitary and the operator H is Hermitian, the expression UHU^{-1} is Hermitian. The proof is given by

$$(UHU^{-1})^\dagger = (U^{-1})^\dagger H^\dagger U^\dagger = UHU^{-1}. \quad (C.145)$$

The projection operator P_n is given by

$$P_n = |\psi_n\rangle \langle \psi_n| \quad (C.146)$$

where $|\psi_n\rangle$ is a unit vector. With P_n an arbitrary vector $|\phi\rangle$ is projected on the unit vector $|\psi_n\rangle$. We obtain

$$P_n |\phi\rangle = \langle \psi_n | \phi \rangle |\psi_n\rangle. \quad (C.147)$$

Projection operators are Hermitian since for any $|\phi\rangle$ and $|\psi\rangle$ we obtain

$$\begin{aligned} \langle \psi | P_n^\dagger | \phi \rangle &= \langle \phi | P_n | \psi \rangle^* = \langle \phi | \psi_n \rangle^* \langle \psi_n | \psi \rangle^* \\ &= \langle \psi_n | \phi \rangle \langle \psi | \psi_n \rangle = \langle \psi | P_n | \phi \rangle. \end{aligned} \quad (C.148)$$

Let $|\psi_n\rangle$ be a complete orthonormal basis. We expand the vector $|\phi\rangle$ into the series

$$|\phi\rangle = \sum_m a_m |\psi_m\rangle. \quad (C.149)$$

We obtain

$$P_n |\phi\rangle = a_n |\psi_n\rangle. \quad (C.150)$$

We also can introduce projection operators on subspaces of the Hilbert space. The operator P_S projects a vector $|\phi\rangle$ of the Hilbert space into the unitary subspace S :

$$P_S = \sum_S |\psi_m\rangle \langle \psi_m|. \quad (C.151)$$

This summation is performed over all basis vectors $|\psi_n\rangle$ of the unitary subspace S . Projection operators are *idempotent*, that is they satisfy the relation

$$P = P^2 = P^n. \quad (C.152)$$

To an operator L of Hilbert space there exist *eigenvectors* $|\psi_n\rangle$ satisfying the *eigenvalue equation*

$$L |\psi_n\rangle = L_n |\psi_n\rangle. \quad (C.153)$$

The c -numbers L_n are called *eigenvalues* of the operator L . If (C.153) is satisfied by several eigenvectors, the set of all corresponding eigenvalues L_n is called the *eigenvalue spectrum* of the operator L . If several eigenfunctions belong to the same eigenvalue,

this eigenvalue is said to be *degenerate*. The eigenvalues of Hermitian operators are real and eigenvectors belonging to different eigenvalues are mutually orthogonal. We obtain for Hilbert space operators

$$(L_n - L_m) \langle \psi_n | \psi_m \rangle = 0. \quad (\text{C.154})$$

If the eigenvectors $|\psi_n\rangle$ of the operator L belong to a complete orthonormal set of eigenvectors in the Hilbert space, we can use these eigenvectors as a *basis*. The matrix representation of the operator L in this system of basis vectors according to (C.130) and (C.153) is given by

$$L_{mn} = \langle \psi_m | L | \psi_n \rangle = L_n \delta_{mn}. \quad (\text{C.155})$$

The matrix L_{mn} is diagonal and its matrix elements are specifying the eigenvalue spectrum L_n of the operator L . Representing the operator given in (C.131) by dyadic products, we obtain with (C.155) and (C.147)

$$L = \sum_n |\psi_n\rangle L_n \langle \psi_n| = \sum_n L_n P_n. \quad (\text{C.156})$$

This representation is called the *spectral representation* of the operator. The following rule holds: An orthonormal system of basis vectors is a system of eigenvectors of an operator, if and only if the matrix representation of the operator is diagonal in this system of basis vectors. The proof for this rule in the inverse direction follows directly from the application of L in spectral representation on $|\psi_n\rangle$.

C.4.2 Function Spaces

A *function space* is a vector space, the points of which are functions [1, 5, 7]. The function space of all complex-valued continuous functions defined on some interval or domain is a Hilbert space. The interval or domain also may be of infinite extension. A suitable *inner product* of two one-dimensional functions $\phi(x)$ and $\psi(x)$ may be defined as

$$\langle \phi(x) | \psi(x) \rangle = \int \phi^*(x) \psi(x) dx. \quad (\text{C.157})$$

An *orthonormal basis* of the function space is given by a *complete* set of basis functions $\psi_n(x)$, fulfilling

$$\langle \psi_m(x) | \psi_n(x) \rangle = \delta_{mn}. \quad (\text{C.158})$$

Any smooth function $f(x)$ can be expanded into a series

$$f(x) = \sum_{n=1}^{\infty} a_n \psi_n(x) \quad (\text{C.159})$$

with the complex coefficients a_n given by

$$a_n = \langle \psi_n | f \rangle . \quad (\text{C.160})$$

The function $f(x)$ can be represented by a Hilbert space vector

$$|f\rangle = \sum_{n=1}^{\infty} a_n |\psi_n\rangle \quad (\text{C.161})$$

where each basis vector $|\psi_n\rangle$ corresponds to a basis function ψ_n and the Hilbert space vector $|f\rangle$ is composed from the basis vectors in the same way as the function $f(x)$ from the basis functions.

Consider a linear differential operator L_{op} , given by

$$L_{\text{op}} = b_0 + b_1 \frac{d}{dx} + b_2 \frac{d^2}{dx^2} + \dots b_k \frac{d^k}{dx^k} . \quad (\text{C.162})$$

Applying the differential operator L_{op} to a function $f(x)$ will map this function into a function $g(x)$,

$$g(x) = L_{\text{op}} f(x) . \quad (\text{C.163})$$

In the basis $\psi_n(x)$ the differential operator has the matrix elements L_{mn} given by

$$L_{mn} = \int \psi_m^*(x) L_{\text{op}} \psi_n(x) dx = \langle \psi_m(x) | L | \psi_n(x) \rangle , \quad (\text{C.164})$$

where L is the operator in Hilbert space corresponding to the differential operator L_{op} . With (C.131) we can write

$$L = \sum_{m,n} L_{mn} |\psi_m\rangle \langle \psi_n| . \quad (\text{C.165})$$

In Hilbert space notation we can write

$$|g\rangle = L |f\rangle . \quad (\text{C.166})$$

From the vector $|g\rangle$ we obtain the corresponding function $g(x)$ with (C.159) and (C.160) as

$$g(x) = \sum_{n=1}^{\infty} \langle \psi_n | g(x) \rangle \psi_n(x) . \quad (\text{C.167})$$

For two differential forms \mathcal{U} and \mathcal{V} of equal order we define an inner product

$$\langle \mathcal{U} | \mathcal{V} \rangle_V = \int_V (\star \mathcal{U}^\star) \wedge \mathcal{V} = \int_V \mathcal{U}^\star \wedge \star \mathcal{V} . \quad (\text{C.168})$$

We call this inner product over a volume a *V-product*. The index V denotes the volume of integration. The index may be omitted when the domain of integration is obvious. If we have for a given domain of integration V a complete *orthonormal set of basis forms* C_m of order p fulfilling the orthonormality relation

$$\langle C_m | C_n \rangle_V = \int_V (\star C_m^*) \wedge C_n = \delta_{mn}, \quad (\text{C.169})$$

we can expand any smooth differential form \mathcal{A} of order p into a series

$$\mathcal{A} = \sum_{n=1}^{\infty} a_n C_n, \quad (\text{C.170})$$

with the expansion coefficients a_n given by

$$a_n = \langle C_n | \mathcal{A} \rangle_V. \quad (\text{C.171})$$

C.4.3 Function Spaces with Biorthogonal Basis

For the integration over a surface A we can define an inner product of two one-forms \mathcal{U} and \mathcal{V} by

$$\langle \mathcal{U} | \mathcal{V} \rangle_A = \int_A \mathcal{U}^* \wedge \mathcal{V}. \quad (\text{C.172})$$

We call this inner product of two one-forms over a surface an *A-product*. From its definition it follows that the A -product has the property

$$\langle \mathcal{V} | \mathcal{U} \rangle_A = - \langle \mathcal{U} | \mathcal{V} \rangle_A^*. \quad (\text{C.173})$$

Since this product vanishes for real $\mathcal{U} = \mathcal{V}$ we need to introduce a *biorthogonal set of basis one-forms* with the basis forms a_n and b_m with the property

$$\langle b_m | a_n \rangle_A = - \langle a_n | b_m \rangle_A = \int_A b_m^* \wedge a_n = \delta_{mn}. \quad (\text{C.174})$$

A set of basis vectors $|a_n\rangle, |b_m\rangle$ fulfilling this relation is called *biorthonormal*. Since this set of basis forms is normalized we call it a *biorthonormal set of basis one-forms*. The biorthogonal basis one-forms are based on biorthogonal functions [9]. If the union set of the dual sets of the basis forms a_n and b_n is a complete set of basis forms, we can expand any smooth one-form on a surface A into a series

$$\mathcal{C} = \sum_{n=1}^{\infty} (c_n^a a_n + c_n^b b_n) \quad (\text{C.175})$$

with the series expansion coefficients c_n^a, c_n^b given by

$$c_n^a = \langle b_n | \mathcal{C} \rangle_A, \quad (C.176a) \quad c_n^b = -\langle a_n | \mathcal{C} \rangle_A \quad (C.176b)$$

in Hilbert space representation (C.175) becomes

$$|\mathcal{C}\rangle = \sum_{n=1}^{\infty} (c_n^a |a_n\rangle + c_n^b |b_n\rangle). \quad (C.177)$$

We introduce the *biorthogonal unit operator*

$$\hat{\mathbf{I}} = \sum_{n=1}^{\infty} (|a_n\rangle\langle b_n| - |b_n\rangle\langle a_n|) \quad (C.178)$$

which has the property

$$\hat{\mathbf{I}} |\mathcal{C}\rangle = |\mathcal{C}\rangle \quad (C.179)$$

for any vector $|\mathcal{C}\rangle$. To represent an operator L by a series of dyadic products we multiply the operator from the left and the right with $\hat{\mathbf{I}}$ and obtain with (C.178)

$$L = \sum_{n=1}^{\infty} \sum_{m=1}^{\infty} (-|a_m\rangle L_{mn}^{aa} \langle a_n| + |a_m\rangle L_{mn}^{ab} \langle b_n| - |b_m\rangle L_{mn}^{ba} \langle a_n| + |b_m\rangle L_{mn}^{bb} \langle b_n|) \quad (C.180)$$

with the matrix elements given by

$$L_{mn}^{aa} = \langle b_m | L | b_n \rangle, \quad L_{mn}^{ab} = \langle b_m | L | a_n \rangle, \quad L_{mn}^{ba} = \langle a_m | L | b_n \rangle, \quad L_{mn}^{bb} = \langle a_m | L | a_n \rangle. \quad (C.181)$$

We say that the set $\{a_k\}$ of all vectors a_k *span* a *subspace* H_A of the Hilbert space H if every vector of this subspace can be represented as a linear combination of a_k . A complete set $\{a_k, b_k\}$ of biorthogonal basis vectors a_k and b_k spans the Hilbert space H . The Hilbert space H can be decomposed in the subspaces H_A and H_B , which are spanned by the sets of basis vectors a_k and b_k , respectively. The projection operators P_a and P_b , given by

$$P_a = \sum_{n=1}^{\infty} |a_n\rangle\langle a_n|, \quad (C.182a) \quad P_b = \sum_{n=1}^{\infty} -|b_n\rangle\langle a_n| \quad (C.182b)$$

project any vector on the subspaces H_A and H_B , respectively. The projection operators have the property

$$P_a |a_n\rangle = |a_n\rangle, \quad P_a |b_n\rangle = 0, \quad P_b |a_n\rangle = 0, \quad P_b |b_n\rangle = |b_n\rangle. \quad (C.183)$$

Consider operators A and B of the form

$$A = \sum_{n=1}^{\infty} \sum_{m=1}^{\infty} |b_m\rangle A_{mn} \langle b_n|, \quad (\text{C.184a})$$

$$B = - \sum_{n=1}^{\infty} \sum_{m=1}^{\infty} |a_m\rangle B_{mn} \langle a_n|. \quad (\text{C.184b})$$

Application of this operator to the basis vectors a_k and b_k yields

$$A|a_n\rangle = \sum_{m=1}^{\infty} A_{mn}|b_m\rangle, \quad (\text{C.185a}) \quad A|b_n\rangle = 0, \quad (\text{C.185b})$$

$$B|a_n\rangle = 0, \quad (\text{C.186a}) \quad B|b_n\rangle = \sum_{m=1}^{\infty} B_{mn}|a_m\rangle. \quad (\text{C.186b})$$

If the matrices A and B are inverse to each other, that is,

$$B = A^{-1}, \quad (\text{C.187})$$

then the operators A and B fulfill

$$AB = P_b, \quad (\text{C.188a}) \quad BA = P_a. \quad (\text{C.188b})$$

If the operators A are only applied to vectors $|\alpha\rangle$ belonging to the subspace H_A and the operators B are only applied to vectors $|\beta\rangle$ belonging to the subspace H_B ,

$$|\alpha\rangle = \sum_{n=1}^{\infty} \alpha_n |a_n\rangle, \quad (\text{C.189a}) \quad |\beta\rangle = \sum_{n=1}^{\infty} \beta_n |b_n\rangle. \quad (\text{C.189b})$$

Then we obtain

$$BA|\alpha\rangle = |\alpha\rangle, \quad (\text{C.190a}) \quad AB|\beta\rangle = |\beta\rangle. \quad (\text{C.190b})$$

In that case the operators A and B can be considered to be inverse to each other. Considering this restriction we can write

$$B = A^{-1}. \quad (\text{C.191})$$

We call A and B to be mutually *pseudoinverse*. An example of this case is the description of the transverse electric and magnetic fields in a waveguide. The electric and magnetic basis forms constitute a biorthogonal set of basis forms. The impedance operator is applied to magnetic field forms only and maps them into electric field forms, whereas the admittance operator acts in the opposite way. Impedance and admittance operators are pseudoinverse to each other.

REFERENCES

- [1] G. Arfken, *Mathematical Methods for Physicists*. New York: Academic Press, 1985.
- [2] C. W. Wong, *Introduction to Mathematical Physics*. Oxford: Oxford University Press, 1991.
- [3] D. S. Watkins, *Fundamentals of Matrix Computations*. New York: John Wiley & Sons, 1991.
- [4] S. Barnett, *Matrices Methods and Applications*. Oxford: Clarendon Press, 1990.
- [5] S. Hassani, *Mathematical Physics*. Berlin: Springer, 2002.
- [6] P. R. Halmos, *Introduction to Hilbert Space*. New York: Chelsea Publishing Company, 1951.
- [7] B. Friedman, *Lectures on Applications-Oriented Mathematics*. New York: John Wiley & Sons, 1969.
- [8] P. A. M. Dirac, *Quantum Mechanics*. Oxford: Oxford University Press, 1956.
- [9] P. Morse and H. Feshbach, *Methods of Theoretical Physics, Part I*. New York: McGraw-Hill, 1953.

Appendix D

Fourier Series and Fourier Transform

D.1 THE FOURIER SERIES

Periodic signals may be expanded into a *Fourier series* [1–3]. A signal for which

$$s(t + nT_0) = s(t) \quad \text{for } n = \dots, -2, -1, 0, 1, 2, \dots \quad (\text{D.1})$$

is valid is called a *periodic signal* with the period T_0 . The fundamental frequency f_0 is given by $f_0 = 1/T_0$ and the corresponding angular frequency is $\omega_0 = 2\pi f_0$. A signal

$$s(t) = \sum_{n=-\infty}^{\infty} a_n e^{jn\omega_0 t} \quad (\text{D.2})$$

which is a superposition of harmonic signals at the fundamental frequency f and the harmonics nf is periodic with T_0 . The series according to (D.2) is called a *Fourier series*. The expansion coefficients a_n are the complex amplitudes at the frequencies $n\omega_0$. The signal $s(t)$ is real if the condition $a_{-n} = a_n^*$ is fulfilled. For real signals $s(t)$ it follows from (D.2) and $a_{-n} = a_n^*$ that

$$s(t) = a_0 + 2\Re \left\{ \sum_{n=1}^{\infty} a_n e^{jn\omega_0 t} \right\}. \quad (\text{D.3})$$

Decomposing a_n in magnitude $|a_n|$ and phase ϕ_n by

$$a_n = |a_n| e^{j\phi_n} \quad (\text{D.4})$$

we obtain from (D.3)

$$s(t) = a_0 + 2 \sum_{n=1}^{\infty} |a_n| \cos(n\omega_0 t + \phi_n). \quad (\text{D.5})$$

We introduce the real amplitudes

$$b_n = a_n + a_n^*, \quad (\text{D.6})$$

$$c_n = j(a_n - a_n^*), \quad (\text{D.7})$$

and obtain from (D.3)

$$s(t) = \frac{1}{2}b_0 + \sum_{n=1}^{\infty} b_n \cos(n\omega_0 t) + c_n \sin(n\omega_0 t). \quad (\text{D.8})$$

Magnitude a_n and phase ϕ_n are obtained from the real amplitudes by b_n and c_n by

$$|a_n| = \frac{1}{2}\sqrt{b_n^2 + c_n^2}, \quad (\text{D.9})$$

$$\phi_n = -\arctan \frac{c_n}{b_n}. \quad (\text{D.10})$$

$$(\text{D.11})$$

The functions $e^{jn\omega_0 t}$ form a complete orthogonal system of basis functions in the interval $[-\frac{1}{2}T_0, \frac{1}{2}T_0]$. Applying

$$\frac{1}{T_0} \int_{-T_0/2}^{T_0/2} e^{j(n-m)\omega_0 t} dt = \delta_{mn} \quad (\text{D.12})$$

to (D.2) we obtain

$$a_n = \frac{1}{T_0} \int_{-T_0/2}^{T_0/2} s(t) e^{-jn\omega_0 t} dt. \quad (\text{D.13})$$

It can be shown that arbitrary periodic functions $s(t)$ with period T_0 , which are smooth with the exception of a finite number of discontinuities and bounded within an interval of length T_0 , may be represented by a Fourier series according to (D.2). At the points of discontinuity t_d of the function $s(t)$ the Fourier series converges to the mean value of the neighboring values on both sides of the discontinuity. Applying this equation to (D.2) we obtain

$$\lim_{\delta \rightarrow 0} \frac{1}{2} (s(t_d + \delta) + s(t_d - \delta)) = \sum_{n=-\infty}^{\infty} a_n e^{jn\omega_0 t_d}. \quad (\text{D.14})$$

From (D.6), (D.7), and (D.8), it follows that

$$b_n = \frac{2}{T_0} \int_{-T_0/2}^{T_0/2} s(t) \cos(n\omega_0 t) dt, \quad (\text{D.15})$$

$$c_n = \frac{2}{T_0} \int_{-T_0/2}^{T_0/2} s(t) \sin(n\omega_0 t) dt. \quad (\text{D.16})$$

We can decompose any function $s(t)$ in an even part $s_e(t)$ and an odd part $s_o(t)$,

$$s(t) = s_e(t) + s_o(t) \quad (\text{D.17})$$

such that $s_e(t)$ and $s_o(t)$ are given by

$$s_e(t) = \frac{1}{2}(s(t) + s(-t)), \quad (\text{D.18})$$

$$s_o(t) = \frac{1}{2}(s(t) - s(-t)). \quad (\text{D.19})$$

From (D.8), (D.17), (D.18), and (D.19), it follows that

$$s_e(t) = \frac{1}{2}b_0 + \sum_{n=1}^{\infty} b_n \cos(n\omega_0 t), \quad (\text{D.20})$$

$$s_o(t) = \sum_{n=1}^{\infty} c_n \sin(n\omega_0 t). \quad (\text{D.21})$$

D.2 THE FOURIER INTEGRAL

In the case of impulsive and transient phenomena in many other cases we have to deal with nonperiodic signals. We start with the consideration of periodic signals and make the transition ΔT to infinity. In this way the distance of spectral lines in the frequency domain Δf given by

$$\Delta f = \frac{\omega}{2\pi} = \frac{1}{T_0} \quad (\text{D.22})$$

is going to zero. We introduce a spectral amplitude density

$$\underline{S}(n\omega_0) = \frac{a_n}{\Delta f} \quad (\text{D.23})$$

and obtain from (D.2)

$$s(t) = \sum_{n=-\infty}^{+\infty} \underline{S}(n\omega_0) e^{jn\omega_0 t} \Delta f \quad (\text{D.24})$$

and from (D.13)

$$\underline{S}(n\omega_0) = \int_{-T_0/2}^{T_0/2} s(t) e^{-jn\omega_0 t} dt. \quad (\text{D.25})$$

Making the transitions $T_0 \rightarrow \infty$ and with this $\Delta f \rightarrow df = d\omega/2\pi$ and $n\omega_0 \rightarrow \omega$, we obtain from (D.24) and (D.25)

$$s(t) = \frac{1}{2\pi} \int_{-\infty}^{\infty} \underline{S}(\omega) e^{j\omega t} d\omega, \quad (\text{D.26})$$

$$\underline{S}(\omega) = \int_{-\infty}^{\infty} s(t) e^{-j\omega t} dt. \quad (\text{D.27})$$

These integrals represent linear functional transformations. The Fourier transformation is given by (D.27) and the inverse Fourier transformation is given by (D.26). The Fourier transformation and its inverse are denoted symbolically by

$$\underline{S}(\omega) = \mathfrak{F}\{s(t)\}, \quad (\text{D.28})$$

$$s(t) = \mathfrak{F}^{-1}\{\underline{S}(\omega)\}. \quad (\text{D.29})$$

Furthermore for the symbolic notation of a pair of Fourier transforms the correspondence symbol

$$s(t) \circ \bullet \underline{S}(\omega) \quad (\text{D.30})$$

is used. Replacing in (D.26) and (D.27) ω and $d\omega$, respectively, with $2\pi f$ and $2\pi df$, respectively, we obtain

$$s(t) = \int_{-\infty}^{\infty} \underline{S}(2\pi f) e^{2\pi j f t} df, \quad (\text{D.31})$$

$$\underline{S}(2\pi f) = \int_{-\infty}^{\infty} s(t) e^{-2\pi j f t} dt. \quad (\text{D.32})$$

A sufficient condition for the existence of a Fourier integral is that $s(t)$ is smooth with the exception of a finite number of discontinuities and is absolutely integrable. The latter condition means that the integral

$$\int_{-\infty}^{\infty} |s(t)| dt \quad (\text{D.33})$$

exists.

The differentiation in the time domain yields a multiplication with $j\omega$ in the frequency domain,

$$\frac{ds(t)}{dt} \circ \bullet j\omega \underline{S}(\omega), \quad (\text{D.34})$$

$$\frac{d^n}{dt^n} s(t) \circ \bullet (j\omega)^n \underline{S}(\omega), \quad (\text{D.35})$$

whereas multiplication with t in time yields a multiplication with j and differentiation in the frequency domain,

$$t s(t) \circ \bullet j \frac{d\underline{S}(\omega)}{d\omega}, \quad (\text{D.36})$$

$$t^n s(t) \circ \bullet j^n \frac{d^n}{d\omega^n} \underline{S}(\omega). \quad (\text{D.37})$$

A shift in the time domain by t_0 yields the multiplication with a phase factor in the frequency domain,

$$s(t - t_0) \circ \bullet e^{-j\omega t_0} \underline{S}(\omega), \quad (\text{D.38})$$

and a shift in the frequency domain by ω_0 yields

$$e^{j\omega_0 t} s(t) \circ \bullet \underline{S}(\omega - \omega_0). \quad (\text{D.39})$$

The complex conjugate functions transform as follows:

$$s^*(t) \circ \bullet S^*(-\omega), \quad (\text{D.40})$$

$$s^*(-t) \circ \bullet S^*(\omega). \quad (\text{D.41})$$

Scaling a function in the time domain by a factor α yields a reciprocal scaling in the frequency domain

$$s(\alpha t) \circ \bullet \frac{1}{\alpha} \underline{S}(\omega/\alpha). \quad (\text{D.42})$$

Interchanging of the time and frequency variables yields

$$\underline{S}^*(\pi t/T^2) \circ \bullet T^2 s^*(\omega T^2/2\pi). \quad (\text{D.43})$$

D.3 THE DELTA DISTRIBUTION

The *delta distribution* has the properties

$$\delta(t) = \begin{cases} 0 & \text{for } t \neq 0 \\ \infty & \text{for } t = 0 \end{cases}, \quad (\text{D.44})$$

$$\int_{-\infty}^{\infty} \delta(t) dt = 1. \quad (\text{D.45})$$

Since the delta distribution vanishes everywhere with an exception at $x = 0$, for an arbitrary function integrable within a neighborhood of $x = 0$, the relation

$$\int_{-\infty}^{\infty} f(x) \delta(x) dx = f(0) \quad (\text{D.46})$$

must hold. For arbitrary smooth functions $f(x)$ we obtain

$$\int_{-\infty}^{\infty} f(x) \delta(x - x_0) dx = f(x_0). \quad (\text{D.47})$$

The proof follows by inserting $f(x+x_0)$ instead of $f(x)$ in (D.46). The delta distribution is not a function but can be considered as a symbol indicating the value of the integral (D.46) or (D.47), respectively. From (D.46) we obtain

$$\int_{-\infty}^{\infty} \delta(t) e^{-j\omega t} dt = 1. \quad (\text{D.48})$$

From (D.27), (D.28), (D.29), and (D.46) it follows that

$$1 = \mathfrak{F}\{\delta(t)\}, \quad (\text{D.49})$$

$$\delta(t) = \mathfrak{F}^{-1}\{1\}. \quad (\text{D.50})$$

We have to consider that the integral for the inverse transformation

$$\delta(t) = \frac{1}{2\pi} \int_{-\infty}^{\infty} e^{j\omega t} d\omega \quad (\text{D.51})$$

does not exist. However, we can consider this integral as a symbol for the inverse Fourier transform according to (D.50). In symbolic notation we can write

$$\delta(t) \circ \bullet 1, \quad (\text{D.52})$$

$$\delta(t - t_0) \circ \bullet e^{-j\omega t_0} \quad (\text{D.53})$$

where (D.53) follows from (D.52) and (D.38) or from (D.27) and (D.47). The argument of the delta distribution may be scaled by

$$\delta(ax) = \frac{1}{a} \delta(x). \quad (\text{D.54})$$

The proof follows from substitution $y = ax$ from

$$\int \delta(ax) dx = \frac{1}{a} \int \delta(y) dy = \frac{1}{a}. \quad (\text{D.55})$$

From this we obtain

$$\delta(\omega) = \delta(2\pi f) = \frac{1}{2\pi} \delta(f). \quad (\text{D.56})$$

For the representation of line spectra the delta function may be used in the frequency domain. From (D.26), (D.48), and (D.56) it follows that

$$1 \circ \bullet 2\pi \delta(\omega) = \delta(f), \quad (\text{D.57})$$

$$e^{j\omega_0 t} \circ \bullet 2\pi \delta(\omega - \omega_0) = \delta(f - f_0), \quad (\text{D.58})$$

$$\cos \omega_0 t \circ \bullet \pi [\delta(\omega - \omega_0) + \delta(\omega + \omega_0)], \quad (\text{D.59})$$

$$\sin \omega_0 t \circ \bullet j\pi [\delta(\omega + \omega_0) - \delta(\omega - \omega_0)]. \quad (\text{D.60})$$

Using the delta distribution we may also represent the Fourier transforms of harmonic signals. For such signals (D.33) is not fulfilled. The sign(x) function is defined by

$$\text{sign}(x) = \begin{cases} -1 & \text{for } x < 0 \\ 0 & \text{for } x = 0 \\ 1 & \text{for } x > 0 \end{cases} . \quad (\text{D.61})$$

The uncertainty of the value of sign(0) has been removed by choosing the value 0. The Fourier transformation of the sign function is

$$\text{sign}(t) \circ \bullet \frac{2}{j\omega} . \quad (\text{D.62})$$

The step function $\sigma(x)$ of the delta distribution is given by

$$\sigma(x) = \int_{-\infty}^x \delta(x_1) dx_1 = \begin{cases} 0 & \text{for } x < 0 \\ \frac{1}{2} & \text{for } x = 0 \\ 1 & \text{for } x > 0 \end{cases} . \quad (\text{D.63})$$

The proof follows from (D.45) if we consider that the delta function gives only a contribution if 0 is within the interval of integration. Since

$$\sigma(x) = \frac{1}{2} + \frac{1}{2} \text{sign}(x) \quad (\text{D.64})$$

the Fourier transform of the σ function is given by

$$\sigma(t) \circ \bullet \frac{1}{j\omega} + \pi \delta(\omega) . \quad (\text{D.65})$$

We also may introduce distributions representing the derivation of the delta function. Applying partial integration yields for a differentiable smooth function

$$\int_{-\infty}^{\infty} f'(x) \delta(x) dx = - \int_{-\infty}^{\infty} f(x) \delta'(x) dx . \quad (\text{D.66})$$

From this we obtain

$$\int_{-\infty}^{\infty} f(x) \delta'(x) dx = -f'(0) , \quad (\text{D.67})$$

$$\int_{-\infty}^{\infty} f(x) \delta^{(n)}(x) dx = (-1)^n f^{(n)}(0) . \quad (\text{D.68})$$

The superscript $^{(n)}$ denotes the n -fold derivative with respect to the argument. The Fourier transformations of the derivatives of the delta function are given by

$$\delta^{(n)}(t) \longleftrightarrow (j\omega)^n. \quad (\text{D.69})$$

REFERENCES

- [1] G. Arfken, *Mathematical Methods for Physicists*. New York: Academic Press, 1985.
- [2] R. Bracewell, *Fourier Transform and its Applications*. New York: McGraw-Hill, 1999.
- [3] B. Friedman, *Lectures on Applications-Oriented Mathematics*. New York: John Wiley & Sons, 1969.

Appendix E

Complex Integration

E.1 ANALYTIC FUNCTIONS

A complex function is an *analytic function* on a region if it is complex differentiable at every point in that region. For analytic functions the terms holomorphic function, regular function, and complex differentiable function are also used [1–4]. An analytic function is infinitely differentiable. An *entire function* is a complex function that is analytic at all finite points of the complex plane. A complex function

$$f(z) = u(x, y) + jv(x, y) \quad (\text{E.1})$$

with $z = x + jy$ is analytic if and only if the *Cauchy-Riemann equations*

$$\frac{\partial u}{\partial x} = \frac{\partial v}{\partial y} \quad \frac{\partial u}{\partial y} = -\frac{\partial v}{\partial x} \quad (\text{E.2})$$

are fulfilled. The complex integral of an analytic function $f(z)$ from z_1 to z_2 along a path C shown in Figure E.1 is given by

$$\int_C f(z) dz = F(z_2) - F(z_1), \quad (\text{E.3})$$

where $F(z)$ is the *antiderivative* of $f(z)$. Since the complex integral of an analytic function is equal to the difference of the antiderivatives of the limits of the integration, the integral of an analytic function over a closed contour vanishes:

$$\oint_C f(z) dz = 0. \quad (\text{E.4})$$

This is the *Cauchy integral theorem*. Consider a function $f(z)$ that is analytic every-

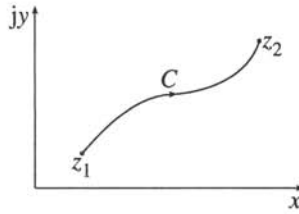
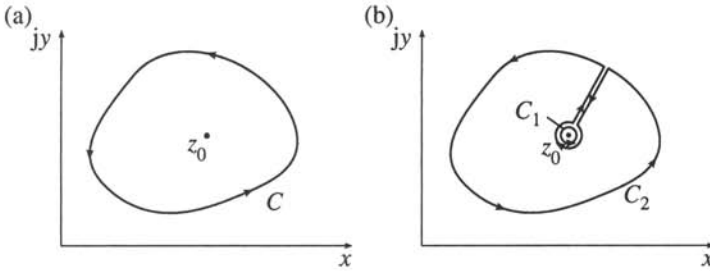


Figure E.1: Path of integration in the complex plane.

Figure E.2: (a) Integration over a closed curve C around a singularity z_0 , (b) subdivision of the path of integration into C_1 and C_2 .

where with the exception of the point z_0 . If a function $f(z)$ fails to be analytic at a point z_0 but is analytic in every neighborhood of the point z_0 this is called a *singular point* or a *singularity*. The integral over a closed path C shown in Figure E.2(a) enclosing the singular point z_0 may be decomposed in two integrals over C_1 and C_2 shown in Figure E.2(b). The path of integration C_1 is a circle of infinitesimal radius ρ_0 enclosing the singular point z_0 , whereas the function $f(z)$ in the region enclosed by the path C_2 is analytic. Therefore the integral over C_2 is zero.

Consider a function $g(z)$ with a pole of first order at z_0 . Such a function may be expressed by

$$g(z) = \frac{f(z)}{z - z_0}, \quad (\text{E.5})$$

with a function $f(z)$ that is analytic and nonvanishing at z_0 . To integrate $f(z)$ around the circle C_2 with radius ρ in counter-clockwise direction we substitute

$$z = z_0 + \rho e^{j\phi} \quad dz = j\rho e^{j\phi} d\phi. \quad (\text{E.6})$$

If we let $\rho \rightarrow 0$, this yields

$$\lim_{\rho \rightarrow 0} \oint_C \frac{f(z)}{z - z_0} dz = j \int_0^{2\pi} f(z_0) d\phi = 2\pi j f(z_0), \quad (\text{E.7})$$

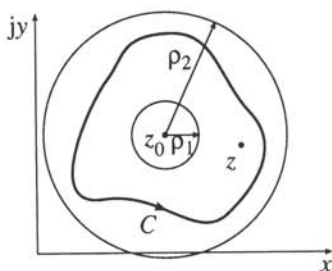


Figure E.3: Annular domain.

This yields the *Cauchy integral formula*, valid for any function $f(z)$ that is analytic in a region enclosed by the contour C and given by

$$f(z_0) = \oint_C \frac{f(z)}{z - z_0} dz \quad f^{(n)}(z_0) = \oint_C \frac{f(z)}{(z - z_0)^{n+1}} dz, \quad (\text{E.8})$$

where $f^{(n)}(z)$ denotes the n th derivative of $f(z)$.

Consider a function $f(z)$ that is analytic in an annular domain $\rho_1 < |z - z_0| < \rho_2$ and exhibiting a singularity at z_0 as shown in Figure E.3. Since the function is singular at z_0 it cannot be expanded into a Taylor series at that point. However, very often it is possible to represent a function with a singularity at z_0 by a *Laurent series*,

$$f(z) = \sum_{n=-\infty}^{\infty} c_n (z - z_0)^n \quad \text{for } \rho_1 < |z - z_0| < \rho_2. \quad (\text{E.9})$$

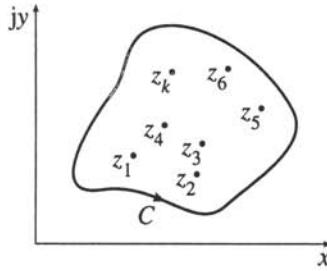
The coefficients c_n of the Laurent series are given by

$$c_n = \oint_C \frac{f(z)}{(z - z_0)^{n+1}} dz. \quad (\text{E.10})$$

E.2 THE RESIDUE THEOREM

Consider a function $f(z)$ that has a finite number n of singularities inside and on a closed contour C , as illustrated in Figure E.4. Let us integrate $f(z)$ over the closed contour in the positive sense; that means counter-clockwise. The *residue theorem* states that the value of the integral of $f(z)$ around the closed contour is $2\pi j$ times the sum of the residues at the singular points enclosed by the contour, hence

$$\oint_C f(z) dz = \sum_{k=1}^n \text{Res} f(z_k). \quad (\text{E.11})$$

Figure E.4: Singular points z_k inside a closed contour C .

For a first-order pole at z_k the *residue* is given by

$$\text{Res } f(z_k) = \lim_{z \rightarrow z_k} (z - z_k) f(z). \quad (\text{E.12})$$

For the special case of $f(z)$ and $g(z)$ analytic in a neighborhood of z_k and $g'(z_k) \neq 0$ we obtain

$$\text{Res } \frac{f(z)}{g(z)} \Big|_{z=z_k} = \frac{f(z_k)}{g'(z_k)}. \quad (\text{E.13})$$

For a pole of m th order the residue is

$$\text{Res } f(z_k) = \frac{1}{(m-1)!} \lim_{z \rightarrow z_k} \frac{d^{m-1}}{dz^{m-1}} [(z - z_k)^m f(z)]. \quad (\text{E.14})$$

E.3 THE SADDLE-POINT METHOD

We investigate integrals of the kind

$$I_0 = \int_{-\infty}^{\infty} C_n(\gamma) H_n^{(2)} \left(\sqrt{k^2 - \gamma^2} \rho \right) e^{-j\gamma z} d\gamma. \quad (\text{E.15})$$

In general it is difficult to evaluate such integrals. For the far-field the evaluation can be simplified by application of the so-called *saddle-point method*. We consider the integral expression

$$I = \int_C f(\zeta) e^{u g(\zeta)} d\zeta, \quad (\text{E.16})$$

which is the generalized form of (E.15). In this integral $f(\zeta)$ and $g(\zeta)$ are complex functions of the complex variable ζ , and u is a positive real number.

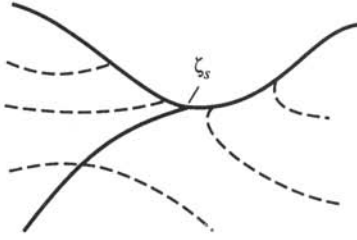


Figure E.5: Surface with saddle-point.

Let us consider one point in the complex ζ -plane for which the condition

$$\frac{dg(\zeta)}{d\zeta} = 0 \quad (\text{E.17})$$

is fulfilled. For real ζ by this condition an extremum value or a turning point is defined. In the complex plane the real part or imaginary part of a regular function can assume an extremum value only at the boundary of a certain domain and not inside of the domain. We expand $g(\zeta)$ at $\zeta = \zeta_s$ in a Taylor series and obtain

$$g(\zeta) = g(\zeta_s) + (\zeta - \zeta_s)g'(\zeta_s) + \frac{1}{2!}(\zeta - \zeta_s)^2 g''(\zeta_s) + \dots \quad (\text{E.18})$$

If the condition (E.17) is fulfilled at $\zeta = \zeta_s$, we obtain in a neighborhood of ζ_s the expansion

$$g(\zeta) = g(\zeta_s) + \frac{1}{2!}(\zeta - \zeta_s)^2 g''(\zeta_s). \quad (\text{E.19})$$

Figure E.5 shows the surface $\Re\{\zeta^2\}$ in a neighborhood of the saddle-point. In the saddle-point method, the path of integration is chosen such that coming from infinity it is going through one of the valleys up to the saddle-point ζ_s , and from there going through the other valley again to infinity. We have to consider that the function

$$e^{ug(\zeta)} = e^{u\Re\{g(\zeta)\}} [\cos(u\Im\{g(\zeta)\}) + j \sin(u\Im\{g(\zeta)\})] \quad (\text{E.20})$$

strongly oscillates with ζ . To suppress these oscillations the path of integration must be selected such that $\Im\{g(\zeta)\}$ is constant. We insert (E.19) into (E.16) and obtain

$$I = e^{ug(\zeta_s)} \int_C f(\zeta) \exp\left[\frac{1}{2}u(\zeta - \zeta_s)^2 g''(\zeta_s)\right] d\zeta. \quad (\text{E.21})$$

In the valley of the saddle surface the real part of $g''(\zeta_s)$ is negative. In (E.19) we have assumed that the positive real number u is sufficiently large that the series expansion

of $g(\zeta)$ can be approximated in a neighborhood of ζ_s by the quadratic term. We are making use of the circumstance that the magnitude of the integrand rapidly converges to zero within a sufficiently small neighborhood of ζ_s . Furthermore we make the assumption that $f(\zeta)$ only is weakly dependent on ζ . Therefore in the region where the integrand gives a contribution, $f(\zeta)$ may be replaced by $f(\zeta_s)$ and moved outside the integral. In this way we obtain

$$I = f(\zeta_s) e^{ug(\zeta_s)} \int_{C_{\text{valley}}} \exp\left[\frac{1}{2}u(\zeta - \zeta_s)^2 g''(\zeta_s)\right] d\zeta. \quad (\text{E.22})$$

Now we express $\zeta - \zeta_s$ by the magnitude η and the phase ψ and obtain

$$\zeta - \zeta_s = \eta e^{j\psi}. \quad (\text{E.23})$$

We choose a path of integration where η is going from $-\infty$ to ∞ and the angle ψ is constant. In this case we obtain

$$d\zeta = e^{j\psi} d\eta. \quad (\text{E.24})$$

This yields

$$I = f(\zeta_s) e^{ug(\zeta_s)} \int_{C_{\text{valley}}} \exp\left[\frac{1}{2}u\eta^2 e^{j2\psi} g''(\zeta_s)\right] e^{j\psi} d\eta. \quad (\text{E.25})$$

Now we are choosing ψ such that

$$e^{j2\psi} g''(\zeta_s) = -p \quad (\text{E.26})$$

is fulfilled, where p is a positive real quantity. With this we obtain

$$I = f(\zeta_s) e^{ug(\zeta_s) + j\psi} \int_{-\infty}^{\infty} \exp\left[-\left(\frac{1}{2}up\right)\eta^2\right] d\eta. \quad (\text{E.27})$$

With the substitution

$$\frac{up}{2}\eta^2 = x^2 \quad (\text{E.28})$$

we obtain from this

$$I \cong f(\zeta_s) e^{ug(\zeta_s) + j\psi} \sqrt{\frac{2}{up}} \int_{-\infty}^{\infty} e^{-x^2} dx = \sqrt{\frac{2\pi}{up}} f(\zeta_s) e^{ug(\zeta_s) + j\psi}. \quad (\text{E.29})$$

REFERENCES

- [1] P. Morse and H. Feshbach, *Methods of Theoretical Physics, Part I*. New York: McGraw-Hill, 1953.
- [2] B. Friedman, *Lectures on Applications-Oriented Mathematics*. New York: John Wiley & Sons, 1969.
- [3] R. V. Churchill and J. W. Brown, *Complex Variables and Applications*. New York: McGraw Hill, 1990.
- [4] C. W. Wong, *Introduction to Mathematical Physics*. Oxford: Oxford University Press, 1991.

List of Symbols

Symbol	Description	Reference
A	Surface	(2.15)
A_e	Effective aperture	(13.97)
∂A	Boundary of a surface A	(2.13)
\underline{a}	Wave amplitude phasor	(8.40a)
$\underline{\underline{a}}$	Incident wave amplitude vector	(10.38)
$A(\mathbf{x}, t)$	Magnetic vector potential	(3.1)
A	Chain matrix	(10.11)
$\mathcal{A}(\mathbf{x}, t)$	Magnetic vector potential form	(3.1)
α	Attenuation coefficient	(3.51)
\underline{b}	Wave amplitude phasor	(8.40b)
$\underline{\underline{b}}$	Scattered wave amplitude vector	(10.38)
$B(\mathbf{x}, t)$	Magnetic flux density vector	(2.23b)
B	Inverse chain matrix	(10.30)
$B(\mathbf{x}, t)$	Magnetic flux density differential form	(2.28)
$\underline{B}(\mathbf{x}, \omega)$	Magnetic flux density differential form phasor	(2.123c)
β	Phase coefficient	(3.51)
C	Capacitance	(5.33)
C_{lk}	Partial capacitance	(5.23)
C'	Capacitance per unit of length	(5.48)
C''	Capacitance per unit of area	(5.52)
c	Speed of light	(2.75)
c	Phase velocity	(7.3)
c_0	Free space speed of light	(2.60)
c_n^m	Normalization constant	(B.53)
d	Differential operator	(2.110)
d	Exterior derivative	(2.110)
d_t	Transverse exterior derivative	(4.136)
\tilde{d}	Covariant derivative	(3.11)
δ_{mn}	Kronecker delta symbol	(A.8)
δ_{xyz}	Kronecker tensor	(A.12)

Symbol	Description	Reference
$\delta(x)$	Delta distribution	(D.47)
$\delta(\mathbf{x} - \mathbf{x}')$	Three-dimensional delta distribution	(5.9)
$\delta_e(\omega)$	Dielectric loss angle	(2.126)
$\delta_m(\omega)$	Magnetic loss angle	(2.127)
$\mathbf{D}(\mathbf{x}, t)$	Electric flux density vector	(2.26)
$\mathcal{D}(\mathbf{x}, \omega)$	Electric flux density differential form phasor	(2.123a)
$\underline{\mathcal{D}}(\mathbf{x}, t)$	Electric flux density differential form	(2.11)
$\mathbf{E}(\mathbf{x}, t)$	Electric field vector	(2.2)
$\underline{\mathbf{E}}(\mathbf{x}, \omega)$	Electric field vector phasor	(2.117)
$\mathbf{e}(x, y)$	Electric structure function	(7.28a)
$\mathcal{E}(\mathbf{x}, t)$	Electric field differential form	(2.11)
$\underline{\mathcal{E}}(\mathbf{x}, \omega)$	Electric field differential form phasor	(2.121)
$\underline{\mathcal{E}}_t(\mathbf{x}, \omega)$	Transverse electric field differential form phasor	(2.175c)
$\underline{\mathcal{E}}_z(\mathbf{x}, \omega)$	Longitudinal electric field differential form phasor	(7.113)
$E(\mathbf{z})$	Electric structure form	(9.97a)
$\mathbf{e}(x, y)$	Electric structure form	(7.29a)
ϵ	Permittivity	(2.23a)
ϵ_r	Relative permittivity	(2.25a)
$\underline{\epsilon}(\omega)$	Complex permittivity	(2.125)
$\underline{\epsilon}_r(\omega)$	Complex relative permittivity	(2.128)
$\epsilon'(\omega)$	Real part of complex permittivity	(2.125)
$\epsilon''(\omega)$	Negative imaginary part of complex permittivity	(2.125)
f	Frequency	(2.84)
$F(\theta, \phi)$	Element characteristics	(13.115)
$\mathbf{F}(\mathbf{x}, t)$	Force vector	(2.7)
$\mathbf{F}^{\text{el}}(\mathbf{x}, t)$	Electric force vector	(2.3)
$\mathbf{F}^{\text{mag}}(\mathbf{x}, t)$	Lorentz force vector	(2.5)
$\mathfrak{F}\{s(t)\}$	Fourier transform	(D.28)
G	Conductance	(9.24a)
G	Antenna gain	(13.94)
G_r	Radiation conductance	(13.172)
G'	Conductance per unit of length	(7.65)
$G_0(\mathbf{x}, \mathbf{x}')$	Green's function	(5.11)
$\mathcal{G}(\mathbf{x}, \mathbf{x}')$	Green's double one-form	(5.56)
$\mathcal{G}_{BS}(\mathbf{x}, \mathbf{x}')$	Green's double one-form	(5.69)
γ	Propagation coefficient	(3.49)
$\mathbf{H}(\mathbf{x}, t)$	Magnetic field vector	(2.23b)
$\underline{\mathbf{H}}(\mathbf{x}, \omega)$	Magnetic field vector phasor	(2.117)
$\mathbf{h}(x, y)$	Magnetic structure function	(7.28b)

Symbol	Description	Reference
$\mathcal{H}(\mathbf{x}, t)$	Magnetic field differential form	(2.14)
$\underline{\mathcal{H}}(\mathbf{x}, \omega)$	Magnetic field differential form phasor	(2.123a)
$\underline{\mathcal{H}}_t(\mathbf{x}, \omega)$	Transverse electric field differential form phasor	(8.117b)
$\underline{\mathcal{H}}_z(\mathbf{x}, \omega)$	Longitudinal electric field differential form phasor	(8.106b)
$H(\mathbf{z})$	Magnetic structure form	(9.97b)
$h(\mathbf{x}, y)$	Magnetic structure form	(7.29b)
$i(t)$	Electric current	(2.13)
\underline{I}	Electric current phasor	(10.1)
$\underline{\mathbf{I}}$	Current vector	(10.3b)
$\Im\{z\}$	Imaginary part of z	(3.50)
$\mathcal{I}(\mathbf{x}, \mathbf{x}')$	Identity kernel	(5.58)
$\mathbf{J}(\mathbf{x}, t)$	Current density vector	(2.21)
$\mathcal{J}(\mathbf{x}, t)$	Current density differential form	(2.21)
$\underline{\mathcal{J}}(\mathbf{x}, \omega)$	Current density differential form phasor	(2.123a)
$\underline{\mathcal{J}}_0(\mathbf{x}, t)$	Impressed current density differential form	(2.62)
$\underline{\mathcal{J}}_0(\mathbf{x}, \omega)$	Impressed current density differential form phasor	(2.124a)
$\mathbf{J}_A(\mathbf{x}, t)$	Surface current density vector	(2.153)
$\mathcal{J}_A(\mathbf{x}, t)$	Surface current density differential form	(2.153)
$\underline{\mathcal{J}}_A(\mathbf{x}, \omega)$	Surface current density differential form phasor	(2.173a)
g	Characteristic impedance square roots	(10.34)
k	Wave number	(3.44)
\mathbf{k}	Wave vector	(3.42)
L	Inductance	(5.78)
L'	Inductance per unit of length	(5.98)
L_{\square}	Inductance of a square parallel plate element	(5.105)
L_{op}	Linear operator	(4.118)
\mathcal{L}	Linear Hilbert space operator	(C.118)
λ	Wavelength	(2.85)
λ_0	Free-space wavelength	(2.88)
λ_c	Cutoff wavelength	(7.233)
λ_g	Waveguide wavelength	(2.85)
$M(\theta, \phi)$	Array factor	(13.123)
M_{ij}	Mutual inductance	(5.76)
$\mathcal{M}_{e0}(\mathbf{x}, t)$	Impressed electric polarization form	(3.22)
$\underline{\mathcal{M}}_{e0}(\mathbf{x}, \omega)$	Impressed electric polarization form phasor	(3.27a)
$\underline{\mathcal{M}}_{e0t}(\mathbf{x}, \omega)$	Impressed transverse el. polarization form phasor	(8.108b)
$\underline{\mathcal{M}}_{e0z}(\mathbf{x}, \omega)$	Impressed longitudinal el. polarization form phasor	(8.108a)
$\underline{\mathcal{M}}_{m0}(\mathbf{x}, \omega)$	Impressed magnetic polarization form phasor	(3.30b)
$\mathcal{M}_{eA}(u, v, t)$	Electric surface polarization form	(2.161)

Symbol	Description	Reference
$\underline{M}_{eA}(u, v, \omega)$	Electric surface polarization form phasor	(2.173b)
$\mathcal{M}_{mA}(u, v, t)$	Magnetic surface polarization form	(2.163)
$\underline{M}_{mA}(u, v, \omega)$	Magnetic surface polarization form phasor	(2.173c)
μ	Permeability	(2.23b)
μ_r	Relative permeability	(2.25b)
$\underline{\mu}(\omega)$	Complex permeability	(2.127)
$\underline{\mu}_r(\omega)$	Complex relative permeability	(2.127)
$\mu'(\omega)$	Real part of complex permeability	(2.129)
$\mu''(\omega)$	Negative imaginary part of complex permeability	(2.127)
n	Normal unit one-form	(2.138)
n	Refractive index	(2.76)
ω	Angular frequency	(2.84)
Ω	Normalized frequency	(11.74)
$p_L(\mathbf{x}, t)$	Power loss density	(4.7)
$\mathcal{P}_L(\mathbf{x}, t)$	Power loss density form	(4.7)
$p_{Le}(\mathbf{x}, \omega)$	Electric power loss density	(4.27)
$\mathcal{P}_{Le}(\mathbf{x}, \omega)$	Electric power loss density form	(4.27)
$p_{Lm}(\mathbf{x}, \omega)$	Magnetic power loss density	(4.29)
$\mathcal{P}_{Lm}(\mathbf{x}, \omega)$	Magnetic power loss density form	(4.29)
$\mathcal{P}_0(\mathbf{x}, t)$	Added power density form	(4.9)
$\overline{\mathcal{P}}_0(\mathbf{x})$	Added time-average power density	(4.34)
P_c	Complex power	(9.1)
$P_{c0}(\mathbf{x}, \omega)$	Added complex power density	(4.32)
$\mathcal{P}_{c0}(\mathbf{x}, \omega)$	Added complex power density form	(4.32)
$\Pi_e(\mathbf{x}, t)$	Electric Hertz vector	(3.16)
$\Pi_e(\mathbf{x}, t)$	Electric Hertz form	(3.16)
$\underline{\Pi}_e(\mathbf{x}, \omega)$	Electric Hertz form phasor	(3.28)
$\underline{\Pi}_m(\mathbf{x}, t)$	Magnetic Hertz vector phasor	(3.33)
$\underline{\Pi}_m(\mathbf{x}, \omega)$	Magnetic Hertz form phasor	(3.34)
ϕ	Normalized potential	(5.19)
ϕ_0	Phase angle	(2.86a)
$\Phi(t)$	Magnetic flux	(2.29)
$\Phi(t)$	Scalar potential	(3.3)
Φ_e	Electrostatic potential	(5.108)
Φ_m	Magnetostatic potential	(5.109)
Φ'	Magnetic flux per unit of length	(7.39)
$\Psi(t)$	Electric flux	(2.27)
$q(t)$	Electric charge	(2.1)
Q'	Electric charge per unit of length	(7.32)

Symbol	Description	Reference
$Q(\mathbf{x}, t)$	Electric charge density differential form	(2.43)
$\underline{Q}(\mathbf{x}, \omega)$	Electric charge density differential form phasor	(2.123d)
$\underline{Q}_A(\mathbf{x}, t)$	Electric area charge density differential form	(2.142)
$\underline{Q}_A(\mathbf{x}, \omega)$	Electric area charge density differential form phasor	(2.172b)
R	Resistance	(9.24b)
R_r	Radiation resistance	(12.25)
R_{ij}	Reaction of field \mathcal{E}_i , \mathcal{H}_i on sources \underline{M}_{e0j} , \underline{M}_{m0j}	(4.66)
$\Re\{z\}$	Real part of z	(2.117)
$\rho(\mathbf{x}, t)$	Electric charge density	(2.43)
ρ_0	Reflection coefficient	(8.47)
$\rho_A(\mathbf{x}, t)$	Electric area charge density	(2.142)
s_i	Unit one-form	(A.109)
$s(t)$	Signal	(D.26)
$\mathbf{S}(\mathbf{x}, t)$	Poynting vector	(4.11)
\mathbf{S}	Scattering matrix	(10.38)
$\mathcal{S}(\mathbf{x}, t)$	Poynting differential form	(4.11)
$\underline{S}(\omega)$	Signal spectrum	(D.27)
σ	Conductivity	(2.62)
$\mathbf{T}(\mathbf{x})$	Complex Poynting vector	(4.19)
\mathbf{T}	Transmission matrix	(10.51)
τ	Transmission coefficient	(10.102)
$\mathcal{T}(\mathbf{x})$	Complex Poynting differential form	(4.19)
$\mathbf{v}(\mathbf{x}, t)$	Velocity vector	(2.7)
$v(t)$	Voltage	(2.9)
\underline{V}	Voltage phasor	(10.1)
$\underline{\underline{V}}$	Voltage vector	(10.3a)
$v_m(t)$	Magnetic voltage	(2.64)
v_g	group velocity	(7.7)
V	Volume	(2.43)
∂V	Boundary of a volume V	(2.45)
\underline{w}	Complex variable	(5.130)
$W(t)$	Energy	(2.8)
$w_e(\mathbf{x}, t)$	Electric energy density	(4.1a)
$\overline{w}_e(\mathbf{x})$	Average electric energy density	(4.23)
$\mathcal{W}_e(\mathbf{x}, t)$	Electric energy density form	(4.2a)
$\overline{\mathcal{W}}_e(\mathbf{x})$	Time-average electric energy density form	(4.23)
$w_m(\mathbf{x}, t)$	Magnetic energy density	(4.1b)
$\overline{w}_m(\mathbf{x})$	Average magnetic energy density	(4.24)
$\mathcal{W}_m(\mathbf{x}, t)$	Magnetic energy density form	(4.2a)

Symbol	Description	Reference
$\overline{\mathcal{W}}_m(\mathbf{x})$	Time-average magnetic energy density form	(4.24)
$W\{f(z), g(z)\}$	Wronskian	(B.11)
\mathbf{Y}	Impedance matrix	(10.6)
y	Normalized admittance	(8.59b)
\overline{Z}_0	Characteristic impedance	(7.37)
Z_F	Wave impedance	(2.79)
Z_{F0}	Free-space wave impedance	(2.80)
Z_{mn}	Impedance matrix elements	(10.4)
\mathbf{Z}	Impedance matrix	(10.5)
\underline{z}	Normalized impedance	(8.59a)
\underline{z}	Complex variable	(5.129)
$\mathbf{0}$	Null matrix	(C.13)
$\mathbf{0}$	Null operator	(C.122a)
$\mathbf{1}$	Unit matrix	(C.17)
$\mathbf{1}$	Unit operator	(C.122b)
$\hat{\mathbf{1}}$	Biorthogonal unit operator	(C.178)
\lrcorner	Contraction	(2.165b)
$\langle\phi $	bra-vector	(C.107)
$ \phi\rangle$	ket-vector	(C.95)
$\langle\phi \psi\rangle$	scalar product	(C.100)
$\langle\mathcal{U} \mathcal{V}\rangle_V$	V-product	(C.168)
$\langle\mathcal{U} \mathcal{V}\rangle_A$	A-product	(C.172)
\wedge	Exterior product	(2.17)
$\circ\!\!\!\rightarrow$	Fourier transform	(D.30)
\in	in	(2.144)
\notin	not in	(2.144)
$*$	Hodge operator	(2.30)
$*_\epsilon$	Permittivity star operator	(2.35a)
$*_\mu$	Permeability star operator	(2.38a)
Δ	Laplace operator	(3.12)
Δ_t	Two-dimensional Laplace operator	(A.138)
$ \mathbf{a} $	Magnitude of the vector \mathbf{a}	(A.4)
∂	Partial differential operator	(2.93)
$\dot{\mathcal{D}}$	Partial derivative of \mathcal{D} with respect to t	(4.3)
$P^\triangleleft \mathcal{A}$	Pullback of \mathcal{A} to the path P	(A.182)
$\overline{\mathcal{S}}(\mathbf{x}, t)$	Time average of $\mathcal{S}(\mathbf{x}, t)$	(4.22)
\perp_n	Twist operator	(2.155)
\times	Vector product	(2.6)

About the Author

Peter Russer received his Dipl.-Ing. degree in 1967 and his Dr. techn. degree in 1971, both in electrical engineering, from the Technische Universität Wien, Austria, where he was assistant professor from 1968 to 1971. In 1971 he joined the Research Institute of AEG-Telefunken in Ulm, Germany, where he worked on fiber-optic communication, broadband solid-state electronic circuits, statistical noise analysis of microwave circuits, laser modulation, and fiber-optic gyroscopes. In 1979 he received the NTG Award for the publication "Electronic circuits for high bit rate digital fiber optic communication systems." Since 1981 he has been a full professor and head of the Institute of High Frequency Engineering at the Technische Universität München (TUM), Germany. In 1990 he was visiting professor at the University of Ottawa and at the University of Victoria in 1993. From October 1992 through to March 1995 he was director of the Ferdinand-Braun-Institut für Höchstfrequenztechnik, Berlin, Germany. In 1994 he was elected Fellow of the IEEE for fundamental contributions to noise analysis and low-noise optimization of linear electronic circuits with general topology. His current research interests are electromagnetic fields, antennas, integrated microwave and millimeter-wave circuits, statistical noise analysis of microwave circuits, and methods for the computer-aided design of microwave circuits. He has published more than 400 scientific papers in refereed journals and conference proceedings.

Peter Russer has developed a variety of courses in RF techniques, microwaves, quantum electronics, and optical communications. He is the program director of the international graduate program "Master of Science in Microwave Engineering" at TUM. Over the years he has graduated more than 400 students, of which more than 50 received their PhD degree.

Peter Russer has served as a member of technical program committees and steering committees of various international conferences (IEEE MTT-S, European Microwave Conference) and as a member of the editorial board of several international journals (*Electromagnetics*, *International Journal of Numerical Modeling*). In 2002 he was elected as Chairman of U.R.S.I. Commission D for a three-year term. He is a member of the German Informationstechnische Gesellschaft (ITG) and the German Physical Society as well as the Austrian Physical Society.

Index

- A-product, 693
- Admittance
 - matrix, 415
 - normalized, 350
 - per unit of length, 336
 - representation, 415
- Admittance matrix
 - surface, 94, 621
- Admittance operator
 - surface, 622
- Ampère's law, 24, 26, 242
- Ampère, André, 2
- Analytic function, 176
- Angle product, 54, 633
- Antenna
 - aperture, 589
 - biconical, 595
 - broadband, 595
 - Cassegrain, 587
 - conformal, 592, 593
 - conformal microstrip, 593
 - dipole, 547, 549, 553
 - frequency-independent, 596
 - gain, 569
 - horn paraboloid, 588
 - lens, 588
 - logarithmic-periodic, 596
 - microstrip, 591
 - monopole, 547
 - parabolic reflector, 587
 - patch, 592
 - planar, 593
 - reflector, 587
 - slot, 589
 - symmetric dipole, 551
- Antenna array, 575
 - array factor, 577
 - circular, 577
 - element pattern, 575
 - linear, 575
 - microstrip, 593
 - multiplicative law, 577
- Antenna gain, 569
- Antiderivative, 705
- Area charge
 - density, 48
 - differential form, 48
- Array factor, 577
- Attenuation coefficient, 69
- Babinet's principle, 123, 591, 596
- Backward wave, 508
- Baker-Hausdorff formula, 683
- Basis
 - three-form, 46
 - two-forms, 46
- Basis form
 - biorthonormal set, 426
 - orthonormal set, 693
- Basis functions, 603, 605
 - complete set of, 147, 606
 - entire domain basis functions, 606
 - subsectional basis functions, 606
- Basis one-form
 - biorthogonal set, 693
 - biorthonormal set, 693

- Bessel differential equation, 99, 659
 - modified, 662
- Bessel function, 99, 659
 - modified, 662
 - modified of the first kind, 662
 - modified of the second kind, 663
 - of the first kind, 99, 659
 - of the second kind, 99, 659
 - spherical, 103, 665
- Biot-Savart law, 163, 203
- Bloch waves, 504
- Booker's relation, 591
- Boundary condition, 47, 54
 - Dirichlet, 272
 - electric field intensity, 53
 - electric flux density, 49
 - magnetic field intensity, 52
 - magnetic flux density, 48
 - Neumann's, 269, 272
 - normal, 47, 49, 50
 - practical, 218
 - tangential, 49, 51, 53
- Brewster angle, 86
- Butterworth response, 482
- Capacitance, 155, 157
 - mutual per unit of length, 252
 - partial capacitance, 156
 - per unit of area, 161
 - per unit of length, 160, 180, 238
- Capacitor, 4, 24, 151
 - spherical, 158
- Cartan, Elie, 5
- Cauchy integral formula, 707
- Cauchy integral theorem, 705
- Cauchy-Riemann equations, 176, 705
- Chain matrix, 92, 416
- Chain representation, 415
- Characteristic equation
 - planar waveguide, 319
- Characteristic impedance, 181, 239, 248, 336
 - coplanar stripline, 266
 - coplanar waveguide, 265
 - matrix, 360
 - microstrip line, 261
 - nonsymmetric two-port, 477
 - symmetric two-port, 475
 - waveguide, 336
- Charge per unit of length, 238
- Chebyshev filter characteristic, 485
- Chebyshev polynomial, 485
- Circulation, 27
- Coaxial line, 229
- Commutation relation, 631
- Complete system of functions
 - spherical, 102
 - spherical harmonics, 671
- Complex
 - amplitude, 286, 338
 - function, 175
 - power, 385
 - wave, 72
- Computer aided design, 603
- Conductance per unit of length, 245
- Conductivity, 28
- Conductor losses, 289
 - rectangular waveguide, 289
- Conformal
 - antenna, 592, 593
 - mapping, 174, 176
 - transformation, 176
- Connection circuit, 427
- Constitutive equations, 19
- Constitutive relations, 19
- Continuity equation, 27
 - differential form, 42
 - integral form, 27
- Contraction, 54, 633
- Controlled source, 434
- Coordinate curve, 46
- Coordinate surface, 46
- Coordinate system
 - Cartesian, 627
 - circular cylindrical, 46, 647
 - curvilinear, 640
 - curvilinear orthogonal, 46
 - general cylindrical, 646
 - orthogonal, 642
 - spherical, 47, 650
 - cartesian, 10
- Coplanar line, 193
 - inhomogeneous coplanar line, 195
- Coplanar stripline, 196, 265
 - inhomogeneous coplanar stripline, 196
- Corrugated surface, 506
- Coulomb force, 9
- Coulomb, Charles, 2
- Coupling

- critical coupling, 403
- overcoupled, 403
- undercoupled, 403
- Covariant derivative, 63, 635
- Cramer's rule, 676
- Crank-Nicolson scheme, 614
- Critical angle, 86
- Crosstalk, 249
- Curl operator, 644, 649, 652
- Current
 - conduction current, 25
 - displacement current, 25
 - generalized, 335, 366
 - irrotational, 106
 - longitudinal, 106
 - modal current, 367
 - solenoidal, 106
 - transverse, 106
- Current density
 - impressed surface, 52
 - surface, 50, 52
- Cutoff frequency, 229, 279
 - material cutoff frequency, 45
- Cutoff phase coefficient, 268
- Cutoff wavelength, 279, 296, 328
 - circular cylindric waveguide, 296
 - radial waveguide, 302
 - rectangular waveguide, 279
- Degenerate modes, 254, 280
- Determinant, 675
 - Jacobian, 641
- Diagonalization, 681
- Dielectric loss, 45
 - rectangular waveguide, 291
- Differential form, 13
 - closed form, 634
 - degree, 42
 - differential form phasor, 43
 - double form, 161, 654
 - electric field differential form, 13
 - exact form, 634
 - exterior differential form, 17
 - inner product, 692
 - magnetic field differential form, 15
- Differential operator
 - curl, 656
 - divergence, 656
 - gradient, 656
- Dipole, 519, 548
 - electric dipole, 158
 - half-wave dipole, 552
 - radiation resistance, 555
- Dirac delta distribution, 48
 - three-dimensional, 129, 153
- Directional coupler, 460
- Directivity, 548
- Dirichlet boundary condition, 272
- Divergence operator, 645, 649, 652
- Double factorial, 660
- Double form
 - double one-form, 161, 654
 - one-two, 163
- Duality, 66
- Dyadic, 654
- Dyadic product, 678
- Effective
 - antenna length, 564, 565
 - aperture, 570
 - area, 570
 - transverse polarization, 366, 451
 - transverse polarization modal amplitude, 367
- Eigenfrequency, 407
- Eigenfunction, 270, 272
- Eigenvalue, 270, 272, 679
 - degenerate, 270
 - discrete spectrum, 269, 272
 - equation, 680
 - matrix, 680
 - problem, 408
- Eigenvector, 679
- Electric charge, 23, 28, 29
 - density, 23, 26
 - density form, 23
- Electric current, 15, 28, 29
 - density, 16–18, 26
 - density form, 18
- Electric displacement, 19
 - two-dimensional form, 179
- Electric displacement form, 20
- Electric field, 10
 - force picture, 14
 - integral equation, 135
 - intensity, 10, 12, 26
- Electric flux, 12, 20, 25, 28, 29
 - density, 19, 20, 25, 26, 48

- form, 20
- Electric force, 11
- Electric polarization
 - impressed, 64, 65
 - impressed form, 64
 - impressed phasor, 65
- Electric potential, 13
 - electric potential difference, 13
- Electric power, 115
- Electromagnetic
 - field, 9
 - interference, 230
 - potentials, 61
 - time-harmonic field, 43
- Electromagnetic wave, 29
 - homogeneous wave equation, 64
 - plane wave, 29, 30, 32, 35
 - time-harmonic, 34
 - wave equation, 36, 61
 - wave front, 30, 31
- Electroquasistatic approximation, 152, 153
- Electrostatic field, 151
- Element pattern, 575
- Elliptic function, 199
 - inverse, 193
 - modulus, 199
- Elliptic integral
 - complete of the first kind, 194, 265
 - complete of the second kind, 194, 265
- Energy, 12, 13
 - electric density, 109
 - magnetic density, 109
- Energy density
 - time-average electric form, 113
 - time-average magnetic form, 113
- Energy picture, 6
- Entire function, 705
- Equivalence principle, 121
- Equivalent
 - circuit, 39, 395
 - sources, 121
- Evanescence
 - field, 88, 89
 - mode, 232
- Exterior derivative, 634
 - curvilinear coordinates, 643
 - transverse, 138, 365, 646
- Exterior differential form, 631
 - p -form, 631
 - one-form, 13, 20
 - three-form, 23
 - two-form, 17, 20
 - zero-form, 23
- Exterior product, 5, 17
- Factorial, 660
- Far-field, 522–524, 526, 527, 552, 553, 561, 563, 572, 581
 - antenna array, 575
 - approximation, 105
 - circular cylindric wave, 102
 - dipole over ground, 538
 - horn antenna, 583
 - linear dipole antenna, 553, 565
 - loop antenna, 563
 - slot antenna, 590
 - surface emitter, 581
- Faraday's law, 4, 26, 42, 44, 242, 287
- Faraday, Michael, 2, 26
- Field
 - concept, 9, 12, 116
 - conservative, 62
 - intensity, 18
 - irrotational, 62
 - line, 14
 - macroscopic, 19
 - magnetic, 10
 - magnetic intensity, 15, 26
 - quasistatic, 152
 - static, 151
 - transverse electric, 76
 - transverse magnetic, 74
- Filter
 - frequency transformation, 492
 - low-pass prototype filter, 492
- Finite
 - difference method, 604, 611
 - element method, 604
 - integration method, 611
- Floquet modes, 504
- Floquet's theorem, 471
- Flux density, 18
 - electric, 19
- Flux linkage, 166
- Force picture, 6
- Foster
 - equivalent circuit, 395
 - reactance theorem, 387, 388

- representation, 394
- Fourier series, 697
- Fractional expansion representation, 394
- Frequency, 34
 - angular frequency, 34
 - band, 1
 - normalized, 482, 485
 - transformation, 492, 493, 495
- Fresnel formula, 82, 85, 88, 89
- Fresnel lens, 589
- Friis transmission formula, 575
- Function
 - complete set of, 145, 146
 - inner product, 144, 691
 - norm, 144
 - orthonormal basis, 691
 - space, 691
 - square integrable, 144
- Fundamental mode polarization sheet, 451
- Gain, 569
- Gamma function, 660
- Gauge
 - Coulomb, 106
 - Lorenz, 63
 - radiation, 106
 - transformation, 62
 - transverse, 106
- Gauss' law, 26
- Generalized
 - current, 408, 429
 - voltage, 408, 428
- Generating function, 662, 664
- Generator impedance, 437
- Goos-Hänchen shift, 88
- Gradient, 643
- Gram-Schmidt orthogonalization method, 145
- Grassmann, Hermann, 5
- Green's form
 - double form, 129
 - double one-form, 161
 - dyadic, 129, 440
 - dyadic, admittance representation, 440
 - dyadic, impedance representation, 440
- Green's function, 128, 129, 147
 - dyadic, 161
 - dyadic, transmission-line, 379, 380
 - microstrip line, 264
 - scalar, 154
- Green's theorem, 128
 - first scalar, 137
 - first scalar two-dimensional form, 139
 - first vector theorem, 140
 - second scalar, 138
 - second scalar two-dimensional form, 140
 - second vector theorem, 141
- Group velocity, 233
- Guide wavelength, 278, 296
 - circular waveguide, 296
 - radial waveguide, 302
 - rectangular waveguide, 278
- Gyration conductance, 436
- Gyration, 435
- Hankel function, 99, 659, 660
 - of the first kind, 99, 659
 - of the second kind, 99, 659
 - spherical, 310, 665
- Hansen form, 96
- Harmonic function, 170
- Helmholtz equation, 65
 - homogeneous, 67, 87
 - inhomogeneous, 66
 - scalar, 95
 - spherical coordinates, scalar, 103
 - two-dimensional scalar, 267, 270
 - vector, 95
- Hermitian form, 678
 - positive definite, 678
 - positive semidefinite, 430, 678
- Hertz differential form
 - electric, 63
 - magnetic, 66
 - retarded electric, 132
 - retarded magnetic, 132
- Hertz vector, 519
 - differential form phasor, 65
 - electric, 63, 65, 66
 - magnetic, 66
- Hertzian dipole, 519, 522-524, 527, 528
 - receiving antenna, 563
 - time domain, 524
- Hilbert space, 144, 683
 - adjoint operator, 688
 - basis, 691
 - degenerate eigenvalue, 691
 - eigenvalue, 690
 - eigenvalue equation, 690

- eigenvalue spectrum, 690
- eigenvector, 690
- hermitian conjugate, 688
- hermitian operator, 689
- inverse operator, 688
- norm of a vector, 685
- null operator, 687
- null vector, 685
- operator, 686
- orthonormal basis vectors, 686
- projection operator, 690
- scalar product, 684
- self-adjoint operator, 689
- spectral representation of an operator, 691
- subspace, 694
- unit operator, 687
- unitary operator, 689
- Hodge operator, 20, 632
 - curvilinear coordinates, 47, 643
- Huygens' principle, 2, 121, 143
- Huygens, Christian, 2
- Hybrid junction, 461
- Hybrid mode, 232
- Hyperbolic cosine-transformation, 181, 182
- Identity kernel, 129, 130, 142, 162
- Image line, 231
- Impedance
 - matrix, 415
 - normalized, 350
 - per unit of length, 336
 - representation, 415
- Impressed current, 371
- Impressed current density, 28
- Impressed voltage, 371
- Inductance, 163, 165–167
 - mutual, 164, 165
 - per unit of length, 167, 168, 181, 238
 - self-inductance, 165
- Inductor, 4, 24, 152
- Inhomogeneous multiconductor transmission-
 - line, 259
- Inner product, 678
 - differential form, 692
 - function space, 691
- Insertion loss, 481
- Integral
 - equation, 135
 - equation method, 603
 - line, 13
 - surface integral, 17
- Kernel, 654
 - function, 144
 - identity kernel, 656
 - Richmond form, 557
- Kirchhoff's laws, 11, 38–40
- Kronecker delta symbol, 628
- Kronecker tensor, 629
- Laplace equation, 169
 - two-dimensional, 175, 235, 262
- Laplace expansion, 676
- Laplace operator, 63, 635
 - one-form, 67, 636
 - one-form, circular cylindric coordinates, 649
 - one-form, curvilinear coordinates, 550
 - one-form, spherical coordinates, 550, 652
 - scalar, circular cylindric coordinates, 649
 - scalar, curvilinear coordinates, 645
 - scalar, spherical coordinates, 652
 - transverse, 646
 - two-dimensional, 267, 646
- Laurent series, 707
- Legendre differential equation, 667
- Legendre function
 - associated, 667
 - associated, first kind, 667
 - associated, fractional degree, 309
 - associated, second kind, 667
 - ordinary, first kind, 667
 - ordinary, second kind, 667
- Legendre polynomials, 667
- Lens, 587
- Loop antenna, 560
 - far-field, 563
 - radiated power, 563
 - receiving antenna, 564, 565
- Lorentz
 - force, 10
 - reciprocity theorem, 125, 126
- Lorenz
 - condition, 62, 63
 - gauge, 63
- Maclaurin series expansion, 682
- Magic T, 461

- Magnetic flux, 12, 20, 28, 29
 - continuity law, 26
 - density, 11, 19, 20, 26, 48, 61
 - form, 20
 - per unit of length, 181, 240
 - two-dimensional density form, 180
- Magnetic force, 11
- Magnetic induction form, 20
- Magnetic loss, 45
- Magnetic polarization
 - impressed magnetic polarization, 66
- Magnetoquasistatic approximation, 152, 153
- Magnetostatic field, 151
- Magnitude, 678
- Main beam direction, 584, 586
- Material
 - equations, 19
 - left-handed, 508
 - macroscopic parameter, 19
- Mathieu
 - characteristic exponent, 474
 - characteristic values, 473
 - differential equation, 473
- Matrix, 673
 - cofactor, 676
 - commutator, 675
 - complex conjugate, 677
 - diagonal, 675
 - exponential of a matrix, 682
 - hermitian, 677
 - hermitian conjugate, 430, 677
 - matrix function, 682
 - null matrix, 674
 - orthogonal, 677
 - orthogonally similar, 681
 - power of a matrix, 681
 - product, 674
 - product with a scalar, 674
 - real, 677
 - singular, 676
 - sum, 673
 - symmetric, 677
 - transpose, 677
 - unit matrix, 675
 - unitarily similar, 681
 - unitary, 430, 678
- Maxwell's equations, 11, 28, 36
 - differential form, 42
 - integral form, 26
 - local form, 41
 - phasor representation, 44
- Maxwell, James C., 2, 26
- Medium
 - anisotropic, 21
 - inhomogeneous isotropic, 467
 - layered, 89
- Metamaterial, 507
 - dispersion relation, 515
- Method of lines, 604
- Method of moments, 603, 605, 617
- Metric coefficient, 46, 642
- Microstripline, 230, 254, 260
 - quasistatic approximation, 262
- Minor, 676
 - leading principal minor, 430, 679
- Mirror, 587
 - antenna, 587
 - principle, 226, 227, 547
- Mittag-Leffler expansion, 393
- Mode, 172
 - degeneration, 300
 - electrostatic, 172
- Mode matching, 604, 617
- Moving frame, 642
- Multiconductor transmission-line, 249
 - impedance matrix, 361
 - inhomogeneous, 259
 - mode current, 358
 - mode voltage, 358
 - power flow, 362
 - reflection coefficient matrix, 360
 - wave amplitude, 362
- Multiconductor transmission-line equations, 252
 - first-order frequency domain, 357
 - first-order time domain, 252, 357
 - second-order frequency domain, 357
 - second-order time domain, 252
- Multiport, 413
 - linear, 413
 - lossless, 430
 - passive, 430
 - port-number symmetric, 415
 - reciprocal, 432
 - source-free linear, 414
- Near field, 521
- Network concept, 11, 12, 116
- Network representation, 427

- Neumann function, 99, 659, 660
- Neumann's boundary condition, 269
- Normalized frequency, 319
- Observation space, 154, 161, 654
- Ohm's law, 28
- One-form
 - fundamental, 14
 - twisted one-form, 51, 653
 - unit one-form, 643
- One-port, 385
 - linear, 385
 - lossless, 430
 - passive, 386
 - reactive, 386
 - source-free, 386
- Operator
 - pseudoinverse, 695
- Operator equation, 606
- Optical fiber, 231
- Orthogonality, 286
- Orthogonality relation
 - associated Legendre function, 670
 - Bessel function, 662
 - Legendre function, 671
- Orthonormal system of eigenfunctions, 145
- Orthonormality relations
 - electric and magnetic structure forms, 274
 - waveguide structure forms, 367
- Parallel wire line, 186, 229
 - symmetric, 186
- Parasitic network elements, 41
 - parasitic capacitors, 41
 - parasitic inductors, 41
- Parseval's Theorem, 146
- Partial derivation, 36
- Partial wave synthesis method, 604
- Per-unit-length matrix
 - admittance, 357
 - conductance, 357
 - impedance, 357
 - resistance, 357
- Periodic signal, 697
- Permeability, 19
 - complex, 45
 - relative, 20, 45
 - space-dependent, 467
 - star operator, 21, 22
 - tensor, 21
- Permittivity, 19
 - complex, 44
 - relative, 20, 45
 - space-dependent, 467
 - star operator, 21
 - tensor, 21
- Permutation, 629
- Phase
 - center, 585
 - coefficient, 69
 - velocity, 232
- Phase plane, 70
- Phasor, 43
 - differential form phasor, 43
 - vector phasor, 43
- Planar transmission-line, 260
- Plane of incidence, 77
- Plane wave, 28, 29
 - time-harmonic, 67, 69
- Pocklington's integral equation, 556
- Poincaré's lemma, 61, 635
- Poisson equation, 153
 - vectorial, 161
- Poisson, Siméon, 2
- Polarization
 - circular, 38
 - direction, 34
 - electric, 19, 133
 - electric surface, 52
 - elliptic, 38
 - impressed electric, 125, 128, 129, 519
 - impressed equivalent, 120
 - impressed magnetic, 128, 129
 - linear, 34
 - linear polarization, 37
 - losses, 44
 - magnetic, 19, 133
 - magnetic surface, 53, 121
 - potential, 65, 66
- Port, 413
- Potential
 - magnetic vector, 61
 - scalar, 61
 - vector, 61
- Power
 - active, 385
 - complex, 385

- loss density, 110
- reactive, 385
- time-average electric dissipation density, 113
- Poynting
 - complex form, 112, 113
 - complex vector, 112
 - differential form, 110
 - theorem, 111, 114
 - time-dependent vector, 112
 - vector, 110, 111
- Product
 - cross, 629, 633
 - inner, 628
 - scalar, 628, 633
 - triple scalar, 630, 633
 - vector, 629
- Propagating mode, 231
- Propagation coefficient, 68, 75, 232, 336
- Propagation factor, 477
- Pseudoscalar, 630, 631
- Pseudovector, 630, 631
- Pullback
 - method of, 653
- Quality factor
 - external, 403
 - loaded, 403
 - resonator, 398
 - unloaded, 403
- Quasi
 - conductor, 45
 - dielectric, 45
- Quasi-TEM mode, 254, 260, 357
- Radiation
 - conductance, 591
 - diagram, 522
 - pattern, 547
 - resistance, 524, 554, 563, 570, 571, 573, 591
- Reactance
 - multiport, 430
 - one-port, 430
- Reaction, 126, 127
- Reciprocity, 125, 126
 - Lorentz theorem, 125, 126
 - theorem, 126, 127, 431
 - theorem, network form, 128
 - theorem, source-free multiports, 431
- Reflection coefficient, 81, 346, 434
- Refractive index, 32, 79
- Residue, 708
- Residue theorem, 707
- Resistance
 - per unit of length, 246
- Resonant circuit, 385
 - damping, 392
 - relative bandwidth, 392
 - series, 389
- Resonant frequency, 407
- Resonator, 385, 395
 - cavity, 395
 - transmission-line, 392
- Return loss, 481
- Ring array, 577
- Saddle-point method, 708
- Scalar, 630, 631
 - true scalar, 23
- Scattering matrix, 422
- Schwarz-Christoffel transformation, 191
- Secular equation, 680
- Signal flow graph, 436
 - loop, 438
 - path, 438
- Signal flow graph, 436
- Singular point, 706
- Singularity, 706
- Skin effect, 212
 - penetration depth, 93, 212, 218
 - surface impedance, 219, 220
 - surface inductance, 220
- Smith chart, 347
- Snell's law, 79
- Solenoid, 151, 165
- Solenoidal field, 61
- Sommerfeld pole, 536
- Sommerfeld radiation condition, 105, 142
- Source space, 154, 161, 654
- Space harmonics, 504
- Spectral domain method, 603
- Speed of light, 9, 28, 32
- Spherical Hankel function, 310
 - fractional order, 310
- Spherical harmonic, 103, 670
- Spherical wave
 - aperiodic, 524
- Spherical waveguide, 309

- Spherical waves
 - transverse magnetic, 104
- Standing wave ratio, 350
- Star operator, 20, 23, 632
 - curvilinear coordinates, 643
- Step function, 703
- Step wave, 32
- Stokes' theorem, 42, 640
 - two-dimensional, 139
- Stripline, 115, 197
- Structure form
 - biorthogonal, 426
 - biorthonormal set, 275
 - electric, 237, 408
 - magnetic, 237, 408
- Structure function, 286
 - biorthonormal, 426
 - electric, 237
 - magnetic, 237
 - TE, 338
 - TEM, 237, 338
 - TM, 338
- Sturm-Liouville differential equation, 143, 146
- Surface
 - current density, 218
 - emitter, 581, 585, 586
 - impedance, 52, 220
 - impedance operator, 222
 - impedance plane, 501
 - induced current, 224
 - resistance, 220
 - wave, 207, 208, 214, 216, 220, 535, 540
 - wave attenuation, 221
- Surface impedance
 - matrix, 94
- Symmetry, 456
 - mirroring, 456
 - rotation, 456
 - symmetry operations, 456
- TE mode, 232
 - propagation coefficient, 267
- Tellegen's theorem, 425
 - field form, 118
 - field representation, 117
 - general network form, 427
 - network form, 425
 - wave amplitude representation, 427
- Three-form, 23
 - fundamental, 23
- TLM node
 - symmetric condensed, 615
- TM mode, 232
 - propagation coefficient, 270
- Transadmittance, 434
- Transformation
 - linear fractional, 347
 - logarithmic, 183
 - orthogonal, 681
- Transformer, 164
- Transimpedance, 434
- Transmission
 - coefficient, 81
 - factor, 574
 - matrix, 424, 620
 - representation, 424
- Transmission coefficient, 434
- Transmission-line, 229
 - antenna mode, 244
 - equation, 242, 246, 335
 - first-order homogeneous equation, 374
 - first-order inhomogeneous equation, 372
 - generalized, 622
 - inhomogeneous, 254, 356
 - left-handed, 509
 - multiconductor, 249
 - radiation loss, 230
 - second-order homogeneous equation, 374
- Transmission-line matrix method, 604, 611
 - TLM cell, 611, 613
 - TLM node, 613
- Transverse
 - electric field, 76
 - electric spherical waves, 104
 - exterior derivative, 646
 - field equations, 366
 - magnetic field, 74
 - wave formulation, 618
- Twist operator, 51, 653
- Twisted one-form, 51, 179, 653
- Two-form, 13, 17
 - fundamental, 18
 - tube representation, 18
- Two-port, 450
 - reciprocal, 433
 - symmetrical, 433, 451
- Two-port current-voltage source, 372, 434

- Uniform plane wave, 68
- Uniqueness theorem, 120
- Unit one-form, 46
- Unit operator
 - biorthogonal, 694
- Unitary transformation, 681
- V-product, 693
- Vector, 627, 631
 - axial vector, 630
 - column vector, 673
 - dyadic product, 678
 - field, 10
 - hermitian conjugate, 430
 - inner product, 678
 - magnitude, 628, 678
 - norm, 678
 - orthonormal basis vector, 629, 642
 - polar vector, 628
 - product, 11
 - row vector, 673
 - tangent vector, 642
 - vector phasor, 43
- Vector space
 - basis, 627
- Voltage, 13, 28
 - electric, 28
 - generalized, 335, 366
 - magnetic, 28
 - modal, 367
 - open-circuit, 436
- Voltage standing wave ratio, 350
- Wave
 - amplitude, 619
 - circular cylindrical, 98
 - complex, 72
 - number, 34
 - packet, 232
 - spherical, 102
 - transverse electric, 73, 76
 - transverse electromagnetic, 72, 235
 - transverse magnetic, 75
- Wave amplitude
 - generator, 437
- Wave equation, 35, 36, 63
 - one-form wave equation, 63
 - scalar wave equation, 63
 - vector, 95
 - vector wave equation, 63
- Wave impedance, 32, 66, 71
 - circular waveguide, 297
 - evanescent field, 88, 89
 - free-space, 32, 213
 - quasi-conductor, 213
 - radial waveguide, 302
 - rectangular waveguide, 281, 284
 - TE wave, 77, 81, 91, 92, 268
 - TEM wave, 76
 - TM wave, 76, 84, 271
- Wave impedance operator, 619
- Wave vector, 67
- Waveguide, 229
 - biconical, 309, 311, 313
 - circular, 230
 - conical, 309, 311
 - coplanar, 254, 265
 - dielectric, 230
 - dielectric circular, 230
 - dielectric loss, 244
 - hollow, 230, 266
 - inhomogeneous, 260
 - junction, 457
 - periodic rectangular, 467
 - phase coefficient, 232
 - planar dielectric, 316
 - power flow, 284
 - radial, 300
 - radiation loss, 244
 - rectangular, 230, 276
 - skin effect losses, 244
 - spherical, 309
 - wedged radial, 307
- Wavelength, 34
 - cutoff, 279
 - guide wavelength, 278, 296
- Wedge product, 17
- Wronskian, 662
- Zenneck surface wave, 208, 535, 539
- Zero-form, 23

Recent Titles in the Artech House Antennas and Propagation Library

Thomas Milligan, Series Editor

Adaptive Array Measurements in Communications, M. A. Halim

Advances in Computational Electrodynamics: The Finite-Difference Time-Domain Method, Allen Taflove, editor

Analysis Methods for Electromagnetic Wave Problems, Volume 2, Eikichi Yamashita, editor

Antenna Design with Fiber Optics, A. Kumar

Antenna Engineering Using Physical Optics: Practical CAD Techniques and Software, Leo Diaz and Thomas Milligan

Applications of Neural Networks in Electromagnetics, Christos Christodoulou and Michael Georgiopoulos

The Art and Science of Ultrawideband Antennas, Hans Schantz

AWAS for Windows Version 2.0: Analysis of Wire Antennas and Scatterers, Antonije R. Djordjević, et al.

Broadband Microstrip Antennas, Girsh Kumar and K. P. Ray

Broadband Patch Antennas, Jean-François Zürcher and Fred E. Gardiol

CAD of Microstrip Antennas for Wireless Applications, Robert A. Sainati

The CG-FFT Method: Application of Signal Processing Techniques to Electromagnetics, Manuel F. Cátedra, et al.

Computational Electrodynamics: The Finite-Difference Time-Domain Method, Second Edition, Allen Taflove and Susan C. Hagness

Electromagnetic Modeling of Composite Metallic and Dielectric Structures, Branko M. Kolundzija and Antonije R. Djordjević

- Electromagnetic Waves in Chiral and Bi-Isotropic Media*,
I. V. Lindell, et al.
- Electromagnetics, Microwave Circuit and Antenna Design for
Communications Engineering, Second Edition*, Peter Russer
- Engineering Applications of the Modulated Scatterer Technique*,
Jean-Charles Bolomey and Fred E. Gardiol
- Fast and Efficient Algorithms in Computational Electromagnetics*,
Weng Cho Chew, et al., editors
- Fresnel Zones in Wireless Links, Zone Plate Lenses and Antennas*,
Hristo D. Hristov
- Handbook of Antennas for EMC*, Thereza MacNamara
- Iterative and Self-Adaptive Finite-Elements in Electromagnetic
Modeling*, Magdalena Salazar-Palma, et al.
- Measurement of Mobile Antenna Systems*, Hiroyuki Arai
- Microstrip Antenna Design Handbook*, Ramesh Garg, et al.
- Mobile Antenna Systems Handbook, Second Edition*, K. Fujimoto
and J. R. James, editors
- Phased Array Antenna Handbook, Second Edition*, Robert J.
Mailloux
- Quick Finite Elements for Electromagnetic Waves*,
Giuseppe Pelosi, Roberto Coccioli, and Stefano Selleri
- Radiowave Propagation and Antennas for Personal
Communications, Second Edition*, Kazimierz Siwiak
- Solid Dielectric Horn Antennas*, Carlos Salema, Carlos Fernandes,
and Rama Kant Jha
- Switched Parasitic Antennas for Cellular Communications*,
David V. Thiel and Stephanie Smith
- Understanding Electromagnetic Scattering Using the Moment
Method: A Practical Approach*, Randy Bancroft
- Wavelet Applications in Engineering Electromagnetics*,
Tapan Sarkar, Magdalena Salazar Palma, and Michael C. Wicks

For further information on these and other Artech House titles,
including previously considered out-of-print books now available through our
In-Print-Forever® (IPF®) program, contact:

Artech House
685 Canton Street
Norwood, MA 02062
Phone: 781-769-9750
Fax: 781-769-6334
e-mail: artech@artechhouse.com

Artech House
46 Gillingham Street
London SW1V 1AH UK
Phone: +44 (0)20 7596-8750
Fax: +44 (0)20 7630 0166
e-mail: artech-uk@artechhouse.com

Find us on the World Wide Web at:
www.artechhouse.com
